

2-0

AD A 0 6 8 9 8 2

PROCEEDINGS

OF THE

FOURTH CONFERENCE

ON THE

CLIMATIC IMPACT ASSESSMENT PROGRAM



EDITED BY

THOMAS M. HARD ANTHONY J. BRODERICK

79 05 24 001

SPONSORED BY THE U.S. DEPARTMENT OF TRANSPORTATION

DOCUMENT IS AVAILABLE THROUGH THE NATIONAL TECHNICAL INFORMATION SERVICE SPRINGFIELD VIRGINIA 22161

HELD AT THE

TRANSPORTATION SYSTEMS CENTER KENDALL SQUARE CAMBRIDGE MASSACHUSETTS 02142 REPRODUCED BY
NATIONAL TECHNICAL
INFORMATION SERVICE
U.S. DEPARTMENT OF COMMERCE
SPRINGFIELD, VA. 22161

NOTICE

The views expressed in these papers are the authors' personal opinions, and do not necessarily reflect those of any organization of which they may be members. The Department of Transportation is distributing this document in the interest of information exchange, and assumes no liability for its contents.

Technical Report Documentation Page

DOT TEC OFT 75 20		2. Government Access		1	
DOT-TSC-OST-75-38				(11)	
Title and Subtitle	manufacture of the second	an Aba Oli and T		August 1976	
Proceedings of the R Assessment Program	C4th),	[43		6. Performing Organiza	tion Code
4-1 tebr	yary 19	75, (A000	0	8. Performing Organiza	tion Report No.
Thomas M. Hard A	nthony J. Broder	ick Cambrio	lge.	DOT TSC-OST-75	
9. Performing Organization DOT Transportation Sy		Massac	husetts	10. Work Unit No. (TRA R6552	
Kendall Square Cambridge MA 02142			The second second second	PRA 06620	
12. Sponsoring Agency Na	me and Address			13. Type of Report and	
Office of the Secretary Department of Transpo			5.71	Conference Procee February 4-7, 1975	
400 Seventh St. SW Washington DC 20590		- 4	5	14. Sponsoring Agency	Code
and edited question an	d-answer eychang	es following some of	the sessions Reports	s on work relevant to	CIAP, though
and edited question-an not sponsored by it, ar Canada, and Japan; bio the aviation industry; t spheric pollution; meas laboratory; and chemis	d-answer exchange included. Amore blogical effects of theoretical models burements of the contents of the contents.	es following some of ing the topics address ultraviolet irradiation of atmospheric com concentrations of trad	the sessions. Reports ed are the related prog n and climate change; position, radiation, ar ce species in the strate	s on work relevant to grams in the United K consequences of NO _x nd climate and their re	CIAP, though ingdom, France restrictions for esponse to strate
and edited question-an not sponsored by it, ar Canada, and Japan; bio the aviation industry; t spheric pollution; meas	d-answer exchange included. Amore blogical effects of theoretical models burements of the contents of the contents.	es following some of ing the topics address ultraviolet irradiation of atmospheric com concentrations of trad	the sessions. Reports ed are the related prog n and climate change; position, radiation, ar ce species in the strate	s on work relevant to grams in the United K consequences of NO _x nd climate and their re	CIAP, though ingdom, France restrictions for esponse to strate
and edited question-an not sponsored by it, ar Canada, and Japan; bid the aviation industry; t spheric pollution; meas laboratory; and chemis laboratory; and chemis ozone atmosphozone emissions SST's aerosols cost/benefit atmosphozone plant re	d-answer exchange included. Amore logical effects of theoretical models surements of the catry and optics of the catry and opt	NO _x climate sampling pollutants stratosphere photochemistry	the sessions. Reports and are the related program and climate change; position, radiation, and the species in the strate	s on work relevant to grams in the United K consequences of NO _X and climate and their reposphere and their reactions. The complete and their reactions are also service springfield.	CIAP, though ingdom, France restrictions for esponse to strate tion rates in the
and edited question-an not sponsored by it, ar Canada, and Japan; bid the aviation industry; t spheric pollution; meas laboratory; and chemis laboratory; and chemis ozone atmospications atmospications SST's aerosols ultravio	d-answer exchange included. Amore logical effects of theoretical models surements of the catry and optics of the catry and opt	NO _x climate sampling pollutants stratosphere	the sessions. Reports and are the related program and climate change; position, radiation, and the strate sees are species in the strate sees. 18. Distribution States DOCUMENT IS A THROUGH THE INFORMATION VIRGINIA 22161	s on work relevant to grams in the United K consequences of NO _X and climate and their reachesphere and their rea	CIAP, though ingdom, France restrictions for esponse to strate tion rates in the

NIIS	White Section
DDC	Buff Section
NANNOUN	CLD []
JUSTI ICAT	ION
BY	MILITAL MARKET STATE
DISTRIBUTE	ON/AVA! ABILITY CODES
	ON/AVAI: ABILITY CODES SPECIAL
DISTRIBUTE	

FOREWORD

In August 1971, the U.S. Department of Transportation initiated its Climatic Impact Assessment Program. Its purpose, then as now, was to investigate the impact on the environment of high-flying aircraft. The progress made since its inception has been reported in three earlier DOT CIAP conferences. These international conferences have provided forums for vigorous discussion by scientists, engineers, and public servants of the scientific and technological results of the many and multidisciplinary studies undertaken during CIAP, as well as the socio-economic implications of these results. The proceedings of this, the fourth and last DOT CIAP conference, contain a summary and a discussion of the CIAP "Report of Findings: The Effects of Stratospheric Pollution by Aircraft." It also contains many papers describing the latest data and designating problem areas of importance.

The analyses described in the "Report of Findings" are based on data compiled in the six DOT CIAP monographs, which were published (subsequent to the Fourth CIAP Conference) in December 1975.

A consequence of the CIAP project has been the discovery that high-flying subsonic aircraft also have an impact on the ozone layer, and that pollutants other than those emitted into the stratosphere by high-flying aircraft have a serious impact on stratospheric ozone. All in all, CIAP has encouraged others to study more comprehensively the effect on man's environment of all pollutants in the atmosphere.

We want to take this opportunity to express our sincere thanks and appreciation to a very large number of persons who have been involved directly, indirectly, and peripherally with this U.S. Department of Transportation Climatic Impact Assessment Program.

Samuel C. Coroniti
Deputy Manager of CIAP
Department of Transportation

Alan J. Grobecker Manager of CIAP Department of Transportation

March 24, 1976

EDITORS' PREFACE

The Fourth Conference on the Climatic Impact Assessment Program, held in Cambridge, Massachusetts February 4 through 7, 1975, was the final conference in a series dedicated to exchange of ideas among scientists, engineers, and others concerned with pollution of the stratosphere by aircraft. We feel that the *Proceedings* of this conference reflect the participants' diverse disciplines and viewpoints, as well as their unifying desire to understand and protect the stratosphere as a resource.

It has taken us longer to get these *Proceedings* to press than we hoped. The principal factor in this was probably the fact that speakers who had prepared only oral presentations were requested months after the conference to produce manuscripts. All but one of them complied, and we very much appreciate the extra effort involved.

In addition, of course, each paper was edited (as was the panel discussion), and the author was sent galley proofs of the final version. The question-and-answer sessions were heavily edited and condensed, and reviewed only by us; we apologize for any errors that may have crept in.

As always, the greatest burden was borne by Ms. Ellen F. Rice of the Raytheon Service Company, who wheedled manuscripts from authors, reviewed them minutely, and shepherded them through the production cycle. That we have a CIAP 4 *Proceedings* of this completeness and quality is in large part her doing.

Thomas M. Hard Anthony J. Broderick Editors

PROCEEDINGS OF THE FOURTH CONFERENCE ON THE CLIMATIC IMPACT ASSESSMENT PROGRAM

U.S. DEPARTMENT OF TRANSPORTATION

FEBRUARY 1975

CONTENTS

CIAP REPORT OF FINDINGS

The Effects of Stratospheric Pollution by Aircraft	1
Panel Discussion	24
OTHER CIAP-TYPE PROGRAMS	
The Committee on Meteorological Effects of Stratospheric Aircraft (COMESA) . R.J. Murgatroyd	39
Principal Activities of COVOS in 1974	45
Stratospheric Ozone Layer Research	55
CIAP-Type Research in Japan	58
BIOLOGICAL AND ECONOMIC IMPACT	
Effects on Plants of Increased UV-B Radiation	62
Estimate of the Effect of Ozone Reduction in the Stratosphere on the Incidence of Skin Cancer in Man	66
Potential Effects on Aquatic Ecosystems of Increased UV-B Radiation D. Stuart Nachtwey	79
A Summary of Estimated Impacts of Climatic Change on Crop Productivity Ray E. Jensen	87
Economic Analyses of Pollution Resulting from Stratospheric Flight: A Preliminary Review Ralph C. d'Arge	97
Discussion	108
ENGINE EMISSIONS AND REGULATORY CONSEQUENCES	
Attainment of Ultra-Low NO _x Emissions Levels in Aircraft Turbine Engines Donald W. Bahr	109
Fleet Projections and What They Mean in Terms of SST Fleet Effluents	
J. Morley English and Gerard L. Kernan	118
Possible Impact of Regulations on Airlines	127
Discussion	130
THEORY OF ATMOSPHERIC MOTIONS AND CLIMATE	
Some Fundamental Limitations of Simplified-Transport Models as Implied by Results from a Three-Dimensional General-Circulation/Tracer Model	132

The Philosophy of One-Dimensional Modeling	147
Use of Excess Carbon-14 Data to Calibrate Models of Stratospheric Ozone Depletion by Supersonic Transports	156
Uncertainties in the Validation of Parameterized Transport in 1-D Models of the Stratosphere Julius S. Chang	175
Climate-Model Results of Stratospheric Perturbations	183
The Design of a Statistical-Dynamical Climate Model, and Statistical Constraints on the Predictability of Climate	195
Ozone Production and Transport with the UCLA General-Circulation Model Yale Mintz and Michael Schlesinger	201
Discussion	223
THEORY OF RADIATIVE TRANSFER	
The Stratosphere: Scattering Effects, a Coupled 1-D Model, and Thermal Balance Effects L.B. Callis, V. Ramanathan, R.E. Boughner, and B.R. Barkstrom	224
The UV Radiation Field in the Stratosphere	234
Results from Recent Solar Radiation Calculations Frederick M. Luther	242
Determining Atmospheric Composition from Vertical Profiles of Daytime Limb Brightness K. Ya. Kondratyev, O.M. Pokrovsky, and M.A. Skorodenok	254
Discussion	263
THEORY OF STRATOSPHERIC CHEMISTRY	
A Two-Dimensional Photochemical Model of the Atmosphere Below 55 km: Estimates of Natural and Man-Caused Ozone Perturbations Due to NO _x	264
Chlorine in the Stratosphere	280
The Chemistry of Atmospheric Bromine	2000
Steven C. Wofsy, Michael B. McElroy, and Yuk Ling Yung	286
On the Production of Nitric Oxide by Cosmic Rays in the Mesosphere and Stratosphere M. Nicolet	292
Chemical Modeling of Perturbations Caused by NO _x Emissions	303
A Two-Dimensional Photochemical Model of the Stratosphere, Including Initial Results of Inert- Tracer Studies	316
Eddy Diffusivity Profiles R.C. Whitten, W.J. Borucki, and R.P. Turco	332
Discussion	333
INTERPRETATION OF LARGE COALE EVERNMENTS	
INTERPRETATION OF LARGE-SCALE EXPERIMENTS	
On the Response of Hemispheric Mean Temperature to Stratospheric Dust: An Empirical Approach	335
The Effect of Atmospheric Nuclear Explosions on Total Ozone	354
Ernest Bauer and Forrest R. Gilmore	354
LANCHESTON	46.5

LABORATORY MEASUREMENTS

Laboratory Studies of Stratospheric OH and Cl Reactions J.G. Anderson, J.J. Margitan, M.S. Zahniser, and F. Kaufman	366
Chlorine-Atom Reactions of Atmospheric Importance R.T. Watson, E.S. Machado, R.L. Schiff, S. Fischer, and D.D. Davis	372
Reaction Rate Data for the Stratosphere: How Good Are They Now? D. Garvin, R.F. Hampson, and M.J. Kurylo	391
Discussion	397
VISIBLE-ULTRAVIOLET RADIOMETRY	
WB57F-Borne Measurements of UV Flux and Ozone Overburden Bach Sellers and Frederick A. Hanser	398
Erythemal Ultraviolet Solar Radiation and Environmental Factors L. Machta, G. Cotton, W. Hass, and W. Komhyr	405
Discussion	411
TRACE-GAS CONCENTRATION MEASUREMENTS	
The AES Stratospheric Balloon Measurements Project: Preliminary Results W.F. Evans, J.B. Kerr, and D.I. Wardle	412
Measurements of NO between 17 and 34.5 km from Churchill, Manitoba B.A. Ridley, J.T. Bruin, H.I. Schiff, and J.C. McConnell	417
Latitudinal Measurements of NO and O ₃ in the Lower Stratosphere from 5.5° to 82° North Max Loewenstein and Howard Savage	422
Seasonal Variations of NO and O ₃ at Altitudes of 18.3 and 21.3 km Max Loewenstein, H.F. Savage, and R.C. Whitten	425
Variation of HNO ₃ Total Column Density with Latitude and Season, and a Measurement of Stratospheric CF ₂ Cl ₂ D.G. Murcray, D.B. Barker, J.N. Brooks, A. Goldman, J.J. Kosters, F.H. Murcray, and W.J. Williams	432
Simultaneous Measurements of NO and NO ₂ in the Stratosphere, and the Partitioning of Odd-Nitrogen Species	438
Spectroscopic Detection and Vertical Distribution of HCl in the Stratosphere Crofton B. Farmer, Odell F. Raper, and Robert H. Norton	449
NO ₂ Measurements by Absorption Spectrophotometer: Observations from the Ground and High-Altitude Balloon, Churchill, Manitoba, July 1974. R.M. Bloxam, A.W. Brewer, and C.T. McElroy	454
The Measurement of Atomic Oxygen and Hydroxyl in the Stratosphere J.G. Anderson	458
Stratospheric Halogen Measurements and In-Situ Determination of Accuracy of Nitric Acid Measurements	465
Discussion	468
THEORIES OF AEROSOL CHEMISTRY AND OPTICS	
Heterogeneous Processes and the Chemistry of Aerosol Formation in the Upper Atmosphere A. W. Castleman, Jr., R.E. Davis, I.N. Tang, and J.A. Bell	470

Can Ions Contribute to Stratospheric Aerosol Formation?	478
Energy Exchange of Aerosols in the Stratosphere	
Giorgio Fiocco, Gerald Grams, and Alberto Mugnai	492
Discussion	496
AEROSOL AND ION CONCENTRATION MEASUREMENTS	
Lidar Observations of the Stratospheric Aerosol: Summary of Results and a Calibration-Error Assessment	497
A Comparison of Dustsonde and Lidar Measurements of Stratospheric Aerosols Ellis E. Remsberg and G. Burton Northam	509
Recent Measurements of Aitken Nuclei in the Lower Stratosphere J. Podzimek, J.B. Haberl, and W.A. Sedlacek	519
In-Situ Measurements at Laramie, Wyoming of the Recent Increase in Stratospheric Aerosol D.J. Hofmann and J.M. Rosen	527
Ion and Aerosol Measurement in the Stratosphere Haruji Ishikawa, Yasuhiro Morita, and Masumi Takagi	530
Discussion	534
Publications of the Climatic Impact Assessment Program	535
List of Registrants	536
Detailed Author Index for All CIAP Conference Proceedings	551
Index of First Authors, This Volume (facing inside back	cover)

THE CIAP REPORT OF FINDINGS: THE EFFECTS OF STRATOSPHERIC POLLUTION BY AIRCRAFT

ALAN J. GROBECKER

Manager, Climatic Impact Assessment Program
U.S. Department of Transportation
Washington, D.C.

HISTORY

This paper will outline the form of the analysis which has led to the conclusions stated in the Report of Findings of the Department of Transportation's Climatic Impact Assessment Program. As can often be the case with such a complicated subject, the data on which all agree may still lead to conclusions or recommendations with which not all agree.

During the discussion of the U.S. supersonic-transport project in 1970, the question was raised, notably by James McDonald, the SCEP study, and Harold Johnston, whether impurities resulting from aircraft flight high in the stratosphere could alter the proportions of atmospheric trace constituents, with harmful results to the earth's environment. The question is an important one.

While they make up only a tiny fraction of the atmosphere, the trace constituents in their natural proportions control the balance of life on Earth, passing light while reducing lethal radiation that would otherwise reach the earth's surface. Flight in the stratosphere, that is, generally above 12 kilometers or 39,000 feet altitude, is of concern; flight in the troposphere below is not. The reason for the distinction is that through turbulence, storms, and rainfall, the troposphere cleanses itself of most water-soluble and particulate impurities in a matter of a few days or weeks, but the stratosphere is virtually stagnant in its vertical dimension and cannot cleanse itself so rapidly. Impurities can remain in the mid-stratosphere for as long as three years, so at any one time there may be as much as a three-year accumulation of contaminants. The horizontal dispersion of contaminants, on the other hand, is worldwide and comparatively rapid. The stratospheric fleet of any nation affects the stratosphere of the entire hemisphere

in which they fly. High-altitude flights over Europe can contaminate the sky over the United States and vice versa.

In 1970, large uncertainties existed in our understanding and knowledge of the stratosphere's constitution, of its dynamic and chemical behavior, and of how the climatic and biological processes are affected by the atmosphere. At that time there was no adequate scientific basis for judging where in the range from negligible to significant the conjectured effects of stratospheric flight operations might fall. However, the questions raised by the scientists at that time were good ones; subsequent studies have shown many of their fears to be justified. During the Congressional debate in July 1970, legislation introduced by Senator H.M. Jackson directed the Department of Transportation to undertake a program to obtain the new knowledge needed for judging how serious the conjectured effects might be, and to report its results to the Congress by the end of calendar year 1974.

The Department of Transportation's Report of Findings, which I am abstracting this morning, describes the results of the ensuing program.

The DOT Climatic Impact Assessment Program (CIAP) has drawn on the work of nine other U.S. Federal Departments and Agencies and seven foreign ones. It has also drawn on the individual talents of some 1000 investigators at numerous universities and other organizations in the United States and abroad. It has of necessity encompassed a wide range of science and technology. A special committee of the National Academy of Sciences and the National Academy of Engineering was organized to review the work of CIAP and to form an independent judgment of the results; its report appears as Environmental Impact of Stratospheric Flight (NAS, 1975). The members of this Climatic Impact

Committee have worked hard on the problems through two years of CIAP. CIAP has harvested many new scientific data and has progressed considerably in synthesizing the data to give a better understanding of the relationships between the aircraft effluents in the stratosphere and their environmental impacts. Although serious uncertainties still exist, their magnitude has been reduced substantially, so that the useful scientific conclusions can be used for establishing approximate technical and operational standards that will assure a chosen level of atmospheric quality in the course of the future development of air travel.

Because of the long lead time involved in preparing remedies, the process of establishing and meeting standards should start now. Only by means of such standards can the future large-scale development of SST operations, by any nation, occur without significant adverse environmental consequences. Moreover, only by means of such standards can the subsonic fleet continue to evolve without similar undesirable consequences.

While the environmental pollutants from aircraft discussed today are important, they are by no means the only causes of undesirable effects at the ground (changes in ultraviolet radiation, temperature, rainfall, etc.). A few examples of contributing causes are aerosol sprays, and industrially generated dust and carbon monoxide. There are many others.

The principal scientific conclusions of CIAP are as follows (Grobecker et al., 1974):

- "1. Operations of present-day SST aircraft and those currently scheduled to enter service (about 30 Concordes and TU-144's) cause climatic effects which are much smaller than minimally detectable.
- "2. Future harmful effects to the environment can be avoided if proper measures are undertaken in a timely manner to develop low-emission engines and fuels in step with the future growth of stratospheric aviation. These measures include:
 - a. The development of new engine technology leading to lower levels of nitrogen oxide emissions (which involves a lead time of 10 to 15

- years for development, fabrication, certification, and introduction into service of the new engines).
- b. Use of jet fuels having a sulfur content smaller than that in current fuels, through the application of state-of-the-art desulfurization processes.
- "3. If stratospheric vehicles (including subsonic aircraft) beyond the year 1980 were to increase at a high rate, improvements over 1974 propulsion technology would be necessary to assure that emissions in the stratosphere would not cause a significant disturbance of the environment.
- "4. The cost of carrying out the measures in conclusion 2, including the operational cost of compliance, is small compared to the potential economic and social costs of not doing so.
- "5. A continuous atmospheric monitoring and research program can further reduce remaining uncertainties, can ascertain whether the atmospheric quality is being maintained, and can minimize the cost of doing so."

The numbers which make these statements of conclusion quantitative are to be found in the Report of Findings, which is due for wide distribution. We hope there will be scientific agreement on these conclusions, which suggest certain courses of action. The suggested courses of action represent recommendations, which are listed below:

- "1. Develop, within the next year, a plan for a proper program for international regulation of aircraft emissions and fuel characteristics for whatever stratospheric flight operations may evolve in the future.
- "2. Accelerate combustion research and engine development programs needed to make stratospheric flight possible with specified nitrogen oxide emission standards.
- "3. Use low-sulfur fuels. Study the implications of utilizing low-sulfur content aviation fuels for stratospheric flight.

"4. Develop a global monitoring system to ensure that environmental protection is being achieved. Continue research (drawing on the monitored data) to reduce the uncertainties in the present knowledge of the stratosphere and improve the methods for estimating climatic change and the biologic consequences."

The remainder of this paper represents the steps of the analysis from which such recommendations and conclusions were derived.

THE STRATOSPHERE

We live in a world which is surrounded by a thin atmosphere which protects it from hostile emissions from the sun and from the galactic cosmic particles. Much of the atmosphere lies in the troposphere, in which are found the cloud structures shown by the photograph of Figure 1, but the gases in the stratosphere (which is above the troposphere) absorb most of the radiation with which we are now concerned.



Figure 1. Earth and its atmosphere.

The stratosphere is defined as that region which has an upward temperature gradient; it ranges from about 8 to 16 kilometers (the altitude of the temperature minimum shown in Figure 2), to about 50 kilometers or 150,000 feet, the temperature maximum. Its lower limit is

an altitude which varies with the season and time of year. It is the positive upward temperature gradient, the distinctive characteristic of the stratosphere, which inhibits vertical mixing so that the stratosphere retains material much longer than the troposphere. The importance of this extended accumulation can be illustrated by comparing the stratosphere to a kitchen. When the garbage is collected every day, the kitchen stays clean. But if it is collected only after a few years, even a tiny bit generated daily builds up to create a real problem.

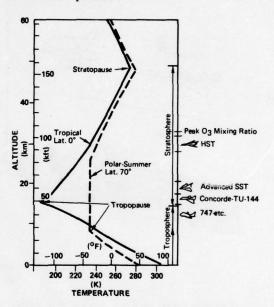


Figure 2. The atmosphere's temperature/altitude profile (after Newell, 1969).

The altitudes at which certain aicraft can fly are shown by the small figures at the right of Figure 2. The 747's and the 707's fly above the lower border of the stratosphere at some times of the year. The Concorde would fly at about 17 or 18 kilometers and the Tupolev-144 at similar altitudes. More advanced later designs may fly even higher in the stratosphere; some future aircraft, such as the hypersonic transport, may fly as high as 35 kilometers.

In the course of the study it was necessary to determine new atmospheric quantities which had not been measured before. Figure 3 illustrates the vehicles which carry measuring instruments, and the atmospheric characteristics which are measured from those vehicles.

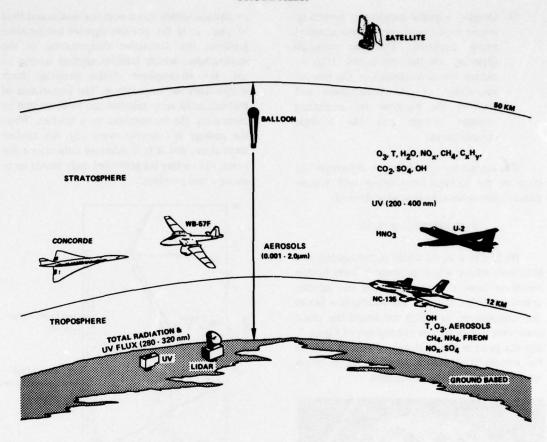


Figure 3. Platforms used and atmospheric characteristics measured in CIAP.

Satellites were used to observe the stratosphere from above. Balloons probed the highest regions of the stratosphere. In the lower stratosphere, the region of most concern, U-2 vehicles, WB-57 aircraft, and the Concorde itself were platforms from which many data were obtained. Lower-flying airplanes, like the NC135 (a military version of the Boeing 707) carried many experiments. Also, some measurements could be made from the ground, such as observations of ultraviolet radiation and of overhead aerosol distributions. Many of these results are described in Figure 4 as vertical profiles of the number density of various constituents, expressed in numbers of molecules per cubic meter. To indicate the scale, at the altitude of 20 kilometers the total number density of all particles is about 10²⁴ m⁻³. The species at the right of the figure, the ozone (O₃) and the water vapor

(H2O), are distributed in the stratosphere in relative concentrations of roughly one part per million. Other trace gases are even more sparse, such as the oxides of nitrogen (NO, NO2, and HNO₃), which are distributed in concentrations of something like one part per billion. There are still others which have not yet been measured (such as the OH radical), which are distributed in concentrations like one part per trillion. All of these trace gases are important because the concentrations of the most dilute, such as the nitrogen oxides, may affect the concentration of the ozone. This mechanism is one of the particular things we want to understand, since the ozone forms a protective barrier which screens out the high-energy part of the solar radiation before it reaches the surface of the earth. Knowing the concentrations of the stratospheric trace gases was thus an essential part of the CIAP task.

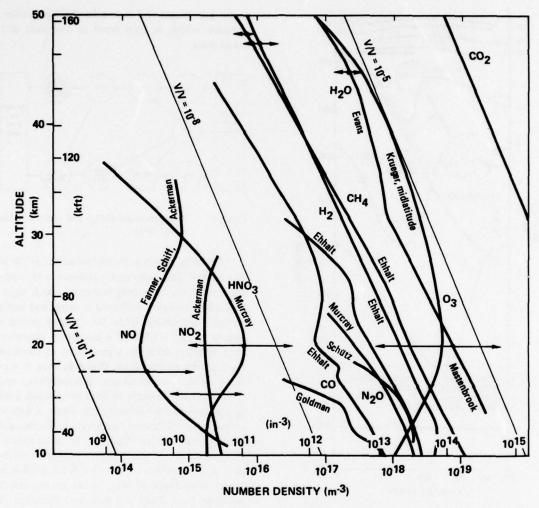


Figure 4. Trace-gas measurements (after Hard, 1975).

In addition, we need to know the patterns of the stratospheric motions, which determine the residence time of materials introduced into the stratosphere. Figure 5 shows estimated residence time as a function of latitude and altitude. Residence time is defined as the length of time required for the concentration of inert material, newly introduced at a given altitude, to be reduced to e⁻¹ (roughly one-third) of its initial value. It is also an inverse measure of the ease with which materials can escape if introduced at that altitude.

In the troposphere (which is below the dot-dash line which marks the mean value of the winter tropopause), residence time is short; the values range from days to weeks. Residence times above the tropopause, however, are much longer, ranging to more than one-and-a-half years. The average residence times for the entire year are two or three times the values of Figure 5, which are measured and derived for the winter period, when the mixing in the stratosphere is the most rapid. Although the numbers of Figure 5 are not the ones used in the CIAP calculations, their relative values illustrate that there is a strong altitude dependence and an important latitude dependence in the region of the tropopause. Both of these dependencies may be taken into account in some way if it becomes necessary to moderate undesirable effects of stratospheric flight in the

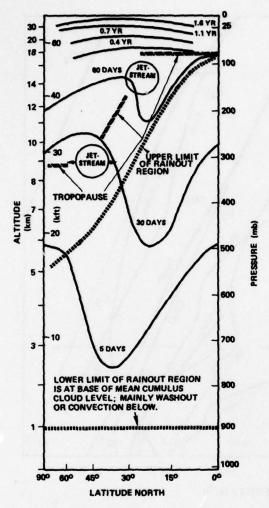


Figure 5. Estimated winter residence times in the atmosphere (after Reiter and Bauer, 1975).

lower stratosphere near the tropopause, since for each 3-kilometer increase of altitude, the sensitivity to a given amount of pollution, as indicated by the residence time, is doubled.

Figure 6 shows the general sequence which we have analyzed in the studies. The analysis primarily considers oxides of nitrogen (NO, NO_2), water vapor (H_2O), and sulfur dioxide (SO_2). The NO_x and SO_2 pollutants are something for which CIAP suggests remedies. For water vapor, there is no remedy other than flight restriction. The NO_x operates in conjunction with the water vapor to deplete the ozone, and this depletion of ozone causes enhancement at ground level of solar ultraviolet-B radiation (290 to 320 nm wavelength), which is destructive to living creatures. This enhanced radiation can

cause skin cancer and have other biologic consequences, which in turn result in economic and social costs.

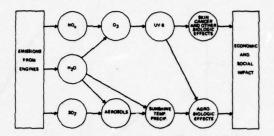
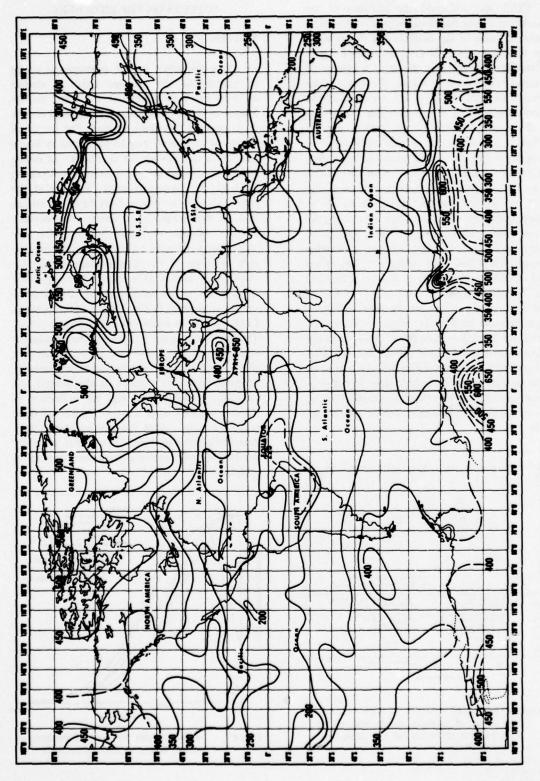


Figure 6. Nitrogen oxide (NO_x) and sulfur dioxide (SO₂) chains.

The SO₂, which is formed when the sulfur in the aircraft fuel is burned, combines with water vapor to form large polymolecules which aggregate after successive collisions to larger and larger particles (aerosols). When the growing particles exceed about 1/10th of a micron in diameter, they interfere with the transmission of sunshine through the stratosphere. This reduction in sunshine affects temperature, precipitation, and other climatic variables close to the ground, with agricultural and other biological results. All these climatic and UV-level changes have economic and social consequences. Changes in stratospheric concentrations of water vapor, oxides of nitrogen, and ozone have climatic effects smaller in degree than those of SO2, so we do not dwell on them here. They are, however, described in the report.

One characteristic which should be borne in mind, of course, is the great natural variability of these constituents. Figure 7 shows the total overhead ozone as measured on 28 April 1969 by the Nimbus satellite. There is large geographic variation; near the equator the Dobson-unit values expressed by the contours drop as low as 200. (A Dobson unit is a value of 10-3 centimeters of ozone at standard temperature and pressure). The greatest thickness of ozone overhead is in the polar regions, where it can be as much as 3.5 times that near the equator. There is also a strong regional variation, apparently controlled by the high-pressure areas in the troposphere. In addition to this large spatial variability, the temporal variability can be as much as ±25% during the year in mid-latitudes. It is supposed that this great natural variability of ozone is paralleled by that of the other trace constituents.



igure 7. Total ozone burden (10⁻³ cm stp), 28 April 1969 (after Prabhakara, 1971).

CIAP also addressed the problem of the calculation of the fractional reduction of vertical ozone in terms of the uniform rate of introduction of nitrogen oxide at various altitudes. Figure 8 describes the differing results of a number of computations (based on values of chemical reaction coefficients, collected and reviewed by the National Bureau of Standards). The differences in the computed results are chiefly due to differing assumptions of vertical eddy-diffusion coefficients (an alternative means of expressing the effect of residence time). When the differences of residence-time assumptions are reconciled, the results (shown in Figure 8) are in strong agreement, except for the items along the dashed line, which represent values computed before the role of nitric acid in scavenging nitrogen oxide had been recognized. The values used in CIAP are more nearly shown by the solid line. Roughly speaking, there is a doubling of sensitivity in the lower stratosphere with each 3-km increase in altitude. Figure 8 shows the values for 20 kilometers; at 17 kilometers the ozone reduction for a given rate of NOx injection is about half as large, and so on. The results of eight one-dimensional models, three two-dimensional models, and one three-dimensional model are in substantial agreement within a factor of three.

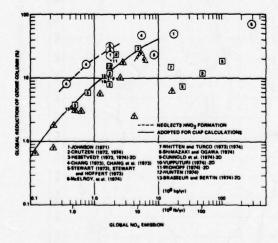


Figure 8. Calculated reduction of vertical ozone in terms of uniform global rate of NO_X addition at 20 km (66 kft) (after Chang, 1974).

EFFECTS ON THE BIOSPHERE

Skin Cancer

Once the effect on the stratospheric ozone of introducing the nitrogen oxide at various altitudes has been computed, the effect on the biosphere of the consequent UV-radiation change at the ground must be examined. The fractional change at earth level may be computed by Beer's Law from the absorption coefficient of ozone and the fractional change in stratospheric ozone. To begin the biological story, we look at the action spectra for minimal erythema of human skin, as determined by a variety of observers, which is shown in Figure 9. Erythema (the reddening of the skin by sunburn) is the perceivable evidence of the skin damage which ultimately may lead to skin cancer. Although there is variation in the responses (as measured by various observers) in the 290 to 320 nm range, CIAP has used a mean value (the dashed curve). The circles of Figure 9 represent the wavelength sensitivity of the Robertson meter, which in a single measurement approximates erythemally weighted radiation received at the ground. An important CIAP project was the collection of Robertson-meter data from a number of these meters, mainly within the United States. Such data, collected over more than a year, generally confirm the estimates that have been derived by calculation.

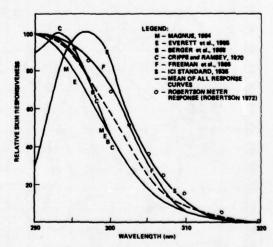


Figure 9. Action spectra for minimal erythema of human skin (after Robertson, 1972).

By using the action spectrum as a weighting function, together with the estimates of solar ultraviolet transmitted through the stratosphere, one may describe, as in Figure 10, the change of vertically incident erythemally weighted radiation as a function of the percent decrease of total ozone. This concave upward curve describes the fact that as the ozone decreases, more and more of the high-energy shorter wavelengths get through to the ground, and the biological effect is proportionally even more intense.

Since one can hardly do laboratory experiments to deliberately induce skin cancer in

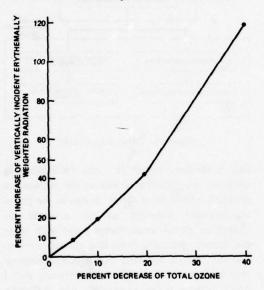
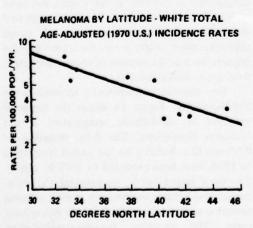


Figure 10. Percent change in dose of vertically incident erythemally weighted radiation vs. percent change in ozone column (after Schulze, 1973).

people, CIAP relied on the epidemiological evidence, supported by a variety of more indirect approaches, to describe the effect of increased UV on people. The epidemiological evidence (principally that gathered by the Third National Cancer Survey) shows that the incidence of skin cancer in the U.S. is a strong function of latitude. The incidence of melanoma in the U.S. white population is shown at the left in Figure 11 for a number of cities; the incidence of the nonmelanomic skin cancer in whites of four U.S. cities is shown on the right. It can be seen that in the middle latitudes there is a doubling of the incidence of non-melanomic skin cancer roughly with every 8 degrees decrease of latitude. Nonmelanomic skin cancer has been directly related to ultraviolet radiation by tests on animals. The considerable scatter of these observations suggests that the estimates of effects which we have used are subject to a considerable amount of uncertainty. However, epidemiological data relating non-melanomic skin-cancer incidence to UV radiation are supported by much other evidence, such as the fact that skin cancer in white-skinned mice and in pigs has been experimentally induced by exposure to ultraviolet radiation. The pigs which were piebald (that is, having melanin splotches on a skin without melanin), when exposed to the ultraviolet radiation, developed skin cancers in the white part of their skin but not on the splotches. People whose skins have more melanin coloring are more immune to non-melanomic skin cancer.

Having developed this deterministic analysis of the effects of stratospheric pollution by aircraft in the inducing of skin cancer, we must



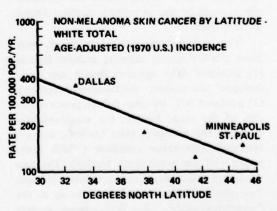


Figure 11. Increase in skin-cancer incidence vs. change in latitude (after Fears et al., 1974).

estimate how incorrect we may be. Some estimates of uncertainty are shown in Figure 12. The values are expressed as fractions indicating the ratios of the standard deviations of observations or calculations to the mean values which are being estimated. For each of the four steps of the estimation, the solid bar represents the uncertainty introduced by that step alone, and the cross-hatched bar represents the cumulative effect as these uncertainties propagate through the succeeding steps. The estimates of nonmelanoma skin-cancer incidence rates are expected to have an uncertainty-to-mean-value ratio of about 0.8. This implies that we may be 95% confident that the estimate is accurate within a factor of 3 to 10.

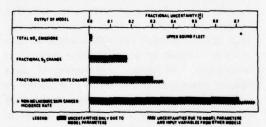


Figure 12. Propagation of fractional uncertainty through NO_x/skin-cancer cascade (after Schainker et al., 1974).

Climatic Impact

The next part of the CIAP study is the climate study. This study was intended to cover the effects of climatic changes (other than changes in the level of ultraviolet radiation) caused by aircraft-effluent pollution as indicated in Figure 13. There are a number of pollutants, only one of which is described as a major problem, because it is the largest of the three. With large enough aircraft fleets, the estimated effects could be serious unless something is done to avoid them.

The stratospheric pollutants which may cause non-UV-related climatic changes include (1) increased SO₂ injection (which can cause increased stratospheric sulfate-aerosol burden), (2) increased NO_x injection (which causes reduction of the ozone burden, but simultaneously increases the nitrogen-oxides burden), and (3) increased water-vapor emissions (which cause increase of the water-vapor burden). The two transparent stratospheric constituents will cause their climatic effect by what is known as the "greenhouse effect." The SO₂-induced aerosols

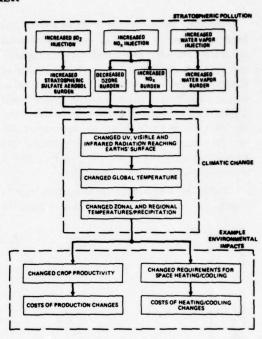


Figure 13. The climate study.

cast a shadow. Hence, by one mechanism or another, the radiation levels at the surface are changed, with a consequent change in the global temperature. Although we can estimate the change in global mean temperature with some confidence, deducing from that change the consequent changes in zonal and regional temperature and precipitation is very difficult, and I don't believe we've succeeded. The difficulty arises because with a decrease in mean global temperature some local regions may get warmer and others may get cooler. There is, however, a strong zonal variation; a change in mean global temperature is felt least in the tropics and most strongly in the polar regions. The CIAP-estimated changes in zonal temperatures were only rough approximations. From these, the environmental impacts, such as the changes of various important food costs, were estimated.

The climatic characteristics themselves are highly variable. Figure 14 shows the temporal variation in mid-latitude temperature in the Northern Hemisphere. The data, compiled by Professor M.I. Budyko for the period from 1880 to 1958, have been extended to 1970 by others. The most jagged curve, representing the mean annual mid-latitude temperature, shows a strong deviation from year to year from the ninety-year mean. The smoother ten-year-running-mean

temperature shows a steady increase from 1880 to about 1940 and a subsequent decrease. From Figure 14, it may be inferred that determining how the world temperature is changing is probably not much easier than determining what's happened to the total ozone.

Figure 15 represents the estimates by a number of experimenters of the change in average global surface temperature which might result from variation of solar radiation. In the

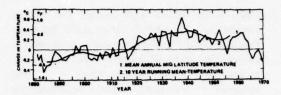


Figure 14. Temporal variation of midlatitude temperature in the Northern Hemisphere (after Budyko, 1974).

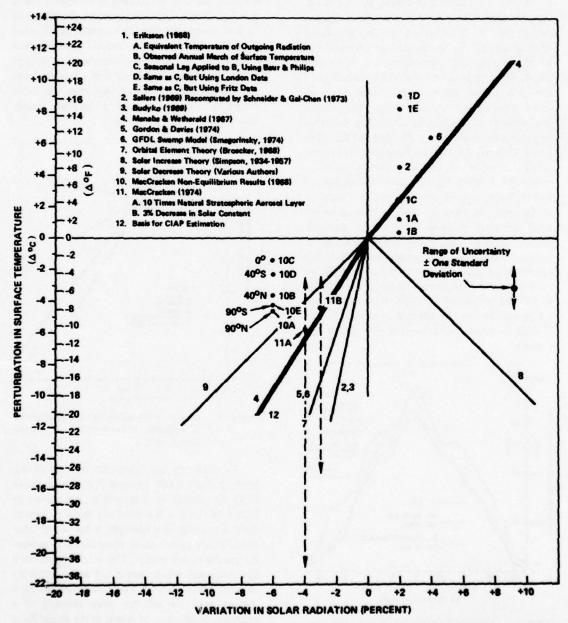


Figure 15. Change in surface temperature as a function of change in the solar radiation (after MacCracken, 1974).

main, these studies were carried out in the interests of the Global Atmospheric Research Program (GARP). They represent a significant contribution to CIAP, however, even though not accumulated at its behest. There is a wide variation of temperature-change sensitivity to change in solar radiation. CIAP chose to use the estimate indicated by the heavy line. The uncertainty of this estimate is large.

Precipitation (rain and snowfall) is controlled to a considerable degree by the zonal temperatures. Figure 16 shows results of computations by M. MacCracken of the latitudinal distribution of the yearly average precipitation for three cases. The topmost curve is the control curve, which represents his model's prediction of the precipitation distribution by latitude zones under present average conditions. The dashed line is the result of decreasing the solar radiation impinging on the earth by 3%, and the solid line below it shows what would happen if the present aerosol content of the stratosphere were increased by a factor 10. For either the change of stratospheric aerosol content or the reduction in the radiation, there is a marked decrease in the total amount of rainfall. However, such an overall decrease would be felt differently in different latitudes. Since local temperature and precipitation changes are affected strongly by local conditions (mountain ranges and so on), it is difficult to predict in detail how the climate where you live will be affected by such a change. Overall, however, global cooling will result in less rainfall.

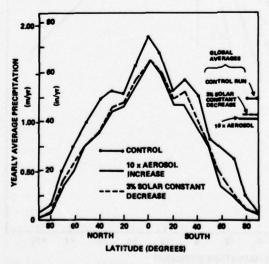


Figure 16. Latitudinal distribution of total precipitation (after MacCracken, 1974).

How the botanical biosphere will react to a decrease in local temperature and precipitation has been estimated by a number of scientists. The effect on the distribution of cultivated crops was especially difficult to estimate, because most cultivated crops are influenced by a number of different factors. One of these may be the constraining factor in a particular region, and another one in a different region.

Non-cultivated plant systems have been naturally selected for survival in the region where they are found. For these systems, the effects of climate change are easier to estimate, as indicated in Figure 17. Nearly all natural systems react unfavorably to a decrease in temperature, except the desert-region ecologies. The latter are constrained by lack of water, and therefore react favorably to factors conserving the water supply such as lowered temperatures.

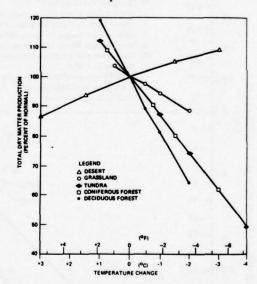


Figure 17. Change in natural-ecosystem productivity as a function of temperature change (after Cooper, 1975).

In exploring the economic impacts of climatic change, CIAP estimated economic sensitivity to change in temperature, as shown in Figure 18. Only a few areas are likely to benefit from a cooling. An example is the world corn crop, which grows more abundantly if average temperatures are cooler. The world production of cotton and wheat seems not to be strikingly affected by a cooling, but production in local regions may be affected very strongly. For example, production of wheat in the Peace River Valley in Canada could be completely wiped out

by shortening of the frost-free season. Certain northern regions of the Soviet Union would also be handicapped, although the Southern regions of the USSR, like those of the United States, might benefit. The world food crop most sensitive to climate cooling is rice.

AREA IMPACTED	NATURE OF COST FOR AT = -1°C*	AMMUAL MAGNITUDE** IN MILLIONS OF DOLLARS FOR AT = -1°C
AGRICULTURE		
1. CORN (ISS WORLD)	NET ADJUSTMENT SENEFIT	-80
2. COTTON (SINS WORLD)	NET ADJUSTMENT COST	+10
2. WHEAT (BO'S WORLD)	NET ADJUSTMENT COST	+62
4. RICE (BUS WORLD)	NET ADJUSTMENT COST	*1000
URBAN AND PHYSICAL RESOURCES		
WAGES DIFFERENTIAL (U.S.A.)	POSSIBLE INCREASE IN COMPENSATING WAGES	-4000
POREST RESOURCES (U.S.A.)	REDUCED PRODUCTION	-700
WATER RESOURCES	SLIGHT NET INCREASE IN WATER SUPPLY	-4
FISHERY RESOURCES (WORLD)	REDUCTION IN FISHERIES YIELD	+1000
PRECIPITATION, 5% INTEREST RAT "ANNUALIZED COST — 1974 (MILLE BENEFIT) N.S. THE ABOVE IMPACTS ARE NOT	AL GLOBAL TEMPERATURE (1880 — 26. R ASSUMED. CRES OF U.S. 1871 DOLLARS; NEGATIVE PREDICTED, THEY WERE ESTIMATED OF R ESTIMATE OF POSSIBLE COSTS.	SIGN DENOTES

Figure 18. Sensitivity of economic impacts to climatic change (after d'Arge, 1974).

Figure 19 shows estimates of the uncertainties of the climatic-impact estimation. These are similar to those shown for the skin-cancer case. In the first five steps the uncertainties of the geophysical estimation are shown, leading to a ratio of uncertainty to mean value which is estimated, for surface temperature, to be about 0.7. The largest contribution is from the step going from the change of radiation to the estimates of surface temperature. Below the surface-temperature estimate are displayed the uncertainties of estimating the costs of the effects of temperature change on various crops. Of these, the largest uncertainty is that in the estimation of wheat costs. In estimating costs of climatic change due to SO₂ pollution of the stratosphere by aircraft, the ratio of uncertainty (as standard deviation) to the mean estimate is about 0.8. That is to say, there is 95% confidence that estimates are covered within a factor of three to ten. Even if one puts in the subjective estimates by modelers of how bad they think their models possibly may be, these factors of uncertainty are not enlarged to more than a factor of 5.

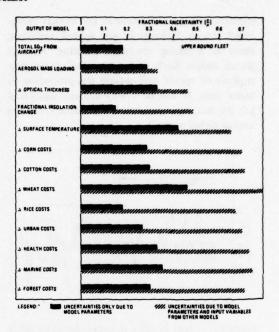


Figure 19. Propagation of fractional uncertainty through SO₂/temperature/costs cascade (after Schainker et al., 1974).

LOOKING AHEAD

Although for science an uncertainty factor of five is very unsatisfactory, knowledge of climate effects within a factor of five may well be adequate for choice of policy today. However, we should not be satisfied with such uncertainty in similar estimates many years from now. We should pursue further investigations with sufficient energy that ten or fifteen years from now we have much more accurate knowledge of the effects of climate change. For the problems of the future, we need to do more monitoring of the causes and effects of climate change.

There are, however, many difficulties in monitoring. Figure 20 illustrates one of them, the temporal variation of total global ozone as measured from the Nimbus satellite. Satellite measurements have the great advantage that one can get many data points in both space and time, as can be seen in Figure 20. Analysis of the data shows a striking variation from day to day. It has been said that some of this variation is actually an artifact of the method of measurement and analysis. Even if it is, there is still a strong

indication that, in addition to the already recognized strong latitudinal and spatial variation, there is a strong temporal variation of total global ozone. Such strong variations mean that analysis of trends will require the processing of many data. It will be a very difficult analytical job to sort out very small variations from the annual global mean.

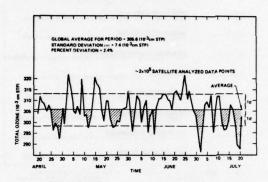


Figure 20. Daily variation in total global ozone (after Lovill, 1974).

Pittock in Australia has made an attempt to analyze, using the data from one station, how long daily observations from a single station would have to be made in order to determine a trend (a certain percent change of overhead ozone in a decade). Figure 21 shows Pittock's conclusions. For 95% confidence, it would take eleven years of daily observations to detect a 5% change in overhead ozone. Pittock's conclusions were derived from the study of observations at a single station at Aspendale. If satellite data were used, contributions from 100 independent "equivalent stations" around the world could be used. With such data, the limit of trend predictability could be improved to one-half percent (rather than 5%) in ten years of observation. This estimate of the limit of detectability has not been demonstrated or otherwise proven; it may be over-ambitious. To try to put discussions on an objective basis, CIAP has undertaken to find out what a one-half-percent change in world ozone would really mean. However, the difficulties for the monitoring systems of the future which result from the large natural spatial and temporal variability of the measurables (the trace-constituent densities, the radiation levels, and so on) are very great.

Figure 22 illustrates another problem, the diversity of possible causes of surface ultraviolet

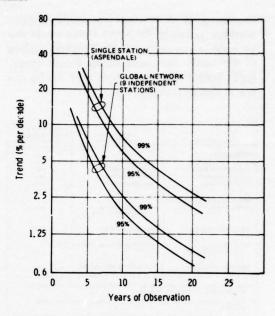


Figure 21. Detectability of trends of change in ozone column (after Pittock, 1974).

change. At the left is an observable quantity: an increase in UVB radiation at the ground. Moving to the right, we see the various possible causes of that change. There are more than thirty such causes, including volcanism, aerosol sprays, atmospheric testing of nuclear weapons, and so on. Only a few of the possible causes are aircraftrelated, such as increased SST or space-shuttle operation. At present, it's not hard to establish that the airplanes are not causing much change in the world ozone, but fifteen years from now it will be more difficult to determine the relative contributions of major causes. The monitoring programs of fifteen years from now will be challenged to define not only the change in world ozone over a time period of considerable duration (like ten years) but how much of that change can be specifically attributed to aircraft flying in the stratosphere.

There is also the problem of determining the causes of other climate changes, as indicated in Figure 23. At the left are two observable changes in mean global climate. To the right are the many possible causes of these climate changes. Only a few (indicated in boxes) of the many possible causes of global temperature change can be attributed to aircraft. At present, we lack the tools for sorting out the causes. Only recently have tools become available for adequately detecting long-term changes in world ozone or

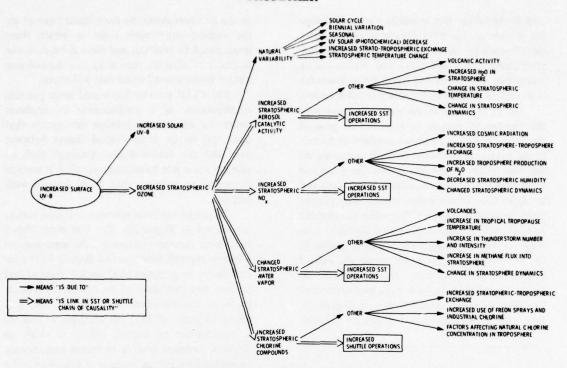


Figure 22. Simplified reverse discrimination tree for surface UV-B increase.

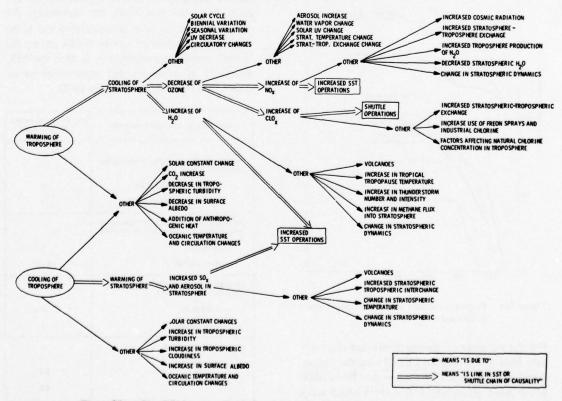


Figure 23. Simplified reverse discrimination tree for tropospheric temperature changes.

climatic variables. But it will be a great challenge for science in the next decade to obtain sufficient knowledge about these processes that longterm changes of world ozone and climate can be recognized in the observed data, and to assess the contribution of each of the many possible causes.

Let us turn now to the question: "How may the number of aircraft be expected to grow in the future?" Figure 24 shows numbers of aircraft in the future, as projected by various studies. At the top of the figure are shown the projected expansion of the subsonic fleet (solid line) and an upper limit of estimates (dashed line). (Upper limit means that there is 95% confidence that the number will be smaller.) Several different estimates of the supersonic aircraft fleet appear in the lower curves (solid lines). Again, the dashed line shows an upper limit. By 1978 about 30 civilian supersonic airplanes may be expected to be flying. If these numbers grow with demand, they may become large in the ensuing decades.

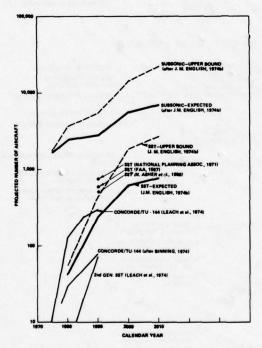


Figure 24. Projected aircraft fleets (references listed in Grobecker et al., 1974).

For the purposes of making worst-case estimates only (not as a projection), CIAP used the "upper limit" growth curves. Remember that this dashed line is not a projection; it is a curve which has a 95% probability of including all possibilities of growth. In other words, the dates corresponding

to the numbers shown by these dashed curves are the earliest conceivable dates at which these levels could be reached, and for a given date, the numbers of aircraft shown by the dashed line almost surely exceed those that will occur.

The CIAP analysis has traced some possible consequences of a proliferation of airpianes under the admittedly dubious assumption that there will be no technological change between now and the future ates. Although such an assumption is not historically justified, it seemed important to portray what could happen with inaction.

Projected oxides-of-nitrogen emission indices are shown in Figure 25. The first entry shows that, with current technology, the emissions of subsonic aircraft (such as the Boeing 747) contain about 16 grams of NO_x per kilogram of fuel burned, and that those of the supersonic vehicles (such as the Concorde and the TU-144) give about 18 grams of NO_x per kilogram of fuel. As a consequence of current efforts to clean up airports, emission indices of future engines may be reduced by 50% in the case of subsonics and a smaller factor in the case of supersonics. But the goals for 1985 and 1990, the technology for which has not yet been demonstrated but is the subject of energetic efforts by NASA and by the aircraft engine manufacturers, is that the NO. emissions of subsonics and supersonics be reduced by a factor of almost 6 by 1990.

ENGINE TYPE (AIRCRAFT SYSTEM)	NO _x EMISSION INDEX: g(NO ₂)/kg FUEL
CURRENT TECHNOLOGY (OPERATIONAL THROUGH 1985)	
- SUBSONIC (JT97D/B747)	16
- SUPERSONIC (CONCORDE)	18
ANTICIPATED REDUCTION TECHNOLOGY (IMPLEMENTED 1980-1985 TIME FRAME)	
- SUBSONIC	8
- SUPERSONIC	12 - 14
ADVANCED REDUCTION TECHNOLOGY (POSSIBLE BY 1985-1990)	
- SUBSONIC	3
- SUPERSONIC	3
PROJECTED MINIMUM	
- SUBSONIC	
- SUPERSONIC	0.3
	0.3

Figure 25. Projected NO, emission indices.

Although the direction this improvement will take is known, it is a far cry from demonstration in the laboratory to having an engine which has been tested and certified for flight operations. The latter represents a task of about \$50,000,000 magnitude at the very least. It will not be done for any reason that we know of except concern for the environment. The projected minimum emission index in Figure 25, which is about 60 times smaller than that of present technology, is a theoretical limit.

Figure 26 shows the possible timing of new development that is required. The upper plot gives fuel burned at high altitude by supersonic aircraft versus ozone reduction in the Northern Hemisphere. Point A denotes the amount that is being produced by present-day aircraft. Point B shows the effect of 140 supersonic aircraft, a level which cannot occur earlier than 1985. Points C, C', and C" show the effect of 820 aircraft, a level which is not expected to be reached before 1995, more probably later. The prime indicates an effect of a sixfold reduction from today's emission levels, a double prime the effect of a sixtyfold reduction.

The upper curve, from A to B to C to D, shows the effect of a fleet which is not regulated, and which continues to use engines of 1974 technology, but proliferates to the sizes indicated. The growth curve passes through a number of levels representing different degrees of change of the Northern Hemisphere ozone. The 0.1% level is the change due to presently existing 1974-type subsonic aircraft.

Supersonics' emissions cannot match those of subsonics at present, but they do reach, before 1985, a level equivalent to about a 0.5% change in ozone, which may be barely discernible in ten years of observation from a complete system using satellites. Some time after 1985 (possibly before the time indicated by C), the effects of pollution by unimproved supersonics may exceed the 5% change in ozone which can be discerned in ten years of observation by a single-station system.

Now, A, B, C, and D represent the effects for unchanged technology. But energetic efforts to change the technology are now going on. The change can't be accomplished overnight; a ten-to-fifteen-year development time is needed to improve engines. The growth curves C' and D'

show the effects of aircraft engines characterized by a sixfold improvement of NO_x emissions. The effects of engines with a sixtyfold improvement are shown by the curves C'' and D''. If the NO_x emission reduction described by the double prime could be achieved by 1990, then the curves stay near the change in ozone which is barely discernible in ten years of observation.

The barely discernible change in ozone, a 0.5% decrease in the Northern Hemisphere, may be characterized in several ways. It is the change caused by about 120 Concordes flying at altitudes between 15 and 17 kilometers, 365 days a year, for 4.5 hours a day. It may cause about a 1% change in the incidence of skin cancer among whites in the United States.

The lower half of Figure 26 shows similarly what the subsonics' emissions growth will do. The table at the left shows the number of airplanes. In 1974, at point P, the subsonics had caused a little less than 0.1% decrease of Northern Hemisphere ozone. By as early as 1985, the change due to subsonics may be as much as 0.5%, a barely detectable value. The solid line shows what happens if we successfully improve those engines, as is thought possible.

Figure 27 shows the effect of sulfur dioxide (SO₂) emissions, due to burning of sulfur in the fuel of supersonic aircraft. The measurable stratospheric barely discernible change is a 10% increase in average stratospheric optical thickness. Flight operations of more than 2000 aircraft would be required to produce a change of this size (10%), which in turn would result in a change of about 0.07°C in the mean global temperature. The impact of a 10% change of stratospheric optical thickness is very small. The growth of the SO₂ effect of supersonics begins to approach the 1974 subsonic level by 1985, and will exceed that value of minimum discernibility (10%) not earlier than 1995. Unless technical remedies are applied, these non-UV climatic effects will occur not much later than the measurable change of ultraviolet radiation. Although we do not have a problem today, we may have serious problems in the foreseeable future unless some action is taken. Ten or fifteen years are required to provide the technical solution; that may be all the time we have for solutions other than the Luddite one of eliminating the machine. It is important that we begin now to anticipate the problem.

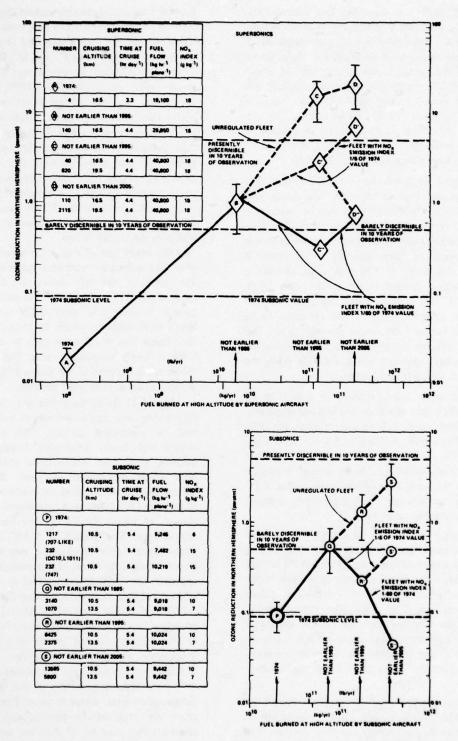


Figure 26. Estimated decrease in ozone vs. fuel burned by aircraft flying in the stratosphere.

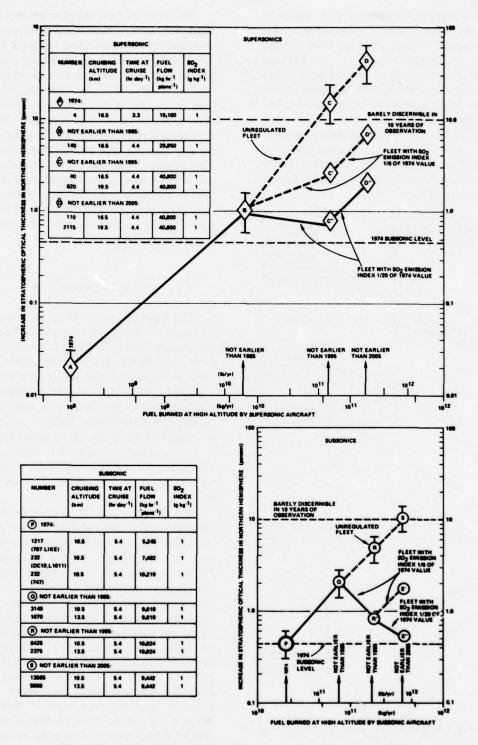


Figure 27. Estimated increase in stratospheric optical thickness vs. fuel burned by aircraft flying in the stratosphere.

Introducing a comparison of costs, Figure 28 shows the present value of some aerosol pollution, projected to years ahead for a few selected indicators under the assumption that airplanes increase in the exaggerated way already described (maximum conceivable growth in numbers without benefit of technological improvement). The dashed lines show the costs of two remedies: the discounted annual cost of a monitoring program, and the total cost of desulfurization. The latter represents about a half-cent per gallon, or 20 cents per barrel, and is a relatively small fraction of the cost of aviation fuel.

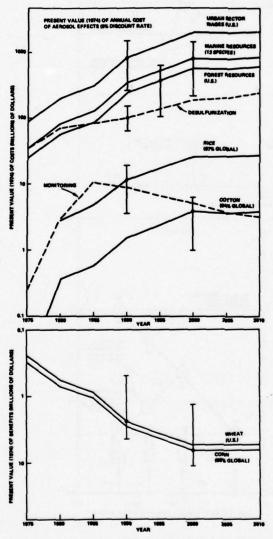


Figure 28. Estimated present value (1974) of annual costs or benefits of SO₂ aerosol effects (5% discount rate).

The costs of these remedies are an order of magnitude smaller than the several ecological consequences estimated. The estimates of economic consequences shown here have uncertainties indicated by error bars. One can choose the most pessimistic, the most optimistic, or, as we have done, the middle value for prediction. Presumably, the sum of all ecological effects of stratospheric pollution is greater than the sum of the few examples that we have shown here, and much greater than the cost of remedies. (We should note, though, that not all the effects are bad; for example, at the bottom of Figure 28 are shown two examples of crops (corn and wheat in the U.S.) that would benefit by the cooling due to increased aerosols.

MEASURES NEEDED

The arguments which I have described so far led to the conclusions described in the beginning of this paper, and the recommendations based on those conclusions. Let us now address what needs to be done. Figure 29 shows steps which need to be taken in the future. As indicated in the figure, CIAP has uncovered many of the problems of stratospheric pollution by aicraft, and suggested some possible technical solutions to those problems. It has tried to do this in such a way that the scientific facts could be debated without regard to our opinions as to the fitting action.

The first step needed is research into and development of non-polluting aircraft engines and fuels. The next most urgent step, which I hope has been begun by the Environmental Protection Agency (EPA), is the establishment of appropriate standards for the quality of stratospheric air. The establishment of air-quality standards, while based on a scientific understanding of the consequences of pollution, must also take into account the subjectively derived criterion of public acceptability. "What is acceptable?" might be phrased in this case as "What is the acceptable deviation from the present annual mean of total overhead ozone?" Would we accept a 1% change? A 0.5% change? A 0.1% change? A 50% change? That is the number that must be determined first by EPA, and then by Congress, and ultimately by the people of the United States.

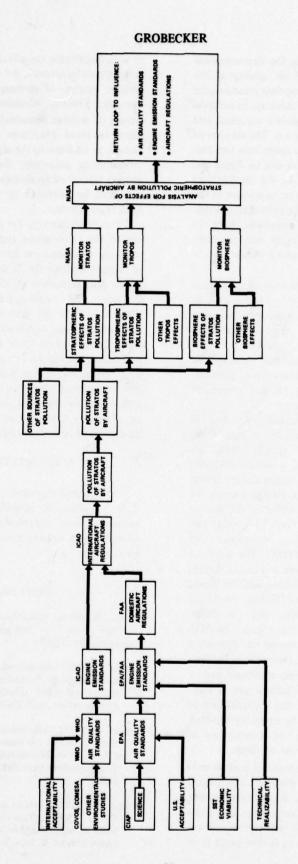


Figure 29. Steps in control of stratospheric aircraft pollution.

The next step following the determination of acceptable standards of air quality is the decision as to what are appropriate standards for aircraft engine emissions. In this step, in addition to meeting the chosen air-quality standard, one must consider some other factors. The number of sources of pollution must be taken into account. The number of airplanes that will be flying and the time of flight of each in the stratosphere become considerations quite as important as the emission characteristics of the individual aircraft. Moreover, engine-emission standards have to be technically realizable. Engine emission standards which cannot be attained should not be prescribed.

In the U.S., the determination of engineemission standards is the role of the EPA in conjunction with the Federal Aviation Administration (FAA). Domestic aircraft regulations based on the standards are established by the FAA in the United States, but stratospheric pollution is really an international problem. Wherever the source may be, the effects of pollution are felt everywhere.

Paralleling the U.S. efforts described in Figure 29, there must be similar activity in the international community. Already there are extensive programs in half a dozen countries whose representatives are here today. These parallel environmental study groups include the U.K. Committee on Meteorological Effects of Stratospheric Aircraft (COMESA), and the French study group on the Consequences des Vols Stratosphériques (COVOS). The work of these groups and similar ones in Canada, Japan, Australia, and the Soviet Union, and the World Meteorological Organization (WMO), the World Health Organization (WHO), and the International Civil Aviation Organization (ICAO), may lead to a world agreement on air-quality standards and the appropriate regulatory action. The parallel studies by institutions abroad and by the National Academies of Science and of Engineering in the U.S. ensure that the questions of stratospheric pollution will be equitably handled, whether they corroborate the conclusions of CIAP reported here or improve on them.

Regulation on an international basis is only the first part of sensible solution. The second part, closing the loop, has to do with determining the true results of the preceding ten or fifteen years of regulated aircraft activity. For loopclosing to be effective ten or fifteen years from now in identifying the effects of pollution of the stratosphere by aircraft, the effects of other, non-aircraft sources of stratospheric pollution (for example, Freons, volcanism, and atmospheric testing of nuclear weapons) must also be recognized to avoid confusion as to the source of change. In addition to the stratospheric effects of stratospheric pollution, there are also tropospheric effects of stratospheric pollution (which may also be confused by multiple causes) and biospheric effects.

Proper monitoring for changes in the stratosphere, the troposphere, and the biosphere seems to imply a requirement for diagnosis as to cause of change. Perhaps the National Aeronautics and Space Administration (NASA) and the National Oceanic and Atmospheric Administration (NOAA) will be the agencies which lead in accomplishing this necessary function. Whoever leads, it is important to the Department of Transportation that the future analysis of the effects of stratospheric change properly identify which effects can be attributed to aircraft. Such analysis will constitute the basis for future reevaluation of air-quality standards, of engine-emission standards, and of aircraft regulation.

ACKNOWLEDGMENT

This report is based on the work of more than a thousand scientist experimenters and authors, whose contributions are individually acknowledged and referenced in the CIAP monograph series.

REFERENCES

- Budyko, M. (1974), Climate and Life, Academic Press, New York, NY, 508 pp. (also 1971, Gidrometeoizdat, USSR).
- Chang J. (1974), "Simulations, perturbations and interpretations," in *Proceedings of the Third Conference on CIAP* (Cambridge, MA), Dept. of Transportation, DOT-TSC-OST-74-15, 330-341.
- Cooper, C. (1975), "Simulation models of the effects of climatic change on natural ecosystems," section 5.7 of CIAP Monograph 5 (Part 2), Dept. of Transportation, DOT-TST-75-55 (part 2), 5-45 5-65
- d'Arge, R.C. (1974), private communication. (See also d'Arge (1976), "Transfrontier pollution: Some issues of regulation," in *Studies in Environmental Economics*, ed. W. Ingo, Wiley, New York, NY.)

- Fears, T., J. Scotto, and M. Schneiderman (1974), "The epidemiology of skin cancer," paper given at the 45th Aerospace Medical Association Meeting (Washington, DC).
- Grobecker, A.J., S.C. Coroniti, and R.H. Cannon, Jr. (1974), Report of Findings: The Effects of Stratospheric Pollution by Aircraft, Climatic Impact Assessment Program, Dept. of Transportation, DOT-TST-75-50.
- Hard, T.M. (1975), "Summary of recent reports of stratospheric trace-gas profiles," section 3.7 of CIAP Monograph 1, Dept. of Transportation DOT-TST-75-51, 3-182 - 3-170.
- Lovill, J.E. (1974), Figure F4 in "Second Annual Report, DOT-CIAP Program," Lawrence Livermore Laboratory Rept. UCRL-51336-74 (Livermore, CA), p. 143.
- MacCracken, M.C. (1974), private communication. (See also MacCracken et al., Chapter 7 of CIAP Monograph 5, Part 2, p. 7-40.)
- NAS (1975), Environmental Impact of Stratospheric Flight: Biological and Climatic Effects of Aircraft Emissions in the Stratosphere, Climatic Impact Committee of the NRC, NAS, NAE, pub. National Academy of Science.
- Newell, R. (1969), "Radioactive contamination of the upper atmosphere," in *Progress in Nuclear Energy*, Ser. 12, *Health Physics*, Vol. 2, Pergamon, Oxford, p. 538.

- Pittock, A.B. (1974), "Ozone climatology, trends and the monitoring problem," in Proceedings of the International Conference on Structure, Composition and General Circulation of the Upper and Lower Atmospheres and Possible Anthropogenic Perturbations (Melbourne), pub. IAMAP, 455-466.
- Prabhakara, C., B.J. Conrad, L.J. Allison and J. Steranka (1971), "Seasonal and Geographic Variation of Atmospheric Ozone Derived from Nimbus III," NASA-TN-D-6643, Goddard Space Flight Center, Greenbelt, MD.
- Reiter, E.R. and E. Bauer (1975), "Residence times of atmospheric pollutants," Appendix A to Chapter 2 of CIAP Monograph 1, Dept. of Transportation, DOT-TST-75-51, 2-125 2-147.
- Robertson, D.F. (1972), "Solar Ultraviolet Radiation in Relation to Human Sunburn," Ph.D. thesis, University of Queensland, Australia.
- Schainker, R., R.W. Atherton, R.P. Brennan, R.W. Lau, J.W. Patmore, and J.E. Wirsching (1974), "CIAP Error Variance Analysis," Interim Rept., Contract DOT-OS-40042, Systems Control, Inc. (Palo Alto, CA)
- Schulze, R. (1973), "Uber die Zunahme der karzinogenen ultravioletten Sonnenstrahlung bei Verminderung der Ozonkonzentration in der freien Erdatmosphäre," University of Hamburg, Germany.

PANEL DISCUSSION

INTRODUCTION

WILLIAM E. STONEY*

Deputy Assistant Secretary for Systems Development and Technology U.S. Department of Transportation

The CIAP study will be terminated in late 1975, when we publish the final six monographs. At that time the Federal Aviation Administration will assume the responsibility for continuing a program based on the scientific conclusions of CIAP.

CIAP has identified NO_x and SO_2 as the two exhaust pollutants that can perturb the natural stratosphere and therefore our living environment. In order to fully understand the effects of these gases, we must first understand the physics and chemistry of the natural stratosphere, and then the interaction of these exhaust gases with the stratosphere.

As Dr. Grobecker mentioned, the measuring and monitoring programs with which the FAA is concerned are designed in the short term to help us better understand the behavior of the stratosphere. Obviously we must establish the baseline for natural stratospheric conditions before the advent of large-scale stratospheric flight. We recognize that even now the stratosphere is being disturbed by exhaust from high-flying subsonic aircraft, and may soon be appreciably affected by the injection of chlorine, which results from the widespread use of "freons" in spray cans.

Some basic contributions to the FAA's monitoring and measurement program will come from NASA's Office of Space Science, which is studying atmospheric pollution. NASA's longrange objectives are to study the physics and chemistry of the stratosphere and to investigate the action of the space shuttle's exhaust on the natural stratosphere. NASA's Office of Applications is initiating a development program for a satellite-borne instrument which will eventually monitor the critical chemical gases and small particles in the stratosphere. The newly developed

instruments will be tested on Nimbus G, which will be flown in 1978 or 1979.

NOAA will continue its present extensive modeling of the atmosphere and its studies of stratospheric pollution. NOAA's laboratories will direct a substantial amount of effort to the study of reaction rates and methods of measurement of minor constituents in the atmosphere. Studies of global ozone will be extended by analysis of satellite observations of the backscattered ultraviolet radiation, from which the daily column of total ozone may be estimated. In addition, data gathered earlier by Nimbus will be analyzed in an attempt to increase our knowledge of the background or baseline data.

In sum, NOAA will operate a world-wide network for obtaining measurements of total ozone column and the aerosol content of the stratosphere.

As a direct result of the CIAP findings, the NASA Lewis Research Center is about to launch a program to develop a combustor with reduced NO_x emissions. NASA Lewis was a major contributor to CIAP Monograph 2, "Propulsion Effluents in the Stratosphere." This monograph predicted the emission levels through the 1990's. On the basis of these predictions, and the recommendations of the CIAP Report of Findings, which you heard here this morning, NASA's Clean Combustor Program, which was initally aimed at reducing NOx during landing and takeoff, was broadened to include some study of the cruise NO_x emissions and possible reductions of them. The NASA commitment to this work includes in-house laboratory work, university research grants, and industry technology contracts.

^{*}Mr. Stoney is now Deputy Director, Office of the Director of Defense Research and Engineering, in the Office of the Secretary of Defense.

PANEL DISCUSSION

The experimental clean-combustor projects for large subsonic engines were expanded in 1974 to study the influence of typical supersonic cruise operating conditions on the NO_x emission levels. Data from these tests show that significant reductions in NO_x can be achieved, but much work is to be done in the future. It is important to remember, too, that any engine changes must also recognize the national need for energy conservation. NASA has a six-year program emphasizing cruise NO_x reduction for both subsonic and supersonic aircraft now in the planning stages.

With regard to sulfur dioxide, Dr. Grobecker mentioned that emissions can be reduced through the use of existing oil-refinery technology. This is a little complicated, since apparently some fuel constituents needed to lubricate portions of the engine are related to the level of sulfur in the fuel. This problem needs to be investigated, and engine manufacturers are aware of it.

In conclusion, DOT and the FAA will continue the research and monitoring aspects of CIAP, and they will work in concert with other United States agencies to do so. DOT considers it mandatory that the momentum generated by CIAP be sustained and applied to solving any related problems that may arise. I think the multi-agency plans I mentioned are moving in the right direction.

EDWARD C. CREUTZ,	Assistant Director for Research
CHAIRMAN	National Science Foundation

and Review
Federal Aviation Administration

California Institute of Technology

Dartmouth College

EDMOND A. BRUN President

Conséquences des Vols Stratosphériques (France)

ROBERT G. MURGATROYD Chairman

Committee on Meteorological Effects of Stratospheric

Aircraft (United Kingdom)

ROBERT W. RUMMEL Vice President, Technical Development

Trans World Airlines

R. BOYD FERRIS Chief, Flight Branch

International Civil Aviation Organization

CREUTZ: I myself did not participate in the Climatic Impact Assessment Program. I did follow it with considerable interest, though, and I'm very pleased to have been asked to serve on this panel which will discuss the CIAP Report of Findings. However, I would like to aim my remarks not so much at the findings, but rather

at where do we go from here? The National Science Foundation has been very interested in CIAP's progress, and in the problems of stratospheric pollution that gave rise to the program in the first place. These matters seem to me to be excellent examples of potentially serious difficulties that require considerable basic research to

help us focus on the real issues and discuss them from the vantage point of reasonably sound understanding of the fundamental phenomena involved.

Let us look a little at what was known about the stratosphere before CIAP was initiated, that prompted scientists and engineers to pose the question of what an SST fleet might do to the ozone layer. It became clear near the start of CIAP that the catalytic reactions involving NO. and HOx were the ones we had to worry about most. Our knowledge of these reactions stems from early basic work in laboratory chemistry for example, that of Professor Johnston at Berkeley, who will speak to us tomorrow. Our awareness of the effects of these catalysts on the ozone layer resulted from basic research on the D-region of the ionosphere. The models of the dynamics of the stratosphere that have been developed recently drew upon earlier models of the general circulation of the atmosphere which had been developed at the National Center for Atmospheric Research, at the National Oceanic and Atmospheric Administration's Geophysical Fluid Dynamics Laboratory, and at the University of California at Los Angeles.

I am impressed with how CIAP successfully coordinated and steered a strong and very wideranging effort in basic stratospheric research, together with a parallel effort in aircraft engine technology and development. But what is the future of atmospheric and stratospheric research? It seems that problems relating to the weakening of the ozone layer are still with us. Freons, the Shuttle emissions, and, as we have more recently realized, the biological reactions involved in denitrification from fertilizers — all require basic research, particularly on the chemistry involved.

I believe that the dynamical modeling of the stratosphere is well under way. Traditionally, the National Science Foundation has supported basic research in this area, as in all areas of science. In the future, the Foundation will continue its support of stratospheric chemistry, with emphasis on measurement of the pertinent trace constituents — an extremely difficult business requiring accuracies of parts per trillion — in laboratory reaction chemistry and in the field of heterogeneous chemistry generally.

I should like to emphasize that it is difficult and indeed scientifically unreasonable to divorce stratospheric chemistry from tropospheric chemistry. An example that comes to mind is the OH radical, which plays an important role in the chemistry of both regions. In the stratosphere, it reacts with trace constituents such as O_3 , HCl, and NO_x ; in the troposphere it is involved in the formation of photochemical smog, reacting with unsaturated hydrocarbons, ozone, and possibly sulfur dioxide.

I believe that CIAP, apart from its very important role in assessing the effects of SST emissions on the stratosphere — and that's what we are hearing most about today, of course — has served in a subtle way as an excellent example of how scientists and engineers have cooperated internationally in responding to a pressing problem. It has pointed clearly to avenues of research which must be followed if we are to avoid recurring "crises" regarding the stratosphere. This example may well make people aware that an ever-increasing knowledge of our environment, which can be acquired only by continually asking questions about how nature really works, is essential for human well-being.

MEISTER: I'd like to take a few minutes to outline for you how we at the FAA view our responsibilities and the nature of the program that we intend to undertake over the course of the next two years.

As Dr. Grobecker said this morning, there are still a good number of scientific uncertainties regarding the effect of SST's on the stratosphere. We know that there are no discernible health hazards now, but more precise knowledge is needed to ensure that they are avoided in the future. In developing environmental regulations, it is the FAA's responsibility to protect public health and welfare. But by law our rules must also not downgrade safety; they must also be economically reasonable and technically practicable. With these various points in mind, we are undertaking our program in high-altitude pollution research and monitoring to provide the technical basis for any eventual regulatory action. Furthermore, the High-Altitude Pollution Program (HAPP) will not be continued in isolation. We are integrating it into our total environmental program, which is also concerned with aircraft noise and low-level aircraft emissions, as well as environmental assessment of airport development projects, including the effect of SST's coming into the United States.

HAPP, our continuing monitoring and research program, will aim at four objectives. First, it will join with other programs in trying to reduce the current scientific uncertainties. Second, it will ascertain whether atmospheric quality is being maintained. Third, it will provide guidance for decisions concerning regulatory actions. Fourth, it will investigate how to minimize the cost of providing any of the required environmental safeguards. In the short term, HAPP's primary concern is simply a better understanding of the natural stratosphere and the effects of aircraft on it.

As Dr. Stoney indicated, after a baseline has been established, the emphasis will shift to directly monitoring the effects of stratospheric flight. Although FAA will maintain some activity in modeling and chemical dynamics in order to better develop our diagnostic tools, the basic contributions to the monitoring efforts will come mainly from NASA and NOAA.

In undertaking the HAPP effort, the FAA proposes to spend in FY75 approximately \$1.7 million, half of which will go for monitoring and experiments. In the FY76 budget recently submitted to the Congress by the President, we are requesting \$2 million, with about \$1 million of that going for monitoring and measurement-related experiments, about \$350,000 for modeling, \$250,000 for chemical-dynamics studies, \$200,000 for engine-emissions work, and \$200,000 for analysis.

In establishing the required standards, of course, we will work very closely with the EPA and international organizations. Ultimately, regulatory action governing emissions from aircraft operating in the stratosphere may be required to avoid significant environmental impacts. As was indicated this morning, this certainly will have to be a joint undertaking by all the nations concerned, and the FAA and EPA will have the task of helping to formulate an international policy on the regulation of fleet operations or aircraft emissions. We will be working with ICAO as early as this spring to do that.

As was also mentioned, aircraft are only one source of high-altitude pollution. Their contribution is a function of the number of engines, the fuel used, the numbers of aircraft flying, and the flight altitude, and we will have to be very careful in our analysis of the fleet forecasts.

Now, as Dr. Grobecker stated in the Report of Findings, CIAP used what might be called the most pessimistic set of assumptions. The FAA estimates that by the year 2000 the maximum market will be 100 Concorde-type aircraft, including TU144's, with up to 200 additional new-technology SST's. On the other hand, the market may be as small as 16 Concorde-type aircraft and 100 new-technology SST's. (For this projected range of Concorde-type aircraft, our best estimate is set at about 40.) This is obviously substantially fewer than the range of 800 to 2500 which appears in the Report. We expect the 2000 subsonic aircraft currently flying in the stratosphere to increase by 50% to 100% by the year 2000 - which should be contrasted with the outer-limit increase of 300% to 1000% projected in the Report.

In short, on the basis of the CIAP study we believe that no substantial environmental hazards are associated with stratospheric flight at present, or probably for many years to come. However, the possibility that they might exist is an important one, and the FAA is undertaking a systematic and comprehensive program of research so that timely policies and plans can ensure that atmospheric pollution by aircraft will never become a hazard.

CANNON: The scientific skill and care and responsible reporting of measurements and calculations which you in this room and your colleagues have brought to this technology assessment have surely been exemplary. They have given us a much better understanding of the important and difficult problem you have addressed. Scientists who carry out technology assessments on other matters from now forward will do well to study the example you have set.

But it is so very difficult to convey to a non-expert — a newsperson, for example, or one's friends — a balanced picture of what the results mean. One is asked the disarmingly simple question, "Is there a problem?" If one answers by saying "There is no serious problem if we take suitable preventive measures," the resulting headline reads *There is No Problem*. If one answers by saying, "There is a serious problem unless we take suitable preventive measures," the resulting headline reads, *There is a Serious Problem*. I suggest that the answer has to begin, "By taking suitable preventive measures, we can avoid a

serious problem." I haven't been able to try that one out yet; I'm looking forward to doing so!

The central issue is prevention. If very large high-altitude fleets, either supersonic or subsonic, ever develop, then only through proper preventive measures can the serious consequences to which Professor Johnston and others have alerted us be avoided. My personal single objective, and I hope that of every person here, is to be sure that the preventive measures, which the CIAP has shown are essential to protecting the environment, are carried out without stint, starting now. The CIAP Report of Findings is clear: While today's aircraft operations are not a threat, engine emission standards will be needed in the future for a safe environment, if SST's are to fly in very large numbers. Such standards may also be needed if subsonic planes are to fly in much larger numbers and at higher altitudes than they do today.

Making clean engines that comply with such standards, and developing them and moving them into the fleets — both subsonics and SST's — will take a decade or more. There is no time to lose in starting the engine research. Any regulation to structure such standards will take years to develop because it must be international. It has to be developed by the nations together, for there is only one stratosphere, and pollution anywhere in it is pollution everywhere in it. There is no time to lose in starting that structuring. Manufacturers and operators need to know many years ahead what the rules are likely to be.

If, for once, we are to prevent a problem instead of confronting a crisis, we all have to dedicate our energies to getting the preventive machinery moving and keeping it moving; to supporting the engine research and the continuing atmospheric research; to supporting the efforts of Fred Meister and Charles Cary of the FAA and their counterparts here and in other countries. That's what we've got to do now that the remarkable research of the scientists in this room and their colleagues has yielded the clear results it has.

What could keep us from succeeding? What could prevent prevention? What could prevent preventive action from getting full support? One thing is a perceived dichotomy among scientists — and I use the word "perceived" advisedly. The preventive actions that have to be taken are going to cost money. Engine research costs money.

Atmospheric research costs money. Regulatory activity and the measurements to support it cost money. The OMB and the Congress have a prime duty to spend money only when it is clear that it is necessary. If scientists appear to disagree, OMB and the Congress will simply conclude that it is not clear that anything should be done, and they will not fund the needed preventive measures.

The misquotation of Dr. Grobecker last month was particularly unfortunate. I should like to take this opportunity to set all of you straight on the exchange that took place. Dr. Grobecker was asked how the study would have been affected if the U.S. had continued development of the SST. He replied that "by this time there might not have been enough airplanes flying to produce a measurable effect." It is difficult to understand how this statement could have been interpreted as saying that a full fleet of U.S. SST's would not affect the ozone layer, particularly, when earlier in the same press conference, he stated that, by our estimates, 120 Concordes would indeed make a perceptible change in the ozone layer.

We need to bring loud and unanimous support to Fred Meister's announcement that the FAA will begin developing with our friends abroad the structure for whatever regulations may be necessary; to James Fletcher's announcement in Congressional testimony last week that NASA intends to pursue a program of continuing atmospheric research to provide a continually improving scientific base for assessing possible harm to the environment from stratospheric operations; and to the continuing enginetechnology program that has just been described.

We have got to make it clear that responsible people are taking responsible action to ensure that the stratosphere will be protected. We need to be sure these actions are supported by the Congress and the people.

MACDONALD: The first point that I should like to make is that CIAP is a prime example of what technology assessment means. It is an examination of a technology and the consequences of its use, and an evaluation of the costs and benefits of its development. As other technologies come along, I hope that we can look back at this study carried out by Dr. Grobecker and Dr. Cannon and their colleagues and see how these techniques can be applied.

My second point is that this study emphasizes the importance of looking at a long-neglected part of the atmosphere: the strato-sphere. The stratosphere is so far up that we don't interact with it on a day-to-day basis. Yet it has an important effect on what happens to the surface on which we live. I think that focusing attention on this part of the atmosphere will substantially increase our understanding of our environment.

The third point is that the CIAP emphasizes the delicate and important interactions between climate and what happens around the world. Small fluctuations in whatever parameter you wish to take — annual average temperature is sometimes used — can influence agricultural productivity and economic welfare in a very, very significant way. The interaction of the atmosphere with the biosphere is part of the story that comes out of CIAP. It's a key part of the story, and one that has not been sufficiently emphasized.

In addition to these three major points, there are others that should be noted. One is the recognition that some of the photochemical reactions which take place in the high atmosphere have analogues that are important in the lower atmosphere. The studies of SO_x and the reactions it undergoes are another valuable contribution. Clearly the points emphasized in the CIAP report, that the stratosphere is a global resource and that control of what happens there can be achieved only through international cooperation, is an extraordinarily important one, and one that we need to bear in mind as we discuss other problems of the atmosphere at lower levels. International law is not nearly so far developed with respect to the atmosphere as it is with respect to the sea, for example.

Finally, there are no black-and-white answers in science. Science deals with probabilities. We don't know for sure what will happen if we have a fleet of 500 SST's flying in the stratosphere. We can make pretty good guesses that the effects are likely to be detrimental, but we can't simply say that you're going to wipe out a certain fraction of the earth's agricultural productivity if you fly 500 SST's eight hours a day. We just don't have that kind of data. We couldn't accumulate the data, even with massive infusions of money over the next ten years, but we can say that there is a high probability that

this will happen. This distinction between saying something is certain and saying it may happen is very difficult to get across in the media, particularly to people who assume that the scientist always has a right answer. This is the kind of problem that we have to face, not only with respect to the SST but with respect to many other issues that relate public policy to science.

I think that the CIAP Report of Findings, together with the analysis by the NAS, the NAE, and the NRC, which substantially agrees with the CIAP report, will serve as a model of the kind of technology assessment we should undertake in a number of fields. I look forward to working with the National Science Foundation and other agencies in developing this kind of assessment of future technologies.

BRUN: A considerable amount of work has been accomplished by CIAP over the last three years. I wish to congratulate not only the Chairman, Dr. Grobecker, and the Deputy Chairman, Mr. Coroniti, but all the authors for the outstanding results documented in the six CIAP monographs.

These monographs, in their provisional form, were studied and commented on by COVOS at the particular request of Dr. Grobecker. The work performed by COVOS is more limited than that of CIAP, and obviously we could not pass judgment on all the results presented in these monographs which, for us, have constituted valuable sources of information. However, we can give our advice on the problems which we have dealt with.

We are glad to see that our conclusions are, in the main, similar. We could discuss a number of details, but so as not to be too long I shall limit myself to the subject of stratospheric flight between 16 and 17 kilometers altitude — which includes flights made by aircraft of the Concorde type. Restricting our remarks to this subject does not mean that the COVOS is interested only in the Concorde problem, however. The scientists who constitute the Committee are not linked in any way to the aeronautical industry, and, like the contributors to CIAP, are interested in promoting knowledge of stratospheric science, engine emission, and the biospheric impact of stratospheric flight.

My first remark concerns the number of aircraft of the Concorde type built by 1990, at which date new combustion chambers emitting

less NOx might be available. Let us make the assumption that 125 Concorde aircraft will be operated in 1990. Assuming a parallel evolution of the TU 144, we would have at that date 250 aircraft of the Concorde type. If each aircraft flies 2000 hours per year and emits 18 grams of NO, per kilogram of fuel, we would have, through 1990, a 0.2 × 109 kg mass of NO_x injected between 16 and 17 km altitude. If one supposes that the American SST will not be in service by 1990 and that the number of military aircraft will not increase significantly, the amount of NO_x emissions in the stratosphere will be essentially equal to this figure, as subsonic aircraft will fly at altitudes under 15 km, and will not contribute in any important manner. Also, by 1990 improvements in engine technology should make it possible to have decreased annual NO_x emissions, even if the number of aircraft continues to increase.

What we are saying here does not contradict the CIAP conclusions. From the data of the CIAP Report of Findings, 0.2×10^9 kg of NO_2 injected annually would cause a reduction of 0.8% to 1% in the column of ozone, using the models adopted for CIAP calculations (see Figures 14 and 16 of the Report and Table 1 of page xvi of the Executive Summary).

A second remark concerns the validity of the models used, both our own and CIAP's. On the one hand, accurate measurements were made in France of the mass of nitrogen oxide constituents actually present in the stratosphere. These measurements, which I shall describe in a later paper, lead to an 8 × 109 kg mass of $NO_y = NO + NO_2 + HNO_3$ between 15 and 40 km. This mass is far higher than that shown in the CIAP conclusions; the discrepancy here seems due simply to CIAP's smaller estimate of the mass of HNO₃. On the other hand, a large discrepancy exists between evaluations of the residence time. For example, at 17 km, Reiter finds a residence time of the order of a few months, and Fabian and Libby one of about eighteen months. Due to the rapid elimination of HNO3 towards the troposphere by the steep gradient of its vertical distribution curve, we can reasonably accept the results of Reiter. Consequently, the total reduction of ozone in 1990 would be rather smaller than 1%.

In view of the above considerations, we have good reason to think that these models, and

consequently the conclusions that may be drawn from them, constitute an upper limit. Thus, it does not seem that in 1990 the decrease in the amount of ozone will reach the threshold of 0.5% considered as barely discernible by CIAP.

COVOS, like CIAP, would like to see in the coming years a program to carefully control and monitor, in an international framework, the evolution of the stratosphere, and to draw up any regulations needed after 1990. France will gladly participate in such a program.

A third remark I make on behalf of the biologists of the COVOS. They want to underline the good agreement among the various computations of the effects of UVB on the skin of the white man (they agree on an increase of 2% in erythemal or carcinogenic activity of solar UV for a decrease of 1% in the amount of ozone). However, they also remark that the *Report* does not attach enough importance to the biological effects which result from the interaction of solar UV with the genetic material of prokaryotes (unicellular organisms) that are the exclusive producers of amino acids.

A fourth remark concerns the economic impact of climate change which might arise from the presence of aerosols in the stratosphere. In this area, many studies have been carried out on risks, and far fewer on benefits. Furthermore, in the assessment of risks, it seems to us that the possibilities of adaptation by change of species in crops, or even by natural adaptation of animals or plants, have not been correctly taken into account. In Canada, during the last twenty years, certain crops have spread northward, that is to say toward average temperatures 4 to 5°C colder. There again, the large effects stated for temperature variations much smaller than 5°C should be considered as a maximum.

I should like to end with two wishes. The first one is that we concern ourselves as much with the presence of ClO_x as with NO_x in the stratosphere. We need further knowledge of the effects of Freons released by spray cans. My second wish is that people be better educated as to the dangers of longer and longer sunbaths by barer and barer people. Could we not inaugurate a nostalgia fashion, where people would wear large hats and be protected by parasols?

MURGATROYD: I would like to start by congratulating Dr. Grobecker and his colleagues on

the important advances that they have made in knowledge and understanding of the atmosphere through the Climatic Impact Assessment Program. The United Kingdom's Committee on Meteorological Effects of Stratospheric Aircraft, COMESA, are also very grateful to the CIAP for the exchange of data and general cooperation of the last three years, and for allowing me the opportunity to make a few comments on the CIAP Report of Findings. My remarks will be brief and mainly limited to a few of the conclusions presented in the Executive Summary, since we received this rather comprehensive report quite recently, and have not been able to study it in as much detail as we might wish.

First, the results of the studies made so far by the COMESA certainly support the finding that operations by present-day SST aircraft would cause climatic effects which are smaller than minimally detectable. Moreover, the evidence is that it will not be possible to measure with any certainty effects which can unambiguously be ascribed to the numbers of SST's thought likely to enter into service in the next one or two decades. According to Table 1 in the Executive Summary of the Report of Findings, 100 Concordes/TU-144's will produce an estimated ozone reduction of 0.39% in the Northern Hemisphere. This figure is two or three times the value we have deduced from the COMESA's one-dimensional model, but if one takes into account all the uncertainties in this work, the disagreement is not large. In any case, values of this order are very much smaller than the natural long-term variations of hemispherical ozone amounts, which are in the region of 5 to 10%.

Second, the CIAP report gives an estimate of 0.5% for the barely discernible change in global mean ozone amount. This estimate seems to be very optimistic, in view of the known wide natural variability of ozone on all time scales and with longitude and latitude. If the aim of the proposed monitoring is to detect a change of this magnitude in a ten-year period, it is very doubtful that it can be achieved. The reproducibility and lack of drift with time of present instruments are not good enough to provide the required accuracy of measurement, even with a vastly expanded observational network. And, what is probably more important, even if such a

change were detected it could not be ascribed to any one cause, since a considerable number of natural and anthropogenic factors may also affect ozone levels: for example, solar variations, cosmic-ray effects, general-circulation variations, and changes in surface source levels of various chemicals such as nitrous oxide, Freons, and other still largely unknown sources and sinks. And finally, it appears that if the differences between hemispheres are taken into account in computing the effect of emissions (it has been argued that since most of the flying will take place in the Northern Hemisphere, ozone will be considerably more affected there), the same differences should be remembered in considering the monitoring problem. The global mean ozone change would not reach 0.5% until a considerably larger change had taken place in the Northern Hemisphere. For this reason, the direct use of the estimates which are given in Table 1 for the Northern Hemisphere, in conjunction with the assumed 0.5% detection limit of global average ozone reduction, leads to an underestimate of the number of aircraft needed to produce a given global change. (See, for example, page xvii of the Executive Summary.)

Third, it should be noted that although CIAP workers have concluded that the climatic effects of small numbers of SST's are likely to be undetectable, they have also concluded that a large increase in stratospheric vehicles would lead to significant disturbances of the environment. The first conclusion is supported by a good deal i independent evidence, such as the large natural variability of the atmosphere and the fact that nuclear tests have had no major effects on total ozone, whereas the second depends basically on theoretical calculations. Once a process has been included in a model, the result of the calculation must have some dependence on it and will be unaffected by other processes not included. The result can to this extent be considered predetermined, and dependent only on the data and the assumptions in that model. For example, the introduction of conversions of NO_x to HNO₃, which were not included in the calculations of only three or four years ago, has reduced significantly the estimated effects of SST operations on the ozone layer. The recent suggestion that Freons and other substances released at the earth's surface may have effects exceeding those estimated to result from aircraft

emissions illustrates the uncertainties in the subject and raises further doubts about predictions which cannot be properly validated. Nevertheless, it is agreed that the CIAP's recommendations, in view of the current state of the subject, are wise and prudent. Research must be continued; improved monitoring, after further detailed evaluation, is desirable to study all the proposed factors which could perturb the ozone layer, not only aircraft; and the development of engine technology in the future must take account of the problems raised by the SST emissions, the growth of stratospheric aviation, and the best current knowledge of the stratosphere.

Fourth, the CIAP has attempted to study the effects on the ozone layer of all stratospheric vehicles. However, most of the calculations contained in its reports refer to large numbers of aircraft flying at 20 km. This situation is not likely to occur for several decades (by which time the technology may have changed considerably), so it hardly constitutes a basis for present decision-making. The practical problem we face right now is to study the more realistic case of a large number of subsonic aircraft flying in the lower stratosphere at 11-13.5 km, together with the small number of SST's flying at 16-17 km anticipated to be in operation in the next 10-15 years. As far as I know, comparatively little effort has been put into modeling the effects of the subsonic aircraft, and the values quoted in the CIAP Report of Findings are less well based than the SST results for 17 and 20 km. So far the continued expansion of subsonic flying has not had significant effects on the environment, so before any decisions to limit operations are made, it should be demonstrated quantitatively (by models) that although the present fleets produce negligible effects the increases expected in subsonic stratospheric flying and the relatively small additions of SST's would cause significant environmental effects. Further numerical work on the effects of subsonic injections, and also on the combined effects of subsonic and SST fleets, is desirable, and it is hoped that the COMESA will be able to make some contribution to this aspect of the problem in the next few months.

Fifth, the climatic aspects have to be considered against the background of natural vari-

ations. Average global temperatures at the earth's surface increased by about 0.6°C from the 1880's to the 1940's, and have since fallen by about 0.3°C. According to the data given in the Executive Summary (pages xxiv-xxv), it appears that 100 Concordes/TU-144's would produce a decrease of 0.003°C, so that even if several thousands of these aircraft were in operation their effects would be small compared to changes due to other causes. It is not known which of the latter are the most important, but it is suspected that dust thrown up by volcanoes, rather than anthropogenic releases of carbon dioxide and other substances from the earth's surface, is the main contributor. It should also be mentioned that effects on the general circulation and the climate will be due to changes in several constituents resulting from the aircraft emissions, i.e., water vapor (possibly with some cloud effects), ozone, and NO2, as well as the aerosols due to SO2, on which the CIAP results are mainly based. When all the other constituents are considered together, these effects will cancel each other out to some degree, so the values given in the Report of Findings are probably overestimates. However, the subject is a very difficult one, with many uncertainties, and the calculations made so far by the COMESA agree in order of magnitude with those of the CIAP. We disagree, however, as regards their interpretation, in that we do not feel they are sufficiently certain - or indeed the effects sufficiently large - to form a proper base for estimating social and economic effects, particularly changes in different regions of the world, considering the wide variability in space and time of the earth's climate.

In conclusion, an administrator concerned with decision-making said to me that what was really needed was a general agreement between scientists on these questions. I think that we have already reached this point in the work of the CIAP and COMESA to the extent that we agree that the introduction of a small number of SST's would have an undetectable effect on the total ozone amount, and also on the earth's climate, by comparison with the natural variations. On the other hand, the possibility of significant effects is not excluded if large increases in stratospheric flight take place with present-day technology. There may later be questions about

the amount of flying that is admissible, but until quantitative understanding improves considerably there will be no sufficiently good scientific basis for formulating any detailed regulation. Meanwhile, since the nature of the potential problems is now well recognized, research should continue and plans should be made for an internationally acceptable monitoring program.

RUMMEL: I think CIAP is on the right track in several respects, specifically with regard to three points:

- Recommending the establishment of an effective global atmospheric monitoring system, in a timely manner
- Recommending the acceleration of combustion technology toward the reduction of potentially harmful emissions in future engines
- Encouraging attention to the question of how, and what kind of, international atmospheric-pollution regulations can be established in the future if they are needed.

Also, the Report of Findings contains a number of reassuring statements. First, the Report indicates that current technology can realize NO, reduction of at least a factor of six while maintaining present engine-performance levels, and that a reduction of a factor of 60 may be foreseen. It also indicates that the use of low-sulfur fuels can adequately solve particulate problems arising from SO₂ engine emissions. Second, the Report of Findings states that current operations with subsonic aircraft do not pose a discernible threat - that in fact current subsonic flight operations could be increased fivefold before the "barely discernible change" level would be reached. Also with respect to future wide-body aircraft, it says that five times the number of 747 aircraft flying today could operate under the "barely discernible level" if NO, were reduced by a factor of only two, not even the factor of six available with present technology.

As for supersonic aircraft, the Report indicates that a fleet of about 30 Concordes and TU-144's would cause climatic effects much smaller than (about 20% of) those considered

•

minimally detectable; operations with over 100 such aircraft would be required to produce detectable results. Also, it implies that even if the "upper-bound" aircraft-fleet size projections should be achieved, sufficient time remains to develop technologies to mitigate the potential problems.

In short, the CIAP Report of Findings is reassuring in that it claims that no discernible problem exists with current subsonic or planned supersonic operations, and that probable advances in technology will be able to cope with any problems arising from future increases in operations.

Now, notwithstanding all this, CIAP urges that a plan for "a proper program for international regulation of aircraft emissions and fuel characteristics" be developed "within the next year." CIAP's own findings indicate that this not only is premature but may never be needed. Giving thought at this time to the structure and content of possible future regulations may prove to be useful in the end, but the early development of a specific plan which would tend to produce over-regulation would be a disservice.

Chapter 6 of the Report of Findings, entitled "Regulations and Controls," considers an appropriate base for the development of regulations to be the "hypothetical worst case" defined by English's upper-bound projections. This worst-case projection shows 1851 large advanced SST's by the year 2000, and 5561 by 2025, along with 14,605 subsonic passenger and cargo aircraft by 2000, and 45,126 such aircraft by 2025. Compare this to no commercial SST's and about 4200 subsonic jet transports in operation today. Setting aside the question of just how unrealistic these high forecasts are, CIAP's own findings indicate that the development of regulations intended to solve the hypothetical problems of 50 years - or even 35 years - from now is not only premature but may be unnecessary. Any regulations that may be required should be developed as the need becomes apparent, and should reflect real-world growth and technology.

CIAP points out that "there are more than 30 possible causes of observable changes in UV radiation at the ground," and that many factors besides aircraft pollution in the stratosphere cause changes in climate. For example, mean surface temperature is affected not only by aircraft exhaust but by industrial pollution,

which is largely responsible for increased accumulation of dust in the troposphere and of CO₂ in the atmosphere. CIAP also points out the importance of identifying all the causes of a particular climatic or biologic impact. If regulations become necessary for the general welfare, all significant contributions to the pollution should be held to the same standard.

In summary, because of the obvious fragility of projections of future world developments and the less-than-complete scientific understanding of the atmosphere that exists, it seems to me that present efforts should be directed toward establishing an effective global monitoring system and developing practical low-NO_v engines.

FERRIS: I have interpreted the request that I speak this morning as a desire to know a little bit more of how ICAO functions, and when, in relation to environmental matters. My job has been made somewhat easier by one of the charts Dr. Grobecker showed earlier this morning. If you remember, it showed four distinct progressive actions in the regulatory chain of activity in the international area: international acceptability, air-quality standards, engine-emission standards, and international aircraft regulations.

On the first of these, international acceptability, ICAO action is triggered once it is recognized that an international problem exists and that there is a desire to solve that problem. You see, the member states in ICAO recognize that if a civil-aviation problem exists which is truly international in scope, it can be solved satisfactorily only through international means.

In the second area, air-quality standards, it was recognized that two other international organizations were involved. The first of these was the World Health Organization, which — to oversimplify — deals with air-quality standards at lower altitudes and around airports. The second was the World Meteorological Organization, which has responsibility for air-quality standards in the upper atmosphere. ICAO keeps in close touch with these two organizations to make sure that we do not get at cross-purposes with each other.

In relation to engine-emission standards, I'd like to refer briefly to the broad environmental activity that ICAO has had under way for many years now. We have had a program embracing aircraft noise, sonic boom, aircraft engine emissions, and airport planning aspects. The aircraft engine-emissions work within ICAO is relevant to the CIAP studies.

At present we are really in the middle of the first three stages in the regulatory chain: We are in the process of establishing international acceptability; air-quality standards are currently being examined and, presumably, developed through the WHO and WMO; and within ICAO we have a group which is working on engine emissions. At this time, there are representatives from France, Japan, the United Kingdom, the United States, and the USSR in this group. It has been given a four-stage program. The first stage was fact-finding. The second was establishing agreement on units of measurement and methods of measurement in relation to exhaust emissions from individual engine types. Third, the group was to investigate whether a certification scheme was needed to control engine emissions. And, finally, it was to proceed with the development of standards, if this proved to be required. I understand that the group is very close to reaching agreement on units and methods of measurement for engine emissions. Later this year, I hope to see agreement on this phase; the group will then be prepared to make recommendations as to requirements for further study and the need for a certification scheme. Any such proposal will next be submitted for consideration by the appropriate standing committee in ICAO. If it is ultimately decided to proceed with the development of standards, such standards would eventually have to be approved by the Council of ICAO, which is its governing body. These standards would then be submitted to Contracting States, and if they were approved, the States would then normally incorporate the substance of these standards in their own national regulations.

This process may seem somewhat cumbersome, but it can — and does — produce results once it is apparent that results are required. As an example, I should mention briefly that ICAO international standards do exist, and have existed for some time now, in the field of aircraft noise, and at this very moment are undergoing further study and development.

OPEN DISCUSSION

JOHNSTON: During the past three years, I've followed all aspects of the CIAP, except for the economics studies. When a couple of weeks ago the newspapers quoted Dr. Grobecker as saying that present SST's would not affect ozone and "a United States fleet of high-flying planes would not weaken the ozone shield either," I knew something was off the track, perhaps a misquotation. When I received a copy of the Executive Summary of the CIAP Report of Findings, and studied it, I developed the following position.

A technical audience, like the one here, can listen to a 1 1/4 hour presentation, such as the excellent one given today by Dr. Grobecker, and keep it all straight, both the conclusions and the uncertainties. However, what the outside world gets - editorial writers and newspapers, members of Congress, the general public - hinges very heavily on just the stated conclusions. It seems to me that the principal conclusion in the Executive Summary represents an adversary position - to be sure, one consistent with the CIAP findings. The order of conclusions, the emphases, the omissions, suggest to me an adversary position in support of the SST. Some questions which could have been simply and clearly answered were not answered. Thus it seemed to me that somebody should write an adversary set of conclusions, consistent with the CIAP findings - that is, anti-SST - for the sake of balance, since the other was not neutral. Now I've never considered it my job to be an anti-SST advocate, but late last week it seemed somebody should do the job for this one time. Thus, I sent off my letter to the New York Times and prepared a short, 10-page "Report of Findings" of my own. This "Report of Findings" agrees with the facts of CIAP, and furthermore agrees with the methodology of the DOT Report of Findings, but has a different set of conclusions - and that's all I'll read.

The following conclusions are derived from the DOT Report of Findings.

- The artificial nitrogen oxides from a fleet of 125 Concordes and TU-144's would reduce ozone in the northern hemisphere by 0.5%. and would eventually increase skin-cancer cases in the United States by 1% - which would be about 5000 per year, or 100,000 over the 20-year life span of the aircraft. The 375 SST's projected for EPA for 1990 would result in threefold greater effects.
- The artificial nitrogen oxides from 500 Boeing SST's as described in 1971, but with the Concorde's emission index for NOx, would decrease ozone by 12% and increase U.S. skin-cancer cases by about 120,000 per year, or about 2.4 million per 20 years.

(These are, I repeat, derived from the Report of Findings, not my own independent calculations.)

3. One future fleet of SST's - this is the big fleet predicted by Dr. Grobecker in Acta Astronautica - predicted for the year 2025 would reduce ozone by substantially more than a factor of three. Even if NOx emissions are reduced by more than a factor of 60, such a fleet would reduce ozone in the northern hemisphere by more than 5%. It appears improbable that very large fleets of SST's can be made safe, even by reduction of the NO. emission index.

My recommendation is to read the whole DOT Report of Findings, not just the statement of conclusions or the headlines!

GROBECKER: Professor Johnston always has a challenging thing to say. While the statements of the Report of Findings are the authors' alone, Dr. Johnston has been a major contributor to the facts on which such analysis, or his own analysis, could be made.

I have prepared a table of equivalences. I don't disagree with those that Professor Johnston has named; that is a perfectly satisfactory way of describing things, although I don't choose to impute unfavorable actions to others. The problem is a little bit like answering the question of whether a cup is half-empty or half-full. The answer can be a matter of taste. Some of the equivalences I will note are on the level assessed as "barely detectable" - that is, without at all relating those levels to standards for regulation. In the future, when discussion of regulation or standards does take place, we would then all be referring to the same physical effects.

We estimated that a "barely detectable" change in world ozone - global ozone, that is, not hemispheric ozone - was one-half percent, a change determinable from 10 years of daily observations. This one-half percent would also be the result, we thought, of 120 Concordes, flying 4.4 hours per day in the northern hemisphere, 365 days per year, with present-day emission indices of 18 g/kg, at altitudes of 15 to 18 km (49 to 59 thousand feet). This same level could cause a change in skin-cancer incidence within the United States of 1%, which I took to be 6000 new additional cases of skin cancer. An equivalence of this might be that the skin cancer - which people may get anyway later in life as a consequence of their skin type and exposure - would occur something like four months earlier, after about 30 years of exposure. It would indeed be the equivalent of 45 minutes at noon once each summer for 30 years at Ocean City, N.J. It might be the equivalent of moving your permanent residence from Baltimore, Maryland to Washington, DC.

A proper question, when we come to addressing air-quality standards, is how many multiples of this effect are tolerable. I can think of people in different parts of the world who would justify different answers to that question. That's why the next point of the

^{*}Alan J. Grobecker, "Research program for assessment of stratospheric pollution," Acta Astronautica 1 (1-2), 179-224 (1974).

discussion now beginning is a matter for the forum of the ICAO that Mr. Ferris talked about.

Dr. Murgatroyd has pointed out that there is confusion as to whether the effect is hemispheric or stratospheric. With NO being emitted by aircraft which in the near future would be flying principally in the northern hemisphere, the "worst-case" effect in the 30° to 60°N latitude band would be about twice the global average, and the effect in the southern hemisphere would be a smaller fraction, suitable to balance out the global average. Many of our early computations were made on an oversimplified global-average basis. If the pollution were introduced principally in one hemisphere, the people of that hemisphere would feel the effects more strongly than the people in the other hemisphere. The number of 120 Concordes that we have used could, if they all flew in the northern hemisphere only, cause the one-half percent change in the 30° to 60° N latitude band, and less in the other hemisphere. So the 120 Concordes that we speak of as giving rise to 1/2% "worst-case" northern-hemisphere change correspond to a figure of about 240 Concordes, distributed globally, needed to produce a 1/2% change in the global

Now, the equivalences for climatic change due to SO₂ also show the effect to be more remote in time. Since many factors can influence changes in global temperature, we have suggested detection of changes in the optical thickness of the stratosphere as the measure of SO₂ pollution effects. I suspect that if the time series of observations of global average temperatures were subjected to the same kind of analytical treatment that Pittock gave the ozone picture, it would show that a long time is needed to determine a small change. We haven't done that analysis; I think it's appropriate to do it. Stratospheric optical thickness is about 0.02, according to Elterman's numbers. The observations and measurements on the record are sparse. The optical thickness of the total atmosphere is about ten times that of the stratosphere. We thought a 10% change in total stratospheric optical thickness, which varies much more than that from year to year, would be a change observable in 10 years of daily or very frequent observations. A change of this size is not suggested in this forum as a standard for regulation at all; it is just a dimension to which I can now describe equivalences.

We think a change of this magnitude would be caused in the hemisphere of injection by about 2070 Concordes flying 4.4 hours per day, 365 days per year, with emission indices of 1 gram of SO₂ per kilogram of fuel burned, cruising at altitudes of 15 to 18 km (49 to 59 kft). This represents a decrease in the mean global temperature, by our system of equivalences, of 0.07°C, or a decrease in mean temperature in the United States of about 1°C. It would perhaps reduce the U.S. rice crop by 2%; the value of the world wheat crop might drop by \$9 million, and that of the world rice crop by \$100 million. It would be the equivalent of one-third of the world temperature decrease from 1940

to 1950. And whether or not we will have at some future time — say ten years from now — the ability to detect either of these so-called "barely detectable" signals is a challenge to technology. These numbers are important today, in my view, as a basis for discussions of how much change would be acceptable and tolerable.

KAUFMAN: I hope my great friendships with Drs. Grobecker and Cannon will not suffer from the blast I am about to deliver. Also, I want to say that although I'm a member of the Climatic Impact Committee, my remarks now have nothing to do with that membership. I have followed CIAP. I think it's wonderful, and I hope the FAA continues it similarly as the High-Altitude Pollution Program. But my criticism concerns the events of the last two weeks. I find it supremely ironic that a program that looks thirty years ahead does so poorly at looking one day ahead: from the day the Report of Findings was released to the next day, when it was reported in the news media. The impression gained by the educated news-follower was that there is no ozone problem. I, of course, agree with Hal Johnston that the Report did a terrible public-relations job, and that you are suffering the consequences. Though most people in this room know what CIAP has accomplished, I was wishing, till Hal came along, that someone would set the record straight the way he has. I also think Dr. Grobecker's remarks about the 45 additional minutes in the sun, and moving from Baltimore to Washington, are frivolous.

To give you an idea of the fallout you are dealing with, I will read you the editorial that appeared in the *Pittsburgh Press* on January 29, 1975. Now you must realize that this is the major morning newspaper serving a metropolitan area of 2.4 million people. The editorial is entitled "FOOTNOTE ON THE SST".

"Remember the supersonic transport SST? It was rejected in a deluge of ecological righteousness nearly four years ago, partly because environmentalists persuaded Congress that a fleet of faster-than-sound aircraft would fatally deplete the layer of ozone that protects Earth from harmful rays of the sun. Peel back the ozone shield, one anti-SST force said, and such radiation-induced diseases as skin cancer would become commonplace. Noise, air pollution, and questionable economics were also advanced against the SST, and now, much too late, we learn each of these arguments. But the ozone argument was a major factor in defeating the SST, and now much too late, we learn that the ozone argument was unscientific nonsense.

"In a carefully documented study prepared for the U.S. Department of Transportation, DOT, scientists have revealed that an SST fleet flying regular schedules for a period of ten years would deplete the ozone shield so little as to be almost undiscernible. Specifically, the DOT report suggests that a fleet of

^{*}Editors' note: The details of this computation may be found in Appendix B of the CIAP Report of Findings.

SST's would thin the ozone layer by as much as one-half of one percent, a figure that shrinks to realistic proportions when it is realized that natural variations in the ozone frequently exceed 30 percent on a daily basis. The DOT report is a powerful argument for using facts and not scare slogans when decisions are to be made. The phony ozone argument has no place in rational scientific discourse, and no place in the SST debate. It is useful to know the facts now, even if exculpatory evidence that arrives after the hanging is of small comfort to the deceased."

The only technical aspect of the Report of Findings I want to discuss is its sudden obsession with the minimum discernible change and with monitoring. Suppose the minimum discernible change in ozone had been 20%? Would that give us license to change it by that much? Would improved monitoring enable us to mitigate pollution that had already occurred? The Report's treatment of these matters is totally unrealistic. Important as monitoring is, it cannot replace prediction.

ELLSAESSER: I would like to take exception to most of what the last speaker said. First, I believe we should inform the public in terms that enable them to evaluate the problem for themselves. I think we have neglected to do that in the past. We should give them information in terms like "moving from Baltimore to Washington," if at all possible. That doesn't mean we shouldn't give other numbers as well, but if we enable the man in the street to decide for himself whether the problem is important, it's the best we can do.

Second, I don't think we can ever hope to guess what the media will do to the statements we give them; I therefore think that our best course of action is to not even consider that aspect when we do make a statement.

Third, I would like to make the point I had in mind before the last speaker got up, which is that our analysis of this particular problem has been made possible to a large extent by previous actions that would not be permitted under today's rules. How far can we go in prohibiting the causes of hypothesized problems, on the basis of what is admittedly incomplete understanding of our environment, without impeding progress? In every technological program that I am aware of, progress can only go so far on the basis of theory before it has to be validated by experimentation. Now, if we stop doing the real-world experiments which tell us conclusively whether our theory is or is not correct, very soon we are going to reach the point from which we can no longer extrapolate. I would only like to recommend that we not preclude the possibility of finding out whether, indeed, we are correct. There are many who argue that we must wait until we know for sure, because once we allow a certain course of action to proceed, it cannot be halted. I think we have demonstrated very clearly in the last few years that this argument is not correct. We discontinued building two prototype SST's at a cost of one hundred million dollars more than it would have cost to produce them. We have stopped the building of power plants in mid-construction. We have, essentially, brought to a halt our nuclear-power industry. There are any number of things like this that we have demonstrated we are capable of doing, and have done in the past few years. So I don't think the argument that we have to stop it before it gets started because we can't stop it later is valid.

GOLDBURG: I speak as an individual who has had a long association with the environmental issues related to the SST. I hope I won't lose my friendship with Fred Kaufman by echoing what Hugh Ellsaesser said: I think we can't be held responsible for what the media do with our statements. I had a very similar experience at The Boeing Company with the CIAP press release. My Vice-President called me and said, "What's this ozone problem you've been telling me about for three years? It doesn't exist!" So I think we all share in that communication gap. In any case, I want to congratulate Dr. Grobecker and his key project managers on carrying out a very difficult program with high technical distinction and sensitivity to the political factors involved.

I have two short comments on the technical issues. First, having watched the development of ozoneperturbation theories over the past six years, I do not believe that NO_x controls ozone perturbations in the stratosphere according to the predictions of the geophysical models based on Professor Johnston's NO. photochemistry. I understand Dr. Cannon's stated need for a scientific-establishment consensus as a result of CIAP, and I understand that NOx is the best explanation we have for ozone observations, but I do not believe that NO_x-based models explain the observed natural variations. In the end, I think the explanation of ozone perturbations will have, as a major component, an aurora hypothesis first mentioned by Willet of MIT in 1968. Therefore, I hope that the validity of NO_x-ozone stratospheric connection will still be a major question in follow-on research.

Second, I also understand the usefulness of the "barely discernible" concept as a criterion, because it gets us off the hook of how much a human life is worth. However, I reel that as the program evolves, we will have to face up to better criteria, for the reasons just mentioned by the previous speakers, since the concept of a "barely discernible change" is artificial and depends upon the sensitivity of the measuring instrument,

In conclusion, I feel the civil air-transportation sector is perhaps being prematurely burdened by an engine-development program for which there is not now a firm technical requirement.

McCLATCHEY: Were interactions between climatic change and ultraviolet change, via cloudiness, considered in CIAP's assessment of biological effects?

GROBECKER: No, even though cloudiness is a major factor in both climate and ultraviolet irradiation. The best available models are just beginning to simulate cloudiness.

NELSON: I would like to correct one misunderstanding: that the aircraft industry could achieve a sixfold NO_x reduction with present technology. The current EPA regulations for Class T-2 aircraft require only about a twofold reduction, and we are still unable to achieve this level in a practical combustor, despite an intensive development effort. A sixfold reduction will require, unfortunately, new inventions or new ideas which we do not have today; even if such a combustor can be developed in a practical aircraft design — and that has not yet been established — expensive long-tenn research and development efforts will be required.

THE COMMITTEE ON METEOROLOGICAL EFFECTS OF STRATOSPHERIC AIRCRAFT (COMESA)

R.J. MURGATROYD British Meteorological Office Bracknell, Berkshire, England

ABSTRACT: The organization and aims of the British COMESA are outlined. COMESA's in-situ and laboratory stratospheric measurement programs are briefly described, and its extensive use of modeling as the best prediction technique available at present is discussed.

The possibility that a large increase in stratospheric flights, particularly by supersonic transports, might lead to atmospheric changes which could significantly affect the human environment has become a matter of great concern in the United Kingdom during the last few years. It was realized that a considerable increase in knowledge and understanding of the stratosphere would be required in order to provide a realistic assessment of the likely magnitude of any changes in terms of operations of the stratospheric aircraft expected to be flying. Accordingly, the British Committee on Meteorological Effects of Stratospheric Aircraft (COMESA) was set up in 1972 to direct and coordinate a program of research, initially of three years' duration, aimed at

- Determining the natural composition of the stratosphere and assessing the changes which might arise from the operation of aircraft (supersonic aircraft in particular), and
- Assessing the meteorological effects, if any, consequent upon these changes.

The members of this committee are appointed by the Director-General of the British Meteorological Office; they include scientists from the Meteorological Office, other Government laboratories, and the Universities. The present members are

Dr. R.J. Murgatroyd (Chairman), Mr. P. Goldsmith (Meteorological Office),

Dr. N.W.B. Stone (National Physical Laboratory),

Dr. J.T. Houghton (Atmospheric Physics Department, University of Oxford) and

Dr. R.P. Wayne (Physical Chemistry Department, University of Oxford),

all of whom are personally responsible for various aspects of the work. Mr. P. Graystone, Mr. R.L. Newson and Miss M.K. Hinds (all of the Meteorological Office) have been coopted as Secretary for different periods. There are no representatives on the Committee from the Concorde Division, Dept. of Industry, or from the aircraft or engine manufacturers, although their experts as well as other U.K. scientists working on relevant subjects have been consulted as necessary and have readily assisted when requested. The Committee will produce a report on its work in 1975; any scientific results obtained by groups associated with this program are also being announced and published in the scientific literature in the normal way. It was of course always intended that there should be full exchange of information and cooperation with our colleagues in other countries to obtain the best possible information and to advance knowledge by mutual discussions on the problems involved. I am very pleased to acknowledge the ready collaboration and express our thanks for the help we have received from both the Comité sur les Conséquences des Vols Stratosphériques (COVOS) in France and the Climatic Impact Assessment Program (CIAP) in the U.S.A.

The COMESA's initial appraisal of the different problems was very similar to that of CIAP in that possible reduction of ozone in the stratosphere as a result of nitrogen oxide emissions appeared to demand the most urgent attention. Emissions of sulfur dioxide were regarded as potentially significant in studies of possible effects on climate, although at the same time water-vapor emissions were considered to be of perhaps comparable importance. In addition, an estimate of likely condensation-trail and cloud formation in the stratosphere was required. A comprehensive solution of these problems clearly could not be achieved within the allocated research period, even by an organization with much larger resources than those available to the COMESA, so it was necessary to concentrate on the most essential features:

- Under the terms of reference, and by its composition, the studies done for the COMESA were confined to atmospheric physics. No new researches were attempted in biological, social, and economic fields, although expert advice was sought and literature surveys made as required. In general, although it was realized that advances were needed in these subjects as well as in atmospheric physics, they were considered to be of second priority since any results could not be used until acceptable solutions of the atmospheric-physics problem had been obtained.
- 2. The studies were concentrated on possible effects of the operation of fleets of subsonic and Concorde-like aircraft in the stratosphere. Further investigations relating to advanced SST's flying at higher altituder and to space vehicles would have led to a wider understanding, but could not be attempted in the time available.
- 3. As far as possible, projects and programs which were known to be effective and to require minimal development work before some results could be obtained were given the highest priority. This criterion was applied to both the measurement techniques and the numerical models, and in fact it was found very difficult to complete some projects which were entirely new within the allocated period.
- Comparatively little effort was devoted to problems which on first examination appeared to be of comparatively minor

importance. For example, it was accepted from other published results that the emissions were relatively unaffected by processes occurring within the aircraft wake and also in mesoscale processes, so that the COMESA model calculations were essentially confined to effects due to the large-scale processes. It is hoped that assumptions of this type can be reexamined as opportunities arise. Even with these limitations the COMESA program is very substantial; only a brief outline can be given here, with references to more detailed descriptions of individual projects.

It is rather widely accepted that the best approach to solving the ozone and climate problems, or at least to obtaining the best estimates of possible effects, is to construct mathematical models which will simulate realistically the natural state of the atmosphere, and then use these models to predict the changes resulting from given perturbations. This approach has its weaknesses. First, it accepts current theory as correct and essentially complete, so the results it gives are at least qualitatively predetermined and will only vary between authors according to the data and differing assumptions they use. Second, although the representations of natural atmospheric conditions can be cheeked to some extent, there is no way of determining whether any predictions are likely to be realistic. Finally, it has not yet proved possible to construct a model that does not have serious deficiencies in either available measured data or simulations of the basic photochemical and transport processes. An experimental program with a fully interactive three-dimensional model of high resolution requires more extensive computer facilities than are presently available, although the COMESA modelers have made some progress with its basic formulation. Nevertheless, keeping the limitations of modeling in mind, the COMESA, like the CIAP, has devoted a major portion of its effort to modeling experiments.

In order to obtain as much external evidence as possible of the likely effects of aircraft emissions, studies have also been made of other phenomena that may have affected the stratosphere. Goldsmith et al. (1973), in agreement with other investigators, have concluded that the

nuclear tests of the 1950's and 1960's injected large amounts of nitrogen oxides into the stratosphere. Although these injections from the 1961 and 1962 tests appear to have been roughly equal to the annual emissions from several hundred SST's, the authors were not able to detect unambiguously any effects on the global ozone amounts. Further work on this subject is continuing. In addition, considerations of the effects of volcanic eruptions on surface temperature have suggested that climatic effects resulting from anticipated SST emissions of particulates and sulfur dioxide are likely to be very small. The progress of the stratospheric measurements and suggestions regarding better assessments of the natural sources of the stratospheric constituents found in aircraft emissions have also been kept under constant review, since the magnitude of the change in stratospheric composition is dependent on the comparative magnitudes of the natural and artificial sources.

COMESA's program of measuring stratospheric gaseous constituents has made extensive use of the National Physical Laboratory's (NPL) submillimeter interferometer technique. The interferometer has been flown both on the Concorde prototype aircraft and, by courtesy of our COVOS colleagues, on large balloons launched from the facilities of the Centre National d'Études Spatiales in France. Measurements of H₂O, O₂, HNO₃, N₂O, and NO₂ column densities above the flight level were made as convenient during tours of the Concorde aircraft to the Far East in 1972 and to South Africa in early 1973. Special flights were made to the north of Scotland in 1973 which included some data on profiles, and later that year series of flights were made on both the French and British Concorde aircraft over the Bay of Biscay. The COMESA measurements on the French aircraft were made during a COVOS flight series on which measurements were also carried out by French scientists and by American scientists from the Jet Propulsion Laboratory (JPL), so that some comparison of results is possible. The latter series of flights, which used the British Concorde, also provided an opportunity for simultaneous measurements by the JPL workers and a Canadian team from the University of Toronto; unfortunately, the planned program could not be completed, and

COMESA was not able to arrange for joint measurements by the French scientists on this occasion. Some of the results of the measurement made during these different series of flights have already been published (Harries et al., 1974; Stone et al., 1975).

In 1974 the work was concentrated on balloon studies, partly because these aircraft were no longer available for this work but mainly because it was decided that good vertical profiles to 30 km or more were the next objective. Ascents were made in France in autumn 1974 and again in spring 1975, and the results are now being analyzed.

In addition to the NPL studies, measurements of H₂O, NO₂, and NO are being made by the Atmospheric Physics Department of the University of Oxford. Their technique is based on the use of pressure-modulator radiometers which are being developed as part of the instrumentation of the Nimbus G satellite. These devices were also used in 1974 for balloon experiments from the French launching facilities, and further flights in 1975 have been arranged. The first results were announced during a Joint COMESA-COVOS Symposium at Oxford in September 1974, and it is hoped that more details will be published in the near future (Chaloner et al., 1975).

In order to obtain data useful for studying the likely effects of aircraft emissions on the stratospheric heat balance, attempts are also being made in the Meteorological Office to construct an apparatus which will measure directly from a balloon the absorption of solar radiation by the gases and aerosols in the stratosphere (Foot, 1975). Laboratory trials demonstrated that a technique using acoustic detectors could provide measurements of heating rates down to about 0.05°C/day. The apparatus has been tested on two balloon flights, but no useful results were obtained on these occasions, due to failures of the sun-seeker used with this apparatus. It now appears that this project will not be completed during the present research period, but it is hoped that its development will be continued later.

Laboratory studies of the basic chemical kinetics of processes taking place in the stratosphere have been carried out in the Physical Chemistry Departments of the Universities of Oxford and Cambridge. The emphasis has been on obtaining new data on various reactions involving NO, NO₂, HNO₃, OH, HO₂, and NH₃, and also SO₂, which are potentially of great importance, and some of which have been comparatively little studied (Chapman et al., 1975; Bemand et al., 1975). In addition to these results, the COMESA modeling studies have made extensive use of the data kindly supplied by the U.S. National Bureau of Standards with the cooperation of the CIAP.

Modeling experiments with various objectives are in progress within the COMESA program:

- time-dependent one-dimensional model containing all the relevant chemical kinetics has been constructed (Tuck, 1975). Further results will be presented by Dr. Tuck at this conference (Tuck, 1976). Apart from runs to compare the ozone content in the model for given continuous SST emissions with the content under 'natural' conditions, studies are being made of the joint effects of subsonic and Concorde-like fleets. Attempts are also being made to simplify the essential chemical kinetics scheme for use in more complicated models while still retaining the more important processes. Interactions involving radiative effects (and hence temperature changes), and the effects of different eddy-diffusion coefficients, are also being investigated.
- 2. A large-scale three-dimensional general-circulation model of the troposphere and stratosphere has also been developed from the Meteorological Office's tropospheric five-level model (Corby et al., 1972; Gilchrist et al., 1973). It has been made global in character and has proved successful in simulating many aspects of the stratospheric circulation, including "sudden warmings". A description of its main features and the type of results it produces was given at the Third Conference on CIAP and also at the joint COMESA-COVOS Symposium in Oxford (Newson, 1974, 1975).

It is intended to form the basis for a fully interactive model, but so far it does not contain any photochemistry. In its earlier version, it had a radiation scheme based on climatology for the solar radiation and Newtonian cooling for the atmospheric radiation. A new radiation scheme has now been developed which is interactive with the composition, and has allowed preliminary studies to be made of effects on the lower atmosphere resulting from changes in stratospheric composition (Mattingly, 1975). The three-dimensional model is also being used to study motions and dispersions of various substances which are treated at present as inert tracers throughout the stratosphere and troposphere, and studies have been made of both ozone and simulated aircraft injections in this context. Finally, efforts are being made to utilize the data on fluxes of these substances within the model as a basis for improved empirical transport parameters in the two- and one-dimensional models.

Satisfactory two-dimensional modeling is in many ways more difficult to accomplish than three-dimensional modeling, as it involves difficult problems of averaging as regards both the photochemical and the transport processes. For the climate studies the interactive radiation scheme, as well as some of the simulations of the tropospheric processes in the three-dimensional model, have been adapted for use in studies of the effects of stratospheric composition changes on surface temperatures. It is possible to study changes in quasiequilibrium states with this type of model; however, there are of course serious disadvantages in using this approach, since the representation of major features such as the large-scale dynamics and the differences between land and sea surfaces cannot be properly simulated. Two-dimensional modeling may produce some representation of all the main atmospheric parameters and provide predictions of wind and tem-

perature as well as composition fields, and studies of this type are being made in the Atmospheric Physics Department, University of Oxford. For the ozone studies a less sophisticated approach is to attempt to solve simultaneously the continuity equations for each constituent, including as comprehensive as possible a representation of the photochemistry and assuming that the transports can be parameterized in terms of known mean winds and eddy motions. Experiments in which the eddy-motion fluxes have been expressed as products of eddy-diffusion coefficients and mixing-ratio gradients have been carried out at the Meteorological Office. Combinations of meridional (K_{yy}) , vertical (K_{zz}) , and slantwise (K_{yz}) eddy coefficients have been chosen, largely empirically, to satisfy the known evolutions of tracer fields such as those of tungsten-185 and strontium-90 injections from nuclear tests, as well as the evolution of the ozone field itself. Other authors have attempted to derive values of these coefficients using different data (heat fluxes, radioactive tracers, etc.) but their work also contains many assumptions. Moreover, efforts made by the COMESA modelers to extract realistic values of Kyy, Kzz, and Kyz from the outputs of the three-dimensional model integrations were not successful, and it appeared that in this model at least the values required were different for different tracers. Thus, although some two-dimensional model results using these coefficients have been obtained, it is clear that further studies are required before such results can be regarded as fully acceptable. The same kind of difficulty applies to the results of one-dimensional models which use the variable (K,) for a vertical diffusion coefficient, and in many ways it is still the use of flux-gradient-transfer theory and the choice of the values for the eddy-diffusion coefficients which present the greatest uncertainty in the oneand two-dimensional model calculations.

Another possible approach (Francis, 1975) is to regard the net meridional flux across latitude circles in the output of a three-dimensional model integration as the result of two fluxes, one northward with values proportional to the mixing ratios in the next grid line south of the latitude considered, and the other southward with values proportional to those in the grid line to the north. The vertical fluxes can be treated in a similar manner in terms of values above and below the level considered. The necessary data can readily be extracted from the three-dimensional model results and the proportionality factors obtained. However, considerable further development along these lines, including studies of the different behavior of different tracers, appears to be necessary before a practical model can be evolved.

The other main uncertainty that is apparent in these models is the effect of the boundaries, particularly the lower boundary. The behavior of the model depends considerably (especially at its lower levels) on the way the boundary conditions are formulated and the values assessed for the tropospheric constituents and natural sources and sinks. Further studies are necessary to clarify this aspect, including more measurements of tropospheric constituents.

In view of the outstanding problems that remain it is hoped that it will be possible to continue research arising from the various aspects of the work now in hand, and that in addition to the COMESA report this year other results of general interest in the way of stratospheric studies obtained from the present data will be published later.

REFERENCES

Bemand, P.P., I.W.M. Smith, and R. Zellner (1975), "Reactions of hydroxyl radicals with nitrogencontaining constituents of the stratosphere," in Proceedings of the Anglo-French Symposium on the Effects of Stratospheric Aircraft (COMESA-COVOS, Oxford), Vol. 2, pub. British Meteorological Office, XXII-1 - 18.

Chaloner, C.P., J.R. Drummond, J.T. Houghton, R.F. Jarnot, and H.K. Roscoe (1975), "Measurement of NO₂ and water vapour in the stratosphere," in *Proceedings of the Anglo-French Symposium on the Effects of Stratospheric Aircraft* (COMESA-COVOS, Oxford), Vol. 1, pub. British Meteorological Office, XII-1 - 2.

- Chapman, C.J., G.W. Harris, and R.P. Wayne (1975), "Kinetics of some reactions of O, H, and OH," in Proceedings of the Anglo-French Symposium on the Effects of Stratospheric Aircraft (COMESA-COVOS, Oxford), Vol. 2, pub. British Meteorological Office, XXI-1-5.
- Corby, G.A., A. Gilchrist, and R.L. Newson (1972), "A general circulation model of the atmosphere, suitable for long period integrations," Quart. J. Roy. Met. Soc. 98, 809-832.
- Foot, J.S. (1975), "An acoustic technique for measuring the absorption of solar radiation in the stratosphere," in *Proceedings of the Anglo-French Symposium on the Effects of Stratospheric Aircraft* (COMESA-COVOS, Oxford), Vol. 2, pub. British Meteorological Office, XXXVII-1 4.
- Francis, P.E. (1975), "Development of a two-dimensional stratospheric model using mean motions and empirical flux terms," in *Proceedings of the Anglo-French Symposium on the Effects of Stratospheric Aircraft* (COMESA-COVOS, Oxford), Vol. 2, pub. British Meteorological Office, XXVI-1 5.
- Gilchrist, A., G.A. Corby, and R.L. Newson (1973), "A numerical experiment using a general circulation model of the atmosphere," Quart. J. Roy. Met. Soc. 99, 2-34.
- Goldsmith, P., A.F. Tuck, J.B. Foot, E.L. Simmons, and R.L. Newson (1973), "Nitrogen oxides, nuclear weapon testing, Concorde and stratospheric ozone," Nature 244, 545-551.
- Harries, J.E., J.R. Birch, J.W. Fleming, N.W.B. Stone,
 D.G. Moss, N.R.W. Swann, and G.F. Neill (1974),
 "Studies of stratospheric H₂O, O₃, HNO₃, N₂O,
 NO₂ from aircraft," in *Proceedings of the Third Conference on CIAP* (Cambridge, Mass.), U.S.
 Dept. of Transportation, DOT-TSC-OST-74-15, 197-212.

- Harries, J.E., and N.W.B. Stone (1973), "Measurements of some hydrogen-oxygen-nitrogen compounds in the stratosphere from Concorde 002," in *Proceedings of the Second Conference on CIAP* (Cambridge, Mass.), U.S. Dept. of Transportation, DOT-TSC-OST-73-4, 78-85.
- Mattingly, S.R. (1975), "Preliminary experiments with an interactive radiation scheme," in *Proceedings of* the Anglo-French Symposium on the Effects of Stratospheric Aircraft (COMESA-COVOS, Oxford), Vol. 2, pub. British Meteorological Office, XXVIII-1-22.
- Newson, R.L. (1974), "An experiment with a tropospheric and stratospheric three-dimensional general-circulation model," in *Proceedings of the Third Conference on CIAP* (Cambridge, Mass.), U.S. Dept. of Transportation, DOT-TSC-OST-74-15, 461-474.
- Newson, R.L. (1975), "Further studies with a threedimensional numerical general circulation model of the stratosphere and troposphere," in Proceedings of the Anglo-French Symposium on the Effects of Stratospheric Aircraft (COMESA-COVOS, Oxford), Vol. 2, pub. British Meteorological Office, XXVII-1-22.
- Stone, N.W.B., J.E. Harries, and J.W. Fleming (1975), "Measurement of stratospheric composition using far infra-red spectroscopy," in Proceedings of the Anglo-French Symposium on the Effects of Stratospheric Aircraft (COMESA-COVOS, Oxford), Vol. 1, pub. British Meteorological Office, X-1 - 15.
- Tuck, A.F. (1975a), "Development and use of a onedimensional stratospheric chemical kinetics model," in *Proceedings of the Anglo-French* Symposium on the Effects of Stratospheric Aircraft (COMESA-COVOS, Oxford), Vol. 2, pub. British Meteorological Office, XXIII-1-24.
- Tuck, A.F. (1976), "Chemical modeling of perturbations caused by NO_x emissions," in this volume.

PRINCIPAL ACTIVITIES OF COVOS IN 1974

EDMOND A. BRUN

Comité sur les Conséquences des Vols Stratosphériques Paris, France

ABSTRACT: This brief presentation will discuss only the principal scientific results obtained during the past year by COVOS, the French committee on the effects of stratospheric aviation.

STRATOSPHERIC MINOR CONSTITUENTS

Absorption Spectrometry

The grille spectrometer previously invented and developed by Girard at ONERA* has been combined with a sun tracker. Its high resolution (limit, 0.1 cm⁻¹) has permitted accurate measurements of stratospheric minor constituents. Figure 1 shows, as an example, an absorption spectrum obtained from the Concorde 001 prototype; the doublet of NO (1890.91, 1890.76 cm⁻¹) is clearly separated. Such spectra can improve the accuracy of NO measurements.

Experiments have been performed with two similar instruments:

- Airborne spectrometer (ONERA): eight flights on the Concorde 001 in June and July 1973, and several flights on a Caravelle airliner, three of which were made at high latitude (65°N, Greenland) in July 1974;
- 300,000-m³ balloon-borne spectrometer (ONERA, IASB): two experiments have been quite successful (May 14, 1973 and May 13, 1974).

The main results of these experiments are summarized in Figures 2 through 5. The curves of Figure 2 show the vertical profile of NO deduced from balloon experiments. In both cases the maximum number density is located at about 30 km; although the experiments were performed at the same place, season, and solar elevation, we can see two different NO distributions. It seems that these large variations are associated with different meteorological condi-

tions; on May 14, 1973 the altitude of the tropopause was 13 km and on May 13, 1974 it was 9 km.

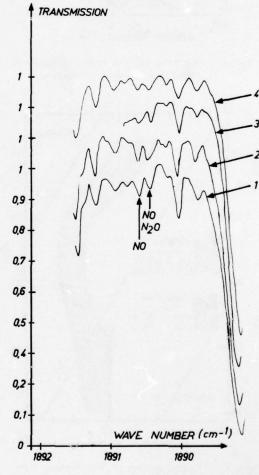


Figure 1. Solar spectra recorded from Concorde 001 near 1890 cm⁻¹. Nitric oxide doublet at 1890.76 and 1890.91 cm⁻¹ is identified. Solar angular elevations: spectrum No. 1, -0.60°; 2, -0.25°; 3, 0.92°; 4, 1.30°.

^{*}Appendix A spells out the acronyms of the various laboratories.

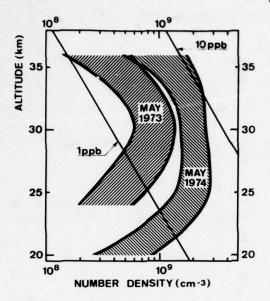


Figure 2. Vertical profiles of nitric oxide deduced from balloon-borne experiments.

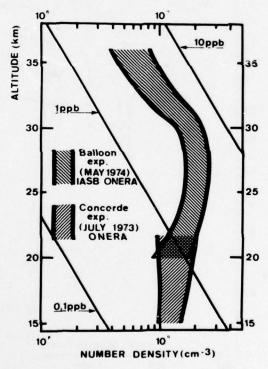


Figure 3. Vertical profiles of NO₂ deduced from balloon-borne and airborne experiments.

The vertical profile of NO₂ concentration shown in Figure 3 has been derived first from

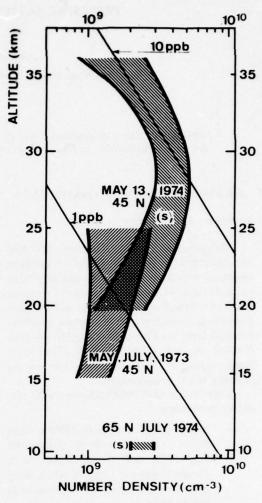


Figure 4. Number density of NO + NO₂ versus altitude deduced from non-simultaneous 1973 and simultaneous 1974 measurements at 45°N and 65°N by IASB and ONERA.

Concorde flights between 15 and 22 km, and second from balloon experiments between 20 and 35 km.

Because of the variation in NO and NO₂ concentrations with time of day, simultaneous measurements of these species are required. Such experiments were performed from balloons at 45°N (May 13, 1974) and from airplanes at 65°N (July 1974). We note that the results of these simultaneous measurements are in good agreement with values deduced from separate NO and NO₂ measurements (made in 1973). In the low stratosphere, the combined number density is

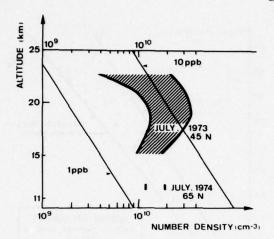


Figure 5. Number density of HNO₃ versus altitude deduced from airborne experiments at 45° N and 65° N.

between 10^9 and 3×10^9 molec cm⁻³ (see Figure 4).

 $\rm HNO_3$ measurements have been made from Concorde in July 1973 at 45°N and from Caravelle at polar latitude. The results are given in Figure 5; the maximum number-density value, 2×10^{10} molec cm⁻³, is located at 20 km. At this altitude, the density of $\rm HNO_3$ is ten times greater than the $\rm NO + NO_2$ density. This predominance of $\rm HNO_3$ is greater than would generally be expected from the model predictions.

If we consider the vertical distribution of odd-nitrogen molecules NO, NO₂, and HNO₃ between 20 and 35 km (Figure 6), the above data suggest an approximately constant volume mixing ratio of $(12\pm3)\times10^{-9}$. Below 20 km, this value decreases rapidly. The low stratosphere appears to be a transition layer between the stratosphere where the $(NO+NO_2+HNO_3)$ concentration is relatively high $(12\ ppb)$ and the troposphere, where, due to the quick mixing process and rain-out of HNO_3 , the concentration of $(NO+NO_2+HNO_3)$ is weaker. This is consistent with a rapid elimination of lower-stratospheric HNO_3 by transport to the troposphere.

From this set of data we can estimate the global values for NO, NO₂, and HNO₃ (Figure 7). The global amount of odd nitrogen between 15 and 40 km is 9×10^{34} molecules, three times higher than the number given in several papers (3×10^{34}).

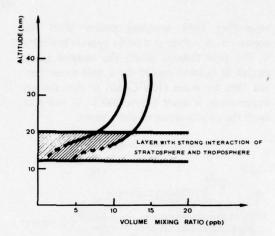


Figure 6. Vertical distribution of odd nitrogen (NO + NO₂ + HNO₃) molecules at midlatitudes suggested by experimental data.

	Vertical	Column Density	Global	Amount
	mol, cm 2	g. cm ²	molecules	grammes
NO	2 10"	10 '	1034	0.5 1012
NO,	3,5 10"	2 10 '	1,8 1034	1,3 1012
HNO,	12 10"	12 10 '	6.2 1034	6.2 1012
Total	17,5 1015	15 10 '	9 1034	8 1012

Figure 7. Estimation of global NO, NO₂ and HNO₃ in the natural stratosphere, from COVOS experimental data.

Emission Spectrometry

Other results have been obtained by emission spectrometry (Marten at CNET). The wide spectral range scanned in the far infrared allowed concentration measurements of many constituents. For instance, the value of the mean mixing ratio of SO_2 between 15 and 30 km is 0.3×10^{-9} ; this value is three times lower than Harries' upper limit.

ENGINE EFFLUENTS

In order to know what would happen to the components of the stratosphere if it were to sustain intense aircraft traffic, it is important to carefully measure the engine effluents.

SNECMA and CEPR have carried out, in a wind tunnel and under stratospheric flight conditions, a study of the effluents of the Olympus engine, the engine used in the Concorde. A strut

supporting eight sampling probes scans the engine jet. A sketch of a probe appears in Figure 8. The pipe through which the sampled gas is carried is quickly cooled by a cold-water flow and then by warm (100°C) air, so that the gas temperature is never below 100°C, in order to avoid the condensation of water vapor.

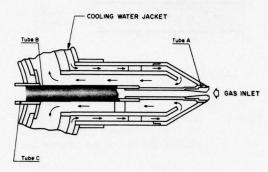


Figure 8. The sampling probe.

The results of this study are not yet final. However, Figure 9 displays the volume mixing ratio of CO_2 as a function of that of NO_x . All the experimental points are well set between two straight lines, the slopes of which define the spread in pollution index, I_E , in grams of NO_x (under the form of NO_2) per kg of fuel. The computation of I_E is carried out under the assumption that all the carbon of the fuel is transformed into CO_2 , which is not far from reality. The index I_E is found to be between 12 and 18 g/kg.

If 16 is taken as the value of this index, a fleet of 250 Concorde airplanes, each flying 2000 hours per year, would then produce every year about 0.2×10^{34} molecules of NO_x , whereas, as we have seen, there exists 9×10^{34} between 15 and 40 km, that is to say 45 times more.

TRANSPORT PROCESSES

Nitrogen oxides, NO_x , are emitted by stratospheric aircraft in the low stratosphere (for the Concorde, up to 18 km). As ozone-destroying reactions with NO_x become significant only above 25 km, it is obvious that it is most important to know the upward vertical transport processes of NO_x .

Below 20 km, vertical transport associated with tropopause breakdowns contributes notably to the renewal of stratospheric air masses, but

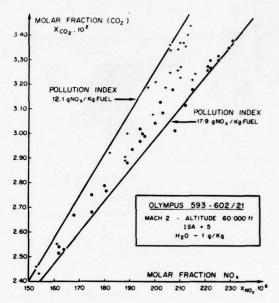


Figure 9. Pollution index at simulated altitude.

clear-air-turbulence phenomena become relatively more important with increased altitude, and it appears that above 20 km turbulent diffusion is an important process that may contribute to the upward transport of NO_v.

Figure 10, taken from the Second Annual Report of the Lawrence Livermore Laboratory to DOT-CIAP, shows the very broad vertical variation of the turbulent transport coefficient of the models presently used. For McElroy, this coefficient increases with altitude above 20 km, while for Chang the variation is the other way around.

COVOS decided to concentrate its effort on these vertical transport problems. Three avenues of research were explored.

Star Scintillation

It is known that the turbulent layers of a clear atmosphere are the cause of deformations of the light waves emitted by a star and, consequently, of phase and intensity fluctuations in a telescope's focal plane. The method developed by Vernin and Roddier at the University of Nice consists in measuring spatioangular correlations between signals received by two photomultipliers, at a distance r from each other, each receiving the light from one of the

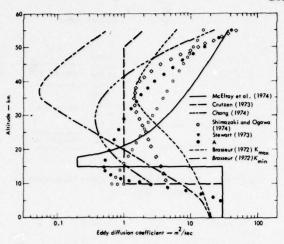


Figure 10. Vertical eddy-diffusion profiles used by various investigators.

elements of a double star (Figure 11). The two lines of sight meet at an altitude $h = r/\theta$ where θ is the angular distance between the two stars. In the case of the Castor star, where $\theta = 2$ arcseconds, the value of h in km is equal to that of r in cm. By varying r from 0 to 20 cm we vary h from 0 to 20 km.

We measure the spatio-angular autocorrelation of the scintillation, as a function of the distance r, parallel (Figure 12a) and perpendicular (Figure 12b) to the line joining the two stars. Theory shows that the difference between these two correlations as a function of r (Figure 12c) passes through maxima when the two beams meet in a turbulent layer. So these maxima give the altitudes h of the turbulent layers, their values providing the turbulence intensities at these various heights. For the exploration represented in the figure, turbulent layers are at 4, 14, and 18 km altitude, corresponding to 4, 14, and 18 cm values for distance r. Precision of altitude readings is on the order of 1 kilometer, due to the width of the spatial autocorrelation.

These measurements allow us to locate the turbulent layers and to get an idea of the importance of their turbulence.

Anemometry

With the method of Jean Barat of CNRS, we were able to measure, from a balloon, the wind-velocity fluctuations at hitherto unexplored

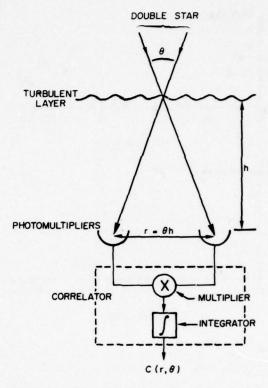
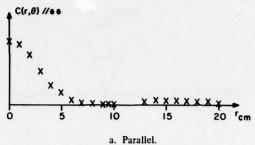


Figure 11. Schematic drawing of optical and electronic apparatus.

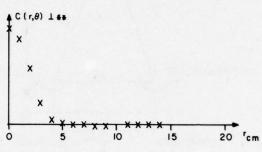
altitudes. Thanks to the sensitivity of the anemometers used (resolving power, 1 cm/sec; time constant, 1 msec), we then can move directly to the microscale and obtain the energy spectrum of the various components in the inertial domain. Using classical Kolmogoroff theory we then determine the turbulence intensity, the energy dissipation rate and the diffusion coefficients.

Figure 13 shows the set-up used: two groups of anemometers, separated vertically by 50 m, are suspended from a balloon 150 m above the higher group. The correlation between the two groups is thus independent of the balloon movements, which are very slow. It is easy, with this set-up, to check the layered structure that characterizes the middle atmosphere.

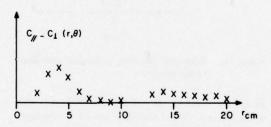
Figure 14 gives recorded curves of velocity fluctuations as a function of time, obtained on October 12, 1974, showing both a turbulent layer at 26,800 m altitude and a calm layer at 26,650 m altitude. Figure 15 gives all the results obtained that same day. This result is quite







b. Perpendicular.



Differences between parallel and perpendicular cross-correlations, showing turbulent layers at 4, 14, and 18 km.

Figure 12. Spatioangular cross-correlations of the double star Castor.

typical. A profile recorded in December of the same year gives approximately the same results, so that it seems reasonable to define a model for such altitudes.

Tracer Release

A medium- and large-scale study is useful, however, to emphasize the passage of the energy of more-or-less organized movements to movements of lesser dimension, where eventually the energy is transformed into heat by viscous effects: such a study was performed by Veret and Bouchardy at ONERA using a passive tracer.

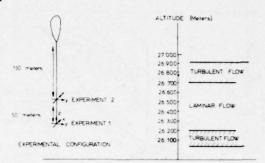


Figure 13. Vertical structure of high-altitude clear-air turbulence (HICAT).

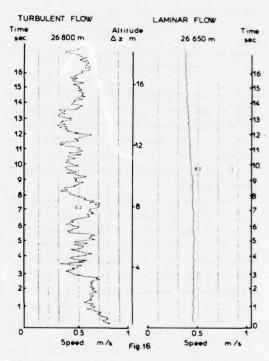


Figure 14. Time variations of HICAT, October 12,

A series of titanium tetrachloride clouds was released from balloons in the low stratosphere. Figure 16 shows the cloud evolution as a function of time at 15 km altitude. From these observations, we can deduce some first results on horizontal diffusion (Figure 17): during the first minutes the cloud expansion is fast, which is compatible with an inertial domain of turbulence; on the other hand, when the cloud is very large with respect to the microturbulence scale, expansion is very much slower. During this latter period, a fine autocorrelation structure is created

inside the cloud, the study of which, presently under way, should soon lead to the determination of the time scale of vertical transport by turbulence.

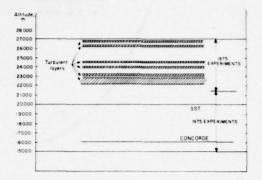


Figure 15. Vertical distribution of HICAT in the middle stratosphere, October 12, 1974.

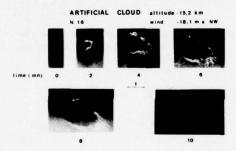


Figure 16. Photographic sequence of an artificial cloud's expansion (ONERA). Altitude, 15.2 km; wind, 18.1 m/sec, NW.

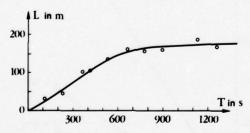


Figure 17. Horizontal (width L in m) evolution of an artificial cloud over time (time T in s) (ONERA).

The stratified structure we just mentioned makes it mandatory to introduce altitude-dependent gradients, and thus to limit the use of diffusion coefficients obtained from a linear theory valid for passive components.

For the current year, it is planned to use the above three methods simultaneously. This experimental effort may open the way to a better knowledge of the dynamic phenomena of the stratosphere.

MODELS OF THE STRATOSPHERE

The help given by the Institut d'Aéronomie Spatiale of Belgium to the SNIAS has permitted us to improve, under the sponsorship of COVOS, three models of the stratosphere, now in progress:

- a. A stationary two-dimensional model (Brasseur and Bertin)
- A non-stationary one-dimensional model (Borghi, Peetermans, Maignan)
- A one-dimensional model of radiative equilibrium, with the radiation of the aerosols taken into account (Bensimon).

As can be seen in Figure 18, which shows the reduction of ozone as a function of the overall emission of NO at 17 km, the Brasseur-Bertin model gives results not far from those of the other stationary models. However, it should be noted that the more realistic non-stationary models yield a much weaker reduction than the above-mentioned ones.

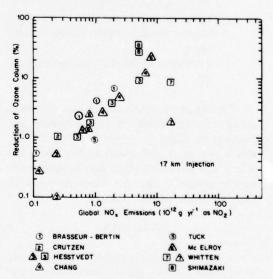


Figure 18. Calculated reduction of vertical ozone column in terms of uniform global rate of NO addition at 17 ± 1 km.

In any event, because of the uncertainty in the dynamic data, the models can yield only rough estimates.

BIOLOGICAL EFFECTS

Relationships between the diminished thickness of the ozone layer and the biological action of the sun's UV radiation (direct or diffused) have been established by a number of authors for erythemal and carcinogenic effects. Latarjet of the Fondation Curie and Chavaudra of the Institut Roussy conclude from their studies that a 2% decrease of the ozone column entails an increase in these effects of 3% ir. the equatorial zone, 4% for the middle-latitudes zone, and 7% for the polar zone, with a corresponding increase in skin cancer for the white population. Let us not forget that, in spite of the enhanced diminution rate with increasing latitude, the danger is more to be feared in equatorial regions.

Moreover, during their work Latarjet and Chavaudra emphasized the importance of the biological effects of UV radiation on the genetic material of prokaryotes (unicellular organisms which generate amino acids), in particular bacteria and algae.

The solar UV radiation may act as:

- an abiotic agent which reduces the prokaryote population,
- a mutagen which can shift genetic equilibrium towards greater radiation resistance.
- a depressor of the photosynthetic capacity.

For the sun at zenith, abiotic and mutagenic activity is comparable to the erythemal and carcinogenic effect, as shown in Figure 19. But this is not so at high zenith angles, where the abiotic and mutagenic effect may become much more important (Figure 20). Obviously the latter effect increases fast with latitude.

AEROSOLS

Aerosol formation from sulfur dioxide seems to us much less important than decrease of the ozone mass, all the more since the fuel could be desulfurized if necessary. However, Bricard and

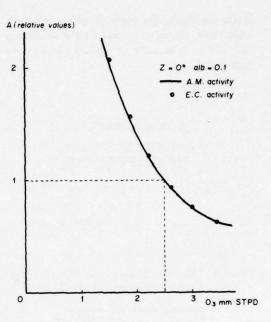


Figure 19. Abiotic and mutagenic (A.M.) and erythemal and carcinogenic (E.C.) effects versus thickness of ozone layer.

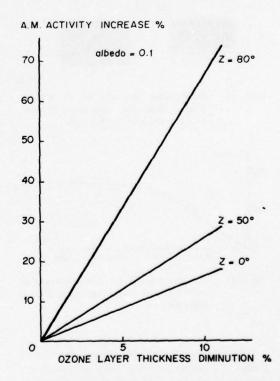


Figure 20. Effects of solar zenith angle (Z) on abiotic and mutagenic activity.

his colleagues at the University of Paris are now ready to use the condensation-nuclei counter with heated oversaturator, which would permit them to assess the concentration of nuclei at stratospheric pressures. Stratospheric balloons will soon be equipped with such counters.

At the same time, the Laboratory of the French Atomic Energy Center (CEA) is constructing a new nucleation chamber that better simulates stratospheric conditions (pressure, temperature, irradiation, gaseous impurities, etc. . . .) for as complete a study as possible of aerosol diffusion and of photolytic reactions entailing condensation-nucleus production.

CONCLUSIONS

COVOS thinks that, in the future, it will be important to monitor the stratosphere's composition.

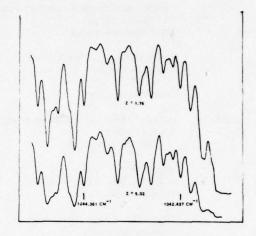
This monitoring can be performed in two ways:

From the ground

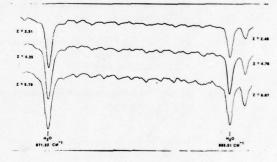
There exists at present at Mont Louis (Prof. Amat) a constant, simultaneous watch on the equivalent thicknesses of ozone and nitric acid (Figure 21);

- From civil aircraft

Instruments for measuring ozone and nitrogen oxides, and possibly also aerosols, are now being selected and developed.



a. Near 1043 cm⁻¹, 13 October 1974, showing ozone absorption.



 b. Near 870 cm⁻¹, 22 December 1974, showing HNO₃ absorption features.

Figure 21. High-resolution atmospheric infrared spectra observed from Mont Louis. $Z = 1/\sin \theta$; $\theta = \text{solar elevation}$.

APPENDIX A

LABORATORIES PARTICIPATING IN COVOS STUDIES

CEPR Centre d'Essais des Propulseurs de Saclay 94100 Orsay, France

CNET Centre National d'Etudes et de Télécommunications 3, ave. de la République 92190 Issy-les-Moulineaux, France

CNRS Service d'Aéronomie du Centre National des Recherches Spatiales Reduit de Verrières 91370 Verrières-le-Buisson, France

CEA Commissariat à l'Energie Atomique, Département de Protection B.P. No. 6
92260 Fontenay-aux-Roses, France

Establissement d'Etudes et de Recherches Météorologiques* 73/77, rue de Sèvres 92100 Boulogne, France

Fondation Curie, Section Biologie Institut du Radium 26, rue d'Ulm 75005 Paris, France

IASB

Institut d'Aéronomie Spatiale de Belgique 3, ave. Circulaire 1180 Bruxelles, Belgique

Institut Gustave Roussy 16 bis, ave. Paul Vaillant-Couturier 94800 Villejuif, France

Laboratoire de Physique des Aérosols Université de Paris VI 7, quai St. Bernard 75005 Paris, France

Laboratoire de Physique Moléculaire des Hautes Energies** 06539 Peymeinade, France

ONERA

Office National d'Etudes et de Recherches Aérospatiales 29, ave. de la Division Leclerc 92320 Châtillon, France

SNECMA

Société Nationale d'Etude et de Construction de Moteurs d'Avion 150, bd. Haussman 75008 Paris, France

SNIAS

Société Nationale Industrielle Aérospatiale 37, bd. de Montmorency 75016 Paris, France

Station Scientifique Citadelle de Mont Louis 66210 Mont Louis, France

Département d'Astrophysique de l'I.M.P.S. Parc Valrose 06034 Nice Cedex, France

^{*}This laboratory participated in stratospheric soundings and in studies of atmospheric circulation.

^{**}This laboratory designed, built, and put into operation a new apparatus for measuring the constituents in a reactor jet.

STRATOSPHERIC OZONE LAYER RESEARCH

B.W. BOVILLE

Atmospheric Environment Service Downsview, Ontario, Canada

ABSTRACT: This paper summarizes the activities and position of the Atmospheric Environment Service (Canada) on the stratospheric ozone problem.

Canada has a long history of research in the atmospheric ozone field. During the sixties the work in the universities of Boville et al. on analysis and modeling, of Brewer in ozone-layer measurements and processes, and of Schiff in atmospheric chemistry, was complemented by expanded government laboratory and network investigations under Godson and Mateer. In addition, fundamental work was carried out by Hampson et al. at CARDE and by a number of upper-atmosphere research groups. This was a period of exciting and innovative work in defining the structure and energetics of the stratosphere and its winter warmings, in modeling these events, in developing vertical profiles and global measurements of ozone, and in refining the Chapman photochemistry and radiation schemes. Out of these came a basic understanding of the interactions between atmospheric dynamics and photochemistry, and of the strong coupling between the stratosphere and troposphere. Stratospheric research then appeared to be proceeding into a lower level of long-term research as an adjunct to global 3-D modeling and observational systems development. The importance of the ozone layer in determining the vertical structure of our atmosphere, and its essential function as an ultraviolet shield, were well known; however, its apparent fragility was not fully appreciated.

In a pure-oxygen system the high-level ozone amount is determined by the solar ultraviolet flux, and the distribution of the total amount of ozone is determined by the rate at which atmospheric circulation moves it out of the high-level source region. (The amount of molecular oxygen is very large compared to that of ozone and is not crucial in the process.) The long-term variations in either solar ultraviolet flux or atmospheric circulation are not yet

known; they are expected to yield some climatological trends in ozone. Although the importance of other trace constituents in determining the precise photochemistry in the upper atmosphere had been rapidly becoming clear, the fragility of the ozone layer was fully realized only with the advent of the supersonic-transport controversy.

The scientific community was brought face to face with the reality that like so many aspects of our environment, the ozone layer, a crucial element to climate and to the existence of all life on earth, is not an inalterable (if variable) natural phenomenon, but is susceptible to significant modification by both man-caused and natural processes. In addition, this layer is only a few tens of kilometers over our heads and is readily accessible for intensive exploration and research.

At the time of the establishment of the United States Climatic Impact Assessment Program, the Atmospheric Environment Service already had a two-dimensional atmospheric model and was operating a network of ozone Dobson stations and ozone-sonde stations as well as the World Ozone Data Centre. A number of Canadian researchers participated in the early work of the CIAP program, and close collaboration and interaction has continued. The AES then launched an expanded Canadian modeling and experimental program with the assistance of an Advisory Committee on Stratospheric Pollution which represented concerned government agencies and the university community.

The theoretical guidance to this program has been based largely on the 2-D model of Vupputuri (1975a). This zonally-averaged steady-state model has the eddy motions parameterized by variable K-coefficients, but all other variables can be made free to interact. The model was expanded in stages from Chapman photochemistry to include fully interactive NO_X and

HO_x schemes based on the CIAP compilation and recommendations. Simulation runs have been made using the standard CIAP injection patterns to provide ready comparison with other model results. The general results are illustrated in Figure 1. The effect of oxides of nitrogen on the ozone layer is clearly dependent on the injection rate and is very sensitive to the injection level. It varies from a small reduction for current low-level aircraft to as high as 16% for a possible future high-level fleet.

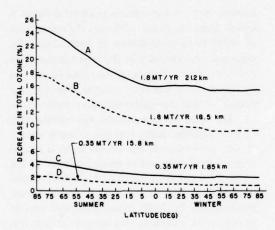


Figure 1. Percentage depletion of total ozone column in the model atmosphere induced by anthropogenic perturbations of nitrogen oxides. Curves A and B represent ozone reduction due to artificial injections of NO_X (1.8 megaton per year at 45°N in the summer hemisphere) at 21.5 and 18.5 km respectively, while the curves C and D denote ozone depletion for a 0.35 Mt/yr i.jection rate at 18.5 and 15.8 km.

More recently, the Freon threat entered the ozone scene, and Vupputuri has added a chlorine photochemistry scheme to the model (Vupputuri, 1975b). Using currently recommended reaction rates and a tropospheric source based on 1972 industrial production rates, the model suggests that the accelerating use of chlorofluorocarbons poses a greater long-term threat to the ozone layer than other anthropogenic activities (see Figure 2).

Although the models have gone through much development in the last decade, they are subject to many approximations and assumptions, and must be validated by and amended

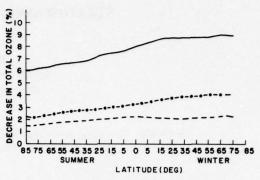


Figure 2. Percentage depletion of the total ozone column in the model atmosphere induced by anthropogenic sources of Freons which correspond to 1972-73 production levels (0.5 and 0.3 Mt/yr for Freon-12 and -11 respectively). The solid curve (top) represents the ozone reduction based on original rate constants (Garvin and Hampson, 1974) for the chlorine chemistry, while the dashed curve (bottom) denotes the revised values of Watson et al. (1976). The dash-dot curve (middle) represents the effect of HCl dissociation with revised rate constants.

with detailed measurements in the atmosphere and the laboratory. A classic example was the apparent discrepancy between the NO2 measurements by Brewer and the NO measurements by Schiff. Further Jetstar and Concorde flights by Brewer and Kerr and balloon flights by Schiff and Ridley did not resolve whether the problem arose from instrumental or atmospheric variability. The most efficient way to resolve many of these problems appeared to be by a series of direct simultaneous measurements of all factors in the ozone balance at stratospheric levels. In early 1973, the AES began plans for a series of such experiments in conjunction with the Skyhook balloon flights out of Churchill, Manitoba. Under the leadership of Evans, the program was successfully planned and launched in the summer of 1974. The two flights, carrying ten AES and university experiments, each flew for about 20 hours in the 25-30 km layer, achieving sunset and sunrise measurements. Results of the flights are still being analyzed. In summer 1975, it is planned to fly two NO, flights and add two more flights with a payload modified to include new chlorine experiments. A proper analysis of these will not be available until early 1976.

BOVILLE

Although the SST problem may have been temporarily allayed (by the economic climate rather than scientific resolution), it is now clear that the full complexity of the stratospheric problem cannot be fully resolved by a three-year crash program—the time required has been extended to five or six years by the chlorine complication, and must be translated into a long-term international cooperative program.

Even though the model results still require considerable verification and the atmospheric measurements are still quite unsatisfactory, it is felt that the following preliminary findings and recommendations can be made at this time.

- A large fleet of SST's flying at 21 km or higher is predicted to have a noticeable effect on the ozone layer, and permissible total aircraft emission levels may have to be defined within a decade.
- Currently planned SST's, due to their lower altitude of 17 km and their small numbers, are not predicted to have an effect which could be distinguished from natural variations.
- 3. The predicted threat from halocarbons is now considered more serious (though unsubstantiated by direct measurement) than that of the SST's, and requires a shift in research emphasis to resolve the chlorine role in the ozone balance.

4. The whole spectrum of threats to the ozone layer constitutes a serious global problem, with many unknowns in chemistry, photochemistry, atmospheric measurements, and atmospheric transports. Continuing active research programs and an international monitoring program are required.

REFERENCES

- Garvin, D., and R.F. Hampson, eds. (1974), "Chemical Kinetics Data Survey, VII: Tables of Rate and Photochemical Data for Modeling of the Stratosphere" (revised), National Bureau of Standards, NBSIR 74-430.
- Vupputuri, R.K.R. (1975a), "The Steady State Structure of the Natural Stratosphere and Ozone Distribution in a 2-D Model Incorporating Radiative and O-H-N Photochemistry and the Effects of Stratospheric Pollutants," Internal Rept. No. APRB 19 N 5, Atmospheric Environment Service, Downsview, Ont.
- Vupputuri, R.K.R. (1975b), "The Impact of Anthropogenic Sources of Freons (Chlorofluoromethanes) on the Meridional Structure of the Stratosphere and Ozone Distribution," AES internal report, in preparation.
- Watson, R.T., G. Machado, S. Fischer, R.L. Schiff, and D.D. Davis (1976), "Chlorine-atom reactions of atmospheric importance," in this volume.

CIAP-TYPE RESEARCH IN JAPAN

TAKAO TOHMATSU

Geophysics Research Laboratory
University of Tokyo
Tokyo, Japan

ABSTRACT: CIAP-type research activities in Japan's scientific and industrial communities are reviewed.

CIAP-type research in the stratosphere is of increasing interest for Japanese scientific and industrial communities. Ongoing research activities can be found in the universities and also some federal agencies.

Routine monitoring of stratospheric parameters using ground-based equipment, together with measurements using meteorological rockets and balloon-borne sondes, have been carried out under the direction of the Japan Meteorological Agency (JMA). Basic experimental research using larger space vehicles is being conducted under the auspices of the Institute of Space and Aeronautical Science, University of Tokyo (ISAS). Table 1 summarizes the aerological networks and monitoring programs in several branches of stratospheric research in Japan.

ATMOSPHERIC OZONE

Ozone in the stratosphere and mesosphere has been an object of study since 1965, using balloons, rockets, and a satellite launched by University of Tokyo. Atmospheric ozone has been measured by three different techniques: (1) the in-situ method using an electrochemical (KI solution) sonde, (2) the attenuation of solar uv radiation through the atmosphere, and (3) the ozone-absorption effect on the atmospheric uv scattering of the solar radiation. The first method is usually applicable to the region of the atmosphere below about 30 km. The optical methods have been attempted on a number of occasions on board large balloons, sounding rockets, and a satellite. They are particularly useful to measure the ozone overburden (or the column density) above (or below) the observer. Standardized comparison of stratospheric ozone measurements

Table 1. Stratosphere Observation Network in Japan

Sonde	18 stations	(JMA)
Rocket	Ryori	(JMA)
	Ozone	
Ground	(Dobson spectrometer) Sapporo Tateno Kagoshima Okinawa	(JMA)
Sonde (with H ₂ O content)	Sapporo Tateno Kagoshima	(JMA) (JMA) (JMA)
Large Balloon	Sanriku	(ISAS)
Rocket	Ryori Uchinoura	(ISAS)
Satellite	(UV scattering) 1975-	(ISAS) 1975-
	Radiation	
Sonde	Sapporo Tateno Kagoshima	(JMA) (JMA) (JMA)
Satellite ("Taiyo")	Feb. 1975-	(ISAS)

obtained with these techniques was made possible by carrying out simultaneous experiments with the three techniques aboard a large balloon. Figure 1 illustrates a standard ozone-density profile (solid curve) in mid-latitude (31°N) in daytime, which was synthesized from the results of various rocket and balloon experiments conducted by GRL (Tohmatsu et al., 1974; Tohmatsu and Watanabe, 1976), and compares it with some theoretical profiles (Shimazaki and Ogawa, 1974, 1975) and a night-time profile after Stair et al. (1975).

TOHMATSU

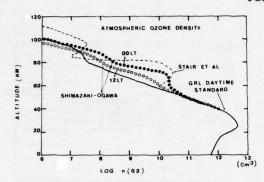


Figure 1. A standardized ozone-density distribution in the vertical in mid-latitudes in daytime (see text).

In the uv-scattering experiment, the optimization of the measuring wavelength is something to be considered carefully. Figure 2 is a comparison of the time variation of local ozone concentration determined by the KI sonde (top) with the overburden values determined in three wavelength bands centered around 290 nm, 320 nm, and 330 nm. The observation was carried out at an altitude of 27 km. The overburden values deduced for the 320 nm and 330 nm bands are in reasonable accord with the local concentration, giving an effective scale height of ozone of 4 to 5 km at 27 km altitude. The overburden deduced for the 290 nm band is too small, however, indicating a possible contamination effect in the wing of the transmission band.

Atmospheric ozone has long been thought to be a good large-scale tracer of atmospheric motions. The flow of ozone associated with the dynamics of the jet westerlies is one of the transport modes to be considered. Figure 3 schematically illustrates a mode of the transport in the vicinity of the jet streams. Observations made with large balloons are particularly suited for studying this kind of local transport effect. Figure 4 is an example of the vertical distribution of ozone density obtained on May 30, 1974 at Sanriku Balloon Center. The two profiles in Figure 4 were obtained at two different locations separated by about 200 km along the trajectory of the balloon. When they are examined with the aid of the simultaneously measured cross-section of winds, shown in Figure 5, we can observe an abrupt change in the ozone-transport behavior across the tropopause. The ozone concentration is strikingly homogeneous below 14 km, but in

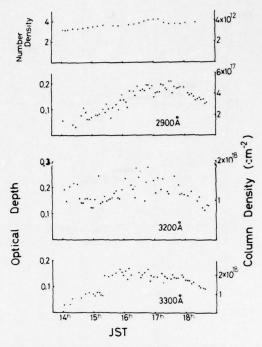


Figure 2. The local ozone density measured by KI sonde (top) compared with the over-burdens deduced from the uv scattering data at three wavelengths. The balloon's altitude was 27 km (May 30, 1974, Sanriku).

the stratosphere we can recognize distinct space and time changes in the same quantity. Furthermore, we notice a small dip in ozone density which was persistent at 21 km; it is related to the wind shear formed between the jet westerlies and their easterly counterflow above 20 km.

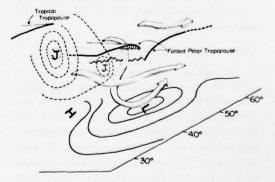


Figure 3. A model of stratospheric air transport through the tropopause breaks associated with the jet streams (courtesy of Dr. H. Kida, Meteorological Research Institute).

TOHMATSU

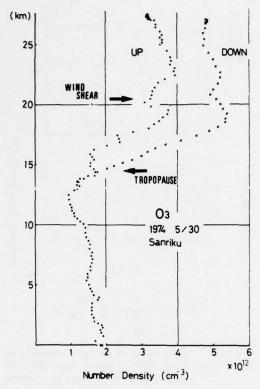


Figure 4. Ozone vertical profiles obtained in two different portions of a balloon trajectory (see text).

The present result is indicative of a number of interesting transport mechanisms near the jet stream. More detailed study of the transport effect is planned in 1975. That experiment will have several droppable sondes aboard a large balloon. They will be released one by one at an appropriate time and distance separation to cover a three-dimensional structure of ozone distribution in the stratosphere.

OTHER STRATOSPHERIC MEASUREMENTS

A balloon-borne mass analyzer which is usable in stratospheric measurements up to altitudes with pressures lower than 10 torr has been developed by Prof. Tomizo Itoh of ISAS. The analyzer is a magnetic-deflection type equipped with an ion-pump evacuating system. To avoid contamnation by degassing from the experimental package, and also to protect the electronic circuits from electrical discharge in high-voltage devices, the whole measuring system is pressurized and isolated in a metallic container.

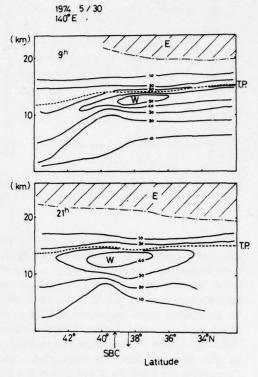


Figure 5. The latitudinal cross-section of the eastwest wind, before and after the ozone profiles in Figure 4 were obtained (courtesy of Japanese Meteorological Agency).

Preliminary experiments in 1974 and 1975 indicated that the analyzer can successfully be used to detect some important minor constituents of the stratosphere.

Measurements of aerosol and ion mobilities in the stratosphere have been carried out by Profs. Haruji Ishikawa and Masumi Takagi of the Research Institute of Atmospherics of Nagoya University. Prof. Ishikawa reviews these topics in his paper in this volume.

INTERNATIONAL PROGRAMS

Following are some of the internationally coordinated programs related to the CIAP investigations that have been conducted under the auspices of the U.S. National Science Foundation and the Japan Society for Promotion of Science. A coordinated experiment on NO and O₃ distributions was carried out by Utah State University, York University, the National Oceanographic and Atmospheric Administration, and

TOHMATSU

the University of Tokyo on November 13, 1973 at Alamogordo, New Mexico (Ridley et al., 1975). Nagoya University cooperated with Wyoming University and the University of Tübingen in the aerosol and ion mobility experiments at Sanriku (Japan), Laramie (USA) and Weisenau (West Germany). Tohoku University and the National Center for Atmospheric Research plan a cooperative experiment on atmospheric radiation in Hawaii.

The stratospheric effect of man-made fluorocarbons is of great concern to some related industries in Japan. The Freon Gas Association of Japan, which is a non-profit organization established by these industries, is participating in the program of the Technical Panel on Fluorocarbon Research of Manufacturing Chemists Association, USA, promoting basic research in chemical and physical properties of fluorocarbons and their related compounds in the stratosphere.

REFERENCES

Ogawa, T. and T. Shimazaki (1975), "Diurnal variations of odd nitrogen and ionic densities in the meso-

- sphere and lower thermosphere: Simultaneous equation of photochemical diffusive equations," J. Geophys. Res. 80, 3945-3960.
- Ridley, B.A., H.I. Schiff, A. Shaw and L.R. Megill (1975), "In situ measurements of stratospheric nitric oxide using a balloon-borne chemiluminescent instrument," J. Geophys. Res. 80, 1925-1926.
- Shimazaki, T., and T. Ogawa (1974), "A theoretical model of minor constituent distributions in the stratosphere including diurnal variations," J. Geophys. Res. 79, 3411-3423.
- Stair, A.T., Jr., J.C. Ulwick, K.D. Baker, and D.J. Baker (1975), "Rocketborne observations of atmospheric infrared emissions in the auroral region," in *Atmospheres of Earth and the Planets*, ed. B.M. McCormac, Reidel, Dordrecht, 335-346.
- Tohmatsu, T., N. Iwagami and T. Watanabe (1974), "An experimental daytime reference ozonosphere," Rep. Ion. Space Res. (Japan) 28, 161-162.
- Tohmatsu, T. and T. Watanabe (1976), "An observational evidence for the seasonal variation of ozone concentration in the upper stratosphere and the mesosphere," Rep. Ion. Space Res., Japan 30, No. 1.2 (in press).

EFFECTS ON PLANTS OF INCREASED UV-B RADIATION

R.H. BIGGS

Institute of Food and Agricultural Sciences
University of Florida
Gainesville, Florida

ABSTRACT: Experiments were conducted in three controlled environments (growth chambers, greenhouses, and a solarium) to determine the response of whole plants to various elevated levels of UV-B radiation. The maximum simulated UV-B regime approximated that of a 50% depletion of the ozone layer (based on a global average ozone column of 0.32 atm-cm). This paper describes the experiments and compares their results.

To provide a data base for the assessment of biological response to increased UV-B irradiation in the biosphere, organisms have to be exposed, and observed, under simulated conditions that approximate as nearly as possible the expected situation in the event of reduced ozone. The biological responses of different organisms to UV radiation depend on their stage of growth and development, and other environmental factors (Bartholic et al., 1974; Caldwell, 1971; Caldwell et al., 1974). This report presents the results of stratified experiments (i.e., with partially controlled environmental conditions) conducted to evaluate response to UV radiation. A list of plants tested for relative sensitivity or resistance to UV-B radiation in growth chambers, greenhouses, and a solarium can be seen in Table 1.

MATERIALS AND METHODS

Plant Materials

Plants having economic importance were selected for testing. They were prepared for growth-chamber, greenhouse, and solarium tests in a manner consistent with cultural practices — for example, Zea mays by germinating the seeds, and cabbage by transplanting young seedlings.

The seeds for most of the plants tested were planted in vermiculite in a medium-sized plastic pot. Prior to seed emergence, the pots were transferred to two environmentally-controlled growth chambers and plants were allowed to grow under two different light regimes at a temperature controlled at $25 \pm 2^{\circ}$ C. During the growth period, the plants were watered daily,

and fertilized weekly with Hoagland's nutrient solution. The plants were placed 20 to 30 cm from the radiation source; they usually were left there without interruption for the duration of the exposure. The plants were observed routinely for possible differences resulting from the treatments.

Growth-Chamber Test Conditions

Light conditions in the two growth chambers were identical except for the supplemental UV radiation. Radiation with a daytime intensity of 310 to 360 microeinsteins m⁻¹ sec⁻², 400-700 nm, was supplied by fluorescent and incandescent lamps for 16 hours daily. The visible portion of the spectrum was supplied by a bank of coolwhite fluorescent and incandescent lamps. For UV-B and UV-A radiation enhancement, four Westinghouse FS40 sunlamps were used in each chamber. The lamps were mounted inside the chamber above the plants but below the Mylar barrier (which was 5 mils, or 0.13 mm, thick) between the main light bank and the chamber. The emission from the FS40 sunlamps was filtered through 5-mil Mylar in one chamber and 5-mil cellulose acetate in the other. The former permits UV-A enrichment only and serves as a control. With the cellulose acetate filter, the UV-B radiation was controlled to correspond to a 0.18-atm cm ozone column at a solar altitude of 45°; plants were exposed to six hours of UV radiation enrichment in the mid-portion of each day. Irradiance for UV-B radiation enhancement was calculated from irradiance detected at the plant-apex level by a UV spectroradiometer (Bartholic et al., 1974).

Table 1. Plants Screened for Response to UV-B Radiation Under Growth-Chamber, Greenhouse, and Solarium Conditions. Sensitivity Ratings Are Given in Terms of Both Plant Height and Biomass Accumulation

Ears Crowtl Chambb Chambb Chambb Chambb Chambb Chambb Chambb Coet peas Cet peas Cet peas Coet peas				S	SENSITIVITY TO UV-B RADIATION	V-B RADIATION		
NAME CULTIVAR Yackson Wonder' beans fit I. Yackson Wonder' beans Harvester' beans Tit I. California Black Eye #5 peas L. Yando' peas L. Yando' peas Yarly Perfection' peas Yarly Perfection' peas Yarly Markel' peas L. Yarly Alaska' peas L. Georgia' collards A. Georgia' collards T. Straight 8' carrot Yarly Scarlet Glove' radish Tearly Golden Summer' squash T. Straight 8' carrot Yarly Golden Summer' squash T. Yarly Scarlet Glove' radish Tearly Golden Summer' squash T. Yarly Scarlet Glove' radish Tearly Golden Summer' squash T. Yarly Tobacco T. Yarly T			Based	Based on Dry-Mass Production	ction		Based on Plant Height	
riz L. 'Jackon Wonder' beans riz L. 'Jackon Wonder' beans 140 L. 'Zapper Cream' peas 2. 'Zapper Cream' peas 2. 'Yando' peas 2. 'Yando' peas 1- 'Early Multiflora' sweet peas 2. 'Little Marvel' peas 3. 'Early Alaska' peas 2. 'Little Marvel' peas 3. 'Little Marvel' peas 4. 'Ceorgia' collards 5. 'Ceorgia' collards 5. 'Ceorgia' collards 6. 'Ceorgia' collards 6. 'Ceorgia' collards 6. 'Early Golden Summer' squash 6. 'Early Golden Summer' squash 6. 'Early Golden Summer' squash 6. 'Chantinay' cucumber 7. 'Silver Skin' onion 6. 'Chantinay' cucumber 7. 'Silver Skin' onion 6. 'Chantinay' cucumber 7. 'Hiki' tobacco 6. 'Horida 501' cars 6. 'Hiki' tobacco 6. 'Caloro' rice 6. 'Yaller' tomatoes 7. 'Hiki' tobacco 6. 'Caloro' rice 6. 'Waller' tomatoes 7. 'Horida 683' celery 6. 'Horida	SCIENTIFIC NAME	CULTIVAR	Growth	Greenhouse	Solarium	Growth	Greenhouse	Solarium
riz L. 'Harvester' beans riz L. 'Zipper Cream' peas L. 'Zipper Cream' peas L. 'Yando peas L. 'Burpee's Blue Bantam' peas L. 'Burpee's Blue Bantam' peas L. 'Early Multiflora' sweet peas L. 'Early Multiflora' sweet peas L. 'Early Multiflora' peas L. 'Early Multiflora' peas L. 'Early Multiflora' peas Tailte Marvel' peas a L. 'Georgia' collards a L. 'Straight 8' carrot 'Early Golden Summer' squash ca L. 'Early Golden Summer' squash ca L. 'Early Golden Summer' squash 'L. 'Silver Skin' onion 'Garor' rye 'Horida 501' oats 'Bragg' soybeans 'ORO-T' sorghum 'Phoneer 3369A' corn ca L. 'Horiumer' peanut 'Great Lake' lettuce 'Yaller' tomatoes 'Purple Top, White Glove' turnip 'Great Lake' lettuce 'Horida 683' celery	Phaseolus lanatus L.	'Jackson Wonder' beans		0			0	
10 C. California Black Eye #5' peas 10 L. 'Zipper Cream' peas 1. 'Wando' peas 1. 'Early Perfection' peas 1. 'Early Multiflora' sweet peas 1. 'Early Multiflora' sweet peas 1. 'Early Multiflora' peas 1. 'Early Alaska' peas 1. 'Georgia' collards 1. 'Straight 8' carrot 1. 'Early Colden Summer' squash 1. 'Early Colden Summer' squash 1. 'Early Golden Sum	Phaseolus vulgaris L.	'Harvester' beans	0	0			0	
L. 'Yando' peas L. 'Wando' peas L. 'Bariy Perfection' peas L. 'Bariy Perfection' peas L. 'Bariy Alaska' peas Little Marvel' peas L. 'Straight 8' carrot Ceorgia' collards a L. 'Straight 8' carrot Tarly Scarlet Glove' radish met L. 'Straight 8' carrot 'Chantinay' cucumber Silver Skin' onion 'Caror' rye 'Horida 501' oats 'Barge' soybeans 'ORO-T' sorghum Phoneer 3369A' corn coa L. 'Hiki' tobacco 'Caloro' rice 'Walter' tomatoes 'Purple Top, White Glove' turnip 'Great Lake' lettuce 'Horida 683' celery 'Horida 683' celery	Vigna unguiculata L.	'California Black Eye #5' peas	‡	0		•	0	
L. 'Wando' peas L. 'Burpee' S Blue Bantam' peas L. 'Early Multilora' sweet peas L. 'Early Multilora' sweet peas L. 'Early Alaska' peas L. 'Early Alaska' peas a L. 'Georgia' collards a L. 'Straight 8' carrot cs L. 'Early Scarlet Glove' radish met L. 'Early Scarlet Glove' radish met L. 'Early Scarlet Glove' radish ca L. 'Early Golden Summer' squash ca L. 'Early Golden Summer' peanut ca L. 'Hiki' tobacco 'Yeloro' rice 'Yeloro' rice 'Yeloro' rice 'Walter' tomatoes 'Purple Top, White Glove' turnip 'Great Lake' lettuce 'Horida 683' celery 'Horida 683' celery	Vigna unguiculata L.	'Zipper Cream' peas	‡	0		•	0	
L. 'Early Perfection' peas L. 'Early Multiflora' sweet peas L. 'Early Multiflora' sweet peas L. 'Early Multiflora' sweet peas L. 'Early Alaska' peas a L. 'Badger Market' cabbage a L. 'Georgia' collards C. 'Georgia' collards a L. 'Straight 8' carrot cs L. 'Early Golden Summer' squash ct. 'Horida 5/01' oats 'Bragg' soybeans ca L. 'Horida 5/01' oats 'Hiki' tobacco 'Teloro' rice	Pisum sativum L.	'Wando' peas		0		0	0	
L. 'Burpee's Blue Bantam' peas L. 'Early Multiflora' sweet peas L. 'Little Marvel' peas L. 'Little Marvel' peas a L. 'Georgia' collards a L. 'Georgia' collards Straight 8' carrot ts L. 'Early Golden Summer' squash mat L. 'Early Golden Summer' squash cl. 'Early Golden Summer' squash cl. 'Straight 8' carrot Silver Skin' onion 'Gator' rye 'Horida 501' oats 'Bragg' soybeans r (L.) 'ORO-T' sorghum 'Phomeer 3369 A' corn red L. 'Hiki' to bacco 'Caloro' rice 'Yeloro' rice 'Walter' tomatoes 'Purple Top, White Glove' turnip 'Great Lake' lettuce 'Horida 683' celery	Pisum sativum L.	'Early Perfection' peas	+	0		•	0	
L. 'Early Multiflora' sweet peas L. 'Early Alaska' peas L. 'Georgia' collards a L. 'Georgia' collards T. 'Straight 8' carrot 'Early Golden Summer' squash i L. 'Early Golden Summer' squash i L. 'Early Golden Summer' squash i L. 'Gator' tye 'Horda 501' oats 'Bragg' soybeans or L. 'Horda 501' oats 'Bragg' soybeans or L. 'Hordant 'Phoneer 3369 A' corn or L. 'Hiki' tobacco 'Caloro' rice 'Yeloro' rice 'Walter' tomatoes 'Purple Top, White Glove' turnip 'Great Lake' lettuce 'Horda 683' celery	Pisum sativum L.	'Burpee's Blue Bantam' peas				0		
L. 'Early Alaska' peas L. 'Little Marvel' peas 'Little Marvel' peas 'Badger Market' cabbage a L. 'Georgia' collards L. 'Straight 8' carrot 'Early Golden Summer' squash re. 'Early Golden Summer' squash re. 'Early Golden Summer' squash re. 'Silver Skin' onion 'Gator' ryce 'Horda 501' oats 'Bragg' soybeans 'ORO-T' sorghum 'Phorner 3369 A' corn ca L. 'Hiki' tobacco 'Caloro' rice 'Yeloro' rice 'Walter' tomatoes 'Purple Top, White Glove' turnip 'Great Lake' lettuce 'Horida 683' celery	Pisum sativum L.	Early Multiflora's weet peas	0			0		
L. 'Little Marvel' peas 'Badger Market' cabbage 'a L. 'Georgia' collards L. 'Straight 8' carrot 'Early Golden Summer' squash 't. 'Early Golden Summer' squash 't. 'Silver Skin' onion 'Gator' ryc 'Thorida 501' oats 'Bragg' soybeans 'ORO-T' sorghum 'Phoneer 3369 A' corn ea L. 'Hiki' tobacco 'Caloro' rice 'Yeloro' rice 'Walter' tomatoes 'Purple Top. White Glove' turnip 'Great Lake' lettuce 'Horida 683' celery	Pisum sativum L.	'Early Alaska' peas		•			0	
a L. 'Badger Market' cabbage a L. 'Georgia' collards set L. 'Straight 8' carrot 'Early Golden Summer' squash "Early Golden Summer' squash "Chantinay' cucumber 'Silver Skin' onion 'Gator' tyce 'Horida 501' oats 'Bragg' sopbeans 'ORO-T' sorghum 'Phoneer 3369A' corn ea L. 'Hiki' tobacco 'Caloro' rice 'Walter' tomatoes 'Purple Top. White Glove' turnip 'Great Lake' lettuce 'Horida 683' celery	Pisum sativum L.	'Little Marvel' peas		0	‡	٠	0	
a L. 'Georgia' collands L. 'Early Scarlet Glove' radish ma L. 'Early Golden Summer' squash i.L. 'Chantinay' cucumber 'Silver Skin' onion 'Gator' rye 'Horida 501' oats 'Bragg' soybeans 'ORO-T' sorghum 'Phoneer 3369 A' corn 'Phoneer 3369 A' corn 'Phoneer 1369 A' corn 'Thoriante' peanut 'Great Lake' lettuce 'Great Lake' lettuce 'Horida 683' celery	Brassica oleracea L. var. capitata	'Badger Market' cabbage		0		0	0	
L. Straight 8' carrot 12. 'Early Scarlet Glove' radish 13. 'Early Golden Summer' squash 14. 'Chantinay' cucumber 15. 'Gator' tye 16. 'Horida 501' oats 18. 'Brage soybeans 17. 'ORO-T' sorghum 18. 'Phomer 3369 A' corn 19. 'Phomer 3369 A' corn 19. 'Caloro' rice 19. 'Walter' tomatoes 19. 'Walter' tomatoes 19. 'Phomer 683' celery 19. 'Phomer 683' celery 19. 'Phomer 683' celery 19. 'Phomer 683' celery	Brassica oleracea L. var. acephata	'Georgia' collards	0	0		0	0	
rs L. 'Early Scarlet Glove' radish mat L. 'Early Golden Summer' squash i.L. 'Chantinay' cucumber 'Silver Skin' onion 'Gafor' ryc 'Horida 501' oats 'Bragg' soybeans 'ORO-T' sorghum 'Phomeer 3369A' corn ea L. 'Hiki' tobacco 'Caloro' rice 'Yeloro' rice 'Walter' tomatoes 'Purple Top, White Glove' turnip 'Great Lake' lettuce 'Horida 683' celery	Pastinace sativa L.	'Straight 8' carrot	‡	0			0	
rad L. 'Early Golden Summer' squash 'I. 'Chantinay' cucumber 'Silver Skin' onion 'Gator' rye 'Horida 501' oats 'Bragg' soybeans 'ORO-T' sorghum 'Phoneer 3369A' corn 'Phoneer 3369A' corn 'T. 'Hiki' tobacco 'Caloro' rice 'Walter' tomatoes 'Purple Top, White Glove' turnip 'Great Lake' lettuce 'Horida 683' celery	Raphanus sativus L.	'Early Scarlet Glove' radish	‡	ŧ	0	‡		0
Chantinay' cucumber Silver Skin' onion Gator' rye 'Piorida 501' oats 'Brage' sopbeans 'ORO-T' sorghum 'Pioneer 3369A' corn 'Pioneer 3369A' corn 'Pioneer 3369A' corn 'Pioneer 1369A' corn 'Cal. 'Hiki' tobacco 'Calero' rice 'Walter' tomatoes 'Purple Top, White Glove' turnip 'Great Lake' lettuce 'Horida 683' celery	Cucurbita moxima L.	'Early Golden Summer' squash	‡			٠		
"Silver Skin' onion "Gator' tye "Horida 501' oats "Bragg' soybeans "ORO-T' sorghum "Phoneet 3369 A' corn "Phoneet 3369 A' corn "Phoneet 3369 A' corn "Cal. "Hiki' tobacco "Caloro' rice "Walter' tomatoss "Purple Top, White Giove' turnip "Great Lake' lettuce "Horida 683' celery	Cucumis sativus L.	'Chantinay' cucumber	‡	0		‡	0	
"Gator' tye "Horida 501' oats "Bragg' soybeans "ORO-T' sorghum "Phoneer 3369 A' corn rea L. 'Horunner' peanut "Walter' tobacco "Caloro' rice "Walter' tomatoes "Purple Top, White Glove' turnip "Great Lake' lettuce "Horida 863' celery	Allium cepa L.	'Silver Skin' onion		0		٠	0	
'Phorida 501' oats 'Bragg' soybeans 'ORO-T' sorghum 'Phoneer 3369 A' corn 'Phoneer peanut 'Phoneer peanut 'Walter' tobacco 'Caloro' rice 'Walter' tomatoes 'Purple Top. White Glove' turnip 'Great Lake' lettuce 'Thorida 683' celery	Secale cereale L.	'Gator' rye	0			0		
Bragg, soybeans 'ORO-T' sorghum 'Ploneer 3369A' corn 'Ploneer 3369A' corn 'Plonener Deanut 'Hiki' tobacco 'Caloro' rice 'Yalre' tomatoes 'Purple Top, White Giove' turnip 'Great Lake' lettuce 'Plonida 683' celery	Avena sativa L.	'Florida 501' oats	0		0	‡		0
r (L.) 'ORO-T' sorghum 'Ploneer 3369A' corn 'Plonener 3369A' corn 'Plorunner' peanut 'Caloro' rice 'Valler' tomatoes 'Purple Top, White Glove' turnip 'Great Lake' lettuce 'Plorida 683' celery	Glycine max L.	'Bragg' soybeans	0		‡	0		
Pioneer 3369 A' corn 'Pioneer 3369 A' corn 'Pioner 1968 Corn 'Caloro' rice 'Walter' tomatoes 'Purple Top, White Glove' turnip 'Great Lake' lettuce 'Pionida 683' celety	Sorghum bicolor (L.) Moench.	'ORO-T' sorghum	‡			:		
red L. 'Phorunner' peanut 1994 L. 'Hiki' tobacco Caloro' rice Walter' tomatoes 'Purple Top, White Glove' turnip 'Great Lake' lettuce 'Phorida 683' celety	Zea mays L.	Pioneer 3369A' corn	0	0		0	:	
tose L. 'Hiki' tobacco 'Caloro' rice 'Walter' tomatoes 'Purple Top. White Glove' turnip 'Great Lake' lettuce 'Horida 683' celery	Arachis hypogaea L.	'Florunner' peanut	0		0			٠
Yealono' rice Yealter' tomatoes Purple Top. White Glove' tumip Great Lake' lettuce 'Plorida 863' celety na L. 'Plorida 863' celety	Nicotiana glutinosa L.	'Hiki' tobacco	0		0			0
rententum "Walter" tomatoes "Purple Top, White Glove' turnip "Great Lake' lettuce "Horida 683' celery	Oryza sativa L.	'Caloro' rice			+			0
. L.	Lycopersicum esculentum Mill.	'Walter' tomatoes	•0	•			0	
ı.	Brassica rapa L.	'Purple Top, White Glove' turnip						0
	Lactuca sativa L.	'Great Lake' lettuce			0			0
var. capitata	Apium graveolena L. var. capitata	'Florida 683' celery			0			0

Code: 0 = not sensitive under test conditions + = sensitivity at the 95% probability level ++ = sensitivity at the 99% probability level

*Fresh weight was measured on this crop

Greenhouse Test Conditions

The greenhouse, constructed of Lascolite (fiber glass), covered 400 square meters. It was equipped with an evaporative cooling system and natural-gas heaters to regulate temperature within the range of 20°C to 30°C. Light conditions were those of sunlight filtered through the Lascolite with the day length extended to 16 hours by incandescent lamps (2 watts/m² at plant height). To enhance radiation in the 280-320 nm region, light fixtures containing three Westinghouse FS40 sunlamps were suspended above the plants (Figure 1). Radiation was filtered through either 5-mil UV-B radiationabsorbing Mylar S (control) or 5-mil UV-B radiation-transmitting cellulose acetate (UV-B radiation-enhanced). Distance between lamps and plants was adjusted to correspond to a 0.18atm-cm ozone column at a solar altitude of 55°. The irradiance was measured at plant-apex level with a UV spectroradiometer (Gamma Scientific, Inc.) and irradiance levels calculated. Plants received UV-B radiation enhancement for six hours daily (1000 to 1600 hours solar time). Measurements were made of rate of growth, fresh and dry weights, and other parameters germane to the type of crop.

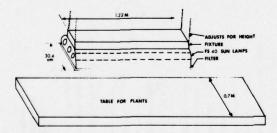


Figure 1. Physical system for supplemental UV-B irradiation of plants under growth-chamber, greenhouse, and solarium conditions.

Solarium Test Conditions

The solarium was a greenhouse whose top had been removed to allow entry of full solar radiation. There were three ground-level pits to house lysometric pots. FS40 sunlamps were mounted over test plants, oriented in a north-south direction to minimize shading. Cellulose-acetate-filtered (+UV-B) and Mylar-filtered (control) sunlamps, as described above, were used to

enhance UV-B radiation (Figure 1) in an otherwise natural day. All plants grown in the solarium were seeded in special lysometric pots directly under the lamps so that radiation was present right from the moment of seeding. The soil mix was constituted of equal parts of vermiculite, Canadian peat, and water-washed gravel to which were added minerals adjusted for the proper nutrient level and pH for each crop. UV-B irradiance was enhanced from 900 to 1600 hours solar time. The UV-B irradiation regime was designed to simulate an 0.11-atm-cm ozone reduction from a base level of 0,30 atm-cm at a solar altitude of 55°. The plant characteristics measured were biomass accumulation, height where appropriate, and other parameters that were considered indicators of an adverse effect on production.

RESULTS AND DISCUSSION

The effects of UV-B radiation on the growth and development of different plant species were tested under growth-chamber, greenhouse, and solarium conditions.

Dry Matter Accumulation

Many observations indicate that dry-matter accumulation is one of the better parameters for evaluation of plant response to UV-B radiation. It is an integrator that reflects a sum of responses through time. Table 1 is a rating of the sensitivity of plants tested under growth-chamber, greenhouse, and solarium conditions. The numerical data for each plant tested have been reported elsewhere (CIAP, 1975). Of the 23 varieties and species tested under growth-chamber conditions, 13 had biomass that was less than that of the controls. In the greenhouse, 4 of 17, and in the solarium, 4 of 10 species had dry-weight accumulations less than that of the controls. Two of these plants could have had lower dry-matter accumulation because of a heavy infestation of insects.

Plant Height

Another parameter closely allied to biomass changes was the effect of UV-B radiation on plant height. As shown in Table 1, significant effects were seen on 15 of 23 plants tested under

growth-chamber conditions, 1 of 16 under greenhouse conditions, and 3 of 7 under solarium conditions. Changes in plant height have been noted by others (CIAP, 1975); they may be related to UV-B-caused inhibition of internode elongation.

Seed Germination and Seedling Growth

UV-B radiation seemed to have no marked effect on seed germination of the species tested. This may be due mainly to the inability of UV-B radiation to penetrate the soil or the seed coats (Shull and Lemon, 1931). However, UV-B radiation had a marked effect on subsequent seedling growth. The rate of seedling emergence was delayed one or two days by UV-B radiation in almost all the varieties tested in the growthchamber and greenhouse conditions. The cotyledons of seeds of some plants such as cow peas and harvester beans, for unknown reasons, seemed to have difficulty in shedding the remanent seed coats, but after they emerged, they were not seen to be seriously injured. Except for plants in the growth chambers, there were no marked abnormal effects such as distorted leaves, leaf bronzing, or chlorosis. The main effect seemed to be one of slowing the rate of seedling growth, and dwarfism. Once beyond the seedling stage, the plants were seemingly more resistant to UV-B radiation.

Plant Survival

Survival rates for the 29 species were not significantly different for plants receiving the UV-B radiation enhancement and the control plants, except in the case of 'Little Marvel' and 'Early Perfection' peas under the lower visible-light intensities of the growth chambers.

Flowering and Other Parameters

Flowering was delayed one or two days in plants grown under UV-B radiation. This may be due to the general effect of UV-B on plant growth. However, the flowers on the UV-B-radiation-treated plants were fewer in number, and smaller in size. The beans and peas were

significantly enough affected that yield could be reduced.

SUMMARY

These short-term growth-chamber, greenhouse, and solarium experiments are indicative of the potential of enhanced UV irradiance to significantly suppress the growth of higher plant species. Yet these experiments must be considered as preliminary, and extrapolations to crop productivity are clearly inappropriate. These experiments by necessity were confined to small numbers of plants. This, combined with the inherent variability of these plant populations, has limited the resolution with which UV-B radiation sensitivity of whole plants can be ascertained. Whether or not plant growth of sensitive species would be reduced under UV-B irradiation enhancement, as would occur with a lesser degree of simulated ozone depletion, remains an open question.

REFERENCES

- Bartholic, J.F., L.H. Halsey, and R.H. Biggs (1974), "Effects of UV radiation on agricultural productivity," in Proceedings of the Third Conference on the Climatic Impact Assessment Program (Cambridge, Mass.), U.S. Dept. of Transportation, DOT-TSC-OST-74-15, 482-497.
- Caldwell, M.M. (1971), "Solar UV irradiation and the growth and development of higher plants," in Photophysiology, vol. 6, ed. A.C. Giese, Academic Press, N.Y., 131-177.
- Caldwell, M.M., W.F. Campbell, and W.B. Sisson (1974), "Plant response to elevated UV intensities," in Proceedings of the Third Conference on the Climatic Impact Assessment Program (Cambridge, Mass.), U.S. Dept. of Transportation, DOT-TSC-OST-74-15, 482-497.
- CIAP (1975), Impacts of Climatic Change on the Biosphere: Part 2 Climatic Effects, ed. M. Caldwell et al., Volume 5, Part 2 of the CIAP monograph series, Dept. of Transportation, DOT-TST-75-55 (Part 2).
- Shull, C.A. and H.B. Lemon (1931), "Penetration of seed coats by ultraviolet radiation," Bot. Gaz. 92, 420-429.

ESTIMATE OF THE EFFECT OF OZONE REDUCTION IN THE STRATOSPHERE ON THE INCIDENCE OF SKIN CANCER IN MAN

FREDERICK URBACH AND RONALD E. DAVIES

Skin and Cancer Hospital
Temple University Health Sciences Center
Philadelphia, Pennsylvania

ABSTRACT: The various models attempting to relate decrease in atmospheric ozone to a possible increase in skin cancer result in the following "amplification factors":

- Increase in UVB due to reduction in ozone concentration in the stratosphere:
 Optical "amplification" factor: 2x (range 1.4 to 2.5)
- Increase in skin-cancer incidence due to increase in UVB radiation at ground level: Biological "amplification" factor: 1x (range 0.5 to 2)
- Increase in skin-cancer incidence due to reduction in ozone concentration in the stratosphere:

Total "amplification" factor: 2x (range 0.7 to 5.0)

If the skin-cancer incidence figures of Scotto et al. (1974) are used as a baseline, with a 2x "amplification" factor, a 5% reduction in ozone concentration could result in an increase of 37 cases of skin cancer per 100,000 population a year at the latitude of Dallas/Fort Worth, Texas, and an increase of 12.4 cases of skin cancer per 100,000 population a year at the latitude of Iowa. On the assumption that the incidence of non-melanoma skin cancer in the United States is approximately 165 per 100,000 (Scotto, 1975), a 5% decrease in stratospheric ozone concentration could result in an average increase in the United States of 16.5 cases of skin cancer per 100,000, or a total of approximately 30,000 new cases per year.

INTRODUCTION

As has been pointed out before, there exists extensive evidence that skin cancer, at least of the non-melanoma type, is caused by cumulative exposure to ultraviolet radiation of wavelengths between 280 and 320 nm, called UVB. This holds true primarily of skin unprotected by significant amounts of melanin (but see Blum, 1969), and thus applies mainly to the white races, or about one-third of the world's population.

All photobiological responses to irradiation by ultraviolet and visible light show a dependence on the energy of the incident photons, with a maximum response at a fairly well-defined photon energy and a somewhat limited range beyond which the lower photon energies are very much less effective. This depends mostly on absorption of UV by specific important molecules, and hence is restricted to the absorption spectra of these molecules.

Skin carcinogenesis by UV radiation is generally assumed to be the result of genetic damage in DNA molecules. The skin-carcinogenesis action spectrum and the DNA absorption spectrum may therefore correspond (Setlow, 1974; Chavaudra and Latarjet, 1973), though there are other possibilities and uncertainties (Blum, 1974). The erythemal spectrum agrees well with the DNA absorption spectrum in the spectral region from 295 to 330 nm, which appears to cause nearly all the response. Hence, either the DNA absorption spectrum or the erythema action spectrum will give nearly the same results for irradiation by sunlight (Setlow, 1974; Chavaudra and Latarjet, 1973; Green and Mo, 1974). Furthermore, the action spectrum for skin carcinogenesis in mice covers the same spectral range as the human erythema action spectrum (Freeman, 1974; Magnus, 1974; Wetzel, 1959); for the purposes of the CIAP studies, the erythema spectrum was taken as equivalent to that for human carcinogenesis. The

weight of the evidence is consistent with the concept that UV-induced photo-damage to skin is the main causative factor in skin cancer, and that there is no threshold effect (Blum, 1959, 1974). Thus a relationship should exist between skin-cancer incidence and cumulative dose governed by a sensitivity function. In mice, the quantitative relationship between UV dose and production of skin cancer has been thoroughly explored: tumor incidence in this experimental model is proportional to the square root of the number of UV doses, their size, and the interval between doses (Blum, 1959).

Blum (1975), using a model that takes into account unresolvable uncertainty in cancer growth, shows by analysis of available data that for men, as for mice, carcinogenesis by repeated doses of ultraviolet radiation is cumulative. The analysis also indicates broad uncertainty in the predictions that may be made from present data. Various factors may contribute to this uncertainty, but these cannot, for the most part at least, be evaluated quantitatively at present. Cumulative dosage or exposure is a function of the amount of ozone in the stratosphere, atmospheric conditions (cloudiness, aerosol, etc.), latitude, and lifestyle (which includes time and type of outdoor activity). Of these, the thickness of the stratospheric ozone layer is a major determinant of the amount and spectral distribution of effective UV radiation which can reach a target at any point on earth.

The question of interest to CIAP is: What is the potential effect of a reduction in stratospheric ozone on the incidence of skin cancer? The most straightforward way to get an answer would be to compare observed skin-cancer incidence to ozone thickness over areas where such epidemiological and meteorological data are available, and extrapolating from this information, making reasonable assumptions to allow for the effects of all factors thought to affect skin-cancer incidence in addition to ozone thickness. Such an approach was used originally by McDonald (1971). It presupposes, however, a knowledge of ozone conditions which is not accurately available at present. Existing ozone maps (1 ondon, 1974; Kohmyr et al., 1973) are based on ozone measurements made at various places (at none of which epidemiologic data for skin-cancer incidence exist) at various times and

with various methods. Extrapolation to specific location and times is difficult. Furthermore, there are known marked seasonal and longitudinal as well as latitudinal changes in ozone (London, 1974). However, since UV radiation is thought to be causally related to skin-cancer production, and can be measured with some accuracy and reliability in many places (Berger et al., 1975) and compared with ozone measurements, it was thought appropriate to use UV data for the estimates reported here.

Utilizing the figures for U.S. skin-cancer incidence obtained by the Third National Cancer Survey (Scotto et al., 1974) and a variety of assumptions about the relationship of UV radiation and skin cancer, several models of the potential effect of reduction of the stratospheric ozone layer have been proposed (McDonald, 1971; Green, 1975; van der Leun and Daniels, 1975; Urbach and Davies, 1975).

Underlying all of these models are several assumptions:

- A decrease in stratospheric ozone will result in an increase in UV radiation shorter than approximately 320 nm.
- An increase in UV radiation shorter than approximately 320 nm will result in an increase in skin cancer in a susceptible human population.
- The observed increase in skin cancer with decreasing latitude is due to several interacting factors, of which ozone thickness and sun angle are two; differences in local atmospheric conditions, genetic background of the population, type, length, and kind of outdoor exposure, and other not-yet-specified conditions make up the rest.

UVB RADIATION AND OZONE

A relationship between ozone-layer thickness and UV radiation which is erythemogenic for untanned white skin has been calculated by a number of investigators, beginning with Latarjet (1935). Table 1 gives summaries of these various computations and the appropriate references. It is striking that the values, except for McDonald's (1971), are so close despite large differences in physical and biological data and in calculation

conditions, such as solar zenith angle. For a 5% decrease in ozone, the increases in UV-B range from 7 to 11.5%. The differences are in part due to the non-linearity of the rate of change of the sunburning capability of solar UV with change in ozone column (see Figure 1). The average increase in UVB effectiveness for a 5% decrease in ozone becomes 9.0% (or an amplification factor of 1.8). Comparisons of UVB meter readings at Hilo, Hawaii and Bismarck, North Dakota with Dobson-meter measurements at these stations showed amplification factors of 2.15 and 2.0 respectively (Berger, 1975).

The nature of the absorptive process is such that the increase in transmission of a particular wavelength will be an exponential function of the change in ozone concentration: The total change in transmission is the integral of the change at each wavelength, and will thus also be related exponentially to the concentration change. The relative magnitude of the change will be strongly dependent on the wavelength region of interest: The greater the overlap between this range and the range of ozone absorption, the greater will be the "amplification factor" relating a given relative change in ozone concentration to

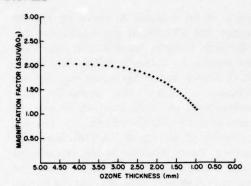


Figure 1. Ratio of change in UVB irradiation to change in total ozone column, as a function of ozone column.

the corresponding relative change in biologically effective ultraviolet transmission. The size of this overlap is defined by the choice of weighting factors, or action spectrum, for the biological effect of interest. In the absence of certain knowledge concerning the action spectrum for cutaneous carcinogenesis (but with the knowledge that UVB wavelengths are relatively more effective carcinogenically than longer wavelengths, at least in animals), the human-skin

Table 1. Relationship Between Ozone-Layer Thickness and Erythemogenic UV

Reference	Estimated Increase of Erythemal UV Effectiveness Due to 5% Decrease of O ₃ Layer Thickness	Comments
Latarjet (1935)	8%	Direct component only - sun at zenith.
Chavaudra and		Direct component only - sun at zenith.
Latarjet (1973)	7%	Using Coblentz and Stair (1934) action spectrum
	9%	Using Cripps and Ramsay (1970) action spectrum
Schulze (1974)		From results for a 10% decrease of O ₃ layer thickness, assuming linearity down to 5%.
	9%	In equatorial zone
	11%	In polar zone
Cutchis (1975)	11.5%	Solar zenith angle 30° . From results for a 10% decrease of O_3 layer thickness.
Mo and Green (1975)	10%	
Setlow (1974)	10%	Evaluation from 2% increase of effects for 1% decrease of O ₃ layer thickness.
van der Leun and Daniels (1975)	21%	Calculated from MacDonald (1971) (opt. amp. factor 4.2).
	9%	Calculated from CIAP data (opt. amp. factor 1.6).

erythema spectrum and a composite DNA photoeffect spectrum have been used as models. A third action spectrum which enters into consideration is that of the UVB meter, designed to approximate the spectrum of human erythema.

The shape and displacement of these spectra is such that for a given initial ozone concentration the amplification factors will be in the order DNA > skin > UVB meter. The absolute magnitude of the factors will also depend on the initial slant-column concentration of ozone as well as the magnitude of the change. It is thus somewhat surprising that the absolute magnitude of the amplification factor can be stated with some confidence. For the model spectra presently in use, for the normal range of ozone concentrations over mid-latitudes, and for relatively small (<20%) changes in concentration, the factors are generally in the range of 1.5-2.5, with a value of 2 providing a not unreasonable approximation. In other words, a 5% reduction in average ozone concentration will result in an increase of approximately 10% in "active" ultraviolet flux at the earth's surface (see Table 1).

Although extensive basic experimental information on the solar spectrum exists, and elegant mathematical models have been produced in this age of high-speed computers, neither can be applied with great certainty to the actual amount of UVB reaching any one area on earth. The atmospheric attenuation processes are too numerous and too ill-defined to be simultaneously quantified with any great degree of accuracy. However, calculations modeling longterm exposures to UVB have been performed (Mo and Green, 1974) and compared to actual measurements. The instruments used in the field measurements were a series of UVB meters (Berger et al., 1975) which were installed at Philadelphia, PA, Des Moines, IA, Minneapolis, MN, Albuquerque, NM, El Paso, TX, Dallas/Fort Worth, TX, Tallahassee, FL, and Oakland, CA.

The major factors affecting transmission of UV radiation of the 290-320 nm range to a terrestrial observer are sun angle (which depends on time of day, season, and latitude), cloud cover, and aerosols and suspended particles. The importance of atmospheric conditions and their variability from hour to hour and day to day are shown in Figures 2 and 3.

Figure 2 gives half-hourly plots of integrated erythemogenic UV as measured by the meters stationed at El Paso (latitude 31.8° north) and Tallahassee (latitude 30.4° north) for the same days of the first week of January 1974. Although Tallahassee is 1.4° farther south than El Paso. and thus would be expected to receive higher daily and cumulative levels of total ultraviolet light because of latitude, this was the case on only one day, January 5, 1974, when both stations had cloud cover for most of the day. The generally lower UVB totals are due to almost daily intermittent-to-major cloud cover at Tallahassee, and generally clear weather at El Paso. In Figure 3, a similar plot is given for El Paso and Albuquerque (35.1° north). Again, repeated cloud cover over Albuquerque magnifies the latitude effect. The sensitivity of the meters to change in local atmospheric conditions is clearly indicated by these figures.

Green et al. (1974), Shettle and Green (1974), and Mo and Green (1974) have performed detailed calculations on systematic relationships of climatic variables and their effects

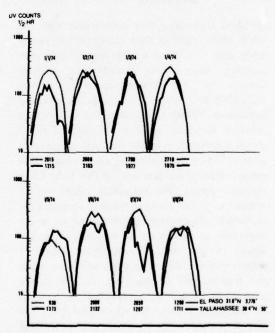


Figure 2. Half-hourly readings taken from sunburning-UV meters in El Paso, Texas and Tallahassee, Florida in January 1974. Note the marked effect of cloud cover at Tallahassee compared to almost daily clear weather in El Paso.

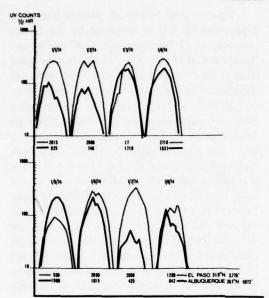


Figure 3. Half-hourly readings from sunburning-UV meters in El Paso and Albuquerque, New Mexico, in January 1974. Again, there is much more cloud cover in Albuquerque than in El Paso.

on local UVB dose. For comparison with the UVB meter readings, they calculated profiles of UVB doses for the exact locations of the meter stations, using their semi-empiric analytic formula for the erythema-spectrum-weighted daily UVB dose, taking into account seasonal and latitudinal dependence of ozone, and assuming a standard turbidity for clear sky only. Table 2 shows a comparison of the calculations of Green et al. (1974) and actual measurements from UVB meters from eight stations in the U.S. for a one-year period. The calculated values are expressed as joules per square meter, weighted for erythemal effectiveness; the measured values are expressed as counts on an empirical scale designed to give maximum expected values of approximately 1000 counts per half-hour inside the tropics. (All graphic data, as well as the material in Table 2, are expressed in these units.) Of the eight stations for which data for a full year are available, for six the slopes of predicted vs. observed data (0.62 ± 0.08) are in reasonable agreement. The exceptions are Philadelphia (slope .85) and Tallahassee (slope .91), presumably caused by local conditions.

The details of the observations, and their correlations with calculations, are reported by

Berger et al. (1975). A crude correlation of 0.910 was observed between the two sets of data, indicating that approximately 83% of the measurement differences were predictable. An examination of the points suggested that the residual variation was not random. Figure 4 presents 12 months of data for three stations separately. Several significant observations arise from the illustration. First, the deviation of observation from prediction is small: residual variation was less than 10%. Second, the agreement is generally better at northern stations than at southern stations, for reasons discussed by Berger et al. Third, there is a systematic deviation of all regression lines from the origin; the deviations are generally greater at southern sta-

The positive x-intercepts are probably due to the difference in the action spectra of UVB meters and human erythema. Relative to the erythema action spectrum used by Green, the UVB meter overestimates longer-wavelength UV (> 320 nm) and somewhat underestimates UV of wavelengths shorter than 300 nm. Since UV irradiation at wavelengths longer than 320 nm varies less with factors such as sun angle and ozone concentration than does UV below 300 nm, the "zero offset" thus can represent an estimate of the contribution of longer UV to the meter readings. This explanation is consistent with the observation that the offset varies inversely with latitude.

Green (1975b) has recently made an additional series of calculations in which the earth-level ultraviolet dose is weighted for an analytical representation of the sunburning-UV meter action spectrum, normalized to 1 at 300 nm. The increased weighting of the range 300-325 nm, and the inclusion of even longer wavelengths, result in amplification (by about one order of magnitude) of the integral dose estimates, compared to the previous erythema-weighted values. Of greater significance is the fact that when these data are compared to the meter readings, the correlations are essentially unchanged but the positive x-intercept virtually disappears.

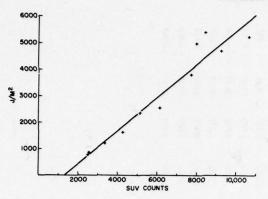
Future temperature corrections of the meters and better estimates of the relative contribution of longer-wavelength radiation to meter readings are expected to make it possible to develop correcting factors for each station,

URBACH AND DAVIES

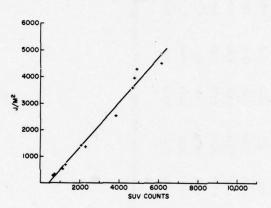
Table 2. Average Daily UVB Doses* by City and Month, for Clear-Sky Conditions (Green and Mo, 1974)

Minneapolis (44.9 N)	Counts	1,627	889	384	280	1,050	1,682	3,271	4,098	5,810	6,414	4,913	3,169
Minne (44.	10 ² 1/m ²	16.8	2.80	1.26	1.46	3.76	9.14	18.91	29.19	36.94	39.05	33.05	20.53
Des Moines (41.7 N)	Counts	2,522	913	653	862	1,264	2,215	3,827	4,810	6,737	7,315	5,042	3,915
Des N	10 ² J/m ²	12.0	4.37	2.18	2.51	5.84	12.75	24.00	34.72	42.21	44.03	38.01	24.98
Philadelphia (40.0 N)	102 J/m ² Counts	2,301	1,137	628	669	1,301	2,092	3,848	4,698	4,891	6,144	4,744	3,497
Philad (40.	10 ² J/m ²	13.56	5.23	2.73	3.11	08.9	14.08	25.40	35.84	43.08	45.51	39.63	26.90
land 3 N)	Counts	2,824	1,403	1,047	1,094	1,889	2,803	5,085	686'9	7,579	7,423	6,238	5,120
Oakland (37.3 N)	10 ² J/m ²	16.27	6.94	3.83	4.25	8.52	16.31	27.59	37.46	44.27	46.60	42.09	30.02
erque (N)	Counts	4,351	2,49	1,49	1,73	2,74	4.96	6,27	8,33	8,84	8,94	66'9	6,39
Albuquerque (35.1 N)	10 ² J/m ²	19.05	8.79	5.17	5.79	11.03	19.99	32.10	41.86	48.07	96.64	45.41	33.32
las N	Counts	3,487	2,002	1,725	1,640	2,877	4,080	5,103	7,365	8,063	7,575	5,800	3,912
Dallas (32.8 N)	10 ² J/m ²	21.69	10.71	6.58	7.24	12.95	22.17	33.93	42.96	48.67	50.83	47.21	35.98
aso	Counts	5,144	3,332	2,494	2,538	4,270	6,156	7,736	9,305	10,695	8,461	8,022	6,380
E	10 ² J/m ²	23.47	12.01	7.63	8.53	15.10	25.39	38.02	47.16	52.41	53.95	49.81	,344 38.17 6,3
assee	Counts	4.228	2.758	1,966	2,255	3,376	4,639	6.416	6,845	7,147	6,337	5.476	5,344
Tallah	10 ² J/m ²	25.09	13.29	8.63	9.57	16.39	26.75	39.08	47.68	52.60	54.30	50.72	39.67 5,344
	Month	Oct	Nov	Dec	Jan	Feb	Mar	Apr	May	Jun	Jul	Aug	Sep

*Doses are given both in joules per square meter of integrated crythema-effective UVB and in Robertson-Berger meter counts (400 counts * 1 minimal crythema dose).



a. El Paso



b. Philadelphia

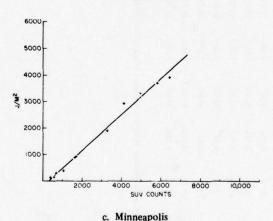


Figure 4. UV radiation, weighted for erythemal effectiveness according to Green et al., 1974, vs. sunburning UV.

which may eventually offer insights into currently unrecognized components of the variation in ultraviolet radiation.

RELATION OF UV FLUX TO CARCINOGENIC ACTIVITY

Available evidence suggests that the latitude gradient of skin-cancer incidence is non-linear. As generally presented, this relationship is described as exponential, relating log of incidence to latitude. Such a representation has two advantages. First, it simplifies the graphic representation of data which vary greatly in magnitude. Second, the exponential relationship is easy to deal with conceptually, since it equates a change in the independent variable to a proportional relative change in the dependent variable; the proportional change is not complicated by the question of the magnitude of the base incidence.

Despite its attractiveness, however, this exponential description has certain disadvantages. Small discrepancies in parameters lead to rather large differences in the appearance of the curve, particularly near its extreme, and to larger differences if extrapolation is attempted. A more fundamental problem is discussed below. Moreover, the data available at present are inadequate in both quality and quantity to provide unambiguous support for an exponential description, although, as indicated, they do suggest a non-linear relationship.

There is obviously a relationship between latitude and solar-energy intensity, and this gradient is greatest in the ultraviolet portion of the spectrum. Although the shape of this relationship is relatively complex and dependent on a number of variables, for a range of mid-latitude values (30°-50°) the form closely approximates a straight line (see, e.g., Green et al., 1974). The integrated weighted measurements of annual dose obtained at eight stations are also in good agreement with a linear latitudinal gradient; although there is considerable scatter in the data. there is no significant improvement in the correlation when simple non-linear (e.g., exponential, second- or third-order) relationships are examined. It thus appears that at least for latitudes corresponding to the continental United States a linear description of the latitude UVdose relationship is adequate.

There is good experimental evidence that changes in UV dose produce changes in skincancer incidence in animals, and presumably in

man (Blum, 1975). Nevertheless, all investigators appear to agree that there are additional latituderelated variables which modify the relation of surface dose to epidemiologic effects. This conclusion is based in part on the indication of non-linearity in the incidence/latitude curves, and in part on the intuitive concept that latituderelated climatic and behavioral effects must modify the dose actually reaching the target population. The factors involved and their magnitude are largely speculative. McDonald (1971) suggested that they contribute about 50% to the observed gradient, and van der Leun and Daniels (1975) consider this a not-unreasonable estimate. To accept such an estimate in conjunction with an exponential incidence/dose relationship, however, implies that these "other factors" are also exponentially related to latitude. If the assumed magnitude of these factors is speculative, an assumed exponential relationship is considerably more so.

If the input of potentially biologically effective UV is linearly related to latitude, and if the factors relating this input to skin cancer are also latitude-dependent, it follows that the relationship of skin-cancer incidence to latitude must be non-linear. If, for example, the modifying factor were a linear function of latitude, skin-cancer incidence would be a second-order function of latitude. While available data are inadequate to argue convincingly for or against such a description, the apparent curvilinearity of the epidemilogic data can be accommodated as well by a second-order relationship as by an exponential relationship.

For modeling purposes, therefore, we have made the following set of assumptions.

- Biologically-active UV dose is a linear function of latitude, within the limits of immediate interest.
- 2. There exists a latitude-dependent "effectiveness factor" which relates the input of biologically-active UV to the biologically effective dose actually reaching the target population. The magnitude of this factor is unknown; in the absence of direct information we assume it to be a linear function of latitude.

3. The incidence of skin cancer is a function of the "effective dose" of biologically-active UV, that portion of the input dose which actually reaches the target population. Again, in the absence of adequate data for man, we assume this relationship to be linear. By inference, therefore, we assume incidence to be second-order with respect to latitude.

The available data from the eight UV meters make it possible to estimate the linear input-dose/latitude relationship, shown in Figure 5. There is no basis for direct estimation of the effectiveness factor; we have made an indirect estimate based in part on the reasoning of Robertson (1972). In one of several attempts to relate UV dose to skin cancer, Robertson considered the number of days on which a certain minimum UV dose was delivered. A daily total dose of 9 minimal erythema doses (MED's) or 3600 counts of the UV meter was considered "ineffective" for skin carcinogenesis if repeated for the adult lifetime of the average susceptible man. (For a description of the reasoning, see Robertson (1972).)

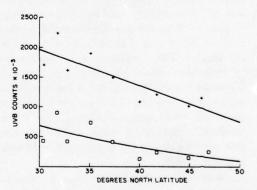


Figure 5. Annual sunburning-UV counts vs. latitude.
+, gross annual SUV, representing data
from Robertson-Berger meters at nine
locations in the U.S. p, effective annual
SUV, representing annual total SUV exceeding 3600 counts/day from the same
Robertson-Berger meters.

Such a formulation has the appearance of a dose "threshold," a concept which is anathema to most photobiologists. Robertson properly described it, however, as a "quasi-threshold" which would be expected if the detection level

for the (quantal) response were greater than zero, or if competing processes (repair, regeneration, rejection, etc.) were operative. As used by Robertson, the "threshold" is simply a go/no-go sorting device, with time intervals being classified as effective or ineffective; the absolute dose is not otherwise considered. For our purposes, however, dose is the component of interest. We therefore adopted Robertson's 3600 counts/day minimum dose as a basis for calculating integral "overdose," the dose in excess of the threshold accumulated at each station. This was accomplished by plotting the mean daily dose for each month, connecting the points, and measuring the area within this curve and above 3600 counts/day (9 × 400 counts, the approximate value of one minimal erythema dose, comparable to Robertson's "sunburn unit"). These integrated values were taken to estimate "effective dose," and are shown fitted to a second-order curve in Figure 5. (Although the second-order fit was not significantly better than a first-order fit, our model requires that "effective dose" be secondorder with respect to latitude.) The ratio of the second-order effective-dose equation to the firstorder total-dose equation is a first-order expression of "effectiveness" as a function of latitude (Figure 6). Both the elevation and the slope of this line are of course dependent on the threshold selected. The 9 units/day value was chosen by Robertson as approximating an average midwinter day in the tropics, and is lower than the midsummer dose in Galway, Ireland, where appreciable skin cancer occurs; if this "quasithreshold" approach is valid, the 9-unit value thus provides about the largest gradient consistent with reality.

With an equation for estimated effective dose in hand, we can relate incidence to effective dose. For the purposes of the present study, the incidence data of Scotto et al. (1974), though limited to four locations, provide the most inter-comparable set of estimates. Best-fit straight lines were calculated for the four experimental incidence values against the expected effective dose (derived from the best-fit second-order equation), for both males and females, and adjusted incidence values for each location were the from these lines. For each latitude the manufacture of the second se

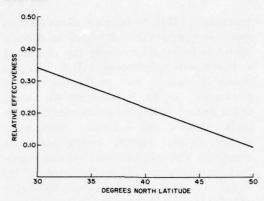


Figure 6. UV effectiveness as a function of latitude, expressed as the ratio of the second-order-fit equation of effective dose (gross annual minus threshold) to the first-order-fit equation of gross annual dose.

increase in effective dose, since the effectiveness factor is a constant at a given latitude. The corresponding incidence was then calculated as a function of the increased effective dose, and expressed relative to the original adjusted incidence. The results (see Table 3) show a small latitude gradient, for both males and females, and represent about a 10-15% increase in incidence for a 10% increase in UV. Taken in conjunction with the previously mentioned 1:2 relation of changes in ozone to changes in UV dose, this indicates a 10-15% increase in skin cancer for a 5% decrease in ozone. In contrast, a calculation based on the assumption of a linear relationship of cancer incidence to total counts (Table 4) suggests a much steeper latitude gradient.

We do not suggest, of course, that the first 3600 counts per day represent ineffective radiation. Instead, we are using an admittedly arbitrary device to estimate the effectiveness of current doses, with the assumption that the same proportionate effectiveness would be observed with increased (or decreased) doses. The use of different "thresholds" (pseudothresholds) for such estimates leads to quantitatively different but qualitatively similar results (in Table 4). The relevant conclusion, independent of the method used to estimate current relative effectiveness, is that if the response (carcinogenesis) is a function of the received dose, and if there are intervening latitude-dependent modifiers of reception (exposure), the response must be a non-linear

Table 3. Effect of a 10% Increase in Biologically Effective Ultraviolet Radiation on Incidence of Skin Cancer*

		Incidence Per 10	00,000	Percent Inc	crease
	Scotto (1974)	Adjusted	Increased	Linear With "Effective SUV"*	Linear With Total SUV
Minneapolis					
Males	179	121.19	137.82	13.72	40.53
Females	104	69.81	77.39	10.85	31.48
Iowa					
Males	157	188.86	212.26	12.38	27.81
Females	74	100.66	111.32	10.59	23.84
San Francisco					
Males	229	303.22	338.06	11.48	21.27
Females	123	152.78	168.66	10.39	19.30
Dallas					
Males	494	445.72	494.80	11.01	18.29
Females	240	217.73	240.10	10.27	16.91

^{*}Based on Urbach and Davies' model (1975)

Table 4. Estimated Effectiveness Factor at Various
Locations for Selected Pseudothreshold
Levels

	Pseudo	threshold l	Level (cou	nts/day)
Location	1200	2400	3600	4800
Minneapolis	0.54	0.31	0.16	0.06
Iowa	0.65	0.42	0.24	0.11
San Francisco	0.70	0.48	0.32	0.18
Dallas	0.72	0.48	0.30	0.17

function of latitude and thus (at least for midlatitudes) of total biologically active dose.

Like all others, this model cannot presently be adequately tested because of the scanty epidemiologic data base. Its virtue, we believe, lies in offering an alternate explanation for a non-linear gradient of skin-cancer incidence with latitude (while avoiding the hazard of postulating an exponential effectiveness factor), and in postulating that equivalent delivered doses have equivalent effects. Its weaknesses include the absence of a clear measure of "effective dose," and the apparent inconsistency between its postulates of linear dose-effect relationship and the results of experimental animal data. With regard to the latter question, however, it is by no means clear that step changes in uniform repeated doses produce the same effects as

equivalent step changes in cumulative annual exposure.

In summary, the various models attempting to relate decrease in atmospheric ozone to a possible increase in skin cancer result in the following "amplification factors":

 Increase in UVB due to reduction in ozone concentration in the stratosphere:

Optical "amplification" factor: 2X (range 1.4 to 2.5)

 Increase in skin-cancer incidence due to increase in UVB radiation at ground level:

Biological "amplification" factor: 1X (range 0.5 to 2)

 Increase in skin-cancer incidence due to reduction in ozone concentration in the stratosphere:

Total "amplification" factor: 2X (range 0.7 to 5.0)

If the skin-cancer incidence figures of Scotto et al. (1974) are used as a baseline, with a 2× "amplification" factor, a 5% reduction in ozone concentration could result in an increase of 37 cases of skin cancer per 100,000 population a year at the latitude of Dallas/Forth Worth, Texas, and an increase of 12.4 cases of skin cancer per 100,000 population a year at the

latitude of Iowa. On the assumption that the incidence of non-melanoma skin cancer in the United States is approximately 165 per 100,000 (Scotto, 1975), a 5% decrease in stratospheric ozone concentration could result in an average increase in the United States of 16.5 cases of skin cancer per 100,000, or a total of approximately 30,000 new cases per year.

It cannot be stressed too strongly that all the calculations by all the authors who have attempted to provide such estimates are subject to great (and at this time not measurable) uncertainty, much of which is inherent in the uncertainty of growth of cell populations in cancer (Blum, 1975). For this reason, until much better data — at least on the effects of shifts in spectral distribution of UV radiation, effects of flux, time-dose relationships, and on-off (seasonal) cycles of irradiation — and much more reliable information on the true incidence of skin cancer are available, all the numerical estimates must be treated as very preliminary, and open to significant correction as new information accumulates.

The skin cancers discussed in the above section are principally the basal- and squamouscell carcinomas. The melanomas have not been included. The incidence of malignant melanomas. although small, also shows a marked latitude gradient, and the death rates from the two broad groups of primary neoplasms of skin are highly correlated in the states and provinces of the United States and Canada. The importance of the malignant melanomas lies in the high proportion of those affected who die (with current methods of treatment it is about 40%, a figure comparable to that of breast cancer). It can be assumed that the extra deaths from squamous-cell carcinomas produced by an environmental change will be associated with an approximately equal number of deaths from malignant melanoma. If the present clinical features of the tumors are unaltered, these melanoma deaths will occur in much younger people than the deaths from other skin cancers.

Furthermore, the preceding observations on the relationship between exposure to sunlight and the incidence of skin cancers and melanomas have largely referred to a static situation. There have been hints that the incidence of skin tumors of all types is rising, but there remains the difficulty of being certain that improving methods of diagnosis and counting have not been largely responsible for this rise. Mortality rates from skin tumors are approximately stable in both the United States white population and in Canada. However, investigation of these rates in both countries shows that the mortality from melanomas is rising rapidly, while that from other skin cancers is declining. Furthermore, the death rates are rising in the younger age groups, and declining in the elderly. The reasonable explanation of these changes is that improvements in medical care (earlier diagnosis, better surgery, and radiotherapy) are reducing the mortality from the squamous-cell carcinomas (better definition of cause of death may also play a part), while the improvements in treatment are failing to keep pace with the rising incidence of melanomas. The changes in the age distribution of the deaths support this, as the average melanoma patient is much younger than the patient with a squamous-cell tumor. Thus, if we are to make projections into the future, we should estimate the incidence of human skin tumors in terms of the levels likely to be reached by the continuation of present trends (which of course are based on human behavior, which is changeable).

Finally, it must be clearly pointed out that all estimates concerning effects of stratospheric ozone depletion on the incidence of skin cancer in man represent conditions which could be expected to exist after a new steady state of both UV radiation and skin-cancer incidence have been reached. Since it is assumed that the development of skin cancer is related to accumulated lifetime UV dose, a new steady state in skin-cancer incidence for a population will not be reached until all members of that population have been exposed to the new level of increased UV over a considerable part of their lifetime. Cutchis (1975) has estimated the manner in which skin-cancer incidence may be expected to build up from an initial to a new equilibrium rate. Assuming a sudden increase in UVB, Cutchis shows that one-quarter of the expected increase in skin-cancer incidence would develop about 10 years after such an event, and that if the UVB irradiance were returned to its original level at this time it would take about 60 years for the skin-cancer incidence to return to its baseline level. Since UVB changes are not likely to occur

suddenly, there will be time in which to carry out pertinent experiments which should allow considerably more accurate estimates of potential risks to man to be made.

ACKNOWLEDGMENTS

The UV meters utilized in these studies were designed and evaluated by Daniel Berger of the Skin and Cancer Hospital in Philadelphia, and Donald F. Robertson of the University of Queensland. The calculations of UVB utilized in this study were performed by Alex E. S. Green and his staff, of the Department of Physics and Astronomy at the University of Florida. The studies were supported by a contract from the DOT Climatic Impact Assessment Program and a grant from the NIH National Institute of Environmental Health.

REFERENCES

- Berger, D. (1975), personal communication.
- Berger, D., D.F. Robertson, and R.E. Davies (1975), "Field measurements of biologically effective UV radiation," Appendix D to Chapter 2 of CIAP Monograph 5, Part 1, U.S. Dept. of Transportation, DOT-TST-75-55, 2-233 2-262.
- Blum, H.F. (1959), Carcinogenesis by Ultraviolet Light, Princeton U. Press.
- Blum, H.F. (1969), "Is sunlight a factor in the geographic distribution of skin color?," Geo. Rev. 69,
- Blum, H.F. (1974), "Uncertainty of growth of cell populations in cancer," J. Theor. Biol. 46, 143.
- Blum, H.F. (1975), "Ultraviolet radiation from the sun and skin cancer in human populations," Appendix A to Chapter 7 of CIAP Monograph 5, Part 1, U.S. Dept. of Transportation, DOT-TST-75-55, 7-87 7-103.
- Chavaudra, J. and R. Latarjet (1973), "Influence des variations de l'ozone atmosphérique sur certaines activités biologiques du rayonnement ultraviolet solaire," Comp. Rend. Acad. Sci. D276, 3841.
- Coblentz, W.W. and R. Stair (1934), "Data on the spectral erythemic reaction of the untanned human skin to ultraviolet radiation," U.S. Bureau of Standards Journal of Research 12, 13-14.

- Cripps, D.J. and C.A. Ramsay (1970), "Ultraviolet action spectrum with a prism-grating monochromator," Brit. J. Derm. 82, 584-592.
- Cutchis, P. (1975), "Estimates of increase in skin cancer incidence with time following a decrease in stratospheric ozone," Appendix D to Chapter 7 of CIAP Monograph 5, Part 1, U.S. Dept. of Transportation, DOT-TST-75-55, 7-141 - 7-169.
- Freeman, R.G. (1975), "Data on the action spectrum of ultraviolet carcinogenesis," J. National Cancer Inst. 55, 1119-1121.
- Green, A.E.S. (1975), "Ultraviolet, ozone and skin cancer," Appendix C to Chapter 7 of CIAP Monograph 5 (Part 1), Dept. of Transportation, DOT-OST-75-55 (part 1), 7-127 7-140.
- Green, A.E.S. and T. Mo (1974), "An epidemiological index for skin-cancer incidence." in *Proceedings of* the Third Conference on CIAF (Cambridge, MA), U.S. Dept. of Transportation, DOT-TSC-OST-74-15, 518.
- Green, A.E.S., T. Mo and J.H. Miller (1974), "A study of solar erythema radiation doses," Photochem. Photobiol. 20, 473-482.
- Green, A.E.S., T. Sawada, and E.P. Shettle (1974), "The middle ultraviolet reaching the ground," Photochem. Photobiol. 19, 251.
- Komhyr, W.D., R.D. Gross, and G. Slocum (1973), "Total ozone increase over North America during the 1960's," Pure Appl. Geophys. 106-8, 981.
- Latarjet, R. (1935), Revue d'Optique Théorique et Instrumentale 14, 398-414.
- London, J. (1974), "Global trends in total atmospheric ozone," Science 184, 987.
- Magnus, I.A. (1974), personal communication.
- McDonald, J.E. (1971), testimony in Congressional Record of March 19, Vol. 117, 3493.
- Mo, T. and A.E.S. Green (1974), "A climatology of solar erythema dose," Photochem. Photobiol. 20, 483-496.
- Mo, T. and A.E.S. Green (1975), "Systematics of climatic variables and implications – local erythemal doses," section 2.2.6 of CIAP Monograph 5, (Part 1), Dept. of Transportation, DOT-OST-75-55 (part 1), 2-74 to 2-78.

- Robertson, D.F. (1972), "Solar Ultraviolet Radiation in Relation to Human Sunburn and Skin Cancer," thesis, University of Queensland.
- Schulze, R. (1974), "Increase of carcinogenic ultraviolet radiation due to reduction in ozone concentration in the atmosphere," in Proceedings of the International Conference on the Structure, Composition and General Circulation of the Upper and Lower Atmospheres and Possible Anthropogenic Perturbations (Melbourne), pub. IAMAP, 479-493.
- Scotto, J. (1975), personal communication.
- Scotto, J., A.W. Kopf, and F. Urbach (1974), "Non-melanoma skin cancer among whites in 4 areas of the U.S.," Cancer 34, 1333.
- Setlow, R.B. (1974), "The wavelength in sunlight effective in producing skin cancer: A theoretical analysis," Proc. Nat. Acad. Sci. 71, 3363.

- Shettle, E.P. and A.E.S. Green (1974), "Multiple scattering of the middle ultraviolet reaching the ground," Appl. Opt. 13, 1567.
- Urbach, F. and R.E. Davies (1975), "Estimated effect of increased UV-B on skin cancer (basal cell and squamous cell cancer)," section 7.4.2 of CIAP Monograph 5 (Part 1), Dept. of Transportation, DOT-OST-75-55 (part 1), 7-46 7-60.
- van der Leun, J. and F. Daniels, Jr. (1975), "The biologic effects of stratospheric ozone decrease: A critical review of assessments," Appendix B to Chapter 7 of CIAP Monograph 5 (Part 1), U.S. Dept. of Transportation, DOT-TST-75-55 (part 1) 7-105 7-124.
- Wetzel, R. (1959), "On the effectiveness spectrum of the carcinogenic features of ultraviolet light," Arch. Geschwulstforsch. 15, 227.

POTENTIAL EFFECTS ON AQUATIC ECOSYSTEMS OF INCREASED UV-B RADIATION

D. STUART NACHTWEY*

Oregon State University Corvallis, Oregon

ABSTRACT: Solar UV-B even at current irradiance levels can kill or detrimentally affect a wide variety of aquatic organisms, e.g., bacteria, algae, protozoans, small invertebrates, and vertebrates (early developmental stages). Populations of organisms survive because they have evolved a variety of mechanisms for coping with solar ultraviolet radiation. Increased UV-B may have effects on natural ecosystems by overwhelming these mechanisms. For example, studies with a model unicellular alga, Chlamydomonas, indicate that the total dose that these organisms can tolerate without significant mortality is much less at increased dose-rates. The dose-rate effect may involve UV damage to repair systems.

As an approach to a first-approximation assessment of the impact of an increase in UV on aquatic ecosystems, I and my colleagues, H. Van Dyke and B.E. Thomson at Oregon State University and John Calkins at the University of Kentucky, have exposed a wide variety of organisms to simulated solar UV-B radiation (290 nm - 315 nm). We initially proceeded on the assumption that if we did not obtain a detrimental effect from UV-B at irradiance levels expected for up to a 50% reduction in the stratospheric ozone layer, then there would be a low probability that any increase in UV-B resulting from a smaller ozone decrease would have a biospheric impact. It soon became apparent, however, that solar UV-B at present irradiance levels can kill a wide variety of aquatic organisms with just a few hours' exposure.

Figure 1 shows a representative sampling of dosage-mortality curves from a survey of basic sensitivities of freshwater algae (McKnight and Nachtwey, 1975). The algae were exposed on agar plates to simulated solar UV-B from Kodacel-filtered FS-20 fluorescent sunlamps (see Sisson and Caldwell (1975) for the spectral output of this lamp/filter combination). The plates were then incubated in alternating 12-hour periods of light and of dark, and scored for mortality after three to five days by counting live colonies and dead cells.

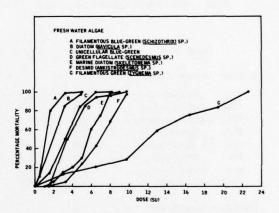


Figure 1. Mortality curves for various algae. The dose is expressed in sunburn units (SU).

From curves such as those in Figure 1, the doses that are lethal to 50% (LD₅₀) or to 90% (LD₉₀) of the population can be interpolated. The doses are expressed in terms of sunburn units (SU), a relatively arbitrary unit which represents 400 counts on a Robertson-Berger sunburning-ultraviolet meter (Berger et al., 1975). For our purposes it will probably suffice to point out that 1 SU is, on average, the amount of solar radiation required to produce a minimally perceptible sunburn on untanned Caucasian skin. For the sake of further reference, consider that in Corvallis, Oregon (latitude

^{*}Dr. Nachtwey is now with the Experiment Definition and Special Projects Branch of the NASA Johnson Space Center in Houston.

44°41′N) in June the peak dose-rate at solar noon is about 3 SU h⁻¹ and the total dose for a summer day is about 20 SU. The LD₅₀ and LD₉₀ values for the algae tested so far are ranked in increasing order in Table 1. Table 2 gives LD₅₀ data for a variety of other aquatic organisms. These latter data were interpolated from the graphically presented results of Calkins (1975b). Inspection of the data reveals a wide range in LD₅₀ values, and shows that the LD₅₀ for most of the organisms falls below 6 SU. This dose is what one would obtain in about 2 hours around noon at mid-latitudes on a clear day in the summertime. The highest LD₅₀, 12 SU, is still less than a day's dose in June in Corvallis.

Table 1. Basic Sensitivities of Various Algae

1	Designation*	LD ₅₀ (SU)	LD ₉₀ (SU)
Filamento	us Algae (Genus)		
FBG-1	(Schizothrix)	1	2.5
FG-6	(Stichococcus)	1.4	3.2
FG-1	(Stigeoclonium)	3.0	≈11
FG-5	(Stigeoclonium)	3.7	4.9
FG-2	(Stigeoclonium)	4.8	8.0
FG-3	(Tribonema)	4.8	8.0
D-6	(Skeletonema)	5.7	7.6
FG-4	(Zygnema)	12.0	20.8
Unicellular	Algae (Genus)		
D-5	(Navicula)	1.8	3.7
D-1	(Navicula)	2.6	4.5
D-2	(Navicula)	3.1	5.9
FL-1	(Scenedesmus?)	3.2	5.9
Chlamy	domonas reinhardi	3.2	4.8
BG-1	(unknown blue-green)	3.2	5.4
D-4	(Navicula)	3.6	6.0
D-3	(Navicula)	3.8	6.0
DES-1	(Ankistrodesmus)	7.0	9.3

^{*}FBG = Filamentous Blue-Green

The mean LD_{50} for both sets of data is 3.8 (\pm a standard deviation of 3.1) SU; the median is 2.4 SU, with 85% of the organisms tested having an LD_{50} below 7 SU. Thus, for a large number

Table 2. Lethal Responses of Bacteria, Yeast, Protozoans, and Invertebrates

	Nominal LD ₅₀ *
Organism or Genus	(SU)
Bacterium A	≈0.2
В	≈0.2
C	≈0.4
D	≈0.5
E	≈0.8
F	1.0
G	9.5
H	≈0.1
I	≈0.2
J	≈0.5
K	≈0.7
L	1.8
M	0.2
N	0.3
0	0.6
P	≈12
Q	0.2
R	0.6
S	1
T	≈12
Shigella	7
Pseudomonas	6
Aeromonas	2.4
Shigella	0.4
Coryneform bacteria	0.4
Yeast	1
Cyclidium	6.5
Tetrahymena (Texas S-12 strain)	7.6
Tetrahymena (Kentucky S-30)	6.4
Paramecium	4
Paramecium	4
Vorticella	3
Roundworm	4.8
Flatworm	≈4
Large rotifer	0.8
Cypris	5.5
Daphnia	3.3
Cyclops	2.6
Aedes aegypti	3.0

^{*}Interpolated from graphs in Calkins (1975b).

of organisms, less than two hours' exposure to solar UV-B at irradiance levels currently found in the mid-latitudes can kill a significant fraction of a population.

The organisms discussed above were irradiated as a single layer of cells on agar and not allowed to avoid the irradiation, so the results reflect the basic sensitivity or the basic tolerance of the organisms. The basic tolerance is the result of several factors:

FG = Filamentous Green

D = Diatom

FL = Flagellate

BG = Blue-Green

DES = Desmid

- a. Screening of the sensitive target molecules by radiation-absorbing nonessential molecules. In the case of algae, there is some absorption of UV-B photons by cell wall material, chlorophyll and other pigments, proteins, and ribonucleic acid (RNA). Absorption of photons by these molecules may lead to damage of the molecule, but for the most part damaged molecules of these kinds are present in large numbers in the cell and are replaceable, so they are not likely to be essential. Photons absorbed by these substances do not reach the presumed critical target molecule, DNA (deoxyribonucleic acid), the carrier of genetic information in the cell. DNA damaged by absorption of photons can be lethal to the cell.
- b. Repair of UV-damaged DNA. Even though some photons get through the screen and are absorbed and damage DNA, almost all cells have enzymatic mechanisms for repairing damaged portions of DNA. At least three repair mechanisms are recognized: photoreactivation, excision-repair, and postreplication repair. The first requires an enzyme and visible light (violet to green) to supply the energy to break apart a bond that formed after the absorption of the UV photon. This bond produces a chemical lesion in DNA, which is called a pyrimidine dimer. The second repair system consists of a cutting away of the damaged portion of one strand of the DNA double helix and replacing the portion with new building blocks (purines and pyrimidines), using the remaining strand as a template. The third enzyme system replicates around the lesions in DNA and then repairs them later, using undamaged strands of the DNA duplex to provide the information for putting in the correct building blocks. The second and third types of repair systems collectively called dark-repair systems.
- c. Cell division delay, possibly for repair time. A prominent feature in the response of almost all cells to UV radiation is a delay of cell division. Certain

- evidence (Nachtwey and Giese, 1968; Hodge and Nachtwey, 1972) indicates that cell division delay may represent an evolved mechanism by which organisms are allowed time for repair of UV-induced damage before it is "fixed" by cell division to become lethal.
- d. Restriction of cell division to night. Many cell types are more sensitive to the lethal effects of UV radiation during cell division than at any other time in their cell cycle (progression from one cell division to the next). Such extra sensitivity may result from damage's being "fixed" in some way before it can be repaired. Many unicellular algae have evolved a complicated reproductive pattern in which they grow quite large during the day (by photosynthesis) and then proceed through a series of rapid cell divisions at night to yield 4, 8, 16 and sometimes 32 cells. This complex pattern of reproduction may have evolved as a mechanism for coping with the increased sensitivity to UV prior to and during cell division (see Figure 2).

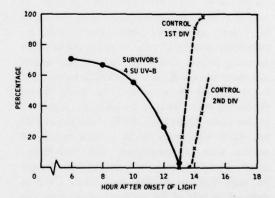


Figure 2. Survival of synchronized Chlamydomonas reinhardi following UV-B irradiation at various times late in the generation cycle. Cells were synchronized and maintained under a 12-hours-light/12-hours-dark regime. Under these conditions, cells divide two (and sometimes three) times in rapid succession during the 13th to the 15th hours after the onset of light. The dashed curves represent the cumulative percentage of control cells that had divided once (1st DIV) or twice (2nd DIV) by the times indicated on the abscissa. Experimental cells were irradiated with 4 SU from Kodacel-filtered FS-20 sunlamps.

At the third CIAP conference Calkins (1974) pointed out that reproduction by survivors could replace organisms killed by UV-B. As long as the dose of UV-B does not exceed a certain "replacement limiting dose" (RLD) for each species of organism, then, according to his model, populations could survive. The computation of the RLD accounts for division delay as well as reproductive death. The RLD's for bacteria, protozoans, and small invertebrates range from approximately 1.25 to 12 SU.

Even when all of the above mechanisms for coping with UV-B are operating, the basic sensitivities or RLD's are still such that a couple of hours of direct solar UV-B can kill most of a population of unicellular organisms. Yet populations of organisms survive in nature. They must therefore rely on additional means to cope with UV-B.

The most important is avoidance. Some organisms hide during the day and are active only at night. The large populations of zooplankton that constitute the sonic scattering layer(s) remain in the darker depths of the ocean during the day and rise to the surface at dusk to feed. (This movement may not represent only an escape from ultraviolet radiation, however; it may also be a mechanism for avoiding predators. If it were merely an escape from UV-B, the organisms would not need to move the hundred or more meters that they do.) Natural waters attenuate the UV-B more than visible light; UV-B is attenuated to a greater or lesser extent depending upon what is dissolved or suspended in the water (Zaneveld, 1975). Calkins (1975a) has made measurements in a wide variety of waters with a submerged Robertson-Berger meter. Table 3 is adapted from his data. It may be seen that, in all but two cases, UV-B is reduced to half of the surface irradiance by less than 60 cm of lake or ocean water (the two exceptions were for particularly clear waters off the coast of Puerto Rico). Note also that in some cases UV-B is halved by less than 10 cm.

Phytoplankton, of course, need light for photosynthesis, and so must remain nearer the surface than zooplankton. But phytoplankton probably use the attenuation of natural waters to some extent to avoid UV-B. Many mobile phytoplankton show a well-developed behavioral response to light: they swim toward a low-to-moderate-intensity light source (positive phototaxis) and away from a high-intensity light source

Table 3. UV-B Transmission Characteristics of Various Waters*

Site and Station	Transmission Per Meter (%)	Z ₅₀ ** (cm)
Puerto Rico		
C	85	436
i	77	271
E	26	51
A	0.6	13
Lake Huron		
C	30	57
В	29	57
A	28	54
Lake Superior		
C	29	56
В	24	49
A	21	45
D	6×10 ⁻³	7
Delaware Bay		
D	26	51
В	22	46
E	19	42
C	16	37
A	10	30
Lake Michigan		
В	26	51
С	21	45
D	21	45
A	19	41
Lake Erie		
D	10	30
В	8	27
C	8	28
E	8	27
F	3	19
Chesapeake Bay		
C	4	21
D	3	20
E	3	19
Patuxent River		
F	3	20
G	3	19
В	2	18
I	2	18
A	2	17
Н	1	16
J	1×10 ⁻²	7.5
Douglass Lake (MI)		
A	9×10 ⁻⁴	6
В	6×10 ⁻⁴	6

^{*}Measured with Robertson-Berger meter (Calkins, 1975a)

^{**}Depth at which surface intensity reduced to half

(negative phototaxis), thus exposing themselves to solar UV-B at a lower dose-rate. Even so, since the daily dose of biologically effective UV-B received at the water's surface is, for a number of organisms, many times the LD50, it is still possible that UV-B will kill organisms at depths where they receive a much reduced dose-rate. For example, in cases where the total daily dose at the surface is 10 times the LD50, the organisms would still be killed at depths where the dose-rate is 10% of the surface dose-rate, provided that reciprocity of exposure duration and dose-rate holds. Reciprocity, however, does not necessarily hold in all cases; it is possible that repair and replacement processes can keep pace with damage processes when the damage is produced slowly enough, so there may be some threshold dose-rate below which killing is not induced. This possibility was examined with a model system, the unicellular organism Chlamydomonas reinhardi. It was found that reciprocity fails.

Figure 3 shows the survival of Chlamydomonas as a function of dose of UV-B administered at a variety of dose-rates. Figure 4 shows the LD_{50} 's and LD_{90} 's, interpolated from the curves in Figure 3, as a function of dose-rate. A strong dose-rate dependency may be noted; if reciprocity had held, a straight line parallel to the abscissa would have been obtained. The LD_{50} 's obtained with varying dose-rates of UV-B show a break in the dose-rate dependency curve, with a marked increase in tolerance below approximately 2.5 SU h⁻¹.

Figure 5 shows the duration of exposure to UV-B required to kill 50% and 90% of a population of *Chlamydomonas* as a function of dose-rate. It may be seen that halving the dose-rate from 2 to 1 SU h⁻¹ results in more than a doubling of the exposure required to kill either 50 percent or 90 percent. Likewise, halving the dose-rate from 4 to 2 SU h⁻¹ again leads to more than a doubling of the exposure needed for a given mortality.

If we accept for the sake of further analysis some level of killing between 50% and 90% as the tolerance level at which a population of *Chlamydomonas* can replace itself overnight by cell division (see Replacement Limiting Dose model of Calkins (1975b)) and if we accept that organisms will be subjected to the maximum dose-rate for only the four hours centered

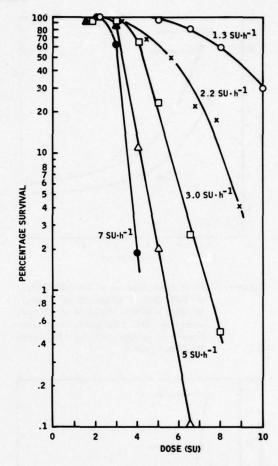


Figure 3. Survival curves of synchronized Chlamydomonas reinhardi irradiated with UV-B from Kodacel-filtered FS-20 sunlamps at various dose-rates.

around geographic noon (Green and Mo, 1975), we can estimate the tolerance dose-rate for Chlamydomonas as being a little less than 2 SU h⁻¹. According to Robertson (1975), between about 45° latitude and the equator, the maximum surface dose-rate might be expected to range from about 3.5 to 5 SU h⁻¹ at sea level on a clear day. Thus, it is reasonable to suppose that organisms must find that depth which reduces the surface UV-B irradiance by about a half to be able to survive under present conditions. As can be determined from the data in Table 3, for most natural waters, this depth would be less than a meter.

It is also reasonable to suppose that an increase in UV-B such as that which might result

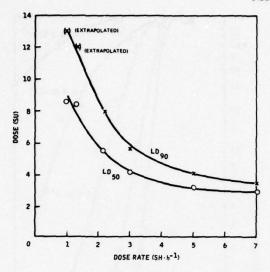


Figure 4. UV-B doses required to kill 50% (LD₅₀) or 90% (LD₉₀) of samples of *Chlamy-domonas reinhardi* irradiated at different dose-rates. The data points were interpolated (or extrapolated) from the curves shown in Figure 3.

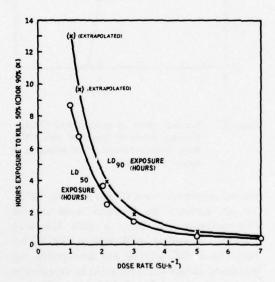


Figure 5. Duration of exposure required to kill 50% (LD₅₀) or 90% (LD₉₀) of Chlamy-domonas reinhardi when irradiated at the dose-rate indicated on the abscissa. The data points were calculated from the values shown in Figure 4.

from a depletion of the ozone layer would just drive organisms deeper. However, microscopic observations show that organisms swim up and down into and out of regions of damaging high-dose-rate UV-B. They also swim in and out of shade and over and under each other in clumps of cells. They are thus exposed to a constantly varying dose-rate or even a fractionated or "flashed" dose: Figure 6 shows that flashing of UV-B radiation at a high dose-rate (3 seconds at 3.4 SU h⁻¹, 3 seconds off) produces the same biological effect as administering the radiation continuously at half the dose-rate. Thus, the lethal effectiveness of UV-B at high dose-rates can be ameliorated by intermittent periods of no, or low-dose-rate, exposure. However, how do organisms "know" when to swim into shade or a low-dose-rate region after they

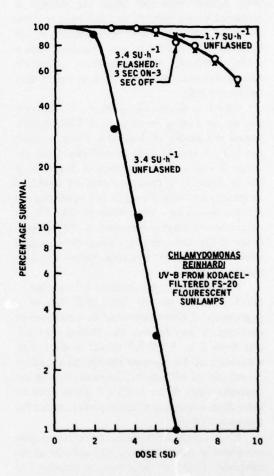


Figure 6. Survival curves for *Chlamydomonas* cells exposed to UV-B at 3.4 SU h⁻¹ (O) or 1.7 SH h⁻¹ (X) continuously (i.e., unflashed) or exposed to 3.4 SU h⁻¹ "flashed" at 3 sec on and 3 sec off.

have accumulated sublethal damage in a high-dose-rate region? It seems unlikely that organisms in some way sense how much damage they have received and spend an appropriate time in the shade to repair it. It seems more likely that their normal behavior pattern in response to light intensity, gravity, O_2 and CO_2 tension, and probably other factors leads to a tolerable exposure situation.

If organisms survive current UV-B irradiances as a result of a complex behavior pattern that has evolved over eons in response to many factors, the key question for assessment of the effect of an increase in UV-B irradiance is, will organisms adapted to a particular zone of depths be able to move deeper in response to a change in one of the factors, UV-B? We don't know. (Of course, if organisms cannot for some reason alter the zone in which they live, they would suffer from the disproportionate increase of the killing effect with increase of UV.)

Even if organisms can move deeper in response to an increase in UV-B, other factors may enter into their ability to survive. Consider that various algae may spend much of their time toward the surface of waters, especially on cloudy days. Consider then what happens when the clouds dissipate. The swimming speed of an organism then becomes a critical factor. For example, Chlamydomonas swims at 6 mm min⁻¹ or 36 cm h-1. If it is at the surface of water with a 50% transmission depth of 60 cm when the clouds move away from a sun emitting at 3 SU h⁻¹, and if it immediately starts swimming down, it can reach a tolerable level of 2 SU h-1 at 32 cm in a little less than an hour. It will have been exposed during its trip to an average doserate of 2.5 SU h-1, but will not have accumulated a lethal dose. (It will have accumulated some sublethal dose, which it may need to compensate for by going down further. However, can cells "know" the dose-rate-weighted dose they have received?) To simplify matters, let us assume that if a cell reaches a 2 SU h-1 region before accumulating a lethal dose it is "safe." Let us also assume that the lethal dose (LD50) is the one for the average dose-rate to which it is exposed. In the scenario just outlined, and with the assumptions just made, the organisms suddenly exposed to 3 SU h⁻¹ sunlight could be safe. Presumably the organisms in such an environment have evolved by natural selection to be able to handle such a contingency; certainly it must

happen frequently in nature. Now consider a 16% reduction in ozone, which, according to an interpolation of Schulze's (1974) estimates, increases the previous 3 SU h-1 sun to 4 SU h-1. With the same scenario and assumptions as above, a Chlamydomonas cell will accumulate a lethal dose before it can get to a safe region: It needs to reach about 60 cm but it can only make it to about 54 cm in the time it takes to accumulate a lethal dose. Although there are gross simplifying assumptions in this analysis, consideration of the problems of avoidance and the time it takes for a unicellular organism to swim a given distance indicate that motile cells with well-developed phototaxic responses are not necessarily resistant to an increase in solar UV-B.

Another factor that may enter the equation is competition. Under a given set of conditions a certain species of organism may predominate in a particular ecosystem. If the conditions are changed - even slightly - the competitive edge may be shifted to another species, which can result in a shift in the entire phytoplankton and zooplankton community. In a recent study by Van Dyke and Thomson (1975), simulated solar UV-B at the irradiance levels to be expected under present conditions caused a shift in the community structure of a simulated marine ecosystem: there was a dramatic shift in predominance from single-celled diatoms to filamentous blue-green algae. The consequence of this shift is that even though productivity may reach about the same level in the UV-irradiated and UV-deficient cases, the small zooplankton cannot eat the large filamentous algae and the larger organisms find blue-green algae less palatable. Thus a shift in community structure can have consequences that transcend the initial effect. It is similar subtle effects that we must seek out and analyze in our assessment of the biospheric impact of an ozone reduction.

REFERENCES

Berger, D., D.F. Robertson, R.E. Davies, and F. Urbach (1975), "Field measurements of biologically effective UV radiation," Appendix D to Chapter 2 of CIAP Monograph 5 (Part 1), Dept. of Transportation, DOT-TST-75-55 (part 1), 2-235 - 2-264.

Calkins, J. (1974), "A preliminary assessment of the effects of UV irradiation on aquatic microorganisms and their ecosystems," in *Proceedings* of the Third Conference on CIAP, Dept. of Transportation, DOT-TSC-OST-74-15, 505-517.

- Calkins, J. (1975a), "Measurements of the penetration of solar UV-B into various natural waters," Appendix E to Chapter 2 of CIAP Monograph 5 (Part 1), Dept. of Transportation, DOT-TST-75-55 (part 1), 2-265 2-296.
- Calkins, J. (1975b), "Effects of real and simulated solar UV-B radiation in a variety of aquatic microorganisms possible implications for aquatic ecosystems," Appendix A to Chapter 5 of CIAP Monograph 5 (Part 1), Dept. of Transportation, DOT-TST-75-55 (part 1), 5-31 5-71.
- Green, A.E.S., and T. Mo (1975), "Erythema radiation doses," Appendix I to Chapter 2 of CIAP Monograph 5 (Part 1), Dept. of Transportation, DOTTST-75-55 (part 1), 2-363 2-407.
- Hodge, F.A., and D.S. Nachtwey (1972), "X-ray-induced delay of cell division in synchronized Tetrahymena pyriformis," Radiat. Res. 52, 603-617.
- McKnight, G. and D.S. Nachtwey (1975), "Natural resistance of freshwater algae to UV radiation a survey," Appendix B to Chapter 5 of CIAP Monograph 5 (Part 1), Dept. of Transportation, DOT-TST-75-55 (part 1), 5-73 5-79.
- Nachtwey, D.S., and A.C. Giese (1968), "Effects of ultraviolet light irradiation and heat-shocks on cell division in synchronized *Tetrahymena*," Exp. Cell Res. 50, 167-176.

- Robertson, D.F. (1975), "Calculated sunburn responses," Appendix J to Chapter 2 of CIAP Monograph 5 (Part 1), Dept. of Transportation, DOT-TST-75-55 (part 1), 2-411 2-424.
- Schulze, R. (1974), "Increase in carcinogenic ultraviolet radiation due to reduction in ozone concentration in the atmosphere," in Proceedings of the International Conference on Structure, Composition and General Circulation of the Upper and Lower Atmospheres and Possible Anthropogenic Perturbations (Melbourne), pub. IAMAP, 479-493.
- Sisson, W.B., and M.M. Caldwell (1975), "Lamp/filter systems for simulation of solar UV irradiance under depleted atmospheric ozone conditions," Appendix C to Chapter 2 of CiAP Monograph 5 (Part 1), Dept. of Transportation, DOT-TST-75-55 (part 1), 2-213 2-231.
- Van Dyke, H. and B.E. Thomson (1975), "Response of a simulated estuarine community to UV irradiation," Appendix D to Chapter 5 of CIAP Monograph 5 (Part 1), Dept. of Transportation, DOT-TST-75-55 (part 1), 5-95 - 5-113.
- Zaneveld, J.R.V. (1975), "Penetration of ultraviolet radiation into natural waters," section 2.4 of CIAP Monograph 5 (Part 1), Dept. of Transportation, DOT-TST-75-55 (part 1), 2-108 - 2-157.

A SUMMARY OF ESTIMATED IMPACTS OF CLIMATIC CHANGE ON CROP PRODUCTIVITY

RAY E. JENSEN*

National Weather Service Environmental Studies Service Center Auburn University Auburn, Alabama

ABSTRACT: This paper reviews recent work on the effects of temperature and precipitation changes on agricultural yields. Rice, wheat, corn, soybeans, cotton, sorghum, and forage crops are considered, and it is found that global generalizations of the effects are unwarranted.

Approximately two years ago, it became apparent that a possibility existed that engine effluents from aircraft in the stratosphere might induce a much larger climatic change at the earth's surface than had been anticipated. At that time the Department of Transportation's Climatic Impact Assessment Program (CIAP) decided to quickly enlarge in scope and effort its limited study to assess the biological impacts of climatic change. This study has resulted in a monograph containing estimates of the effect of climate on food and fiber production (CIAP, 1975), although in some instances the estimates are admittedly preliminary and incomplete. It should prove to be an excellent source document for those in government and elsewhere who have to make some value judgments now concerning the effect of climate on food and fiber production and on natural ecosystems.

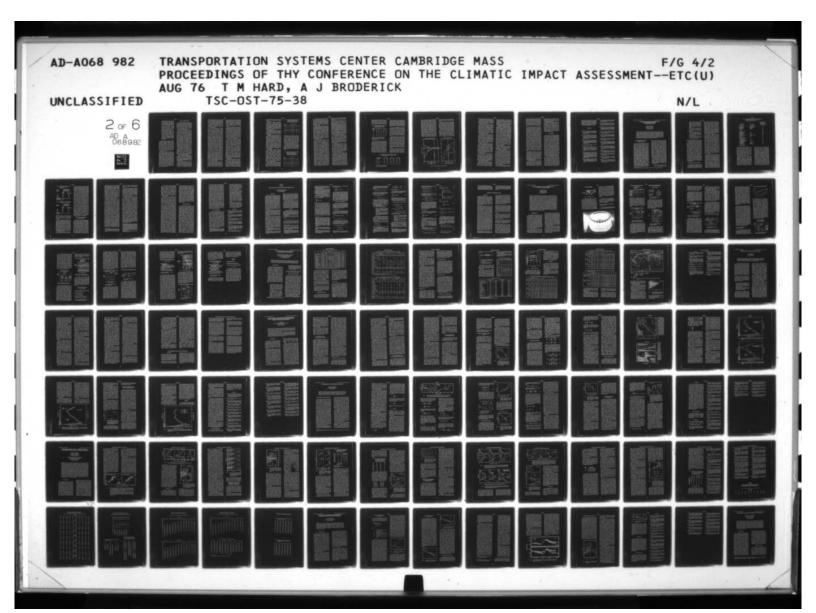
This paper will try to summarize, as objectively as possible, some of what over 60 agricultural, ecological, and agricultural-meteorological experts have written in Part 2 of CIAP Monograph 5 about the effect of climatic change on food and fiber crops. (The effect of climatic change on some natural ecosystems is also assessed in the monograph, but this paper will not attempt to deal with this topic too.)

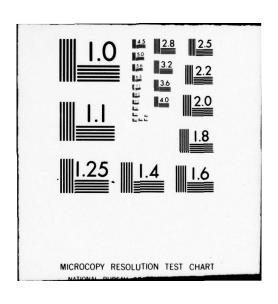
METHODOLOGY

Certain arbitrary assumptions were made concerning the nature of the climatic change to be studied because specific inputs from scientists working on the perturbed-atmosphere panel could not be made available soon enough. These assumptions were:

- 1. That the mean values would stay within the range of observed natural variations for either the global cooling or warming to be studied. It was also assumed that the variances about the means of the climatic elements being considered would remain within the range of observed variation, that the changes in mean temperature would apply equally to both the mean maximum and minimum temperature, and that precipitation distribution and variability would fall within actual observed ranges.
- 2. That of the many climatic elements which affect crop production and ecosystems, those of primary importance were temperature, precipitation and solar radiation. In the case of these three climatic elements, it was assumed that for any climatic change global temperature changes would not exceed ±3°C from present normals, global precipitation changes would not depart more than ±30% from present normals, and that solar radiation would not decrease more than 3% at the mid-latitude point at noon. Other meteorological elements, such as wind, humidity, and snow cover, were placed in a secondary role as to both change and probable effects upon agriculture. These elements, at cer-

^{*}Dr. Jensen is now Director of the NWS Environmental Studies Service Center at Texas A&M.





tain thresholds and periods, may have considerable impact on agricultural and natural ecosystems — for example, the effect of wind and humidity on disease and insect outbreaks, and the effects of snow cover on winter-kill of small grains. However, present climatic-assessment techniques do not allow more than a preliminary qualitative appraisal of effects such as these on crop production and ecosystems.

3. That the assessment of climatic change be based on present technology, management, and plant cultivars. In other words, no attempt was made to assess the possible degree of substitution of one crop for another in a changing climate, or the yield changes that would result with the substitution of earlier or later varieties of a crop for those presently grown.

The effects of climatic change on production were assessed by means of literature reviews, by regression models usually relating monthly temperature and precipitation to yield, by state-of-the-art simulation models, and by studies of how historical climatic changes have affected crop production and natural ecosystem boundaries. These natural-ecosystem and historical studies were reported at the Third Conference on CIAP by Drs. Charles Cooper and Clarence Sakamoto, and appear in those Proceedings (Cooper et al., 1974; Sakamoto, 1974).

Analyses in these studies have emphasized a climatic change consisting of lower global temperatures and precipitation than present normals, since this was the climatic scenario given to the panel members when the studies were initiated. However, about a year ago, because of the uncertainties in the estimates of aircraft-induced climatic change, the panel participants were asked to enlarge their studies and deliberations to include four combinations of positive and negative temperature and precipitation changes about present-day normals. Although there is still more analysis of, and material for, the case of decreasing global temperatures and precipitation, nearly all the studies have made assessments of the effects of climatic change on productivity for the other three combinations.

RESULTS AND DISCUSSION

The postulated changes in temperature, precipitation, and solar radiation will not only have direct effects on plant growth and development throughout the growing season, but will affect other factors related to productivity, such as the length of the freeze-free period, soil temperatures, evapotranspiration, the soil moisture balance, and the hydrological balance.

Changes in mean temperature will have a profound effect on the length of the growing season. Studies in this monograph used as a rule-of-thumb the assumption that a temperature change of 1°C would cause a change of approximately ten days in the length of the freeze-free period. However, a study just completed by Bollman and Hellyer (1974) indicated that the change in the length of a freeze-free period as the result of a change of mean temperature depended on the initial duration of the freeze-free period. Their calculations for the spring-wheat area of Canada showed that a 1°C cooling of mean temperature would shorten an 80-day freeze-free period on the order of 20 days, and a 120-130 day freeze-free period by about six days. Such changes would have pronounced effects on cropping patterns and choice of cultivars in areas of the world where crop production is now a marginal enterprise, as will be discussed later.

Soil temperatures are determined largely by ambient temperatures, solar radiation, and precipitation, and to a lesser extent wind. The greatest impacts of soil-temperature changes on agriculture would be seen at the ends of the growing season, insofar as soil temperature relates to soil thawing and freezing, germination of seeds, and the depth of soil freezing.

Two other factors figure prominently in the assessment of the effect of climatic change on productivity. They are the soil water balance and the overall hydrological balance. Both are strongly affected by precipitation and the actual evapotranspiration, that is, the loss of water from both plant and soil.

Actual evapotranspiration for most of the earth's surface would be affected less by climatic change than projected, because most surfaces are not sufficiently wet to evaporate fully all year. The amount of time during a year that agricultural areas can be considered as freely evapo-

rating surfaces will depend on the frequency and amount of precipitation, the type and density of plant cover, the extent of sub-freezing temperatures, and the water-holding capacity in the soil root zone. Because the soil, plant, and climatic factors influencing evapotranspiration are not independent, it is difficult to draw a general conclusion about how climate changes would affect evapotranspiration.

As a specific example of how a soil water balance might be influenced by a climatic change, a tested soil water-balance model developed by Richardson and Ritchie (1973) was used to calculate daily soil water-balance changes over a three-year period for a Riesel, Texas location. The soil water balance was computed for a crop rotation characteristic of that area: grain sorghum, oats, and cotton, with fallow between the growing seasons (Ritchie and Holton, 1975). Climatic change was simulated by changing the original daily observations. Temperatures were lowered by 1°C, precipitation by 5%, and solar radiation by 2.5%. The calculations showed that the water balance resulting from the simulated climatic change was essentially similar to the original calculated water balance. This similarity indicated that at this location over the three-year period the reductions in rainfall were largely offset by reduced evapotranspiration. The model simulation verified earlier conclusions in the study, based on empirical and theoretical relationships, that reduction in evapotranspiration because of lower temperatures would tend to offset reductions of precipitation resulting in little change in the soil water balance and, therefore, little change in drought conditions. However, the model calculations showed that drainage of soil water through the root zone would be decreased rather drastically in years with below-average precipitation, but would be changed little in years with above-normal precipitation. This result could bode serious consequences if the climatic change persisted for a number of years, since drainage of water through the root zone in agricultural areas is the major source of ground-water recharge.

The hydrological implications of climatic change were studied with a Department of Agriculture watershed hydrology model reported by Holton and Lopez (1973). The model was run for four watersheds representing several rather dissimilar climatic regimes. The watersheds were

located at Coshocton, Ohio; Upper Taylor Creek, Florida; Bush Creek, Riesel, Texas; and Hastings, Nebraska. The model was run for five years for the Florida watershed and for eight years at the other three locations. Climatic conditions used were ten combinations of $\pm 2^{\circ}$ C temperature, $\pm 15\%$ and $\pm 30\%$ precipitation, and $\pm 1\%$ solar radiation.

The model results indicated that changes in temperature had little effect on runoff from the watersheds (Ritchie and Holton, 1975). Analysis of the runoff response showed that runoff from all the watersheds was for practical purposes essentially linear with precipitation changes. In the Coshocton, Riesel, and Hastings watersheds runoff measured in inches increased by about a factor of four when precipitation was increased from 30% below normal to 30% above normal. The agricultural implications are obvious in areas where runoff water is directed into stock ponds or impounded for later use in irrigation.

Let us now turn our attention to the effects of climatic change on specific crops, beginning with rice. The major climatic impact of any temperature change on world rice production would be on length of growing season, which determines the geographical areas in which rice can be grown (Stansel and Huke, 1975). The growing season begins and ends when mean temperatures move across 15°C. Temperature change would have only a minor influence on yield within the major rice-producing areas. In non-tropical areas, however, where temperature is limiting, not only would the growing season be shortened, but plant growth and development would also be slowed. For instance, a 1°C temperature decrease would lengthen the time required to grow a crop from seven to eleven days, while at the same time shortening the growing season by about ten days. This dual effect would cause serious production problems where present cultivars are pushing the limits of the growing season.

Increases in mean temperatures would generally increase the areas where rice could be grown, thereby increasing world production. More significantly, however, higher temperatures may allow multiple cropping in the vast rice areas of the intermediate latitudes. The longer growing season would also allow more flexibility in planting time, resulting in better use of climatic conditions, mainly solar radiation. However, this

JENSEN

would be offset by some decrease in yields of rice grown in the tropics, due to the higher temperatures.

Each type of rice culture is influenced to varying degrees by changes in precipitation. Production of both rainfed upland and rainfed lowland cultures would be directly correlated with precipitation change, though to different levels. Deep-water culture is negatively correlated with precipitation change, because depth of flood water has an inverse influence on the production of floating rice.

Irrigated cultural systems, being controlled, would be influenced less by precipitation change than other cultures. However, the amounts of water available for irrigation would be influenced by precipitation.

Precipitation changes would probably result in solar-radiation changes. In irrigated cultures or where water was not limiting, an increase in solar radiation due to decreased precipitation would increase yields. Studies have shown a 1% change in available solar energy in the plant community would increase production 1.4%, if other factors were not limiting. Assuming that a 1% change in precipitation would result in at least a 0.5% change in solar energy reaching the earth's surface, the magnitude of the potential yield change due to increased radiation could be large. In rainfed upland, rainfed lowland, and deepwater cultures, changes in solar energy would not have a large influence on yield because other factors are limiting.

The influences of temperature change and precipitation change on world rice production appear to be additive. Table 1 summarizes the effects of several combinations of temperature and precipitation change on world rice production. In general, the main effects of precipitation are a decrease in yields with decreasing precipitation, and an increase in yields with increasing precipitation. The main effects of temperature are that mean temperature decreases greater than 0.5°C would result in decreased yields. The most favorable combination for world rice yields would be increased precipitation and higher temperatures.

Stansel and Huke (1975) also investigated the effect of climatic change on United States rice production. They concluded that with no change in present cultivars and management practices, and with 2°C reduction in mean

Table 1. Deviation from World Rice Production Base (300 million metric tons) for Various Temperature and Precipitation Changes, in Percent (after Stansel and Huke, 1975)

Precipi-		Temperature Change								
tation Change	-2°C	-1°C	5°C	0°C	+.5°C	+1°C	+2°C			
-15%	-19	-13	-8	-8	4	0	3			
-10%	-17	-11	-6	-6	-2	2	5			
-5%	-13	-7	-2	-2	2	6	9			
0%	-11	-5	0	0	4	8	11			
+5%	-9	-3	2	2	6	10	13			
+10%	-5	1	6	6	10	14	17			
+15%	-3	3	8	8.	12	16	19			

temperature and a 15% increase in precipitation, the United States rice industry as we know it today could not exist. There would be no rice industry in California, and if the industry survived in Arkansas, production would be cut 50%. Rice production could survive in Texas and Louisiana, but yields would be reduced by 20%. Each of the four states now produces approximately 25% of the United States rice crop.

Stansel and Huke also looked at the effect of the same climatic change, also occurring in the United States in 1990, but under the assumption that new programs dealing with the effects of climatic change would be established. These estimated agronomic yield factors are given in Table 2.

Table 2. Deviation from U.S. Average Rice Production (5 million metric tons) for Various
Temperature and Precipitation Changes by
1990 (after Stansel and Huke, 1975).
Development of Early Season Assumed

Precipi-		Temperature Change										
Change Change	-2°C	-1°C	5°C	0°C	+.5°C	+1°C	+2°C					
-15%	2	5	8	8	11	15	20					
-10%	-1	2	5	6	8	12	18					
-5%	- 4	-1	2	2	5	9	14					
0%	-9	-4	-1	0	4	7	12					
+5%	.9	-6	-3	-2	0	4	9					
+10%	-14	-10	-7	-6	-3	0	6					
+15%	-18	-14	-10	-9	-6	-2	3					

A climatic change of a 2°C reduction in mean temperature accompanied by a 15% increase in precipitation could reduce yields by 18% even with cultivars adapted to cool temperature conditions. A significant research breakthrough like increasing the photosynthetic efficiency of rice cultivars could easily overcome this yield depression.

Ramırez, Sakamoto, and Jensen (1975) investigated the potential effects of temperature and precipitation changes on wheat yields for the Great Plains and midwestern states in the United States, as well as for leading non-domestic wheat-producing areas of the world, including China, Europe, Canada, the USSR, and Argentina. Multiple-regression models were used to analyze the climatic effects for most of these areas. In the cases of China and Europe, a historical approach rather than a statistical approach was used to study the effects of climatic change on wheat production; the results were reported by Dr. Sakamoto at last year's meeting (Sakamoto, 1974).

It was clear from that study that the response of wheat yield to changes in temperature and/or precipitation depended on the prevailing climate of a particular region. For example, in the case of the Plains and midwestern states, it was found that precipitation increases of 10 to 30% could increase wheat yield from about one to four bushels per acre in the semi-arid area of the Great Plains (which includes North Dakota, South Dakota, Kansas and Oklahoma). On the other hand, in Illinois and Indiana, where precipitation is much higher, a 10 to 30% increase in precipitation decreased wheat yield by one to four bushels per acre. When temperature and precipitation changes were simulated simultaneously in the statistical models, maximum yields were achieved in the relatively drier Great Plains areas when decreased temperature was coupled with increased precipitation. In the wetter areas, such as Illinois and Indiana, maximum yields were achieved when temperature decrease was coupled with precipitation decrease. Yield increases with these combinations of temperature and precipitation ranged as high as over five bushels per acre. Increases or decreases in yield responses also varied for different areas within a state. An excellent example was in North Dakota, where increases in precipitation produced small reductions in yield in the wetter Red River Valley, while large increases in yield occurred elsewhere in the state.

In the USSR, eight combinations of temperature and precipitation change, over the temperature range of -1 to +1°C and over the precipitation range of -10 to +10%, were critically analyzed for yield responses in 27 regions. The most favorable overall response, according to the models, was associated with a cooling of 1°C coupled with a 10% precipitation increase. This combination would increase yield more than 20% in the major USSR wheat-production regions. The most deleterious effect on Russian wheat vield was associated with a 1°C temperature increase and a precipitation decrease of 10%. In this case yields could decrease as much as 20% in the Russian breadbasket, with even larger decreases in the drier regions such as Kazakh.

As a cautionary note, it should be pointed out that the effects of climatic change on Russian wheat yields are based on multiple-regression equations developed with only 10 years of climatic and yield data. However, the responses of the USSR yields to certain combinations of temperature and precipitation were much like those in the United States where soils and climate are similar.

In Argentina, wheat production would be favored by cooler temperatures. A 1°C temperature decrease would increase yield from about 3 to 7.5%. Yield responses to change in rainfall were much less than responses to change in temperature, except in the warm, wet province of Entre Rios located in northeast Argentina. In this province a 10% decrease in rainfall would boost yields by 28%, and if coupled with a 1°C cooling would increase yields 35%.

The effect of climatic change on corn production in the corn belt of the United States was investigated by means of statistical models and state-of-the-art physiological models (Benci et al., 1975). A statistically based crop/weather/soil-moisture model developed by Leeper, Runge, and Walker (1974) was used to perform the most extensive analysis for CIAP on climate and corn relationships. Working from the average long-term (1901-1969) "corn belt" weather, they found that corn yield would change approximately 11.3% for each 1°C change in average maximum temperatures and about 1.5% for each 10% change in precipitation. Other parametric

combinations of climatic changes and the associated yield responses are shown in Table 3. In general, according to this model, cooler and wetter conditions will increase corn yields, and warmer and drier conditions will decrease them.

Table 3. Estimated Percent Change in Corn Yield as a Result of Changes in Temperature and Precipitation (after Benci et al., 1975)

Temperature Change	Change	e in Prec	ipitation	(% of No	ormal*)
(°C)	-20%	-10%	0	+10%	+20%
-2°	19.8	21,2	22.7	24.2	25.6
-1.0	8.4	9.8	11.3	12.8	14.2
0	-2.9	-1.5	0	1.5	2.9
+1.0	-14.2	-12.8	-11.3	-9.8	-8.4
+2.0	-25.6	-24.2	-22.7	-21.2	-19.8

*Normal = 85 ± 16 bu/acre, 1901-72 average for selected stations in Missouri, Illinois, Indiana, Nebraska, Iowa and Kansas, where 65% of U.S. corn production is located.

The effect of climatic change on corn yields was also estimated using the multiple-regression equations described by Dr. L.M. Thompson (1969), with the coefficients updated through 1972. These estimates and those from the Leeper et al. model, for three states and four combinations of temperature and precipitation, are compared in Table 4. Both models predict that a warming of 0.75°C will decrease yields by a few percent. The discrepancies in the estimates are associated with cooler-than-normal temperatures and decreasing precipitation. The Leeper et al. models predict that yields will continue to

increase in all three states for a cooler and drier climate. Estimates from the Thompson model suggest that in Iowa any cooling trend associated with decreasing precipitation will cause yield decreases, and that in Illinois and Indiana, yields will increase by only a few percent at best before decreasing when the temperature change reaches -3°C.

A third, physiologically based model developed by Dr. W.G. Duncan of the University of Kentucky was run for three corn-belt locations with 1972 data. Although the yield output of the Duncan model is not exactly comparable with that of the other two models, for the same four combinations of temperature and precipitation it shows a pattern like that of the Thompson model, supporting its general trends (Benci et al., 1975).

The Thompson and the Leeper et al. models, although both statistical, are very different. The Thompson model was built on long-term climate and yield data. The Leeper et al. model was developed by growing corn under appropriate field conditions at several locations over a period of three years, and using these data as inputs to develop a yield-predicting model. Many explanations can be given as to why the discrepancies may arise, but they should be the subject of further research and testing. In the meantime, the yield response in Table 3 should be used with caution.

The effects of climatic change on soybean yields have been estimated for the states of Ohio, Indiana, Illinois, Iowa, and Missouri by the use of multiple-regression equations developed by Thompson (1970). The results are plotted in

Table 4. Comparison of Predictions by Two Models of the Effect of Climatic Change on Corn Yields, in Percent of Normal (after Benci et al., 1975)

Climate Combination	Ic	owa	Ind	iana	llir	nois
Evaluated	D&S*	B&R**	D&S	B&R	D&S	B&R
+0.75°C	-0.01	-0.07	-0.03	-0.08	-0.03	-0.08
-0.75°C, -2.5%P	-0.02	+0.07	+0.02	+0.08	+0.01	+0.07
-1.5°C, -5%P	-0.05	+0.14	+0.03	+0.15	0.00	+0.15
-3.0°C, -10%P	-0.19	+0.27	+0.01	+0.30	-0.07	+0.29

^{*}Estimate using the Thompson model.

^{**}Estimate using the Leeper et al. model.

JENSEN

Figure 1. It can be seen that sovbean yields will be increased by lower temperatures in Illinois. Indiana, and Missouri. However, in Iowa and Ohio, lower temperatures will be deleterious; yield decreases of about 20% will result if temperatures drop by as much as 3°C. A physiological soybean model developed by Dr. R.B. Curry of the Ohio Agricultural Research and Development Center at Wooster was used by Curry and Baker to simulate the effects of climatic change at that location. Their results (Curry and Baker, 1975) lend credibility to the estimates made with the Thompson equation, as well as shedding light on the nature of the large decreases in yields with decreasing temperature in Ohio and Iowa. In three of the four years, simulations of a 2°C temperature decrease caused frost-kill of the plants before maturity. Maps of freeze-free periods for these five states showed

that growing seasons in both Iowa and Ohio were somewhat shorter than those in the other three states.

Soybeans can be grown in a shorter growing season than corn, and therefore would probably be less affected than corn by a cooling trend. Other model simulations by Curry show that a slight warming might be helpful in increasing yields at some locations, and that in general decreases in rainfall lower yields while increases in rainfall of up to at least 15% increase yields.

Cotton production would not be materially affected by a warming or cooling of about 2°C (Baker et al., 1975). However, in order to maintain production at present levels with a 2°C cooling, some changes in cultural production and nitrogen fertilization would probably be required. A 2°C decrease in temperature could shift the cropping zone as much as 160 km

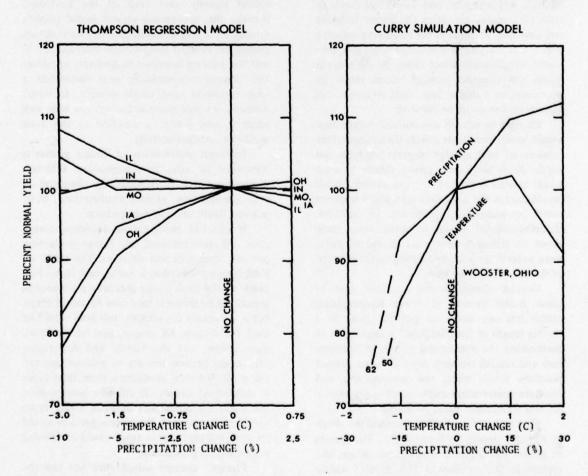


Figure 1. Effect of climatic change on soybean yields.

further south except in Russia and California. In the United States, this would affect production in Tennessee, North Carolina, Missouri and Kentucky, primarily because of the shortened growing season, but these areas account for only 8% of U.S. cotton production.

Grain sorghum, a crop of tropical origin, is adapted to areas of high temperature and low rainfall. Most of the sorghum is grown at latitudes of less than 40°. Sorghum ranks fourth among the cereals in world production. It is normally grown in areas where temperatures are too high or rainfall too low for production of other summer crops, such as corn or soybeans. Therefore, changes in temperature or rainfall would probably affect both the area in which sorghum is grown, and its yield.

Vanderlip and Ritchie (1975) suggest that reduced temperatures would primarily delay planting and maturity, and would not result in reduced acreages except at the higher latitudes and altitudes. In much of the sorghum-producing area a 1 or 2°C decrease in temperature probably would not seriously affect yields. In the areas in which the effective growing season might be shortened, an earlier hybrid could be grown, but yield potential would be reduced.

Changes in rainfall amount and distribution would have much larger effects than temperature changes on both acreage of grain sorghum and yields. Since sorghum is grown mostly in areas where rainfall is limited, changes in the rainfall would change the size of the area where sorghum could be successfully produced. In addition, changing rainfall would in many cases bring about an almost proportional change in yield, since water is the primary limiting factor in much of the sorghum production.

Genetic change in the sorghum plant to allow better growth at lower temperatures, utilize less soil water, or produce grain in a shorter length of time are possible approaches to overcoming the detrimental effects of temperature and rainfall changes. Also, soil-management practices which affect soil temperatures and moisture conservation might possibly help alleviate minor climate-induced problems.

Hart and Carlson (1975) discussed the effect of climatic change on forage crops. The species of grasses and legumes used for hay, silage, and pasture in the continental U.S. exhibit widely varying adaptation to environmental conditions. The area of usefulness of a forage crop is considerably smaller than the area in which it can survive; a species may survive in marginal areas of its range, but its production will vary considerably from year to year. Other forage crops will be better adapted to the changed climate and more productive, and will be grown instead.

North-south distribution of forage species is governed largely by temperature. High summer temperatures set a southern limit to the range of cool-season grasses, and low winter temperatures limit the northward range of warm-season grasses. If average daily temperatures decreased by 2.5°C, the range of the warm-season grasses would move south only about 150 miles, but the range of the cool-season grasses would extend south to the Gulf of Mexico, excepting only southern Texas and Florida. Orchard-grass and tall fescue might replace bermuda and bahiagrass almost entirely over most of the Southeast, because the cool-season grasses would provide grazing for a longer season than the warm-season grasses. However, if temperatures increased 2.5°C and the existing north-south gradients of winter and summer temperatures were maintained, a wide transition zone would develop, to which neither cool- nor warm-season grasses were well adapted, and forage production in this zone would be curtailed severely.

East-west distribution of forage grasses is controlled by effective precipitation. Effective precipitation can be changed by alteration of total precipitation, of evapotranspiration, or of seasonal distribution of precipitation.

If effective precipitation decreases, forage grass will move eastward, and forage production per unit land area will decrease. The effect on total forage production is not as easy to predict. Much of the land in the area where introduced grasses can be grown is used now for cereal crops, but if it became dry enough, this land would be used for forages. Of course, part of the shortgrass prairie, and the bunch- and desert-grass area, might become too dry to produce any forage at all, but total production from these types is quite small already. If effective precipitation increased, the boundaries between forage types would shift westward. Production per acre would increase, but land now in range would be diverted to cereal-crop production.

Climatic changes would alter not just the area in which a particular forage crop is grown,

but also the yield of that crop. For example, in Iceland the mean temperature of the warmest six months was 7.65°C in the late 1950's, but only 6.83°C in 1966 and 1967. Hay yields for the same periods were 4.33 and 3.22 t/ha, respectively. A temperature drop of 0.8°C produced a 25% reduction in degree days above a base of 5°C, and a 26% reduction in hay yields (Bryson, 1974).

Cereals, ryegrass, and clovers are important sources of winter forage in the Southeast, but production is strongly affected by temperature and precipitation. A model developed by Hart and Burton (1965) was used to predict the effect of temperature and precipitation changes on the forage yields of oats. Total production would change ±5% with a ±10% change in precipitation, but there would be little change in the seasonal pattern of production, because moisture is not limiting for most of the season. A 2.5°C increase in temperature would make forage available about a month earlier in the winter, but would decrease total forage production, because growth of the crop would end about a month earlier in the spring. A 2.5°C decrease would increase total production, because growth would continue further into the spring, when other conditions are more favorable. However, in the latter case, forage production would be cut to almost nothing in winter, a time when it is needed badly. Lower precipitation would delay seeding in the fall in some years, and increase chances of failure in establishment. Lower temperatures would increase the chances of winter kill, and could result in a total loss of production in some years.

Unfavorable environments may decrease forage production by means other than direct interference with growth. Plant diseases spread more rapidly when humidity is high, so disease losses would increase if precipitation increased or solar radiation and perhaps temperature decreased. Very short exposure to ultraviolet radiation inhibits pollen germination; an increase in ultraviolet radiation could reduce seed production of wind-pollinated grasses.

Forage utilization, as well as forage production, would be affected by climatic change. Grazed pastures may be damaged severely by trampling when the soil is wet; increased rainfall would increase the number of days when this kind of damage would occur. More days in

winter with snow cover would result in fewer days when livestock could graze, but on the other hand increased snow cover might reduce winter-killing of the forage stand.

Higher rainfall and decreased solar radiation would make it more difficult to make hay. If increased rainfall and decreased radiation were accompanied by cooler temperatures and a shorter grazing season, as seems likely, the need for hay would increase at the same time that hay production became more difficult. In the southern U.S., this might be offset by the increased production of winter forage from cool-season grasses, but such an increase would not be possible farther north.

CONCLUSION

CIAP's study of the effects of climatic change on selected natural and agricultural ecosystems demonstrated that broad generalizations on the subject are seldom possible. It also showed that the response of an entity to climatic change within those systems, whether it be plant or animal, had to be examined with respect to the particular climatic niche that it occupied. Therefore, the response function of a specific livestock or crop enterprise to climatic change depended heavily upon the climatic regime in which the enterprise was being pursued. For example, the same postulated climatic change may produce very different response functions in northern and southern Russian wheat-growing areas, or for Alberta and Manitoba, Canadian wheat-growing areas; in some cases, the response functions may even be of opposite sign. Thus, we cannot make a generalization, such as that a cooler and wetter climate regime will favor wheat production in a particular area, or in the world, until the prior climatic regimes have been specified and the appropriate methodology applied.

Man has the ability and the tools to overcome much of the climatic change discussed here. By genetic manipulation and crop and cultivar substitution, the challenge posed by decreased temperature could be met, except on the extreme northern and southern boundaries of the world where the growing season would become too short to grow any crop. Droughtresistant cultivars could partially recoup the lower yields caused by reduced precipitation. Irrigation and drainage projects might be re-

JENSEN

quired to offset the remaining effects of precipitation decrease. However, to offset climatic change of some of the magnitudes discussed in Monograph 5, commitment to worldwide crop research and engineering projects would have to be made soon, and a high priority given them.

REFERENCES

- Baker, D.N., J.R. Lambert, and J.N. Jenkins (1975), "Cotton," section 4.1.5 of CIAP Monograph 5 (Part 2), Dept. of Transportation, DOT-TST-75-55 (part 2), 4-147-4-163.
- Benci, J.F., E.C.A. Runge, R.F. Dale, W.G. Duncan, R.B. Curry, and L.A. School (1975), "Effects of hypothetical climatic changes on production and yield of corn," section 4.1.1 of CIAP Monograph 5 (Part 2), Dept. of Transportation, DOT-TST-75-55 (part 2), 4-3 - 4-37.
- Bollman, F. and G. Hellyer (1974), "The Economic Consequences of Projected Temperature Changes in Climatically Sensitive Wheat-Growing Areas of the Canadian Prairie," Development and Resources Corp., Sacramento, CA.
- Bryson, R.A. (1974), "A perspective on climatic change," Science 184, 753-760.
- CIAP (1975), "Impacts of Climatic Change on the Biosphere. Part 2 Climatic Effects," Volume 5 of the Climatic Impact Assessment Program monograph series (Part 2), ed. J. Bartholic and R.E. Jensen, Dept. of Transportation, DOT-TST-75-55 (part 2).
- Cooper, C.F., T.J. Blasing, H.C. Fritts, Oak Ridge Systems Ecology Group, F.M. Smith, W.J. Parton, G.F. Schreuder, P. Sollins, J. Zich, and W. Stoner (1974), "Simulation models of the effects of climatic change in natural ecosystems," in Proceedings of the Third Conference on CIAP (Cambridge, MA), Dept. of Transportation, DOT-TSC-OST-74-15, 550-562.
- Curry, R.B. and C.H. Baker (1975), "Climatic change as it affects soybean growth and development," section 4.1.4 of CIAP Monograph 5 (Part 2), Dept. of Transportation, DOT-TST-75-55 (part 2), 4-132 4-147.

- Hart, R.H. and G.W. Burton (1965), "Effect of weather on forage yields of winter oats, rye, and wheat," Agron. J. 57, 588-591.
- Hart, R.H. and G.E. Carlson (1975), "Forages," section 4.1.6 of CIAP Monograph 5 (Part 2), Dept. of Transportation, DOT-TST-75-55 (part 2), 4-163 4-173.
- Holton, H.N. and N.C. Lopez (1973), "USDAHL-73 Revised Model of Watershed Hydrology," Plant Physiology Institute Rept. No. 1, USDA Agricultural Research Service, Beltsville, MD 20705, 110 pp.
- Leeper, R.A., E.C.A. Runge, and W.M. Walker (1974), "Effect of plant available stored moisture on corn yields," Agron. J. 66, 723-733.
- Ramirez, J.M., C.S. Sakamoto, and R.E. Jensen (1975), "Wheat," section 4.1.2 of CIAP Monograph 5 (Part 2), Dept. of Transportation, DOT-TST-75-55 (part 2), 4-37 4-90.
- Richardson, C.W. and J.T. Ritchie (1973), "Soil water balance for small watersheds," Trans. Amer. Soc. Agri. Eng. 16, 72-77.
- Ritchie, J.T. and H.N. Holton (1975), "Soil-water balance, drought, and other hydrological implications," section 2.2.5 of CIAP Monograph 5 (Part 2) Dept. of Transportation, DOT-TST-75-55 (part 2), 2-52 2-61.
- Sakamoto, C. (1974), "Effect of climate on nondomestic wheat production," in Proceedings of the Third Conference on CIAP (Cambridge, MA), Dept. of Transportation, DOT-TSC-OST-74-15, 539-548.
- Stansel, J. and R.E. Huke (1975), "Rice," section 4.1.3 of CIAP Monograph 5 (Part 2), Dept. of Transportation, DOT-TST-75-55 (part 2), 4-90 4-132.
- Thompson, L.M. (1969), "Weather and technology in the production of corn in the U.S. corn belt," Agron. J. 61, 453-456.
- Thompson, L.M. (1970), "Weather and technology in the production of soybeans in the central United States," Agron, J. 62, 232.
- Vanderlip, R.L. and J.T. Ritchie (1975), "Grain sorghum," section 4.1.7 of CIAP Monograph 5 (Part 2), Dept. of Transportation, DOT-TST-75-55 (part 2), 4-173 4-176.

ECONOMIC ANALYSES OF POLLUTION RESULTING FROM STRATOSPHERIC FLIGHT: A PRELIMINARY REVIEW*

RALPH C. D'ARGE
Department of Economics
University of Wyoming
Laramie, Wyoming

ABSTRACT: Under the general auspices of the DOT Climatic Impact Assessment Program, a substantial amount of theoretical and applied economic research was conducted on pollution that may result from stratospheric flight. This research can be classified into four broad categories: (1) impact analyses concerned with the economic costs and benefits of climatic and ozone modification, (2) costs of emissions control and monitoring programs, (3) responsibility for, and other issues of, emissions regulation, and (4) models of decision-making designed to analyze stratospheric pollution problems (and provide guidance in solving them). This paper contains a brief summary of progress in each of these categories, along with a discussion of research needs. (For a complete tabulation of the results of the CIAP research, the reader is advised to consult CIAP Monograph 6 (1975).)

THE STRATOSPHERIC POLLUTION PROBLEM: A SKETCH

From an economic perspective, the stratospheric pollution problem differs little from other types of pollution problems. The stratosphere, being a common-property resource, is likely to be inefficiently utilized as a sink for pollutants. To achieve economic efficiency, stratospheric emissions should be regulated and, in simple economic terms, controlled up to the point at which costs of regulation at the margin equal social damages at the margin associated with emissions that remain. However, this simple rule cannot be applied unless three empirical relationships are well defined: (1) a complete and concise damage function relating societal damages to the atmospheric effects for various rates of pollutant emissions, (2) a relationship between costs of pollutant control and regulation and pollutant emissions, and (3) an empirically accurate relationship between rates of pollutant emissions and atmospheric effects. The central problem for stratospheric regulation is that neither the sign nor the magnitude of any of these relationships is known with a high degree of certainty. However, estimates to date as regards the third relationship suggest that aircraft emissions will tend to reduce global temperature and the O3 concentration. Best estimates to date also indicate that on balance a global cooling will be costly to society, but they are based on intensive examination of only about 20% of the world's economy. Finally, direct costs of regulation for regulating some pollutants, SOx, have been estimated with some degree of precision, while for others, including NOx, suggested methods of control presuppose such radical redesign of jet engine combustors that accurate estimates of costs are not foreseeable. Thus, the traditional benefit-cost analytical approach cannot be applied to the stratospheric pollution problem except in a rather crude and limited form. For example, "best" estimates of the three relationships can be tabulated and the order-ofmagnitude of the damages and costs of regulation can be evaluated; this is done in the next section of this paper. However, the current uncertainties place substantial qualifications on these results.

Given the inherent uncertainties and possibilities for large errors in measurement, how should the stratospheric pollution problem be analyzed from an economic perspective? First, one might characterize the major distinguishing attributes as follows:

 There are large uncertainties in the effects on surface climate of various

^{*} This paper is an extended version of the notes used for the presentation at the Fourth Conference on CIAP.

levels of emission in the stratosphere of oxides of nitrogen, oxides of sulfur, particulates, and water vapor. Some changes may involve irreversibilities in the natural environment, although no substantive evidence of this is now available.

- There are extremely large uncertainties in the translation of tropospheric climatic changes into quantitative biological effects.
- There are very high uncertainties as to how social communities and the economic system adjust to large-scale climatic change or even small climatic shifts in the biosphere.
- 4. None of these substantial uncertainties is likely to become a near-certainty in less than one or two decades.

Given these underlying assumptions, efforts were concentrated on defining the decision problems.

The essential economic decision problem is one of analyzing a class of problems, in which the transfer function between cause and effect is subject to extreme uncertainty at the point of initial decision, but a process of learning over time can be anticipated. The decision process is sequential: decisions made in the next decade can be continued or revoked in future times, and not all decisions on the utilization of the stratosphere need be made at one point in time. Also, impacts of both biological and social consequences may not be observed for one or more human generations after the perturbation of the stratosphere. The monitoring and emissions-control costs range from low-cost current techniques such as fuel desulfurization to very high-cost methods of reducing emissions and detecting subtle climatic changes. The direct economic costs of substantial climatic perturbations are likely to be high when adaptation to environmental changes is not explicitly included in the assessment.

ESTIMATES OF ECONOMIC IMPACTS

The fundamental interdependence of economic activity and the atmospheric environment is well understood by everyone either adapting to or living in adverse climates, and it is obvious

that climate is one of the underlying determinants in economic systems. The location and density of human settlements, value of agriculture, physical health, and even recreational pursuits are partly the result of climatic changes. For example, increased temperatures could mean decreased heating costs, but increased airconditioning costs. Lower temperatures may mean a decrease in productivity of agriculture. In the past two years there has been an attempt by researchers to examine costs and benefits associated with climatic change under the auspices of the Climatic Impact Assessment Program of the U.S. Department of Transportation.

It is impossible to examine all economic effects without a complete global generalequilibrium analysis of benefits and costs. The approach taken was that of examining a more or less representative sample of major agricultural crops, fisheries, and commercial forests in order to assess their (partial-equilibrium) adjustment to climatic change and the implied associated benefits and costs. Studies were completed on world corn, cotton, wheat, and rice production; on forest production in the U.S., Canada, and the USSN; and on thirteen commercial-fishery species worldwide. For assessing effects in the non-natural-resource area, cost and benefit measures were made for residential, commercial, and industrial fossil-fuel demands, for electricity in commercial and residential buildings, for housing and clothing costs, for road-repair and snowremoval costs, and finally for aesthetic costs (or benefits) associated with preferred weather patterns. In addition, studies were made of the health-cost impacts.

Cost or benefit measures were developed by utilizing the concept of consumer surplus where applicable, and calculating direct changes in costs or savings where consumer surplus appeared to be not applicable. For comparative purposes, a 1°C change in mean annual global temperature is assumed to occur over a 30-year interval from 1990 to 2020. Of course, the interval 1990 to 2020 is entirely arbitrary; it is dependent upon the pollutant injection rate assumed. Table 1 is presented only to illustrate magnitude of benefits and costs of this arbitrary global temperature change. For those categories of economic activity analyzed, net cost is approximately 8.5 billion dollars on an annual basis, or 170 billion dollars

D'ARGE

Table 1. Estimates of Economic Costs of Climatic and Biologic Changes (-1°C change in mean annual temperature, no change in precipitation, 5% interest rate assumed)

. Impact Studied	Investigators	Annualized Cost, 1974 (in millions of U.S. dollars; negative sign denotes benefit)
Corn Production	Schulze, Ben-David	-21
Cotton Production	Schulze, Ben-David	11
Wheat Production	Mayo, McMillan	92
Rice Production	Bollman	956
Forest Production	Schreuder	
U.S.		661
Canada		268
U.S.S.R.		
(softwood only)		1383
Douglas-Fir Production	Schmidt	475
Marine Resources	Bell	1431
Health Impacts		
(excluding skin cancer)	Anderson, Lave, Pauly	2386
Water Resources	Bollman	-2
Urban Resources		
Wages	Hoch	3667
Residential, Commercial and Industrial Fossil		
Fuel Demand	Nelson	176-232
Residential and Commercial		
Electricity Demand	Crocker et al.	-748
Housing and Clothing		
Expenditures	Crocker et al.	507
Public Expenditures	Sassone	24
Aesthetic Costs	Bradley, Larsen	-219

Source: d'Arge (1975).

on a present-value basis. It is important to note that there is incomplete coverage of some economic sectors as well as omission of other sectors, except perhaps for rice and cotton production. Each estimate was developed independently, so there are no corrections for sectoral or categorical interdependence such as the effect of increasing scarcity of rice on the demand for wheat, and there is no consideration of possible future technological changes.

Tables 2 and 3 give a very preliminary benefit-cost analysis based on the *measured* damages and control costs. Table 2 contains estimates of the damages (from climatic change induced by aerosols) avoided by desulfurization of the jet fuel used in supersonic aircraft, along with the costs associated with sulfur removal. It can be seen that for various fleet sizes of supersonic aircraft flying in the year 2000, the benefit-cost ratio for desulfurization exceeds 2.5.

However, it is to be noted that damages avoided are computed on the basis of assuming proportionality over the range 0 to -1°C and examining the range 0 to -0.007°C. The mean temperature change resulting from the various possible fleets is very uncertain at present. Some scientists have indicated that the most likely change is negative but very slight, between 0.007 and 0.014°C (see Appendix K of the NAS study (1975)). It is conceivable, but not probable, that the negative change could be as high as 0.5°C. An additional problem is that fuel desulfurization is intended to prevent climatic cooling by aerosols, but the countervailing impact from injection of water vapor, which on balance is predicted to raise surface temperature via the "greenhouse effect," is not considered. Desulfurization alone could conceivably induce an even greater warming effect than water-vapor injections. Until more precise global meteorological models can be

Table 2. Climate Change – Preliminary Estimates of Costs and Benefits for Fuel Desulfurization

Number of Planes*	Present-Value Cost, 1974, with 5% Interest Rate (millions of U.S. dollars)						
	Damages Avoided	Desulfurization					
200	240	92					
400	480	186					
600	720	278					
1000	1200**	464					

^{*}Second-generation supersonic aircraft flying in the year 2000.

Table 3. Ozone Depletion – Preliminary Estimates of Costs and Benefits for Engine Redesign

Number of Planes*	5% Is	alue Cost, 1974, nterest Rate of U.S. dollars)
	Damages Avoided	Redesign Costs
200	560	110
400	1040	150
600	1600	190
1000	2760	270

^{*}Second-generation supersonic aircraft flying in the year 2000.

constructed so that the joint effect of water vapor and aerosols can be more accurately predicted, the benefit-cost ratio calculated here for sulfur removal must be viewed with skepticism.

Economic costs induced by alteration in the amount of UV radiation reaching the earth were estimated for skin cancer (non-melanoma) and materials. Materials-weathering costs associated with increased UV radiation were estimated for plastics, textiles, paints, and other surface finishes. Many other potential impacts, including increased skin aging, sunburn, and biological processes dependent on the UV spectrum, were not measured. In Table 3 are listed measured damages avoided and estimated costs associated with redesigning jet-engine combustors to reduce NO_x emissions by a factor of 6.

For fleet sizes from 200 to 1000 airplanes, all computed benefit-cost ratios exceed 4. Ozone-

depletion effects in various countries are highly diverse, since incidence rates for skin cancer are much greater for light-skinned Caucasians and for individuals who spend large amounts of time in the sun. For countries where there is relatively little activity out of doors, changed UV radiation should have only minor effects on incidence rates. For nations with very substantial levels of outdoor recreation, incidence rates are likely to increase. Because of the negative impacts of ozone depletion on areas that were not included, and the method of estimating damages, a greater degree of confidence might be placed in the estimated benefit-cost ratios exceeding 1, than in those for temperature change. In the benefit-cost estimates presented for ozone depletion and for climatic change, there is a substantial difference in the sheer magnitude of damages that may occur, but the climatic estimates appear to be subject to a much greater degree of uncertainty.

It should be clear from these very preliminary benefit-cost analyses that (1) the stratosphere is a resource which is potentially sensitive to man's activities, and not enough is known about it to accurately predict consequences with regard to either efficiency or distribution, and (2) suspected impacts tend to be negative and of a long-term character. Increased exposure to UV radiation today means an increased probability of contracting skin cancer in 30 years, and a gradual buildup of aerosols in the atmosphere may require 60 years to be noticeably reflected in long-term trends of surface temperature.

INSTITUTIONS FOR REGULATION AND MONITORING

Both common law and international agreement (implied in the Chicago Convention of 1944) state that airspace above each sovereign nation is controlled exclusively by that nation. However, airspace over the oceans is not subject to control of use or access by any nation. The stratospheric pollution problem, at least in terms of an institutional setting, can be viewed as somewhat analogous to the pure mining problem in which any owner of land above a common pool can tap it. Pumping by one owner will affect all other owners directly, since it reduces both pumping pressures and future supplies. Conventional economic wisdom asserts that each mine owner will have very strong incentives to

^{**}Probable change of -0.007°C.

exploit the resource and use it more intensively than is socially desirable. In the case of stratospheric pollution, there is the added dimension that each individual nation's decisions will affect not only others but also itself—i.e., if an individual nation should decide to pollute the stratosphere, it would influence not only the climate of other nations but also its own. Consequently, there would be some incentive for each nation, acting individually, to restrict its emissions.* For truly global common-property resources like the oceans and stratosphere, positive or negative impacts are unlikely to be one-directional in effect and incentive, but are more likely to have this feedback effect.

With regard to guiding international principles - who pays, and how much - it appears that there are no existing precedents except the various observations on conflicts over nuclear testing. Individual nations, through their sovereign rights, and with some degree of individual autonomy, have the right to impose regulations on the airspace above them provided these individual countries are willing to accept some sort of potential retaliation, economic or otherwise, on supersonic flights or subsonic flight elsewhere. Individual nations also have the right, through bilateral agreement outside of the International Civil Aviation Organization (ICAO), to prohibit landing of any form of aircraft that they believe constitutes present danger.** The upper limit to airspace is roughly defined by customary international law and precedent set during the first decade of the space age. It was recognized. that the U2 aircraft flying reconnaissance flights at 60,000 feet (18.3 kilometers) was within sovereign airspace. This altitude was accepted as sovereign airspace because it was navigable by aircraft. (On the other hand, states have tolerated spacecraft satellites over their territory without claiming violation of their sovereign rights.) Thus, it appears that individual states can regulate emissions from stratospheric flight that occur within their sovereign boundaries, including boundaries at sea. What individual states will not be able to control are emissions over the oceans,

which do not constitute sovereign airspace, and over nations agreeing to allow stratospheric flight.†

A legal question is emerging as to whether an agreement among the ICAO nations to regulate emissions from supersonic flights and aircraft outside sovereign territories can be made without conflicting with other international agreements. The 1958 Geneva Convention on the High Seas provides for freedom of flight over the high seas. ‡ Whether this agreement will be honored cannot at this time be foreseen.

Most dimensions of the natural environment on a regional or global scale are resources without rigidly defined or enforceable international ownership rights. The atmosphere, especially the stratosphere, is a prime example. This resource can be viewed as being commonly owned or not owned at all. A nation which agreed to a particular pattern of ownership of this resource could potentially lose some of its implicitly controlled resources and thereby its national wealth. As long as international entitlements are obscure, any nation can lay implicit claim to the stratospheric resource exceeding any equitable share it might presume to receive if entitlement were made explicit. This is not to say that once some other nation impinges on a country's perceived implicit entitlement, it will not find a negotiated settlement, and thereby explicit entitlement, to be superior to an implicit one. However, the affected nation, in negotiating, must revise downward its own perceived ownership of the common-property resource. In consequence, proceeding from a situation of implicit entitlements of common-property resources to explicit regulation, and thereby ownership, means that some (or all) nations must revise downward their expectations of national wealth stemming from the resources that each implicitly believes it controls.

^{*}Generally, restriction by nations acting in isolation will lead to inefficient reduction in emissions because of the common-property character of the resource.

^{**}This section draws heavily on Larsen and Faggen (1975).

[†]This might lead one to speculate on the feasibility of flying from Moscow using the Arctic Ocean as a pivotal point for entering other oceanic airspaces and being able to land at almost any coastal city in the world without violating sovereign airspace. It appears unrealistic to assume that stratospheric flight can be regulated through assertions of the rights and laws of sovereign airspace, even though the aircraft typically will be flying at altitudes within currently recognized sovereign boundaries.

^{*}Convention on the High Seas signed at Geneva, Switzerland (April 29, 1958).

A second aspect of major importance arises from the concept of national sovereignty. National sovereignty implies that, aside from variations in political or economic power or information, governments will achieve the greatest welfare for all by independently pursuing autonomous goals and interacting with each other through international markets. The belief in national sovereignty as an ideal is so ingrained in the world's cultures that it is impractical to presume it will be easily given up or seriously modified.

The concept of national sovereignty in decision, combined with the idea that implicit (as opposed to explicit) entitlement of the stratosphere yields a greater perceived wealth for nations, suggests that resolution of stratospheric pollution problems will generally be subject to the following constraints. First, no nation will easily accept international agreement on entitlement of this significant common-property resource without receiving compensation to retain its perception of national wealth. Hence, the classical answer to such problems, internalizing or developing an independent commission to aid the decision-making process for the resource, is not easily transferable to the stratospheric pollution problem; a new overriding element of distributional gains and losses must be simultaneously included. Second, international court settlements for regulating pollution of the stratosphere are not likely to yield satisfactory results. There appear to be three almost insurmountable problems. To begin with, how are damages to be measured and damage payments assessed? The victim nation's social values may be strikingly different from those of the polluting country, and there may not be a social-welfare index that is applicable to both. For the victim nation, international trading prices, at least at the margin, offer a measure of welfare loss. However, if the impact is felt by individual citizens, and no market prices can be attached to their losses, then a measure of welfare loss is available only through direct examination and questioning, with consequent "free-rider" difficulties. A second problem is that the actual magnitude of the loss may be uncertain unless stratospheric pollution is allowed to continue to the point of observable damages, e.g., threshold levels of skin cancer. Given the sovereign rights of nations, no nation can be forced to pay environmental

damages. The tradeoff here may be in terms of loss of international prestige and good will, or increasing the possibility of conflict, versus monetary payments based on possibly misrepresented public preferences in the victim nations. Third, there is also the problem of assigning damages when more than one nation's stratospheric pollution contributes to total damages. If the different nations' residuals are synergistic, or if damages are non-linearly related to pollutant injection, then there is no easy method of determining how much responsibility each nation should take even under the "Trail Smelter" guidelines (see Reports of International Arbitral Awards, 1938). Thus, it can be anticipated that international courts or international commissions will have difficulty in arbitration even if such institutions are given some degree or level of regulatory powers.

DECISION PROCESSES

On the basis of "best" estimates, it seems that substantial numbers of aircraft should be allowed to fly in the stratosphere, but only in compliance with standards on pollutant emissions. Small numbers of such aircraft now flying in the stratosphere apparently do not constitute a significant enough pollutant load to be scientifically detectable. Given the sequential nature of both learning and pollutant loading, the immediate question is, what type of regulatory strategy is likely to be reasonably valid? Without flights in the stratosphere, stratospheric constituents are not going to be perturbed (except through chlorofluorocarbons and perhaps nitrogen fertilizers used at the earth's surface), and therefore man can learn nothing directly about the stratosphere's capacity to "absorb" pollutants. Alternatively, permitting stratospheric flight without undertaking serious monitoring efforts may lead to unacceptable terrestrial changes. Since the stratosphere can apparently regain its chemical balance even after substantial loadings of NO_x and SO_x, a reasonable policy would seem to be one that allowed some experimentation but balanced it with extensive monitoring programs. As new information becomes available over the next decade from monitoring and laboratory studies, and nonmarket measures of economic values are improved, this learning process may be expected

to provide greater insight as to feasible regulatory actions, even if such actions take a minimum of one decade for implementation. Professors W.R. Porter and M.L. Cropper from the University of California, Riverside, provide one model of such a sequential decision process (see Appendix A), in which the decision-maker adjusts choices according to the latest scientific, technical, and economic information and its estimated accuracy. They use what is essentially a variant of stochastic dynamic programming processes. With this model and other work, it is at least conceptually feasible to design a reasonable operating strategy for regulating emissions into the stratosphere. It remains to be seen whether viable international institutions for managing the stratospheric pollution problem exist, or will exist. An important initial question is how nations will divide the relatively large outlays for baseline and continuous monitoring of the stratosphere, and for research and development efforts on reducing aircraft pollutant emissions. Perhaps an equitable division would be for the polluting nations to finance R&D with United Nations supervision, and for each nation to contribute to financing global monitoring efforts according to the United Nations funding shares.

RESEARCH NEEDS

There appears to be sufficient evidence that pollutants from stratospheric flight are potentially a serious global environmental problem. There is also some evidence that fleet sizes of SST's and subsonics flying in the stratosphere must be at least an order of magnitude larger than the size of current subsonic fleets to induce substantial pollution-related damage to the global economy. Thus, critical decisions on emission rates, flight altitude and location, and number and duration of flights can be postponed for at least five to ten years.* The essential problem, then, is to design an efficient set of research studies for the next five to eight years to provide the data needed for consistent and adequate international regulatory policies. I think an efficient and successful research design would include the following components:

- More intensive examination of the costs and benefits to urban and rural communities of climatic changes, including the effect of latitude and climatic variability – i.e., hourly, weekly, and seasonal variations in micro-climates.
- A historical examination of how societies have adjusted to long-term trends in climate. Such analyses would offer insight on how non-market considerations influence benefits and costs.
- 3. A continued effort to objectively relate changes in ultraviolet radiation to changes in humans, animals, and plants. Perhaps most important, a net effect of UV-B on skin-cancer incidence rates should be striven for, with mitigating influences of behavior, socio-economic class, race, and so on taken into account.
- 4. The development of quantitative economic models for designing and implementing a short- and a long-term stratospheric monitoring program which would consistently integrate data on source, ambient change, and effects.

REFERENCES

- CIAP (1975), Economic and Social Measures of Biologic and Climatic Change, ed. d'Arge et al., Vol. 6 of CIAP monograph series, Dept. of Transportation, DOT-TST-75-56.
- Cropper, M.L. (1975), "Optimal use of the stratosphere with irreversibilities," section 2.5 of CIAP Monograph 6, Dept. of Transportation, DOT-TST-75-56, 2-88 - 2-101.
- d'Arge, R.D. (1975), "Introduction and overview," Chapter 1 of CIAP Monograph 6, Dept. of Transportation, DOT-TST-75-56, 1-1 - 1-37.
- Larsen, P.B. and E.S. Faggen (1975), "Regulation of stratospheric flights to control adverse environmental effects," section 2.9 of CIAP Monograph 6, Dept. of Transportation, DOT-TST-75-56, 2-157 2-181.
- NAS (1975), Environmental Impact of Stratospheric Flight: Biological and Climatic Effects of Aircraft Emission in the Stratosphere, Climatic Impact Committee of the NRC, NAS, and NAE, pub. National Academy of Science.
- (1938), Reports of International Arbitral Awards, Vol. III, pub. International Couet of the Hague.

^{*} This statement must be qualified if the ozone profile and climate are affected by other anthropogenic sources, including chlorofluorocarbons. If this is the case, then regulating decisions may be needed much sooner.

D'ARGE

APPENDIX A

NOTE ON OPTIMAL POLICIES FOR MONITORING STRATOSPHERIC FLIGHT

W.R. PORTER AND M.I. CROPPER University of California, Riverside Riverside, California

INTRODUCTION

The problem in monitoring stratospheric flight is to decide how often and at what locations to measure the effects of flight on the environment. Since the purpose of monitoring is to improve decisions regulating flight, any treatment of the monitoring problem must be based on a model for the control of stratospheric flight. One approach which has proved useful is to view the problem of regulating flight as a problem in stochastic dynamic programming. In this framework the decision-maker determines how much flight to permit in each period to maximize net benefits from flight over some horizon. Net benefits in any period depend on the control variable, amount of flight, and the state of the system being controlled. In the SST problem the state of the system may be interpreted either as a pollution stock (e.g., the stock of NO_x, SO_x, or some other effluent discharged during flight) or as some measure of environmental quality, such as the density of the ozone laver.

Stratospheric flight affects net benefits directly through a benefit function and indirectly by increasing the pollution stock. The relationship between amount of flight and level of pollution is embodied in a state transformation, which gives the pollution stock at the end of period t as a function of the pollution stock at the end of the previous period and the amount of flight in the tth period.

Under certain general conditions, the problem described here may be solved to yield the optimal amount of flight each period as a function of the pollution stock at the beginning of that period. To implement the optimal policy, the decision-maker has only to determine what the state of the system will be at any point in time and then compute the optimal amount of flight allowed. It is important to realize that if all the relationships in the model are deterministic, the decision-maker need know only the size of the initial pollution stock in order to compute what the state of the system will be at any point in time. Thus, in the absence of uncertainty, the policymaker need measure the state variable only at the beginning of the planning horizon. The monitoring problem, as described above, simply does not exist.

The monitoring question is, however, important if the relationship between the control variable and the state variable is uncertain. In this case, it is still In most stochastic control models it is assumed that the decision-maker can costlessly observe the state of the system before announcing his choice of the control variable. In practice, however, measuring the state variable is costly, and it is therefore meaningful to ask how often the state of the system should be observed. The remainder of the paper provides a method of determining the optimal pattern of monitoring activity when monitoring is costly and the amount of pollution generated by stratospheric flight is uncertain.

THE MODEL²

At the beginning of each period of his horizon the policy-maker must determine a_t , the number of hours of flight permitted during the period. For reasons given below, it is convenient to measure the number of hours of flight in terms of pollutants discharged per hour. Thus a_t represents the number of ppm of NO_x or SO_x resulting from flight.

As flight occurs, X, the stock of the pollutant in the environment, increases according to the state equation

$$X_t = X_{t+1} + a_t + w_t, \quad t = T-1, T-2, \dots, 0.$$
 (1)

Equation (1) states that X_t , the pollution stock at the end of period t, is equal to X_{t+1} , the state of the system at the end of the previous period, 4 plus a_t , the increment in pollution caused by flight during the t^{th}

² The model presented here is similar to the model

possible to solve for the optimal level of flight as a function of the state of the system. However, given knowledge of the initial pollution stock and of the random state transformation, it is no longer possible to determine the state of the system for all future time. Instead the decision-maker can only compute a probability distribution over future pollution stocks. Thus, in the uncertainty case, the state of the system can be known only if it is actually observed.

developed by one of the authors in Cropper (1975).

This is equivalent to assuming that emission-cont

³ This is equivalent to assuming that emission-control standards for aircraft engines have already been imposed, so that the amount of pollution resulting from an hour of flight is fixed.

⁴ Following the dynamic programming convention, all periods are numbered backwards. T refers to the time at the beginning of the T-period horizon and T-I to the first period of the horizon. Period 0 is the last period of the horizon.

This will be the case if the amount of effluents discharged during flight is uncertain or if the effect of effluents on the state variable (e.g., the ozone layer) is uncertain.

period, plus w_t , an exogenous periodic change in the accumulated pollutant. The $\{w_t\}$ are assumed to be independently and identically distributed random variables with known distribution.⁵

Within each period society derives benefits $B(a_t)$, which are assumed to be an increasing, concave function of the number of hours of flight. At the same time the pollution which accompanies flight imposes costs $D(X_t)$, which increase at an increasing rate with the size of the pollution stock. Net benefits, $B(a_t) - D(X_t)$, are defined to be the difference between benefits and costs.

If at the end of each period the decision-maker could observe X_t without charge, he would be faced with the problem of selecting control variables a_{T-1} , a_{T-2} , ..., a_0 to maximize the sum of expected net benefits over a T-period horizon

$$\sum_{t=0}^{T-1} B(a_t) - ED(X_t) , \qquad (2)$$

subject to (1).⁶ The expectation operator appears in equation (2), since at the time a_t is chosen X_t , the pollution stock at the end of period t, is random.

If X_{t+1} is costlessly observable at the end of period t+1 before a_t is chosen, then the decision-maker should solve equation (2) for a_t as a function of X_{t+1} , t=T-1, T-2, ..., 0. When monitoring is costly, the decision-maker, given the initial pollution stock X_T , must determine when he will next pay to observe the state of the system, as well as the amount of flight to permit in each period until the first observation is taken. In order to determine when X should first be observed, however, the decision-maker must determine an optimal monitoring strategy for the entire horizon, as well as the number of hours of flight allowed in each period. The wedenote the total number of observations by n, 0 < n < T, and the cost of each observation by n, then the decision-

maker will choose a_{T-1} , a_{T-2} , ..., a_0 and the times at which monitoring will occur to

$$\max \sum_{t=0}^{T-1} B(a_t) - ED(X_t) - nq.$$
 (3)

Once this problem has been solved, the decision-maker will know when (if at all) he next plans to observe X, and how much flight to permit in each period before this observation is taken. Suppose that the decision-maker first plans to monitor X at the end of period T- τ . Once $X_{T-\tau}$ has been observed, the decision-maker will again solve the problem described above, with $T = T-\tau$ and with $X_{T-\tau}$ replacing X_T as the initial pollution stock. In this manner the optimal monitoring policy is determined sequentially, with the decision-maker deciding, on the basis of his most recent information, when next to monitor the pollution stock.

THE SOLUTION TO THE PROBLEM

The solution to the monitoring problem described above can be obtained using a backwards-recursive procedure frequently employed in solving dynamic programming problems. To illustrate clearly how this is accomplished, we solve the monitoring problem first for a two-period horizon, then for a three-period horizon, and, finally, for the general T-period case.

The Two-Period Model

In the two-period case the decision-maker knows X_2 , the pollution stock at the beginning of the horizon, and must select a_1 , the amount of flight during period one, and a_0 , the amount of flight in the final period, to maximize

$$B(a_1) - ED(X_1) + B(a_0) - ED(X_0),$$
 (4)

where

$$X_1 = X_2 + a_1 + w_1$$
 and $X_0 = X_1 + a_0 + w_0$.

The decision-maker can pick a_0 and a_1 solely on the basis of his knowledge of X_2 , or, at a cost of q, he can observe X_1 before choosing a_0 . If the decision-maker chooses a_0 and a_1 without observing X_1 , his maximal expected utility over both periods is

$$V_{10}(X_2) = \max_{a_0, a_1} E[B(a_0) - D(X_2 + a_1 + w_1 + a_0 + w_0) + B(a_1)$$

$$- D(X_2 + a_1 + w_1)].$$
(5)

⁵ In the case of NO_X or aerosols, it is probably not unreasonable to assume that the pollutant stock is affected by some exogenous noise in the manner indicated by equation (1). However, more complicated forms of the state transformation could be employed without altering the validity of the results described below. For example, the state equation could be written $X_t = X_{t+1} + a_t + b_t X_{t+1}$, with b_t representing an uncertain pollution decay rate. Alternatively, the uncertain increment to the pollution stock could be made to depend on a_t . For expository purposes, however, it is convenient to work with equation (1).

⁶ The method of determining an optimal monitoring policy is not altered if a positive discount rate is assumed. A zero rate is assumed only for notational simplicity.

We assume throughout that if the policymaker pays to observe X_t he will in fact observe the true state of the system. We thereby ignore any problems posed by random measurement error.

⁸ The strict concavity of B(·) and the strict convexity of D(·) guarantee that this maximum exists and is unique.

If the decision-maker plans to observe X_1 before choosing a_0 , using a backwards-recursive procedure, he will choose a_0 as a function of X_1 and will receive an expected return of

$$W_0(X_1) = \max_{a_0} E[B(a_0) - D(X_1 + a_0 + w_0)]$$
 (6)

in period 0. In period 1 the decision-maker will select a 1 (as a function of X_2) to maximize $E[W_0(X_1) + B(a_1) - D(X_1)]$ and will receive an expected payoff of

$$V_{11}(X_2) = \max_{a_1} E[W_0(X_2 + a_1 + w_1) + B(a_1) - D(X_2 + a_1 + w_1)]$$
(7)

over the two-period horizon, before deducting the cost of observing X_1 . Since the decision-maker's objective is to maximize the expected value of net benefits minus monitoring costs, he will choose to observe X_1 if and only if $V_{11}(X_2) - q > V_{10}(X_2)$. Equivalently, the decision-maker will monitor X_1 iff $V_{11}(X_2) - V_{10}(X_2)$, the expected gain from monitoring, exceeds the cost of taking an observation.

The value-of-monitoring function, $V_{11}(X_2) - V_{10}(X_2)$, possesses two important properties.

- 1. $V_{11}(X_2) V_{10}(X_2) > 0$ for all X_2 . This follows from the definition of a maximum, with the strict inequality holding if the distribution of w_t is non-trivial, if $B(\cdot)$ is strictly concave and if $D(\cdot)$ is strictly convex and increasing.
- V₁₁(X₂) V₁₀(X₂) is an increasing function of X₂, provided marginal damages increase at a faster rate than marginal benefits, i.e., provided B" < D".

The last condition is likely to be satisfied whenever X is large in absolute terms, especially if X can be thought of as approaching a catastrophe level. Intuitively, when a catastrophic pollution level has been reached the rate of increase in marginal pollution damage is very high.

In view of properties (1) and (2) the monitoring decision may be expressed very simply in terms of X₂:

Monitor if
$$X_2 > \alpha$$
 (8)

Do not monitor if $X_2 < \alpha$

where $\alpha = \max \{X_2 | V_{11}(X_2) - V_{10}(X_2) \le q\}$ and where $\alpha = \infty$ if no such maximum exists.

If the decision-maker decides to monitor, then a_1 will be chosen to satisfy (7) and a_0 will be found by maximizing $B(a_0) + ED(X_1 + a_0 + w_0)$. If it is not optimal to monitor, then a_0 and a_1 are chosen to satisfy (5). The resulting two-period expected return will be written

$$W_{1}(X_{2}) = \begin{cases} V_{10}(X_{2}) & , X_{2} \leq \alpha \\ V_{11}(X_{2}) - q & , X_{2} > \alpha \end{cases}$$
 (9)

The Three-Period Model9

In the three-period case, X_3 , the pollution stock at the beginning of the first period, is assumed known and a_2 , a_1 , and a_0 must be chosen to maximize

$$\sum_{t=0}^{2} B(a_{t}) - ED(X_{t})$$
 (10)

subject to $X_t = X_{t+1} + a_t + w_t$, t = 2, 1, 0.

The monitoring problem is to determine whether monitoring should occur at all and, if so, whether X_2 or X_1 should be the first state variable observed.

We shall define, analogous to the two-period case,

$$V_{22}(X_3) = \max_{a_2} E[W_1(X_2) + B(a_2) - D(X_2)]$$
 (11)

$$V_{21}(X_3) = \max_{a_2, a_1} E[W_0(X_1) + B(a_1) - D(X_1) + B(a_2) - D(X_2)]$$
(12)

$$V_{20}(X_3) = \max_{a_2, a_1, a_0} E[B(a_0) - D(X_0) + B(a_1) - D(X_1) + B(a_2) - D(X_2)]$$
(13)

In view of (11)-(13) the maximum expected return from each monitoring strategy is

- V₂₂(X₃) q if X₂ is the first state variable observed and an optimal policy is followed with respect to X₂, the state observed at the end of period 2;
- V₂₁(X₃) q if X₁ is the first variable monitored and an optimal policy is followed with respect to X₁;
- 3. V₂₀(X₃) if neither X₂ nor X₁ is observed.

The decision-maker will select the monitoring strategy with the highest expected return and will choose values of a_2 , a_1 , and a_0 which satisfy the appropriate $V_{2t}(X_3)$, t=2, 1, 0. For computational purposes the maximum of 1.-3. can be determined by simple pairwise comparison of $V_{22}(X_3) - q$, $V_{21}(X_3) - q$, and $V_{20}(X_3)$. However, we conjecture

Using a backwards-recursive procedure, the threeperiod model is formed from the two-period model by adding an additional period at the beginning of the horizon. Period 2 is now the first period of the horizon and period 0 the last period.

that under certain reasonable conditions 10 the optimal monitoring strategy will have the form

Monitor
$$X_2$$
 next if $\alpha_{21} < X_3$

Monitor
$$X_1$$
 next if $\alpha_{20} < X_3 < \alpha_{21}$ (14)

Do not monitor if $X_3 \le \alpha_{20}$

where $\alpha_{20} = \{ \max X_3 N_{21}(X_3) - V_{20}(X_3) \le q \}$, and $\alpha_{21} = \max \{ X_3 N_{22}(X_3) \le V_{21}(X_3) \}$.
Assuming that this is the case, the maximal

three-period return can be written

$$W_{2}(X_{3}) = \begin{cases} V_{20}(X_{3}) & \text{if } X_{3} < \alpha_{20} \\ V_{21}(X_{3}) - q & \text{if } \alpha_{20} < X_{3} < \alpha_{21} \end{cases} (15)$$

$$V_{22}(X_{3}) - q & \text{if } \alpha_{21} < X_{3}$$

The monitoring strategy in (14) has the intuitively appealing property that the decision-maker will monitor X sooner the larger the initial pollution stock is. This property seems, upon reflection, to characterize a variety of everyday monitoring problems. A driver is likely to check his gas gauge more often when his tank is near empty than when it is full. An individual is more likely to have a physical examination when he is feeling ill than when he is feeling well.

The T-Period Model

In the T-period case, X_T, the pollution stock at the end of period T, is known and the decision-maker must select $a_{T-1}, a_{T-2}, \ldots, a_0$ to maximize

$$\sum_{t=0}^{T-1} B(a_t) - ED(X_t) , \qquad (16)$$

where $X_t = X_{t+1} + a_t + w_t$, $t = T-1, T-2, \dots, 0$. The monitoring problem is to determine which of T possible monitoring strategies yields the highest expected net return.

As in the two- and three-period cases, we shall let $W_t(X_{t+1})$ represent the maximal expected return over periods t, t-1, ..., 0 if X_{t+1} is the state at the end of period t+1. $V_{ts}(X_{t+1})$ represents the return received over periods t, t-1, ..., 0 if X is first observed at the end of period s, s < t, and an optimal policy is followed with respect to X_s, the state variable observed. Formally,

(i)
$$0 > V'_{22}(X_3) > V'_{21}(X_3) > V'_{20}(X_3)$$

and

(ii)
$$V_{20}(\alpha_{20}) > V_{21}(\alpha_{20}) - q > V_{22}(\alpha_{20}) - q$$
.

$$W_{-1}(X_0) = 0 (17)$$

$$W_0(X_1) = \max_{a_0} E[B(a_0) - D(X_0)]$$
 (18)

$$W_{t}(X_{t+1}) = \begin{cases} V_{t0}(X_{t+1}) & \text{if } X_{t+1} \leq \alpha_{t0} \\ V_{t1}(X_{t+1}) - q & \text{if } \alpha_{t0} < X_{t+1} \leq \alpha_{t1} \\ & \ddots & & \\ \vdots & & \ddots & \\ V_{tt-1}(X_{t+1}) - q & \text{if } \alpha_{tt-2} < X_{t+1} \leq \alpha_{tt-1} \\ V_{tt}(X_{t+1}) - q & \text{if } \alpha_{tt-1} < X_{t+1} \end{cases}$$

where

$$V_{ts}(X_{t+1}) = \max_{a_t, \dots, a_s} E[W_{s-1}(X_s) + \sum_{r=s}^{t} B(a_r) - D(X_r)]$$
(20)

$$\alpha_{t0} = \max \left\{ X_{t+1} | V_{t1}(X_{t+1}) - V_{t0}(X_{t+1}) \le q \right\}, \quad (21)$$

$$t = T-1, \dots, 1.$$

$$\begin{aligned} \alpha_{ts} &= \max \left\{ X_{t+1} \big| V_{ts+1}(X_{t+1}) - V_{ts}(X_{t+1}) < 0 \right\}, \ (22) \\ &t = T\text{-}1, \ldots, 1 \\ &s = t, \ldots, 1. \end{aligned}$$

The decision-maker will choose X_t as the first variable to be monitored if the strategy "observe X, next" yields the highest expected return. Thus, to find the optimal monitoring strategy the decision-maker will pick the maximum of $\{V_{T-1,T-1}(X_T) - q, V_{T-1,T-2}(X_T) - q, \dots, V_{T-1,1}(X_T) - q, V_{T-1,0}(X_T)\}$. This may be accomplished by making T-1 pairwise comparisons among the $V_{T-1,t}(X_T)$. However, under appropriate conditions the optimal monitoring strategy will have the form:

Monitor
$$X_{T-1}$$
 next if $\alpha_{T-1,T-2} < X_T$
Monitor X_{T-2} next if $\alpha_{T-1,T-3} < X_T < \alpha_{T-1,T-2}$

(23)

Monitor
$$X_1$$
 next if $\alpha_{T-1,0} < X_T < \alpha_{T-1,1}$

¹⁰ Sufficient conditions for the optimal monitoring strategy to have the form (14) are that

D'ARGE

where the $\{\alpha_{T-1,t}\}$ are defined by (21) and (22).

Once the optimal monitoring strategy has been selected, the number of hours of flight permitted in each period before monitoring occurs will be obtained as the solution to the corresponding V_{T-1,t}(X_T). Note that after the first X has been observed, the problem

described by equations (16)-(23) will be solved again, with T now indicating the number of periods remaining in the horizon. In this manner the optimal monitoring policy is determined sequentially, with each monitoring decision based on the decision-maker's most recent information.

BIOLOGICAL AND ECONOMICAL IMPACT

DISCUSSION

GWIAZDOWSKI: In the absence of other questions, I have one that I would like to address to Dr. Urbach. You indicated that the effect of ozone on skin cancer was real and important. Now the Environmental Protection Agency is trying to remove ozone, oxides of nitrogen, and particulates from the atmosphere of the urban areas, where most of our people live. As I understand the meteorology, that will lead to an increase in ultraviolet radiation in all of those areas and therefore, presumably, toward an increase in skin cancer. Now, if this is an important problem, has EPA asked you about this?

URBACH: EPA has not asked me anything, for which I should perhaps be thankful. However, as regards the amount of ozone and nitric oxides and such, you may recall a slide I showed you of actual measurements taken in Philadelphia. If you remember, there was a nice notch which made the curve smooth and symmetrical: that was the end of July and August in Philadelphia. And that rather nice notch is probably due not to ozone but to the various other mobile-source air effluents and climatic conditions. Completely cleaning up a city like Los Angeles is probably like governing New York impossible. But even if you could, the change would not really be very great. The reason for this is that many factors contribute to the relatively low amount of skin cancer among city dwellers. In any area with high buildings, about 50% of the ultraviolet radiation is excluded. This was shown by Schulze back in about 1925. You would get about twice the sunburn in the same period of time on top of Rockefeller Center that you would in the ice-skating rink 300 feet below because half the radiation is absorbed by the buildings. Years ago, 'this was called the "biologic darkness" of cities; they get so little ultraviolet that most of the people who do get skin cancer in big cities either are very fair or are people who work outdoors all the time. I think cleaning up the air in the cities would probably not lead to a measurable increase in skin cancer. The change would be orders-of-magnitude different from what would happen if the ozone level changed, I think the benefits of cleaning up cities, given the ill effects of pollution on eyes, lungs, and so on, would certainly outweigh a very few more cases of skin cancer.

(UNIDENTIFIED): It seems to me from what we know about climatic changes over the last hundred years, and in particular the last 25 years, that the climatic studies we have seen from CIAP on grain production and the like are very valuable, although a 1°C change is really a climatic fluctuation, not a major climatic change. Since the climatic fluctuations are regional, we can't take a globally-averaged climatic change and integrate the economic cost. There may be simultaneous cooling in the Ukraine and warming over the U.S. From 1949 to 1972 there was a very dramatic cooling over the U.S., while many parts of the world experienced a warming. It seems to me a fluctuation of 1°C globally would be very non-linear locally, and I don't see how you could possibly integrate the economic effects.

D'ARGE: I agree with you that there are regional variations. They are accounted for in the following sense: The kinds of statistical models that were used predict changes in yields, and they reflect these shifts within regions over time. Obviously, a global change of -1°C may not mean a change of -1°C in every area, but we just don't have a better set of numbers. If you can give me the regional figures – I'll make this a challenge – I'll give you the regional economic effects tomorrow.

(UNIDENTIFIED): I would like to comment on one aspect I haven't heard addressed here at the CIAP conference. It's fairly obvious from some of the findings of the agricultural programs that ozone has quite an influence on crop production. I should like to know whether there might be some beneficial aspects of stratospheric ozone reduction.

(UNIDENTIFIED): As I understand it, Dr. d'Arge, the actual price structure used for your various crops was what existed in 1972. In what direction would your results change due to the energy crisis and the resulting price differentials in the agricultural market?

D'ARGE: Well, in general the costs for the crops we studied are underestimates today, as are the heating costs and urban costs (which reflect 1972 fuel prices) and all of the indirect costs involved, such as construction (which are based on the 1972 prices). There is a new price structure now. One can argue that those values should be adjusted upwards to reflect the new price structure, but a logical argument can also be made that what we are observing now is a brief anomaly relative to the length of time involved in climatic change, and therefore one should look at long-run values, which are better illustrated by 1972 figures.

ATTAINMENT OF ULTRA-LOW NO_x EMISSIONS LEVELS IN AIRCRAFT TURBINE ENGINES

DONALD W. BAHR

Aircraft Engine Group General Electric Company Cincinnati, Ohio

ABSTRACT: The attainment of ultra-low oxides-of-nitrogen (NO_x) emissions levels in aircraft turbine engines, at cruise and other high-power operating conditions, will require combustors which are significantly different and more complex than current combustors. Specifically, in ultra-low-NO_x combustors, features will be needed to vaporize the fuel and fully mix it with all of the available combustion air upstream of the combustion zone, since both theoretical considerations and experimental investigations show that very low NO_x levels may be obtained in combustors if the combustion process is carried out with uniform, all-gaseous, and very lean fuel-air mixtures. The use of such provisions will, in turn, probably require variable combustor-airflow-distribution capabilities so that satisfactory performance may be obtained at low-power operating conditions, as well as at cruise and the other high-power operating conditions. Ultra-low-NO, combustors will thus embody major departures from the combustor design technology used in the most modern operational engines, and will also be much more advanced than the low-emissions combustors currently being developed to meet the emissions standards prescribed for ground-level engine operating conditions. The apparent necessity for fuel-air premixing to obtain ultra-low NO_x emissions levels is a particularly significant departure from current combustor design practice; it is an area of considerable concern because of fuel pre-ignition, flame flashback, and carbon-deposition problems and their serious consequences. Accordingly, extensive applied research and exploratory development efforts appear to be needed to establish the feasibility and practicality of obtaining ultra-low NO_x emissions levels in combustors, to evolve suitable ultra-low-NO_x combustor design concepts and to provide the required designtechnology base for this totally new type of combustor.

INTRODUCTION

The combustors used in modern aircraft turbine engines must be capable of meeting stringent performance and operational requirements over wide ranges of engine operating conditions. Based on design technology acquired over a period of many years, combustors in current use have been successfully designed and developed to meet these exacting requirements. The need for reduced pollutant-emissions levels adds a new set of requirements to those already imposed. Extensive efforts to develop technology for the design of combustors with reduced carbon monoxide (CO), unburned-hydrocarbons (C_xH_y), and oxides-of-nitrogen (NO_x) emissions levels are, therefore, under way.

The primary intent of this paper is to provide a brief description of the combustor design-technology advances needed to obtain ultra-low NO_x emissions levels in future aircraft turbine engines. This presentation summarizes

the typical combustor performance requirements of modern operational aircraft turbine engines and the status of the NASA/General Electric Experimental Clean Combustor Program, which is presently under way to develop low-emissions combustors for use in these engines. The conceptual combustor design features needed to obtain NO_x emissions levels significantly lower than those provided by the combustor design concepts evolved in the NASA Experimental Clean Combustor Program are also outlined, along with brief descriptions of the key development concerns associated with these advanced conceptual design features.

Originally, this presentation was prepared only as a lecture to be delivered at the CIAP 4 conference, and no written text for publication was composed. However, copies of the slide charts used in the presentation are given in the following pages. They are supplemented by brief accompanying descriptions of the key points contained in each chart.

BAHR

CF6-50 ENGINE COMBUSTOR

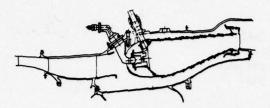


Chart 1 - CF6-50 Engine Combustor

A cross-sectional illustration of a current-technology combustor, typical of those in use in modern aircraft turbine engines, is shown in Chart 1. This specific combustor is used in the General Electric CF6-50 turbofan engine, which is a commercial transport aircraft engine in the 50,000-pound (224 kN) thrust class. This annular combustor is an advanced, short-length, long-life design which has been developed to meet the performance requirements of the CF6-50 engines and to operate with very low smoke-emission levels. In this annular combustor design, the fuel

is introduced by 30 pressure-atomizing fuel nozzles. As in almost all current-technology combustors, the fuel is injected directly into the primary combustion zone, where it is atomized and mixed with the primary-zone airflow, and where most of the combustion process occurs. With this basic design, the very hot combustion gases are carefully confined within the cooling liners of the combustor, so that any possibilities of combustor hardware burnout problems due to pre-ignition or flame-flashback phenomena are avoided.

A photograph of the CF6-50 combustor is shown in Chart 2. In this photograph may be seen the 30 dome swirl cups, into which the 30 fuel nozzles are installed, and the details of the inner and outer cooling liners.

Chart 3 – Key Performance/Operating Requirements – CF6-50 Engine Combustor

Some of the important steady-state performance and operating requirements of the CF6-50

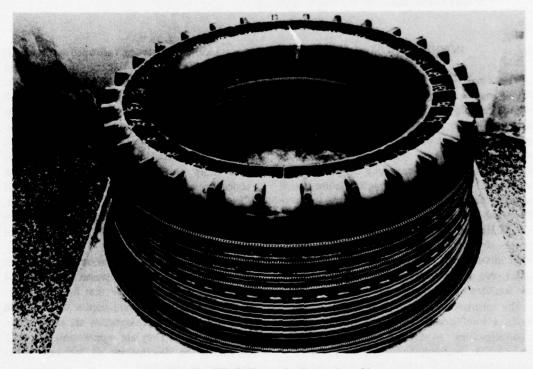


Chart 2 - CF6-50 Engine Combustor Assembly

KEY PERFORMANCE/OPERATING REQUIREMENTS

CF6-50 ENGINE COMBUSTOR

STANDARD DAY OPERATING CONDITIONS
 FUEL: KEROSENE

	GROUND	TAKEOFF	CLIMBOUT	CRUISE (35K-0.85 MACH)	APPROACH
PERCENT OF RATED POWER	3.5	100	85	21	30
INLET AIR TEMPERATURE (%)	313	1014	955	859	674
INLET AIR PRESSURE (psia)	42.8	426	372	168	172
FUEL-AIR RATIO	0.0117	0.0235	0.0214	0.0205	0.0144
FUEL-AIR EQUIVALENCE RATIO	0. 172	0.345	0 315	0.302	0.212
MIN. COMBUSTION EFFICIENCY (%)	96.0	99,9+	99.9+	99.9+	99.0
MAX. EXIT TEMPERATURE PATTERN FACTOR	0.30	0.22	0,22	0.22	0.25
MAX. TOTAL PRESSURE	4.5	4.5	4.5	4.5	4.5

engine combustor are shown in Chart 3, as an illustration of the stringent performance and broad operational capabilities typically required of combustors used in modern aircraft turbine engines. As is illustrated, these combustors must be capable of operating over wide ranges of inlet air temperatures, inlet air pressures, and fuel-air ratios, and must be able to meet exacting performance requirements over these wide ranges.

EXIT TEMPERATURE DISTRIBUTION REQUIREMENTS

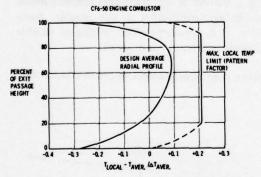


Chart 4 - Exit Temperature Distribution Characteristics - CF6-50 Engine Combustor

Among the most stringent sets of performance requirements of the combustors used in modern aircraft turbine engines are those relating to exit temperature distribution. For example, the exit temperature distribution requirements of the CF6-50 engine combustor are shown in Chart 4. As is illustrated, the average exit radial profile must conform to a specified shape to meet turbine-rotor operating requirements. Also, local peak temperatures must be minimized to protect the turbine-stator parts.

GROUND START REQUIREMENTS

CF6-50 ENGINE COMBUSTOR

OPERATING CONDITION	RANGE
INLET AIR TEMPERATURE	-30°F to 140°F
	(239 ⁰ K) to (333 ⁰ K)
INLET AIR PRESSURE	0.7 ATM. to 1.2 ATM.
FUEL-AIR RATIO	0.015 to 0.020

Chart 5 - Ground-Start Requirements - CF6-50 Engine Combustor

Additional stringent sets of performance requirements imposed on the combustors used in modern aircraft turbine engines are the ignition, or ground-start, requirements. As is illustrated by the operational requirements of the CF6-50 engine combustor, presented in Chart 5, these combustors must be capable of satisfactorily igniting and providing acceptable engine acceleration characteristics over wide ranges of combustor operating conditions.

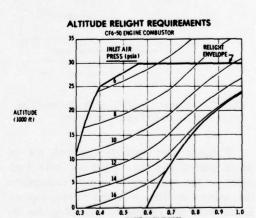


Chart 6 - Altitude Relight Requirements - CF6-50 Engine Combustor

Still other stringent performance requirements imposed on the combustors used in modern aircraft turbine engines are those governing altitude relight. As an illustration, the altitude operating flight envelope of the CF6-50 engine and its associated combustor-inlet airpressure levels are shown in Chart 6. The CF6-50

engine combustor must be capable of satisfactorily igniting and providing acceptable engine acceleration characteristics at any point within this envelope, which includes some severe sub-atmospheric-pressure operating conditions.

The combustors presently in use in modern operational aircraft turbine engines have been successfully developed to meet these requirements and those previously described. They have also been developed to operate with low smokemission levels, and to have long life. However, this advanced development status has required a number of years to attain, and is the direct result of the increasingly extensive design technology that has been steadily acquired during the past twenty or more years.

EFFECT OF PRIMARY ZONE STOICHIOMETRY ON NOx LEVELS

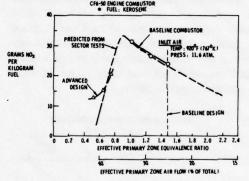


Chart 7 - Effect of Primary-Zone Stoichiometry on NO_x Levels - CF6-50 Engine Combustor

Within recent years, requirements for reduced gaseous-pollutant emissions have been added to the requirements already imposed on the combustors used in aircraft turbine engines. Extensive efforts to develop technology for the design of combustors with reduced levels of the emissions of concern - CO, C_xH_y, and NO_x are, therefore, being conducted both by government agencies and by aircraft engine manufacturers. Progress has already been made in the definition of approaches for reducing CO and C_xH_y emissions levels. In the investigations conducted to date, the attainment of significantly lower NO_x emissions levels has been found to be the most formidable emissions problem associated with aircraft turbine engines - especially in the cases of the newer, high-performance subsonic-transport engines and the supersonic transport engines, because of their high combustor-inlet air temperatures.

Investigations conducted at General Electric have shown that the only fundamental combustor design approach for significantly reducing NO_x emissions levels involves the use of much leaner prima—mbustion-zone fuel-air mixtures than those used in current-technology combustors. Some typical results of these investigations are presented in Chart 7. Operation with primary-zone mixtures richer than those used in modern combustors results in modest NO_x-emissions-level reductions, but also causes objectionable increases in smoke emission levels.

The use of leaner-than-stoichiometric primary-combustion-zone mixtures, while effective in reducing NO_x emissions levels, results in excessively lean mixtures at low-engine-power operating conditions. As a result, the reduced NO_x emissions levels are accompanied by large increases in CO and C_xH_y emissions levels and unacceptable losses in ignition performance. Thus, the use of this basic approach in current-technology combustors is not feasible. Some form of combustion-process staging or variable combustor geometry is required.

NASA ECCP DOUBLE ANNULAR CF6-50 COMBUSTOR

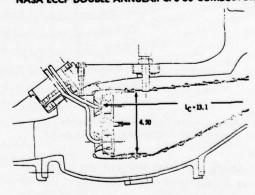


Chart 8 - NASA ECCP Double-Annular CF6-50 Combustor

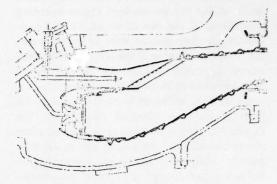
In the light of findings like those shown in Chart 7, the efforts of the NASA/General Electric Experimental Clean Combustor Program have, from the outset, been focused on the definition and development of advanced combustors with the combustion-process-staging design features needed to provide the required lean primary-combustion-zone fuel-air mixtures at high-power engine operating conditions and the required richer mixtures at low-power engine operating conditions. The overall objective of this program is to develop technology for the design of advanced combustors for use in commercial-transport aircraft-engine applications, to permit compliance by these engines with the presently defined EPA standards which set limits on the pollutant emissions quantities that may be discharged in and around airports. In this program, the advanced combustors are being specifically sized for use in the General Electric CF6-50 engine. However, the technology being generated in this program is intended to be generally applicable to all advanced engines in the largethrust category.

One of the two most promising advanced combustors evolved in this program is depicted in Chart 8. This combustor features the use of two primary combustion zones, or domes, separated by a short centerbody. In this staged-combustor design concept, the outer dome is designed to operate with airflows lower than those supplied to the inner dome. Only the outer dome is fueled at idle and other low-engine-power operating conditions. In this manner, near-stoichiometric fuel-air mixtures and long residence times, due to the low air velocities, are maintained in the outer dome at the low-engine-power operating conditions. As a result, low CO and CxHv emissions levels at these operating conditions are obtained. At high-engine-power operating conditions, both stages are fueled and most of the total fuel flow is supplied to the inner dome. Consequently, lean fuel-air mixtures are obtained in both domes, and very short residence times are obtained in the inner dome due to its high air velocities. Low NO_x and smoke emissions levels result.

Chart 9 – NASA ECCP Radial/Axial Staged CF6-50 Combustor

The other promising advanced combustor evolved in this program is depicted in Chart 9. This combustor also features the use of two combustion stages, or zones. Here the stages are more nearly in series, and the operation of the

NASA ECCP RADIAL/AXIAL STAGED CF6-50 COMBUSTOR



main (downstream) stage is very dependent on the pilot (upstream) stage. In this staged-combustor design concept, only the pilot stage is fueled at idle and other low-engine-power operating conditions. Because of its relatively low airflows, near-stoichiometric fuel-air mixtures and long residence times are maintained in this stage at the low-engine-power operating conditions. As a result, low CO and C_xH_y emissions levels are obtained. At the high-engine-power operating conditions, both stages are operated, and high proportions of the total fuel flow are supplied to the main stage. In this latter stage, which handles a high percentage of the total combustor airflow, the fuel is premixed to some degree with its airflow, and therefore the resulting fuel-air mixtures that flow into its combustion zone are lean and relatively uniform. The burning of these lean mixtures is stabilized by the pilot stage of the combustor. Because of these main-stage design features, low NOx and smoke emissions levels are obtained.

NASA ECCP CF6-50 COMBUSTORS

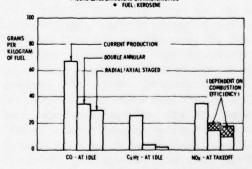


Chart 10 - NASA ECCP CF6-50 Combustors - Ground-Level Emissions Characteristics

BAHR

The typical gaseous-pollutant emissions levels, at the key ground-level engine operating conditions, of the two advanced CF6-50 combustors, in their present state of development, are compared to those of the current-productionengine combustor in Chart 10. In the case of NO_x emissions at takeoff operating conditions, a range of NO_x emissions levels is obtained with both of the two advanced combustors. The highest NO, emissions levels were obtained when the combustion-process staging was adjusted to provide combustion efficiencies comparable to those of the current production combustor. However, even the highest NO_v emissions levels of these advanced combustors are well below those of the current-production combustor, as are the CO and C_xH_y emissions levels.

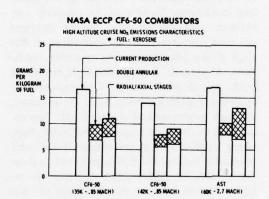


Chart 11 - NASA ECCP CF6-50 Combustors - High-Altitude-Cruise NO_x-Emissions Characteristics

The typical NO_x emissions levels at highaltitude-cruise operating conditions of the two combustors, both in the CF6-50 engine and in an assumed Advanced Supersonic Transport (AST) engine, are shown in Chart 11. Relative to the current production combustor, NOx emissionslevel reductions of about 50%, with acceptable combustion-efficiency performance, have been obtained with the two advanced combustors. Significant trade-offs between NO_x emissions level and combustion efficiency have been observed with these combustors; they are indicated in Chart 11 by the cross-hatched bands. The NO. emissions levels shown at the lower edges of these bands were obtained with combustion efficiencies of about 99%. The NO_x emissions levels at the upper edges were obtained with combustion efficiencies of 99.7% or higher. A combustion efficiency of at least 99.5% is considered to be essential at cruise conditions to minimize fuel consumption.

NASA ECCP RADIAL/AXIAL STAGED CF6-50 COMBUSTOR

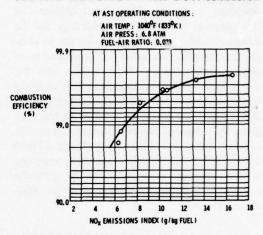


Chart 12 - NASA ECCP Radial/Axial Staged CF6-50 Combustor - At AST Operating Conditions

The radial/axial staged-combustor design concept has been found to have particularly sensitive NO_x -emissions-level combustion-efficiency-performance trade-off characteristics, as is illustrated in Chart 12. Although quite low NO_x emissions levels are obtainable at cruise operating conditions with this combustor design concept, the combustion-efficiency levels associated with these very low NO_x emissions levels are not satisfactory.

NASA ECCP CF6-50 COMBUSTORS

KEY DESIGN / DEVELOPMENT CHALLENGES

- COMBUSTION EFFICIENCY PERFORMANCE AT PART POWER OPERATING CONDITIONS
- . CONTROL OF EXIT TEMPERATURE DISTRIBUTIONS
- FLAME FLASHBACK PREVENTION (R / A STAGED)
- . FUEL SUPPLY / CONTROL SYSTEMS COMPLEXITY
- EFFECTS ON ENGINE ACCELERATION / DECELERATION CHARACTERISTICS
- . PREVENTION OF THRUST TRANSIENTS DURING FUEL STAGING CHANGES

Chart 13 - NASA ECCP CF6-50 Combustors - Key Design/Development Challenges

Considerable progress has been made in the development of technology for the design of these advanced combustors. However, they are considerably more complex and sophisticated than current-technology combustors, and they embody significant departures from the combustor design practices and technology currently found in even the newer operational engines. Accordingly, many aspects of their performance and operating capabilities are unknown, and only very limited technology and criteria for their design and development are in hand. Because of these factors, several more years of technology development appear to be needed before versions of these advanced staged-combustor design concepts may be considered for use in operational engines. Some of the key design and development concerns that must be resolved are shown in Chart 13. Efforts to provide the technology to meet these challenges are under way.



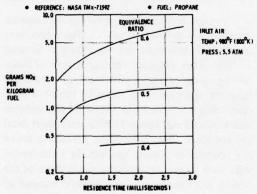


Chart 14 - NO_x Levels Obtainable with Lean Fuel-Air Mixtures

Even with advanced combustor design concepts like those being evolved in the NASA Experimental Clean Combustor Program, high-altitude-cruise NO_{X} emissions-levels reductions by much more than a factor of two do not appear likely. From theoretical considerations, an ideal combustion process involving lean, all-gaseous, and uniformly mixed fuel-air mixtures would be expected to provide lower NO_{X} emissions levels at mixture pressure and temperature operating conditions similar to those in the ECCP. The feasibility of obtaining very low NO_{X} emissions levels with such fuel-air mixtures has

already been experimentally demonstrated in laboratory combustors. Some results of a significant investigation of this kind are shown in Chart 14. With very lean mixtures, NO_x emissions indices below 2 were obtained, with realistic combustion-zone residence times and with reasonable combustion efficiencies. All NO. emissions indices shown in this plot were obtained with combustion efficiency levels of 99.25% or higher, with the higher efficiencies being obtained with the longer residence times. For a combustion efficiency of 99.7%, residence times of about 1.8 and 1.1 milliseconds, respectively, were needed with the 0.4 and 0.5 equivalence-ratio mixtures. These results suggest that the NO_x emissions levels of aircraft turbine engines, at high-altitude-cruise operating conditions, could possibly be reduced by a factor of 10 or more.

ULTRA-LOW NOX COMBUSTOR-CONCEPTUAL DESIGN

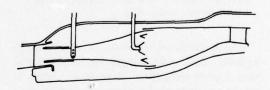


Chart 15 – Ultra-Low-NO_x-Combustor Conceptual Design

The application of these ideal-combustionprocess approaches in engine combustors will involve provisions for vaporizing the fuel and fully mixing it with all of the available combustion air upstream of the combustion zone - at cruise and other high-engine-power operating conditions. A conceptual combustor design with such provisions is shown in Chart 15. Since such a design would not provide satisfactory performance at ignition and low-engine-power operating conditions, additional provisions for injecting the fuel into part of the combustion zone, at these low-engine-power operating conditions, would also be needed. Even with such fuel-injection capabilities, variable-geometry features to reduce the quantities of air admitted into the combustion zone at low-engine-power operating conditions would probably also be needed. A combustor with these design features

would be very different from current-technology combustors, and even much more advanced than the combustors being evolved in the NASA Experimental Clean Combustor Program. The use of fuel-air premixing upstream of the combustion zone, which is an essential feature of such a combustor design concept, is a particularly significant departure from current design practice.

MAJOR DESIGN/DEVELOPMENT CONCERNS

ULTRA-LOW NO_x COMBUSTORS

- COMPLEXITY OF OPERATION
 - COMBUSTION AIRFLOW MODULATION
 - FUEL FLOW STAGING
 - SYNCHRONIZATION OF AIRFLOW / FUEL CONTROL CONTROLS
- . THRUST TRANSIENTS DURING AIRFLOW/FUEL FLOW STAGING
- EFFECTS ON ENGINE ACCELERATION / DECELERATION CHARACTERISTICS
- COMBUSTION STABILITY WITH LEAN MIXTURES
- . FUEL PRE-IGNITION
- . FLAME FLASHBACK INTO FUEL-AIR MIXING CHAMBER
- FUEL DECOMPOSITION/CARBON DEPOSITION ON HOT PARTS

Chart 16 - Major Design/Development Concerns - Ultra-Low-NO_X Combustors

Such advanced combustors would be inherently much more complex and sophisticated than current-technology combustors. Some of the key design and development concerns associated with such combustors are shown in Chart 16. Providing for and accommodating upstream fuel-air premixing would necessitate provisions for both fuel-flow staging and airflow modulation. The development of such capabilities is expected to be a very formidable challenge. The basic combustion-process stability obtainable with very lean mixtures is also a major area of concern. Such mixtures are near the lean inflammability limits of hydrocarbon-air mixtures, and, in addition, are very susceptible to combustionprocess oscillations, which have a variety of causes. Foremost among the concerns are the possible consequences of upstream fuel-air premixing, which opens the possibility of fuel pre-ignition, flame flashback, and/or carbondeposition problems in the premixing zone. Any such occurrences can have catastrophic consequences. Thus, the feasibility and practicality of incorporating such advanced design concepts and features into the combustors of operational engines cannot be accurately assessed at this time. Major research and technology development efforts will be needed before these feasibility and practicality questions can be satisfactorily answered.

Chart 17 - Fuel Pre-Ignition Design Criteria

INLET AIR TEMPERATURE (OF

Typical ignition-delay data for kerosene-air mixtures are shown in Chart 17. These data were obtained in investigations conducted at General Electric. They illustrate the importance of maintaining short average and local gas residence times in the premixing zones of ultra-low-NO_x combustors. At pressures above 10 atmospheres and temperatures above 1100°F, very short local gas residence times within the premixing zones are essential to prevent ignition. In a combustor with such premixing features, pre-ignition of the fuel-air mixtures could result in rapid burnout of the downstream combustor parts.

FLAME FLASHBACK TEST DATA (PREMIXING COMBUSTOR) • FUEL KEROSPIE

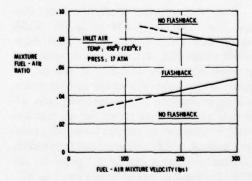


Chart 18 - Flame-Flashback Test Data (Premixing Combustor)

BAHR

Typical flame-flashback data, obtained in General Electric investigations, are shown in Chart 18. These data illustrate the importance of maintaining high average and local gas velocities in the premixing zone to minimize flashback tendencies. In a combustor with premixing features, any flame flashback into the premixing zone could result in rapid burnout of the downstream combustor parts.

ULTRA-LOW NOx COMBUSTORS

TECHNOLOGY DEVELOPMENT

- RESEARCH & EXPLORATORY DEVELOPMENT
 - FUEL PRE-IGNITION/FLAME FLASHBACK SUPPRESSION
 - FUEL PRE-MIXING METHODS
 - LEAN MIXTURE COMBUSTION CHARACTERISTICS
- EXPLORATORY COMBUSTOR DEVELOPMENT
 - FUEL FLOW/AIR FLOW STAGING NEEDS
 - PERFORMANCE ATTAINABLE
- PROTOTYPE COMBUSTORS DESIGN/DEVELOPMENT
- . PROTOTYPE FUEL CONTROL SYSTEMS DESIGN/DEVELOPMENT
- . ENGINE DEVELOPMENT/ DEMONSTRATION TESTING

Chart 19 – Ultra-Low-NO_x Combustors – Technology Development

Extensive applied research and technology-development efforts will be needed to establish the feasibility and practicality of obtaining ultra-low NO_x emissions levels in combustors, to

evolve suitable ultra-low- NO_x combustor design concepts, and to provide the required design technology base for this very new and different type of combustor. The key sequential steps envisioned for these needed research and development efforts are shown in Chart 19.

SUMMARY

- . FORMIDABLE TECHNICAL CHALLENGE
- NEW COMBUSTOR DESIGN TECHNOLOGY BASE NEEDED
- MAJOR COMBUSTOR/ENGINE DEVELOPMENT EFFORTS REQUIRED

Chart 20 - Summary

The attainment of ultra-low NO_x emissions levels at high-altitude-cruise operating conditions in future aircraft turbine engines is expected to be a very major and challenging task. Compared to the levels obtainable with current-technology combustors, NO_x emissions-levels reductions of about 50% appear to be obtainable with advanced staged combustors, like those currently being evolved in the NASA Experimental Clean Combustor Program. Significantly greater reductions will require the use of totally new and different combustor-design approaches and technology. These approaches will require very substantial technology-development efforts.

FLEET PROJECTIONS AND WHAT THEY MEAN IN TERMS OF SST FLEET EFFLUENTS

J. MORLEY ENGLISH AND GERARD L. KERNAN*

School of Engineering and Applied Science University of California, Los Angeles Los Angeles, California

ABSTRACT: This paper briefly describes the model used in selecting aircraft fleet mixes for various 1990-2000 scenarios, discusses the scenarios, and presents the passenger and cargo distribution by plane type for each scenario. It then explains the model and base data used to calculate the emission of various pollutants for each fleet, and gives the results broken down by altitude and latitude band.

INTRODUCTION

This paper describes the geographical location and altitude distribution of aircraft in the stratosphere in the 1990-2000 decade. The methodology of predicting air travel using a scenario approach was described at the Third Conference on CIAP (English, 1974), so the emphasis here will be on the size of future supersonic fleets and the estimation of emissions.

Also, in addition to satisfying the upperbound traffic demand with no constraints on supersonic technology (excepting the ban on overland flights), other supersonic scenarios were considered. The primary scenario assumed that an advanced supersonic transport would be built and that the demand for air travel would be divided between subsonic and supersonic modes. However, other possibilities that were considered were:

- a. No Supersonic Transport. This scenario assumes that for technical or market reasons, or because of prohibition on its operation, the SST is just a transient phase in air-transport development, and by 1990 it has disappeared completely from the scene.
- b. No Advanced Supersonic Transport.

 This scenario falls between the primary scenario and that of no supersonic transport. Due to primarily economic reasons, no country is prepared to undertake the expensive research and development program to build an ad-

vanced long-range supersonic transport. Accordingly, the present Concorde and Tupolev supersonic transports will be the only types available to compete with subsonic transports.

Both of the above scenarios were treated only for the upper-bound traffic predictions.

AIRCRAFT SELECTION MODEL

Future aircraft fleets were selected to service the demand on each route according to a profit criterion. A supersonic premium of 1.4 times the average subsonic fare was used in the model. (A higher fare for supersonic travel is essential to recover the anticipated higher fuel and capital costs for supersonic aircraft.) Supersonic flight within the contiguous U.S. and Europe was not permitted, but it was allowed within the U.S.S.R., South America, Africa, and parts of Asia. Supersonic flight was permitted for ocean crossing and over lightly populated areas. In addition, supersonic flight was allowed on routes where it would be necessary to have subsonic segments at each end to avoid sonic booms over populated areas. A subroutine was used to allocate passenger demand to supersonic aircraft on the basis of the passengers' willingness to pay the incremental cost for time saved. The value of time used was that developed by Lockheed (1973). The specifications of aircraft that will be flying from 1990-2000 are given in Table 1.

Suitable aircraft are filled with passengers at variable load factors and passenger revenue for

^{*}Dr. Kernan is now with the Irish Development Agency, Dublin.

Table 1. Characteristics of Available Flight Systems*

Transport	Range (km)	Passenger Capacity	All-Cargo Capacity (kg)	Secondary Cargo (kg)	Cruise Mach	Gross Weight (kg)	Operational Date
Extended small 3-jet	4,000	170	0	0	0.82	99,000	1977
SST	6,100	105	0	0	2.00	174,000	1975
Narrow-body 4-jet	9,500	145	40,800	9,000	0.82	152,000	Present
Large 4-jet	9,500	380	108,000	45,000	0.86	350,000	Present
Large 3-jet	5,500	270	56,600	18,000	0.83	200,000	Present
Long-range 3-jet	9,200	270	70,000	36,200	0.83	252,000	Present
Small 3-jet	3,200	140	0	2,200	0.82	70,000	Present
Large 2-jet	3,500	230	0	11,000	0.82	150,000	1975
Long-range 4-jet	10,000	285	72,500	11,000	0.87	299,000	1978
Large advanced SST	7,400	295	0	0	2.70	350,000	1987
Very large 4-jet	12,000	600	140,000	54,000	0.89	420,000	1981
Hypersonic	7,400	235	0	0	6.00	210,000	2015
Advanced very large	12,000	1,000	187,000	82,000	0.82	590,000	1990

*Sources: Boeing (1973), Petersen and Waters (1972), Douglas (1974), NASA (1973)

the single-route cycle computed. If the aircraft can carry belly cargo, the cargo demand for the route is served first by carrying belly cargo in the passenger aircraft, before assignment of any cargo to an all-cargo aircraft. The remainder of the route cargo demand is then served by all-cargo aircraft of the same type, providing an all-cargo aircraft of the passenger type is available within the set. If not, an all-cargo aircraft is selected on the basis of profitability to serve the remainder of the route's cargo demand.

The net route profit on this flight system subset is computed as a single value. Profit for all other combinations of passenger and cargo aircraft are then computed, and the subset with the maximum net route profit is selected to serve the route.

The number of aircraft needed to serve the route demand is determined on the basis of route flight time and the daily utilization which may be expected from each aircraft. The world fleet is obtained by summing the aircraft requirements over all of the world routes.

PREDICTED AIR FLEETS

The total number of aircraft required on the basis of the selection model to service the different scenarios described previously is shown in Tables 2 and 3. The fleet is calculated to carry

the summer peak traffic level, which traditionally runs 25% above the yearly demand. It should be noted that this represents an additional element of conservatism. Actually, peak loads may be accommodated in part by reduced load factors in the off-season period and corresponding crowding during the peak season. Also, no allowance is made for changed route demands that might occur. For example, the southern hemisphere's traffic demand pattern will be out of phase with the northern hemisphere's.

Upper-Bound Fleet

Even with the economic climate extremely favorable for growth of air transport, it is difficult to conceive that the air-transport industry, on a world scale, will account by 1990 for more than 1700 billion passenger-kilometers for passengers and 300 billion tonne-kilometers for cargo. Most of the passenger travel and all of the cargo will still be accommodated by subsonic jets flying at altitudes well below 12 km. This traffic translates into 5300 aircraft on routes longer than 700 km (the route segment length at which an aircraft may fly in the stratosphere for an appreciable time). All of these aircraft are large, averaging approximately 440 seats per airplane. A significant part of the traffic will be carried in an advanced re-scale aircraft, exceeding the

Table 2. Predicted Commercial World Fleets for Upper-Bound and Most-Likely Scenarios

Scenario	Hi	storical	l	Upper-Bound					Most-Likely						
Transport Type	1970 Actual*	Pred	Model- licted Cargo	1	80 Cargo		90 Cargo		00 Cargo		80 Cargo		90 Cargo		00 Cargo
Subsonic															
Twin engine**	1200	Service.													
Narrow-body 4-jet	1500	82	24	216	13					166	11			-	
Small 3-jet	1200	266		100						71					
Large 2-jet				20		149		1623		21		87		763	
Large 3-jet		18	18	31	2	324	114	1641	1031	31	4	183	78	674	460
Long-range 3-jet				2906	15	57	141	3985	569	2033	14	69	94	1523	267
Extended small 3-jet				27		259		768		23		161		374	
Large 4-jet		531	3	37	105	3060	217	601	1388	10	85	1490	130	156	646
Very large 4-jet					3	10	50	106	215	1		14	26	3	108
Long-range 4-jet						152	9 .	103			2	75	11	1	7
Advanced very large						465	270	1213	1362			246	177	342	528
TOTAL	3900	897	45	3337	138	4476	801	10040	4565	2355	116	2325	516	3836	2016
Supersonic															
SST				51						42					
LASST						440		1855				241		615	
TOTAL				51	March 1	440		1855		42		241		615	

Table 3. Commercial World Fleets for No-Advanced-SST and Supersonic-Ban Scenarios

Scenario	No Adva	nced SST		Supersonic Ban						
Year Transport	19	990	19	990	2000					
Туре	Pass.	Cargo	Pass.	Cargo	Pass.	Cargo				
Subsonic										
Large 2-jet	151		48		1562					
Large 3-jet	178	98	52	4	2046	11				
Long-range 3-jet	53	145	133	33	4890	4				
Extended small 3-jet	206		146		387					
Large 4-jet	3490	238	3412	265	1111	2219				
Very large 4-jet	3	36	55	14	150	189				
Long-range 4-jet	120	1	51							
Advanced very large	542	203	679	244	1860	938				
TOTAL	4743	721	4576	560	12006	3361				
Supersonic	e savenel									
SST	379									
Large advanced SST										
TOTAL	379	0	0	0	0	0				

^{*}Sources: World Airline Record (1971), World Aviation Directory (1971)
**A short- to medium-range jet with 80-130 passenger capacity, which almost never flies in the stratosphere.

capacity of the present Boeing 747 by a factor of more than two. Even with the industry reaching or approaching maturity by the year 2000, traffic could be more than double that of 1990.

The 1990 supersonic fleet will consist of 440 large advanced supersonic transports. This corresponds to 20% of traffic on admissible routes being captured by an SST.

The advanced SST would supersede the present Concorde and Tupolev types and be flying at an altitude of 18-21 km during the supersonic flight regime. Of the reasonably high utilization time -8 hours per day - only slightly more than half would be at this high altitude. Nevertheless, the fuel burned, predominantly over the North Atlantic, would amount to 26×10^9 kg/year.

The study was carried out by considering the market potential only, without consideration for the significant technological difficulties attached to development and production of an advanced SST. Even if a crash SST program were initiated today, it is highly unlikely that there would be significant numbers of large advanced SST's in operation by 1990. On the other hand, it is conceivable that the market might demand 440 SST aircraft, and the precise time at which production could catch up to this need is not important. If the urgency were sufficient, it could certainly be some time before 2000. Cargo aircraft will play an increasingly important role, since the demand for air cargo is predicted to grow at a faster rate than for passenger travel. In 1990 the cargo fleet will be comprised of 801 aircraft, of which the dominant types will be the large 4-jets and the ACX, the large advanced transport. These aircraft types will also be dominant in 2000 when the total cargo fleet will have increased to 4565 aircraft, approximately half the subsonic passenger fleet.

Most-Likely Fleet

The most-likely fleet will be similar in composition to that of the upper-bound fleet, though the numbers will be smaller. A fleet of 2355 subsonic and 42 supersonic aircraft is predicted for 1980. By 1990 the supersonic fleet will have increased to 241 LASST's, approximately half the upper-bound fleet. The subsonic passenger-fleet size in 1990 will drop slightly below the 1980 number, though the productivity

will have increased due to the selection of larger-capacity aircraft. The 1990 subsonic and supersonic passenger fleet will also be approximately half the 1990 upper-bound fleet. A cargo fleet of 516 aircraft is predicted for 1990. Again, the dominant types will be the L4J and the ACX. The 1990 supersonic fleet of 241 aircraft will increase to 615 aircraft by the year 2000.

No-Advanced-SST Scenario

The scenario for the case in which no large advanced SST is built was also examined from 1990. The aircraft fleet needed to carry the upper-bound traffic estimate is given in Table 3. The supersonic fleet chosen comprises 379 SST's, as compared with 440 LASST's for the scenario where the LASST was allowed. The subsonic passenger fleet increases from 4476 aircraft for the upper-bound case to 4743, to provide additional capacity in the absence of the LASST. The number of cargo aircraft, however, is decreased from 801 in the upper-bound case to 721 in this case. This is due to the additional belly-cargo space available in the larger subsonic fleet.

Supersonic-Ban Scenario

For this scenario, a complete ban on supersonic flight is examined for 1990. This case was also based on the upper-bound traffic prediction. Comparing it again with the upper-bound case, there is a small increase in the passenger aircraft fleet in 1990, from 4476 to 4576 aircraft. In addition, there is a change in the types of aircraft, with the number of ACX increasing from 465 for the upper-bound case to 670 for the supersonic-ban scenario. This is necessary in order to carry the traffic that was formerly carried supersonically. In addition, there is a drop in the number of cargo aircraft from 801 for the upper-bound case to 560 for the supersonic-ban scenario. This is again attributable to the increased belly-cargo capacity of the allsubsonic fleet. (The same effect is also obvious for the fleets in the year 2000.)

EMISSIONS CALCULATION MODEL

Given a particular route, the model determines the grids through which it passes and the route length through each grid. The emission rate

in tonnes/day in each grid is calculated as follows:

$$E_i = \sum_{j=1}^{n} n_j I_{i,j} F_j \times \frac{Distance in Grid}{Cruise Speed} (n=1,...9)$$

where

E_i = emission rate for ith emission species

I_{i,j} = emission index of ith species for jth aircraft type

F_j = fuel flow rate for jth aircraft type

n; = number of aircraft of jth type

The emission rate was estimated for an average day during the period July to August, when air traffic is at peak levels. The yearly average emission rate equals 0.75 of the peak summer rate.

The emission indices used for calculating engine emissions are given in Table 4. These indices are typical of present subsonic and supersonic engines. In the case of supersonic aircraft, two NO_x emission indices were used, 10 g/kg for the 9-12 km band (for subsonic climbing speed) and 18 g/kg for higher altitude bands (for supersonic cruise speed). The fuel

flows used to calculate total emissions, as shown in Table 5, are also based on present estimates of future engine technology.

The basic flight profiles used to determine the altitudes at which emissions occur are shown schematically in Figure 1.

Table 4. Engine Emission Indices (g/kg fuel)

Emission Species	Subsonic	Supersonic	Hypersonic
NO _x		HAME OF	7 17
9-12 km	10	10	17
12-15 km	7	18	17
15-18 km and above	-	18	17
со	3	3	-
Total Hydrocarbons	0.5	0.5	-
Soot	0.02	0.02	-
H ₂ O	1.25×10^{3}	1.25 × 10 ³	8.9 × 10 ³
CO ₂	3.22×10^{3}	3.22 × 10 ³	_
SO ₂	1.0	1.0	-
Total Trace Elements	0.01	0.01	-
Lubricating Oil	0.1	0.1	-

Table 5. Aircraft Characteristics

Transport Types	Cruise Speed (km/hr)	year 1980	Fuel Flow (kg/hr) year 1990	year 2000
Advanced very large	870	16100	16100	16100
Advanced subsonic 4-jet	990	13200	13200	13200
Large 2-jet	870	5400	5400	6200
Large 3-jet	880	6600	6600	7300
Large 4-jet	900	10400	10900	10900
Very large 4-jet	930	11800	11800	11800
Long-range 3-jet	890	7700	7700	8200
Long-range 4-jet	930	9500	9500	10400
Extended small 3-jet	900	3900	3900	3900
Small 3-jet	870	3600	3600	3600
Narrow-body 4-jet	870	4500	4500	4500
SST	2130	19100	19100	19100
Large advanced SST	2880	40800	40800	40800
Hypersonic	5410*/6960	100900*/39200	100900*/39200	100900*/3920

*Specifications during climbing period.

Sources: Becker and Kirham (1974), NASA (1973), BAC (1973)

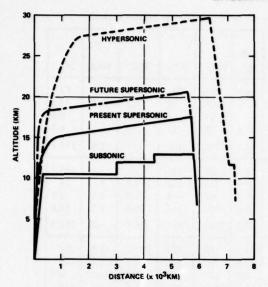


Figure 1. Representative flight profiles.

The subsonic flight profile has a maximum cruising altitude of 13 km (42,600 ft), which is higher than that reached by present subsonic types; at present they rarely go above 40,000 ft. However, it is anticipated that succeeding genera-

tions will be certificated to operate at higher altitudes than are used at present.

For supersonic aircraft, two flight profiles are used. The profile for present supersonic types is based on the Concorde. It will have a maximum cruising altitude of 17.5 km (57,000 ft), which will be reached in the final cruise stage. Future supersonic types are expected to fly faster (Mach 2.7) and higher, cruising at a maximum altitude of 20.5 km (67,000 ft).

EMISSIONS

A summary of emissions by altitude band and aircraft type for each scenario is given in Tables 6, 7, and 8. It can be noted that in terms of mass alone, CO₂ is the largest. The lowest emissions were for trace elements and lubricating oil. The insignificant supersonic emissions in the 9-12 km band were excluded from consideration to simplify modeling.

 NO_X emissions above 15 km are calculated to increase from 0 tonnes per day in 1970 to 94 in 1980. By 1990, this will have increased rapidly to 1810, and will reach 7658 tonnes per day by the year 2000.

Table 6. Upper-Bound Global Emissions by Altitude Band (tonnes/day, summer season)

Year	Aircraft Type	Altitude Band (km)	H ₂ O× 10 ³	CO ₂ ×	Trace	Lub Oil	NO _x	со	тнс	Soot	SO ₂
1970	Sub	9-12	50	1250	0.4	3.9	388	116	19.4	4 0.8 7 0.3 1 1.1 8 2.8 0.9 4 - 6 0.1 6 3.8 0 6.0 1 2.1 5 0.1 8 1.9	38.8
	Sub	12-15	20	40	0.1	1.3	94	40	6.7	0.3	13.3
		Total	70	1290	0.5	5.2	482	156	26.1	1.1	52.1
1980	Sub	9-12	170	440	1.4	13.8	1380	413	68.8	2.8	138.0
	Sub	12-15	57.5	150	0.5	4.6	322	138	23	1000000	46.0
	Sup	12-15	0.9	2.4	-	-	14	- 2	0.4	-	0.8
	Sup	15-18	6.5	16.8	0.1	0.5	94	16	2.6	0.1	5.2
		Total	235.0	610.0	2.0	18.9	1810	569	94.6	3.8	190.0
1990	Sub	9-12	370.0	960.0	3.0	29.9	2990	897	150.0	6.0	299.0
	Sub	12-15	130.0	340.0	1.0	10.4	729	312	52.1		104.0
	Sup	15-18	6.3	1.6	0.1	0.5	90.4	15	2.5	0.1	5.0
	Sup	18-21	120.0	310.0	1.0	9.6	1720	287	47.8	1.9	95.6
	mere Ch	Total	630	1620	5.0	50.0	5530	1500	252.0	10.0	503.0
2000	Sub	9-12	890	2230	7.1	71.0	7100	2130	355.0	14.2	710.0
	Sub	12-15	350	900	2.8	27.8	1950	835	139.0	5.6	278.0
	Sup	15-18	26	66	0.2	2.1	368	61	10.2	0.4	20.5
	Sup	18-21	510	1300	4.1	40.5	7290	1210	202.0	8.1	405.0
	Marine State	Total	1770	4560	14.0	142.0	16708	4236	706	29	1410.0

Table 7. Most-Likely Global Emissions by Altitude Band (tonnes/day, summer season)

Year	Aircraft Type	Altitude Band (km)	H ₂ O× 10 ³	CO ₂ ×	Trace	Lub Oil	NO _x	со	тнс	Soot	SO ₂
1980	Sub	9-12	120	320	1	9.8	977	293	48.9	2	97.7
	Sub	12-15	40.7	110	0.3	3.3	228	98	16.3	0.7	32.5
	Sup	15-18	0.8	2	-	_	11	2	0.3	-	0.6
	Sup	18-21	5.4	13.9	-	0.4	78	13	2.2	0.1	4.3
		Total	160	440	1.3	13.5	1294	406	67.7	2.8	135.1
2000	Sub	9-12	200	520	1.6	16	1600	480	79.9	3.2	160.0
	Sub	12-15	70	180	0.6	5.6	392	168	28.0	1.1	56
	Sup	15-18	3.4	8.8	-	0.3	49	8	1.4	0.1	2.7
	Sup	18-21	67	170	0.5	5.4	965	161	26.8	1.1	53.6
		Total	340	870	27.3	27.3	3006	817	136.1	5.5	272.3
2000	Sub	9-12	340	880	2.8	27.5	2750	824	137	5.5	275
	Sub	12-15	140	350	1.1	10.9	762	326	54.4	2.2	109
	Sup	15-18	8.4	21.6	0.1	0.7	121	20	3.4	0.1	6.7
	Sup	18-21	170	440	1.4	13.7	2460	410	68.3	2.7	137
		Total	650	1690	5.4	52.8	6093	1580	263.1	10.5	527.7

Table 8. Upper-Bound Global Emissions by Altitude Band for Supersonic-Ban and No-Advanced-SST Scenarios (tonnes/day, summer season)

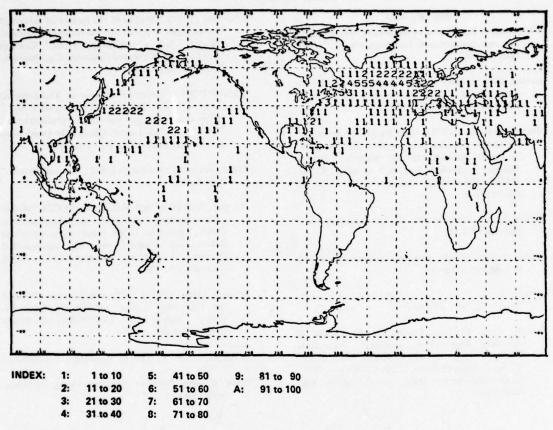
Scenario	Year	Aircraft Type	Altitude Band (km)	H ₂ O× 10 ²	CO ₂ × 10 ³	Trace	Lub Oil	NO _x	со	тнс	Soot	SO ₂
No Advanced SST	1990	Sub	9-12	390	1010	3.1	31.4	3140	943	157	6.3	314
		Sub	12-15	150	380	1.2	11.7	822	352	58.7	2.4	117
		Sup	12-15	5.9	15.3	-	0.5	85	14	2.4	0.1	4.7
		Sup	15-18	51.5	130	0.4	4.1	741	123	20.6	0.8	41.2
			Total	597	1535	4.7	47.7	4788	1432	238.7	9.6	476.9
Supersonic Ban	1990	Sub	9-12	390	1010	3.1	31.4	3140	941	157	6.3	314
		Sub	12-15	150	380	1.2	11.9	830	356	59.3	2.4	119
			Total	540	1390	4.3	43.3	3970	1297	216.3	8.7	433
	2000	Sub	9-12	980	2530	7.9	78.6	7860	2360	393	15.7	786
		Sub	12-15	410	1050	3.3	32.8	2290	983	164	6.6	328
			Total	1390	3580	11.2	111.4	10150	3343	557	22.3	1114

For the no-advanced-SST scenario, emissions will be confined below 18 km; in the case of the supersonic-ban scenario, there will be no emissions above 15 km.

The geographical distribution of NO_X in the 18-21 km band for the upper-bound scenario is given in Figure 2. Only emission rates higher than 1 tonne per day were indexed, to facilitate readability. The highest emissions will occur in the rectangle bounded by latitude $40^\circ N$ to $60^\circ N$

and longitude 80°W to 20°E. This zone covers North America, the North Atlantic, and Europe; it corresponds with the heavily trafficked air routes.

The highest subsonic NO_x emission is 41 tonnes per day in the 9-12 km band which occurs at 40°N, 95°W near Chicago; it is due to the cumulative effect of many subsonic intercontinental flights in the United States. The highest supersonic NO_x emission is 63 tonnes per day in



UNIT: TONNES/DAY

Figure 2. NO_x emissions for supersonic aircraft in the 18 to 21 km altitude band in 1990 (summer season).

the 18-21 km band at 45°N, 65°W over Prince Edward Island in Canada, because many supersonic flights between North America and Europe are routed through this region.

The latitude distribution of NO_x in the 18-21 km band for the upper-bound case is given in Figure 3. It can be observed that there are no emissions above 85°N and below 40°S; no air traffic is expected in these latitudes. The pattern of latitude distributions for 2000 is expected to be similar to that for 1990.

The bulk of NO_x emissions in 1990 for the 9-12 km band will occur in latitudes 20°N to 60°N. For the 12-15 km band, 77% of the emissions will be in the same latitude band, with 93% for the 15-18 km band and 87% for the 18-21 km band. Similar concentrative effects in this latitude band can be expected for the year 2000. The latitude band 50°N to 55°N will have the highest concentration of emissions for the

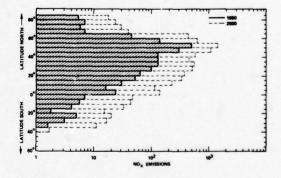


Figure 3. Upper-bound NO_x latitude distribution; 18-21 km altitude band, years 1990 and 2000 (tonnes/day, summer season).

18-21 km band, with 500 tonnes per day in 1990 and 1480 tonnes per day in 2000.

98% of the total emissions will occur in the northern hemisphere.

REFERENCES

- Air Transport Association of America (1967), Engineering and Maintenance Memorandum No. 67-81, October 1967.
- Becker, John V. and Frank S. Kirham (1974), "Hypersonic aircraft 21st century transports?," ICAO Bulletin, February 1974, 8-11.
- Boeing Company (1973), "Studies of the Impact of Advanced Technologies Applied to Supersonic Transport Aircraft: Interim Summary Report, Volume 3: Market Analysis," Contract NAS-1-11938, Commercial Aircraft Group, Seattle, DG-22529-2.
- British Aircraft Corporation (1973), unpublished data supplied to DOT.
- Crilly, William (1973), personal correspondence with Pan American Airways.
- Douglas Corp. (1974), General Performance Report, Report No. MDC J5806/01.
- Douglas Corp. (1973), "Studies of the Impact of Advanced Technologies Applied to Supersonic Transport Aircraft: Task II, Market Analysis and Economic Ground Rules," Contract NAS-1-11939, McDonnell-Douglas Corp., Long Beach, CA, MDC-J4378.

- Lockheed (1973), "Studies of the Impact of Advanced Technologies Applied to Supersonic Transport Aircraft: Task II, Market Analysis," Contract NAS-1-11940. Lockheed-California Co, Burbank, CA, LR-25827-2.
- NASA (1973), "Advanced Supersonic Technological Concept Study, Reference Characteristics AST," National Aeronautics and Space Administration, Langley Research Center, CR-132374 (work done by LTV Aerospace Corp, Hampton, VA).
- Pan American World Airways (1973), "Annual Report,". New York.
- Petersen, Richard H. and M.H. Waters (1972), "Hypersonic transports: Economics and environmental effects," presented at the Eighth Congress of the International Council of the Aeronautical Sciences, Amsterdam, Aug-Sept 1972 (ICAS Report No. 72-32).
- Stoessel, Robert (1970), "A Proposed Standard Method for Estimating Airline Indirect Operating Expense," Report No. LW70-500R, Lockheed-Georgia Co., May 1970.
- World Airline Record (1971), Roadcap and Associates.
- World Aviation Directory (summer 1971), Ziff-Davis Publishing Co.

POSSIBLE IMPACT OF REGULATIONS ON AIRLINES

R.W. RUMMEL Trans World Airlines New York, New York

ABSTRACT: The global atmospheric monitoring system and the emphasized low- NO_x combustion technology recommended by CIAP are very reasonable. However, promulgation of regulations on the basis of either today's incomplete knowledge or the "maximum conceivable" future levels of operation used in many estimates would be unjustified and highly inadvisable.

I have been asked to talk on the possible impact of regulations which do not exist, and which may never be needed, against a backdrop of possible engine technology developments which, if realized, might or might not result in compliance with these non-existent regulations. If the regulations existed, and if I knew the degree to which contemporary hardware would or would not comply with those regulations, then I could better assess the possible impact of regulations on airlines. Since neither is so yet, I can only discuss whether there is justification for regulations, and what their consequences might be.

Because of the obvious uncertainties in projections of future world developments, and our less-than-complete scientific understanding of the atmosphere, it seems reasonable and appropriate that two objectives recommended by CIAP be pursued. These are:

First, an effective global atmospheric monitoring system should be established. (Both the stratosphere and troposphere should be monitored for a number of reasons besides aerospace activities.)

Second, combustion technology aimed at developing practical engines which generate less NO_x should be accelerated.

Most important, the promulgation of regulations should wait until it is more certain that a problem requiring regulation will exist. Giving prior thought to the structure and content of possible future regulations may or may not prove finally to be useful, but the early development of a specific plan which produces over-regulation

would be a disservice. CIAP points out that "there are more than 30 possible causes of observable changes in UV radiation at the ground" and that many factors besides aircraft pollution in the stratosphere cause changes in annual mean surface temperature, such as accumulation of carbon dioxide from fossil fuels burned by industry and increased accumulation of dust in the troposphere, also from industry. CIAP also notes the importance of identifying whether a particular climatic or biologic impact is caused by aircraft or by some other source.

If regulations are necessary for the general welfare, all significant sources of pollution should be restricted concurrently; no one significant source of pollutants should be singled out for special treatment. Moreover, any regulations that may be required should be tuned to the reality of advances in technology, industry, air transportation, and real-world dynamics.

CIAP has concluded, on the basis of solid scientific information, that regulations would have to be global in nature to be effective - that only by international agreement could the natural composition of the stratosphere be maintained, and that vigorous efforts would be needed to achieve this goal. CIAP mentions the International Civil Aviation Organization (ICAO), the World Meteorological Organization (WMO), and the United Nations Environmental Program (UNEP) as key existing international organizations. Presumably, CIAP has in mind the establishment of worldwide standards for maintaining the quality of the stratosphere, and the enforcement of them by the governments of the world's states. There are presently 128 members of ICAO, 138 members in the U.N., 58 of which are members of the UNEP, and there are 136

states and territories which are members of the WMO. (Except in air-traffic affairs, the ICAO convention imposes only a moral obligation on member states to implement rules at the national level.) Obtaining early international agreement on atmospheric standards and rules among so many parties when the need for them remains controversial seems nearly impossible.

Consider the regulatory problem of establishing and enforcing compliance with a world annual tonnage limit on NOx injection. Imagine the difficulty of getting 128 members of ICAO to agree on the allocation of this tonnage among them, not to mention distributing each nation's allocation amongst its various carriers. This would probably impel direct federal control of flight schedules and services at the national and international levels. International flight scheduling would be particularly troublesome because services between nations are controlled by bilateral agreements, not ICAO or the U.N. or any other world organization. In most countries, authority for direct federal control of flight schedules and frequency of service simply does not exist.

Economic and social impacts must also be considered. Dr. Grobecker has pointed out that some kinds of stratospheric pollution would probably benefit certain crops in some parts of the world and be detrimental to the same crops in other areas. Wheat is one such example; it could cost some nations hundreds of millions of dollars annually while simultaneously adding to the wealth of others. This agricultural aspect of atmospheric modification would become, I believe, more than a minor problem in establishing either standards or compliance rules so long as the need for such agreements remains problematical.

Setting arbitrary limits, either directly or indirectly, on air transportation will tend to limit, confuse, and stifle what would otherwise be the orderly evolution of air transportation systems to serve the world's market needs. While difficult to quantify, this aspect itself could generate severe economic and social impacts which should be carefully considered and weighed against alternative courses of action. If and when regulations are needed, they should penalize or restrict this normal growth as little as possible, in the interests of the general welfare.

I mentioned NO_x tonnage limits only as an example of the kind of regulation which seems to

me to be wholly impractical and most undesirable. Another approach falling in the same general category would be the setting of latitude limits for operations in the stratosphere. If it is a near-impossibility to allocate NO_x tonnage between countries and then between airlines, it is a near-impossibility squared to subdivide air operations by confining them to various latitude bands. The latitudes of primary concern probably contain the most densely populated areas - the ones that require air transportation the most. In short, I do not see how, as a practical matter, either NO_x tonnage limits or latitude limits of operation could be equitably imposed at either the national or the international level.

If emissions of NO_X from aircraft must be regulated, then a much more manageable solution would be to make the level of NO_X emissions an aircraft certification requirement in each new aircraft type. This might be done through the ICAO convention.

Certification limits for aircraft NO, generation could reflect such operational parameters as altitude and range, as well as the reasonable ability of the manufacturers to incorporate advanced technology. Aircraft certification standards could be tightened from time to time in response to advances in technology and to the climatic need. This course would necessitate establishing global aircraft-certification requirements sufficiently in advance of aircraft design to permit the manufacture of complying power plants and aircraft, without resorting to retrofit. The manufacturer could then proceed in the assurance that the enormous investments required to develop and produce new aircraft would not be undercut or voided by after-thefact rules. Similarly, airlines could better undertake the large commitments required by fleet replacement or expansion programs.

CIAP has shown clearly that the stratosphere will not yield easily or quickly to man's activities. And I believe that further rigorous review and analysis would indicate that using reasonable and realistic fleet projections, rather than the CIAP "upper bound" fleets, would show that sufficient time is left to alleviate any effects of aircraft effluents by the application of certification rules.

I want to make it quite clear that I am not advocating the regulatory approach of certification. I am merely saying that if controls are

indeed needed, certification of new aircraft designs, with firm emission requirements in existence when the design is undertaken, is more plausible and manageable than many other regulatory approaches.

The imposition of limits on operating altitude is still another regulatory possibility, but I see no reason to impose them on current subsonic aircraft. Jet aircraft operating today are certified for maximum-altitude operations. For example, the Boeing 747 is certified for a maximum operating altitude of 45,100 feet and the Lockheed L1011 at 42,000 feet. However, for performance reasons, the practical operating altitude limits for each of these aircraft is considered to be only 39,000 feet. What with air traffic control and other problems such as aircraft operational weights, the 747's and L-1011's normally operate at a maximum altitude of between 31,000 and 35,000 feet. The operation altitude of the Douglas DC-10 is similar. In all probability, SST's would generally operate well within the stratosphere, at the 50,000 to 60,000 foot level. If compliance with altitude limits should become advisable for new types of high-altitude aircraft, this could be handled either by air-traffic-control systems or by aircraft certification through ICAO. In the interest of leaving air transportation unshackled to the maximum degree, as nearly everyone agrees is desirable, operating altitude limitations should be avoided, if possible.

Incidentally, I do not believe that CIAP's "upper bound" fleets would ever be attained if altitude limits were imposed, because the growth of these fleets would be arrested by air traffic saturation. I do not believe they are likely to be attained in any event.

CIAP bases its climatic impact analyses on these "upper bound" fleet size projections, the "maximum conceivable demand rather than practicability for construction, [which] provides a basis for considering the worst that could conceivably happen when assessing the possible consequences." The use of "maximum conceivable" levels of aircraft operations may be sound for determining whether or not atmospheric problems could ever develop. However, use of the "upper bound" projections for regulatory purposes would be unrealistic, unnecessary, and punitive — a major disservice to all.

The CIAP Report of Findings also mentions "expected subsonic" and "expected supersonic" fleets, which are appreciably smaller than the "upper bound" fleets. However, all of CIAP's computations on emissions and other environmental factors appear to be based on the "upper bound" fleets.

The CIAP "upper bound" world fleets number 3,475 subsonic passenger and cargo aircraft in 1980, 5,277 in 1990, 14,605 in 2000, and 45,126 by 2025. Only 37 747-sized passenger aircraft are shown for 1980, whereas 245 have been manufactured to date. On the other hand, 2,906 long-range passenger trijets are shown for 1980, whereas only 258 have been manufactured to date. The 2,906 trijets shrink to 57 in 1990 and increase to 3,985 in the year 2000. CIAP projects an enormous number, 3,060, of 747sized passenger aircraft for 1990. Aberrations and large fluctuations like these, especially at ten-year intervals, do not make sense for aircraft capable of 18 to 20 years of service. I understand that these projections reflect a demand model working backward from a future date. Unquestionably, history will show them to be major excursions from reality. CIAP's SST projections total 51 by 1980, 440 by 1990, 1,885 by 2000, and an astounding 5,561 by 2025! Total projected subsonic and supersonic fleets would consist of 50,687 aircraft by 2025!

Where will the fuel for such enormous fleets come from? CIAP shows that each "large advanced supersonic transport" would burn about four times as much fuel per hour as the 747-type aircraft. Using an arbitrary four-to-one ratio for advanced SST's, the 50,687-plane projected fleet of both subsonic and supersonic aircraft would use as much fuel as 67,370 subsonic aircraft — about 14 times the total number of jet transports operated today. How can we believe that air transportation will be able to command such an enormous amount of energy in an energy-limited world?

Moreover, where will the airports for these huge numbers of planes come from? And what air-traffic-control system could cope with this volume plus the growing general-aviation sector? Surely if the enormous demand envisioned by CIAP really develops, it will be accommodated not by 50,000 airplanes but by some other solution.

RUMMEL

The need for regulations should be appraised on the basis of much smaller fleet projections than those used by CIAP for emission computations. One needs only to consider the low airtransportation growth rates experienced in the past few years, the currently dismal fuel availability and cost outlook, and airport and airtraffic saturation to understand that 1980-1985 air-fleet size as envisioned by CIAP is enormously overstated. Regulations, if required at all, should be promulgated to solve real-world problems — not exaggerated hypothetical ones.

CIAP states that current operations with subsonic aircraft do not pose a discernible threat - that in fact current subsonic flight operations could be increased fivefold before the "barely discernible change" level of the stratosphere would be reached. Also – without respect to future wide-body aircraft, which may fly at higher altitudes - five times the number of 747 aircraft flying today could operate under the "barely discernible level" if NOx were reduced by a factor of only two, and CIAP says that available technology can achieve a factor of six. Since under the best of circumstances it would take many years to increase subsonic flight operations fivefold, retrofitting on the current types of subsonic aircraft with lower-NO_x burners should not be needed.

Some amplification of the retrofit costs implicit in the CIAP report is appropriate. For this the "upper bound" fleet projections must be used, since they are the only detailed fleet projections available to me. However, the rela-

tionship of costs shown here will also be substantially valid for more reasonably sized fleets. CIAP indicates that retrofit kits should cost about 25% of the price of new power plants and about \$50 million in non-recurring costs; this does not include kit-installation labor and added maintenance expense. Each large new subsonic engine will cost about \$1 million in 1976. The cost of each new engine for an advanced SST is anybody's guess; my guess is \$1.4 million. The CIAP Report of Findings shows 5,277 subsonic passenger and cargo aircraft and 440 advanced SST's in 1990. Adding 15% for labor and 17% to cover spare engines, retrofit cost for the 1990 subsonic fleet would total approximately \$7.1 billion in 1976 dollars. Retrofitting the 440 SST's would cost about \$0.8 billion in 1976 dollars. Thus, the subsonic fleet which is estimated to contribute only around 20% of the pollution would bear a disproportionate 90% of a very big bill. The high cost and low return from the retrofitting of subsonic fleets seem to have been passed over lightly in the Report of Findings. Clearly, the focal point of attention must remain prospective SST fleets.

Finally, CIAP observes that implementation of its findings will "presumably include the establishment of standards for stratospheric air quality..." To reiterate a main point here, without prior agreement on international atmospheric standards, the monitoring system advocated by CIAP could lead too easily to precipitous, ill-advised, or unnecessary regulatory actions.

ENGINE EMISSIONS AND REGULATORY CONSEQUENCES

DISCUSSION

(UNIDENTIFIED): I have a question for Bob Rummel. You stated, I think, that the CIAP upper-bound fleet could be used for environmental analysis of possible effects, but that it shouldn't be used for any regulatory type of "what if" analysis. Could you please expand on that? What type of fleet projection would you recommend be used for regulatory analysis, if some upper upper bound based on demand ought not to be used?

RUMMEL: Use of the upper-bound limits by scientists to determine whether or not a potentially harmful problem exists seems to be reasonable. The development

of regulations, however, should be tuned to the evolutionary advances of *real* fleets. After all, the upperbound limits are postulated for a very distant period — 35 to 50 years in the future. (You can take your choice, because both are presented.) Regulations, if promulgated, should deal with the level of activity that exists now and what is expected for the immediate future, with consideration of changes in level of technology. Then you can determine what actions need to be taken. This is a dynamic situation. I don't think we can have rules promulgated now that will stand for 50 years in any event. Let's develop rules as they are needed, and then change them as required to cope with evolving circumstances.

ENGINE EMISSIONS AND REGULATORY CONSEQUENCES

KAUFMAN: What are the prospects for NO_x emissions from the engines which will have still higher bypass ratios, those designed for the wide-body jets that will be flying somewhat higher? Is there something in the works that will make the emissions considerably higher?

BAHR: As the bypass ratio increases, the compressorpressure ratio goes up, of course. If you do nothing, the combustor-inlet temperatures also increase, and then the NO_x levels increase. However, the approaches I described, such as those being developed for the NASA Clean Combustor Program, will certainly provide NO, reductions even for these higher-pressure-ratio engine cycles. Those approaches can be refined further, so I think we can expect to see, with sufficient development work, a reduction on the order of a factor of 2 with that kind of design concept. Now the pressure ratios that people are talking about for the future aren't a whole lot higher than the 30-to-1 pressure ratio I discussed this morning. The possibility of increasing this to 35 is being discussed and studied, and somewhere there's even talk of 40 to 1, but the change in NO_x in going from 30 to 1 to 40 to 1 isn't really all that large.

(UNIDENTIFIED): I'd like to ask Mr. Rummel whether there isn't a certain inconsistency between his comment about waiting to develop regulations till the problem is really with us and his other comment that there is a long lead time in developing advanced engine designs. It seems to me that the two have to be put together in some realistic way.

RUMMEL: I don't think there is any inconsistency. I fully support the advancement of technology to the maximum reasonable extent to reduce engine emissions, and I think we should get on with that and find out what in fact can be done. I think what the CIAP Report of Findings does is raise a large red flag to indicate a possible problem, and we should seek ways to solve it in case aviation grows so far that the problem actually comes into existence. I didn't comment directly on the lead time for power plants or retrofit, but again if you look at the current state of air transportation it is clear that for many, many years the fleets are going to be very much smaller than those CIAP projected. It is for this reason that I believe sufficient time exists to cope

with this problem, and I suggest that these growth scenarios be analyzed in depth before a lot of money is needlessly spent.

ELLSAESSER: In going through our program, I don't see any space that has been devoted to the problem of removal of sulfur. Would any of the people who spoke this morning care to say what impact the removal of sulfur from fuel would have on the aircraft engine or industry?

RUMMEL: It's a fairly simple calculation. You start with about \$100 million a year in added cost, but the greater part of the problem is due to the limits of the "fuel farm" capacity at most airports. At most of the major airports, these "fuel farms" – the storage tanks – can handle only one type of fuel. Unless all airplanes use a common fuel, additional major investments in tanks and plumbing systems will be required to handle both types of fuel. Here again I think further analysis of the effects from fleets of some realistic size is needed before we make the investment required.

E. LOEWENSTEIN: Mr. Rummel, I believe you said that certification should in effect constitute a license to operate the aircraft through its useful life. You also said that certification should be based upon the technology current at the time the aircraft comes up for certification, which may be fair enough. But what if the aircraft has a useful life of 20 years, and after 10 years we find that it poses a real menace to the atmosphere, perhaps not of itself but in conjunction with spray cans or something else we find out about in the next few years? Do you really feel that the airline industry would refuse to perform modification or retrofit of the aircraft?

RUMMEL: No. I mean that in general we should be able to assume that the rules won't be changed in the middle of the evolution phase of an aircraft, but that progress would be made by making each type of aircraft better than the preceding one. Of course, if it should turn out that some major hazard is attributable to aircraft, the operators and others involved would certainly respect the need for change. But as I read the CIAP report, such a hazard is not apparent at present.

SOME FUNDAMENTAL LIMITATIONS OF SIMPLIFIED-TRANSPORT MODELS AS IMPLIED BY RESULTS FROM A THREE-DIMENSIONAL GENERAL-CIRCULATION/TRACER MODEL

J.D. MAHLMAN

NOAA Geophysical Fluid Dynamics Laboratory
Princeton University
Princeton, New Jersey

ABSTRACT: The answers to a number of important environmental questions depend quite critically upon our capability for providing reliable descriptions of large-scale atmospheric transport of trace substances. In many cases it is useful to try to provide meaningful answers by using highly simplified models of tracer transport. In this paper, an attempt is made to provide some assessments of the fundamental uncertainties inherent in such models.

The approach used is the analysis of results of a comprehensive three-dimensional general-circulation/tracer model in order to examine the validity of various transport hypotheses. Evaluations are made of various one-dimensional, two-dimensional, and low-resolution three-dimensional transport hypotheses. The analyses indicate that some of the basic assumptions utilized in these simpler models are often not satisfied. This leads to some fundamental uncertainties which cannot easily be reduced without significant conceptual reformulations of the simpler models.

INTRODUCTION

Evaluation of the environmental impact of operating supersonic aircraft in the stratosphere depends crucially upon a reliable assessment of the atmospheric dispersion of various trace constituents. This is also the case for a number of other important environmental questions. The need for such assessments invariably leads to a reliance upon numerical models of trace-constituent transport.

The numerical models currently in use vary drastically in their complexity, number of empirical prescriptions, and computational requirements. At present, all models employ empirical prescriptions to some degree. They range from models which are totally empirical to models which attempt to simulate the basic physical mechanisms as much as possible. Because of this extreme range of modeling philosophies, it is important to understand the inherent uncertainty in a given model when applying it to a given problem. At present, this is not readily possible, mainly because large uncertainties also exist in the data sets used to evaluate the validity of the various models.

In this paper, an alternative approach for evaluating the uncertainties of various transport models is utilized. The results from a highresolution, three-dimensional (3-D) general-circulation/tracer model are analyzed in order to examine the validity of the basic hypotheses employed in some of the simpler transport models.

The use of a model to evaluate other models is immediately susceptible to criticism on the grounds that even the more complex model cannot claim to provide an exact duplication of the behavior found in the actual atmosphere. This, of course, is quite true. In fact, it is very possible that a simpler model will provide a more realistic reproduction of some "observed" feature, especially since it may have been specifically designed to agree with that particular "observation". However, if the more complex model is able to simulate the essential transport mechanisms acting in the atmosphere, it should still be possible to evaluate the accuracy of more simplified transport hypotheses within the model framework. In short, the more complex model may be regarded as a plausible "atmosphere" in which all the data is available everywhere and at all times. As a result, all tracer mixing ratios, fluxes, gradients, integrals, and meteorological quantities are at the researcher's disposal.

By using such an approach, one cannot claim to be able to provide a definitive evaluation of the applicability of the simpler transport models. Rather, this approach helps to provide an independent check upon the validity of a given simplified-transport assumption in terms of how well it is able to provide predictions of transport as calculated explicitly by the complex model. However, if such a simplified transfer assumption is shown to be only partially valid, or not generally applicable, then this provides some insight into the inherent fundamental uncertainties of that simple model when it attempts to predict tracer behavior.

Also in this paper, an evaluation will be made of some key aspects of the assumptions involved in the following types of simplified models: low-resolution 3-D models, 2-D models, "standard" 1-D models, and "tropopause"-coordinate 1-D models. In addition, some limitations of the model used for preparing these evaluations will be briefly reviewed.

DESCRIPTION OF THE GENERAL-CIRCULATION MODEL

The general-circulation model used in this research was designed and constructed by S. Manabe and J.L. Holloway, Jr. A more complete description of the model framework than that given here is presented in Holloway and Manabe (1971) and Manabe and Holloway (1975). This model employs finite-difference approximations over the global domain up to a height of about 31 km. The equations solved are the hydrostatic "primitive" equations of motion, the first law of thermodynamics, the ideal gas law, the masscontinuity equation, and the water-vaporcontinuity equation. Primary dependent variables are the three velocity components, temperature, surface pressure, and water-vapor mixing ratio (the ratio of water-vapor density to air density). Other variables calculated are soil moisture, precipitation, snow depth, ground temperature, evaporation, and precipitation runoff.

The model has an average horizontal grid spacing of about 265 km. It contains eleven levels in the vertical, with a mean spacing of about 3 km from the middle troposphere to the lower stratosphere. Large-scale topography is included through use of the so-called "sigma" system, where the vertical coordinate levels are specified as pressure normalized by surface pressure (Phillips, 1957).

Radiative transfer is computed using a seasonally varying solar radiation with distributions of ozone and clouds specified according to their zonal-mean, seasonally varying climatic values. Infrared radiative transfer is included by using the scheme of Manabe and Strickler (1964). Carbon dioxide is assumed to be constant everywhere for purposes of radiative-transfer calculations, while water vapor is taken from the model-determined local mixing ratios. The land surface temperature is calculated through an equation of ground heat balance, while the ocean surface temperature is specified according to observed seasonally varying values.

In any model there is a requirement for considering the possible influence of phenomena which exist below the chosen grid resolution. At the present time fully acceptable methods do not exist for including these sub-grid-scale effects in terms of the resolved phenomena. Thus, the only real advantage this type of high-resolution model possesses relative to coarser resolutions is that a much smaller fraction of the total processes is dependent upon the poorly understood sub-gridscale specifications. To crudely include the effects of vertical heat and moisture transport by cloud-scale convection, the so-called "moist convective adjustment" of Manabe, Smagorinsky, and Strickler (1965) is utilized. The effects of mixing of quantities on scales below the grid resolution are approximated by the non-linear diffusion method of Smagorinsky (1963).

This model has been run through several annual cycles so that the last simulation year is essentially at statistical equilibrium, i.e., quite small trends of important global-mean properties such as temperature, energy, precipitation, etc. are observed. However, only one model year is included in these studies. Therefore, the possibility of interannual variability in the circulation is precluded, since this same year of general-circulation model data is used in successive years of the tracer experiments.

DESCRIPTION OF THE TRACER MODEL

The tracer model utilizes time-dependent winds, temperatures, and surface pressures from the general-circulation model to solve the trace-constituent continuity equation for any globally transported tracer. To increase research flexibility and conserve computer resources, the

tracer model operates independently of the general-circulation model. This is accomplished by saving the pertinent data from the general-circulation model on a series of tapes which are read as input by the tracer model. Because of this, all of these tracer experiments are fully passive, i.e., they do not affect the results of the general-circulation model in any way.

To calculate transport by the large-scale winds, the Eulerian form of the tracer continuity equation is combined with the mass continuity equation so that all transport terms are written as flux divergences. This ensures that no unwanted global tracer sources or sinks are present except for computer roundoff error. The horizontal and vertical winds are then used to solve for the three-dimensional flux divergence of the tracer at each grid box (about 78,000 in the grid) and at each finite time step (about 25 minutes in length). In the horizontal plane, centered second-order finite differencing is used (Kurihara and Holloway, 1967), while a centered fourth-order scheme is employed in the vertical.

Occasionally, space or time truncation error in calculating the tracer flux divergence by the large-scale winds leads to situations in which the tracer mixing ratio becomes negative. This situation tends to occur locally when the upstream tracer values near a grid box point are much smaller than the downstream ones. Such negative mixing ratios are "corrected" back to zero by "borrowing" tracer from the downstream grid box in the axis of the flux-divergence component most responsible for producing the negative value. This is always done in such a manner that the process conserves the total mass of the tracer.

The horizontal transfer of trace material on scales below the grid resolution is modeled crudely by a highly scale-selective eddy-diffusion formulation in which the transfer coefficient is locally dependent upon properties of the wind and tracer fields. This has the effect of ensuring that the net transfer by this somewhat arbitrary process is more than an order of magnitude smaller than the transport by model-resolved motion scales.

In the vertical, specification of sub-grid-scale processes is not included. This does not imply that such processes are unimportant in vertical trace-substance transport. Rather, it is currently a test of the capability of the motions resolved by the model to accomplish the required vertical

transports. In the troposphere, vertical transport by small-scale processes is quite important. However, this is still a subject of some controversy for the stratosphere.

The experiments run to date with this model suggest that a quite small value of the vertical sub-grid-scale transfer . coefficient would be appropriate for the model stratosphere, say, of the order of 10²cm²sec⁻¹. This value is almost two orders of magnitude smaller than the typical values required to account for all of the vertical transfer in the stratosphere (e.g., Chang, 1974; McElroy et al., 1974). Use of this lower value would be consistent with results from a recent observational study of small-scale stratospheric turbulence by Lilly, Waco, and Adelfang (1973). In the troposphere, the values should be significantly larger because of the presence of cloud-scale convective transports not explicitly resolved by the model.

The modeling of sources and sinks in the tracer continuity equation can be varied arbitrarily according to the processes acting to locally create or destroy a given trace constituent. In the two major experiments executed to date, physical removal mechanisms are the only non-conservative processes included in the troposphere. At the surface layer, dry removal is assumed to be proportional to the tracer mixing ratio and a removal coefficient of magnitude 1/20 per day. The effects of tracer removal by precipitation are crudely included by assuming that the removal in the troposphere is a function of tracer amount, precipitation intensity, and a removal coefficient which diminishes up to about 8 km and is zero at higher levels. A more complete description is given in Mahlman (1973a). For a fully detailed description of all modeling approaches and equations used in this tracer model, see Mahlman and Moxim (1976).

SOME LIMITATIONS OF THE GENERAL-CIRCULATION/TRACER MODEL

As was stated earlier, the purpose of this study is to evaluate some aspects of simpler transport models in the light of results from a higher-resolution 3-D general-circulation/tracer model. Since a basic assumption of this study is that this complex model has managed to capture the significant transport mechanisms explicitly, it is important to establish what features of the

model simulation are somewhat unlike the behavior of the actual atmosphere. Thus, almost paradoxically, the very great number of successful features of this simulation experiment are of no further direct interest in this paper. Needless to say, however, an evaluation of this kind is vitally dependent upon the utilization of a model simulation which is mostly successful in reproducing the important features of the atmospheric circulation. Further information on this model simulation and how the results compare with the characteristics of the actual atmosphere are given in Mahlman and Manabe (1972), Mahlman (1973a), Hayashi (1974), Manabe, Holloway, and Hahn (1974), Hahn and Manabe (1975), Manabe and Holloway (1975), Manabe and Mahlman (1976), and Mahlman and Moxim (1976).

Most of the qualitatively observable model simulation limitations for stratospheric tracer-dispersion problems seem to be related to the placement of the top model level at about 31 km. This choice appears to be too low to allow a very successful simulation of the middle stratospheric circulation. Also, the model's vertical grid length in this region is more than a factor of two larger than that employed in the lower stratosphere.

The above resolution limitations might be related to a number of simulation difficulties in the model middle stratosphere. The simulated wintertime mid-latitude westerly winds are almost a factor of two stronger than the observed. Also, the model does not predict the mid-winter sudden stratospheric warming events often observed in the Northern Hemisphere. Thus, at best this simulation must be viewed as being possibly representative of a year in which no sudden stratospheric warming occurred. Consistent with this limitation, the model predicts the transition from winter westerlies to summer easterlies to occur somewhat later than actually observed. This effect is also consistent with the fact that the model-simulated summer easterly circulation does not last as long as actually observed.

In contrast, the simulation of nearly all features of the lower-stratospheric/upper-tropospheric circulation appear to be satisfactory. One minor exception to this is that the amplitude of the simulated extratropical cyclonic disturbances appears to be slightly underestimated. The work of Miyakoda et al. (1971)

suggests that a model with higher computational resolution than that used here would produce cyclonic disturbances of greater amplitude. This could somewhat affect the amount of tracer being brought through the tropopause in association with these cyclonic disturbances. For more details on these cross-tropopause transport phenomena, as well as pertinent references, see Danielsen (1968), Reiter (1972), and Mahlman (1973b).

In the tracer model, the transport rate through the surface boundary layer appears to be somewhat underestimated due to the lack of any vertical sub-grid-scale transfer processes in the model. This particular deficiency has no apparent effect upon the simulated transport phenomena in the stratosphere and upper troposphere.

BRIEF DESCRIPTION OF THE TRACER EXPERIMENTS

The tracer experiments used for the evaluations presented here have been described in some detail in Mahlman (1973a). Thus, they will be only described briefly in this paper.

a. "Mid-Latitude Point Source" Tracer Experiment. In this experiment, a diffuse instantaneous source is introduced at the beginning of the integration. The center of this source is at about 36°N, 180°E, and 18.8 km (65 mb). After the start of the experiment, the tracer is completely conserved in the stratosphere and is subject to destruction when it comes into contact with the tropospheric removal processes. The tracer in this experiment may thus be regarded as being somewhat analogous to the constituents injected by a nuclear-weapons detonation, which are subject to rapid tropospheric removal processes.

b. "Vertical Stratification" Tracer Experiment. This experiment is designed to provide a very simple way to examine the transport of a tracer which is highly stratified in the vertical by virtue of a photochemically maintained equilibrium in the middle stratosphere and a sink in the lower troposphere. It may thus be thought of as being qualitatively similar to atmospheric ozone. The tropospheric sink is exactly the same as in the previous experiment. A net implicit source of tracer is established at the top model level by

setting the mixing ratio at a constant normalized value of 1.0 for the entire length of the experiment. This means that the tracer flux due to motions out of or into this level is always instantaneously balanced by a local tracer source or sink. This can be physically visualized as an extremely rapid damping back to its simple photochemical equilibrium value (1.0) after it has been locally disturbed by a vertical transport process. Below this top level and above the middle troposphere, no tracer sources and sinks are included.

For a discussion of some of the tracer evolutions and transport mechanisms in these two experiments, see Mahlman (1973a).

LOW-RESOLUTION THREE-DIMENSIONAL MODELS

The most obvious simplification of the three-dimensional dynamics as simulated by a general-circulation model is just a reduction in the computational resolution. Such an expedient is clearly attractive because a factor-of-two reduction in the horizontal resolution leads to a factor-of-eight reduction in the computational burden.

The use of lower-resolution models offers a strong possibility for examining transport problems in the stratosphere, since the apparent spatial scales of meteorological phenomena in that region are much larger than those typical of the troposphere. An example of a low-resolution model in this category is the quasi-geostrophic spectral model of Cunnold et al. (1975).

It has long been clear that excessively low computational resolution in a general-circulation model acts to suppress the development of the all-important cyclone-scale waves in the troposphere. As suggested earlier, such a suppression may also inhibit cross-tropopause tracer transport in a model. What is not as generally recognized is that low computational resolution also inhibits and distorts the simulation of the very-largest-scale tropospheric disturbances as well (Manabe et al., 1970). Since it is these long waves that provide the source of energy for disturbances in the stratosphere, it is not clear whether or not a low-resolution model will provide a fully valid simulation of the stratospheric circulation.

A useful way to gain some insight into potential hazards involved in using low-resolution 3-D models for tracer transport problems is to examine the simulated distribution of tracer as a function of spatial scale in the high-resolution 3-D model. For this evaluation, zonal-harmonic analyses were computed for a number of latitude circles and times from the high-resolution tracer experiment data.

Figure 1 shows an example of a computed power spectrum of R²(n), where R is the tracer mixing ratio, and n is the planetary wave number (number of waves around a latitude circle). The tracer data is taken at 50.4°N from six days of April in the first year of integration of the "Vertical Stratification" tracer experiment. The power spectrum of Figure 1 at 65 mb shows three features worthy of note. First, a significant power peak shows up at n = 3 and 4. This is consistent with the very large scale of meteorological phenomena commonly observed in the stratosphere. Next, a significant peak is observed at n = 7 and 8. This peak is due to the stratospheric remnants of tropospheric extratropical cyclones. As mentioned earlier, such transient disturbances are known to be instrumental in effecting transport of tracer in the lower stratosphere and through the tropopause.

At the smallest scales (n = 10-48), the dropoff of power with increasing wavenumber is

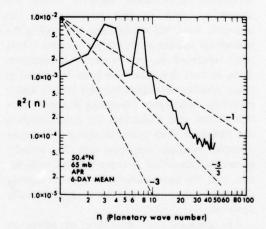


Figure 1. Zonal spectra of R² as a function of planetary wavenumber (n). Data are taken from the "Vertical Stratification" experiment of Mahlman (1973a) at 50.4°N and 65 mb for the first six days of April (9th month of experiment).

rather slow. The spectral slopes of -1 and -5/3, which connote a freely cascaded passive scalar in two and three dimensions, respectively, are included in the figure to provide a frame of reference. The data are consistent with the case of a strong transfer of tracer fluctuations to higher wave numbers (smaller scales). This indicates that a non-negligible fraction of the tracer structure exists at relatively small spatial scales. This is the case even though the model kinetic energy is almost totally contained in scales corresponding to very low planetary wave numbers.

On the basis of the information given by Figure 1, it seems reasonable to hypothesize that low-resolution models may lead to considerable uncertainty when applied to tracer transport problems. This uncertainty might be reduced significantly if the model could fully resolve spatial scales out to, say, n = 10. It appears that models with less resolution than this may have to include a carefully designed "parameterization" of the important unresolved phenomena.

TWO-DIMENSIONAL MODELS

In response to various atmospheric tracerdispersion problems, a number of investigators have developed 2-D transport models. These are models in which only zonal-mean variables are specifically included in the calculation. In the context of the previous section, this can be thought of as a model which does not explicitly include any planetary wavenumbers greater than n = 0.

Because of the well-recognized and obvious importance of zonally asymmetric parts of the motion field ("eddies") in meridional and vertical transport, it is necessary in a 2-D model that the transport by these "eddies" be "parameterized" in terms of properties of the explicitly calculated zonal-mean quantities. The approach used in recent models almost invariably follows the lead established by Reed and German (1965) in which the net "eddy" tracer fluxes are assumed, through use of the mixing-length hypothesis, to be transferred locally down the zonal-mean gradient at all points in space and time. A countergradient flux in one coordinate direction is permitted in this formulation as long as the net "eddy" flux vector is down the net zonal-mean gradient. Additional implicit assumptions in such formulations are that the "eddy" tracer fluxes are independent of the "eddy" tracer distribution, and that the "eddy" fluxes and the fluxes by the mean meridional circulation are independent of each other.

Through use of the high-resolution general-circulation/tracer model, it is possible to examine these assumptions independently because the model generates its "eddy" fluxes explicitly, without any direct dependence upon zonal-mean quantities. In this paper, only the relationship between the eddy fluxes and the mean gradients will be examined. Thus, only the degree of fundamental applicability of the basic mixing-length assumptions will be examined. The problem of empirical suitability of 2-D transport models for applied problems is beyond the purpose of this paper.

According to the simple mixing-length formulation in two-dimensions, the "eddy" fluxes are related to the mean gradients by

$$\overline{v'R'}^{\lambda} = -K_{yy} \frac{\partial \overline{R}^{\lambda}}{\partial y} - K_{yz} \frac{\partial \overline{R}^{\lambda}}{\partial z}$$
 (1)

$$\overline{w'R'}^{\lambda} = -K_{zz} \frac{\partial \overline{R}^{\lambda}}{\partial z} - K_{yz} \frac{\partial \overline{R}^{\lambda}}{\partial y}$$
 (2)

where $(\)^{\lambda}$ is a zonal average, $\overline{v'R'}^{\lambda}$ the zonal-mean horizontal "eddy" flux, $\overline{w'R'}^{\lambda}$ the zonal-mean vertical "eddy" flux, and K_{yy} , K_{zz} , and K_{yz} are the horizontal, vertical, and off-diagonal "eddy" diffusion coefficients, respectively. By assuming that $K_{yz} = (\overline{w'R'}^{\lambda}/\overline{v'R'}^{\lambda})$ K_{yy} , the various "eddy" diffusion coefficients can be written in terms of "eddy" fluxes and mean gradients as

$$K_{yy} = \frac{\overline{v'R'}^{\lambda^2}}{\overline{v'R'}^{\lambda}} \frac{\partial \overline{R}^{\lambda}}{\partial y} - \overline{w'R'}^{\lambda} \frac{\partial \overline{R}^{\lambda}}{\partial z}, \quad (3)$$

$$K_{zz} = \frac{\overline{w'R'^{\lambda^2}}}{\overline{-v'R'^{\lambda}}} \frac{\partial \overline{R}^{\lambda}}{\partial y} - \overline{w'R'^{\lambda}} \frac{\partial \overline{R}^{\lambda}}{\partial z}, \quad (4)$$

$$K_{yz} = \frac{\overline{v'R'^{\lambda}} \overline{w'R'^{\lambda}}}{\overline{-v'R'^{\lambda}} \frac{\partial \overline{R}^{\lambda}}{\partial y} - \overline{w'R'^{\lambda}} \frac{\partial \overline{R}^{\lambda}}{\partial z}}$$
(5)

Thus, if all fluxes and gradients are known, the proper "eddy" diffusivities can, in principle, be evaluated from the model data. It is of interest to recognize that the denominator of Eqs. (3), (4), and (5),

$$\overline{-v'R'}^{\lambda} \ \frac{\partial \overline{R}^{\lambda}}{\partial y} - \ \overline{w'R'}^{\lambda} \ \frac{\partial \overline{R}^{\lambda}}{\partial z} \, ,$$

(or $\overline{-v'R'}^{\lambda}$ $\partial \overline{R}^{\lambda}/\partial y_p - \overline{\omega'R'}^{\lambda}$ $\partial \overline{R}^{\lambda}/\partial p$ in pressure coordinates) has a special physical significance in the balances for the global mean-squared tracer mixing ratio

$$\overline{R^2}^G = \overline{R^{\lambda^2}}^G + \overline{\overline{R'^2}}^G.$$

A sample calculation of $\overline{-v'R'^{\lambda}}$ $\partial \overline{R}^{\lambda}/\partial y_p - \overline{\omega'R'^{\lambda}}$ $\partial \overline{R}^{\lambda}/\partial p$ is presented in Figure 2. It is the mean of the month of November (month 11) from the "Mid-Latitude Point Source" experiment described in Mahlman (1973a).

Figure 2 shows large areas in which this quantity is indeed *negative*, that is, the *net* local "eddy" flux vector is countergradient. In these regions, the implied "eddy" diffusivities K_{yy} and K_{zz} then must both be *negative* as required by Eqs. (3) and (4). The shaded areas of Figure 2 thus indicate situations in which the usual mixing-length assumptions are *not* satisfied.

It follows from the above result that the usual "eddy" flux parameterizations in 2-D models probably do not provide an accurate calculation of the horizontal and vertical "eddy" fluxes as they occur in the actual stratosphere. This implies that the mixing-length framework should be regarded only as an "empirical"

approach which may be utilized as a method for providing a plausible agreement with observed net tracer behavior (not observed "eddy" fluxes).

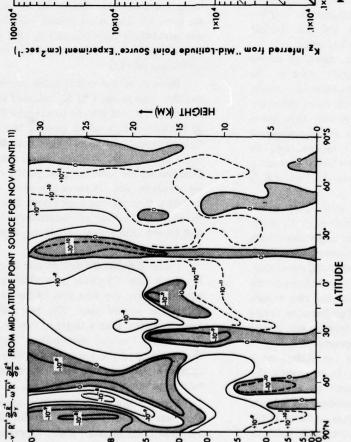
The regions of inferred negative values of Kyy and Kzz from the results of Figure 2 imply rather strongly that other processes in the 3-D model are acting to prevent these countergradient fluxes from leading to grossly unphysical results. Careful analysis of this experiment shows clearly that the local tracer values are sustained in such regions by a strong downgradient flux caused by the mean meridional circulation. This is yet another way of illustrating that the large-scale "eddies" and the mean-meridional circulation constitute a highly interactive system with respect to stratospheric tracer transport. Such interactions were demonstrated in previous tracer studies by Hunt and Manabe (1968) and Mahlman (1973a), and suggested theoretically by Dickinson (1969).

Since the meridional circulation and "eddy" transports are a highly coupled system, and since Figure 2 indicates that the mixing-length hypothesis doesn't provide a dependable parameterization of the "eddy" fluxes, it also follows that, in this type of 2-D transport model, the actual meridional circulation is not necessarily the best choice for use in the model. Using the actual meridional circulation would tend to lead to a net tracer change which is incorrect because it is not consistent with the "eddy" fluxes derived from use of the mixing-length hypothesis. This leads to the conclusion that the meridional circulation in such a model should also be empirically determined to provide the best "fit" to a set of observed data. Such an argument suggests that, in such 2-D transport models, no real physical significance should be given to the calculated transports by mean circulation and "eddies". The only valid test of this kind of model is whether or not the empirically determined net behavior is consistent with observations of actual tracer behavior.

ONE-DIMENSIONAL MODELS

An extremely simple kind of transport model which can still produce quite useful results is the so-called 1-D model. In these models either the horizontal coordinates are systematically averaged over, or transport in these dimensions is ignored. In consistent one-dimensional models,





PRESSURE (MB)

Figure 2. Monthly mean meridional cross-sections of $\overline{-v'R'}^{\lambda} \partial \overline{R}^{\lambda}/\partial y - \overline{\omega'R'}^{\lambda}$ $\partial \overline{R}^{\lambda}/\partial p$ from the "Mid-Latitude Point Source" experiment of Mahlman (1973a). Data is taken from November (11th month of experiment). Shading indicates regions where the net "eddy" flux vector is countergradient.

A STATE OF THE STA

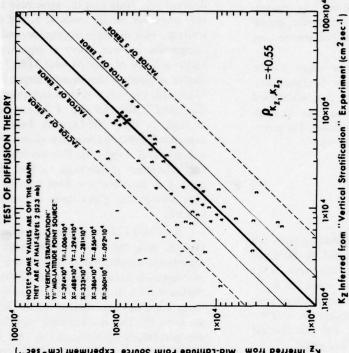


Figure 3. Scatter diagram of 1-D K_z values calculated separately from the two 3-D tracer experiments described by Mahlman (1973a). Values are monthly means for eleven separate months. In each comparison the advecting wind fields are identical. Numbers indicate model levels (1 = 27.6 mb, 2 = 52.3 mb, 3 = 80.7 mb, 4 = 149.9 mb, 5 = 240.6 mb, 6 = 412.0 mb). Heavy solid line gives axis of "perfect" agreement. Thin solid line indicates a factor-of-2 disagreement.

315

the global mean vertical flux \overline{wR}^H is "parameterized" through use of the mixing-length hypothesis. Here, $(\overline{\ })^H$ is a global average over a horizontal surface.

As in previous sections, some insight into the relative validity of this simple "parameterization" of atmospheric transport can be obtained by analysis of results from the general-circulation/tracer model experiments. The procedure employed has been to calculate

$$K_{z} = -\frac{\overline{w}\overline{R}^{H}}{\frac{\partial \overline{R}^{H}}{\partial z}}$$
 (6)

for various periods of time, averaging from the two tracer experiments described by Mahlman (1973a) and reviewed briefly in this paper. In the mixing-length hypothesis, the value of K_z is assumed to be a function of only the transporting motion field, and independent of both the details of the tracer field and the specific structure of the tracer sources and sinks.

There appears to be no reason to expect such assumptions to be rigidly valid in the atmosphere. The only real question of concern here is the degree to which such assumptions are violated. If this can be assessed, then some insight can be gained into the fundamental limitations inherent in 1-D models, i.e., an assessment of the basic uncertainty in such a model even when the "best possible" set of K_z's has been determined.

One way to check on such basic uncertainties is to calculate the values of K_z independently from the two tracer experiments with the same model. Since the advecting wind fields are identical in the two experiments, the mixinglength hypothesis asserts that the independently calculated values of K_z from the two experiments should be the same. This has been tested at monthly intervals for an eleven-month period common to the two tracer experiments.

The results of this test are plotted on a scatter diagram in Figure 3. In this figure the K_z 's from the two experiments are entered as ordinate and abscissa. The numbers 1-6 indicate the model levels (see the figure caption). If the mixing-length hypothesis is completely valid, all data points should lie on or very near the heavy

diagonal line. Note that the agreement is reasonably close for model levels 4, 5, and 6. These levels are near the mean tropopause, and, for this comparison at least, show a mean agreement within a factor of two. At level 3 (80.7 mb), the scatter of points is significantly larger. At level 2 (52.3 mb), the values deviate significantly from the "ideal". Also, for five of the eleven months at level 2, the "Mid-Latitude Point Source" experiment indicated negative values of K_z (see upper left of Figure 3). This occurred because the calculated global-mean vertical flux was upward at this level for April through August, even though the global-mean tracer increased upward.

At level 1 (27.6 mb) the discrepancy is very evident, with the "Mid-Latitude Point Source" experiment showing values of K_z nearly an order of magnitude larger. The cause of this will be discussed later. It is of interest to note that the linear correlation coefficient for this entire data set is +0.55. This is statistically significant, but not particularly high considering that the basic hypothesis assumes the existence of a correlation coefficient of +1.0.

Because of the considerable scatter in the monthly comparisons of K_z calculations shown in Figure 3, it is of interest to examine the nature of calculated K_z 's when most of the temporal meteorological behavior has been averaged out – i.e., one-year averages. Recall that in these experiments the same one-year period of advecting winds is used for successive years. It should be noted that the real atmosphere thus provides an additional source of uncertainty due to its well-known interannual variability, especially in the stratosphere.

Figure 4 shows the distribution of calculated K_z from the "Vertical Stratification" tracer experiment for the first year of the experiment versus the second year. The two calculations agree by better than a factor of two everywhere. Thus, in the "vertical stratification" experiment, the evolution of the tracer field in time does not appear to have a large effect upon the model-calculated values of global-mean K_z .

Figure 5 shows the same kind of calculation that was seen in Figure 4, but for the "Mid-Latitude Point Source" tracer experiment. This figure shows very large year-to-year differences in

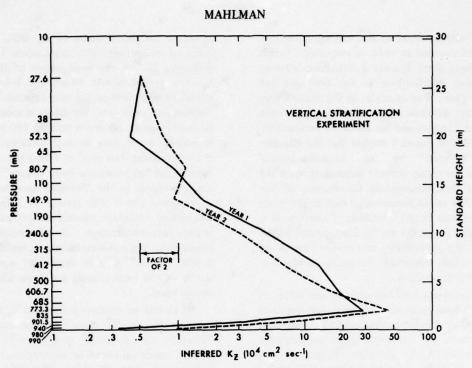


Figure 4. Comparison of successive one-year average values of 1-D K_z inferred from the 3-D "Vertical Stratification" experiment. In each case the advecting wind fields are identical.

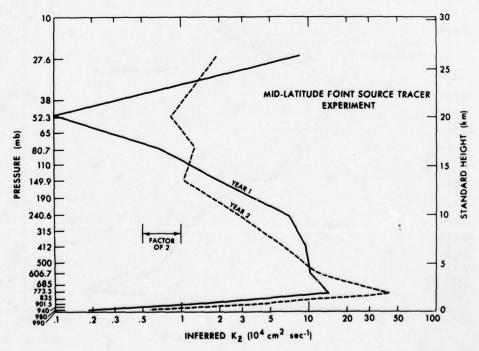


Figure 5. Comparison of successive one-year average values of 1-D K_z inferred from the 3-D "Mid-Latitude Point Source" experiment. In each case the advecting wind fields are identical.

the calculated values of Kz, varying between a factor of two and an order of magnitude. In this experiment there is quite a difference between the tracer distributions in the first and the second years. For example, in the second year significant amounts of tracer are located in the equatorial regions and the Southern Hemisphere. The result of Figure 5 implies that the effective K,'s "selected" by the three-dimensional motions are rather strongly dependent upon the model's three-dimensional distribution of the tracer. The model meteorology that leads to such circumstances is quite realistic. Therefore, it is reasonable to expect similar fundamental limitations in the applicability of the one-dimensional mixing-length hypothesis to tracer problems in the actual atmosphere.

A comparison of two-year average values of K_z from each tracer-model experiment is shown in Figure 6. This shows that longer-term averages of K_z from the two experiments are generally quite similar. A very significant exception to this occurs at the top model half-level (27.6 mb).

Here the calculated values of Kz differ by an order of magnitude. The explanation for this difference lies in the basic design of the two tracer experiments. At 38 mb and below, the model formulations in the two experiments are identical. In each case, the tracer is assumed to be inert from 38 mb down through 190 mb, and is subject to the same removal specifications in the troposphere. However, at 10 mb the tracer is inert in the "Mid-Latitude Point Source" experiment, whereas in the "Vertical Stratification" experiment, tracer fluctuations at 10 mb are assumed to be instantaneously damped back to a time/space-independent chemical-equilibrium value. Thus, the one-dimensional K, which a 3-D model "selects" is also dependent upon the nature of the local sources and sinks which act on the tracer.

It should be cautioned that the K_z 's calculated in Figures 3-6 should not be used as a "correct" set for direct application to atmospheric tracer problems in preference to other independent determinations. The calculations

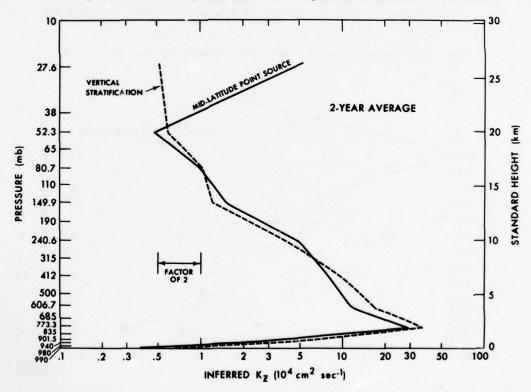


Figure 6. Comparison of two-year average values of 1-D K_z from the 3-D "Vertical Stratification" experiment and the "Mid-Latitude Point Source" experiment. In each case the advecting wind fields are identical. (Note significant difference at 27.6 mb).

and tests performed here were designed to avoid that question by examining only the basic transfer assumptions as viewed from the framework of a more complex model.

Some investigators have recently suggested that some of the ambiguities inherent in 1-D models might be reduced significantly if the term "horizontal" were redefined to mean parallel to lines of mean height of the tropopause (e.g., Johnston et al., 1976; Hunten, 1976). This suggestion is based upon the general observation that mixing-ratio isolines of many tracers tend to lie parallel to the mean tropopause. Thus, if a parcel of air on one of these surfaces is vertically transported independently of its "horizontal" position on this surface, the one-dimensional transport concept would be valid. Consequently, the ambiguity so evident in Figures 3-6 would be eliminated.

This idea has been examined in a cursory manner by performing a calculation of the zonal-mean K_z on such a coordinate surface (1.5 km above the model mean tropopause). The results of this calculation are given in Figure 7. This suggests that the tracer vertical transfer is a strong function of "horizontal" position in this coordinate system. For example, in the tropics tracer is being transported upward against its mean gradient, while in mid-latitudes tracer is being transported strongly toward the troposphere.

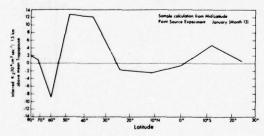


Figure 7. Sample calculation of model-computed K_Z along a "horizontal axis" 1.5 km above the mean tropopause. Data is taken from the "Mid-Latidude Point Source" experiment and is a monthly mean for January (13th month of experiment).

However, the "tropopause coordinate" 1-D model may still represent an improvement over the usual kind of 1-D model discussed in Figures 3-6, even though a remaining unsolved problem

in this concept is how to define the global tracer amount consistently at each coordinate level in such a model without ambiguity.

BEHAVIOR OF TRACERS WITH AND WITHOUT TROPOSPHERIC SINKS

Some recent work by Johnston et al. (1975) has indicated that significant differences exist between the behavior of nuclear-weaponsproduced particulate radioactive tracers and gaseous carbon-14. Although large uncertainties are present in both data sets, the apparently more rapid removal of the particulate tracer has been interpreted as being due to the effect of preferential gravitational settling of particles in the stratosphere. This is a definite possibility, although the earlier data of Telegadas and List (1969) appears to be inconsistent with this concept. Further discussion on this point is found in Chang (1976). Since the oxides of nitrogen emitted by a fleet of supersonic aircraft exist in gaseous form, it has been suggested that, for this problem, the gaseous carbon-14 behavior provides the most appropriate analog for calibrating empirical transport models. However, it may also be important to consider that the particulate tracers are strongly removed in the troposphere. while gaseous carbon-14 experiences only very weak tropospheric removal.

In the previous section, evidence was presented which indicates that the "proper" choice of K_z in a 1-D transport model can depend rather strongly upon the specific types of sources and sinks acting on a given tracer. This naturally leads to the question of whether or not a set of K_z 's determined for a given tracer with a given distribution and "chemistry" can be reliably used for a tracer with different properties. More specifically, are the effective K_z 's for stratospheric tracers with and without tropospheric removal mechanisms the same or different?

Again, the general-circulation/tracer model provides a tool for examining this question. As a test, the tropospheric sink mechanism was discontinuously removed from the "Mid-Latitude Point Source" tracer experiment code at the start of October, year 2 (month 22). As before, the model-determined one-dimensional K_z's were calculated and the "No Sink" values of K_z were

compared against those of the regular "Control" experiment.

The comparison values of K_z for the second month of the "No Sink" experiment are shown in Figure 8. This shows that the tropospheric values of K_z diminish significantly in the "No Sink" experiment relative to the "Control" experiment. Thus, even though the tropospheric tracer values are strongly increasing, the downward tracer flux decreases relatively faster than the global mean gradient is reduced. This is yet another example of how the transport of a tracer is affected by its sources and sinks.

The effect of this process on the long-term removal of tracer from the stratosphere is not clear at the present time. These experiments are currently being run for a much longer time interval in order to study this problem.

The question naturally arises as to the physical reasons why the effective K_z appears to be noticeably dependent upon the nature of the sources and sinks acting on the tracer. The case shown in Figure 8 happens to be one in which

the physical explanation is reasonably clear. In the "Mid-Latitude Point Source" tracer experiment, the tropospheric removal processes are dependent upon the model-calculated precipitation rate. Because precipitation is strongly coupled with ascending air parcels, this produces a tendency for the ascending air to have very strong local tracer removal associated with it. As a result, the transport is such that the tracer amount in the upward-moving air is not at all typical of the level mean tracer amount. This is inconsistent with the mixing-length hypothesis. Note in Figure 8 that this effect is significant even though the mean gradient between the middle troposphere and the lower stratosphere is rather large. (The "No Sink" level mean at 110 mb is 12.6 times that at 500 mb.)

SUMMARY

The high-resolution general-circulation/ tracer model described by Mahlman (1973a) has been used to evaluate some of the assumptions

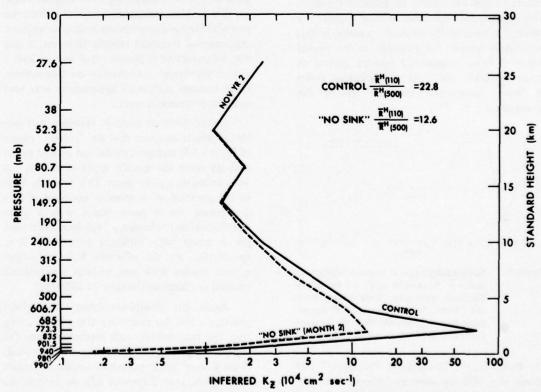


Figure 8. Comparison of monthly mean 1-D K_z values calculated from the 3-D "Mid-Latitude Point Source" (control) experiment with the "No Sink" results for the second month after sink removal.

employed in less comprehensive transport models. By evaluating within the framework of the comprehensive model, the question of which model is the most suitable for current application has been deferred.

For low-resolution 3-D models, evidence was presented which indicates that significant distortions in the tracer transport may occur unless the model is able to resolve scales down to about ten planetary wavenumbers. Furthermore, the model results indicate that a considerable amount of tracer "power" exists at even smaller scales (n = 10-48) in the high-resolution 3-D model. This is interpreted as being indicative of a strong transfer of tracer fluctuations to smaller spatial scales.

Some aspects of the mixing-length hypothesis as applied to 2-D models were examined. The results indicate that the commonly invoked 2-D mixing-length assumptions are seriously violated, in the sense that negative horizontal and vertical "eddy" diffusivities are frequently indicated. This suggests rather strongly that both the "eddy" transport and meridional-circulation specifications should be regarded as being inherently empirical in character as long as the "eddy" mixing-length hypothesis is used in such models. It was thus concluded that the only acceptable test of this type of 2-D transport model is whether or not the net behavior of the calculated tracer is consistent with observations.

The tests of 1-D transport assumptions indicate frequent violations of the mixing-length hypothesis, in the sense that the calculated values of K_z were shown to be dependent upon the three-dimensional tracer distribution and upon the nature of the specific sources and sinks acting on a tracer. These results suggest that even the "best" set of K_z 's derived to "explain" a given tracer may not be applied with high confidence to a tracer with a different distribution and different sources and sinks.

It may be found that some of these fundamental uncertainties can be reduced without abandoning the simpler model frameworks. To do so will require transport "parameterizations" with a firmer physical basis than that provided by the traditional mixing-length hypotheses.

ACKNOWLEDGMENTS

The author is extremely indebted to W.J. Moxim whose highly productive work has been

absolutely essential to the success of this project. Gratitude is also expressed to S. Manabe for his instrumental role in making this project possible, to J. Smagorinsky for his efforts to provide an environment where such research can be conducted, and to H. Levy II for a number of stimulating discussions.

REFERENCES

- Chang, J.S. (1974), "Simulations, perturbations, and interpretations," in Proceedings of the Third Conference on the Climatic Impact Assessment Program (Cambridge, Mass.), U.S. Dept. of Transportation, DOT-TSC-OST-74-15, 330-341.
- Chang, J.S. (1976), "The application of radioactive tracers," in this volume.
- Cunnold, D., F. Alyea, N. Phillips, and R. Prinn (1975), "A three-dimensional dynamical-chemical model of atmospheric ozone," J. Atmos. Sci. 32, 170-194.
- Danielsen, E.F. (1968), "Stratospheric-tropospheric exchange based on radioactivity, ozone, and potential vorticity," J. Atmos. Sci. 25, 502-518.
- Dickinson, R.E. (1969), "Theory of planetary wavezonal flow interaction," J. Atmos. Sci. 26, 73-81.
- Hahn, D.G., and S. Manabe (1975), "The role of mountains in the South Asian monsoon circulation," J. Atmos. Sci. 32, 1515-1541.
- Hayashi, Y. (1974), "Spectral analysis of tropical disturbances appearing in a GFDL general circulation model," J. Atmos. Sci. 31, 180-218.
- Holloway, J.L., Jr., and S. Manabe (1971), "Simulation of climate by a global general circulation model: 1. Hydrologic cycle and heat balance," Mon. Wea. Rev. 99, 335-370.
- Hunt, B.G., and S. Manabe (1968), "Experiments with a stratospheric general-circulation model. II. Largescale diffusion of tracers in the stratosphere," Mon. Wea. Rev. 96, 503-559.
- Hunten, D.M. (1976), "The philosophy of onedimensional modeling," in this volume.
- Johnston, H.S., D. Kattenhorn, and G. Whitten (1976), "Use of excess carbon-14 data to calibrate models of stratospheric ozone depletion by supersonic transports," in this volume.
- Kurihara, Y., and J.L. Holloway, Jr. (1967), "Numerical integration of a nine-level primitive-equations model formulated by the box method," Mon. Wea. Rev. 95, 509-530.

- Lilly, D.K., D.E. Waco, and S.I. Adelfang (1974), "Stratospheric mixing estimated from high-altitude turbulence measurements," J. Appl. Met. 13, 488-493.
- Mahlman, J.D. (1973a), "Preliminary results from a three-dimensional general-circulation/tracer model," in *Proceedings of the Second Conference on the Climatic Impact Assessment Program* (Cambridge, Mass.), U.S. Dept. of Transportation, DOTTSC-OST-73-4, 321-337.
- Mahlman, J.D. (1973b), "On the maintenance of the polar front jet stream," J. Atmos. Sci. 30, 544-557.
- Mahlman, J.D., and S. Manabe (1972), "Numerical simulation of the stratosphere: Implications for related climate change problems," in *Proceedings of the Survey Conference* (Cambridge, Mass.), Climatic Impact Assessment Program, U.S. Dept. of Transportation, DOT-TSC-OST-72-13, 186-193.
- Mahlman, J.D., and W.J. Moxim (1976), "Experiments with a global general-circulation/tracer model. I. Tracer model description and results from a mid-latitude point source experiment," in preparation.
- Manabe, S., D.G. Hahn, and J.L. Holloway, Jr. (1974), "The seasonal variation of the tropical circulation as simulated by a global model of the atmosphere," J. Atmos. Sci. 31, 43-83.
- Manabe, S., and J.L. Holloway, Jr. (1975), "The seasonal variation of the hydrologic cycle as simulated by a global model of the atmosphere," J. Geophys. Res. 80, 1617-1649.
- Manabe, S., and J.D. Mahlman (1976), "Simulation of seasonal and interhemispheric variations in the stratospheric circulation," J. Atmos. Sci. 33, to be published.

- Manabe, S., J. Smagorinsky, J.L. Holloway, Jr., and H.M. Stone (1970), "Simulated climatology of a general circulation model with a hydrologic cycle. III. Effects of increased horizontal computational resolution," Mon. Wea. Rev. 98, 175-212.
- Manabe, S., J. Smagorinsky, and R.F. Strickler (1965), "Simulated climatology of a general circulation model with a hydrologic cycle," Mon. Wea. Rev. 93, 769-798.
- Manabe, S., and R.F. Strickler (1964), "Thermal equilibrium of the atmosphere with a convective adjustment," J. Atmos. Sci. 21, 361-385.
- McElroy, M.B., S.C. Wofsy, J.E. Penner, and J.C. McConnell (1974), "Atmospheric ozone: Possible impact of stratospheric aviation," J. Atmos. Sci. 31, 287-303.
- Miyakoda, K., R.F. Strickler, C.J. Nappo, P.L. Baker, and G.D. Hembree (1971), "The effect of horizontal grid resolution in an atmospheric circulation model," J. Atmos. Sci. 28, 481-499.
- Phillips, N.A. (1957), "A coordinate system having some advantages for numerical forecasting," J. Met. 14, 184-185.
- Reed, R.J., and K.E. German (1965), "A contribution to the problem of stratospheric diffusion by large-scale mixing," Mon. Wea. Rev. 93, 313-321.
- Reiter, E.R. (1972), "Atmospheric Transport Processes:
 Part 3. Hydrodynamic Tracers," AEC Critical
 Review Series, U.S. Atomic Energy Commission,
 Office of Information Services, 212 pp (available
 as TID-25731 from NTIS; \$3.00).
- Smagorinsky, J. (1963), "General circulation experiments with the primitive equations: I. The basic experiment," Mon. Wea. Rev. 91, 99-164.
- Telegadas, K., and R.J. List (1969), "Are particulate radioactive tracers indicative of stratospheric motions?", J. Geophys. Res. 74, 1339-1350.

THE PHILOSOPHY OF ONE-DIMENSIONAL MODELING*

DONALD M. HUNTEN Kitt Peak National Observatory Tucson, Arizona

ABSTRACT: Vertical transport of inert tracers (or grouped constituents such as odd nitrogen) is discussed. It is argued that useful results can be obtained in a coordinate system based on the mean tropopause. A method of determining the eddy coefficient K is presented. A vertical profile of K is obtained from methane observations; it is incorporated into a simple transport model and used to predict odd-nitrogen mixing ratios for several fleets of aircraft, both supersonic and subsonic.

STRATOSPHERIC VERTICAL TRANSPORT

The discussion of the "hierarchy of models" in CIAP Monograph 3 (CIAP, 1975) gives an interesting intellectual framework for the description of transport in stratospheric modeling. In this framework, a one-dimensional representation is derived by averaging its three-dimensional "parent" over latitude and longitude. Satisfying as this may be, it is not really much help, and may even be a hindrance, to development of an understanding of the atmosphere. Actually, onedimensional models have an existence independent of this framework, and have been used for the past 20 years. They may perhaps be regarded as an engineering approach to the problems of vertical transport, difficult or perhaps impossible to derive from fundamental principles, but obtained instead by a physically reasonable shortcut. In this approach, we make the assumption that the flux of a substance is proportional to the gradient of its mixing ratio, and give the proportionality constant the unfortunate name "eddy diffusion coefficient". (The name is not fully descriptive, and conjures up in some minds the idea of small-scale turbulence, which is not really appropriate. Indeed, much of the vertical transport seems to be performed by motions of very large scale; and on the other hand, some motions can carry material up and then back again without giving any mixing to speak of.)

The need to assess scientific questions that have immediate societal import has placed a lot of emphasis on the engineering aspects of theory. It is thus worth reminding ourselves of its more normal role, which is particularly important to those of us who think about other planetary atmospheres besides the Earth's. Theory is a kind of armchair exploration, in which we can test various ideas and see which ones seem most worth following up observationally. At the same time, we can hope to improve our insight into how the atmosphere really works. Of course, one-dimensional models will not teach us much about atmospheric motions, but that is not their purpose: they are aimed at deriving a usable, tractable description of atmospheric chemistry.

For a one-dimensional formulation to make sense, the mixing ratio f must be a global, or at least hemispheric, average; it is best if f is uniform worldwide. The natural tracers CH₄ and N₂O obey this last restriction very well, for they originate in the ground and are well distributed by motions in the troposphere. As they move up through the stratosphere, these molecules are slowly destroyed by photochemical processes at a calculable rate. The resulting gradient of their mixing ratio has been observed, and they are therefore particularly valuable as tracers for the rate of the mixing process. (This application is discussed below in some detail.)

Most artificial sources of odd nitrogen within the stratosphere are fairly concentrated geographically (e.g., aviation corridors), so the applicability of a one-dimensional eddy treatment must be questioned. The situation is not nearly so bad as might be expected, as has been seen in the behavior of radioactive clouds from

^{*}A shorter version of this paper appeared in the Proceedings of the National Academy of Sciences (Vol. 72, pp 4711-4715, 1975).

nuclear tests (e.g., Gudiksen et al., 1968; Johnston et al., 1973, 1976). In a few months, material spreads all around a latitude circle, with somewhat slower north-south spreading. This horizontal spreading is able to give fair uniformity within a hemisphere before a large amount of vertical motion can take place.

A more serious difficulty is found in the nature of the tropopause and the stratospheric motions just above it. The tropopause is defined as the level at which the tropospheric vertical lapse rate of several degrees Celsius per kilometer gives way to a height-independent temperature, characteristic of the stratosphere. The tropopause height is around 9 km in polar regions, and 17 km over the equator. To a first approximation, horizontal mixing takes place along surfaces parallel to the tropopause (Davidson et al., 1966; Reed and German, 1965). Thus, at least at the heights reached by aircraft, the important height is the distance above the tropopause, not above the ground. Although this picture is oversimplified, it is probably the best available for quantitative use. Two-dimensional models offer a considerable improvement in principle, but I have little faith in their results, because of the difficulty in prescribing realistic eddy coefficients in the absence of large amounts of tracer data. The assumption that material spreads over a hemisphere, while cruder in principle, at least reproduces the general features of the observed behavior of radioactive clouds.

In transport calculations, the "tropopause" is a level at which the eddy-diffusion coefficient changes from a large tropospheric value to a small stratospheric value. There are reasons, both theoretical and empirical, for associating this level with the tropopause defined from the temperature profile. But there is no assurance that the two are the same, especially in the data from a particular vertical sounding; to avoid confusion, we should really use a different name, such as "transport tropopause".

In a one-dimensional model, the vertical flux ϕ (molecules cm⁻² sec⁻¹) of tracer is assumed to be proportional to the gradient of its mixing ratio f; the proportionality constant is Kn_a , where K is the eddy-diffusion coefficient and n_a is the number-density of air molecules:

$$\phi = -Kn_a \frac{df}{dz}.$$
 (1)

K is a purely empirical quantity, to be determined (as shown in examples below) by substituting observed quantities for the other variables in (1). To simplify the description, we model the atmosphere as isothermal, with a constant scale height H; thus, its number-density or concentration n_a varies as $\exp(-z/H)$. It is convenient to measure the height z from the tropopause level z_t , where $n_a = n_{at}$; we write $h = (z - z_t)/H$, a nondimensional height in units of H, and $n_a = n_{at} \exp(-h)$. The solution of the differential equation (1) is

$$f = -\int \frac{\phi}{Kn_a} dz, \qquad (2)$$

and the integral can be evaluated if suitable functional forms are chosen for ϕ and K. In a region of the atmosphere where they are constant, Eq. (2) becomes

$$f = A - \frac{\phi H}{K n_a}, \qquad (3)$$

where A is the constant of integration; or, since $f = n/n_a$,

$$n = An_a - \frac{\phi H}{K}. \tag{4}$$

According to Eq. (3), f = A if $\phi = 0$; this constancy does not depend on our simplifying assumptions, as may be seen from Eq. (1). Conversely, the second term in Eqs. (3) and (4) gives a constant term in the number density for a downward flux.

Figure 1a shows an illustrative model for the troposphere and stratosphere; at the tropopause, K changes from 105 to 3 × 103 cm² sec⁻¹. In each region Eq. (3) or (4) can be applied with a different value of A, and the solutions can be made to agree at the interface between the two regions. The source is taken to have a strength, averaged over the globe, of Q molecules cm⁻² sec-1 at the nondimensional height hq. At greater heights, $\phi = 0$ once a steady state has been attained, and therefore f is constant. Below ha, \$\phi\$ has the constant value -Q. We assume that the pollutant is removed at the surface; removal in rain would give a similar result. Tropospheric (subscript t) density profiles for two values of A, are shown in Figure 1b. The density at the tropopause is insensitive to At, which can be

HUNTEN

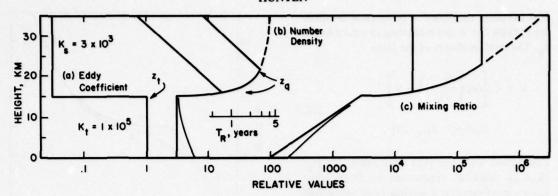


Figure 1. The simple two-layer model. (a), the eddy-diffusion coefficient K; (b), the density of a minor constituent for equal sources at z_q = 16 and 22 km; also the residence time (Hunten, 1975); (c), the corresponding mixing ratios of the minor constituent.

taken as zero; then $n_t = QH/K_t$ (cf. Hunten, 1969). With this density as the lower boundary condition for the stratosphere (subscript s), the stratospheric profile up to height h_a is:

$$n_{s} = \frac{QH}{K_{s}} \left[1 - \left(1 - \frac{K_{s}}{K_{t}} \right) e^{-h} \right]$$

$$= \frac{QH}{K_{s}} (1 - 0.97e^{-h}).$$
(5)

Above h_q , the aforementioned constant value of f is obtained by substituting h_q for h in Eq. (5). The result is

$$f_q = \frac{QH}{K_s n_{at}} (\exp h_q - 0.97).$$
 (6)

Examples are shown in Figures 1b and c, for sources 1 and 7 km above the tropopause.

It is useful to represent the results of a transport model by an "injection coefficient" α , following a suggestion by McElroy et al. (1974). As Figure 1c illustrates, the mixing ratio above the source is independent of height; we shall call it f_q . f_q is related to the source strength Q by the definition of α ,

$$f_{\alpha} = \alpha Q, \qquad (7)$$

where α depends on the source height h_q. A typical value for α at 18 km is 5×10^{-17} cm² sec. A source strength Q = 10^8 molecules cm⁻² sec⁻¹ then gives a mixing ratio 5×10^{-9} , or 5 ppb. If several sources are present, perhaps

including natural ones, their contributions to f at each height are simply added. The reduction of ozone by odd nitrogen occurs mainly by reactions above 25 km. Thus, for a source at any lower height, the injection coefficient permits an immediate calculation of the corresponding change of odd-nitrogen mixing ratio. A curve of α as a function of height has the same form as the envelope in Figure 1c.

More interesting than the oversimplified stratospheric model so far discussed is one in which K varies exponentially with height. A similar variation of ϕ can also be included, by an obvious extension. If the scale height for K is $H_K = -H/a$, we have

$$K = K_0 \exp(ah) \tag{8}$$

$$Kn_a = K_0 n_{at} \exp (1-a)h$$
. (9)

K₀ is the value of K at the lower boundary, usually the tropopause. The scale height of the product Kn_a in Eq. (9) is H_p, and

$$\frac{1}{H_{\rm p}} = \frac{1}{H} + \frac{1}{H_{\rm K}} = \frac{1-a}{H} \ . \tag{10}$$

It is found below that H_K is negative (K increases with height) and a, as defined, is therefore positive. The solutions (3) and (4) remain the same, but with K a function of z, and H replaced by H_n ; for example,

$$f = A - \frac{\phi H_p}{K n_a} = A - \frac{\phi H}{K n_a (1-a)}$$
. (11)

The injection coefficient α is obtained by dividing (11) by $Q = -\phi$ and evaluating at source height z_q . The result is always of the form

$$\alpha = C \left[exp \left(\frac{z_q - z_t}{H_p} \right) - D \right]$$

$$= C \left[exp(1-a)h_q - D \right].$$
(12)

Comparison with Eq. (11) shows that $C = H_p/(K_0 n_{at})$. Algebraic expressions for D are often fairly complicated; it is usually most easily evaluated by matching the value of α at the lower boundary of the layer with the value at the top of the next lower layer. Table 1 shows values of C, D, z_t , and H_p for the models derived below, and Figure 2 shows the corresponding profiles of α .

Table 1. Model Parameters for Use in Eq. (12)

	All Models	2-Layer Model		Layer odel
Layer	t*	s	b	s
z _t (Km)	11	15	10	14
$H, H_p(Km)$	6.2	18.1	6.2	18.1
C*	0.082	20	0.29	16.7
D	0	0.992	0.7	0.979

*t = troposphere $(K = 10^5 \text{ cm}^2 \text{ sec}^{-1})$

b = boundary layer (4 km deep, $K = 3 \times 10^4$)

s = stratosphere (K from Figure 3)

**C is in units of 10⁻¹⁷ cm² sec.

Residence times can also be calculated in the present framework (Hunten, 1975), though they must be used with caution. The residence time is conveniently defined as the ratio of stratospheric burden to the source strength.

USE OF NATURAL TRACERS

The eddy-diffusion coefficient K in Eq. (1) is a parameter to be determined from observations of appropriate natural tracers. Here we shall focus on methane, CH₄, which is the best-observed of the suitable substances. The relevant data are shown as points in Figure 3. Inspection of these results shows a small but distinct gradient of the mixing ratio starting at the tropopause. The measurements, obtained by

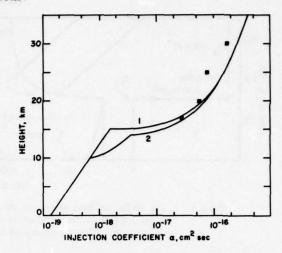


Figure 2. Injection coefficients for the two models of Table 1. The squares were taken from the papers of McEiroy et al. (1974) and McConnell and McEiroy (1973).

Ehhalt et al. (1972) and Ehhalt and Heidt (1973), are of exceptional quality. Samples, obtained by balloons (or, at 50 km, by a rocket), were analyzed on the ground by gas chromatography. Methane can also be observed spectroscopically (Kyle et al., 1969; Cumming and Lowe, 1973), the results confirm the ones used here, be do not define the gradients well enough for the present analysis.

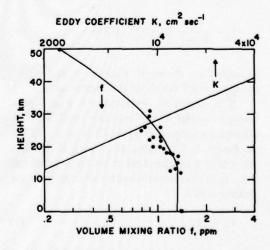


Figure 3. Methane mixing ratios from the balloon data and the 50-km rocket measurement of Ehhalt et al. (1972). The curved line, drawn by eye, was used to obtain the profile of K.

Since Figure 3 is a semilogarithmic plot, the slope is the logarithmic derivative, which may be written

$$d \ln f/dz = (1/f) (df/dz) = -1/H_f$$
,

so that H_f is the scale height of the mixing ratio. Then Eq. (1) may be written

$$K(z) = \frac{\phi(z)}{n_a(df/dz)} = \frac{\phi(z)H_f(z)}{n(z)}$$
. (13)

The number density n(z) is taken directly from the measurements shown in Figure 3; to get $H_f(z)$ we must estimate the slopes, which are obviously rather uncertain. The curve shown is typical of those that can be drawn through the points; they all give similar results for K, within a factor of two or so. The flux $\phi(z)$ is derived from the observed profile with the use of a computed photochemical lifetime $\tau(z)$, discussed further below. For a constituent that is destroyed but not produced in the atmosphere, the continuity equation and its integral are

$$\frac{d\phi}{dz}$$
 = -loss rate = - $\frac{n(z)}{\tau(z)}$

$$\phi(z) = \int_{-\infty}^{z} (n/\tau) dz.$$
 (14)

This expression is readily evaluated in steps, working down from the top, where $\phi = 0$, and using the observed n(z).

Substitution into Eq. (13) gives a somewhat scattered set of points, which are well represented by the straight line and upper scale of Figure 3. Many other representations of the data could have been picked, but this one, an exponential function of height, is convenient because it allows the analytic solution of the eddy equation used here. It is represented by

$$K = 2200 \exp(z-14)/9.43 \text{ cm}^2 \text{sec}^{-1}$$
, (15)

which is $2200 \text{ cm}^2\text{sec}^{-1}$ at 14 km and 3.5×10^4 at 40 km. H_K is -9.43 km, H_p is 18.1 km, and a is 0.657.

The same methane data have already been analyzed by Wofsy and McElroy (1973); their

technique was to postulate various profiles of K and pick the one that predicted the best methane profile. The resulting K's are greater by a factor of four above 30 km, and differ only slightly below 20 km. Another analysis, with data from an additional balloon flight, has been mentioned by Ehhalt et al. (1974); see also Crutzen (1974). These values are somewhat larger yet. Probably much of this spread comes from differing estimates of the photochemical lifetimes; another reason for it is Crutzen's use of daytime values for $\tau(z)$ instead of diurnal means.

Since the photochemical lifetime is a principal source of uncertainty, it is worth some discussion. Methane is attacked by OH and O(1D). The latter also produces most of the OH, at the heights of concern here, from water vapor. Both O(1D) and OH are absent at night, and a diurnal-average concentration must be used. Calculation of the OH density is discussed in detail by Wofsy et al. (1972), and another treatment valid above 40 km is given by Hunten and Strobel (1974). Both papers show good agreement with rocket dayglow observations above 45 km by Anderson (1971). Some uncertainty follows from the need to extrapolate to low temperatures the rate coefficient for the reaction of OH with CH4. Wofsy et al. adopt a result based on Greiner (1970), recently confirmed by Margitan et al. (1974). The values used here (Wilson, 1972) are about half as large at stratospheric temperatures, and lead to a slight underestimate of the eddy coefficients. Another difficulty in calculating OH concentrations is the loss rate of odd hydrogen, controlled by the reaction of OH and HO2.

The source of $O(^1D)$ atoms in photolysis of ozone, and their principal sink in collisional quenching by N_2 and O_2 , are both readily evaluated. Current estimates for the lifetimes of CH_4 , and also of N_2O and CO, are shown in Figure 4. N_2O is destroyed primarily by photolysis (Bates and Hays, 1967; McConnell and McElroy, 1973); a minor branch, attack by $O(^1D)$, is an important source of odd nitrogen, as discussed below. CO is a less valuable tracer than the others, because it is both produced and destroyed by OH reactions in the stratosphere.

Only one profile of N₂O is available so far (Ehhalt et al., 1974); the eddy coefficients derived from CH₄ fit it fairly well, but several more

HUNTEN

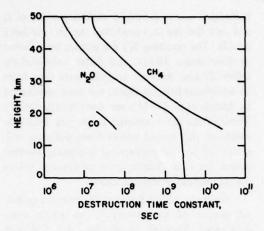


Figure 4. Loss time constants, τ , for use in Eq. (14). The N₂O results are from Bates and Hays (1967), and the others were calculated with the OH and O(¹D) concentrations of McElroy et al. (1974).

flights seem needed to define an average situation. The virtue of the CO profile is that it clearly points to a discontinuity of K at the tropopause (Seiler and Warneck, 1972). Its lifetime, as seen in Figure 4, is short compared to transport times; thus, it is difficult to get any more information about K from it.

Seiler and Warneck (1972) also point out the utility of ozone in transport calculations, since it approximates a conserved tracer in the vicinity of the tropopause. According to Eq. (1), K(df/dz) should not change as this boundary is crossed, if ϕ is constant. From averaged ozone observations, it is found that Af/dz increases by a factor of 38. This figure would be rised to 50 by a rough allowance for the change of na between the regions in which the two slopes were estimated. Thus, if K is 1×10^5 in the troposphere, then it is 2×10^3 just above the tropopause. Downwardflowing tracers have the great virtue of showing large, readily-observable gradients of f, but ozone must be used with caution because it is far from inert at some altitudes.

It is an obvious conclusion that the potential value of tracers for defining transport parameters in the stratosphere has barely begun to be realized. The techniques exist to make the measurements; they simply have not been used on an adequate scale. Although the situation is not so bad for methane, more data would still be valuable. Calibration of 2-dimensional models is a nearly hopeless task at present.

The natural tracers have been observed almost exclusively at a latitude near 30° N, where the height of the tropopause is 15 km. For other latitudes, it has been argued above that the relevant height scale should be based on the tropopause height. In addition, a boundary layer can be inserted in the region 10-14 km, using an intermediate value of K, 3×10^4 cm² sec⁻¹. Such a 3-layer model (see Table 1) has been adopted with considerable success in a very recent study (Johnston et al., 1976) of the transport of carbon-14 from nuclear tests, and will be used here as the standard.

ODD NITROGEN, NATURAL AND ARTIFICIAL

Before one can have confidence in predicted effects of artificial sources, one should be able to show that the natural situation is adequately described. Such a description is a bit beyond the simple method discussed here, but it can be used to illuminate an existing computation, that of McElroy et al. (1973). N₂O, discussed above as a tracer, is also the principal source of odd nitrogen in the stratosphere. Its lifetime, shown in Figure 4, is almost entirely determined by photolysis into $N_2 + O$. This process gives even nitrogen, but a slower one, attack by O(1D), gives odd nitrogen (2 molecules of NO) or even nitrogen (N2 + O2) at equal rates. According to McConnell and McElroy (1973), the resulting natural source strength Q is about 7 × 107 molecules cm-2 sec-1, spread mainly over the 20-40 km range. For their profile of K, the injection coefficient at 30 km is $\alpha = 17 \times 10^{-17}$ cm² sec; the product αQ gives a mixing ratio f = 12×10^{-9} , or 12 ppb. This result is insensitive to the assumed values of K: with faster transport the source Q is larger, but α is smaller because the loss of odd nitrogen is greater.

Another possible source of odd nitrogen is destruction of NH₃, though the actual end product is not known. McConnell (1973) finds that the source, if such it is, has an effective height around 20 km, and a magnitude very close to that for N₂O. But the injection coefficient is smaller than that of N₂O by a factor of 7; thus the source from NH₃ makes at most only a minor contribution to odd nitrogen at higher altitudes, as McConnell also points out.

The response of the ozone concentration [O₃] to an increment of odd nitrogen is complicated by feedback effects, which are analyzed by McElroy et al. (1974) and found to be small but not negligible. No attempt is made here to discuss the chemistry of odd nitrogen, which is treated merely as a conserved tracer. Instead, the computed results by McElroy et al. (1974) are adopted. McElroy's result (their Table 5) is represented by

- 100
$$\frac{\Delta[O_3]}{[O_3]} = \delta = 1.405 \text{ f} - .0105 \text{ f}^2$$
, (16)

where f in parts per billion is equal to f_q in Table 2. Thus, an increment of 1 ppb in f_q would reduce the ozone abundance by $\delta = 1.4\%$.

Artificial sources must be treated carefully because they are not spread worldwide like the natural tracers. Most of the remarks here will be confined to air traffic in the northern hemisphere at about 45°N. The material is assumed to spread uniformly over the whole hemisphere. In truth, there is some leakage across the equator, but there will also be a tendency for a maximum amount to be near the source. These two effects come close to compensating for each other, and the estimates should be valid for middle latitudes. There may indeed be a considerable "corridor effect" at the heights where the aircraft fly. But the odd nitrogen must move upwards to 25-30 km to significantly affect the stratospheric ozone production. Ozone in turn spreads outwards and downwards from this same region. These two smoothing processes will almost certainly eliminate any substantial corridor effect in reduction of the total ozone column (Cunnold et al., 1975).

The area of each hemisphere is 2.55×10^{18} cm². Odd-nitrogen emissions are usually expressed in 10^9 g/year, or kilotons/year, in the form of NO₂. One kT/y (which is the amount produced by a Concorde or TU-144 flying 7 hours a day) therefore corresponds to a source strength of 1.62×10^5 molecules cm⁻² sec⁻¹. With the injection coefficient α in units of 10^{-17} cm⁻² sec⁻¹ and the source Q' in units of kT/y, we obtain for the mixing ratio

$$f_q = 0.0016 \alpha Q'$$
 parts per billion. (17)

Table 2. Predicted Effects of Various Assumed Fleets of Aircraft.

	Subsonic		Present SST	Advanced SST
Number	1000	1000	60	200
Q' (kT/y)	600	600	60	800
Height (km)	12	13	16	20
Effective height	14	15	18	22
$\alpha(10^{-17}\mathrm{cm}^2\mathrm{sec})$	0.35	1.27	4.45	9.6
f _q (ppb)	0.34	1.22	0.43	12.3
O3 loss (%)	0.47	1.7	0.60	17

NOTES: The "advanced SST" is arbitrarily taken to produce four times the odd nitrogen of a Concorde. The 2-km difference between the actual and effective heights allows for the translation from high-latitude flight paths to a model for 30° latitude. The last three lines give the injection coefficient for the three-layer model, the odd-nitrogen mixing ratio, and the expected ozone reduction for one hemisphere.

Most long-distance air traffic is at high latitudes, where the height of the tropopause is 10-12 km (Jocelyn et al., 1973). It is assumed that the 12-km boundary should be converted to 14 km for use with Model 2 of Table 1; thus, 2 km is added to all heights to give "effective heights." Predictions for several assumed fleets are given in Table 2. The number of "jumbo" jets' is 2.5 times the 1974 fleet, and has been assumed to fly somewhat higher. The prediction is extremely sensitive to the exact height, as illustrated by the two assumed heights for the subsonic fleet in the table. The effects shown are beginning to be appreciable, but one can be fairly sure that today's smaller fleet has not yet made a serious dent in the ozone. A relatively modest fleet of Concordes and TU-144's could be significant, and a larger fleet of advanced aircraft very serious indeed. Needless to say, the effects from different groups of aircraft are additive.

These predictions are considerably greater than those of McElroy et al. (1974), who deliberately adopted a highly conservative approach. Their tropopause was high, 16 km, and no adjustment was made to actual flight altitudes. Emissions were averaged over the globe, rather than half of it. For flights primarily over the North Atlantic, the present assumptions should be realistic.

HUNTEN

SUMMARY

The effect of odd nitrogen on stratospheric ozone can be estimated with good accuracy by breaking down the problem into its parts. The sources and sinks of odd nitrogen are first treated as discussed above. Second, the partitioning among the major forms NO, NO₂, and HNO₃ is calculated. Finally, the destruction of O₃ by NO₂ is obtained. The second and third steps can be represented by Eq. (16), obtained from the detailed results of McElroy et al. (1974). This simplified method belongs more to the domain of a hand calculator than to that of a computer.

Although one can be confident regarding the general behavior of the eddy-diffusion coefficient up to 40 km or so, it would be valuable to have many more observations of natural tracers, especially CH₄, N₂O, and CO. Another important quantity is the OH concentration, needed for interpreting the CH₄ and CO distributions. The region just above the tropopause is especially tricky, and especially important because of the possible impact of subsonic aviation. At present this impact is negligible, but as air traffic grows and aircraft fly higher, a noticeable depletion of ozone is a real possibility. To protect the stratosphere, subsonic jet engines, as well as their supersonic cousins, may have to be modified to produce less odd nitrogen.

ACKNOWLEDGMENTS

Kitt Peak National Observatory is operated by the Association of Universities for Research in Astronomy, Inc., under contract to the National Science Foundation. I thank A.J. Broderick, D.H. Ehhalt, and H.S. Johnston for valuable communications.

REFERENCES

- Anderson, J.G. (1971), "Rocket measurements of OH in the mesosphere," J. Geophys. Res. 76, 7820-7824.
- Bates, D.R. and P.B. Hays (1967), "Atmospheric nitrous oxide," Planet. Space Sci. 15, 189-197.
- Crutzen, P.J. (1974), "Estimates of possible future ozone reduction from continued use of fluoro-chloro-methanes (CF₂Cl₂, CFCl₃)," Geophys. Res. Lett. 1, 205-208.

- Cumming, C. and R.P. Lowe (1973), "Balloon-borne spectroscopic measurement of stratospheric methane," J. Geophys. Res. 78, 5259-5264.
- Cunnold, D., F. Alyea, N. Phillips, and R. Prinn (1975), "A three-dimensional dynamical chemical model of atmospheric ozone," J. Atmos. Sci. 32, 170-194.
- Davidson, B., J.P. Friend, and H. Seitz (1966), "Diffusion and rainout of stratospheric radioactive material," Tellus 18, 301-315.
- Ehhalt, D.H., L.E. Heidt, and E.A. Martell (1972), "The concentration of atmospheric methane between 44 and 62 kilometers altitude," J. Geophys. Res. 77, 2193-2196.
- Ehhalt, D.H. and L.E. Heidt (1973), "Vertical profiles of CH₄ in the troposphere and stratosphere," J. Geophys. Res. 78, 5265-5271.
- Ehhalt, D.H., L.E. Heidt, R.H. Lueb, and N. Roper (1974), "Vertical profiles of CH₄, H₂, CO, N₂O and CO₂ in the stratosphere," in *Proceedings of the Third Conference on CIAP* (Cambridge, Mass.), U.S. Department of Transportation, DOT-TSC-OST-74-15, 153-160.
- Greiner, N.R. (1970), "Hydroxyl radical kinetics by kinetic spectroscopy. VI. Reactions with alkanes in the range 300-500°K," J. Chem. Phys. 53, 1070-1076.
- Gudiksen, P.H., A.W. Fairhall, and R.J. Reed (1968), "Roles of mean meridional circulation and eddy diffusion in the transport of trace substances in the lower stratosphere," J. Geophys. Res. 73, 4461-4473.
- Hunten, D.M. (1969), "The upper atmosphere of Jupiter," J. Atmos. Sci. 26, 826-834.
- Hunten, D.M. (1975), "Residence times of aerosols and gases in the stratosphere," Geophys. Res. Lett. 2, 26-28.
- Hunten, D.M. and D.F. Strobel (1974), "Production and escape of terrestrial hydrogen," J. Atmos. Sci. 31, 305-317.
- Jocelyn, B.E., J.F. Leach, and P. Wardman (1973), "The effect of growth in stratospheric flight operation," Water, Air, Soil Pollution 2, 141-153.
- Johnston, H.S., D. Kattenhorn, and G. Whitten (1976), "Use of excess carbon-14 data to calibrate models of stratospheric ozone depletion by supersonic transports," J. Geophys. Res. 81, 368-380; see also this volume.
- Johnston, H., G. Whitten, and J. Birks (1973), "Effect of nuclear explosions on stratospheric nitric oxide and ozone," J. Geophys. Res. 78, 6107-6135.

HUNTEN

- Kyle, T.G., D.G. Murcray, F.H. Murcray, and W.J. Williams (1969), "Abundance of methane in the atmosphere above 20 kilometers," J. Geophys. Res. 74, 3421-3425.
- Margitan, J.J., F. Kaufman, and J.G. Anderson (1974), "The reaction of OH with CH₄," Geophys. Res. Lett. 1, 80-81.
- McConnell, J.C. and M.B. McElroy (1973), "Odd nitrogen in the atmosphere," J. Atmos. Sci. 30, 1465-1480.
- McComell, J.C. (1973), "Atmospheric ammonia," J. Geophys. Res. 78, 7812-7821.
- McElroy, M.B., S.C. Wofsy, J.E. Penner, and J.C. McConnell (1974), "Atmospheric ozone: possible impact of stratospheric aviation," J. Atmos. Sci. 31, 287-303.

- Reed, R.J. and K.E. German (1965), "A contribution to the problem of stratospheric diffusion by largescale mixing," Mon. Wea. Rev. 93, 313-321.
- Seiler, W. and P. Warneck (1972), "Decrease of the carbon monoxide mixing ratio at the tropopause," J. Geophys. Res. 77, 3204-3214.
- Wilson, W.E. (1972), "A critical review of the gas-phase reaction kinetics of the hydroxyl radical," J. Phys. Chem. Ref. Data 1, 535-573.
- Wofsy, S.C., J.C. McConnell, and M.B. McElroy (1972), "Atmospheric CH₄, CO, and CO₂," J. Geophys. Res. 77, 4477-4493.
- Wofsy, S.C. and M.B. McElroy (1973), "On vertical mixing in the upper stratosphere and lower mesosphere," J. Geophys. Res. 78, 2619-2624.

USE OF EXCESS CARBON-14 DATA TO CALIBRATE MODELS OF STRATOSPHERIC OZONE DEPLETION BY SUPERSONIC TRANSPORTS

HAROLD S. JOHNSTON

Department of Chemistry University of California, Berkeley Berkeley, California

DAVID KATTENHORN AND GARY WHITTEN

Inorganic Materials Research Division Lawrence Berkeley Laboratory Berkeley, California

ABSTRACT: During 1974, at least seven one-dimensional models of vertical eddy transport and photochemistry have been used to predict the reduction of ozone by nitrogen oxides from supersonic transports. Chang (1974) has shown that these predictions are sensitive to the assumed values for the vertical eddy-diffusion coefficient K₂. In this article, an effort is made to calibrate the one-dimensional K₂ functions against quantitative data for the dissipation of excess carbon-14 from the stratosphere during the period 1963-70. The data for excess carbon-14, following the nuclear-bomb test series of 1961-62, were published in 1971 and 1972, but they have not been used to derive the various K, functions. Tables of these data are presented in a form that may be useful to others in calibrating two-dimensional and three-dimensional models of stratospheric motion. In checking the onedimensional models, the direct observations by balloons at 30°N are primarily used. Also, these data are interpreted as a special hemispherical average (averaging along lines parallel to a standard, sloping tropopause). The carbon-14 data and strontium-90 data differ in many important respects, and it is judged that the carbon-14 data give the better estimate of air motion in the stratosphere. The seven K. models give predictions that differ strongly from one model to another. The models that give a fairly realistic prediction of carbon-14 distribution and persistence are those with minimum K, between 15 and 20 km and with increasing K₂ from 20 to 50 km. Models with these features, as recalculated by Chang (1974), agree with each other as to ozone reduction by artificial nitrogen oxides from SST's. These models are used to predict the ozone reduction by SST's according to Grobecker's (1974) upper-bound projection out to the year 2025. Very large reductions of global ozone are indicated more than a factor of two - for traffic of that magnitude.

INTRODUCTION

The catalytic reduction of stratospheric ozone by nitrogen oxides from supersonic transport (SST) exhausts was calculated earlier by means of a "box model" and steady-state photochemistry (Johnston, 1971). At that time, the natural background of nitrogen oxides (NO_x) was not known, the quantity of NO_x expected to be emitted by future SST fleets was uncertain, and the photochemical-atmospheric model was primitive, though efficient. By the end of 1974, these uncertainties had been greatly reduced. During 1974, a substantial number of measurements of NOx in the stratosphere were reported, and were summarized by Hard (1975). Grobecker (1974) has published a projection for the years 1990-2025 of future SST traffic in the stratosphere, and he gave an estimate of the amounts of nitrogen oxides that would be emitted in the stratosphere at various altitude bands if future SST's emit NOx at the same rate as present ones (per kilogram of fuel consumed). At least seven modelers have made different one-dimensional-model calculations of the natural stratosphere and the stratosphere as perturbed by SST's, including vertical eddy transport and extensive O, N, H chemistry (Crutzen, 1974; Chang, 1974; Stewart, 1973; McElroy et al., 1974; Whitten and Turco, 1974; Shimazaki and Ogawa, 1974; Hunten, 1975). Similar calculations which include two-dimensional motions have been made by at least three groups (Hesstvedt, 1974; Vupputuri, 1974; Widhopf, 1974). One group has successfully carried out calculations of the SST perturbation problem

with a model of three-dimensional atmospheric motions (Cunnold et al., 1974). Model calculations of ozone reduction by injection of NO_x at 20 km are given by Figure 1, panel a.

To a considerable extent, these twelve calculations of the SST perturbation (1971-1974) are in agreement; ten out of twelve agree within better than a factor of three. Two of them fall far outside this range, however. Chang (1974) undertook a systematic investigation of the reasons for the discrepancies between the onedimensional models. He found that Stewart (model 5) had carried out integrations of the SST perturbation for only 18 months, whereas at least 10 years are needed to attain a steady state; this correction brought model 5 into line with ten others. Chang (1974) used his chemical model, his set of boundary conditions, and his computer program to recalculate the predicted SST effect for the seven models involving onedimensional motions (see Figure 1, panel b). The seven vertical eddy-diffusion functions, K2, are given in Figure 2 and in Table A1 of the appendix. The maximum rate of insertion of nitrogen oxides in Figure 1b corresponds to Grobecker's (1974) upper-bound projection for the year 2025.

The curves in Figure 1b differ only with respect to vertical eddy-diffusion function, K_z . At low values of NO_x injection rate, there is a spread of a factor of six between model 7 and model 12; at high rates of NO_x injection this spread is a factor of three. The purposes of this paper are to see whether an independent evaluation can be made of the accuracy of the seven K_z functions, and to narrow the spread of predictions in Figure 1b.

During and after the period of massive nuclear-bomb tests of 1961-62, there was extensive sampling of the stratosphere for radioactive tracers, including those lodged on solid particles, such as strontium-90, and those which are gases, such as excess carbon-14. There are detailed, zonal-average, contour maps of observed excess carbon-14 in the stratosphere and troposphere every three months (with a few exceptions) from 1955 to 1967 (Telegadas, 1971) and some further data out to 1971 (Telegadas et al., 1972). These data were only recently published in the form of Health and Safety Laboratory (HASL) Reports of the U.S. Atomic Energy Commission. It appears that none of the modelers of the SST perturbation made detailed, quantitative use of these extensive data. After the test series ended

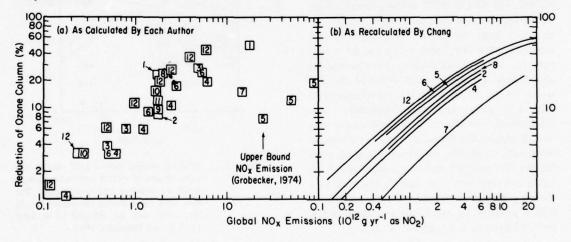


Figure 1. Calculated percentage reduction of the average global ozone column as a function of the mass of NO_x inserted at 20 km. a. Results available for each of twelve different groups. b. Seven one-dimensional models of vertical eddy-diffusion function K_z were recalculated on a uniform basis by Chang (1974). The upper limit of NO_x insertion is the upper bound projected by Grobecker (1974) for the year 2025.

The modelers are identified by number code: (1) Johnston, 1971; (2) Crutzen, 1974; (3) Hesstvedt, 1974, 2-D model; (4) Chang, 1974; (5) Stewart, 1973; (6) McElroy et al., 1974; (7) Whitten and Turco, 1974; (8) Shimazaki and Ogawa, 1974; (9) Vupputuri, 1974, 2-D model; (10) Widhopf, 1974, 2-D model; (11) Cunnold et al., 1974, 3-D model; (12) Hunten, 1975.

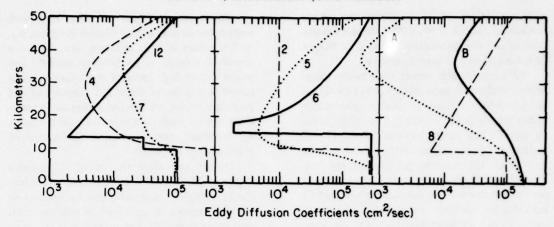


Figure 2. Vertical eddy-diffusion functions, K_z, for seven one-dimensional models numbered as in Figure 1. A and B are Brasseur (1972) Kmin and Kmax.

in December 1962, there was a cloud of carbon-14 covering the northern hemisphere with peak concentration at about 19 or 20 kilometers and with a fairly narrow vertical spread. This case is an appropriate analogy to the SST problem.

In this article, we develop the data in a form that may be useful for testing two- and threedimensional models of stratospheric motion, and tables are given in the appendix for this purpose. We take the data at 30°N as the primary source for testing the one-dimensional models. However, we also average over the northern hemisphere to supplement the direct observations at 30°N and, perhaps, to interpret what a one-dimensional model does. We then take an observed distribution of excess carbon-14 as the initial condition. and we solve the time-dependent, onedimensional, vertical eddy-diffusion equations for subsequent distributions of excess carbon-14, using each of nine K, functions (the seven used for the SST problem and two more). Numerous initial and final states are treated. The merit of a given K, function is judged with respect to how well it predicts the magnitude and shape of the carbon-14 profile as a function of time.

PRIMARY DATA

An example of the observed distribution of excess carbon-14 from the HASL Reports of the U.S. Atomic Energy Commission is shown in Figure 3 (Telegadas, 1971). The units are 10⁵ atoms of excess carbon-14 per gram of air and are proportional to mixing ratio or mole fraction.

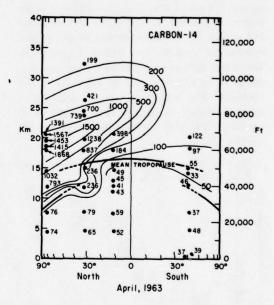


Figure 3. Relative mixing ratios (10⁵ atoms per gram of air) of excess carbon-14 as measured by balloons and U-2 aircraft. The data were taken during the period March-May 1963 and are referred to as April 1963. (From Telegadas, 1971.)

By multiplying by 4.82 × 10⁻¹⁸, one can convert these units to mixing ratio by volume. The data are from balloons, U-2 aircraft, and ordinary aircraft. Balloons were launched at 30°N for the period 1963-70 (after 1970, balloons were launched at latitudes of 65°N, 30°N, and 34°S), and the observed excess carbon-14 is given on Figure 3. Extensive sampling was done by U-2

aircraft in the stratosphere and by ordinary aircraft in the troposphere, and carbon-14 was measured at numerous ground-level stations.

It is important to emphasize that the numerical data points shown on Figure 3 comprise all the carbon-14 data observed for this time period (except for ground-based measurements). The only observations above 22 km are the balloon soundings at 30°N. It might appear that contour lines above 22 km are largely the product of imagination on the part the authors of the report, but such an appearance is not quite correct. More extensive data were obtained by balloon for other radioactive species, and these data were some guide to where bomb debris did and did not go. Data were obtained every 3 months before and after this period, and continuity between one period and another was of some guidance in drawing the contour lines. Also, the total stratospheric burden of carbon-14 was known. The bombs of high total yield (above 10 Mt) had a smaller fraction of fission yield relative to total yield than smaller bombs. One bomb with about 60 Mt total yield was fired at 75°N in October 1961, and it may constitute a hidden reservoir of carbon-14 above 35 or 40 km. The subsequent analysis of data depends primarily on the direct observations at 30°N, and these data are supplemented by a hemispherical average that is significant only below 22 km.

The balloon measurements of 14C at 30°N (actually 31°N) for the period January 1963 to January 1966 (Telegadas, 1971) and for November 1970 (Telegadas et al., 1972) are listed in the Appendix, Table A2. From a series of contour maps similar to Figure 3, the mixing ratios were converted to concentration of excess carbon-14 by use of air-density data from the Table of Standard Atmospheres (AFCRL, 1960). Vertical profiles were drawn at each 10 degrees of latitude, and these profiles were read at each kilometer elevation to give the values in the Appendix, Table A3. This analysis was carried out for January 1963, April 1963, July 1963, October 1963, January 1964, and January 1965. These data were replotted as zonal-average contour maps of excess carbon-14 concentration, five of which are given in Figure 4.

An example of the observed distribution of strontium-90 for April 1963 is shown in Figure 5 (Telegadas, 1967). The units are disintegrations per minute per thousand cubic feet of standard

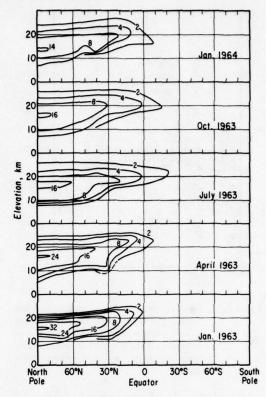


Figure 4. Concentration of excess carbon-14 (units of 10³ molecules cm⁻³) for the indicated times. These zonal-average maps of ¹⁴C concentration were derived from mixing-ratio maps such as Figure 3.

air, and are proportional to mixing ratio. The elevations for various values of strontium-90 mixing ratios at 30°N are given in the Appendix, Table A4. From these data, profiles of strontium-90 mixing ratios are readily obtained.

COMPARISON OF CARBON-14 AND STRONTIUM-90 AS TRACERS FOR STRATOSPHERIC AIR MOTIONS

Johnston, Whitten, and Birks (1973) showed that the bulk "residence time" of carbon-14 in the stratosphere (1963-65) was twice as long as that for strontium-90. There must be factors that cause strontium-90 to have a spuriously short residence time, or that cause carbon-14 to have (or appear to have) a spuriously long residence time, or both.

Carbon-14 is formed by a nuclear reaction between a neutron and molecular nitrogen. The initial product is probably ¹⁴CO, not ¹⁴CO₂. The

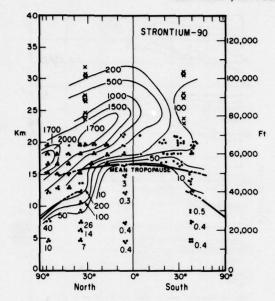


Figure 5. Relative mixing ratios (disintegrations per minute per 1000 cubic feet of standard air) of strontium-90 for April 1963. (From Telegadas, 1967.) × and O, observations from balloons; •, observations from aircraft

nuclear bombs of the 1961-62 test series were fired on the surface or in the troposphere, and the fireball was lifted into the stratosphere by thermal buoyancy. Before rising, the fireball cooled to about 6000K by emission of radiation and by expansion. The rising fireball was further cooled, largely by entrainment of cold air. The gases transported into the stratosphere were subjected to a wide range of temperatures, from 6000K to ambient. Carbon monoxide is burned to carbon dioxide by hot air. Measurements by Hagemann et al. (1965) showed that much less than 1% of the carbon-14 was in the form of carbon monoxide, and at least 99% was carbon-14 dioxide.

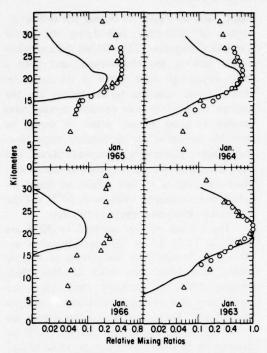
Strontium-90 was lodged on solid particles. One immediately suspects that the difference in stratospheric residence times between carbon-14 and strontium-90 is that particulate strontium-90 underwent gravitational settling. However, Telegadas and List (1969) calculated the settling velocity of strontium-90 on the basis of estimates and some measurements of the size of the solid particles containing the radioactive tracer; they concluded that the settling velocity would be slow below 30 km. Their calculations did not consider the possibility that the radioactive

particles would ionize the surrounding air and act as condensation nuclei for aqueous sulfuric acid in the stratosphere. Such enlarged particles would settle faster than the "dry" particles considered by Telegadas and List.

The carbon-14 and strontium-90 clouds at 30°N are directly compared with each other in Figure 6, using the data in Table A2, A4, and A6. For strontium-90, the maximum mixing ratio in April 1963 was 1700 disintegrations per minute per 1000 ft³ of standard air. All strontium-90 mixing ratios for April 1963 and later times were divided by 1700 to normalize all observations to the maximum as of April 1963. For carbon-14 the maximum mixing ratio in April 1963 was 74.2 units (X10-16), and all carbon-14 mixing ratios were normalized by this value. The curves in Figure 6 are the normalized strontium-90 mixing ratios for April 1963, January 1964, January 1965, and January 1966. The circles in Figure 6 are normalized average carbon-14 mixing ratios (Table A6): the triangles are normalized, directly observed carbon-14 mixing ratios (Table A2) for the same times as the strontium-90 curves.

In April 1963 the relative carbon-14 and strontium-90 profiles are very nearly the same above 14 km (strontium-90 is washed out by rain in the troposphere, carbon-14 is not, and the difference between C-14 and Sr-90 in the troposphere is due to this feature). The agreement in relative mixing ratios is good both above and below the point of maximum mixing ratios - for the April 1963 data. However, above 30 km strontium-90 is less than carbon-14. In January 1964 the carbon-14 and strontium-90 clouds agree fairly well below the maximum (15 to 20 km), but the relative mixing ratio of strontium-90 is substantially less than that of carbon-14 in the range 23 to 30 km. By January 1965, the strontium-90 is less than the carbon-14 over the 18 to 30 km range, and they are together from 15 to 18 km. By January 1966, the relative mixing ratio of strontium-90 is at least a factor of two less than that of carbon-14 at all elevations.

The separation of the strontium-90 and carbon-14 clouds in Figure 6 appears to be due to gravitational settling. However, Chang (1975) offers an alternate explanation. Most of the tests of the 1961-62 series were made at the polar USSR station, Table 1. The bomb debris deposited in the polar stratosphere would require time



to appear at 30°N. The largest test was a 60-Mt bomb, October 1961, which had an unusually small fission yield (strontium-90) but normal carbon-14 yield. This large bomb probably rose high in the stratosphere. As this debris was transported downwards, its high ¹⁴C/⁹⁰Sr ratio would cause an apparent separation of the carbon-14 and strontium-90 clouds. This explanation concerns a region of the stratosphere where no observations were made. We believe that the difference between the C-14 and Sr-90 profiles in Figure 6 is too great to be explained quantitatively by this mechanism.

If the separation of clouds in Figure 6 is due to particulate settling by the strontium-90, then the carbon-14 data would be superior to the strontium-90 data (and probably to other solid, particulate, radioactive tracers) for the purpose of calibrating models of stratospheric motion.

ANALYSIS OF THE CARBON-14 DATA

These data are based on a fairly thin grid so far as global coverage is concerned. There was

Table 1. Approximate Times and Yields (Mt) of Nuclear-Bomb Tests in 1961-62, and Months from Bomb Explosion to Various Later Times

Time			Months	from '	Test to:
(mo/yr)	Location*	Mt	1/63	1/64	1/65
9/61	P	9.2	16	28	40
10/61	P	90.5	15	27	39
5/62	T	2	8	20	32
6/62	T	10	7	19	31
7/62	T	2	6	18	30
8/62	P	54	5	17	29
9/62	P	96	4	16	28
10/62	P,T	17	3	15	27
12/62	P	23	1	13	25
	Total:	304			
	Weighted avoid of debris (m		8	20	32

^{*}P, polar, USSR; T, tropical, US or UK. (Seitz et al., 1968)

detailed sampling by aircraft up to 22 km, but there was only one balloon profile of carbon-14 at higher elevation until 1970 (compare Figure 3). There were more extensive balloon samples of strontium-90 than carbon-14, especially in the polar region (Telegadas, 1967). Seitz et al. (1968) tabulated each explosion of the 1961-62 series (their Tables 2-4) with respect to date, yield, and vertical distribution. Seitz et al. pointed out that the observed distributions after the polar tests were quite different from those calculated on the basis of previous experience (1954-58) for tropical tests. If we assume a uniform distribution of nuclear-bomb materials over their quoted vertical spread, then only 35 Mt out of 304 Mt of the large bombs was deposited above 22 km - that is, about 88% of the nuclear cloud was deposited in the region that was densely searched by aircraft. According to the tables by Seitz et al., the portion of the nuclear debris above 33 km (the upper limit of the balloon measurements) was 4 Mt out of 304 Mt. If Seitz et al. are correct, the amount of excess carbon-14 completely outside the range of observation altitudes was not large, but the two-dimensional distribution of material between 22 and 33 km is not accurately known.

There is a large error of measurement associated with any one contour map of carbon-14, and no conclusions should be based on minor features. There was slow transport of carbon-14

from the northern hemisphere to the southern hemisphere, as seen in Table 2. This north-to-south movement of carbon-14 can be treated by a two- or a three-dimensional model of atmospheric motions. To a one-dimensional model, however, this loss to the southern hemisphere may appear as a faster-than-real loss to vertical transport.

Table 2. Distribution of Stratospheric Carbon-14
Between the Northern Hemisphere and
the Southern Hemisphere from January
1963 to December 1970 (in units of
10²⁶ atoms) (from Telegadas, 1971)

Date	N.H.	S.H.	% N.H.
1/63	310	(46)	87
7/63	243	(58)	81
1/64	203	(52)	80
7/64	128	(55)	70
1/64	113	(57)	66
7/65	92	(59)	61
1/66	88	(58)	61
7/66	73	(55)	57
7/69	45	(41)	52

It was suggested by Seitz et al. (1968) that nuclear-bomb debris be averaged over the northern hemisphere, not at equal heights above the ground but at equal heights above a sloping tropopause. The sloping lines of constant mixing ratio of carbon-14 are evident in Figure 3, and these lines more or less parallel the tropopause. Of course, there is a time-and-place-varying gap in the tropopause. On a year-long basis it is possible to define and use the concept of a "standard tropopause", which we take to be:

90°N, 8 km	40°N, 13 km
80°N, 9 km	30°N, 14 km
70°N, 10 km	20°N, 15 km
60°N, 11 km	10°N, 16 km
50°N, 12 km	0°. 16 km

The observed concentrations in Table A3 of the Appendix were averaged by the cosine function to give equal weight to equal area over the three-dimensional globe along lines at equal heights above this "standard tropopause". This average over the northern hemisphere was assigned to 30°N latitude, the latitude of midarea between the equator and the pole.

This choice of tropopause height is based on the observed slope with latitude of the maximum carbon-14 mixing ratio for a large number of maps, such as Figure 3, during the test moratorium of 1959-1961, and during the period 1963-67 (Telegadas, 1971). Within the somewhat coarse grid of the observations, and given a fairly substantial noise factor in the data, the simple linear function (given above) for the average slope of lines of constant mixing ratio seemed as good as any other. It would be desirable to derive an appropriate slope from independent meteorological considerations, but such a study is beyond the scope of this article. Most conclusions of this article are based on actual observations by balloons at 30°N, not the hemisphere averages deduced in this way.

The average profiles ascribed to 30°N are listed in Table A5 of the appendix; they are plotted in Figure 7 for the periods of January 1963, April 1963, July 1963, October 1963, January 1964, and January 1965. There are insufficient data to support this detailed analysis after 1965. These average concentrations are converted to average mixing ratios at 30°N by dividing by total air concentration. These mixing ratios are listed in Table A6 of the appendix.

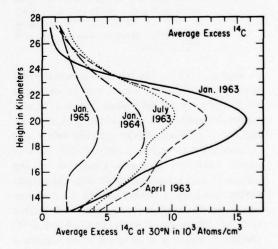


Figure 7. Northern-hemisphere average (see text) concentration of excess carbon-14 as a function of height between January 1963 and January 1965. These averages are ascribed to the geographical average latitude of the northern hemisphere, namely 30°N.

In Figure 8, the hemisphere-average mixingratio profiles (Table A6) are plotted as circles and the 30°N local profiles (Table A2) as triangles. Comparisons between these two pro-

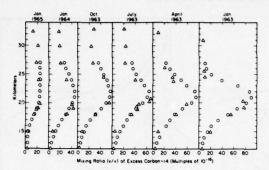


Figure 8. Comparison of average (Figure 7) mixing ratios and locally observed (by balloon soundings) mixing ratios of excess carbon-14 at 30°N. Ο, hemispherical average; Δ, local observation at 30°N.

files are interesting only below 22 km, where aircraft carried out measurements at different latitudes (above 22 km, all data are based on balloons operated at only one latitude, with interpolation to aircraft measurements at lower elevations). It can be seen that these two profiles are similar.

The similarity of the two sets of profiles in Figure 8 is a matter of interest in itself: the carbon-14 concentrations averaged to 30°N along lines equidistant above the standard, sloping tropopause are very nearly the same as the actual concentrations at 30°N. A one-dimensional vertical eddy-diffusion model located at 30°N is, in this sense, an approximate model for the northern hemisphere.

CALIBRATION OF ONE-DIMENSIONAL MODELS AGAINST OBSERVED CARBON-14 DATA

The profiles of excess carbon-14 for January 1963 were extended to the surface of the earth on the basis of observed carbon-14 in the troposphere, and were extended from the observed point of highest elevation to 50 km by a decreasing exponential function. This extended mixing-ratio profile was used as the initial condition for calculations using the various K_z functions. The vertical grid was spaced every kilometer from 0 to 50. The lower boundary condition used was that observed at 1 km, which remained constant for several years at a mixing ratio near 3×10^{-16} . The upper boundary condition was that the concentration at 51 km was

one-half that at 50 km. The vertical eddydiffusion problem was set up in terms of firstorder differencing, which guarantees conservation of mass even with the non-continuous K, functions of Figure 2. The problem was thus one of 50 simultaneous linear equations with constant coefficients. The problem was solved by the Gear method (Hindmarsh, 1972) on the Lawrence Berkeley Laboratory's CDC 7600 computer. With the boundary conditions specified, with the initial profile specified, and with use of a given K, function, it was a simple matter to compute the predicted carbon-14 distribution at any future time. Typically the future profiles were calculated every 3 months for 2 years and then every year to a total of 10 years. These calculated profiles, for each Kz function, are then compared with the observed ones. This procedure was repeated with the initial distribution taken to be April 1963 instead of January 1963, and then for July 1963, January 1964, and January 1965 also.

These calculations were made for the seven K_z functions shown in Figure 2 and for Brasseur's (1972) "Kmax" and "Kmin", all of which are listed in Table A1 of the appendix. We have made a large number of plots of calculated profiles and observed profiles for the nine K_z functions. Four sets of these plots are given by Figures 9, 10, 11, and 12. Each of these plots is of special interest for one reason or another, and they are all discussed below.

In Figure 9, the initial profile is that of January 1963 and the predicted profiles are January 1964. This period is of interest in that it represents the case of maximum gradients, and the sharpest initial distribution. There was a substantial change in one year in the northern-hemisphere profile, and there was relatively little loss to the southern hemisphere. The different K_z models give strongly different predictions, relative to one another. (The predictions of the models will be discussed below.)

In Figure 10, the initial profile is that of January 1964 and the observed points are from the balloon measurements directly observed at 30°N in January 1966. Again, there are strong differences in prediction by the nine models, and the sense of the differences is the same in Figure 10 as in Figure 9.

In Figure 11, the initial profile is that observed locally by balloon in January 1965, and

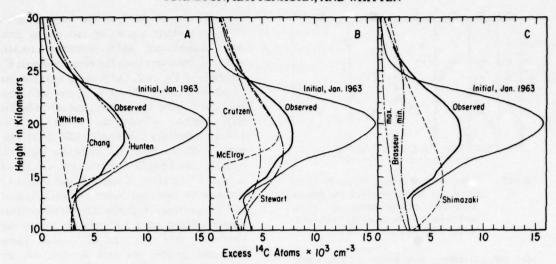


Figure 9. Comparison of average observed excess carbon-14 on January 1964 with that calculated by nine models of K₂ (Figure 2, Table A1) for January 1964. The initial distribution for calculation was the observed distribution for January 1963. Both initial and final conditions correspond to ○ in Figure 8.

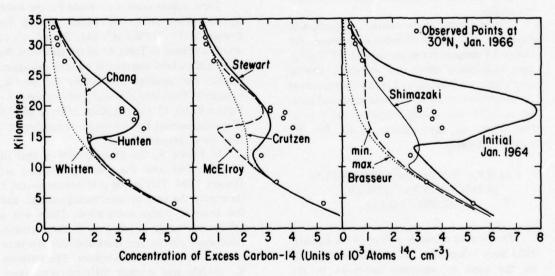


Figure 10. Comparison of directly observed excess carbon-14 on January 1966 with that calculated by nine models of K_z for January 1966. The initial distribution for each computation was the observed distribution on January 1964.

the observed data are those obtained directly by balloon in December 1970. In January 1965, 66% of the stratospheric carbon-14 was in the northern hemisphere and 34% was in the southern hemisphere, but in December 1970 it was essentially equal in the two hemispheres (Table 2). This transport to the southern hemisphere

was allowed for, as follows: The magnitude of the initial condition was taken to be the average between the northern and southern hemispheres, rather than the actual value in the northern hemisphere. From consideration of Table 2 the actual concentrations of January 1965 were reduced by the factor 0.75. The observed

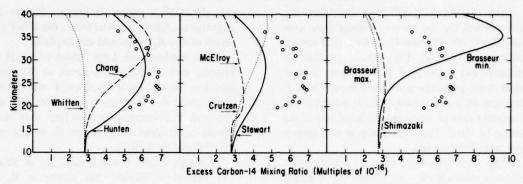


Figure 11. Comparison of directly observed carbon-14 mixing ratios on November 1970 with those calculated by nine models of K_z for January 1971. The initial distribution for each computation was the global-average observed distribution on January 1965. According to Telegadas et al.(1972), this excess carbon-14 was left over from the 1961-62 test series, and it was not a part of the 1967-70 series of relatively small bombs, which deposited their debris in the stratosphere between 14 and 18 km.

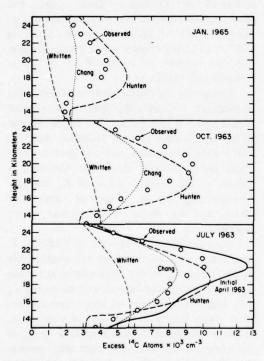


Figure 12. Comparison of average observed excess carbon-14 on July 1963, October 1963, and January 1965 with results of models whose initial conditions are based on April 1963.

carbon-14 in November 1970 is spread between 20 and 35 km, with a maximum mixing ratio at about 25 km. There were French and Chinese atmospheric tests of nuclear bombs between

1967 and 1970. According to Telegadas et al. (1972), the 1967-70 tests inserted radioactive debris between 14 and 18 km in the northern hemisphere and between 15 and 19 km in the southern hemisphere; they also stated that the carbon-14 above 20 km in December 1970 was primarily contributed by the bomb-test series that ended in December 1962.

The predictions of the nine K_z functions are compared with each other and with observed carbon-14 distributions in Figures 9, 10, and 11. Similar comparisons were made with other observed carbon-14 distributions taken as the initial values and with all later observed carbon-14 distributions taken as comparison for predicted versus observed profiles. The pattern shown by Figure 9-11 is confirmed by all of these comparisons, but Figure 12 gives the example that departs the most from the general pattern. This figure gives the poorest agreement between observed profiles and those calculated by Hunten's model.

DISCUSSION

The excess carbon-14 cloud, spread over the northern hemisphere by the atmospheric nuclear-bomb test series of 1961-62, appears to provide a useful calibration for theories of stratospheric motions. The observations of carbon-14 provide direct data for large-scale stratospheric sweep-out times in the region 15 to 25 kilometers.

The vertical eddy-diffusion functions, K_z , were derived by the various authors from considerations of: (1) heat-flux data; (2) vertical profiles of ozone; (3) vertical profiles of methane; (4) radioactive fallout from nuclear-bomb tests, primarily particulate tracers such as strontium-90 and tungsten-185; (5) other factors. It appears that no one made detailed use of the carbon-14 data. Thus this study is an independent test of the models.

The nine models using vertical eddy-diffusion constants K_z as a function of height give markedly different predictions, relative to each other, concerning the dissipation of the carbon-14 cloud during the period 1963-70. The relative and absolute predictions made by the nine K_z models are very nearly the same for the four time intervals of Figures 9-12.

Figure	Time Interval	
9	Jan. 1963 - Jan. 1964	
10	Jan. 1964 - Jan. 1966	
11	Jan. 1965 - Nov. 1970	
12	Apr. 1963 - Jan. 1965	

The model associated here with an investigator is often not the only model considered by that investigator. For example, Crutzen has used several other K_z models, and he has used a different, preferred model in recent calculations. The model associated with Whitten is an early one that he considered and rejected; it is retained here as an extreme example, not as a test of Whitten's recent work. For present purposes, it is necessary to adhere to these models, even if they do not represent the investigators' latest, best judgment, because these models were used in Chang's (1974) comparative study (Figure 1b) of the effect of model K, on SST perturbation, and it is desirable to compare predictions of carbon-14 with those for the SST's. Crutzen's model used here is valuable in showing the effect of making K, constant with height in the stratosphere. Whitten's model is of interest in showing what a large difference in stratospheric sweep-out time is caused by differences in K, function (Figure 2). Brasseur's "Kmin" shows the effect of a very low K, value high in the stratosphere. McElroy's or Hunten's model shows the effect of a region of low K_z low in the stratosphere. Chang's model shows the effect of a region of low K_z in the mid-stratosphere.

The models with large values of K_z at all heights, such as Brasseur's Kmax or Whitten's function, sweep excess carbon-14 out of the stratosphere at a rate very much faster than was observed. This discrepancy is so large that line 7 should be dropped from Figure 1b in any realistic discussion of SST's.

Chang's model has minimum K_z at 30 km and Brasseur's "Kmin" has minimum K_z at 37 km. These models sweep out the region 17 to 21 km at much too fast a rate, but they build up relatively large mixing ratios near 35 km over a long period of time. Chang's peak mixing ratio at 35 km in Figure 11 agrees with the observed carbon-14, but Brasseur's "Kmin" retains too much carbon-14 at 35 km. If there were a large hidden source of carbon-14 above 35 km in 1963, then Chang's model would greatly overpredict the amount of carbon-14 at 35 km in November 1970 (Figure 11).

Except for the discontinuity at 10 km in the troposphere, Crutzen's K_z function is constant with height. It sweeps out the region around 20 km at a much faster rate than was observed, and it gives a long-term profile (Figure 11) of a shape rather different from that observed. A change of the absolute value of K_z can give approximately correct sweep-out times near 20 km, but the shape of the profile is not improved.

Four functions (5, Stewart; 6, McElroy; 8, Shimazaki; and 12, Hunten) are qualitatively similar: large Kz in the troposphere, minimum K, in the lower stratosphere, and increasing K, with height from lower to upper stratosphere. They differ largely as to height of tropopause, height of minimum Kz, and magnitude of Kz at the minimum. The relatively small differences in these K, functions (Figure 2) lead to substantial differences in predicted history of carbon-14 in the stratosphere. The height of Shimazaki's region of small K, is too low (note the low elevation of peak carbon-14 in Figures 9 and 10), and the average value of his K, appears to be too large (note the almost totally swept-out stratosphere by 1970). Stewart's model gives a fairly good representation of the shape of the carbon-14 profile and very nearly the correct

height of maximum carbon-14 in the various comparisons, but the magnitude of his K_z function between 15 and 25 km appears to be too large, because it always predicts too little carbon-14 in the stratosphere. McElroy's function gives many predictions in approximate agreement with observations (his function is best for the interval January 1964 to January 1965); but the tropopause is about 2 kilometers too high; also, this K_z function appears to be too large on the average, since it has swept too much carbon-14 out of the stratosphere over the long time period (Figure 11).

Hunten's model of K_z gives a reasonably correct prediction of the shape, elevation of the maximum, and magnitude of the carbon-14 cloud for all initial and final profiles tested. Figure 12 gives its poorest prediction. Hunten's K_z model appears to be superior to other models tested here. However, even this model somewhat underestimates the persistence of carbon-14 after 8 years (Figure 11).

We have explored the effects of introducing small changes in some of the models. The long-term predictions of the carbon-14 distribution are very sensitive to small perturbations of assumed K_z . The predictions are strongly dependent on both the shape and the magnitude of the K_z function. The long-term carbon-14 peak concentration near 20 km (Figure 10, for example) appears to require the qualitative features of McElroy's or Hunten's model, that is, low values between 15 and 20 km and rapidly increasing values above 25 km.

In view of the considerable success of Hunten's model in describing the carbon-14 data, it is of interest to examine the full predictions of his model for the eight-year period, taking the initial distribution as of January 1963. In terms of mixing ratios from 0 to 50 km, these predictions are given for January 1964, January 1965, January 1966, and November 1970 (Figure 13). The lower boundary value was taken to be 2.8 × 10⁻¹⁶ at all times. The upper boundary condition is that the concentration at 51 km is half that at 50 km. For each calculated profile, the initial distribution of January 1963 was reduced to correct for subsequent transport of carbon-14 to the southern hemisphere. For example, the initial distribution of January 1963 was reduced by the factor .66/.87 for the calculated curve for January 1965 (note the "%

N.H." column in Table 2). The triangles are direct observations at 30°N and the circles are the specially-defined northern-hemisphere average. This K_z function is fairly successful in predicting the history of the carbon-14 over the eight-year period. The terminal prediction for November 1970 is very similar for January 1963 as initial state (Figure 13) and for January 1965 as initial condition (Figure 11). The agreement of this terminal prediction with observations, regardless of initial time, is regarded as evidence against the existence of a large pocket of carbon-14 above the polar region which would cause the separation of carbon-14 and strontium-90 in Figure 6.

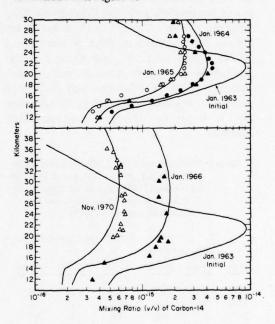


Figure 13. Calculated and observed excess carbon-14 mixing ratios in the stratosphere, one, two, three, and eight years after January 1963 (corrected for transport to southern hemisphere). The curves were calculated by Hunten's model. Ο, • northern-hemisphere averages; Δ, A direct observations at 30°N.

There is a strong correlation between the correctness of predicting the carbon-14 profile in Figures 9 and 10 (but not so much so for the long-term case of Figure 11) and the magnitude of the reduction of ozone by the SST perturbation, Figure 1b. In Figures 9 and 10, the best predictions of carbon-14 are made by Hunten, Stewart, and McElroy; in Figure 1b these also predict the three largest reductions of ozone by

SST's. Crutzen, Chang, and Shimazaki give comparable predictions of carbon-14 in Figures 9 and 10, and they give about the same magnitude of ozone depletion, which is about a factor of two less than the Hunten-McElroy-Stewart group. However, the predicted ozone reduction by SST's is less sensitive to the K_z function than is the sweep-out of the cloud of carbon-14.

Finally, it is of interest to consider the reduction of ozone as a function of added NO. using Hunten's Kz function, Chang's calculation with Hunten's Kz function (Figure 1b), and Grobecker's (1974) projected injection of NO_x (this projection applies if there is no reduction of the NO_x emission index from supersonic transports). Grobecker's projected upper-bound NO, injections at both 17 km (15 to 18) and at 20 km (18 to 21) are given in Table 3. Grobecker's (1974) upper-bound NO_x and Chang's (1974) one-dimensional photochemical model with Hunten's (1974) K_z function give very large reductions of global ozone, substantially greater than a factor of two after the year 2010 (Table 3).

Table 3. Global Projections of NO_x Insertion (units of 10¹²g NO₂ yr⁻¹) at 17 km and at 20 km (Grobecker, 1974) and Ozone Reduction as Calculated by Chang (1974) Using Hunten's K_z Function (1974)

	NO _x in	sertion	% ozone o	om NO,	
Year	17 km	20 km	17 km	20 km	Total
1990	0.45	0.22	3.0	2.5	5.5
1996	0.60	1.3	4.0	13	17
2000	0.70	3.0	4.5	23	27
2006	1.0	6.5	6.2	37	33
2010	1.1	9.0	6.7	43	49
2015	1.2	12	7.2	47	54
2020	1.5	20	8.7	52	61
2025	1.6	27	9.2	60	69

ACKNOWLEDGMENT

This work was supported by the Climatic Impact Assessment Program by means of an interagency agreement between the Department of Transportation and the Atomic Energy Commission through the Inorganic Materials Research Division, Lawrence Berkeley Laboratory. We wish to express our appreciation to James

Friend, a co-author of the paper by Seitz et al. (1968), who suggested the idea of averaging the carbon-14 data along non-horizontal lines.

REFERENCES

- Air Force Cambridge Research Laboratories (1960), Handbook of Geophysics, rev. ed., Macmillan, New York, NY.
- Brasseur, G. (1972), "Stratospheric chemistry," Aeronomica Acta B41.
- Chang, J.S. (1974), "Simulations, perturbations, and interpretations," in *Proceedings of the Third Conference on the Climatic Impact Assessment Program* (Cambridge, Mass.), U.S. Dept. of Transportation, DOT-TSC-OST-74-15, 330-341.
- Chang, J.S. (1975), "Uncertainties in the validation of parameterized kinetics and transport models," in this volume.
- Crutzen, P. (1974), "A review of upper atmospheric photochemistry," Can. J. Chem. 52, 1569-1581.
- Cunnold, D.M., F.N. Alyea, N.A. Phillips, and R.G. Prinn, "First results of a general circulation model applied to the SST-NO_x problem," in Preprints of the AMS/AIAA Second International Conference on the Environmental Impact of Aerospace Operations in the High Atmosphere (San Diego), pub. AMS, 187-193.
- Grobecker, A.J. (1974), "Research program for assessment of stratospheric pollution," Acta Astron. 1, 179-224.
- Hagemann, F.T., J. Gray, Jr., and L. Machta (1965), "Carbon-14 Measurements in the Atmosphere – 1953 to 1964," Health and Safety Laboratory Report 159, U.S. Atomic Energy Commission, 11.
- Hard, T.M. (1975), "Summary of recent reports of stratospheric trace-gas profiles," section 3.7 of Volume 1 of the CIAP monograph series, Dept. of Transportation, DOT-OST-75-51, 3-162-3-170.
- Hesstvedt, E. (1974), "A simplified time-dependent two-dimensional photochemical model of the stratosphere," in Proceedings of the International Conference on Structure, Composition, and General Circulation of the Upper and Lower Atmospheres and Possible Anthropogenic Perturbations (Melbourne), pub. IAMAP, 1097-1106.
- Hindmarsh, A.C. (1972), "GEAR: Ordinary Differential Equation System Solver," Lawrence Livermore Laboratory Report UCID-30001, Rev. 1.

- Hunten, D.M. (1975), "Estimates of stratospheric pollution by an analytic model," Proc. NAS 61. (See also "The philosophy of one-dimensional modeling," in this volume.)
- Johnston, H.S. (1971), "Reduction of stratospheric ozone by nitrogen oxide catalysts from supersonic transport exhaust," Science 173, 517-522; "Catalytic Reduction of Stratospheric Ozone by Nitrogen Oxides," UCRL Report No. 20568, 1-106.
- Johnston, H.S., G. Whitten, and J. Birks (1973), "The effect of nuclear explosions on stratospheric nitric oxide and ozone," J. Geophys. Res. 78, 6107-6135.
- McElroy, M., S. Wofsy, J. Penner, J. McConnell (1974), "Atmospheric ozone: Possible impact of stratospheric aviation," J. Atmos. Sci. 31, 287-300.
- Shimazaki, T., and T. Ogawa (1974), "Theoretical models of minor constituents' distributions in the stratosphere and the impact of the SST exhaust gases, in Proceedings of the International Conference on Structure, Composition and General Circulation of the Upper and Lower Atmospheres and Possible Anthropogenic Perturbations (Melbourne), pub. IAMAP, 1062-1092.
- Seitz, H., B. Davidson, J.P. Friend, and H.W. Feeley, (1968) "Numerical Models of Transport, Diffusion, and Fallout of Stratospheric Radioactive Material: Final Report on Project Streak," Report No. NYO-3654-4, Isotopes (Teledyne), (50 van Buren Ave., Westwood, NJ).
- Stewart, R. (1973), "Response of stratospheric ozone to the simulated injections of nitric oxide," presented at the AGU Fall Meeting, San Francisco.
- Telegadas, K., J. Gray, Jr., R.E. Sowl, and T.E. Ashenfelter (1972), "Carbon-14 Measurements in the Stratosphere from a Balloon-Borne Molecular

- Sieve Sampler," Health and Safety Laboratory Report 246, U.S. Atomic Energy Commission, 69-106.*
- Telegadas, K. (1967), "The Seasonal Stratospheric Distribution of Cadmium-109, Plutonium-238, and Strontium-90," Health and Safety Laboratory Report 184, U.S. Atomic Energy Commission, 53-118.*
- Telegadas, K., and R.J. List (1969), "Are particulate radioactive tracers indicative of stratospheric motions?", J. Geophys. Res. 74, 1339-1350.
- Vupputuri, R.K. (1974), "The role of stratospheric pollutant gases (H₂O, NO_x) in the ozone balance and its implications for the seasonal climate of the stratosphere," in *Proceedings of the International Conference on Structure, Composition and General Circulation of the Upper and Lower Atmospheres and Possible Anthropogenic Perturbations* (Melbourne), pub. IAMAP, 905-931.
- Whitten, R.C. and R.P. Turco (1974), "The effect of SST emissions on the earth's ozone layer," in Proceedings of the International Conference on Structure, Composition and General Circulation of the Upper and Lower Atmospheres and Possible Anthropogenic Perturbations (Melbourne), pub. IAMAP, 971-983.
- Widhopf, G.F., and T.D. Taylor (1974), "Numerical experiments on stratospheric meridional ozone distributions using a parameterized two-dimensional model," in *Proceedings of the Third Conference* on the Climatic Impact Assessment Program (Cambridge, MA), Dept. of Transportation, DOT-TSC-OST-74-15, 376-389.

APPENDIX

TABLES OF MODEL EDDY-DIFFUSION COEFFICIENTS AND OBSERVED RADIOACTIVE TRACER DATA

Table A1. Vertical Eddy-Diffusion Function K_z (in units of 10³ cm² sec⁻¹)

				Kil	ometers				
1	2	3	4	5	6	7	8	9	10
11	12	13	14	15	16	17	18	19	20
21	22	23	24	25	26	27	28	29	30
31	32	33	34	35	36	37	38	39	40
41	42	43	44	45	46	57	48	49	50

^{*}The HASL reports are available on microfilm from the AEC Health and Safety Laboratory, 376 Hudson St., New York, NY 10014.

Table A1. Vertical Eddy-Diffusion Function K_z (in units of $10^3~{\rm cm}^2~{\rm sec}^{-1}$) (cont.)

				H	unten				
100.	100.	100.	100.	100.	100.	100.	100.	100.	30.
30.	30.	30.	2.3	2.3	2.7	3.0	3.3	3.7	4.2
4.5	5.2	5.6	6.4	7.2	0.0	9.0	10.	11.	12.
13.	15.	16.	18.	20.		24.	28.	30.	34.
38.	41.	47.	52.	59.	63.	72.	80.	90.	100.
				C	hang				
300.	300.	300.	300.	300.	300.	300.	300.	300.	300.
23.	18.	15.	12.		9.7	8.6	7.4	6.6	6.0
5.3	5.0	4.5	4.2	4.0	3.9 5.0	3.7	3.7	3.7	3.7
3.8	3.9	4.0	4.2	4.5		5.4	6.1		8.0
9.2	11.	13.	15.	18.	22.	26.	33.	42.	54.
				St	ewart				
300.	300.	300.	300.	270.	220.	150.	90.	42.	23.
13.	8.2	6.0	5.1	5.0	5.1 8.2	5.2	5.4	5.6	6.0
6.2	6.6	7.0	7.3	7.8	8.2	8.9	9.1	9.9	11.
12.	13.	14.	15.	16.			22.	26.	30.
33.	40.	45.	56.	66.	78.	93.	120.	140.	160.
				Wh	itten				
100.	100.	100.	100.	100.	100.	100.	100.	100.	44.
		38.	35.	34.	32.	31.	28.	27.	26.
25.	23.	22.	21.	20.	19.	18.	17.	16.	15.
15.	14.	14.	14.	14.	14.	15.	16.	17.	18.
20.	22.	25.	3.0	35.	42.	56.	75.	100.	130.
				Shir	nazaki				
100.	100.	100.	100.	100.	100.	100.	100.	100.	6.4
7.0	7.5	8.1	8.9	9.2	10.	11.	12.	13.	14.
14.	15.	16.	17.	18.	20.	23.	24.	25.	27.
29.	31.	33.	35.	39.	42.	44.	48.	51.	55.
6.0	63.	69.	73.	80.	85.	91.	99.	110.	120.
				Mo	Elroy				
300.	300.	300.	300.	300.	300.	300.	300.	300.	300.
300.	300.	300.	300.	300.	2.0		2.0	4.0	7.0
9.0	12.		19.	22.	25.		35.	40.	45.
52.	59.	65.	7.2	81.	90.		110.		130.
140.	150.	160.	170.	180.	200.	220.	230.	240.	260.
				Cri	utzen				
300.	300.	300.	300.	300.	300.	300.	300.	300.	300.
10.	10.	10,	10.	10.	10.	10.	10.	10.	10.
10.	10.	10.	10.	10.	10.	10.	10.	10.	10.
10.	10.	10.	10.	10.	10.	10.	10.	10.	10.
10.	10.	10.	10.	10.	10.	10.	10.	10.	10.
				Brasser	ur Kmin				
190.	180.	170.	150.	140.	130.	120.	98.	82.	70.
58.	45.	38.	31.	25.	21.	18.	14.	12.	10.
8.1	6.5	5.5	4.3	3.4	2.8	2.3	1.9	1.5	1.3
1.1	0.80	0.75	0.62	0.54		0.51	0.52	0.54	0.58
0.65	0.74	0.83	0.95	1.1	1.2	1.4	1.7	2.0	2.2
					ır Kmax				
190.	180.	170.	160.	150.	145.	140.	135.	130.	127.
124.	120.	115.	110.	98.	91.	84.	78.	71.	64.
60.	53.	48.	43.	38.	34.	30.	26.	23.	22.
20.	17.	15.	14.5	14.	14.	14.	14.5	15.	16.
17.	18.	21.	22.	23.	25.	28.	32.	34.	38.

Table A2. Mixing Ratios α (V/V) of Excess Carbon-14 (in multiples of 10^{-16})

a. Mixing Ratios at 30°N, Based on Directly Observed Local Values

km	1/63	4/63	7/63	10/63	1/64	1/65	1/66
36							
35							
34							
33			20.6	18.5	16.9	12.1	14.3
32	7.58	9.55					
30			24.0	23.8	19.2	21.4	14.1
27		20.2	22.1	26.7	20.2	18.0	14.1
26	9.60						
25	10.0	33.6		44.6			
24		35.5	39.8		30.7	22.4	16.7
22							
21							
20	77.1	59.4	46.8	55.1	40.4	24.9	15.0
19	73.0		43.8			18.3	14.2
18	55.7	40.2	33.6	30.9	31.7	14.3	
15	20.8	9.84	5.23	8.48	7.54	4.85	
12	5.81	11.3	3.02	3.36	3.98	3.93	
8	2.92	3.79	3.12	2.98	3.60	3.17	
4	2.98	3.12	2.93	2.93	3.65	2.93	
0		2.10	2.91	2.77	2.84	2.75	

c. Mixing Ratios Observed by Balloon, and Contour Lines as Inferred from Balloon Plus Aircraft Sampling, November 1970

b. Mixing Ratios as Observed at Various Latitudes and Heights, January 1966

9°	N	30°	'n	70°N		
km	<u>α</u>	km	<u>α</u>	km	<u>α</u>	
4.5	2.84	4.5	3.18	1.0	3.18	
8.5	2.80	8.3	2.99	4.3	3.08	
12.0	2.99	11.8	3.42	7.5	3.18	
14.8	3.13	15.0	4.34	11.9	7.04	
18.0	3.90	16.2	11.7	15.0	13.0	
19.0	4.58	17.8	13.4	17.8	16.1	
19.5	4.63	18.8	17.1	18.5	15.3	
		19.0	14.2	18.8	19.4	
		19.5	15.0	19.2	18.4	
		24.0	16.7			
		27.2	14.1			
		30.0	14.1			
		31.0	15.8			
		32.8	14.3			

9°	N	30	°N	42	N
km	<u>\alpha</u>	km	<u>a</u>	km	<u>α</u>
20.8	3.71	19.6	5.30	19.6	5.78
21.0	3.86	20.3	5.78	20.9	6.03
21.4	4.34	21.0	6.51	21.3	6.27
22.0	4.82	21.2	6.17	23.3	6.75
23.0	5.30	22.2	6.27	24.0	6.89
23.7	5.78	23.9	6.84	27.2	6.75
27.2	5.35	24.3	6.75	27.4	6.65
30.6	5.30	24.4	6.70	30.8	6.46
31.5	5.11	26.5	6.75	31.5	6.27
		27.2	6.31	36.0	6.03
34	°S	27.6	6.84		
le ma		31.2	6.27	65	°N
km	<u>a</u>	32.5	5.59	len.	
20.0	5.78	32.8	6.17	km	<u>\alpha</u>
20.0	5.74	33.0	6.27	20.3	6.27
		34.0	5.78		
21.1	6.17	35.5	5.30	22.3	6.75
21.7	6.27	36.3	4.63	24.0	6.70
23.9	6.27	50.5		26.9	6.80
24.2	6.51			27.0	6.75
27.0	6.46			30.0	6.27
27.2	6.27			31.0	5.78
27.3	5.78				
32.3	5.78				

Table A3. Concentration of Excess Carbon-14 (10³ molecules cm⁻³)

a. January 1963

km	80° N	70°N	60° N	50° N	40°N	30°N	20° N	10°N	<u>0° N</u>	10°S	<u>20°S</u>	30°S
29								0.3	0.3	0.3		
28							0.4	0.5	0.5	0.5	0.4	
27						0.4	0.6	0.6	0.6	0.6	0.6	0.4
26					0.6	0.6	0.8	0.8	0.8	0.8	0.8	0.6
25				0.8	0.8	0.8	1.0	1.4	1.2	1.0	0.8	0.8
24		0.9	1.0	1.2	1.0	1.4	2.8	3.0	1.6	1.2	1.0	0.8
23	1.2	1.2	1.4	1.6	2.0	5.6	6.4	4.2	1.8	1.2	1.0	1.0
22	1.8	1.8	2.8	4.4	9.4	11.6	10.4	4.4	1.8	1.4	1.2	1.0
21	3.8	5.6	10.2	12.0	15.8	14.8	12.2	4.2	1.8	1.6	1.2	1.0
20	12.6	13.4	16.4	18.4	18.2	16.4	12.6	3.6	1.6	1.4	1.2	1.2
19	19.4	20.6	20.8	21.4	18.6	16.0	11.4	3.0	1.4	1.4	1.4	1.2
18	25.0	25.2	24.8	22.8	17.0	14.8	6.8	2.2	1.2	1.2	1.4	1.2
17	30.4	28.6	27.0	21.2	15.2	12.2	5.8	1.4	1.2	1.0	1.4	1.2
16	33.6	30.6	25.0	19.2	13.0	9.2	5.0	1.2	1.0	1.0	1.4	1.4
15	32.8	28.2	22.0	16.4	10.8	7.4	4.2	1.0	0.8	0.8	1.2	1.2
14	28.8	23.8	18.0	12.0	8.8	6.4	3.6				1.2	1.2
13	21.4	16.0	12.6	9.2	6.2	5.4						1.2
12	14.0	11.6	9.8	6.2	3.6							
11	11.4	9.8	4.6	3.4								
10	9.8	7.6	4.0									
9	8.0	4.2										
8	4.4											

b. January 1964

km	80° N	70°N	60° N	50°N	40°N	<u>30°N</u>	20° N	<u>10°N</u>	<u>o</u> °	<u>10°S</u>	20°S	30°S
29								0.9	0.9	0.9		
28							1.0	1.0	0.9	0.9	0.8	
27						1.2	1.2	1.1	1.0	1.0	0.8	0.7
26					1.6	1.6	1.8	1.2	1.3	1.0	0.8	0.8
25				2.1	2.2	2.4	2.4	1.5	1.6	1.2	0.9	0.8
24			2.6	2.8	3.2	3.2	3.4	2.0	1.7	1.4	0.9	0.9
23		3.2	3.6	3.8	4.4	4.6	4.6	3.4	1.8	1.6	1.0	0.9
22	4.2	4.4	4.8	5.2	5.6	6.0	5.6	3.8	1.9	1.6	1.1	1.0
21	5.4	6.0	6.6	7.0	7.8	7.4	6.4	3.6	1.9	1.6	1.2	1.1
20	7.2	7.6	8.2	8.6	8.6	8.2	6.6	3.4	1.8	1.6	1.1	1.1
19	9.0	9.0	10.0	9.4	9.4	8.8	6.4	2.8	1.8	1.4	1.1	1.0
18	11.4	10.8	11.0	10.2	10.0	8.2	5.4	2.4	1.8	1.4	1.0	1.0
17	13.0	12.0	11.2	11.0	9.6	7.2	3.2	2.0	1.7	1.4	1.0	1.0
16	14.2	12.2	9.2	10.2	9.0	4.8	2.3	1.7	1.6	1.4	1.2	1.1
15	14.8	13.0	11.4	6.8	9.0	3.4	1.9	1.6	1.6	1.4	1.3	1.2
14	15.2	13.8	12.6	7.8	10.4	3.4	1.8				1.5	1.4
13	14.6	13.0	11.6	8.2	8.4	2.6						
12	13.0	12.0	8.8	2.4	4.0							
11	11.2	10.4	6.2	3.0								
10	9.6	7.0	4.4									
9	7.6	5.4										
8	5.8											

Table A3. Concentration of Excess Carbon-14 (10³ molecules cm⁻³) (cont.)

c. January 1965

km	80° N	70° N	60° N	50° N	40° N	30° N	20° N	10° N	<u>o</u> °	10°S	20° S	30°S
29								0.9	0.5	0.5		
28							1.2	1.0	0.6	0.6	0.5	
27						1.6	1.4	1.2	0.8	0.8	0.6	0.7
26					1.5	1.8	1.8	1.4	1.0	1.0	0.8	0.8
25				2.0	1.8	2.1	2.0	1.7	1.2	1.2	1.0	0.9
24			2.0	2.2	2.2	2.4	2.4	2.0	1.4	1.4	1.2	1.0
23		2.4	2.4	2.7	2.6	2.8	2.8	2.4	1.7	1.7	1.5	1.2
22	3.0	2.8	2.9	3.2	3.2	3.4	3.2	2.6	2.0	2.0	1.8	1.4
21	3.4	3.3	3.4	3.6	3.8	3.9	3.8	2.7	2.4	2.2	2.0	1.7
20	4.0	3.8	4.0	4.2	4.4	4.4	3.8	2.6	2.6	2.4	2.2	1.9
19	4.6	4.6	4.8	5.2	5.0	4.4	3.4	2.6	2.3	2.2	2.3	2.0
18	5.4	5.4	5.6	5.8	5.0	3.8	2.6	1.2	1.4	1.4	1.8	1.8
17	6.0	5.8	5.9	5.4	4.4	3.0	1.6	1.0	0.8	0.9	1.3	1.6
16	6.3	6.0	5.8	5.2	3.4	1.8	1.4	1.0	0.9	1.0	1.0	1.4
15	6.3	6.0	5.8	4.0	2.6	1.4	1.2	1.1	1.1	1.2	1.0	1.2
14	6.0	6.0	5.2	2.6	2.2	1.6	1.2				1.0	1.0
13	5.7	4.8	4.0	2.5	2.1	1.7						1.0
12	5.4	4.4	3.6	2.4	2.2							
11	5.0	4.0	3.4	2.6								
10	4.6	3.8	3.2									
9	4.2	3.4										
8	4.0											

Table A4. Relative Mixing Ratio* of Strontium-90 at $30^{\circ}\,\text{N}$

April 1963		July	July 1963		October 1963		January 1964		January 1965		January 1966	
km	90Sr	km	90Sr	km	90Sr	km	90Sr	km	90Sr	km	90Sr	
30.3	200	29.0	300	32.0	200	29.5	100	30.3	30	32.5	10	
28.0	500	28.0	400	28.5	300	26.5	200	26.8	50	29.8	20	
24.3	1000	26.5	500	26.5	500	25.2	300	25.2	100	28.2	30	
23.2	1500	23.9	1000	23.7	1000	23.6	500	21.8	200	27.0	40	
21.8	1700	22.8	1500	21.9	1200	22.4	800	21.4	300	26.0	50	
19.3	1700	21.8	1700	21.2	1500	21.6	900	20.9	350	24.6	100	
18.5	1500	19.2	1700	19.4	1500	20.6	1000	19.2	350	22.2	150	
17.7	1000	18.6	1500	19.1	1200	19.2	1000	17.9	300	20.0	150	
16.2	500	17.8	1000	18.5	1000	18.7	900	16.7	200	18.3	130	
14.0	200	16.5	500	17.2	500	18.3	800	16.2	100	17.8	100	
10.8	100	16.0	200	16.2	300	17.2	500	15.8	50	17.9	50	
9.5	50	15.5	100	15.8	200	16.2	300	14.0	10	12.0	10	
7.3	26	14.9	50	15.6	100	15.7	200					
6.0	14	14.1	10	15.2	50	13.5	100					
4.5	7			14.0	10	12.0	50					
						10.5	22					

^{*}In units of disintegrations per minute per 1000 cubic feet of standard air.

Table A5. Average Concentration of Excess Carbon-14 at 30° N (units of 10³ atoms cm⁻³)

km	1/63	4/63	7/63	10/63	1/64	1/65
27	0.61	1.38	2.09	2.14	1.58	1.48
26	0.89	2.08	2.52	2.84	2.05	1.70
25	1.72	3.11	3.42	3.75	2.80	2.07
24	3.69	4.65	4.71	4.87	3.70	2.40
23	7.76	6.77	6.45	6.19	4.81	2.85
22	11.9	9.91	8.71	7.75	6.11	3.36
21	14.6	11.9	9.98	8.92	7.13	3.89
20	15.7	12.6	10.0	9.37	7.70	4.31
19	14.8	11.4	9.07	9.12	7.85	4.28
18	13.1	10.1	8.07	8.02	7.76	4.03
17	10.1	9.10	7.95	6.73	6.88	3.35
16	7.7	8.44	7.30	5.19	6.00	2.28
15	6.25	7.85	6.16	4.50	5.40	1.96
14	4.59	6.00	4.77	3.71	3.86	1.90
13	3.25	4.47	3.73	3.17	2.87	1.94

Table A6. Mixing Ratios (V/V) of Excess Carbon-14 at 30° N (multiples of 10^{-16}), Based on Average Values from Table A5

km	1/63	4/63	7/63	10/63	1/64	1/65
27	10.2	22.9	34.5	35.4	26.2	24.4
26	12.5	29.3	35.6	40.1	28.9	24.0
25	20.7	37.4	41.1	45.0	33.6	24.8
24	38.3	48.4	49.0	50.6	38.4	24.9
23	67.0	58.5	55.7	53.4	41.6	24.6
22	87.6	72.6	63.8	56.7	44.7	24.6
21	90.9	74.2	62.0	55.4	44.3	24.1
20	82.8	66.5	53.1	49.3	40.6	22.7
19	66.3	51.3	40.5	40.8	35.1	19.1
18	49.8	38.4	30.7	30.5	29.5	15.3
17	32.9	29.5	25.8	21.8	22.3	10.8
16	21.6	23.4	20.2	14.4	16.6	6.3
15	14.9	18.7	14.7	10.7	12.8	4.6
14	9.4	12.3 .	9.8	7.6	7.9	3.9
13	5.8	8.0	6.6	5.6	5.1	3.4

UNCERTAINTIES IN THE VALIDATION OF PARAMETERIZED TRANSPORT IN 1-D MODELS OF THE STRATOSPHERE

JULIUS S. CHANG Lawrence Livermore Laboratory Livermore, California

ABSTRACT: The extensive use of parameterized, coupled-chemical-kinetics-and-transport models in the CIAP program has focused a great deal of attention on the need to validate these models. Due to the lack of experiments designed to test model predictions directly, it has become necessary to seek indirect and partial confirmations of the ability of the models to represent the structure of the stratosphere. Of particular importance is the quantitative validity of the extensively parameterized vertical transport in the 1-D models. Unfortunately, great uncertainties exist even for this limited objective. We shall discuss some of the limitations of the existing experimental data in providing conclusive quantitative evidence.

INTRODUCTION

The two basic components of any theoretical model of the stratosphere are the photochemical-kinetic processes and the dynamictransport processes. In constructing a model we attempt to describe all the essential photochemistry and to represent the principal transport mechanisms in the stratosphere. Due to various limitations, we are forced to simplify and parameterize many of the detailed physical processes. For example, we are forced to choose a limited, manageable subset of photochemical reactions from the full known kinetics system. In this choice we are limited by our current knowledge, and can never rule out future modifications. This is illustrated by the growth of the list of essential stratospheric reactions from the pure O_x system to O_x - HO_x , O_x - HO_x - NO_x and now Ox - HOx - NOx - ClOx systems (Chapman, 1930; Nicolet, 1970; Crutzen, 1970, 1971; Johnston, 1971; Stolarski and Cicerone, 1974; Wofsy and McElroy, 1974).

In matters of transport, the level of parameterization in these models is often extensive. For example, in two-dimensional models the net atmospheric motions are necessarily (but also somewhat arbitrarily) represented by the concepts of mean motion and turbulent eddy diffusion. These concepts, as formulated for present two-dimensional models, are not mutually independent. The observationally deduced values for these parameters are limited by further

assumptions (Reed and German, 1965; Mahlman, 1975). In one-dimensional models the net vertical atmospheric motion is represented by a diffusive-transport mechanism, while the other motions are assumed to be averaged out. Hence, not only is the parameterization severe, but the character of the net motions may even be misrepresented. Thus, the only justification for such parameterization of the net vertical transport is that it is expedient, and apparently works "reasonably well". But utilizing these models for predictions of perturbations to the stratosphere is always suspect. This is especially apparent now that it has been demonstrated that differences in the predictions of various models are principally due to the differences in the parameterization of the vertical transport process (Chang and Johnston, 1974; Chang, 1974).

Better quantification is needed of the uncertainties in the model predictions of the possible perturbations of the ozone by supersonic transport operations in the stratosphere. Therefore, a thorough analysis of the parameterized transport used in these models is required. Both natural chemical tracers and man-made radionuclides may be used in assessing the accuracy of the model transport, and each will be discussed in turn. It should be obvious that almost all conclusions apply equally well to the multi-dimensional models, although the present discussions are centered on one-dimensional models.

VERTICAL EDDY-DIFFUSION COEFFICIENTS

As was mentioned before, the net vertical motion in the one-dimensional model is represented by an altitude-dependent diffusion coefficient K(z) in the species-continuity equation

$$\frac{\partial C_i}{\partial t} = \frac{\partial}{\partial z} \left[\rho K(z) \frac{\partial}{\partial z} (C_i/\rho) \right]$$
$$+ P_i - L_i C_i + S_i,$$

where

C_i = C_i(z,t) is the concentration of the ith constituent;

 ρ = ambient air density;

P_i = production of C_i due to photochemical interactions;

L_iC_i = loss of C_i due to photochemical interactions;

S_i = any other possible sinks or sources of C_i,

t = time

In general, K(z) is characterized by a rather large value in the troposphere (≈105 cm²/sec), followed by a low-value region (≈103 - 104 cm²/sec), and then a fast rise to a high value again ($\approx 10^5$ cm²/sec). This is in keeping with the observed stability (or relatively long residence time) of the stratospheric region. However, detailed structures of the preferred K(z) for various models are quite different; three of them are shown in Figure 1. Curve A is based on the vertical eddy-diffusion coefficients derived from heat-flux data by Gudiksen et al. (1968). Because the original values were derived for a twodimensional model including mean vertical wind, it was necessary to adjust the values so that we would have approximately a two-year residence time at 20 km. For the regions above 30 km, a smooth connection was made to the high values of 2×10^5 cm²/sec in the 50-55 km region. This is quite arbitrary and differs greatly from curves B and C. Both curves B and C are derived from the same type of data, namely, stratospheric measurements of CH₄. Wofsy and McElroy (1973) assumed K(z) to have the form $\alpha \rho^{-1/2} + \beta$

above 18 km, chose α and β to match prescribed values at 18 and 60 km, and obtained curve B. which fits the observed CH₄ concentration at 50 km (Ehhalt, 1972). This calculation is reliable if, and only if, the chemical lifetime for CH4 (as derived in the given model) is reliable. This lifetime depends on not only the photolysis rate for CH₄ but also its measured kinetic reaction rates with OH and O(1D). Concentrations of OH and $O(^{1}D)$ depend on the K(z) in the model, so we are back to where we started. Curve C as furnished by Hunten (1975) was derived by drawing a curve through the measured CH4 values, estimating a boundary flux for CH₄, and using the chemical lifetime of CH₄ from Wofsy and McElroy (1973) to calculate K(z) from Eq. (1). After that, some adjustment was made at the tropopause to simulate the seasonal variation in tropopause heights. As a result, this K(z) profile not only inherited the uncertainties of profile B. but due to its marked differences from B, it raises the question of self-consistency, in that we would not expect the OH and O(1D) concentrations based on profiles B and C to agree.

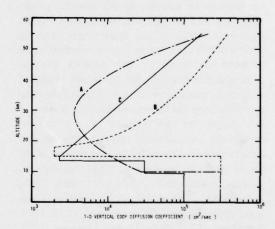


Figure 1. Examples of vertical eddy-diffusion profiles for 1-D models.

It is clear that all attempts at "deriving" eddy-diffusion coefficients are burdened with arbitrary assumptions and uncertain input data. The same is true for two-dimensional models, as was discussed by Mahlman (1975). In the absence of solid theoretical bases, the usefulness of models must then rest with direct comparison with known tracers in the stratosphere.

CHEMICAL TRACE SPECIES AS TRACERS

As was indicated in the above discussion, in considering chemically active tracers it is necessary to know all the relevant production and loss mechanisms. By definition, the chemically reactive tracers undergo chemical transformation in the stratosphere. Thus, any analysis involving these tracers must be sensitive to uncertainties in our knowledge of the chemical cycles and to the calculated or measured photolytic and chemicalkinetic reaction-rate coefficients. Therefore, only the chemical tracers with the simplest chemical cycles are suitable as tracers in validating models. Two major tracers are CH₄ and N₂O. Their chemical cycles are rather simple (Wofsy and McElroy, 1973; Wofsy and McConnell, 1971) and available measurements are reliable. Unfortunately, they do not serve to differentiate among the profiles A, B, and C in Figure 1. Figures 2 and 3 show that given identical chemistry, boundary conditions, etc., all three K(z)'s provide equally good results in the important range of 10-30 km. Above 40 km, only profile B can predict the CH4 measurement. For profile C our computed results differ from the original claim of Hunten that profile C fits all CHA data, including the high-altitude data. As a check of our calculation we also computed a CH4 distribution (case D) based on a profile first suggested by Crutzen (1971). Comparison of both distributions B and D with the original publications confirms the accuracy of our calculation.

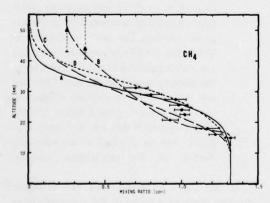


Figure 2. Comparison of measured CH₄ vertical profiles and some theoretical profiles.

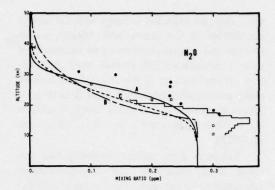


Figure 3. Comparison of measured N₂O vertical profiles and some theoretical profiles.

It should also be pointed out that all CH₄ data used here have been collected at one station, Palestine, Texas (32°N). When they are compared to the infrared data of Ackerman and Muller (1973), differences as large as a factor of two are found in the 20-30 km range. Similarly, the N2O measurements are also somewhat scattered. In both sets of data it is the critical region just above the tropopause that shows the most uncertainty. Other trace species such as NO, NO2, HNO3, and O3 are not good tracers, because they are highly variable in natural concentration and highly dependent on model input parameters such as solar zenith angle, diurnal and seasonal processes, etc. The recently measured chlorofluorocarbons (CF₂C1₂, CFC1₃) (Lovelock, 1974; Molina and Rowland, 1974) promise to be better tracers than any of the above trace species due to their apparently perfectly simple chemical cycle (i.e., they are totally inert except for photolysis). The stratospheric measurement of these chlorofluorocarbons has great potential usefulness, except perhaps for the added complication that the non-steady-state nature of chlorofluorocarbons' atmospheric concentrations may not provide sufficient sensitivity to test the parameterized profiles A, B, C, and others.

RADIONUCLIDES AS TRACERS

Atmospheric nuclear-weapons tests inject an easily identifiable amount of radionuclides into the atmosphere. These radionuclides are injected either as fine particulates (e.g., Sr⁹⁰, W¹⁸⁵, Rh¹⁰², and Cd¹⁰⁹) or as true gas (C¹⁴). As

such, they are expected to move with the natural circulations of the atmosphere. Ideally, a continuous and regular program of measurement of these radionuclides can provide much information on the motions of the atmosphere. Indeed, many investigators have used these data to good advantage (List and Telegadas, 1969; Machta et al., 1970; Telegadas and List, 1969; Johnston et al., 1975).

Although these radioactive-debris data provided good qualitative and semi-quantitative information in the past, their most recent use (Johnston, 1975) may have demanded more details than are available. In contrast to the chemical tracers, these radionuclides are nonreactive and undergo well-understood radioactive decay only. Unfortunately, this advantage over chemical tracers is almost totally overshadowed by the difficulties caused by the transient nature of the radionuclides. Detailed quantification of any given radionuclide depends not only on the exact knowledge of the initial state (i.e., amount, location, spatial distribution, meteorology at the time of injection, etc.), but also on the accuracies of subsequent global-scale measurements at all levels of the atmosphere and at the surface. Consequently, we are limited by the available measurement platforms. During past atmospheric nuclear tests we often had extensive and regular aircraft data below ≈21 km but only a few balloon samples at discrete altitudes above that (up to ≈32 km) (Telegadas and List, 1969). Therefore, only those tests in which the initial stabilized nuclear debris is below 20 km can be quantified reasonably well. On the basis of the estimated total yields from the individual tests in the early sixties and the estimated cloud stabilization heights (Petersen, 1970), we believe that more than half of the radioactive debris could have been placed well above 20 km. This clearly would significantly affect the quantitative accuracy of Sr90 and C14 data.* Since these are the principal radioactive tracers, with the most extensive data, we shall now limit our discussions to them.

As stratospheric tracers Sr^{90} and C^{14} differ in three essential characteristics:

- 1. Production Mechanism, Sr90 is a fission product with a half-life of 28 years. Each megaton of fission yield is estimated to produce about 0.1 megacurie of Sr90. C14 is produced through the interaction of neutrons with atmospheric nitrogen (proportionally to total yield) and has a half-life of 5600 years. If we assume the natural, cosmic-ray-produced background C14 to be uniformly mixed in the atmosphere, then the difference between the observed and the background C14 is the tracer, known as excess C14. While the net stratospheric deposition of Sr90 is dependent on the extent of local fallout, net C14 injected per test depends on the degree of surface absorption of the neutrons. Unfortunately these estimates are rather uncertain (Machta et al., 1963).
- 2. Loss Mechanism. In addition to the natural decay, Sr⁹⁰ can be removed from the atmosphere through rainout scavenging. On the other hand, atmospheric C14 (in the form of CO2) can at most be exchanged with the natural reservoir in the ocean and the biosphere (Machta et al., 1963). This difference in removal mechanism means that once Sr⁹⁰ enters the troposphere, it is prevented from reentering the stratosphere. However, the tropospheric excess C14 can be recirculated into stratosphere.
- 3. Enhanced Downward Motion. Sr⁹⁰ in finite-size particles can undergo gravitational settling, whereas C¹⁴ in the gas phase will not. The analysis of List and Telegadas (1969) apparently indicates no such separation above 25 km, due to the initially small particle size. They did not examine the possibility of nucleation and particle growth below 25 km. This possibility still has not been analyzed, due to the lack of an adequate theory of the nucleation process.

It has been observed that the effective residence times of a tracer in the stratosphere as deduced from Sr⁹⁰ and C¹⁴ data, 2 and 4 years respectively, differ by a factor of two (Telegadas,

^{*}The other tracers mentioned above are special, one-time-only tracers (List and Telegadas, 1969),

1967, 1971). The question is why, and which best represents the behavior of NOx from the SST in the stratosphere? Pointing out that NO, is gaseous like C14 and that Sr90 may undergo particulate settling. Johnston et al. (1975) suggest that C14 data should be used to validate the vertical transport in 1-D models. In fact, Johnston's analysis indicates that profile C in Figure 1 gives the best agreement with observed data. This would favor the high estimates among the current range of estimated ozone perturbations. However, a detailed consideration of the Sr⁹⁰ and C¹⁴ tracer data suggests that his results are not conclusive, and that a literal interpretation of the published C14 data may be quite inappropriate.

Figure 4 shows the trends in C¹⁴ and Sr⁹⁰ at 20 km as a function of time at 60°-75°N and at 24 km as a function of time at 31°N. These are direct measurements independent of extrapolations. It is seen that for the two periods 1960-61 and 1964-65 there are marked differences in the relative trends of C¹⁴ and Sr⁹⁰. If we are to interpret the 1964-65 differences in

trends to be a manifestation that Sr90 is undergoing nucleation and particulate settling, then we are at a loss to explain the very good agreement in the 1960-61 trends. The same relative behavior of trends is also observed in the estimated global stratospheric burdens. But this global burden is subject to data extrapolations and subjective estimates by the data analysts. For the present purpose of considering any possible evidence of particulate settling in Sr⁹⁰, the local directlymeasured data are much more sensitive and reliable. It should be stressed at this time that all the published latitudinal contours of C14 and Sr⁹⁰ are smooth interpolations of known data points. The dashed lines indicate the portion of the data that is based strictly on intuitive guesses. If we go back to the original data and apply the abovementioned characteristics of C14 and Sr90 injection processes (characteristics 1 and 2 above) we can construct a hypothetical scenario in which all the major characteristics of the observations can be explained without recourse to the particulate-settling conjecture (characteristic 3).

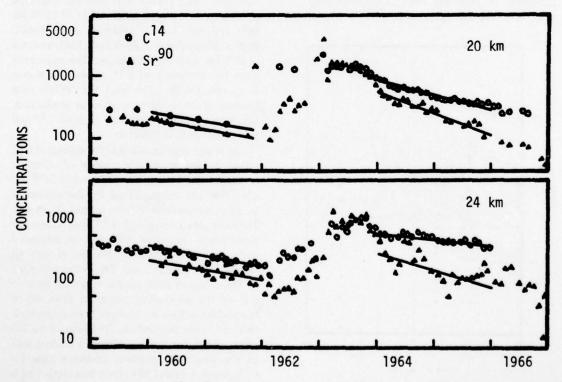


Figure 4. Trends in C¹⁴ (10⁵ atoms per gram of air) and Sr⁹⁰ (disintegrations per minute per 1000 standard cubic feet of air) concentration as a function of time at 20 km (60°-75°N) and at 24 km (31°N).

THE HIDDEN-SOURCE HYPOTHESIS

It is known that more than half the 1961-62 USSR tests were high-yield weapons (>10 Mt). The best available estimates for the stabilized cloud height (Petersen, 1970) would place these nuclear clouds above 20 km in the polar region. where there were no direct measurements of either C14 or Sr90. As a result, any tabulation of stratospheric burdens based on contours of the type shown in Figure 5 would greatly underestimate the true burden. Indeed, this was shown by Machta et al. (1963). Prior to the large polar tests of 1961-62 very little of the injection was placed above 20 km, and consequently the observed burden and estimated productions agree to within ±10% in both 1960 and 1961. In 1963, after the last of the high-yield tests, the measured additional burden for C14 was 54% less than the estimated new production. This agrees well with the unmeasured C14 estimated at that time. It is true that estimates of C14 production may not be accurate (with up to ±50% error on the absolute scale). But if we consider the good agreement in 1960 and 1961 as the normalization, then the discrepancies in 1963 would be

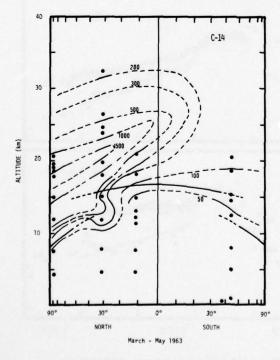


Figure 5. Examples of the estimated latitudinal cross-sections of mean seasonal excess C¹⁴ concentrations.

more real than not. Furthermore, this agrees well with the existence of a hidden source, which we have postulated on the basis of completely different reasoning.

If we accept this hidden-source hypothesis, then the trends in Figure 4 are easily explained. As was pointed out above, Sr90 production is proportional to the fission yield, while the C¹⁴ production is proportional to the total vield. For the 1957-58 test series, it was estimated that approximately half of the total yield was due to fission, while in the 1961-62 test series less than 30% of the total yield was due to fission (Federal Radiation Council, 1963). Since it is known that the high-yield tests (i.e., those that may be deposited above 20 km) are especially low in fission yield, we would expect the cumulative vertical distribution of C14 to be different from that of Sr90. Through a careful tabulation of the estimated deposition heights of C¹⁴ and Sr⁹⁰ from the 1961-62 tests, taking into account the relative ratio of fission and fusion yields, we estimate that approximately 20% more of the C14 was above 20 km than was the case with Sr90. This checks well with the estimated differences in the missing Sr⁹⁰ and C¹⁴ (31% for Sr⁹⁰ and 46% for C¹⁴) (Machta et al., 1963). With a differentiated high-altitude hidden source of C14 for the 1961-62 tests, we then expect the local measurements of C14 to show a slower decay rate. On the other hand, the 1957-58 tests have no apparent differentiation in production, and, hence, similar local decay rates for C14 and Sr⁹⁰. This explains Figure 4.

It is also well-known that the estimated C14 global burden showed a change of effective residence time (Telegadas, 1971) while Sr90 did not. This can be explained by the difference in loss mechanisms (characteristic 2 above). The facts that tropospheric C14 may reenter the stratosphere, and that C14 has an estimated surface loss rate of only 20% per year of the total tropospheric burden, argue for an eventual shift of the observed stratospheric residence time to that of the tropospheric residence time. All of the profiles in Figure 1 estimate the stratospheric residence time for altitude 20-30 km to be 2-3 years. Hence, by 1965 we expect a gradual shift to the longer tropospheric residence time for C¹⁴, about 5 years (20% yearly loss rate). This is in qualitative agreement with Figure 6.

In this section we have suggested a hypothesis which would by itself explain much of the

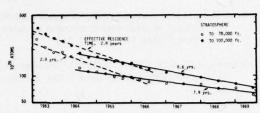


Figure 6. Observed effective residence times for stratospheric C¹⁴.

observed behavior of C¹⁴ and Sr⁹⁰. Although the evidence is somewhat indirect, it is based on known physical processes. Much of the qualitative discussion could be directly tested with a multidimensional global model. However, this would still lack conclusiveness, since these models themselves must be beyond reproach. Nevertheless, it should be clear that there exist well-founded uncertainties in the radionuclide data such that the data alone could not provide sufficient evidence to determine the preferred parameterization of vertical transport in the 1-D models.

CONCLUSION

We have discussed some of the major uncertainties in the experimental data on the available stratospheric tracers. It is concluded that both the chemical tracers and the radionuclides cannot provide sufficient sensitivity to limit the uncertainty in representing 1-D vertical transport to within a factor of two or three. Consequently, at present we must accept a factor of two or three as the uncertainty in the model-predicted stratospheric ozone perturbation. Furthermore, it is also apparent that greater future effort should be dedicated to the quantitative interpretation of experimental data, with clear delineation of their global implications.

ACKNOWLEDGMENTS

I would like to thank H.H. Johnston for pointing out the problem and for many illuminating discussions. I also would like to thank K. Telegadas for helping me to appreciate the data.

The work reported here was performed under the auspices of the U.S. Energy Research and Development Administration under contract No. W-7405-Eng-48.

REFERENCES

- Ackerman, M. and C. Muller (1973), "Stratospheric methane and nitrogen dioxide from infrared spectra," Pure Appl. Geophys. 9, 1325.
- Chang, J.S. (1974), "Simulations, perturbations, and interpretations," in Proceedings of the Third Conference on the Climatic Impact Assessment Program (Cambridge, Mass.), U.S. Dept. of Transportation, DOT-TSC-OST-74-15, 330.
- Chang, J.S. and H.S. Johnston (1974), "The effect of NO_x effluents on ozone," in *Proceedings of the* Third Conference on the Climatic Impact Assessment Program (Cambridge, Mass.), U.S. Dept. of Transportation, DOT-TSC-OST-74-15, 323.
- Chapman, S. (1930), "A theory of upper-atmosphere ozone," Mem. Roy. Meteorol. Soc. 3, 103.
- Crutzen, P.J. (1970), "The influence of nitrogen oxides on the atmospheric ozone content," Quart. J. Roy. Meteorol. Soc. 96, 320.
- Crutzen, P.J. (1971), "Ozone production rates in an oxygen-hydrogen-nitrogen oxide atmosphere," J. Geophys. Res. 76, 7311.
- Elhalt, D.H., L.E. Heidt, and E.A. Martell (1972), "The concentration of atmospheric methane between 42 and 62 kilometers altitude," J. Geophys. Res. 77, 2193.
- Federal Radiation Council (1963), "Estimates and Evaluation of Fallout in the United States from Nuclear Weapons Testing Conducted Through 1962," Report No. 4.
- Gudiksen, P.H., A.W. Fairhall, and R.J. Reed (1968), "Roles of mean meridional circulation and eddy diffusion in the transport of trace substances in the lower stratosphere," J. Geophys. Res. 73, 4461.
- Hunten, D.M. (1975), "Estimates of stratospheric pollution by an analytic model," Proc. NAS 72, 4711; also (1976) in this volume.
- Johnston, H.S. (1971), "Reduction of stratospheric ozone by nitrogen oxide catalysts from supersonic transport exhaust," Science 173, 517.
- Johnston, H.S., D. Kattenhorn, and G. Whitten (1975), "Use of excess carbon-14 data to calibrate models of stratospheric ozone depletion by supersonic transports," in this volume.
- List, R.J. and K. Telegadas (1969), "Using radioactive tracers to develop a model of the circulation of the stratosphere," J. Atm. Sci. 26, 1128.
- Lovelock, J. (1974), "Atmospheric halocarbons and strato pheric ozone," Nature 252, 292.

CHANG

- Machta, L., R.J. List, and K. Telegadas (1963), "Inventories of Selected Long-lived Radioisotopes Produced During Nuclear Testing," Health and Safety Laboratory Report, US AEC, HASL-142, 243.
- Machta, L., K. Telegadas, and R.J. List (1970), "The slopes of surfaces of maximum tracer concentration in the lower stratosphere," J. Geophys. Res. 75, 2279.
- Mahlman, J.D. (1975), "Some fundamental limitations of simplified-transport models as implied by results from a three-dimensional, general-circulation/tracer model," in this volume.
- McElroy, M.B. and J.C. McConnell (1971), "Nitrous oxide: A natural source of stratospheric NO," J. Atmos. Sci. 28, 1095.
- Molina, M.J. and F.S. Rowland (1974), "Stratospheric sink for chlorofluoromethanes: Chlorine atomcatalysed destruction of ozone," Nature 249, 810.
- Nicolet, M.(1970), "Ozone and hydrogen reactions," Ann. Geophys. 26, 531.
- Petersen, K.R. (1970), "An empirical model for estimating world-wide deposition from atmospheric nuclear detonations," Health Physics 18, 357.

- Reed, R.J. and K.E. German (1965), "A contribution to the problem of stratospheric diffusion by largescale mixing," Mon. Wea. Rev. 93, 313.
- Stolarski, R.S. and R.J. Cicerone (1974), "Stratospheric chlorine: Possible sink for ozone," Can. J. Chem. 52, 1610.
- Telegadas, K. and R.J. List (1969), "Are particulate radioactive tracers indicative of stratospheric motions?", J. Geophys. Res. 74, 1339.
- Telegadas, K. (1967), "The Seasonal Stratospheric Distribution of Cadmium-109, Plutonium-238 and Strontium-90," Health and Safety Laboratory Report, US AEC, HASL-184, I-53.
- Telegadas, K. (1971), "The Seasonal Atmospheric Distribution and Inventories of Excess Carbon-14 from March 1955 to July 1969," Health and Safety Laboratory Report, US AEC, HASL-243.
- Wofsy, S.C. and M.B. McElroy (1973), "On vertical mixing in the upper stratosphere," J. Geophys. Res. 78, 2619.
- Wofsy, S.C. and M.B. McElroy (1974), "HO_x, NO_x and ClO_x: Their role in atmospheric photochemistry," Can. J. Chem. 52, 1582.

CLIMATE-MODEL RESULTS OF STRATOSPHERIC PERTURBATIONS*

MICHAEL C. MACCRACKEN

Lawrence Livermore Laboratory
University of California
Livermore, California

ABSTRACT: The ZAM2 zonal climate model has been used to simulate the climatic effects of several stratospheric perturbations proposed in the CIAP context. Two control runs are being carried out in order to clarify the effect of using annual average solar radiation instead of seasonally and daily varying solar position. Preliminary perturbation experiments with reduced ozone, increased stratospheric aerosol, reduced solar constant, and increased water vapor have been run to equilibrium using annual average solar radiation at each latitude. Reduced ozone leads to a surface warming (in part because the effects of nitrogen dioxide absorption of solar radiation and of ozone absorption and reemission of infrared radiation are not included). Increased aerosol and an approximately equivalent reduction in solar radiation lead to comparable reductions in surface temperature and an unusually strong effect on the hydrologic cycle. Increased stratospheric water vapor results in slight stratospheric cooling, and slight surface warming.

INTRODUCTION

Since the beginning of CIAP, a primary goal has been the development of reliable estimates of the climatic effect of aerospace utilization of the stratosphere. Development of such estimates has proven extremely difficult for a number of reasons. First, climate is a complex phenomenon; observed climate has displayed variations over all spatial and temporal scales that have been studied. And we have very little understanding of why these past changes occurred. Second, this complexity manifests itself through a wide number of atmospheric processes. (The investigation and simulation of each of these is a subject of intensive study in its own right.) Combining this variety of inadequately understood individual processes, from radiation to convection, from precipitation to large-scale transport, into a single model poses extremely difficult problems of both a physical and a computational nature. Thus we have seen a diversity of modeling approaches, from one to three dimensions, each with its own capabilities and limitations. And so a third difficulty comes in trying to interpret the diversity of results, for no one model treats the whole problem. In some cases this has led (and is still

leading) to the sign of the simulated climatic effect being different in different models.

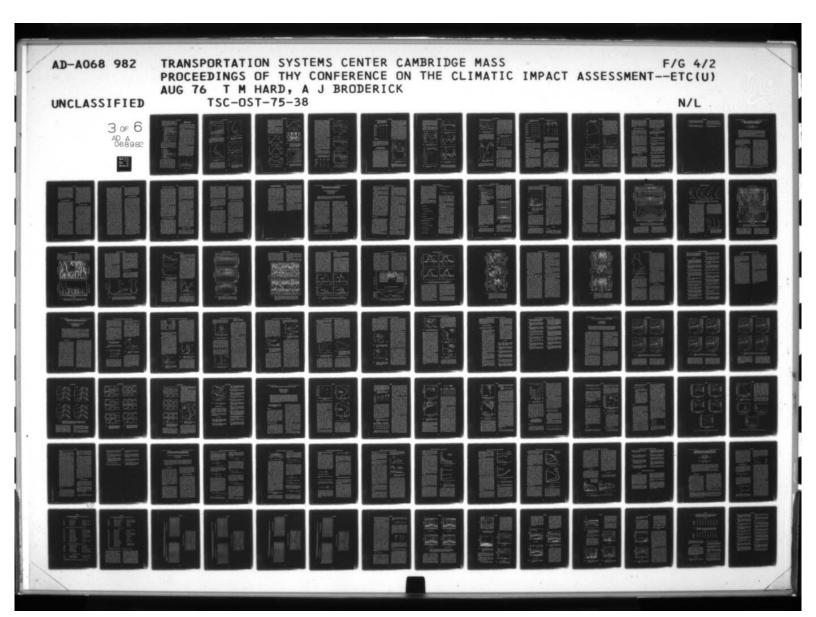
As a result, conclusions as to the climatic change which might result from SST fleet operation have had to be either very general indications, or, at best, estimates with broad error bars.

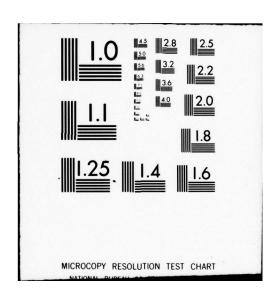
The results presented here must be viewed in the context of this diversity — I do not claim they are the result, only that with the variety of processes that the ZAM2 model includes, and in the fashion that it treats them, these are the climatic changes which the model is indicating. Their validity relative to other results must then be judged in terms of the processes included, adequacy of treatment, and similar other factors.

MODEL STRUCTURE

The basic structure and validation of some of these processes have been discussed at the last two CIAP conferences (MacCracken, 1973; Luther and MacCracken, 1974). The ZAM2 model is a two-dimensional global climate model with a 10° grid. The atmospheric motions are treated through the use of the so-called "primitive" equations, with the meridional transport of temperature and water vapor by horizontal

^{*}Work performed under the auspices of the U.S. Energy Research and Development Administration and supported in part by the Climatic Impact Assessment Program, U.S. Department of Transportation.





eddies simulated with Stone's formulation in the troposphere and Luther's prescription in the stratosphere. Eddy-momentum transport is represented by a simple diffusion approximation. The atmospheric processes included in the atmospheric calculations are:

- Solar radiation (ozone, water vapor, aerosol, clouds, earth's surface)
- Terrestrial radiation (water vapor, clouds, aerosol, CO₂, surface)
- Hydrologic cycle (evaporation, clouds, convective precipitation, large-scale precipitation, snow, reevaporation of falling rain)
- Clouds (convective, layered at four levels)
- Mean meridional transport (vertical, latitudinal)
- Eddy transport (vertical, latitudinal, cross-term)
- Convection (temperature, water vapor)
- Adiabatic overturning.

The surface at each latitude is divided into land (which may be partly mountains) and oceans, parts of each of which may be snow-and/or ice-covered. The lowest layer of the atmosphere is differentiated according to the underlying surface type. The processes treated at the surface include:

- Sensible heat
- Evaporation
- Terrestrial radiation
- Solar radiation
- Surface energy storage (land and ocean)
- Sea ice buildup and melting
- Mountains (obstruction, full surface treatment)
- Albedo variations
- Meridional ocean transport.

The processes in both the atmosphere and surface are highly inter-coupled. We have endeavored to validate most processes separately (such as, for example, the solar and longwave radiation). Although careful examination of each of the simulated processes is required for evaluation of the results, in the time available I will only be able to contrast model results for the control case with the observed atmosphere, and then show the results of some of our simulations.

SIMULATION OF THE OBSERVED CLIMATE

Before a climate model is used to study the effects of perturbations to the natural climate, it is appropriate to compare model results for the control case with the observed climate. The ZAM2 model is being run in two modes for the control climate.

In an attempt to determine whether the model's climate is stable, and to conserve computer time, the first mode chosen was to run with annual average solar radiation until an equilibrium climate was reached. This has been accomplished, and the model has not tended toward either an ice age or a melting of the ice caps. Certain of the results, however, do not—and probably should not be expected to—correspond very closely to the observed climate.

In the second mode, the model is run with seasonally and diurnally varying solar radiation. Much longer simulations are required to achieve an annual equilibrium than when the annual average sun is used. We are just beginning these simulations, but they seem to show much closer agreement with the observed climate in such variables as the zonal wind.

With that preface, let me show some results from the ZAM2 model with annual average radiation and contrast them with observations. The atmospheric temperature field is shown in Figure 1, and contrasted with observed values as compiled by Manabe and Hunt (1968) in Figure 2. The agreement is quite good except in the lower polar stratosphere, where the model pattern is warmer and more ragged. The tropical tropopause temperature minimum is in excellent agreement in terms of both height and value.

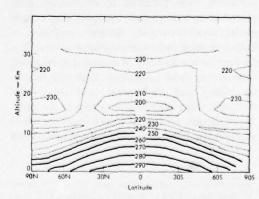


Figure 1. Control-run temperature (°K).

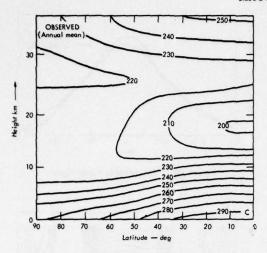


Figure 2. Observed temperature (°K).

Another indication of the temperature structure is the lapse rate, shown in Figure 3. Figure 4 shows typical values based on observations from Manabe and Hunt (1968). Again, except in the lower polar stratosphere, the agreement is excellent.

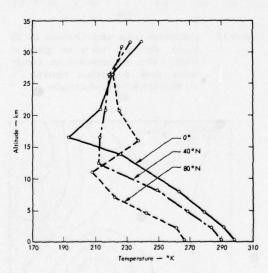


Figure 3. Lapse rate for various latitudes (control, average annual sun).

Water-vapor mixing ratio is another important measure of climatic behavior. As shown in Figures 5 and 6, agreement with the tropospheric observations from Oort and Rasmusson (1971) is reasonably good. Other measures of the hydrologic cycle include the precipitation and evaporation rates, which are compared to values from

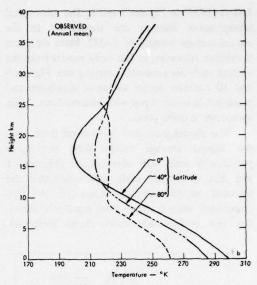


Figure 4. Observed lapse rate, from Starr and collaborators as presented by Manabe and Hunt (1968).

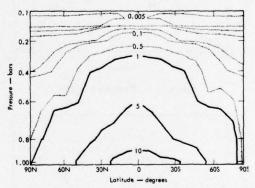


Figure 5. Control-run water-vapor mixing ratio (gm/kg).

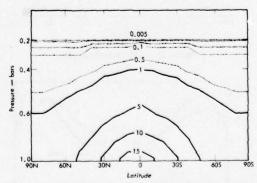


Figure 6. Observed water-vapor mixing ratio (gm/kg), from Oort and Rasmusson (1971).

Southern hemisphere is reflection of northern-hemisphere data.

Sellers (1965) in Figures 7 and 8. The subtropical precipitation minima are suppressed in the annual-average version of ZAM2. More structure is evident, however, in the early results from the version with the seasonally varying sun. Figures 9 and 10 contrast model values of cloudiness and precipitable water vapor with observations. Again agreement is quite good.

The model-generated zonal-wind field from the annual average model does not agree particularly well with observations (Figures 11 and 12). There are early indications that the seasonal model corrects some of the discrepancies, since it shows both equatorial easterlies and mid-latitude stratospheric westerlies.

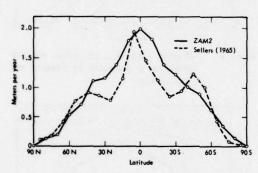


Figure 7. Precipitation rate.

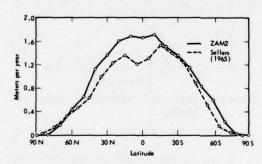


Figure 8. Evaporation rate,

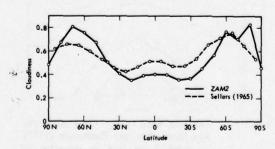


Figure 9. Total cloudiness in tenths.

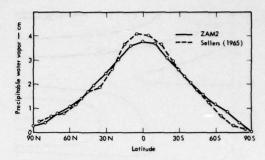


Figure 10. Precipitable water vapor.

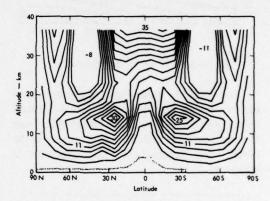


Figure 11. Control-run zonal wind. Contours are 10 km/hr, numerical values are given in m/sec. Values are instantaneous; average values show no surface easterlies in northern-hemisphere mid-latitudes.

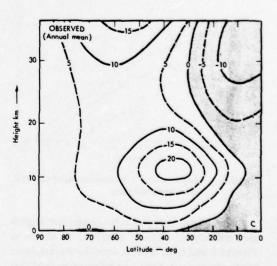


Figure 12. Observed zonal wind (m/sec). Based largely on data from Starr and collaborators as presented by Manabe and Hunt (1968).

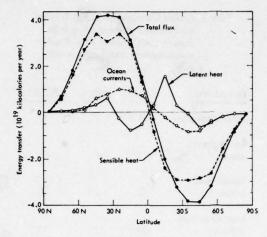
Since zonal winds do not participate in the transport processes in the model (although they are a sensitive measure of the temperature pattern), the real question concerns the validity of the simulated meridional-vertical wind structure. In contrast to observations, the annual average model tends to show a single-Hadley-cell circulation rather than the observed three-cell structure. The Ferrel cell should perhaps not be expected in a zonal model, as it is largely a statistical result of eddy averaging. In a zonal model it is more appropriate to look at the net effect of the meridional wind pattern, as illustrated by the components of the meridional energy transports. Figure 13 contrasts the model results with annual average values from Sellers (1965). The total transport is in quite good agreement. It can be seen that mean-motion advection dominates in low latitudes and eddy transport in mid- and high latitudes.

Global energy-balance components are also important variables to compare with observations, as shown in Tables 1 and 2. The model's planetary albedo is lower than Sellers' value (the latter is not confirmed by satellite evidence, which indicates about 0.30) and lower than the more recent estimates given in the NAS/NRC study (NAS/NRC, 1974). This is in part due to the fact that annual average solar radiation restricts the growth of seasonal snow cover at high latitudes. The lower albedo leads primarily to an increase in intensity of the hydrologic cycle over that observed.

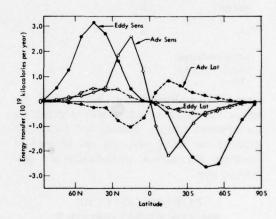
As I indicated earlier, these results come from our model with annual-average solar radiation. We expect to have a control case with seasonal and diurnal sun soon, which may clear up

Table 1. Global Surface-Energy-Balance Components (normalized so solar input = 100), Control Run. Positive values indicate surface energy gain.

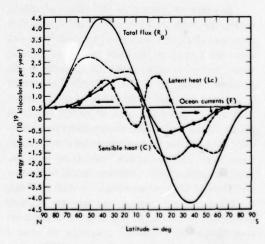
Component	ZAM2	Sellers	NRC/NAS
Sensible	-5	-5	-7
Evaporation	-28	-22	-23
Longwave	-22.5	-20	-21
Solar	55.5	47	51
Net	0	0	0



a. Control run.



b. Atmospheric portion of control run.



c. Observed values (from Sellers, 1965).

Figure 13. Meridional energy-flux components.

Table 2. Global Atmospheric-Energy-Balance Components (normalized so solar input = 100), Control Run. Positive values indicate atmospheric energy gain.

Component	ZAM2	Sellers	NRC/NA
Solar absorption	16.5	17	19
Longwave to			
space	-72	-64	-70
Latent heat			
release	28	22	23
Longwave from			
surface	22.5	20	21
Sensible from			
surface	5	_5	7
Net	0	0	0
Diffuse reflected			
to space (albedo)	28	36	30

some of the discrepancies. But, overall, we believe the annual-average version is simulating the observed energy, thermal, and hydrologic structure reasonably well, and can be used to investigate stratospheric perturbations in a preliminary way.

CLIMATIC EFFECT OF STRATOSPHERIC AEROSOLS

In order to investigate the effect of stratospheric aerosols we have run model simulations with zero (0x), one (1x), two (2x), and four (4x) times the normal global mass loading of aerosol, where normal is taken to be $0.43 \mu g/cm^2$ in the pressure interval from 75 to 150 mb. The aerosol is assumed to have a real index of refraction of 1.45 and an imaginary part of -0.005 (which is mildly absorbing). ZAM2 incorporates parametrically the effective aerosol properties (backscatter, forescatter, and absorption) calculated with the detailed spectral solar-radiation model of Braslau and Dave (1973) as modified by Luther (1974a). In the long-wave regime, we use an analytic expression based on the small-optical-depth limit to determine an emissivity, assuming the aerosol layer acts as a blackbody (Luther, 1974b). The aerosol simulations are compared to a simulation which has normal aerosol loading with a 1%

reduction in the solar constant in order to facilitate comparison with other model experiments which have been interpreted as applicable to the problem of increased aerosol. Remember that each run used the annual-average-solar-radiation version of ZAM2. Steady state has essentially been achieved in each case.*

First, Figures 14 and 15 show the departure from the control run of surface temperature and of lowest-layer air temperature as a function of latitude, averaged over surface type, for the various cases. Note that the surface-temperature patterns are reasonably consistent, with increasing stratospheric-aerosol loading resulting in decreasing temperatures. The effects appear to be generally larger and more irregular at the poles than at lower latitudes. The extreme variations at 70°N were due to formation of snow cover on land at sea level where none existed in the control run. It is interesting that there seems to be a warming on the mid-latitude edge of the

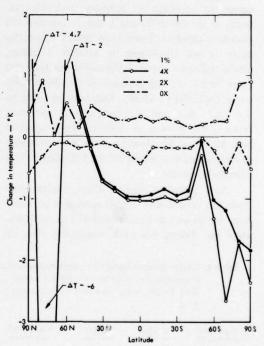


Figure 14. Change in surface temperature, perturbed run minus control run.

^{*}In looking at the results, it should be noted that the model results give precise numbers. The fact that several significant figures are given does not imply the same accuracy in predicting how the real climate will respond.

cooling polar regions. This seems to be correlated with decreased cloudiness and planetary albedo, as shown in Figures 16 and 17. These in turn seem to result from the decreased evaporation in mid-latitudes, as shown in Figure 18. Precipitation has also decreased in a similar pattern (Figure 19).

A smoother measure of tropospheric temperature change is the 600-mb temperature change (Figure 20). For the zero-aerosol case, the exaggerated polar effect is obvious. In the

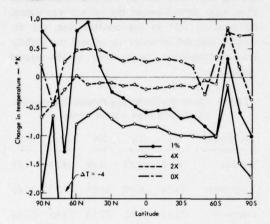


Figure 15. Change in surface-layer air temperature, perturbed run minus control run.

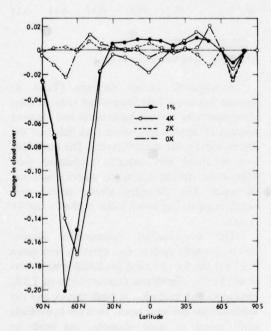


Figure 16. Change in cloud cover, perturbed run minus control run.

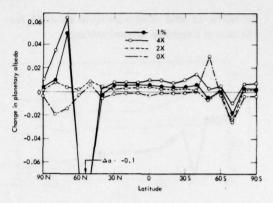


Figure 17. Change in planetary albedo, perturbed run minus control run.

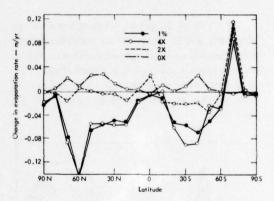


Figure 18. Change in evaporation rate, perturbed run minus control run,

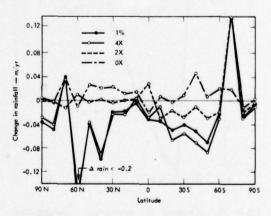


Figure 19. Change in precipitation rate, perturbed run minus control run.

increased-aerosol cases, with the polar temperature inversion, there seems to be little change. In the lower stratosphere, the temperatures in the aerosol layer tend to increase up to about 4K for the case of four-times aerosol loading.

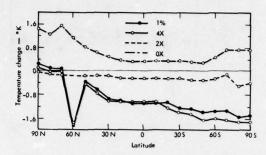


Figure 20. 600-millibar temperature difference, perturbed run minus control run.

In terms of the pattern of meridional energy transport, ZAM2 leads to a dramatic change, with generally reduced poleward fluxes in regions where a general cooling has occurred (Figure 21). In the northern polar regions some shifting has gone on due to the change in latitude of the snow limit.

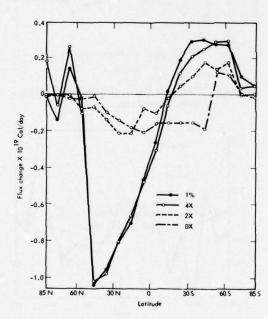


Figure 21. Changes in atmospheric sensible-pluslatent-heat meridional fluxes, perturbed run minus control run.

To measure the global effects of stratospheric aerosols we can look at various factors on a global basis, recognizing that this hides large latitudinal variations.

Surface energy balances (Table 3) show that increased aerosol loading leads to less sensibleheat loss and less evaporation from the surface with increased net loss from long-wave radiation. (This is because, although the surface is cooler, there is less back radiation since there is less water vapor in the atmosphere.) Solar radiation absorbed by the surface (even with a reduced solar constant) was essentially unchanged. This is due in part to the decreased water vapor in the atmosphere. Note that for the four-times aerosol case, solar absorption at the surface was almost identical to that in the control case; the decreased amount of water vapor and the slightly reduced cloudiness compensated for the aerosol obstruction.

Table 3. Global Surface-Energy-Balance Components (normalized so solar input = 100)

Component	0X	1X	2×	1%*	4X
Sensible	4.72	4.78	4.59	4.54	4.50
Evaporation	-28.33	-28.08	-28.04	-27.52	-27.05
Longwave	-22.43	-22.62	-22.72	-23.65	-24.05
Solar	55.50	55.49	55.24	55.60	55.49
Net**	+0.02	+0.01	-0.11	-0.11	-0.11

^{*}Normalized to full solar constant

Atmospheric energy balances (Table 4) showed less latent-heat release and reduced solar absorption (the aerosol backscatter and lessened amount of water vapor more than balanced the absorption by the aerosol layer). The long-wave loss to space was virtually unchanged even though the surface long-wave radiation loss was increased. The planetary albedo stayed very nearly constant (up about 0.002 in the 2x and 4x cases).

The water-budget components showed rather dramatic results. Precipitation was down 3.6% for the 4x case, and precipitable water was down 10.2%. Cloudiness decreased almost 1.5%, mostly in high latitudes, in both the 4x and the reduced-solar-constant cases. Thus the hydrologic cycle seems to react strongly, and tends to diminish the temperature changes induced by the aerosol layer through reduced cloudiness.

^{**}Includes trend and round-off error

Table 4. Global Atmospheric-Energy-Balance Components (normalized so solar input = 100)

Components	<u>0x</u>	<u>1x</u>	2x	1%*	4X
Solar					
absorption	16.57	16.52	16.54	16.13	16.32
Longwave					
to space.	-72.21	-72.02	-72.02	-71.96	-72.01
Latent heat					
release	28.39	28.09	28.07	27.55	27.08
Longwave					
from surface	22.43	22.62	22.72	23.65	24.05
Sensible					
from surface	4.72	4.78	4.59	4.54	4.50
Net**	-0.10	-0.01	-0.11	-0.20	-0.26
Diffuse reflected					
to space (albedo)	27.9	28.0	28.2	27.5	28.2

^{*}Normalized to full solar constant

reduced atmospheric absorption of solar radiation, and less back radiation to the surface. In the long-wave, the increased planetary loss that might be expected due to reduced atmospheric water content and cloudiness is apparently limited by both the aerosol layer and reduced atmospheric temperatures.

As summarized in Table 5, the net effect on surface and sea-level atmospheric temperatures is less than seems to result from the Sellers model (which has no hydrologic cycle) and the radiative-convective and GFDL models (which have fixed cloudiness) as reported in CIAP Monograph 4 (1975). Two additional early ZAM2 simulations, with a 3% solar-constant reduction and ten-times-normal aerosol loading are also included.

It is very difficult to decide in which model and which answer one should place the most confidence. Not only must one weigh heavily the effects of dimensionality and of representation of transport and radiation processes, but, as shown by the ZAM2 results, the hydrological cycle, clouds, and convective processes are also very important. And we all still have a long way to go before we can model these processes satisfactorily in global models.

Table 5. Change in Global Average Surface
Temperature

	Temperature	Sensitivity Ratio*			
	Difference	Global	Rai	Range	
Run	from Control	Average	Low	High	
0 X	+0.293	73	5	225	
1X	0			-	
2X	-0.188	47	5	145	
1%	-0.424	42	-200	610	
4X	-0.969	81	-180	605	
3%**	4.73	158	65	665	
10X**	-5.86	163	105	610	

^{*}For comparison with solar-constant (σ) calculations where background aerosol loading (0.43 μ g/cm²) is assumed to be equivalent to an \approx 0.4% reduction in solar constant ($\Delta\sigma$) on the basis of simple calculations from Luther. Sensitivity ratio = $\Delta T/(\Delta\sigma/\sigma)$.

On the basis of these simulations, it seems apparent that increased stratospheric aerosol loading and a reduced solar constant both lead to surface coolings of similar extent when reasonable equivalences are used. But the sensitivity of the climate to specific aerosol amounts is not yet certain.

OZONE REDUCTION

In addition to the aerosol simulations, we have treated one case of ozone reduction. The total global reduction and the pattern of the percentage reduction in the vertical was taken from Chang's (1974) one-dimensional model results for SST's at 21 km (Figure 22). The latitudinal pattern of the reduction is taken from Cunnold's (1974) study using the MIT model (Figure 23). Both simulations assumed the equivalent of the Boeing 500-plane SST fleet. Due to some differences in amount of natural ozone and normalization considerations, our study ended up treating an 11.7% global average reduction in ozone (Chang had 11.1%).

The ZAM2 model does not yet include either solar absorption by NO₂ or long-wave emission by ozone, both important processes

^{**}Includes trend and round-off error

^{**}Runs made earlier.

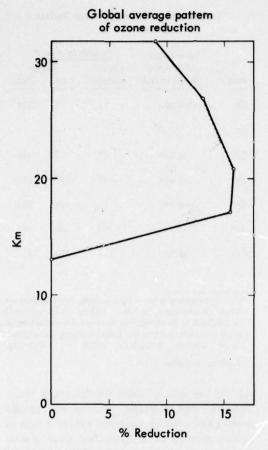


Figure 22. Global-average pattern of ozone reduction.

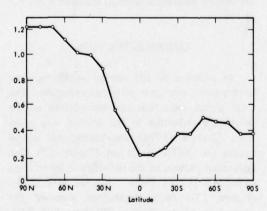


Figure 23. Latitudinal pattern (normalized to 40°N) of ozone reduction.

which radiative-convective models indicate may change the sign of the result when ozone is reduced. We expect to include these effects in ZAM2 in the near future. Our model does include, however, the very important effect of reduced ozone on the albedo, which was virtually ignored until Luther pointed it out a little more than six months ago, and which also seems to be a factor that can control the sign of the effect.

The global-average surface and sea-level air temperatures in the ZAM2 simulation increased about 0.24K, with mid-latitude northern-hemisphere temperatures increasing by about twice the global average (Figure 24). Global-average temperatures in the stratosphere decreased on the average between about 0.5 to 1.5K depending on latitude and altitude, with values exceeding 2K common in the northern-hemisphere stratosphere.

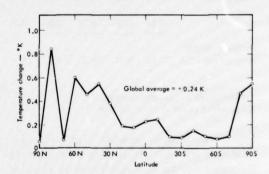


Figure 24. Change in surface temperature, perturbed ozone run minus control run.

In terms of the global integrals, the planetary albedo decreased slightly. This is because a slight reduction in cloudiness more than compensated for the albedo increase expected from the ozone decrease alone. This cloudiness decrease, in turn, seemed to result from the increased convection induced by increased adiation and a steeper lapse rate, and from some latitudinal redistribution of clouds in various layers. It occurred despite increased precipitable water vapor (1.6%), increased precipitation (0.6%), and a longer water-vapor residence time in the atmosphere (0.9%). The increased water vapor did not compensate for the decreased ozone absorption of solar energy, with total atmospheric absorption of solar energy dropping

Thus, again, as for aerosols, the treatment of the hydrologic cycle is of crucial importance in ozone-perturbation studies. Radiative-convective

models which fix the clouds, fix the relative humidity, or fix other parts of the hydrologic cycle may thus give misleading answers, as may ZAM2 by leaving out some processes. I think all we can say is that a reasonable ozone reduction is likely to cause a temperature change of a few tenths of a degree — and the sign of the effect is not yet clear.

WATER-VAPOR PERTURBATION

Finally, we have used ZAM2 to simulate in a very simple way the effects of a 1-ppm increase in water-vapor mixing ratio above 150 mb, treating the effects only through the interaction with the solar and long-wave radiation calculations.

The resulting effects were quite small. The global-average surface temperature increased 0.094K. Temperatures throughout the troposphere also increased about a tenth of a degree. Stratospheric temperatures dropped about 0.2K, except in some regions just above the tropopause where the reduction was a little more than a degree. From the heating rates, it is evident that the change in long-wave cooling caused by the increased water vapor is almost a hundred times larger than the additional solar heating which is induced.

The net effect on planetary, atmospheric, and surface energy-balance components is very small. For example, the albedo increases by a few hundredths of a percent, and cloudiness changes by less than 0.001%. The precipitable water increases about 0.5% because of the warmer tropospheric temperatures, but the relative humidity is essentially unchanged.

SUMMARY

The ZAM2 model has been applied to aerosol, ozone, and water-vapor perturbations. From the aerosol and ozone calculations it is clear that the atmospheric hydrologic cycle plays an important role in determining what the net effect is likely to be. Because no climate models are generally agreed to represent convection, cloudiness, water vapor, and the rest of the hydrologic cycle particularly realistically, it seems clear that the uncertainty of what the climatic effects would be in the real atmosphere may still be quite large. I might add that while

incorporating a large number of feedback mechanisms in a complex model is nice in principle, in practice it poses many difficult problems in interpretation and the need for extensive sensitivity studies. Because of these and other oftrepeated caveats, the results of the ZAM2 model, and all other present models, should be viewed primarily as indications of the range of the likely effects, not absolute indicators.

ACKNOWLEDGMENT

I would like to thank Fred Luther and Gerald Potter for their contributions in developing the model, and Gerald Potter for his carrying out of the model simulations.

REFERENCES

- Braslau, N. and J.V. Dave (1973), "Effects of aerosols on the transfer of solar energy through realistic model atmospheres," J. Appl. Meteorol. 12, 601.
- Chang, J. (1974), Lawrence Livermore Laboratory, personal communication.
- CIAP (1975), The Natural and Radiatively Perturbed Troposphere, ed. Leith et al., Volume 4 of the CIAP monograph series, Dept. of Transportation, DOT-TST-75-54.
- Cunnold, D.M., F.N. Alyea, N.A. Phillips and R.G. Prinn (1974), "First results of a general circulation model applied to the SST-NO_x problem," in *Preprints* of the AMS-AIAA Second International Conference on the Environmental Impact of Aerospace Operations in the High Atmospheres, (July 8-10, 1974, San Diego, CA), pub. AMS, 187.
- Luther, F.M. (1974a), "Solar Radiation Model RAD1"," Lawrence Livermore Laboratory Rept. UCID-16572.
- Luther, F.M. (1974b), "Effect of Stratospheric Aerosol on Longwave Radiative Fluxes: Variation with Latitude and Season," Lawrence Livermore Laboratory Rept. UCID-16559.
- Luther, F.M. and M.C. MacCracken (1974), "Initial validation studies for ZAM2 radiation and largescale eddy transport mechanisms," in *Proceedings* of the Third Conference on CIAP (Cambridge, MA), Dept. of Transporation, DOT-OST-74-15, 437-449.
- MacCracken, M.C. (1973), "Zonal atmospheric model ZAM2," in *Proceedings of the Second Conference* on CIAP (Cambridge, MA), Dept. of Transportation, DOT-TSC-OST-73-4, 298-320.

- Manabe, S. and B.G. Hunt (1968), "Experiments with a stratospheric general circulation model. 1: Radiative and dynamic aspects," Mon. Wea. Rev. 98(8), 477.
- National Research Council/National Academy of Sciences (1974), "Understanding Climate Change: A
- Program for Action," United States Committee for the Global Atmospheric Research Program,
- Oort, H.H., and E.M. Rasmusson (1971), "Atmospheric Circulation Statistics," NOAA Professional Paper No. 5.
- Sellers, W.D. (1965), *Physical Climatology*, University of Chicago Press, Chicago, Illinois.

THE DESIGN OF A STATISTICAL-DYNAMICAL CLIMATE MODEL, AND STATISTICAL CONSTRAINTS ON THE PREDICTABILITY OF CLIMATE*

C.E. LEITH

National Center for Atmospheric Research† Boulder, Colorado

ABSTRACT: This paper deals with two general topics. The first is a prescription for the design of a climate model that combines an internal statistical and an external dynamical component. The theoretical basis for making such a separation is a somewhat special definition of climate, which is discussed at some length. The external dynamical model is like traditional general-circulation models in using deterministic equations; the internal statistical model, however, is based on statistical-hydrodynamical equations for the evolution of statistical moments.

The second topic is the logical statistical consequence of the well-known limited predictability of the weather as it relates to the predictability of the climate. The problem is described in terms of a signal of possibly predictable climate change, as compared to the noise coming from unpredictable weather fluctuations.

This paper describes a personal view of the approach to the design of a climate model. As such, it contains much conjecture about future developments which will perhaps be proved false, but some definite position must be taken as a starting point for discussion.

DEFINITION OF CLIMATE

Before the design of a numerical model of climate is discussed, it is necessary to be as precise as possible in the definition of the word "climate". We generally think of climate as the average behavior of the land-ocean-atmosphere system over relatively long times, rather than the detailed daily fluctuations that we call the weather. The main problem of definition is making precise the dividing line between weather and climate. On the basis of recent results of computer experiments on the predictability of the weather, we might somewhat arbitrarily set the dividing time scale at two weeks. Climate should not, however, be defined in terms of two-week time averages, for these would retain a large and unpredictable noise component from the weather fluctuations. Instead we must try to make another division into what I shall call an internal system (say, the atmosphere) characterized by relatively rapid fluctuations, which is embedded in an external system (including, say, the ocean) that provides relatively slowly changing external influences on the internal system. We may then define the climate in terms of averages over an imagined ensemble of internal states which is in equilibrium with the slowly changing external influences. The internal ensemble consists of a myriad of atmospheric states, all under the influence of the same external conditions of sea-surface temperature, ice cover, solar radiation, etc. Such a definition, familiar from classical statistical mechanics, provides theoretically well-defined ensemble averages free from the statistical fluctuations of any individual realization. The ergodic presumption is that the ensemble averages would be equal to individual time averages over infinite time under constant external conditions. Yet we may consider ensemble averages changing in response to changing external conditions on a finite time scale, and be able to speak of climate change.

The boundary between the internal and the external systems is itself hard to define precisely. A dry land surface with its rapidly changing temperature should certainly be considered as part of the internal system, and most of the ocean as part of the external system, but we are

^{*}This paper was also published as Appendix 2.2 in "The Physical Basis of Climate and Climate Modelling," GARP Publication Series No. 16, WMO/ICSU, Geneva, 1975.

[†]The National Center for Atmospheric Research is sponsored by the National Science Foundation.

less certain about land moisture, or fluctuating snow cover, or ocean surface layers. However, in any particular numerical model used specifically for short-range weather prediction, a distinction is always made between the internal system variables, computed by the model, and the external system variables, for which it is considered adequate that values be specified and not depend on the internal state. Although somewhat different choices are made in different models, any such choice can also serve to define internal and external systems so far as climate is concerned.

THE CLIMATE ENSEMBLE

We are defining the climate in terms of an ensemble of internal states, so that all internal climatic properties are determined by the probability distribution of the climate ensemble. For a fixed external state we assume that there is a single stationary ensemble toward which any other ensemble tends with time. Without such an assumption (which may, of course, be false) we cannot speak of the climate associated with any given external state. We shall need, in fact, the somewhat stronger assumption that for any given history of external state changes there is a unique history of associated climate ensembles toward which any other ensemble history tends with time. The most obvious example of this more general situation is given by the annual cycle of solar heating, which leads by our assumption to a unique annual climate cycle, other external influences being unchanged. We expect that at any point in time the climate ensemble associated with a given history will be similar but not identical to that corresponding to the current external state treated as stationary.

There are, of course, important feedback mechanisms by which the internal system can influence the evolution of the external state, and here we are forced to make a crucial approximation if we are to separate the two systems. We shall assume that the time scale of internal system behavior is so much shorter than that of the external system that we may use internal averages over intermediate times for computing the feedback influences, and, further, that we may approximate such time averages by ensemble averages. (The errors of so doing will be discussed in a later section.) We shall assume

therefore that the external state history is dependent at most on the statistical properties of the internal climate ensemble, and not on the detailed properties of an individual realization.

The problem of designing a numerical model of climate change therefore becomes twofold. First, we must devise a statistical model for the internal system that will provide reliable information on at least the first and second moments of the climate ensemble, and second, we must devise a dynamical model of those parts of the exterior system, such as the ocean circulation and snow and ice cover, that are influenced by the average behavior of the internal system as given by its statistical model. It will be the coupling of these two submodels that will provide a complete numerical model for studying climate change.

THE INTERNAL SYSTEM

The most ambitious models of the internal system constructed to date have been the atmospheric general-circulation models (GCM's). These have not been statistical models as such, but rather dynamical models following individual realizations, from which statistical information has been extracted by time-averaging. Such models have been run for simulated times of the order of a year, at great expense in computer time, and are proving to be quite successful in their ability to reproduce the observed first- and second-moment statistics of the real atmosphere.

A statistical model of the atmosphere is used in order to avoid the laborious computation of a rapidly changing individual realization by computing directly the slowly-changing moment statistics characterizing the climate ensemble. A statistical model is usually approached through a moment-expansion procedure based on the underlying dynamics equations, and here one runs up against the closure problem. The quadratic nonlinearity, arising in particular from the advection terms in the dynamics equations, leads to a dependence of the evolution of the moments of a given order on the value of moments of one higher order. We must close this otherwise infinite hierarchy of moment equations by making a closure approximation which relates a moment of some order to others of lower order.

A simple approach to this problem has been to seek a closure after the first moment (or mean

equations for the atmosphere) by relating second-moment quantities (such as eddy transports) to first-moment quantities (such as mean temperature gradients) through various combinations of ingenuity, physical intuition, and empiricism. This approach, sometimes called parameterization, has been seriously complicated by the somewhat two-dimensional nature of the atmosphere with its associated counter-gradient eddy transports, but it has led already to a number of reasonable statistical models, while closure on the next higher level is still under development.

The closure problem on a higher level has been dealt with at some length for the far simpler but analogous problem of devising a statistical model for solutions of the Navier-Stokes equations, that is, for turbulence models. For the simplest possible case of homogeneous isotropic turbulence, both two- and three-dimensional, there now exist closures after the secondmoment equation in spectral representation that have been compared to direct numerical simulations and found to be reasonably good. Promising results have also been obtained for three-dimensional inhomogeneous turbulence in a grid-point representation with equations for the evolution of local second moments. But much remains to be done to convert these simple results for turbulence into a reliable closure scheme for a statistical model of the atmosphere.

The essential problem in devising a model for the climate ensemble is not that we do not know what the underlying probability-evolution equations are, but rather that we must find the best approximate solutions to these equations with the limited computing power available to us. A key question therefore is how few degrees of freedom N are needed to describe the climate adequately. There are several reasons to believe that this may be of order N = 100 rather than the 100,000 found in some full-fledged GCM's. For example, studies with empirical orthogonalfunction expansions have been able to account for most of the observed variance of the temperature and geopotential height fields with about 100 functions, and it is known that most of the horizontal eddy transport is effected by the largest scales of motion. The use of the smallest possible N is particularly important in schemes that include equations for second moments of which, in general, there are N(N+1)/2. Although the second-moment matrix for any particular

ensemble could be diagonalized (reducing the number of non-zero elements to N) by the use of an empirical orthogonal-function base, we cannot count on its remaining in diagonal form when we are studying climate change. Incidentally, the reason, that the turbulence problem has been so relatively tractable is that the symmetries of homogeneity and isotropy have tremendously reduced the number of equations involved.

THE EXTERNAL SYSTEM

Most aspects of the design of a dynamical model of the external system are quite straightforward, and have been considered at length in the design of GCM's. The treatment of snow and ice, for example, involves relatively simple budget equations. The greatest practical problem seems to be posed by the proper design of an ocean-circulation model. What is needed, of course, is a dynamical model for the slowly evolving ocean circulation that in many ways is analogous to an atmospheric model. But designing a model of the circulation for the ocean is far more difficult than designing one for the atmosphere, because of the far greater range of important space and time scales. Important transport is carried in narrow boundary currents, the Rossby deformation scale is smaller so that relatively more kinetic energy is found at the 100 km scale than in the atmosphere, and there seems to be a continuum of important time scales from weeks in the surface layers to millennia in the abyss. Unfortunately, there seems to be no way to avoid the necessity for an ocean model as part of a climate model. It is known, for example, that the poleward heat transport in the oceans is as important to the global energy balance as that in the atmosphere, and also that the ocean surface temperature is a dominant external influence, through sensible and latent heat transfer, in determining the behavior of the atmosphere.

Although other aspects of the physical interaction between the internal and external systems require further refinement, none of them seems to pose specifically numerical problems as severe as those of an ocean model. The treatment of solar and terrestrial radiation transfer, for example, is quite reliable already in clear air; aerosols present more of a problem here, especially the most common and erratic aerosol of all, made up of cloud water droplets.

PRESENT AND FUTURE MODELS

The simplest climate models have involved only a few degrees of freedom and have been used to describe the globally averaged heat balance. Important as these have been in establishing gross constraints, they are unsatisfying in their lack of detail. The next level of complexity is found in zonally symmetric models, in which it is assumed that climate statistics are homogeneous in the longitudinal direction. Most present zonal models involve closure after the first moment or mean equations, and a natural direction for future work is the extension of these to include equations for the evolution of second moments, such as eddy kinetic energy and eddy poleward transport. It may turn out, however, that the improvement arising from such a higherlevel closure will not be great enough to be worth the extra computation, considering the inherent limitations in zonal models.

It seems unlikely that a climate model will be truly satisfactory unless it can describe the inhomogeneous climate arising from continentality and non-zonal ocean surface temperatures. Our goal, then, should be the construction of a three-dimensional model that includes a statistical version of an atmospheric GCM and a dynamical model of the wind-driven and thermohaline circulation of the oceans. As has been pointed out already, the design of these two components faces major difficulties, and one can only guess at how they might be overcome.

STATISTICAL ATMOSPHERIC MODEL

The starting point for development of a statistical atmospheric model should, of course, be any present dynamical GCM which is already known to be simulating the atmosphere well. Such models have, in fact, a statistical component in them at present, in that various eddy viscosity and diffusion prescriptions are used to simulate the average influence of small unresolved scales of motion on the larger scales that are explicitly computed. In recent years, increases in available computing power have permitted an increase in model resolution, so that the details of the eddy-diffusion process have become relatively unimportant. But the way to a statistical model lies in the reversal of this process with the development of coarseresolution models and a more careful treatment of the statistical influence of unresolved scales. We know that eddy-diffusion terms by themselves are inadequate because they do not preserve the statistical properties of the system, as indicated by, for example, the deficiencies in the energy spectrum for earlier coarse-mesh models. Here an interesting possibility is suggested by our experience with turbulence models: namely, that in addition to an eddy viscosity term there should also be introduced a random eddy forcing term, and that a combination of viscous damping and random forcing may better simulate the statistical influence of unresolved scales of motion.

In any case, the task will be to reduce a GCM to a minimum number of degrees of freedom while preserving its time-averaged statistics. If successful, we shall have a model with enough scales of motion resolved to characterize the mean fields and to provide enough covariances for determining most of the eddy transports. The unresolved scales will be assumed to have vanishing means and be characterized at most by variance and covariance spectra.

The final step will be to convert our loworder dynamical model into a purely statistical one for computing means and covariances of the resolved scales. This might be accomplished with a second-level closure of moment-expansion equations of the sort used in stochastic dynamic forecasting models. Since the low-order dynamical model can be computed relatively rapidly, we must always consider the simple alternative of a Monte Carlo approach, by which statistics are obtained from a combination of time- and sample-ensemble averaging. Such in fact was the approach of the most ambitious climate model run to date at the Geophysical Fluid Dynamics Laboratory (GFDL), in which time-averaged statistics taken from single runs of a full atmospheric model were used to drive a deterministic oceanic model which in turn provided changing external influences on the atmospheric model.

DYNAMIC OCEANIC MODEL

The development of a reliable oceaniccirculation model seems to be more straightforward but could, in fact, turn out to be far more difficult. Principally because of the difficulty of acquiring adequate observations, the state of knowledge of the oceanic circulation is primitive compared to that of the atmosphere. What observations do exist suggest that the problem of treating small spatial scales statistically will be more severe. It is to be hoped that the techniques worked out for the atmosphere will be applicable here. An additional difficulty will arise when we become interested in climate change over very long time scales, for then we will want to shift some of the more rapidly fluctuating oceanic motions into the internal system, and the boundary between the internal and external systems will become harder to define.

It is evident that the computing power required for oceanic models is at least as great as it is for atmospheric models. There is, fortunately, rapidly increasing interest and involvement in oceanic-circulation models in a number of oceanographic research centers, stimulated in large part by observational programs such as MODE and NORPAX.

LINEAR SENSITIVITY THEORY

One of the first uses of any statistical model of the internal system is the determination of small changes in internal statistical properties in response to small changes in external parameters. For sufficiently small changes about the present climate we would expect a linear analysis to be appropriate, and in mathematical terms the problem becomes one of determining a response matrix whose elements are sensitivity coefficients. Of course, for larger changes second-order effects will become important and a linear analysis is inadequate, but many questions of climate stability could be answered from a knowledge of the linear-response matrix.

A key question here is how resistant climate means are to being changed by incremental external forcing. In the case of a Maxwell-Boltzmann equilibrium distribution for a dynamical system with N degrees of freedom, the fluctuation-dissipation theorem of statistical mechanics provides the following answer: If a small forcing term δf_{α} is added to the dynamical evolution equation for a mode u_{α} , i.e., $\dot{u}_{\alpha} = Q_{\alpha}$ $(u_1, \ldots, u_N) + \delta f_{\alpha}$, then the shift in the mean $\mu_{\alpha} = \langle u_{\alpha} \rangle$ will be $\delta \mu_{\alpha} = \tau_{\alpha} \delta f_{\alpha}$, where $\tau_{\alpha} = \sigma_{\alpha} \delta f_{\alpha}$

 $\int_0^\infty R_\alpha(\sigma) d\sigma$ and $R_\alpha(\sigma)$ is the time- σ -lagged correlation coefficient for the mode u_α . The climate ensemble is not a Maxwell-Boltzmann ensemble, but experience with such nonequilibrium distributions in turbulence theory suggests that the fluctuation-dissipation theorem continues to provide a fair approximation. Since for many meteorological variables we know that $\tau_\alpha \approx 3$ days, we can make a rough estimate that the stabilizing influence of the nonlinear dynamics is such that an external influence perturbs the climate mean of a meteorological variable by the amount that the latter would change in about three days if it were not coupled to the rest of the system.

NOISE IN FINITE TIME AVERAGES

The advantage in using an ensemble-average definition of climate properties has been described already, and is that such properties are then slowly changing and free from the day-today fluctuations of individual realizations. But the real atmosphere is, of course, only one member of the ensemble, and the usual operational definition of climate is based on finite time averages of this single realization. From sampling-theory considerations, we know that finite time averages of a random time series have random fluctuations about the ensemble average, with a standard deviation given asymptotically by $\sigma_T = \sigma(T_0/T)^{1/2}$, where T is the averaging time, $T_0 = \int_{-\infty}^{\infty} R(\tau) d\tau$ is an effective independence time, and σ and $R(\tau)$ are the standard deviation and time-\u03c4-lagged correlation, respectively, for the time series.

Since To is about six days for many atmospheric variables, we see that, for example, a 90-day seasonal time average will have a fluctuation about the ensemble mean of about onequarter of the daily fluctuation. Inasmuch as the detailed daily fluctuations are known to be unpredictable in that time range, so also must the related fluctuations in the seasonal mean be unpredictable, and thus may properly be called noise in the communication-engineering sense. In contrast, the slowly-changing ensemble mean we may call a signal which we may hope to be able to predict through the use of climate models. The practical value of such predictions will depend in the usual way, of course, on the ratio of signal to noise.

POTENTIAL PREDICTABILITY OF CLIMATE FLUCTUATIONS

The question of the potential predictability of climate fluctuations can also be approached through an examination of frequency spectra of atmospheric variables. Observations indicate that the time series of weather fluctuations of meteorological variables, such as temperature, seems to be reasonably well modeled by a first-order Markov process with time-7-lagged correlation $R(\tau) = \exp(-\nu/\tau/)$ characterized by a constant decay rate ν of the order of 0.3 day-1. The corresponding power spectrum as a function of frequency ω is given by $P(\omega) = A/(\nu^2 + \omega^2)$ where A is a constant. As $\omega \rightarrow 0$ for such a spectrum we have $P(\omega) \rightarrow A/\nu^2$, a constant, and the spectrum appears white at its low-frequency end. There is thus some contribution to fluctuations at any frequency, no matter how low, by the fluctuations of the weather.

We may pose then some key questions for climate studies. What parts, if any, of climate fluctuations are potentially predictable, and not just the unpredictable statistical fluctuations of unpredictable weather? In a power spectrum analysis is there extra potentially-predictable power above the white, low-frequency end of the

daily weather fluctuations? Is it possible (although it seems highly unlikely) that some long-term compensation process might depress the real weather spectrum below its white extension to $\omega = 0$?

Answers to such questions require detailed examination of lagged correlations and of power spectra. A preliminary study of Manley's 250-year record of monthly mean temperatures in central England shows small lagged correlations significantly above that of weather out to about six months, small but probably significant lagged correlations at two and four years, and a generally white spectrum with evidence of extra spectral power for periods of a few decades and longer. The six-month lagged correlation may well be a reflection of North Atlantic sea-surface-temperature anomalies, and the two-year period is the quasibiennial oscillation which has shown up in many other records.

Although this preliminary study does not provide much hope for, say, a clearly useful forecast of seasonal climate a year in advance, such studies should be continued, with statistical tests being made not only of the pessimistic null hypothesis that nothing is predictable, but also of hypotheses that are framed more optimistically.

OZONE PRODUCTION AND TRANSPORT WITH THE UCLA GENERAL-CIRCULATION MODEL

YALE MINTZ AND MICHAEL SCHLESINGER*

Department of Meteorology University of California Los Angeles, California

ABSTRACT: Ozone production and transport are calculated with a three-dimensional troposphericstratospheric general-circulation model in which the circulation, radiational heating, and ozone photochemistry are fully coupled and interactive. Some results are presented from the early part of a calculation for the northern-hemisphere winter season.

Early in 1971, the UCLA general-circulation research group began development of a global atmospheric general-circulation model whose upper boundary is the stratopause. The motivation was the need for a model which explicitly simulates the large-scale three-dimensional motions of the stratosphere as well as the troposphere, and which has ozone as a prognostic variable. A grant from the Department of Transportation's Climatic Impact Assessment Program, in addition to the longer-term support by the National Science Foundation Atmospheric Sciences Section and the NASA Goddard Space Flight Center Institute for Space Studies, enabled us to develop such a model. To our knowledge, this is the only three-dimensional global general-circulation model in which the circulation, radiational heating, and ozone photochemistry are fully coupled and interactive.

A detailed account of the design of the model is given in the Workshop Notes on The UCLA Atmospheric General Circulation Model (Arakawa and Mintz, 1974). Here we present only a brief description of the model and some results from the early part of a calculation for the northern-hemisphere winter season.

DESCRIPTION OF THE MODEL

Variables of the Model

The primary prognostic variables of the model are horizontal velocity, temperature, and surface pressure, governed respectively by the

horizontal-momentum equation, the thermodynamic-energy equation, and the surfacepressure-tendency equation. With appropriate boundary conditions, these so-called "primitive equations" form a closed system for an atmosphere that is adiabatic and frictionless.

But the general circulation of the atmosphere is the large-scale thermally driven motion, with frictional dissipation, in which there are strong interactions between the heating field and the motion field. Therefore, a number of auxiliary prognostic variables, with corresponding governing equations and appropriate boundary conditions, must be added to simulate the heating. The most important of these auxiliary prognostic variables is water vapor, which is governed by the water-vapor continuity equation. Because the source and sink terms in the water-vapor continuity equation and in the thermodynamic-energy equation greatly depend on sub-grid-scale cumulus convection, the UCLA model has a parameterized penetrative cumulus convection which interacts with a parameterized planetary boundary layer. The planetary boundary-layer depth, and the magnitudes of the temperature discontinuity and moisture discontinuity at the top of the boundary layer, are prognostic variables of the model.

Because there can be an appreciable diurnal heat storage in the ground, because water stored in the ground can be a significant source of water vapor for the atmosphere, and because snow lying on the ground can have a large influence on the surface albedo and also be a significant

^{*}Mr. Schlesinger is also affiliated with The Rand Corporation in Santa Monica, California.

water-vapor source, the ground temperature, ground-water storage, and mass of snow on the ground are prognostic variables of the model, governed by energy- and water-budget equations for the ground.

Because it strongly influences the radiational heating of the stratosphere, ozone was made a prognostic variable of the model, governed by an ozone continuity equation with parameterized sources and sinks.

In addition to the prognostic variables, the model has many diagnostic variables (physicalstate variables whose presence and whose magnitudes, rather than whose time rates of change of magnitude, are determined by the governing equations). Among the more important of these diagnostic variables are the different types of clouds, which form with the release of latent heat, and whose presence affects the shortwave and the longwave radiational heating of the air. In the model, any tropospheric layer which is saturated is taken to be filled with cloud. In addition, if the top of the planetary boundary layer is saturated it has a sub-layer of stratus cloud. Furthermore, if the parameterized cumulus convection has penetrative cumulonimbi which detrain at levels higher than 400 mb, the layer in which the detrainment takes place is taken to be filled with cloud. For the radiation calculations, clouds warmer than -40°C are taken to be water-droplet clouds, and clouds colder than -40°C are taken to be ice-crystal clouds.

Physical Processes

In addition to the three-dimensional gridscale transports of the prognostic variables, the sources and sinks of the variables are calculated according to the governing physical processes.

For the prediction of the horizontal velocity, the horizontal momentum equation has, in addition to the pressure-gradient force and coriolis force, a frictional force which is made to depend on a frictional drag at the surface of the earth with sub-grid-scale vertical eddy flux of horizontal momentum within the planetary boundary layer, and on a sub-grid-scale vertical eddy flux of horizontal momentum within the free atmosphere which is a function of the parameterized cumulus convection.

For the prediction of temperature, the heating term in the thermodynamic energy equation

consists of a solar and infrared radiational heating, a sensible heat flux across the earth's surface with a sub-grid-scale vertical eddy flux of heat and a release of heat of condensation within the planetary boundary layer, a sub-grid-scale vertical eddy flux of sensible heat and release of heat of condensation by the parameterized cumulus convection, and a heating by large-scale condensation and a cooling by evaporation of the falling raindrops.

For the prediction of water vapor, the source (and sink) term in the water-vapor continuity equation consists of an evaporation at the earth's surface with a sub-grid-scale vertical eddy flux of water vapor within the planetary boundary layer, a sub-grid-scale vertical eddy flux of water vapor and condensation by the parameterized cumulus convection, and a large-scale condensation and evaporation.

The planetary boundary layer (PBL) for the UCLA model was originally designed by Deardorff (1972), who parameterized the vertical structure of the PBL by its bulk properties and made its depth a prognostic variable. Subsequently, Arakawa and Randall (see Chapter XI of the Workshop Notes (Arakawa and Mintz, 1974)) made many modifications of this parameterization, the most important of which are the addition of the jumps of moisture and moist static energy at the top of the PBL as prognostic variables, the interaction of the PBL with the cumulus ensembles, and the inclusion of boundary-layer stratus clouds.

The parameterization of cumulus convection that was used in the earlier UCLA models has been replaced by a new scheme, based on the theory of Arakawa and Schubert (1974). In the new scheme (see Chapter X of the Workshop Notes), the cumulus-cloud ensemble interacts with the subcloud planetary boundary layer as well as with the cloud environment above the PBL. The scheme predicts the spectral distribution of the cumulus cloud types in quasi-equilibrium with the large-scale processes. The parameterized cumulus convection produces sub-grid-scale vertical transfers of heat, moisture, and horizontal momentum.

The basic radiation parameterization scheme, described in Chapter XV of the Workshop Notes, is a modification of the scheme developed by Katayama (1972) for the UCLA tropospheric models. This scheme treats the

transfers of both solar and longwave radiation. For the solar radiation the effects of clouds, water-vapor absorption, and molecular scattering are included. For the longwave radiation, the emission and absorption by water vapor and carbon dioxide are included, and the clouds are treated as effective black bodies. Since the documentation in the Workshop Notes, the scheme has been extended to include the radiative effects of ozone, and has been modified to treat the absorption of near-infrared solar radiation by large optical paths of water vapor, and the absorption and emission of longwave radiation by small optical paths of carbon dioxide (Schlesinger, 1976b).

Ozone production and transport have also been added to the model (Schlesinger, 1976b). The production of ozone is based on a photochemical model comprised of the Chapman reactions

$$O_2 + h\nu \xrightarrow{j_1} 2O$$
,
 $O + O_2 + M \xrightarrow{k_1} O_3 + M$,
 $k_1 = 6.6 \times 10^{-35} \exp(510/T)$,
 $O_3 + h\nu \xrightarrow{j_2} O_2 + O$,
 $O + O_3 \xrightarrow{k_2} 2O_2$,
 $k_2 = 1.9 \times 10^{-11} \exp(-2300/T)$,

and the NO-NO2 catalytic cycle

NO + O₃
$$\stackrel{k_3}{\rightarrow}$$
 NO₂ + O₂,
 $k_3 = 9 \times 10^{-13} \text{ exp } (-1200/\text{T}),$
NO₂ + O $\stackrel{k_4}{\rightarrow}$ NO + O₂,
 $k_4 = 9.1 \times 10^{-12},$
NO₂ + h $\nu \stackrel{j_3}{\rightarrow}$ NO + O,

where the photodissociation rates j; are

$$j_{i}(z) = \int_{0}^{\infty} \alpha_{\lambda,i} I_{\lambda,\infty}$$

$$\cdot \exp \left[-\sec \zeta \sum_{k} \alpha_{\lambda,k} \int_{z}^{\infty} n_{k}(z) dz \right] d\lambda.$$

Here $I_{\lambda\infty}$ is the extraterrestrial monochromatic photon flux per unit wavelength, $\alpha_{\lambda,i}$ is the absorption cross-section of species i at wavelength λ , $n_k(z)$ is the number density of species k at altitude z, ξ is the solar zenith angle, and the summation extends over all species k that absorb in the spectral region where species i photodissociates.

The distribution of NO₂ is prescribed. It varies only in the vertical, following the profile calculated by McElroy et al. (1974) but with absolute concentrations reduced by 43.5% (for the reason given below).

The photochemical ozone production is calculated only in the layers above 100 mb because below 100 mb the production rate is small. The photodissociation rates $j_i(z)$ are computed by a linear bivariate table interpolation. The destruction of ozone at the earth's surface, due to heterogeneous chemical reactions, is parameterized following Cunnold et al. (1975).

The transport of ozone by the horizontal wind components is calculated with a space-centered scheme. For a down-gradient transport, an arithmetic mean of the two ozone mixing ratios is used; for an up-gradient transport, a harmonic mean is used. This eliminates the spurious generation of negative ozone mixing ratios due to time truncation error. The scheme has a generally diffusive character because, for given ozone mixing ratios and mass transport, the ozone transport is greater with the arithmetic mean than with the harmonic mean; however, the computational diffusion is small because the horizontal gradient is small.

The transport of ozone by the vertical velocity is calculated with a space-centered scheme which is based on the conservation of the global integral with respect to mass of the logarithm of the ozone mixing ratio (Schlesinger, 1976b). This is done because the extremely large vertical gradient of ozone makes it undesirable to

use the arithmetic/harmonic-mean scheme, which is diffusive.

Prescribed Parameters

The prescribed parameters of the model are:

- Radius, surface gravity, and rotation speed of the planet
- Solar constant and orbital parameters of the planet
- Total atmospheric mass
- Thermodynamic and radiation constants
- Geographical distributions of open ocean, ice-covered ocean, ice-free land, and land covered by glacial ice
- Surface elevation
- Surface roughness
- Thickness of the sea ice
- Ocean surface temperature
- Distribution of NO₂.

For the present study, the prescribed oceansurface temperature is the observed annual mean ocean-surface temperature. Ice-free ocean is assigned an albedo of 0.07, and the sea ice and snow-free glacial ice an albedo of 0.40. The albedo of the predicted snow cover is taken as 0.65 when the snow is colder than its melting temperature, and as 0.50 when it is at its melting temperature. For snow-free land, the albedo is made to vary with the amount of water in the plant-root zone of the soil: from an albedo of 0.28 where there is no evapotranspirationavailable soil water, to an albedo of 0.12 where the soil water is equal to or exceeds one-third of the maximum amount of evapotranspirationavailable water that the soil can hold (which is taken as 15 gm of water/cm²). This dependence of the surface albedo on the water stored in the soil simulates the dependence of surface albedo on vegetation cover. It is intended to be a simple parameterization of the feedback of the biosphere to climate.

Vertical Structure of the Model

Figure 1 shows the vertical structure of the model. The lower boundary follows the earth's topography, where surface pressure is defined. The upper boundary is the 1-mb pressure surface

and is approximately at the height of the stratopause (about 50 km). The model atmosphere is divided into twelve layers; the boundaries of these layers follow the coordinate surfaces of a generalized σ -coordinate. From 100 mb upward, these coordinate surfaces are also constant-pressure surfaces. The lowest four layers have equal depth in pressure p, and the uppermost seven layers have equal depth in log p. The broken lines in the figure show the levels at which the prognostic variables of horizontal velocity, temperature, water vapor, and ozone are carried for each of the layers. These levels are centered in p for the layers below 100 mb, and in log p for the layers above 100 mb.

Z(km)		p(mb)
48.5		- 1.00
****	(SPONGE LAYER)	- 1.39
43.0		1.93
		2.68
38.0 —		- 3.73
		- 5.18
33.4 —		- 7.20
	STRATOSPHERE	- 10.0
29.0 —	O THE THE TENE	- 13.9
		- 19.3
24.7 —		- 26.8
20.5		- 37.3 - 51.8
20.5		- 720
16.3 —		- 100
10.3		
12.0		- 150.
12.0		- 200
8.0 —	TROPOSPHERE	- 300. - 400.
4.5	- Automatical Control	600.
0.0		800 .

Figure 1. Vertical structure of the model. The prognostic variables of horizontal velocity, temperature, water vapor, and ozone are carried on the σ-surfaces shown by the broken lines.

The top layer of the model, called the "sponge layer", has a damping term designed to absorb upward-propagating wave energy and thus prevent spurious reflections of wave energy at the upper boundary.

Figure 2 shows the lowest five layers of the model. The parameterized planetary boundary layer, whose depth varies in space and time,

may contain stratus cloud. Above the PBL there may extend a cumulus-cloud ensemble. The boundary-layer depth may be less than, equal to, or greater than one or more of the model layers.

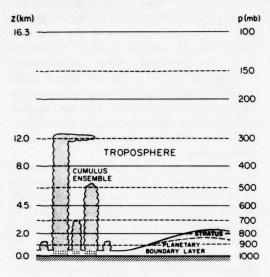


Figure 2. The lowest five layers of the model, showing the parameterized planetary boundary layer which may contain stratus cloud and above which there may extend a cumulus-cloud ensemble.

Horizontal Coordinates, Grid Size, and Time Step

The horizontal coordinates are longitude and latitude. The grid size is 5° of longitude and 4° of latitude, which makes the two linear grid distances equal at 37° latitude. To avoid having to use an extremely short time step because the meridians converge toward the poles, selected terms in the prognostic equations are longitudinally averaged (Schlesinger, 1976a). The basic time step is 6 minutes, but the source and sink terms and the vertical advection of water vapor and ozone use a time step of 30 minutes.

Mathematical Aspects of the Model

Arakawa (1970; see also the Introduction to the Workshop Notes (Arakawa and Mintz, 1974)) developed the principle that the statistical properties of the finite-difference solution of the governing equations of atmospheric motion will approximate those of the continuous solution if the important integral constraints are maintained. The integral constraints that are maintained by the UCLA model are: conservation of total mass, conservation of total kinetic energy during inertial processes, conservation of enstrophy (mean square vorticity) during vorticity advection by the nondivergent part of the horizontal velocity (on a plane), the integral constraint on the pressure-gradient force, conservation of total energy during adiabatic and non-dissipative processes, and conservation of total entropy and total potential enthalpy during adiabatic processes.

In this model, the distribution of the variables over the horizontal grid points was changed to the scheme which best simulates inertiagravity waves and the geostrophic adjustment process (Workshop Notes, Chapter V, Section I). Consequently, solutions with this scheme are free from the highly non-geostrophic computational noise which commonly exists in solutions obtained with other schemes.

In addition, the extension of the model to the stratopause required a change from the previous vertical differencing scheme. The new scheme is superior, when the stratosphere is included, because it has an integral constraint on the distribution of total entropy and a very accurate finite-difference hydrostatic equation (Workshop Notes, Chapter II, Section 5, and Chapter III, Section 8). Furthermore, an analytical study showed that the new vertical differencing scheme, when applied to levels equally spaced in log p, guarantees that the vertical wavenumber of a planetary wave, for a given equivalent depth, is constant in height for an isothermal atmosphere, just as it is in the continuous case. This is one of the important advantages of the model: namely, that there will be little or no spurious internal reflection of vertically propagating wave energy due to the discretization (Workshop Notes, Chapter IV, Section 4).

RESULTS

Initialization

The prognostic variables of this tropospheric-stratospheric model were initialized in the following way. For the σ -surfaces below 100 mb, the horizontal velocity, temperature,

and water-vapor mixing ratio were obtained by a vertical interpolation of these fields from a day at the beginning of December which was the result of a long integration that had been made with the UCLA three-level tropospheric model. The surface pressure, ground temperature, ground-water storage, and mass of snow on the ground were also taken from the three-level model results for that day. (The initial state for the integration of the three-level model was one in which the temperature field was threedimensionally isothermal, the velocity was zero everywhere, the surface pressure was everywhere equal to the global mean surface pressure, and there was no water vapor in the air, no water stored in the ground, and no snow on the ground.) For the o-surfaces above 100 mb, the initial temperature for the tropospheric-stratospheric model was taken to vary only with pressure, according to the mid-latitude spring/fall profile of the 1966 U.S. Standard Atmosphere. The initial horizontal velocity above 100 mb was set equal to the geostrophic velocity (except at the equator, where it was made equal to the mean of the velocities at 4°N and 4°S). The initial watervapor mixing ratio above 100 mb was taken as zero. Because the residence time of atmospheric ozone is very long, the ozone mixing ratio was initialized from the observed zonal-mean ozone number density, on the basis of the Ozone Data for the World for December (1960-72) and on the initial air density of the model. The initial sun declination and distance were taken for the beginning of December. The prescribed NO2 profile was taken from McElroy et al. (1974).

Several times during the first 60 simulated days of the integration, small programming and coding errors were detected and corrected. At these times the sun's declination and distance were set back some days (re-initialized), but no re-initialization was made of the prognostic variables.

By Day 60, however, it was clear that a large error was being produced in the ozone field as a result of our original formulation for the vertical ozone transport, which was the arithmetic/harmonic-mean scheme. That scheme was producing a large, computationally false, net downward transport of ozone. To correct this computational error, the above-described logarithmic scheme was designed. The logarithmic

scheme was introduced on Day 60, and at that time the ozone number density was re-initialized to what it had been on Day 0. A lower bound of $0.04 \,\mu g$ O_3/g air was set for the re-initialized ozone mixing ratios for the levels below 400 mb, following the observations of Hering and Borden (Wu, 1973). The magnitude of the prescribed NO_2 profile was reduced by 43.5% in order to make the calculated global photochemical ozone-production rate on Day 60 the same as the rate of the surface destruction of ozone given by Tiefenau and Fabian (1972). The sun's declination and distance were set back, for the last time, to December 20, near the northern-hemisphere winter solstice.

The integration has now reached a total of 76 days (January 5), which is 16 days since the ozone was re-initialized. This is not long enough for the model atmosphere to have reached its statistically-steady equilibrium state: neither in its production and transport of ozone, nor for such slow dynamical processes as the upward propagation of wave energy through the stratosphere. As computer time becomes available (the model requires three hours of IBM 360/91 computer time per day of simulated time), we will continue with the integration until the equilibrium state is reached, and will analyze and publish those results. But to make the potentialities of the model more widely known through this CIAP publication, we are presenting here the results already obtained.

Zonally-Averaged Temperature and Circulation

Figures 3 and 4 show meridional crosssections and vertical profiles of the zonallyaveraged simulated temperatures, averaged for the last two days of the 76-day integration, together with the observed normal temperatures for Dec-Jan-Feb, according to Newell et al. (1972). In the cross-section of the observed field, the vertical scale is linear with height and the field is shown up to the 31-km (10-mb) level. In the cross-section for the simulated field, the vertical scale is linear in pressure between 1000 mb and 200 mb, and is linear in log p between 100 mb and 1 mb, which is the top of the model (at about 48 km).

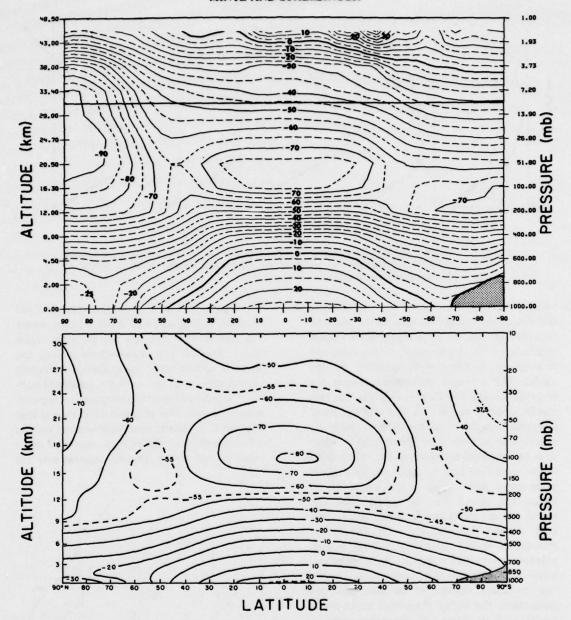


Figure 3. Meridional cross-sections of the zonally averaged temperature. Top: simulated temperature, averaged for the last two days of the integration (Jan 4-5). Bottom: observed normal temperature for Dec-Jan-Feb (from Newell et al., 1972), Units: degrees Celsius.

One can draw only zeroth-order conclusions from a comparison of the simulated and observed fields that are shown here, because the model atmosphere has not reached its statistically-steady equilibrium state and because, for those fields in which there are large time variations, the comparison of a short-term mean (a two-day

average) with a long-term mean (the seasonal normal) may involve a large sampling error.

Comparing the gross features of the simulated and the observed fields that are shown here, one may say that the 3-level and then the 12-level model atmosphere evolved from an extremely unrealistic initial state into a state

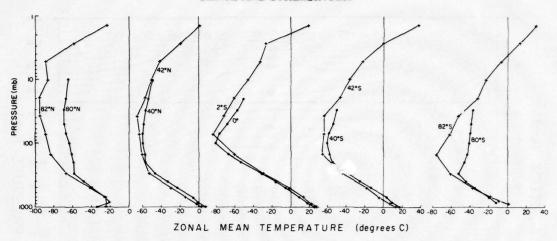


Figure 4. Vertical profiles of the zonally averaged temperature, Crosses: simulated temperature, averaged for the last two days of the integration. Circles: observed normal for Dec-Jan-Feb (from Newell et al., 1972).

which correctly reproduces the zeroth-order features of the real atmosphere. In the temperature cross-section, shown in Figure 3, the general structure of the troposphere, tropopause, and stratosphere is fairly well simulated by the model. The principal difference between the observed normal for Dec-Jan-Feb and the two simulated days, Jan 4-5, is that the simulated temperature in the upper troposphere and lower stratosphere at both poles is about 20°C colder than the observed temperature. An examination of the wind field (see, for example, the 500-mb geopotential height map in the lower part of Figure 12), shows that, up to this time, the model has not developed large-amplitude ultralong waves. This indicates that the model atmosphere is not producing a large enough poleward eddy heat transport. Whether largeramplitude long waves will develop as the integration continues remains to be seen. (In this connection, the earlier three-level tropospheric model, with its "rigid lid" upper boundary at 100 mb, developed a strong and permanent ultra-long wave blocking pattern, which also is not correct.) But although the simulated temperature on Days 75-76 is too cold in the upper troposphere and lower stratosphere near the poles, the temperature pattern in the stratosphere, especially in the northern hemisphere, is very similar to what is observed in the period that precedes sudden warming, as shown by Barnett (1974, Figure 8a).

Figures 5 and 6 show the simulated and observed zonally-averaged zonal velocity. Again, the zeroth-order features are correctly reproduced. The fact that the simulated easterly and westerly surface zonal winds are approximately correct shows that the vertically integrated poleward angular-momentum transports are approximately correct. The principal deficiency is that the two tropospheric west-wind maxima and the winter-hemisphere stratospheric west-wind maximum are too strong. This is consistent with the

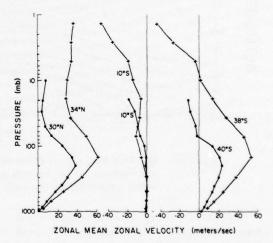


Figure 6. Vertical profiles of the zonally-averaged zonal velocity. Crosses: simulated velocity, averaged for the last two days of the integration, Circles: observed normal for Dec. Jan-Feb (from Newell et al., 1972),

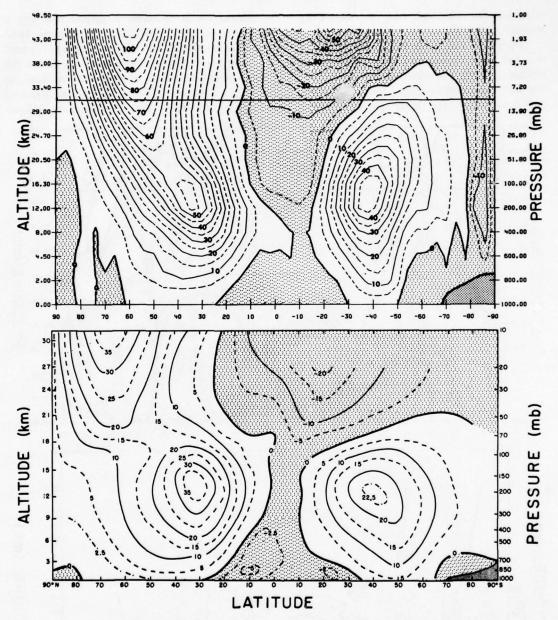


Figure 5. Meridional cross-sections of the zonally-averaged zonal velocity. Top: simulated velocity, averaged for the last two days of the integration (Jan 4-5). Bottom: observed normal for Dec-Jan-Feb (from Newell et al., 1972). Units: meters/sec.

temperature's being too cold in the upper troposphere and lower stratosphere in the higher latitudes of both hemispheres. In the real atmosphere, the three-dimensional jet streams are narrow and have a high speed, but, because these jet streams meander with respect to latitude, the zonal average along latitude circles shows broad

maxima with much lower maximum speeds. The model atmosphere has not yet developed large-amplitude ultra-long waves, so that its jet streams do not meander much; its zonally-averaged west-wind maxima are therefore too narrow and too strong. In the upper stratosphere of the summer hemisphere, the simulated east wind maximum

resembles the observed one, as shown by Murgatroyd (1969).

Figures 7 and 8 show the simulated and observed mean meridional mass circulation and profiles of the zonally-averaged meridional velocity. The zonally-averaged meridional velocity, from which the mean meridional mass

circulation is obtained, is ageostrophic and is therefore very difficult to determine from observations. In fact, Newell et al. (1972) used wind observations directly only to obtain the northern-hemisphere mean meridional mass circulation shown in Figure 7. For the southern hemisphere they used the so-called indirect

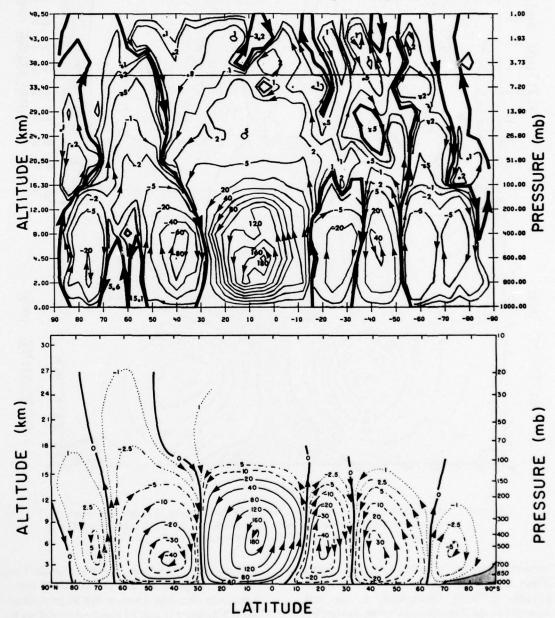


Figure 7. Meridional cross-sections of the mean meridional mass circulation, Top: simulated circulation, averaged for the last two days of the integration (Jan 4-5). Bottom: observed normal for Dec-Jan-Feb (from Newell et al., 1972). Units: 10¹² gm/sec,

method to obtain the mean meridional mass circulation (and from that the corresponding profiles of the mean meridional velocity) as a residual term in the zonal angular-momentum budget. This method, which was first proposed and used by Mintz and Lang (1955), uses the observed poleward eddy angular-momentum flux, which is quasi-geostrophic, plus a number of assumptions, and gives only approximate results. It is remarkable, and most likely coincidental, that the simulated mean meridional mass circulation matches the observed circulation as closely as is shown in Figure 7.

The simulation shows the two tropospheric tropical Hadley cells, with the northern-hemisphere cell broader and stronger and extending across the equator; the two tropospheric middle-latitude Ferrel cells; a direct cell, with a double center, in the higher latitudes of the southern hemisphere; and a complex pattern of direct and indirect cells poleward of the Ferrel cell in the northern hemisphere which does not match the observed field. In the stratosphere, the simulated two-day average shows a complex pattern of mass circulation, especially in the summer hemisphere. In the winter-hemisphere stratosphere, a prominent large-scale feature is

the upward current whose axis crosses the 100-mb and 10-mb levels near 70° north. This current then turns equatorward and, reinforced by flow from the south, descends across the 10-mb level at about 45°N and across the 100-mb level at about 35°N, where it merges with the converging upper branches of the tropospheric Hadley and Ferrel cells. This feature of the simulated stratospheric circulation resembles the one which Vincent (1968) obtained for the winter season, using the angular-momentum budget and observations of the poleward eddy angular-momentum flux in the northern-hemisphere stratosphere. The strong sinking motion of this circulation feature coincides with the temperature maximum in the winter-season middle-latitude lower stratosphere shown in Figure 3.

Preliminary Ozone Results

Figure 9 shows the global photochemical production rate of ozone, the global surface-destruction rate of ozone, and the global-mean total ozone as functions of time. Immediately following the ozone re-initialization on Day 60, the photochemical production rate increased by

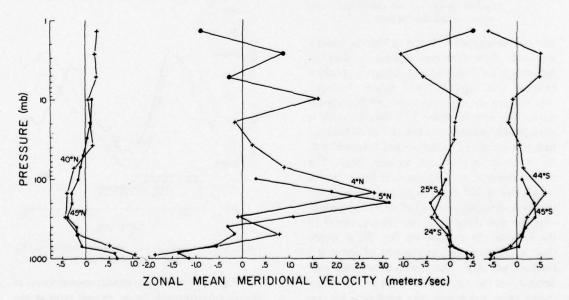


Figure 8. Vertical profiles of the zonally-averaged meridional velocity at the central latitudes of the tropospheric Hadley and Ferrel cells. Crosses: simulated velocity, averaged for the last two days of the integration. Circles: observed normal for Dec-Jan-Feb (from Newell et al., 1972). (The circled crosses denote that the velocity scale must be multiplied by 10.)

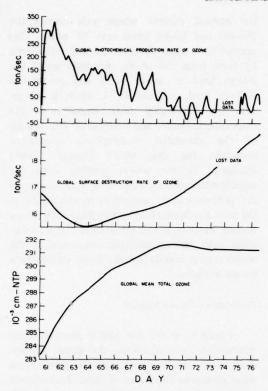


Figure 9. The global photochemical production rate of ozone, the global surface destruction rate of ozone, and the global mean total ozone, as functions of time.

an order of magnitude. It stayed high for about a day and then decreased toward a state of high-frequency oscillations, between positive (source) and negative (sink) values. Averaged over the last six days, the global photochemical production rate is about 13 tons/sec, which is substantially smaller than the rate of 64 tons/sec that was calculated by Brewer and Wilson (1968) for a moist atmosphere without NOx. The surface destruction rate (shown in Figure 9 with a scale that is 100 times larger than the scale for the photochemical production) decreased slightly over the first three days, and then increased to the value of 19 tons/sec on Day 76, at which time it was increasing at the rate of about 0.5 tons/sec per day. The surface-destruction rate depends on the amount of ozone in the lowest model layer, and it may take some time for this to reach equilibrium. The global-mean total ozone increased from the initial value of 283.4 Dobson units (1 D.U. = 10-3 cm-NTP) on Day 60, to 291.7 D.U. on Day 70. It then fell slightly, and has about leveled off at the value of 291.3 D.U. on Day 76. This is about the same as the observed value of 291.4 D.U. $(4 \times 10^{37} \text{ molecules})$ for January 1964, given by Brewer and Wilson (1968).

Figure 10 shows the latitudinal distribution of total ozone at the initial time and averaged over the last two days of the simulation (Days 75-76). The observed distributions for the northern-hemisphere winter (London, 1963) and the southern-hemisphere summer (Sticksel, 1970) are also shown for comparison. During the simulation, in both hemispheres, the total ozone decreased in the high latitudes and increased in the tropics and in the middle latitudes. The large decreases in the polar regions have caused the high-latitude maxima to be displaced equatorward. We suspect that the decrease of total ozone in the two polar regions, which makes the amounts there less realistic now than at the re-initialization time, occurs for the same reason that the temperatures are too cold in the polar regions - namely, the poleward eddy transports of heat and ozone are too small because the model has not yet developed large-amplitude tropospheric and stratospheric ultra-long waves. Whether these transports will become larger as the simulation proceeds remains to be seen.

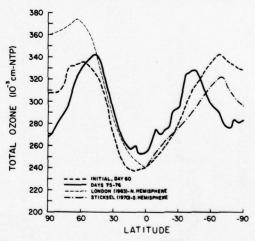


Figure 10. Simulated and observed latitudinal distributions of total ozone.

Figure 11 shows meridional cross-sections of the zonally-averaged ozone mixing ratio at the re-initialization time and averaged over the last two days of the simulation. The observed field for Dec-Jan-Feb from Newell et al. (1974) is also shown. During the simulation, the ozone maximum at 10 mb became more intense and its

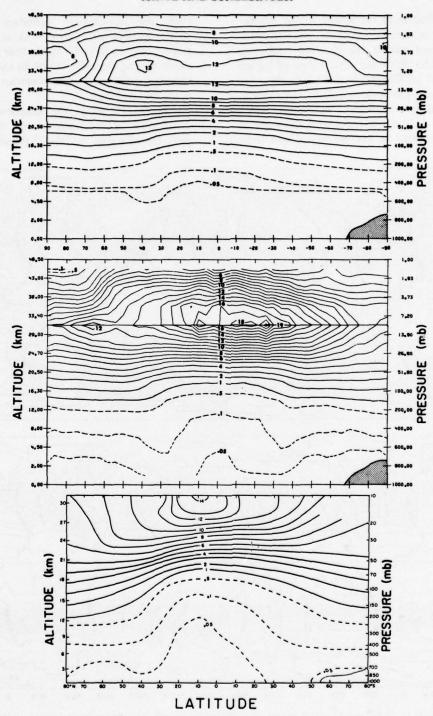


Figure 11. Meridional cross-sections of the zonally-averaged ozone mixing ratio. Top: simulated ozone at the re-initialization time (Day 60).

Middle: simulated ozone averaged for Days 75-76. Bottom: observed normal for Dec-Jan-Feb (from Newell et al., 1974). Units: µg/g.

center shifted from the winter to the summer side of the equator. Although this location of the center is not seen in the observed field from Newell et al. (1974), the observations of Dütsch (1969) and of Krueger et al. (1973) show the maximum on the summer side of the equator. The simulated secondary maximum which developed at 10 mb at 66° N with the value of $12 \mu g/g$ is similar to, but one model level lower

than, the high-latitude secondary maximum shown by Krueger et al. (1973). In the lower troposphere, by Days 75-76, the lines of constant ozone mixing ratio dip closest to the ground in the tropics and subtropics, somewhat as they do in the observed field.

Figure 12 shows the simulated synoptic distribution of total ozone and the 500-mb geopotential height on Day 75 (Hour 21 GMT).

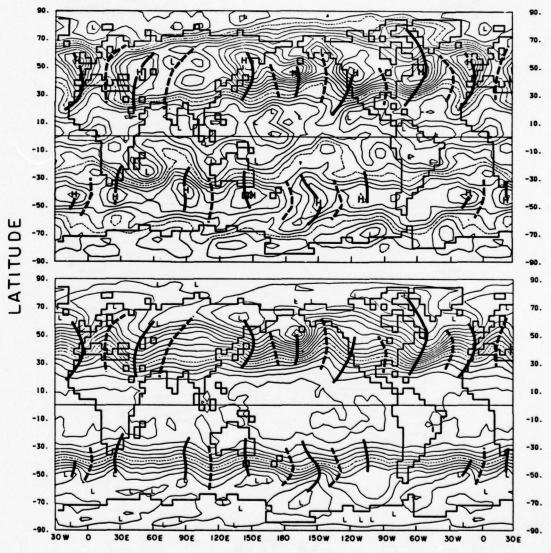


Figure 12. Simulated synoptic distribution of total ozone and 500-mb geopotential height, on Day 75 (Hour 21 GMT) of the integration. Top: total ozone, where the dashed contour line is 290 Dobson units and the contour interval is 10 D.U. Bottom: 500-mb height, where the dashed contour line is 5600 meters and the contour interval is 60 meters. The 500-mb trough lines (solid lines) and ridge lines (dashed lines) are also shown superposed on the field of total ozone.

The significant feature shown here is the pronounced zonal variation of total ozone, especially in the middle latitudes of the northern hemisphere. The differences between adjacent maxima and minima along a latitude circle are of the order of tens of Dobson units and, in some places, are almost as large as the difference between the equatorial minimum and middlelatitude maximum of the zonally-averaged total ozone, shown in Figure 10. The 500-mb geopotential height field shows the simulated baroclinic waves which move slowly eastward. By superposing the trough and ridge lines of these waves on the total ozone field, we see that the maxima and minima of total ozone coincide, respectively, with the trough and ridge lines of the 500-mb waves. It is gratifying that both the amplitude of this zonal variation of total ozone, and its phase relationship to the baroclinic disturbances at 500 mb (and at 300 mb), are precisely what are observed in the real atmosphere, as shown for example by Normand

(1953). Because the model provides complete information on its ozone production and transport, we shall be able to determine the exact reason for this correlation between total ozone and the tropospheric waves.

Figure 13 shows the latitudinal distribution of the vertically integrated photochemical production rate and the surrace destruction rate of ozone, averaged for two days, at four times during the integration. All of the photochemical production-rate curves have the same qualitative character: positive production (source) in the tropics and the southern-hemisphere middle latitudes, negative production (sink) in the high latitudes of the southern hemisphere and middle latitudes of the northern hemisphere, and zero production in the northern-hemisphere polar night. During the simulation, the production rate near the equator and in the lower and middle latitudes of the summer hemisphere became much smaller. As has already been seen in Figure

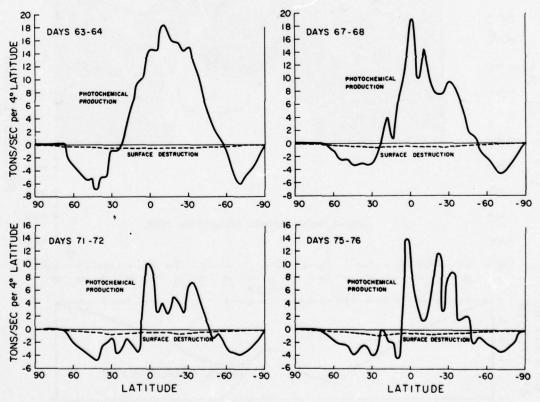


Figure 13. Latitudinal distribution of the vertically integrated photochemical production rate and the surface destruction rate of ozone, averaged for two days, at four times during the simulation.

9, the net global photochemical production rate is small from Day 70 on.

. Figure 14 shows a meridional cross-section of the photochemical ozone-production rate, and a latitudinal profile of the surface destruction rate, averaged for Days 75-76. There is photochemical production of ozone in almost all latitudes in the upper two layers of the model (except in the latitudes of the polar night), and in a tropical zone in the lower stratospheric layers. (No photochemical production of ozone was calculated for the layers below 100 mb in the model.) In the middle latitudes of the winter hemisphere and in the high latitudes of the summer hemisphere, the strength and vertical extent of the sink dominate the overlying source and, as shown in Figure 13, the production rate summed vertically over the atmosphere is negative in these latitudes. The surface destruction rate has maxima near 25°N and 20°S. These are close to the latitudes of the largest rate of ozone transport to the ground.

Figure 15 shows latitudinal profiles of the vertically integrated northward transports of ozone by the mean meridional circulation, $\Sigma[G_{\varrho}]$ [q_{ϱ}], by the zonal eddies, $\Sigma[G_{\varrho}^*q_{\varrho}^*]$, and the total transport, $\Sigma[G_{\varrho}q_{\varrho}]$. Here q_{ϱ} is the ozone mixing ratio in layer ℓ and $G_{\ell} = (2\pi a \cos \theta)$ ϕ) $\Pi v_0 \Delta \sigma_0$, where a is the earth's radius, ϕ is the latitude, II is the normalization pressure used to define the vertical σ -coordinate (99 mb for layers above the 100-mb level and p_s - 100 for layers below the 100-mb level, where p_s is the surface pressure), v_Q is the meridional velocity component in layer ℓ , and $\Delta \sigma_{\ell}$ is the thickness of layer ℓ in σ -space. The summation extends over all model layers. The brackets denote the zonal average, the asterisks denote the local deviation

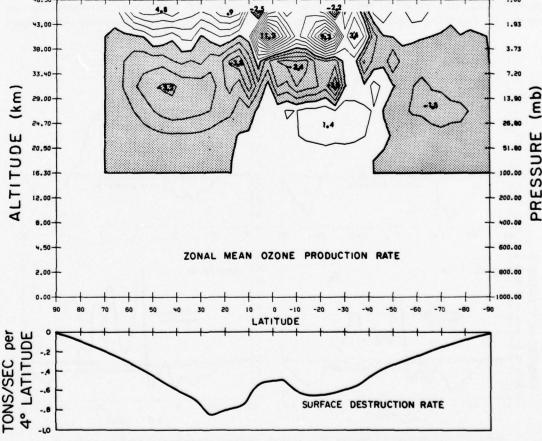


Figure 14. Top: meridional cross-section of the photochemical ozone production rate, averaged for Days 75-76. Units: tons/sec per 4° latitude per model layer. Bottom: latitudinal profile of the surface destruction rate of ozone, averaged for Days 75-76.

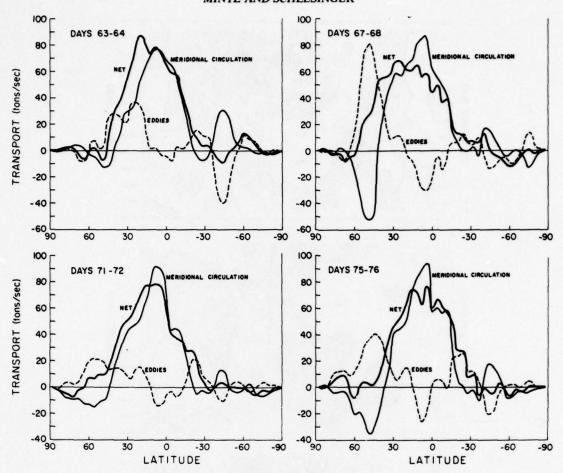


Figure 15. Vertically integrated northward transports of ozone by the mean meridional circulation and by zonal eddies, averaged for two days, at four times during the simulation.

from the zonal average, and the superior bars denote the time average. This model has no horizontal transport of ozone by sub-grid-scale diffusion. The transports shown are two-day averages at four times during the simulation. The transports are highly variable in time. Throughout the period of integration, the transport by the mean meridional circulation dominates in the tropics and carries ozone from the summer hemisphere into the winter hemisphere, with only a weak counter-transport by the eddies. In the middle latitudes of both hemispheres, the two transports have about equal magnitude, with the mean meridional circulation transporting ozone away from the poles and the eddies transporting ozone toward the poles.

Figure 16 shows meridional cross-sections of the northward ozone transport by the mean meridional circulation and by the zonal eddies, and the sum of the two transports, averaged for the last two days of simulation. The direction of the transport by the mean meridional circulation agrees closely with the sign of the time-averaged mean meridional mass circulation shown in Figure 7. This suggests that the so-called "oscillating-cell" component of the ozone transport is small (in this two-day average). The largest transports by the mean meridional circulation are in the tropical stratosphere, and the maxima there are several times greater than the eddy transports.

The northward ozone transport by the eddies, shown in the middle part of Figure 16, also has a complex structure. The eddy transport of ozone is toward the poles in the middle and lower stratosphere and toward the equator in the

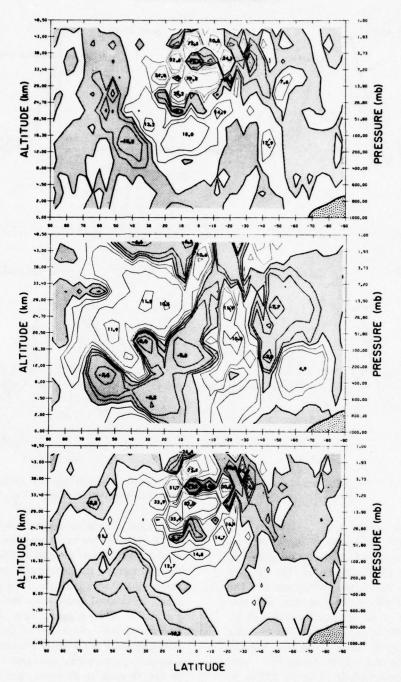


Figure 16. Meridional cross-sections of the northward transports of ozone, averaged over the last two days of the simulation (Days 75-76). Top: northward transport by the mean meridional circulation; contours shown for 0, 5, 10, 20, and 50 tons/sec per model layer. Middle: northward transport by zonal eddies; contours shown for 0, 1, 2, 5, and 10 tons/sec per model layer. Bottom: total northward transport; contours shown for 0, 5, 10, 20, and 50 tons/sec per model layer.

upper and middle troposphere. This distribution is consistent with the known energetics of the atmosphere. In the troposphere, eddy available potential energy is converted into eddy kinetic energy by the poleward-moving (warm) air rising and the equatorward-moving (cold) air sinking, and we expect the sinking air to contain more. ozone than the rising air. On the other hand, in the lower and middle stratosphere, eddy kinetic energy is converted into eddy available potential energy by the poleward-moving (warm) air sinking and the equatorward-moving (cold) air rising, so that the eddy transport of ozone there should be poleward. The vertically integrated eddy transport of ozone, shown in Figure 15, is the small difference between the large poleward eddy transport in the stratosphere and the large equatorward eddy transport in the troposphere.

The total northward ozone transport, shown at the bottom of Figure 16, has roughly the same pattern as the transport by the mean meridional circulation in the tropical latitudes, but in the middle and higher latitudes it is somewhat more like the eddy transport.

Figure 17 shows meridional cross-sections of the vertical transports of ozone by the mean meridional circulation, [S][q], by the zonal eddies, [S*q*], and the total transport, [Sq], averaged for the last two days of the simulation. Here $\dot{S} = (2\pi a \cos\phi) (a\Delta\phi) \Pi \dot{\sigma}$, where $\Delta\phi$ is the angular increment in the meridional direction (4°) , $\dot{\sigma}$ is the vertical σ -velocity, and the other symbols are as defined above. This model has no vertical transport of ozone by sub-grid-scale diffusion. In the two-day average, the vertical transport of ozone by the mean meridional circulation shows the alternations in sign that correspond closely (but not exactly) with the sinking and rising branches of the two-day averaged mean meridional mass circulation. In the troposphere, the downward-moving branches of the circulation cells carry the ozone into and through the lowest model layer where there is surface destruction of ozone; consequently, the branches of the cells which move upward, out of the lowest model layer, carry much less ozone. The largest downward ozone transports in the troposphere are in the adjacent descending currents of the Ferrel and Hadley cells in each hemisphere. In the northern hemisphere, this

strong downward ozone transport is the continuation of a downward transport of ozone by the descending branch of the stratospheric mean meridional mass circulation that was described above. In the summer stratosphere, this part of the ozone transport, like the circulation itself, has a very complex structure.

The vertical transport of ozone by zonal eddies, shown in the middle part of Figure 17, is downward almost everywhere in the troposphere and in the lower stratosphere, and is upward almost everywhere in the upper stratosphere. Comparing these vertical eddy transports with the zonally-averaged ozone mixing ratios shown in Figure 11 shows that they are downgradient eddy transports.

The bottom part of Figure 17 shows the total vertical ozone transport. It indicates that it is the combined effect of the mean meridional transport and the eddy transport which supports the large surface destruction rates near 25°N and 20°S shown in Figure 14.

Figure 18 shows the global mean of the vertical ozone transports. These are the sums, from pole to pole, of the transports shown in Figure 17. We see that for the globe as a whole the vertical ozone transport by the grid-scale eddies is several times larger than the transport by the mean meridional circulation.

Because the model has no ozone source or sink between the 100-mb level and the top of the lowest model layer (where the average pressure is about 800 mb), the vertical ozone transport will be constant with height through this part of the domain when the ozone field is in a steady state. But, as Figure 18 shows, this is not yet the case. Between 100 mb and 400 mb, the vertical ozone transport is diverging at the rate of 36 tons/sec; and between 400 mb and the top of the lowest model layer, it is converging at the rate of 36 tons/sec. The downward transport at the top of the lowest model layer is 34 tons/sec, which is about 15 tons/sec larger than the rate of the surface destruction at this time. We shall continue the simulation until the ozone approaches its statistically steady equilibrium state, but we do not expect the directions and the relative magnitudes of the vertical ozone transports to differ very much from what is shown in Figure

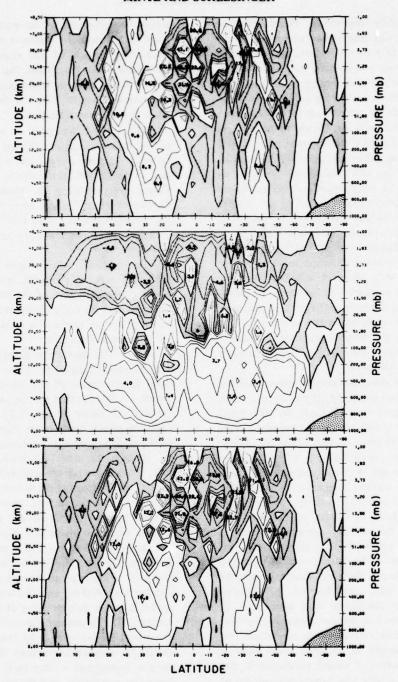


Figure 17. Meridional cross-sections of the vertical transports of ozone, averaged over the last two days of the simulation (Days 75-76). Top: downward transport by the mean meridional circulation; contours shown for 0, 2, 5, 10, and 20 tons/sec per 4° latitude. Middle: downward transport by zonal eddies; contours shown for 0, 0.5, 1, 2, and 5 tons/sec per 4° latitude. Bottom: total downward transport; contours shown for 0, 2, 5, 10, and 20 tons/sec per 4° latitude.

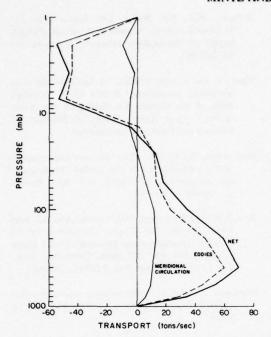


Figure 18. Vertical profiles of the global vertical ozone transport. Positive values are downward.

SUMMARY AND CONCLUSIONS

We have described a three-dimensional global atmospheric general-circulation model which extends from the earth's surface to the stratopause. Its circulation, radiational heating, and ozone photochemistry are fully coupled and interactive. We have also presented some results from the early part of a simulation of the general circulation that was made with this model, showing the zonally-averaged temperature and velocity fields and the ozone production and transport.

The simulation has not yet been carried far enough for the prognostic variables of the model to have reached their long-term, statistically-steady equilibrium states. But the results, at this stage, with certain exceptions, are already in fairly good agreement with what we know about the real atmosphere from observations. We are therefore inclined to accept those parts of the results which are not known from observations, and which are very difficult to obtain from observations, as being correct zeroth-order approximations of the real atmosphere. With respect to ozone, these results are: that the

vertically integrated latitudinal transport of ozone in the tropics consists almost entirely of a large transport from the summer to the winter hemisphere by the mean meridional circulation, but in the middle and higher latitudes it is the small difference between a large poleward transport by the eddies and a large equatorward transport by the mean meridional circulation; that the vertically integrated latitudinal transport by the eddies is, itself, the small difference between a large eddy transport toward the poles in the middle and lower stratosphere and a large eddy transport toward the equator in the upper and middle troposphere; and that in the zonal average the largest vertical transports of ozone are in the descending branches of the mean meridional circulation, but in the global average the vertical eddy transport of ozone is several times larger than the vertical transport by the mean meridional circulation.

The principal deficiency of the model is that both the ozone amounts and the temperatures are somewhat too low in the upper troposphere and in the stratosphere in the polar regions of both hemispheres. This seems to be the result of the model atmosphere's not having yet developed tropospheric and stratospheric ultra-long waves of sufficiently large amplitude, so that the poleward eddy transports of heat and of ozone are too small. Whether the ultra-long waves will grow in amplitude and produce larger poleward transports of heat and ozone as the simulation continues remains to be seen.

ACKNOWLEDGMENTS

The authors wish to thank the many members of the research group who participated in the construction of the UCLA General-Circulation Model. In particular, they are grateful to Professor A. Arakawa, the principal architect of the model, and Professor S.V. Venkateswaran, Drs. A. Katavama, J.-W. Kim, W. Schubert and T. Tokioka, and Messrs. W. Chao, D. Randall, and S. Lord. They thank Mmes. D. Hollingworth and D. Conti and Mr. C. Kurash for their programming contributions. They also thank Professor R. Newell for the figures reproduced here. The research was supported by the National Science Foundation, Atmospheric Sciences Section, under Grant GA-34306; the Department of Transportation, Climatic Impact Assessment

Program, under Grant GA-34306X; and the National Aeronautics and Space Administration, Institute for Space Studies, Goddard Space Flight Center, under Grant NGR 05-007-328.

REFERENCES

- Arakawa, A. (1970), "Numerical simulation of largescale atmospheric motion," in Numerical Solution of Field Problems in Continuum Physics, Vol. 2, SIAM-AMS Proceedings, ed. Birkhoff and Varga, pub. American Mathematical Society, Providence, RI, 24-40.
- Arakawa, A., and Y. Mintz (1974), "Workshop Notes on The UCLA Atmospheric General Circulation Model (24 March-4 April 1974)," Department of Meteorology, University of California, Los Angeles, California, 404 pp.
- Arakawa, A., and W.H. Schubert (1974), "Interaction of a cumulus cloud ensemble with the large-scale environment, Part I," J. Atmos. Sci. 31, 674-701,
- Barnett, J.J. (1974), "The mean meridional temperature behaviour of the stratosphere from November 1970 to November 1971 derived from measurements by the selective chopper radiometer on Nimbus IV," Quart. J. Roy. Met. Soc. 100, 505-530.
- Brewer, A.W., and A.W. Wilson (1968), "The regions of formation of atmospheric ozone," Quart. J. Roy. Met. Soc. 94, 249-265.
- Cunnold, D., F. Alyea, N. Phillips, and R. Prinn (1975), "A three-dimensional dynamical-chemical model of atmospheric ozone," J. Atmos. Sci. 32, 170-194.
- Deardorff, J.W. (1972), "Parameterization of the planetary boundary layer for use in general circulation models," Mon. Wea. Rev. 100, 93-106.
- Dütsch, H.U. (1969), "Atmospheric ozone and ultraviolet radiation," in World Survey of Climatology, Vol. 4, ed. Rex, Elsevier, New York, 383-432.
- Katayama, A. (1972), "A Simplified Scheme for Computing Radiative Transfer in the Troposphere," Technical Report No. 6, Department of Meteorology, University of California, Los Angeles, 77 pp.
- Krueger, A.L., D.F. Heath, and C.L. Mateer (1973), "Variations in the stratospheric ozone field inferred from Nimbus satellite observations," Pure Appl. Geophys. 106-108, 1254-1263.
- London, J. (1963), "The distribution of total ozone in the northern hemisphere," Beitr. Phys. Atmos. 36, 254-263.

- McElroy, M.B., S.C. Wofsy, J.E. Penner, and J.C. McConnell (1974), "Atmospheric ozone: Possible impact of stratospheric aviation," J. Atmos. Sci. 31, 287-303.
- Mintz, Y. and J. Lang (1955), "A model of the mean meridional circulation," Article VI in "Investigations of the General Circulation of the Atmosphere," Final Report, Dept. of Meteorology, University of California, Los Angeles.
- Murgatroyd, R.J. (1969), "The structure and dynamics of the stratosphere," in *The Global Circulation of the Atmosphere*, ed. Corby, pub. Roy, Meteor. Soc., London, 159-195.
- Newell, R.E., J.W. Kidson, D.G. Vincent, and G.J. Boer (1972, 1974), The General Circulation of the Tropical Atmosphere and Interactions with Extratropical Latitudes, MIT Press, Cambridge, Mass., Vol. 1 (1972), 258 pp.; Vol. 2 (1974), 371 pp.
- Normand, C. (1953), "Atmospheric ozone and the upper-air conditions," Quart. J. Roy. Met. Soc. 74, 39-50.
- Ozone Data for the World, 1960-72, compiled by Canadian Department of Transport in cooperation with WMO.
- Schlesinger, M.E. (1976a), "A Fast Numerical Method for Explicit Integration of the Primitive Equations Near the Poles," P-5507, The Rand Corporation, Santa Monica, CA (in preparation).
- Schlesinger, M.E. (1976b), "A Numerical Investigation of the General Circulation of Atmospheric Ozone," Ph.D. dissertation, Dept. of Meteorology, University of California, Los Angeles (in preparation).
- Sticksel, P.R. (1970), "The annual variation of total ozone in the southern hemisphere," Mon. Wea. Rev. 98, 787-788.
- Tiefenau, H., and P. Fabian (1972), "The specific ozone destruction at the ocean surface and its dependence on horizontal wind velocity from profile measurements," Arch. Met. Geoph. Biokl. A21, 399-412.
- U.S. Standard Atmosphere Supplements (1966), prep. for ESSA, NASA, and USAF.
- Vincent, D.G. (1968), "Mean meridional circulations in the northern hemisphere lower stratosphere during 1964 and 1965," Quart. J. Roy. Met. Soc. 94, 333-349.
- Wu, M.-F. (1973), "Observation and Analysis of Trace Constituents in the Stratosphere," Annual Report, Contract No. DOT-OS-20217, Environmental Research and Technology, Lexington, MA, 218 pp.

THEORY OF ATMOSPHERIC MOTIONS AND CLIMATE

DISCUSSION

A. MILLER: Because of the interest shown in the transport of tracer substances, I feel I should mention that we at the National Weather Service are starting a program in which we are actually going to calculate the vertical and horizontal transports of ozone in the middle stratosphere, utilizing the ozone mixing ratios from the backscattered-ultraviolet ozone experiment on the Nimbus 4 spacecraft.

CRUTZEN: I am disappointed that we haven't resolved the question of eddy-diffusion coefficients. One of the things which Dieter Ehhalt and I have done with methane - and Don Hunten referred to this - has been to try to get the eddy-diffusion profiles from the methane and N2O data. Now, the model which Dieter was using for that was the model which I had developed in Stockholm. We had a small computer, and we simply couldn't afford to do extensive time-dependent calculations. So, I had the sun fixed at about 45° in that model. We let the chemistry work, and then Dieter tried to fit his diffusion profile to the measurements. Now, as Don said, in that model the sun is on for 24 hours. You must be careful when using eddy-diffusion coefficients derived in that way. If you are going to use a model similar to the simple one which I had, okay. But if you are going to apply the coefficients to a model which has a diurnal cycle in it, or which has transport working for 24 hours and chemistry for 12 hours, then I recommend that you divide these eddy-diffusion coefficients by 2. That's probably the best thing you can do. If you do that in Harold Johnston's case, you would probably get a little better correspondence with the carbon-14 data.

I also claimed in that same paper that most of the carbon-14 was dumped in the stratosphere not as ¹⁴CO₂, but as ¹⁴CO. So I was wrong there. Forget that point. The reason for the formation of ¹⁴CO₂ is that there is a lot of radiation chemistry going on. In fact,

reactions between carbon and nitrogen are involved, which was very surprising to me.

CHANG: Paul just described some of his calculations. In our calculation, we used McElroy's loss rate for CH₄. In fact, I compared Crutzen's CH₄ loss rate, as it appeared in his 1971 JGR paper, with my own and McElroy's CH₄ loss rates. Between 15 and 40 kilometers, the three loss rates seem to agree within 5% or so. Indeed, as Don Hunten suggested, on the top – from 45 to 55 kilometers, say – if you don't consider diurnal sun, you are indeed doubling this loss rate, which was just verified.

ACKERMAN: I have been surprised to see CH₄ being used so much to try to evaluate these eddy-diffusion coefficients. There has been no use of the spectroscopic results obtained by Lowe and McKinnon, and by Muller and myself, on vertical profiles of CH₄. I would like to add that recently, using the Girard spectrometer to look for NO and NO₂, we got new information on methane. Within experimental error, these methane data do not indicate any decrease of mixing ratio below 25 kilometers.

CALLIS: We have performed some one-dimensional calculations to estimate the sensitivity of surface temperature to ozone reduction, and our model says that if you reduce ozone the surface temperature has to decrease, while Mike MacCracken's model says that the surface temperature has to increase. I think the basic difference is not because one is 1-D and the other 2-D. Mike MacCracken has neglected the 9.6-micron band of ozone. When you reduce ozone, you reduce the greenhouse effect of this band. In fact, we have also performed calculations with the 1-D model neglecting this band, and in that case we predict an increase in the surface temperature. So I think the difference between the two models is in the treatment of the 9.6-micron band and not in the number of dimensions.

MacCRACKEN: I agree.

THE STRATOSPHERE: SCATTERING EFFECTS, A COUPLED 1-D MODEL, AND THERMAL BALANCE EFFECTS

L.B. CALLIS, V. RAMANATHAN, R.E. BOUGHNER, AND B.R. BARKSTROM

NASA Langley Research Center Hampton, Virginia

ABSTRACT: The present paper describes results in three problem areas: (1) the effect of Rayleigh scattering on the photodissociation rates in the stratosphere, (2) use of a 1-D stratospheric model which calculates atmospheric temperature profiles from profiles of optically active constituents determined within the model, and (3) the effect of perturbations of stratospheric constituents on surface temperature and the earth/atmosphere energy balance.

It is shown that Rayleigh scattering may substantially alter the stratospheric photodissociation rates. The effects of these changes are examined with the aid of a 1-D photochemical model. This model is also used to examine the effect of coupling the determination of the optically active species in the stratosphere (O₃, NO₂, H₂O, and CO₂) with the determination of the atmospheric temperature profile, by means of a radiative-convective model. The sensitivity of the surface temperature of the earth to changes in the stratospheric O₃ and NO₂ is examined. The "albedo effect" associated with the O₃ and NO₂ concentration changes is accounted for and discussed.

INTRODUCTION

During the course of the CIAP studies, substantial effort has been devoted to the accurate determination of the chemical and photochemical rate constants. These constants constitute an important body of input data to the 1-, 2-, and 3-D stratospheric models from which impact assessments are drawn. One of the considerations of this paper is the determination of the importance of Rayleigh scattering to the calculation of stratospheric photodissociation rates within the wavelength interval 0.175 ≤ \lambda ≤ 0.73 µm. Scattering can affect the determination of these rates by: (1) reducing the intensity of the direct solar beam at various levels of the atmosphere, and (2) providing a diffuse intensity field via the multiple molecular scattering. These effects tend, respectively, to decrease and increase the stratospheric photodissociation rates. The section on Rayleigh-scattering effects examines the question of the net results of increase and decrease of dissociation rates, as well as effects on clouds, surface reflectivity, and zenith angle. This question was first discussed by Callis (1974). The present work expands upon these results and examines the effect of these rate changes on the stratospheric constituent profiles as determined by a 1-D photochemical model.

The present paper also discusses solutions which result from the coupling of a 1-D photochemical model with an equilibrium radiativeconvective model. The solutions are coupled in the sense that the temperature profile between 0≤z≤50 km is derived from specified profiles of CO2 and H2O and with profiles of O3 and NO2 determined from the photochemical model. The coupling between the temperature structure and the photochemistry is of interest, since changes in the O3 profile will be reflected in a changed temperature. The meridional temperature distribution is dynamically and climatically significant. Studies with a 1-D model represent a necessary first step in the development of an understanding of these interactions. Others who have examined these interactions (McElroy et al., 1974; Blake and Lindzen, 1973; Rao, 1970) have used thermal codes, in conjunction with photochemical models, but they do not account for effects associated with the hot bands of CO2, Doppler broadening, and surface temperature, all of which can be significant. In addition, these codes are usually formulated as parameterizations and are not sensitive to local perturbations of the stratospheric constituents. The present work is not limited in this manner. The thermal code (Ramanathan, 1974) accounts for contributions due to the 9.6-µm band of O3, the fundamental bands of four CO2 isotopes as well as six

hot bands of CO_2 , and the vibration-rotation and pure rotation bands of H_2O (important for tropospheric and thermal-balance considerations). The method is efficient and sensitive to local constituent perturbations, and its results compare favorably with the more detailed results of Dickinson (1973) and Manabe and Strickler (1964).

The paper also presents preliminary results of an analysis (Ramanathan et al., 1975) of the effects of perturbations of stratospheric O₃ and NO₂ on the earth/atmosphere energy balance. The calculations were conducted using the abovementioned thermal code and a multiple-scattering code from Callis (1972). This work provides preliminary information on the sensitivity of the surface temperature of the earth, T_s, to changes in stratospheric constituents. Despite the inherent limitations of using globally averaged radiative-convective models in such analyses, important trends can be exposed and sensitivity factors generated.

EFFECT OF RAYLEIGH SCATTERING ON PHOTODISSOCIATION

The photodissociation rate of the i^{th} species, J_i , at a given altitude z is given by the following expression:

$$J_{i}(z) = n_{i}(z) \left\{ \int_{\Delta \lambda} I^{\infty}(\lambda) \sigma_{i}(\lambda) \eta_{i}(\lambda) \exp \left[\left(\tau_{s}^{\infty}(\lambda) - \tau_{s}(\lambda, z) + \tau_{a}^{\infty}(\lambda) - \tau_{a}(\lambda, z) \right) / \mu \right] d\lambda + \int_{\Delta \lambda} \overline{I}(\lambda, z) \sigma_{i}(\lambda) \eta_{i}(\lambda) d\lambda \right\}$$
(1)

where n_i is the number density, σ_i the absorption cross-section, η_i the quantum efficiency, μ the cosine of the solar zenith angle, I^{∞} the solar intensity at the top of the atmosphere, \overline{I} the diffuse intensity integrated over all solid angles, τ_s^{∞} and τ_a^{∞} the total optical depth due to scattering and absorption respectively, and where τ_s and τ_a are the optical depths due to scattering

and absorption at the altitude of interest. It is to be expected that scattering processes will be significant if $\tau_s^{\infty} = O(\tau_a^{\infty})$.

Figure 1 presents the variation of τ_s^{∞} and $\tau_s^{\infty} + \tau_a^{\infty}$ as a function of wavelength, λ . The absorption and scattering properties of the atmosphere were calculated as follows: number densities from the *U.S. Standard Atmosphere*, 1962, O₃ number-density profile from McClatchey's (1972) midlatitude summer distribution, spectral intervals and cross-sections of O₂ and O₃ and flux of solar photons from Ackerman (1971), and the Rayleigh-scattering cross-sections from Penndorf (1957). Figure 1 indicates that, for $0.20 \le \lambda \le 0.73 \ \mu m$, τ_s represents a non-negligible part of the total optical depth of the atmosphere, the minimum relative contribution occurring at $0.255 \ \mu m$.

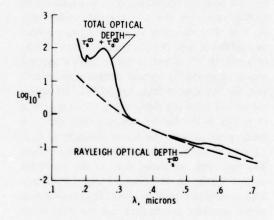


Figure 1. Spectral variation of atmospheric normal optical depth due to scattering and absorption.

An anisotropic multiple-scattering radiation-transfer code (Callis, 1972) has been employed to calculate the diffuse intensity field at 40 equally spaced altitude intervals between 0 and 50 km and for 170 frequency intervals (Ackerman, 1971) between 0.175 μ m and 0.735 μ m. The diffuse field and the attenuated solar beam were then used in conjunction with equation (1) to calculate photodissociation rates as a function of zenith angle and surface reflectivity, as well as cloud cover and cloud reflectivity. Calculations were performed for the reactions shown as equation (2)

$O_2 + h\nu \rightarrow 2O(^3P)$	$0.1750 \le \lambda \le 0.2420$	
$O_3 + h\nu \rightarrow O(^3P) + O_2$	λ ≤ 0.3100	
$O_3 + h\nu \rightarrow O(^1D) + O_2$	λ ≤ 0.3100	
$NO_2 + h\nu \rightarrow NO + O$	λ ≤ 0.3980	
$NO_2 + h\nu \rightarrow NO + O(^1D)$	$\lambda < 0.2440$	
$HNO_3 + h\nu \rightarrow OH + NO_2$	$0.2000 < \lambda \le 0.3200$	(2)
$HNO_2 + h\nu \rightarrow OH + NO$	$0.3000 < \lambda \le 0.4000$	
$H_2O + h\nu \rightarrow OH + H$	$0.1170 < \lambda \le 0.1980$	
$H_2O_2 + h\nu \rightarrow 2OH$	$0.1870 < \lambda \le 0.4358$	
$NO_3 + h\nu \rightarrow NO + O_2$	$0.4525 < \lambda \le 0.6750$	
$N_2O + h\nu \rightarrow N_2 + O(^1D)$	$0.1163 < \lambda \le 0.3125$	

where the spectral intervals in which photodissociation takes place are indicated. Typical results are presented in Figures 2-5.

Figure 2 presents the variation of the ratio of the photodissociation rate with scattering to the rate without scattering, J/J₀, as a function of altitude for $\mu = -0.6$ and a surface reflectivity $R_s = 0$. For purposes of explanation, consider two of the curves, the photodissociation of NO2 to yield O(3P), which occurs within a spectral region of moderate optical thickness ($\tau \approx 0.3$), and the breakup of NO₂ to yield O(¹D), which occurs in a relatively thick region of the spectrum $(\tau \approx 30)$. In the former case, the solar radiation easily penetrates to the lower atmosphere (z ≤ 12 km) where the bulk of the scattering occurs. The reflected radiation, due to the moderate optical depths above 12 km, is transmitted with little attenuation back to space. The combination of the resultant diffuse field, and the small effect of scattering on the direct beam above 15 km, leads to substantial increases in the photodissociation rates. For NO₂ [→O(³P)], a 45% increase is noted at 15 km; for O³ [→O(³P)] the increase is 26 percent.

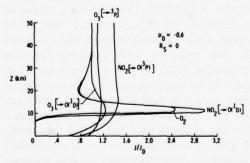


Figure 2. Rayleigh-scattering effects on photodissociation rates of $O_3[\rightarrow O(^1D)]$, $O_3[\rightarrow O(^3P)]$, and $NO_2[\rightarrow O(^3P)]$ as a function of altitude.

For the photodissociation of O₃ and NO₂ yielding O(1D), and of O2, the results are substantially different. These processes occur in a part of the spectrum where the absorption processes are substantially stronger and the optical depths larger. Due to the large τ , radiation scattered in the lower layers is strongly attenuated between 10 and 20 km and little diffuse radiation is experienced above 20 km. The result is a decline in the ratio J/J₀ (due to radiation scattered out of the incident beam) between 50 and 20 km. The increase in the ratio below 20 km is attributed to the presence of a small diffuse field and the rapidly diminishing intensity of the direct beam. Below 10 km, the absorption is such that the diffuse field is driven to zero more strongly than the direct beam. From a practical point of view, the excursion of the ratio J/J₀ between 10 and 20 km is inconsequential since, due to the large optical depths, these photochemical rates are extremely small at altitudes below about 25 km. Figure 3 shows similar curves for the remainder of the reaction rates. Similar changes in the rates due to scattering are noted.

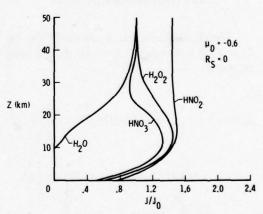


Figure 3. Rayleigh-scattering effects on photodissociation rates of H₂O, HNO₃, H₂O₂, and HNO₂ as a function of altitude.

Figure 4 represents the variation of the ratio, J/J_0 , with variation in zenith angle. The profiles for the photodissociation of O_2 and NO_2 yielding $O(^3P)$ are typical of photodissociation processes that occur in parts of the spectrum which are respectively optically thick and moderately thick. The lower sun effectively increases the optical depth of the atmosphere. This leads to a decrease in those rates which are determined in the "thin" part of the spectrum. For rates in the

"thick" part of the spectrum, a decrease in the upper levels is noted with an increase in the regions below 25 km. Once again, these increases are of academic interest only, for reasons already discussed.

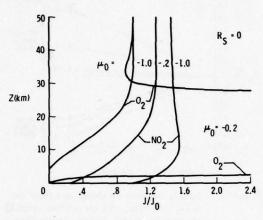


Figure 4. Effect of zenith angle on photodissociation rates as a function of altitude.

Figure 5 presents results obtained with a layer having reflectivity of 0.4 at 5 km. The radiation field is not calculated for lower heights in this case. This configuration approximates the effect of a cloud layer at 5 km on photodissociation rates, which is substantial. The increased diffuse-intensity field due to the clouds raises the maximum value of J/J₀ for NO₂ from 1.45 to 1.64; for O₃ the increase is from 1.16 to 1.51.

It is clear that the effects of Rayleigh scattering and scattering from clouds substantially affect the photodissociation rates within the stratosphere. The sensitivity of 1-D model results to such changes in the photochemical rates will be discussed in a later section.

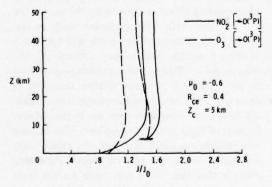


Figure 5. Effect of cloud cover on photodissociation rates as a function of altitude.

THERMAL-STRUCTURE AND THERMAL-BALANCE STUDIES

In order to gain a more complete understanding of the impact of perturbations of stratospheric constituents, work at Langley has been directed toward the development of codes which would permit the determination of the temperature structure with either given or calculated profiles of O₃, NO₂, CO₂, and H₂O. Preliminary results have been reported by Ramanathan (1974). The present section presents additional results on the thermal structure obtained from this model. Results are also presented of studies of the earth/atmosphere thermal balance, conducted with the previously discussed solar-scattering code used in conjunction with the thermal code.

Figure 6 (Ramanathan et al., 1975) shows results for the atmospheric thermal structure for three cases: the unperturbed atmosphere, the atmosphere with a 30% O₃ reduction between 12 and 40 km for $\delta = 0$, and the same reducedozone atmosphere for $\delta = +6$. The parameter δ is the negative of the ratio of the change in NO2 to the change in O_3 . For $\delta = +6$, the NO_2 is 180% of the ambient values. Calculations for ΔO_3 = -30% and δ = +6 indicate general reduction of the stratospheric temperature with small decreases in the tropospheric and ground temperatures, T_s. The maximum ΔT is seen to be -4.5K near 37 km with a temperature change at 16 km of -2.5K. For $\Delta O_3 = -30\%$ and $\delta = 0$, which indicates no change in ambient levels of NO2, the reduction of temperature is somewhat larger, up to -7K at 37 km and -3.5K at 16 km. The difference between the two cases is due to the compensating effect of absorption by NO2 in the solar part of the spectrum. These calculations assume an O₃ distribution given by Krueger and Minzner (1973), an NO₂ distribution from the modeling work of Chang (1974), and a cloud cover of 44.6%, cloud reflectivity R_c = 0.515, ground reflectivity $R_o = 0.105$, and cloud-top altitude $z_c =$ 6.25 km. The potentially most significant result from such changes, should they be experienced in the tropical regions, may be the effect on stratospheric H2O levels. If one subscribes to the theory that the tropical tropopause temperature minimum provides an effective "cold trap" for upwelling H2O, then changes of 2-3K can be significant relative to the upward H2O flux into the stratosphere. For example, at 15°N latitude,

the annual-average value of T at 16.5 km is 193K. The corresponding mass mixing ratio for H₂O saturation is 3.44(10⁻⁶). A reduction of temperature by 3K results in a saturation mixing ratio of 2.08(10⁻⁶), a 40% drop. If the tropical tropopause temperature does play a major role in establishing the levels of stratospheric water vapor, then a 3K drop in temperature could be significant. Mastenbrook (1971) reports that measurements of the water-vapor cycle in the stratosphere indicate that such a correlation of the stratospheric concentrations of H₂O with the tropical tropopause temperature indeed exists. Thermal-balance calculations indicate that a reduction of the stratospheric H2O mass mixing ratio to levels of 2.0(10-6) would result in a cooling of the surface temperature by 0.28K under the assumptions of a radiative-convective model.

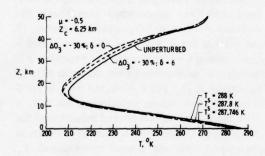


Figure 6. Perturbed and unperturbed radiativeconvective equilibrium temperature profiles for constant cloud-top altitude, average cloudiness, and half day of full sun. (From Ramanathan et al., 1975.)

The NASA Langley scattering and thermal codes were also used in an examination of the effect on surface temperature of O3 reductions in the presence of NO2. Calculations were carried out under the assumptions of a radiativeconvective model with previously described unperturbed profiles of O3, NO2, and atmospheric number density. The results are shown in Figure 7 for a constant cloud-top altitude of 6.25 km for $\delta = 0$, +6, and +10, with and without the "albedo effect." The "albedo effect" refers to the fact that with a reduction of the stratospheric O3, the solar beam will be allowed to penetrate more effectively to the Rayleigh scattering layer. The backscattered radiation, as a result of the diminished column density of O3

above it, is more easily able to escape to space. Consequently, the O_3 reduction results in an increase of the albedo of the earth/atmosphere system.

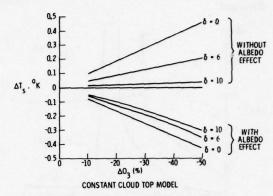


Figure 7. Surface temperature change as a function of O_3 reduction and δ for constant-cloud-top-altitude model. (From Ramanathan et al., 1975.)

The results shown in Figure 7 indicate an increase in surface temperature, Ts, with decreasing O3 in the absence of the scattering or the "albedo effect." This is explained by noting that with a decrease in O3, the stratospheric temperatures decrease. A corresponding decrease in the outward longwave flux is observed. To compensate for this and restore thermal balance, T, must increase. The largest increases are shown for δ = 0, that is, without a compensating effect of the NO2 solar absorption. Differences in the results when the overriding "albedo effect" is included are dramatic, with ozone reductions now leading to a reduction in the surface temperature of the earth. The largest differences are for the case where $\delta = 0$, $\Delta T_s = -0.43$ K for a 50% O_3 reduction. Once again, the NO2 provides a compensating effect, as shown by the curves for δ = +6 and +10. The predicted shift in the surface temperature of the earth will lead to a difference in the water-vapor content of the troposphere. Since the radiative-convective model assumes a constant relative humidity, a decrease of the average tropospheric temperature will lead to an attendant decrease in the column density of H2O in the troposphere. This in turn will provide an additional "albedo effect" not accounted for in the present results. Estimates indicate that this effect will cause further temperature drops, changing ΔT_s by approximately

8%. Thus, the importance of the molecular scattering processes in atmospheric thermal-balance studies related to the O_3 - NO_x problem is not to be overlooked.

Figure 8 provides additional perspective on the role of scattering in thermal-balance studies when O₃ is being reduced in the presence of NO_2 . The albedo change Δa is plotted as a function of percentage O_3 reduction with $\delta = 0$, +6, and +10. The major change in a occurs when δ = 0, or in the absence of the compensating NO₂ absorption. This indicates that a given reduction of O₃ due to interactions with C1O_x $(\delta = 0)$ will have more of an impact on the thermal balance than a similar reduction of O₃ due to interaction with NO_x ($6 \le \delta \le 10$). It is also interesting to note that the albedo changes associated with the decrease in O3 are as large as, or larger than, the changes noted by Herman (1974) due to the direct effect of sulfate aerosols in the altitude range 15-25 km. An obvious area for future investigation is an assessment of the combined effect of stratospheric aerosols and perturbations of O3 and NO2 on the earth/ atmosphere albedo.

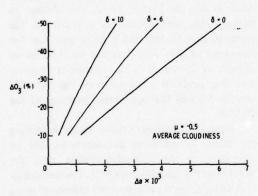


Figure 8. Earth/atmosphere albedo change as a function of ΔO_3 and δ for average cloudiness. (From Ramanathan et al., 1975.)

In addition to its role in the "albedo effect" and the well-known "greenhouse effect," it has been shown (Ramanathan et al., 1975) that the atmospheric thermal balance is sensitive to changes in the vertical distribution of O₃ for a given column amount. Using Green's distribution (Lacis and Hansen, 1974) for the unperturbed O₃, this sensitivity is illustrated in Figure 9 by the parameter F_{O₃}. This parameter is the difference between the flux emitted by the atmo-

spheric column and the total absorption by the atmospheric column of the surface radiation in the 9.6-µm-band region. The negative values indicate that more radiation is absorbed by the column than is emitted by it in that band. Figure 9 illustrates the sensitivity of this parameter to the altitude of peak ozone concentration. The upper curve indicates that for increasing peak altitude, zmax, the outward longwave flux is also increased. This is a result of a decrease in the effective broadening pressure, which in turn decreases the band absorptance, permitting the additional flux to escape. Also shown on the figure is the curve labeled $\Delta O_3 = -30\%$, referring to a 30% reduction of the O3 between 12 and 40 km. The two curves illustrate clearly the relative roles of the two phenomena in the earth/ atmosphere thermal balance: the arrows show that a 2.8-km increase in z_{max} provides a change in Fo3 comparable to that caused by a 30% reduction of O3.

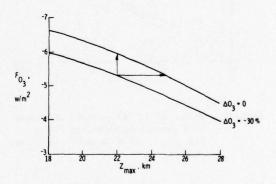


Figure 9. Effect of O₃ peak-concentration altitude on O₃ 9.6-\(\mu\) m band flux at top of atmosphere. Green's distribution of O₃ used with column density = 0.344 cm STP, average cloudiness, and T_S = 288K. (From Ramanathan et al., 1975.)

COUPLED-MODEL INVESTIGATIONS

The coupled, steady-state photochemical model used in the current work was developed by Boughner (1975); it extends from 0 to 50 km, has 40 equally spaced layers, and includes 19 species and 41 reactions. Essentially, the eddy-diffusion coefficients, chemistry, and rates of Chang (1974) were used. The model is coupled with the previously discussed thermal code, and hence can determine atmospheric temperatures from calculated O₃ and NO₂ profiles with

appropriate CO₂ and H₂O distributions. The mixing ratio for CO₂ is taken to be 320 ppm. Water-vapor content in the troposphere is determined by an assumed relative humidity. In the stratosphere, the minimum mass mixing ratio of H₂O is taken to be 3.0 ppm. A tropospheric lapse rate of -6.5 K/km is used up to the calculated tropopause. The model is interactive in the sense that calculated temperatures are used to determine temperature-dependent rate constants, and calculated species distributions are used to determine the temperature structure. Typical results are presented in Figures 10 through 12.

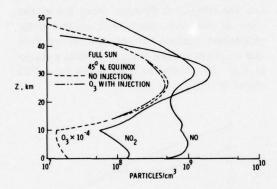


Figure 10. Profiles of O₃, NO₂, and NO determined with coupled photochemical model for full sun at 45°N latitude, during the equinox.

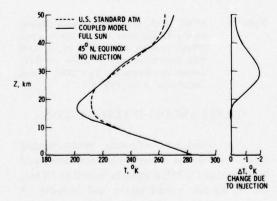


Figure 11. Comparison of vertical temperature profile determined by coupled photochemical model. Temperature change due to NO_x injection by 500 SST's.

Figure 10 represents ambient distributions of NO, NO₂, and O₃ determined with the coupled model. Also shown is the O₃ profile resulting from the injection of NO at 20 km by 500 SST's. The bulk of the O₃ destruction, as expected, occurs above the injection altitude and results in a column decrease of O₃ of approximately 8%. Our studies indicate that the effect of the temperature coupling in injection studies is to reduce the O₃ loss by approximately 10%. This is in agreement with McElroy (1974) and is attributed to the fact that the reduction of O₃ leads to a temperature reduction, thus decreasing the rate at which NO reacts with O₃.

The temperature profile corresponding to the ambient case is shown on Figure 11 in comparison with the 1962 Standard Atmosphere. Agreement is excellent above 22 km where the temperature structure is less affected by atmospheric dynamics. Below the 22-km level, transport processes have a larger impact on the thermal structure. These processes cannot be simulated by a photochemical model. Below 10 km there is no disagreement, since the lapse rate in the model has been selected as -6.5 K/km. Also shown in Figure 11 is the change in stratospheric temperature as a result of the injection due to 500 SST's. It is seen that the maximum change is a decrease by 2.0K at an altitude of 29 km. It is this change in temperature that leads to a reduction of the NO + O3 rate by 5% and the subsequent lessening of the O3 loss.

Figure 12 presents model results indicating the effect of including perturbations, due to scattering, in the photodissociation rates for $NO_2[\rightarrow O(^3P)]$ and $O_3[\rightarrow O(^3P)]$. Photodissociation rates, J, for these cases were calculated using solar transmission functions averaged over 24 hours. These perturbations were included as a constant multiplicative factor at all altitudes. The NO₂ rate was increased by 1.5 and the O₃ rate by 1.3. Consideration of Figure 5 indicates that above 10 km, the perturbed photodissociation rates are only weakly dependent upon altitude. photodissociation rates Other were left unchanged. The results (which are approximate) indicate that the effects of scattering cause up to 50% increases in concentrations of NO, and up to 25% reductions of NO2 at 40 km, ranging down to a 7% decrease at 30 km. An illustration of the

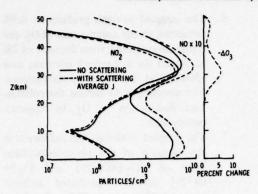


Figure 12. Effect of Rayleigh scattering on coupled photochemical model constituent profiles.

percentage of O3 change due to scattering for the ambient case is also shown. The maximum change is a decrease of approximately 6%. The distribution shown corresponds to an O2 column-sum decrease, due to the inclusion of scattering, of 2.3%. Work to date has indicated that the effect of scattering on the O₃ column sum lost (due to injection of NO by 500 SST's) is to reduce the amount of O3 lost by approximately 1-2%. In view of the large changes in the ambient NO and NO2 due to scattering, this is somewhat surprising. The explanation lies in the fact that due to the temperature dependence of the NO + O₃ rate, most of the O₃ loss occurs at altitudes above injection. At these altitudes, the ambient concentrations of NO2 are perturbed only slightly relative to perturbations at the injection altitude. Consequently, the effects of scattering are small. The fact that the scattering actually leads to less of a reduction in the O3 column sum is attributed to the attendant slight reduction of temperature between 25-30 km that causes a reduction in the NO + O3 rate.

From the foregoing, it appears that the effect of scattering in the presence of injection at altitudes below 20 km will be small. Note, however, that account has been taken only of changes in the rate for $NO_2 [\rightarrow O(^3P)]$ and $O_3 [\rightarrow O(^3P)]$, and these only approximately. Effects of changes in the other photodissociation rates are being examined. It should also be clear from the previous discussion that if injection of NO occurs at altitudes between 25-30 km, the role of scattering would be substantially enhanced.

Figures 13 and 14 present NO and HNO₃ profiles, determined with the present model, in comparison with observational data and with the calculations of Chang (1974). Figure 13 shows good agreement between the present NO profiles and the data of Ackerman (1973) between 20 and 40 km, but the results are smaller by as much as a factor of two than those of Chang at 20 km. At the higher altitudes, agreement with Chang is good. The data by Ridley et al. (1975) are generally lower, by one-half, than the present calculations.

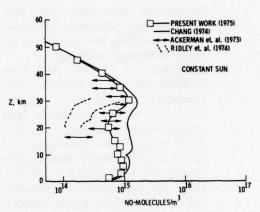


Figure 13. Comparison of present work with NO observational data.

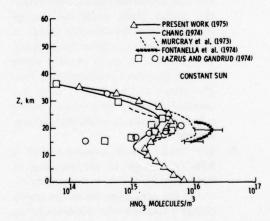


Figure 14. Comparison of present work with HNO₃ observational data.

Figure 14, for the HNO₃, indicates the agreement between the present model results and data of Murcray et al. (1973) to be good above 22 km. Below this level, the data are generally higher than our calculated values. The data of

Fontanella (1974) is substantially higher than the calculated results. Comparison with the work of Chang shows the present levels of HNO₃ to be nearly twice as large between 12-35 km. Both sets of calculations fall within the range of data by Lazrus and Gandrud (1974).

CONCLUDING COMMENTS

On the basis of the present work, the following conclusions have been reached:

- Stratospheric photodissociation rates are substantially affected (both increased and decreased) by the inclusion of the effects of Rayleigh scattering.
- 2. Reductions of O₃ by 30% from 12-40 km can lead to decreases in the tropopause temperature of approximately 3K. If the stratospheric H₂O concentrations are assumed to be determined by the tropical tropopause temperature, such a change could decrease stratospheric H₂O levels by one-third. Under the assumptions of a radiative-convective model, the surface temperature would then be reduced by 0:28K.
- 3. The reduction of O₃ in the presence of Rayleigh scattering, clouds, and a reflective surface leads, under the assumptions of a radiative-convective model, to a reduction of the surface temperature. The presence of levels of NO₂ above ambient provides a compensating effect. The effect is 1.6 times as large if a constant-cloud-top-temperature model is used rather than a constant-cloud-top-altitude model.
- 4. The albedo change associated with a 30% O_3 change in the presence of scattering, for $\delta = -6$, is comparable to, and in the same direction as, the albedo change associated with the direct effect of stratospheric sulfate aerosols between 15-25 km.
- 5. The thermal balance of the earth/ atmosphere system is sensitive to the altitude of the O₃ peak for a given column sum. This is due to the sensitivity of the longwave flux at the top of the atmosphere to the effective broadening pressure of the 9.6-μm band of O₃.

- 6. The coupled analysis predicts an 8.3% reduction of the column sum of O₃ and a maximum temperature decrease of 2K at 30 km for a standard injection case (500 SST's). The effect of the temperature coupling is to reduce the column-sum destruction of O₃ by approximately 10%.
- The coupled model studies indicate that the increase of the photodissociation rates of NO₂ [→O(³P)] and O₃ [→O(³P)] increases predicted ambient levels of NO by up to 50% and reduces predicted NO₂ levels by up to 25%.
- 8. The coupled-model studies indicate that perturbations of the O₃ and NO₂ photodissociation rates do not substantially alter the total O₃ destruction due to injection of NO by 500 SST's at 20 km or below. For injection at higher altitudes, the rate perturbations due to scattering can have an appreciable effect upon the O₃ column-sum destruction.

REFERENCES

- Ackerman, M. (1971), "Ultraviolet solar radiation related to mesopheric processes," in *Mesospheric Models and Related Experiments*, ed. Fiocco, Reidel Pub. Co., Dordrecht, 149-159.
- Ackerman, M., D. Frimout, C. Muller, D. Nevejans, J.-C. Fontanella, A. Girard, and N. Louisnard (1973), "Stratospheric nitric oxide from infrared spectra," Nature 245, 205.
- Blake, D., and R.S. Lindzen (1973), "Effect of photochemical models on calculated equilibria and cooling rates in the stratosphere," Mon. Wea. Rev. 101 (11), 783-802.
- Callis, L.B. (1972), "The radiative transfer equation and environmental effects in the upper atmosphere," AIAA Paper No. 72-663 (presented at the AIAA 5th Fluid and Plasma Dynamics Conference, Boston).
- Callis, L.B. (1974), "The importance of Rayleigh scattering on photochemical processes in the stratosphere," presented at the 1974 Fall Annual Meeting, Dec. 12-17, American Geophysical Union.
- Chang, J.S., D.J. Wuebbles, W.H. Duewer, A.C. Hindmarsh, N.K. Madsen, and R.L. Tarp (1974), "Second Annual Report, DOT-CIAP Program," Lawrence Livermore Laboratory, UCRL-51336-74, 25-59.

- Dickinson, R.E. (1973), "Method of parameterization for infrared cooling between altitudes of 30 and 70 kilometers," J. Geophys. Res. 78, 4451-4457.
- Fontanella, J.-C., A. Girard, L. Gramont, and N. Louisnard (1975), "Vertical distribution of NO, NO₂, and HNO₃ as derived from stratospheric absorption infrared spectra," Appl. Opt. 14, 825-839.
- Krueger, A.J., and R.A. Minzner (1973), "A Proposed Midlatitude Ozone Model for the U.S. Standard Atmosphere (Summary)," Goddard Space Flight Center, X-651-73-22.
- Lacis, A.A., and J.E. Hansen (1974), "A parameterization for the absorption of solar radiation in the earth's atmosphere," J. Atmos. Sci. 31, 118-133.
- Lazrus, A.L., and B.W. Gandrud (1974), "Distribution of stratospheric nitric acid vapor," J. Atmos. Sci. 31, 1102.
- Manabe, S., and R.F. Strickler (1964), "Thermal equilibrium of the atmosphere with a convective adjustment," J. Atmos. Sci. 21, 361-385.
- Mastenbrook, H.J. (1971), "The variability of water vapor in the stratosphere," J. Atmos. Sci. 28, 1495-1501.
- McClatchey, R.A., R.W. Fenn, J.E.A. Selby, F.E. Volz, and J.S. Garing (1972), "Optical Properties of the Atmosphere," AFCRL-72-0497, Environmental Research Papers No. 411.
- McElroy, M.B., S.C. Wofsy, J.E. Penner, and J.C. McConnell (1974), "Atmospheric ozone: Possible impact of stratospheric aviation," J. Atmos. Sci. 31, 287.

- Murcray, D.G., A. Goldman, F.H. Murcray, W.J. Williams, J.N. Brooks, and D.B. Barker (1973), "Vertical distribution of minor atmospheric constituents as derived from airborne measurements of atmospheric emission and absorption infrared spectra," AIAA Paper No. 73-103 (presented at the AIAA 11th Aerospace Sciences Meeting, Washington, DC); also in the CIAP 2 Proceedings.
- Penndorf, R. (1957), "Tables of the refractive index for standard air and the Rayleigh scattering coefficient for the spectral region between 0.2 and 20.0 and their application to atmospheric optics," J. Opt. Soc. Am. 47, 176-182.
- Ramanathan, V. (1974), "A simplified stratospheric radiative transfer model: Theoretical estimates of the thermal structures of the basic and perturbed stratosphere," in Preprints of the Second International Conference on the Environmental Impact of Aerospace Operations in the High Atmosphere (San Diego), pub. AMS, 147-154.
- Ramanathan, V., L.B. Callis, and R.C. Boughner (1976), "Sensitivity of surface temperature and atmospheric temperature to perturbations in stratospheric concentration of ozone and nitrogen dioxide," J. Atmos. Sci., in press.
- Rao, V.R. Krishna (1970), "A Numerical Experiment on the Steady State Meridional Structure of the Stratosphere," Ph.D. Thesis, Dept. of Meteorology, McGill University.
- Ridley, B.A., H.I. Schiff, A. Shaw, and L.R. Megill (1975), "In-situ measurement of stratospheric NO using a balloon-borne instrument," J. Geophys. Res. 80, 1925-1929; also (1974) in CIAP 3 Proceedings.

THE UV RADIATION FIELD IN THE STRATOSPHERE

N. SUNDARARAMAN Operations Research, Inc. Silver Spring, Maryland

ABSTRACT: The variations, with altitude and with latitude, of the direct and the diffuse solar UV fluxes, for selected wavelengths in the stratosphere, are presented. These fluxes are obtained from radiative-transfer calculations in an atmosphere with ozone absorption and molecular multiple scattering. It is shown that the diffuse fluxes add significantly to those directly received, and hence to the atmospheric heating rates, at stratospheric altitudes. The calculations use observed ozone data.

A knowledge of the climatology of solar ultraviolet (UV) radiation fluxes in the stratosphere is desirable both for the photochemical considerations of the region and for atmosphericheating rate calculations. In this paper, the distributions in altitude and in latitude of stratospheric UV fluxes, obtained from radiativetransfer calculations, are presented; the calculations assume a cloudless and aerosol-free atmosphere, stratified in plane-parallel layers, which is illuminated at the top by a parallel beam of unpolarized monochromatic radiation and which is bounded at the bottom by a surface of zero reflectivity. In addition, the effect of molecular scattering on atmospheric heating rates is illustrated.

The wavelength region considered extends from 240 nm (1 nm = 10^{-9} m) to 340 nm and includes almost all of the solar UV spectrum which penetrates to levels below the stratopause (≈ 50 km). (The wavelengths around the oxygen window at 200 nm, which are of interest because of their importance to the dissociation of chlorofluoromethanes in the upper stratosphere (Rowland and Molina, 1975), have not been included.)

The main atmospheric absorber of the radiation considered in this paper is ozone. There is also some absorption due to nitrogen dioxide; however, the amount of nitrogen dioxide occurring in the natural stratosphere is so small that its effects have been ignored in this study. In addition to absorption by ozone, the incident radiation suffers attenuation through multiple scattering by air molecules. The radiation reaching any level in the atmosphere does so in the form of a direct beam (F_e) and in the form of

diffuse or multiply-scattered radiation. The latter has both upward (F_u) and downward (F_d) components and is influenced by ground reflection. Obviously, as we ascend to higher altitudes in the stratosphere, the direct component assumes increasing importance.

The absorption coefficients of ozone in the UV region are known to be temperature-dependent (Vigroux, 1953, 1967). The temperature profiles for the different latitude zones and seasons tabulated in the U.S. Standard Atmosphere Supplements, 1966, have been used in this work to calculate this temperature dependence; the air-density profiles from the Supplements have been used in calculating scattering effects.

To calculate the direct fluxes, Beer's law is assumed:

$$F_s(z, \lambda) = \mu_0 F(\alpha, \lambda) e^{-[\tau_{\lambda}(z)/\mu_0]}$$

where $\mu_0 = \cos \theta_0$ with $\theta_0 = \text{solar zenith angle}$, $F(\alpha, \lambda)$ = solar flux for the wavelength λ incident at the top of the atmosphere (the values used are those tabulated by Ackerman (1971), and $\tau_{\lambda}(z)$ is the optical depth of the atmosphere at the altitude z, which includes both absorption and scattering effects. Figure 1 shows the values of the direct solar flux (F_s) varying with altitude for ten wavelengths and for four values of μ_0 : 0.8, 0.6, 0.4, and 0.2. The inset in this figure illustrates the ozone profile used; a description of the method of obtaining such ozone profiles is given below. Figures 2 and 3 show F_s variations for two other ozone amounts. The ozone amounts are representative of middle, low, and high latitudes respectively.

SUNDARARAMAN

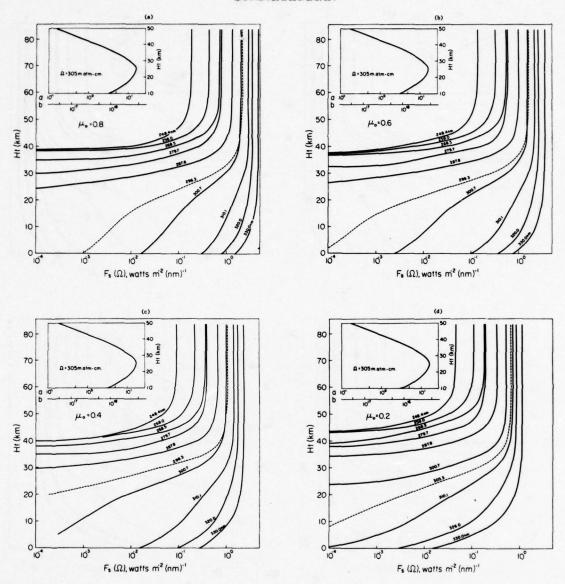


Figure 1. Height variation of the direct solar flux for a total ozone amount of 305 matm-cm. The inset shows the ozone profile used: scale a is matm-cm per km; scale b is molecules per m³.

Using umkehr data on the vertical distributions of ozone, Bojkov (1969) noted a close correlation between total ozone amount (Ω) and its vertical distribution. Bojkov's analysis has been extended in this study to include all vertical ozone data available up to 1972, taken from Ozone Data for the World (1957-1972) and

regression relations of the form $p_3(\ell) = A(\ell) + B(\ell) \Omega$ have been derived for each station where vertical ozone distribution is observed. Here $p_3(\ell)$ is the average partial pressure (nb) of ozone in layer ℓ, Ω is the total ozone amount (matm-cm) and $A(\ell)$ and $B(\ell)$ are constants for each layer. These constants are found to be

SUNDARARAMAN

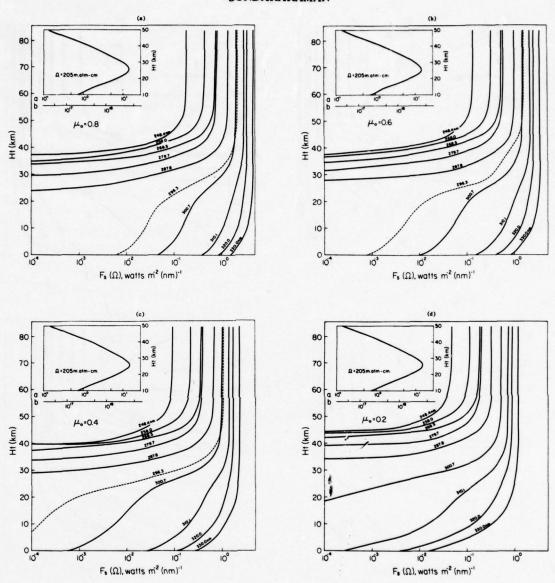


Figure 2. Height variation of the direct solar flux for a total ozone amount of 205 matm-cm. The inset shows the ozone profile used: scale a is matm-cm per km; scale b is molecules per m³.

functions of latitude, with little dependence on either longitude or season. Isolines of Ω , $A(\ell)$, and $B(\ell)$ can be drawn, and for any geographic point, values of Ω , $A(\ell)$, and $B(\ell)$ can be interpolated. From these values, an average altitude distribution of ozone for that point can be inferred. This procedure is found to be good

up to 35 km. Between 35 and 50 km, the latitude-height cross-sections of ozone amounts derived by Krueger et al. (1973), have been used. Above 50 km, all rocket and satellite observations reported in the literature were fitted to yield a smooth ozone height profile which is assumed to be independent of latitude and

SUNDARARAMAN

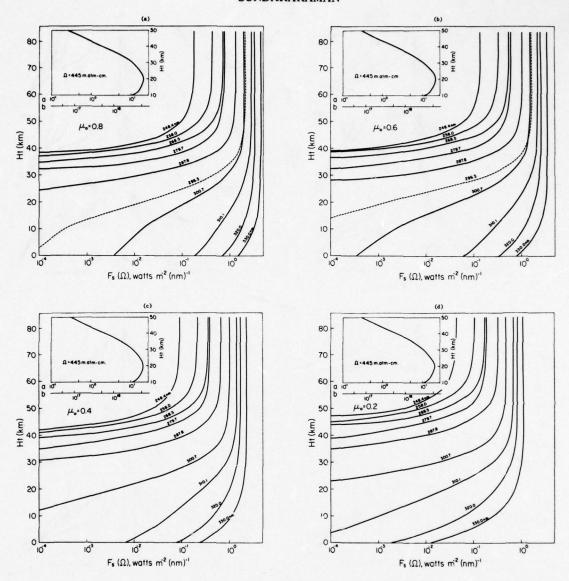


Figure 3. Height variation of the direct solar flux for a total ozone amount of 445 matm-cm. The inset shows the ozone profile used: scale a is matm-cm per km; scale b is molecules per m³.

longitude. In this profile, the ozone concentration decreases by approximately an order of magnitude for every 10-km height increase (Sundararaman, 1973; Sundararaman et al., 1973). This paper is the first effort, to the best of the author's knowledge, which thus uses available ozone climatology to derive stratospheric UV-flux climatology.

The diffuse component of the solar flux is arrived at by solving the equation of radiative transfer using well-known numerical iterative techniques (Herman and Browning, 1965; Dave and Furukawa, 1966; Sundararaman and Venkateswaran, 1975). Figure 4 depicts F_s and the ratios (F_d/F_s) and (F_u/F_s) as functions of altitude for three values of μ_0 (0.8, 0.6, and 0.4)

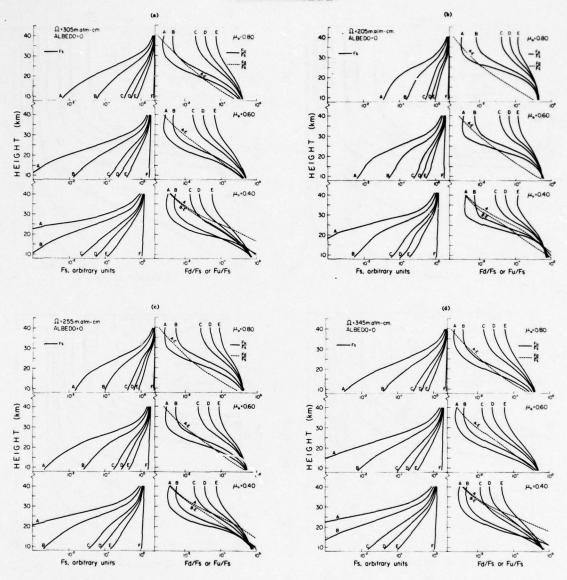


Figure 4. Height variation of the direct solar flux, and the relative contributions of the upward and downward fluxes. The fluxes are normalized to π units for vertical incidence at the top. Labeling: A, 296.7 nm; B, 300.4 nm; C, 305.5 nm; D, 308.8 nm; E, 311.4 nm; F, 600 nm. (The last is not discussed in this paper.)

and for four ozone amounts (with their inferred profiles). It may be seen that at 20 km, for example, and for Ω =305 matm-cm, the directly received energy is augmented as much as 25% by radiation which is scattered upward from the troposphere into the stratosphere. This fraction depends upon the wavelength, the solar zenith angle, and the ozone amount. The downward-

scattered component generally makes a smaller percentage contribution except for large absorption, which occurs either at shorter wavelengths or at larger solar zenith angles, for a given ozone amount.

Figures 5, 6 and 7 show the variation, with latitude, of the daily average values of the direct (\overline{F}_s) , the upward-scattered (\overline{F}_u) and the

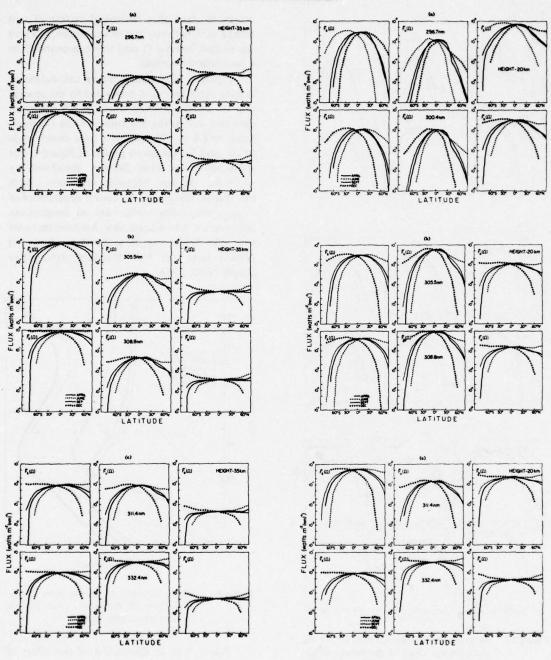


Figure 5. Latitudinal and seasonal variation of the daily average values of the direct, and the upward and downward diffuse, fluxes for selected wavelengths at 35 km altitude.

Figure 6. Latitudinal and seasonal variation of the daily average values of the direct, and the upward and downward diffuse, fluxes for selected wavelengths at 20 km altitude.

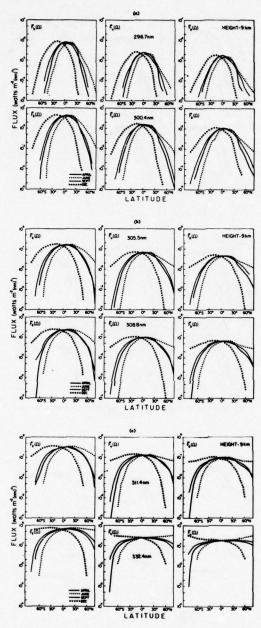


Figure 7. Latitudinal and seasonal variation of the daily average values of the direct, and the upward and downward diffuse, fluxes for selected wavelengths at 9 km altitude.

downward-scattered (\overline{F}_d) fluxes for six wavelengths and for four months at 35 km, 20 km, and 9 km respectively. These maps are good for 0° longitude. The daily average value is a quantity, which, when multiplied by the number of seconds in a mean solar day (86,400) gives the

energy incident on a horizontal surface of unit area (1 m²), between sunrise and sunset, in a unit wavelength interval (1 nm) which is centered on a particular wavelength.

Figure 8 illustrates a model calculation of heating rates (per unit mass) due to the absorption of several selected bands of UV radiation (and also due to the absorption of the Chappuis band, 497.5 to 695 nm) for a solar zenith angle of 60° and for the ozone profile of Figure 1. For wavelengths less than 240 nm, absorption by molecular oxygen becomes important. Such absorption, along with the known dependence of oxygen absorption coefficients on temperature and pressure, where applicable, has been included here. The model oxygen profile (not shown) is derived from the U.S. Standard Atmosphere Supplements, 1966.

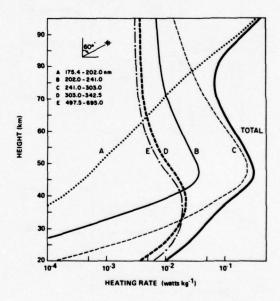


Figure 8. Height variation of heating rates due to absorption of the direct solar flux in selected wavelength bands.

Figure 9 is an illustration of the effect of molecular multiple scattering on atmospheric heating rates. The height distribution of the heating rate (in μ W m⁻³ nm⁻¹) is shown for $\lambda = 311.4$ nm for five values of μ_0 (1, 0.8, 0.6, 0.4 and 0.2) and for the ozone profile of Figure 1. An increase in the heating rate may be noticed when the effects of scattering are included (Panel B), which is quite marked when the sun is at or close to the zenith sky.

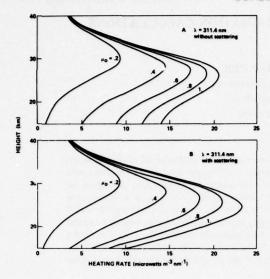


Figure 9. The effect of multiple scattering at 311.4 nm on atmospheric heating rates.

ACKNOWLEDGMENT

I am deeply grateful to Professor S.V. Venkateswaran of the University of California, Los Angeles, for his guidance and continued encouragement. I thank Mr. D.E. St. John of UCLA for his valuable assistance in computing these fluxes.

This work was supported by the Department of Transportation under the Climatic Impact Assessment Program.

REFERENCES

Ackerman, M. (1971), "Ultraviolet solar radiation related to mesospheric processes," in *Mesospheric Models and Related Experiments*, ed. G. Fiocco, pub. D. Reidel, Dordrecht, 149-159.

Bojkov, R.D. (1969), "Computing the vertical ozone distribution from its relationship with total ozone amounts," J. Appl. Meteor. 8, 284-292.

- Dave, J.V., and P.M. Furukawa (1966), "Scattered radiation in the ozone absorption bands at selected levels of a terrestrial Rayleigh atmosphere," Meteor. Monographs 7, (29).
- Herman, B.M., and S.R. Browning (1965), "A numerical solution to the equation of radiative transfer," J. Atmos. Sci. 22, 559-566.
- Krueger, A.J., D.F. Heath, and C.L. Mateer (1973), "Variations in the stratospheric ozone field inferred from Nimbus satellite observations," Pure Appl. Geophys. 106-108, 1254-1263.
- Ozone Data for the World (1957-1972), Meteorological Branch, Canadian Department of Transportation, Toronto, Canada.
- Rowland, F.S., and M.J. Molina (1975), "Chlorofluoromethanes in the Environment," Rev. Geophys. Space Phys. 13(1), 1-35.
- Sundararaman, N. (1973), "Some Consequences of the Absorption of Solar Ultraviolet Radiation by Atmospheric Ozone," Ph.D. thesis, University of California, Los Angeles.
- Sundararaman, N., and S.V. Venkateswaran (1975), "Radiation in the natural and perturbed troposphere," section 5.3 of Volume 4 of the CIAP monograph series, U.S. Dept. of Transportation, DOT-TST-75-54, 5-6 - 5-44.
- Sundararaman, N., D. St. John, and S.V. Venkateswaran (1973), "The characteristics of the solar ultraviolet radiation at Arosa," AIAA Paper No. 73-523, presented at the AIAA/AMS International Conference on the Environmental Impact of Aerospace Operations in the High Atmosphere (Denver).
- U.S. Standard Atmosphere Supplements, 1966, sponsored by ESSA, NASA, and the USAF, pub. by the U.S. Government Printing Office.
- Vigroux, E. (1953), "Contribution à l'étude experimentale de l'absorption de l'ozone," Ann. de Phys. 8, 709-762.
- Vigroux, E. (1967), "Détermination des coéfficients moyens d'absorption de l'ozone en vue des observations concernant l'ozone atmosphèrique à l'aide du spectromètre Dobson," Ann. de Phys. 2, 209-215.

RESULTS FROM RECENT SOLAR RADIATION CALCULATIONS

FREDERICK M. LUTHER

Lawrence Livermore Laboratory
University of California
Livermore, California

ABSTRACT: Results are presented from an extensive theoretical investigation aimed at evaluating (1) the effect of increased NO_2 concentrations on solar absorption as compared to that of reduced ozone concentrations and (2) the effect of molecular multiple scattering and ground reflection on photodissociation rates. In (1), we considered 17-km and 20-km injections of NO_x . In both cases, the increase in solar absorption by NO_2 was approximately 40% of the decrease in solar absorption caused by reduced ozone. The effect of changes in ozone and NO_2 concentrations on solar heating rates and planetary albedo are also shown as functions of solar zenith angle and surface albedo. In (2), results are compared with similar calculations typical of most atmospheric models which include absorption only in the direct solar beam. The functional dependence of the results on wavelength, height, solar zenith angle, and ground albedo is shown.

SOLAR ABSORPTION BY NO_2 IN THE STRATOSPHERE PERTURBED BY NO_{x} INJECTION

Introduction

While much attention has been directed toward nitrogen dioxide as a chemical reactant affecting the destruction of ozone in the stratosphere, little attention has been directed toward its property as an absorber of solar radiation. Hesstvedt and Isaksen (1974) were among the first to quantitatively study solar absorption by NO₂ and its role in the energy budget of the atmosphere. In this paper, we report the results of a theoretical study of the effect of increased NO₂ concentrations on solar absorption as compared to the effect of reduced ozone concentrations.

The Radiative-Transfer Model

The same radiative-transfer model was used for both studies described in this paper. The radiative-transfer model assumes a cloudless, plane-parallel atmosphere in which there is molecular multiple scattering and gaseous absorption above a Lambert ground. We consider only the wavelength region between 187.2 nm and 735 nm, in which molecular oxygen, ozone, and nitrogen dioxide are the dominant gaseous absorbers. The spectral

region is divided into 119 spectral intervals, of which 9 are in the Schumann-Runge bands of oxygen. The atmosphere between zero and 55 km is divided into 43 layers, the thickness of a layer being 1 km up to 35 km, then 2.5 km up to 55 km. Each atmospheric layer is subdivided into sublayers such that the optical depth of each layer, including scattering and absorption, is less than 0.02. There may be as many as 500 sublayers, depending upon the total optical depth of the atmosphere. The Gauss-Seidel iterative scheme (see Braslau and Dave, 1973) is used to solve the radiativetransfer equation to obtain the intensity of the radiation at increments of 6° in the local zenith angle for each level. Components of the intensity are then integrated over the upper and lower hemispheres to obtain the diffuse fluxes. The absorption cross-sections were derived from a variety of sources described in Gelinas at al. (1973).

The absorption cross-sections for ozone and NO₂ are shown in Figure 1. The peak in the NO₂ cross-section occurs near 400 nm, which is between the Huggins and Chappuis bands of ozone. The ozone cross-section is strongly peaked near 250 nm, and the peak in the cross-section for the weaker Chappuis band occurs near 600 nm.

The vertical profiles of temperature, pressure, and oxygen concentration correspond to those of the U.S. Standard Atmosphere

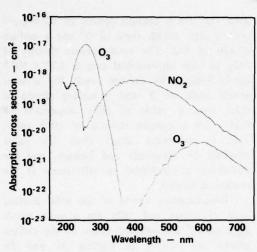
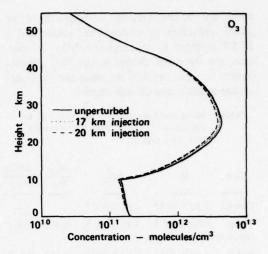


Figure 1. Absorption cross-sections for ozone and NO₂.

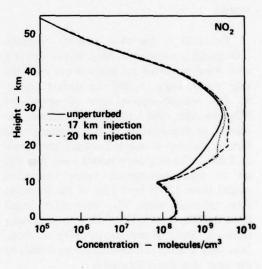
(1962). The concentration profiles for ozone and NO₂ were derived from Chang's (1974b) one-dimensional transport-kinetics model. The fact that the profiles of ozone and NO₂ concentration are not independent, but rather are coupled kinetically, ensures that the two profiles are at least consistent with our present understanding of the kinetics.

The perturbations which we consider are injections of NO2 at a source rate of 2000 molec/cm3 uniformly distributed over a 1-km-thick layer, at separate injection heights of 17 km and 20 km. (This annual injection rate (2.5 × 1012 g/yr) corresponds to a fleet of 4000 Concorde-type SST's). The ozone and NO2 concentration profiles for the unperturbed case, along with the 17-km and 20-km injection cases, are shown in Figure 2. The unperturbed ozone profile corresponds to 0.305 atm-cm of ozone. The unperturbed concentration profiles for ozone and NO2 both fall within the range of midlatitude stratospheric observations (LLL, 1974), although the tropospheric values of NO2 concentration are somewhat smaller than observed. However, this difference does not have a significant effect on the stratospheric heating rates because the attenuation due to solar absorption by NO2 is

Hesstvedt and Isaksen (1974) used three types of NO₂ profiles in their calculations. For two of their profiles, they assume a total



a. For ozone.



b. For NO2.

Figure 2. Vertical concentration profiles.

column density of 6×10^{15} cm⁻² at the tropopause. They did not state the height of their tropopause, but we have assumed it to be 13 km. The integrated column densities above 13 km for each of the three cases used in the present calculation are shown in Table 1. Hesstvedt and Isaksen's stratospheric column density for NO₂ lies between the 17-km and 20-km injection cases. The 17-km injection corresponds to a 5.3% reduction in stratospheric ozone and a 33.7% increase in stratospheric NO₂,

while the 20-km injection corresponds to an 11.2% reduction in stratospheric ozone and a 67.5% increase in stratospheric NO₂. In each case, the fractional change in the NO₂ column density is approximately six times the fractional change in the ozone column density.

Table 1. Integrated Column Densities Above 13 km (molec cm⁻²) and Relative Changes with NO_x Injection

Case	03	NO ₂	$\frac{\Delta O_3}{O_3}$	NO ₂
Control	7.92 × 10 ¹⁸	4.06 × 10 ¹⁵	_	_
17-km injection	7.50×10^{18}	5.43 × 10 ¹⁵	-0.053	0.337
20-km injection	7.03×10^{18}	6.80 × 10 ¹⁵	-0.112	0.675

Results

For each of the three sets of concentration profiles, ozone and NO2 solar-absorption rates were computed for selected values of the solar zenith angle, θ , and the surface albedo, R. The solar-absorption rates of ozone and NO₂ for the total atmospheric column, expressed as a percentage of the incoming solar flux at the top of the atmosphere, are shown in Table 2 for the unperturbed case. For this set of input parameters, ozone absorption ranged from 2.95% to 7.23% of the incoming solar radiation, while NO2 absorption ranged from 0.072% to 0.365% of the incoming solar radiation. Solar absorption by NO2 is, therefore, only a small fraction (0.024 to 0.050) of the solar absorption by ozone.

Table 2. Solar Absorption by Ozone and NO₂ for the Unperturbed Case, in Percent of the Incoming Solar Flux

Surface	Ozon	e Abso	orption	(%)	NC	2 Abso	rption (%)
Albedo	0°	30°	60°	78°	0°	30°	60°	78°
0.00	2.95	3.14	4.00	6.25	0.072	0.083	0.104	0.304
0.25	3.28	3.46	4.28	6.48	0.091	0.101	0.157	0.318
0.50	3.63	3.80	4.58	6.72	0.111	0.122	0.175	0.332
0.75	4.01	4.16	4.90	6.97	0.134	0.144	0.195	0.348
1.00	4.43	4.56	5.25	7.23	0.160	0.169	0.218	0.365

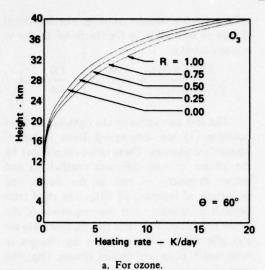
Hesstvedt and Isaksen (1974), using a simplified radiative-transfer model, computed NO₂ absorption to be 0.13% of the incoming

solar flux for a column density of 10^{16} cm⁻² with a solar zenith angle of 0° and a surface albedo of 0.2. The total column density of NO₂ for our unperturbed case is 4.27×10^{15} cm⁻². Scaling the present result for a solar zenith angle of 0° and a surface albedo of 0.25 gives a value of NO₂ absorption of 0.21% for a column density of 10^{16} cm⁻². This is somewhat larger than the value obtained by Hesstvedt and Isaksen, and the difference is attributed to differences in the numerical models.

Instantaneous values of the solar heating rates of ozone and NO2 for a solar zenith angle of 60° and selected values of the surface albedo are shown in Figures 3a and 3b respectively. The ozone heating rate increases monotonically with height through 40 km, while the NO₂ heating rate peaks near 32 km. Virtually no radiation reaches the earth's surface at wavelengths less than 290 nm, which means that surface albedo can affect ozone heating rates only through the Huggins and Chappuis bands. Consequently, changes in surface albedo do not cause large relative changes in the ozone heating rates. The NO2 heating rates, on the other hand, are much more sensitive to changes in surface albedo. Because there is almost complete atmospheric transmission at wavelengths greater than 330 nm (see the second half of this paper), the NO₂ heating rate nearly doubles as the surface albedo increases from 0.0 to 1.0.

The change (with respect to the unperturbed case) in the NO₂ absorption rate is compared to the change in the ozone absorption rate for the 17-km and 20-km injection cases in Table 3. The increase in NO2 absorption compensates for between 38% and 50% of the decrease in ozone absorption for the 17-km injection, and for between 34% and 47% for the 20-km injection. The increase in NO₂ absorption, therefore, significantly compensates for the decrease in sclar absorption by ozone. The values in Table 3 are only weakly sensitive to changes in surface albedo (particularly for large solar zenith angles). Even with the reductions in ozone concentration considered here, virtually all of the solar radiation in the Hartley band of ozone is absorbed, resulting in little change in the solar absorption in this band. Since the atmosphere is almost transparent in the Huggins and Chappuis bands,

LUTHER



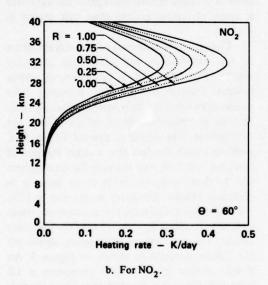


Figure 3. Unperturbed heating rates for selected values of surface albedo and a solar zenith angle of 60°.

ozone absorption in these bands is roughly proportional to the ozone column density. Since NO₂ absorption overlaps this spectral region, the changes in solar absorption by ozone and NO₂ depend similarly on surface albedo.

The changes in the instantaneous solar heating rates of ozone and NO₂ (as compared to the unperturbed case) for a solar zenith angle of 60° are shown in Figures 4a and 4b for the 17- and 20-km injections, respectively. We see that the injection at 20 km leads to changes in the heating

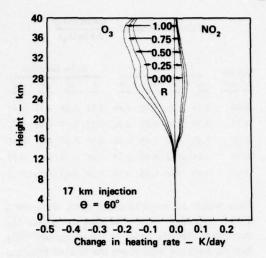
Table 3. Values of $-\frac{\Delta Abs(NO_2)}{\Delta Abs(O_3)}$

Surface	1	7-km l	njectio	on	2	0-km l	njectio	on
Albedo	<u>0°</u>	30°	60°	78	0°	30°	60°	78
0.00	0.38	0.39	0.45	0.49	0.34	0.36	0.41	0.47
0.25	0.38	0.40	0.45	0.50	0.35	0.37	0.41	0.47
0.50	0.40	0.41	0.45	0.50	0.36	0.38	0.41	0.47
0.75	0.41	0.42	0.45	0.50	0.38	0.39	0.42	0.47
1.00	0.43	0.43	0.45	0.50	0.39	0.40	0.42	0.47

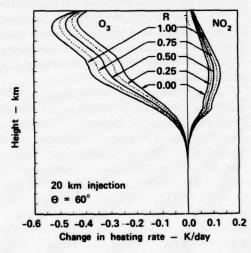
rates which are approximately twice those for a 17-km injection. The altitudes at which the maximum changes occur in the ozone and NO_2 heating rates are well above the level of injection of NO_x in both cases, the maximum change occurring near 37 km for ozone and near 27 km for NO_2 . Below 23 km the changes in the ozone and NO_2 heating rates are approximately equal in magnitude, although opposite in sign. Above 23 km the change in the ozone heating rate clearly is dominant.

An appreciation of how the change in NO2 absorption can be such a significant fraction of the change in ozone absorption, when NO2 absorption was such a small fraction of ozone absorption for the unperturbed case, can be obtained by considering the major elements which work together to bring this about. The significance of these elements, rather than being apparent prior to these calculations, is understood as a result of these calculations. An important element is that the change in NO2 column density is several times the change in ozone column density (in this case 6 times). Other kinetics calculations (see Chang, 1974a) predict factors ranging from 4 to 10 depending upon the magnitude and height of the injection. Another element is that there is not a one-to-one correspondence between the fractional change in the ozone column density and the fractional change in ozone absorption. For the cases considered here, the fractional change in ozone absorption was approximately 0.6 times the fractional change in ozone column density. Because of the non-linear relationship between ozone absorption and ozone column density, which results primarily from the strong absorption in the Hartley band, this factor would increase as the fractional reduction in ozone

LUTHER



a. Injection at 17 km.



b. Injection at 20 km.

Figure 4. Changes in ozone and NO₂ heating rates for an injection of NO_x.

column density increases, approaching a value of 1.0 as the ozone column density approaches zero. On the other hand, because NO₂ absorption is weak, there is approximately a one-to-one relationship between the fractional change in NO₂ absorption and the fractional change in NO₂ column density. The ratio of changes in NO₂ and ozone absorption can be estimated by multiplying the ratio of NO₂ absorption to ozone absorption for the unperturbed case (0.04) by the ratio of the fractional changes in column densities and the ratio of

correspondence factors relating the fractional change in absorption to the fractional change in column density.

$$-\frac{\Delta Abs(NO_2)}{\Delta Abs(O_3)} \approx \frac{0.04}{1} \times \frac{6}{1} \times \frac{1.0}{0.6} \approx 0.4 \tag{1}$$

The first two ratios on the right-hand side of equation (1) are determined from transport-kinetics calculations. These ratios are affected by the choice of eddy-diffusion coefficients and model chemistry as well as the height and magnitude of injection of NO_X . The third ratio depends principally upon the magnitude of the ozone reduction. This ratio and the first ratio are also affected to a lesser degree by changes in solar zenith angle and surface albedo. Thus, the ratio of changes in solar absorption can vary over a range of values greater than that shown in Table 3.

Changes in the amount of gaseous absorbers in the stratosphere will affect the planetary albedo. For example, a reduction in ozone column density allows more incoming solar radiation to enter the troposphere, resulting in an increase in upward-scattered radiation from the troposphere. The increased upward diffuse flux, embined with the fact that a larger fraction of this flux will now pass through the stratosphere and be jost to space, leads to an increase in planetary albedo. Similarly, an increase in NO2 column density decreases the atmospheric transmissivity, resulting in a decrease in the planetary albedo. The net increase in planetary albedo for the 20-km injection is shown in Figure 5. An albedo change of 3 X 10-3 represents a 1% change in the global mean albedo. These changes in planetary albedo represent significant perturbations to the global energy budget, as evidenced by their effect on surface temperature (Callis et al., 1975). The effect of the reduction in ozone column alone is approximately twice that of the combined effect shown in Figure 5. The effect of the increase in NO2 column density alone, being roughly half that of the ozone reduction, is approximately equal to the combined effect, although opposite in sign.

Conclusions

The amount of solar radiation absorbed by NO₂ is only a few percent of that absorbed by

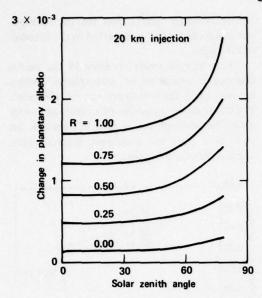


Figure 5. Change in planetary albedo vs. solar zenith angle for a 20-km injection of NO_x.

ozone for an unperturbed atmosphere, yet the change in NO₂ absorption resulting from the stratospheric injection of NO_x may be a significant fraction (on the order of 0.4) of the change in ozone absorption. This fraction, although dependent on many factors, is only weakly dependent on surface albedo and solar zenith angle. For these perturbations, the change in stratospheric solar heating rate is on the order of a few tenths of a degree Kelvin per day, with the most significant changes in the net solar heating rate occurring well above the level of injection of NO_x. Perturbations to the ozone and NO₂ column densities can also significantly affect the planetary albedo.

EFFECT OF MOLECULAR MULTIPLE SCATTERING AND SURFACE ALBEDO ON ATMOSPHERIC PHOTODISSOCIATION RATES

Introduction

At present, only the most elementary radiative-transfer calculations are incorporated in atmospheric models containing photochemically active species. This is primarily due to nothing more than computer running time and capacity limitations. For example, even the simplest atmospheric kinetics models are beset with computational constraints that normally lead one to invoke the assumption of a purely absorbing atomic and molecular atmosphere when determining solar fluxes for the evaluation of photodissociation rates. Because of these factors, the roles of multiple scattering, of the earth's surface reflection, and of clouds and aerosols in photochemical rates have remained a side-issue in atmospheric photochemical trace-gas models. However, it is well known that these radiative aspects can be significant in determining stratospheric and tropospheric radiative intensities at photodissociative wavelengths.

We present some results from the application of a reasonably general radiative-transfer model to the calculation of photodissociation rates. The model includes multiple molecular scattering and the earth's surface albedo. The effects of clouds and aerosols are not considered at this time. Photodissociation rates are computed for several reactions, representing different photodissociation spectral types, as a function of altitude, z, surface albedo, R, and solar zenith angle, θ , in order to provide a quantitative guide for sensitivity analysis on the pure-absorption photodissociation rates that are presently in use.

The Radiative-Transfer Applications in Atmospheric Photochemical Models

Stratospheric and tropospheric models that contain photochemically active species have almost universally invoked an assumption of pure absorption for computing solar fluxes and photodissociation rates. We will briefly review the elements of that approach and describe the pure molecular-absorption calculations that we perform for reference.

The solution of the one-dimensional, purely absorbing, source-free radiative-transfer equation at a particular altitude, z, solar zenith angle, θ , and atmospheric composition, $\left\{N_A(z)\right\}$, is given by

$$F_{\lambda}(z,\theta,\{N_A\}) = F_{\lambda}(\infty) \exp\left[-\tau_{\lambda}(z,\theta,\{N_A\})\right], \quad (2)$$

where $F_{\lambda}d\lambda$ is the flux of photons (cm⁻² sec⁻¹) in the wavelength interval $d\lambda$ about λ . $F_{\lambda}(\infty)$

represents the solar flux at one astronomical unit, and the optical depth, τ_{λ} , is given by

$$\tau_{\lambda}(z,\theta,\{N_A\}) \equiv \int_{z}^{\infty} dz' \sum_{A} N_{A}(z') \sigma_{T}^{A}(\lambda,T(z')) \sec\theta.$$
 (3)

In equation (3), the summation on A includes all atmospheric absorbers, each having number density $N_A(z)$ cm⁻³ and a total absorption cross-section $\sigma_A^T(\lambda, T(z))$ cm². Most generally, $\sigma_A^T(\lambda, T(z))$ is a function of the temperature, T(z). Since we consider only the spectral region of 187.2 nm to 735 nm, we include only absorption by O_2 , O_3 , and NO_2 , with only σ_{O_2} being dependent upon T(z).

The photodissociation rate for transforming species i to species j is denoted by

$$J_{i \rightarrow i}(z,\theta) N_{i}(z)$$
,

where

$$J_{i \to j}(z,\theta) \equiv \int_{\text{all } \lambda} d\lambda \, \sigma_D^i(j,\lambda,T(z)) \, F_{\lambda}(z,\theta,\left\{N_A\right\}) , \quad (4)$$

is expressed in terms of the microscopic photodissociation cross-section, $\sigma_D^i(j,\lambda,T(z))$ cm². Given microscopic cross-section data $F_{\lambda}(\infty)$, $\left\{N_A(z)\right\}$, and θ , it is a straightforward matter to compute photodissociation coefficients. In our calculations, we use $F_{\lambda}(\infty)$ derived from Ackerman's (1970) data, T(z) and N_{O_2} from the U.S. Standard Atmosphere (1962), and microscopic data from a variety of sources described in Gelinas et al. (1973). Values of $N_{O_3}(z)$ and $N_{NO_2}(z)$ are the same as those used in the first part of this paper for the unperturbed case.

When molecular multiple scattering and surface reflection are included in the calculation of photodissociation coefficients, the F_{λ} in Equation (4) includes the direct solar component plus the contribution by diffuse radiation, which is given by

$$\int_{4\pi} I_{\lambda} d\omega ,$$

where I_{λ} is the spectral intensity of the radiation (angle-dependent) and ω is solid angle. The

radiative-transfer model used for the multiplescattering calculation is described in the first half of this paper.

It is not necessary to show all the photodissociation reactions of atmospheric interest because basic spectral types can be identified. The transmission properties of a purely absorbing molecular atmosphere, as seen in Figure 6, are used as a basis for classifying spectral types. Three distinct regimes occur:

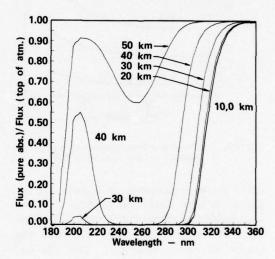


Figure 6. Transmission properties of a purely absorbing molecular atmosphere.

Regime 1: 187 nm $\leq \lambda \leq$ 290 nm

Virtually no radiation is transmitted to the lower elevations (0-10 km) for wavelengths shorter than 290 nm. Molecular species such as O₂, for which the dominant part of the photodissociation cross-section lies in this spectral region, are, therefore, not directly photochemically active in the lower atmosphere. At higher altitudes (≥ 20 km), there is the well-known O₂-O₃ window at about 200 nm-210 nm. Above 30 km, there is significant transmission through this upperatmospheric window.

Regime 2: 290 nm $\leq \lambda \leq 330$ nm

This is a transition region; virtually no solar radiation reaches the earth's surface at 290 nm, but there is almost complete transmission at 330 nm.

Regime 3: 330 nm $\leq \lambda \leq 735$ nm

In this spectral region there is virtually complete transmission at all altitudes for a purely absorbing atmosphere.

The effects of molecular multiple scattering and surface reflectivity on photodissociation rates are analyzed both in terms of their effect on the photodissociation coefficients for individual reactions and in terms of their effect on the flux entering Equation (4). An understanding of the spectral variation of their effect on the flux will aid in the interpretation of their effect on the photodissociation coefficients which result from a spectral integration.

Results

Extensive numerical calculations were performed while parametrically varying the solar zenith angle and surface albedo. In studying the spectral dependence of the effect on F_{λ} , we present only the results for a solar zenith angle of 60° , but these are qualitatively typical of the results for other zenith angles.

The ratio F_{λ} (multiple scattering)/ F_{λ} (pure absorption) is shown in Figure 7 for selected altitudes. At an altitude of 40 km, there is little change in the flux for wavelengths less than 290 nm. There is actually a slight decrease in the flux in this spectral region except in the vicinity of the local peak near 250 nm, at which point there is large attenuation of the solar flux. Since no solar radiation reaches the earth's surface at wavelengths less than 290 nm, there is no dependence on surface albedo in this spectral region.

The results for a surface albedo of 0.0 demonstrate the effect of molecular multiple scattering alone, which is shown to have its maximum effect near 330 nm. Molecular multiple scattering may cause as much as a 50% increase in F_{λ} , but this occurs over a relatively narrow spectral region. At wavelengths greater than 300 nm there is a strong dependence upon surface albedo, which may lead to as much as a

doubling of the flux for this solar zenith angle. For a surface albedo of 0.3 (approximate global mean), the flux is increased between 30% and 60% at wavelengths greater than 330 nm.

The ratio of fluxes for 30 km and 20 km shows little change compared to the results for 40 km at wavelengths greater than 300 nm. There is a significant change in the ratio of fluxes at wavelengths less than 300 nm, however. Large increases in the ratio of fluxes occur as large vertical optical depths ($\tau \approx 10$) are approached. Although these ratios are large, the magnitude of the flux is so small at these optical depths that the change in flux should have a negligible effect on species concentrations at these altitudes. This is demonstrated by the photodissociation of molecular oxygen, which is shown in Figure 8.

In the lower atmosphere, the downward solar flux is reduced due to increased back-scatter. On the other hand, the upward-scattered radiation from below tends to increase F_{λ} . As one moves downward from 10 km to the earth's surface, the downward flux is reduced, and the amount of atmosphere available to scatter the radiation upward is also reduced. Consequently, in moving from 10 km to the earth's surface, there is a dramatic decrease in F_{λ} for the multiple-scattering case. For most wavelengths, however, surface reflection is more than adequate to make up for the decrease in downward flux due to molecular scattering.

We now consider the effect of molecular multiple scattering and surface reflection on the photodissociation coefficients for specific reactions. Although we shall restrict our discussion to only a few reactions, they represent the variation in behavior that occurs as the spectral region of primary importance moves from Regime 1 to Regime 3:

$$O_3^{h\nu} O(^1D) + O_2$$
 (5a)

$$NO_2 \stackrel{h\nu}{\rightarrow} NO + O$$
 (5b)

$$O_3^{h\nu} O(^3P) + O_2$$
 (5c)

The ratio J (multiple scattering)/J (pure absorption) is shown for each of these reactions in Figure 9. The results are parameterized over height, surface albedo, and solar zenith angle (0, 30, 60, and 78°).

LUTHER 2.8 2.8 2.6 2.6 Z = 40 kmZ = 30 km2.4 2.2 2.0 1.8 Flux(mult. scat.)/Flux(pure abs.) 2.4 Flux(mult. scat.)/Flux(pure abs.) $\tau > 10$ 2.2 R = 1.00R = 1.00 2.0 0.75 0.75 1.8 1.6 0.50 1.6 0.50 1.4 0.25 1.4 0.25 1.2 1.2 0.00 0.00 1.0 1.0 0.8 0.8 0.6 0.6 0.4 0.4 0.2 0.2 0.0 0.0 300 200 400 500 600 700 200 300 400 500 600 700 Wavelength - nm Wavelength - nm 2.8 2.8 2.6 2.6 Z = 20 kmZ = 10 km2.4 2.4 Flux(mult. scat.)/Flux(pure abs.) $\tau > 10$ 2.2 R = 1.00R = 1.002.0 0.75 0.75 1.8 0.50 0.50 1.6 0.25 1.4 0.25 1.2 0.00 0.00 1.0 0.8 0.6 0.4 0.2 0.2 0.0 0.0 200 300 700 200 300 400 500 600 400 500 600 700 Wavelength - nm Wavelength - nm 2.8 2.6 Z = 0 km2.4 Flux(mult. scat.)/Flux(pure abs.) 2.2 R = 1.002.0 0.75 1.8 > 10-1.6 0.50 1.4 0.25 1.2 0.00 1.0 0.8 0.6 0.4 0.2 0.0 200 300 700 400 500 600 Wavelength - nm

Figure 7. Ratio of fluxes vs. wavelength at selected altitudes for a solar menith angle of 60°.

LUTHER

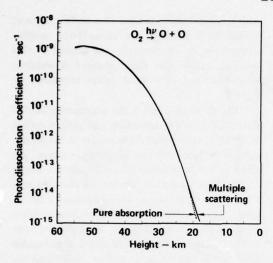
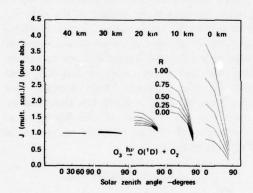


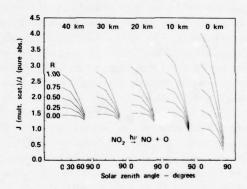
Figure 8. Photodissociation coefficients for the reaction $O_2 \stackrel{h\nu}{\rightarrow} O$ + O for a solar zenith angle of 60° .



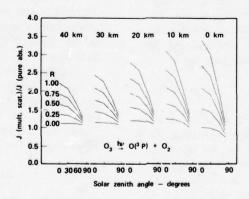
a. For the reaction $O_3 \stackrel{h\nu}{\rightarrow} O(^1D) + O_2$.

Reaction (5a) overlaps spectral Regimes 1 and 2. In Regime 1, there is no dependence upon surface albedo, so for altitudes greater than 35 km, the behavior of this reaction is typical of Regime 1. Molecular multiple scattering has a negligible effect on the photodissociation coefficient above 35 km because there is little scattering of the incoming radiation at these levels, and the tropospheric attenuation is so large that little radiation is scattered upward from below. As the flux in Regime 1 is depleted, the relative contribution of flux in Regime 2 increases. Consequently, the sensitivity of results to surface albedo increases markedly with decreasing altitude.

Reaction (5b) spans Regimes 2 and 3. Consequently, the photodissociation coefficients at all altitudes depend strongly on surface albedo. The values for R = 0.0 show that molecular scattering alone significantly increases



b. For the reaction $NO_2 \stackrel{h\nu}{\rightarrow} NO + O$.



c. For the reaction $O_3 \stackrel{h\nu}{\rightarrow} O(^3P) + O_2$.

Figure 9. Ratio of photodissociation coefficients, with and without scattering, vs. solar zenith angle.

the stratospheric values of the photodissociation coefficients.

Reaction (5c) is in Regime 3. In this case, the effect of molecular scattering alone on the stratospheric values of the photodissociation coefficients is significantly reduced.

There are certain features which are common to all three sets of results. In each case, the ratio of photodissociation coefficients decreases with increasing solar zenith angle, and at a given altitude the curves for different values of surface albedo converge as the solar zenith angle increases. Remember that F_{\(\lambda\)} for the multiplescattering case consists of two components: the direct solar flux and the contribution due to downward and upward diffuse radiation. The direct solar flux differs from the pure absorption flux only in terms of the additional attenuation due to the molecular-scattering optical depth. The gaseous-absorption optical thickness is the same for both cases. Contributions to the diffuse radiation field come from two sources: scattering out of the direct solar beam and scattering at the earth's surface. The diffuse radiation is strongly dependent upon the flux of photons incident at the top of the atmosphere, which varies as the cosine of the solar zenith angle. As the solar zenith angle increases, a larger fraction of the total flux is diffuse, but the incident flux at the top of the atmosphere is reduced. As the solar zenith angle increases, the direct solar flux decreases more rapidly for the multiple-scattering case because of the molecular-scattering optical depth. The net effect is a decrease in the ratio of photodissociation coefficients. Because less radiation is incident at the earth's surface at large solar zenith angles, the photodissociation coefficients corresponding to different values of the surface albedo at a given altitude tend to converge as the solar zenith angle increases.

Conclusions

There is a strong spectral variation in the effect which molecular multiple scattering and surface reflection have on photodissociation rates. We have analyzed these effects for three basic spectral regimes: 187 nm $\leq \lambda \leq$ 290 nm, 290 nm $\leq \lambda \leq$ 330 nm, and 330 nm $\leq \lambda \leq$ 735 nm. In Regime 1, surface albedo has no effect on photodissociation rates because vir-

tually no radiation reaches the earth's surface. Molecular scattering can cause large relative changes in F_{λ} at large optical depths in this spectral region, but these changes in absolute magnitude are very small when compared to $F_{\lambda}(\infty)$.

For Regimes 2 and 3, the combined effect of molecular multiple scattering and surface reflection can cause severalfold increases in the stratospheric values of the photodissociation coefficient for large values of surface albedo, which implies that significant changes in photodissociation rates might occur over extensive areas of snow, ice, or cloud cover. The results are highly sensitive to solar zenith angle, especially for large values of surface albedo. The effect of molecular multiple scattering and surface reflection decrease with increasing solar zenith angle.

Changes in the concentration profiles used in the calculation will alter these results at wavelengths where there is strong attenuation due to gaseous absorption. In Regime 1, the ratio F_{λ} (multiple scattering)/ F_{λ} (pure absorption) will be affected by changes in ozone concentration at large optical depths. Changes in ozone concentration will also affect values of this ratio near 600 nm (the Chappuis band). Because solar absorption by NO_2 is much less than that by ozone (see the first part of this paper), these results are only weakly sensitive to changes in NO_2 concentration.

ACKNOWLEDGMENTS

The author would like to thank Dr. Robert J. Gelinas for his contribution to the work described in the second half of this paper. Dr. Gelinas helped to develop the numerical model, and he provided very valuable guidance in its application.

This work was performed under the auspices of the U.S. Energy Research and Development Administration, under contract No. W-7505-Eng-48, and was supported in part by the Climatic Impact Assessment Program of the U.S. Department of Transportation.

REFERENCES

Ackerman, M. (1970), "Ultraviolet solar radiation related to mesospheric processes," Aeronomica Acta A 77.

LUTHER

- Braslau, N. and J.V. Dave (1973), "Effects of aerosols on the transfer of solar energy through realistic model atmospheres," J. Appl. Meteor. 12, 601-619.
- Callis, L.B., V. Ramanathan, R.E. Boughner, and B. Barkstrom (1975), "The stratosphere: Scattering effects, a coupled 1-D model, and thermal balance effects," in this volume.
- Chang, J.S. (1974a), "Simulations, perturbations, and interpretations," in Proceedings of the Third Conference on the Climatic Impact Assessment Program (Cambridge, MA), U.S. Dept. of Transportation, DOT-TSC-OST-74-15, 330-341.
- Chang, J.S. (1974b), private communication.
- Gelinas, R.J., R.P. Dickinson, and K.E. Grant (1973), "Solar Flux and Photodissociation Calculations for

- LLL Atmospheric Physics Programs," Rept. UCRL-74944, Lawrence Livermore Laboratory (Livermore, CA).
- Hesstvedt, E. and I.S.A. Isaksen (1974), "On NO₂-Absorption of Solar Radiation and Its Role in the Heat Budget of the Lower Atmosphere," Institute Report Series, No. 6, Institutt for Geofysikk, Universitetet i Oslo.
- LLL (1974), "Second Annual Report, DOT-CIAP Program," Rept. UCRL-51336-74, Lawrence Livermore Laboratory (Livermore, CA).
- U.S. Standard Atmosphere (1962), U.S. Government Printing Office, Washington, D.C. Also see U.S. Standard Atmosphere Supplements (1966), prepared for ESSA, NASA, and the USAF.

DETERMINING ATMOSPHERIC COMPOSITION FROM VERTICAL PROFILES OF DAYTIME LIMB BRIGHTNESS

K.YA. KONDRATYEV, O.M. POKROVSKY, AND M.A. SKORODENOK

University of Leningrad

Leningrad, USSR

ABSTRACT: Using the model of solar radiation transfer in a spherical atmosphere described in Newell and Gray (1972), formulas were obtained for the characteristics of the information content of vertical profiles of the daytime horizon brightness, in connection with the formulation and solution of the inverse problems. The results of the calculations revealed the optimal experimental conditions (solar zenith angle and wavelength) for the reconstruction of the vertical distribution of the concentration of three optically-active atmospheric components (aerosol, ozone, air density) from brightness data in the wavelength region of 0.2-0.7 μ m.

INTRODUCTION

The ever increasing interest in the problem of climate change, and in the factors causing it (see Pokrovsky, 1972), attracts the attention of scientists to another problem - that of estimating the role of various optically active (gaseous and aerosol) components of the atmosphere. This is the main reason for recent intensification of studies of the influence of aerosol on radiative transfer in the atmosphere (Kondratyev et al., 1973) and the development of methods for remote sensing from space of minor gaseous and aerosol atmospheric components (Kondratyev et al., 1974). This paper discusses the possibilities of determining the vertical profiles of some minor gaseous and aerosol components of the atmosphere from measurements of the brightness field of the daytime horizon.

The problem of interpreting data on the brightness field of the daytime horizon in the visible and infrared spectral regions is of interest because it is possible that such information can be used to determine the vertical profiles of the optically-active components of the troposphere, stratosphere, and mesosphere (Kondratyev, 1972; Kondratyev et al., 1974; Marchuk and Mikhailov, 1967; Newell and Gray, 1972; Rosenberg and Sandomirsky, 1967). Ozone and aerosol are among the dominant optically-active components in the abovementioned spectral regions. Of great importance also is the determination of

the density of the air which is responsible for molecular scattering. The interaction between solar radiation and the atmosphere is for present purposes determined by the processes of scattering and absorption. However, fluorescence is another possible process, and should be kept in mind in interpreting measurement data.

FORMULATING THE PROBLEM

To obtain information on the vertical profiles of the abovementioned atmospheric components, it is necessary to solve a problem which is the inverse of calculating the radiation field from the transfer equation. In the case of a spherical model of the atmosphere, even the latter problem is very difficult to solve because of the many complications connected with multiple radiation scattering (Marchuk and Mikhailov, 1967). Apart from the fact that such problems have no analytical solution, even their approximate numerical solution requires, as a rule, considerable computing time. Under these circumstances, a strict formulation of the inverse problem is practically impossible. In this case the only alternative is to select arbitrary concentration profiles, obtain the corresponding solution of the direct problem, and then improve the concentration profiles by an iterative procedure until the calculated brightness profiles agree with the measured ones. However, since the final variations of the vertical profiles of the components sought may correspond to negligibly small quantitative variations of the radiation field, the

abovementioned approach can lead to substantial errors.

Newell and Gray (1972) offer a simplified model of radiative transfer in a spherical atmosphere which makes it possible to establish the analytical relationship between atmospheric composition and the brightness of the daytime horizon. Here is its brief description. By introducing the optical thickness τ along the path (x_1, x_2) in the atmosphere

$$\tau_{\lambda} (x_1, x_2) = \sum_{\kappa} \int_{x_1}^{x_2} \rho_{\kappa} (x) + (\sigma_{s\kappa} (\lambda) + \sigma_{a\kappa} (\lambda)) dx$$
(1)

where ρ_{κ} (x) is the density (concentration), and $\sigma_{s\kappa}$ (λ), $\sigma_{a\kappa}$ (λ) are the scattering and absorption coefficients of the κ -component at wavelength λ , we obtain the following expression for the vertical profile of brightness:

$$I(\lambda, \psi, h) = \int_{L(h)} B(\lambda, \psi, h, x)$$

$$\cdot \{ \exp -\tau_{\lambda} (x_{s}, x) \} dx$$
(2)

Here L (h) is the length of the sighting line in the atmosphere, with tangent height h and boundary point (on the observer's side) x_s ; ψ is the solar zenith angle, and x is the running coordinate of a point on the sighting line (Figure 1). The value of the source function B (λ, ψ, h, x) is determined by the intensity of radiation coming to point x and scattered along the sighting line. B can be represented as the sum of three terms B_S , B_A , B_M , which determine respectively 1) the contribution of direct solar radiation (primary scattering), 2) the contribution of radiation reflected by the underlying surface, and 3) the contribution of multiple-scattered radiation. The following representation is valid for function B:

$$\mathbf{B}_{S}(\lambda,\psi,\mathbf{h},\mathbf{x}) = \sum_{\kappa} \mathbf{P}_{\kappa}(\psi) \cdot \sigma_{S\kappa}(\lambda) \cdot \rho_{\kappa}(\mathbf{x})$$

$$\cdot \mathbf{S}(\lambda) \cdot \sigma_{S\kappa}^{-\tau_{i}}(\mathbf{x}^{*},\mathbf{x})$$
(3)

Here S (λ) is the intensity of solar radiation at the point for the wavelength λ , and P_{ν} (ψ) is the

scattering phase function of the κ -component. Supposing that the underlying surface reflects solar radiation according to Lambert's law, Newell and Gray (1972) used for B_A the following representation:

$$B_{A}(\lambda,\psi,h,x) = A(\lambda,\psi,h,\omega_{s})$$

$$\cdot B_{S}(\lambda,\psi,h,x)$$
(4)

Here function A is connected analytically with both ω_s (the underlying surface albedo) and the values of ρ_κ (x) for the lower (relative to L (h)) atmospheric layers. The calculations of Newell and Gray for the direct problem by the Monte Carlo method have shown that for a number of atmospheric models the source function B_M can be represented approximately by the following formula:

$$B_{M} (\lambda, \psi, h, x) = m (\lambda, \psi, h)$$

$$\times (B_{S} (\lambda, \psi, h, x) + B_{A} (\lambda, \psi, h, x))$$
(5)

Here the empirical multiplier m is a function of λ , ψ , h only, and it is independent of the variations of profiles $\rho_{\kappa}(x)$ within a given ensemble of functions. Now, if we designate by $I_S(\lambda,\psi,h)$ the radiation intensity corresponding to the source function B_S , the total radiation intensity will take the form of

$$I(\lambda, \psi, h) = (1 + m(\lambda, \psi, h)) \times$$

$$(1 + A(\lambda, \psi, h, \omega_s)) I_s(\lambda, \psi, h)$$
(6)

If we now insert (3) into (2) and also take into account (4), (5), and (6), we can easily obtain explicit expressions for the dependence of I (λ, ψ, h) on ρ_{κ} (x), which will be determined by a system of non-linear integral equations of the first kind. Therefore, assuming that the characteristics of the interaction between radiation and atmospheric components $\sigma_{s\kappa}$ (λ), $\sigma_{a\kappa}$ (λ), and P_{κ} (ψ) are absolutely known, it becomes possible to formulate strictly the problem of finding the ρ_{κ} (x) by inversion of the integral equations mentioned above.

Naturally, for the conditions of the real atmosphere we cannot have precise information

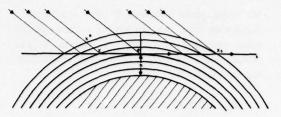


Figure 1. Diagram of the experiment.

on, for instance, the spatial distribution of aerosol optical parameters (scattering function, absorption and scattering coefficients) which vary due to the spatiotemporal variations of the chemical composition and microstructure of the aerosol. In this most difficult situation it appears worthwhile to analyze, at the first stage of the investigations, the possibilities of obtaining the information required about each of the variable parameters in turn, supposing that every other parameter is known precisely and is fixed. In recent years considerable experience in solving such problems in connection with the consideration of inverse problems for the infrared region been accumulated (Pokrovsky Timofeyev, 1972). Therefore, in formulating the problem of determining atmospheric composition as shown above, it appears worthwhile to perform the investigations according to the usual scheme (for inverse problems) (Pokrovsky, 1972). The first important stage of such an investigation should be the study of the information content of the experiment, and the determination of optimal measurement conditions: i.e., the determination of those values of the controllable variables λ , ψ , h at which the measured function I (λ, ψ, h) contains the largest amount of information about one or another atmospheric component. This paper presents the results of such an investigation, based on the supposition that vertical distributions ρ_s (h) (s = 1,2,3) of three atmospheric components are taken as the unknown parameters.

INFORMATION CHARACTERISTICS OF THE EXPERIMENT

In the numerical solution of the problem, the initial system of integral equations should be approximated by the corresponding system of algebraic equations. For this purpose, the interval of the variation of each of the independent variables (λ, ψ, h, x) is covered with a finite net of the values of these variables $(\{\lambda_i\}, \{\psi_j\}, \{h_k\}, \{x_i\})$, and the integral expressions are replaced by the corresponding quadratic sums. The algebraic system can formally be expressed as follows:

$$I(\lambda_i, \psi_i, h_k) = A[\rho_s(x_l)] + \epsilon_{ijk}$$
 (7)

$$(i = 1, ..., I; j = 1, ..., J; l = 1, ..., L; k = 1, ..., K; s = 1, 2, 3)$$

Here ϵ_{ijk} is the sum of errors of the experiment and those of the model used with λ_i, ψ_j, h_k . The unknown parameters form three L-dimensional vectors ρ_1, ρ_2, ρ_3 . These distributions fluctuate at random relative to the known mean $\bar{\rho}_1, \bar{\rho}_2, \bar{\rho}_3$. Let us assume that the deviation vectors $\Delta \rho_s = \rho_s - \bar{\rho}_s$ (s = 1,2,3) are distributed according to the normal law with the known covariance matrices K_1, K_2, K_3 , respectively. Radiation variations corresponding to component deviations $\Delta \rho_s$ (s = 1,2,3) are described by the following system of equations

$$\Delta I_{ijk} = \sum_{s=1}^{3} \sum_{l=1}^{L} A_{sl}^{ijk} \Delta \rho_{sl} + \widetilde{\epsilon}_{ijk}$$
 (8)

containing the operators of partial derivatives

$$A_{sl}^{ijk} = \frac{\partial A_{ijk}}{\partial \rho_{sl}} \ [\overline{\rho}_{sl}] \ ; \ (\rho_{sl} = \rho_{s} (x_{l})) \tag{9}$$

calculated with the mean values of the distributions sought for $\overline{\rho}_s$ (s = 1,2,3). Making use of (8), we come to the conclusion that ΔI_{ijk} are also random values having covariance matrices

$$K_{I}^{ijk} = \sum_{s=1}^{3} \left\{ A_{sl}^{ijk} \cdot K_{s}^{lm} \cdot \left(A_{sl}^{ijk} \right)^{*} \right\} + K_{\epsilon}^{ijk}$$
(10)

 (K_s^{lm}) is an element of matrix K_s (s = 1,2,3)). Here and below, summation over every index met twice is supposed. Now, in accordance with the results of Pokrovsky (1972), it is possible to calculate the information content (in Shannon's

sense) about one or another of the $\rho_s(h)$ components sought, contained in the results of measuring I.

Due to the non-linear character of system (7), the set of operators A_{sl}^{ijk} contains all the possible information on the sensitivity of measured values Iiik to variations of the unknown parameters $\Delta \rho_{sl}$. However, as can be seen from (9), the array of partial derivatives depending on five indices has a rather complex structure, allowing no possibility of direct analysis and clear (for instance, graphic) presentation. The only way to overcome this difficulty is index contraction, a procedure well known in tensor calculus. Let us use this procedure to obtain several information characteristics of the experiment. According to Pokrovsky (1972), the total information content extracted from measurements of Iiik is determined by the relationship

$$J(I_{ijk}) = \frac{1}{2} \cdot \log_2 \frac{|K_I^{ijk}|}{|K_c^{ijk}|}$$

(|A| is the determinant of matrix A).

By introducing the reduced covariance matrix of signal

$$K_I^{ijk}(s) = K_I^{ijk} - A_{sl}^{ijk} \cdot K_s^{lm} \cdot (A_{sm}^{ijk})^*$$
,(11)

we obtain the formula for the informant J, the amount of information about ρ_s contained in I_{iik} ,

$$J(I_{ijk}, \rho_s) = \frac{1}{2} \cdot \log_2 \frac{|K_I^{ijk}|}{|K_I^{ijk}(s)|}$$
 (12)

It is also possible to introduce a more detailed characteristic relating to component ρ_s in the mth atmospheric layer. For this purpose, the operation of reduction for only the mth diagonal element of matrix K_I^{ijk} in (11) is necessary. The substitution of the result of K^{ijk} (sm) into (12) will give the following formula for the informant:

$$J(I_{ijk}, \rho_{sm}) = \frac{1}{2} \cdot \log_2 \frac{|K_1^{ijk}|}{|K_1^{ijk}(sm)|}$$
 (13)

Indices i,j,k correspond to values of the controlled variables λ , ψ , h (on a discrete net), the choice of which determines the conditions of the experiment. By making use of formulae (12) and (13) it is possible to set up the problem of finding the optimal values of the controlled variables.

Let us investigate the dependence of the informant on one of the three such variables. In this case, the contraction of matrices over the other two variables should be performed in the right part of (12) and (13) by summation over the corresponding indices. If the value of one of the controlled variables has already been fixed, the contraction is performed over one index only. Combining the operation of contraction and fixation for various indices and components in formulas analogous to (12) and (13), we obtain a whole series of informants which fully characterize the information content of the experiment, and provide the basis for its optimal planning.

OPTIMAL MEASUREMENT CONDITIONS

The above set of information functions was used in the analysis of the information content of the data on vertical distributions of the daytime horizon brightness profiles in the 0.2-0.7 μ m region.

Let us dwell on the elements of the atmospheric optical model used, proceeding from the fact that in the spectral range considered it is necessary to take into account the two kinds of interaction between solar radiation and atmospheric components, i.e., scattering and absorption. Both molecular and aerosol atmospheric components scatter light. The Rayleigh scattering determines the law of interaction between radiation and the molecular component. The optical characteristics of aerosol (the coefficient and scattering function) were calculated by making use of the parameters n = 1.35, $\nu = 3$. (n is the refractive index; it is assumed that aerosols are a purely scattering component, and that their

microstructure is described by Junge's formula with the value $\nu = 3$.)

In the region considered, ozone absorbs solar radiation much more intensely than do other gaseous components and aerosol and may be considered to be the only absorbing component. Thus, this model contains three components which actively influence the formation of the brightness field.

For the purposes of calculation, the real atmosphere was approximated by a stratified spherically-symmetrical model. The 80-km atmospheric thickness considered was divided into 32 elementary layers 2.5 km thick.

As follows from the results of the above section, in order to calculate the information characteristics it is necessary to give the vertical distributions of the density of the components considered, as well as the covariance matrices describing natural variations of these distributions relative to the mean values. The corresponding data on air density were borrowed from Groves (1970). The data on ozone concentration were borrowed from Wu (1970). Elterman's "synthetic model", which was the basis of the work in Newell and Gray (1972), was used as the mean distribution of the aerosol attenuation coefficient. The elements of the corresponding covariance matrix were calculated under the assumption that within the 3 σ dispersion interval the attenuation coefficient can vary by one order of magnitude. All the calculations, with the exception of some specified cases, were based on the assumption that the sensitivity of the receivers of the spectral instruments constituted $10^{-5} \mu W/m^2$ nm ster.

As has already been mentioned above, the scheme of the experiment (illustrated in Figure 1) is determined by the choice of values of the three controlled variables λ , ψ , h. By the use of index contraction, the dependences of information content on each of the variables were obtained.

Figure 2 shows the graphs of the dependences on wavelength of the information content of the measurement data (separately for each of the components) for a number of solar zenith angles with $\omega_s = 0$. According to these data, it can be concluded that measurements of the brightness field of the daytime horizon contain

considerable information on the vertical distribution of aerosol, much less information on the ozone concentration, and still less information on variations of the air density.

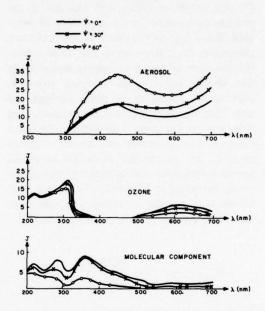


Figure 2. Dependence of the information content J of measurements on the wavelength λ , for three solar zenith angles ψ .

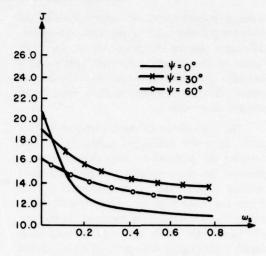
Analysis of the data presented in Figure 2 makes it possible to determine the values of λ which are optimal from the point of view of remote sounding of each of the atmospheric components considered. With respect to ozone, wavelengths near $\lambda = 300 \text{ nm}$ are most informative. The 220-nm wavelength is somewhat less informative. It should be noted that neither of these optimal wavelengths coincides with the position of maximum absorption in the Hartley-Huggins bands (265 nm). In the Chappuis band, $\lambda = 590 \text{ nm}$ appears to be optimal for ozone sounding. Consideration of the aerosol informant shown in Figure 2 makes it possible to conclude that the maximum of information is contained in the measurement data near $\lambda = 700$ nm and near 440 nm. Both of these spectral regions correspond to local minimums of absorption by ozone. Measurements near $\lambda = 700$ nm appear to be more informative, because the contribution of molecular scattering decreases abruptly with wavelength. However, the data of Figure 2 make

it possible to conclude that with the increase of the solar zenith angle ψ , the difference in the information content between wavelengths $\lambda = 440 \text{ nm}$ and $\lambda = 700 \text{ nm}$ diminishes, and is already negligible at $\psi = 60^{\circ}$.

With respect to the vertical distribution of air density, the most informative measurements occur in the 350-370 nm spectral interval. Consideration of the dependences of the information on λ at different solar zenith angles ψ makes it possible to discover certain regular features. Information on the aerosol component increases with the increase of ψ , which is due to the growing radiation intensity, determined by the primary scattering on aerosol particles. Due to the elongated aerosol scattering function, the relative contribution of aerosol scattering increases. This circumstance accounts for the decrease of the molecular and ozone informants with increasing ψ . It should be emphasized that these results are for a non-reflecting underlying surface, whose albedo is $\omega_s = 0$. For real conditions the surface albedo varies between 0.1 and 0.8. Therefore, let us now consider the results of investigating the dependence of the information content on ω_{ς} .

Figure 3 shows the graphs of such dependences of the aerosol and ozone informants on ω_s at three solar zenith angles. In considering these data, two opposed regular trends should be noted: as ω_s increases, the aerosol informant increases and the ozone informant decreases. The increase of information on the aerosol component can easily be accounted for by the increasing intensity of solar radiation reflected by the underlying surface and scattered along the sighting line. Here the relative contribution of radiation single-scattered by aerosol particles increases.

As can be seen from formulae (11) and (12), the informants obtained are relative characteristics, in the sense that they are normalized for the total amount of information (on the three components simultaneously). It is to this circumstance that the decrease of the ozone informant with increasing ω_s is due. The calculations made show that with the increase of ω_s , discrepancies in the values of the ozone informant between $\lambda = 220$ nm and $\lambda = 310$ nm are reduced, and have already disappeared completely at $\omega_s = 0.6$.



a. For aerosol, $\lambda = 700$ nm.

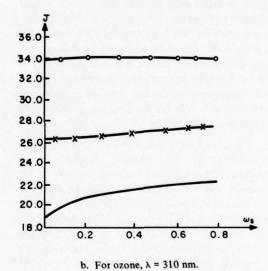


Figure 3. Dependence of the information content J of measurements on the underlying surface albedo ω_s , for three solar zenith angles ψ .

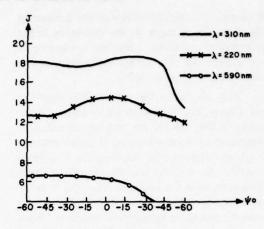
The data shown in Figure 3 reveal that with the increase of ψ , the dependence of the information content of the experiment on the value of the albedo ω_s weakens notably. Beginning with $\psi=60^\circ$, the aerosol informant becomes completely independent of ω_s . It has already been mentioned above that the optimal conditions for measuring the aerosol component are characteristic of high values of ψ . Therefore, in determining the aerosol vertical profile from

optimal measurements, the contribution of the underlying surface may be neglected. The ozone informant remains dependent on ω_s for small values of the albedo. Since low zenith angles provide more favorable conditions for measuring ozone, here underlying surfaces with small albedos are preferable.

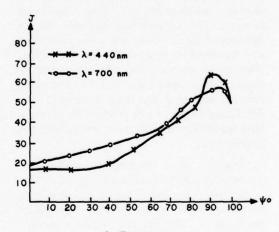
The dependence of the informants on solar zenith angle was mentioned earlier. Let us now consider the problem in more detail. Figure 4 presents the characteristics of the information content of the experiment as functions of ψ . Under the assumption that the optical characteristics of aerosol are known precisely, the increase of the aerosol informant with growing solar zenith angle (Figure 4a) can easily be accounted for by the elongation of the scattering function. In accordance with (3), (4), and (5), the source function (along the line of sight) depends linearly on the value of the scattering function for a fixed zenith angle. The data of Figure 4a also make it possible to conclude that with the increase of ψ the differences between the information content of measurements at the optimal wavelengths 440 nm and 700 nm remain, but appear to be negligible in the region of optimal angles 90-95°.

It should be noted, however, that the actual variability in the physical properties and chemical composition of aerosol particles causes considerable variations in their optical properties. In particular, fluctuations in the size distribution of particles lead to considerable variations of the scattering function. Here the greatest variations occur for scattering angles 0-20°, corresponding to zenith angles 70-90°. On the other hand, the relative contribution of multiple-scattered radiation decreases with the increase of ψ . Therefore, errors connected with the use of approximation (5) will also be much smaller with large values of U. Since the above-mentioned factors tend to compensate for each other, it may be supposed that their effect on the position of optimal values is insignificant.

Since the Rayleigh scattering function is much less elongated than the aerosol scattering function, the relative contribution of radiation scattered by aerosol increases more rapidly with the angle ψ than does the contribution of the molecular component. This results in the decrease of the molecular informant with the



a. For aerosol.



b. For ozone.

Figure 4. Dependence of the information content J of measurements on the solar zenith angle ψ .

increase of ψ . Therefore, zenith angles close to $\psi = 0^{\circ}$ are most favorable for determining air density.

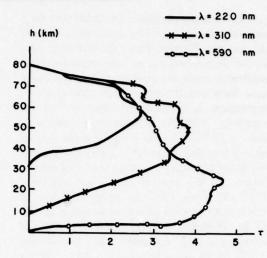
Figure 4b shows angular dependences of the ozone informants for three optimal wavelengths: 310, 220, and 590 nm. Most characteristic of these functions is their weak dependence on ψ in the interval between -60° and +10°, and a considerable decrease of the information content with $\psi > 30^\circ$. For measurements with $\lambda = 310$ nm the greatest information content corresponds to solar zenith angles close to $\psi = 20^\circ$. For other wavelengths the maximums of information take place at $\psi = 0^\circ$ and -30°. It

can be seen from the data of Figure 4b, however, that the range of angles from -10° to +20° may be considered favorable for simultaneous measurements at two or more wavelengths.

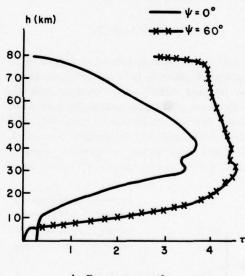
The foregoing considerations are derived from formulae like (12). The corresponding information characteristics give an idea of the total information content of remote sensing (under various experimental conditions) relative to the whole vertical distribution of the atmospheric component considered. However, it is also important to have data on the information content for individual atmospheric layers. The corresponding informants for various experimental conditions can be calculated using formulae like (13).

Figure 5 shows the results of calculations of the information content of the experiment for determining aerosol and ozone profiles. As can be seen from Figure 5a, the measurement data for $\lambda = 700$ nm contain the largest amount of information on the aerosol concentration in the 30-60 km layer. Below 15-20 km and above 70 km the experiment yields practically none of the necessary information. In the height interval 20-65 km, with increasing ψ the information content increases uniformly. The vertical structure of the aerosol informant for $\lambda = 440 \text{ nm}$ (not shown) differs from that described above, in that its upper limit of sounding is lower (40-50 km), corresponding to an increase of information content in the 10-30 km layer. Thus, the basic information on the aerosol distribution can be obtained from the data of measurements with $\lambda = 700$ nm. The use of measurement results for $\lambda = 440$ nm may appear worthwhile in connection with the sensing of aerosol layers at heights around 20 km.

The vertical profiles of the information content of the experiment for the ozone component for the optimal value of $\lambda = 310$ nm and two quasi-optimal values of $\lambda = 220$, 590 nm (Figure 5b) differ markedly. Measurements at $\lambda = 310$ nm chiefly contain information on atmospheric layers in the 30-65 km height interval. The data obtained from the brightness profile at $\lambda = 590$ nm in the less intense Chappuis absorption band relate to the height range 15-45 km. It can be seen from the data of Figure 5b that, with



a. For aerosol, $\lambda = 700$ nm.



b. For ozone, $\psi = 0^{\circ}$.

Figure 5. Vertical profiles of the information content of the experiment.

regard to its information content, the spectral region at $\lambda = 220$ nm is somewhat analogous to the optimal interval at $\lambda = 310$ nm. Taking account of the importance of the problem of sensing the ozone layer located at the height of 20-25 km, it may be concluded that it is necessary to use the data of measurements at both wavelengths (310 nm) and (590 nm) to reconstruct the vertical profile of ozone.

The above estimates were calculated for a radiation-sensor sensitivity level of 10-5 µW/ m² nm ster. Figure 6 shows the vertical profiles of the aerosol and ozone informants for other sensitivity levels of the instruments. The above data show that the information content of the experiment is substantially dependent on the sensitivity. With the decrease of the sensitivity level to $10^{-4} \mu \text{W/m}^2$ nm ster., the upper limit of aerosol sounding decreases to 50-55 km, whereas the lower boundary of ozone sounding rises to 30 km. In the case of very poor sensitivity $(10^{-2} \mu \text{W/m}^2 \text{ nm ster})$ the upper boundary of this indirect method of aerosol sounding appears to be 35-40 km, and the lower boundary of ozone sounding, determined by the vertical profile of the ozone informant, is 35 km. With a decrease in sensitivity, the information content of the experiment also decreases.

CONCLUSION

Since this paper describes the solution of the problem of planning the experiment, its results can be used directly in connection with the development of instrumentation. We have determined optimal measurement conditions (the solar zenith angle, the wavelength) for each of the three atmospheric components (aerosol, ozone, the molecular component) which are of

interest to us. It has been found that the brightness profiles provide the most information for the aerosol component. They provide the least for air density. The influences of the underlying surface albedo and of the measurement error level have been investigated. The distribution of information for each of the components in different atmospheric layers has been analyzed. These results make it possible to assess the possibilities of the considered method of remote sensing. However, to estimate the accuracy of the method, it is necessary to compare the atmospheric-component vertical profiles, reconstructed from the data on brightness profiles using this model, with those obtained from direct concentration measurements. It appears desirable to assess the dependence of the information content of brightness measurements on the parameters of the microstructure of aerosol (particle size distribution, complex index of refraction). Of great interest is the problem of the information content of the polarization characteristics of the radiation field.

REFERENCES

Groves, G.V. (1970), "Seasonal and Latitudinal Models of Atmospheric Temperature, Pressure and Density," Air Force Surveys in Geophysics, No. 218

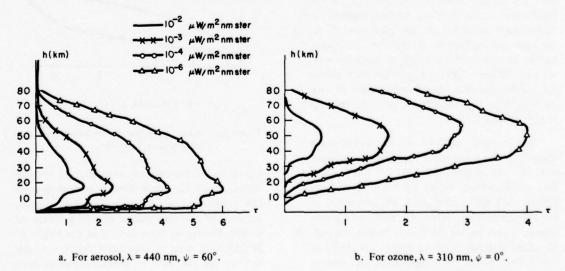


Figure 6. Vertical profiles of the information content of the experiment with four sensitivity levels of the measurement instruments.

- Kondratyev, K.Ya. (ed.) (1972), Investigation of the Environment from Manned Orbital Stations, Gidrometeoizdat, Leningrad.
- Kondratyev, K.Ya., O.B. Vassilyev, L.S. Ivlev, G.A. Nikolsky, and O.I. Smokty (1973), Influence of Aerosol on Radiation Transfer: Possible Climatic Consequences, Leningrad University Press.
- Kondratyev, K.Ya., A.A. Grigoryev, A.G. Pokrovsky, O.M. Pokrovsky, O.I. Smokty, Yu.M. Timofeyev (1974), Remote Sensing of Minor Gaseous and Aerosol Components of the Atmosphere from Space, Leningrad University Press.
- Marchuk, G.I., and G.A. Mikhailov (1967), "Results of the solution of some problems of atmospheric optics by the Monte-Carlo method," Izvestia USSR Acad. Sci., Fiz. Atmos. Okean. 3 (4).

- Newell, R.E., and C.R. Gray (1972), "Meteorological and Ecological Monitoring of the Stratosphere and Mesosphere," Contr. Rept. CR-2094, National Aeronautics and Space Administration, Washington, D.C.
- Pokrovsky, O.M. (1972), "On the optimal conditions of indirect sounding of the atmosphere," Izvestia USSR Acad. Sci., Fiz. Atmos. Okean 8 (10).
- Pokrovsky, O.M., and Yu.M. Timofeyev (1972), "A general statistical approach to the solution of the inverse problems of atmospheric optics," Meteorol. Hydrol. 1.
- Rosenberg, G.V., and A.B. Sandomirsky (1967), "Determination of the scattering coefficient vertical variation from photographs of the Earth's daytime horizon," Izvestia USSR Acad. Sci., Fiz. Atmos. Okean. 3 (2).
- Wu, M.F. (1970), "Ozone Distribution and Variability," MIT Aeronomy Program Internal Rept. No. AER 1-2.

THEORY OF RADIATIVE TRANSFER

DISCUSSION

VUPPUTURI: I have a comment on ozone and temperature coupling. Depending upon where you reduce the ozone in the stratosphere, it can produce heating or cooling of the surface. For example, in my 2-D model, if you reduce the ozone in the upper stratosphere, the radiation that is not being absorbed there (because of the ozone reduction) is being absorbed at a lower level. This produces a shift in the tropopause of about 5 kilometers, and where this shift occurs, it produces a heating effect. Also, Dr. Callis, you mentioned that the albedo effect is comparable to the aerosol effect, as I understand it. Did you incorporate the aerosols into your model? If so, did you still get the same effect?

CALLIS: I did not calculate the aerosols in the model. The comparisons that I was alluding to were the work of Herman, which was reported here last year and appears in the CIAP 3 *Proceedings*. I took a look at the change in the albedo, based on his calculations which were

carried out at 1/2 micron, for various particulate loadings between 15 and 25 kilometers. On the basis of his conclusions, it seems that the change he observes is of the same order of magnitude as the change associated with the decrease in ozone. We are now in the process of including aerosols in a calculation of our own so that we can do parametric studies of this particular problem.

(UNIDENTIFIED): Dr. Callis, what method do you and your co-workers use for your multiple-scattering calculations?

CALLIS: The method we use is a calculation routine that I developed and reported in 1972. The radiative-transfer equation becomes a hyperbolic equation, and solution techniques that are well adapted to hyperbolic systems apply. It turns out that this solution is unconditionally stable and convergent, and can be as accurate as you choose to make it, depending on your selection of the zenith angle, the azimuthal coordinates, and the vertical coordinates.

A TWO-DIMENSIONAL PHOTOCHEMICAL MODEL OF THE ATMOSPHERE BELOW 55 KM: ESTIMATES OF NATURAL AND MAN-CAUSED OZONE PERTURBATIONS DUE TO NO_x*

PAUL J. CRUTZEN
Aeronomy Laboratory
NOAA Environmental Research Laboratories
Boulder, Colorado

and

National Center for Atmospheric Research**
Boulder, Colorado

ABSTRACT: A two-dimensional photochemical model of the troposphere and stratosphere is formulated. Calculated meridional and seasonal distributions of important constituents are presented, and it is shown that there is often a very good correspondence between theoretical and observed concentrations. Transport of water vapor, its evaporation at ground level, and its removal by precipitation, as well as rainout processes for gases in the troposphere, are considered. The transport parameterization derived in this study yields a 'dry' stratosphere.

It is calculated that variations in NO production from galactic cosmic rays over the 11-year solar cycle may cause variations in the total ozone content at high latitudes of at most 0.5%, which is about 10 times less than observed. Estimates are presented of the effect on the ozone layer of aircraft flying in the stratosphere.

INTRODUCTION

One-dimensional models have given a remarkably accurate description of the average vertical distribution of a number of photochemically reactive gases in the atmosphere (see, e.g., Crutzen (1973, 1974) and Wofsy and McElroy (1974)). Such models have formed, therefore, much of the basis for the assessment of the possible future environmental impact of aircraft operations in the stratosphere (Grobecker et al., 1974; NAS, 1975). The published estimates of future ozone reductions obtained with higher-order models (e.g., Hesstvedt, 1974; Cunnold et al., 1975) do not differ grossly from those obtained with the one-dimensional models. Nevertheless, it is clear that further development of higher-order models is extremely important, mainly because such models allow a better interpretation of observational data. Ideally models should be developed which permit detailed studies of full interactions between radiative, photochemical, and hydrodynamical processes. Among the simplest higherorder models should be ranked the twodimensional, zonally-averaged models in which the transport of the chemical constituents is prescribed by sets of empirically-derived transport parameters, while temperatures are chosen to be equal to the average observed temperatures. In such models it is assumed that, to a first approximation, any changes to the chemical composition of the stratosphere (e.g., caused by human activities) do not alter the average temperatures and transport parameters of the unperturbed state.

In this paper a two-dimensional, timedependent photochemical model is presented,

^{*}This article does not cover exactly the same material that was presented at the Fourth Conference on CIAP. In particular, since the effect of halogen compounds on stratospheric ozone has been treated in a number of recent papers, it seemed more worthwhile to devote the present discussion to the original CIAP-related issues, which centered around the effects of oxides of nitrogen (natural or man-made) on the ozone layer.

Due to time limitations, this presentation is rather short and the author apologizes for the fact that the number of references has been kept to a minimum. A more extensive version of this article will be prepared in the near future.

^{**}NCAR is sponsored by the National Science Foundation.

which incorporates the photochemistry and meridional transport of a great number of important gaseous compounds from ground level to about 55 km. A set of transport parameters (eddy-diffusion coefficients) is derived, which seems to describe satisfactorily the meridional and seasonal distributions of ozone and other constituents. This model is used to calculate the global variations in total ozone caused by periodic variations in the intensity of galactic cosmic rays. Estimates will also be presented of reductions in total ozone which would be caused by the operation of large fleets of supersonic aircraft in the stratosphere.

MODEL DESCRIPTION

The set of photochemical reactions used in this model is given in Table 1. The continuity equation which describes the rate of change with time (t) of the zonal-average concentration of any constituent or combination of constituents (X) at a given latitude (ϕ) and height (z) can be written in the following way:

$$\frac{\partial(X)}{\partial t} = -\frac{\partial}{\partial z} F_z - \frac{1}{a \cos\phi} \frac{\partial}{\partial \phi} (\cos\phi F_y)$$

$$+ P(X) \qquad (1)$$

In this expression P(X) is the net production of X (which includes both photochemistry and rainout), a is the radius of the earth, and F_y and F_z are the northward and upward components of the meridional flux of X, which, considering mean motions and eddy diffusion, may be approximated by the following formulae (Reed and German, 1965):

$$F_{y} = -K_{yy}(M) \frac{\partial}{\partial y} \mu_{x} - K_{yz}(M) \frac{\partial}{\partial z} \mu_{x}$$

$$+ v(X)$$

$$F_{z} = -K_{yz}(M) \frac{\partial}{\partial y} \mu_{x} - K_{zz}(M) \frac{\partial}{\partial z} \mu_{x}$$

$$+ w(X)$$
(2)

((M) = concentration of air molecules; $\mu_X = (X)/(M)$; dy = ad ϕ ; v, w are northward and upward components of the mean meridional

winds; K_{yy} , K_{yz} , and K_{zz} are eddy-diffusion coefficients.) $K_{yz} = 0$ when upward and downward motions are statistically uncorrelated; otherwise, mixing occurs preferentially along surfaces which slope with an angle α with regard to the horizontal plane. In that case we may write, to a first-order approximation (Reed and German, 1975),

$$K_{yy} = K_{11}$$

$$K_{yz} = \alpha K_{11}$$

$$K_{zz} = K_{22} + \alpha^2 K_{11}$$

$$(3)$$

where K₁₁ and K₂₂ denote the diffusion coefficient along and perpendicular to the main diffusion axis. With the aid of expression (3) it is easy to derive the diffusion coefficients applying to any arbitrary coordinate system. The values for K_{11} , α , and K_{22} applied in this study are shown in Table 2-5. These values were obtained by "trial and error" to give the best agreement between the observed and calculated temporal and latitudinal distributions of ozone and water vapor. Insufficient information is available on trace-gas distribution above about 30 km, so the evaluation of eddy-diffusion coefficients in these regions is quite arbitrary. Mean-wind data for the four seasons were adopted from Louis (1974). In order to satisfy mass-continuity requirements, the wind components were expressed as meridional derivatives of the stream function,

Pressure coordinates were adopted as the vertical coordinates in this study. This is again important to satisfy the mass-continuity requirements, which seems essential since we are interested in relatively small (of the order of 1%) changes in total ozone due to anthropogenic influences. Typically, in two-dimensional models, climatological-mean temperatures are prescribed for each season (or sometimes month). Air parcels may be considered to follow constantpressure surfaces, changing the temperature distributions, with no change in the mixing ratios of the different chemicals. By comparison, neither concentrations nor mixing ratios are conserved at constant height surfaces. The pressure levels were chosen to correspond to height intervals of about 2 km, except for the lowest two kilometers,

Table 1. Reaction Scheme and Coefficients. A number of heterogeneous reactions in the troposphere were also considered.

Oxygen reactions

R1	$O_2 + h\nu \rightarrow O + O$	λ < 242 nm
R2	$O + O_2 + M \rightarrow O_3 + M$	$k_2 = 1.1 \times 10^{-34} \exp(500/T)$
R3a	$O_3 + h\nu \rightarrow O_2 + O(^1D)$	$\lambda < 319 \text{ nm}$
R3b	$O_3 + h\nu \rightarrow O_2 + O$	$\lambda < 1140 \text{ nm}$
R4	$O_3 + O \rightarrow O_2 + O_2$	$k_4 = 1.9 \times 10^{-11} \exp(-2300/T)$
R5	$O(^1D) + M \rightarrow O + M$	$k_5 = 6.0 \times 10^{-11}$

Reactions defining relative concentrations of OH, H, HO $_2$, H $_2$ O $_2$, and HNO $_3$

R6	$O + OH \rightarrow H + O_2$	$k_6 = 4.2 \times 10^{-11}$
R7	$O_3 + OH \rightarrow HO_2 + O_2$	$k_7 = 1.6 \times 10^{-12} \exp(-1000/T)$
R8	$CO + OH \rightarrow H + CO_2$	$k_8 = 2.1 \times 10^{-13} \exp(-75/T)$
R9	$H_2 + OH \rightarrow H + H_2O$	$k_9 = 2.3 \times 10^{-11} \exp(-2450/T)$
R10	$O_3 + H \rightarrow OH + O_2$	$k_{10} = 2.6 \times 10^{-11}$
R11	$O_2 + H + M \rightarrow HO_2 + M$	$k_{11} = 2.1 \times 10^{-32} \exp(290/T)$
R12	$O + HO_2 \rightarrow OH + O_2$	$k_{12} = 2.0 \times 10^{-11}$
R13	$O_3 + HO_2 \rightarrow OH + 20_2$	$k_{13} = 1.0 \times 10^{-13} \exp(-1250/T)$
R14	$NO + HO_2 \rightarrow OH + NO_2$	$k_{14} = 2.2 \times 10^{-13}$
R15	$OH + NO_2 (+ M) \rightarrow HNO_3 (+ M)$	
R16	$HNO_3 + h\nu \rightarrow OH + NO_2$	$\lambda < 546 \text{ nm}$
R17	$HO_2 + HO_2 \rightarrow H_2O_2 + O_2$	$k_{17} = 3.0 \times 10^{-11} \exp(-500/T)$
R18	$H_2O_2 + h\nu \rightarrow OH + OH$	$\lambda < 565 \text{ nm}$

Production and loss reactions for odd hydrogen and nitric acid

R19a	$H_2O + O(^1D) \rightarrow OH + OH$	$k_{19a} = 3.0 \times 10^{-10}$
R19b	$CH_4 + O(^1D) \rightarrow CH_3 + OH$	$k_{19b} = 4.0 \times 10^{-10}$
R19c	$H_2 + O(^1D) \rightarrow H + OH$	$k_{19c} = 3.0 \times 10^{-10}$
R20	$OH + OH \rightarrow H_2O + O$	$k_{20} = 1.1 \times 10^{-11} \exp(-500/T)$
R21	$OH + HO_2 \rightarrow H_2O + O_2$	$k_{21} = 6.0 \times 10^{-11}$
R22	$OH + H_2O_2 \rightarrow H_2O + HO_2$	$k_{22} = 1.7 \times 10^{-11} \exp(-900/T)$
R23	$OH + HNO_3 \rightarrow H_2O + NO_3$	$k_{23} = 6.0 \times 10^{-13} \exp(-400/T)$

Methane oxidation reactions

R24	$OH + CH_4 \rightarrow H_2O + CH_3$	$k_{24} = 2.5 \times 10^{-12} \exp(-1660/T)$
R25	$CH_3 + O_2 + M \rightarrow CH_3O_2 + M$	$k_{25} = 2.6 \times 10^{-31}$
R26	$CH_3O_2 + NO \rightarrow CH_3O + NO_2$	$k_{26} = 1.5 \times 10^{-12} \exp(-500/T)$

^{*}Units: Two-body reactions: cm³ molecules⁻¹ s⁻¹; three-body reactions: cm⁶ molecules⁻² s⁻¹

Table 1. Reaction Scheme and Coefficients. A number of heterogeneous reactions in the troposphere were also considered. (cont.)

R27 R28 R29 R30a	$CH_3O_2 + HO_2 \rightarrow CH_3O_2H + O_2$ $CH_3O_2H + h\nu \rightarrow CH_3O + OH$ $CH_3O + O_2 \rightarrow CH_2O + HO_2$ $CH_2O + h\nu \rightarrow H_2 + CO$	$k_{27} = 3.0 \times 10^{-11} \text{ exp(-500/T)}$ $J_{\text{CH}_3\text{O}_2\text{H}} = J_{\text{H}_2\text{O}_2} \text{ (assumed)}$ $k_{28} = 4.2 \times 10^{-13} \text{ exp(-3000/T)}$ $\lambda \le 350 \text{ nm}$
R30b	$CH_2 O + h\nu \rightarrow H + CHO$	λ ≤ 350 nm
R31	$CH_2O + OH \rightarrow H_2O + CHO$	$k_{31} = 1.4 \times 10^{-11}$
R32	$CHO + O_2 \rightarrow HO_2 + CO$	$k_{32} = 1.7 \times 10^{-13}$
	Nitrogen reactions	
R33	$NO + O_3 \rightarrow NO_2 + O_2$	$k_{33} = 9.0 \times 10^{-13} \exp(-1200/T)$
R34	$NO_2 + O \rightarrow NO + O_2$	$k_{34} = 9.2 \times 10^{-12}$
R35	$NO_2 + h\nu \rightarrow NO + O$	$\lambda < 400 \text{ nm}$
R36	$N + O_3 \rightarrow NO + O_2$	$k_{36} = 3.0 \times 10^{-11} \exp(-1200/T)$
R37	$N + O_2 \rightarrow NO + O$	$k_{37} = 1.1 \times 10^{-14} \exp(-3150/T)$
R38	$N + OH \rightarrow NO + H$	$k_{38} = 5.3 \times 10^{-11}$
R39	$N + HO_2 \rightarrow NO + OH$	$k_{39} = 2.0 \times 10^{-10}$
R40	$NO + h\nu \rightarrow N + O$	$\lambda < 191 \text{ nm}$
R41	$N + NO \rightarrow N_2 + O$	$k_{41} = 2.7 \times 10^{-11}$
R42	$N_2O + h\nu \rightarrow N_2 + O$	$\lambda < 337 \text{ nm}$
R43a	$N_2O + O(^1D) \rightarrow NO + NO$	$k_{43a} = 1.1 \times 10^{-10}$
R43b	$N_2O + O(^1D) \rightarrow N_2 + O_2$	$k_{43b} = 1.1 \times 10^{-10}$
R44	$NO_3 + NO_2 + M \Rightarrow N_2O_5 + M$	
R45	$N_2O_5 + h\nu \rightarrow NO_2 + NO_3$	Johnston and Graham (1974)
R46	$NO_2 + O_3 \rightarrow NO_3 + O_2$	Johnston and Graham (1974)
R47	$NO_3 + NO \rightarrow 2NO_2$	
R48	$NO_3 + h\nu \rightarrow NO_2 + O$	

^{*}Units: Two-body reactions: cm3 molecules-1 s-1; three-body reactions: cm6 molecules-2 s-1

where a finer height resolution of about 0.5 km was chosen. The pressures at the boundary levels were chosen to be 980 mb and 0.415 mb.

To avoid the necessity for a prohibitively large number of very short computation time steps, reactants were grouped together so that "compound" X in equation (1) may denote either a particular constituent or the sum of a number of constituents. In this study the following "compounds" were considered: $(X) = (O) + (O_3)$, $(X) = (N) + (NO) + (NO_2)$, $(X) = (HNO_3)$, $(X) = (NO_3) + 2(N_2O_5)$, $(X) = (H) + (OH) + (HO_2) + 2(H_2O_2)$, $(X) = (CH_4)$, (X) = (CO), $(X) = (H_2O)$, $(X) = (H_2)$. The

concentrations of the individual compounds within each group of constituents are derived from the photochemical steady-state assumption. The photochemical and advective terms in equation (1) were integrated explicitly, while the diffusive part of the right-hand side in equation (1) was solved by the "leapfrog" method. A 10° latitudinal resolution and a two-hour time step were used to integrate equation (1), which permitted a full one-year integration on the CDC 7600 computer in 15 minutes (18 × 31 gridpoints). Mean daytime dissociation probabilities were calculated at the start of each 15-day period (the year was assumed to have 360

Table 2. Two-Dimensional Model Transport Coefficients as a Function of Latitude and Altitude for December-February. The power of 10 by which each number on a particular height level should be multiplied is given in the right-hand column.

b. Slope of main diffusion axis (α). a. Eddy-diffusion coefficients $(K_{11}, units cm^2s^{-1})$ along the main diffusion axis.

in thin (Am)	0.00 0.00 0.00 00.00 0.00 0.00 0.00 0.00 0.00 00.0 00.0 00.0	0.00 0.00 0.00 0.00 0.00 0.00 00.0	0.00 0.00 0.00 0.00 0.00 0.00 0.00 0.00 0.00 0.00 0.00	0.00 0.00 0.00 0.00 0.00 0.00 0.00	0.00 0.00 0.00 0.00 0.00 0.00 0.00 0.00 0.00 0.00	0.00 0.00 0.00 0.00 0.00 0.00 0.00 0.00 0.00	0.00 0.00 0.00 0.00 0.00 0.00 0.00 0.00 0.00 0.00 0.00	0.00 0.00 0.00 0.00 0.00 0.00 0.00 0.00 0.00 0.00 0.00	6.64 0.09 6.64 0.09 6.00 0.00 0.00 0.00	.60 1.32 1.73 1.87 1.35 .86 0.00 0.00	.72 1.20 7.64 3.47 3.73 2.70 1.71 0.00	1.80 3.45 5.20 5.40 4.05 7.57 0.00 0.00	1.44 2.40 5.28 6.93 7.47 5.40 7.43 0.00 0.00	3.00 4.40 8.67 9.33 6.75 4.29 0.00 0.00	.36 .79 1.04 1.12 .81 .51 0.00 0.00	00.0 00.0 04 11.1 15.1 59.	1.06 1.39 1.49 1.08 .67 0.00 0.00 0.0053	1.19 1.56 1.68 1.23 .59 0.00 0.00 0.0047	1.32 1.71 1.84 .49 7.00 0.00 0.00 0.00	1.40 1.34 1.45 0.00 0.00 0.00 0.00 0.00 0.00	.42 1.02 0.00 0.00 0.00 0.00 0.00 0.00 0.0	.25 U.n0 0.00 0.0020	0.00 0.00 0.00 0.0006 1.67 0.00 0.00 0.00-1.33	.83 0.00 0.00 0.00 .83	0.00 0.00 0.00 0.00 0.00	0.00 0.00 0.00 0.00 0.00	-5.00 0.00 0.00 0.00 0.00 0.00	0.00 0.00 0.00 0.00 0.00	4 05 05 01 0 01 05- 05- 04- 05- 04- 07- 08-	
	2.00	100	100	100		100	.00 10	100	.06 10	100	-00 10	.00	.00 10	7.80 10	.00 10	.00 10	.00 10	.00 10	.60 13	7.00 10	.00 10	.00 10	.00 10	.00	.00	7.00 10	1.50 10		00	
	2 00	7.00.7					7.00.7		7.68 7							7.00 7									. 60 7	7.00.7			0,	
	22.72	6.72		5.72 7	6.72	6.72	6.72 7						6.72 7	6.72 7		6.72 7			6.81 7		7.00 7	7.00 7	7.00 7		7.00 7				9	
:	5.76	5.76	5.76	5.76	5.76	5.76	5.75	5.76	5.76	5.76	5.76	5.76	5.76	5.76	9.16	5.76	5.76	5.80	6.43	2.00				2.00			3.50		20	
		. 30										4.90	** 90	4:30	4. 90	80	** 99	4.30	5.31	7.00						3.53	26.5		•	
:	3.30	3.30	3.30	3.30	3.30	3.30	3.33	3.30	3.38	3.33										2000		2.00	5.34	3.90	2.66	2.11	2.04		36	
	2.05	2.05	2.65	2.65	2.05	2.05	2.05	2.05	2.05	2.05	2.05	2.05	2.05	2.15	2.05	2.65	5.06	2.36	3. 30	4.25	4.25	4.25			1.73	1.29	1.22		50	
1		. 80		. 80	. 80	. 80	. 80	. 80	. 80		. 30	98.			38.			26.	1.36	1.50	1.50	1.50	1.35		. 80	. 45	9.		10	2
		. 90	. 80	. 90	. 86	. 90		. 80	. 90		. 80		. 80	. 90	. 80		. 36	*6.	1.37	1.50	1.50	1.56	1.35	96.		54.	04.		•	ATITUD
		. 30		.90		. 33	. 3.5	.30	.90	. 30	. 30			. 33			. 30			1.50									07-	-
			100	-				107	-	-	-								1.53	1.92						. 39			-50	
0	04	44	16.	16	16.	.97	. 97	. 97		.97	.97	46.	44	26.	16.	. 47	16.	1:14	1.64	2.33	2.67	2.34	1.70	.21		.66	3.		-30	
																	-		*					•					,	

c. K₂₂ perpendicular to the main diffusion axis.

10 10 10 10 10 10 10 10	. 70	68. 44.	.58 .80	. 52	.47	.43 .60	36. 68.	3.49 4.87	3.16 4.41	2.86 3.49 c	2.59 3.61	2.34 3.27	2.12 2.96	1.52 2.12	1.09 1.52	. 78 1.09	. 56 . 78	46. 04.	04. 04.	*0. *0.	04. 04.	*0. *0.	54. 54.	1.40 1.80	1.80 1.80	1.80 1.83	6.40 5.40	6.40
2	.36	. 33	. 30	.27	. 24	.22	.20	1.79	1.42	1.47	1.33	1.20	1.00	. 78			. 12	.12		.01	4.50	1.80	1.80	1.80	1.80	.36	1.04	1.08
2	.26	.23	.21	61.	.17	91.	.1.	1.28	4.16	4.05	· +5	. 46	. 78	94.	0**	.12	.12	.12	.12	6.20	05.0	6.20	6.20	6.20	6.20	**:	1.32	1.32
	.50	90.		.37	.34	.31	.28	2.50	2.26	50.2	1.85	1.68	1.52	1.09	.78	.56	0.	1.50	1.50	.15	1.50	.08	.30	.30	. 30	90.	.18	.14
D000001-0-10000000000000000000000000000														-	-									~	77	~	•	-
								-	•					•	_	_		_	_		-				-	_	•	

Table 3. Two-Dimensional Model Transport Coefficients as a Function of Latitude and Altitude for March-May. The power of 10 by which each number on a particular height level should be multiplied is given in the right-hand column.

ng the main diffusion axis.	main diffusion
the main diffi	1 along the main diffi
the	1 along the
	a I

b. Slope of the main diffusion axis (α).

		**	16. 79.	**
70 10 5 13 1 10 1 10 1 10 1 10 1 10 1 10			1. 10 . 01 . 1	1.50 1.10 .07
March 1997 199			1. 10 . 07 . 1	1. 10 . 07 . 1
20			1. 30 .07 .99	1. 30 .07 .99
20			1.30 .97 .84	1.30 .97 .84
2			1 6. 51.1	1 6. 51.1
10			16. 79. 31.	16. 79. 31.
### 19			1. 10. 11. 11.	1. 10. 11. 11.
M. 1. 1. 1. 1. 1. 1. 1. 1. 1. 1. 1. 1. 1.	•		00. 00. 00. 00.	00. 00. 00. 00.
A 20 1 1 2 1 2 1 2 1 2 1 2 1 2 1 2 1 2 1	• •		1. 30 .0. 19	1. 30 .0. 19
7.0 1165 1.30 1.30 2.16 2.26 2.44 1.20 1.00 1.30 1.30 1.30 1.30 1.30 1.30 1.3		:4:	26. 19. 19. 21.1	1.5: 1.1: .9981
7.0 1.05 1.30 1.02 2.16 2.2 2.8 0.1 1.2 1.0 1.0 1.0 1.0 1.0 1.0 1.0 1.0 1.0 1.0	•		1. 10 . 07 . 44 . 40	1.40 1.73 1.16 .07 .44 .40
100 110 110 110 110 110 110 110 110 110	•	.90	1.30 .97 50	1.50 1.30 .97
47, 121, 145, 147, 216, 516, 244, 124, 135, 147, 211, 514, 214, 214, 214, 214, 214, 214, 214, 2	•	÷.	1. 10 . 97 . 42	1.59 1.57 1.10 .97
1.10 1.77 2.12 1.70 7.13 2.73 2.74 1.72 1.72 1.72 1.72 1.72 1.72 1.72 1.72	•	06.	1. 10 1.14 1.13 .90	1.49 1.50 1.10 1.14 1.13 .90
15: 2.55 140 2.50 1.33 2.51 1.22 1.32 1.32 1.32 1.32 1.32 1.32 1.3	:	1.16	1.42 1.61 1.47 1.34 1	1.69 1.63 1.42 1.61 1.47 1.14 1
110 0 2 0 2 0 2 0 0 0 0 0 0 0 0 0 0 0 0	:	1.56	1.95 2.29 1.93 1.56 1	1. 44 2.32 1.75 7.29 1.93 1.55 1
11.0 2.0 3.0 3.0 4.0 5.4.0 5.0 5.0 5.0 5.0 5.0 5.0 5.0 5.0 5.0 5	:	1.50	2.41 2.47 7.54 1.50 1	2.67 3.17 2.41 2.47 7.04 1.50 1
1.37 1.40 2.23 1.48 4.59 6.50 7.10 7.10 7.10 7.10 7.10 7.10 7.10 7.1	:	1.59	3, 25 2, 34 1, 03 1,59 1	1, 20 1,74 1,75 7, 34 1,03 1,59 1
76 1.27 1.37 1.27 1.27 1.27 1.27 1.27 1.27 1.27 1.2	:	1.36 1	2.41 1.71 1.51 1.16 1	** 22 1.10 2.41 1.71 1.51 1.15 1
. 40 .95 1113 134 2.27 3.61 4.35 5.28 . 40 .65 .37 1.33 1.57 2.52 2.94 4.44 . 40 .62 .94 1.99 1.51 1.73 1.97 1.55 10 .20 .30 .40 .50 .60 .70 .80	•	36.	2. 30 1.21 1. 14 . 34	3. 14 2.22 2.30 1.21 1.14 .74
.45 .66 .97 1.33 1.57 2.52 2.94 4.44 .40 .62 .54 1.09 1.31 1.73 1.47 1.55 .10 .20 .30 .40 .50 .60 .70 .80	•	. 33	1.40 .84 .67 .53	2, 16 1.53 1.40 .84 .67 .53
140 .62 .54 1.09 1.31 1.73 1.97 1.55 10 20 20 30 40 50 60 70 80	•	42	\$4. 85. AA. Ar.	1.64 1.7 . 76 . 66 . 56 . 45
30 40 50 60 70	•	05.	95. 65. 49. 07.	03. 65. 49. 07. 19.
		-20 =10	-40 -30 -20	-30 -20

c. K₂₂ perpendicular to the main diffusion axis.

Table 4. Two-Dimensional Model Transport Coefficients as a Function of Latitude and Altitude for June-August. The right-hand column gives the power of 10 by which each number of a particular height level should be multiplied.

a. N ₁₁ along the main diffusion axis.	b. Slope of main diffusion axis (α) .
	History
6.53 6.45 6.12 6.50 3.10 1.95 .90 .90 .90 .99 .97 1.30 1.56 1.92 2.04	
7.10 6.43 6.46 6.14 6.56 8.10 6.06 6.0 6.0 6.0 6.0 6.0 10.30	52 0.00 0.00 0.00 0.00 0.00 0.00 0.00 0.
6.5 3 5.46 6.11 6.60 1.00 1.00 1.00 1.00 1.00 1.0	0.00 0.00 0.00 0.00 0.00 00.00 00.00
6. 1 5. 4. 6. 1 1 1 1 1 1 1 1 1 1 1 1 1 1 1 1 1 1	00.0 00.0 00.0 00.0 00.0 00.0 00.0
6.53 6.46 6.14 6.56 7.10 .00 .00 .00 .00 .00 1.56 1.92 2.08	0.00 0.00 0.00 0.00 0.00 0.00 0.00 0.00
5.5 F. 1 F	00.0 00.0 00.0 00.0 00.0 00.0 00.0
6. F.	0.00 0.00 0.00 0.00 0.00 0.00 0.00 0.00
5.43 E. 46 F. 14 L. F. T. 11 L. 56 L. 50 L. 50 L. 50 L. 56 L	00-00-00-00-00-00-00-00-00-00-00-00-00-
6.53 6.46 6.14 6.60 2.40 6.00 6.00 6.00 6.00 6.00 1.30 1.56 1.02 2.00	000000000000000000000000000000000000000
7.37 6.48 6.48 6.48 1.48 1.48 1.48 1.48 1.56 1.92 2.08	26 1.20 1.54 1.17 1.18 1.10 0.10 0.10 0.10 0.10 0.10 0.10
7.35 6.47 4.46 4.14 4.5 3 4.5 1.5 1.5 1.5 1.5 1.6 1.6 2.5 08	00.0 00.0 00.0 00.1 00.1 00.1 00.1
T. 70 A. C. T. B. C. T. C. T. C.	00.0 00.0 1.10 0.10 0.10 0.00
7 7 6 6 7 8 8 8 8 9 9 9 9 9 9 9 9 9 9 9 9 9 9 9	00.0 00.0 2.2 2.37 0.00 0.00
2 - 1 - 2 - 1 - 2 - 1 - 2 - 2 - 2 - 2 -	6.18 4.80 6.64 7.47 5.40 3.43 U.00 0.00
7	6.75 4.29 0.00 0.00
2. 1. 30 1. 30 1. 1. 10 1. 90 . 90 . 90 . 90 . 1. 30 . 1. 56 . 1. 56 . 1. 50 . 1. 30 .	0.00 0.00 18. 18. 51.1 57. 66.
20 C 2 C 2 C 2 C 2 C 2 C 2 C C C C C C C	.38 .A4 1.04 1.31 .94 .50 0.00 0.30
2 - 1 - 1 - 1 - 1 - 1 - 1 - 1 - 1 - 1 -	96 1.25 1.49 1.08 .67 0.00 0.00
201 201 101 101 101 101 101 101 101 101	. 49 1.09 1.40 1.68 1.23 .58 0.00 0.00
5-81 6-00 5-84 46 4-41 3-14 1-36 1-36 1-35 1-47 1-59 1-40 1-40 1-40 1-40 1-40	00.000.0
7.16 7.00 6.47 7.30 6.41 7.00 4.25 1.50 1.50 1.50 1.84 2.24 1.46 2.24 1.46 2.24	.00 0.00 00.
7.10 7.60 7.00 7.00 7.00 7.00 4.25 1.50 1.50 1.50 2.62 2.62 2.62 2.62	.60 1.32 1.22 0.00 0.00 n.00 0.00 0.00
7-33 7-11 7-36 7-31 7-36 6-95 4-23 1-53 1-56 1-69 1-05 2-41 7-95 4-05	.50 0.00
7-00 7-06 7-00 7-00 5-03 3-19 1-36 1-36 1-36 1-66 1-67 1-67 1-67 1-67 1-67	0.00 0.00 0.00 0.00 0.00 0.00 0.00 0.00
7.90 7.10 7.31 6.40 3.64 7.77 .96 .96 .06 .10 1.10 2.41 3.42 4.59 5.26	0.00 0.00 3.00-1.11-2.53 . 83 0.00 0.00
5.32 L.74 2.50 1.56	0.00 0.00 0.00 - F-00 - F-00 - O - O - O - O
5. 4. 3.73 3.74 3.00 5.20	200 - 100 -
6.3 t. m t. 1 2.7 t. 102 t. 1.16 1.86 2.11	00.5 00.5 00.6 00.0 00.0 00.0 00.0
90. 25. 05. 05. 07. 25.	0.00 0.00 0.00 0.00 5.00 5.00
-80 -70 -60 -50 -40 -30 -20 -10 0 10 20 30 40 50 60 70 60	
	200 - 200 - 200
LATITUDE	
	LATTROBL

c. K₂₂ perpendicular to the main diffusion axis.

•		•	2	ď	1	•	•	•	•		•	•	•	•	•	•	•	•		•	•	•	2	•	u	ď			n 1	•	•
1 00		200	00.1	1.00			8.31	7.52	A. A.				2.00	4.56	4.12	2.04	2					. 20	•	04.	*0.	40				00.1	2000
80	9		. 80	. 73	. 68		2.95	5.39	4.87					3.27	2.96	2.12	1.52	00						04.	.0.	.0	90			00.	200
. 98	. 80	:	.80	.73	4.58		2.42	2.39	4.87		00		10.5	3.27	5.96	2.12	1.52	00.1	. 78				.0.	. 40	.15	.15					
.70				. 52	4.7		4.66	3.86	3.49	3.14	2. 44	1		4:34	2.15	1.52	1.09	. 7.	45	•				0	*	.45	1.80	. 8			
.70	*		. 20	.52	4.71			3.86	3.49	3.16	2.04			5.34	2.15	1.52	1.09	. 78	\$:			46.	.45	1.80	. 80			
00.				.3	3.36		3.00	4.1	2.50	2.26	2.05				1.50	1.04	.78	90	00					1.50	90.	.30	.30	90	40		
. 36	:			.27	2.42			1.48	1.70	1.62	1.67			1.60	1.09	.78	.56	. 40	. 13					00.	1.90	1.80	1.90	1.80	*		
.26	. 23				1.73			•	1.28	1.15	1.05	50			. 78	.56		. 12	.12	. 12	2	200		2.30	2.40	2.20	2.20	2.20		1.32	32
.26	. 23	31		61.	1.73			**	1.28	1.16	1.05	90			. 78	.56	0.	. 12	.12	. 12		00		00.0	07.7	2.20	2.20	2.20		1.32	1.33
.26	. 23	10.	3	-	1.73	1.67		*	82.1	1.16	1.05	57.		06.	. 78	• 50	04.	.12	.12	-15	.12			2	07.	6.20	6.20	6.20	**	1.32	1.32
.36	.33	30			2.45	01.0			1.79	1.62	1.47	1.33	30	200	60.	. 78	.56	.40	.12	.12	.12			000	000	1.80	1.80	1.87	34	1.0A	1.08
000	•				3.38	400			5.50	2.26	50.2	1.85	1.68	000	75.	1.09	.78	.56		1.50	1.50					. 30	.30	.30	90.	.18	. 18
.70	4	. 58	23	200		4.24			3.49	3.16	2.86	5.59	2.34		21.5	1.52	1.09	. 78	.56	04.	04.	*0	4			.43	1.80	1.90	1.80	5.40	5.40
86.	60.	.80	7.		9.38	5.95	30			:	3.99	3.61	3.27	6		2:15	1.52	1.09	. 78	. 56	0.	*0.					1.80	1.80	1.80	2.40	2.40
00.	000.	1.00	1.00			8.31	7.63		000	9.15	5.57	\$0.6	45.4			900	2.15	1.52	60.	1.50	1.50		. 60			. 15	. 45	1.80	1.80	2.40	60.5
00.	1.00	1.00	1.00			8.31	7.52		0	6.15	2.57	2.04	4.50			2.40	2:10	7:35	60.1	.78	. 54	.0.					.25	00.1	1.00	3.00	3.00
					:	8.3	1.42			2.0	2.47	2.04	4.56	4.12				25.	60.1	. 78	. 24	40.	. 40	*			. 25	1.00	1.00	3.00	3.00
	35	200	48		9	7	42		2 5	99	36	34	32	30	30	22	07	7.4	77	20	18	16	14	1.0	15	2	x	9	4	77	0

LATITUME

Table 5. Two-Dimensional Model Transport Coefficients as a Function of Latitude and Altitude for September-November. Each number at a particular height should be multiplied by the power of 10 listed in the right-hand column.

b. Slope of the main diffusion axis (α) .	Leasif (4a)	0.00 0.00 0.00 0.00 0.00 0.00 0.00 0.00 0.00	55 0.00 0.00 0.00 0.00 0.00 0.00 0.00 0	00.0 00.0 00.0	10 0 0 0 0 0 0 0 0 0 0 0 0 0 0 0 0 0 0	1.09 2.41 3.12 3.73 2.77 1.71 0.00	2.73 6.00 7.80 9.33 6.75 4.29 U.00	84 - 46 - 66 - 66 - 14 - 00 0 00 0 00 0 00 15 18 211 - 20 - 46 - 46 - 46 - 46 - 46 - 46 - 46 - 4	1.56 1.94800 0.00	32 1-22 1-32 1-32 0.00 0.00 0.00 0.00 0.00 0.00 0.00 0.	0.00 0.00-1.33 .61	00.400 4.00 4.00 0.00 0.00 4.00 5.00 0.00 0	0.00 0.00 0.00 5.00 5.00 5.00 5.00 5.00	
a. K ₁₁ along the main diffusion axis.	F. 48 2.61 2.15 2.17 1.40 1.30 1.05 .10 .10 .60 1.35 1.40 2.70 2.0	2.46 2.41 2.44 2.47 1.40 1.30 1.05 .40 .90 .80 1.35 1.90 2.70 3.27 2.46 2.45 2.44 2.47 1.40 1.30 1.30 1.30 1.30 1.30 1.30 1.30 1.3	2.44 2.41 2.44 2.07 1.40 1.40 1.05 .40 .40 .40 1.49 1.40 2.48 2.41 2.44 2.47 1.40 1.45 1.05 .40 .40 .40 1.45 1.40	2-44 2-41 2-44 2-47 1-40 1-30 1-05 -90 -80 -80 1-35 1-90 2-70 3-20 2-44 2-41 2-44 2-47 1-90 2-70 3-20 2-40 2-41 2-41 2-42 2-42 2-42 2-42 2-42 2-42	2.48 2.41 2.42 2.41 1.40 1.30 1.05 .40 .40 .40 1.35 1.90 2.70 3.24 2.41 2.41 2.44 2.41 2.44 2.41 2.44 2.41 2.44 2.41 2.44 2.41 2.44 2.41 2.44 2.41 2.44 2.41 2.44 2.41 2.44 2.41 2.44 2.41 2.41	7.44 2.41 2.34 2.07 1.40 1.30 1.05 .80 .86 .80 1.35 1.90 2.70 3.24 2.40 2.70 3.24 2.40 2.70 3.24 2.40 2.70 3.24 2.40 2.70 3.24 2.40 2.70 3.24 2.40 2.70 3.24 2.40 2.40 2.40 2.40 2.40 2.40 2.40 3.24 2.40 2.40 2.40 3.24 2.40 2.40 3.24 2.40 2.40 3.24 2.40 2.40 3.24 2.40 2.40 3.40 2.40 3.40 2.40 3.40 2.40 3.40 3.40 3.40 3.40 3.40 3.40 3.40 3	**51 2*44 2*47 1*47 1*10 1*10 **80 **80 1*35 1*90 2*70 3*24 **********************************	7.44 7.51 2.34 2.07 1.90 1.30 1.05 .90 .80 .86 1.35 1.90 2.70 3.27 7.48 2.51 2.32 1.90 2.70 3.22 7.48 2.51 2.32 1.90 2.70 3.22 7.48 2.52 7.52 7.52 7.52 7.52 7.52 7.52 7.52	3.05 2-72 2.31 2-31 1.71 1.72 1.21 .30 .90 .91 1.55 2.19 2.70 3.21 3.21 3.21 3.21 3.21 3.21 3.21 3.21	.53 1.44 4.75 3.90 1.50 2.50 1.50 1.60 1.50 3.25 5.00 5.73 7.00 1.65 5.66 5.77 4.60 7.09 7.29 1.50 1.60 1.50 2.97 4.45 6.75 7.00 1.63 6.86 6.26 7.00 7.09 7.29 1.50 1.60 1.50 2.97 4.45 6.75 7.00	1.56 1.25 2.14 1.33 1.16 .95 .46	1.74 1.6 1.2 1.3 1.4 . 65 . 45 . 45 . 45 . 45 . 46 1.24 2.00 2.86 1.74 1.67 1.97	10 20 30 40 50 60 70	LATITUDE

c. K₂₂ perpendicular to the main diffusion axis.

ULIGHT (Su)

•	•			•		•	•					,		,						,	•				•	ď	•	u		•			
1.00	1.00	1.00				8.3	7.52				2000	2.00	4.56	4.12	40 0		21.5	20.1	1.09	. 78	.56	.04				*0.	*0.	35		00.1	3.00	3.00	
86.	. 49	. 80	7.3			0.40	5.34	4.87		7		1000	3.27	4.96	11	25				. 20	04.	.04	. 40			.0.	. 25	1.00	000		2.00	3.00	70
.98																																	90
.7.																																	20
. 70																																	
00.																																	30
.3																																	50
45.																																	10
95																																	0
. 23																																	0
.33																																	63-
000				200	3.05	2.17	2.50	2. 24		60.0	50.	90.	1.52	1.00				04.	1.50	1.50		. 50			. 30	. 30	. 40	40		97.			200
B 6																																01-	
1.00																																04-	
																																-70	
	1.0	1.00	4.18	A. 21	7 63		9.00	6.15	5.57	5.00	4.5			2.04	2.13	1.52	1.00	7.8							36		1.00	20.1	3.00	3.00		-80	
22.5	30	48	46	44	4.2			38	36	34	32	360	2 5	97	26	7.4	22	20	18		107	14	12	10	X		0	4	7	0			

days) and were applied during the sunlit hours of each such period. At night photochemistry was "frozen," except for the conversion of NO_x to NO_3 and N_2O_5 . The variation of solar position over the year was closely simulated.

The distribution of water vapor is dependent on condensation processes and removal by rainfall. At each gridpoint the concentration of water vapor was calculated by integrating equation (1). The probability of cloud formation is determined in the following way. At each gridpoint temperatures are assumed to have a Gaussian distribution. In the present study the mean and the standard deviation of temperatures were derived from observations (Oort and Rasmusson, 1971; Louis, 1974). At each gridpoint it is possible to determine the temperature T_s , so that $q = q_s(T_s)$, where q denotes the calculated humidity and q_s(T_s) is the saturation humidity at the temperature T_s . For all temperatures $T \leq T_s$ the air will be supersaturated, and the probability for cloud formation can be determined from the Gaussian temperature-distribution function at each gridpoint. By this method it is also possible to determine the rate of precipitation at each gridpoint. For the sake of simplicity, it is incorrectly assumed that all precipitation reaches the ground without re-evaporation. As it does not seem impossible to estimate the standard deviation of temperatures within each gridbox using large-scale stability criteria, an extension of the method presented may make it feasible to estimate sub-grid-scale mean cloudiness in fullyinteractive dynamic models of the atmosphere.

With knowledge of the probability of cloud formation (p_c) , it is possible to estimate the rainout rates P_r for gaseous compounds in the atmosphere, so that

$$P_r(X) = -p_c(X) t^{-1}(X)$$
.

We have adopted the following values for the residence times of some water-soluble gases in clouds: $t(NO_x) = 2$ days, $t(N_2O_5) = 8$ hours, $t(HNO_3) = 8$ hours, $t(H_2O_2) = 2$ days, $t(CH_3O_2H) = 2$ days. A variety of boundary conditions were adopted in this study. The mixing ratios for a number of constituents were prescribed at the lower boundary, and were set equal to the average measured mixing ratios $(CH_4:1.5 \times 10^{-6}; N_2O:2.5 \times 10^{-7}; H_2:5 \times 10^{-7}; H_2O:$ see listing in Telegadas and London

(1954)). For HNO_3 , NO_x , and CO the lower boundary condition was determined from the equation

$$F_z = -K_{zz}(M) \frac{d\mu_x}{dz} = -w_d(X) + I_z(X),$$

where I_z denotes the industrial and biological release rates of a constituent as a function of latitude (Robinson and Robbins, 1970; Seiler, 1974) and w_d is the deposition velocity, which was assigned different values over land and sea (average values of w_d were derived at each latitude, taking into account the areas covered by land $(w_d \varrho)$ and water and ice (w_{ds})). The following values for w_d (cm s⁻¹) were used in this study:

Species	$\mathbf{w}_{d\ell}$	w _{ds}
HNO ₃	0.2	1
O_3	0.2	0.05
NO _x	0.2	0.5
со	0.1	0

At the upper boundary (0.415 mb, ≈ 55 km), fixed mixing ratios of 10^{-8} were prescribed for NO_X , which is mostly NO at that altitude. For all other compounds, no vertical eddy flux through the upper boundary was allowed to occur $(\partial \mu_V/\partial z = 0)$.

RESULTS (UNPERTURBED ATMOSPHERE)

A set of empirically-derived diffusion coefficients which was found to explain quite satisfactorily the seasonal and meridional distribution of ozone is listed in Tables 2-5. In Figure 1 the model-calculated meridional and seasonal cross-sections of ozone are shown. Measured average distributions of ozone above 25 km (Krueger et al., 1973) and below 25 km (Dütsch, 1971) agree everywhere with calculated ozone concentrations to within 20%. The present model also simulates very well the latitudinal and seasonal distributions of total ozone, particularly the differences between the seasonal distributions in the Southern and Northern Hemispheres (Figure 2).

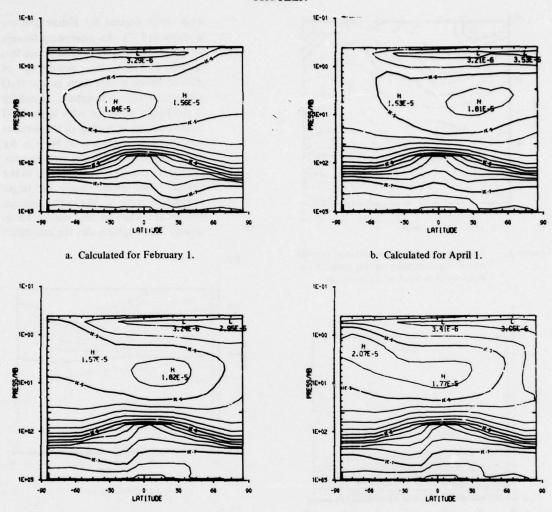


Figure 1. Cross-sections of mass mixing ratios of ozone. Contour intervals are 0.20 orders of magnitude. (In this and all succeeding figures, the unlabeled inner horizontal and vertical coordinate marks identify the gridpoints of the model: 10° latitude steps and approximately 2-km height intervals, except for 0.5-km intervals in the lowest 2 km.)

Water vapor is a very important tracer for the transfer of air between stratosphere and troposphere, and the amount of stratospheric water vapor is very sensitive to the correct parameterization of the diffusion processes. This is especially true at latitudes poleward of 30°, where average temperatures in the lower stratosphere are sufficiently high to permit a far-toolarge transfer of water vapor into the stratosphere, if vertical diffusion is overestimated. Indeed, application of published eddy-diffusion

c. Calculated for July 1.

coefficients (Luther, 1973; Gudiksen and Fairhall, 1968; Louis, 1974) clearly leads to excessive stratospheric water-vapor mixing ratios (and unsatisfactory ozone distributions as well). The distributions of water vapor derived with the presented diffusion coefficients, as shown in Figure 3, for example, are much more satisfactory, although the calculated concentrations still seem to be about twice too high (Mastenbrook, 1974; Harries, 1973). Clearly, finer tuning of the eddy diffusion would cer-

d. Calculated for October 1.

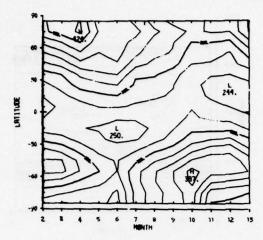


Figure 2. Latitudinal and seasonal variation in total ozone as calculated with this model. Contours are at intervals of 20 matm-cm.

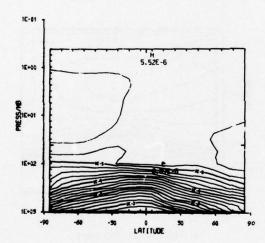
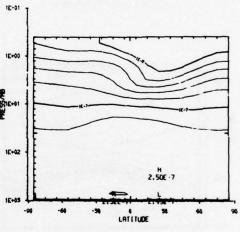


Figure 3. Calculated volume mixing ratios of water vapor in the stratosphere for February 1. Contour intervals are 0.20 orders of magnitude.

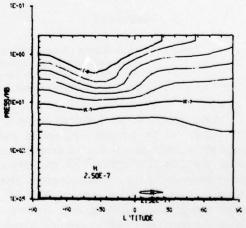
tainly have been possible, but this has still not been attempted because of lack of accurate information on the mean circulation, and mean temperatures and standard deviations of temperatures.

Calculated distributions of N_2O , $NO + NO_2$, N_2O_5 , HNO_3 , OH, HO_2 , H_2O_2 , CO, and CH_4 are presented in Figures 4 through 10. The following features merit notice:

 a. The vertical distribution of N₂O at 30°N (see Figure 4) agrees fairly closely with those derived by Ehhalt and coworkers (1975). An interesting feature of the results presented here is that this model indicates the possibility of marked seasonal variations in the N₂O content of the stratosphere, especially at the higher altitudes, with larger N₂O concentrations occurring in the summer season. Since oxidation of N₂O is the main source of NO in the stratosphere, the larger concentrations of N₂O in the summer stratosphere imply far larger production rates of NO in the summer hemisphere than in the winter hemisphere. This explains also the calculated



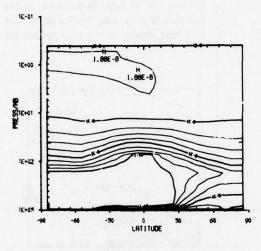
a. For February 1.



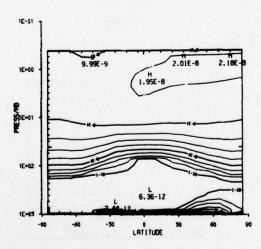
b. For September 1.

Figure 4. Volume mixing ratios of N₂O. Contour intervals are 0.20 orders of magnitude.

seasonal variations in NO_x (Figure 5). There is, therefore, the possibility of significant transport of N_2O and NO_x from the stratosphere into the lower mesosphere during the summer months. The possible presence of N_2O with rather high mixing ratios in the mesosphere may be of aeronomic importance, since the photodissociation at short wavelengths may lead to interesting products.



a. For February 1.



b. For September 1.

Figure 5. Volume mixing ratios of NO + NO_2 . Contour intervals are 0.25 orders of magnitude.

b. The calculated latitudinal distribution of nitric acid (Figure 6) during the spring season agrees rather satisfactorily with the distribution observed by Lazrus and Gandrud (1974). There is also generally good agreement between calculated and optically-determined concentrations of NO and NO₂ (Patel et al., 1975; Ackerman, 1975). However, the calculated mixing ratios of NO are generally about a factor of two to three times as large as those measured in situ with the chemiluminescence NO sonde (Ridley et al., 1976).

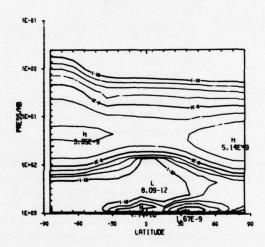


Figure 6. Volume mixing ratios of HNO₃ for February 1. Contour intervals are 0.25 orders of magnitude.

A significant portion of NO and NO2 is converted to NO3 and N2O5 (see Figure 7), the latter especially during periods with long nights. Since in effect two NO or NO2 molecules are stored per N2O5 molecule formed, the formation of N2O5 protects ozone from otherwise significantly larger catalytic destruction. Unfortunately, the kinetic and photochemical data that describe the formation of N2O5 in the atmosphere have been determined under laboratory conditions rather far from those prevailing in the stratosphere, so the application of these data may introduce significant errors. For example, it

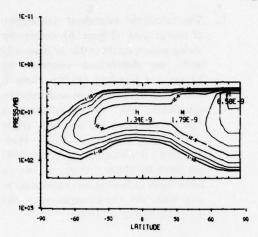


Figure 7. Calculated volume mixing ratios of N₂O₅ at noon for February 1. No calculations of N₂O₅ were performed below 15 km and above 36 km. Contour intervals are 0.25 orders of magnitude.

is possible that the absorption cross-section of N_2O_5 in the ultraviolet is temperature-dependent.

c. The calculated concentrations of the odd-hydrogen species OH, HO₂, and H₂O₂ are shown in Figures 8 and 9. Observations of the distribution of H₂O₂ are important because they provide information on the distribution of HO₂, which is an important odd-hydrogen compound that is more

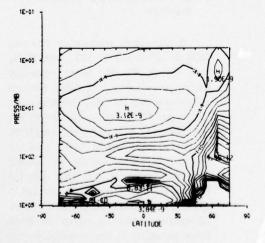
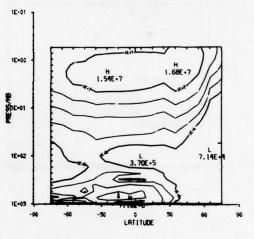


Figure 8. Calculated volume mixing ratios of H₂O₂ for February 1. Contour intervals are 0.20 orders of magnitude.

difficult to measure. The mixing ratios of $\rm H_2O_2$ reach values in the ppbv (10^{-9}) range near 25 km and in the lower troposphere. This species may be important in heterogeneous oxidation processes, leading to the formation of sulfates, nitrites, and nitrates from $\rm SO_2$ and $\rm NO_x$.

The average calculated daytime concentrations of OH for the fall season are presented in Figure 9. These concentrations are of large importance, as the OH radical is the only known significant attaching species in the troposphere for



a. For OH.

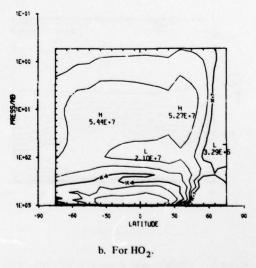
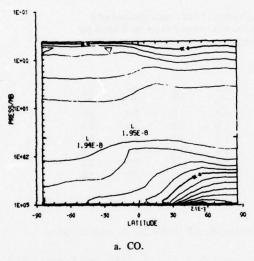


Figure 9. Calculated mean daytime concentrations, February 1. Contour intervals are 0.25 orders of magnitude.

a number of atmospheric gases of low solubility, e.g., CH₄, CO, and hydrogen-containing halocarbons.

d. The fact that the calculated distribution of CO in the troposphere (see Figure 10) is very similar to the measured distribution (Seiler, 1974) indicates that the calculated OH concentrations cannot deviate grossly from the real atmosphere values. For instance, if the real OH concentrations were far larger than those calculated with the present model, the calculated industry-related



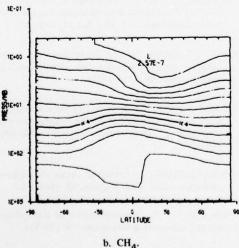


Figure 10. Calculated volume mixing ratios for February 1. Contours are at intervals of 1.5×10^{-8} .

CO at mid-latitudes in the Northern Hemisphere would have been far lower than the observed one. With the present model we calculated an average global CO production of 1.9×10^{11} molecules cm⁻²s⁻¹ in the atmosphere from the oxidation of methane, which should be compared with an average industrial CO input of about 9.3×10^{10} molecules cm⁻²s⁻¹. It follows that the industrial and natural productions of CO in the Northern Hemisphere are about equal.

PERTURBATIONS OF ATMOSPHERIC OZONE

Starting with the work by Johnston (1971) and Crutzen (1971), there has been general concern about the possibility of significant damage to the ozone shield by a number of human activities. With the present model we have calculated the percentage reductions in total ozone that would result from the operations of large fleets of supersonic aircraft (see Tables 6 and 7). We have assumed that all flights would take place at mid-latitudes in the Northern Hemisphere and that each aircraft would cruise on the average 7 hours per day in the stratosphere. The number of flight hours may be closer to 4 hours/day (Broderick, 1975; Grobecker et al., 1974) and other fleet sizes may also be far more likely. However, it is permissible to scale the results collected in Tables 6 and 7 for any particular fleet size or number of flight hours per day.

The results in these two tables show significant reductions in ozone due to aircraft operations, with reductions in the Southern Hemisphere being a little more than half of the reductions in the Northern Hemisphere. On the average, the reductions in total ozone derived with this model are in rather good agreement with previous studies made using onedimensional models. In order to study another possible effect on the ozone layer, we have also tried to simulate the variations in NO production due to the action of galactic cosmic rays, which exhibits a 11-year periodicity. Contrary to the hypothesis of Ruderman and Chamberlain (1975), our calculations give at most a 0.5% variability in ozone. Our conclusion is, therefore,

CRUTZEN

Table 6. Percentage Reduction in Total Ozone by a Fleet of 450 Boeing SST's of pre-1971 Design (assumed NO₂ emission index of 18 g/kg) Calculated with the Present Model. Each plane was assumed to fly for 7 hours per day at an altitude of 20 km. Positive latitudes are north, negative ones south.

			L	ATITUDE				
	<u>-75</u>	-55	-35	-15	15	35	55	75
Jan. 1	4.9	4.0	3.2	3.2	4.9	6.1	7.5	8.1
March 1	5.4	4.3	3.3	3.2	4.5	5.5	6.7	7.4
May 1	5.3	4.6	3.6	3.5	4.3	5.3	6.6	7.8
July 1	4.7	4.4	3.9	3.5	4.2	5.4	7.3	9.3
Sept. 1	4.4	4.0	3.5	3.3	4.1	5.8	8.6	11.3
Nov. 1	4.5	3.9	3.3	3.1	4.5	6.2	8.5	9.9

Table 7. Percentage Reduction in Total Ozone by a Fleet of 290 Concordes (assumed NO₂ emission index of 21 g/kg). Each plane was assumed to fly for 7 hours per day at an altitude of 18 km. Positive latitudes are north, negative ones south.

			L.	ATITUDE				
	<u>-75</u>	<u>-55</u>	-35	-15-	15	35	55	75
Jan. 1	1.6	1.4	1.2	1.1	1.5	1.8	2.0	2.1
March 1	1.9	1.5	1.2	1.2	1.6	1.8	2.1	2.3
May 1	1.9	1.6	1.3	1.3	1.5	1.7	2.0	2.3
July 1	1.6	1.5	1.4	1.3	1.4	1.7	2.1	2.6
Sept. 1	1.5	1.4	1.3	1.2	1.3	1.7	2.3	3.1
Nov. 1	1.5	1.3	1.2	1.1	1.4	1.8	2.3	2.6

that the observed periodic changes in total ozone (±5%) at high latitudes cannot be explained by changes in stratospheric NO input from galactic cosmic rays.

ACKNOWLEDGMENTS

This study was begun in the fall of 1973 at the Institute of Meteorology of the University of Stockholm under a grant from the Svenska Riksbankens Jubileumsfond. Dr. W. Jessen assisted in the initial phase of the study. After August 1974 the work was continued at NCAR, Boulder, Colorado. A small grant was obtained from the Climatic Impact Assessment Program of the Department of Transportation.

REFERENCES

Ackerman, M. (1975), "NO, NO₂ and HNO₃ below 35 km in the atmosphere," J. Atm. Sci. 32, 1649-1657.

Broderick, A.J. (1975), private communication.

Cunnold, D., F. Alyea, N. Phillips and R. Prinn (1975), "A three-dimensional dynamical-chemical model of atmospheric ozone," J. Atm. Sci. 32, 170-194.

Crutzen, P.J. (1971), "Ozone production rates in an oxygen-hydrogen-nitrogen oxide atmosphere," J. Geophys. Res. 76, 7311-7327.

Crutzen, P.J. (1973), "A discussion of the chemistry of some minor constituents in the stratosphere and troposphere," Pure Appl. Geophys. 106-108, 1385-1399.

Crutzen, P.J. (1974), "A review of upper atmospheric photochemistry," Can. J. Chem. 52, 1569-1581.

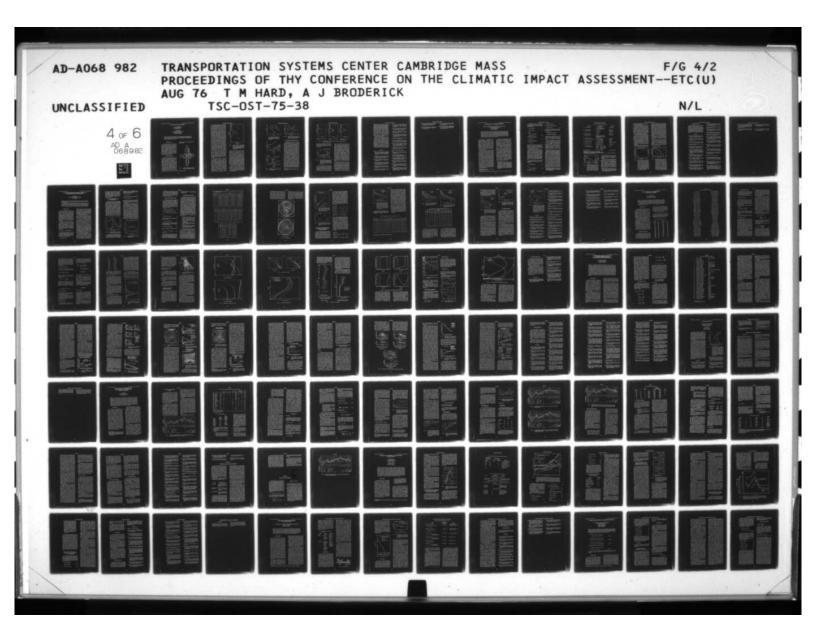
Dütsch, H.U. (1971), "Photochemistry of atmospheric ozone," Advances in Geophysics 15, 219-322.

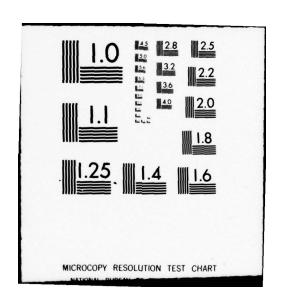
Ehhalt, D., L.E. Heidt, R.H. Lueb, and E.A. Martell (1975), "Concentrations of CH₄, CO, CO₂, H₂, H₂O, and N₂O in the upper stratosphere," J. Atm. Sci. 32, 163-169.

CRUTZEN

- Grobecker, A.J., S.C. Coroniti, and R.H. Cannon, Jr. (1974), Report of Findings: The Effects of Stratospheric Pollution by Aircraft, Climatic Impact Assessment Program, U.S. Dept. of Transportation, DOT-TST-75-50.
- Gudiksen, P.H., A.W. Fairhall, and R.J. Reed (1968), "Roles of mean meridional circulation and eddy diffusion in the transport of trace substances in the lower stratosphere," J. Geophys. Res. 73, 4461-4473.
- Harries, J.E. (1973), "Measurements of stratospheric water vapor using far-infrared techniques," J. Atm. Sci. 30, 1691-1698.
- Hesstvedt, E. (1974), "Reduction of stratospheric ozone from high-flying aircraft, studied in a two-dimensional photochemical model with transport," Can. J. Chem. 8, 1592-1598.
- Johnston, H.S. (1971), "Reduction of stratospheric ozone by nitrogen oxide catalysts from SST exhaust," Science 173, 517-522.
- Johnston, H.S., and R. Graham (1974), "Photo-chemistry of NO_x and HNO_x compounds," Can. J. Chem. 52, 1415-1423.
- Krueger, A.J., D.F. Heath, and C.L. Mateer (1973), "Variations in the stratospheric ozone field inferred from Nimbus satellite observations," Pure Appl. Geophys. 106-108, 1254-1263.
- Lazrus, A.L., and B.W. Gandrud (1974), "Distribution of stratospheric nitric acid vapor," J. Atm. Sci. 31, 1102-1108.
- Louis, J.-F. (1974), "A Two-Dimensional Transport Model of the Atmosphere," Ph.D. thesis, Astro-Geophysics Department, University of Colorado, Boulder.
- Luther, F.M. (1973), "Monthly mean values of eddy diffusion coefficients in the lower stratosphere," presented at the AIAA-AMS International Conference on the Environmental Impact of Aerospace Operations in the High Atmosphere (Denver), AIAA paper 73-498.

- Mastenbrook, H.J. (1974), "Water-vapor measurements in the lower stratosphere," Can. J. Chem. 52, 1527-1531.
- NAS (1975), Environmental Impact of Stratospheric Flight, Climatic Impact Committee of the NRC, NAS, and NAE, pub. National Academy of Science.
- Noxon, J.F. (1975), private communication.
- Oort, A.H., and E.M. Rasmusson (1971), "Atmospheric Circulation Statistics," NOAA Professional Paper 5, U.S. Dept. of Commerce, Rockville, MD, 324 pp.
- Patel, C.K.N., E.G. Burkhardt, and C.A. Lambert (1974), "Spectroscopic measurements of stratospheric nitric oxide and water vapor," Science 184, 1173-1176.
- Reed, R.J., and K.E. German (1965), "A contribution to the problem of stratospheric diffusion by large scale mixing," Mon. Wea. Rev. 93, 313-328.
- Ridley, B.A., J.T. Bruin, and H.I. Schiff (1976), "Measurements of NO between 17 and 34.5 km from Churchill, Manitoba," in this volume.
- Robinson, E., and R.C. Robbins (1970), "Gaseous atmospheric pollutants from urban and natural sources," in Global Effects of Environmental Pollution, ed. Singer, D. Reidel Pub., Dordrecht, 50-64.
- Ruderman, M.A., and J.W. Chamberlain (1975), "Origin of the sunspot modulation of ozone: Its implications for stratospheric NO injection," Planet. Space Sci. 23, 247-268.
- Seiler, W. (1974), "The cycle of atmospheric CO," Tellus 26, 116-135.
- Telegadas, K., and J. London (1954), "A Physical Model of the Northern Hemisphere Troposphere for Winter and Summer," Scientific Report No. 1, Dept. of Meteorology and Oceanography, New York University.
- Wofsy, S.C., and M.B. McElroy (1974), "HO_x, NO_x, and ClO_x: Their role in atmospheric photochemistry," Can. J. Chem. **52**, 1582-1591.





CHLORINE IN THE STRATOSPHERE

R.S. STOLARSKI* NASA Johnson Space Center Houston, Texas

R.J. CICERONE Space Physics Research Laboratory The University of Michigan Ann Arbor, Michigan

ABSTRACT: The present understanding of the chemistry and budget of stratospheric chlorine is reviewed. The available data on OCIO indicate that its role is negligible. Various stratospheric chlorine sources are investigated, and it is concluded that the dominant source is the dissociation of halocarbons diffusing from the Earth's surface.

INTRODUCTION

Most of the attention at CIAP conferences has been focused on NO_{X} and its role in the chemistry of the natural ozone layer, and on the perturbation of this natural balance by additional sources. This paper will review the chemistry and budget of stratospheric chlorine, which has received considerable attention recently as a potential perturber of the ozone layer. Current understanding seems to indicate that chlorine is only a minor factor in the present ozone balance, but is potentially an efficient catalyst for the destruction of stratospheric ozone.

CHLORINE CHEMISTRY

The chemistry of gaseous chlorine in the stratosphere has been discussed by a number of authors (e.g., Stolarski and Cicerone, 1974; Crutzen, 1974a,b; Wofsy and McElroy, 1974; Molina and Rowland, 1974a; Cicerone et al., 1974; Wofsy et al., 1975; and Rowland and Molina, 1975), and the available rate constants have been reviewed by Watson (1974). We will briefly describe these reactions and then focus upon some of the outstanding questions and uncertainties. Figure 1 represents the basic reaction scheme, which involves HCl, Cl, ClO, ClOO, and OClO. Not shown in this scheme are molecules which are certainly formed but are likely to

dissociate under visible irradiation (e.g., Cl₂, NOCl, NO₂Cl).

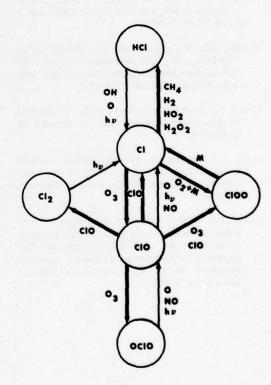


Figure 1. Basic chlorine reaction scheme for HCl, Cl, ClO, OClO, and ClOO in the stratosphere.

^{*}Dr. Stolarski is now with the NASA Goddard Space Flight Center, Greenbelt, Maryland.

Most authors agree that the basic scheme is OH and O reacting with HCl to form Cl, followed by Cl reacting with H2 or CH4 to re-form HCl. But Cl also reacts with O₃ to form ClO, which can react with NO to re-form Cl, or with O to catalytically destroy two odd oxygens. In addition, Cl atoms can combine with O2 in a three-body reaction to form ClOO, which is rapidly dissociated by thermal collisions with any atmospheric molecule, yielding very small concentrations of ClOO (Watson, 1974). Figure 2 shows relative concentrations of HCl, Cl, and ClO for this simple reaction scheme, using the rates given in Watson (1974) and the concentrations for OH, NO, O₃, and O of Wofsy and McElroy (1974). Figure 3 shows diurnally-averaged chemical reaction times for HCl, Cl, and ClO, respectively, for the same assumed reaction rates and concentrations. The HO2 curves in Figure 3b were calculated with an assumed rate constant for Cl + $HO_2 \rightarrow HC1 + O_2$ of 2×10^{-11} cm³ molecule⁻¹ sec-1. The solid curve used the HO₂ profile of Wofsy and McElroy (1974), while the dashed curve used an HO₂ profile from the calculations of the model being developed by the University of Michigan group. Somewhat different reaction rates were used for the latter HO2 profile; in particular, OH + HO₂ → H₂O + O₂ was assigned the lower value of 2 × 10⁻¹¹ cm³ molecule⁻¹ sec-1. The dashed curve for H2O2 was also generated from the profile in the Michigan model and a rate constant of 6.6 × 10⁻¹³ cm³ molecule-1 sec-1 (Watson et al., 1976). The reactions of Cl with HO2 and H2O2 appear to be of minor significance if OH + HO₂ is fast, but their importance increases rapidly as the OH + HO2 rate decreases.

The possible significance of the reaction $CIO + O_3$, whether it slows down catalysis through formation of OCIO or speeds it up through CIOO, has been pointed out by some authors in their discussions of chlorine chemistry. These discussions are based on the upper limit of 5×10^{-15} cm³ molecule⁻¹ sec⁻¹ to the reaction rate, set by Clyne and Coxon (1968). Indeed, if the reaction proceeds at that rate and the products are OCIO and O_2 , then significant quantities of OCIO are built up in the middle stratosphere, as indicated by the chemical time constant shown in Figure 4 and the resultant splitting ratios shown in Figure 5a. In this calculation, OCIO was destroyed by reaction

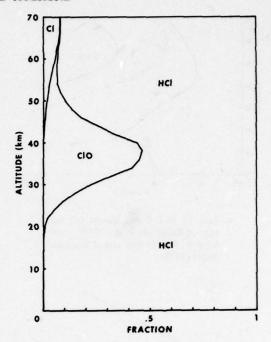
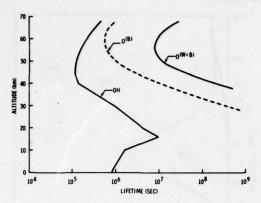


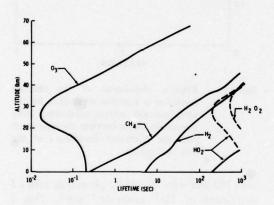
Figure 2. Relative abundances of the chlorine species as a function of altitude for the basic reaction scheme (excluding OCIO formation). Areas between the lines represent the fractional abundances of the indicated species.

with NO and with O, and by photolysis with a J coefficient of 10-4 molecule-1 sec-1. This J coefficient is at present arbitrary. Figure 5b shows the splitting ratios for $J_{OCIO} = 10^{-2}$. As can be seen, this choice of value causes a significant reduction in predicted OCIO concentration. To refine J_{OCIO}, a careful consideration of the predissociated bands below 375 nm is necessitated (see, e.g., Watson, 1974). Recent efforts by Rundel and Stolarski (1976) at modeling the Cl2-O3 photolysis experiment (Norrish and Neville, 1934) indicate that the rate coefficient of ClO + O3 is much less than the Clyne and Coxon (1968) upper limit. A coefficient of 10-18 cm3 molecule-1 sec-1 or less is indicated, with the principal channel going to $Cloo + O_2$.

Figure 5b shows the splitting ratios when k_{O_3+C1O} is 5×10^{-18} cm³ molecule⁻¹ sec⁻¹ (with OClO as the product) and J_{OClO} is 10^{-4} molecule⁻¹. As can be seen, such a small reaction rate for ClO + O₃ effectively removes that reaction as a significant factor in the catalytic ozone destruction by chlorine.



 Loss of HCl. Curve labeled (B) uses rate of Balakhnin et al. (1971). Curve labeled (W & B) uses rate of Wong and Belles (1971).



b. Loss of CL

Figure 3. Chemical reaction time constants for loss of various species.

c. Loss of CIO.

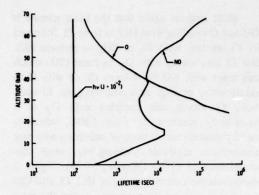


Figure 4. Chemical reaction time constants for loss of OCIO. Time constant for photolysis shown is for arbitrary J of 10⁻² sec⁻¹.

STRATOSPHERIC CHLORINE BUDGET*

Stratospheric chlorine must come either from extraterrestrial sources (i.e., meteoritic debris) or from the surface of the Earth. Meteoritic debris is usually not significant below the mesosphere, thus implying that the Earth's surface is the ultimate source of all stratospheric chlorine. The main problem is how it reaches the stratosphere. As can be seen from Figures 2, 5a, and 5b, the chlorine is almost entirely HCl in the troposphere if released as HCl, Cl, ClO, OClO, or Cl₂ (which photodissociates in the visible). Since HCl is highly soluble, it is efficiently rained out in the troposphere (see Stedman et al. (1975) for more complete discussion). Residence times are not more than a few days, leading to large negative gradients of concentration versus altitude throughout the troposphere. Farmer's (1975) infrared measurement of column content of HCl is consistent with this interpretation if ground-level mixing ratios are around the 1-ppb level, as deduced by Junge (1957). Lazrus' (1975) upper limit of 0.05 ppbm at 14 km also supports this view. Figure 6 indicates a reasonable profile for tropospheric CIX. The dashed line, constant at 0.02 ppb, shows the stratospheric mixing ratio due to ground-level CIX sources. The most likely ground-level source for this profile is release of HCl from sea-salt spray in

^{*}Much of this section is based on the paper of Cicerone et al. (1975).

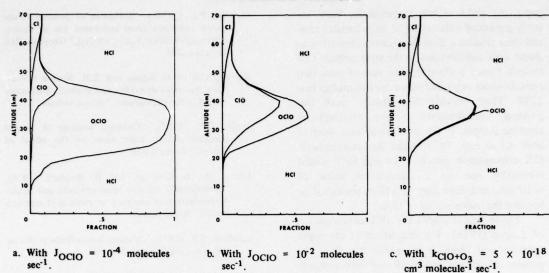


Figure 5. Relative abundances of the chlorine species as a function of altitude, as in $k_{CIO+O_3} = 5 \times 10^{-15}$ cm³ molecule⁻¹ sec⁻¹.

the presence of less volatile acids, as discussed by Wofsy and McElroy (1974). It does not, however, constitute a significant source of stratospheric chlorine.

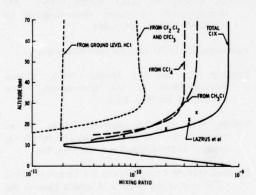


Figure 6. Predicted late 1974 stratospheric chlorine concentrations versus altitude according to source (solid and dashed lines). HCl observational data of Lazrus (1975) is shown for comparison (see also Cicerone et al., 1975).

Molina and Rowland (1974a) have shown that a more important source is the chlorine-containing molecules which are stable in the troposphere. These molecules are insoluble and hence immune to rainout, they are not dissociated by visible and near-UV radiation, and they

do not react with OH, O, O₃, or other tropospheric molecules or free radicals. These molecules are the halogenated hydrocarbons of the general formula CnHxClyFz. The most important appear to be CH₃Cl, CCl₄, CF₂Cl₂, and CFCl₃. Methyl chloride (CH₃Cl) is probably of natural origin; it has been measured in the troposphere at levels of 400-600 parts per trillion by Rasmussen (1975) and Lovelock (1974). It is attacked slowly by OH in the troposphere (Watson, 1975), which causes it to decrease slightly in mixing ratio through the troposphere. Due to its probably natural source, it is likely to provide a CIX mixing ratio in the stratosphere almost equal to the 400-600 ppt at the ground, the decrease corresponding to that small fraction which reacts with tropospheric OH, leading to HCl which eventually rains out. The resulting CIX profile is shown in Figure 5b for 400 ppt ground-level CH₃Cl.

Carbon tetrachloride, CCl₄, has been used industrially for more than 50 years, and may also have a natural source. There is some question regarding the magnitude of the source and the existence of possible sinks. Figure 6 shows the CIX profile calculated for CCl₄ with the steady-state assumption discussed by Molina and Rowland (1974b) and by Cicerone et al. (1975).

Fluorocarbons 11 and 12, CFCl₃ and CF₂Cl₂, have no known natural sources or any

important sinks in the troposphere. They are being produced industrially at an increasing rate, and thus require a time-dependent calculation to assess their contribution to the stratospheric CIX budget. Figure 6 illustrates the sum of these two contributions as predicted for approximately late 1974. They provide a relatively small but growing contribution to the stratospheric chlorine budget. If the production rate were to level off at early-1975 values, the stratospheric CIX contribution due to F-11 and F-12 would eventually rise to a steady-state value of ≈ 10 ppb, and thus they would be predicted to become the major source of CIX.

Figure 6 also shows the HCl measurements of Lazrus (1975). The magnitude at his upper measurement levels is somewhat less than the present calculation, but is still well within experimental and prediction uncertainties. The significant aspect of these measurements is the shape of the altitude profile, clearly indicating an effective high-altitude source such as the halogenated hydrocarbons are calculated to be. More measurements are still needed, both to verify the chemical relationships among the CIX species and to further elucidate the source-sink relationships.

REFERENCES

- Balakhnin, V.P., V.I. Egorov, and E.I. Intezarova (1971), "Kinetics investigation of the elemental reactions of oxygen atoms in the gas phase by epr:

 II. The reaction O + HCl → OH + Cl," Kinet. Catal.
 12, 258.
- Cicerone, R.J., R.S. Stolarski, and S. Walters (1974), "Stratospheric ozone destruction by man-made chlorofluoromethanes," Science 185, 1165.
- Cicerone, R.J., S. Walters, and R.S. Stolarski (1975), "Chlorine compounds and stratospheric ozone," Science 188, 375.
- Cicerone, R.J., D.H. Stedman, and R.S. Stolarski (1975), "Estimate of late 1974 stratospheric concentration of gaseous chlorine compounds (CIX)," Geophys. Res. Lett. 2, 219.
- Clyne, M.A.A., and J.A. Coxon (1968), "Kinetic studies of oxy-halogen radical systems," Proc. Roy. Soc. A303, 207.
- Crutzen, P.J. (1974a), "A review of upper atmospheric chemistry," Can. J. Chem. 52, 1569.

- Crutzen, P.J. (1974b), "Estimates of possible future ozone reduction from continued use of fluoro-chloro-methanes (CF₂Cl₂, CFCl₃)," Geophys. Res. Letters 1, 205.
- Farmer, C.B., O.F. Raper, and R.H. Norton (1976), "Spectroscopic detection and vertical distribution of HCl in the stratosphere," in this volume.
- Junge, C.E. (1957), "Chemical analysis of aerosol particles and of trace gases on the island of Hawaii," Tellus 9, 528.
- Lazrus, A., B. Gandrud, and R. Woodard (1976), "Stratospheric halogen measurements and in-situ determination of accuracy of nitric acid measurements," in this volume.
- Lovelock, J.E. (1975), "Natural halocarbons in the air and in the sea," Nature 256, 193.
- Molina, M.J. and F.S. Rowland (1974a), "Stratospheric sink for chlorofluoromethanes: Chlorine atom catalysed destruction of ozone," Nature 249, 810.
- Molina, M.J. and F.S. Rowland (1974b), "Predicted present stratospheric abundances of chlorine species from photodissociation of carbon tetrachloride," Geophys. Res. Lett. 1, 309.
- Norrish, R.G.W. and G.H.J. Neville (1934), "The decomposition of ozone photosensitized by chlorine," J. Chem. Soc., 1864.
- Rasmussen, R. (1975), personal communication.
- Rowland, F.S. and M.J. Molina (1975), "Chlorofluoromethanes in the environment," Rev. Geophys. Space Phys. 13, 1.
- Rundel, R.D. and R.S. Stolarski (1976), "A reexamination of the photochemistry of the Cl₂-O₃ system," to be published in J. Geophys. Res.
- Stedman, D.H., W. Chameides and R.J. Cicerone (1975), "The vertical distribution of soluble gases in the troposphere," Geophys. Res. Lett. 2, 233.
- Stolarski, R.S. and R.J. Cicerone (1974), "Stratospheric chlorine: A possible sink for ozone," Can. J. Chem. 52, 1610.
- Watson, R.T. (1974), "Rate Constants of CIO_x of Atmospheric Interest," Chemical Kinetics Data Survey, Vol. VIII, National Bureau of Standards, NBSIR 74-516.
- Watson, R.T. (1975), "Chlorine, chlorine oxides and other halogen species," section 5.75 of CIAP Monograph 1, U.S. Dept. of Transportation, DOT-TST-75-51, 5-125 - 5-152.

- Watson, R.T., G. Machado, S. Fischer, R.L. Schiff, and D.D. Davis (1976), "Chlorine-atom reactions of atmospheric importance," in this volume.
- Wofsy, S.C. and M.B. McElroy (1974), "HO_x, NO_x, and ClO_x: Their role in atmospheric photochemistry," Can. J. Chem. **52**, 1582.
- Wofsy, S.C., M.B. McElroy, and N.D. Sze (1975), "Freon consumption: Implications for atmospheric ozone," Science 187, 535.
- Wong, E. L. and F.E. Belles (1971), "Rate Measurements for the Reaction of Hydrogen Chloride and Deuterium Chloride with Atomic Oxygen," NASA Technical Note TN-D-6495.

THE CHEMISTRY OF ATMOSPHERIC BROMINE*

STEVEN C. WOFSY, MICHAEL B. MCELROY, AND YUK LING YUNG

Center for Earth and Planetary Physics Harvard University Cambridge, Massachusetts

ABSTRACT: Bromine may act as a catalyst for recombination of ozone and could be more efficient than either nitric oxide or chlorine. The lower atmosphere contains small concentrations of gaseous bromine produced by marine activity, by volatilization of particulate material released during the combustion of leaded gasoline, and by the use of methyl bromide as an agricultural fumigant. Observations by Lazrus et al. (1975) indicate small concentrations of bromine, $\approx 10^{-11}$ (v/v), in the contemporary stratosphere, and appear to imply a reduction of approximately 0.3% in the global budget of O₃. Estimates are given for reductions in O₃ which might occur if the use of CH₃Br as an agricultural fumigant were to continue to grow at present rates.

The chemistry of atmospheric ozone may be influenced to a remarkable extent by exceedingly small quantities of select stratospheric gases. Attention has focused in recent years on nitric oxide released by SST's (Johnston, 1971; Crutzen, 1972) and on chlorine produced by photodecomposition of chlorofluoromethanes (Molina and Rowland, 1974). This paper is devoted to a discussion of bromine. As we shall see, concentrations of bromine as small as 1 part in 10^{11} (v/v) can have an appreciable influence on ozone.

There are indications that the mixing ratio of gaseous forms of acidic bromine, represented most probably by HBr, according to the discussion below, may approach 10-11 in today's stratosphere (Lazrus et al., 1975) with similar values observed in the troposphere (see below). The mixing ratio of acidic bromine appears to increase with increasing altitude between 15 and 19 km, and there is evidence for similar behavior in the height distribution of particulate bromine (Lazrus et al., 1975; Delany et al., 1974). It is difficult to escape the conclusion that there must be a stratospheric source for particulate and gaseous acidic bromine.** Decomposition of methyl bromide offers a plausible explanation. Methyl bromide has been detected recently in surface waters of the ocean and in Antarctic snow (Rasmussen, 1975). It is used extensively as a fumigant and there may be additional natural sources as discussed below.

† The contribution from gasoline to the gaseous bro-

mine budget of the northern hemisphere could be as large as 20%. In carrying out the computations

summarized here we assumed a gasoline-related bromine source of 1.8 × 10⁵ tons yr⁻¹ (Klingman, 1974)

and estimated that half of this bromine would be volatilized before removal from the atmosphere. We

adopted a lifetime of 2 weeks for inorganic gaseous

bromine, consistent with the analysis by Moyers and

Duce (1972).

Bromine is present in both gas and particulate phases in the troposphere, with the gas phase dominant by a factor which ranges typically between 4 and 20. The mixing ratio of gaseous bromine is about 1.5 × 10-11 over Hawaii (Moyers and Duce, 1972) and it seems probable that the major constituent is HBr (see below). Measurements near the South Pole (Duce et al., 1973) suggest values smaller by about a factor of 5. There are indications that the gaseous component is derived primarily from volatilization of bromine carried into the atmosphere as a component of marine aerosols (Duce et al., 1963, 1965), with additional contributions from decomposition of CH₂Br and from particles released during the combustion of leaded gasoline (Moyers and Duce, 1972; Cadle, 1972; Martens et al., 1973). Using available data for the gasoline source strength, and empirical values for the atmospheric lifetime of HBr, we estimate a source strength for total gaseous bromine of 1.1 × 106 tons yr⁻¹, of which approximately 80% is derived from marine aerosols, 10% from CH₃Br, and 10% from automobiles.†

^{**}Gaseous BrO could contribute to the "particulate"

bromine found on neutral filters.

^{*}This paper appeared in nearly identical form in Geophysical Research Letters (Vol. 2, No. 6, pp. 215-218), in June 1975.

The importance of bromine in the stratosphere relates to its potential role as a catalyst for recombination of ozone. Catalysis can take place either through

$$Br + O_3 \rightarrow BrO + O_2$$

$$BrO + O \rightarrow Br + O_2$$
(1)

or through

$$2 \left\{ Br + O_3 \rightarrow BrO + O_2 \right\}$$

$$BrO + BrO \rightarrow 2Br + O_2$$
(2)

The sequence (1) is equivalent to

$$0 + 0_3 \rightarrow 20_2$$
 (1)

The sequence (2) is equivalent to

$$O_3 + O_3 \rightarrow 3O_2$$
 (2')

Reaction (2) could evolve Br₂ rather than Br. The efficiency of the cycle would not be greatly affected by uncertainties in the identity of the bromine product, since Br₂ will photolyze rapidly in the presence of sunlight.

Chlorine-atom chains are terminated in the stratosphere by reactions with CH_4 and H_2 , which tie up the gas in the relatively unreactive form HCl. The analogous reactions of bromine with CH_4 and H_2 are endothermic, and Watson (1975) was led to conclude that BrO might be the major form of gaseous bromine over an extensive height range. The efficiency of the catalytic cycles (1) and (2) could be exceedingly large in this case, and mixing ratios of bromine as small as 10^{-12} would have appreciable effects on O_3 .

It seems more likely, however, that HBr should dominate. Hydrogen bromide could be produced by

$$Br + HO_2 \rightarrow HBr + O_2 \tag{3}$$

and

$$Br + H_2O_2 \rightarrow HBr + HO_2 \tag{4}$$

and would be removed by

$$OH + HBr \rightarrow H_2O + Br \tag{5}$$

with an additional contribution from

$$h\nu + HBr \rightarrow H + Br.$$
 (6)

The chemical model adopted for this study, taken for the most part from Watson (1975), is given in Table 1.

Methyl bromide is removed by

$$OH + CH3Br \rightarrow H2O + CH2Br.$$
 (7)

The bromine atom is subsequently released, and inorganic bromide (HBr + Br + BrO) is carried out of the lower atmosphere by rain as discussed earlier.

The major uncertainties in the chemical model relate to reactions (3) and (7), for which we adopt rate constants 10^{-11} cm³ sec⁻¹ and 2×10^{-12} exp(-1200/T) respectively. The rate for (3) was suggested by a consideration of high-temperature data reported by Day et al. (1971). The rate for (7) is consistent with preliminary measurements for the reaction at 300K (Watson and Davis, 1975) and agrees also with the high-temperature data by Wilson (1965).

Height profiles computed for major bromine species are given in Figure 1. The computations summarized by this and subsequent figures were carried out using procedures described elsewhere (McElroy et al., 1974; Wofsy and McElroy, 1974; Wofsy et al., 1975), with the eddy-diffusion profile taken from Hunten (1975), but multiplied by 1.5 above 16 km to obtain agreement with CH₄ observations. The chemical scheme allowed for 95 reactions, including those listed in Table 1, The flux of inorganic bromine at ground level was taken equal to 5.3 × 107 molecules cm-2 sec-1*, and the flux of CH3Br was adjusted to agree with Lazrus et al. (1975). The surface flux of CH3Br was estimated in this manner to be 3.0 × 106 molecules cm⁻² sec⁻¹, approximately four times the value we inferred from Klingman (1974) for the net amount of bromine consumed in the manufacture of CH3Br during

^{*} This is the value of the flux derived from a calculation using the washout profile given in Table 1, a mean ground-level mixing ratio of 1 × 10⁻¹¹, and Hunten's (1975) eddy-diffusion profile.

WOFSY, MCELROY, AND YUNG

Table 1. Chemical Reactions Used in the Model

	Reaction	Rate Expression (a)	Reference
k ₁	$Br + O_3 \rightarrow BrO + O_2$	$1.2 \times 10^{-12} (300^{\circ} \text{K})$ $1 \times 10^{-10} \text{ exp } (-1320/\text{T}) [A, C]$ $2.5 \times 10^{-11} \text{ exp } (-900/\text{T}) [B]$	Watson (1975)
k ₂	$NO + BrO \rightarrow NO_2 + Br$	2 × 10 ⁻¹¹	Watson (1975)
k ₃	$Br + HO_2 \rightarrow HBr + O_2$	1 × 10 ⁻¹⁰ [C] 1 × 10 ⁻¹¹ [B] 0. [A]	Day et al. (1971) (see text)
k ₄	$BrO + O \rightarrow Br + O_2$	8 × 10 ⁻¹¹	Watson (1975)
k ₅	$BrO + BrO \rightarrow 2Br + O_2$	6.4×10^{-12}	Watson (1975)
	BrO + $h\nu \rightarrow$ Br + O	rate unknown in the atmosphere, probably slower than k ₂ according to Watson (1975)	
k ₆	$OH + HBr \rightarrow H_2O + Br$	$3.7 \times 10^{-11} \exp(600/T)$	Watson (1975)
k ₇	$OH + CH_3 Br \rightarrow H_2O + CH_2Br (b)$	$2 \times 10^{-12} \text{ exp (-1200/T)}$ 5.5 × 10 ⁻¹² exp (-1900/T)	(see text)
k ₈	$Br + H_2O_2 \rightarrow HBr + HO_2$	$1 \times 10^{-11} \exp (-1200/T)$	(see text)
J ₁	$HBr + h\nu \rightarrow H + Br$ (c)	$0, 0, 2.8 \times 10^{-9}, 4.9 \times 10^{-6}, 3.8 \times 10^{-6}, 6.7 \times 10^{-6}$	Romand and Vodar (1948)
J ₂	$CH_3Br + h\nu \rightarrow CH_3 + Br$	$0, 0, 2.2 \times 10^{-9}, 4.1 \times 10^{-8}, 7.3 \times 10^{-6}, 1.8 \times 10^{-5}$	Davidson (1951)
R ₁	HBr + rain, aerosol → removed from atmosphere	$\begin{array}{lll} 1.7 \times 10^{-6} & 0 < Z < 4 \text{ km} \\ 8.5 \times 10^{-7} & 4 \text{ km} < Z < 6 \text{ km} \\ 4.3 \times 10^{-7} & 6 \text{ km} < Z < 8 \text{ km} \\ 1.7 \times 10^{-7} & 8 \text{ km} < Z < 10 \text{ km} \\ 0 & 10 \text{ km} < Z \end{array}$	(see text)
kg	$O + HBr \rightarrow OH + Br$	4.0 × 10 ⁻¹² erp (-1360/T)	Brown and Smith (1975)

^aUnits are cm³ sec⁻¹. Letters A, B, C refer to curves in Figure 2.

bBr atom is assumed to be released during subsequent chemistry of CH₂Br.

^cPhotodissociation rate is given as a function of altitude (in km), units of sec⁻¹ (0, 10, ..., 50 km). A 24-how average is used at 30° latitude, 0° solar declination.

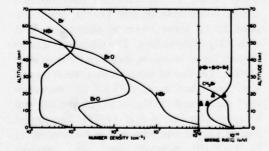


Figure 1. Height profiles for Br, HBr, BrO, and (Br + HBr + BrO). The data (4) are from Lazrus et al. (1975). Computations allow for transport of N₂O, NO_x, CH₄, CO, O₃, (HBr + Br + BrO), and CH₃Br, and account for complete HO_x and NO_x chemistry. The mean lifetime calculated for CH₃Br (column concentration/flux) is 1.1 yr.

1974. Plonka (1975) is of the opinion that only 25% of the industrial CH₃Br is released to the atmosphere, mainly as a byproduct of fumigation.

Taken at face value, the analysis given here implies both natural and industrial sources of CH₃Br. The sea is the most probable natural source, providing 75-95% of the CH₃Br shown in Figure 1.* However, we cannot exclude the possibility of additional anthropogenic contributions to stratospheric bromine, associated for example with the escape of (CH₂Br)₂ from gasoline storage tanks or with the production of

^{*} Burreson et al. (1975) reported very recently that CHBr₃ is an important component of certain seaweeds. If released to the atmosphere, CHBr₃ would play a role analogous to that attributed to marine CH₃Br in the present context.

relatively insoluble bromine species during the combustion of leaded gasoline.

According to the model, the mixing ratio of inorganic bromine decreases by only a factor of 5 between ground and tropopause. This profile results from the choice of heterogeneous loss coefficient (cf. Wofsy et al., 1972), and is consistent with observational data for other soluble species, HCl (Farmer, 1975), NH₃ (Georgii and Muller, 1974), and HNO₃ (Lazrus et al., 1974), and is in agreement also with radioactivity removal rates summarized by Junge (1963).

The results in Figure 1 imply a reduction on the order of 0.3% in the global concentration of O_3 due to bromine catalysis, of which approximately 0.2% may be attributed to CH_3Br and 0.02% to bromine release from auto exhausts. Reductions in O_3 , computed with various values for k_1 and k_3 , are shown in Figure 2. The results in Figure 2 were derived subject to the constraint of a height-independent value for the mixing ratio of (HBr + Br + BrO), and illustrate the dependence of the computed ozone deficit on this parameter.

Figure 3 gives several conceivable time profiles for the ozone deficit associated with agri-

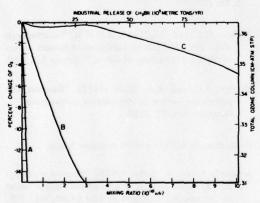


Figure 2. Ozone reduction as a function of (HBr + Br + BrO). Different curves refer to different combinations of rate expressions for k_3 and k_1 , as shown in Table 1. Curve B combines "best estimates" for these rates. Curve A shows a model where HBr formation does not occur (k_3 and k_8 set at zero). Curve C illustrates the effect of a choice for k_3 and k_1 designed to minimize the ozone perturbation. The upper axis shows the approximate industrial release rate of CH_3Br which would produce the given stratospheric perturbation, using $k_7 = 2 \times 10^{-12}$ exp (-1200/T).

cultural use of CH3Br. Curves D and E differ in choice of rate constant for reaction of OH with CH₃Br. Curve E employs the value suggested by analogy with the OH-CH3Cl reaction and is consistent also with the preliminary measurement by Watson and Davis. Curve D uses the OH - CH₄ reaction rate. Production and use of CH₃Br is assumed to grow in curves D7 and E7 at a rate of 7% per annum, a value close to the historical trend. Curves D15 and E15 envisage a somewhat larger growth rate, approximately 15% per annum. The latter growth rate may not be unreasonable, since cost factors currently limit fumigation to a very few high-value crops. Approximately 10% of world bromine production is used in the manufacture of CH₂Br, and roughly 63% in the production of ethylene dibromide.

It seems clear that an unconstrained growth in the use of methyl bromide could cause future problems for ozone. Measurements of bromine compounds in the atmosphere, together with laboratory studies of several key reactions, notably k_1 , k_3 , and k_7 , should be pursued in order to clarify these matters.

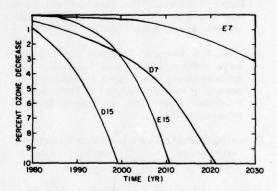


Figure 3. Reduction in ozone due to release of anthropogenic CH3Br. Curves D and E differ in the values assumed for k7: D, same rate as CH4; E, preliminary measurement reported by Watson and Davis (1975). Other rates are the same as curve B, Figure 2. 7% and 15% annual increases are modeled by D7, E7, and D15, E15 respectively. The anthropogenic release was set equal to 104 tons in 1974, approximately 50% of the total global production. The release rate estimated by Plonka (see text) would imply a shift of the time axis by approximately 10 years for D7 and E7, 5 years for D15 and E15.

WOFSY, MCELROY, AND YUNG

ACKNOWLEDGMENTS

We are indebted to C. Kolb, I. Chet, and R. Mitchell for valuable discussions, and to S. Coroniti and J. Plonka for useful communications. This work was supported by the National Aeronautics and Space Administration under Grant NASA NSG 2031, and by the Atmospheric Sciences Division of the National Science Foundation under Grant GA33990X to Harvard University.

REFERENCES

- Brown, F.D.H. and I.W.M. Smith (1975), "Absolute rate constants for the reactions of O(³P) atoms with HCl and HBr," Int. J. Chem. Kin. 7, 301.
- Burreson, B.J. and R.E. Moore (1975), "Haloforms in essential oil of the alga A. Taxiformis," Tetrahedron Lett. 7, 473.
- Cadle, R.D., (1972), "Composition of the stratospheric "sulfate" layer," Trans. Am. Geophys. U., 53, 812.
- Crutzen, P.J. (1972), "SST's, a threat to the earth's ozone shield," Ambio 1, 41.
- Davidson, N. (1951), "The ultraviolet absorption spectra and the refractive indices of some fluorobromomethanes," J. Am. Chem. Soc. 73, 468.
- Day, M.J., D.V. Stamp, K. Thompson, and G. Dixon-Lewis (1971), "Inhibition of hydrogen-air and hydrogen-nitrous oxide flames by halogen compounds," in *Proceedings of the 13th Symposium on Combustion*, pub. The Combustion Institute (Pittsburgh), 705.
- Delany, A.C., J.P. Shedlovsky, and W.H. Pollock (1974), "Stratospheric aerosol: the contribution from the troposphere," J. Geophys. Res. 79, 5646.
- Duce, R.A., J.T. Wasson, J.W. Winchester, and F. Burns (1963), "Atmospheric iodine, bromine and chlorine," J. Geophys. Res. 68, 3943.
- Duce, R.A., J.W. Winchester, and T.W. Van Nahl (1965), "Iodine, bromine and chlorine the Hawaiian marine atmosphere," J. Geophys. Res. 70, 1775.
- Duce, R.A., W.H. Zoller, and J.L. Moyers (1972), "Particulate and gaseous halogens in the Antarctic atmosphere," J. Geophys. Res. 78, 7802.
- Farmer, C.B., O.F. Raper, and R.H. Norton (1975), "Spectroscopic detection and vertical distribution of HC1 in the stratosphere," in this volume.

- Georgii, H.W., and W.J. Muller (1974), "On the distribution of ammonia in the middle and lower troposphere," Tellus XXVI 1-2, 180.
- Hunten, D.M. (1975), "Philosophy of one-dimensional modeling," in this volume.
- Johnston, H.S. (1971), "Reduction of stratospheric ozone by nitrogen oxide catalysts from SST exhaust," Science 173, 517.
- Junge, C.E. (1963), Air Chemistry and Radioactivity, Academic Press, New York, New York, 298ff.
- Klingman, C.L. (1974), "U.S. Bureau of Mines Mineral Yearbook," U.S. Dept. of the Interior.
- Lazrus, A., B. Gandrud, R. Woodard, and W. Sedlacek (1975), "Stratospheric halogen measurements and in-situ determination of accuracy of nitric-acid measurements," in this volume.
- Martens, C.S., J.J. Wesolowski, R. Kaifer, and W. John (1973), "Lead and bromine particle size distribution in San Francisco Bay area," Atmospheric Environment 7, 905.
- McElroy, M.B., S.C. Wofsy, J.E. Penner, and J.C. McConnell (1974), "Atmospheric ozone: Possible impact of stratospheric aviation," J. Atmos. Sci. 31, 287.
- Molina, M.J., and F.S. Rowland (1974), "Stratospheric sink for chlorofluoromethanes: Chlorine atom-catalysed destruction of ozone," Nature 249, 810.
- Moyers, J.L. and R.A. Duce (1972), "Gaseous and particulate iodine in the marine atmosphere," J. Geophys. Res. 77, 5229.
- Rasmussen, R. (1975), private communication.
- Romand, J. and B. Vodar (1948), "Spectre d'absorption de l'acide chlorodydrique gazeux dans la région de Schumann," Comptes Rendus (Acad. Sci.) 226, 238.
- Watson, R.T. (1975), "Chlorine, chlorine oxides and other halogen species," section 5.7.5 in Vol. 1 of the CIAP monograph series, U.S. Dept. of Transportation, DOT-OST-75-51, 5-125 - 5-152.
- Watson, R.T., D.D. Davis, E.S. Machado, and R. Schiff (1975), "The temperature dependence of some chlorine and bromine atom reactions of stratospheric interest," presented at a meeting of the American Chemical Society, Philadelphia, April 1975.

WOFSY, MCELROY, AND YUNG

- Wilson, W.E. (1965), "Structure, kinetics, and mechanism of a methane-oxygen flame inhibited with methyl bromide," in *Proceedings of the 10th Symposium on Combustion*, pub. The Combustion Institute (Pittsburgh), 47.
- Wofsy, S.C., J.C. McConnell and M.B. McElroy (1972), "Atmospheric CH₄, CO and CO₂," J. Geophys. Res. 77, 4477.
- Wofsy, S.C. and M.B. McElroy (1974), "HO_x, NO_x, and ClO_x. Their role in atmospheric photochemistry," Can. J. Chem. 52, 1582.
- Wofsy, S.C., M.B. McElroy, and N.D. Sze (1975), "Freon consumption: Implications for atmospheric ozone," Science 187, 535.

ON THE PRODUCTION OF NITRIC OXIDE BY COSMIC RAYS IN THE MESOSPHERE AND STRATOSPHERE

M. NICOLET Institut d'Aéronomie Spatiale de Belgique Brussels, Belgium

ABSTRACT: Nitric oxide is formed in the atmosphere through the ionization and dissociation of molecular nitrogen by galactic cosmic rays. One NO molecule is formed for each ion pair produced by cosmic-ray ionization.

The height-integrated input (day and night) to the lower stratosphere is of the order of 6×10^7 NO molecules cm⁻² sec⁻¹ in the auroral zone (geomagnetic latitude $\Phi > 60^\circ$) during the minimum of the sunspot cycle, and 4×10^7 NO molecules cm⁻² sec⁻¹ in the subauroral belt and auroral region ($\Phi > 45^\circ$) at the maximum of solar activity. The tropical production is less than 10^7 NO molecules cm⁻² sec⁻¹ above 17 km, and at the equator the production is only 3×10^6 NO molecules cm⁻² sec⁻¹.

INTRODUCTION

Oxides of nitrogen formed in the thermosphere by reactions involving charged species (Nicolet, 1965b; Norton and Barth, 1970; Strobel et al., 1970; Nicolet, 1970a; Strobel, 1971a, b, 1972) cannot penetrate down into the stratosphere (Brasseur and Nicolet, 1973). The photodissociation of nitric oxide (Strobel, 1972; Brasseur and Nicolet, 1973) is more important in the mesosphere than its transport rate, and the normal presence of oxides of nitrogen in the stratosphere must be due to their formation in that region.

Among the various possible processes leading to the formation of nitrogen oxides in the stratosphere, we may consider as the principal process the decomposition of nitrous oxide (Bates and Hays, 1967; Crutzen, 1970, 1971; Nicolet, 1970b, 1971; McElroy and McConnell, 1971; Nicolet and Vergison, 1971; Nicolet and Peetermans, 1972). However, direct photodissociation such as

$$N_2O + h\nu (\lambda < 2515 \text{ Å}) \rightarrow N(^4S) + NO(^2\Pi)$$
 (1)

is aeronomically impossible (Nicolet and Peetermans, 1972) and the exclusive primary dissociation process of N₂O yields oxygen atoms. But, as introduced by Nicolet (1970b, 1971), nitric oxide is generated only by the reaction

$$N_2O + O(^1D) \rightarrow 2 \text{ NO.}$$
 (2)

The O(¹D) atoms are formed by the photodissociation of stratospheric ozone. The calculated vertical distribution of N₂O in the stratosphere depends strongly on the values adopted for the eddy-diffusion coefficient (Nicolet and Vergison, 1971; McElroy and McConnell, 1971; Crutzen, 1971; Nicolet and Peetermans, 1972).

The oxidation of NH₃ has also been proposed as a dominant stratospheric source of NOx (McConnell, 1973; McConnell and McElroy, 1973). It requires a NH₃ mixing ratio of the order of at least 10-9 in the lower stratosphere if it is to play a role in the production of nitric oxide molecules (Nicolet, 1973 (Figure 10), 1974 (Figure 8)). Since NH₃ has not been observed in the stratosphere, such a source is probably not important. According to Crutzen (1974), NH₃ can be removed efficiently by heterogeneous processes in the troposphere. A recent analysis of the solar spectrum by Kaplan (1973) shows that the mixing ratio could be much smaller than 8 × 10-11. However, recent measurements by Georgii and Muller (1974) lead to mixing ratios as low as 5 × 10-10 to 1 × 10-9 in the polar maritime air and to about 5 × 10-9 over the continent. In any case, an accurate analysis of this problem is still required.

Finally, recent independent studies (Warneck, 1972; Nicolet and Peetermans, 1972) have proposed the production of nitric oxide by cosmic rays acting on N₂. Brasseur and Nicolet (1973) have indicated that the production of nitric oxide molecules is of the order of one

molecule per ion pair produced by cosmic rays. The production of nitric oxide by cosmic rays is also a nighttime process, and its rate is related to the geomagnetic latitude. An attempt will be made here to estimate the world-wide mesospheric and stratospheric production of nitric oxide by this process.

IONIZATION AND DISSOCIATION BY COSMIC RAYS

Ionization due to cosmic rays (Dalgarno, 1967) is produced mostly by secondary electrons ejected by heavy particles. The experimental results of Rapp et al. (1965) give the crosssections for dissociative ionization of molecules by electron impact from threshold up to 1000 eV (Figure 1). The dissociative ionization cross-section rises from threshold to a maximum near 100 eV and decreases with increasing energy. The cross-section for the dissociative ionization process $N_2 \rightarrow N + N^+$ corresponds to about 20% of the total ionization cross-section for electron energies greater than 100 eV, and to about 25% for $O_2 \rightarrow O + O^+$ under the same conditions. Thus, the ratios of N2+/N+ and O₂⁺/O⁺ ion production are 4 and 3, respectively.

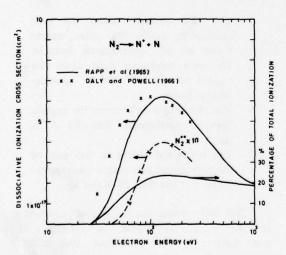


Figure 1. Dissociative ionization cross-section of molecular nitrogen versus electron energy.

The production of *molecular* nitrogen ions in the air is, therefore, $4/5 \times 0.8 = 0.64$ of an ion pair, and the production of *atomic* nitrogen ions is $4/5 \times 0.2 = 0.16$ under the same conditions.

Assuming that the N⁺ ions (Dalgarno, 1967) are immediately converted by a charge-transfer reaction into neutral nitrogen atoms

$$N^+ + O_2 \rightarrow O_2^+ + N$$
 (3)

or indirectly transformed through the reaction

$$N^+ + O_2 \rightarrow O + NO^+$$
 (4)

the production of nitrogen atoms through the dissociative ionization process must be $0.16 \times 2 = 0.32$ nitrogen atoms per ion pair produced by cosmic rays.

The total dissociation cross-section has been measured (Figure 2) by Winters (1966). The average cross-section for electron energies between 30 and 300 eV is of the order of 1.75 × 10-16 cm², corresponding to about three times the average dissociative ionization crosssection (5 × 10-17 cm²) in the same energy range. Thus, the production of nitrogen atoms by direct dissociation is $0.32 \times 2 = 0.64$ per ion pair produced by cosmic rays. The total yield of nitrogen atoms produced by dissociation and dissociative ionization of N2 is therefore approximately one (0.96) nitrogen atom for every ion pair produced by cosmic rays. The accuracy of this ratio can be improved when more precise experimental data are obtained. If O+ ions have an effect, it will not change the approximate value

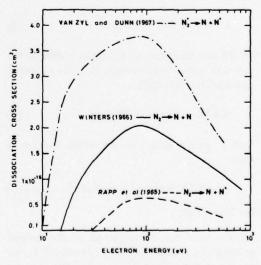


Figure 2. Dissociation cross-section of N₂ and N₂⁺ versus electron energy.

of 1.00 adopted for the production of nitrogen atoms. The total yield of odd nitrogen would, however, increase above one nitrogen atom for one ion pair produced by cosmic rays if a reaction such as $O_2^+ + N_2 \rightarrow NO^+ + NO$ were accepted at stratospheric levels.

REACTION OF NITROGEN ATOMS

The dissociative ionization and dissociation of N₂ and the dissociative recombination of molecular ions may lead to a production of nitrogen atoms in the normal ⁴S state and in the excited states ²D and ²P. Since the lifetime of the excited state ²D is long (9.4 × 10⁴ sec), a direct reaction between N(²D) and O₂ must be considered. Thus, after its production, atomic nitrogen reacts as follows

$$N(^4S) + O_2 \rightarrow O + NO + 32 \text{ kcal}$$
 (5)

with a rate coefficient (Becker et al., 1969)

$$b_7 = 7.5 \times 10^{-15} \text{ T e}^{-3000/\text{T}} \text{ cm}^3 \text{ sec}^{-1}$$
 (6)

or

$$N(^2D) + O_2 \rightarrow O + NO$$
 (7)

with a rate coefficient (Lin and Kaufman, 1971; Slanger et al., 1971)

$$b_7 * = 6 \times 10^{-12} \text{ cm}^3 \text{ sec}^{-1}$$
. (8)

Of the various aeronomic processes leading to the union of odd-nitrogen atoms, only the following reaction (Nicolet, 1965a)

$$N + NO \rightarrow O + N_2 + 75 \text{ kcal}$$
 (9)

with a rate coefficient known within a factor of two

$$b_6 = 1.5 \times 10^{-12} \text{ T}^{1/2} \text{ cm}^3 \text{ sec}^{-1}.$$
 (10)

can play a role.

Its role can be neglected in the normal processes of NO formation by (5) and (7); for an excess of nitrogen atoms, reaction (9) must be considered. In a perturbed atmosphere, the reactions $N + NO_2 \rightarrow NO + NO$, $N_2O + O$, and $N_2 + O$

O₂ should be considered for a complete analysis of NO production.

THE COSMIC-RAY VARIATIONS

The galactic cosmic radiation, which is essentially isotropic as observed on the Earth, is modulated by the interplanetary magnetic field; hence, its effect on NO production is related to solar activity. Since its intensity depends on the geomagnetic field, there is an ionization or dissociation effect which varies strongly with latitude. Table 1 gives the production of ion pairs, nitrogen atoms, or nitric oxide molecules between 85 km and 35 km for a solar activity cycle. The minimum value is reached near the maximum of the solar activity and the maximum value corresponds with minimum solar activity. There is a solar-activity effect which is greater than a factor of two at high latitudes. In fact, the variation with solar activity depends on the geomagnetic regions. Figure 3 shows the geomagnetic regions; they are defined as follows, using geographic coordinates of $\varphi_0 = 78.5^{\circ}N$ and $\lambda_0 = 69^{\circ} \text{ W}$ for the north geomagnetic pole (Nicolet, 1959):

- 1. The two auroral regions for each hemisphere cover the polar regions down to 60° geomagnetic latitude.
- The two subauroral belts cover the regions between 60° and 45° geomagnetic latitudes.
- The minauroral belt covers the regions between geomagnetic latitudes 45°N and S.
- The equatorial region is that part of the minauroral belt with a geomagnetic latitude of less than 20°N and S.

The NO production is almost constant in the equatorial region (see Figure 4 and Table 1); the latitudinal and solar-activity effects are very small. In the other part of the minauroral belt $(20^{\circ} < \Phi < 45^{\circ})$ there is a rapid increase of the NO production with latitude with smaller differences due to the solar activity effect. In the subauroral belt $(45^{\circ} \le \Phi \le 60^{\circ})$ the production rate of nitric oxide almost reaches its maximum, and the variation with solar activity is particularly large

Table 1. Cosmic-Ray Production of Nitric Oxide [(or Ion Pair or Atomic Nitrogen) (cm⁻³ sec⁻¹)] in the Mesosphere and Upper Stratosphere

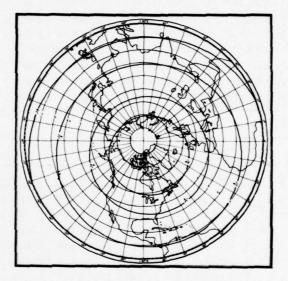
Altitude		Latitue	de Φ	
(km)	0°	15°	30°	40°
85	$(3.3 \pm 0.1) \times 10^{-4}$	$(3.6 \pm 0.1) \times 10^{-4}$	$(6.0 \pm 0.3) \times 10^{-4}$	(9.6 ± 0.4) × 10 ⁻⁴
80	$(8.0 \pm 0.2) \times 10^{-4}$	$(8.8 \pm 0.2) \times 10^{-4}$	$(1.5 \pm 0.1) \times 10^{-3}$	(2.3 ± 0.1) × 10-
75	$(1.8 \pm 0.05) \times 10^{-3}$	$(2.0 \pm 0.05) \times 10^{-3}$	$(3.3 \pm 0.2) \times 10^{-3}$	(5.2 ± 0.3) × 10-
70	$(3.7 \pm 0.1) \times 10^{-3}$	$(4.1 \pm 0.1) \times 10^{-3}$	$(6.9 \pm 0.4) \times 10^{-3}$	(1.1 ± 0.1) × 10
65	$(7.2 \pm 0.2) \times 10^{-3}$	$(8.0 \pm 0.2) \times 10^{-3}$	$(1.3 \pm 0.1) \times 10^{-2}$	(2.1 ± 0.1) × 10 ⁻⁵
60	$(1.3 \pm 0.05) \times 10^{-2}$	$(1.5 \pm 0.05) \times 10^{-2}$	$(2.4 \pm 0.2) \times 10^{-2}$	(3.4 ± 0.2) × 10 ⁻³
55	$(2.3 \pm 0.05) \times 10^{-2}$	$(2.6 \pm 0.15) \times 10^{-2}$	$(4.3 \pm 0.2) \times 10^{-2}$	(6.8 ± 0.3) × 10
50	$(4.3 \pm 0.1) \times 10^{-2}$	$(4.7 \pm 0.1) \times 10^{-2}$	$(7.8 \pm 0.5) \times 10^{-2}$	$(1.2 \pm 0.1) \times 10^{-}$
45	$(7.9 \pm 0.2) \times 10^{-2}$	$(8.7 \pm 0.2) \times 10^{-2}$	$(1.4 \pm 0.1) \times 10^{-1}$	(2.3 ± 0.1) × 10
40	$(1.5 \pm 0.5) \times 10^{-1}$	$(1.7 \pm 0.05) \times 10^{-1}$	$(2.8 \pm 0.1) \times 10^{-1}$	(4.4 ± 0.2) × 10
35	$(3.1 \pm 0.1) \times 10^{-1}$	$(3.4 \pm 0.1) \times 10^{-1}$	$(5.6 \pm 0.3) \times 10^{-1}$	$(9.0 \pm 0.4) \times 10^{-1}$

Altitude		$\Phi = 50^{\circ}$			Φ = 60°	
(km)	Min	Mean	Max	Min	Mean	Max
85	1.4 × 10 ⁻³	1.7 × 10 ⁻³	·2.0 × 10 ⁻³	1.6 × 10 ⁻³	1.8 × 10 ⁻³	3.3 × 10-3
80	3.5×10^{-3}	4.2×10^{-3}	4.0×10^{-3}	3.9 × 10 ⁻³	4.4 × 10 ⁻³	8.0 × 10-
75	7.8×10^{-3}	9.3 × 10 ⁻³	1.1×10^{-2}	8.8 × 10 ⁻³	9.8 × 10 ⁻³	1.8 × 10-2
70	1.6 × 10 ⁻²	2.0×10^{-2}	2.3×10^{-2}	1.8 × 10 ⁻²	2.1×10^{-2}	3.8 × 10-2
65	3.2 × 10 ⁻²	3.8×10^{-2}	4.5 × 10 ⁻²	3.6 × 10 ⁻²	4.0×10^{-2}	7.3 × 10-
60	5.8 × 10 ⁻²	7.0×10^{-2}	8.2 × 10 ⁻²	6.5 × 10 ⁻²	7.3 × 10 ⁻²	1.3 × 10-1
55	1.0×10^{-1}	1.2×10^{-1}	1.4×10^{-1}	1.1 × 10 ⁻¹	1.3 × 10 ⁻¹	2.3 × 10 ⁻¹
50	1.9×10^{-1}	2.2×10^{-1}	2.6×10^{-1}	2.1 × 10 ⁻¹	2.4×10^{-1}	4.3 × 10-1
45	3.5 × 10 ⁻¹	4.1×10^{-1}	4.9 × 10 ⁻¹	3.9 × 10 ⁻¹	4.4 × 10 ⁻¹	7.9 × 10
40	6.6 × 10 ⁻¹	7.9 × 10 ⁻¹	9.3 × 10 ⁻¹	7.4 × 10 ⁻¹	8.3 × 10 ⁻¹	1.5
35	1.3	1.6	1.9	1.5	i.7	3.1

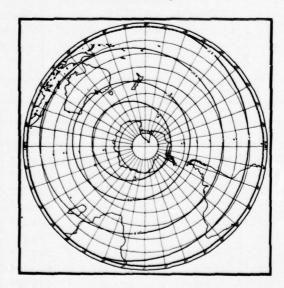
Altitude		$\Phi = 70^{\circ}$	
(km)	Min	Mean	Max
85	1.6 × 10 ⁻³	2.8×10^{-3}	4.0 × 10 ⁻³
80	3.9 × 10 ⁻³	6.8×10^{-3}	9.6 × 10 ⁻³
75	8.8 × 10 ⁻³	1.5 × 10 ⁻²	2.2 × 10 ⁻²
70	1.8 × 10 ⁻²	3.2×10^{-2}	4.5 × 10 ⁻²
65	3.6 × 10 ⁻²	6.2×10^{-2}	8.8 × 10-2
60	6.5 × 10 ⁻²	1.1 × 10 ⁻¹	1.6 × 10 ⁻¹
55	1.1 × 10 ⁻¹	2.0×10^{-1}	2.8 × 10 ⁻¹
50	2.1 × 10 ⁻¹	3.7×10^{-1}	5.2 × 10 ⁻¹
45	3.9 × 10 ⁻¹	6.7×10^{-1}	9.5 × 10 ⁻¹
40	7.4 × 10 ⁻¹	1.3	1.8
35	1.5	2.6	3.7

at the border of the auroral zone ($\Phi = 60^{\circ}$). In the auroral zone ($\Phi > 60^{\circ}$) the production rate of nitric oxide is constant for the same solar-activity conditions but varies strongly with solar activity. The values covering the solar maximum (1958) and solar minimum (1965) cause the minimum and maximum production of nitric oxide molecules in the auroral regions and in a part of the subauroral belt ($\Phi < 60^{\circ}$) for high solar-activ-

ity conditions. A knee in the curves for 20 km (Figure 4) occurs at $\Phi < 60^\circ$ at solar maximum and at $\Phi > 60^\circ$ at solar minimum. An example of the variation in the auroral region is given in Figure 5 for two solar cycles from 1955 to 1970. The production of nitric oxide molecules at 20 km varies from a minimum of about 15 molecules cm⁻³ sec⁻¹ to a maximum of about 25 molecules cm⁻³ sec⁻¹.



a. Northern hemisphere.



b. Southern hemisphere.

Figure 3. Geomagnetic regions.

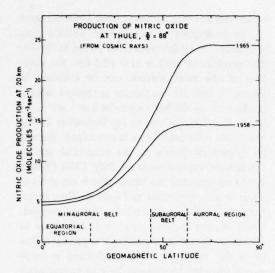


Figure 4. Nitric oxide production at 20 km by cosmic rays versus latitude for conditions of solar-activity maximum (1958) and minimum (1965). Cosmic-ray data deduced from Neher (1961, 1967).

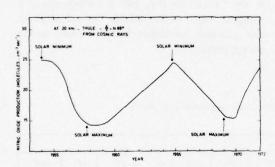


Figure 5. Nitric oxide production at 20 km in the northern auroral region at Thule, Φ = 88°. Cosmic-ray data deduced from Neher (1971):

THE VERTICAL DISTRIBUTION OF THE PRODUCTION OF NITRIC OXIDE IN THE STRATOSPHERE

From measurements of cosmic rays in the stratosphere at high latitudes covering several solar maxima and minima (Neher, 1971) it is possible to deduce the maximum and minimum production rates of nitric oxide in the entire auroral region. Figure 6 is an illustration of various NO production rates. The vertical distributions at different solar minima (1954, 1965)

and at different solar maxima (1958, 1969) are not very different, respectively. The variation of the nitric oxide production with altitude is particularly large above the production peak, which is at $12.5 \text{ km} \pm 1 \text{ km}$ depending on the latitude and on the solar cycle. Below the peak, the results (Figure 6) for cosmic-ray ionization obtained by George (1970) on January 10-11, 1968 at constant geomagnetic latitude 44°N (near the beginning of the subauroral belt) do not differ very much from the value for the auroral region $(\Phi > 60^{\circ})$ near a maximum of solar activity. The following values can be used at $\Phi \geqslant 44^{\circ}$ for the minimum production of nitric oxide molecules:

Altitude (km)	0	1	2	3	4
NO (cm ⁻³ sec ⁻¹)	2.6	3.3	4.2	5.3	7.0
Altitude (km)	5	6	7	8	9
NO (cm ⁻³ sec ⁻¹)	9.1	12.0	15.8	19.5	23.1
Altitude (km)	10	11	12	12.5	
NO (cm ⁻³ sec ⁻¹)	26.2	29.3	30.6	30.8	

There is, therefore, significant stratospheric production of NO molecules (day and night) in the region of $\Phi \geqslant 45^\circ$. Another detailed observation of the cosmic-ray ionization (Neher, 1967) at Bismarck, $\Phi = 56^\circ$, in 1965 from June 28 to August 4 leads to values of nitric oxide production (Figure 6) which are not too different from the observations made at Thule ($\Phi = 88^\circ$), particularly below the production peak. Considering the values observed at $\Phi = 44^\circ$ for maximum solar activity and at $\Phi = 56^\circ$ for minimum solar activity, the following average values for the production of nitric molecules can be adopted for the upper troposphere and lower stratosphere at $\Phi \geqslant 45^\circ$:

Altitude (km)	5	6	7
NO (cm ⁻³ sec ⁻¹)	10.4±1.3	13.4±1.4	16.7±1
Altitude (km)	8	9	10
NO (cm ⁻³ sec ⁻¹)	21.1±1.5	25.4±2	29.2±3

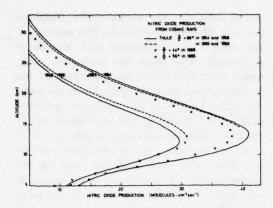


Figure 6. Production of nitric oxide at high geomagnetic latitudes during various solar cycles. 1954 and 1965 are minimum solar activity; 1958 and 1969 are maximum solar activity. Cosmic ray data from Neher (1971). Φ = 44° in 1968 are from measurements made by George (1970) and Φ = 56° by Neher (1967) at Bismarck Φ = 56° and φ = 47°.

A latitude survey of the cosmic-ray ionization (Neher, 1967) was made during July 1965 corresponding to a minimum of solar activity which was not very different from 1954 in regard to the production of nitric oxide. Table 2 gives the values for all latitudes from 10 km to 30 km. The production peak is near 12.5 km; the variation of the peak altitude can be followed in Figure 7, and the maximum is reached with a production of 40 NO molecules cm⁻³ sec⁻¹. As far as the absolute cosmic-ray ionization during maximum solar conditions is concerned, there is no systematic survey in the equatorial region. From observations made in July 1958 (Neher, 1961) we obtained the values which are given in Table 3 and illustrated in Figure 8. They represent a low minimum for nitric oxide production. From the production peak (≈ 12.5 km) up to 30 km. there is an extension of the auroral region $(\Phi \ge 60^{\circ})$, where the NO production is maximum) into the subauroral belt to geomagnetic latitudes $\Phi \approx 50^{\circ}$ and $\Phi \approx 55^{\circ}$, respectively. Below the production peak, there is an extension into the whole subauroral belt ($\Phi \ge 45^{\circ}$). This characteristic (last column of Table 3) referred to as the "knee" (Neher, 1961) corresponds at a constant height to the latitude beyond which as one proceeds to higher latitudes little or no change occurs.

Table 2. Maximum Production of Nitric Oxide Molecules (cm⁻³ sec⁻¹)

Altitude					Latit	ude Ф						
(km)	0°	10°	15°	20°	25°	30°	35°	40°	45°	50°	55°	≥60°
10	(13)	(14)	15.2	17.0	18.8	20.4	22.8	25.2	27.6	30.9	32.0	32.0
12.5	(14)	(15)	16.1	17.4	19.4	22.1	25.0	29.0	32.1	35.9	38.8	39.3
15	(10.5)	(11.5)	12.2	13.5	15.3	17.3	21.3	25.3	28.5	32.0	36.0	37.5
17.5	(7.5)	(8.0)	8.5	9.5	10.6	12.3	15.2	18.3	21.6	25.4	28.9	31.2
20	(5.0)	(5.2)	5.4	6.0	6.9	8.0	10.1	12.4	15.0	18.1	21.0	23.2
22.5	(2.7)	(2.8)	3.1	3.6	4.2	4.9	6.2	7.6	9.8	12.0	14.7	16.7
25	(1.7)	(1.8)	1.9	2.2	2.5	3.1	3.6	4.6	6.2	8.0	10.0	11.6
27.5	(1.0)	(1.0)	1.1	1.3	1.6	1.9	2.4	3.1	4.1	5.3	6.4	8.0
30	<1	<1	<1	<1	<1	1.1	1.5	2.0	2.6	3.2	4.1	5.4

Values in parentheses are extrapolations from data at higher latitudes.

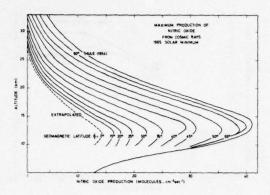


Figure 7. Production of nitric oxide during a minimum of solar activity. Cosmic-ray data deduced from Neher (1967, 1971).

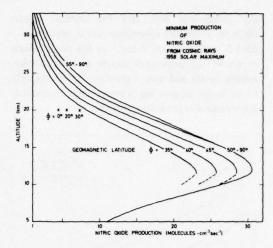


Figure 8. Production of nitric oxide during a maximum of solar activity. Cosmic-ray data deduced from Neher (1961).

Table 3. Minimum Production of Nitric Oxide Molecules (cm-3 sec-1)

414iad.		I	Latitude Φ				
Altitude (km)	35°	40°	45°	50°	55-90°	Knee	
10	21.0	24.0	26.0	26.0	26.0	44°	
12.5	27.5	25.3	28.2	30.5	30.5	49	
15	18.2	21.2	24.2	27.0	27.0	49	
17.5	13.3	15.8	18.2	20.6	21.2	51	
20	8.2	10.2	12.2	14.2	15.5	53	
22.5	5.0	6.2	7.2	8.8	10.1	55	
25	3.1	3.9	4.9	5.9	6.8	55	
27.5	1.9	2.5	3.2	3.8	4.5	56	
30	1.1	1.6	2.1	2.6	3.0	56	

The latitude of the knee increases with altitude. During maximum solar conditions, the knee occurs at a geomagnetic latitude of about 40° at sea level, at $\Phi = 44^{\circ}$ (see Table 3) at an altitude of 10 km, and at $\Phi = 56^{\circ}$ at an altitude of 30 km. During minimum solar conditions, the knee occurs at higher latitudes, for example, at $\Phi = 52^{\circ}$ at an altitude of 10 km, at $\Phi = 55^{\circ}$ for the production peak at 12.5 ± 1.0 km, and $\Phi = 60^{\circ}$ at an altitude of 20 km.

If we compare (Figure 9) the vertical distributions of the nitric oxide production during conditions of minimum and maximum solar activity, we can see that there are several regions to be considered. In the equatorial region $(\Phi < 20^{\circ})$, the maximum production of nitric oxide is less than 17.5 molecules cm⁻³ sec⁻¹ at the peak. In the minauroral belt, the increase is such that the minimum peak production is about 28 NO molecules cm⁻³ sec⁻¹. It is clear that in

the subauroral belt and the auroral region $(\Phi > 45^\circ)$ this NO formation rate is important – 35 ± 5 molecules cm⁻³ sec⁻¹ at the peak, which represents an important source at lower stratospheric levels and may, therefore, be comparable to or larger than other sources since cosmic-ray ionization also is present at night.

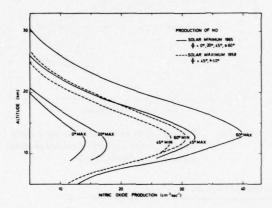


Figure 9. Comparison of the production of nitric oxide molecules for minimum and maximum solar activities in the equatorial region ($\Phi \le 20^{\circ}$), in the subauroral belt ($45^{\circ} \le \Phi \le 60^{\circ}$) and in the auroral region ($\Phi \ge 60^{\circ}$).

The ionization and dissociation of molecular nitrogen by cosmic rays provide (Figure 10) a height-integrated input to the stratosphere of 6 × 107 NO molecules cm-2 sec-1 (day and night) in the auroral zone ($\Phi \ge 60^{\circ}$) during minimum solar-activity conditions, and 4 X 107 NO molecules cm⁻² sec⁻¹ in the subauroral belt and auroral region ($\Phi \ge 45^{\circ}$) during maximum solar-activity conditions. The extension of the polar tropopause to geomagnetic latitudes of 35° inside the minauroral belt leads (Figure 10) to NO production greater than 2 × 107 molecules cm⁻² sec⁻¹. As far as the equatorial and tropical stratosphere is concerned, the production is less than 10⁷ NO molecules cm-2 sec-1, since the tropopause reaches an altitude of 17 km. At the tropopause break, the stratospheric production may increase by a large factor according to the synoptic situation. At mean latitudes it is well known that the tropopause height is very variable with no special concentration near the mean value.

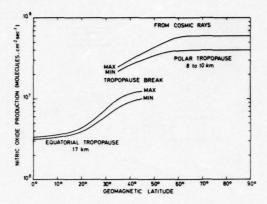


Figure 10. Production in the stratosphere of nitric oxide molecules (cm⁻² sec⁻¹) versus geomagnetic latitude for conditions of minimum (NO_{max}) and maximum (NO_{min}) solar activity.

CONCLUDING REMARKS

It may be concluded that the production of nitric oxide molecules by the ionization and dissociation of molecular nitrogen in the mesosphere and stratosphere is negligible in the mesosphere (NO production less 1 cm⁻³ sec⁻¹) but increases to a maximum in the lower stratosphere in the polar regions. The distribution of the ionization and dissociation of N₂ by cosmic rays implies that the NO production is greater than 10^7 molecules cm⁻² sec⁻¹ throughout the lower stratosphere for geomagnetic latitudes $\Phi \ge 45^\circ$ (Figure 10), from 2×10^7 to 6×10^7 cm⁻² sec⁻¹. In the equatorial region $\Phi < 20^\circ$ the NO production is small, 3×10^6 molecules cm⁻² sec⁻¹.

If the vertical distribution of the production of nitric oxide by cosmic rays (Figure 11) and by the reaction of $O(^1D)$ with N_2O are compared, it can be seen that production by cosmic rays is important below 20 km between 45° latitude and the pole. Since cosmic rays cause both daytime and nighttime NO production, the process is particularly important during the winter at high latitudes. It is necessary that production of about 5×10^7 NO molecules cm⁻² sec⁻¹ be introduced in the computation of stratospheric models and that correct lower-boundary conditions be used.

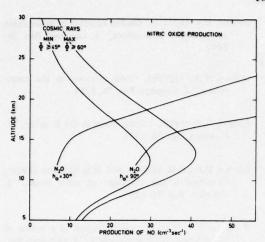


Figure 11. Comparison of the production of nitric oxide molecules in the lower stratosphere by cosmic-ray ionization and dissociation of N_2 and by oxidation of N_2 0. The "cosmic ray curves" are given for maximum and minimum conditions at geomagnetic latitudes $\Phi \ge 60^\circ$ and $\Phi \ge 45^\circ$, respectively. The " N_2 0 curves" are given for an overhead sun $h_{\odot} = 90^\circ$ and an average height $h_{\odot} = 30^\circ$.

REFERENCES

- Anderson, H.R. (1973), "Cosmic ray total ionization 1970-1972," J. Geophys. Res. 78, 3958.
- Bates, D.R. and P.B. Hays (1967), "Atmospheric nitrous oxide," Planet. Space Sci. 15, 189.
- Becker, K.H., W. Groth, and D. Kley (1969), "The rate of the aeronomic reaction N + O₂," Z. Naturf. 24A, 1280.
- Brasseur, G. and M. Nicolet (1973), "Chemospheric processes of nitric oxide in the mesosphere and stratosphere," Planet. Space Sci. 21, 939.
- Crutzen, P.J. (1970), "The influence of nitrogen oxides on the atmospheric ozone content," Quart. J. Roy. Met. Soc. 96, 320.
- Crutzen, P.J. (1971), "Ozone production rates in an oxygen-hydrogen-nitrogen oxide atmosphere," J. Geophys. Res. 76, 7311.
- Crutzen, P. (1974), "A review of upper atmospheric photochemistry," Can. J. Chem. 52, 1569.
- Dalgarno, A. (1967), "Atmospheric reactions with energetic particles," Space Research (pub. North Holland, Amsterdam), Vol. VII, 849.

- Daly, N.R. and R.E. Powell (1966), "Electron collision in nitrogen," Proc. Phys. Soc. 89, 273.
- George, J.M. (1970), "New data on the absolute cosmic ray ionization in the lower atmosphere," J. Geophys. Res. 75, 3693.
- Georgii, H.W. and W.J. Muller (1974), "On the distribution of ammonia in the middle and lower troposphere," Tellus 26, 180.
- Kaplan, L.D. (1973), "Background concentration of photochemically active trace constituents in the stratosphere and upper troposphere," Pure and Appl. Geophys. 106-108, 1341.
- Lin, C.L. and F. Kaufman (1971), "Reactions of metastable nitrogen atoms," J. Chem. Phys. 55, 3760.
- McConnell, J.C. (1973), "Atmospheric ammonia," J. Geophys. Res. 78, 7812.
- McConnell, J.C. and M.B. McElroy (1973), "Odd nitrogen in the atmosphere," J. Atmos. Sci. 30, 1465.
- McElroy, M.B. and J.C. Connell (1971), "Nitrous oxide: A natural source of stratospheric NO," Atmos. Sci. 28, 1095.
- Neher, H.V. (1956), "Low-energy primary cosmic-ray particles in 1954," Phys. Rev. 103, 228.
- Neher, H.V. (1961), "Cosmic-ray knee in 1958," J. Geophys. Res. 66, 4007.
- Neher, H.V. (1967), "Cosmic-ray particles that changed from 1954 to 1958 to 1965," J. Geophys. Res. 72, 1527.
- Neher, H.V. (1971), "Cosmic rays at high latitudes and altitudes covering four solar maxima," J. Geophys. Res. 76, 1637.
- Nicolet, M. (1959), "Geographical distribution of the International Geophysical Year Stations," Ann. Int. Geophys. Year, Vol. III.
- Nicolet, M. (1965a), "Nitrogen oxides in the chemosphere," J. Geophys. Res. 70, 679.
- Nicolet, M. (1965b), "Ionospheric processes and nitric oxide," J. Geophys. Res. 70, 691.
- Nicolet, M. (1970a), "The origin of nitric oxide in the terrestrial atmosphere," Planet. Space Sci. 18, 1111.
- Nicolet, M. (1970b), "Aeronomic reactions of hydrogen and ozone," Aeronomica Acta A79 and (1971) in Mesospheric Models and Related Experiments, Reidel, Dordrecht, 1-51.

- Nicolet, M. (1973), "An overview of aeronomic processes in the stratosphere and mesosphere," Aeronomica Acta A121 and (1974) Can. J. Chem. 52, 1381.
- Nicolet, M. and W. Peetermans (1972), "The production of nitric oxide in the stratosphere by oxidation of nitrous oxide," Ann. Géophys. 28, 751.
- Nicolet, M. and E. Vergison (1971), "L'oxyde azoteux dans la stratosphère," Aeronomica Acta A91.
- Norton, R.B. and C.A. Barth (1970), "Theory of nitric oxide in the Earth's atmosphere," J. Geophys. Res. 75, 3903.
- Rapp, D., P. Englander-Golden, and D.D. Brighin (1965), "Cross-sections for dissociative ionization of molecules by electron impact," J. Chem. Phys. 42, 4081.
- Slanger, T.C., B.J. Wood, and G. Black (1971), "Temperature coefficients for N(²D) quenching by O₂ and N₂O," J. Geophys. Res. 76, 8430.

- Strobel, D.F. (1971a), "Diurnal variation of nitric oxide in the upper atmosphere," J. Geophys. Res. 76, 2441.
- Strobel, D.F. (1971b), "Odd nitrogen in the mesosphere," J. Geophys. Res. 76, 8384.
- Strobel, D.F. (1972), "Nitric oxide in the D-region," J. Geophys. Res. 77, 1337.
- Strobel, D.F., D.M. Hunten, and M.B. McElroy (1970), "Production and diffusion of nitric oxide," J. Geophys. Res. 75, 4307.
- Warneck, P. (1972), "Cosmic radiation as a source of odd nitrogen in the stratosphere," J. Geophys. Res. 77, 6589.
- Winters, H.F. (1966), "Ionic absorption and dissociation cross-section for nitrogen," J. Chem. Phys. 44, 1472.

CHEMICAL MODELING OF PERTURBATIONS CAUSED BY NO_x EMISSIONS

A.F. TUCK

British Meteorological Office Bracknell, Berkshire, England

ABSTRACT: A one-dimensional, time-dependent model has been developed for the purpose of investigating the chemical kinetics of the stratosphere in a manner as complete as current knowledge permits. The formulation of stratospheric transport processes is rudimentary, consisting as it does of vertical eddy diffusion, and this must be borne in mind in interpreting any results which are quoted.

As a predictive tool in its own severely limited context, the model shows a reduction which varies seasonally from 1.2% in late winter to 0.8% in late summer, caused by an annual injection of 9.5×10^{11} grams of NO_2 at 16-18 km.

INTRODUCTION

A time-dependent, one-dimensional model of stratospheric chemical kinetics has been developed to study the processes determining the stratosphere's natural composition and the changes which might be caused by large-scale injections of minor constituents from aircraft exhausts. The representation of the physicochemical processes is as complete as present knowledge permits; this is achieved at the expense of incorporating a rudimentary dynamical scheme, namely, vertical eddy diffusion.

The model is being developed not only as a test bed to improve both qualitative and numerical understanding of the chemical aspects of the overall problem, but also to provide tested, simplified chemical kinetics for use in two- and three-dimensional models. It will also provide a prediction in its own right of the change in total ozone column density caused by emission of NO₂, H₂O, CO₂, CO, and CH₄ from the engines of an SST fleet. This prediction must be viewed with the reserve appropriate to the model's minimal representation of atmospheric dynamics.

THE MODEL STRUCTURE

The chemical kinetics are listed in Table 1. Rate coefficients were selected where possible from the NBS Chemical Kinetic Data Survey tables (Garvin and Hampson, 1974). The temperature and pressure-column distributions were taken from US Standard Atmosphere publica-

tions (1962, 1966); the eddy-diffusion coefficients are listed in Table 2. The model has a vertical resolution of one kilometer, and extends from 10 to 50 km. The time t is incorporated in the variation of solar zenith angle ϕ with season and local hour angle. ϕ is expressed by

$$\cos \phi = \cos \Lambda \cos \delta \cos \theta + \sin \Lambda \sin \delta \quad (1)$$

where Λ = latitude (kept constant at 45°N in the experiment described here), δ = solar-declination angle, and θ = t/240°, where t is in seconds measured from noon of the vernal equinox.

Table 2. The Eddy-Diffusion Coefficients

10 ⁻⁴ K	Z	10 ⁻⁴ K	Z
(cm ² sec ⁻¹)	(km)	(cm ² sec ⁻¹)	(km)
2.87	48.5	0.367	28.5
2.33	47.5	0.372	27.5
1.91	46.5	0.382	26.5
1.58	45.5	0.397	25.5
1.33	44.5	0.417	24.5
1.13	43.5	0.443	23.5
0.965	42.5	0.476	22.5
0.837	41.5	0.517	21.5
0.734	40.5	0.568	20.5
0.652	39.5	0.631	19.5
0.585	38.5	0.708	18.5
0.530	37.5	0.805	17.5
0.487	36.5	0.925	16.5
0.452	35.5	1.07	15.5
0.424	34.5	1.26	14.5
0.402	33.5	1.50	13.5
0.386	32.5	1.80	12.5
0.375	31.5	2.19	11.5
0.368	30.5	2.69	10.5
0.365	29.5		

TUCK

Table 1. The Chemical-Kinetic Mechanism

$O_2 + h\nu \rightarrow O + O$	$OH + NO + M \rightarrow HNO_2 + M$
$O_3 + h\nu \rightarrow O + O_2$	$OH + NO_2 + M \rightarrow HNO_3 + M$
$O_3 + h\nu \rightarrow O + O_2(^1\Delta)$	$OH + O_3 \rightarrow HO_2 + O_2$
$O_3 + h\nu \to O(^1D) + O_2(^1\Delta)$	$HO_2 + O_3 \rightarrow OH + O_2 + O_2$
$NO + h\nu \rightarrow N + O$	$H + O_3 \rightarrow OH(\nu=1-9) + O_2$
$NO_2 + h\nu \rightarrow NO + O$	$O + OH \rightarrow O_2 + H$
$N_2O + h\nu \rightarrow N_2 + O(^1D)$	$O + HO_2 \rightarrow OH + O_2$
$NO_3 + h\nu \rightarrow NO + O_2$	$OH + OH \rightarrow O + H_2O$
$N_2O_5 + h\nu \rightarrow O + NO_2 + NO_2$	$OH + H_2 \rightarrow H \div H_2O$
$H_2O + h\nu \rightarrow H + OH$	$H + HO_2 \rightarrow OH + OH$
$HNO_2 + h\nu \rightarrow OH + NO$	$H + HO_2 \rightarrow H_2 + O_2$
$HNO_3 + h\nu \rightarrow OH + NO_2$	$H + OH \rightarrow O + H_2$
$HCHO + h\nu \rightarrow H_2 + C$	$O(^{1}D) + H_{2}O \rightarrow OH + OH$
$HCHO + h\nu \rightarrow H + HCO$	$O(^{1}D) + H_{2} \rightarrow H + OH$
$CO_2 + h\nu \rightarrow O + C$	$H + OH + M \rightarrow H_2O + M$
$H_2O_2 + h\nu \rightarrow OH + OH$	$OH + OH + M \rightarrow H_2O_2 + M$
$HO_2 + h\nu \rightarrow O + OH$	$H + O_2 + M \rightarrow HO_2 + M$
$CH_3O_2 + h\nu \rightarrow O + CH_3O$	$OH + H_2O_2 \rightarrow H_2O + HO_2$
$CH_3NO + h\nu \rightarrow CH_3 + NO$	$O + H_2O_2 \rightarrow OH + HO_2$
$CH_3ONO + h\nu \rightarrow CH_3O + NO$	$HO_2 + HO_2 \rightarrow O_2 + H_2O_2$
$O(^1D) + M \rightarrow O + M$	$OH + HNO_2 \rightarrow H_2O + NO_2$
$O_2(^1\Delta) + M \rightarrow O_2 + M$	$OH + HNO_3 \rightarrow H_2O + NO_3$
$O_2(^1\Sigma_g^+) + M \rightarrow O_2 + M$	$OH + CO \rightarrow CO_2 + H$
$OH(\nu=1-9) + M \rightarrow OH + M$	$H + NO_2 \rightarrow NO + OH$
$O + O_2 + M \rightarrow O_3 + M$	$N + OH \rightarrow NO + H$
$0 + 0_3 \rightarrow 0_2 + 0_2$	$NO + HO_2 \rightarrow OH + NO_2$
$O(^{1}D) + O_{3} \rightarrow O_{2} + O_{2}$	$N + O_3 \rightarrow NO + O_2$
$O(^{1}D) + O_{3} \rightarrow O + O + O_{2}$	$N + NO \rightarrow N_2 + O$
$O({}^{1}D) + O_{3} \rightarrow O + O_{2}({}^{1}\Sigma_{g}^{+})$	$N + O_2 \rightarrow NO + O$
$O(^{1}D) + O_{2} \rightarrow O + O_{2}(^{1}\Sigma_{g}^{+})$	$N + NO_2 \rightarrow N_2O + O$
$O_2(^1\Delta) + O_2(^1\Delta) \rightarrow O_2 + O_2(^1\Sigma_g^+)$	$N + NO_2 \rightarrow NO + NO$
$O_2(^1\Sigma_g^+) + O_3 \rightarrow O + O_2 + O_2$	$O(^{1}D) + CH_{4} \rightarrow OH + CH_{3}$
$O_2(^1\Delta) + O_3 \rightarrow O + O_2 + O_2$	$OH + CH_4 \rightarrow H_2O + CH_3$
$NO + O_3 \rightarrow NO_2 + O_2$	OH + HCHO \rightarrow H ₂ O + HCO
$O + NO_2 \rightarrow NO + O_2$	$HCO + O_2 \rightarrow HO_2 + CO$
$NO_2 + O_3 \rightarrow NO_3 \div O_2$	$CH_3 + O_2 + M \rightarrow CH_3O_2 + M$
$NO_2 + NO_3 + M \rightarrow N_2O_5 + M$	$CH_3 + NO + M \rightarrow CH_3NO + M$
$O + N_2O_5 \rightarrow NO_2 + NO_2 + O_2$	$CH_3O_2 + NO \rightarrow CH_3O + NO_2$
$NO + NO_3 \rightarrow NO_2 + NO_2$	$CH_3O_2 + CH_3O_2 \rightarrow CH_3O + CH_3O + O_2$
$O + NO + M \rightarrow NO_2 + M$	$CH_3O + NO \rightarrow CH_3ONO$
$O + NO_2 + M \rightarrow NO_3 + M$	$CH_3O + NO_2 \rightarrow CH_3ONO_2$
$O(^1D) + N_2O \rightarrow NO + NO$	$CH_3 + NO_2 \rightarrow CH_3NO_2$ $CH_3 + NO_2 \rightarrow CH_3NO_2$
$O(^{1}D) + N_{2}O \rightarrow N_{2} + O_{2}$	
	$CH_3O + O_2 \rightarrow HCHO + HO_2$

THE MODEL EQUATIONS

A chemical-kinetic scheme permits modeling of the temporal evolution of the composition of a reacting gas through the time derivatives of the number densities of the species involved.

A set of simultaneous equations of the form

$$\frac{dY(i)}{dt} = P(i) - Q(i) Y(i)$$
 (2)

is obtained, where Y(i) is the number density of the ith constituent, and P(i) and Q(i) are functions of the other Y's; P(i) is a source and Q(i) Y(i) a sink term. Integration of these equations forward in time yields the number densities Y(i) as functions of t.

The one-dimensional eddy-diffusion equation used was

$$\frac{\partial Y(i)}{\partial t} = \frac{\partial}{\partial Z} K_z \rho_z \frac{\partial}{\partial Z} \frac{Y(i)}{\rho_z}$$
 (3)

where Z is the altitude coordinate, ρ_Z is the air density, and K_Z is the vertical eddy-diffusion coefficient, specified as a function of the model altitude Z.

INTEGRATION OF THE MODEL EQUATIONS

Chemical-Kinetic Equations

The chemical-kinetic equations have widely different characteristic time constants; this poses severe problems if integration is to be performed conservatively, accurately, and with computational economy. Conservation of the total numbers of oxygen, nitrogen, hydrogen, and carbon atoms is essential, otherwise spurious sources and sinks of various species may be introduced. High accuracy (say to better than the 10-2 or 10-3 over the whole integration period) is not essential in view of the other uncertainties in the calculations, but computational economy is a *sine qua non* in view of the model complexity.

In principle, one should in this case solve the 34 equations arising from the reactions listed in Table 1 simultaneously, either by a multistep Gear method or by a fully implicit matrix method. These approaches were ruled out on the grounds of computational cost and of probable

mathematical and numerical difficulties associated with the necessary matrix inversions. In a model which correctly treats diurnal variations, the chemical scheme changes radically at dawn and dusk, and finding a matrix inversion which would be sufficiently flexible and efficient enough appeared difficult.

king the equations one at a time still offers a strictly conservative scheme - for example, by the use of an explicit Euler firstorder forward time step. However, the stability requirements for such an integration demand a time step of the order of microseconds for stratospheric chemical kinetics. This is computationally unacceptable; employing a stationarystate approximation for those species which have small characteristic times permits relaxation of this restraint, but at the expense of conservation. In addition, one must arrange for repeated testing in space and time to test the validity of a stationary-state approximation. This leads to difficulties if long integrations are performed, since one needs a "correct" solution against which to make the tests.

Equation (4), derived from an integration over the time step t with the assumption of constant P and O over this interval

$$Y_{n+1}(i) = Y_n(i)e^{-Q_n(i)\Delta t} + \frac{P(i)}{Q(i)}(1 - e^{-Q_n(i)\Delta t})$$
 (4)

was found to be unsuitable, since it leads to loss of conservation and introduces artificial sinks of, for example, odd nitrogen.

After considerable experimentation, a semiimplicit relation

$$Y_{n+1}(i) \approx \frac{Y_n(i) + P(i) \Delta t}{1 + Q(i)\Delta t}$$
 (5)

was employed. The subscript n refers to time level. This is in fact a non-conservative algorithm, but in operation steps were taken to improve its performance to an acceptable level. This was achieved by holding $Y_n(i)$ constant, and iterating the other Y(i)'s to recalculate P(i) and Q(i) and hence a new value $Y_{n+1}(i)$. After careful investigation of the chemical-kinetics scheme running without dynamics, it was decided that a time

step of 30 seconds and 4 iterations during daylight, and 60 seconds and 2 iterations at night, would suffice, with the modification that the time step would be 1 second for 10-minute periods after sunrise and sunset. This reduced spurious sources and sinks of odd nitrogen to levels which were small compared to the natural sources and sinks.

Photodissociation Coefficients

The rate at which photon-absorbing molecules dissociate is computed from the equation

$$J(Z) = \sum_{\lambda} Q(\lambda) \, \sigma(\lambda) \, L(Z,\lambda)$$

where Z = altitude, λ = wavelength of solar radiation, Q = quantum yield, σ = absorption cross-section, and

$$L(Z) = L_0 e - (\Sigma_i \sigma_i N_i(Z)M)$$

where L_0 is the solar flux at the top of the atmosphere, N_z is the column density, and the subscript i* refers to absorbing species. The magnification factor M allows for the variation in path length with solar angle ϕ , and is expressed by

$$M = \left(1 + \frac{Z}{R}\right) \left(1 + \frac{2Z}{R} - \cos^2\phi\right)^{-1/2}$$

where R = radius of Earth.

The solar fluxes are calculated and stored at each level, permitting the ready computation of solar-UV heating rates if desired.

Photodissociation coefficients are calculated every half-hour during daylight, except during the 30-minute periods which respectively precede and follow dusk and dawn, when the J's are computed more frequently.

Eddy-Diffusion Equations

The eddy-diffusion equations were integrated separately using a simple forward time

step of 3600 seconds, operating on the number densities generated during the last dynamical step by the chemical equations. Spatially the treatment was based on levels halfway between the chemical levels, using the relation

$$\frac{\partial Y_{\ell}}{\partial t} = \frac{1}{(\Delta Z)^2} \frac{K_{\ell+1/2} \rho_{\ell+1/2} Y_{\ell+1}}{\rho_{\ell+1}} - \frac{K_{\ell+1/2} \rho_{\ell+1/2} + K_{\ell-1/2} \rho_{\ell-1/2}}{\rho_{\ell}} Y_{\ell} + \frac{K_{\ell-1/2} \rho_{\ell-1/2} Y_{\ell-1}}{\rho_{\ell-1}} \tag{6}$$

where 1 is the space index. (The values for K are shown in Table 2.)

The boundary conditions employed to date involved assuming a photochemical stationary state at the top level (50 km); the chemical reactions but not the dynamic processes were permitted to change the composition at the bottom level (10 km).

The complete model, which is programmed in ASSEMBLER but with FORTRAN I/O, takes 112 seconds per day (averaged over a year) for its 40 levels, on an IBM 360/195 machine.

EXPERIMENTS

Starting Conditions

Currently, no set of measurements is available which enables one to choose stratospheric-constituent distributions close to those which the model generates without making large changes. This is probably caused by shortcomings in both the measurements and in the model; in any case, the model has to generate fields of the more reactive intermediate species, for which there are no measurements.

Initially, the different species were assigned the following volume mixing ratios, constant throughout the stratosphere, selected more or less according to available measurements of their mixing ratios:

N ₂	0.781		
02	0.209		
CO ₂	3 × 10 ⁻⁴		
H ₂ O	5 × 10 ⁻⁶		
N ₂ O	2.5×10^{-7}		
HNO ₃	3×10^{-9}		
NO	10-9		
NO ₂	3 X 10 ⁻⁹		
H ₂	5 × 10 ⁻⁷		
CO	4×10^{-8}		
CH ₄	1.5 × 10 ⁻⁶		

Ozone was assigned a profile synthesized from the data of Hering and Borden (1967) in the lower stratosphere, and from Krueger (1973) above 22 km. All other species were set to zero.

Tests of the Chemical Kinetics

An integration using the chemical kinetics only was performed with the above initial values, and was taken to 40 days of simulated time. During this period substantial changes took place in certain of the profiles, including the expected reduction of N_2O at higher altitudes, through reaction with $O(^1D)$. The distributions of the 34 species at the end of this 40-day run were then taken as the starting values for actual experiments.

An experiment in which the chemistry alone was operative was then run to 80 days, making 120 days in all for this version of the model. The profiles were beginning to show roughnesses, especially those of the species which were undergoing photodissociation; this experiment was then terminated since the results clearly indicated that some treatment of vertical transport should be included.

Tests of the Vertical-Transport Scheme

The one-dimensional eddy-diffusion formulation was then tested and used in two experiments in which the chemical kinetics were omitted; the same initial 40-day profiles were used. In the first experiment, which related to the natural conditions, the species were transported vertically in the expected manner, with a marked tendency for the transport to minimize the number-density gradients. This experiment

served as a control integration for a second experiment in which injections of NO_2 , H_2O , CO_2 , CO, and CH_4 were made. One-quarter of each injectant was inserted at the 16- and at the 18-km levels, and one-half at 17 km. The amounts injected are listed in Table 3; they correspond to an emission of 9.5×10^{11} grams of NO_2 annually in the stratosphere. The difference in the NO_2 profiles, for this pair of experiments which use dynamics only, is plotted as a function of time in Figure 1. These curves delineate the way in which the model transports the artificial injection in the vertical. Of particular import is the rate at which the artificial injectant is transported upwards from the flight

Table 3. Injectants and Injection Rates

Molecule	NO ₂	н ₂ о	со	CO ₂	CH ₄
Total injection rate (molec. cm ⁻³ sec ⁻¹)	768	172 800	267	91 200	77

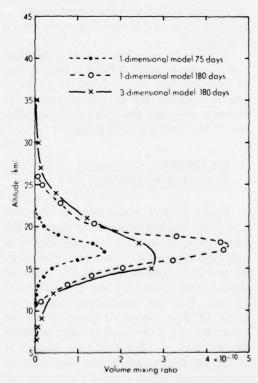


Figure 1. Vertical transport of NO₂ tracer in COMESA one- and three-dimensional models.

altitudes to the regions of net photochemical production in the upper levels of ozone layer.

A comparison of the results of the injection experiment with vertical transfer only with the vertical spread of the same quantity of an inert tracer injected in the three-dimensional general-circulation model of Newson (1974) reveals reasonable agreement, as is illustrated in Figure 1. This provides evidence for some degree of validity in the choice of vertical eddy-diffusion coefficients in the one-dimensional model.

Representation of the Natural and Perturbed Stratospheres

Two experiments have been mounted to date, with the separately tested component parts of the chemical-kinetic and dynamic schemes combined to form a single model in which Equations (2) and (3) were integrated forward in time.

The first experiment was an initial attempt with this model to compute vertical profiles of the constituents in a one-dimensional representation of the chemical composition of the natural stratosphere.

The second experiment included the injection of exhaust emissions listed in Table 3. Half of these amounts were injected at 17 km, a quarter at 18 km, and the remaining quarter at 16 km, at every time step. The total annual injection of NO_2 was 9.5×10^{11} grams.

The Simulation of the Natural Stratospheric Composition

Figure 2 gives model profiles from this experiment. Bearing in mind the effect of different averaging methods, compare Figure 2a with Figure 3, in which Ackerman (1974) shows the envelopes covering all currently published measurements of NO, NO₂, and HNO₃. One may conclude that the order-of-magnitude abundances of these species are consistent for the measurements and the model calculations (which are for noon at 1250 days (late August) at 45°N). The uncertainties in this comparison are very large, and do not constitute a rigorous test of the model.

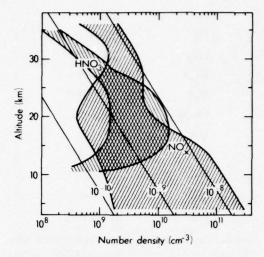
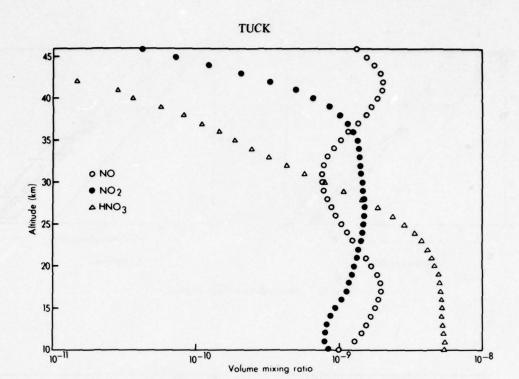


Figure 3. Envelopes including the data on NO_x (NO + NO₂) and HNO₃ (from Ackerman, 1974).

The profiles of the N₂O and CH₄ molecules, which are, with H₂O, the principal sources for the reactive species which characterize stratospheric chemical kinetics, are depicted in Figure 2b and in Figure 4 (measurements). There is clear qualitative agreement in the shape of the profiles of the N₂O and CH₄ mixing ratios, which decrease with increasing altitude because of reaction and photodissociation.

The model's water-vapor profile in Figure 2b may be compared with the global-average profile compiled by Harries (1975), shown in Figure 5a. The model profile shows a clear increase as altitude increases, caused by the methane oxidation; this effect is not unequivocally present in the average measured profile. However, the individual profile of Houghton (1975) obtained at 44°N 0°W on 9 July 1974 between 20 and 30 km (see Figure 5b) shows qualitative agreement with the model profile; significance should not be attached to the detailed numerical agreement, but rather to the fact that there is an increase at high altitude.

The model ozone profiles (Figure 6) show a wide seasonal variation; the agreement with observations is reasonably good, but there is a tendency for the maximum to be too high, possibly because the quantitative altitude dependence of penetration of solar UV, and hence of molecular-oxygen photodissociation, is





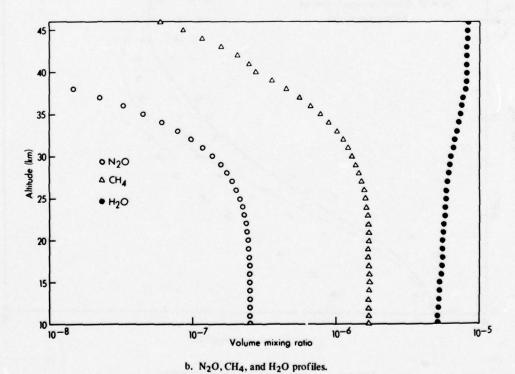


Figure 2. Model profiles for various species at 1250 days.

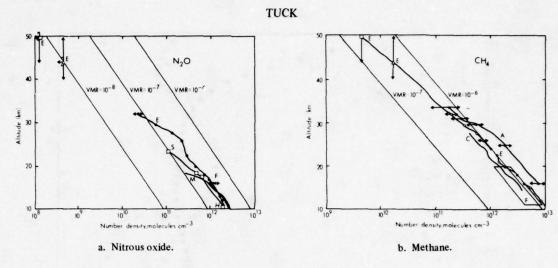


Figure 4. Stratospheric number densities.

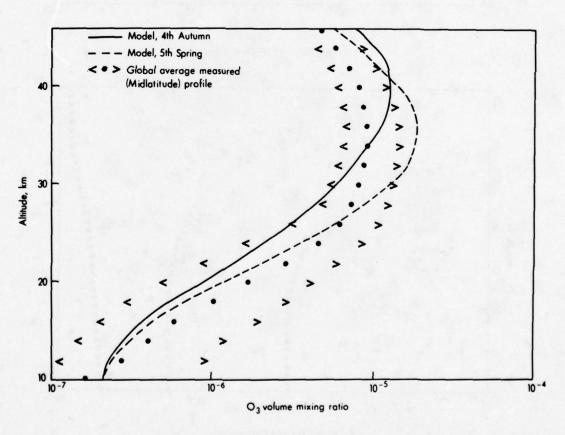
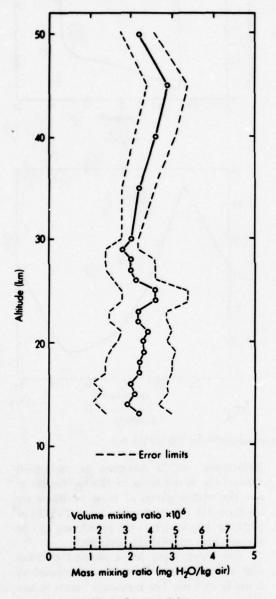


Figure 6. Ozone, model and measured profiles.

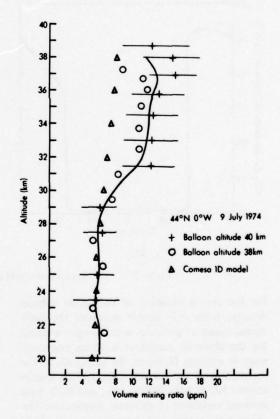
difficult to calculate. The production of nitrogen atoms by cosmic rays in the lower stratosphere and photodissociation of NO higher up is important because some of the reaction paths of the nitrogen and oxygen atoms with NO and NO₂ provide a sink for odd nitrogen; this is again difficult to compute accurately.



a. Mean of measured data.

Figure 7 shows the diurnal variation of NO, NO_2 , NO_3 , and N_2O_5 . The diurnal variation of NO_2 is consistent with observations which show less NO_2 after dawn than before dusk, but not with a maximum at noon. Since this run was started, new data on the photodissociation of NO_3 has appeared; it is not completely clear what effect this will have on the data, but a first inspection suggests that the changes will be minor. It should be noted that Figures 6 and 7 suggest that a computationally economic squarewave approximation to the diurnal variation will not be valid for N_2O_5 .

Figure 8 displays the model-computed temporal behavior of total column densities, during a span of 6 years. The first obvious point is the familiar one that a one-dimensional chemical-kinetic model cannot obtain the correct phase



 b. Comparison of model and measured profiles, at 44°N 0°W, 9 July 1974.

Figure 5. Stratospheric water-vapor profiles.

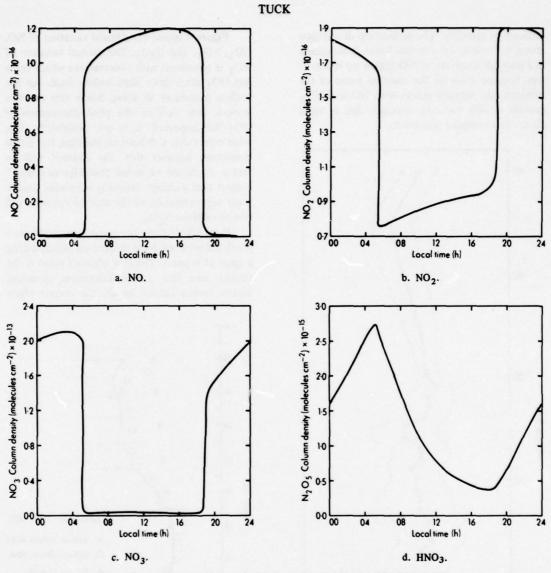


Figure 7. Diurnal variation of odd nitrogen species for day 336 (20 Feb 00).

for the annual variation in the ozone column density, because it cannot represent the meridional transport processes which largely account for the observed maximum in spring and minimum in autumn. However, the amplitude of the variation is of the correct scale. All the species shown, NO + NO₂, HNO₃, O₃, and H₂O, have seasonal variations of different amplitudes. The phase relationships are interesting, particularly those between the NO + NO₂, HNO₃, and O₃. The NO + NO₂ is at a maximum just before

midsummer, and a minimum in midwinter, whereas the reverse holds for HNO₃. Whether or not the relative phases of these variations are maintained in a two-dimensional model will be of particular importance in the partitioning of odd nitrogen between NO, NO₂ and HNO₃.

The water vapor has a seasonal variation with an amplitude of about 3% superimposed on a steady increase. The maximum occurs in late autumn/early winter, and the minimum in late spring/early summer. The long-term increase

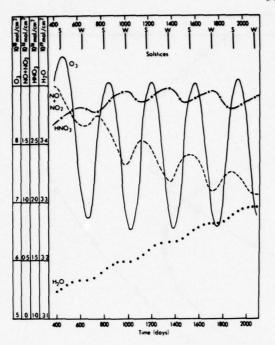


Figure 8. Column densities above 10 km as a function of time.

probably reflects a combination of the slow upward transport of methane to levels where it is oxidized, and the rate of flux of water vapor itself through the top boundary.

The figure also shows the long time required by stratospheric chemical-kinetic models to attain a seasonally varying stationary state, starting from data selected from experimental measurements.

The Concorde Injection Experiment

The results of the experiment in which the emissions were injected between 16 and 18 km are displayed in Figures 9 and 10.

Figure 9 shows, for late August, conditions of insolation, the ozone column, the percentage of reduction of the ozone column as a function of height, and the percentage of ozone below a given level. The curves illustrate the point that the reactions

$$NO + O_3 \rightarrow NO_2 + O_2$$

$$NO_2 + h\nu \rightarrow NO + O$$

$$NO_2 + \overline{O} \rightarrow NO + O_2$$

$$O_3 + h\nu \rightarrow O + O_2$$

require only visible light to be effective as a catalytic cycle, and thus reduce the vertical ozone column over a wide range of altitudes at and above the levels of the injection. The maximum ozone reduction occurs at the heights where most of it is located, and does not depend solely, as is often claimed, upon injected nitrogen oxides' reaching the regions where net ozone production occurs by the reactions

$$O_2 + h\nu \rightarrow O + O$$

 $O + O_2 + M \rightarrow O_3 + M$

This argument of course depends critically upon the rate of vertical transfer at these levels, and whether the transport of a species is determined by its gradient.

Figure 10 shows the seasonal variation of the ozone reduction, ranging from 0.8% in late summer to 1.2% in late winter.

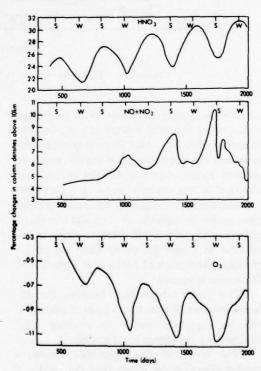


Figure 10. Percentage changes in HNO₃, NO + NO₂, and O₃ as a function of time.

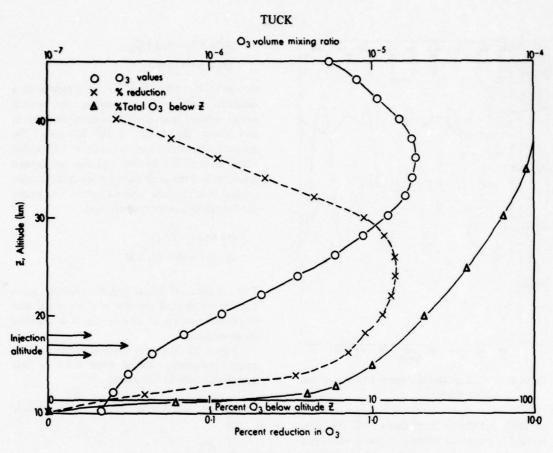


Figure 9. Effects on ozone at 1220 days with SST injection (late summer).

The maximum reduction as a percentage occurs when the total column is least, and the minimum when the total column is greatest. This is because the one-dimensional model cannot, as outlined earlier, correctly describe the seasonal variation in the ozone column at a particular latitude, because the meridional transport processes cannot be represented. It is also true that a given amount of injected nitrogen oxide is less effective as a sink for ozone when the photochemical production of ozone is at a maximum; this occurs in summer.

The phase relationships between the different species in Figure 10 are again of interest; it will be especially useful to examine their behavior in a two-dimensional model.

The result of this experiment shows a smaller effect on the ozone than the results of other workers. The fact that the model described

here has a completely time-dependent, diurnally varying sun probably accounts, at least in part, for the somewhat lower reduction in the total ozone column. The calculated total (NO + NO₂ + HNO₃) is rather higher than that of most other models in the stratosphere, giving an average column density above 12 km of about 2.5 × 1016 molecules cm-2. Such a column density corresponds to total NO + NO2 + HNO3 amounts comparable to these given by recent measurements (see Figure 3). However, the significant information is the partitioning between these three molecules between about 15 and 30 km; this shows a behavior depending upon altitude and time in a complicated manner, which of course cannot be represented in stationary state models. The greater the proportion of HNO3 during sunlit periods, the less will be the reduction in the ozone layer.

TUCK

FURTHER DEVELOPMENTS

A reduced chemical scheme, using approximately half the number of species and reactions in the chemical-kinetic mechanism described here, is being tested for use in a two-dimensional model. A rapid scheme, using 13 species and 18 reactions, is also undergoing trials, with a vertical resolution of 2 km and an altitude range of 0-48 km in its one-dimensional form.

Further experiments under way with the one-dimensional model include one using the solar absorption in the model with an atmospheric radiation scheme to compute heating rates and hence temperatures, for application to the reaction rates. Experiments are also planned to investigate the effects of nuclear-weapon testing on the ozone layer, and to test the sensitivity of the model to variation of certain key rate coefficients.

REFERENCES

Ackerman, M. (1974), "NO, NO₂, and HNO₃ Befow 35 km in the Atmosphere", prep. for Office of Naval Research and Climatic Impact Assessment Program under contract N00014-73-C-0076.

- Garvin, D. and R.F. Hampson, eds. (1974), "Chemical Kinetics Data Survey, VII: Tables of Rate and Photochemical Data for Modeling of the Stratosphere" (revised), National Bureau of Standards, NBSIR 74-430,
- Harries, J.E. (1975), private communication (U.K. National Physical Laboratory).
- Hering, W.S. and T.R. Borden, Jr. (1967), "Ozonesonde Observations over North America, Volume 4", Air Force Cambridge Research Labs (Bedford, MA), AFCRL-64-30 (IV).
- Houghton, J.T. (1975), private communication (Oxford University, Atmospheric Physics Dept.).
- Krueger, A. (1973), "The mean ozone distribution from several series of rocket soundings to 52 km at latitudes from 58°S to 64°N", Pure Appl. Geophys. 106-108, 1278-80.
- Newson, R.L. (1974), "An experiment with a tropospheric and stratospheric three-dimensional general-circulation model", in *Proceedings of the Third Conference on the Climatic Impact Assessment Program* (Cambridge, Mass.), U.S. Dept. of Transportation, DOT-TSC-OST-74-15, 461-474.
- U.S. Standard Atmosphere (1962), U.S. Government Printing Office; U.S. Standard Atmosphere Supplements (1966), prep. for ESSA, NASA, and USAF.

A TWO-DIMENSIONAL PHOTOCHEMICAL MODEL OF THE STRATOSPHERE, INCLUDING INITIAL RESULTS OF INERT-TRACER STUDIES

GEORGE F. WIDHOPF The Aerospace Corporation Los Angeles, California

ABSTRACT: A time-dependent meridional photochemical model of the lower regions of the atmosphere has been developed to calculate the distributions of trace chemical species in the atmosphere. Large-scale eddy transport and mean meridional advective transport are included in the model. The species considered are O(¹D), O(³P), O₂, O₃, N₂O, NO₂, NO, NO₂, HNO₃, N, H, OH, HO₂, H₂O₂, H₂O, and CH₄. Steady-state distributions of O₃, N₂O, NO₂, NO, and HNO₃, calculated in the entire meridional plane, where the season in the northern hemisphere is autumn, are in relatively good agreement with available atmospheric observations. Agreement between the calculated and observed meridional variations of the total ozone column is also good. Initial estimates of the potential change in the chemical structure of the stratosphere resulting from the deposition of pollutants in typical North Atlantic flight corridors by SST's are presented. Significant decreases in the total ozone column were found in both hemispheres for a deposition of 1.65(10)¹² grams of NO₂ per year in flight corridors centered at 50°N latitude and at altitudes of 20 and 17 km, respectively. The results of some initial inert-tracer studies performed to test the adequacy of the time-dependent transport data used in the model are in relatively good agreement with available distribution data of tungsten-185 and carbon-14.

INTRODUCTION

Since the stratosphere is a very stable region, characterized by a residence time on the order of a few years, the accumulation of pollutants deposited by a fleet of SST's flying in the stratosphere may, through photochemical reactions, alter the concentration of ozone in this region of the atmosphere. This, in turn, can change the amount of ultraviolet radiation reaching the surface of the earth, which may significantly affect our biosphere. Consequently, it is necessary to determine what effects these pollutants will have on the chemical state of the "natural" atmosphere.

In order to adequately assess the effect on the ozone layer of pollutants deposited in the lower regions of the atmosphere by future SST aircraft, a consistent numerical model of the existing "natural" atmosphere must initially be developed and verified. This paper describes a two-dimensional meridional photochemical model* of the lower regions of the atmosphere, which parameterizes the meridional thermo-

Any model which is ultimately to be used to model the effect of SST pollutants on the distribution of trace species in the atmosphere must initially be able to reproduce the "natural" atmosphere reasonably well, especially in the regions in which the effect of the pollutants is likely to be significant. It is evident that any such model of the atmosphere has to be verified by comparing the numerical results with available experimental data for the trace species of interest. These comparisons should include detailed examination of the meridional distribution of ozone, together with the meridional variation of the total ozone column. This is necessary because the total ozone column can be in reasonable agreement with the observed data even when the detailed meridional distributions are not.

Recently, more detailed information has become available which can be used to improve the transport data necessary for this type of model. Some preliminary calculations using these

dynamic structure and the advective and turbulent eddy transport, and solves for the transient and spatial distributions of the important trace species, using a comprehensive chemical system.

^{*}Brief discussions of other reported modeling efforts are included in Widhopf (1974) and Widhopf and Taylor (1974).

transport data together with simplified chemical systems (Chapman cycle including the NO, effect) were reported by Widhopf and Taylor (1974) from an initial study evaluating the adequacy of this type of model. The results presented in this paper are a continuation of this previous study, using a more complete O-H-N chemical system. Since the comparison of calculated distributions with observed distributions for trace species other than ozone is a more stringent test of the model, these types of comparisons are also discussed in this paper. The results of these specific calculations and the associated comparisons with observed data are discussed in the first part, and the model is briefly described. Some calculations of the perturbed atmosphere resulting from the deposition of pollutants from a hypothetical fleet of SST's are also presented. A description of some inert tracer studies which were performed to further evaluate the transport data used in the model are presented in the second part of this paper. Both of these studies are preludes to the running of a time-dependent calculation of the distribution of trace species in the atmosphere throughout the complete cycle of seasons.

GOVERNING EQUATIONS

The governing species-conservation equation is derived following the general procedure outlined by Reed and German (1965) for representing the turbulent transport flux due to large-scale eddies. In the meridional plane this equation, written in terms of the mass mixing ratio, Y_i, is of the form

$$\rho \frac{\partial Y_{i}}{\partial t} + \rho w \frac{\partial Y_{i}}{\partial z} + \frac{\rho v}{r} \frac{\partial Y_{i}}{\partial \phi}$$

$$= \frac{1}{r} \frac{\partial}{\partial \phi} \left\{ \rho k_{\phi z} \frac{\partial Y_{i}}{\partial z} \right\}$$

$$+ \frac{1}{r} \frac{\partial}{\partial \phi} \left\{ \frac{\rho}{r} k_{\phi \phi} \frac{\partial Y_{i}}{\partial \phi} \right\}$$

$$+ \frac{\partial}{\partial z} \left\{ \rho k_{zz} \frac{\partial Y_{i}}{\partial z} \right\}$$

$$+ \frac{\partial}{\partial z} \left\{ \frac{\rho}{r} k_{z\phi} \frac{\partial Y_{i}}{\partial \phi} \right\}$$

$$(1)$$

+
$$2 \frac{\rho}{r} \left\{ k_{zz} \frac{\partial Y_i}{\partial z} + k_{z\phi} \frac{\partial Y_i}{r \partial \phi} \right\}$$

 $\frac{\rho}{r} \tan \phi \left\{ k_{\phi z} \frac{\partial Y_i}{\partial z} + k_{\phi \phi} \frac{\partial Y_i}{r \partial \phi} \right\}$
+ $\omega_i + S_i$ (i = 1,2...NI)

where Y_i is the mass mixing ratio, ρ_i/ρ , of the ith chemical species; ρ is the local mean atmospheric density; t is the temporal variable; $r=z+R_e$, where R_e is the mean radius of the earth and z is the altitude measured from and normal to the earth's surface; ϕ is the latitude; ω_i is the photochemical rate of production/depletion of the ith species; and S_i is the local source/sink effect. The components of the tensor, $k_{\alpha\beta}$, represent the diffusion coefficients in the respective directions arising from large-scale eddy motions, while v and w are the components of the mean circulation in the meridional and vertical directions, respectively. This equation is solved for each of the trace species considered.

PART I: STRATOSPHERIC PHOTOCHEMICAL MODEL

Chemical Model

The chemical system which is considered in this investigation includes the following species: $O(^{1}D)$, $O(^{3}P)$, O_{2} , O_{3} , NO, $N_{2}O$, NO₂, OH, H₂O, HO₂, H₂O₂, HNO₃, N, H, N₂, and CH₄. The distributions of H2O and CH4 are fixed in time as interpreted from the studies of Mastenbrook (1971), Ashby et al. (1972) and Ehhalt and Heidt (1973). The specific reaction system and the associated reaction-rate coefficients used in this investigation are tabulated in Table 1. This O-H-N chemical system is essentially the one recommended by the CIAP chemical panel (Johnston, 1974), as outlined in the first and third volumes of the Climatic Impact Assessment Program monograph series (1975). The rates are those recommended in the Survey of Reaction Rate Data, edited by Garvin and Hampson (1974).

The local photodissociation rates are calculated using the solar-flux data compiled by Ackerman (1971). The absorption cross-sections for O_2 in the Schumann-Runge bands are taken

Table 1. Chemical Reactions and Rate Coefficients

1.	$O(^3P) + O_3 \rightarrow 2O_2$	1.9(10) ⁻¹¹ exp(-2300/T)
2.	$O_2 + h\nu \rightarrow 2O(^3P)$	J ₂
3.	$O_3 + h\nu \rightarrow O(^3P) + O_2$	J ₃
4.	$NO_2 + h\nu \rightarrow O(^3P) + NO$	J ₄
5.	$O(^{3}P) + O_2 + M \rightarrow O_3 + M$	$1.07(10)^{-34} \exp(510/T)$
6.	$O(^3P) + NO_2 \rightarrow O_2 + NO$	9.1(10) ⁻¹²
7.	$O_3 + NO \rightarrow O_2' + NO_2$	9(10) ⁻¹³ exp(-1200/T)
8.	$O_3 + NO_2 \rightarrow 2O_2 + NO$	1.23(10) ⁻¹³ exp(-2470/T)
9.	$O_3 + OH \rightarrow O_2 + HO_2$	$1.6(10)^{-12} \exp(-1000/T)$
10.	$NO + HO_2 \rightarrow OH + NO_2$	2.3(10) ⁻¹³
11.	$O(^3P) + H_2O \rightarrow OH + OH$	0.0
12.	$OH + NO_2 + M \rightarrow HNO_3 + M$	$8.5(10)^{-13} \exp(360/T) \div \{(M) + 1.5(10)^{18}\}$ *
13.	$HNO_3 + h\nu \rightarrow OH + NO_2$	J ₁₃
14.	$HO_2 + O_3 \rightarrow OH + O_2 + O_2$	$1(10)^{-13} \exp(-1250/T)$
15.	$HO_2 + O(^3P) \rightarrow OH + O_2$	1(10)-11
16.	$OH + HO_2 \rightarrow H_2O + O_2$	2(10)-10
17.	$OH + HNO_3 \rightarrow H_2O + NO_2 + O(^3P)$	1.3(10) ⁻¹³
18.	$H_2O_2 + h\nu \rightarrow OH + OH$	J ₁₈
19.	$H_2O_2 + OH \rightarrow H_2O + HO_2$	1.7(10) ⁻¹¹ exp(-910/T)
20.	$HO_2 + HO_2 \rightarrow H_2O_2 + O_2$	3(10) ⁻¹¹ exp(-500/T)
21.	$O_3 + h\nu \rightarrow O_2 + O(^5D)$	J ₂₁
22.	$O(^1D) + M \rightarrow M + O(^3P)$	5.9(10) ⁻¹¹
23.	$N_2O + h\nu \rightarrow N_2 + O(^1D)$	J ₂₃
24.	$N_2O + O(^1D) \rightarrow N_2 + O_2$	1.1(10) ⁻¹⁰
25.	$N_2O + O(^1D) \rightarrow NO + NO$	1.1(10)-10
26.	$NO + h\nu \rightarrow N + O(^{3}P)$	J ₂₆
27.	$N + O_2 \rightarrow NO + O(^3P)$	$1.1(10)^{-14}$ T exp(-3150/T)
28.	$N + NO \rightarrow N_2 + O(^3P)$	2.7(10)-11
29.	$N + NO_2 \rightarrow NO + NO$	6(10) ⁻¹²
30.	$N_2 + O(^1D) + M \rightarrow N_2O + M$	2.8(10)-36
31.	$NO_2 + N \rightarrow N_2O + O(^3P)$	9(10) ⁻¹²
32.	$O(^1D) + H_2O \rightarrow OH + OH$	3.5(10)-10
33.	$O(^{1}D) + CH_{4} \rightarrow OH + CH_{3}$	4.0(10)-10
34.	$OH + O(^3P) \rightarrow O_2 + H$	4.2(10)-11
35.	$H + O_2 + M \rightarrow HO_2 + M$	2.08(10) ⁻³² exp(290/T)
36.	$H + O_3 \rightarrow OH + O_2$	2.6(10) ⁻¹¹
37.	$NO + O(^3P) + M \rightarrow NO_2 + M$	3.96(10) ⁻³³ exp(940/T)
38.	$OH + OH \rightarrow H_2O + O(^3P)$	1(10) ⁻¹¹ exp(-550/T)
39.	$N + O_3 \rightarrow NO + O_2$	5.7(10) ⁻¹³

^{*}Fit of Tsang's data, Prinn et al. (1974)

from the tabulated values of Hudson and Mahle (1972), while the cross-sections for the Herzberg continuum are obtained from data compiled by Ackerman (1971). The quantum yields in the wavelength regime near 310 nm were obtained from the data of Lin and DeMore (1973).

The cross-sections for O₃ in the Hartley, Huggins, and Chappuis bands are from the data compiled by Ackerman (1971), while the photodissociation cross-sections for NO2 were taken from Johnston et al. (1973). The quantum yields for the photodissociation of NO2 were obtained from Garvin and Hampson (1973). The photodissociation cross-sections and quantum yields for HNO3 are those reported by Johnston and Graham (1972). The corresponding data for H₂O₂ were obtained from the work of Schurgers and Welge (1968) and Urey et al. (1929), whereas the data for NO were obtained from Strobel (1971). The N₂O photodissociation cross-sections were interpreted from the measurements of Romand and Mayence (1949).

Using these sets of data, the photodissociation rates are calculated throughout the computational field at every time step in order to ensure proper coupling of the photochemistry and the dynamics.

Boundary Conditions

The computational domain considered in this particular aspect of the investigation extends from the North to the South Pole, with a ten-degree meridional resolution, and from 10 km to 50 km, with a vertical resolution of $\Delta z = 2$ up to 16 km, $\Delta z = 1$ from 16 to 35 km, and $\Delta z = 2.5$ from 35 km to the upper boundary. At the polar regions, a zero latitudinal flux is assumed.

A fixed ozone concentration was imposed at the lower boundary with values obtained from the meridional distributions compiled by Dütsch (1971) and Hering and Borden (1964a,b, 1965, 1967), as summarized in the data compilation of Wu (1973). The concentration of N₂O at the lower boundary was prescribed as an average value interpreted from the tropospheric measurements of Schütz et al. (1970) and Goldman et al. (1973), while the mass mixing ratio of HNO₃ at this boundary was interpreted from the measurements of Lazrus and Gandrud (1974). NO and NO₂ mass mixing ratios were specified at the

lower boundary as interpreted from one-dimensional-model results, while the species O(³P), O(¹D), OH, HO₂ H₂O₂, N, and H were taken to be in photochemical equilibrium at the lower boundary.

 $O(^{3}P)$, $O(^{1}D)$, O_{3} , OH, HO_{2} , $H_{2}O_{2}$, N, and H were assumed to be in photochemical equilibrium at the upper boundary, while the mass mixing ratios of NO2, N2O, and HNO3 were analytically continued to the upper boundary by a second-order extrapolation in space and time described in Widhopf (1974) and Widhopf and Taylor (1974). This extrapolation allows the use of centered spatial differencing at this boundary while also eliminating the necessity for specifying a boundary condition for these species at this location. It is an accurate and stable method of evaluating conditions at computational boundaries (Victoria and Widhopf, 1972) when the physical mechanisms interior to the computational domain govern the boundary value. This is the case for N2O, NO2, and HNO3 which are being transported up into the higher regions of the stratosphere.

Transport Data

As stated in the Introduction, the meridional distributions of temperature, density, mean meridional circulation, and the components of the turbulent-diffusivity tensor are specified functions of time and space. Details about the structure of the stratosphere are difficult to obtain, due to the scarcity of experimental data. The data that are available do not completely encompass the entire region of the atmosphere which is of interest, and knowledge of the large-scale temporal variations is also incomplete. Thus, the accuracy of the parameterization is directly dependent upon the availability and reliability of observational data. The data used in this study are believed to be both the most recent and the most reliable presently available.

The meridional distributions of both the mean density and temperature were specified using the data obtained from ten years of observations which were analyzed and compiled by Louis (1973). These averaged data are specified from the surface to 68 kilometers for the entire meridional plane for each of the four yearly seasons.

Luther (1973a) has recently analyzed the heat-transfer, temperature, and wind-variance

data of Oort and Rasmusson (1971), using the procedure outlined by Reed and German (1965) for defining the components of the anisotropic turbulent-eddy-diffusivity tensor. The three components, $k_{\phi\phi}$, $k_{\phi z}$, and k_{zz} , are specified for the northern hemisphere from the surface to 60 kilometers. Values for the components of the diffusivity tensor in regions where observational data were not available were obtained by Luther (1973a,b) by extrapolation, using the results of Wofsy and McElroy (1973) and Newell et al. (1966). These coefficients are specified for each month, as well as seasonally, and were used to parameterize the components of the turbulentdiffusivity tensor. The values for the southern hemisphere were obtained by using the northernhemisphere values of six months later.

The mean meridional circulation was obtained from the work of Louis et al. (1974), who calculated the circulation patterns by solving the continuity and energy equations using compiled observations of the local meridional temperature distributions and heat-transfer rates. These are the same data sources used to define the thermal structure of the atmosphere, as previously discussed. The circulation patterns are specified for the entire meridional plane for each season from the surface to 50 kilometers. In order to ensure that total mass conservation would be satisfied, the vertical wind component obtained by Louis was used as specified and the meridional component calculated from the global continuity equation. Small differences (a few percent except near the poles) were noted between the respective values obtained for the meridional component; they result mainly from the different numerical methods used in each solution.

Numerical Scheme

An accurate (second-order in space and time) time-dependent numerical finite-difference scheme developed by Widhopf and Victoria (1973), which efficiently overcomes the "stiff" nature of the chemical system, is used to solve the governing individual-species conservation equations. Details of the scheme as applied to this problem are discussed in Widhopf (1974) and Widhopf and Taylor (1974).

Discussion of Results

Computations of the distributions of atmospheric trace species were carried out for the entire meridional plane during northern-

hemisphere autumn. The local photodissociation rates were computed by using an average local daylight zenith angle and weighting this resultant local rate with respect to the local daylight ratio. The calculations were relaxed in time until a steady-state distribution was obtained. It must be remembered that in the troposphere the time scale for changes in the background hydrodynamic structure of the atmosphere is much shorter than the local chemical relaxation time, so a steady-state assumption is not a good approximation in this region. Therefore, the lower boundary for these particular computations was selected to be above the surface, but away from the region of primary interest.* No modifications were made to the parameterized data as they were prescribed by the respective data sources except, as noted, to assure overall mass conservation.

The meridional distribution of the total ozone column in Dobson units (10⁻³ cm, stp) is presented in Figure 1 for the fall season in the northern hemisphere (October). Here the computation is compared to the data of Sticksel (1970) (southern hemisphere) and London (1963) (northern hemisphere) which are averaged for the fall season. Additional data of Gebhart et al. (1970), which represent average values for the month of October for the entire meridional plane, are included in the figure for comparison.

^{*}A calculation was performed subsequent to the CIAP 4 conference for this same case but with the lower boundary at the surface. A comparison of the results of the two methods for the natural atmosphere shows a maximum difference of 10% in the species concentrations above 18 km, and in most cases much less.



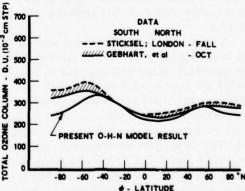


Figure 1. Comparison of the calculated and observed latitudinal variations of the total ozone column.

Since the data represent the entire ozone column, whereas the computations were carried out for the altitude regime of 10 to 50 km, inclusive, the ozone column reported by Gebhart et al. (1970) for the 0-15 km altitude regime was added to the computed results for the 15-50 km region. As can be seen in Figure 1, between 60°S and 90°N latitude the computed latitudinal variation of the total ozone column is in good agreement with observations, both in magnitude and in the shape of the distribution.

The calculated meridional variation of the ozone concentration is in relatively good agreement with compiled ozone observations. This is exemplified in Figure 2 which depicts, at selected latitudes, vertical ozone profiles compared with corresponding ozone measurements of Hering and Borden (1964a,b, 1965, 1967), as summarized in the data compilation of Wu (1973) the northern hemisphere and the data of Dütsch (1971) in the southern hemisphere. The individual rocket measurements of Krueger (1973) are depicted at the higher altitudes. Relatively good agreement with data is obtained at each latitude shown except that, in general, the calculated results tend to underpredict the magnitude of the ozone peak.*

Comparisons of the calculated distributions of N₂O, NO₂, NO, and HNO₃ with the limited number of available measurements of these species show relatively good agreement with the data.** Specifically, a comparison of the calculated distributions of N₂O at 30°N and 30°S latitude with various measurements is given in Figure 3. Here the 30°N profile should be compared with the measurements of Ehhalt et al.

ments. This will be discussed in detail in subsequent reports of the results of the complete annual-

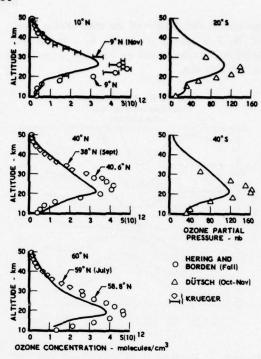


Figure 2. Comparison of the calculated and observed vertical profiles of ozone at selected latitudes.

(1974) which were made at 32°N latitude during September. The agreement is very good up to 30 km, whereas above 40 km the 30°S latitude distribution agrees much better with the data. However, it should be pointed out that the data above 40 km are represented by only two data points which have rather large error bands. The

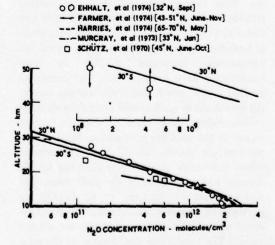


Figure 3. Comparison of the calculated N2O distributions with available measurements.

^{*}Subsequent calculations (surface to 50 km) performed after this meeting for these same conditions show that the manner of the evaluation of the photodissociation rate accounts for the difference between the computational results and the measurements. A complete 24-hour-average evaluation of the photodissociation rate, rather than the evaluation at an average daylight zenith angle used here, yields ozone profiles in excellent agreement with observations, filling in the profiles depicted in Figure 2. The corresponding changes for N₂O are insignificant and the resulting profiles for NO₂, NO and HNO₃ are in relatively good agreement with available measure-

solar-cycle calculation. **A much more detailed comparison of the calculated results and available measurements is found in Widhopf (1974). Calculated meridional distributions of these species are also included therein.

meridional distribution of the mass mixing ratio of N_2O is shown in Figure 4; a significant latitudinal variation can be observed, especially at high altitudes.

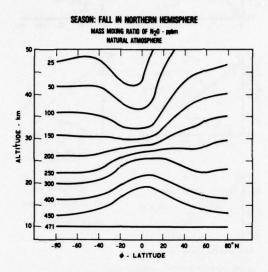


Figure 4. Meridional distribution of N₂O mass mixing ratio.

The calculated distributions of NO₂ at 30°N and 40°N latitude are in general agreement with the measurements of Ackerman and Muller (1972, 1973), Murcray et al. (1974), and Fontanella et al. (1974) made between 33°N and 51°N. The computed distribution of NO at 40°N latitude is in relatively good agreement with the data of Ackerman et al. (1973) above 25 km.

Figure 5 shows comparisons of profiles of the mass mixing ratio of HNO3 at various latitudes with the measurements of Lazrus and Gandrud (1974). These measurements were made in both hemispheres during the spring season; for comparison, calculated profiles in both hemispheres have been plotted. The computed profiles at 30° north and south latitude for the fall season are in good overall agreement with the corresponding measurements for the spring season in the opposite hemisphere. Similar comparisons are shown for 10° and 60° latitude, where reasonable agreement is observed for the altitude and magnitude of the peak value. The measurements of Murcray et al. (1973) are generally of greater magnitude than the measurements of Lazrus and Gandrud (1974) and are not shown. The meridional distribution of the mass mixing ratio of HNO3, shown in Figure 6, exhibits a significant meridional variation.

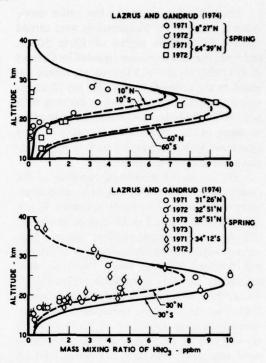


Figure 5. Comparison of the calculated HNO₃ distributions with the measurements of Lazrus and Gandrud (1974).

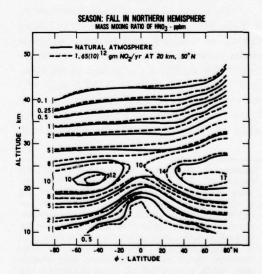


Figure 6. Meridional distribution of HNO₃ mass mixing ratio for the "natural" atmosphere and with 1.65(10)¹² grams of NO₂ injected per year.

The meridional variation of the mass mixing ratio of NO_x (NO + NO_2) is shown in Figure 7. High levels of NO_x are seen to be concentrated above the tropical regions. The corresponding

latitudinal variation of OH is very slight except in the region near the North Pole, which is in a polar nighttime condition where OH tends to disappear.

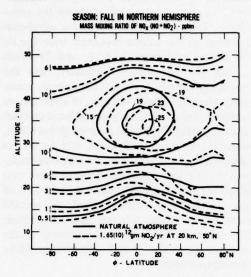


Figure 7. Meridional distribution of NO_x mass mixing ratio for the "natural" atmosphere and with 1.65(10)¹² grams of NO₂ injected per year.

On the basis of these results, the model appears to adequately predict the meridional distribution of ozone as well as the relative distributions of other important trace species. In order to make an initial assessment of the effect of the deposition of SST pollutants on the chemical structure of the atmosphere, a set of calculations, in which a hypothetical amount of pollutants was injected into the atmosphere, was performed for this same season. For these calculations, a North Atlantic flight corridor was assumed to be centered at 50°N latitude at an altitude of 20 km. NO2 was injected at this spatial location at the rates of 1.65(10)12* and 0.275(10)12 grams per year. Another calculation was performed for an injection rate of 1.65(10)¹² grams per year, where the corridor was assumed to be centered at an altitude of 17 km. These calculations were run until an equilibrium situation was attained. In this regard, the "natural" atmospheric calculation, as well as the perturbed cases, was run for a "real" time of 7.5 years.

The latitudinal variations of the subsequent ozone-column depletion for these "perturbed" atmospheres are shown in Figure 8.* Here, it should be emphasized that this is the ozone depletion calculated for the altitude regime of 10 to 50 km, and that the percentage of depletion is calculated on the basis of the corresponding calculated value for the "natural" atmospheric case for this altitude regime. This procedure does increase the effect of the NO_x in the polar regions, since the calculated ozone concentration for the "natural" atmosphere is low in this region. Also shown in this figure are the global average decreases of the ozone column, which are 14.7 and 3.2% for the two 20-kminjection cases, and 9.8% for the 17-km-injection simulation. These values are higher than corresponding values obtained from one-dimensional models (see Chang and Johnston (1974) and Chang (1974) for a compilation of these model results); this is probably mostly a result of the models' different stratospheric residence times. The corresponding global average increases in NO_x column for these cases are 82.2, 12.1 and 65.0%, respectively. When these values are compared with a correlation of various one-dimensional-model decreases in ozone column with the corresponding increases in NO_x column, compiled by Chang and Johnston, the values agree very well, falling on or near the center line of the correlation. This indicates that the various

*Value recommended by DOT on the basis of Johnston's (1971) estimates of the magnitude of future SST fleet NO_x injection rates.

SEASON: FALL IN NORTHERN HEMISPHERE (Oct)

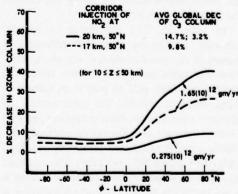


Figure 8. Latitudinal variation of the reduction of the ozone column (10 < z < 50 km) for various North Atlantic SST corridor calculations.

^{*}The meridional variations are very similar in shape to those calculated by Widhopf and Taylor (1974) for a simple Chapman-NO_x chemical system.

chemical models yield the same relative changes in global ozone concentration with respect to global changes in NO_X concentration. However, it should be noted that the ozone-column depletion for the 17-km-injection case is approximately one-third less than that obtained for the same injection rate at 20 km, being nearly invariant with latitude. A decrease of one-half is obtained from one-dimensional models, the difference probably being a result of the respective model stratospheric vertical-diffusion time scales.

It should be pointed out that in the onedimensional-model situation the injected pollutant is assumed to be uniformly distributed in a 1-km-thick global shell, whereas in this twodimensional-model simulation the global amount is injected in a specified flight corridor. Thus, even though the pollutants were injected in the mid-latitude North Atlantic flight corridor, the effect in the southern hemisphere is still significant. However, on the average, it is lower than the corresponding effect in the northern hemisphere by a factor of approximately 3.3.

The larger effect in the northern hemisphere is obviously due largely to the location of the flight corridor, and the larger percentage decrease in the northern polar region is due to blockage by these pollutants. (However, it is also a result of the fact that the ozone column for the unperturbed state is lower in this region.) Since most of the ozone is produced near the equatorial region and is then transported to the higher latitudes, the deposition of the SST pollutants in this North Atlantic corridor has effectively blocked this transport of ozone, resulting in a high percentage decrease of the ozone column near the northern polar region.

In order to find the effect of initially uniformly distributing the SST effluents, as assumed in the one-dimensional models, a calculation was performed for a uniform volumetric injection rate from pole to pole at an altitude of 20 km. Here, of course, the total amount of pollutants injected into the atmosphere per unit of time is the same as in the corresponding North-Atlantic-corridor simulation previously described (1.65(10)¹² grams NO₂ per year). The resultant latitudinal depletion of the total ozone column is shown in Figure 9. The latitudinal variation is quite different in this case, being similar in shape to the natural latitudinal variation in the ozone column. The global average is also less than for

the corresponding North-Atlantic-corridor case, yielding a 12.6% decrease of ozone for a corresponding increase in NO_x of 63.3%. Thus, the mode of injection affects not only the distribution, but the global-average effect on the atmosphere. This is a result of the strong meridional variation of the various important trace species (as shown in Figures 2, 4, 6, and 7) which control the atmospheric chemistry, and the meridional variation of the atmospheric transports which result in a variation of stratospheric residence times. Thus, a North-Atlantic-corridor calculation slightly overpredicts the global effect, since in reality not all traffic will be in this specified corridor. However, the maximum variation of the global average between these two simplified calculations is approximately 14% of the corresponding corridor result. At specific latitudes, the effect is much larger. Therefore, the effect of the meridional variation of the mode of deposition of SST effluents should be investigated further.

SEASON: FALL IN NORTHERN HEMISPHERE

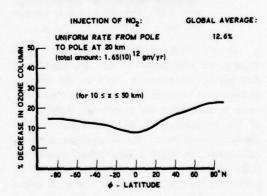


Figure 9. Latitudinal variation of the reduction of the ozone column (10 < z < 50 km) for uniform volumetric deposition of SST pollutants.

When the meridional variations in ozone reduction for the corridor simulations were normalized with respect to their corresponding global averages, the resulting distributions were essentially reduced to a single curve, demonstrating that the nonlinear chemical effect for different injection rates is not very significant so long as the mode of injection is similar.

It is interesting to examine the changes in the meridional distributions of various trace species due to the deposition of SST pollutants. Superimposed on the calculated "natural" atmospheric meridional distributions of HNO₃ and NO_x, shown in Figures 7 and 6 respectively, are the equilibrium distributions calculated for the case in which 1.65(10)¹² grams of NO₂ are injected in the North Atlantic flight corridor centered at 50°N and 20 km.

It can be seen that the level of HNO3 has risen considerably in the northern hemisphere in the region of the flight corridor, and its peak value has increased by approximately a factor of two. The same general distribution pattern of HNO3 is noted in the northern mid-altitude regime, except that the levels have increased considerably. Corresponding large changes are noted for NO_x (similar results are true for NO₂), the largest of which occurs in the general region of the corridor and toward the high northern latitudes. The peak values of both of these constituents have moved northward, away from the equator and toward the flight corridor, as a result of the deposition of NO2. Corresponding changes of OH and N2O were found to be insignificant. The major reduction in the ozone concentration occurs in the region near the point of injection; the reduction can be perceived up to an altitude of 45 km in the high northern latitudes.

Conclusions

A time-dependent meridional photochemical model of the atmosphere has been developed which considers a comprehensive chemical system. Steady-state calculations were carried out for the "natural" atmosphere during northern-hemisphere autumn. Comparisons of these results with available measurements of O3, N2O, NO2, NO, and HNO3 show good agreement with the data. The meridional variation of the total ozone column is also in good agreement with the observed distribution. These comparisons show that the model adequately predicts the "natural" chemical state of the stratosphere. Initial estimates of the effect of the pollutants deposited in the stratosphere by a hypothetical fleet of SST's flying in a North Atlantic corridor show it to be significant: a 14.7% average global ozone depletion for a deposition rate of 1.65(10)12 grams of NO2 per year in a corridor centered at 20 km and 50°N. Deposition at an

altitude of 17 km shows a similar effect, except that its magnitude is approximately two-thirds of that for 20-km injection. Even though the total quantity of pollutants was injected in a specified North Atlantic corridor, a measurable effect was calculated in the southern hemisphere. The latitudinal variation of the effect of these pollutants on the ozone column is significant, and the volume-averaged hemispheric ratio is approximately a factor of 3.3. The spatial location of the initial deposition of the pollutants has been shown to affect not only the latitudinal variation of the resultant ozone depletion, but the global average as well.

It should be emphasized that these calculations are initial estimates which will be refined when the complete time-dependent annual model is fully developed. The inert tracer studies discussed in Part II of this paper are an independent evaluation of the adequacy of the transport data to be used in the computation of the distribution of the trace species throughout the complete annual cycle of the seasons.

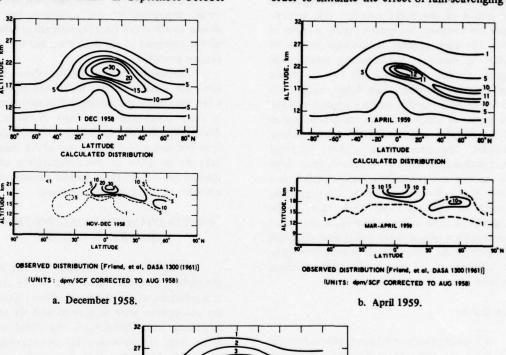
PART II: INITIAL RADIOACTIVE-TRACER DISPERSION RESULTS

In order to have an independent test of the atmospheric-transport data used in the model, computations of the dispersion of inert tracers in the atmosphere were performed and the results compared with observations. As stated above, these tests are necessary for determining the adequacy of the time-dependent transport data which are to be used in a complete yearly seasonal calculation of the distribution of trace species in the atmosphere. For these inert-tracer computations, the measured distribution of the radioactive nuclear debris, which resulted from past nuclear-weapon testing, was utilized as an initial condition. The time-dependent model described in Part I (without the chemistry) was utilized to compute the global atmospheric dispersion of these tracers, with the transport data fitted with a periodic function in order to allow a continuous variation throughout the year. The procedure used to specify the transport data ensured mass conservation at every computation point throughout the year. (Here it should be emphasized that these numerical experiments are independent tests of the transport data, since the transports were originally obtained from

atmospheric observations of temperature, heattransfer rates, and local wind variances.)

The initial numerical experiment was performed for radioactive tungsten-185 which was injected into the lower stratosphere at approximately 11°N latitude and 18 km altitude as a result of some nuclear testing (Hardtack Test Series) in the summer of 1958. The first detailed set of measurements of the distribution of tungsten-185 was made in September-October

1958, so these measurements were used as initial conditions for the present calculations. Comparisons of the computational results and the observations are shown in Figure 10, where the meridional contours of the tracer concentration are shown in units of disintegrations per minute/standard cubic foot, corrected for radioactive decay to 15 August 1958. In this calculation, a rainout lower-boundary condition was utilized in order to simulate the effect of rain-scavenging of



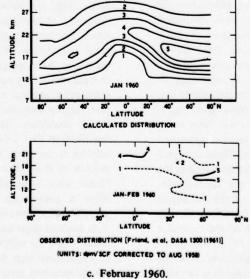


Figure 10. Comparison of the calculated and observed mean distributions of tungsten-185.

debris in the real atmosphere. A 0.5-km vertical and 5° latitudinal resolution was used in the computation.

As can be seen from these contours, the calculation of the relative dispersion of this inert tracer agrees reasonably well with the available data, especially in the decay of the equatorial maximum and the evolution of the mid-latitude secondary maximum. The relative time variation of the concentration of tungsten-185 is seen to be fairly well reproduced by the model. In all of these comparisons, it should be remembered that the accuracy of the data is not very good, due to the distribution, frequency, and methods of measurements, and that these distributions are an interpretation of the specific local measurements reported by Friend et al. (1961). However, the global trends should be relatively correct. A plot of the decay of the equatorial maximum with time is shown in Figure 11. Here the bimonthly average values of the measured concentrations are indicated, along with the number of the individual measurements comprising each data point. The calculated values are seen to be in good agreement with the data. Plotted as well are the results of Gudiksen et al. (1968), who also investigated the stratospheric dispersion of tungsten-185 using a parameterized two-dimensional transport model. Gudiksen et al. (1968) had to modify the transport coefficients of Reed and German (1965) in an arbitrary manner in order to make their calculation agree with this set of data. Their modification was successful in predicting the decay of the equatorial maximum; however, it was not at all successful in predicting the observed secondary maximum in the midnorthern latitudes. The present calculation, however, does predict the observed secondary maximum reasonably well. (It should be reiterated here that in the calculations reported herein no arbitrary modifications were made to the prescribed transport data as obtained from the sources described in Part I.)

As an additional comparison with observed data, the rise of the equatorial maximum with time is shown in Figure 12. The same type of bimonthly information is shown in this figure, where the present calculation shows an initial fast rise and then a leveling off at a constant altitude, as do the observations. The calculations of Gudiksen et al. (1968) indicate a constant rise with time. It should be noted that the highest

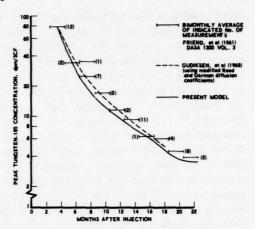


Figure 11. Comparison of the calculated and observed decreases of the equatorial peak concentration of tungsten-185 with time.

altitude at which measurements were made was approximately 21.5 km. This fact somewhat limits the interpretation of this aspect of the data; however, the present calculations do indicate that the height of maximum concentration levels off with time, a trend which is also indicated by the measurements.

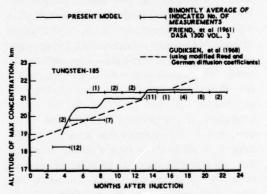


Figure 12. Comparison of the calculated and observed altitudes of the equatorial peak concentration.

These comparisons indicate that the transport data used in this study are indeed indicative of the actual average transport of the atmosphere. To examine this question further, an additional investigation was pursued with respect to the dispersion of radioactive carbon-14.

For these computations, the distributions interpreted by Johnston et al. of the carbon-14 data presented by Telegadas (1971) and Telegadas et al. (1972) were used for comparison and

initial conditions. The calculation was started at April 1963, using the data described in these documents to prescribe the distribution of carbon-14 in the entire meridional plane. The lower regions of the troposphere were taken to be fully mixed at latitudinal values indicated by the measurements. A constant mass mixing ratio of 1.35 (10)-16 was interpreted from the measurements near the surface, and was prescribed as the lower boundary condition at the surface. An upper boundary condition of zero concentration was assumed at 50 km. The integration was carried out for seven complete yearly seasonal cycles; some of the results at 30°N are shown in Figure 13. Here the results are compared with the profiles interpreted by Johnston et al., and also with the measurements made at this latitude for the time period of April 1963 to January 1966. Reasonable agreement between the calculated results and the measured distribution can be seen. Additional comparisons for January 1965 at a number of latitudes are shown in Figure 14. The initial condition for this particular calculation was the measured distribution in January 1964. As in the previous case, it should be pointed out that due to the distribution, frequency, and method of measurement, as well as the interpretation of distributions between the isolated measurements, the accuracy of the data is not expected to be particularly good. The calculation seems to overpredict the downward vertical transport below approximately 20 km, resulting in an underprediction of the peak values with time. However, due to the questionable accuracy of the data, it is difficult to fully evaluate how serious this situation may be. In order to approximate the error in the vertical transport, the data were assumed to be accurate and the vertical diffusion coefficient, kzz, was altered to bring the calculation into agreement with the data. Decreasing k, by approximately 35% at 20 km and below, and decreasing this alteration by successive 5% increments every kilometer above 20 km up to 27 km, brought the calculation into very good agreement with the data. This gives an indication of the approximate mean accuracy of the vertical transport. Thus, the estimates of the potential ozone reductions by SST NO, emissions presented in Part I are fairly reasonable on the whole. Much more comprehensive studies are examining the transport data, the

question of particulate versus gaseous debris dispersion, and the coordination of the calculations of the dispersion of tungsten-185 and carbon-14 with the calculation of the annual variation of the distribution of trace species in the atmosphere.

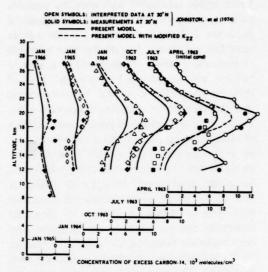


Figure 13. Comparison of the calculated and observed distributions of carbon-14 at 30°N.

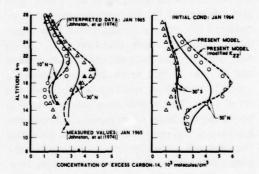


Figure 14. Comparison of the calculated and observed distributions of carbon-14 at various latitudes.

These results do indicate that the model transport data are reasonable representations of the mean atmospheric transport. Therefore, work is now in progress to compute the distribution of the trace species in the atmosphere continuously throughout the entire seasonal cycle, using the coupled photochemical model previously described in Part I. The results of all of these computations will be used to evaluate the currently prescribed transport, and if any modifications are deemed necessary after all of the results

have been examined, they will be implemented only in a manner consistent with the distributions of these inert tracers and of trace species in the atmosphere.

ACKNOWLEDGMENTS

The author would like to acknowledge the work of Mr. Raymond F. Kramer of The Aerospace Corporation, who constructed a very efficient computer code to carry out these numerical calculations. He is also indebted to Dr. William S. Helliwell, formerly of The Aerospace Corporation, who assisted in the initial construction of this computer code, and to Dr. Thomas D. Taylor of The Aerospace Corporation for his continued encouragement and constructive criticism.

This work has been supported in part by the Climatic Impact Assessment Program, U.S. Department of Transportation, and in part by The Aerospace Corporation Research Program.

REFERENCES

- Ackerman, M. (1971), "Ultraviolet solar radiation related to mesospheric processes," in Mesospheric Models and Related Experiments, ed. G. Fiocco, Springer-Verlag, New York, 149-159.
- Ackerman, M. and C. Muller (1972), "Stratospheric nitrogen dioxide from infrared spectra," Nature 240, 300-301.
- Ackerman, M., D. Frimout, C. Muller, D. Nevejans, J.C. Fontanella, A. Girard, and N. Louisnard (1973), "Stratospheric nitric oxide from infrared spectra," Nature 245, 205-206.
- Ackerman, M. and C. Muller (1973), "Stratospheric methane and nitrogen dioxide from infrared spectra," Pure and Appl. Geophys. 106-108, 1325-1335.
- Ashby, R.W., T. Shimazaki, and J.A. Weinman (1972), "Effect of water vapor and oxides of nitrogen on the composition of the stratosphere," in *Preprints* of the International Conference on Aerospace and Aeronautical Meteorology, Washington, D.C., pub. AMS, 417-421.
- Chang, J.S. (1974), "Simulations, perturbations and interpretations," in Proceedings of the Third Conference on the Climatic Impact Assessment Program (Cambridge, Mass.), U.S. Department of Transportation, DOT-TSC-OST-74-15, 330-341.

- Chang, J.S. and H.S. Johnston (1974), "The effect of NO_x effluents on ozone," in *Proceedings of the Third Conference on the Climatic Impact Assessment Program* (Cambridge, Mass.), U.S. Department of Transportation, DOT-TSC-OST-74-15, 323-329.
- CIAP (1975a), The Natural Stratosphere of 1974, ed. Reiter et al., Volume 1 of the CIAP monograph series, Dept. of Transportation, DOT-TST-75-51.
- CIAP (1975b), The Stratosphere Perturbed by Propulsion Effluents, ed. Robinson et al., Volume 3 of the CIAP monograph series, Dept. of Transportation, DOT-TST-75-53.
- Dütsch, H.C. (1971), "Photochemistry of atmospheric ozone," in Advances in Geophysics, Vol. 15, ed. H.E. Landsberg and J. Van Meighem, Academic Press, New York, 219-322.
- Ehhalt, D.H. and L.E. Heidt (1973), "Vertical profiles of molecular H₂ and CH₄ in the stratosphere," AIAA Paper No. 73-518, presented at AIAA/AMS International Conference on the Impact of Aerospace Operations in the High Atmosphere (Denver, Colorado).
- Ehhalt, D.H., L.E. Heidt, R.H. Lueb, and N. Roper (1974), "Vertical profiles of CH₄, H₂, CO, N₂O and CO₂ in the strotosphere," in *Proceedings of the Third Conference on the Climatic Impact Assessment Program* (Cambridge, Mass.), U.S. Department of Transportation, DOT-TSC-OST-74-15, 153-159.
- Farmer, C.B., O.F. Raper, R.A. Toth, and R.A. Schindler (1974), "Recent results of aircraft infrared observations of the stratosphere," in Proceed-dings of the Third Conference on the Climatic Impact Assessment Program (Cambridge, Mass.), U.S. Department of Transportation, DOT-TSC-OST-74-15, 234-245.
- Fontanella, J.C., A. Girard, L. Gramont, and N. Louisnard (1974), "Vertical distribution of NO, NO₂, and HNO₃ as derived from stratospheric absorption infrared spectra," in *Proceedings of the Third Conference on the Climatic Impact Assessment Program* (Cambridge, Mass.), U.S. Department of Transportation, DOT-TSC-OST-74-15, 217-232.
- Friend, J.P., H.W. Feely, P.W. Krey, J. Spar, and A. Walton (1961), "Discussion of HASP Results," Vol. 3, DASA 1300, Defense Atomic Support Agency, Washington, D.C.
- Garvin, D. and R.F. Hampson (1973), "Atmospherical modeling and the chemical data problem," AIAA Paper No. 73-500, given at AIAA/AMS International Conference on the Environmental Impact of Aerospace Operations in the High Atmosphere (Denver, Colorado).

- Garvin, D. and R.F. Hampson, eds. (1974), "Chemical Kinetics Data Survey VII. Tables of Rate and Photochemical Data for Modeling of the Stratosphere (revised)," NBSIR 74-430, National Bureau of Standards.
- Gebhart, R., R. Bojkov, and J. London (1970), "A comparison of observed and computer models," Beitrage zur Physik der Atmosphäre 32, 209-227.
- Goldman, A., D.G. Murcray, F.H. Murcray, and W.J. Williams (1973), "Balloon-borne infrared measurements of the vertical distribution of N₂O in the atmosphere," J. Opt. Soc. Am. 63 (7), 843-845.
- Gudiksen, P.H., A.W. Fairhall, and R.J. Reed (1968), "Roles of mean meridional circulation and eddy diffusion in the transport of trace substances in the lower stratosphere," J. Geophys. Res. 73(14), 4461-4473.
- Harries, J.E., J.R. Birch, J.W. Fleming, N.W.B. Stone, D.G. Moss, N.R.W. Swann, and G.F. Neill (1974), "Studies of stratospheric H₂O, O₃, HNO₃, N₂O and NO₂ from aircraft," in Proceedings of the Third Conference on the Climatic Impact Assessment Program (Cambridge, Mass.), U.S. Department of Transportation, DOT-TSC-OST-74-15, 197-212.
- Hering, W.S. (1964), "Ozonesonde Observations over North America, 1," AFCRL Research Report AFCRL-64-30(I).
- Hering, W.S. and T.R. Borden, Jr. (1964), "Ozonesonde Observations over North America, 2," Environmental Research Paper No. 38, AFCRL-64-30(II).
- Hering, W.S. and T.R. Borden, Jr. (1967) "Ozonesonde Observations over North America, 3," Environmental Research Paper No. 133, AFCRL-64-30(III).
- Hering, W.S. and T.R. Borden, Jr. (1967), "Ozonesonde Observations over North America, 4," Environmental Research Paper No. 279, AFCRL-64-30(IV).
- Hudson, R.D. and S.H. Mahle (1972), "Interpolation Constants for Calculation of Transmittance and Rate of Dissociation of Molecular Oxygen in the Mesosphere and Lower Thermosphere," National Aeronautics and Space Administration TM X-58084.
- Johnston, H.S. (1971), "Catalytic Reduction of Stratospheric Ozone by Nitrogen Oxides," Lawrence Radiation Laboratory Report UCRL-20568, Berkeley, California.

- Johnston, H.S. and R. Graham (1973), "Gas phase ultraviolet absorption spectrum of nitric acid vapor," J. Phys. Chem. 77, 62-63.
- Johnston, H.S., D. Kattenhorn, and G. Whitten (1975), "Use of Excess Carbon-14 Data to Calibrate Models of Stratospheric Ozone Depletion by Supersonic Transports," Lawrence Berkeley Laboratory, LBL-3548, Berkeley, California.
- Johnston, H.S., Shih-Ger Chang, and G. Whitten (1973),
 "Photolysis of Nitric Acid Vapor," Lawrence
 Berkeley Laboratory, LBL-1865, Berkeley,
 California.
- Krueger, A.J. (1973), "The mean ozone distribution from several series of rocket soundings," Pure Appl. Geophys. 106-108 (5-7), 1272-1280.
- Lazrus, A.L. and B.W. Gandrud (1974), "Distribution of stratospheric nitric acid vapor," J. Atmos. Sci. 31, 1102-1108.
- Lin, C.L. and W.B. DeMore (1973), "O(¹D) production in ozone photolysis near 3100A," J. Photochem. 2, 161-164.
- London J. (1963), "The distribution of total ozone in the northern hemisphere," Beitrage zur Physik der Atmosphäre, 26, 254-263.
- Louis, J.-F. (1973), National Center for Atmospheric Research, private communication.
- Louis, J.-F., J. London, and E. Danielsen (1974), "The interaction of radiation and the meridional circulation in the stratosphere," in Proceedings of the International Conference on Structure, Composition and General Circulation of the Upper and Lower Atmospheres and Possible Anthropogenic Perturbations (Melbourne), pub. IAMAP, 1205.
- Luther, F.M. (1973a), "Monthly Values of Eddy Diffusion Coefficients in the Lower Stratosphere," UCRL Report 74616; also AIAA Paper No. 73-498, presented at the AIAA/AMS International Conference on the Environmental Impact of Aerospace Operations in the High Atmosphere (Denver, Colorado).
- Luther, F.M. (1973b), Lawrence Livermore Laboratory, private communication.
- Mastenbrook, H.J. (1971), "The variability of water vapor in the stratosphere," J. Atmos. Sci. 28, 1495-1501.
- Murcray, D.G., A. Goldman, A. Csoeke-Poeckh, F.H. Murcray, W.J. Williams, and R.N. Stocker (1973), "Nitric acid distribution in the stratosphere," J. Geophys. Res. 78, 7033-7038.

- Murcray, D.G., A. Goldman, F.H. Murcray, W.J. Williams, J.N. Brooks, and D.B. Barker (1973), "Vertical distribution of minor atmospheric constituents as derived from airborne nieasurements of atmospheric emission and absorption spectra," in Proceedings of the Second Conference on the Climatic Impact Assessment Program (Cambridge, Mass.), U.S. Department of Transportation, DOTTSC-OST-73-4, 86-98.
- Newell, R.E., J.M. Wallace, and J.R. Mahoney (1966), "The general circulation of the atmosphere and its effects on the movement of trace substances, Part 2," Tellus 18, 363-380.
- Oort, A.H. and E.M. Rasmussen (1971), "Atmospheric Circulation Statistics," National Oceanic and Atmospheric Administration Prof. Paper 5.
- Prinn, R.G., F.N. Alyea, D.M. Cunnold, and A. Katz (1974), "The distributions of odd nitrogen and odd hydrogen in the natural and perturbed atmosphere," in Preprints from the Second International Conference on the Environmental Impact of Aerospace Operations in the High Atmosphere (San Diego, Calif.), 180-186.
- Reed, R.J. and K.E. German (1965), "A contribution to the problem of stratosphere diffusion by large-scale mixing," Mon. Wea. Rev. 93, 313-321.
- Romand, J. and J. Mayence (1949), "Spectre d'absorption de l'oxyde azoteux gazeux dans la région de Schumann," Comptes Rendus 228, 998-1000.
- Schurgers, M. and K.H. Welge (1968), "Absorption Koeffizient von H₂O₂ and N₂H₄ Zwischen 1200 und 2000 A," Z. Naturforsch 23A, 1508-1510.
- Schütz, K., C. Junge, R. Beck, and B. Albrecht (1970), "Studies of atmospheric N₂O," J. Geophys. Res. 75, 2230-2246.
- Sticksel, P.R. (1970), "The annual variation of total ozone in the southern hemisphere," Mon. Wea. Rev. 98 (10), 787-788.
- Strobel, D.F. (1971), "Odd nitrogen in the mesosphere," J. Geophys. Res. 76 (34), 8384-8393.
- Telegadas, K. (1971), "The Seasonal Stratospheric Distribution and Inventories of Excess Carbon-14

- from March 1955 to July 1969," in Health and Safety Laboratory Report 243, U.S. Atomic Energy Commission, 3-86.
- Telegadas, K., J. Gray, Jr., R.E. Sowl, and T.E. Ashenfelter (1972), "Carbon-14 Measurements in the Stratosphere from a Balloon-Borne Molecular Sieve Sampler," in Health and Safety Laboratory Report 246, U.S. Atomic Energy Commission, 69-106.
- Urey, H.C., L.H. Dawsey, and F.O. Rice (1929), "The absorption spectrum and decomposition of hydrogen peroxide by light," J. Amer. Chem. Soc. 51, 1371-1383.
- Victoria, K.J. and G.F. Widhopf (1972), "Numerical solution of the unsteady Navier-Stokes equations in curvilinear coordinates: The hypersonic blunt body merged layer problem," presented at the Third International Conference on Numerical Methods in Fluid Mechanics, University of Paris-Orsay, published in Lecture Notes in Physics, No. 19, Vol. II, Springer-Verlag, Berlin.
- Widhopf, G.F. and K.J. Victoria (1973), "On the solution of the unsteady Navier-Stokes equations including multicomponent finite rate chemistry," in Computers and Fluids, Vol. 1, 159-184.
- Widhopf, G.F. (1974), "Meridional distributions of trace species in the stratosphere and the effect of SST pollutants," presented at the American Geophysical Union Fall Annual Meeting, San Francisco, California, 12-17 December 1974.
- Widhopf, G.F. and T.D. Taylor (1974), "Numerical experiments on stratospheric meridional ozone distributions using a parameterized two-dimensional model," in *Proceedings of the Third Conference on the Climatic Impact Assessment Program* (Cambridge, Mass.), Dept. of Transportation, DOT-TSC-OST-74-15, 376-389.
- Wofsy, S.C. and M.B. McElroy (1973), "On vertical mixing in the upper stratosphere and lower mesosphere," J. Geophys. Res. 78, 2619-2624.
- Wu, Mao-Fou (1973), "Observations and Analysis of Trace Constituents in the Stratosphere," Environmental Research and Technology, Inc., Annual Report, Contract DOT-OS-20217.

EDDY DIFFUSIVITY PROFILES

R.C. WHITTEN AND W.J. BORUCKI NASA Ames Research Center Moffett Field, California

R.P. TURCO
R and D Associates
Santa Monica, California

The Report of Findings of the Climatic Impact Assessment Program (Grobecker et al., 1974, Figure 14) and the Proceedings of the Third Conference on the Climatic Impact Assessment Program (Chang and Johnston, 1975, Figure 1; Chang, 1974, Figure 5) reported values of ozone depletion attributed to various investigators, including the authors of this paper. Points designated "7" in the first two figures and designated by a solid triangle in the third represented ozone depletion values supposedly characteristic of our models (e.g., Whitten et al., 1974).

In fact, these points do not represent our results. The results of our calculations are higher than those shown and actually lie just below the values calculated by Chang (1974) with his own model and diffusivity profile. In particular, we calculate a 4% ozone reduction for a global NO_x emission rate of 1.5 NO^{12} gm/yr injected at 20 km, instead of the 2.5% reduction attributed to us in Figure 5 of Chang (1974). Similarly, the points shown in Figure 14 of Grobecker et al. (1974) attributed to us are also too low. The reason for this discrepancy is believed to be the use by Chang (1974) and Chang and Johnston (1974) of an eddydiffusion profile mentioned in some of our recent papers (Whitten and Turco, 1974a, b, and Whitten et al., 1974), but not actually used by us to calculate ozone depletions. The eddy profile that we used in our computations is shown in our Figure 1 as profile B. Chang (1974) assumed that we had used profile A. This mistake led to the anomalously low values of residence time and ozone depletion attributed to us. Our results are actually close to Chang's (1974) results. We should also like to note that if we use the Wofsy-McElroy (1973) eddy-diffusivity profile, we obtain results consistent with Chang's computations with the Wofsy-McElroy profile.

REFERENCES

Brasseur, G. and M. Nicolet (1973), "Chemospheric processes of nitric oxide in the mesosphere and stratosphere," Planet. Space Sci. 21, 939-61.

Chang, J.S. (1974), "Simulations, perturbations, and interpretations," in Proceedings of the Third Conference on the Climatic Impact Assessment Program (Cambridge, Mass.), U.S. Department of Transportation, DOT-TSC-OST-74-15, 330-34.

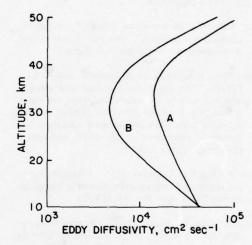


Figure 1. Eddy diffusivity profiles. A – Whitten and Turco (1974a,b), high. The upper portion of this profile was suggested by Zimmerman (1974). It was extended down into the stratosphere by following the general shape of profile B and joining it to the tropospheric value of 4 × 10⁴ cm sec⁻¹ at 10 km altitude. B – Whitten and Turco (1974a,b), low. This profile was suggested by Hays and Olivero (1970), and is bracketed by those suggested by Brasseur and Nicolet (1973).

Chang, J.S. and H.S. Johnston (1974), "The effect of NO_x effluents on ozone," in *Proceedings of the* Third Conference on the Climatic Impact Assessment Program (Cambridge, Mass.), U.S. Department of Transportation, DOT-TSC-OST-74-15, 323-29.

Grobecker, A.J., S.C. Coroniti, and R.H. Cannon, Jr. (1975), Report of Findings: The Effects of Stratospheric Pollution by Aircraft, U.S. Department of Transportation, DOT-TST-75-50.

Hays, P.B. and J.J. Olivero (1970), "Carbon dioxide and monoxide above the troposphere," Planet. Space Sci. 18, 1729-34.

WHITTEN, BORUCKI AND TURCO

Whitten, R.C., and R.P. Turco (1974a), "The effect of SST emissions on the earth's ozone layer," in Proceedings of the International Conference on Structure, Composition and General Circulation of the Upper and Lower Atmospheres and Possible Anthropogenic Perturbations (Melbourne), pub. IAMAP, 971-83.

Whitten, R.C., and R.P. Turco (1974b), "Perturbations of the stratosphere and mesosphere by aerospace vehicles," AIAA J. 12, 1110-17. Whitten, R.C., W.J. Borucki, and R.P. Turco (1974), "One-dimensional model studies of ozone depletion," in *Proceedings of the Third Conference on* the Climatic Impact Assessment Program (Cambridge, Mass.), U.S. Department of Transportation, DOT-TSC-OST-74-15, 342-58.

Wofsy, S.C. and M.B. McElroy (1973), "On the vertical mixing in the upper stratosphere and lower mesosphere," J. Geophys. Res. 78, 2619-24.

Zimmerman, S.P. (1974), AFCRL, private communication.

THEORY OF STRATOSPHERIC CHEMISTRY

DISCUSSION

(UNIDENTIFIED): How do you make sure that all chlorofluorocarbon sinks have been accounted for?

ROWLAND: You can look for overt sinks, like reactions of hydroxyl radicals, effects in biological systems, dissolving in the ocean, et cetera; all of these seem to be negligible. You can look for undetected sinks by the rate of disappearance of atmospheric fluorocarbons. If you compare Ray McCarthy's best estimates of how much Freon-11 has been produced with Lovelock's and Wilkniss's measurements of how much is in the atmosphere, within the accuracy of the measurement, you find that all the Freon-11 that has been produced is still in the atmosphere. There has been a doubling time of about six years in the production of Freon-11; half of it has been produced in the last six years, and threequarters of it in the last twelve years. What kind of lower limit does that put on the lifetime of Freon-11? Stretching the errors as far as I can I get 20 years as the minimum lifetime, but it is more likely at least 30 years. Almost everything reacts faster with Freon-11 than with Freon-12, so Freon-12 must have an even longer lifetime. In sum, there is no evidence, overt or indirect, that Freon-11 and Freon-12 are going away.

(UNIDENTIFIED): Bob Watson has measured the reaction rate of hydroxyl with methyl chloride, and he has calculated an approximate lifetime for it of less than a year.

ROWLAND: Lovelock measured methylchloroform (1,1,1-trichloroethane) concentrations in Western Ireland and Capetown — as a matter of fact, the "Capetown Station" is Jim Lovelock sitting on a cliff. You can compare the relative amounts of methylchloroform in the northern and southern hemispheres. At the same time he measured Freon-11, and you can use that to calibrate the interhemispheric mixing. If you do, you get a lifetime in the atmosphere for methylchloroform of about two years. The same calculation for trichloroethylene gives you a lifetime of a few months. I think

this means that almost all carbon-hydrogen compounds have lifetimes of, at the most, several years; those molecules that have carbon-carbon double bonds have lifetimes of less than a year.

(UNIDENTIFIED): Has anyone considered attack by electrons as a tropospheric sink for fluorocarbons?

ROWLAND: Lovelock was able to detect such small amounts of Freon-11 just because it has a very high electron-attachment cross-section. (He uses an electron-capture detector.) For molecules which have about the same electron-attachment cross-section as Freon-11, you know that their lifetime with respect to that process is at least 20, 25, or 30 years. Carbon tetrachloride has an even higher electron-attachment cross-section, but is still very long-lived. So, although the electron-attack sink is a good hypothesis, the persistence of CCl₄ probably proves that there is less than one electron per cubic centimeter in the troposphere.

CRUTZEN: I would like to show you the results of some calculations which Ivar Isaksen, George Reid, and I have performed, estimating the production of nitrogen oxides during certain solar proton events. [Here Dr. Crutzen gave a brief summary of "Solar Proton Events: Stratospheric Sources of Nitric Oxide", by Crutzen, Isaksen, and Reid, which subsequently appeared in Science, Vol. 189, pp. 457-459 (1975). He emphasized the importance of comparing nitrogen oxide production by such events with ozone observation records.]

UNIDENTIFIED: I would like to know how significant the cosmic-ray sources of odd nitrogen in the stratosphere are.

HARD: Ruderman and Chamberlain have offered a causal mechanism to explain the observed correlation of total ozone at high-latitude stations with the solar cycle. The solar wind modulates cosmic-ray penetration into the atmosphere at high latitudes, and the resulting modulation in the production of nitric oxide in the polar stratosphere may account for a small periodic variation in ozone. I don't know the magnitude of their

THEORY OF STRATOSPHERIC CHEMISTRY

estimate. Dr. Nicolet's paper today was the first attempt to provide an essential link in this causal mechanism. Ruderman and Chamberlain have also suggested that this natural experiment might calibrate the response of the stratosphere to artificial injections of nitrogen oxides.

SCHAINKER: Two comments. First, agreement of some of these 1-D models with measured data is not sufficient reason to stop looking for other mechanisms. Second, the sensitivity of a model's output to the uncertainty in one of its input data can be much larger or much smaller than that uncertainty.

ON THE RESPONSE OF HEMISPHERIC MEAN TEMPERATURE TO STRATOSPHERIC DUST: AN EMPIRICAL APPROACH

R.C. OLIVER
Institute for Defense Analyses
Arlington, Virginia

ABSTRACT: The cooling effects of stratospheric dust, and response times for the resulting hemispheric mean temperature changes, are estimated using an empirical approach and a simple time-dependent formulation. The approach couples estimates of stratospheric dust injections by volcanic eruptions to an available record of mean-temperature anomalies. The time period examined is 1883-1968. The effort is exploratory; nevertheless, the results strongly suggest that large volcanic eruptions do lead to short-term climatic cooling effects that, with frequent eruptions, would tend to be cumulative. The many uncertainties are noted, as are difficulties introduced by apparent underlying temperature trends. The cooling coefficients and response times found are compared to values developed elsewhere. The apparent climatic significance of stratospheric dust, and the fact that climatic changes involve integrals over time, suggest that long-term records of stratospheric dust, as well as other climate-determining factors, should be developed and maintained.

INTRODUCTION

In this paper, a simple, empirically calibrated, time-dependent formulation is used to estimate the effects of stratospheric dust on hemispheric mean temperatures. The formulation utilizes a "cooling coefficient" per unit mass of stratospheric dust that applies to a "steady-state" change - in a time frame of years to decades* but which is developed from the dynamic changes that occur following large volcanic eruptions. The temperature changes are obtained from an available record of mean temperature anomalies over the period 1883-1968. The cooling effect of an eruption depends on the response time of the ocean-land surface-atmosphere system; thus, a lumped response time is also developed empirically. The results so obtained are compared to theoretical results reported or developed elsewhere (Hidalgo, 1974; Budyko, 1974b). Because of the uncertainties involved, this paper is exploratory in nature; however, it is believed that the method should be sufficiently sensitive to show up any serious inconsistencies between theory and available data.

The approach used here differs from that used in prior studies; it is described in detail following a discussion of the climatic and volcanic records. In essence, however, it is a time-integrated approach, in which it is assumed that volcanic eruptions are a major factor in short-term climate change, and that such eruptions provide valuable, if unfortunately not completely satisfactory, indications of the dynamics of climatic temperature changes. Other possible causes of climatic change are discussed briefly, but are not treated quantitatively.

Many previous investigators have considered the question of cooling effects of volcanic dust, as evidenced by the climatic record, generally considering each eruption independently, but apparently without reaching an established consensus (see, e.g., Arakawa et al., 1955; Mitchell, 1961, 1971; Humphreys, 1964; Reitan, 1971; Budyko, 1974b; Landsberg and Albert, 1974; Bauer and Oliver, 1975). Budyko (1974b) has also considered briefly the averaged effects of frequent volcanic activity, arguing that the volcanically active period 1883-1912 was cooler than the subsequent similar period because of greater stratospheric dust. In addition, very recent data from deep-sea drilling sections (Kennett and Thunnel, 1975) suggest a correlation between strong volcanic activity and ice ages, tending to confirm speculations often made in the past.

^{*}Possible very long-term effects, such as the postulated ice-albedo feedback effect (which may require thousands of years to be significant (Budyko, 1974a)) are not included. Climate undoubtedly responds on a variety of time scales.

THE CLIMATIC AND VOLCANIC RECORDS

A Northern Hemisphere yearly mean-annual-temperature-anomaly record over the period 1880-1968 is shown in Figure 1, along with a record of major volcanic events; a more detailed listing of volcanic events is given in Table 1. The temperature-anomaly curve is from a tabulation by Budyko (1969), updated by T. Asakura* in 1974, and provided in digital form by Mitchell (1974). The validity of this temperature-anomaly curve has been questioned (Landsberg, 1975), but here, with minor exception, it is accepted without further examination.

The volcanic data are from several sources, but are based largely on the tabulation published by Mitchell (1970); however, Mitchell's dust-mass estimates have generally been adjusted downward by a factor of two, on the basis of independent estimates for several of the events (Deirmendjian, 1972; Junge, 1974), and have been further adjusted for the latitude of the event, as discussed below. The volcanic-dust data are discussed briefly in Appendix A. In general, the well-known dust-veil-index (D.V.I.) concept of Lamb was not utilized in the tabulation in view of its incorporation of time, dust quantity,

and area factors (as well as, in certain circumstances, resultant climate change); for the purposes here, dust quantities were of primary interest. The uncertainties in the volcanic dust numbers are large: a factor of two or more. Furthermore, the listing may well be incomplete; the comprehensive work by Macdonald (1972) suggests additional, possibly important, events, but no estimates of stratospheric dust injections are provided.

The latitude, strength, and probably season of an eruption can all be expected to play a role in determining the effect of the eruption on the mean annual hemispheric temperature anomaly. Dust in the polar night, for example, would be expected to have an effect on the radiation balance quite different from that of dust in the tropics. The physical phenomena involved are far beyond the scope of this paper. Nevertheless, two corrections for latitude effects were felt to be necessary and were utilized. These related to (1) the fraction of total dust reaching the Northern Hemisphere, and (2) the time delay between the event and its impact on the Northern Hemisphere mean-annual-temperature anomaly. The assumptions made are shown in Table 2.

^{*}Japan Meteorological Agency (unpublished results).

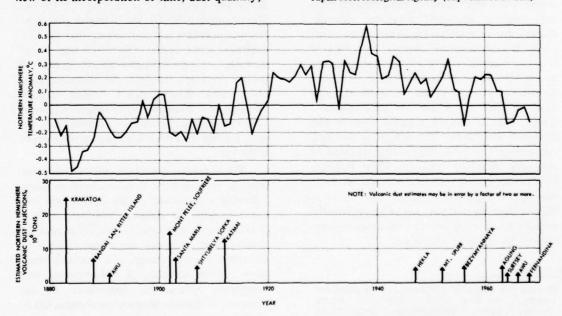


Figure 1. The climatic record (Budyko and Asakura, via Mitchell (1974)) and principal volcanic dust injections (various sources, cf. Table 1 and Appendix A).

OLIVER

Table 1. Estimates of Stratospheric Dust Injections from Volcanic Eruptions

						Lamb	1970)	Megat	in Assigned	Assigne Year
			Class, 10 ⁶ Tons	Deirmen- djian,	Sapper's	Total Dust,	D.V.I. Northern		rn Hemisphere	N.H. Climate
Year	Eruption	Latitude	(Mitchell)	1970(1)	Class(2)	km ³	Hemisphere	Event	Year's Total	Affected
1883	Krakatoa	6°S	100	30	1	5.0	1000	25	25	1884
1885	Falcon Island	20°S	1		2(?)	-	100	0.1	0.1	1886
1886	Tarawera	38.5° S	10	_	1	1.5	$(400)^{(3)}$	0.5		
1886	Niafu	16°S	1	-	2	-	100	0.2	0.7	1887
1888	Bandai San	38°N	10	_	1	3.0	(250)	5	5.0	1888
1888	Ritter Island	5.5°S	10	-	1	1.7	(125)	2.5	2.5	1889
1890	Bogoslov	54°N	1	-	_	-	(50)	0.5	0.5	1890
1892	Awu	3.5°N	10	-	-	-	$(100)^{(3)}$	2.5	2.5	1892
1898	Una Una	9°S	1	-	3	_	70	0.3	0.3	1899
1902	Mont Pelée	15°N	10		2	_	$(100)^{(3)}$	3.8		
1902	Soufrière	13.5°N	10	-	1	1.0	$(300)^{(3)}$	3.8		
1902	Santa Maria	14.5°N	20(4)	-1		(7.5	15.1	1902
1903	Santa Maria	14.5°N	20(4)	-}	1	5.4	$(600)^{(3)}$	7.5	7.5	1903
1904	Minami Iwoshima	24°N	-		2(?)	,_	30	0.3	0.3	1904
1907	Shtyubelya Sopka	52° N	10		1	3	150	5	5.0	1907
1911	Taal	14°N	1		2	-	15	0.4	0.4	1911
1912	Katmai	58° N	10	13.4	1	(0.006-21)	150	13	13	1912
1914	Sakurashima	31.5°N	1	_	2	0.5	20	0.5	0.5	1914
1929	Asama	36.5°N	0.1	_		0.1	4	0.1	0.1	1929
1931	Klyuchev	56° N	0.1	-	_	0.1	2	0.1	0.1	1931
1947	Hekla	64° N	10		_	0.18	(20)	5	5	1947
1951	Mt. Lamington	9°S	_	_	-	-	10	0.5	0.5	1952
1953	Mt. Spurr	61°N	10		_	7 -	2	5	5	1953
1956	Bezymyannaya	56°N	10	_	_	1.0	(10)	5	5	1956
1963-										
1965	Surtsey	63°N	1	-	-	0.7	15	0.5	0.5	1963
1963	Agung	8.5°S	30	9	_	_	400	5	5	1964
1966	Awu	3.5°N	10	_	_	≈3	150-200	2.5	2.5	1966
1968	Fernandina	0.5°S	10	_		1-2 (?)	50-100	2.5	2.5	1969

⁽¹⁾ Assumes dust in stratosphere at density of 1.0 gm/cc.

Table 2. Assumed Latitudinal Effects

Eruption	Northern Hemisphere Dust	Year Affecting Northern Hemisphere Mean
Latitude	Fraction	Temperature
90° N-20° N	1.0	Same
20° N-10° N	0.75	Same
10° N- 0°	0.5	Same
0° -10°S	0.5	1 year later
10°S-20°S	0.33	1 year later
20°S-40°S	0.1	1 year later
40°S-90°S	Ignore	•

These assumptions should be examined, and the use of a finer time resolution considered, in more detailed work.

Several points should be noted from Figure 1 and Table 1:

 The quantity of the dust injected from major volcanic eruptions is indeed very great. The 1883 Krakatoa eruption, for example, apparently put 50 to 100 million tons of dust into the global stratosphere; for the purposes here, an initial Northern Hemisphere value of 25 million tons is assigned (see Appendix A). The effects, which were noted essentially worldwide, lasted for several years. Losses in direct solar beam of 20 to 30% were noted, although about 85% of this (Budyko, 1974b; Herman, 1974) was regained due to an increase in scattered light. This event was extensively studied at the time and is described in detail by various authors (Lamb, 1970; Deirmendjian, 1972).

- A short cooling wave apparently followed the Krakatoa eruption and several of the later eruptions. Other fluctuations, however, showed no evident relation to volcanic events.
- The overall climatic trend from the 1880s to the 1930s was one of warming.
 Furthermore, this warming trend apparently took place even in the early

⁽²⁾ Sapper's scale for explosive eruptions: Magnitude 1 = >109 m³ ejected, Magnitude 2 = 108-109, etc. Only explosive eruptions are considered here. Source: Lamb, 1970.

⁽³⁾World value. No Northern Hemisphere value given.

⁽⁴⁾Timing split according to Mitchell (1974).

part of this period, a time during which a number of major eruptions occurred.

A period of several decades existed (about 1915-1945) in which volcanic activity was unusually light and, as mentioned earlier, the temperatures were higher than during the preceding or, in fact, the subsequent (current) period.

Volcanic eruptions and dust in the stratosphere can, or could, affect climate in a variety of possible ways, including alteration of planetary albedo, heating of the stratosphere by absorption of solar radiation (with alteration of the radiation balance), changes in cloud nuclei (Wexler, 1951), and changes in snow albedo due to deposition of tropospheric dust (Landsberg, 1970). Volcanoes put a variety of materials into the stratosphere, e.g., mineral dust, water, CO2, HCl, and SO₂, any of which could contribute to climatic change. The SO2, however, on conversion to sulfuric acid, is believed to be the most important component in a climatic sense.* These are all complex effects; the goal here is to estimate empirically the net effect. In doing so, it is necessary to at least mention other possible causes of climatic effects, as follows.

Numerous possible causes of climate change have been discussed in the literature, including both anthropogenic and natural factors. Two principal anthropogenic sources are often considered: changes in atmospheric carbon dioxide and changes in tropospheric dust. These and other factors, such as changes in stratospheric water vapor, changes in ozone, changes in solar constant, changes in sun spots, and changes in orbital parameters have been reviewed by various authors (e.g., Mitchell, 1961, 1970, 1975; Reitan, 1971; Dyer, 1974; Lamb, 1972; Bryson, 1974). The possible effects due to changes in carbon dioxide are perhaps most readily subject to analysis, for good data do exist on atmospheric CO2 and its increase over recent decades. Thus, according to Reitan (1971), on the basis of a calculation by Manabe and Wetherald (1967), the increase in CO2 between the 1880's and the 1960's could have caused an increase of 0.3°C. Unfortunately, however, such computations are based on an assumption of constant cloudiness, and possible changes in cloud cover are exceedingly important. Manabe and Wetherald (1967) show, for example, that a 1% increase in low cloudiness would cause an 0.8°C decrease in mean temperature; thus, a 0.3°C warming could be compensated for by a change of about 0.4% in low cloudiness. A change of only 0.4% in low cloudiness would obviously be exceedingly difficult to detect. The influence, or even the sign, of other possibly significant factors, such as tropospheric dust, is less easy to establish than that of CO₂, and might well compensate for CO₂ changes. In view of these many uncertainties, no attempt is made here to correct for these other factors. In any event, Mitchell (1975) concluded that neither tropospheric particulates nor atmospheric CO2, in concert or separately, could have accounted for the major part of the observed temperature changes in the past century.

THE APPROACH

Development

The approach was developed following a suggestion by Budyko (1974b) to the effect that the earth's surface temperature may respond to perturbations in a simple fashion, according to

$$\frac{dT}{dt} = -\lambda (T - T_R) .$$
(1)

For the purposes at hand, T is used to represent mean temperature and, in fact, in view of data availability (as will be discussed further), mean annual temperature in the Northern Hemisphere, at time t; λ is a climatic response constant (yr^{-1}) , and T_R is the reference or equilibrium mean temperature towards which the mean temperature T is "moving".

For conditions following a volcanic eruption, T_R clearly varies with time. To account for this, it is assumed that

$$T_{R} = T_{0} - \alpha M(t) , \qquad (2)$$

^{*}Friend (1972) gives an "average" analysis for volcanic gases of 95% H₂O, 4% CO₂, and 1% SO₂ by volume for a mass ratio of H₂O/SO₂ of 53 to 1. In CIAP studies (Hidalgo, 1974), it has been found that the effect of water vapor is roughly equal to (about one-half as great as) the effect of SO₂ (and of opposite sign) at a mass ratio of 1250 to 1. Thus, the SO₂ and other dust quantities should generate the dominant

where T_0 is an (unknown) equilibrium mean temperature in the long-term absence of stratospheric dust, α is a cooling coefficient (here in °C/million tons of dust), and M(t) is the mass of dust as a function of time.*

As Eq. (2) is written, T_0 is implied to be a constant. In fact, T_0 will certainly vary with time, because of CO_2 and other factors unrelated to volcanic eruption change. Since the manner in which T_0 has varied with time is unknown, it is necessary to make either arbitrary assumptions as to the functional relationship of T_0 with time, or limiting assumptions; one arbitrary relationship is included briefly in Appendix B, but the remainder of this paper involves two limiting assumptions:

- T₀ is constant over a 10- or 20-year period and is estimable from the mean temperature existing after 5 or 10 years of light volcanic activity.
- T₀ is constant over an 80- to 100-year period and is estimable from the mean temperatures prevailing after several decades of very light activity.

The first assumption gives small values for the cooling coefficient and the response time, and the second assumption gives higher values for both. Presumably, "true" values would be between these limiting values, but this cannot be proven to be the case, because of the many variables that could affect climate.

The first assumption is used in exploring two periods near the turn of the century; the second is used for the full period (1883-1968). In effect, the second assumption implies either that the lower temperatures prevailing prior to 1883 were due to previous volcanic activity,* or that an underlying, fairly rapid warming trend began about 1883, with the increase in measured

Under both of the above assumptions, T_0 is treated as a constant, so that the same mathematical formulation applies. For convenience, the quantities θ and β are now defined, where θ is the anomaly relative to the reference line used by Budyko, and β represents a constant difference between this reference line and T_0 , that is:

$$T(t) - T_0 = \theta(t) - \beta , \qquad (3)$$

so that Eq. (1) becomes

$$\frac{dT}{dt} = -\lambda [T - T_0 + \alpha M(t)] , \qquad (4a)$$

or

$$\frac{d(\theta-\beta)}{dt} = -\lambda[\theta - \beta + \alpha M(t)] . \qquad (4b)$$

Equation (4b) leads to

$$\theta = (\theta_0 - \beta) e^{-\lambda(t-t_0)} + \beta$$

$$+ \int_{t_0}^{t} e^{-\lambda(t-\tau)} [-\lambda \alpha M(\tau)] d\tau ,$$
(5)

where θ_0 is the value of the temperature anomaly at the beginning of the integration period being considered. To integrate Eq. (5), M(t) is needed; for simplicity, volcanic dust loadings were assumed to follow a relationship of the form:

$$M(t) = M_0 e^{-k(t-t_0)}$$
, (6)

where M_0 represents the mass of dust in the stratosphere at the beginning (t_0) of the time period in question, and k^{-1} represents a dust residence time. Substituting Eq. (6) into (5) and integrating gives:

$$\theta = (\theta_0 - \beta) e^{-\lambda(t-t_0)} + \beta$$

$$-\frac{\lambda \alpha M_0}{\lambda - k} \left[e^{-k(t-t_0)} - e^{-\lambda(t-t_0)} \right] . \tag{7}$$

temperature delayed by volcanic activity. The effects of rapidity of change are explored briefly in Appendix B.

^{*}In principle, of course, if data on CO₂, H₂O, tropospheric dust, cloudiness, etc., over the course of time were available, and cooling or warming factors were known for each one, their effects in the treatment could be included.

^{*}For example, Lamb (1972) lists an eruption of Ghaie (4°S, 152°E) in 1878 with a possible D.V.I. 25% greater than that of Krakatoa. It is doubtful, however, that volcanic eruptions were of sufficient frequency or magnitude to depress mean temperatures, prior to the Krakatoa event, to the values measured, relative to temperatures in the 1930's.

Note that by either Eq. (2) or (7), the steady-state temperature reductions caused by M_0 tons maintained continuously would be αM_0 . Note that M_0 is usually estimated from radiation measurements, and that the product αM_0 can be estimated from these measurements and theoretical radiative-equilibrium (heat-balance) arguments. In one sense, therefore, this work can be considered to be a test of these theoretical arguments.

Again, for simplicity, in order to use Eq. (7) for sequential events, it was assumed that all dust injections could be characterized by the same value of k; i.e., by the same residence time (k^{-1}) . With this assumption, Eq. (7) was applied on a yearly step basis, taking M₀ at the beginning of each time step as the sum of residual old dust and new dust added during the year. Treating residence-time values as being reasonably known quantities, empirical values of λ and α were sought to obtain a fit to the temperature record (Figure 1). In most cases, the computation was begun at the 1883 point and the analytical curve was forced, by selection of α , for an assumed λ , to pass from the -0.14°C point in 1883 through a minimum value of -0.48°C, which the data show was reached a year or so later. Dust estimates were used from Table 1. The only exception to this general procedure was made in a study of the period 1901-1920 (described later).

For convenience in the following discussion, the terms "climatic response time," C, equal to λ^{-1} , and "dust residence time," R, equal to k^{-1} , both in years, are utilized.

Some Characteristics of the Formulation

Before proceeding, it is of interest to note the manner in which the initial anomaly, $(\theta_0-\beta)$ in Eq. (7), affects the relative shape of the climatic response to a given volcanic event. The point is illustrated in Figure 2 for an arbitrary set of assumptions. In Figure 2, all curves are normalized to start at the same point. Note that where the initial anomaly is negative (i.e., the climate, without volcanic eruptions, is in a warming trend*), the downward displacement is

much less than if no trend exists or if a cooling trend is under way. Note also that the time to minimum temperature is reduced in the presence of a warming trend. With a small eruption and a strong warming trend, it is conceivable that no cooling below the initial value might be noted; similarly, with a strong cooling trend, no recovery might result, and the mean temperature might simply drop to the new equilibrium value, accelerated in the process by the volcanic eruption.

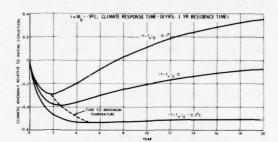


Figure 2. Apparent climatic response, by formulation, for the same volcanic eruption under three assumptions as to initial temperature anomaly with the same arbitrary value for climatic response time.

Another point of interest with regard to Eq. (7) is that the time-integrated cooling effect of a given eruption (from t_0 to ∞) is simply $\alpha M_0/k$, and is independent of λ . It is evident then that the residence time (k^{-1} or R) is fully as important as M_0 in determining the effects of a given eruption. (The Lamb (1970) D.V.I. clearly incorporates this concept, but not in a manner directly usable here.) The uncertainties introduced by the assumption of a constant residence time for all eruptions are discussed in a later section; clearly, however, the assumption will overstate the effects of some eruptions and understate the effects of others. The effects of variation in λ are illustrated below.

Preliminary Utilization of the Formulation – The Need for an Empirical Evaluation of Constants Specific to This Formulation

The formulation shown in Eq. (7) involves several constants, for all of which it might appear that estimates are available from the literature or by reasonable assumption. As a preliminary

^{*}Note that these "trends" take place with a constant value of T₀; the temperature at the beginning of the period is simply assumed to be displaced from its equilibrium value.

exercise, it is of interest to see how well these values might apply to the period following the Krakatoa eruption in 1883. Thus Budyko (1974b), on the basis of the seasonal march of temperatures, developed a value of λ of 0.4 yr⁻¹, or a 2.5-year response time. Mitchell (1970) assumed a residence time for stratospheric dust of 14 months, but a considerable variability is involved (Mitchell, 1961); a figure of one year seems reasonable as a working figure here. The value of β over a short period might reasonably be taken as zero.

As discussed later, a value for α of 0.53°C/Mt can be derived from results of the CIAP effort, as reported by Grobecker et al. (1974); this figure is for a hypothesized 10-year steady-state loading of SO_2 -derived stratospheric dust. (Note, however, that CIAP studies also recommend that about one-third of this value should be used for one-year changes (see Hidalgo, 1974, p. F-122). This smaller figure, however, includes the effects of nonequilibrium response.)

The above constants and an M_0 value of 25 million tons were used with Eq. (7) to develop the dotted curve in Figure 3; the dashed curve was developed for the same values of α and M_0 , but it assumes a 10-year response time. Data (arrow) from a RAND (Mintz-Arakawa) model run (Batten, 1974) that simulates a Krakatoa cloud, which apparently did not include oceanic thermal inertia, are also indicated as a matter of interest. Note that the computational results show far larger displacements than do the actual

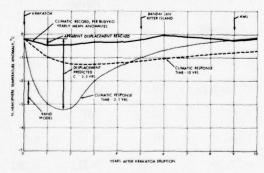


Figure 3. Climatic record and certain analytical results, treating the Krakatoa eruption as an isolated event and ignoring any underlying trends. The Bandai San and Awu events are not included. This plot shows that constants from the literature apparently cannot be used in the formulation developed here.

data. With a climatic response time of 10 years, the displacement is greatly reduced, but the duration of the effect is greatly increased; however, the total time-integrated effect as noted above would be unchanged by changes in λ .

A number of factors could enter into the apparent poor agreement in Figure 3 between computed and measured changes in mean temperature; it appears, however, that an alternative empirical approach may be useful in finding what values of these constants would be required to fit the historical data. Given these data, the empirical and theoretical results will then be reexamined.

RESULTS AND DISCUSSION

Results from Short-Period Studies – Possible Long-Term Trends Ignored

Two short-period (\approx 20 years) cases were examined to determine empirical constants. In these cases, possible underlying long-term trends were ignored.

The 1883-1900 Period

The first set of results is given in Figure 4, in which analytical curves with several sets of constants are shown. In these cases, the starting point was as shown, and the zero-anomaly reference value was taken as the appropriate value for T_0 — i.e., β was set equal to zero. As noted earlier, values of α were selected to force

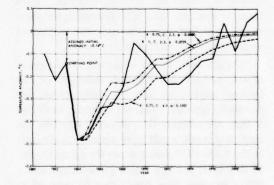


Figure 4. Climatic record and model results using constants shown. Initial anomaly set at -0.14°C. No other trends. Period 1883-1900.

OLIVER

the analytical curves through a minimum at -0.48° C; the precise time at which this occurred was allowed to "float." Note that a reasonable fit is given by a climatic response time of 2.5 years, a residence time of 1 year, and an α of 0.0739 (an α considerably smaller than that used in Figure 3).

Note that the assumption of shorter residence times leads to larger values for α . By inspection of the three curves, it is evident that a climatic response time of about 3 years and an α of about 0.1 would, with a residence time of 0.75 years, approximately duplicate the middle curve. It is clear, therefore, that one of the variables in Eq. (7) must be taken as a known value to avoid multiple apparent solutions; here, residence time is taken as a known value, normally one year.

The 1901-1902 Period

For the 1901-1902 short-term case, β was taken as +0.08°C, so that the initial anomaly $(\theta_0-\beta)$ was zero. (A step change in T_0 of 0.08°C from the previous plot is implied.) In this case, the curves were forced through -0.24°C by selection of α . In this case, a climatic response time of 2.5 years does not give nearly so good a fit as one of 5 years, at least in the period before the Katmai eruption in 1912. The large swing in temperature following the Katmai eruption makes any comparison in this latter period rather suspect.

Note that doubling the climatic response time from a value of 2.5 years to one of 5 years leads, in this case, to a 50% increase in the value of α , an effect which is opposite to that of increasing the residence time.

As discussed in the approach, these figures should provide lower-bound estimates of the cooling effects, in that warming trends are essentially ignored. Note, for example, in Figure 5 that the addition of a warming trend to the analytical result would raise the analytical curves in the 1906-1910 period above the values shown; in this case, a larger cooling coefficient and a longer response time would then be required to force the curves through the recorded data. These facts will become evident in the next section.

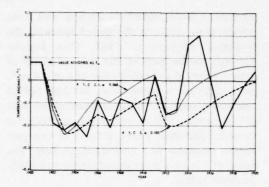


Figure 5. Climatic record and model results using constants shown. Underlying trends not considered. Period 1900-1920.

Full-Period Results

Principal Results

Under the second assumption, T_0 in 1883 was based on temperatures being approached in the 1930's. Values of β of 0.26 and 0.36 ($\theta_0 - \beta$ or $T-T_0$ of -0.4 or -0.5 in 1883) were used.

Several results are shown in Figures 6, 7, and 8. Again, the curves are the result of stepwise par-by-year application of Eq. (7), using dust mass as in Table 1, with events adjusted in a time sense according to Table 2. The following constants were used in the three figures.

	Figure				
Constant	6	7	8		
β,°C	0.36	0.36	0.26		
$(T-T_0)_{1883}$	-0.5	-0.5	-0.4		
R, yr	1.0	1.0	1.0		
C, yr	10	9	6.5		
α, °C/Mt	0.227	0.211	0.162		

Note that the analytical results all seem to follow the full curve in a general way, although deviating somewhat in recent years in a quantitative sense. Note also that the C and α values are about twice those found previously.

OLIVER

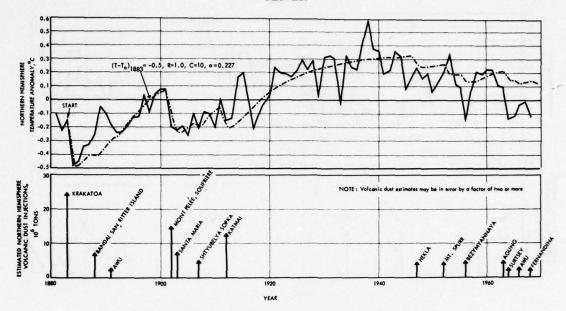


Figure 6. Analytical result, using $(T-T_0)_{1883} = -0.5$, R = 1.0, C = 10, and $\alpha = 0.227$, superimposed on the climatic record.

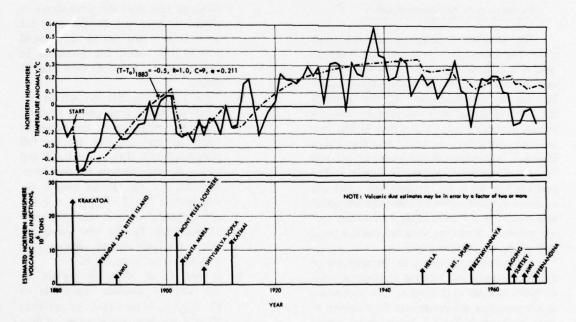


Figure 7. Analytical result, using $(T-T_0)_{1883} = -0.5$, R = 1.0, C = 9, and $\alpha = 0.211$, superimposed on the climatic record. The effect of a shorter climatic response time can be seen by comparing this figure to Figure 6.

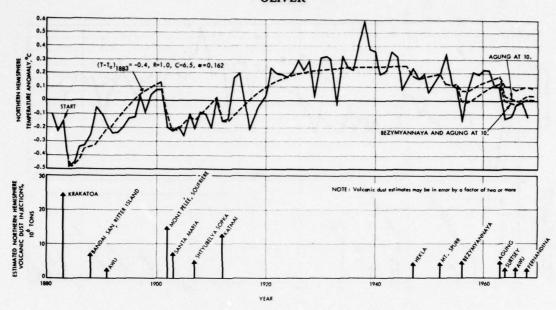


Figure 8. Analytical result, using $(T-T_0)_{1883} = -0.4$, R = 1.0, C = 6.5, and $\alpha = 0.162$, superimposed on the climatic record. The assumed initial temperature anomaly is smaller $(-0.4^{\circ}C)$ than in Figure 7; a shorter climatic response time and smaller cooling coefficient result.

Exploratory Optimization Studies

The question of preferred constants, even under the assumptions made in this long-term case, is a difficult one, and merits some discussion. Note first, in Figure 6, the large deviation between the analytical curve and the record in the 1885-1890 period, unmatched by any off-setting deviation later. This effect is less pronounced with a shorter limatic response time in Figure 7, and is even better balanced out with the set of constants shown in Figure 8. The post-1945 period is not matched well under any of the assumptions: either a new trend was under way — perhaps the most likely explanation — or the masses of dust used were too small, a point that will be discussed shortly.

To reduce subjectivism in the selection of preferred curves, but without attempting a full multidimensional optimization, the root-mean-square deviation was determined for a number of cases, as shown in Table 3. Several points should be noted:

 As is visually apparent on comparing Figures 6 and 8, if the entire 1883-1968 period is to be fitted, a value of (Γ-T₀)₁₈₈₃ smaller than -0.5°C (i.e., about -0.4°C) gives a smaller standard deviation than does the curve shown in Figure 6, since the deviations in the latter half of the period are reduced considerably. Also, the constants in Figure 8 give a better fit than those in Figure 7.

- These data show that the best fit is a function of the time period selected. Thus, the minimum in the tabulated values of rms deviation for the full period is for $(T-T_0)_{1883} = -0.4^{\circ}C$ and with a 6.5-year climatic response time; however, for the shorter period, the minimum is for $(T-T_0)_{1883} = -0.5^{\circ}C$ and a climatic response time of about 9 years (Figure 7). The best overall fit, among the cases studied, appears to be the case plotted in Figure 8.
- It was found that, in general, as the assumed absolute magnitude of (T-T₀)₁₈₈₃ is increased, the optimum climatic response time increases, as does the value of α that forces the curve through the -0.48°C minimum selected. This can be seen in the α column in Table 3. Also, as was noted carlier, if climatic response time is held constant and R is varied, α increases with decreasing R.

Table 3. Some Exploratory Optimization Results

		Constants		Root-Mean-Square (rms) Deviation			
$(T-T_0)_{1883}$	R	<u>c</u>	α	1883-1968	1883-1942	Plotted As	
-0.5	1.0	8	0.1949	0.1363	0.1232		
-0.5	1.0	9	0.2109	0.1325	0.1202	Fig. 7	
-0.5	1.0	10	0.2267	0.1332	0.1242	Fig. 6	
-0.5	0.9	10	0.2441	0.1319	0.1208		
-0.4	1.0	6	0.1537	0.1233	0.1233		
-0.4	1.0	6.5	0.1619	0.1220	0.1220	Fig. 8	
-0.4	1.0	7	0.1700	0.1222	0.1228		
-0.4	1.25	5.5	0.1269	0.1242	0.1250		
-0.4	1.25	6	0.1337	0.1233	0.1243		
-0.4	1.25	6.5	0.1405	0.1240	0.1257		

Sensitivity and Uncertainties

- a. Sensitivity to Dust Masses, Post-1945 Period. In view of the deviation of the analytical results for post-1945 from the climatic curve, it was of interest to explore briefly the sensitivity of the analytical results to the dust-injection numbers used from this period. Two arbitrary cases were considered:
 - The Agung value was doubled from 5 to 10 million tons.
 - The Agung and the Bezymyannaya values were both doubled from 5 to 10 million tons.

The results are shown in Figure 8. In both cases, considerable change is noted in the analytical curve, as would be expected. It seems clear that, if the formulation is valid, and if by chance all or most post-1945 eruptions have been underestimated relative to those near the turn of the last century by a factor of about two, i.e., by factors that are probably within the uncertainty of the injected masses, then the post-1945 analytical result would show a greater displacement than does the measured curve (see, however, subsection b below). This observation suggests a need for a more detailed examination of the events or of dust masses in the stratosphere during this period. Note that fair precision is needed, a factor of two evidently being unacceptable.

b. Uncertainties in Residence Times. It was noted in an earlier section that dust residence times are as important as initial dust masses in

determining total cooling effects, and that the use of a constant residence time for all eruptions overstates the effects of some eruptions and understates the effects of others. In effect, since smaller eruptions would be expected to have residence times lower than those of larger eruptions, this work may well overstate the effects of small eruptions. Also, if latitude plays a part in residence times, as may well be the case, with high-latitude eruptions possibly having lesser residence times (Mitchell, 1961) than those of tropical eruptions, then the effects of small northern-latitude eruptions may be overstated on two counts. These points need further study.

c. Uncertainty of and Sensitivity to the Climate Record. A ground rule of this paper, as noted at the outset, was that the temperature record would not be questioned in detail. The absolute accuracy of this curve is unknown. Nevertheless, a few comments may be in order.

First, it may be noted that extreme short-term positive swings seem to be balanced by short-term negative swings. These fluctuations may arise from the use of land-dominated averages, i.e., of too few stations to get a valid hemispheric average. For changes of the magnitudes noted to be valid, either strong (and unknown) perturbations must occur, or thermal inertial (response time) estimates come into question.

Second, it was noted earlier that all full-term computations, as well as the short-term computations from 1883-1900, involved starting at -0.14°C with a forced minimum at -0.48°C. If this difference of -0.34°C had been in serious

error, however, the subsequent curve fits would have been poor. However, the sensitivity of the results to errors in these two data points was given some study by considering two possibilities:

- The 1883 initial point was erroneously low by 0.1°C, but all other points were correct.
- The 1883 point and the minimum temperature reached following the Krakatoa eruption were both erroneously low by 0.1°C.

In case 1, the effect was to increase α , inasmuch as the Krakatoa eruption, under this assumption, caused a cooling of 0.44°C instead of 0.34°C. Small effects were noted on optimum response time, etc., but the predominant effect was to create a corresponding excess displacement in the 1901-1903 period. The larger α , of course, made the post-1945 analytical curve look better relative to the data measured.

In case 2, the displacement created by Krakatoa was still taken as 0.34° C, so α was not strongly affected. Optimum response times were increased by a year or so, but no dramatic effect was evident.

These brief examples suggest that the overall results are not extremely sensitive to absolute uncertainties in the temperature-anomaly record near the initiation period.

d. Other Uncertainties. Uncertainties obviously exist in all facets of this work, ranging from questions as to the basic validity of the formulation used to questions of dust masses used, volcanic eruptions not recognized, residence times after and differences between eruptions, etc. Analysis of all these factors has not been attempted; the justification is, of course, that this paper is intentionally exploratory.

Two points should be noted with regard to dust masses and the values found for the cooling coefficient. First, what is actually used in the computations is the product αM_0 , which is in units of temperature. The entire work could have been done in some unit of this type, with different eruptions rated in terms of each other or in radiation loss, etc., a point that is discussed later. Obviously, if the dust masses used are, say,

twice as high as they should be, then the α figures are half as large as they should be Second, the density question should be noted. The optical effects of a given mass of dust of given particle size and properties are inversely related to particle density. Deirmendjian (1972) gives masses in unit density; other authors do not quote the densities being used. Unit densities may be suitable for porous tephra particles; sulfuric acid particles, however, which would be expected to have longer-lasting effects, have densities near 1.7 gm/cc.

COMPARISON OF RESULTS

Summarized Results

The two approaches, as just described, lead to two sets of results:

Period Considered	°C/Mt	C, years	
Short term	0.07-0.10	2.5-5	
Long term	0.16-0.21	6-9	

It is important to note that these results were developed, and should always be taken, in pairs, i.e., a small value of α should be used with a short response time, and a larger value of α with a longer response time.

As pointed out earlier, the two assumptions on which these figures were developed may represent limiting values, in that in the short-term case, long-term trends are ignored, and in the long-term case, the effects of long-term trends are probably overstated. Of course, the question arises as to which set may be more realistic, and this question cannot be answered absolutely. Insight may, however, be gained by comparing these sets of numbers to results of other investigators. These arguments will favor the larger numbers.

Cooling Coefficients

The α results can be compared to theoretical values developed under the CIAP program on the basis of radiation calculations, on the effects of added dust, and on resultant theoretical temperature changes. One value of α was used for

illustrative purposes in Figure 3. Other values from various authors' work are reported by Hidalgo (1974). These results indicate the change in equivalent solar constant $(\delta \sigma/\sigma)$ assuming a uniformly distributed aerosol over the Northern Hemisphere in a 10-km thick layer; this change in equivalent solar constant is then converted to an estimated temperature change, if maintained for certain lengths of time. The equivalent solarconstant-change computations are made assuming an average solar zenith angle of 60 degrees, which doubles the normal value of optical depth. Given the change in effective solar constant, the change in steady-state temperature is obtained, using an estimated x proportionality constant, according to

$$\Delta T = \chi \frac{\delta \sigma}{\sigma} \quad , \tag{8}$$

where ΔT is the temperature change in $^{\circ}C$ after specified time periods, and $\delta \sigma/\sigma$ is the fractional effective change in solar constant.

A value of χ of 150°C (per percent change in equivalent solar constant) is recommended by Leith et al. (as reported by Hidalgo (1974)) and by Budyko (1974a) for time periods of perhaps a decade; a value of 250 that incorporates ice-

albedo feedback effects is recommended for a time period of the order of 1000 years. A smaller value (50) is recommended for a time period of one year. The different values recognize the thermal inertia and feedback effects. While the empirical and theoretical approaches are not strictly comparable, it would appear that the appropriate value for comparison here is the quasi-steady-state value of 150 (see also subsection below).

The various workers' results are summarized in Table 4, using a χ value of 150 and converting to common units. As before, the term ΔS_d in Table 4 refers to a hypothetical particulate concentration, assuming uniform dispersal of added aerosol over a 10-km thick band; the units are $\mu g/m^3$. The value of α is obtained from χ , $\delta \sigma/\sigma$, and the stratospheric volume involved (2.55 \times 10¹⁸ m³), correcting for the units employed.*

Table 4 includes reference to values of ω and β , which describe assumed optical properties of the particles. The term $(1-\omega)$ defines the probability of absorption, and $\beta\omega$ the probability

$$\alpha = \frac{150 \times 0.009 \, [^{\circ}\text{C/(\mu gm/m}^{3})]}{2.55 \, [\text{Mt/(\mu gm/m}^{3})]} = 0.53^{\circ} \, \text{C/Mt}$$

Table 4. Comparison of Results^a

Author	ω	β	-80/0	<u>α</u>	Remarks
Grobecker	_	18 0 <u>2</u> 18 1	0.0094S _d	0.53	b
Herman ^c	1.0	0.19	0.010 _d S _d	0.59	$\lambda = 0.5 \mu m$, nonabsorbing
Herman ^c	0.9	0.18	0.016 \(S_d \)	0.94	
Pollack-Toon ^c	0.99	0.12	0.0061 \Delta S _d	0.36	Wavelength integration
Coakley- Schneider ^c	1.0	0.10	0.0046 \(S_d \)	0.27	Wavelength integration
Luther ^c	0.95	0,095	0.0114S _d	0.65	Wavelength integration
This work				0.07-0.23	

^aThe variations in theoretical numbers include differences in assumed particle-size distribution and density, as well as in computational technique. The "now-preferred" value is that of Pollack & Toon (Hidalgo, 1975).

^{*}Thus, in the first case in Table 4,

bAs used in Grobecker et al. (1974), p. 43.

^cTaken from Hidalgo (1974).

of backscattering. It is now believed (Hidalgo, 1975) that ω for sulfuric acid particles is very near to 1.0; values of 0.9, one value used by Herman in studying effects parametrically, or 0.95, used by Luther, are too low and lead to values of $\delta \sigma / \sigma$, and thus α , which are too high. Thus, the CIAP most-applicable values can be quoted as being about 0.27 to 0.36, versus values found here of about 0.07 to 0.2. The midpoint of the empirical values (if taken as 0.14 ± 0.07) is clearly within a factor of about two to three of the theoretical values when a χ value of 150 is used, and is probably within the uncertainties in the dust masses. Also, quite obviously, the theoretical results themselves involve a number of uncertainties; longwave effects, which reduce the values by 10-25 percent, are not included and, of course, the value of χ can be questioned. (Grobecker et al. (1974) give a range of values that, in terms of α , would be expressed as 0.5 ± 0.7 .) Also, it should be remembered that the α value developed here includes the net effect of all the material injected by volcanic eruptions, including water vapor, and perhaps certain feedback effects (such as changes in cloudiness, or tropical tropopause warming with resultant water-vapor enhancement), which could cause some countervailing warming effects. Thus, the empirical value might well be somewhat lower than the theoretical values that result from consideration of aerosols only, all other factors remaining constant.

This comparison can also be phrased somewhat differently. Thus, it was noted earlier that the term αM_0 , by definition, represents a steadystate change in temperature, which would result if Mo were to be maintained indefinitely (decades) at a constant level. Also, as noted earlier, the masses of stratospheric dust have in fact been estimated from the optical properties of aerosol clouds, and with the aid of the same theoretical arguments these radiation-loss measurements can be used to estimate the product αM_0 . Thus, in the case of the Krakatoa eruption, direct-beam losses of 20-30% were measured, even after the dust had become well dispersed. If it is assumed, following Budyko (1974b), that net losses were about 15% of the direct losses, the fractional net loss received at the ground would have been 0.03 to 0.045. With a x value of 150, as above, the Krakatoa dust cloud (25 Mt assumed as the initial northern-hemisphere loading), if maintained indefinitely, should have

resulted, by these arguments, in a 4.5 to 6.75° C* loss in surface temperature. By comparison, the equivalent steady-state loss using the short-term results for this event would be (0.07 to 0.10) \times 25, or 1.75 to 2.5°C, and for the long-term case (0.16 to 0.21) \times 25, or 4.0 to 5.25°C. This argument would favor the larger pair of numbers (assuming, of course, that the χ value of 150 is correct).

As a separate matter, it might be noted that a cooling coefficient, but of a completely different sort, can be developed from a plot given by Mitchell (1970) noting stratospheric volcanic loadings versus time and equivalent cooling for each event. This coefficient, which can be converted to about 0.02°C/million tons of stratospheric dust, relates to the short-term climatic displacement following an eruption, not to the steady-state value. An analogous value based on the Krakatoa data used here would be 0.34°C/25 million tons, or about 0.014°C/million tons.

Climatic Response Times

Response times in the sense used here are not treated explicitly by Leith et al. (1975) in the studies on which the previous comparison was made; rather, responses as a function of time were given. The first two χ values (50 at 1 year, 150 at 10 years), however, are fitted by $\chi =$ 152.9 $(1 - e^{-0.396t})$, implying a short-term response time (1/0.396) of about 2.5 years, which is in agreement with Budyko, who estimated a response time based on the seasonal march of temperatures. A figure in this range was found to fit short-term events (Figures 4 and 5) reasonably well, but this comparison should be treated with caution. Budyko refers to a response time for less-than-yearly changes, whereas here the response time refers to changes in mean annual temperatures. It would seem reasonable that annual mean values might respond more slowly than seasonal values.

A response time comparable to that used here was developed by Reitan (1971), intercomparing five-year periods, in an attempt to achieve estimates of the relative importance of volcanic

^{*}In fact, figures twice these values could be developed by CIAP methodology, if the 20-30% loss were assumed to represent losses with a direct overhead sun, rather than losses at the average solar zenith angle of 60 degrees.

dust, tropospheric dust, and carbon dioxide in the stratosphere. He found, after some study, that a climatic half-response time (as in Eq. (1), but not carried through as in Eq. (7)) of five years was most appropriate. A half-time of five years corresponds to an e-folding time of 5/0.693 = 7.2 years, very similar to the 6.5-year preferred value found in this work in the full-period study.

Effect of Trends, and Other Pitfalls

Values of α , k, and λ alone, even if precisely known, would be insufficient to predict the "effect" of a given volcanic eruption or of any other specified perturbation, unless underlying trends were understood. This point was made in Figure 2; the ignoring of a warming trend accounted for part of the wide deviation of "predicted" from measured values in Figure 3. Other reasons for the deviation shown there can be postulated, including, if the work here is accepted, too large a value for α (or χ). An important point, however, is that use of a large value of α (0.5) with a short response time (2.5 years), as in one of the curves in Figure 3, seems never to be appropriate.

CONCLUDING COMMENTS

First, the results strongly suggest that large volcanic eruptions do lead to significant short-term cooling effects, which would tend to be cumulative with frequent eruptions. Thus, there is qualitative compatibility between available theoretical calculations and observations on the cooling effects of stratospheric aerosols. Quantitatively, the theoretical values imply a greater cooling per unit mass of dust than do empirical values developed here, but under certain of the assumptions made, values obtained from the two approaches are within what is probably the severalfold uncertainty range.*

Second, deducing climatic effects of volcanic eruptions from climatic data taken within a period of a few years following the eruption Third, lags in climatic changes of, say, 6 (±3) years have implications in view of man's possible inadvertent alteration of the climate. If the climate were in a warming trend, it might warm for a significant number of years before some man-induced (cooling) pollutant could reverse the trend.

Finally, the time-integrated aspects of climate changes should be noted. If theory is eventually to be tied to observation, accurate long-term records will be needed of all the factors, of which stratospheric dust is certainly only one, that may control climate.

ACKNOWLEDGMENTS

The author wishes to express his appreciation to a number of individuals who have been of considerable assistance in carrying out this work. Dr. J. Murray Mitchell, Jr., of NOAA, provided general encouragement, as well as invaluable assistance by supplying much of the necessary data. He is also indebted to several of his coworkers here at IDA, notably Dr. R.G. Finke for critical review, helpful discussions, and aid with computational techniques, and Mr. Henry Hidalgo and Drs. E. Bauer and W. Wasylkiwskyj for help with data interpretation, data sources, and mathematics.

This work was supported by the Climatic Impact Assessment Program of the U.S. Department of Transportation under Contract No. DOT-OS-30057. It was presented in preliminary form at the Fourth Conference on CIAP under the title "On the Response of Hemispheric Mean Temperature to Volcanic Eruptions, and Related Matters: An Empirical Approach."

REFERENCES

Arakawa, A., T. Fujita, H. Itoo, Y. Masuda, S. Matsumoto, T. Murakami, T. Ozawa, E. Suzuki, M. Takeuchi, and K. Tomatsu (1955), "Climatic abnormalities as related to the explosions of volcano and hydrogen-bomb," Geophys. Magazine (Tokyo) 26 (4), 231-255.

without considering underlying longer-term trends may well result in erroneous estimates of the cooling effects of stratospheric aerosols. If the climate were in a warming trend, a volcanic eruption might merely slow the process, and the climatic record could show almost no temperature effect. Conversely, if the climate were in a cooling trend, the event might have great apparent effect.

^{*}Note added in proof: In theoretical work published subsequent to the preparation of this paper, Pollack et al. find the cooling effects of sulfuric acid aerosols to be (in units used here) $\approx 0.1^{\circ}$ C/Mt, close to the values found with the "short term" studies herein. (See J.B. Pollack, O.B. Toon, A. Summers, W. van Camp, and B. Baldwin, "Estimates of the climatic impacts of aerosols produced by space shuttles, SST's, and other high flying aircraft," J. Appl. Meteorol. 15, 247-258.)

OLIVER

- Batten, E.S. (1974), "The Atmospheric Response to a Stratospheric Dust Cloud as Simulated by a General Circulation Model," Report No. R-1324-ARPA, RAND Corporation, Santa Monica, Calif.
- Bauer, E., F.R. Gilmore, and R.C. Oliver (1975), "Response of the stratosphere to impulsive loads," Chapter 8 of CIAP Monograph 1, Dept. of Transportation, DOT-TST-75-51.
- Bryson, R.A. (1974), "A perspective in climate change," Science 184, 753-760.
- Budyko, M.I. (1969), "The effect of solar radiation variations on the climate of the earth," Tellus 21, 611-619.
- Budyko, M.I. (1974a), private communication to A.J. Grobecker, U.S. Department of Transportation, 10 July.
- Budyko, M.I. (1974b), Climate and Life, Academic Press, New York (see in particular 249, 294, 295, 298, and 299).
- CIAP (1975), The Natural and Radiatively Perturbed Troposphere, ed. C.E. Leith et al., Volume 4 of the CIAP monograph series, Dept. of Transportation, DOT-TST-75-54.
- Deirmendjian, D. (1972), "On Volcanic and Other Particulate Turbidity Anomalies," P-4782, RAND Corporation, Santa Monica, Calif.
- Dyer, A.J. (1974), "The effect of volcanic eruptions on global turbidity and an attempt to detect long-term trends due to man," Quart. J. Roy. Met. Soc. 100, 563-571.
- Friend, J.P. (1972), Yearbook of Science and Technology, McGraw-Hill, New York, 411-413.
- Grobecker, A.J., S.C. Coroniti, and R.H. Cannon, Jr. (1974), Report of Findings: The Effects of Stratospheric Pollution by Aircraft, Climatic Impact Assessment Program, Department of Transportation, DOT-TST-75-50, Washington, D.C.
- Hidalgo, H. (1974), "Summary, Monograph 4," Appendix F in Grobecker et al. (1974).
- Hidalgo, H. (1975), private communication.
- Humphreys, W.J. (1964), Physics of the Air, Dover Publications, Inc., New York (originally published 1920 by the Franklin Institute, but with 1929 and 1940 updates).
- Junge, C.E. (1974), "Important problems of global pollution," in Proceedings of the International Conference on Structure, Composition and General

- Circulation of the Upper and Lower Atmospheres and Possible Anthropogenic Perturbations (Melbourne), pub. IAMAP, 1-16.
- Kennett, J.P. and R.C. Thunell (1975), "Global increase in quaternary explosive volcanism," Science 187, 497-503.
- Lamb, H.H. (1970), "Volcanic dust in the atmosphere with a chronology and assessment of its meteorological significance," Phil. Trans. Roy. Soc. London A266, 425-533.
- Lamb, H.H. (1972), Climate: Present, Past and Future, Vol. I: "Fundamentals and Climate Now," Methuen & Co., Ltd.
- Landsberg, H.E. (1970), "Man-made climatic changes," Science 170, 1265-1274.
- Landsberg, H.E., and J.M. Albert (1974), "The summer of 1816 and volcanism," Weatherman 27, 63-66.
- Landsberg, H.E. (1975), private communication, 2 January.
- Macdonald, G.A. (1972), Volcanoes, Prentice-Hall, Inc., Englewood Cliffs, NJ.
- Manabe, S., and R.T. Wetherald (1967), "Thermal equilibrium of the atmosphere with a given distribution of relative humidity," J. Atmos. Sci. 24 (3), 241-259.
- Mitcheil, J.M., Jr. (1961), "Recent secular changes of global temperature," Ann. N.Y. Acad. Sci. 95, 235-250.
- Mitchell, J.M., Jr. (1970), "A preliminary evaluation of atmospheric pollution as a cause of the global temperature fluctuation of the past century," in Global Effects of Environmental Pollution, S.F. Singer (ed.), Springer-Verlag, N.Y., 139-155.
- Mitchell, J.M., Jr. (1971), "The effect of atmospheric aerosols on climate with special reference to temperature near the earth's surface," J. Appl. Meteorol. 10 (4), 703-714.
- Mitchell, J.M., Jr. (1974), private communication, 18 November.
- Mitchell, J.M., Jr. (1975), "A reassessment of atmospheric pollution as a cause of long-term changes of global temperature," in *The Changing Global Environment*, S.F. Singer (ed.), Reidel, Dordrecht, 149-175.

OLIVER

Reitan, C.H. (1971), "An Assessment of the Role of Volcanic Dust in Determining Modern Changes in the Temperature of the Northern Hemisphere," Ph.D. Thesis, University of Wisconsin.

Volz, F.E. (1972), "Normal and volcanic turbidity from Smithsonian mountain solar spectrobolometry 1905 to 1950 and comparison with recent data," personal preprint cited in Junge (1974).

Wexler, H. (1951), "On the effects of volcanic dust on insolation and weather," Bull. Amer. Meteorol. Soc. 32, 1.

APPENDIX A

COMMENTS ON CERTAIN VOLCANIC ERUPTIONS

The large eruption of Krakatoa, on which much of the discussion in this paper is based, took place 26-27 August 1883 at 6°S and 105.5°E, although smaller explosive phases started 20 May 1883 (Lamb, 1970). Estimates of the amount of solid matter blown up range from 6 to 18 km³ (Lamb, 1970). Lamb suggests that 6 km³ ($\approx 10^{10}$ tons) and Deirmendjian (1972) that 4 km³ were dispersed as dust in the atmosphere; only a small portion, however, went into the stratosphere (1/100 used by Mitchell, 1970; 1/600 according to Deirmendjian, 1972; recognized but not given by Lamb). Losses of 20-30% in the direct solar beam were noted essentially worldwide, occurring as long as two or three years after the eruption; much of this loss (about 85% (Budyko, 1974b)) was made up by an increase in the diffuse radiation.

Several estimates of the stratospheric dust loading from this event are available (although it is not clear as to what degree they are independent), as follows:

Author	Global Stratospheric Burden
Mitchell (1970)	10 ⁸ tons initially; however, only half this value was assumed to be effective the first year (50 million tons)
Junge (1974), based on Volz (1972)	32×10^6 tons, global, a year after the event; apparently roughly the same in both hemispheres
Deirmendjian (1972)	30 × 10 ⁶ tons, assuming unit density, computed from optical criteria (a "few months" after the event)

Portions of the dust reached great heights (< 27 km) according to Lamb (1970); however, the mean stratospheric cloud height must have been much less. Mitchell (1970) ascribes a residence time of 14 months to the dust so injected. Junge (1974), quoting Volz (1972), gives a worldwide loading of 32 million tons one year after the event; correcting for an assumed exponential decay (14 months' residence time), an initial figure of 75 million tons results. Deirmendjian,

however, assuming unit density, estimates 30 million tons, which, correcting for say three months' time, would imply 37 million tons initially; if a density of say 1.7 gm/cc is used, the corrected initial value would be 63 million tons. Presumably, somewhat less than half these global figures should be used for Northern Hemisphere loadings - in fact, much less if the Agung experience (see below) is representative. However, on the basis of the fact that Junge (1974) implies substantially equal radiation-loss values in both hemispheres a year after the event, the split may have been almost equal. Any assigned value involves some arbitrariness; a Northern-Hemisphere value of 25 million tons was selected, or half of Mitchell's first-year global value, decaying directly from this value thereafter. This figure was then used in prorating subsequent events, using Mitchell's tabulation of magnitudes (see Table 1, main text), except as noted below for Katmai and Agung.

Two small (0.5 million tons each) northernhemisphere events also took place in 1883. However, under the assumptions of this work (Table 2, main text), they were supposed to have already affected the 1883 starting-point climatic anomaly and were ignored relative to Krakatoa for the subsequent period.

No independent studies of the large eruptions of 1902-04 were available. Mitchell's estimates, prorated, and his split, in terms of the years involved, were used.

In the case of Katmai (1912), Deirmendjian (1972) gives an estimate of 13.4 million tons (at unit density). This particular eruption involved very great discrepancies in estimates, ranging, according to Lamb (1970), from 0.006 to 21 km³ of solid ejecta. Deirmendjian estimated Katmai at 44% of Krakatoa in total dust output, which would have given Katmai a magnitude in the Northern Hemisphere roughly equal to Krakatoa's. Junge (1974) quotes a figure of 16 million tons, 0.2 years after the eruption, which, at 14 months' residence time, corrects to 19 million tons initially. Junge's (Volz's) quoted value, as noted earlier, for the Krakatoa event on a global basis corresponds (at 14 months' residence time) to 75 million tons initially, thereby putting Katmai at about 25% of Krakatoa, or 50% in the Northern Hemisphere. Normalizing, by using 50% of the value used for Krakatoa (25 million tons), a figure of 12.5 million tons is obtained. Lamb's D.V.I. for Katmai in the Northern Hemisphere is only 15% of that for Krakatoa. A figure of 13 million tons was used.

OLIVER

In the case of Agung (1963), it has been reported that most of the dust remained in the Southern Hemisphere: Junge (1974) quotes a value for the Northern Hemisphere as 2 million tons, 0.8 years after the eruption (versus 12 million tons in the Southern Hemisphere). If the total of 14 million tons is corrected, assuming 14 months' residence time, to the initial injection, a figure of 28 million tons is found, in essential agreement with the 30 million tons quoted by Mitchell (1970). Deirmendjian, however, gives only 9 million tons at unit density; at a density of 1.7 gm/cc, the figure would be 15.3 million tons. By the rules of Table 2, 15 million tons at the latitude of Agung should have put 7.5 million tons on the Northern Hemisphere; however, the Junge (1974) figure of 2 million tons corrects only to 4 million tons initially. These data could not all be rationalized. A figure of 5 million tons was assigned, with a figure twice this also considered (see Figure 8).

Considerable question also exists in the Hekla (1947), Mt. Spurr (1953), and Bezymyannaya (1956) eruptions, all in the far north. The values shown for Hekla and Mt. Spurr were again prorated from Mitchell's figures. Much smaller values would be estimated from the small total-dust figures quoted by Lamb. The Bezymyannaya figure of 5 million tons was also doubled (Figure 8) for illustrative purposes.

In view of the large uncertainties in the dust estimates, no attempt was made to adjust these figures as residence-time assumptions were varied in the main text.

APPENDIX B

EFFECTS OF A TIME-VARYING TO

As discussed in the main text, any assumption as to how T_0 , the hypothetical steady-state temperature in the absence of stratospheric dust, might have varied with time over the 1883-1968 period would be somewhat or totally arbitrary. In general, any such assumptions involve additional constants, and additional constants are always to be avoided in an empirical study. (A sinusoidal relationship, for example, would involve constants for phase, amplitude, and period.) It was, however, desired to obtain some comprehension of the effects of such changes, using some approach compatible with that used in the rest of the study. For this purpose, the assumption was made of an exponential relationship involving one additional constant (γ) , of the following type.

$$T_0 = T_{0(1883)} + \beta \left[1 - e^{-\gamma(t-t_0)}\right]$$
, (B.1)

where t-t₀ represents the number of years after 1883. With $\gamma = \infty$, this expression reduces to that given earlier; with γ finite and not equal to λ , the expression becomes

$$\theta = (\theta_0 - \beta) e^{-\lambda(t-t_0)} + \beta$$

$$-\frac{\lambda \alpha M_0}{\lambda - k} \left[e^{-k(t-t_0)} - e^{-\lambda(t-t_0)} \right]$$
(B.2)

$$+\frac{\lambda\beta}{\gamma-\lambda}\left[e^{-\gamma(t-t_0)}-e^{-\lambda(t-t_0)}\right]$$

For sequential (yearly-steps) use, the value of β in the last term must be reduced after each period by $\beta_{(t-1)}e^{-\gamma}$, just as the dust masses must be reduced by $M_{t-1}e^{-k}$.

If a value β is taken, based on the difference between mean temperature in the 1930's and the reference temperature used by Budyko (≈ 0.3°C), then values of γ can be assumed, and the various results will show the difference between a square-wave (or preexisting-anomaly) assumption ($\gamma = \infty$) and finite rates of warming. One such set of results is shown in Figure B-1. In general, it is found that a finite warming rate (G = γ^{-1} = 10 to 20 years) had only moderate impact (17%) on the required value for a with a given climatic response time, but considerable effect on the shape of the resulting curve. The formulation (B.2) was studied briefly to see when a short residence time (four years in Figure B-1) could be made to fit the full 1883-1968 curve. A rough fit was found with G = 20 years and C = 4 years, with $\alpha = 0.10$, showing that short- and long-period results may be compatible (and the shortperiod values about correct) if underlying trends can be quantified. It should be stressed, however, that Eq. (B.1) is completely arbitrary.

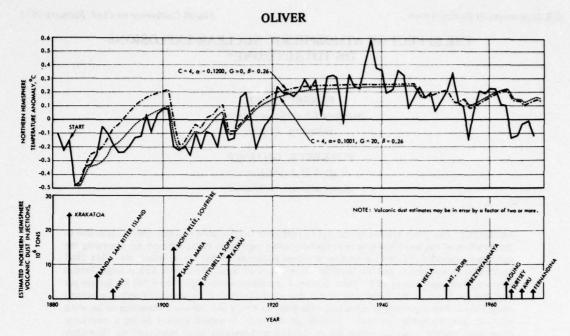


Figure B-1. Analytical results illustrating the effects of a change in equilibrium mean temperature with time according to a specified path.

THE EFFECT OF ATMOSPHERIC NUCLEAR EXPLOSIONS ON TOTAL OZONE*

ERNEST BAUER
Institute for Defense Analyses
Arlington, Virginia

FORREST R. GILMORE R & D Associates Santa Monica, California

ABSTRACT: This paper reviews the current knowledge of the depletion of stratospheric ozone due to the injection of oxides of nitrogen from thermonuclear explosions in the atmosphere, discussing the theoretical calculations, the ground-based observations of global ozone after the 1961-1962 multimegaton test series, and the satellite observations of local effects following a single French thermonuclear explosion in 1970. There is general agreement on the approximate NO production per megaton yield and on the subsequent ozone depletion expected to be associated with the various nuclear tests. This depletion, as calculated principally by Chang and Johnston, extending earlier work of Foley and Ruderman, is small – typically of the order of several percent during a reasonable observation interval – and lies within the probable error of available ozone measurements. Thus while there is no real disagreement between prediction and observations and no reason to doubt the validity of the predictions of ozone depletion, existing atmospheric data do not provide a statistically significant demonstration of the catalytic destruction of ozone by oxides of nitrogen.

INTRODUCTION

Johnston (1971) pointed out a potential major environmental hazard due to stratospheric aircraft flight. Aircraft engines emit oxides of nitrogen (NO_x = NO + NO₂), which under stratospheric conditions will decrease the amount of ambient ozone by a catalytic reaction cycle. A reduction of ambient atmospheric ozone will lead to an increase in solar ultraviolet (UV) flux at ground level. Since most of the biologically harmful radiation is normally filtered out by ozone absorption, such an increase in solar UV could have a variety of deleterious effects, ranging from increased levels of skin cancer and possible decreases in crop plant yields to accelerated deterioration of rubber and some plastics.

As a result of this and other environmental concerns, the Department of Transportation's Climatic Impact Assessment Program (DOT/CIAP) was established in 1971

...in order to determine regulatory constraints on flights in the stratosphere such that no adverse environmental effects result. Thus DOT/CIAP will assess, by 1974 report, the impact of climatic changes resulting from propulsion effluents of vehicles in the stratosphere, as projected to 1990.

In view of the short time scale of the program, the principal method of attack on the problem has consisted of measurements of ambient stratospheric NO_x and other potentially relevant species, supplemented by extensive computer modeling. To augment our confidence in these predictions, any kind of partial experimental simulation is worthy of investigation. Thus the suggestion by Foley and Ruderman (1972) that the injection of NO_x into the stratosphere by Soviet and U.S. thermonuclear explosions in the atmosphere in 1961-1962 provided such a simulation was both appropriate

^{*}This paper appeared in nearly identical form in Reviews of Geophysics and Space Physics (Vol. 13, No. 4, pp 451-458) in August 1975.

and timely, and has been the subject of considerable investigation.

The present paper reviews the current evidence on this problem. After a discussion of the total yield of NO per megaton (Mt) in an atmospheric nuclear explosion, and of the predicted global reduction of total ozone as a result of the multimegaton Soviet and U.S. nuclear tests of 1961-1962, the nature of ground-based global ozone measurements during the period 1957-1970 is reviewed. Predicted decreases in total ozone column are of the order of a few percent and would be extremely hard to extract from the noisy signal.

An opportunity for local observation of ozone reduction due to a specific thermonuclear explosion is provided by Nimbus IV satellite observations of the area above the French and Chinese thermonuclear tests in 1970. These data are reviewed; once again the results are not clearcut: in the one event in five tests in which the nuclear cloud was certainly viewed, an apparent local ozone decrease was observed, although it lies within the statistical error of the measurements.

A qualitative discussion of the chemistry and dispersion of the point release of a large amount of NO (corresponding to an atmospheric megaton nuclear explosion) is given to illustrate the difficulty of drawing useful conclusions from measurements on such a release.

The present discussion may prove disappointing to the reader in that its conclusions are neither clear-cut nor positive. Nevertheless, it has been written to point out to the physical scientist some of the limitations and complexities inherent in analyzing large-scale geophysical phenomena of this kind.

THE PRODUCTION OF NITRIC OXIDE (NO) BY ATMOSPHERIC NUCLEAR EXPLOSIONS AND ITS PREDICTED EFFECTS

When air is heated to a temperature of the order of 2000-4000K, which process requires an energy of ≈ 1 kt per 1000 tons of air (1 kt = 10^9 kcal $\approx 4.2 \times 10^{12}$ J = 1.2×10^6 kWh), 1-2% of the total air is transformed into NO. Figure 1 shows the equilibrium composition of heated air as a function of temperature at 0.1-atm pressure.

As the air cools below 2000K, those chemical reactions which tend to deplete the NO concentration become very slow, so that the net NO concentration stabilizes at about 1%. This heating and cooling of air is the dominant mechanism by which NO is produced in a nuclear explosion. The amount of NO thus produced has been calculated by a number of investigators, whose conclusions are listed in Table 1; for a more detailed review of the problem, see Gilmore (1975). All investigators agree that the net yield is in the range 1000-10,000 tons of NO per megaton yield.

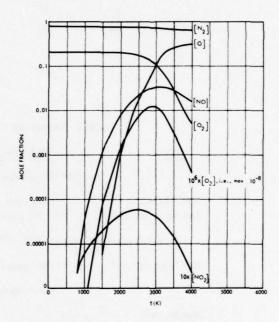


Figure 1. Equilibrium composition of hightemperature air ($\rho = 0.1$ atm; CO₂, H₂O, and their decomposition products are omitted).

During 1961-1962, massive thermonuclear atmospheric tests were carried out by both the United States and the USSR, and in 1970-1973, much smaller test series were carried out by France and China. The times, locations, and yields of these test series are listed in Table 2.

The degree of atmospheric ozone reduction depends significantly on the altitude of NO injection. Accordingly, estimates of fireball rise height are given in Figure 2.

Table 1. Calculated NO Production by Low-Altitude Nuclear Explosions

NO Produce of Yie		Calcul	ation Includes	
Molecules	kt	Shock	Late Fireball	Reference
0.5×10^{32}	3	x		Zeldovich and Raizer (1967)
0.3-2	1.5-10		x	Foley and Ruderman (1972)
0.17-1	1-5		x	Johnston et al. (1973)
0.3-1.5	1.5-8		x	Foley and Ruderman (1973)
1-2.5	5-12		x	Simons and Caledonia (1973)
1	5	x		Goldsmith et al. (1973)
0.4-1.5	2-8	x	x	Gilmore (1975)

Table 2. Atmospheric Thermonuclear Tests Since 1961

Date	Total Yield, Mt	Reference
	USSR (Novaya Zemlya, 72°-	77°N, 52°-58°E)
Sept. 14-Oct. 31, 1961	120 (25, 58 Mt, etc.)	Foley and Ruderman (1973, Table 5)
Aug. 5-Dec. 24, 1962	180 (20, 30 Mt, etc.)	Foley and Ruderman (1973, Table 5)
U.S.A. (Christmas	Island, 1.5°N, 157°W, and.	Johnston Island, 16.5°N, 169°W)
May 2-Oct. 31, 1962	37 ('Mt range')	Foley and Ruderman (1973, Table 5)
	France (Mururoa, 22°	S, 139°W)
May 30, 1970	1	Telegadas (1974a, Table 8)
July 3-4, 1970	2	Telegadas (1974a, Table 8)
Aug. 14, 1971	2	Telegadas (1974a, Table 8)
	China (Lop Nor, 40°	N, 90°E)
June 17, 1967	3	Zander and Araskog (1973)
Dec. 27, 1968	3	Zander and Araskog (1973)
Sept. 29, 1969	3	Zander and Araskog (1973)
Oct. 14, 1970	3	Telegadas (1974, Table 8)
June 27, 1973	2-3	Telegadas (1974b)

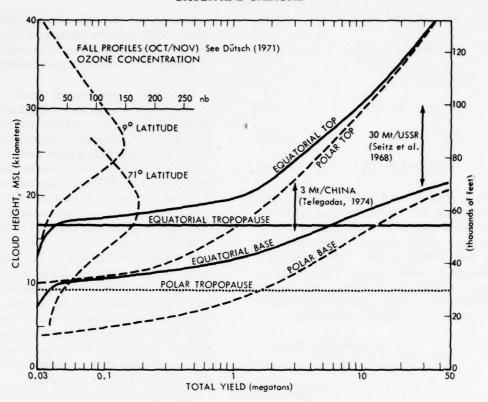


Figure 2. Fireball rise height as a function of yield (from Peterson, 1970) compared with the ambient ozone profile (from Dütsch, 1971) for both equatorial and polar conditions. For the nuclear cloud 'equatorial' refers to 0°-30° latitude; 'polar' refers to 30°-90°. Peterson's polar estimates of cloud rise appear to be too high, as judged by radioisotopic measurements of Soviet tests: see, in particular, the results of Seitz et al. (1968) for a 30-Mt test. The results of Telegadas (1974) for Chinese mid-latitude 3-Mt tests are also shown.

The practical question, which was first raised by Foley and Ruderman (1972), is the following: Since the amounts of NO produced by these bombs – especially by the very large Soviet test series of 1961-1962 – are of geophysically significant magnitude, how large a decrease of atmospheric ozone would be expected, and was such a decrease observed?

Our present understanding of the atmospheric ozone photochemical balance is outlined in Table 3 and the equations below (Johnston, 1975).

-Chapman's oxygen-only scheme

$$O_2 + h\nu(UV) \rightarrow 20 \tag{1}$$

$$0 + 0 + X \rightarrow 0_2 + X$$
 (2)

$$0 + O_2 + X \rightarrow O_3 + X$$
 (3)

where X is the third-body molecule.

$$O_3 + h\nu(UV \text{ or visible}) \rightarrow O_2 + O$$
 (4)

$$0 + 0_3 \rightarrow 20_2$$
 (5)

-Water cycle (important at high altitudes)

$$HO + O_3 \rightarrow HO_2 + O_2 \tag{6}$$

$$HO_2 + O \rightarrow OH + O_2 \tag{7}$$

Net:
$$O + O_3 \rightarrow 2O_2$$
 (8)

$$NO + O_3 \rightarrow NO_2 + O_2 \tag{9}$$

$$NO_2 + O \rightarrow NO + O_2$$
 (10)
 $Net: O + O_3 \rightarrow 2O_2$ (11)
 $-ClO_x \text{ cycle}$ (12)
 $ClO + O \rightarrow Cl + O_2$ (13)

Net: $0 + O_3 \rightarrow 2O_2$ (14)

Table 3, which is based on the above reactions, indicates that the Chapman or 'oxygen-only' set of chemical reactions, which produce all the atmospheric ozone, account for the removal of only about 18% of the ozone. The largest single mechanism for removing ozone from the atmosphere is provided by the NO_x species, through the reaction cycle (9)-(11), which is several times faster than the direct oxygen reaction (5).

Table 3. Global Ozone Balance for Formation and Destruction of Ozone by Various Mechanisms (Johnston, 1974a)

Mechanism	Relative Rate, %	
Formation, O ₂ + sun	+100	
Transport to troposphere	-1	
Destruction by O and O ₃	-18	
Destruction by water reactions	-11	
Destruction by NO _x catalysts	-50 to -70	
Destruction by CIO _x , MO _x ,* or other	-20 to 0	

^{*}M denotes metal.

The effects of the 1961-1962 test series on atmospheric ozone have been estimated by Foley and Ruderman (1972, 1973), Johnston et al. (1973), and Chang and Duewer (1973). Nitric oxide production is of the order of 10³² molecules or 5000 tons per Mt (Table 2). In 1961-1962, some 300 Mt were exploded, principally in the Soviet test series of fall 1961 and fall 1962, so that the net injection rate per year was of the order of 10³⁴ molecules NO. Many of these bombs were very large (see Table 2) and produced fireballs that rose above 20 km (Figure 2), where the mean atmospheric residence time

for injectants is of the order of 1-5 yr (Reiter and Bauer, 1975). Thus the atmospheric burden due to bomb tests is comparable to the total amount of natural NO_x , which is approximately 2 \times 10^{34} molecules.

By simply comparing the amount of NO injected from the bomb tests with the amount of ambient NO, (which at that time was estimated to be 4 X 1034 molecules), Foley and Ruderman (1972, 1973) suggested, without making calculations, that the total-ozone reduction should be greater than 10%. The first model calculation of the ozone decrease due to the 1961-1962 nuclear tests was carried out by Johnston et al. (1973). They used a production rate of 1×10^{32} NO molecules, Mt and assumed that the NO would have the same distribution as the radioactive debris. From the observed distribution of strontium 90 in the summer of 1963, they derived the corresponding distribution of nitrogen oxides and calculated steady-state ozone reductions from 3.5 to 6.3% as a function of latitude in the Northern Hemisphere. The average ozone reduction was 5% in the Northern Hemisphere and less than 1% in the Southern Hemisphere.

A more detailed model calculation was carried out by Chang and Duewer (1973). They assumed a production rate of 0.5×10^{32} NO molecules/MT and computed the effects of the pulsed input of nuclear bursts from 1957 through 1962, including the vertical transport and removal of the nitrogen oxides, in a timedependent one-dimensional model of the Northern Hemisphere. They predicted an ozone reduction in the Northern Hemisphere of 4% in 1963, falling to 2% by late 1965. However, they used formulas for the nuclear injection altitudes suggested by Foley and Ruderman (1972, 1973) without the latter's correction for the fact that the polar tropopause lies lower than the equatorial tropopause. Thus their injection altitudes are higher than those given by Peterson (1970) and considerably higher than those suggested by radioactive-debris data (see Figure 2). This difference tends to give an overestimate of the ozone depletion.

The reduction of ozone is calculated to be small because most of the tests were at high latitudes (> 70°N) during or just before the polar night. Most ozone near the poles arrives there by transport from the ozone formation region,

which is above 23 km in the tropics, above 28 km in the summer temperate or polar zones, and nonexistent in and near the winter pole. Relatively little nitric oxide injected into the lower polar stratosphere ever reaches the ozone source region.

To compare these calculated effects with observations, it is necessary to survey existing data on worldwide ozone distribution, and this is done in the following section.

GROUND-BASED GLOBAL OZONE OBSERVATIONS AND THE 1961-1962 ATMOSPHERIC NUCLEAR EXPLOSIONS

Prior to the International Geophysical Year (1957-1958) there were very few stations worldwide providing long-term records on total atmospheric ozone. Indeed, only the relatively closely spaced stations at Arosa, Oxford, and Tromsö have obtained fairly continuous data since the 1930's, although several other stations have records for a few of these early years. Selected stations since 1960 have been analyzed by Komhyr et al. (1971) and by Goldsmith et al. (1973), and the complete body of data since 1957 has been analyzed by London and Kelley (1974) and by Johnston et al. (1973). The data since the 1950's have also been considered by Angell and Korshover (1973) and Christie (1973). Like most meteorological data, these ozone records show variability on a variety of scales of time and distance: Figure 3 indicates the nature of the global data after the smoothing introduced by taking a 12-month running mean.

One significant source of error in the data is that the Soviet-bloc instrument, the M-83 filter ozonometer, gives results that are not strictly comparable with those of the Dobson prism spectrophotometer used elsewhere. A side-byside comparison of an M-83 and a Dobson meter has shown that the filter instrument reports systematically greater amounts of ozone (up to 30%) than the prism meter at low solar angles (winter) and lower amounts (about 6%) for nearly overhead sun (summer). Also, the filter instrument overestimates ozone relative to the prism instrument under hazy conditions and has a standard deviation of readings about five times as great as the Dobson meter (Bojkov, 1969). Moreover, the global coverage of ground-based

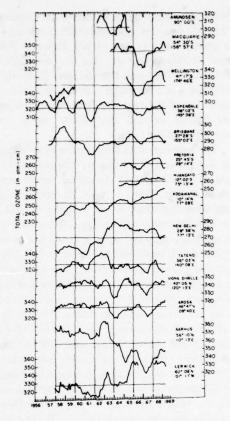


Figure 3. Twelve-month running mean of total ozone (Newell, 1972). During the period from mid-1961 to late 1962 there was massive nuclear testing in the atmosphere, but no unambiguous effect of this on ozone can be seen in the figure.

ozone instrumentation is far from adequate. In many cases, a ground-based station was operated for a few years only; the coming and going of stations at various parts of the world is capable of introducing large distortions in a global-trend analysis. These features suggest possible large systematic errors in a trend analysis.

One general conclusion of all the workers cited above is that during the 1957-1970 time period there was an overall increase of 5-10% in total ozone in the Northern Hemisphere but no significant change in the Southern Hemisphere.

More specifically, Johnston et al. (1973) find a decrease for 1957-1961, followed by a substantial increase in 1962-1970. A comparable effect is found by other workers (in particular, London and Kelley (1974)). H.S. Johnston

(1974a; see Appendix A of Bauer and Gilmore, 1975) suggests that this minimum is related to the nuclear tests of 1961-1962. However, J.K. Angell (1974) points out that the March 1961 minimum in the 'quasi-biennial' (or '26-month') oscillation was a particularly strong one; indeed, Angell and Korshover (1973) in their analysis were unable to find any effect due to the 1961-1962 nuclear tests.

The long-term data were examined by Angell and Korshover (1973) and by Christie (1973), especially with respect to cyclic trends with periods longer than 1 year. It seems wellestablished that there is a quasi-biennial oscillation in total ozone amounting to about 4% for the stations considered by Angell and Korshover (1973). At Tromsö and at Arosa before 1957 there was a strong correlation of total ozone with the 11-year solar cycle. The full amplitude of this change was almost 10% at Tromsö and about 5% at Arosa (Angell and Korshover, 1973). The amplitude of this change for Christie's 'global ozone' (largely Arosa, Oxford, and Tromsö) was greater than 10% for two complete solar cycles, 1933-1955. In the Southern Hemisphere, Angell and Korshover found a correlation of total ozone with the solar cycle with an amplitude of just over 1% for the period 1957-1970. For the period 1957-1970 in the Northern Hemisphere the correlation of total ozone with the solar cycle is very uncertain.

The whole problem of the correlation of ozone with the solar cycle is quite controversial (see Willett, 1962; London and Haurwitz, 1963; London and Oltmans, 15 73; Paetzold, 1973). An explanation of the phase-shifted correlation between solar activity and global ozone has been offered by Ruderman and Chamberlain (1975) and Nicolet (1975), following up Warneck's (1972) suggestion that cosmic rays produce ionization and thus nitrogen atoms and nitric oxide molecules in the stratosphere. Cosmic rays are steered into the earth's polar regions by magnetic fields. These magnetic fields are modulated by the stream of charged particles from the sun, which varies with an 11-year sunspot cycle, and the NO molecules produced in this way reduce the ozone concentration by the wellknown NO_v-O₃ catalytic cycle.

Johnston et al. (1973; see also Appendix A of Bauer and Gilmore, 1975) think that these statistical analyses of long-term global ozone data

indicate that ozone was affected by the nuclear tests of 1961-1962, especially since no effect was seen in the Southern Hemisphere but an ozone minimum occurred in the Northern Hemisphere between 1961 and 1963.

There were two other processes operating during this 1961-1963 time period, however, which might have affected the ozone, namely, a massive volcanic eruption of Mt. Agung (8.5°S, 115.5°E, February 10-March 17, 1963) and a breakdown of the 'quasi-biennial oscillation' in the atmospheric motion about this time. Thus Angell and Korshover (1973), in an analysis of quasi-biennial and long-term fluctuations in total ozone, suggest that the Mt. Agung eruption caused a breakdown of the quasi-biennial, total-ozone oscillation in the Southern Hemisphere subtropics, with anomalously high ozone values a few months after the eruption.

A major volcanic eruption might change the ozone level directly, due to the heterogeneous decomposition of ozone on dust and other material injected into the stratosphere by the eruption, as well as indirectly, by affecting the atmospheric motions. It is, of course, not clear how a volcanic eruption in the Southern Hemisphere subtropical region can affect the ozone level in the Northern Hemisphere, except possibly through dynamics. For an indication of some of the other complexities of this situation, see Hofmann et al. (1974), which relates changes in tropopause height to the stratospheric aerosol burden and ozone level.

We do not feel that presently available data permit us to decide between such divergent explanations of changes in ozone. The ground-based data available during this time (1957-1970) have not yet proved adequate to provide an unambiguous interpretation; it may be hoped that satellite data, with their far more detailed global coverage, will resolve this discrepancy.

SATELLITE OBSERVATIONS: NIMBUS IV RECORDS OF THE FRENCH AND CHINESE TESTS OF 1970 AND LATER

It is clear from the previous section that it is very difficult to detect significant bomb-induced changes in total ozone from ground-based instruments. However, in April 1970 the Nimbus IV

satellite was launched with both UV and IR sensors for total ozone, providing essentially global coverage. This raises the possibility of detecting changes in total ozone column by directly observing the nuclear cloud several hours or days after the detonation. A simple calculation of the ozone depletion by J.S. Chang of the Lawrence Livermore Laboratory (see Appendix B of Bauer and Gilmore, 1975) indicates a 5-10% local depletion in ozone under these conditions. Even this is not a simple measurement, however, because the ozone data show considerable natural fluctuations. Accordingly, independent nuclear cloud-tracking data are desirable to distinguish local ozone minima due to explosions from those due to natural atmospheric processes.

Of the five thermonuclear tests that could have been observed by Nimbus IV, useful data

were obtained only for the French test of May 30, 1970. Here Miller et al. (1974) observed, 3 hours after detonation, a small ($\approx 1\%$) minimum on the UV ozone sensor near the position of the nuclear cloud, as located by an IR sensor on the same satellite. This minimum was not observed on the previous or following day (see Figure 4). A comparable signal was also observed with an IR ozone sensor. To interpret the signals, we quote from the summary of Miller et al. (1974):

To summarize, we have presented one (1) case where the BUV ozone sensor field of view happened to co-locate with a stratospheric cloud resultant from an atmospheric nuclear test. This particular ozone value happened to be lower than either of the points to the north or south and does not appear to be associated with any other rela-

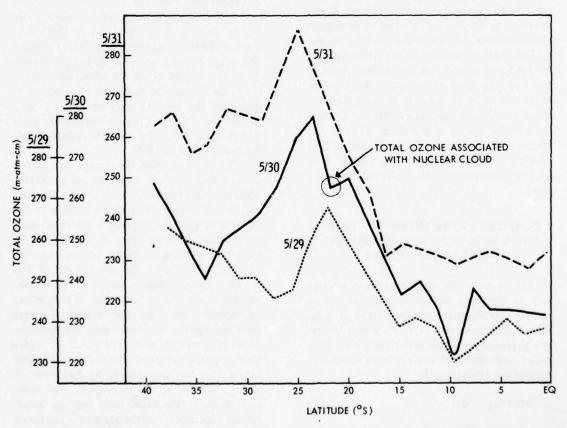


Figure 4. Meridional cross-sections of total ozone on May 29-31, 1970 (Miller et al., 1974). Note the minimum in total ozone at 22°S latitude on May 30, which has no corresponding feature on May 29 or 31. This feature is interpreted as being due to the French thermonuclear explosion which had occurred 3 hours earlier.

tive minimum in this region. However, because the ambient ozone is not defined in this region, we cannot assign an accurate relative number to this minimum. In addition, as the results of both the BUV and IRIS measuring techniques are model dependent, we do not feel that a definite statement can be made, at this time; that this minimum was caused by the increase of nitric oxide by the nuclear weapons test. As Chang (private communication) has estimated that for a device of this magnitude (about 1 megaton) the ozone depletion should be less than 1% from ambient at 3 hours from detonation, it is our view that we must await further results to clarify the situation.

The following supplementary information has been provided by Miller and Krueger. On May 30, 1970, there were IR pictures of the nuclear cloud which showed that the satellite was actually looking at the cloud; in this case the local ozone minimum shown in Figure 4 was observed. By May 31 the nuclear cloud was no longer observed, and there was no evidence for the local ozone minimum on the orbit closest to the predicted position of the nuclear cloud at that time. In none of the other four nuclear events was there comparable tracking evidence which would have established that the satellite was actually looking at the cloud. Thus on the French test of July 4, 1970, Christie (1974) observed nothing significant, presumably as a result of inadequate tracking information on the cloud.

QUALITATIVE DISCUSSION OF NITRIC OXIDE INJECTIONS BY ATMOSPHERIC NUCLEAR EXPLOSIONS

Let us now ask specifically what we can learn by observing the ozone reduction associated with atmospheric thermonuclear explosions. Table 3 and reactions (1)-(10) show that laboratory photochemistry and analysis of atmospheric species concentrations and residence times suggest that the catalytic cycle

$$NO + O_3 \rightarrow NO_2 + O_2 \tag{9}$$

$$NO_2 + O \rightarrow NO + O_2 \tag{10}$$

Net:
$$0 + 0_3 \rightarrow 20_2$$
 (11)

is the principal mechanism for the removal of atmospheric ozone. It would be very desirable to obtain a verification of this statement by measurements taken after atmospheric nuclear explosions. It would be even more useful if such measurements could give information on the mean residence time of NO_x in the lower stratosphere, since this residence time is important for predicting the effects of stratospheric aircraft on total ozone but is very difficult to obtain by other means.

A 100-Mt test series, like that of 1961 or 1962, injects a total amount of NO_x equal to perhaps 10-25% of the ambient atmospheric burden and has been predicted by Johnston et al. (1973) and by Chang and Duewer (1973) to produce a 4-5% reduction in total ozone in the Northern Hemisphere. Unfortunately, the data are not good enough either to confirm or to contradict this prediction.

A 2-Mt atmospheric nuclear explosion in the tropics, such as the French test of 1970, produces a cloud containing about 10,000 tons of NO, whose top rises to about 20 km (see Figure 2). In the tropics, about 9% of the total ozone lies below 20 km, and as a result of atmospheric dispersion the concentration of injected NO $_{\rm X}$ equals the ambient ozone concentration near 20 km some 2-3 days after the injection (cf. Bauer and Gilmore, 1975).

The direct reaction (9) is quite fast, with a characteristic time of some minutes at 20 km, while reaction (10) is very much slower. Thus the dip in total ozone observed on Nimbus IV by Miller et al. (1974) and possibly associated with the nuclear explosion (see Figure 4) can be explained entirely in terms of reaction (9) without reference to the other parts of the catalytic cycle. This is rather disappointing, because if several parts per billion of NO, in the stratosphere control the concentration of several parts per million of ozone, each NO molecule must be recycled some thousands of times through reactions (9) and (10) or their equivalent before it is lost (presumably by formation of HNO₃, diffusion to the troposphere, and eventual rainout). One might hope that an 'atmospheric experiment' of the scale of a release of the order of 10,000 tons of NO would be large enough to verify this catalytic cycle and loss rate of NOx, but in fact we see that the observations

of Nimbus IV at best merely verify the direct reaction (9), which is well established in the laboratory.

It is simple to do a comparable analysis for a much smaller release (see, e.g., Bauer and Gilmore, 1975), and one can show that smaller releases, whose identity and integrity (i.e., observability) are dissipated much faster than those of a bigger release, cannot serve to demonstrate anything other than the well-known direct reaction (9).

CONCLUSIONS

- 1. There exist worldwide ozone data from about 1957 onward that can be used to determine long-term global trends, on a scale of a decade or a solar 11-year cycle. The introduction of satellite data from 1970 onward provides a dramatic improvement in the quality of the data, insofar as they are continuous.
- 2. There is general agreement within a factor of 3 up or down on the predicted ozone depletion due to NO_x injection by the 1961-1962 atmospheric thermonuclear explosions, and the predicted depletion falls within the random variability of the available data. While there is certainly no disagreement between observations and predictions, this is not the same as a positive confirmation.
- 3. Satellite observations from Nimbus IV of the French and Chinese thermonuclear explosions of 1970 and later provide little definite information; in only one out of five events has any effect been observed, and this was small (within the observational error) and, if real, can be explained in terms of the well-studied direct reaction between NO and O_3 . Thus again these satellite observations provide no confirmation or refutation of the stratospheric NO_x - O_3 cycle, nor do they provide the lifetime of NO_x injected into the stratosphere.

ACKNOWLEDGMENTS

This work was supported by the Climatic Impact Assessment Program of the Department of Transportation under contract DOT-OS-30057. Many people have helped in providing data and critical comments: we should particularly like to thank J.K. Angell (NOAA-ARL), J.S.

Chang (LLL), P. Cutchis (IDA-STD), P. Gold-smith (U.K. Meteorological Office), H.S. Johnston (University of California), A.J. Krueger (NASA-GSFC), R. Penndorf, and M. Ruderman (Columbia University).

REFERENCES

- Angell, J.K. (1974), private communication.
- Angell, J.K., and J. Korshover (1973), "Quasi-biennial and long-term fluctuations in total ozone," Mon. Wea. Rev. 101, 426-443.
- Bauer, E., and F.R. Gilmore (1975), "Effect of atmospheric nuclear explosions on total ozone," Institute for Defense Analyses Paper IDA 1076, done for U.S. Dept. of Transportation, DOT-TST-75-67.
- Bojkov, R.D. (1969), "Differences in Dobson spectrophotometer and filter ozonometer measurements of total ozone," J. Appl. Meteorol. 8, 362-368.
- Chang, J.S., and W.H. Duewer (1973), "The possible effect of NO_x injection in the stratosphere due to past atmospheric nuclear weapons tests," presented at the International Conference on the Environmental Impact of Aerospace Operations in the High Atmosphere (Denver), AIAA paper 73-538.
- Christie, A.D. (1973), "Secular or cyclic change in ozone," Pure Appl. Geophys. 106-108, 1000-1009.
- Christie, A.D. (1974), "The use of BUV satellite observations to study ozone depletion processes," in Proceedings of the International Conference on Structure, Composition and General Circulation of the Upper and Lower Atmospheres and Possible Anthropogenic Perturbations (Melbourne), pub. IAMAP, 494-508.
- Dütsch, H.U. (1971), "Photochemistry of atmospheric ozone," Advances in Geophysics 15, 219-322.
- Foley, H.M., and M.A. Ruderman (1972), "Stratospheric nitric oxide production from past nuclear explosions, and its relevance to projected SST pollution," Institute for Defense Analyses Paper P-984 (Arlington, Va.).
- Foley, H.M., and M.A. Ruderman (1973), "Stratospheric NO production from past nuclear explosions," J. Geophys. Res. 78, 4441-4450.
- Gilmore, F.R. (1975), "The production of nitrogen oxides by low-altitude nuclear explosions," J. Geophys. Res. 80, 4553-4554.

- Goldsmith, P., A.F. Tuck, J.S. Foot, E.L. Simmons, and R.L. Newson (1973), "Nitrogen oxides, nuclear weapon testing, Concorde and stratospheric ozone," Nature 244, 545-551.
- Hofmann, D.J., J.M. Rosen, and T.J. Pepin (1974), "Influence of the tropopause height on the global stratospheric aerosol burden and implications for the recent increase in ozone," J. Appl. Meteorol. 13, 734-737.
- Johnston, H.S. (1971), "Reduction of stratospheric ozone by nitrogen oxide catalysts from supersonic transport exhaust," Science 173, 517-522.
- Johnston, H.S. (1974a), "Pollution of the stratosphere," Environ. Conserv. 1, 163-176.
- Johnston, H.S. (1974b), private communication.
- Johnston, H.S. (1975), "An overview of stratospheric chemistry," section 5.2 of CIAP Monograph 1, U.S. Dept. of Transportation, DOT-TST-75-51, 5-7-5-36.
- Johnston, H.S., G. Whitten, and J. Birks (1973), "Effect of nuclear explosions on stratospheric nitric oxide and ozone," J. Geophys. Res. 78, 6107-6135.
- Komhyr, W.D., E.W. Barrett, G. Slocum, and H.K. Weickmann (1971), "Atmospheric total ozone increase during the 1960's," Nature 232, 390-391.
- London, J., and M.W. Haurwitz (1963), "Ozone and sunspots," J. Geophys. Res. 68, 795-801.
- London, J., and J. Kelley (1974), "Global trends in total atmospheric ozone," Science 184, 987-989.
- London, J., and S. Oltmans (1973), "Further studies of ozone and sunspots," Pure Appl. Geophys. 106-108, 1302-1307.
- Miller, A.J., A.J. Krueger, C. Prabhakara, and E. Hilsenrath (1974), "Nuclear weapons tests and short-term effects on atmospheric ozone," in Preprints of the Second International Conference on the Environmental Impact of Aerospace Operations in the High Atmosphere (San Diego), pub. AMS, 81-84.
- Newell, R.E. (1972), "Climatology of the stratosphere from observations," in Proceedings of the Survey Conference (Cambridge, Mass.), U.S. Dept. of Transportation, Climatic Impact Assessment Program, DOT-TSC-OST-72-13, 165-185.

- Nicolet, M. (1975), "On the production of nitric oxide by cosmic rays in the mesosphere and stratosphere," Planet. Space Sci. 23, 637-649; also (1976), in this volume.
- Paetzold, H.K. (1973), "The influence of solar activity on the stratospheric ozone layer," Pure Appl. Geophys. 106-108, 1308-1311.
- Peterson, K.R. (1970), "An empirical model for estimating world-wide deposition from atmospheric nuclear detonations," Health Phys. 18, 357-378.
- Reiter, E.R., and E. Bauer (1975), "Residence times of atmospheric pollutants," Appendix A to Chapter 2 of CIAP Monograph 1, U.S. Dept. of Transportation, DOT-TST-75-51, 2-125 - 2-147.
- Ruderman, M., and J. Chamberlain (1975), "Origin of the sunspot modulation of ozone: Its implication for stratospheric NO injection," Planet. Space Sci. 23, 247-268.
- Seitz, H., B. Davidson, J.P. Friend, and H.W. Feely (1968), "Final Report on Project Streak: Numerical Models of Transport, Diffusion and Fallout of Stratospheric Radioactive Material," Rept. NYO-3654-4, prepared for the Atomic Energy Commission, by Isotopes, Inc., Westwood, NJ.
- Simons, G.A., and G. Caledonia (1973), private communication.
- Telegadas, K. (1974a), "Radioactivity Distribution in the Stratosphere from Chinese and French High Yield Nuclear Tests (1967-1970)," AEC Health and Safety Laboratory (N.Y.), Rept. HASL-281, 1-57, 1-107, 1-108.
- Telegadas, K. (1974b), private communication, November 1974.
- Warneck, P. (1972), "Cosmic radiation as a source of odd nitrogen in the stratosphere," J. Geophys. Res. 77, 6589-6591.
- Willett, H.C. (1962), "The relationship of total atmospheric ozone to the sunspot cycle," J. Geophys. Res. 67, 661-670.
- Zander, J., and R. Araskog (1973), "Nuclear Explosions 1945-1972, Basic Data," FOA4 Rept., Research Institute of National Defense, Stockholm, Sweden.
- Zeldovich, Y.B., and Y.P. Raizer (1967), Physics of Shock Waves and High Temperature Phenomena, Academic Press, New York (Vol. 2, 566-571).

INTERPRETATION OF LARGE-SCALE EXPERIMENTS

DISCUSSION

MACHTA: We've looked at three of the Chinese events, using meteorological trajectories to determine when the debris passed over Japan. In one case we actually confirmed this by monitoring radioactivity in the lower

stratosphere over Japan. In each case, the ozone level rose. In a case confirmed by radioactivity measurements, total ozone rose 30%, which is one of the largest rises we've ever seen from day to day. It did not occur at just one station; all the stations in Japan responded in the same way.

LABORATORY STUDIES OF STRATOSPHERIC OH AND CI REACTIONS

J.G. ANDERSON*, J.J. MARGITAN, M.S. ZAHNISER, AND F. KAUFMAN

University of Pittsburgh

Pittsburgh, Pennsylvania

ABSTRACT: Results of laboratory studies are presented for six OH-radical reactions and one Cl-atom reaction, $Cl + O_3 \rightarrow ClO + O_2$, using the discharge-flow configuration with resonance-fluorescence detection of either OH or Cl. The recombination reactions of OH with NO and NO₂ and the bimolecular reactions with O_3 , CH_4 , HCl, and HNO₃ were investigated over temperature ranges from about 230 to 450K (290 to 450K for CH_4 and HNO₃). Their stratospheric importance is pointed out. New data are presented for the $Cl + O_3$ reaction, the first step in the catalytic ClO_x chain, which show it to be about 40% slower at stratospheric temperatures than an earlier published estimate.

INTRODUCTION

It has become increasingly clear that the principal loss processes for "odd oxygen" (O + O₃) in the mid- and upper stratosphere, the region where the local steady state is controlled by photochemistry, consist of intricately interlocking catalytic cycles which involve the species O_X, HO_X, NO_X, ClO_X, and possibly still others, as well as many of their cross-products and combinations. From the simplicity of the Chapman scheme with its 4 steps we have advanced to the complexity of the O-H-N system with about 50 steps, 10-15 of which are of major importance, and to the Cl system with an additional 40 steps, 8-10 of which need to be known fairly accurately. As if that task were not enough to keep a battery of laboratory kineticists busy for many years, there are many other-processes whose rates must be known even though they are not directly involved in ozone catalysis, such as those which remove precursors of potential catalysts or others which represent source or loss processes for species whose measured altitude profiles may be used to deduce a one-dimensional eddy-diffusion coefficient.

In view of this urgent need it is well to set down the principal requirements for the acquisition of reliable rate data: (1) Elementary reactions ought to be measured as directly as possible, rather than being calculated from the results of bulk rate measurements in terms of complicated, assumed mechanisms. (2) The temperature dependence should be established experimentally over a sufficiently large range so as to make long empirical or theoretical extrapolations unnecessary. (3) Those molecular states (electronic, vibrational) which are not easily relaxed by collisions with inert carrier gas should be clearly identified and their course of reaction followed. (4) The pressure dependence should be investigated for those reactions (recombinations and dissociations) in which energy transfer is one of the major steps of the overall process.

This is not to say, of course, that bulk thermal or photochemical reaction studies cannot provide interesting and useful results when enough information is available on the overall mechanism, but the more direct methods whose versatility, sensitivity, and accuracy have been greatly improved in recent years - are clearly to be preferred. Two principal ones, the flash-photolysis and discharge-flow techniques, are compared in Table 1; it can be seen that these methods complement each other very well: Flash photolysis is relatively free from surface interference and operates well at high pressures; discharge-flow, on the other hand, is able to generate and bring together almost any desired species and follow their reaction under steadystate conditions by variation of the spatial position of a movable injector of one of the reactants or by similar variation of the source or detector. The work described here uses the

^{*}Dr. Anderson is now at the Department of Atmospheric and Oceanic Science of the University of Michigan.

discharge-flow technique in the fixed-source, fixed-detector, movable-reactant-injector configuration, and derives its high sensitivity from the application of resonance-fluorescence detection, a method also employed by some recent flash-photolysis studies. The present paper consists of two parts: (i) a brief review of the published results of kinetic data on six reactions of OH radicals, carried out mainly in an older apparatus, and (2) new work on the ${\rm Cl} + {\rm O}_3$ reaction in a new system.

Table 1. Comparison of Experimental Kinetics Techniques

Method	Advantages	Disadvantages
Flash photolysis	High sensi- tivity	Photolytic generation
	Absence of surface effects Wide pressure	Interference by diluents, reactants
	range	Reactive initial mixture
Discharge-flow	Wide range of	Surface effects
	production and detection methods	Limited pres- sure range
	High sensi- tivity	Data analysis in fixed detector configuration
	Steady-state measurement	- Comparation
	Short "mixed time" of reactants	

EXPERIMENTAL

The principle of our measurements has been described in several earlier publications (Anderson and Kaufman, 1972; Anderson et al., 1974; Anderson and Kaufman, 1973; Margitan et al., 1974; Margitan et al., 1975; Zahniser et al., 1974) and will be reviewed very briefly. Reactive species are generated upstream of the 2.54-cm-diameter flow tube in microwave discharges either directly (as for Cl atoms in dilute ($\leq 0.01\%$) Cl₂-He mixtures) or indirectly (as for OH radicals, which are produced by the H + NO₂ reaction from dilute, discharged H₂-He mixtures). At total pressures of 1 to 10 torr in inert carrier gas (He, Ar, N₂), i.e., densities of about 10^{17} cm⁻³, atom/radical reactants are thus

produced at densities of about 10¹¹ cm⁻³ and excess stable reactant is added at about 10¹³ cm⁻³ through a movable injector. High detection sensitivity for either OH or Cl of ≥ 10⁹ cm⁻³ thus keeps the reactive species at mole fractions of 10-8 to 10-6 and the other reactants at 10-3 to 10-4, and minimizes the perturbation of flow parameters by added reactants. Linear flow velocities range from 1 to 4 X 10³ cm sec⁻¹, and surface reactions are inhibited by coating the flow tube with metaphosphoric acid and heating it to 450K under vacuum. Under normal experimental conditions, the desired atom or radical reaction is studied under pseudo-first-order conditions and the competing surface removal reaction cancels out in the analysis, provided such removal is not affected by the added reactant. Nevertheless, its rate constant, kw, was measured repeatedly by generating the reactive species at varying positions in the flow tube. Values of kw of 10 to 15 sec-1 for OH and about 2 sec-1 for Cl were obtained, much smaller than the effective firstorder rate constants for the desired gas-phase reactions.

The OH + HCl measurements (Zahniser et al., 1974) and the present results on CI + O₃ were carried out in the new modular flow-tube apparatus shown in Figure 1, which is fitted with a vacuum uv monochromator and detector (McPherson, Model 218) and several fluorescence-scattering cells. For Cl-atom fluorescence measurements, the emission of a He-plus-trace-Cl₂ microwave discharge lamp was used at 134.72 nm, the strongest line of the ²P-²P transition. Under the chosen conditions this emission was slightly self-absorbed, but it maximized the ratio of signals in the presence and absence of Cl-atoms in the flow tube, where the optical depth was always kept very low, i.e., [Cl] < 10¹¹ cm⁻³. A typical semi-logarithmic

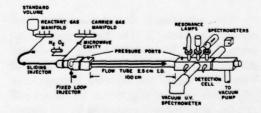


Figure 1. Diagram of apparatus.

decay plot of Cl due to its reaction with O_3 is shown in Figure 2. It covers a full two orders of magnitude. 65 such experiments were run at temperatures from 200 to 360K, as shown in the Arrhenius plot of Figure 3, with a least-squares fit given by the expression 2.17×10^{-11} exp [-338 cal mole⁻¹/RT] cm³ sec⁻¹. The random errors in repeated experiments at any one temperature were in the 8 to 10% range, but when systematic errors of all measured variables are included, the above rate-constant expression is thought to give values accurate to 20% (single standard deviation) over the experimental temperature range.

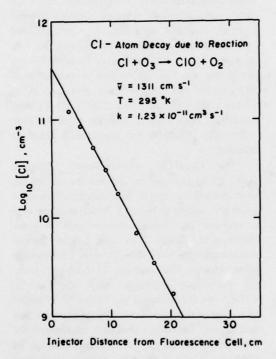
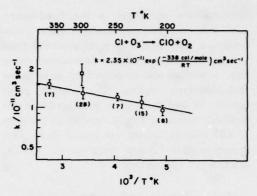


Figure 2. Typical experimental decay plot.

DISCUSSION

The earlier work on OH reactions is summarized in Table 2. The two recombination reactions with NO and NO_2 were investigated essentially at their low-pressure, third-order limit where they display the expected M-dependence (N_2 about twice as effective as He or Ar) and negative T-dependence controlled by the energy-dependent redissociation of the HNO_2^{\ddagger} or



O Clyne and Watson, (1.85 ± 0.36) x 10⁻¹¹ cm³ sec⁻¹

Figure 3. Arrhenius plot for Cl + O₃ reaction. D, Clyne and Watson, (1.85 ± 0.36) × 10⁻¹¹ cm⁻³ sec⁻¹. Figures in parentheses indicate the number of experiments averaged to give each point.

HNO₃[‡] collision complex. The recombination rate constants are large, showing the processes to be fully allowed, as expected, and the complex to be loose. RRKM calculations have been reported for several assumed geometries of the activated state (Tsang, 1973).

Of the two recombinations, the one with NO₂ is much the more important, since it links the HO_x and NO_x cycles and forms the stable molecule HNO₃, whose atmospheric concentration has been measured repeatedly and which is water-soluble and thereby rained out of the troposphere. It is interesting to note, moreover, that this recombination is in its "fall-off" regime at the pressures of the lower stratosphere (Anderson et al., 1974) and that a reasonably realistic and sophisticated kinetic model must be used for the recombination in order to attain the accuracy required in stratospheric modeling.

The OH + O_3 reaction has been invoked as well as eliminated from stratospheric consideration several times during the past 15 years, on the basis of various estimates of its rate constant, which have ranged from $\leq 5 \times 10^{-13}$ cm³ sec⁻¹ by one of us (Kaufman, 1964) to $< 10^{-16}$ by Langley and McGrath (1971). The value reported by us more recently (Anderson and Kaufman, 1973) has since been further confirmed by DeMore and Tschuikow-Roux (1974) and is qualitatively supported by the work of Simonaitis and Heicklen (1974). The HO_x cycle

Table 2. Hydroxyl-Reaction Studies ($1 \le P \le 10$ Torr)

Reaction	Temperature Range Dependence	Reference
$OH + NO + M \rightarrow HNO_2 + M$	$230 \le T \le 450K$	(Anderson and Kaufman, 1972;
$k^{III} = 3.3, 3.4, 5.8 \times 10^{-31} \text{ cm}^6/\text{sec}$	T-2.4	Anderson et al., 1974)
He, Ar, N ₂		
$OH + NO_2 + M \rightarrow HNO_3 + M$	$230 \le T \le 450K$	(Anderson and Kaufman, 1972;
$k^{III} = 1.0, 1.0, 2.3 \times 10^{-30} \text{ cm}^6/\text{sec}$	T ^{-2.5}	Anderson et al., 1974)
He, Ar, N ₂		
$OH + O_3 \rightarrow HO_2 + O_2$	$220 \leqslant T \leqslant 450K$	(Anderson and Kaufman, 1973)
$k^{II} = 1.3 \times 10^{-12} \exp \left[\frac{-1900 \text{ cal/mole}}{\text{RT}} \right] \text{cm}^3/\text{sec}$		
$OH + CH_4 \rightarrow H_2O + CH_3$	$290 \le T \le 440K$	(Margitan et al., 1974)
$k^{II} = 3.8 \times 10^{-12} \exp \left[\frac{-3600 \text{ cal/mole}}{\text{RT}} \right] \text{ cm}^3/\text{sec}$		
$OH + HNO_3 \rightarrow H_2O + NO_3$	$295 \leqslant T \leqslant 464K$	(Margitan et al., 1975)
$k^{II} = 0.89 \times 10^{-13} \text{ cm}^3/\text{sec}$		
OH + HCl → H ₂ O + Cl	$224 \le T \le 460K$	(Zahniser et al., 1974)
$k^{II} = 2.0 \times 10^{-12} \exp \left[\frac{-620 \text{ cal/mole}}{\text{RT}} \right] \text{cm}^3/\text{sec}$		

is thereby back in contention; it acquires major importance in the upper stratosphere but accounts for only about one-sixth of the total ${\rm O}_3$ loss processes.

The CH₄ reaction is of indirect importance as one of two major loss processes for methane, which is unreactive in the troposphere and whose altitude profile has been used to determine an effective eddy-diffusion coefficient for onedimensional modeling calculations. The result summarized here (Margitan et al., 1974) is in good agreement with two other studies, but disagrees with Wilson's review (1972), in which the activation energy was obtained by combining high-temperature and room-temperature results of different investigations. Even so, the activation energy suggested by Wilson was only 1.3 kcal mole-1 higher than ours, and his extrapolated rate constant at 200K was a factorof-two lower than that of the three most direct studies.

The successful study of the OH + HNO2 reaction shows the versatility of the experimental method as it involves a highly corrosive, normally liquid, and strongly adsorbed reactant. The latter property brings about a positive intercept in the extrapolated plot of observed pseudo-first-order rate constant vs. HNO3 concentration as [HNO₃] approaches zero. This intercept is due to the reaction of OH with adsorbed HNO₃, but it begins to interfere seriously with the kinetic analysis only at the lowest temperature of this study (272K), where the surface reaction accounts for about half of the total OH loss. The result, a temperature-independent value of $(0.89 \pm 0.13) \times 10^{-13}$ cm³ sec⁻¹ is in excellent agreement with that of a flash-photolysis investigation by Zellner and Smith (1974). In the lower stratosphere, HNO3 is formed by the recombination of OH with NO2 discussed above, and is destroyed by photolysis and by the OH + HNO2 reaction. During the day, the last reaction may

be a minor branch; however, if the OH + $\rm HO_2$ reaction rate constant turns out to be lower than the improbably high value of 2×10^{-10} cm³ sec⁻¹, the stratospheric hydroxyl concentration will be greater and the OH + $\rm HNO_3$ reaction relatively more important. At night, it is the only major $\rm HNO_3$ loss process, of course.

The last of the OH reactions, that with HCl, which was investigated in the new apparatus, is part of the ClOx scheme, where it is the major step regenerating catalytically active Cl species from the relatively inactive and more easily rained-out HCl. The reaction is therefore of major importance, since there would be little cause for alarm about any Cl-catalyzed ozone removal if HCl were irretrievable, i.e., if the OH + HCl reaction were very slow. Unfortunately, this is not the case, as Table 2 shows: the reaction is quite rapid and has a negligible energy barrier. Again, there is very good agreement with the results of a flash-photolysis study by Smith and Zellner (1974). The present measurements extend to 224K at their low-temperature end, so only very slight extrapolation is required for stratospheric modeling calculations.

Last, the new results on the Cl + O3 reaction need to be discussed, compared with other studies, and assessed for their stratospheric importance. As Figures 2 and 3 show, this reaction removes Cl-atoms rapidly and cleanly, has virtually no activation barrier, and is not followed by other steps (such $ClO + O_3 \rightarrow Cl + 2O_2$) which would regenerate Cl-atoms. It does show a slight temperature dependence, which amounts to a decrease from 1.3 to 1.0×10^{-11} cm³ sec⁻¹ as the temperature is lowered from 300 to 200K. The present value is 30% lower than the only published result of 1.85×10^{-11} at 298K (Clyne and Watson, 1974), but since the older value was also used at stratospheric conditions, in the absence of lowtemperature data, the necessary correction factor becomes larger. Other, as yet unpublished results confirm the lower values: a re-measurement giving $(1.33 \pm 0.26) \times 10^{-11}$ at 298K by Clyne and Nip (1975), and a temperature-dependence study by Watson et al. (1976) who report an Arrhenius expression of $(3.08 \pm 0.3) \times 10^{-11}$ $\exp \left[-(576 \pm 60)/RT\right]$ at 220 to 350K. The latter is in good agreement with our findings at 300K but falls about 25% below ours at 200K. All of these measurements have the effect of

confirming the large rate of this, the first step in the catalytic CIO_{X} scheme, but they show it to be a factor of 1.7 to 2 slower than had earlier been estimated and used in modeling calculations. The full evaluation of the CIO_{X} scheme awaits additional kinetic results on $\text{Cl} + \text{CH}_{4}$ as well as on ClO + O and ClO + NO.

ACKNOWLEDGMENT

This work was supported by the National Aeronautics and Space Administration under Grant No. NGR 39-011-161.

REFERENCES

- Anderson, J.G. and F. Kaufman (1972), "Kinetics of the reaction OH + NO₂ + M → HNO₃ + M," Chem. Phys. Lett. 16, 375.
- Anderson, J.G. and F. Kaufman (1973), "Kinetics of the reaction OH(v=0) + O₃ → HO₂ + O₂," Chem. Phys. Lett. 19, 483.
- Anderson, J.G., J.J. Margitan, and F. Kaufman (1974), "Gas phase recombination of OH with NO and NO₂," J. Chem. Phys. 60, 3310.
- Atkinson, R., D.A. Hansen, and J.N. Pitts, Jr. (1975), "Rate constants for the reaction of the OH radical with H₂ and NO (M = Ar and N₂)," J. Chem. Phys. 62, 3284.
- Clyne, M.A.A. and W. Nip (1975), unpublished results.
- Clyne, M.A.A. and R.T. Watson (1974), "Kinetic studies of diatomic free radicals using mass spectrometry," J. Chem. Soc. Faraday Trans. I 70, 2250.
- Davis, D.D. and R.T. Watson (1975), "Kinetic review of chlorine and bromine chemistry," unpublished.
- DeMore, W.B. and E. Tschuikow-Roux (1974), "Temperature dependence of the reactions of OH and HO₂ with O₃," J. Phys. Chem. 78, 1447.
- Kaufman, F. (1964), "Aeronomic reactions involving hydrogen; a review of recent laboratory studies," Ann. Géophys. 20, 106.
- Langley, K.R. and W.D. McGrath (1971), "The ultraviolet photolysis of ozone in the presence of water vapour," Planet. Space Sci. 19, 413.
- Margitan, J.J., F. Kaufman, and J.G. Anderson (1974), "The reaction of OH with CH₄," Geophys. Res. Lett. 1, 80.

- Margitan, J.J., F. Kaufman, and J.G. Anderson (1975), "Kinetics of the reaction OH + HNO₃ → H₂O + NO₃," in Proceedings of the First Symposium on Chemical Kinetics Data for the Upper and Lower Atmosphere (Warrenton, VA), ed. Benson et al., pub. Wiley for Int. J. Chem. Kinet., 281.
- Simonaitis, R. and J. Heicklen (1974), "The mechanisms of the H₂O-catalyzed chain photodecomposition of O₃ and the reaction of HO with O₃," J. Photochem. 2, 309.
- Smith, I.W.M. and R. Zellner (1974), "Rate measurements of reactions of OH by resonance absorption," J. Chem. Soc. Faraday Trans. II 70, 1045.
- Tsang, W. (1973), "Comparisons between experimental and calculated rate constants for dissociation and combination reactions involving small polyatomic molecules," Int. J. Chem. Kin. 5, 947.

- Watson, R.T., G. Machado, R.L. Schiff, S. Fischer, and D.D. Davis (1976), "Chlorine-atom reactions of atmospheric importance," in this volume.
- Wilson, W.E., Jr. (1972), "A critical review of the gas-phase reaction kinetics of the hydroxyl radical," J. Phys. Chem. Ref. Data 1, 535.
- Zahniser, M.S., F. Kaufman, and J.G. Anderson (1974), "Kinetics of the reaction of OH with HCI," Chem. Phys. Lett. 27, 507.
- Zellner, R. and I.W.M. Smith (1974), "Rate constants of the reactions of OH with NH₃ and HNO₃," Chem. Phys. Lett. 26, 72.

CHLORINE-ATOM REACTIONS OF ATMOSPHERIC IMPORTANCE

R.T. WATSON,* E.S. MACHADO, R.L. SCHIFF, S. FISCHER, AND D.D. DAVIS Chemistry Department University of Maryland College Park, Maryland

ABSTRACT: The technique of flash photolysis/resonance fluorescence has been utilized to study the temperature dependences of three chlorine-atom reactions of considerable fundamental importance to stratospheric chemistry. These reactions have been studied under a wide range of experimental conditions to ensure the absence of complicating secondary processes. The reactions of interest (with their corresponding rate constants) are expressed in units of cm³ molecule⁻¹ s⁻¹:

$$\begin{array}{c} k_1 \\ \text{Cl} + \text{O}_3 \stackrel{k}{\to} \text{ClO} + \text{O}_2; \quad \Delta \text{U}_{298}^\circ = -164 \text{ kJ mol}^{-1} \\ k_1 = (3.08 \pm 0.30) \times 10^{-11} \text{ exp-}(576 \pm 50/\text{RT}) \\ \text{Cl} + \text{CH}_4 \stackrel{k_2}{\to} \text{CH}_3 + \text{HCl}; \quad \Delta \text{U}_{298}^\circ = +6.4 \text{ kJ mol}^{-1} \\ k_2 = (7.44 \pm 0.75) \times 10^{-12} \text{ exp-}(2437 \pm 110/\text{RT}) \\ \text{Cl} + \text{H}_2 \stackrel{k_3}{\to} \text{H} + \text{HCl}; \quad \Delta \text{U}_{298}^\circ = +4.0 \text{ kJ mol}^{-1} \\ k_3 = (5.50 \pm 0.5) \times 10^{-11} \text{ exp-}(4750 \pm 100/\text{RT}) \\ \end{array} \tag{213-350K}$$

In addition, the following reaction was studied at 300K:

Cl + H₂O₂
$$\rightarrow$$
 HCl + HO₂; $\Delta U_{298}^{\circ} = -56.8 \text{ kJ mol}^{-1}$
 $k_4 \approx 5.8 \times 10^{-13} \text{ (\pm factor 2.0)}$ (300K)

A direct implication of the new rate data is the need to revise downward by a factor of ≈ 2.5 the magnitude of the ClO_x -caused stratospheric ozone perturbation predicted by earlier model calculations.

INTRODUCTION

Within the past year, a series of papers has appeared in the literature dealing with the possible effects of the presence of chlorine-containing species of natural (e.g., CH₃Cl) and anthropogenic (e.g., CF₂Cl₂) origin in the stratosphere (Cicerone et al., 1974, 1975; Crutzen, 1974; Crutzen and Isaksen, 1976; Molina and Rowland, 1974; Rowland and Molina, 1975; Wofsy and McElroy, 1974; Wofsy et al., 1975). It

has been proposed that these contaminants, many of which have been observed in the troposphere and lower stratosphere, can photolyze, or react with free radicals, producing Cl atoms or ClO radicals, and thus promoting the destruction of odd oxygen (odd oxygen $\equiv O(^3P)$ and O_3). The results of some model calculations predict that the presence of ClO_x ($ClO_x \equiv ClO$, HCl, Cl, OClO, ClOO) in the stratosphere at concentration levels in excess of 1 ppb (v/v) would cause a significant (> 2%) perturbation of

^{*}Dr. Watson is now with the Jet Propulsion Laboratory of the California Institute of Technology.

the integrated ozone column density. Quantitative model calculations require knowledge of the net upward flux of chlorine-containing species through the tropopause, and their subsequent fate in the stratosphere, as well as accurate rate-constant data for the key reactions.

The key chlorine reactions which participate in stratospheric chemistry are:

$$Cl + O_3 \rightarrow ClO + O_2 \tag{a}$$

$$ClO + O \rightarrow Cl + O_2$$
 (b)

$$NO + CIO \rightarrow NO_2 + CI$$
 (c)

$$Cl + RH \rightarrow R + HCl$$
 (d)

$$OH + HCl \rightarrow H_2O + Cl$$
 (e)

where RH \equiv CH₄; H₂; H₂O₂; or HO₂. In the ClO_x system, reactions (a) and (b) are those primarily responsible for the conversion of odd oxygen into molecular oxygen. It can be shown that the efficiency (ρ) of the ClO_x catalytic cycle is governed by the rate of reaction (b):

$$\rho \propto 2k_b[O][CIO] \tag{I}$$

If steady-state conditions are assumed for [O] and [ClO], the following alternate expression can be derived:

$$\rho \propto \frac{2k_{a}k_{b}k_{e}J_{a}[O_{3}]^{2}[HCI][OH]}{k_{d}[RH]\{k_{b}J_{a}[O_{3}] + k_{c}k_{f}[NO][O_{2}][M]\}}$$
(II)

where J_a is the photodissociation constant for O_3 , and k_f is the rate constant for the third-order recombination reaction of oxygen atoms with molecular oxygen. From equation (II) it can be seen that the catalytic efficiency is highly dependent upon several rate constants, many of which have received only limited study.

The present work provides an absolute determination of the rate constants of the chlorine-atom reactions with ozone, methane, and hydrogen, over a wide range of temperature and pressure, to insure that the results can be directly applied to atmospheric model calculations. In addition, a limited study of the reaction of Cl with H_2O_2 was performed at 300K to ascertain whether this reaction is important in the strato-

sphere. The experimental technique used in this study was flash photolysis/resonance fluorescence.

EXPERIMENTAL

The experimental details and operating principles of the flash-photolysis/resonance-fluorescence techniques have been fully described in the literature (Davis and Klemm, 1972; Davis et al., 1972, 1974). Consequently, only recent modifications and essential details will be discussed.

Two reaction cells were used in this work: (1) a black-anodized aluminum cell with an internal volume of ≈ 850 cm3 for methane and hydrogen, and (2) a Pyrex cell with an internal volume of ≈ 150 cm³ for ozone and hydrogen peroxide, due to their susceptibility to heterogeneous decomposition on metal surfaces. The cell temperature was controlled to within ± 0.5K by flowing methanol (235-325K) or ethylene glycol (298-400K) from a thermostated circulating bath through the outer jackets of the reaction vessels. Temperatures below 235K could be controlled to within ± 2K using cooled dry N2. An ironconstantan thermocouple was used in conjunction with a wheatstone-bridge resistance box to measure temperature, with a precision of better than 0.5K.

Atomic chlorine was produced from the flash photolysis of CCl₄ or CF₂ClCFCl₂ by a N₂ spark-discharge lamp in the presence of a reactive reagent (e.g., CH₄, H₂, O₃, H₂O₂) and a large excess of the diluent gas He or Ar. The mechanism for CCl₄ photodecomposition has been shown to be (Davis et al., 1975):

$$CCl_4 + h\nu (\lambda > 165 \text{ nm}) \rightarrow CCl_3 + Cl$$

 $\rightarrow CCl_2 + 2Cl (\text{or } Cl_2)$

The spark-discharge lamp was equipped with a window made of LiF, MgF₂, sapphire, or Suprasil, depending upon the reagent present in the reaction cell. A Suprasil window was usually chosen to eliminate the production of reactive intermediates from the photodecomposition of the added reagent (e.g., $CH_4 + h\nu \rightarrow CH_2 + H_2$) (Ausloos et al., 1964; Braun et al., 1966; Leighton and Steiner, 1936; Mahan and Mandal, 1962)

whose presence could lead to kinetic complications. Chlorine atoms formed in the $^2P_{1/2}$ state should be rapidly quenched into the $^2P_{3/2}$ ground state by collision with CCl₄ (Donovan et al., 1969). Chlorine atoms thermally equilibrated at 300K should then have a population of 0.8% in the $^2P_{1/2}$ state (the $^2P_{1/2}$ state lies $\approx 800 \text{ cm}^{-1}$ above the $^2P_{3/2}$ state).

Using published absorption cross-section data for CCl₄ (Watson, 1974, 1976) and flash-lamp fluxes (flash energy 80 J) based on ethylene actinometry, it was calculated that typical chlorine-atom concentrations of $\approx 5 \times 10^{10}$ atoms cm⁻³ were produced with a CCl₄ concentration of 2×10^{15} molecules cm⁻³. Initial chlorine-atom concentrations were varied from 10^{10} to 2×10^{11} atoms cm⁻³ by varying the flash energy from 20 to 250 J ([CCl₄] = 2×10^{15} molecules cm⁻³), and from 10^{10} to 10^{11} atoms cm⁻³ by varying [CCl₄] from 3 to 50 × 10^{14} molecule cm⁻³ (flash energy = 80 J).

Chlorine atoms were detected with a discharge-flow chlorine resonance lamp, the gas mixture consisting of < 1% of Cl_2 in Ar. As in previous studies (Davis and Klemm, 1972; Davis et al., 1972, 1974), photon-counting electronics were used throughout this study. The linear relationship between chlorine-atom concentration and the observed fluorescence intensity was established by varying the [CI] via a variation in the flash energy over a range of a factor of 20.

Each reaction was studied using pseudo-first-order kinetic conditions, i.e., [Reagent] $_0/[Cl]_0 \ge 600$; as expected, the chlorine-atom concentration decayed exponentially with time. Because the initial chlorine-atom concentration was kept low, multiple flashes (5-200) on a single gas mixture were required to produce a single smooth kinetic decay curve. However, the number of flashes per gas mixture was limited such that the decomposition of the added reagent (CH_4, H_2, H_2O_2, O_3) was always less than 3%. In some cases, therefore, several fillings of an identical gas mixture were used to develop a single experimental decay curve.

Gas pressures of less than 6 torr were measured using an MKS Baratron pressure gauge which was periodically checked against a dibutyl phthalate manometer. The high-pressure measurements (20-800 torr) were made with a two-turn Bourdon gauge (Wallace and Tiernan type

FA-145). It was estimated that the precision to which CH4/He and H2/He gas mixtures could be prepared was better than ≈ 1%, but was only ≈ 3-5% for O₃/He mixtures because of uncertainties in the determination of ozone concentration caused by small but significant amounts of heterogeneous decomposition and by experimental error in the measurement of [O₃] by uv absorption at 260 nm. The CCl4 and CF2ClCFCl2 pressures were measured somewhat less precisely at low temperatures in the aluminum cell due to surface adsorption effects. However, an uncertainty in these quantities does not lead to any inaccuracy in the reported rate data, since the latter species only act as precursors of atomic chlorine, and their absolute concentration is not required in the data analysis.

The CH₄ used in this study was of two types: Matheson "Gold Label Ultra High Purity" (stated purity of 99.97%), mass-spectrometrically analyzed for C_2H_6 (70 ppm) and C_3H_8 (20 ppm), and research grade (stated purity of 99.99%), mass-spectrometrically analyzed for C_2H_6 (20 ppm) and C_3H_8 (< 5 ppm). The CH_4 was thoroughly degassed in liquid N2 (77K) before use. Two types of H2 were used in this study, with no observable difference in the results obtained: Matheson "Research Purity" (stated purity of 99.9995%), containing less than 0.5 ppm of CH4, and Matheson "Ultra High Purity" (stated purity of 99.999%). These were used without further purification. The helium was Matheson "Gold Label Ultra High Purity" (stated purity of 99.999%), which was also used without further purification. The ozone was generated by flowing molecular oxygen through a commercial ozonizer, and was collected on silica gel at 196K. Molecular oxygen was removed from the ozone by vacuum-pumping the silica gei for 10-15 minutes. When needed, the ozone was collected in a Pyrex bulb and diluted as required with He. The purity of the ozone was measured by uv spectrophotometry at 255.3 nm and was typically $\approx 90\%$ (10% O₂). The ozone cross-section at 255.3 nm was taken from published data (DeMore and Raper, 1964) to be 137 (atm at 273K)-1 cm-1, base 10. Excellent agreement exists between several investigations of the published absorption cross-section data for O₂ at 253.7 nm (Becker et al., 1974; DeMore and Raper, 1964; Hudson, 1971).

Although there was no significant (<5%) variation of the bimolecular rate constant with total pressure, there was one with temperature. A least-squares fit of the data, weighted according to the number of experiments and the reliability of the results, was performed at each temperature to determine the bimolecular rate constant at that temperature. A weighted least-squares fit of the bimolecular rate constants then produced the following Arrhenius expression:

$$k_1 = (3.08 \pm 0.30) \times 10^{-11} \times$$

exp-(576 ± 50 cal mol⁻¹/RT)

(220-350K)

The results of 60 experiments were used to compute this expression. The most probable systematic error in this study is that of overestimating the ozone concentration by neglecting a small amount of heterogeneous and/or photolytic decomposition (total < 7%).

Possible complicating secondary reactions which must be considered are:

$$ClO + O_3 \rightarrow Cl + 2O_2$$
 (f)

$$ClO + O \rightarrow Cl + O_2$$
 (b)

$$C1 + O_2 + M \rightarrow C1OO + M$$
 (g)

$$Cl + O_3 + M \rightarrow ClO_3 + M$$
 (h)

$$C1 + C1 + M \rightarrow C1_2 + M \tag{j}$$

These reactions can be rejected for the following reasons. The rate constant for reaction (f) has recently been reported (Clyne et al., 1975) to be $\leq 5 \times 10^{-15} \text{ cm}^3 \text{ molecule}^{-1} \text{ s}^{-1}$, which eliminates any possibility that this reaction could regenerate atomic chlorine within the time scale of the experiment. Atomic oxygen could be formed from the photolysis of ozone or molecular oxygen (impurity in the ozone); however, the rate of reaction (b) should be dependent upon the square of the flash energy. The observed first-order rate constants showed no dependence upon flash energy, precluding the need to consider this reaction (in agreement with calculations). The absence of a pressure dependence in the bimolecular rate constant is also in

agreement with calculations which indicate that complications due to reactions (g), (h), and (j) should be of negligible importance.

RESULTS AND DISCUSSION

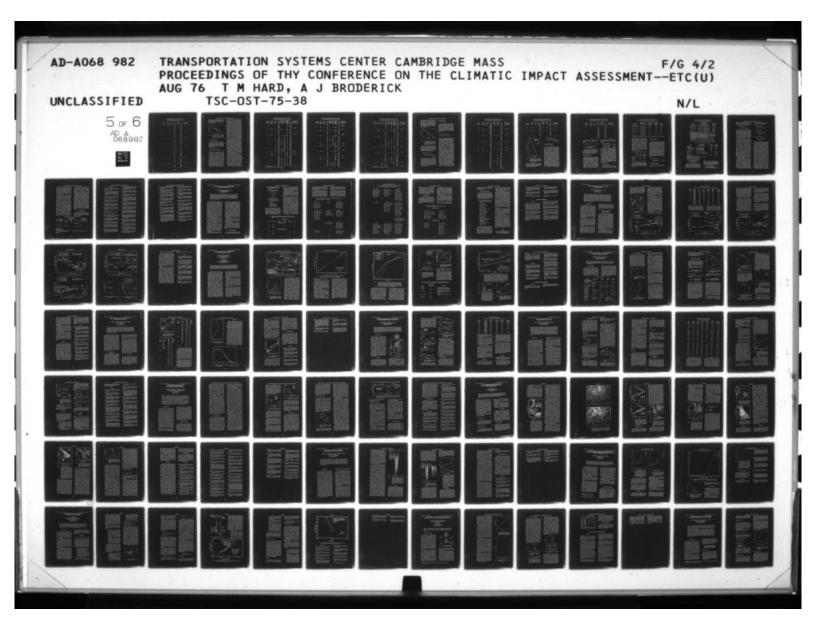
(i)
$$Cl + O_3 \xrightarrow{k_1} ClO + O_2$$

Table 1 and Figure 1 summarize studies of reaction 1 made over a range of temperature (218-350K), pressure (5-40 torr), and other experimental parameters. Pseudo-first-order kinetic conditions $[O_3]_0 > [CI]_0$, ($[CI]_0 \approx 5 \times 10^{10}$ atoms cm⁻³; $[O_3]_0 \approx (2.5-25) \times 10^{13}$), were utilized so that equation (III) could be used to analyze the data.

$$-d[C1]/dt = k_1[C1][O_3] + k_{diffusion}[C1]$$

$$ln([C1]_0/[C1]_t) = (k_1[O_3] + k_{diffusion}) \times t$$
(III)

Numerous preliminary experiments were performed to show that heterogeneous decomposition of ozone on the reactor surfaces was less than 5%. The first-order rate constant, k'1, was determined for a particular gas mixture after the gas had been allowed to reside in the reaction cell for different times (0, 2, 5, 10 minutes) before the experiment was initiated. After an initial "aging" period, it was found that k' was independent of residence time. However, when the two resonance lamps were on, it was observed that k' decreased with increasing residence time, indicating photolytic decomposition of the ozone. Consequently, the time taken to perform an experiment was limited to < 2 minutes, to eliminate inaccuracies in the measurement of k'1 due to photolytic decomposition of the ozone. Experiments were performed which showed that there was no observable dependence of k'₁ upon the flash energy or CCl₄ concentration (Table 1). These experiments verified that there was no dependence of the bimolecular rate constant upon initial chlorine-atom concentration, and that there was no "flash" decomposition of ozone. Experiments in which the number of flashes per filling of a particular gas mixture were varied showed a decrease in k'1 as the number of flashes increased. This was not due to regeneration of atomic chlorine, but rather to photolytic decomposition of ozone caused by the increased



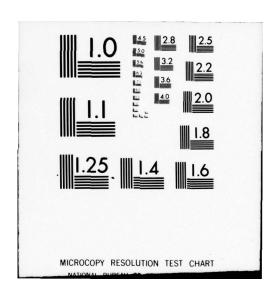


Table 1. Reaction-Rate Data for the Process Cl + $O_3 \rightarrow ClO + O_2$

emperature (°K)	Diluent (torr)	CCl ₄ (mtorr)	O ₃ (mtorr)	Flash Energy (joules)	K' ₁ (sec ⁻¹)	10 ¹² K _{bimolecular} (cm ³ molecule ⁻¹ s ⁻¹
220	5 (He)	65	0.00	88	100	
	- ()		1.11		443	
			1.67		580	
			2.12		925	
			2.51		1111	
			3.13		1325	
			3.65		1570	
			4.38		1620	
			4.46		1710	
			4.70		1940	8.57 ± 0.62
239	5(He)	65	1.11	88	730	
			2.12		1075	
			3.28		1550	
			3.92		1702	
			4.33		1870	
			5.45		2425	
			6.39		2873	
			7.65		2900	8.95 ± 1.17
259	5(He)	65	0.80	88	436	
			1.24		595	
			1.67		775	
			2.09		794	
			2.45		1008	
			2.48		1111	
			3.13		1272	
			3.82		1560	
			5.27		2080	
			6.57		2590	10.04 ± 0.5
298	5 (He)	65	0.82	88	442	
			1.04		601	
			1.66		740	
			1.71		691	
			2.11		935	
			2.19	20	1040	
			2.19	88	1083	
		100000000000000000000000000000000000000	2.19	180	928	
		20	2.19	88	1020	
		130	2.19	88	944	
		65	2.58		1048	
			3.13		1366	
			3.23		1344	
			3.44		1425	
			4.38		1818	
			4.97 6.26		2200 2450	11.98 ± 0.8
200	40.4			0.0		
298	40(Ar)	65	0.00	88	40 547	
			1.57 2.17		696	
			3.13		1060	
			3.81		1320	
			4.18		1445	
			5.22		1984	
			7.31		2800	11.44 ± 0.50
350	5(He)	65	1.12	88	540	
330	3(He)	03	1.72	00	800	
			2.23		1052	
			3.00		1250	
			3.42		1465	
			0.74		1403	

length of time required to complete the experiment. Consequently, the number of flashes per single filling of the reaction cell was limited to $\leq 20 \ (\approx 90 \text{ seconds})$.

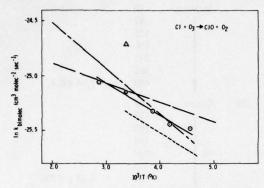


Figure 1. Arrhenius plot for the Cl + O₃ reaction: Δ, Clyne and Watson, 1974; ---, Nip and Clyne, 1976; --, Anderson et al., 1976; ---, Kurylo and Braun, 1976; O, this work.

(2)
$$Cl + CH_4 \xrightarrow{k_2} CH_3 + HCl$$

The results for reaction (2) are presented in complete detail in Table 2. This reaction was again studied using pseudo-first-order conditions, $[CH_4]_0 \gg [Cl]_0$, so that the individual plots of chlorine-atom decay with time could be analyzed using equation (IV):

$$-d[C1]/dt = k_2[C1][CH_4] + k_{diffusion}[C1]$$

$$\therefore \ln([C1]_0/[C1]_t) = (k_2[CH_4]_0 + k_{diffusion}) \times t \quad (IV)$$

Reaction (2) was thoroughly studied over a range of temperature (218-401K) and pressure (20-100 torr He, 50 torr Ar). The bimolecular rate constant k2, and the individual pseudofirst-order rate constants k'2 (after correction due to differences in the chlorine-atom diffusion rates for differing total pressures and diluent gases), were found to be invariant with diluentgas pressure and the nature of the diluent gas (Table 2). These observations verify that the reaction studied was bimolecular, as expected, and that complications due to secondary processes, which are third-order in nature, were not important under the experimental conditions of low (≈ 1011 atom cm-3) chlorine-atom concentration as used in this study. Experiments uti-

lizing variations in CCl₄ concentration (15-150 mtorr) were performed, with no significant deviations in the experimental first-order rate constants being observed. A series of experiments was performed at 239 and 401K where CF2ClCFCl2 was substituted for CCl4 as the precursor of atomic chlorine. The concentration of this C2F3Cl3 was varied by a factor of 20 (10-200 mtorr). The bimolecular rate constant, k2, was shown to be independent of C2F3Cl3 concentration at each temperature, and within the expected experimental uncertainty of our results (< 10%) yielded a value for k2 similar to that achieved with CCl_4 . Variations in the flash energy by a factor of ≈ 12 (20-250 joules) also resulted in no significant variations of the bimolecular rate constant. The observation that variations in initial chlorine-atom concentration by factors of $\approx 13 (1.1-14 \times 10^{10} \text{ at } 299\text{K})$ and $\approx 34 \ (0.43-15 \times 10^{10} \text{ at } 238\text{K}), \text{ produced by}$ varying CCl₄ (or C₂F₃Cl₃) and flash energy, resulted in no significant variation in the firstorder rate constants, is strong evidence that complicating secondary kinetic processes are of no importance in this study. As noted earlier, the flash lamp was equipped with either a sapphire or a quartz window to prevent the photolysis of CH₄ below 140 nm, which would have resulted in the production of CH2 radicals (whose presence in concentrations of ≥ 10¹² radicals cm⁻³ could cause serious kinetic complications). The experiments which were performed with a large variation in flash energy (20-245 joules at 299K, and 25-245 joules at 238.5K) showed no variation in first-order rate constant, thus eliminating the possibility of kinetic complications caused by labile photolytic fragments' reacting rapidly enough with atomic chlorine to result in an erroneous interpretation of the rate data.

A third series of experiments was performed, in which the number of consecutive flashes per single filling of a particular gas mixture was varied. At 299 and 401K, the number of flashesper single filling was varied by a factor of 20 (5-100 and 10-200 respectively), and at 239K by a factor of 10 (20-200), with no significant variation in the observed first-order rate constants. These experiments tend to eliminate kinetic complications due to a buildup in the concentration of a "reactive" stable product.

As stated in the experimental section of this paper, two samples of CH₄ were used in this

Table 2. Reaction-Rate Data for the Process Cl + CH₄ → CH₃ + HCl

Temperature	Diluent (torr)	CCl ₄ (mtorr)	CH ₄ (mtorr)	Flash Energy (joules)	Flashes per Filling	Flashlamp Window Material	K' ₂ (sec ⁻¹)	10 ¹⁴ K _{bimolecular} (cm ³ molecule ⁻¹ s ⁻¹)
218	20 (He)	65	0	88		Sapphire	40	
0.00	20 (110)		50			1	82	
			100				135	
			150				200	
			200				271	
			250				355	
			300			+	400	2.98 ± 0.4
220	40 (He)	65	50	88	25	Quartz	84	
			50				117	
			100				169	
			125				191	
			150				240	
			175				272	
			200			1	322	3.31 ± 0.33
238.5	40 (He)	65	25	88	25	Quartz	94	
			31		15		95	
			31.65		25		.105	
			50		25		122	
			75		25		181	
			99		35		212	
		15	100	45	50		187	
		65	100	88	50		198	
			150		125		283	
			150		25		324	
			150	88	25		268	
			150	25	75 10		267	
			150 150	210 88	150		301 289	
		15	150	00	100		253	
		65	200		50		382	
			200		50		407	
		15	200	45	100		328	
		15	200	20	100		326	
		65	200	88	50		338	
		15	200	30	100		348	
		65	200	106	100		400	3.86 ± 0.3
239	40 (He)	10*	25	88	50	Quartz	70.3	
			100			1	193	
			250		75	•	417	3.79 ± 0.09
	40 (He)	50*	25	88	50	Quartz	90.5	
			25				105.8	
			100				210	
			100		75		221	
			100		1-1-		207	
			100	20	150		203	
			100	245	20		240	
			160	88	50		313	
			250		75		450	
			250				467	
			250	25	150		431	
			250	245	25		446	
			250	88	20		397	
			250		200		398	
			268		100		543	4.15 ± 0.5

^{*}For this experiment, TF13 (C2Cl3F3) was used instead of CCl4.

Table 2. Reaction-Rate Data for the Process Cl + $CH_4 \rightarrow CH_3 + HCl$ (cont.)

Temperature (°K)	Diluent (torr)	CCl ₄ (mtorr)	CH ₄ (mtorr)	Flash Energy (joules)	Flashes per Filling	Flashlamp Window Material	K' ₂ (sec ⁻¹)	10 ¹⁴ K _{bimolecular} (cm ³ molecule ⁻¹ s ⁻¹)
	40 (He)	200*	25		50	Quartz	138.9	
	()		100			1	245	
			250				483	3.81 ± 0.02
								3.99 ± 0.18
245	40 (He)	65	20	88	25	Quartz	89	
2.0	10 (110)	•	40			1	137	
			60				172	
			98.5				247	4.94 ± 0.30
245	40 (He)	65	25	88	25	Quartz	87	
243	40 (He)	05	50	00	~	Quarte	146	
			75				192	
			100				231	
			125				282	
			150				342	5.00 ± 0.26
			130				342	4.97 ± 0.3
250	20 (He)	65	0	88	30	Sapphire	40	
200	20 (110)	00	20	00	30	Jappine	90	
			30		50		117	
			40		50		138	
			40		100		138	
			40	45	100		135	
			40	211	35		144	
			50	88	50		168	
			60	00	50		177	
			70		50		216	
			80		50	+	225	6.01 ± 0.29
	200 (He)	65	0	88	40	Sapphire	18	
	(,		40	-	75	Jappinae	133	
			80		100		212	6.29 ± 0.29
273	20 (He)	65	20	88	50	Sapphire	116	
	20 (110)		30	- 00		Jappine	145	
			50				185	
			60				224	
			70				267	
			80				278	7.92 ± 0.98
298	20 (He)	65	0	88	25	Sapphire	36	
270	20 (110)	03	15	00	50	Sappine	122	
			30		30		180	
			45				225	
			45				230	
			60				290	
			75				331	11.90 ± 1.0
	***							11.90 1 1.0
	50 (Ar)	65	20 40	88	25	Sapphire	100 175	
			60				248	11.4 ± 0.9
	20 (He)	65	0.0			Complies	46	11.410.5
	20 (Ne)	65	0.0			Sapphire	46	
			15				123	
			30				180	
			30		5		196	
			30		100		188	
			30	45	25		185	
			30	215	20		174	
			45	88	25		240	
			45				232	
			45		100		218	

Table 2. Reaction-Rate Data for the Process Cl + CH₄ → CH₃ + HCl (cont.)

remperature	Diluent (torr)	CCl ₄ (mtorr)	CH ₄ (mtorr)	Flash Energy (joules)	Flashes per Filling	Flashlamp Window Material	K' ₂ (sec ⁻¹)	10 ¹⁴ K _{bimolecular} (cm ³ molecule ⁻¹ s ⁻¹)
		100	60	4	25	Sapphire	290	
			60			i	282	
			60		100		300	
			75		25		330	
			90				408	
			90				380	11.50 ± 0.6
	200 (He)	65	0	88	30	Sapphire	31	
	200 (110)		30	-	100	•	151	12.36
	40 (He)	65	0	88	25	Quartz	45	
			15			1	103	
			30				165	
			45				220	
			60				280	
			90				383	
								11.4.02
			120				485	11.4 ± 0.2
299	40 (He)	65	20	88	25	Quartz	182	
			20				155	
			70				375	
			70				369	
			70		100		374	
			70		10		345	
			70		25		368	
			70	20	25		342	
			70	245	10		340	
			70	45	25		363	
			70	88	25		386	
		150	150	88			653	
		65	150			+	707	12.08 ± 0.03
350	100 (He)	65	0	88	25	Sapphire	77	
550	100 (110)	00	7		25	Juppine	125	
			14		50		157	
			21		30		221	
			28				258	
			35				295	
			42				330	21.83 ± 1.9
								21.00 - 1.0
401	40 (He)	65	25	95	50	Quartz	460	
			25				462	
			50				676	
			75				933	
			100				1104	
			100				1004	
			100		200		1082	
			100		10		1042	
		15	100	45	50		1118	
		65	150	95			1577	
			200		100		1905	
			268				2564	35.4 ± 1.19
401	40 (He)	50*	25	95	50	Quartz	526	
401	40 (He)	20	100	,,	30	Qualtz	1203	
		50	100				1199	
		100	100			1	1205	20.45 . 2.55
		50	268				2778	38.45 ± 0.38

^{*}For this experiment, TF13 (C2Cl3F3) was used instead of CCl4.

study. Analysis of the first showed 70 ppm of C_2H_6 and 20 ppm of C_3H_8 , whereas the second contained 20 ppm of C_2H_6 and < 5 ppm of C_3H_8 . There was no discernable dependence of the bimolecular rate constant on the particular batch of CH_4 used (see Figure 2), indicating that these low impurity levels cause no inaccuracy in the reported rate data.

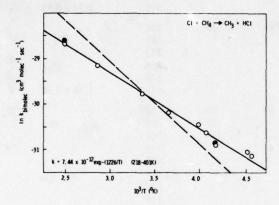


Figure 2. Arrhenius plot for the Cl + CH₄ reaction:

--, Clyne and Walker, 1973; O, this work where CCl₄ was used as the Cl-atom precursor; •, this work where CFCl₂CF₂Cl was used as the Cl-atom precursor.

Whereas the bimolecular rate constant showed no variation with diluent pressure, flash energy, or initial chlorine-atom concentration, it varied significantly with temperature. A weighted least-squares fit of all the data shown in Table 2 yields the following Arrhenius expression:

$$k_2 = (7.44 \pm 0.7_5) \times 10^{-12} \times$$
 $exp-(2436 \pm 100 \text{ cal mol}^{-1}/RT)$
(218-401K)

In summary, a total of about 180 experiments were performed under a wide range of conditions chosen to detect possible complicating secondary kinetic processes. In view of the results, the probability that such processes significantly affected the Arrhenius expression seems very low. Moreover, it should be noted that there is no observable curvature in the Arrhenius plot of Figure 2.

(3)
$$Cl + H_2 \stackrel{k_3}{\rightarrow} HCl + H$$

The results obtained for reaction (3) are shown in Table 3 and Figure 3. Pseudo-first-order conditions, $[H_2]_0/[Cl]_0 \ge 10^4$ (e.g., at 298K $[Cl]_0 \approx 5 \times 10^{10}$ and $[H_2]_0 = (1.7 \text{ to } 15) \times 10^{15}$), were used throughout this study to minimize the complications of secondary kinetic processes. Equation (V) was used to analyze the individual decay plots of atomic chlorine concentration with time:

$$-d[C1]/dt = (k_3[H_2] + k_{diffusion})[C1]$$

$$\therefore \ln([C1]_0/[C1]_t) = (k_3[H_2] + k_{diffusion}) \times t \qquad (V)$$

Reaction (3) was thoroughly studied over ranges of temperature (213-350K), pressure (20-50 torr), and other experimental parameters. The bimolecular rate constant, k3, was observed to be invariant with total pressure and the nature of the diluent gas, verifying that the reaction was bimolecular as expected, and that complications due to third-order secondary processes were unimportant under the experimental conditions used in this study. Variations in the flash energy by a factor of ≈ 5 (45-211 J) resulted in no significant variation in the observed individual first-order rate constants, k'3, for a constant H2 concentration. These observations strongly indicate that complicating secondary processes, due to rapid reactions of atomic chlorine with either labile photolytic fragments or labile reaction intermediates, were not important. A series of experiments was performed in which the number of consecutive flashes per single filling of a particular gas mixture was varied. At 298K, the number of flashes per single filling was varied by a factor of 10 (15-150) with no significant variation in the observed first-order rate constants. These experiments tend to eliminate the possibility of kinetic complications due to the formation of a significant concentration of a reactive stable photolytic or reaction product.

Whereas the bimolecular rate constant showed no variation with diluent pressure, the nature of the diluent gas, or flash energy (initial

Table 3. Reaction-Rate Data for the Process $Cl + H_2 \rightarrow HCl$

Temperature	Diluent (torr)	CCl ₄ (mtorr)	H ₂ (mtorr)	Flash Energy (joules)	Flashes per Filling	K ₃ (sec ⁻¹)	10 ¹⁵ K _{bimolecular} (cm ³ molecule ⁻¹ s ⁻¹ ;
213	20 (He)	50	1,500	88	50	82	
213	20 (He)	30	3,000	00	30	122	
			4,500			172	
			6,000			231	
			8,000			316	
			10,000			372	0.73 ± 0.03
220	20 (He)	65	2,000	88	50	128	
			3,000			161	
			4,000			223	
			5,000			255	
			7,000			378	
			8,000			423	1.16 ± 0.06
250	20 (He)	65	200	88	50	66	
			300		75	83	
			400		100	102	
			400			106	
			500			106	
			500			114	
			600			127	
			700			136	
			800			151	3.46 ± 0.25
273	20 (He)	65	0	88	75	40	
			200		50	102	
			400		100	150	
			500			170	
			600			210	
			700			232	
			800			273	7.94 ± 0.76
298	50 (Ar)	65	100	88	75	60	
			200		100	116	
			300			185	19.3 ± 2.3
298	20 (He)	65	0	88	50	45	
			50			80	
			50			83	
			100			108	
			100			110	
			100		100	112	
			150		50	125	
			150 150			133	
			150		160	123	
			200		150 50	137 170	
			200		30	180	
			200				
			200	45	100	181	
			200	45 211	100 50	171	
			250		30	155	
			250	88	15	196	
			250		150	191	
			300		50	196	
			300		30	214 240	
			300			215	
			350			215	
			350			250	
			330			250	

Table 3. Reaction-Rate Data for the Process Cl + H₂ → HCl (cont.)

Temperature	Diluent (torr)	CCl ₄ (mtorr)	H ₂ (mtorr)	Flash Energy (joules)	Flashes per Filling	K ₃ (sec ⁻¹)	10 ¹⁵ K _{bimolecular} (cm ³ molecule ⁻¹ s ⁻¹)
			400			294	
			450			307	
			450		100	350	18.8 ± 0.5
298	40 (He)	65	100	88	50	75	
			250			165	
			400			345	
			600			355	17.2 ± 0.5
350	100 (He)	65	0	88	50	60	
			25			85	
			50			128	
			75			169	
			100			221	
			125			268	
			150			305	64.7 ± 2.2

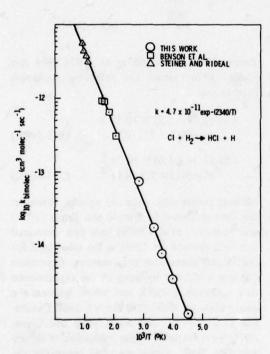


Figure 3. Arrhenius plot for the CI + H₂ reaction:

O, this work; □, Benson et al., 1969; Δ,

Steiner and Rideal, 1939. The solid line represents the evaluated expression of 4.7 × 10⁻¹¹ exp-(2340/T).

chlorine-atom concentration), it varied significantly with temperature. A weighted leastsquares fit of the data shown in Table 3 yields the following Arrhenius expression:

$$k_3 = (5.50 \pm 0.5) \times 10^{-11} \times$$

 $exp-(4750 \pm 100 \text{ cal mol}^{-1}/RT)$
(213-350K)

(4)
$$Cl + H_2O_2 \xrightarrow{k_4} HCl + HO_2$$

The results of reaction (4) are shown in Table 4. As in the case of reactions (1), (2), and (3), the study of H₂O₂ was performed under first-order conditions where [H2O2]0/[Cl]0 ranged from 9 × 103 to 8 × 104. The results of the study of reaction (4) were found to be less reproducible than would normally be acceptable, presumably due to heterogeneous decomposition of H2O2 on the reactor surfaces. Consequently, the uncertainty limits placed upon the final result obtained for the bimolecular rate constant have been made much larger than normal (a factor of 2). A pressure of 50 torr of argon was used to slow diffusion to the reactor surfaces and thus minimize heterogeneous wall loss. The H₂O₂ concentration was determined by UV spectrophotometry using published absorption cross-section data (Calvert and Pitts, 1967). These measurements were normally made on the vapor phase above a 90% H₂O₂ aqueous solution, immediately before mixtures of the vapor with Ar were prepared in preconditioned bulbs.

Table 4. Reaction-Rate Data for the Process Cl + H₂O₂ → HCl + HO₂

Temperature (°K)	Diluent (torr)	CCl ₄ (mtorr)	H ₂ O ₂ (mtorr)	Flash Energy (joules)	K ₄ (sec ⁻¹)	K _{bimolecular} (cm ³ molecule ⁻¹ s ⁻¹)
298	50(Ar)	65	0	100	15.5	
			6.7		46.5	
			11.7		92.4	
			16.7		138	
			16.7		155	
			20.0		260	
			20.0		216	
			21.65		226	
			21.65		333	
			21.65		256	
			21.65		282	
			26.65		370	
			26.65		445	
			33.3		534	
			33.3		295	
			83.25		1000	
			116.6		1667	5.8×10^{-13}

A least-squares fit of the data in Table 3 produces the following bimolecular rate constant:

$$k_A = 5.8 (\pm factor 2) \times 10^{-13}$$
 (300K)

COMPARISON WITH PREVIOUS RESULTS

Previous work will be referred to here, but not discussed in detail. Critical discussions of the results obtained for reactions (1)-(4) in this and previous studies have been presented elsewhere (Watson, 1976; Watson et al., 1976a, b).

(1)
$$Cl + O_3 \xrightarrow{k_1} ClO + O_2$$

Figure 1 and Table 5 summarize the Arrhenius expressions obtained in this and other studies of the kinetic behavior of the chlorine-atom/ozone reaction (Anderson et al., 1976; Clyne and Watson, 1974; Kurylo and Braun, 1976; Nip and Clyne, 1976). From Table 5, it can be seen that a variety of techniques have been employed to study reaction (1) within the temperature range of the stratosphere (200-270K). A least-squares fit of the individual bimolecular rate constants reported in this and three other recent studies (Kurylo and

Braun, 1976, Anderson et al., 1976; Nip and Clyne, 1976) yields the following Arrhenius expressions:

(A)
$$(2.69 \pm 1.2) \times 10^{-11} \times$$

exp-(511 ± 211/RT) (205-298K)

(B)
$$(3.34 \pm 1.0) \times 10^{-11} \times$$

exp-(615 ± 150/RT) (205-466K)

All data points were weighted equally. However, the data published by Kurylo and Braun (1976) and Anderson et al. (1976) have been corrected due to a revision (≈ 7.5%) in the value used for the ozone absorption cross-section. Expression (A) was evaluated by using all the experimental data collected at 298K and below, whereas the data points at 350K (this study), 366K (Anderson et al., 1976), and 452K (Nip and Clyne, 1976) were included in the evaluation of expression (B). Both expressions yield essentially the same bimolecular rate constants between 220 and 298K (e.g., k_1 (240K): (A) = 9.21 × 10⁻¹²; (B) = 9.20×10^{-12}). Expression (A) is recommended for use in stratospheric model calculations (discussed later).

(2)
$$Cl + CH_4 \stackrel{k_2}{\rightarrow} CH_3 + HCl$$

Table 6 presents the results of the competitive chlorination studies (Knox and Nelson,

Table 5. Summary of Arrhenius Expressions for the Process Cl + O3 - ClO + O2

Reference	Arrhenius Expression (cm ³ molecule ⁻¹ s ⁻¹)	10 ¹¹ k ₁ (298K) (cm ³ molecule ⁻¹ s ⁻¹)	Temperature Range (°K)	Technique*
Clyne and Watson (1974)	-	1.85 ± 0.36	298	DF/MS
Kurylo and Braun (1976)	$(2.72 \pm 0.45) \times 10^{-11}$ × exp-(592 ± 78/RT)	1.02 ± 0.05	213-298	FP/RF
Anderson et al. (1976)	$(2.17 \pm 0.43) \times 10^{-11}$ × exp-(340 ± 60/RT)	1.22	205-366	DF/RF
Nip and Clyne (1976)	$(5.15 \pm 0.5) \times 10^{-11}$ × exp-(831±55/RT)	1.33 ± 0.26	221-629	DF/RA
This study	(3 08 ± 0.3 × 10 ⁻¹¹ × exp-(576 ± 50/RT)	1.20 ± 0.10	220-350	FP/RF

^{*}DF, discharge flow; FP, flash photolysis; MS, mass spectrometry; RF, resonance fluorescence; RA, resonance absorption.

1959; Pritchard et al., 1954) in two forms: the ratio of pre-exponential A factors, and the difference in activation energies. The two results differ only by $\approx 7\%$ in the magnitude of the pre-exponential factor, so their mean will be used for comparison with the results of the more recent direct studies. Table 7 summarizes the evaluated Arrhenius expressions for the Cl + H₂ reference reaction (Benson et al., 1969; Clyne and Walker, 1973; Fettis and Knox, 1964; Watson, 1976; Watson et al., 1976), showing considerable variance among the Arrhenius parameters for k_3 . This leads to a variety of derived expressions for k_2 .

Table 6. Summary of Arrhenius-Expression Ratios (k_{H2}/k_{CH4})

	A _{CH₄} / A _{H₂}	Е _{Н2} - ЕСН ₄	Temperature Range (°K)
Knox and Nelson (1959)	0.30	1650 ± 60	193-593
Pritchard et al. (1954)	0.32	1650 ± 150	293-488
Mean Value	0.31	1650 ± 100	193-593

Table 8 compares the Arrhenius expressions for k_2 derived from Tables 6 and 7 with those obtained from the present experiments and other direct studies (Clyne and Walker, 1973; Poulet et al., 1974).

(3)
$$Cl + H_2 \stackrel{k_3}{\rightarrow} H + HCl$$

Table 7 summarizes the evaluated Arrhenius expressions for the kinetic behavior of atomic chlorine with molecular hydrogen (references are given for the data used for these evaluations). A critical review (Watson, 1976; Watson et al., 1976b) of the earlier results for k3 and k-3 concluded that the results obtained in studies of the reverse reaction (-3) are in error due to experimental difficulties. Of the direct studies of reaction (3), the results obtained in this study are in good agreement with those of Steiner and Rideal (1939) (modified, see Watson, 1976), and Benson et al. (1969) (see Figure 3). From the data obtained in this study, and Benson et al. (1969) and Steiner and Rideal (1939), the following evaluated Arrhenius expression was derived:

$$k_3 = (4.7 \pm 0.4) \times 10^{-11} \times$$

exp-(4676 ± 59/RT) (213-1071K)

(4)
$$C1 + H_2O_2 \xrightarrow{k_4} HC1 + HO_2$$

No other studies of this reaction have been reported.

Table 7. Summary of Arrhenius Expressions for kCl+H2

Reference	Arrhenius Expression k _{Cl+H2} (cm ³ molecule ⁻¹ s ⁻¹)	Temperature Range (°K)
Fettis and Knox (1964) ^a	$(1.38 \pm 0.1) \times 10^{-10} \exp(5500 \pm 140/RT)$	273-1071
Benson et al. (1969) ^b	$(8.0 \pm 2.0) \times 10^{-11} \exp{-(5275 \pm 400/RT)}$	273-1071
Clyne and Walker (1973) ^c	A. $(3.7 \pm 0.6) \times 10^{-11} \exp(4264 \pm 100/RT)$ B. $(5.6 \pm 1.2) \times 10^{-11} \exp(4485 \pm 137/RT)$	195-610 195-496
Watson et al. (1976b) ^d	A. $(5.5 \pm 1.0) \times 10^{-11} \exp(4750 \pm 100/RT)$ B. $(4.7 \pm 0.4) \times 10^{-11} \exp(4676 \pm 59/RT)$	213-350 213-1071

^aEvaluation based on all previous data (Ashmore and Chanmugam, 1953; Fettis and Knox, 1964; Rode-Bush and Klingelhoefer, 1933; Steiner and Rideal, 1939).

Table 8. Summary of Arrhenius Expressions for k_{Cl+CH_A}

Reference	Arrhenius Expression kCl+CH ₄ (cm ³ molecule ⁻¹ s ⁻¹)	10 ¹⁴ k ₂₉₈ (cm ³ molecule ⁻¹ s ⁻¹)	Temperature Range (°K)
Competitive			
chlorination:	$4.28 \times 10^{-11} \exp{-(3850/RT)^a}$	6.42	193-593
Knox and Nelson (1959)	$2.48 \times 10^{-11} \exp{-(3625/RT)^b}$	5.44	
Pritchard et al. (1954)	$1.74 \times 10^{-11} \exp{-(2835/RT)^{c}}$	14.5	
	$1.45 \times 10^{-11} \exp-(3026/RT)^d$	8.75	
Clyne and Walker (1973)	$5.1 \times 10^{-11} \text{ exp-}(3560 \pm 37/\text{RT})$	13.0	300-686
Poulet et al. (1974)	$(1.84 \pm 0.14) \times 10^{-11} \text{ exp-}(2800 \pm 200/\text{RT})$	13.6	295-490
This work	$(7.44 \pm 0.7) \times 10^{-12} \exp(2437 \pm 100/RT)$	11.6	218-401
Davis et al. (1970)		15.0	298

^a Based on the Fettis and Knox (1964) evaluation of Cl + H₂ (see Table 7).

ATMOSPHERIC IMPLICATIONS OF NEW RATE DATA

Numerous model calculations have demonstrated that the injection of chlorinated compounds into the stratosphere results in the selective destruction of odd oxygen at midaltitudes (≈ 25-45 km) (Cicerone et al., 1974,

1975; Crutzen, 1974; Crutzen and Isaksen, 1976; Molina and Rowland, 1974; Rowland and Molina. 1975; Wofsy and McElroy, 1974; Wofsy et al., 1975), where the catalytic efficiency (ρ) can be expressed via equation II:

$$\rho \propto \frac{2k_{a}k_{b}k_{e}J_{a}[O_{3}]^{2}[HCI][OH]}{k_{d}[RH]\{k_{b}J_{a}[O_{3}] + k_{c}k_{f}[NO][O_{2}][M]\}}$$
(II)

bEvaluation based on their own data, and reinterpreted data taken from Ashmore and Chanmugam (1953), Clyne and Stedman (1966), Fettis and Knox (1964), Rode-Bush and Klingelhoefer (1933), Steiner and Rideal (1939), and Westenberg and deHaas (1968).

^cA. Evaluation based on determinations of both k_{H2} and k_{H2} (Benson et al., 1969; Clyne and Stedman, 1966; Davis et al., 1970; Westenberg and deHaas, 1968).

B. Evaluation based on k_{H2} (Clyne and Stedman, 1966; Davis et al., 1970; Westenberg and deHaas, 1968).

 $^{^{\}rm d}$ A. Direct determination of $k_{\rm H_2}$ using flash photolysis/resonance fluorescence (Watson et al., 1976b).

B. Evaluation based on (A), and on data from Benson et al. (1969) and Steiner and Rideal (1939).

^bBased on the Benson et al. (1969) evaluation.

^c Based on the Clyne and Walker (1973) evaluation.

dBased on the Watson et al. (1976b) evaluation.

The present study reinvestigated the kinetic behavior of processes (a), $(Cl + O_3 \rightarrow ClO + O_2)$, and, in part, (d), where k_d [RH] can be written:

$$k_d[RH] = k_2[CH_4] + k_3[H_2]$$

+ $k_4[H_2O_2] + k_5[HO_2]$

New results are reported for k_2, k_3 , and k_4 . The most expedient approach to evaluating the effect of the new rate-constant data upon the published results of the model calculations is to assume that the altitude most sensitive to the injection of ClO_{x} , the altitude of maximum ozone reduction, is 35 km, and to discuss the consequences of the new kinetic information at that altitude. The temperature of the standard stratosphere at 35 km is taken to be 237K.

The early model calculations (Cicerone et al., 1974, 1975; Crutzen, 1974; Wofsy and McElroy, 1974) used a temperature-invariant rate constant of 1.85 × 10⁻¹¹ cm³ molecule⁻¹ s⁻¹ for k_a . A value of 9.06 \times 10⁻¹² cm³ molecule⁻¹ s⁻¹ was derived for k_a at 237K from the Arrhenius expression obtained in the present study. This is in close agreement with the value of 9.09 X 10-12 cm3 molecule-1 s-1 which was obtained from the "evaluated" Arrhenius expression (see discussion of reaction (1)) (Watson, 1976; Watson et al., 1976b). The new value of ka at 237K is a factor of 2.0 lower than that used in the early calculations. Consequently, the use of equation II would predict that the catalytic efficiency (ρ) would be reduced by a factor of 2; however, this simplistic approach predicts the maximum possible change. The actual change will probably be less than a factor of 2, due to an increase in the ozone density at lower altitudes produced by the "self-healing" effect.

The greater the magnitude of k_d [RH], the lower the catalytic efficiency of ClO_x , due to the "tying up" of chlorine in an inactive form, HCl. Although concentration profiles for both CH_4 and H_2 have been experimentally determined up to ≈ 50 km in the stratosphere (Ehhalt and Heidt, 1973, 1974) neither HO_2 nor H_2O_2 has been directly detected. Consequently, the only profiles which exist for $[HO_2]$ and $[H_2O_2]$ are those predicted by the one-dimensional photochemical models. Considerable uncertainty exists in the rate-constant data for the reactions which

exert control over the atmospheric concentrations of HO₂ and H₂O₂ (and OH), e.g.,

OH + HO₂
$$\stackrel{k_i}{\rightarrow}$$
 H₂O + O₂;
 $k_{(i)} = 2 \times 10^{-11} \cdot 2 \times 10^{-10}$
O + HO₂ $\stackrel{k_{ii}}{\rightarrow}$ OH + O₂;
 $k_{(ii)} = 8 \times 10^{-11}$ exp-(500/T)
 $\stackrel{t}{\pm}$ factor 4
HO₂ + HO₂ $\stackrel{k_{iii}}{\rightarrow}$ H₂O₂ + O₂;
 $k_{(iii)} = 3 \times 10^{-11}$ exp-(500/T)
 $\stackrel{t}{\pm}$ factor 2

The magnitude of [HOx], and its partitioning $(HO_x \equiv H + OH + HO_2 + H_2O_2)$, are dependent upon the selection of rate-constant data for reactions (i)-(iii). The majority of model calculations have been performed using a high value $(2 \times 10^{-10} \text{ cm}^3 \text{ molecule}^{-1} \text{ s}^{-1})$ for $k_{(i)}$, the predominant chain-termination process for HOx, resulting in a low $[HO_x]/([H_2O] + [CH_4] +$ [H2]) ratio. Recent rate data (Davidson et al., 1976) for $O(^{1}D)$ quenching by N_{2} and O_{2} , and $O(^{1}D)$ reaction with $H_{2}O$, CH_{4} , $N_{2}O$, and H_{2} , increase the uncertainty in the accuracy of the published [HO_x] profiles. Model calculations which have used high values for k(i) and k(ii) (2 × 10⁻¹⁰ and 6 × 10⁻¹¹ respectively) predict that [HO₂] at 35 km has a value of $\approx 1.7 \times 10^7$ molecules cm-3 (Wofsy and McElroy, 1974), whereas the model calculations which have used low values for $k_{(i)}$ and $k_{(ii)}$ (2 × 10⁻¹¹ for each) predict that the concentration of HO2 at 35 km is $\approx 7.8 \times 10^7$ molecules cm⁻³ (Cicerone, 1976). The H₂O₂ concentration is predicted to range from about 2 to 10 × 108 molecules cm-3 at 35 km. Unfortunately, not only is the HO2 concentration uncertain because of a lack of reliable rate-constant data for the above processes, but k_5 (Cl + HO₂ \rightarrow HCl + O₂) has not been experimentally measured. The most probable value for k_5 is estimated to be $\approx 2 \times 10^{-11}$ cm³ molecule⁻¹ s⁻¹; however, a range of values

from 1×10^{-11} to 1×10^{-10} cm³ molecule⁻¹ s⁻¹ has been used in the model calculations. Table 8 presents the range of magnitudes that can be expected for atomic-chlorine reaction rates. The mixing ratio for both H_2 and CH_4 was taken to be 0.67 ppm (v/v) (Ehhalt and Heidt, 1973, 1974). It is unlikely that the mixing ratios are significantly inaccurate, although there is a lack of data above 35 km.

From Table 8 it can be seen that reaction with either CH4 or HO2 is expected to be the dominant sink for atomic chlorine. Crutzen (1974) used the values of Clyne and Walker for $k_2(CH_4)$ and $k_3(H_2)$, 1 × 10⁻¹⁰ cm³ molecule⁻¹ s⁻¹ for $k_5(HO_2)$, 2 × 10⁻¹⁰ and 2 × 10⁻¹¹ cm³ molecule-1 s-1 for k(i) and k(ii) respectively, resulting in an HO₂ concentration of 2.6 × 10⁷ molecules cm-3 at 35 km. Therefore, the relative rates for Cl-atom destruction were 2.9 × 10-3 (CH_4) , 4.5 × 10⁻⁴ (H_2) , and 2.6 × 10⁻³ (HO_2) . The new rate data for k2 and k3 would increase k_2 [CH₄] to 4.6 × 10⁻³, and decrease k_3 [H₂] to 2.5 × 10-4. Thus, k_d [RH] would increase from 5.95 to 7.25 \times 10⁻³ (\approx 22%). Wofsy and McElroy (1974) used the values of Clyne and Walker (1973) for k₂(CH₄), and of Westenberg and deHaas (1968) for k₃(H₂), 1 × 10⁻¹¹ cm³ molecule-1 s-1 for $k_5(HO_2)$, and 2 × 10-10 and 6×10^{-11} cm³ molecule-1 s⁻¹ for $k_{(i)}$ and $k_{(ii)}$. This resulted in an HO₂ concentration of ≈ 1.7 X 107 molecules cm⁻³ at 35 km. Therefore, the relative rates for chlorine-atom destruction were

 2.9×10^{-3} (CH₄), 2.4×10^{-4} (H₂), and $1.7 \times$ 10-4 (HO₂). The new rate data for k₂ and k₃ would increase $k_2[CH_4]$ to 4.6×10^{-3} , but leave $k_3[H_2]$ the same. Therefore, $k_d[RH]$ is increased from 3.3 to 5.0 \times 10⁻³ (\approx 52%). Consequently, it is evident that the new rateconstant data causes a small but significant decrease in the catalytic efficiency, p. A conclusion of this paper is that the Cl + H₂O₂ reaction is not a significant sink (< 0.05 kd [RH]) for atomic chlorine for any combination of HOx rate constants, whereas experimental data are required for the Cl + HO2 reaction to determine its importance. If the rate constants for k(i), $k_{(ii)}$, and $k_{(iii)}$ are 2 × 10⁻¹¹, 2 × 10⁻¹¹ and 3 × 10-12 cm³ molecule-1 s-1 respectively, then the [HO₂] profile will be the maximum possible. Under these conditions, if $k_5 \ge 6 \times 10^{-11} \text{ cm}^3$ molecule-1 s-1, then the magnitude of ks [HO₂] ≥ k₂ [CH₄]. However, the greatest perturbing effect of this combination of values for k(i), k_(ii), and k_(iii) would be an increase in [OH], leading to an enhancement of ρ by accelerated regeneration of atomic chlorine via the OH + HCl reaction.

ACKNOWLEDGMENT

One of the authors, D.D. Davis, would like to express his appreciation to the National Aeronautics and Space Administration for their support of this research.

Table 9. Magnitudes of Various Atomic-Chlorine Sinks at 35 km

		k(2371	K) cm ³ molecule	-1 _S -1	104	k[reagent]	s ⁻¹
Species	Concentration (molecules cm ⁻³)	This Study	Clyne & Walker	Others	This Study	Clyne & Walker	Others
CH ₄	1.1 × 10 ¹¹	4.2 × 10 ⁻¹⁴	2.6 × 10 ⁻¹⁴	-	46	29	-
H ₂	1.1×10^{11}	2.3 × 10 ⁻¹⁵	4.1 × 10 ⁻¹⁵	1.1×10^{-15} (a) 2.2×10^{-15} (b)	2.5		1.2 2.4
H ₂ O ₂	$(2-10) \times 10^8$	≈2.5 × 10 ⁻¹³ (c)	-	-	0.5 to 2.5		-
HO ₂	$(1.5 - 8) \times 10^7$	$\approx 2 \times 10^{-11} (d)$	-	(1 - 10) × 10-11(e)	3 to 16	-	1.5 to 80

^aBenson et al. (1969)

bWestenberg and deHaas (1968)

^cCalculated using an estimated Arrhenius expression of 1×10^{-11} exp-(875/T) which is compatible with a mean value of \approx 5.8 \times 10⁻¹³ cm³ molecule-1 s⁻¹ at 298K.

dAuthor's estimate.

eEstimates.

REFERENCES

- Anderson, J.M., F. Kaufman, and M.S. Zahniser (1976), "Kinetics of the reaction Cl + O₃ → ClO + O₂," Chem. Phys. Lett. 37, 226.
- Ashmore, P.G. and J. Chanmugam (1953), "Reactions in the system hydrogen, chlorine, nitric oxide, and nitryl chloride. Part 1. The reaction between hydrogen and chlorine in the presence of nitric oxide and nitrosyl chloride," Trans. Faraday Soc. 49, 254.
- Ausloos, P.R. Gorden, and S.G. Lias (1964), "Effect of pressure in the radiolysis and photolysis of methane," J. Chem. Phys. 40, 1854.
- Becker, K.H., U. Schurath, and H. Seitz (1974), "Ozone-olefin reactions in the gas phase. I. Rate constants and activation energies," Int. J. Chem. Kinet. 6, 725.
- Benson, S.W., F.R. Cruickshank, and R. Shaw (1969), "Iodine monochloride as a thermal source of chlorine atoms: The reaction of chlorine atoms with hydrogen," Int. J. Chem. Kinet. 1, 29.
- Braun, W., K.H. Welge, and J.R. McNesby (1966), "Flash photolysis of methane in the vacuum ultraviolet, I. End product analysis," J. Chem. Phys. 45, 2650.
- Calvert, J.G. and J.N. Pitts, Jr. (1967), Photochemistry, Wiley, New York, 201 pp.
- Cicerone, R.J. (1976), private communication.
- Cicerone, R.J., R.S. Stolarski, and S. Walters (1974), "Stratospheric ozone reduction by man-made chlorofluoromethanes," Science 185, 1165.
- Cicerone, R.J., D.H. Stedman, and R.S. Stolarski (1975), "Estimate of late 1974 stratospheric concentrations of gaseous chlorine compounds (ClX)," Geophys. Res. Lett. 2, 219.
- Clyne, M.A.A. and D.H. Stedman (1966), "Reactions of atomic hydrogen with hydrogen chloride and nitrosyl chloride," Trans. Faraday Soc. 62, 2164.
- Clyne, M.A.A. and R.F. Walker (1973), "Absolute rate constants for elementary reactions in the chlorination of CH₄, CD₄, CH₃Cl, CH₂Cl₂, CHCl₃, CDCl₃ and CBrCl₃," J. Chem. Soc. Faraday Trans. I 69, 1547.
- Clyne, M.A.A. and R.T. Watson (1974), "Kinetic studies of diatomic free radicals using mass spectrometry. Part 2 Rapid bimolecular reactions involving the ClO(X ²Π) radical," J. Chem. Soc. Faraday Trans. 1 70, 2250.

- Clyne, M.A.A., D. McKenny, and R.T. Watson (1975), "Reactions of chlorine oxide radicals. Part 5 – The reaction 2ClO(X ²Π) → Products," J. Chem. Soc. Faraday Trans. I 71, 322.
- Crutzen, P.J. (1974), "Estimates of possible future ozone reductions from continued use of fluoro-chloro-methanes (CF₂Cl₂, CFCl₃)," Geophys. Res. Lett. 1, 205.
- Crutzen, P.J. and I.S.A. Isaksen (1976), "The impact of the chlorocarbon industry on the ozone layer," J. Geophys. Res., in press.
- Davidson, J.A., C.M. Sadowski, H.I. Schiff, G.E. Streit, C.J. Howard, A.L. Schmeltekopf, and D.A. Jennings (1976), "Absolute rate constant determinations for the deactivation of O(¹D) by timeresolved decay of O(¹D) → O(³P) emission," J. Chem. Phys. 64, 57.
- Davis, D.D. and R.B. Klemm (1972), "A flash photolysis-resonance-fluorescence kinetics study of ground-state sulfur atoms: I. Absolute rate parameters for reaction of $S(^3P)$ with $O_2(^3\Sigma)$," Int. J. Chem. Kinet. 4, 367.
- Davis, D.D., W. Braun, and A.M. Bass (1970), "Reactions of Cl(²P_{3/2}). Absolute rate constants for reaction with H₂, CH₄, C₂H₆, CH₂Cl₂, C₂Cl₄ and c-C₆H₁₂," Int. J. Chem. Kinet. 2, 101.
- Davis, D.D., R. Huie, J. Herron, W. Braun, and M. Kurylo (1972), "Absolute rate constants for the reaction of atomic oxygen with ethylene over the temperature range 232-500°K," J. Chem. Phys. 56, 4868.
- Davis, D.D., S. Fischer, and R. Schiff (1974), "Flash photolysis-resonance fluorescence kinetics study: Temperature dependence of the reactions OH + CO → CO₂ + H and OH + CH₄ → H₂O + CH₃," J. Chem. Phys. 61, 2213.
- Davis, D.D., J.F. Schmidt, C.M. Neeley, and R.J. Hanrahan (1975), "Effect of wavelength in the gas-phase photolysis of carbon tetrachloride at 253.7, 184.9, 147.0, and 106.7 nm," J. Phys. Chem. 79, 11.
- DeMore, W.B. and O.J. Raper (1964), "Hartley band extinction coefficients of ozone in the gas phase and in liquid nitrogen, carbon monoxide, and argon," J. Phys. Chem. 68, 412.
- Donovan, R.J., D. Husain, A.M. Bass, W. Braun, and D.D. Davis (1969), "Kinetic spectroscopic studies of Cl(3p⁵ ²P_{3/2},1/2) in the vacuum ultraviolet," J. Chem. Phys. 50, 4115.
- Ehhalt, D.H. and L.E. Heidt (1973), "The concentration of molecular H₂ and CH₄ in the stratosphere," Pure Appl. Geophys. 106-8, 1352.

- Ehhalt, D.H. and L.E. Heidt (1974), "Vertical profiles of molecular H₂ and CH₄ in the stratosphere," AIAA J. 12, 822.
- Fettis, G.C. and J.H. Knox (1964), "The rate constants of halogen atom reactions," in "Progress in Reaction Kinetics," Pergamon Press, Vol. 2, 1.
- Hudson, R.D. (1974), "Absorption cross-sections of stratospheric molecules," Can. J. Chem. 52, 1465.
- Knox, J. and R. Nelson (1959), "Competitive chlorination reactions in the gas phase: Hydrogen and C₁-C₅ saturated hydrocarbons," Trans. Faraday Soc. 55, 937.
- Kurylo, M.J. and W. Braun (1976), "Flash photolysis resonance fluorescence study of the reaction Cl + O₃ → ClO + O₂ over the temperature range 213-298K," Chem. Phys. Lett. 37, 232.
- Leighton, P.A., and A.B. Steiner (1936), "The photochemical decomposition of methane," J. Am. Chem. Soc. 58, 1823.
- Mahan, B.H. and R. Mandal (1962), "Vacuum ultraviolet photolysis of methane," J. Chem. Phys. 37, 207.
- Molina, M.J. and F.S. Rowland (1974), "Stratospheric sink for chlorofluoromethanes: Chlorine atomcatalysed destruction of ozone," Nature 249, 810.
- Nip, W.S. and M.A.A. Clyne (1976), "Study of elementary reactions by atomic resonance absorption with a non-reversed source. I. The reaction Cl + O₃ → ClO + O₂," J. Chem. Soc. Faraday Trans. II 72, 838.
- Poulet, G., G. LeBras, and J. Combourieu (1974), "Etude cinétique des réactions du chlore atomique et du radical ClO avec le méthane par la technique du réacteur à écoulement rapide, couplé à un spectromètre de masse," J. Chimie Phys. 71, 101.
- Pritchard, H.O., J.B. Pyke, and A.F. Trotman-Dickenson (1954), "A method for the study of chlorine atom reactions: The reaction Cl + CH₄ → CH₃ + HCl," J. Am. Chem. Soc. 76, 1201.

- Rode-Bush, W.H. and W.C. Klingelhoefer (1933), "Atomic chlorine and its reaction with hydrogen," J. Am. Chem. Soc. 55, 130.
- Rowland, F.S. and M.J. Molina (1975), "Chlorofluoromethanes in the environment," Rev. Geophys. Space Phys. 13, 1.
- Steiner, H. and E.K. Rideal (1939), "The exchange reactions between deuterium and hydrogen halides. I: Hydrogen chloride," Proc. Roy. Soc. (London), Ser. A 173, 503.
- Watson, R.T. (1974), "Reactions of CIO_X of Atmospheric Interest (Part I)," Chemical Kinetics Data Survey VIII, National Bureau of Standards NBSIR 74-516.
- Watson, R.T. (1976), "Reactions of ClO_X of Atmospheric Interest (Part II)," to appear in J. Phys. Chem. Ref. Data.
- Watson, R.T., E.S. Machado, S. Fischer, and D.D. Davis (1976a), "A temperature dependence kinetics study of the reactions of $Cl(^2P_{3/2})$ with O_3 , CH_4 and H_2O_2 ," J. Chem. Phys., in press.
- Watson, R.T., E.S. Machado, B.C. Conaway, Y. Oh, R.L. Schiff, and D.D. Davis (1976b), "A kinetic study of the reaction of Cl atoms with several simple molecules: Comparison of competitive and direct experimental techniques," manuscript in preparation.
- Westenberg, A.A. and N.J. deHaas (1968), "Atommolecule kinetics using ESR detection. IV. Results for Cl + H₂ ≠ HCl + H in both directions," J. Chem. Phys. 48, 4405.
- Wofsy, S. and M. McElroy (1974), "HO_x, NO_x, and ClO_x: Their role in atmospheric photochemistry," Can. J. Chem. **52**, 1582.
- Wofsy, S., M. McElroy, and N. Sze (1975), "Freon consumption: Implications for atmospheric ozone," Science 187, 535.

REACTION RATE DATA FOR THE STRATOSPHERE: HOW GOOD ARE THEY NOW?

D. GARVIN, R.F. HAMPSON, AND M.J. KURYLO

National Bureau of Standards Gaithersburg, Maryland

ABSTRACT: The reaction-rate and photochemical data currently available for use in modeling of stratospheric chemistry are reviewed. They are characterized in terms of their quality and applicability. Of 46 "important" chemical reactions, the data for 33 are adequate. For 82 "less important" reactions, the data are generally less reliable, but in many cases sufficient. A similar pattern exists for photochemical processes. The data are adequate for 8 of 16 "important" processes and are adequate for 5 of 16 "less important" processes. A list of reactions for which more measurements are needed is supplied.

Quantitative models of stratospheric chemistry require a large amount of numerical data as input, in the form of rate constants, optical absorption coefficients, and quantum yields. These data become useful after the likely chemical mechanism has been identified. The results predicted by the models are very sensitive to some of the input data. The results are much less sensitive to certain other input data, which nonetheless represent important processes in the mechanism, such as catalytic cycles and the formation and destruction of atoms and free radicals. Still other data are needed for reactions that have been included for the sake of completeness. Finally, there are numerical data that are needed for the decision-making process of developing the mechanism for the complex system, but are not included in the models.

The quality and applicability of the available data are analyzed in this paper in order to show the present status of the field and to point out needs for new measurements. The starting point is the information in Chapter 5 of "The Natural Stratosphere of 1974" (CIAP, 1975).

Section 3 of Chapter 5 is a list of reactions that "need to be considered in the modeling of the stratosphere" (Johnston et al., 1975). The list includes both chemical reactions and photochemical processes. It was annotated to indicate which ones are "considered to be important by modelers". These selections were based more on a knowledge of plausible chemistry than on sensitivity analysis.

A slightly revised version of this list is used in this paper. The revisions allow for new data

and new ideas about which processes are important. This new list includes 128 chemical reactions and 32 photochemical processes. 46 of the chemical reactions and 16 of the photochemical processes are considered to be important. This revised list is given in tables in an arrangement pertinent to the analysis to be described shortly.

Section 9 of the same chapter contains a table of rate constants and photochemical data for about 300 processes (Garvin and Hampson, 1975). The preferred values given for 160 of these reactions are recommended for use by modelers. Where possible, estimates of the likely accuracy of the data are given. These are subjective judgments, usually based on consideration of the degree of agreement among measurements made in several laboratories and on an assessment of the methods used.

Information on accuracy, temperature range of measurement, and extent of the data base contained in this table are used to analyze the list of reactions that need to be considered in stratospheric modeling.

The chemical-kinetic data were put into five classes according to their likely renability, and into three classes according to the temperatures at which the data had been obtained. For photochemical processes, a simple twofold classification was used. These categories are listed in Table 1.

CHEMICAL KINETICS

The reliability classification for chemical reactions generally follows the estimates of likely

Table 1. Definition of Classification Scheme Used in Analysis of Chemical-Kinetic and Photo-Chemical Data

Rate-Constant Reliability Classification

lo	g ₁₀ l	(=	×	£	x
A	0	<	x	<	0.1
В	0.1	<	x	<	0.3
C	0.3	<	x	<	1
D		1	<	x	
E		no	d	ata	a

Temperature Range of Measured Data

- 1 includes stratospheric temperatures
- 2 range of $T \ge 300$ K
- 3 300K only

Photochemical Processes

- α σ_{λ} and ϕ_{λ} well characterized
- β further study desirable

accuracy. However, no reaction was placed in the top category, A, unless there were measurements for it from two or more laboratories. This category is for data good to 25% or better. Measurement differences between laboratories are often of this order unless there is a deliberate cooperative program of intercomparison. Cate-

gories B and C are for data known to within factors of two and ten, respectively. Category D means that an order-of-magnitude estimate or an upper or lower limit has been obtained. Category E means that no reliable data exist.

Table 2 presents the statistics on distribution of the chemical-kinetic data according to reliability and temperature range of measurements. The individual reactions are listed in Tables 3 and 4 in groups keyed to the classification scheme in Table 1.

The overall status of the rate data for the 46 important chemical reactions is presented in Table 2. Consideration of the data for the individual reactions indicates that for the 33 reactions in categories A and B the rate-constant data are in good shape from room temperature down to the stratospheric temperature regime. The six rate constants indicated as measured to within 25% at 300K only (A3) are actually known reliably at stratospheric temperatures, since they are rate constants for O(1D) reactions which occur with nearly unit collision efficiency. They will have very small temperature coefficients. Recent (unpublished) measurements on some of them as a function of temperature (Schmeltekopf, 1975) will shift this set to another category in the A and B series. The reactions in category B3 are either radical-radical or combination reactions. Their temperature

Table 2. Summary of Rate-Constant Data for 46 Important Chemical Reactions and 82 Less Important Chemical Reactions Categorized According to Reliability and Temperature Range

		<u>T</u>	emperature Range		
Category	δ log ₁₀ k	Strat. Temp.	> 300K	3 300K only	Total
		Important Chemic	cal Reactions		
A	0.1	6	1	6	13
В	0.3	9	5	6	20
C	1		2	6	8
D	>1			3	3
E	no data			2	2
		Less Important Che	mical Reactions		
A	0.1				
В	0.3	8	7	11	26
C	1	1	9	12	22
D	>1			4	4
E	no data			30	30

coefficients also will be small. The overall good status of the rate data for these reactions reflects the intensive efforts made recently by experimental kineticists.

For the less important chemical reactions, summarized in Table 2 and listed in Table 4, the reaction-rate data are in poorer shape. None are in category A. For 30 of the 82 there are no data. There are several reasons for this. Many of these reactions are minor paths. The models are unlikely to be sensitive to them. Rough data can

be accepted until a reaction is shown to be important. It is not surprising that there has been no intensive effort to improve the data on these reactions.

Also, the situation is not so bad as it appears from Table 2. There is no evidence, to date, that certain of these reactions occur. They were included in the survey in an attempt to cover the possible interactions of the trace species known (or suspected) to play roles in stratospheric chemistry. For example, 12 reactions of HSO_x

Table 3. Important Chemical Reactions Categorized According to Reliability and Temperature Range (see Table 1 for description of categories)

<u>A1</u>	<u>A2</u>	<u>A3</u>
$O + O_2 + M \rightarrow O_3 + M$	$N + NO \rightarrow N_2 + O$	$N_2O + O(^1D) \rightarrow N_2 + O_2$
$O_3 + O \rightarrow O_2 + O_2$		$N_2O + O(^1D) \rightarrow NO + NO$
$NO_2 + O \rightarrow NO + O_2$		$O(^{1}D) + O_{2} \rightarrow O + O_{2}(^{1}\Sigma)$
$NO_2 + O_3 \rightarrow NO_3 + O_2$		$O(^1D) + H_2O \rightarrow 2HO$
$H + O_2 + M \rightarrow HO_2 + M$		$O(^1D) + H_2 \rightarrow H + HO$
$HO + CH_4 \rightarrow H_2O + CH_3$		$O(^{1}D) + CH_{4} \rightarrow CH_{3} + HO$
<u>B1</u>	<u>B2</u>	<u>B3</u>
$NO + O_3 \rightarrow NO_2 + O_2$	$N + O_2 \rightarrow NO + O$	$O(^1D) + M \rightarrow O + M$
$HO + NO_2 (+ M) \rightarrow HNO_3 (+ M)$	$H + O_3 \rightarrow HO^* + O_2$	$HO_2 + HO_2 \rightarrow H_2O_2 + O_2$
$HO + HNO_3 \rightarrow H_2O + NO_3$	$HO + O \rightarrow H + O_2$	H ₂ CO + O → HO + HCO
$HO + O_3 \rightarrow HO_2 + O_2$	$H_2O_2 + HO \rightarrow H_2O + HO_2$	$NO_2 + O + M \rightarrow NO_3 + M$
$HO_2 + O_3 \rightarrow HO + 2O_2$	$H_2CO + HO \rightarrow HCO + H_2O$	$ClO + O \rightarrow Cl + O_2$
$HO + CO \rightarrow CO_2 + H$		CIO + NO → CI + NO ₂
$Cl + O_3 \rightarrow ClO + O_2$		
$CI + CH_4 \rightarrow HC1 + CH_3$		
HCl + HO → H ₂ O + Cl		
	<u>C2</u>	<u>C3</u>
	$HO_2 + NO \rightarrow HO + NO_2$	$NO_3 + NO \rightarrow 2NO_2$
	$CH_3O + O_2 \rightarrow CH_2O + HO_2$	$HO_2 + NO_2 \rightarrow HNO_2 + O_2$
		$HO + HO_2 \rightarrow H_2O + O_2$
		$CH_3 + O_2 \rightarrow CH_3OO$
		$CH_3 + O_2 \rightarrow CH_2O + HO$
		$HCO + O_2 \rightarrow CO + HO_2$
<u>E</u>		<u>D3</u>
$HO_2 + O \rightarrow HO + O_2$		CH3OO + NO - + CH3O + NO2
$CI + HO_2 \rightarrow HCI + O_2$		CIO + O3 - OCIO + O2
My males areas (2)		$ClO + O_3 \rightarrow ClOO + O_2$

Table 4. Less Important Chemical Reactions Categorized According to Reliability and Temperature Range (see Table 1 for description of categories)

<u>B1</u>	<u>B2</u>	<u>B3</u>
$O + O + M \rightarrow O_2 + M$	$2NO + O_2 \rightarrow 2NO_2$	$N + O_3 \rightarrow NO + O_2$
$NO + O + M \rightarrow NO_2 + M$	$HO + NO + M \rightarrow HNO_2 + M$	$N + NO_2 \rightarrow N_2O + O$
$O_2(^1\Delta) + O_3 \rightarrow 2O_2 + O$	$O_2(^1\Delta) + M \rightarrow O_2 + M$	$N + HO \rightarrow NO + H$
$NH_3 + HO \rightarrow NH_2 + H_2O$	$HO + HO \rightarrow H_2O + O$	$O_2(^1\Sigma) + M \rightarrow O_2 + M$
HO + H ₂ → H ₂ O + H	$HO + HO + M \rightarrow H_2O_2 + M$	$O_2(^1\Sigma) + O_3 \rightarrow O_2 + O_2 + O$
H ₂ S + O → HO + HS	$O + CH_4 \rightarrow CH_3 + HO$	$H_2S + HO \rightarrow H_2O + HS$
$SO_2 + O + M \rightarrow SO_3 + M$	OCIO + CI → 2CIO	$SO_2 + HO_2 \rightarrow HO + SO_3$
$C1 + H_2 \rightarrow HC1 + H$		$SO_2 + HO + M \rightarrow HSO_3 + M$
		OCIO + O → CIO + O ₂
		$CF_2Cl_2 + O(^1D) \rightarrow products$
		$CFCl_3 + O(^1D) \rightarrow products$
<u>C1</u>	<u>C2</u>	<u>C3</u>
$SO + O_3 \rightarrow SO_2 + O_2$	$NO_2 + NO_3 (+ M) \rightarrow N_2O_5 (+ M)$	$HO + HNO_2 \rightarrow H_2O + NO_2$
	$N_2O_5 (+ M) \rightarrow NO_2 + NO_3 (+ M)$	$HO_2 + NO + M \rightarrow HNO_3 + M$
	$NO_3 + NO_2 \rightarrow NO + O_2 + NO_2$	$O(^{1}D) + O_{3} \rightarrow O_{2} + O_{2}$
	$H_2O_2 + O \rightarrow HO + HO_2$	$O(^{1}D) + O_{3} \rightarrow O_{2} + 2O$
	$HO_2 + H \rightarrow HO + HO$	$HO(v > 2) + O_3 \rightarrow H + 2O_2$
	$HO_2 + H \rightarrow H_2 + O_2$	$HO(v > 2) + O_3 \rightarrow HO_2 + O_2$
	$SO_3 + O \rightarrow SO_2 + O_2$	$HO(v > 3) + O_3 \rightarrow HO + O_2 + O$
	CIO + CIO → products	$HO_2 + H \rightarrow H_2O + O$
	HCl + O → HO + Cl	$SO_3 + H_2O \rightarrow H_2SO_4$
		$Cl + O_2 + M \rightarrow Cloo + M$
		$Cloo + M \rightarrow Cl + O_2 + M$
		$Cl + H_2O_2 \rightarrow HCl + HO_2$
		<u>D3</u>
		$N_2O_5 + O \rightarrow 2NO_2 + O_2$
		$N_2O_5 + H_2O$ (on particles) \rightarrow 2HNO
		$CH_3OO + NO_2 \rightarrow CH_3OONO_2 \xrightarrow{hp} ?$
		$SO_2 + NO_3 \rightarrow SO_3 + NO_2$
E	<u>E</u>	<u>E</u>
$N + HO_2 \rightarrow HO + NO$	$HSO_3 + HSO_3 \rightarrow H_2SO_3 + SO_3$	$HSO_6 + NO \rightarrow HSO_5 + NO_2$
$NH_2 + oxides \rightarrow NO_x$	$HSO_3 + HO \rightarrow H_2O + SO_3$	$HSO_6 + SO_2 \rightarrow HSO_5 + SO_3$
$CH_3OO + HO_2 \rightarrow CH_3OOH + O_2$	$HSO_3 + HO (+ M) \rightarrow H_2SO_4 (+ M)$	$Cl + O_3 (+ M) \rightarrow ClO_3 (+ M)$
$CH_3O + HO_2 \rightarrow CH_3OH + O_2$	HSO ₃ + surface → products	$HO_2 + CIO \rightarrow HCIO + O_2$
CH ₃ OH + HO → H ₂ O + CH ₂ OH	$HSO_3 + O_2 + M \rightarrow HSO_5 + M$	$HO_2 + OCIO \rightarrow HCIO_2 + O_2$
$+1S + oxides \rightarrow SO_2$	$HSO_5 + NO \rightarrow HSO_4 + NO_2$	CIO + OCIO → CI ₂ O + O ₂
SO ₂ + surface → ?	$HSO_4 + HO_2 \rightarrow H_2SO_4 + O_2$	$OCIO + CO \rightarrow CIO + CO_2$
SO ₃ + H ₂ O (surface) → ?	$HSO_4 + HSO_4 \rightarrow H_2S_2O_8$	C100 + C0 → C10 + CO ₂
0. + CO + CO + SO	HSO ₄ + surface → ?	HCl + surface → products
$SO_3 + CO \rightarrow CO_2 + SO_2$		HO + CIO - HCIO

HO + ClO₃ → HClO₄

HSO₄ + O₂ → HSO₆

SO + NO₂ - SO₂ + NO

radicals in category E, though mechanistically interesting, are unlikely to be important. Five more in category E are reactions forming or destroying ClO₂ or ClO₃, both of which are currently thought to be of minor importance in the stratosphere. Probably no more than a dozen of these "no data" reactions deserve any attention in modeling the stratosphere.

PHOTOCHEMISTRY

The species that can undergo photochemical decomposition are listed in Table 5, arranged in groups reflecting the quality of the data. The analysis made here simply divides the processes into those for which the data are acceptable and those for which more laboratory studies would be helpful.

In general, the input data required for photochemical processes consist of photoabsorption cross-section data, primary quantum-yield data for all photodissociative channels, and identification of secondary reactions of the primary fragments. The last item is needed both for construction of mechanisms of stratospheric chemistry and also for the interpretation of the laboratory experiments.

Of the 32 photochemical processes shown, 16 are considered important by modelers. Of these 16 processes, eight are well characterized while eight require further study. The table also includes 16 photochemical processes considered to be less important, 11 of which need further study.

For most of those processes characterized as needing further study, absorption cross-section

Table 5. Photochemical Processes Categorized According to Quality of Data (see Table 1 for definition of categories)

Important Processes

<u>α</u>	β
$O_2 + h\nu \rightarrow O + O$	$NO_3 + h\nu \rightarrow NO_2 + O$
$O_3 + h\nu \ (\lambda = 450-650 \text{ nm}) \rightarrow O_2 + O$	$NO + h\nu \rightarrow N + O$
$O_3 + h\nu (\lambda = 310-340 \text{ nm}) \rightarrow O(^3P) + O_2$	$H_2O_2 + h\nu \rightarrow 2HO$
$O_3 + h\nu \ (\lambda < 310 \text{ nm}) \rightarrow O_2(^1\Delta) + O(^1D)$	$CH_3OO + h\nu \rightarrow ?$
$NO_2 + h\nu \rightarrow NO + O$	HCHO + $h\nu \rightarrow H_2 + CO$
$N_2O + h\nu \to N_2 + O(^1D)$	$HCHO + h\nu \rightarrow H + HCO$
$HNO_3 + h\nu \rightarrow HO + NO_2$	$CF_2Cl_2 + h\nu \rightarrow Cl + CF_2Cl_2$
$HNO_2 + h\nu \rightarrow HO + NO$	$CFCl_3 + h\nu \rightarrow Cl + CFCl_2$

Less Important Processes

α	β
$Cl_2 + h\nu \rightarrow Cl + Cl$	$NO_2 + h\nu (\lambda < 245 \text{ nm}) \rightarrow ?$
$HCl + h\nu \rightarrow H + Cl$	$N_2 + h\nu \rightarrow N + N$
$O(^{1}D) \rightarrow O(^{3}P) + h\nu$	$O_3 + h\nu \ (\lambda < 200 \text{ nm}) \rightarrow ?$
$O_2(^1\Sigma) \rightarrow O_2 + h\nu$	$CH_3OH + h\nu \rightarrow ?$
$O_2(^1\Delta) \rightarrow O_2 + h\nu$	$ClO_2 + h\nu \rightarrow Cl + O_2$
	$OCIO + h\nu \rightarrow CIO + O$
	$CIO + h\nu \rightarrow CI + O$
	$N_2O_5 + h\nu \rightarrow ?$
	$SO_3 + h\nu \rightarrow SO + O_2$
	$SO_3 + h\nu \rightarrow SO_2 + O$
	$HSO_3 + h\nu \rightarrow ?$

data already exist, but primary quantum-yield values and characterization of secondary reactions are needed.

MEASUREMENTS NEEDED

Although it is useful to have a summary of the status of a field, it is more helpful to show what needs to be done. Such lists have been compiled by various workers and distributed informally during the past few years of intensive study of the stratosphere. Our current choices for more work now are given in Table 6.

Table 6. Chemical Reactions and Photochemical Processes for which New Measurements are Needed

HO + HO2 → H2O + O2 C1 + HO2 - HC1 + O2 CI + CH₄ → HCI + CH₃ CIO + O - CI + O2 $C10 + O_3 \rightarrow OC10 + O_2$ $ClO + O_3 \rightarrow [ClOO + O_2] \rightarrow Cl + 2O_2$ CIO + NO → CI + NO2 $CCl_xF_v + h\nu \rightarrow Cl + CCl_{x-1}F_v$ CI + NO2 + M - CINO2 + M $CINO_2 + O \rightarrow CINO + O_2$ CINO2 + hv -> CINO + O HO₂ + O₃ → HO + 2O₂ HO2 + O → HO + O2 HO2 + NO - HO + NO2 HO + halogenated organics → products $CH_3OO + NO \rightarrow NO_2 + CH_3O$ HSO₃ → H₂SO₄ $HSO_x + NO \rightarrow HSO_{x-1} + NO_2$ H2CO + hv - H2 + CO H2CO + hv → H + HCO

The reactions were selected on the basis of several criteria. First, there are some reactions for which new, accurate measurements will be needed in order to resolve ambiguities in the existing data. Second, there are reactions to which the models appear to be very sensitive. Third, there are reactions that are becoming increasingly important in the thinking of atmo-

spheric scientists. In putting this list together, we used the analysis of the status of the field presented here, and also the recommendations of others (CIC, 19.75; IMOS, 19.75).

The individual reactions will not be discussed here. Instead some general remarks are offered as a guide to the reader. Much of the current emphasis in stratospheric chemistry is on reactions of Cl, ClO, and the photochemistry of organic halides. Very few reactions of Cl or of the chlorine oxides have been studied except at room temperature. Measurements at temperatures down to 230K are desirable. Also, the study of the photochemical decomposition of chlorocarbons is incomplete. Absorption coefficients are needed as a function of temperature for each chlorocarbon that can reach the stratosphere. Quantum yields should be checked (many probably will be near unity) and the fate of the organic radicals formed in the photolysis should be determined. This may lead to recognition of the need for further photochemical studies

Rate constants for reactions of hydroxyl with halocarbons are needed because these reactions appear to control the chemical lifetimes of these molecules in the troposphere and thus may be used to estimate the acceptability of substitutes proposed for the halocarbon propellants and refrigerants presently in use.

The hydroperoxyl radical appears prominently in the list. As a radical it is not very reactive. But it is important in cycles that control the concentration of hydroxyl. Indeed, any studies of reaction rates for gas-phase reactions of HO₂ will help in the interpretation of stratospheric chemistry. Those to be emphasized now are reactions of HO₂ with itself, HO, O, and Cl.

Finally, we must warn the reader that this list will rapidly become out of date because of the continuing high level of laboratory activity related to stratospheric chemistry. From our point of view as data evaluators, the sooner this list becomes a dead issue, the better we will like it.

REFERENCES

CIAP (1975), The Natural Stratosphere of 1974, ed. E. Reiter et al., Vol. 1 of the CIAP monograph series, U.S. Dept. of Transportation, DOT-TST-75-51.

- CIC (1975), Interim Report of the Panel on Atmospheric Chemistry, Climatic Impact Committee, NRC Assembly of Mathematical and Physical Sciences, National Academy of Sciences, Washington, DC, July 1975.
- Garvin, D.G. and R.F. Hampson (1975), "Rate and photochemical data," section 5.9 of CIAP Monograph 1, Dept. of Transportation, DOT-OST-75-51, 5-195 - 5-262.
- IMOS (1975), Fluorocarbons and the Environment, Report of Federal Task Force on Inadvertent

- Modification of the Stratosphere, Council on Environmental Quality, Federal Council for Science and Technology, GPO 038-000-00226-1.
- Johnston, H.S., D.D. Davis, and P.J. Crutzen (1975), "Summary of reactions that need to be considered in modeling the stratosphere," section 5.3 of CIAP Monograph 1, Dept. of Transportation, DOT-OST-75-51, 5-36 - 5-42.
- Schmeltekopf, A. (1975), private communication (NOAA, Boulder).

LABORATORY MEASUREMENTS

DISCUSSION

UNIDENTIFIED: In stratospheric chemical models there seems to be a consistent over-prediction of ozone at about 25 kilometers. The effect of atmospheric scattering of sunlight on oxygen atom production, if taken into account, might reduce that overprediction by something like six percent, which is not enough. Does anyone have another explanation? In the photochemically dominated region, chemical models ought to achieve much better agreement with observation.

HEICKLEN: A possible reaction which hasn't been considered in stratospheric models is the reaction of ozone with nitrous acid to give nitric acid. We haven't yet been able to measure its rate, though we have a lot of indirect evidence that it might occur.

SCHIFF: Jack McConnell has calculated the possible effects of that reaction, $HNO_2 + O_3$. When taken by itself, its effects on stratospheric chemistry are small. But when it is taken with another reaction, $HO_2 + NO_2 \rightarrow HNO_2 + O_2$, which you have suggested elsewhere as a source of nitrous acid, the effects are large.

HEICKLEN: The best values for the rate coefficient of $HO_2 + NO \rightarrow HO + NO_2$ is now about $10^{-12} \text{ cm}^3 \text{ sec}^{-1}$. The rate coefficient of $HO_2 + NO_2$ is one-seventh of that — we've rechecked it recently — which means roughly $2 \times 10^{-13} \text{ cm}^3 \text{ sec}^{-1}$.

SCHIFF: If $HO_2 + NO_2$ is 2×10^{-13} , and if $HNO_2 + O_3$ is as fast as 10^{-15} , then their combined effect on the partition among stratospheric odd-nitrogen compounds is significant. Neither reaction is important by itself.

GARVIN: That should remind us of the need for good absolute rate coefficients for the reactions of HO₂.

UNIDENTIFIED: I was glad to see Dr. Garvin's emphasis on uncertainties in measurement, because the error is really about as important as the value itself in assessing the validity of models in stratospheric chemistry.

UNIDENTIFIED: Well, in our formal experiments, the random measurement errors are between 5 and about 8 percent. But there are surely larger systematic errors. I have yet to see — except in extraordinarily special cases — interlaboratory comparisons that agreed to better than 25%.

WB57F-BORNE MEASUREMENTS OF UV FLUX AND OZONE OVERBURDEN

BACH SELLERS AND FREDERICK A. HANSER

Panametrics, Inc.
Waltham, Massachusetts

ABSTRACT: A filter-wheel UV spectrophotometer has been used to measure the vertical downward solar UV flux over the 200 to 400 nm region. Several high-altitude WB57F flights have provided solar UV data over the latitude range 50° south to 60° north. The decrease in flux from the 320-300 nm region allows the ozone overburden to be calculated and latitudinal ozone overburden profiles are thus obtained. Profiles have been obtained for altitudes of 10 to 19 km, and show the general pattern of a minimum near the equator with increasing levels of ozone toward the poles. At times, the equator-to-pole ozone profiles tend to increase in steps over a degree or two in latitude, and occasional profiles show the presence of ozone bands several degrees wide. While the general trend of the equator-to-pole profiles appears to be stable over the course of a few weeks, the ozone bands show significant variations in about one week.

INTRODUCTION

The stratospheric ozone layer shields the earth's surface from solar UV radiation at wavelengths less than 320 nm. It is thus essential for most life forms, since it absorbs precisely those wavelengths which are most damaging to them. Because of the possible effect of SST emissions on the ozone layer, measurements of the solar UV flux and ozone overburden have been an important part of CIAP. A filter-wheel UV spectrophotometer (UVS) has therefore been built and flown on several of the CIAP flights in the Airstream series. The instrument has been described by Sellers et al. (1973) and by Sellers and Hanser (1973).

The results of our first four Airstream flights were presented in tabular form by Hanser and Sellers (1974). Here, we present most of these results in graphic form and point out some of the major features of the predominantly north-south flight measurements. It has also been possible to calculate several ozone densities from changes in the overburden measured at various aircraft altitudes.

The results discussed here, together with additional data still in analysis, form an important baseline measurement for monitoring future ozone-layer changes. Because of natural variability, it is important that as much data as possible be obtained. Recent calculations of the possible reduction of the ozone overburden by

fluorochloromethanes (e.g., Crutzen (1974) and references cited therein) show that the ozone shield also faces potential reduction from several sources in addition to SST emissions, and thus should be carefully monitored in the decades ahead.

OZONE RESULTS DERIVED FROM UV FLUX DATA

The UVS was designed for high-altitude solar UV measurements, where the Rayleigh-scattered light forms a small part of the instrument response. The measured UV fluxes, examples of which have been presented by Sellers and Hanser (1973), show the expected fall-off below 320 nm, caused by the ozone overburden. From the measured UVS intensities, the ozone overburden is calculated as described by Hanser and Sellers (1974). Once the ozone overburden is known, the UV intensities can then be recalculated from the solar zenith angle and the pressure altitude. Thus, the calculated ozone overburden is a good summarizing parameter for the measured UV fluxes. While the complete UV flux data have been presented in tabular form by Hanser and Sellers (1974), here we discuss only the calculated ozone overburdens.

Much of the UVS data obtained thus far covers the Albuquerque-Panama flight path for the CIAP WB57F. This flight path is shown in Figure 1. The best data for this path were

obtained on 22 and 31 January 1974, and are plotted in Figure 2. The ozone-overburden values have an uncertainty of about 10%, which is usually systematic, as shown by the small spread in Figure 2. The statistical variation of the points is usually determined by noise in the aircraft data-recording system, and occasionally is quite severe.

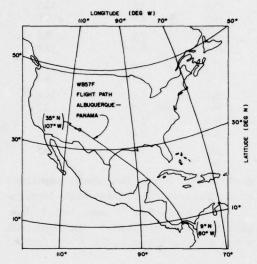


Figure 1. Map showing typical WB57F Albuquerque-Panama flight path.

The results in Figure 2 were obtained from data taken at constant altitude except for the indicated periods. The altitude shifts that occurred with small horizontal change lead to measurable ozone densities, and are presented as the first three lines in Table 1. The errors in the ozone density in Table 1 are a few \times $10^{17}/\text{m}^3$ The ozone density values are in reasonable agreement with measurements summarized in a report by Wu (1973).

The most noticeable feature in Figure 2 is the ozone band between about 27° and 33°N latitude. A detailed study of the raw data has shown that an instrumental effect did not cause this structure, and we are confident that it is real. A check of the National Weather Service 200-mb-height isotach map for 1200 GMT on 31 January 1974 shows a close correlation of the ozone band with greater-than-70-knot eastwardflowing winds. This is in agreement with the findings of Prabhakara et al. (1971) that an ozone maximum over southern Asia was correlated with the track of the easterly jet. Their ozone data were obtained from infrared measurements on Nimbus 3. Another interesting feature is the step in ozone overburden at about 14°N in the 22 January data.

Ozone results for the 23 September 1973 flight over the path of Figure 1 are shown in

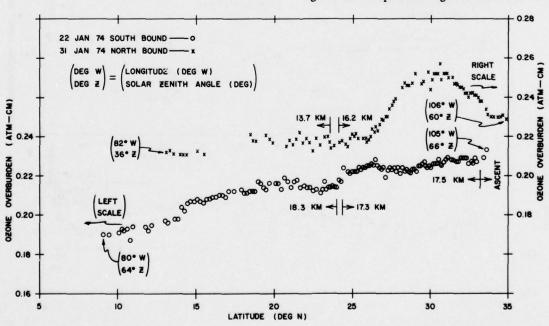


Figure 2. Ozone overburden data from 22 and 31 January 1974 flights.

Table 1. Measured Ozone Densities from UVS Data on Several CIAP Airstream Flights

Data in Figure No.	Date of Data (yr-mo-day)	Lat. (deg N)	Long. (deg W)	Average Altitude (km)	Altitude Range (km)	Ozone Density (10 ¹⁷ /m ³)
2	740122	33.1	104	16.9	1.2	9.0
2	740122	24.2	89	17.8	1.0	22.1
2	740131	23.8	89	***	2.5	1.5
3	730923	31.3	101	18.0	1.7	14.6
3	730923	33.3	105	18.1	1.5	12.3
3	730923	34.2	105	15.0	4.7	6.0
4	730602	24.9	90	18.4	0.6	28.2
4	730607	33.8	106	13.1	6.3	15.4
5	730907	-11.0	79	17.1	3.6	7.0
5	730912	-13.6	72	17.0	3.5	5.3
6	740127	-43.9	67	16.8	1.4	24.8
6	740127	41.5	67	14.9	2.4	3.3
6	740127	-35.5	66	16.8	1.4	19.7
6	740128	-14.8	76	16.8	1.6	10.1
7	730605	16.5	63	16.9	2.2	10.5

Figure 3. Here, the overburden shows only a very gradual rise to about 25°N; some structure at 31 to 34°N, due solely to aircraft altitude changes, is illustrated by the calculated interpolated values shown in the enlarged insert. The slight decrease

north of 25°N is most likely due to penetration of the ozone layer as its mean height decreases.

Ozone results for 2 June and 7 June 1973 are shown in Figure 4. The flight path is that shown in Figure 1. The 7 June data for

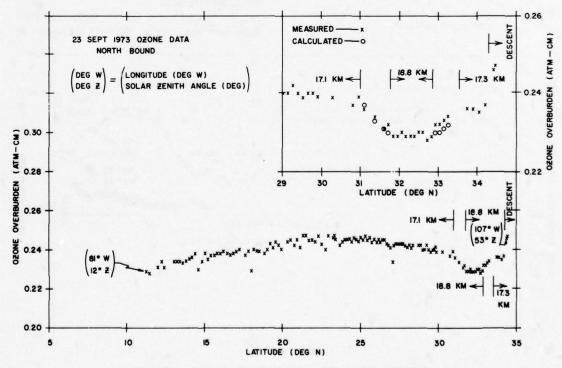


Figure 3. Ozone overburden data from 23 September 1973 flight.

16.4 km show a gradual overburden increase away from the equator, while the 2 June data, available for only the northern half of the flight, show a decrease north of $25^{\circ}N$. The latter effect is again probably due to penetration of the ozone layer, as the 2 June flight was above 18 km. The altitude step near $25^{\circ}N$ for the 2 June data gives an ozone density of about $28\times10^{17}/m^3$ at 18.4 km, and while this is a reasonable value, the large statistical variations evident in the 2 June data make it uncertain by perhaps a factor of two.

Ozone results from the southern hemisphere for early September 1973 are shown in Figure 5. The data are from a total of four flights, at a number of altitudes. Ozone densities calculated from altitude changes are shown in Table 1. Gaps in the results are due to either aircraft maneuvering, UVS malfunction, aircraft tape-recorder malfunction, or extremely noisy data. The most noticeable features are the ozone minimum near 10° to 20°S latitude, and the ozone band at 40° to 47°S. Southern-hemisphere results for late January 1974 are shown in Figure 6. Here, the ozone layer appears to be nearly constant over a large latitude range, although there seem to be

sharp changes near 5°N, possibly near 40°S, and also at 30° to 35°S. The results from Figures 5 and 6° for a north-south path at about 70°W longitude. Measurable ozone densities from altitude shifts are given in Table 1.

Ozone results from flights from Panama to Antigua are shown in Figure 7. The 30 January 1974 data show a continuous rise toward northern latitudes. The 5 June 1973 data show a possible peak at 12° to 15° N, but this may be due to penetration of the ozone layer north of 15° N. The altitude change during the return portion of the June flight gives an ozone density of about $11 \times 10^{17}/\text{m}^3$ at 16.5° N and 16.9 km, as is shown in Table 1.

Results from a 1 November 1973 flight are shown in Figure 8. Here, an ozone step is observed at 41° to 42°N, although lack of data beyond 46°N makes it impossible to tell whether this is a true step or a band associated with the jet stream. Figure 9 shows ozone overburden from a number of early June 1973 flights near Panama. Here, a possible weak ozone minimum at 7° to 9°N is evident.

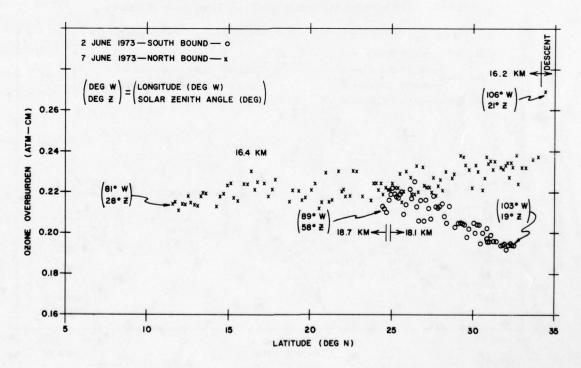


Figure 4. Ozone overburden data from 2 and 7 June 1973 flights.

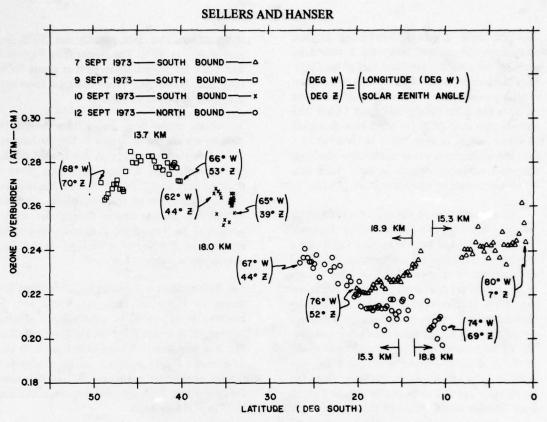


Figure 5. Ozone overburden data from 7, 9, 10, and 12 September 1973 flights.

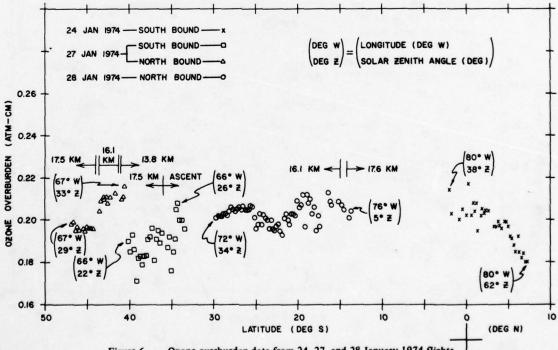


Figure 6. Ozone overburden data from 24, 27, and 28 January 1974 flights.

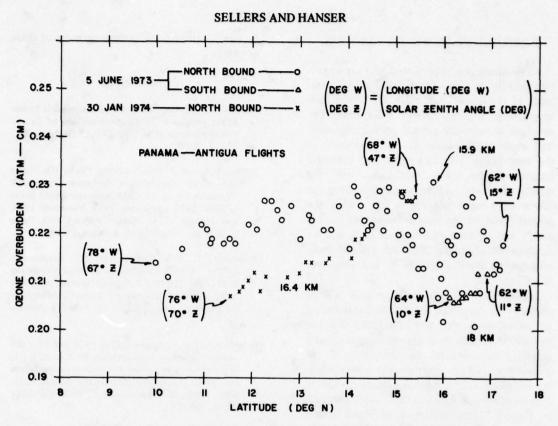


Figure 7. Ozone overburden data from 5 June 1973 and 30 January 1974 flights.

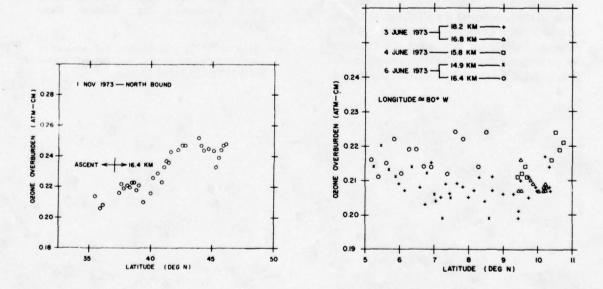


Figure 8. Ozone overburden data from 1 November 1973 flight.

Figure 9. Ozone overburden data from 3, 4 and 6, June 1973 flights.

DISCUSSION AND CONCLUSIONS

The ozone results presented here are important because they give a high-resolution measurement of the ozone overburden for a long path length over a comparatively short time. The structure occasionally present provides information about the dynamics of ozone transport in the atmosphere. The data show that structural features in the ozone overburden can vary rapidly with time — changing significantly in the course of a week (see Figure 2) — while the general trend of the ozone overburden is only slowly varying (compare Figures 2, 3, and 4). Analysis of additional data will provide more information about these short- and long-term variations.

Monitoring for long time periods will be necessary to determine the natural variability of the ozone overburden and its detailed time and latitude structure. Such monitoring is clearly necessary in order to evaluate the effect of potential or actual anthropogenic atmospheric perturbations. It may be that gradual changes in a long-path-length ozone measurement (as, e.g., in Figure 3) are indicative of stable ozone conditions for the particular season and geographical location, and this type of measurement may be best for monitoring long-term changes in the ozone overburden. The presence of steps and bands in the ozone overburden (as, e.g., in Figure 2) may indicate a changing ozone pattern at that particular latitude and time which is not suitable for comparison against a baseline measurement. It is hoped that analysis of additional data and

future monitoring will provide answers to these questions.

REFERENCES

- Crutzen, P.J. (1974), "Estimates of the possible future ozone reductions from continued use of fluoro-chloro-methanes (CF₂Cl₂, CFCl₃)," Geophys, Res. Lett. 1, 205-8.
- Hanser, F.A. and B. Sellers (1974), "Solar UV Fluxes and Ozone Overburdens Obtained from UVS Measurements on the CIAP Airstream Flight Series of June 1973, September 1973, November 1973, and January 1974," Report PANA-UVS-4, Panametrics, Inc., Waltham, Mass. (August 1974).
- Prabhakara, C., E.B. Rodgers, and V.V. Salomonson (1971), "Global Distribution of Total Ozone Derived from Nimbus 3 Satellite During April-July 1969 and its Implication to Upper Tropospheric Circulation," Report NASA TM X-65774 (November 1971).
- Sellers, B. and F.A. Hanser (1974), "UV flux level and ozone overburden from latitudes 60°N to 60°S," in Proceedings of the Third Conference on the Climatic Impact Assessment Program (Cambridge, MA), U.S. Dept. of Transportation, DOT-TSC-OST-74-15, 129-136.
- Sellers, B., F.A. Hanser, and J.L. Hunerwadel (1973), "Design, Fabrication and Flight of an Ultraviolet Interference-Filter Spectrophotometer Aboard a WB57F High Altitude Aircraft," Report PANA-UVS-1, Panametrics, Inc., Waltham, Mass. (October 1973).
- Wu, Mao-Fou (1973), "Observation and Analysis of Trace Constituents in the Stratosphere," Report No. DOT-TST-74-7 (July 1973).

ERYTHEMAL ULTRAVIOLET SOLAR RADIATION AND ENVIRONMENTAL FACTORS

L. MACHTA, G. COTTON, AND W. HASS Air Resources Laboratories NOAA Environmental Research Laboratories Silver Spring, Maryland

W. KOMHYR

Air Resources Laboratories NOAA Environmental Research Laboratories Boulder, Colorado

ABSTRACT: Field measurements of erythemal ultraviolet radiation by several sensors yield both a climatology of this fraction of the solar spectrum and the relationship of the observed intensities to environmental factors such as cloudiness, air mass, ozone, turbidity, and ground albedo. In general, the results conform to expectation, but the provisional magnification factor (ratio of percentage change in ultraviolet radiation to percentage change in ozone) is slightly less than the commonly quoted value of two.

For the past few years, the Department of Transportation's Climatic Impact Assessment Program has supported a series of measurements of erythemal ultraviolet radiation (hereafter called UV-B) at a number of locations within the United States. These data have provided the first observational climatology of UV-B radiation in the U.S.A. Comparison of the UV-B data with environmental factors permits a quantitative assessment of their effects on UV-B radiation.

Figure 1 shows the location of the 12 Temple University dosimeters, the two Air Resources Laboratories dosimeters, the two Smithsonian Radiation Biology Laboratory filter-wheel radiometers, and the Dobson spectrophotometers (total-ozone measuring instruments). The Temple device depends upon the fluorescence of a magnesium tungstate stratum caused by UV-B radiation. It is a simple, relatively inexpensive instrument based on a design of Dr. D.F. Robertson of Australia (1972). The ARL dosimeters are modified Dobson spectrophotometers which respond to UV-B radiation in proportion to the Urbach and Berger (1972) erythemal action spectrum (shown in Figure 6). Finally, the Smithsonian Radiation Biology Laboratory has installed a filter-wheel radiometer at Tallahassee, Florida. The transmission through

the eight filters may be seen in Figure 2. By properly weighting the signal from each of the filters, it is possible to approximate any ultraviolet action spectrum desired. This will be useful if and when an experimentally measured carcinogenic spectrum replaces the erythemal or sunburning action spectrum that is now used to approximate it.

Figure 3 shows the high correlation between measurements of UV-B by the modified Dobson instrument and those made with the Temple sensor. In fact, the high correlation of 0.96 at Bismarck shown in Figure 3 is exceeded by the correlation at Tallahassee (0.98). This graph also permits the conversion of the Temple meter readings to joules/m² (2.8 "counts" equals 1 joule/m²).

Using the conversion just noted, the provisional results for nine stations with the Temple instruments during 1973-74 appear in Figure 4. This figure displays the decrease in UV-B from south to north. The annual pattern shows a more marked northward gradient than do the summer points. But there are irregularities in the latitudinal trend which, in large part, reflect differences in cloudiness, a prime environmental factor controlling the amount of UV-B radiation reaching the ground.

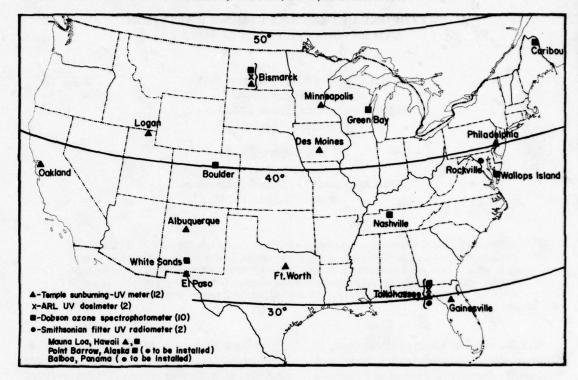


Figure 1. Location of instruments to measure ultraviolet solar radiation and total ozone.

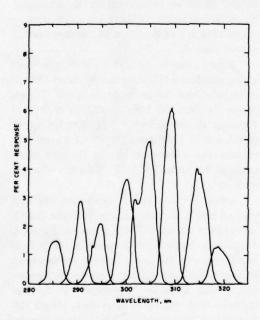


Figure 2. Filter transmission curves for the Smithsonian Radiation Biology Laboratory filter-wheel radiometer at Tallahassee, Florida.

A second very obvious factor controlling the quantity of UV-B radiation received at the ground is the zenith angle of the sun, or air mass (the secant of the zenith angle). But the air-mass variation changes the amount of solar radiation differently at each UV-B wavelength. Figure 5, reproduced through the courtesy of Dr. R. Lehman of NOAA, shows the relative intensity of direct solar radiation at various air masses between 1.05 (sun near the zenith) and 2.2 (sun closer to the horizon). The intensities of solar radiation have been normalized at 308.5 nm. The non-normalized values can be recovered by multiplying the appropriate air-mass values by the number under s.f. in the upper left-hand corner of the figure. It follows, then, that solar radiation decreases with increasing air mass. However, it decreases more rapidly at shorter wavelengths than at longer wavelengths. Since, as seen in Figure 6, the erythemal action spectrum peaks at about 296 nm (2960 Angstrom units), the decrease in erythemal solar energy due to increasing air mass (greater solar zenith angle) is much more rapid than that due simply to

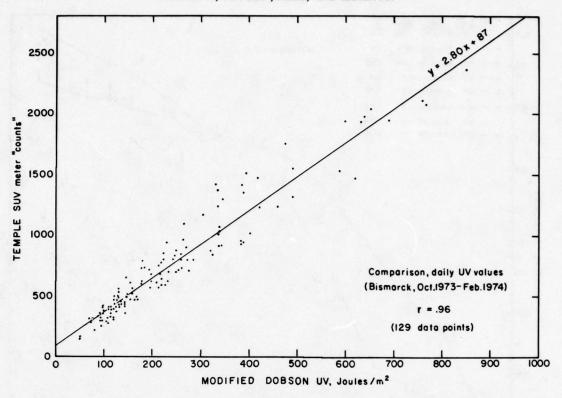


Figure 3. The relationship between the daily total "counts" of the Temple dosimeter and the daily integrated measurements of the ARL modified Dobson spectrophotometer.

increasing the length of the air column between the sensor and the sun.

Figure 6 shows the Urbach and Berger (1972) erythemal action spectrum. The ARL modified Dobson spectrophotometer has a mask which admits radiant energy proportionally to this spectrum. The ozone absorption coefficient as a function of wavelength also appears on the figure. Thus, the shorter UV-B wavelengths between, say, 290 and 300 nm, which are most effective in producing sunburn, are also those strongly absorbed by ozone.

Using this absorption coefficient, several investigators have deduced theoretical attenuation factors which include UV-B scattering in varying degrees of sophistication. Table 1 lists some of the more recent results. The magnification factors — that is, the ratio of the percentage change in UV-B to that of ozone — range from about 1.5 to a little over 2.0.

Figure 7 presents the magnification factor as a function of ozone amount. The heavy solid line

reflects Shettle and Green's (1974) theory and is very close to the often-quoted value of 2.0. The remaining lines and points depend on empirical fits to observed UV-B and total ozone data collected at Bismarck, N.D. The pairs of solid and dashed lines vary with air mass, the lowest set being for air mass 1.0 and the upper set for air mass 1.6. Several features of these lines are to be noted. First, the magnification factor increases with increasing ozone amount. Typical total-ozone readings in the U.S. lie in the range 0.300 to 0.400 atm-cm. The fairly well-marked dependence of magnification factor on ozone amount results from their assumed functional relationship, shown in the lower right-hand side of Figure 7. A few trial-and-error calculations suggest that a single exponential form fits the data best, but this conclusion must be provisional for the time being. The second feature shown by the figure is the lower magnification factor for clear-plus-cloud conditions compared with clear weather.

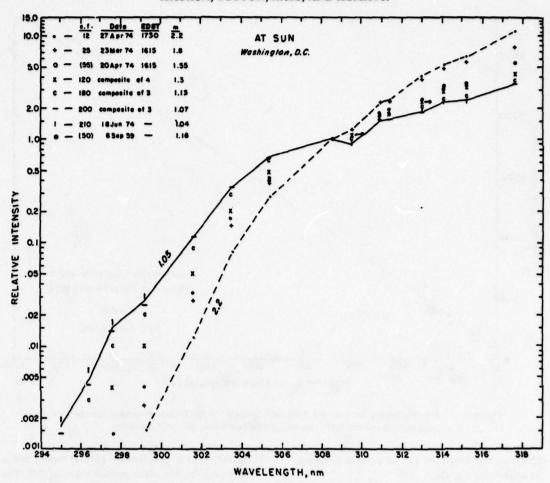


Figure 4. A plot of relative intensity of ultraviolet radiation looking directly at the sun with different air masses. All readings from a double spectrophotometer have been normalized to a common reading of unity at 308.5 nm. The "absolute" values at each air mass (m) may be found by multiplying the relative values by the scale factors under s.f. in the upper left side of the figure. (This figure is reproduced through the courtesy of Dr. R. Lehman of NOAA, who took the measurements in the Washington, D.C. area.)

When the empirical relationship for various air masses and ozone amounts is applied to daily, clear-sky UV-B data, one obtains the values indicated by the crosses in Figure 7 (the dates appear adjacent to the crosses). The magnification factor at any one location (Bismarck in this case) varies with the day of the year because of the variation in air mass. The provisional results of these data suggest that the magnification factor may be between 1.5 and 2.0 rather than the commonly accepted value of 2.0.

Atmospheric turbidity also attenuates the UV-B radiation received at ground level. Figure 8

relates the UV-B radiation in the body of the figure to turbidity and ozone amount at Tallahassee. Theory suggests that changes in turbidity at low readings will have a smaller impact on the UV-B than the same percentage change in turbidity at higher values of turbidity. This expectation is confirmed at the low-turbidity station, Bismarck, where the UV-B dependence on turbidity cannot be given with certainty. But at Tallahassee, Figure 8, there is a fairly clear-cut decrease of UV-B with increasing turbidity. However, despite these results, the dependence of UV-B solar radiation on turbidity, keeping all

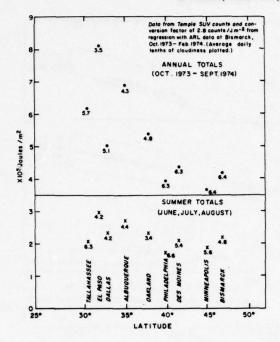


Figure 5. The annual and summer values of erythemal ultraviolet radiation reported for the Temple dosimeter. Numbers near dots and crosses provide average cloudiness, in tenths of sky covered (taken from National Weather Service records for the indicated periods).

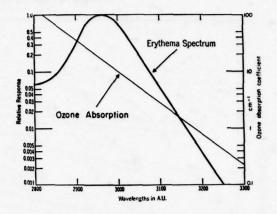


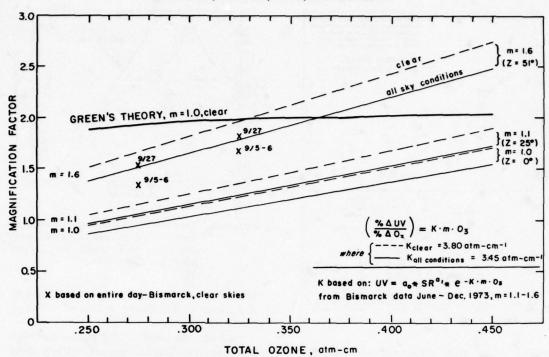
Figure 6. The Urbach-Berger erythemal action spectrum (heavy curve) and the ozone absorption curve (thin straight line). (From Shettle and Green, 1974.)

other factors constant, is not as easy to demonstrate even at Tallahassee as that of UV-B on total ozone.

Finally, the albedo of the ground also plays a role in controlling the amount of UV-B global radiation (both the Temple and ARL instruments measure global or direct-plus-diffuse radiation). This may be seen in Figure 9, in which the amount of UV-B radiation is stratified according to the presence or absence of snow on the ground. The figure again shows the dependence of UV-B on total ozone, but it also illustrates the increase in UV-B on days with snow cover (high

Table 1. Theoretical Ratio of Percent Increase of Erythemal Ultraviolet Radiation to Percent Decrease in Thickness of Total Ozone Column (Magnification Factor) (adapted from Urbach and Davies, 1975)

Reference	Magnification Factor for 5% O ₃ Decrease	Comments
Chavaudra and		Direct component only - sun at zenith
Latarjet (1973)	1.40	Using Coblentz and Stair (1934) action spectrum.
	1.80	Using Cripps and Ramsay (1970) action spectrum.
Schultze (1974)		Evaluation from results for a 10% decrease of O ₃ layer thickness, assuming a linear law down to 5%.
	1.80	In equatorial zone.
	2.20	In polar zone.
Green et al. (1974)	2.00	Evaluation from Figure 8, for Gainesville, Florida at noon.
Green et al. (1975)	2.00	
	2.06	
	1.55	



Variation with ozone amount of the UV-B-to-ozone magnification factor. The solid heavy line is a theoretical estimate by Green for unit air-mass unity and clear skies, suggesting a magnification factor of two. The thin dashed lines are empirical fits to the data collected at Bismarck for clear skies; the thin solid lines apply to both clear and cloudy conditions. The extinction factor for ozone, K, has been found to vary slightly between periods of clear and cloudy skies. The crosses show the magnification factors for the entire day with no clouds, as computed from the same empirical formula noted in the lower right. In the formula $\mathbf{a_0}$ and $\mathbf{a_1}$ are empirically derived parameters, SR stands for the solar radiation from about 300 to 3000 nm, K is an empirically derived ozone-extinction coefficient, m is air mass, and O_3 stands for the ozone in atm-cm.

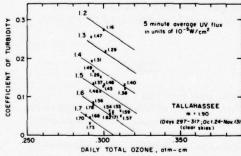


Figure 7.

Figure 8. The dependence of UV-B radiation on turbidity at Tallahassee. (The coefficient of turbidity increases as the air becomes more turbid.) The numbers in the body of the figure are the fluxes of UV-B radiation at air mass 1.90 and the indicated ozone amount. The sloping lines derive from a bilinear regression analysis of the plotted values. The figure shows a decrease of UV-B radiation with increasing turbidity at the same air mass and ozone amount.

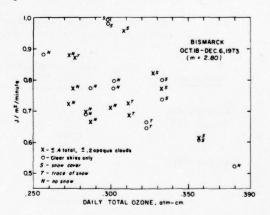


Figure 9. The effect of snow cover on the UV-B radiation. This figure shows that, at Bismarck, the global (direct plus diffuse) UV-B radiation increases when snow cover, with its higher albedo, replaces the bare ground.

albedo) as opposed to those with bare ground (low albedo).

In conclusion, the findings of the CIAP-sponsored UV-B measurement program generally conform to expectation. The provisional, empirical magnification factors relating UV-B and total ozone are slightly smaller than the usually quoted value of 2.0.

REFERENCES

- Chavaudra, T. and R. Latarjet (1973), "Influence des variations de l'ozone atmosphérique sur certaines activités biologiques du rayonnement ultraviolet solaire," Comp. Rendus Acad. Sci. Paris, Ser. D 276, 3481-3485.
- Coblentz, W.W. and R. Stair (1934), "Data on the spectral erythemic reaction of the untanned human skin to ultraviolet radiation," Research Paper RP631, Bureau of Standards Journal of Research, Vol. 12, January.
- Cripps, D.J. and C.A. Ramsay (1970), "Ultraviolet action spectrum with a prism-grating monochromator," Brit. J. Dermatol. 82, 584-592.
- Green, A.E.S., T. Sawada, and E.P. Shettle (1974), "The middle ultraviolet reaching the ground," Photochem. & Photobiol. 19, 251-259.

- Green, A.E.S., T. Sawada, E.P. Shettle, D.S. Nachtwey, M.L. Nack, J.H. Miller, and T. Mo (1975), "Expected changes in the middle UV and biologically effective doses," section 2.2 of CIAP Monograph 5 (Part 1), Dept. of Transportation, DOT-TST-75-55 (part 2), 2-26 - 2-78.
- Robertson, D.F. (1972), "Solar Ultraviolet Radiation in Relation to Human Sunburn and Skin Cancer," Thesis, University of Queensland, Australia.
- Schultze, R. (1974), "Increase of carcinogenic ultraviolet radiation due to reduction in ozone concentration in the atmosphere," in Proceedings of the International Conference on Structure, Composition, and General Circulation of the Upper and Lower Atmospheres and Possible Anthropogenic Perturbations (Melbourne), pub. IAMAP, Vol. 1, 479-493.
- Shettle, E.P. and A.E.S. Green (1974), "Multiple scattering calculation of the middle ultraviolet reaching the ground," Appl. Opt. 13, 1567-1581.
- Urbach, F. and D. Berger (1972), private correspondence; see also D. Berger, F. Urbach and R.E. Davies (1968), "The action spectrum of erythema induced by ultraviolet radiation," in *Proceedings of the 13th Congressus Internationalis Dermatologicae* (Munich, 1967), Springer-Verlag, Berlin, 112-117.
- Urbach, F. and R.E. Davies (1975), "Estimate of the effect of ozone reduction in the stratosphere on the incidence of skin cancer in Man," in this volume.

VISIBLE-ULTRAVIOLET RADIOMETRY

DISCUSSION

(UNIDENTIFIED): Dr. Hanser, is there any possibility that some of the features you see are due to changes in underlying albedo, such as might occur over bright clouds?

HANSER: I don't think so, since we fly at high altitude and use more than one bandpass filter to discriminate among the wavelength-dependent components of scattered light.

THE AES STRATOSPHERIC BALLOON MEASUREMENTS PROJECT: PRELIMINARY RESULTS

W.F. EVANS, J.B. KERR, AND D.I. WARDLE

Atmospheric Environment Service Downsview, Ontario, Canada

ABSTRACT: Measurements of HNO₃, NO₂, NO, O₃, solar ultraviolet flux, and infrared and submillimeter spectra were obtained from balloons launched from Churchill, Manitoba in July 1974. The results are summarized and the concentration ratios of the various species are compared with theoretical calculations.

INTRODUCTION

The stratospheric models which are used to predict the effects of future fleets of SST's and halomethane usage on the stratospheric ozone layer are extremely dependent on the photochemical reaction sets used to model the distributions of minor nitrogen constituents. Two years ago, the Atmospheric Environment Service undertook a project to obtain a set of simultaneous measurements of key stratospheric con-

stituents in order to verify the currently accepted photochemical schemes. The project consisted of a large, complex balloon payload with ten scientific experiments; five were conducted by AES scientists, and five by experimenters in Canadian universities. Detailed information on the experiments, the experimenters, and the parameters measured with each instrument are given in Table 1. The payload engineering and field support of gondola systems were carried out by SED Systems Ltd., Saskatoon.

Table 1. AES Balloon Project

Experiment	Experimenters	Affiliation	Wavelength (μm)	Item Measured
I. SOLAR ABSORPTION				
Scanning solar radiometer	W. Evans, S. Bain	A.E.S.	2 to 14	H ₂ O, O ₃ , N ₂ O
NO ₂ spectrophotometer	A. Brewer, J. Kerr, T. McElroy	U. of Toronto, A.E.S.	0.44	NO ₂ , O ₃
NO ₂ scanning photometer	D. Wardle	A.E.S.	0.44 to 0.45	NO ₂
UV flux spectrometer	D. McEwen	U. of Saskatchewan	0.19 to 0.31	UV flux, O3
II. EMISSION				
HNO ₃ radiometer	W. Evans, C. Lin	A.E.S.	11.3	HNO ₃
Scanning emission radiometer	W. Evans, C. Midwinter	A.E.S.	4 to 8	H ₂ O, O ₃
Far IR Michelson interferometer	T. Clark, D. Kendall	U. of Calgary	80 to 300	$\mathrm{O_3,H_2O,HNO_3}$
IR spectrometer	E. Llewellyn	U. of Saskatchewan	1 to 4	$OH^*, O_2(^1\Delta)$
III. SAMPLING				
NO snooper	H. Schiff, B. Ridley	York University	Chemiluminescent	NO
O ₃ sampler	R. Olafson, J. Kerr	A.E.S.	Chemiluminescent	03
Ozonesonde		A.E.S.	Sampling	P, T, H ₂ O, O ₃

FLIGHT MEASUREMENTS

Two flights were conducted from Churchill, Manitoba, on July 8 and July 22, 1974. Only partial measurements were obtained from the first flight, but most experiments functioned well on the July 22 flight. The altitude/time profile for the July 22 flight is shown in Figure 1. Measurements of the altitude profiles of nitric acid, nitric oxide, and ozone, shown in Figure 2, were made during the balloon ascent; remotesensing measurements of nitrogen dioxide, water vapor, ozone, and other gases were made during sunset by long-path solar absorption. Similar measurements were made during the sunrise

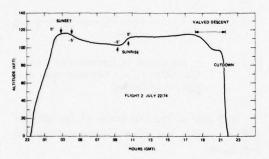


Figure 1. The altitude-time profile for the July 22 balloon flight from Churchill, Manitoba (58.6°N, 94°W).

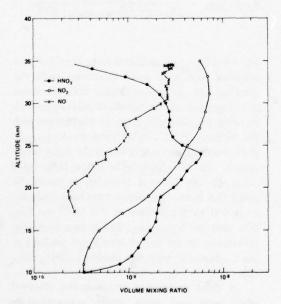


Figure 2. Mixing-ratio profiles of HNO₃, NO₂, and NO measured on the July 22 flight.

period, and further profile information was obtained during the valved descent in the late afternoon.

A series of four ozonesondes was flown in conjunction with the main scientific gondola launch to provide meteorological and ozone data; they were flown six hours before, during, six hours after, and twelve hours after the main launch. In addition, a rocketsonde was fired from Churchill on July 23, 1974, which provided information on temperature and winds up to 60 km. The mean temperature structure was quite similar to the U.S. Standard Atmosphere for 60°N, July, with the tropopause located at 11 km. An analysis of the ozonesonde profiles indicated that the measured ozone distribution was similar to the mean ozone distribution at Churchill for July obtained earlier (Hering and Borden, 1965) with the exception of a higher peak mixing ratio of 7 ppmv. The total ozone amount, as determined from the ground-based Dobson-spectrophotometer measurement, was 0.35 atm cm.

The nitric acid profile shown in Figure 2 was obtained with a liquid-nitrogen-cooled multichannel radiometer which measured atmospheric thermal emission in the 11.3-µm band of HNO₃ during the balloon ascent. The radiance profiles obtained were consistent with those measured by Murcray et al. (1973) at other latitudes. The HNO₃ mixing-ratio vertical profile showed a broad layer peaked at 24 km with a peak mixing ratio of 6 ppbv. The total amount of HNO₃ measured above the tropopause was 0.32 matm cm.

The NO_2 profile was obtained from our inversion analysis of measurements taken by C.T. McElroy of the University of Toronto (see Bloxam et al., 1975) of the differential absorption of the solar spectrum in the 4500-Å region during sunset. The F value varied by 0.08 at 94°, corresponding to a path length of \approx 10 matm cm of NO_2 ; this long absorption path produced an excellent signal-to-noise ratio. The NO_2 mixing ratio varied slowly from 0.2 ppbv at the tropopause to more than 6 ppbv above 30 km.

The NO profile was measured by B. Ridley and H. Schiff of York University (Ridley et al., 1975) with their direct-sampling chemiluminescence technique. The NO mixing ratio varied from 0.25 ppbv at 19 km up to 3 ppbv at the float

EVANS, KERR, AND WARDLE

altitude of 34.5 km. When converted to concentrations, this represents an approximately constant number-density profile, with a "bite" taken out in the region of the ozone layer.

COMPARISON WITH THEORY

A simulation of the ratios of the constituents has been carried out, using the rate coefficients and photodissociation parameters recommended in Table 5.39 of CIAP Monograph 1 (1975) in a diurnally-averaged steady-state calculation.

The OH concentrations were calculated from a parameterization suggested by McConnell (1975):

[OH] =
$$\frac{[k_{H_2O+O(^1D)}] [O(^1D)] [H_2O] / R}{k_{OH+HO_2}}$$

where $R = [HO_2]/[OH]$

The ratio of NO₂ to NO was calculated from the expression:

$$R_{NO_2/NO} = \frac{[k_{NO+O_3}] [O_3]}{J_{NO_2} + [k_{NO_2+O}] [O]}$$

It should be noted that this ratio was calculated using the measured ozone number density and the measured temperature. The observed ratio of NO2/NO, as calculated from the measured NO2 and NO profiles, is shown in Figure 3. (The time lag between the observations of NO and NO₂ has been taken into account in this calculation.) The calculated ratio, when compared with the observed ratio of NO2/NO, has a similar altitude variation; it would be in absolute agreement if the observed NO concentrations were increased by a factor of 1.8 or if the observed NO₂ concentrations were decreased. Alternately, one could postulate that the laboratory value for the rate constant for the NO + O2 reaction is too small, although the difference from theory is within the experimental accuracy of the NO and NO₂ measurements.

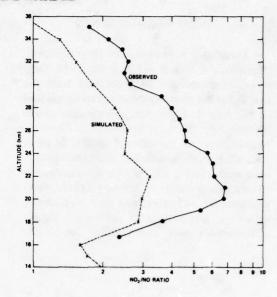


Figure 3. A comparison of the measured ratio of NO₂/NO with the simulated ratio as a function of altitude.

In Figure 4, the simulation of the ratio of HNO₃ to NO₂ has been calculated from the expression:

$$R_{\text{HNO}_3/\text{NO}_2} = \frac{[k_{\text{OH}+\text{NO}_2}] \text{ [OH] [M]}}{[J_{\text{HNO}_3}] + [k_{\text{OH}+\text{HNO}_3}] \text{ [OH]}}$$

The ratio (k_{CIAP}) calculated using the CIAP rate indicates uniformly good agreement with the observed ratio at most altitudes; both the shape and magnitude of the calculated ratio agree with those of the observed ratio. A calculation with the McElroy et al. (1974) value for k_{OH+NO_2} gives poorer agreement; although the shape is still similar, the calculated ratio is too large by a factor of two at most altitudes. It should be noted that these calculations have been made for a low-OH model; a value of 2×10^{-10} cm³/sec was used for k_{OH+HO_2} . Larger hydroxyl concentrations in the model would not produce as good agreement with the observed HNO₃/NO₂ ratio.

A third comparison involving the observed nitric acid and nitric oxide concentrations is shown in Figure 5. The simulated ratio

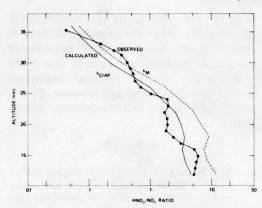


Figure 4. A comparison of the measured ratio of HNO₃/NO₂ with the simulated ratio as a function of altitude.

 $R_{HNO_3/NO}$ can be obtained from the previous calculations:

$$R_{HNO_3/NO} = R_{HNO_3/NO_2} \times R_{NO_2/NO}$$

The ratio calculated with the recommended CIAP value (k_{CIAP}) has an altitude variation similar to that of the observed ratio, R_{HNO_3/NO_2} , but is somewhat smaller at most altitudes. The ratio calculated with the McConnell and McElroy (1973) value (k_M) shows improved but not complete agreement with the observed ratio. The observed ratio falls between the two calculated cases at altitudes below 25 km.

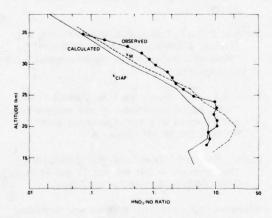


Figure 5. A comparison of the measured ratio of HNO₃/NO with the simulated ratio as a function of altitude.

Again, the discrepancy is within the error limits of the measurements and laboratory rate-

constant values; no serious flaw in current photochemical theory is indicated.

Of prime interest to the problem of the ozone balance is the mixing ratio of odd nitrogen (≈ NO_v). As shown in Figure 6, model calculations indicate that this should be approximately constant as a function of altitude from 20 to 40 km. The observed NO, NO2, and HNO3 mixing ratios have been summed to derive the NO_v mixing-ratio profile (Curve A). Overall, the observations indicate an odd-nitrogen mixing ratio of about 10 ppbv. This should be compared with the 11 ppbv of the Vupputuri (1975) model (Curve E) and the 10 ppbv of the McConnell model (McElroy et al., 1974) (Curve D). These two models have been plotted on the right-hand side of Figure 5 with their tropopause heights (16 km) adjusted to the observed tropopause altitude (11 km).

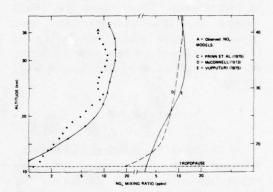


Figure 6. The observed odd-nitrogen mixing ratio in comparison with the distribution of NO_y from several stratospheric computer models used to predict stratospheric pollution effects.

The odd-nitrogen mixing ratio from the two-dimensional model of Prinn et al. (1975) (Curve C) gives an opportunity for a comparison at 60° N in July; there is excellent agreement with the shape of the observed NO_y profile, although the peak mixing ratio of their model is 14 ppbv.

SUPPLEMENTARY MEASUREMENTS

Measurements of the solar ultraviolet flux in the wavelength interval from 1900 to 3000 Å with a resolution of 2 Å were obtained on the

EVANS, KERR, AND WARDLE

first flight by D.J. McEwen (University of Saskatchewan). The radiation in the 2100-Å window produces O₃ and dissociates fluorocarbons. Measurements at a float altitude of 29 km were made over a range of solar zenith angles from 40° to 85°. A theoretical simulation of the ultraviolet flux measurements, using the observed ozone, temperature, and density distributions, is currently under way.

Measurements of the submillimeter thermalemission spectrum over the range 30 to 120 cm⁻¹ with a resolution of ≈ 0.3 cm⁻¹ were obtained with a Michelson interferometer by T.A. Clark (University of Calgary). Lines from O_3 and H_2O are readily identifiable and lines from HCl, NO_2 , and HNO_3 may be present.

Atmospheric spectra in the range from 1.0 to 3.1 μ m were measured with a scanning infrared spectrometer by E.J. Llewellyn (University of Saskatchewan). These include the diurnal variation of chemiluminescent emissions from vibrationally excited hydroxyl and $O_2(^1\Delta)$; the $O_2(^1\Delta)$ measurements will be used to infer the ozone distributions above the balloon float altitude.

SUMMARY

In conclusion: The altitude profiles of HNO3, NO2, and NO have been measured on the same balloon flight. The NO2/NO ratio is a factor of two larger than predicted. An increase in the NO densities by a factor of 1.8 would bring the observed ratio for NO2/NO into exact agreement with the theoretical value. The HNO3/NO2 and HNO₃/NO ratios are close to the ratios calculated for a low-OH model with the exception of a factor-of-two discrepancy at 30 km. There is no significant disagreement between currently accepted photochemical schemes and these observations, considering the uncertainties in the rate constant for the OH + NO2 reaction and the OH densities; a measurement of OH is probably essential for a complete experiment. In relation to the validity of models, the measured NO, mixing ratio verifies that the odd-nitrogen content of the stratosphere is approximately 10 ppbv, close to the mixing ratios calculated or assumed in most models. It should be cautioned that this is a preliminary analysis of most of the experimental data, and the final constituent profiles may change somewhat; however, it is not anticipated that the main conclusions will be altered.

REFERENCES

- Bloxam, R.M., A.W. Brewer, and C.T. McElroy (1975), "NO₂ measurements by absorption spectrophotometer: Observations from the ground and high-altitude balloon, Churchill, Manitoba, July 1974," in this volume.
- CIAP (1975), "The Natural Stratosphere of 1974," ed. Reiter et al., Volume 1 of the CIAP monograph series, U.S. Dept. of Transportation, DOT-TST-75-51.
- Hering, W.S., and T.R. Borden (1965), "Mean Distributions of Ozone Density Over North America 1963-1964," Air Force Cambridge Research Labs. Rep. No. 65-913.
- McConnell, J.C., and M.B. McElroy (1973), "Odd nitrogen in the atmosphere," J. Atmos. Sci. 30, 1465-1480.
- McConnell, J.C. (1975), private communication:
- McElroy, M.B., S.C. Wofsy, J.E. Penner, and J.C. McConnell (1974), "Atmospheric ozone: Possible impact of stratospheric aviation," J. Atmos. Sci. 31, 287.
- Murcray, D.G., A. Goldman, A. Csoeke-Poeckh, F.H. Murcray, W.J. Williams, and R.N. Stocker (1973), "Nitric acid distribution in the stratosphere," J. Geophys. Res. 78, 7033.
- Prinn, R.F., F.N. Alyea, and D.M. Cunnold (1975), "Stratospheric distribution of odd nitrogen and odd hydrogen in a two dimensional model," J. Geophys. Res. 80, 4997-5004.
- Ridley, B.A., J.T. Bruin, and H.I. Schiff (1975), "Measurements of NO between 17 and 34.5 km from Churchill, Manitoba," in this volume.
- Vupputuri, K.R. (1975), "Seasonal and latitudinal variation of N_2O and NO_x in the stratosphere," J. Geophys. Res. 80, 1125.

MEASUREMENTS OF NO BETWEEN 17 AND 34.5 KM FROM CHURCHILL, MANITOBA

B.A. RIDLEY, J.T. BRUIN, H.I. SCHIFF, AND J.C. McCONNELL

Department of Chemistry

York University

Downsview, Ontario, Canada

ABSTRACT: NO was measured on two balloon flights made from Churchill $(58^{\circ}N, 95^{\circ}W)$ during July 1974 with a chemiluminescence sampler. One flight, made during high-sun conditions, found mixing ratios increasing from 0.3 to 2.7 ppbv between 17 and 29.5 km. The second flight found values increasing from 0.25 to 2.7 ppbv between 17 and 30.5 km, and a constant mixing ratio of 2.7 ppbv between 30.5 and ≈ 34.5 km. Measurements were also made during a sunset, and the decay of NO (measured down to the instrument's detection limit) is compared with that calculated from a 1-dimensional stratospheric model.

At present it is believed that reactions involving odd nitrogen, NO_x, form the dominant catalytic cycle for O₃ destruction in the stratosphere below about 45 km. As part of a program to continue measurements of NO in the atmosphere, we have completed two balloon flights from Churchill, Manitoba which enabled us to make mixing-ratio measurements between about 17 and 34.5 km. On one of these flights, the NO experiment was incorporated into the multiexperiment gondola of the Canadian Atmospheric Environment Service which was designed to obtain simultaneous measurements of several NO_x species. Comparisons of various data obtained from this flight were presented in Dr. Evans' paper. In this note, in-situ NO measurements during high-sun conditions and during sunset are presented.

EXPERIMENTAL

The NO/O₃ chemiluminescence instrument for in-situ NO sampling and the payload configuration for balloon transport have been described in detail elsewhere (Ridley and Howlett, 1974; Ridley et al., 1974, 1975). Experimental tests to confirm that no significant sampling errors are encountered with this payload configuration have also been described (Ridley et al., 1974, 1975). Provision is made for on-board calibration of the instrument by the addition of small known flows of NO to the air sample flow from a high-pressure tank containing a few ppm of NO

in N₂. Analysis of this flight calibration bottle before and after the balloon flights gave NO concentrations which agreed to 5%. The estimated accuracy of the data presented below is 30%.

The balloons were launched from Churchill, Manitoba, at 58°N, 95°W. Flight 1 took place on July 16, 1974; it used a 2.3 × 104 m³ balloon with the payload suspended some 30 m below. Measurements were made between 22:00 and 01:00 GMT during ascent and float. Flight 2 was made on July 22, 1974; a 3.1 × 105 m³ balloon with the payload suspended about 100m below was used. Measurements were made from 00:30 to 04:00 GMT and for an additional 2.5 hours after visible sunset. Visible sunset on the balloon occurred near 04:08 GMT. For flight 2 some problems were encountered in the determination of the balloon float altitude. This note assumes that float was near 34.5 km; there is a possibility that this figure is about 1 km low.

RESULTS

The NO mixing ratios obtained for solar zenith angles, χ , less than 90° are shown in Figure 1 and in Tables 1 and 2. The tabulated number densities were calculated from atmospheric density data determined from radiosonde releases. The O_3 profile for flight 1, shown in Figure 2, was obtained from an ozonesonde release from the Churchill station just after the launch of the NO instrument.

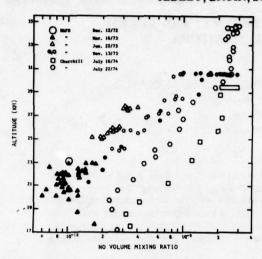


Figure 1. Vertical NO volume mixing-ratio profiles obtained from Churchill and Holloman AFB, New Mexico with $\chi < 90^{\circ}$.

Table 1. NO Data for Flight 1, July 16, 1974

		Mixing	Number
Time	Altitude	Ratio	Density
(GMT)	(km)	(ppbv)	(cm ⁻³)
22:05	17.5	0.35	0.94×10^{9}
	18.6	0.32	0.72
	19.6	0.42	0.82
	21.2	0.75	1.1
	23.2	1.2	1.3
22:30	24.8	1.4	1.2
	25.75	2.0	1.5
	26.8	2.2	1.4
	28.8	2.1	1.1
	29.4 ± 0.3	2.7	1.3
		2.3	1.1
		2.2	1.1
23:04		2.1	1.0
		2.6	1.2
		2.7	1.3
		2.7	1.3
		2.3	1.1
23:31		2.8	1.4
		2.6	1.2
		3.1	1.5
		2.3	1.1
24:00		3.0	1.5
		3.1	1.5
		3.0	1.5
		2.8	1.4
		3.1	1.5
		2.9	1.4
		3.0	1.5
24:30		2.5	1.2
		2.7	1.3
		2.9	1.4
		2.7	1.3
24:50		2.3	1.1

Table 2. NO Data for Flight 2, July 22, 1974

Time (GMT)	Altitude (km)	Mixing Ratio (ppbv)	Number Density (cm ⁻³)
00:33	17.2	0.27	7.9 × 10 ⁸
	18.9	0.24	5.5
	19.7	0.23	4.6
	20.6	0.27	4.7
	21.5	0.37	5.6
01:02	22.9	0.46	5.6
	23.5	0.58	6.4
	24.1	0.57	5.8
	24.6	0.76	7.1
	25.9	0.91	7.0
	26.7	0.99	6.7
01:30	27.5	0.90	5.4
	28.2	1.2	6.5
	29.4	1.9	8.5
	29.9	2.2	9.1
	30.5	2.6	9.7
	31.0	2.6	9.1
02:03	31.8	2.5	7.7
	32.0	2.5	7.5
	32.4	2.7	7.6
	32.8	2.7	7.1
	33.5	2.3	5.4
	33.7	2.4	5.5
02:31	34.0	2.7	5.9
	34.1	2.9	6.0
	≈ 34.5	2.6	5.3
		2.4	4.9
		2.8	5.7
		2.8	5.7
03:04		3.0	6.0
		2.8	5.7

In both cases, the NO mixing ratio increases strongly with altitude between 19 and 29 km, a trend in agreement with data of earlier flights from New Mexico. Flight 1 exhibits significantly higher mixing ratios between 20 and 28 km, though the profiles converge at the higher altitudes. At float, with $\chi < 90^{\circ}$, there is little variation in the mixing ratio during the measurement period. For flight 1 the average value is 2.7 ± 0.2 ppbv for the two-hour period. For flight 2 the average value is again 2.7 ± 0.2 ppbv but the measurement time is only about 26 minutes.

Flight 2 also permitted measurements to be made during sunset while the balloon was at float. The open circles of Figure 3 show the ratio of NO during sunset to the average high-sun value of 2.7 ppbv. The instrument operated for an additional 2.5 hours after visible sunset, but the NO mixing ratio remained below the limit of detection of the instrument (ca. 0.06 ppbv).

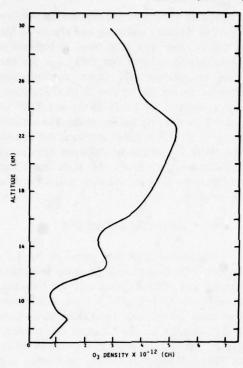


Figure 2. Vertical ozone number-density profile for the July 16, 1974 NO balloon flight.

DISCUSSION

Figure 1 compares the Churchill data with that obtained from Holloman AFB, New Mexico (Ridley et al., 1974, 1975). The New Mexico data was obtained during fairly high sun conditions. All of the data in Figure 1 was obtained with two essentially identical instruments using similar payload configurations. Although the profiles exhibit similar trends, with mixing ratio increasing with altitude between about 20 and 30 km, there is a difference of up to a factor of 10 in the 20 to 26 km region. If possible seasonal and latitude effects are neglected for the moment, this difference seems to indicate that there is considerable short- and long-term variability in NO. Short-term variability is indicated by the Churchill profiles, which were taken only six days apart. Still shorter-term variability was observed at float on the November 13th flight, where NO at first increased and then decreased with time over the float duration of about two hours. Similar observations of variability have been noted by Ackerman et al. (1974, 1975) and by Loewenstein and coworkers (Loewenstein et al., 1974, 1975; Savage et al., 1975). Also, Murcray et al. (1974) and Lazrus and Gandrud (1974) have observed considerable variations in

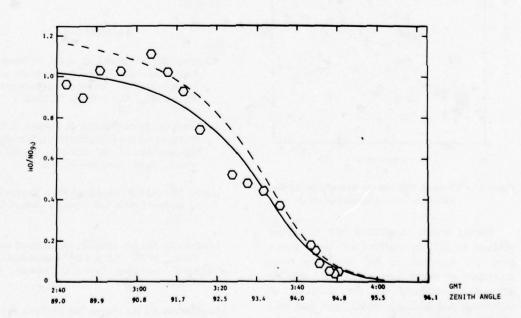


Figure 3. The decay of NO during sunset for the July 22, 1974 Churchill flight. Upper scale, GMT; lower scale, zenith angle.

 HNO_3 , the predominant NO_x species below about 30 km.

Because of the short-term variations in NO observed, it is and will be difficult to unequivocally ascertain seasonal and latitude trends from the limited amount of data obtained so far by various groups. Loewenstein and coworkers (Loewenstein et al., 1974, 1975; Savage et al., 1974) have presented data which may indicate higher NO mixing ratios in the lower stratosphere in summer. From our scanty data we cannot confirm this possibility.

Figure 4 gives a plot of our data relative to height above the tropopause. Overall, this improves the agreement of the Churchill and New Mexico data. It is not easy to interpret such a plot of data from two latitudes, however. A general lowering of the tropopause as northern latitudes are approached is not the only factor in the agreement, because O_3 , temperature, transport and solar insolation are all changing.

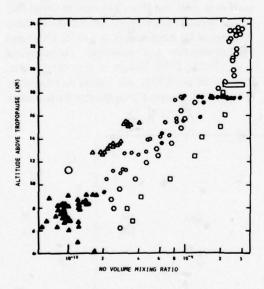


Figure 4. Vertical NO volume mixing-ratio profiles relative to the tropopause (see text).

During sunset conditions NO is rapidly oxidized to NO₂ by reaction with O₃. Figure 3 gives the variation of NO from the time-dependent photochemical model of J. McConnell, which includes all the reactions of McConnell and McElroy which have time constants short enough to be of importance in the diurnal variation. The calculation employs

straight-path photolysis and neglects the possible effects of Rayleigh scattering and albedo on the photolysis rates. The solid curve in Figure 3 is the calculated ratio of $NO_\chi/NO_{\chi=90^\circ}$ for the actual temperature and ozone concentration measured during the balloon float. Calculations with a variation of $\pm 30\%$ in O_3 and $\pm 10^\circ$ in temperature give very similar results. The normalization to $\chi=90^\circ$ is rather arbitrary; the dashed curve gives the results of the same calculation normalized at $\chi=91.7^\circ$. In both cases the agreement between the calculation and the data is quite good.

ACKNOWLEDGMENTS

Considerable help was given us by L.C. Howlett, F.N. Foulds, and the group from SED Systems Ltd., Wayne Evans and the Canadian Atmospheric Environment Service, and Raven Industries. Ozone and radiosonde data were kindly obtained by the Churchill Meteorology Station. The flight operations were supported by the National Research Council of Canada and the Atmospheric Environment Service. Instrument construction was supported by the U.S. Department of Transportation through NOAA, as part of the Climatic Impact Assessment Program.

REFERENCES

Ackerman, M., D. Frimout, C. Muller, D. Nevejas, J.C. Fontanella, A. Girard, L. Gramont and N. Louisnard (1974), "Recent stratospheric spectra of NO and NO₂," Can. J. Chem. 52, 1532.

Ackerman, M., J.C. Fontanella, D. Frimout, A. Girard, N. Louisnard and C. Muller (1975), "Simultaneous measurements of NO and NO₂ in the stratosphere," Planet. Space Sci. 23, 651.

Lazrus, A.L. and B.W. Gandrud (1974), "Distribution of stratospheric nitric acid vapor," J. Atmos. Sci. 31, 1102.

Loewenstein, M., J.P. Paddock, I.G. Poppoff and H.F. Savage (1974), "NO and O₃ measurements in the lower stratosphere from a U-2 aircraft," Nature 249, 817.

Loewenstein, M., H.F. Savage and J.P. Paddock (1975), "Stratospheric measurements of NO and O₃ from 0° to 82° north latitude," in this volume.

RIDLEY, BRUIN, SCHIFF, AND McCONNELL

- Murcray, D.G., A. Goldman, W.J. Williams, F.H. Murcray, J.N. Brooks, R.N. Stocker, and D.E. Snider (1974), "Stratospheric mixing ratio profiles of several trace gases as determined from balloon-borne infrared spectrometers," in Proceedings of the International Conference on Structure, Composition and General Circulation of the Upper and Lower Atmospheres and Possible Anthropogenic Perturbations (Melbourne, Jan. 14-25, 1974), pub. IAMAP, 292.
- Ridley, B.A. and L.C. Howlett (1974), "An instrument for nitric oxide measurements in the stratosphere," Rev. Sci. Instrum. 45, 742.
- Ridley, B.A., H.I. Schiff, A.W. Shaw, L.R. Megill, L. Bates, C. Howlett, H. LeVaux and T.E. Ashenfelter

- (1974), "Measurements of nitric oxide in the stratosphere between 17.4 and 22.9 km," Planet. Space Sci. 22, 19.
- Ridley, B.A., H.I. Schiff, A. Shaw and L.R. Megill (1975), "In-situ measurements of stratospheric nitric oxide using a balloon-borne chemiluminescent instrument," J. Geophys. Res. 80, 1925.
- Savage, H.F., M. Loewenstein and R.C. Whitten (1974),
 "In-situ measurements of NO and O₃ in the lower
 stratosphere," in Preprints of the Second International Conference on the Environmental Impact
 of Aerospace Operations in the High Atmosphere
 (AMS/AIAA, San Diego), pub. AMS, 5.

LATITUDINAL MEASUREMENTS OF NO AND O₃ IN THE LOWER STRATOSPHERE FROM 5.5° TO 82° NORTH

MAX LOEWENSTEIN AND HOWARD SAVAGE NASA Ames Research Center Moffett Field, California

ABSTRACT: Latitudinal measurements of NO and O_3 concentrations were carried out in June and October of 1974 at altitudes between 18.3 and 21.3 km using in-situ measuring techniques. The observed NO number densities range from 4×10^8 to 1.8×10^9 cm⁻³ and are consistent with other recent in-situ and remote observations of NO concentrations in the lower stratosphere. High values of NO were observed near 5.5°N and in the 60° to 80° north latitude range, with generally lower and steady values observed in the 20° to 60° north latitude range. Ozone measurements show the well-known increase of ozone toward the pole.

INTRODUCTION

In this note we report some early results of a program undertaken to determine the lower-stratosphere concentrations of NO and O₃ as functions of latitude in the Northern Hemisphere. Measurements are carried out in situ by instruments carried on a U-2 aircraft flying in the 18.3 to 21.3 km altitude range. Details of the chemiluminescence-type detector for the nitric oxide measurements and the ultraviolet-absorption photometer for ozone measurements are described elsewhere (Savage et al., 1974).

The results presented here were obtained from two experimental flight series: (1) flights made in June 1974 covering latitudes from 38° to 82°N, and (2) flights made in October 1974 covering latitudes from 5.5° to 37°N. Most of the flight data were obtained near 157° west longitude along a meridian through Honolulu, Hawaii and Barrow, Alaska. Between 38° and 65°N the flight tracks deviate from this meridian by a maximum of 36° to the east, as indicated on the map of Figure 1.

RESULTS

The NO and O₃ data from the June 1974 and October 1974 flight series are summarized in Figures 2 through 4, and important flight parameters are given in Table 1. The latitudinal measurement coverage is continuous from 5.5° to 82° north latitude. Each NO data point is the result of a three-minute observation of the

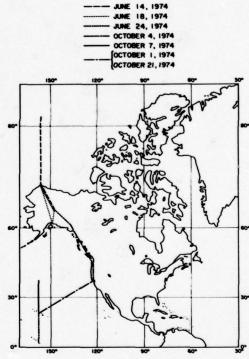


Figure 1. Flight path map.

atmosphere, during which time the NO chemiluminescence analyzer output is recorded once per second, followed by a six-minute instrument-calibration cycle. At the aircraft speed of 206 m/sec the resolution of the data is one degree of latitude per data point. Ozone data are acquired at a rate of one data point per ten seconds; thus, O₃ is measured on a nearly

LOEWENSTEIN AND SAVAGE

continuous basis. A sampling of this quasi-continuous O₃ record is shown in Figures 2 through 4. Figure 4 shows data obtained on the flights between Moffett Field, California and Hickam AFB, Hawaii; for operational reasons, these sampling flights were carried out at an altitude of 19.8 km. The NO data from the 21 October flight show a greater-than-normal scatter, due to excess noise in the NO instrument on that day. This instrument malfunction was subsequently corrected.

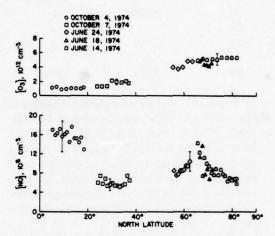


Figure 2. NO and O₃ concentrations at 18.3 km altitude as a function of latitude at 122° to 158° west longitude.

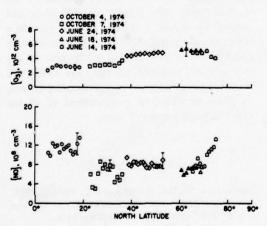


Figure 3. NO and O₃ concentration at 21.3 km altitude as a function of latitude at 122° to 158° west longitude.

The accuracy of the NO data varies, depending on details of the operating condition of the NO instrument and on the NO level being

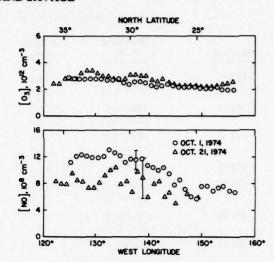


Figure 4. Measurements at 19.8 km in October 1974. Ozone concentrations are a function of latitude, NO concentrations a function of longitude.

detected. Typical O₃ and NO error limits are shown in Figures 2 and 3 for each flight.

Data presented elsewhere (Loewenstein et al., 1976) indicate that between mid-June early October at mid-latitudes (33°-40°N/122°W) about a 25% decrease in NO concentration is observed in the 18 to 21 km altitude range. Thus, assuming that this seasonal variation occurs at all longitudes between 122° and 157°W, there will be a small discontinuity in the data of Figures 2 and 3 at 36°N. All data for latitudes north of 36°N were acquired in June 1974; data for latitudes south of 36°N were taken in October 1974. The seasonal variation of NO has not yet been well enough documented to allow accurate correction of our latitudinal data for this seasonal effect. This discontinuity of the data should be kept in mind in the following discussion.

Some important features of the data to be noted are the following:

1. NO concentrations increase in a southerly direction from 30°N at both the 18.3 and 21.3 km altitudes; however, the most striking increase, by a factor of nearly three, occurs at 18.3 km. The data for latitudes south of 20°N were acquired on 4 October 1974 and the data for latitudes between 20° and 36°N were acquired on 7 October 1974. Thus it cannot be

LOEWENSTEIN AND SAVAGE

Table 1. Corollary Data for the Flights in the Latitudinal Survey of NO and O3

Day-Year	Run Time (UT)	Altitude (km)	Avg. Temp. (K)	N Latitude Range	W Longtitude Range
165-74	1917-2242 2300-0035	18.3 21.3	229 232	65-82	148-157
169-74	1955-2041 2104-2240	18.3 21.3	227 229	61-71	148-157
174-74	1720-1850 1906-2141	18.3 21.3	226 220	38-64	122-144
274-74	1845-2331	19.8	211	22-37	124-155
277-74	1815-2035 2047-2300	18.3 21.3	202 212	5.5-20	158
280-74	1825-2044 2057-2300	18.3 21.3	206 215	23-37	158
294-74	1727-2229	19.8	209	22-36	122-156

ruled out that natural fluctuations of NO over a period of two to three days contribute to the measured latitudinal effects that are shown in Figures 2 and 3.

- 2. The NO data for latitudes between 20° and 82° N are fairly constant, lying generally between 6×10^8 and 1×10^9 cm⁻³ at 21.3 km, and between 5×10^8 and 1×10^9 cm⁻³ at 18.3 km. Peaks in the measured NO can be seen in both the 18.3 and 21.3 km data above 60° N latitude; however, these are not observed at the same latitude for the two altitudes.
- 3. The data of 1 October and 21 October (shown in Figure 4) are not part of the latitudinal survey. They are shown to provide a comparison of nitric oxide concentrations measured at the same altitude along the same flight track but 20 days apart. Note that the flight altitude is 19.8 km, which is different from that of the data in Figures 2 and 3.
- 4. The ozone data show an expected increase toward northerly latitudes, partly due to the natural increase of ozone toward the pole and partly because the flight altitude is approaching the altitude of the ozone peak in the region of 70° to 80°N latitude.

SUMMARY

We have presented data on the latitudinal distribution of NO in the altitude range of 18-21 km. These are early results of a program undertaken to determine the global distribution

of important stratospheric minor constituents. High values of NO were observed at latitudes south of 20°N compared with the rather steady values observed between 20° and 80°N. The data coverage for NO represents about one data point per degree of latitude. More data of this kind must be collected to reveal any average stratospheric structure of the NO latitudinal distribution.

We are currently planning to repeat this kind of latitudinal survey to accomplish two objectives: first, to acquire data from 5° to 80°N latitude in a short time span to eliminate the seasonal split now present in the data; and second, to acquire sufficient data to provide a better average distribution of NO in the altitude range of 18 to 21 km. Also, in the near future, measurement capability for NO₂ and HNO₃ will be added to the airborne in-situ sampling system, to allow simultaneous measurement of all the important odd-nitrogen species.

REFERENCES

Loewenstein, M., H.F. Savage, and R.C. Whitten (1976), "Stratospheric measurements of NO and O₃ from 5° to 82° north latitude," in this volume.

Savage, H.F., M. Loewenstein, and R.C. Whitten (1974), "In situ measurements of NO and O₃ in the lower stratosphere," in *Preprints of the Second International Conference on the Environmental Impact of Aerospace Operations in the High Atmosphere* (San Diego), pub. AMS, 5-10.

SEASONAL VARIATIONS OF NO AND O₃ AT ALTITUDES OF 18.3 AND 21.3 KM

MAX LOEWENSTEIN, H.F. SAVAGE, AND R.C. WHITTEN NASA Ames Research Center Moffett Field, California

ABSTRACT: Nitric oxide and ozone concentrations have been measured in situ from a high-altitude research aircraft based at the NASA Ames Research Center. Data which show the variations of NO and O_3 with the time of year are presented for 18.3- and 21.3-km altitudes. The extreme values of the observed NO concentrations at 21.3 km are 1.2×10^9 cm⁻³ in summer and 2×10^8 cm⁻³ in winter. At 18.3 km the extreme values are 1.6×10^9 cm⁻³ in summer and 1×10^8 cm⁻³ in winter. The smoothed NO seasonal data show variations of about a factor of 2.5 at 21.3 km and a factor of 4 at 18.3 km. The ozone data show the generally expected concentrations and seasonal variation.

We have used a photochemical model employing the measured ozone concentrations, the mean solar zenith angle, and seasonal HNO₃ data reported by others to predict the seasonal NO variation at 20 km. The result is a summer-to-winter NO ratio of 2.5 which is in fair agreement with the observed ratios.

INTRODUCTION

The importance of the oxides of nitrogen in the chemistry of the atmospheric ozone layer has been discussed by Crutzen (1971) and Johnston (1971). Both authors pointed out the possibility that the ozone layer could be affected by nitric oxide injection from supersonic-transport operations in the lower stratosphere. The suggestion of such an effect has motivated various efforts in modeling and measurements of the ambient stratosphere. Recently, several workers (McElroy et al., 1974; Whitten and Turco, 1974) have presented one-dimensional atmospheric models including transport and chemistry, in an attempt to provide a more realistic assessment of the effect of nitric oxide on the ozone layer.

The first direct NO_x measurement ($NO_x \equiv NO + NO_2$) in the lower stratosphere was reported in 1971 (Hale and Pontano, 1971). Since then, a number of workers have reported measurements of NO and NO_2 by various techniques at altitudes ranging from 15 to 30 km (Ackerman and Muller, 1972; Ackerman et al., 1973, 1974; Fontanella et al., 1974; Ridley et al., 1974a, 1974b; Toth et al., 1974; Loewenstein et al., 1974a, 1974b; Savage et al., 1974; Patel et al., 1974; Murcray et al., 1974). These authors measured only NO or NO_2 in a particular experiment, except for a simultaneous measure-

ment of NO and NO₂ carried out by Ackerman et al. (1974).

Discrepancies which have existed between various NO measurements are now beginning to be resolved as a pattern of seasonal variations unfolds from our data. For example, Ackerman's measurements (Ackerman et al., 1973), which had appeared to disagree with our early measurements (Loewenstein et al., 1974a), now appear, because of the seasonal variation of NO, to agree well with our new data.

A measurement of stratospheric NO (or NO₂) yields useful information about NO₂ (or NO) because the NO/NO₂ ratio is given approximately by photochemical theory. The time constant for interconversion of NO and NO₂ is about 100 sec at 20 km; therefore, these species are in photochemical equilibrium at this altitude. An additional factor in the photochemistry of NO_x is its conversion to nitric acid by reaction with OH. Because the time constant for such conversion is $\approx 10^6$ sec at 20 km, HNO₃ is not in photochemical equilibrium with the other oddnitrogen compounds, NO and NO₂. Hence, measurement of NO or NO₂ alone does not yield complete data on odd-nitrogen abundance.

A continuing measurement program, which will also yield data on NO₂ and HNO₃ concentrations, is necessary in order to completely establish seasonal and geographical behavior of NO₈ concentrations in the lower stratosphere.

INSTRUMENTATION

Our measurements of nitric oxide and ozone are made in situ with instruments carried on a U-2 aircraft flying at altitudes of 18.3 and 21.3 km. A flow of ambient air is brought into the experiment bay of the aircraft by an airscoop extending beyond the aircraft boundary layer. At a 21.3-km cruise altitude, where the true airspeed of the aircraft is 206 m sec⁻¹, the pressure developed at the inlet scoop is 12 Torr in excess of ambient pressure. Inside the experiment bay, a flexible line carries the airflow to a manifold from which flows are distributed to the measuring instruments.

Nitric Oxide Sensor

Nitric oxide in the air sample is detected by the chemiluminescence method, based on the reactions

$$NO + O_3 \rightarrow NO_2 + O_2$$
, (1a)

$$\rightarrow NO_2 + O_2, \tag{1b}$$

$$NO_2^* \rightarrow NO_2 + h\nu$$
, (2)

$$NO_2 * + M \rightarrow NO_2 + M$$
, $M = O_2$ or N_2 . (3)

At 300K, 7% of NO molecules that undergo reaction with ozone will react via path (1a), leading to excited-state NO_2^* molecules which then decay radiatively via reaction path (2), or are quenched via reaction path (3). The spectrum of emitted radiation lies between 0.6 and 3 μ m, with a broad peak near 1.2 μ m. A portion of this radiation is detected in the NO chemiluminescence instrument.

The signal observed with the nitric oxide chemiluminescence instrument is proportional to the rate at which NO molecules enter the reaction chamber in the instrument; thus,

$$S_{atm} = K F_{atm} X_{atm}, \tag{4}$$

where S_{atm} is the observed signal from the atmosphere with NO volume mixing ratio X_{atm} flowing through the instrument at a rate F_{atm} . K is a constant of the instrument for a fixed set of operating conditions, and it is determined by introducing into the instrument, during the flight

measurements, a metered flow F_{cal} of NO in nitrogen, whose mixing ratio X_{cal} is known. The observed instrument response is

$$S_{cal} = K F_{cal} X_{cal}$$
 (5)

where S_{cal} is the measured calibrator signal. The instrument constant K is periodically determined during atmospheric measurements.

The linear relationship between signal and mixing ratio expressed by Eqs. (4) and (5) is assured by using a large excess of ozone reactant relative to the nitric oxide being measured.

In the chemiluminescence instrument (Figure 1), the atmospheric sample and ozone reactant are introduced through concentric injector tubes into a cylindrical flow reactor which is 20 cm long and 5 cm in diameter. The reactor is glass with an interior gold plating to enhance light collection by the detector. The reactionchamber end window opposite the gas injector is a Corning 2-62, 6200-Å long-pass filter. An EMI 9659 photomultiplier, which has a photocathode with "extended red" sensitivity, views the reaction chamber through the 2-62 filter. The photomultiplier tube is operated at dry-ice temperature. Pulse-counting electronics are used to process the output from the tube, and linear count-rate circuits provide full-scale analog outputs equivalent to 104 and 3 × 104 counts per second, each with a one-second electronic time constant.

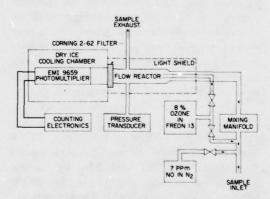


Figure 1. Schematic diagram of the NO detection apparatus.

Ozone reactant is provided from a 1-liter stainless-steel bottle containing a mixture of nominally 8 mole percent ozone in liquid Freon 13. Typical reactant flow is 30-50 g hr⁻¹ of the

O₃-Freon solution. NO calibrator gas is carried in a 500-cm³ stainless-steel bottle which is filled to 500 psi from a master calibrator-gas cylinder prior to each flight. The NO mixing ratio of the calibrator currently being used is 6.7 ppm in nitrogen. Calibrator gas flows of 4 and 10 cm³ min⁻¹ STP are used for the periodic instrument calibration. Air sample flow through the instrument is typically 19 × 10³ cm³ min⁻¹ STP at a 21.3-km cruise altitude.

The NO instrument has three operating modes: calibrate, null, and measure. Each mode is allotted 3 min, which yields a 9-min cycle for one complete atmospheric NO measurement. Alternate 9-min cycles employ the high and low calibrator flows as a check on the linearity of the instrument response.

In the calibrate mode, the calibrator gas flow is added into the atmospheric gas flow upstream of the mixing manifold. In the null mode, the ozone reactant is added into the atmospheric flow upstream of the mixing manifold. To check the nulling of the atmospheric NO in this mode, an overlap of 1 min between high-calibrator and null modes is provided. This gives a direct measurement of the nulling efficiency once every 18 min. If less than 99% nulling is observed, the NO data are corrected correspondingly. The minimum detectable NO mixing ratio is dependent on the instrument operating conditions and is generally in the range 0.02 to 0.04 ppb, which is 3 × 10⁷ to 7 × 10⁷ molecules cm⁻³ at 21.3 km.

Ozone Sensor

Ozone is measured in a commercial ultraviolet photometer (Bowman and Horak, 1972) by monitoring the transmission of the 2537-Å Hg radiation through a 71-cm airpath. This wavelength lies close to the peak of the strong Hartley-continuum absorption of ozone. A temperature-controlled Hg lamp is used as the 2537-Å source, and the absorption cell is continuously flushed with ambient air at a flow of 250 cm³ min⁻¹ STP. A vacuum photodiode with a CsTe cathode is used to detect the transmitted 2537-Å radiation. A second identical photodiode detector viewing the Hg source directly is incorporated into a servo loop to control the output intensity of the lamp.

The instrument operates in two modes, measure and null. In the null mode, an MnO_2 scrubber removes ozone from the airflow and a signal I_0 , proportional to the unattenuated 2537-Å intensity, is measured and stored. In the measure mode, a signal I, proportional to the attenuated 2537-Å intensity, is measured and stored. The I and I_0 values are used to obtain the ratio

$$\frac{I_0 - I}{I_0} = 1 - e^{\alpha p \ell} \tag{6}$$

where $\alpha = 306 \text{ cm}^{-1} \text{ atm}^{-1}$ is the ozone absorption coefficient at 2537 Å, p is the STP partial pressure of ozone, and $\ell = 71 \text{ cm}$ is the absorption-tube length.

The measure and null modes are of 5 sec duration each; thus, an ozone measurement is completed in 10 sec. The instrument sensitivity is 3 nbar STP of ozone, or 8×10^{10} molecules cm⁻³.

Atmospheric Temperature Sensor

Outside air temperature is measured with a resistance thermometer and is recorded by the pilot every 15 min during the flight. The accuracy of the measurements is ±2K, and the average temperatures measured are listed in Table 1.

MEASUREMENTS AND CALIBRATIONS

One complete nitric oxide measurement is made every 9 min of flight; therefore, the spatial resolution of the nitric oxide measurements is 110 km. The mean mixing ratio of NO is calculated using Eqs. (4) and (5):

$$X_{NO} = \frac{S_{atm} F_{cal}}{S_{cal} F_{atm}} X_{cal}$$
 (7)

where S_{atm} and S_{cal} are the signals from the atmospheric nitric oxide and the nitric oxide calibrator as derived from the flight data. The uncertainty in the ratio of these signals is due to the counting statistics of the measure, null, and calibrate determinations. This uncertainty ranges from 1% to 20%, depending upon the size of the NO signals being detected on a particular flight.

Table 1. Summary of the Flight Parameters

Day-Year	Start Run (UT)	End Run (UT)	Altitudes (km)	Avg. Temp. (K)	N Latitude Range	W Longitude Range
320-73	1800	2030	18.3 21.3	218 221	38	117-123
340-73	1900	2200	18.3 21.3	210 213	37.5-47.5	121-123
352-73	1830	2200	18.3 21.3	210 215	37.5-49	122-123
022-74	1800	2100	18.3 21.3	220 219	37.5-47.5	121-123
032-74	1700	2030	21.3	221	37.5-49	122-123
070-74	1745	1930	21.3	221	37.5-40.5	106-122
099-74	1830	1930	18.3	19 S 20 40 1	35-37.5	120-122
125-74	1700	2130	18.3 21.3	212 217	33-37.5	112-122
151-74	1730	2130	18.3 21.3	212 221	33-37.5	112-122
175-74	1900	2140	21.3	220	37.5-53	122-130
221-74	1715	1920	18.3 21.3		37.5-40	119-122
234-74	1715	1915	18.3 21.3	211 227	37.5-40	119-122
242-74	1615	1815	18.3 21.3	-	37.5-40	119-122
263-74	1730	1900	21.3	222	37.5-40	119-122
329-74	1915	2230	18.3 21.3	208 211	33-37.5	112-122
345-75	1915	2230	21.3	220	33-37.5	112-122
352-74	1815	2130	18.3 21.3	222 225	33-37.5	112-122
010-75	1815	2130	18.3 21.3	221 224	33-37.5	112-122
028-75	1815	2130	18.3 21.3	219 222	33-37.5	112-122
044-75	1815	2130	18.3 21.3	216 221	33-37.5	112-122
045-75	1845	1945	18.3	221	36-37.5	118-122

 F_{cal} , the nitric oxide calibrator flow rate, is measured by monitoring the differential pressure across a calibrated capillary, and the pressure and temperature within the capillary. Calibrator flows are fixed by a pressure regulator and critical orifices. F_{atm} is determined by measuring the differential pressure across the NO instrument, and the pressure and temperature in the reaction chamber. The uncertainty in the ratio of these flows is estimated to be $\pm 10\%$.

 X_{cal} is the mixing ratio (of nitric oxide in nitrogen) of the calibrator gas used in the flight experiments. The mixing ratio of the master calibrator bottle has been determined recently (January 1975), using an NO_x analyzer which was calibrated against an NO_2 permeation tube. The result is $X_{cal} = 6.7 \pm 0.7$ ppm NO in N_2 . A previous determination of the mixing ratio in the same bottle was made by the manufacturer in February 1974 and found to be 6.34 ± 0.13

ppm. The agreement of these two measurements indicates that the NO-in- N_2 mixture we are using is stable, and we have adopted our own measurement and uncertainty estimate of X_{cal} for the calculations in this paper.

A number of systematic effects on the atmospheric NO determinations have been identified and are accounted for in the data analysis. Briefly, these are:

- Depletion of NO in the flight calibrator bottle has been measured to be 3% d⁻¹; this bottle is normally filled within 24 hr prior to a flight, and a correction for the depletion is made to the data.
- When incomplete nulling is observed, a correction is made as discussed in the previous section.
- Loss of NO due to reaction with ambient ozone in the inlet lines to the NO detector has been computed and a correction amounting to about 2% is made.
- Wall losses within the system have been measured and are found to be negligible.

After the data have been corrected for these systematic effects, there remains a residual systematic uncertainty in the NO data of $\pm 3\%$.

Combining the error estimates above, we can give a range of uncertainties for the data presented here. When the counting statistics contribute much less than 10% uncertainty, the flows and the NO-calibrator mixing ratio fix the uncertainty at $\pm 15\%$. For a statistical uncertainty as large as 20%, which is sometimes observed, the overall uncertainty becomes $\pm 25\%$.

One complete ozone measurement is made every 10 sec of flight; therefore, the spatial resolution of the ozone measurements is 2 km. The data from the ozone ultraviolet photometer are corrected for line losses, which have been determined to be stable at 15% after a system conditioning time of 30 min under simulated atmospheric conditions. The estimated uncertainty in the ozone data is ±15%.

RESULTS

Figures 2 and 3 and Table 1 summarize the results of flights made between November 1973

and January 1975 and show the seasonal variations of O₃ and NO at altitudes of 18.3 and 21.3 km. Each plotted point for NO and O3 is the average value observed at that altitude on that day. Each NO point is typically the average of 8 to 12 observations. The size of the rectangle for each NO point shows the spread in the values measured on that day and is not related to the uncertainty of the individual observations. The small spread shown for some of the flights at 18.3 km is due to the small number of observations at that altitude. Also shown for comparison are the NO data of Ackerman et al. (1975) and Ridley et al. (1974a,b). The spread of the O₃ data is not shown in Figures 2 and 3, since many of the spreads are of the order of the size of the symbols.

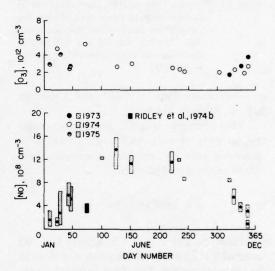


Figure 2. Average NO and O₃ concentrations at 18.3 km altitude versus time of year. See Table 1 for range of latitude and longitude. Symbol size for the NO data is determined by actual spread of values (not uncertainty).

Figures 2 and 3 show a seasonal variation in nitric oxide concentrations at both 18.3 and 21.3 km. At 21.3 km NO concentrations are typically 1×10^9 cm⁻³ in midsummer and 4×10^8 cm⁻³ in winter, although extreme values range from 1.2×10^9 cm⁻³ in summer to 2×10^8 cm⁻³ in winter. At 18.3 km the same trend is observed, with 1.2×10^9 cm⁻³ being a typical midsummer NO concentration, decreasing to 3×10^8 cm⁻³ in winter. In this case the

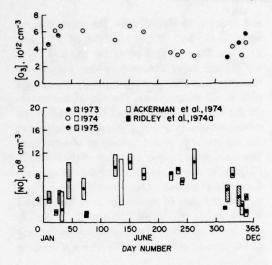


Figure 3. Average NO and O₃ concentrations at 21.3 km altitude versus time of year. See Table 1 for range of latitude and longitude. Symbol size for the NO data is determined by actual spread of values (not uncertainty).

extremes observed are 1.6×10^9 cm⁻³ in summer and 1×10^8 cm⁻³ in winter.

The observed seasonal change of ozone concentration at both 18.3 and 21.3 km is in agreement with the well-known seasonal variation of ozone at mid-latitudes.

DISCUSSION

From Figures 2 and 3 it appears that NO varies over the year by about a factor of three at the altitudes studied. The effect is slightly larger at 18.3 km than at 21.3 km, and the variation is more clearly defined at the lower altitude.

We have considered various possible causes of an NO seasonal variation with the observed phase and magnitude. They are:

- Increased oxidation of NO to HNO₃, due to increased winter ozone and decreased winter photolysis of HNO₃.
- Increased oxidation of NO to HNO₃, due to increased water vapor in winter.
- Increased transport of N₂O from the tropics in spring.
- Increased transport of NO_x and HNO₃ into the troposphere in winter.

Of the possible effects listed, only the first one can account for the magnitude and phase of the NO variation as well as the observed ≈35% winter increase of the nitric acid overburden (Murcray et al., 1975).

Production of nitric acid from NO_x is related to the ozone concentration by the reactions

$$O_3 + h\nu \rightarrow O(^1D) + O_2,$$
 (7)

$$O(^{1}D) + H_{2}O \rightarrow 2OH,$$
 (8)

$$OH + NO_2 + M \rightarrow HNO_3 + M, \qquad (9)$$

whereas the principal destruction mechanism is photolysis,

$$HNO_3 + h\nu \rightarrow OH + NO_2$$
. (10)

 NO_x equilibrium is established by the reactions

$$O_3 + NO \rightarrow O_2 + NO_2 \tag{11}$$

$$NO_2 + h\nu \to NO + 0.$$
 (12)

For an assumed condition of photochemical equilibrium in the 20-km altitude region, we can derive a proportionality between NO and HNO₃ from the foregoing six chemical reactions, namely,

[NO]
$$\approx \frac{J_{10} [HNO_3]}{[O_3]^2}$$
 (13)

where J_{10} is the photolysis rate for reaction (10).

From our ozone data we find about a 50% increase in midwinter ozone concentration over the summer value. From some of our one-dimensional model results, we estimate the HNO₃ photolysis rate at 40°N to be about 1.5 times greater in summer than in winter. If we take the HNO₃ winter increase at 20 km to be 35%, as suggested by the data of Murcray et al. (1976), then from Eq. (13) the summer-to-winter ratio of nitric oxide is 2.5, in rough agreement with our observations.

A more definitive treatment of the seasonal variation of stratospheric nitric oxide awaits

further studies with our two-dimensional stratospheric model and simultaneous measurements of O₃, NO, NO₂, HNO₃, and OH.

REFERENCES

- Ackerman, M., and C. Muller (1972), "Stratospheric nitrogen dioxide from infrared spectra," Nature 240, 300-301.
- Ackerman, M., D. Frimout, C. Muller, D. Nevejans, J.-C. Fontanella, A. Girard and N. Louisnard (1973), "Stratospheric nitric oxide from infrared spectra," Nature 245, 205-206.
- Ackerman, M., J.-C. Fontanella, D. Frimout, A. Girard, N. Louisnard and C. Muller (1975), "Simultaneous measurements of NO and NO₂ in the stratosphere," Planet. Space Sci. 23, 651-660.
- Bowman, L.D. and R.F. Horak (1972), "A continuous ultraviolet absorption ozone photometer," in Air Quality Instrumentation, Vol. 2, ed. John W. Scales, Instr. Soc. Am., Pittsburgh, 305.
- Crutzen, P.J. (1971), "Ozone production rates in an oxygen-hydrogen-nitrogen oxide atmosphere," J. Geophys. Res. 76, 7311-7327.
- Fontanella, J.-C., A. Girard, L. Gramont and N. Louisnard (1974), "Vertical distribution of NO, NO₂, and HNO₃ as derived from stratospheric absorption infrared spectra," in *Proceedings of the Third Conference on the Climatic Impact Assessment Program* (Cambridge, Mass.), U.S. Dept. of Transportation, DOT-TSC-OST-74-15, 217-233.
- Hale, L.C. and B.A. Pontano (1971), "A photoionization measurement in the stratosphere" (abstract), Trans. Amer. Geophys. Union 52, 869.
- Johnston, H. (1971), "Reduction of stratospheric ozone by nitrogen oxide catalysts from supersonic transport exhaust," Science 173, 517-522.
- Loewenstein, M., J.P. Paddock, I.G. Poppoff and H.F. Savage (1974a), "NO and O₃ measurements in the lower stratosphere from a U-2 aircraft," Nature 249, 817-818.
- Loewenstein, M., J.P. Paddock, I.G. Poppoff and H.F. Savage (1974b), "In-situ NO and O₃ measurements in the lower stratosphere from a U-2 aircraft," in *Proceedings of the Third Conference on the Climatic Impact Assessment Program* (Cambridge,

- Mass.), U.S. Dept. of Transportation, DOT-TSC-OST-74-15, 213-215.
- McElroy, M.B., S.C. Wofsy, J.E. Penner and J.C. McConnell (1974), "Atmospheric ozone: Possible impact of stratospheric aviation," J. Atmos. Sci. 31, 287-303.
- Murcray, D.G., A. Goldman, W.J. Williams, F.H. Murcray, J.N. Brooks, J. VanAllen, R.N. Stocker, J.J. Kosters, D.B. Barker and D.E. Snider (1974), "Recent results of stratospheric trace-gas measurements from balloon-borne spectrometers," in *Proceedings of the Third Conference on CIAP* (Cambridge, Mass.), Dept. of Transportation, DOTTSC-OST-74-15, 184-192.
- Murcray, D.G., D.B. Barker, J.N. Brooks, J.J. Kosters and W.J. Williams (1976), "Variation of stratospheric nitric acid vapor with latitude and season," in this volume.
- Patel, C.K.N., E.G. Burkhardt and C.A. Lambert (1974), "Spectroscopic measurements of stratospheric nitric oxide and water vapor," Science 184, 1173-1176.
- Ridley, B.A., H.I. Schiff, A. Shaw, and L.R. Megill (1974a), "In-situ measurements of NO in the stratosphere using chemiluminescence," in Proceedings of the Third Conference on the Climatic Impact Assessment Program (Cambridge, Mass.), U.S. Dept. of Transportation, DOT-TSC-OST-74-15, 193-196.
- Ridley, B.A., H.I. Schiff, A.W. Shaw, L.R. Megill, L. Bates, C. Howlett, H. Levaux and T.E. Ashenfelter (1974b), "Measurement of nitric oxide in the stratosphere between 17.4 and 22.9 km," Planet. Space Sci. 22, 19-24.
- Savage, H.F., M. Loewenstein and R.C. Whitten (1974), "In-situ measurements of NO and O₃ in the lower stratosphere," in Preprints of the Second International Conference on the Environmental Impact of Aerospace Operations in the High Atmosphere (San Diego), pub. AMS, 5-10.
- Toth, R.A., C.B. Farmer, R.A. Schindler and O.F. Raper (1974), "Aspects of infrared detection of nitric oxide in the stratosphere" (abstract), Trans. Amer. Geophys. Union 55, 384.
- Whitten, R.C. and R.P. Turco (1974), "Perturbations of the stratosphere and mesosphere by aerospace vehicles," AIAA J. 12, 1110-1117.

VARIATION OF HNO₃ TOTAL COLUMN DENSITY WITH LATITUDE AND SEASON, AND A MEASUREMENT OF STRATOSPHERIC CF₂Cl₂

D.G. MURCRAY, D.B. BARKER, J.N. BROOKS, A. GOLDMAN, J.J. KOSTERS, F.H. MURCRAY, AND W.J. WILLIAMS

Department of Physics and Astronomy
University of Denver
Denver, Colorado

ABSTRACT: A sensitive spectral-radiometer system capable of measuring the atmospheric emission in the 6.5- μ m to 13.0- μ m region has been constructed for use on the WB57F aircraft used on the Department of Transportation Climatic Impact Assessment Program. The data obtained with this instrument on a number of flights have been analyzed to determine the total HNO₃ column density above the aircraft at various latitudes and seasons. Examination of these data indicates a definite variation of HNO₃ column density with latitude, and possible seasonal variations.

In view of the current interest in the fluorocarbon pollution problem, infrared laboratory absorption spectral measurements of CF_2Cl_2 and $CFCl_3$ were performed and the results applied to balloon flight data of August 12, 1968. A volume mixing ratio of 5×10^{-11} v/v is derived for CF_2Cl_2 and a probable volume mixing ratio of 2×10^{-11} v/v is estimated for $CFCl_3$. These values are compared with calculations by Crutzen and by Cicerone et al. for 21 km. Also, an upper limit for HF in the lower stratosphere up to 30 km is set at 3×10^{-10} v/v for September 30, 1965.

INTRODUCTION

The initial detection of stratospheric HNO₃ (Murcray et al., 1968) was based on an absorption feature at 1325 cm⁻¹ observed in solar spectra obtained at sunset from 30 km using balloon-borne instrumentation. Laboratory studies, verified by subsequent balloon flights, indicated that absorption features in the 11.3-µm region were much better suited for measuring the stratospheric concentration of HNO3. All of the quantitative results we have presented previously (Murcray et al., 1969b; Williams et al., 1972; Brooks et al., 1973) have been based on observations made in this spectral region. These studies indicated that infrared atmospheric emission spectra could also be used to obtain HNO3 data if the spectral-radiometer systems were made sensitive enough. The relative advantages of these two techniques were discussed in a previous article (Murcray et al., 1973). The earlier data were all obtained during balloon flights made from Holloman AFB, New Mexico or Fairbanks, Alaska.

As part of the Climatic Impact Assessment Program (CIAP) of the Department of Transportation we constructed a sensitive spectralradiometer system for use on the WB57F aircraft. With this system it is possible to obtain data over a wide geographic area in a short time. Data on the total column density of HNO3 above flight altitude have been derived from the measurements made during a number of flights, and are presented below. These show a definite dependence on latitude, and possible trends of seasonal dependence. The aircraft has the disadvantage that the peak flight altitude obtainable is well below the peak of the HNO3 layer; hence, information concerning the distribution with altitude of HNO3 is difficult to obtain from these data. Therefore, only total column densities of HNO3 are presented here.

INSTRUMENTATION

The spectrometer used in this study is a 0.38-meter Littrow-type grating spectrometer in which the radiation is double-passed and interrupted after the first pass by means of a tuning-fork chopper. Chopping the optical beam improves the spectral purity and provides an absolute radiometric reference. A small telescope narrows the spectrometer's field of view to 1° by 4°. The spectrometer and telescope assemblies

are mounted in a liquid helium dewar so that all components in the detector's field of view are cooled to less than 10K, with the exception of the dewar vacuum window. For maximum instrumental sensitivity the window should also be cooled, but if the window is cooled provision has to be made to keep frost (H₂O or CO₂) from forming on it. Due to the time and weight constraints it was not possible to incorporate such a system into the unit. Instead the window was partially cooled by the ambient air flowing over the nose section of the aircraft.

The ac signal developed at the Ge:Cu detector from the chopped radiation is amplified by a JFET preamplifier contained in the dewar. It is then further amplified and synchronously rectified outside the dewar using operational amplifiers. The total system gain is adjustable from the instrument control panel; the system can also be operated in an automatic gain-control mode which adjusts the gain so that the peak voltage is between 2.8 and 4.8 Vdc (which is within the recording range of the aircraft data-handling system). A second channel of the data system is used to record the detector signal at high gain, while a third channel is used to record the commutated housekeeping data. For the flights reported here, the detector was equipped with a filter which passes radiation from 6.5 µm to 13.0 µm. This wavelength region contains emission features due to CH₄, N₂O, O₃, HNO₃, H₂O and CO₂. Only the data concerning the HNO₃ distribution have been reduced to date.

DATA REDUCTION

The signal voltage as measured is proportional to the difference between the incident spectral radiance, from both the atmosphere and the dewar window, and the reference blackbody radiance at the temperature of the instrument. Since the internal temperature is iess than 10K, the internal radiance is taken as zero. The window used in the dewar is chosen for low emissivity, and operates at ambient air temperature; however, at the higher altitudes this emission becomes a significant portion of the observed signal in the $11-\mu m$ region. The data are reduced using calibration factors determined from pre- and post-flight instrument calibrations. The window radiance is calculated on the basis of

its temperature and a curve of emissivity versus wavelength determined from laboratory calibrations, and is subtracted from the total measured radiance data. The remaining radiance is due to atmospheric gases and particulates.

Once the data have been obtained in this form, two additional steps are required to determine the HNO₃ column density above the aircraft. The first step is to determine the emissivity at 11.2 μ m, and the second is to determine the HNO3 amount from this emissivity. The amount of HNO3 present above the aircraft is small and the radiance observed at the aircraft comes from all altitudes above the airplane. Since the temperature varies with altitude, one has to make some assumption about the distribution of HNO3 and temperature above the airplane. The mean height of the HNO3 column density was determined for the profiles derived from the balloon flight data. This mean height was 22 km with very little variation with latitude or time of year. In view of this, the total HNO₃ above the aircraft was assumed for the calculation to be at 22 km and the temperature at that altitude was determined from rawinsonde data obtained at various stations close to the aircraft flight path. By using a blackbody radiance for this temperature, it is possible to determine the HNO3 emissivity from the data. Since the HNO3 emissivity is small, it lies in the linear absorption region, and the total column density of HNO₃ above the aircraft is directly proportional to the emissivity. The constants of proportionality have been determined in laboratory measurements (Goldman et al., 1971).

The results obtained for the January Airstream flights are given in Figure 1. Note that the points represent data obtained on different days, at different altitudes, and in different latitudes. There is some local variation in the observed data. Nevertheless, a definite dependence of the HNO3 column density on latitude is evident, increasing from the equator to high latitudes. The latitude dependence in the northern hemisphere is different from that in the southern hemisphere, and appears to indicate higher HNO₃ values in the winter than in the summer. However, more data are needed before a definite seasonal dependence can be established. The data points that fall below the line one would draw to fit the dependence, particularly in the southern

hemisphere, were obtained when the aircraft was flying at 18 km; and it appears that at these latitudes the aircraft has penetrated into the HNO₃ layer, and the decrease is due to this rather than any decrease in total HNO₃ amounts. (On the average, about 75% of the HNO₃ lies above 18 km). The balloon data are also plotted on this graph; they tend to confirm the latitudinal and possibly the seasonal dependence one would infer from the aircraft data.

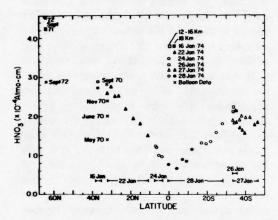


Figure 1. Variation of HNO₃ column density with latitude from the January Airstream series.

The data from the April Airstream series are given in Figure 2. The latitudinal dependence is again evident, and it appears that we are still in a winter regime in the Northern hemisphere; however, it is evident that the layer is now lower in the Northern hemisphere, and the high-altitude flights are penetrating the HNO₃ layer at the high latitudes.

It should be emphasized that these conclusions are based on a limited amount of data, and that significant day-to-day variations in total HNO₃ column density have been observed. Therefore, more data are required to verify the conclusions drawn here. The estimated error in the HNO₃ amounts presented here is approximately 25%.

These results are in agreement with the conclusions reached by Lazrus and Gandrud (1974) on the basis of their filter measurements. Fontanella et al. (1975) have deduced a similar HNO₃ total column density from solar spectra in the 1330 cm⁻¹ spectral region recorded from aircraft at 16 km altitude. Harries et al. (1974)

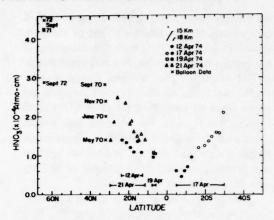


Figure 2. Variation of HNO₃ column density with latitude from the April Airstream series.

have derived similar total HNO₃ amounts from atmospheric emission spectra recorded from aircraft. The spectra were obtained in the 20 cm⁻¹ region at 15 km altitude. However, no significant latitudinal variations were observed in their study.

The latitudinal and seasonal variations presented here appear to show trends similar to those predicted theoretically by Rao-Vupputuri (1975). However, more data are needed before a detailed comparison between experiment and theory can be made.

FLUOROCARBONS

Recent interest in certain fluorocarbons and the associated photochemical derivatives which may occur in the stratosphere prompted us to re-examine earlier balloon flight data to determine what information could be obtained relevant to these constituents. According to the one-dimensional photochemical models used by Molina and Rowland (1974), Crutzen (1974a), and Cicerone et al. (1974), the introduction of fluorocarbons into the stratosphere in large quantities will alter the ozone chemistry, and could reduce total ozone amounts. Verification of these models as representative of the atmospheric processes requires quantitative measurements to determine first whether the fluorocarbons are present in the stratosphere at predicted concentrations, and second whether the intermediate- and end-product constituents are present.

Many of these constituents are identifiable, both qualitatively and quantitatively, using infrared spectral techniques. We have recently completed laboratory and theoretical studies of a number of these constituents, and have identified spectral regions where quantitative information can be obtained against the natural spectral background of the stratosphere (Goldman et al., 1974). We have applied these results to selected balloon flight data and have derived a value for the mixing ratio of CF_2Cl_2 , a probable value for $CFCl_3$ and an upper limit for HF.

Identification of Fluorocarbons

Both CF₂Cl₂ and CFCl₃ exhibit strong absorption features in the 800-950 cm⁻¹ spectral region (see Figure 3). CF₂Cl₂ has two sharp spectral features at 921.9 ± 0.2 cm⁻¹ and 923.2 ± 0.2 cm⁻¹ in addition to the broad-band absorption, while CFCl3 has only a broad band centered at 847 cm⁻¹ (at the instrumental resolution of 0.4 cm⁻¹). The CF₂Cl₂ band at 922 cm⁻¹ and the CFC13 band at 847 cm⁻¹ occur in stratospheric "windows" between minor absorptions by HNO3 and weak CO2 bands. Absolute gas amounts can be obtained from broad-band features, but positive identification of weak absorbers is best obtained by identifying two or more spectral features, usually sharp lines or line groups.

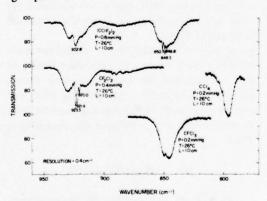


Figure 3. Laboratory absorption spectra of selected halogenated hydrocarbons in the 780-950 cm⁻¹ region.

We have re-examined selected balloon flight measurements of spectral absorptions in the 800-950 cm⁻¹ region. On one such flight (August

12, 1968, over Holloman AFB, New Mexico) this region was observed during sunset, thus enhancing the optical path for minor absorbers. These observations have been reported earlier (Murcray et al., 1969a); they consist of several consecutive spectra as developed during sunset. The final spectral scan, at a zenith angle of 93.5°, shows spectral features which we are attributing to CF2Cl2 and possible CFCl3 (Figure 4). Justification of these identifications is contained in the following paragraph. Since this identification derives from a single spectral scan it requires additional confirmation; however, the current need for stratospheric measurements of the flurocarbons has caused us to publish these data on a "most probable" basis.

The primary identification of CF₂Cl₂ in the spectrum of Figure 4 is based on coincidence of the position of a previously unidentified line (marked with an arrow) at a measured position of 923.2 ± 0.15 cm⁻¹ and the 923.2 cm⁻¹ feature of the laboratory spectrum of CF₂Cl₂. This position is measured from the adjacent P-branch lines of the 10.4- μ m (ν_3 - ν_1) CO₂ band. The absorption at 923.2 cm⁻¹ is too strong to be due to the P42 line of this CO₂ band at 923.0 cm⁻¹, although this line must be considered for the quantitative analysis of CF2Cl2. There are two weak atmospheric H2O lines at 922.2 cm-1 and 925.1 cm⁻¹, but comparisons with neighboring H₂O lines of similar magnitude show that these do not have measurable absorptions in the spectrum of Figure 4, so we do not attribute the unidentified line to either of the water lines. There is a second blended absorption feature which we measured at 921.6 cm⁻¹, and attribute to the 921.9 cm⁻¹ feature measured in the laboratory for CF₂Cl₂. In addition, the ≈2% broad-band absorption at about 930 cm-1 is consistent with the nature of the CF2Cl2 laboratory data, and examination of the original voltage traces of the balloon data shows that the broad-band feature was present in the data, and was not introduced in the reduction process.

Once convinced of the CF₂Cl₂ absorptions at 923 and 930 cm⁻¹, we further examined the spectra at 847 cm⁻¹ for CFCl₃. We were careful to use the balloon spectrum as it was originally reduced, so that no prejudice towards measuring fluorocarbons could have been introduced. Since the depression around 847 cm⁻¹ cannot be

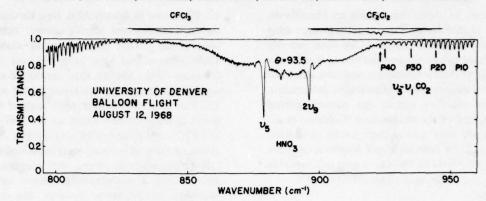


Figure 4. Solar spectrum observed at a height of 30.5 km and a zenith angle of 93.5°. The height of the tangent path is 18.4 km and the optical path is 6.0 air masses. The approximate height of the trop pause is 14 km. The volume mixing ratio for CF_2Cl_2 is 5×10^{-11} v/v, and that for $CFCl_3$ is 2×10^{-11} v/v.

attributed to the wings of the HNO₃ bands, we have considered it due to CFCl₃.

Mixing Ratios of Fluorocarbons

Absorption coefficients for CF₂Cl₂ at 923.3 and 930 cm⁻¹ and for CFCl₃ at 847 cm⁻¹ were measured from laboratory spectra similar to those shown in Figure 3. A few spectra were measured in the 5% absorption range to ensure that the absorption coefficients were derived from spectral absorptions closely matching that of the balloon data.

Measurements of atmospheric absorption were then made at the same three frequencies from the balloon flight spectrum in Figure 4. The absorption at 923.2 cm-1 was linearly corrected for the $(\nu_3-\nu_1)$ CO₂ P42 line and the wing of the HNO₃ band. The absorption coefficients were adjusted to an appropriate atmospheric temperature and used in conjunction with the atmospheric absorption measurements to calculate volume mixing ratios for CF₂Cl₂ and CFCl₃. The values thus derived are 5×10^{-11} v/v (at 930 cm⁻¹) and 6×10^{-11} v/v (at 923.2 cm⁻¹) for CF₂Cl₂ and 2 × 10⁻¹¹ v/v (at 847 cm⁻¹) for CFCl3. These values are derived for an optical path tangent at 18.4 km and measured from 30.5 km. The altitude of the tropopause was approximately 14 km.

It is difficult to assess the accuracy of this measurement due to the small absorptions involved. The largest error is probably directly associated with the measurement of absorption from the balloon flight data, and for now we place ±50% as an estimated error.

It is useful to compare these results with Crutzen's model for the end of 1968 (Crutzen, 1974b) and with Cicerone's model for 1972 (Cicerone et al., 1974). Crutzen's values are 5.6 \times 10⁻¹¹ v/v for CF₂Cl₂ and 1.8 \times 10⁻¹¹ v/v for CFCl₃ at an altitude of 21 km. The Cicerone model for 1972 predicts \approx 9 \times 10⁻¹¹ v/v for CF_xCl_y at 21 km, which results in an adjusted estimate of \approx 6 \times 10⁻¹¹ v/v for 1968. Most of the optical path for the balloon measurement occurs near the minimum altitude traversed; thus, the measured mixing ratio nearly represents a layer a few kilometers thick just above that minimum altitude (18.4 km).

It is gratifying that all the mixing ratios are consistent with theory, but the main results of the measurement are that there were fluoro-carbons present in the stratosphere in 1968, and that an additional measurement is required both to confirm this and to measure the change since 1968.

HF - AN UPPER LIMIT

In addition to measuring the fluorocarbons, we have attempted to place an upper limit on the amount of HF (a possible end product of the fluorocarbon photochemistry) present in the stratosphere by comparing the detection limit of a previous balloon flight with calculated atmospheric spectra containing trace amounts of HF (Goldman et al., 1974). Two lines of HF can be

measured at 4001.2 cm⁻¹ and 4039.1 cm⁻¹ with minimal atmospheric interference. On a balloon flight from Chico, California on September 30, 1965 (Murcray et al., 1966) we scanned this spectral region but did not take data into the sunset. No absorption (<1%) was measured at either frequency at altitudes of observation from 7 to 30 km. From these data we have set an upper limit for the mixing ratio of $3 \times 10^{-10} \text{ v/v}$ throughout the lower stratosphere to slightly above 30 km. It is uncertain at this time what level of HF concentration is expected in the stratosphere. Sunset observations of HF would, however, provide at least a tenfold improvement in the minimum detection limit.

ACKNOWLEDGMENTS

Acknowledgment is made to the National Center for Atmospheric Research, which is sponsored by the National Science Foundation, for computer time used in this research.

We wish to thank P. Crutzen for providing fluorocarbon height profiles for our comparison. This research was supported in part by the National Science Foundation, NASA Ames Research Center, Air Force Cambridge Research Laboratories, and the Department of Transportation.

REFERENCES

- Brooks, J.N., A. Goldman, J.J. Kosters, D.G. Murcray, F.H. Murcray, and W.J. Williams (1973), "Balloon-borne infrared measurements," in *Physics and Chemistry of the Upper Atmosphere*, ed. B.M. McCormac, D. Reidel Pub., Dordrecht, 278-285.
- Cicerone, R.J., R.S. Stolarski, and S. Walters (1974), "Stratospheric ozone destruction by man-made chlorofluoromethanes," Science 185, 1165-1167.
- Crutzen, P. (1974a), "Estimates of possible future ozone reductions from continued use of fluoro-chloro-methanes (CF₂Cl₂, CFCl₃)," Geophys. Res. Lett. 1, 205-208.
- Crutzen, P. (1974b), NCAR, private communication.
- Fontanella, J.C., A. Girard, L. Gramont, and N. Louisnard (1975), "Vertical distribution of NO, NO₂ and HNO₃ as derived from stratospheric absorption infrared spectra," Appl. Opt. 14, 825-839.
- Goldman, A., T.G. Kyle, and F.S. Bonomo (1971), "Statistical band model parameters and integrated

- intensities for the 5.9μ , 7.5μ and 11.3μ bands of HNO₃ vapor," Appl. Opt. 10, 65-73.
- Goldman, A., W.J. Williams, and D.G. Murcray (1974),
 "Measurement of Trace Constituents from Atmospheric Infrared Emission and Absorption Spectra

 a Feasibility Study," Final Report prepared under Contract NAS2-8200 for NASA Ames Research Center by the Department of Physics and Astronomy, University of Denver.
- Harries, J.E., J.R. Birch, J.W. Fleming, N.W.B. Stone, D.G. Moss, N.R.W. Swann, and G.F. Neill (1974), "Studies of stratospheric H₂O, HNO₃, N₂O and NO₂ from aircraft," Proceedings of the Third Conference on the Climatic Impact Assessment Program (Cambridge, Mass.), Department of Transportation, DOT-TSC-OST-74-15, 197-212.
- Lazrus, A.L. and B. Gandrud (1974), "Distribution of stratospheric nitric acid vapor," J. Atmos. Sci. 31, 1102-1108.
- Molina, M.J. and F.S. Rowland (1974), "Stratospheric sink for chlorofluoromethanes: Chlorine atom-catalysed destruction of ozone," Nature 249, 810-812.
- Murcray, D.G., F.H. Murcray, and W.J. Williams (1966), "High Altitude Atmospheric Transmittance as Observed over Northern California," AFCRL-66-410, Scientific Report No. 3, Department of Physics, University of Denver.
- Murcray, D.G., T.G. Kyle, F.H. Murcray, and W.J. Williams (1968), "Nitric acid and nitric oxide in the lower stratosphere," Nature 218, 78-79.
- Murcray, D.G., F.H. Murcray, W.J. Williams, T.G. Kyle, and A. Goldman (1969a), "Variation of the infrared solar spectrum between 700 cm⁻¹ and 2240 cm⁻¹ with altitude," Appl. Opt. 8, 2519-2536.
- Murcray, D.G., T.G. Kyle, F.H. Murcray, and W.J. Williams (1969b), "Presence of HNO₃ in the upper atmosphere," J. Opt. Soc. Am. 59, 1131-1134.
- Murcray, D.G., A. Goldman, A. Csoeke-Poeckh, F.H. Murcray, W.J. Williams, and R.N. Stocker (1973), "Nitric acid distribution in the stratosphere," J. Geophys. Res. 78, 7033-7038.
- Rao-Vupputuri, R.K. (1975), "Seasonal and latitudinal variations of N₂O and NO_x in the stratosphere," J. Geophys. Res. 80, 1125-1132.
- Williams, W.J., J.N. Brooks, D.G. Murcray, and F.H. Murcray (1972), "Distribution of nitric acid vapor in the stratosphere as determined from infrared atmospheric emission data," J. Atmos. Sci. 29, 1375-1379.

SIMULTANEOUS MEASUREMENTS OF NO AND NO₂ IN THE STRATOSPHERE, AND THE PARTITIONING OF ODD-NITROGEN SPECIES

MARCEL ACKERMAN

Institut d'Aéronomie Spatiale de Belgique Brussels, Belgium

ABSTRACT: The recording of infrared solar spectra at sunset from a balloon gondola at 38 km altitude has led to the determination of the vertical distributions of stratospheric NO and NO_2 . The measured NO_2 -to-NO ratio indicates the limited validity of sunset observations of these two species. This determination of NO_x levels, in conjunction with other data available on HNO₃, allows a better definition of the partitioning of the odd-nitrogen species in the low stratosphere.

Research on the stratosphere has remained rather academic until recently. In 1971, it was assumed (Johnston, 1971) that the projected increase in oxides of nitrogen from aircraft flying in the stratosphere could reduce the ozone shield by about a factor of 2, thus permitting the harsh radiation below 300 nanometers to permeate the lower atmosphere, and consequently endangering life at the earth's surface. The interest of aeronautical industries and of governmental agencies in the problem has changed the level of activity in stratospheric research. The emphasis of this research has become measuring and modeling the natural stratosphere for the prediction of possible modifications.

Ozone is formed from atomic oxygen resulting from the dissociation of molecular oxygen by solar ultraviolet radiation,

$$O_2 + h\nu \to O + O \tag{1}$$

$$O + O_2 + M \rightarrow O_3 + M$$
 (2)

An ozone reduction would result from increased scavenging of odd-oxygen atoms in a catalytic set of reactions involving increased nitric oxide and nitrogen dioxide, as follows:

$$NO_2 + O \rightarrow NO + O_2 \tag{3}$$

$$NO + O_3 \rightarrow NO_2 + O_2$$
 (4)

It is currently accepted that nitric oxide is formed in the stratosphere by reaction of nitrous oxide which originates from biological activity at ground level. Since odd-nitrogen molecules apparently do not build up continuously, a removal mechanism by nitric acid rain-out has been suggested.

Three years of experimental work have only transformed our ignorance of the real natural abundance of NO, NO₂, and HNO₃ in the stratosphere into a preliminary knowledge. It is time, however, to assess the available results and to compare them with theoretical predictions.

NITR'C CXIDE

Detection of nitric oxide in the stratosphere has been reported by various authors (Toth et al., 1973; Ridley et al., 1973; Girard et al., 1973). Vertical distributions of this constituent have been derived by absorption spectrometry using the sun as a source (Ackerman et al., 1973, 1975) and by chemiluminescence with O₃ (Ridley et al., 1974). After sunset, reaction (4) should transform nitric oxide into nitrogen dioxide. Nitric oxide has been observed (Patel et al., 1974) to reappear after sunrise, due to the photodissociation process

$$NO_2 + h\nu \rightarrow NO + O \tag{5}$$

which regenerates atomic oxygen, making it available for ozone formation by reaction (2). Chemiluminescence has also been used on board high-flying aircraft (Loewenstein et al., 1974) to measure stratospheric NO. This method indicates large variations at 18 and 20 km over a period of several months (Savage et al., 1974).

The concentration of nitric oxide has also been determined in the mesosphere and in the lower thermosphere.

Most of the experimental NO concentration data are illustrated in Figure 1. They indicate higher number densities in the stratosphere than in the mesosphere, suggesting different production regimes, as was postulated on theoretical grounds (Nicolet, 1971). A steep decrease is observed below 30 km, and possibly an increase in the vicinity of the tropopause, below which no observation is available. The abundance of NO is, however, known (Ackerman et al., 1974; Ridley et al., 1974; Savage et al., 1974) to vary with

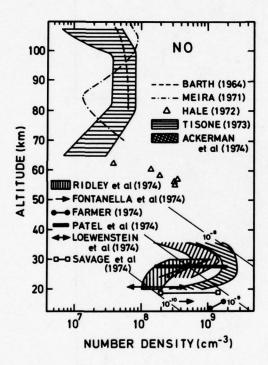


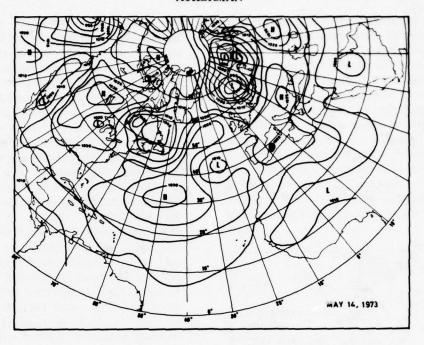
Figure 1. Measured nitric oxide number densities versus altitude in the chemosphere. In the stratosphere, Ackerman et al. (1974) have reported two very different vertical profiles, measured on May 14, 1973 (low) and on May 13, 1974 (high). Patel et al. (1974) have observed the NO variation at sunrise to be more than one order of magnitude. The variation of NO in the vicinity of 20 km altitude over a few days, reported by Savage et al. (1974), is also illustrated. Constant volume mixing ratios are roughly indicated by the straight lines marked 10⁻⁸, 10⁻⁹ and 10⁻¹⁰.

time and location. Loewenstein et al. (1975) have simultaneously measured NO and O_3 at two altitudes over a wide latitude range. In the troposphere over tropical areas (as indicated by low ozone number densities) they observed an NO bulge with values as high as 1.8×10^9 cm⁻³ at 18.3 km. At 21.3 km, it can be seen from their O_3 abundances that the data were gathered in the stratosphere at all latitudes (5° to 75° north), and NO values were generally larger there except over tropical areas where the bulge was reduced.

The nitric oxide observations at 19 km made by Savage et al. (1974) from November 1973 to June 1974, from 75° to 120° west and from 33° to 49° north, indicate a sudden NO increase of a factor of 7, leading to a high value of 1.4×10^9 cm⁻³ persisting until the end of May. This should probably be attributed to transport by motion of air masses, since the difference is too large to be accounted for by ozone fluctuations' changing the NO₂/NO ratio by reactions (4) and (5). It is thus not astonishing that two vertical distributions observed (Ackerman et al., 1974) by means of the same instrumentation under the same experimental conditions, but separated by almost exactly one year, exhibit a difference of a factor of 2 to 10 at 24 km, as shown by Figure 1. The meteorological situations shown in Figure 2 were very different at the two dates at the observation sites (44° north; -1° to 3° west). These situations were rather typical for the period preceding the experiments; namely, low pressures reached lower latitudes in May 1974 than in May 1973. It might also be interesting to notice that soundings made over Arosa showed a very different behavior of the ozone layer below the peak during the first experiment (May 14, 1973) and the second experiment (May 13, 1974), as shown in Figure 3. A well-marked tropospheric airinjection process into the stratosphere was taking place from 10 to 18 km in the second case; a well-marked variability also existed from 22 to 28 km, as illustrated in Figure 3b.

There are, however, too few measurements of nitric oxide at present for us to attempt quantitative evaluations of the observed variations. However, these variations are real, and their interpretations obviously require the simultaneous observation of several parameters, including minor constituents and dynamic processes, on a synoptic basis of reasonable extent.

ACKERMAN



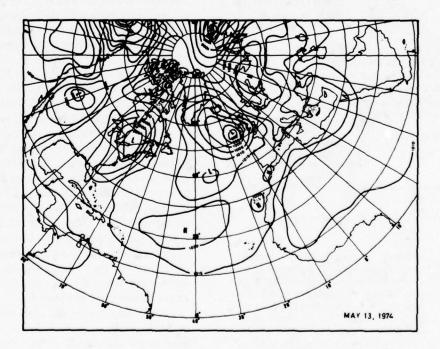


Figure 2. Surface-pressure maps at the dates of the NO measurements reported by Ackerman et al. (1974). Low pressures were extending more towards lower latitudes on May 14, 1974 (Figure 2a) than in the case of May 13, 1973 (Figure 2b). These situations were rather characteristic of the two periods.

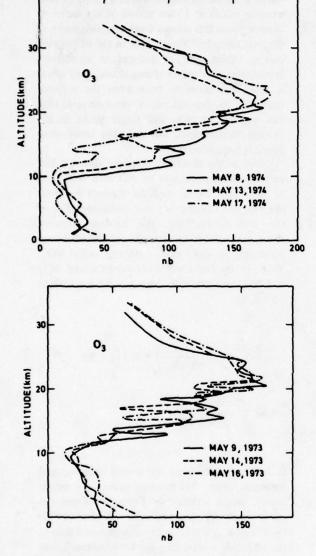


Figure 3. Ozone partial pressure versus altitude over Switzerland at the two periods of NO observations by Ackerman et al. (1974). In 1973 (a) ozone appears to vary from day to day at random, while in 1974 (b) a trend is observed in the ozone below 18 km; an organized decrease occurs from May 8 to May 17.

NITROGEN DIOXIDE

The observations of nitrogen dioxide number densities available for the troposphere and for the stratosphere are plotted in Figure 4. Chemical analyses (Moore, 1974; Nash, 1974; Georgii and Jost, 1964) of air samples performed from ground level up to 6 km altitude, as well as remote spectrometry (Brewer et al., 1973), have been used in the troposphere to determine NO2. The experimental values are spread over almost two orders of magnitude. Measurements of supposedly unpolluted ground-level air indicate values that differ by more than a factor of 100. Georgii and Jost (1964) conclude from their measurements made on board aircraft that tropospheric NO₂ originates partly from biological activity in soils. The latter source would explain why the values observed in summer are higher than those observed in winter. The enrichment in N¹⁴ observed (Moore, 1974) for tropospheric NO2 could be due to the biological contribution. A significant variability of tropospheric NO2 seems to be firmly established, as well as the influence of human activities. Robinson and Robbins (1971) propose a latitudinal variation (4 ppb over tropical and temperate land areas, 0.5 ppb over polar land areas and oceans).

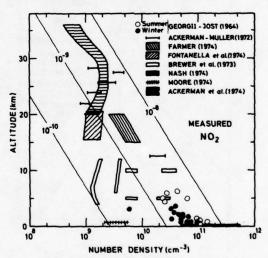


Figure 4. Number densities of nitrogen dioxide versus altitude measured by means of ground-based and aircraft- and balloon-borne instruments. Constant volume mixing ratios are roughly indicated by the straight lines marked 10⁻⁸, 10⁻⁹, and

The abundance of NO₂ in the stratosphere is known from infrared remote spectrometry (Ackerman and Muller, 1972, 1973; Farmer, 1974; Ackerman et al., 1974; Fontanella et al., 1974) performed from balloon gondolas and

from aircraft. As is the case for NO, the few determinations are also at mid-latitudes, limiting the possible comparison with theoretical models at roughly 45° north which could be representative of average conditions.

Several models have yielded NO and NO₂ vertical distributions for average conditions and even for specific latitudes and seasons. Some of the results are illustrated in Figure 5. Models in which various sets of possible vertical distributions are proposed can hardly be compared with experimental results. In one of the cases represented in Figure 5 (Levy, 1973) a tropospheric abundance of NO₂ was assumed in order to deduce other parameters. At 30 km altitude the modeling data are consistent with each other and with experimental results. The situation is different at lower altitudes. It should be pointed out that the various models considered give NO₂

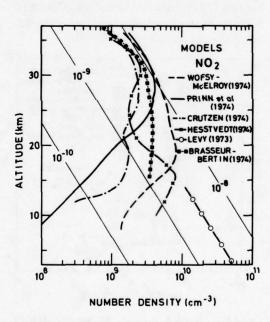


Figure 5. Theoretically evaluated NO₂ number densities versus altitude. Only models yielding unique distributions have been used. Where various latitudes have been considered, only the numbers for 45° latitude are shown. Levy (1973) did not compute NO₂ but introduced a distribution to compute other parameters. Constant volume mixing ratios are represented by straight lines marked 10⁻⁸, 10⁻⁹, and 10⁻¹⁰.

values at 30 km that agree within a factor of two, whereas values at 15 km spread over a factor of twenty. Does this mean a weak coupling between the two altitudes? Particularly in the tropopause region, values used or deduced in models are spread over two orders of magnitude, even where it does not seem to have been the authors' intention to demonstrate a variability. Models can produce double and single peaks in the vertical distributions, but only the latter situation has been observed.

Due to the short characteristic time (≈ 100 sec) for interconversion of NO into NO₂ and of NO₂ into NO in daylight through reactions (4), (5), and (3), the last one being negligible in the low stratopshere, the balance between these two oxides of nitrogen can better be represented by their sum, currently called NO_x. This can be evaluated from experimental NO₂ and NO data available from ground level up to 36 km, by

$$NO_x = NO_2 \left(\frac{1+R}{R}\right) = NO(1+R)$$

where
$$R = \frac{k_4 [O_3]}{J_5 + k_3 [O]}$$

R has been evaluated by several authors, and measured once. The various values are represented versus altitude in Figure 6. From the curve given by Brasseur and Nicolet (1973) (which best agrees with the experimental data at the altitudes where they can be compared), and from the NO2 and NO measurements shown in Figure 1 and in Figure 4, a possible envelope of NO, values has been derived; it is shown in Figure 7. It will be discussed later. The measured values of R are strikingly smaller than those deduced in models. This could be attributed to an underestimate of J₅, which has always been computed without taking Rayleigh scattering into account. As already pointed out (Ackerman, 1974), diffuse radiation can in some cases contribute as much to photodissociation as direct solar radiation, yet only the latter has been considered in models up to now.

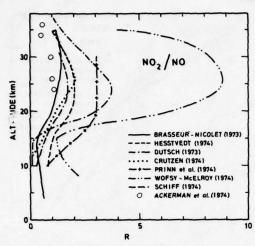


Figure 6. NO₂/NO ratios versus altitude computed in various models. The circles represent measurements taken at low solar elevation that have nonetheless been considered by the authors to represent daytime values.

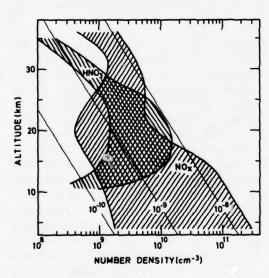


Figure 7. Envelopes including the available data on NO_x (NO + NO₂) and on HNO₃. Constant volume mixing ratios are roughly represented by the straight lines marked 10⁻⁸, 10⁻⁹ and 10⁻¹⁰.

NITRIC ACID

Absorption spectra have led to the detection (Murcray et al., 1969) of HNO₃ in the stratosphere, and to several determinations of its profile. A rather large number of measurements make this odd-nitrogen molecule the most

measured in the stratosphere of the three that are considered here. High-resolution absorption spectroscopy performed from ground level (Vigroux, 1973) has indicated (on the basis of the narrowness of the observed lines) that HNO2 is more in the upper than in the lower layers of the atmosphere. By means of aircraft-borne emission spectroscopy (Harries, 1974), a sharp increase in nitric acid has been observed above the tropopause. The same method used at shorter wavelengths, on board balloon gondolas (Murcray et al., 1974), has yielded vertical distributions of the abundance of nitric acid in the stratosphere at various latitudes. The chemical analysis of in-situ-collected samples (Lazrus and Gandrud, 1974) has also demonstrated the variability of nitric acid with time and latitude, with higher values towards the pole than towards the equator. The concentrations obtained by this method tend to be the lowest, particularly at low altitudes, while absorption spectroscopy from aircraft (Fontanella et al., 1974) has a tendency to give higher concentrations, and so do some interpretations of emission measurements (Fried and Weinman, 1970).

No optical measurement seems to have been reported for HNO₃ in tropospheric air. We have used spectra taken by absorption spectrometry during balloon ascents, and published by Murcray et al. (1969), to evaluate one tropospheric upper limit corresponding to a volume mixing ratio smaller than 10⁻¹⁰. The result is shown in Figure 8 with envelopes representing the data obtained by means of the various methods at various times and locations. All results are included in the broad envelope illustrated in Figure 7.

Examples of theoretically deduced vertical distributions of HNO₃ are shown in Figure 9. Values given for altitudes higher than 15 km represent the experiments rather well, while below 12 km theory appears to overestimate abundances of HNO₃.

DISCUSSION

Nitric acid is known, like any very polar molecule, such as HCl, to have an extremely low activity in dilute aqueous solutions. On the other hand, Warneck (1974) has shown that the time constant for collisions of trace constituents with

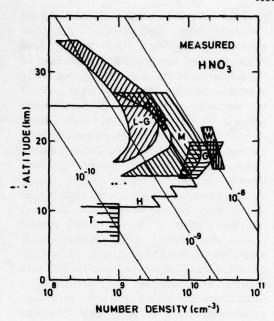


Figure 8. Envelopes representing the measured nitric acid number densities versus altitude. L-G corresponds to the data of Lazrus and Gandrud (1974), M to those of Murcray et al. (1974), G to those of Fontanella et al. (1974), W to those of Fried and Weinman (1970) and H to those of Harries (1974). The values represented by the circles and by the upper limit marked T have been evaluated by the present author on the basis of the atmospheric experiments of Murcray et al. (1969) and of the laboratory data published by Fontanella et al. (1974). Constant volume mixing ratios are roughly illustrated by the straight lines marked 10⁻⁸, 10⁻⁹, and 10⁻¹⁰.

cloud elements is less than five seconds. These considerations would explain a low concentration of HNO₃ in the tropospheric gas phase. They have not been taken into account in models where rain-out times longer than a few days have been introduced to represent the evacuation of odd nitrogen from the stratosphere to the troposphere. They might, however, improve the agreement between theory and experiment in the region of the tropopause and below. This would probably need adjustments to maintain the computed concentrations of NO₂ at the level indicated by the observations, requiring other sources of odd nitrogen in the low stratosphere.

NO_x obviously presents an important variability with time in the stratosphere. Seasonal

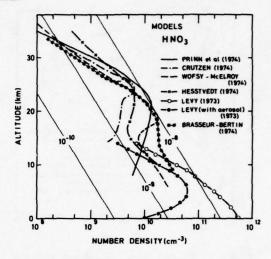


Figure 9. Theoretically evaluated HNO₃ number densities versus altitude. Only models yielding unique distributions have been used. Where various latitudes were considered, only the numbers for 45° are shown.

variations have been considered in models, as well as the possibility (Ruderman and Chamberlain, 1975) of the interpretation of the apparent correlation of ozone variation with the eleven-year cycle of solar activity in terms of the effect of nitrogen-oxides modulation by cosmic rays. Even if doubts have been cast on the significance of such correlations (London and Oltmans, 1973), such investigations are very interesting. There is, however, no conclusive demonstration of the direct role of oxides of nitrogen as an intermediate in these phenomena that would allow firm assessments (Johnston, 1974) to be made of the possible effects of stratospheric aircraft on ozone. Large variations of NO have been observed, as described in a previous section. The NO abundances observed by Ackerman et al. in May 1973 and in May 1974 differ markedly. Total ozone data for the two months are shown in Figure 10. In May 1973, total ozone appears to vary from day to day randomly around mean values which are larger at high latitudes. The latitudinal variation is also present in May 1974, but a pronounced decrease of 10 to 20% appears over one week. The observations indicate the occurrence of a well-organized modification of large geographic extent, from at least 51° north to 39° north, including the area of high NO observations. The

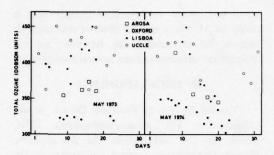


Figure 10. Total ozone versus time measured over various European stations in May 1973 and in May 1974. In this latter case, the beginning of the summer minimum occurs while May 1973 is still in the spring maximum.

decrease in total ozone is suggested to be due to the replacement of ozone-rich air below 20 km by ozone-poor air. This suggestion stems from the vertical profiles observed over Switzerland which were shown in Figure 3. The umkehr observations made over Lisbon show the same trend, which is not unusual near the end of the ozone spring maximum at this station (Figueira, 1973) — namely, during the total-ozone minimum in the month of May 1974, levels 2 and 3 (12 and 16.5 km) exhibit minimum values, while maximum values for the whole month are observed at levels 5, 6, and 7 corresponding respectively to 25, 30, and 35 km.

The ozone reduction below 20 km, which is responsible for the reduction in total ozone, cannot be attributed to NO_x chemistry, since the currently accepted atomic-oxygen content at these altitudes implies a characteristic reaction time longer than a year. It should also be remarked that this ozone decrease in the lower stratosphere occurred concurrently with an increase in the middle stratosphere. All these observations suggest that the variability with time of total ozone, that could be related in this case with NO_x on the basis of chemical interactions in a simple correlation, was actually entirely under the control of transport processes.

Determinations of tropospheric NO_2 indicate a wide range of NO_x values, tentatively illustrated in Figure 7. Low values are usually thought to be characteristic of unpolluted air and are much smaller than those used in models (Levy, 1973; Chameides and Walker, 1974). The

reduction of NO_x in these models would reduce the production of HNO₃ that has been considered by Warneck (1974) as being too high in comparison with the observed global precipitation of nitric acid in rain. On the other hand, high values of NO_x concentrations, suggested by the observations of Georgii and Jost (1964), who have indicated a seasonal variation (summer values higher than winter ones) that could hardly be explained on the basis of human activities, could have consequences for the stratosphere. They could lead to injections of tropospheric NO_x into the stratosphere when its mixing ratio at the stratospheric heights is smaller than that in the troposphere. This could be supported by the isotopic composition of HNO3 observed between 21 and 27 km (Moore, 1974), which shows about the same N14/N15 ratio as for standard N2. If stratospheric HNO3 is all derived from N2O having a marked N15 enrichment, this should also appear in nitric acid as a product of NOx, provided that the reactions

$$N_2O + O(^1D) \rightarrow N_2 + O_2$$
 (6)

and

$$N_2O + O(^1D) \rightarrow NO + NO \tag{7}$$

have no differential isotopic effects. This is a reasonable assumption that should, of course, be checked experimentally to allow a firm interpretation of the stratospheric isotopic measurements.

Considering the replacement time (Danielsen, 1968) of stratospheric air by tropospheric air and the high HNO₃ amounts derived by absorption spectrometry (Fontanella et al., 1974), a downward flux of nitric acid larger than 5×10^8 cm⁻² sec⁻¹ should be accepted. Such a flux would imply another source of odd stratospheric nitrogen besides reaction (7), whose odd-nitrogen production has been estimated as $(0.29\text{-}1.5) \times 10^8$, $(0.25\text{-}0.65) \times 10^8$, $(0.5\text{-}1.3) \times 10^8$, and $(0.8\text{-}1.0) \times 10^8$ cm⁻² sec⁻¹ by Crutzen (1974), Wofsy and McElroy (1974), Brasseur and Nicolet (1973), and Isaksen (1973), respectively.

On the other hand, the low HNO₃ values of Figure 7 would imply, given the same interchange time between tropospheric and stratospheric air, a flux equal to $.8 \times 10^8$ cm⁻² sec⁻¹. The average value, $(2.9 \pm 2.1) \times 10^8$ cm⁻² sec⁻¹,

shows clearly that the actual uncertainty in the HNO $_3$ n₁easurements is unsatisfactory. If it were admitted that HNO $_3$ abundances derived from in-situ sampling were systematically too low, and if, on the basis of such an argument, they were rejected, an average flux value of $(3 \pm 2) \times 10^8$ cm⁻² sec⁻¹ would be derived, which would exclude several of the theoretical values. An additional source of stratospheric odd nitrogen would have to be introduced, particularly if the absolute quantum yield for the formation of O(¹D) in O $_3$ photolysis, the value of which has always been assumed (Welge, 1974), is in fact smaller than currently accepted.

CONCLUSION

Measurements of the chemically related oddnitrogen molecules in the atmosphere appear to be particularly good tests for models designed to predict the possible modifications of the stratosphere under natural and artificial constraints. Measurements are at present too sparse to provide a thorough check. However, they indicate possibilities of improving the evaluation of vertical distributions and temporal variations of NO_x and HNO_3 that are required for the lower stratosphere and for the troposphere. In particular, diffuse as well as direct solar radiation should be taken into account when certain photodissociation rates are evaluated in models.

Fundamental matters, such as the sources and fate of odd nitrogen above the average tropopause height as well as in the troposphere, seem to require further high-priority investigations. Quasi-horizontal transport should be considered in more detail, since it can lead to injection of tropospheric NO_x-rich air from the tropics into the middle-latitude stratosphere over periods of time that are short (Piaget, 1971) compared with the conversion time of NO, into HNO3. This could be a partial cause of the short time and small scale of observed NO, variations, and could represent an additional natural source of stratospheric odd nitrogen. Certain experimental methods have contributed most of the available information. Their use should be intensified. But the use of other methods has perhaps not been emphasized enough up to now.

As far as the prediction of a possible reduction of ozone by a factor of two is

concerned, some models now predict that it could be 1% for a similar fleet of stratospheric aircraft. Present models can, however, scarcely describe the variations of the natural stratosphere.

ACKNOWLEDGMENTS

Thanks are due to Professor Dütsch, at the Laboratorium für Atmosphärenphysik ETH, Zürich; to Dr. Walshaw, at the Atmospheric Physics Department, Oxford University; to Dr. Figueira from Servicio Meteorological Lisbõa; and to Dr. Maenhout and Mr. Lebrun at the Royal Meteorological Institute of Belgium for having kindly provided ozone data.

REFERENCES

- Ackerman, M. and C. Muller (1972), "Stratospheric nitrogen dioxide from infrared absorption spectra," Nature 240, 300-301.
- Ackerman, M. and C. Muller (1973), "Stratospheric methane and nitrogen dioxide from infrared spectra," Pure Appl. Geophys. 106-108, 1325-1335.
- Ackerman, M., D. Frimout, C. Muller, D. Nevejans, J.-C. Fontanella, A. Girard and N. Louisnard (1973), "Stratospheric nitric oxide from infrared spectra," Nature 245, 205-206.
- Ackerman, M. (1974), "Solar ultraviolet flux below 50 kilometers," Can. J. Chem. 52, 1505-1509.
- Ackerman, M., J.-C. Fontanella, D. Frimout, A. Girard, N. Louisnard and C. Muller (1975), "Simultaneous measurements of NO and NO₂ in the stratosphere," Planet. Space Sci. 23, 651-660.
- Barth, C.A. (1964), "Rocket measurement of the nitric oxide dayglow," J. Geophys. Res. 69, 3301-3303.
- Brasseur, G. and M. Bertin (1974), "Un modèle bidimensionnel de la stratosphère," in Proceedings of the Anglo-French Symposium on the Effects of Stratospheric Aircraft (Oxford), pub. British Meteorological Office, XXIV-1.
- Brasseur, G. and M. Nicolet (1973), "Chemospheric processes of nitric oxide in the mesosphere and stratosphere," Planet. Space Sci. 21, 939-961.
- Brewer, A.W., C.T. McElroy, and J.B. Kerr (1973), "Nitrogen dioxide concentrations in the atmosphere," Nature 246, 129-133.
- Chameides, W. and J.C.G. Walker (1973), "A photochemical theory of tropospheric ozone," J. Geophys. Res. 78, 8751-8760.

ACKERMAN

- Crutzen, P. (1974), "A review of upper atmospheric photochemistry," Can. J. Chem. 52, 1569-1581.
- Danielsen, E.F. (1968), "Stratospheric-tropospheric exchange based on radioactivity, ozone and potential vorticity," J. Atm. Sci. 25, 502-518.
- Dütsch, H.U. (1973), "Recent developments in photochemistry of atmospheric ozone," Pure Appl. Geophys. 106-108, 1361-1384.
- Farmer, C.B. (1974), "Infrared measurements of stratospheric composition," Can. J. Chem. 52, 1544-1559.
- Figueira, M.F. (1973), "Atmospheric ozone and flow field variations over Lisbon," Pure Appl. Geophys. 106-108, 1586-1599.
- Fontanella, J.-C., A. Girard, L. Gramont and N. Louisnard (1974), "Vertical distribution of NO, NO₂ and HNO₃ as derived from stratospheric absorption infrared spectra," in *Proceedings of the Third Conference on CIAP* (Cambridge, Mass.), U.S. Department of Transportation, DOT-TSC-OST-74-15, 217-233; and Appl. Opt. 14, 825 (1975).
- Fried, P.M. and J.A. Weinman (1970), "Vertical distribution of HNO₃ vapor in the stratosphere," Bull. Amer. Meteorol. Soc. 51, 1006.
- Georgii, J.-W. and D. Jost (1964), "Untersuchung über die Verteilung von Spurengasen in der freien Atmosphäre," Pure Appl. Geophys. 59, 217-224.
- Girard, A., J.-C. Fontanella and L. Gramont (1973), "Détection de l'oxyde azotique dans la stratosphere," C.R. Acad. Sci. Paris 276, 845.
- Hale, L.C. (1972), as discussed in M.B. McElroy (1972), "Conference Summary," in Proceedings of the Survey Conference, Climatic Impact Assessment Program, Dept. of Transportation, DOT-TSC-OST-72-13, on pp. 262 and 266.
- Harries, J.E., D.G. Moss and N.R. Swann (1974), "H₂O, O₃, N₂O and HNO₃ in the arctic stratosphere," Nature 250, 475-476.
- Hesstvedt, E. (1974), "Reduction of stratospheric ozone from high-flying aircraft, studied in a twodimensional photochemical model with transport," Can. J. Chem. 52, 1592-1598.
- Johnston, H. (1971), "Reduction of stratospheric ozone by nitrogen oxide catalysts from supersonic transport exhaust," Science 173, 517-522.
- Johnston, H.S. (1974), "Photochemistry in the stratosphere with applications to supersonic transports," Acta Astronaut. 1, 135-156.

- Lazrus, A.L. and B.W. Gandrud (1974), "Distribution of stratospheric nitric acid vapor," J. Atm. Sci. 31, 1102-1108.
- Levy, H. II (1973), "Photochemistry of minor constituents in the troposphere," Planet. Space Sci. 21, 575-591.
- London, J. and S. Oltmans (1973), "Further studies of ozone and sunspots," Pure Appl. Geophys. 106-108, 1302-1307.
- Loewenstein, M. and H.F. Savage (1975), "Latitudinal measurements of NO and O₃ in the lower stratosphere from 5.5° to 82° North," in this volume.
- Loewenstein, M., J.P. Paddock, I.G. Poppoff and H.F. Savage (1974), "NO and O₃ measurements in the lower stratosphere from a U-2 aircraft," Nature 249, 817-818.
- Loewenstein, M., H.F. Savage, and R.C. Whitten (1975), "Seasonal variations of NO and O₃ at altitudes of 18.3 and 21.3 km," in this volume.
- Meira, L.G., Jr. (1971), "Rocket measurements of upper atmospheric nitric oxide and their consequences to the lower ionosphere," J. Geophys. Res. 76, 202-212.
- Moore, H. (1974), "Isotopic measurement of atmospheric nitrogen compounds," Tellus 26, 169-174.
- Murcray, D.G., T.G. Kyle, F.H. Murcray and W.J. Williams (1968), "Nitric acid and nitric oxide in the lower stratosphere," Nature 218, 78-79.
- Murcray, D.G., F.H. Murcray, W.J. Williams, T.G. Kyle and A. Goldman (1969), "Variation of the infrared solar spectrum between 700 cm⁻¹ and 2240 cm⁻¹ with altitude," Appl. Opt. 6, 2519-2536.
- Murcray, D.G., A. Goldman, W.J. Williams, F.H. Murcray, J.N. Brooks, R.N. Stocker and D.E. Snider (1974), "Stratospheric mixing ratio profiles of several trace gases as determined from balloon-borne infrared spectrometers," in Proceedings of the International Conference on Structure, Composition and General Circulation of the Upper and Lower Atmospheres and Possible Anthropogenic Perturbations (Melbourne), pub. IAMAP, 292-306.
- Nash, T. (1974), "Nitrous acid in the atmosphere and laboratory experiments on its photolysis," Tellus 26, 175-179.
- Nicolet, M. (1971), "Aeronomic reactions of hydrogen and ozone," in Mesospheric Models and Related Experiments, ed. G. Fiocco, Reidel Pub., Dordrecht, 1-15.

ACKERMAN

- Patel, C.K.N., E.G. Burkhardt and C.A. Lambert (1974), "Spectroscopic measurements of stratospheric nitric oxide and water vapor," Science 184, 1173-1176.
- Piaget, A. (1971), "Utilisation de l'ozone atmosphérique comme traceur des échanges entre la troposphère et la stratosphère," Veröffentlichungen der Schweizerischen Meteorologischen Zentralanstalt, Zürich, 21, 1-71
- Prinn, R.G., F.N. Alyea, D.M. Cunnold and A. Katz (1974), "The distribution of odd nitrogen and odd hydrogen in the natural and perturbed stratosphere," in Preprints of the Second International Conference on the Environmental Impact of Aerospace Operations, in the High Atmosphere (San Diego), pub. AMS 180-186.
- Ridley, B.A., H.I. Schiff, A.W. Shaw, L. Bates, L.C. Howlett, H. Levaux, L.R. Megill and T.E. Ashenfelter (1973), "Measurements in-situ of nitric oxide in the stratosphere between 17.4 and 22.9 km," Nature 245, 310-311.
- Ridley, B.A., H.I. Scaiff, A. Shaw and L.R. Megill (1974), "In-situ measurements of NO in the stratosphere using chemiluminescence," in Proceedings of the Third Conference on CIAP (Cambridge, Mass.), Department of Transportation, DOT-TSC-OST-74-15, 193-196.
- Robinson, E. and R.C. Robbins (1971), "Sources, Abundance, and Fate of Gaseous Atmospheric Pollutants," Amer. Petrol. Inst., Washington D.C., 77 pp.

- Ruderman, M.A. and J.W. Chamberlain (1975), "Origin of the sunspot modulation of ozone: Its implications for stratospheric NO injection," Planet. Space Sci. 23, 247.
- Savage, H.E., M. Loewenstein and R.C. Whitten (1974), "In-situ measurements of NO and O₃ in the lower stratosphere," in Preprints of the Second International Conference on the Environmental Impact of Aerospace Operations in the High Atmosphere (San Diego), pub. AMS, 5-10.
- Schiff, H.I. (1974), "Measurements of NO, NO₂ and HNO₃ in the stratosphere," Can. J. Chem. 52, 1536-1543.
- Tisone, G.C. (1973), "Measurements of NO densities during sunrise at Kauai," J. Geophys. Res. 78, 746-750.
- Toth, R.A., C.B. Farmer, R.A. Schindler, O.F. Raper and P.W. Schaper (1973), "Detection of nitric oxide in the lower stratosphere," Nature Phys. Sci. 244, 7-8.
- Vigroux, E. (1973), "High resolution analysis of the sun's radiation received at the ground from 9μ to 11.6μ," Pure Appl. Geophys. 106-108, 1336-1340.
- Warneck, P. (1974), "On the role of OH and HO₂ radicals in the troposphere," Tellus 26, 39-46.
- Welge, K.H. (1974), "Photolysis of O_x, HO_x, CO_x and SO_x compounds," Can. J. Chem. 52, 1424-1435.
- Wofsy. S.C. and M.B. McElroy (1974), "HO_x, NO_x and ClO_x: Their role in atmospheric photochemistry," Can. J. Chem. **52**, 1582-1591.

SPECTROSCOPIC DETECTION AND VERTICAL DISTRIBUTION OF HCI IN THE STRATOSPHERE

CROFTON B. FARMER, ODELL F. RAPER, AND ROBERT H. NORTON

Jet Propulsion Laboratory California Institute of Technology Pasadena, California

ABSTRACT: HCl has been observed in the stratosphere by airborne spectroscopic measurements of the 1-0 band at 3 μ m wavelength. The results, which are specific to the HCl molecule in the gas phase, show a rapid increase with altitude in the lower stratosphere. The stratospheric layer, which commences at about 15 km, reaches its maximum concentration at an altitude above 21 km (the limiting height of the observations to date). The local value for the volume mixing ratio at 21 km is $7 \pm 1 \times 10^{-10}$. However, the zenith column abundance observed above 21 km (6.3 \times 10¹⁴ molecules cm⁻²) implies that the mixing ratios at greater altitudes are unlikely to reach values much in excess of the local value at 21 km.

INTRODUCTION

We have detected HCl in the stratosphere through spectroscopic observations of the 1-0 fundamental band in the 2700 to 3000 cm-1 region of the telluric solar spectrum. The spectra covering this region were obtained during the course of the CIAP studies from an Air Force NC-135 (at 11 to 12 km), from both the British and French Concorde SST prototypes (at 15.5 km), and, more recently, from the NASA U2 (at 21 km) in connection with stratospheric background studies performed for the NASA Office of Aeronautics and Space Technology. The reduction of the spectra has required a complete reanalysis of the telluric solar spectrum over the 3- to 4-um wavelength range in order to confirm that the suspected HCl features were not in fact weak, previously unassigned, transitions due to the known infrared-active constituents of the atmosphere, and to permit the quantitative treatment of those HCl features which are spectrally blended with lines of these other gases. The combined results of the observations made to date have provided spectra from which the detailed profile in the stratosphere up to 21 km has been derived, together with the column abundance above this altitude. The present paper summarizes the results of the stratospheric observations and presents the initial determination of the vertical distribution of HCl.

OBSERVATIONS AND SPECTRAL ANALYSIS

The observations reported here were made with a high-speed stepped Michelson interferometer having unapodized spectral resolution of 0.13 cm⁻¹; for the present measurements, the spectral range covered was from 1750 to 3050 cm⁻¹. The instrumentation for the U2 observations was essentially the same as that described for the earlier NC135 and Concorde flights (Farmer et al., 1973). For the more recent observations, however, the spectral signal-tonoise ratio was significantly improved by internal modulation of the infrared radiation, which reduced the effects of turbulence, and also by improvements to the solar tracking system. The noise in the spectra obtained from the U2 measurements was typically 2 × 10-3 of the signal at 100% transmission.

The 1-0 band of HCl consists of regularly spaced pairs of lines covering the frequency range from approximately 2700 to 3000 cm⁻¹ (3 to 3.5 µm region). Each pair of lines corresponds to a transition of the ³⁵Cl and ³⁷ Cl isotopes of HCl. The stronger members of the band thus span a region of the atmospheric spectrum which is characterized by absorptions of several other naturally occurring gases (CH₄, H₂O, N₂O, CO₂ and O₃) but is dominated by CH₄ and the isotopic variants of water vapor. It is clear from examination of the atmospheric spectrum over

this region that several of the HCl lines are completely masked by the strong absorptions of the more abundant atmospheric constituents; of the remaining candidate HCl lines which can be used for detection and measurement, most are blended to some degree with weak absorptions of the other gases. For the stratospheric spectra, R1, R2, R3, P5, and P6 of H35Cl and R1, R2, and R3 of H37Cl are the most useful for analysis. In both tropospheric and stratospheric cases the R1 line of the main isotope is completely free of interference from any known atmospheric species within a distance of several resolution elements, although the pressure-broadened wing of the strong P9 manifold of v3 CH4 overlaps the R1 line for tropospheric conditions.

As stated previously, for the correct identification of HCl and the subsequent quantitative analysis of the spectra it is necessary to ensure that the observed features are not due to weak transitions of the known atmospheric trace gases. To this end, use was made of the AFCRL line listing (McClatchey et al., 1973) together with the results of extensive laboratory measurements (Toth et al., 1975; Brown et al., 1976) which were made to supplement the published data where these were incomplete or incorrect. The laboratory measurements included samples which exceeded the maximum column abundances of the gases in the atmospheric observations, in order that all transitions which might contribute significantly to the observed atmospheric spectra could be included in the analysis. Using the revised spectral-line listing of transition frequencies and intensities obtained in this way, the observed spectra were analyzed by a process of numerical fitting. A synthetic spectrum was generated for the appropriate conditions of the optical-path geometry for each of the observations and compared with the observed spectrum. HCl was then added to the synthetic spectrum until it matched the observed absorptions. The transition strengths used for HCl were taken from the values given by Toth et al. (1970). An example of a set of synthetic spectra generated by this technique, discussed in greater detail below, is shown in Figure 1. Further evidence of the correct identification of the HCl features is the fact that all of the absorptions attributed to HCl in any one observed spectrum are reproduced with the correct relative strengths for the unique HCl abundance determined for that observation.

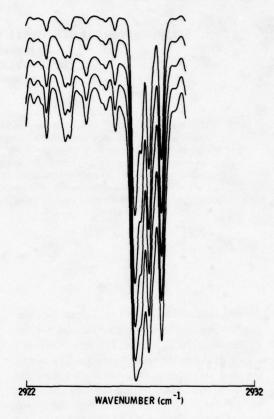


Figure 1. Synthetic stratospheric spectra computed for the region of the HCl R1 lines. The zero and 100% transmission levels for the individual spectra have been offset for clarity. The observational conditions are chosen to match the geometry of the measured spectra shown in Figure 2 with the derived HCl profile of Figure 3 (see text).

RESULTS

Measurements of stratospheric halogens of low molecular weight have been made by Lazrus et al. (1975), using an in-situ sampling technique. Apart from these, no other experimental data are available which contain information pertaining to the stratospheric abundance of HCl. From the combined results of the NC135, Concorde, and U2 flights, the presence of HCl in the stratosphere can be firmly established and a preliminary vertical mixing profile determined. Figure 2 is a reproduction of portions of a set of

stratospheric spectra covering the R1 and R2 lines; for purposes of clarity, the spectra have been ordered in increasing air mass. For comparison, the synthetic spectra in Figure 1 were generated for the same observational conditions. The result of the analysis of the stratospheric spectra shows the HCl is present in a layer having its lower bound at an altitude of about 14 km, with the mixing ratio increasing up to the maximum altitude of the observations, the upper bound of the layer being at some higher altitude.

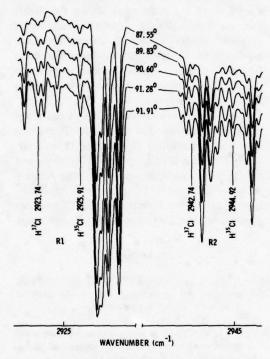


Figure 2. Stratospheric spectra obtained from the U2 observations, at the indicated solar zenith angles, showing the HCl R1 and R2 lines.

The detailed reduction of the spectra yields the profile shown in the upper part of Figure 3. This figure also includes the tropospheric profile determined earlier by the authors (Farmer et al., 1975) based on spectroscopic observations and the in-situ values obtained by Junge (1957). The stratospheric values reported by Lazrus vary from less than 0.04 ppbv at 13.7 km to 0.4 ppbv in the region from 20 to 27 km. Although these results are somewhat lower than those obtained from the spectroscopic observations, it should be pointed out that the two techniques are con-

siderably different from each other; in particular, one samples a single point at a given altitude while the other samples over an extended horizontal region. With this in mind, the two sets of results can be said to be in agreement, but only if HCl is the predominant species in the samples analyzed by Lazrus.

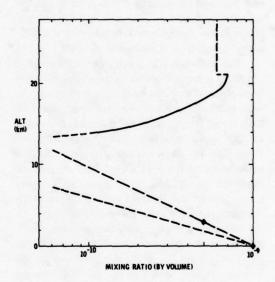


Figure 3. Vertical distribution of HCl in the atmosphere. The lower dashed lines represent the tropospheric variation with height for the two limiting values of the HCl scale height deduced from Junge's in-situ measurements (diamonds) and the total column abundance obtained from the previous tropospheric observations. The detailed profile derived from the stratospheric observations is shown by the solid line extending up to 21 km; the distribution is shown as uniformly mixed at a concentration consistent with the observed column abundance above this altitude. The true profile reaches a maximum at some point above the maximum observation height.

CONCLUSIONS

The relatively small scale height for HCl in the troposphere derived from the earlier results implies that tropospheric HCl is insignificant as a source for HCl in the stratosphere. Thus, apart from the possibility of the direct injection of chlorine into the stratosphere following volcanic eruptions, it might be expected that chlorine species would not be found as natural trace constituents of the stratosphere. Indeed, the

current concern over the potential depletion of the stratospheric ozone layer by the continued release into the atmosphere of large quantities of fluorochloromethanes ("Freons"), a stable molecular form which can act as the carrier to transport halogen atoms to the stratosphere (Molina and Rowland, 1974), implies the assumption that the catalytic destruction of ozone by chlorine from natural sources is not a significant factor in the dynamic equilibrium of the unperturbed ozone layer (Cicerone et al., 1975).

The extent to which volcanic eruptions are a source of gaseous chlorine in the atmosphere has been pursued with renewed vigor in recent years, with particular emphasis on the direct injection into the stratosphere. Most of the computations to date have suggested that the contribution from this source results in stratospheric HCl abundances an order of magnitude less than are measured here (Cadle, 1975), but, in a recent paper Ryan and Mukherjee (1975) estimate amounts comparable to those reported here. As the latter authors point out, however, the principal difference between their result and those published earlier lies in the value derived for the fraction of the total gaseous chlorine released during an eruption which is directly injected into the stratosphere. While the earlier estimates of 3-5% for this value may be too low, Ryan and Mukherjee's value of 55% is almost certainly too high. In any event, as most workers attempting these calculations point out, the limited sources of reliable data which are available render the results valuable only as order-of-magnitude estimates.

With the data presently available, it is not possible to resolve the question of whether the stratospheric source for the HCl observed here is direct injection of gaseous chlorine by volcanoes or the introduction of chlorine-containing compounds which are anthropogenic in origin. In either case, however, the only explanation for a profile of this type is that the HCl observed at 20 km is formed at or above this level, probably from photodissociation of other chlorinecontaining species. The profile reproduced here for the lower side of the stratospheric HCl layer, together with the limiting values obtained earlier for the tropospheric distribution, should be sufficient to test current models in these regions. It is of crucial importance now to extend this profile upwards as far as possible in order to

determine the altitude of the maximum in the HCl distribution and the shape of the profile above this altitude.

ACKNOWLEDGMENTS

We are indebted to R.A. Toth, R.H. Hunt, J.S. Margolis, and L. Brown for their generosity in allowing us to make use of recently obtained spectral data prior to publication, and to B. Robbins for assistance with the data analysis. The development and continuously reliable operation of the instrument during the flights was the result of the determined efforts of H. Geise, R. Wilson, and R. Perrin. We thank especially the NASA Flight Group at the Ames Research Center, without whose enthusiastic support the U2 observations could not have been successfully carried out.

This paper presents the results of one phase of research carried out at the Jet Propulsion Laboratory, California Institute of Technology, under Contract Number NAS 7-100, sponsored by the National Aeronautics and Space Administration, and under Contract DOT-AS-20094, sponsored by the Climatic Impact Assessment Program of the Department of Transportation.

REFERENCES

- Brown, L., R.A. Toth, and R. Hunt (1976), "Line positions and strengths of CH₄ in the 2700 to 3000 cm⁻¹ region," in preparation.
- Cadle, R.D. (1975), "Volcanic emissions of halides and sulfur compounds to the troposphere and stratosphere," J. Geophys. Res. 80, 1650.
- Cicerone, R.J., D.H. Stedman, and R.S. Stolarski (1975), "Estimate of late 1974 stratospheric concentration of gaseous chlorine compounds (CIX)," Geophys. Res. Lett. 2, 219.
- Farmer, C.B., R.A. Toth, R.A. Schindler, and O.F. Raper (1973), "Near-infrared interferometric measurements of stratospheric composition to be made from the Concorde," in *Proceedings of the Second Conference on CIAP* (Cambridge, Mass.), U.S. Dept. of Transportation, DOT-TSC-OST-73-4, 65-77.
- Farmer, C.B., O.F. Raper and R.H. Norton (1976), "Spectroscopic detection and vertical distribution of HCl in the troposphere and stratosphere," Geophys. Res. Lett. 3, 13-16.

- Junge, C.E. (1957), "Chemical analysis of aerosol particles and of gas traces on the island of Hawaii," Tellus 9, 528.
- Lazrus, A., B. Gandrud, R. Woodard and W. Sedlacek (1975), "Stratospheric halogen measurements," Geophys. Res. Lett. 2, 439-441.
- McClatchey, R.A., W.S. Benedict, S.A. Clough, D.E. Burch, R.F. Calfee, K. Fox, L.S. Rothman, and J.S. Garing (1973), "AFCRL Atmospheric Absorption Line Parameters Compilation," Air Force Cambridge Research Labs Report TR-73-0096, Environmental Research Paper 434.
- Molina, M.J. and F.S. Rowland (1974), "Stratospheric sink for chlorofluoromethanes: Chlorine atom catalyzed destruction of ozone," Nature 249, 810.
- Ryan, J.A., N.R. Mukherjee (1975), "Sources of stratospheric gaseous chlorine," Revs. Geophys. Space Phys. 13 (5), 650-658.
- Toth, R.A. and J.S. Margolis (1975), "Spectra of H₂¹⁸O in the 2900 to 3400 cm⁻¹ Region," J. Mol. Spec. 57, 236-245.
- Toth, R.A., R.H. Hunt and E.K. Plyler (1970), "Line strengths, line widths, and dipole moment function for HCl," J. Mol. Spec. 35, 110.

NO₂ MEASUREMENTS BY ABSORPTION SPECTROPHOTOMETER: OBSERVATIONS FROM THE GROUND AND HIGH-ALTITUDE BALLOON, CHURCHILL, MANITOBA, JULY 1974

R.M. BLOXAM, A.W. BREWER, AND C.T. MCELROY

Department of Physics University of Toronto Toronto, Ontario

ABSTRACT: Nitrogen dioxide measurements made by a balloon-borne spectrophotometer operating at an altitude of 35 km have been found to corroborate the conclusions concerning stratospheric NO_2 which we have published in previous reports. The comparison of the balloon observations with those obtained by means of a ground-based instrument at the launch site provides continuing support for the accuracy of the NO_2 data we have published, including the noontime maximum.

Measurements of the concentration of atmospheric nitrogen dioxide and its vertical distribution, by ground-based differential spectrophotometry, have already been reported (Brewer et al., 1973, 1974a-c; Johnston, 1974). The theory of the technique is discussed at some length in these references, and is similar in principle to the "umkehr" method, which has been used for many years to measure the vertical distribution of atmospheric ozone (Dobson, 1957; Mateer and Dütsch, 1964).

The measurements obtained give vertical distributions at sunrise and sunset only, but have indicated the existence of a strong midday maximum of the total stratospheric nitrogen dioxide.

As has been discussed in the Brewer et al. and Johnston references, when the sun is relatively high in the sky the total atmospheric nitrogen dioxide in the optical path is given by the difference between the instrument readings and the value of the instrument absorption function* which would be observed if there were no NO_2 between the observation point and the sun. This is the F_0 of the instrument. The value of F_0 is derived by determining the vertical distribution which, in a single-scattering model, fits the observed morning and evening observations. The

observations of both direct sun and zenith sky are plotted as functions of zenith angle for angle greater than $\approx 80^{\circ}$, and different vertical NO₂ distributions are tried until a satisfactory fit is obtained. The value of the instrument F₀ is also determined by this "fit." The accuracy of the value of F₀ depends on the reliability of the deduced sunrise and sunset distributions of NO₂, and consequently so does the midday amount of NO₂ (Brewer et al., 1974c; Johnston, 1974).

To assess the reliability of previous conclusions, measurements made by a ground-based spectrophotometer and a similar balloon-borne instrument have been compared.

It should be noted that most of the NO_2 is assumed to lie below an observation point at 35 km, and hence the deduced distribution of most of the nitrogen dioxide will be independent of F_0 .

OBSERVATIONAL PROGRAM

The balloon flight was made from Churchill, Manitoba $(59^{\circ} \text{N} \times 94^{\circ} \text{W})$ in July of 1974. Also, during the period July 7 to July 23, a series of observations was made from the ground at Churchill. The average of the sunrise and the sunset curves, observed from the ground, are presented as Figures 1 and 2 respectively. In these diagrams the curved lines have been calculated with a "single scattering" model from the NO_2 distributions given in Figure 4. (Figure 5 gives daytime data.)

 $F = \log_{10}(I_1/I_2) - 1.46 \log_{10}(I_2/I_3)$

For full information see Brewer et al. (1973, 1974a, b).

^{*}The instrument function is computed as follows:

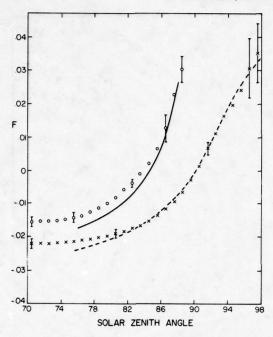


Figure 1. Mean sunrise observations of the variation of our absorption function F. Clear-sky ground observations from Churchill. ○, observed direct sun; X, observed zenith sky; —, calculated direct sun, ---, calculated zenith sky. The "error bars" represent day-to-day changes in the NO₂ profile, except for large zenith angles (≈95°) where Poisson noise dominates.

The "error bars" indicated on Figures 1, 2, and 5 represent the extremes of variations in the observations taken on different days. Except for zenith angles greater than $\approx 95^{\circ}$, differences in the curves due to statistical noise are smaller than the day-to-day fluctuations in the NO₂ distributions.

The actual data received from the balloon spectrophotometer is depicted in Figure 3. It has been corrected for the electronic and photomultiplier dead time, but is otherwise unfiltered. The error bars represent the effects of Poisson noise on the individual intensities measured.

RESULTS

Figure 4 compares the average vertical distribution determined from the balloon data with that deduced by the curve-fitting method from the ground observations.* The total NO₂

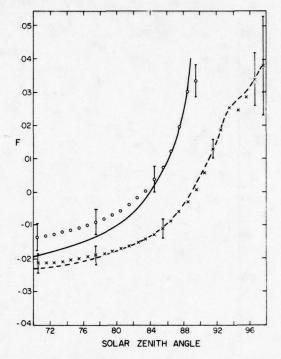


Figure 2. Mean sunset observations at Churchill.

Clear sky. O, observed direct sun; X,
observed zenith sky; —, calculated direct
sun; ----, calculated zenith sky. Calculated
Fo for Figures 1 and 2 equals -.032.

amounts are about 0.5×10^{-3} cm stp. Figure 5 plots the variations of the total NO_2 overhead throughout the day, derived from the ground observations taken at Churchill.

The deduced concentrations above 40 km are very uncertain. These results suggest that for the given place and time the crossover of the morning and evening curves is real — that is to say, above about 40 km the morning NO₂ concentrations are greater. The earlier published measurements of Brewer et al. did not show this, but they were derived from fewer data and referred to Southern Ontario.

The concentrations shown for the balloon measurement are totally independent of the

^{*}The volume mixing-ratio curves presented in certain papers of Brewer et al. (1973, 1974a, b) are in error. The concentration curves, which are correct, were not properly converted to mixing ratio. We apologize for any inconvenience this may have caused, and thank Dr. D.M. Hunten for bringing this error to our attention.

BLOXAM, BREWER, AND McELROY

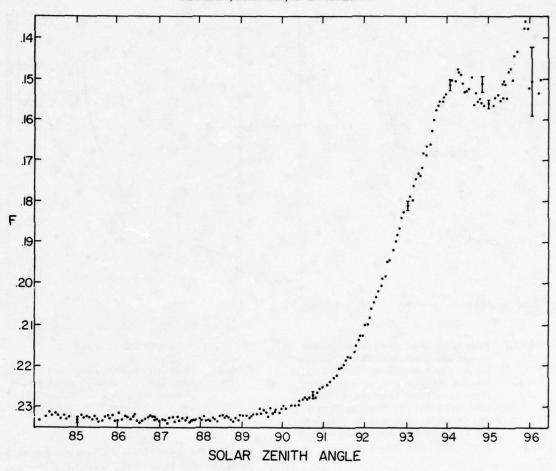


Figure 3. Balloon observation of direct sunlight at sunset from an altitude of 35 km over Churchill, July 22, 1974. The error bars represent the expected error due to Poisson statistics.

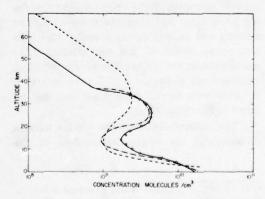


Figure 4. Comparison of distributions calculated from Figures 1, 2, and 3. —, balloon sunset observations, July 22, 1974; ---, ground average sunrise observations, ----, ground average sunset observations.

"umkehr" technique, and thus confirm the results obtained with the latter. They apply to July 22, 1974 only.

CONCLUSIONS

Spectrophotometric remote sensing gives, with reasonable accuracy, the amount and vertical distribution of the NO₂ at sunrise or sunset.

The comparison between balloon and ground-based observations confirms the earlier estimates of F_0 , and therefore the existence of the midday maximum in the total stratospheric nitrogen dioxide.

More complete analysis of the data presented here, particularly in its relation to earlier observations, will be presented elsewhere.

BLOXAM, BREWER, AND McELROY

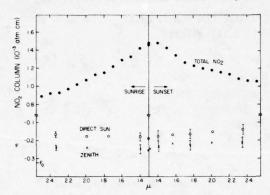


Figure 5. Average observed values of F and calculated columnar amount of NO_2 overhead at Churchill for July 7-23, 1974, throughout the day, derived from the mean ground observations. $\mu = \sec \left\{ \arcsin \left[(R/R+h)\sin \chi \right] \right\}$, $R = \operatorname{earth's}$ radius, h = 20 km, $\chi = \operatorname{solar}$ zenith angle. For comparison, the total NO_2 amount overhead in Southern Ontario at noon August 3, 1973 was 3.5×10^{-3} cm (Brewer et al., 1973).

ACKNOWLEDGMENTS

We are indebted to Dr. J. B. Kerr of the Atmospheric Environment Service of Canada for his aid in carrying out this experiment.

This research was supported by the National Research Council of Canada, and the Atmospheric Environment Service of Canada.

REFERENCES

Brewer, A.W., J.B. Kerr, and C.T. McElroy (1973), "Nitrogen dioxide concentrations in the atmosphere," Nature 246, 129-133.

Brewer, A.W., C.T. McElroy, and J.B. Kerr (1974a), "Spectrophotometric nitrogen dioxide measurements," in Proceedings of the International Conference on Structure, Composition and General Circulation of the Upper and Lower Atmospheres and Possible Anthropogenic Perturbations (vol. 1), 307-314.

Brewer, A.W., C.T. McElroy, and J.B. Kerr (1974b), "Spectrophotometric nitrogen dioxide measurements," in *Proceedings of the Third Conference on* the Climatic Impact Assessment Program (Cambridge, MA), U.S. Department of Transportation, DOT-TSC-OST-74-15, 257-263.

Brewer, A.W., C.T. McElroy, and J.B. Kerr (1974c), "Reply to Dr. Johnston's paper," in *Proceedings of the Third Conference on the Climatic Impact Assessment Program* (Cambridge, MA), U.S. Department of Transportation, DOT-TSC-OST-74-15, 271-272.

Dobson, G.M.B. (1975), "Observers' handbook for the ozone spectrophotometer," Ann. I.G.Y. 5, 46.

Johnston, H.S. (1974), "Alternative interpretation of umkehr data for nitrogen dioxide," in Proceedings of the Third Conference on the Climatic Impact Assessment Program (Cambridge, MA), U.S. Dept. of Transportation, DOT-TSC-OST-74-15, 264-270.

Mateer, C.L. and H.U. Dütsch (1964), "Proposed Standard Umkehr Evaluation Techniques,"
National Center for Atmospheric Research (Boulder, CO).

THE MEASUREMENT OF ATOMIC OXYGEN AND HYDROXYL IN THE STRATOSPHERE

J.G. ANDERSON

Department of Atmospheric and Oceanic Science Space Physics Research Laboratory University of Michigan Ann Arbor, Michigan

ABSTRACT: Measurements of ground-state atomic oxygen $O(^3P)$ between 25 and 43 km, and of ground-state hydroxyl $OH(X^2\pi)$ between 40 and 70 km, in the earth's atmosphere are presented. At a solar zenith angle of 51°, atomic oxygen is found to decrease from 2×10^9 cm⁻³ at 43 km to 2×10^7 cm⁻³ at 25 km, with statistically-significant local structure evident in the profile below 35 km. Hydroxyl is found to increase from 4×10^6 cm⁻³ at 70 km to 1×10^7 cm⁻³ at 45 km at a solar zenith angle of 86° , and to reach 2×10^7 cm⁻³ at 40 km at a solar zenith angle of 80° .

INTRODUCTION

The upward transport of stable species that originate at the earth's surface, most notably CH₄, H₂, H₂O, N₂O, CCl₄, CFCl₃, CF₂Cl₂, and HCl, is followed by photodissociation and oxidation in the stratosphere, resulting in the formation of an extensive system of atomic and molecular fragments (radicals) which are highly reactive chemically.

The extreme homogeneous reactivity of these radicals requires that the chemical environment be carefully defined in the region of the measured sample; this implies that simultaneous in-situ measurements are needed. The extreme heterogeneous reactivity of these radicals, on the other hand, requires either that they be sampled remotely or that particular care be taken to insure complete isolation of the sample from the measurement device.

These requirements motivated the development of instrumentation capable of performing simultaneous, in-situ measurements in unperturbed samples over extended altitude regions. The method, here termed the Laminar Flow-Through/Resonance-Fluorescence Technique, has been previously discussed (Anderson, 1975) but will be treated briefly here. For completeness, a rocket-borne resonance-fluorescence airglow technique is also described; it has previously been used to determine the absolute concentration of OH in the upper stratosphere and mesosphere.

Results are presented on measurements of

ground-state atomic oxygen $O(^3P)$ and ground-state hydroxyl $OH(X^2\pi)$, and a brief discussion of those measurements in the context of present photochemical theories of the stratosphere is offered.

EXPERIMENTAL

The Resonance-Fluorescence Airglow Technique

Classical studies of the upper atmospheres of planets have used and are continuing to use airglow features excited by ultraviolet radiation from the sun (Barth, 1966; Barth et al., 1971). Three criteria must in general be satisfied in order to extract an absolute concentration from such data, assuming that the spectroscopic details of the electronic transitions as well as the solar flux at the resonance wavelength are known:

- 1. The atmosphere must be optically thin at the center of the resonance line.
- Resonance fluorescence must be the dominant mode of excitation.
- 3. The ratio of the total atmospheric Rayleigh-scattering cross-section to the atomic or molecular resonance crosssection must be less than the mixing ratio of species under investigation over the altitude range of interest.

Although the above conditions are generally satisfied for a wide range of species in the

thermosphere and upper mesosphere, (1) and (3) are often not satisfied in the stratosphere. For example, atomic oxygen violates condition (1) throughout the stratosphere, the mesosphere, and most of the thermosphere if the sun is used as a source, because the atmosphere is optically deep at the center of the oxygen resonance line at 130.4 nm. Moreover, hydroxyl violates condition (3) throughout the entire stratosphere and most of the mesosphere because of its exceedingly small concentration (approaching a part per trillion).

In order to extend the airglow technique to lower altitudes for the purpose of measuring the absolute concentration of OH, two points were exploited:

- a. At various regions within the OH (0,0) band of the A² Σ-X²π transition at 309 nm, the rotational line spectrum exhibits an overlapping structure at the "heads" of the individual branches, thereby providing an enhancement in the ratio of the resonance-scattering cross-section.
- b. Rayleigh scatter is polarized perpendicular to the plane containing the sun, scattering center, and instrument (see Goody, 1964), whereas molecular resonance fluorescence is virtually unpolarized at the appropriate branch heads.

Thus, mounting a polarized, high-resolution scanning spectrometer in the nose of a zenith-oriented spin-stabilized rocket made it possible to make observations of the OH airglow between 45 and 70 kilometers (Anderson, 1971). Data from that experiment are presented in the following section. Although the measurement was successful, several shortcomings were inherent in the technique.

- The altitude regime of the measurement is restricted to the upper stratosphere and above, because of the exceedingly small mixing ratio of OH.
- The data represent a total column emission rate above the instrument, and thus
 they must be differentiated in order to
 extract a local volume density. This

- significantly complicates the interpretation of the data and precludes the possibility of simultaneously measuring chemically related species.
- Use of the sun as a source prevents study of the diurnal behavior of OH.

In order to overcome these shortcomings a new approach was taken.

The Laminar Flow-Through/Resonance-Fluorescence Technique

Figure 1 presents a schematic of the flowthrough/resonance-fluorescence technique. A beam of photons which are resonant with an allowed electronic transition from the ground state of an atom or diatomic molecule is passed through the sample gas. The rate of absorption and subsequent isotropic reemission of those photons is proportional to the concentration of scattering centers within the beam, thus providing a direct means of determining the absolute concentration of atoms and diatomics which are characterized by large electronic absorption cross-sections out of the ground state. Photons are collected in a direction perpendicular to the source beam and the gas-flow direction and are counted with a photomultiplier/pulse-counting system. This configuration, using mutually perpendicular directions of flow, irradiation, and observation, has been used successfully in the laboratory for gas-phase kinetic studies of atoms and radicals (Clyne and Cruse, 1972; Anderson

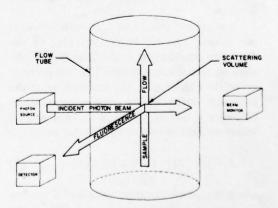


Figure 1. Schematic of the flow-through/resonancefluorescence geometry.

Absolute calibration of the flight instrument is accomplished in the laboratory using a fast-flow reactor of which the flight instrument is an integral part (Anderson, 1975). A large-capacity Roots blower (Leybold Heraeus Model WA2000) is used to achieve flow velocities and pressures corresponding to those encountered during flight. The formation of a known quantity of the atom or radical upstream of the instrument is achieved by using, in the case of atomic oxygen, the well-known titration seaction (Morse and Kaufman, 1965),

$$NO + N \rightarrow O + N_2$$

and for OH the reaction (Golden et al., 1963)

$$H + NO_2 \rightarrow OH + NO.$$

Both reactions combine an atom, formed in the microwave discharge, with a stable molecule added in calibrated amounts through a movable injector. Sufficient atom concentrations are used to insure that (a) the reaction is driven to completion in a distance small compared with the distance between the injection point of the stable molecule and the optical axis of the instrument, and (b) the atoms are in excess over the added stable molecule, insuring that a single atom or radical is produced for each added molecule.

The photon count rate S, in units of counts per second, can be written in terms of the resonance cross-section σ , the lamp flux F, the atom or radical concentration [X], the detector collection efficiency ϵ , the transmission of the collection optics T, the phototube quantum efficiency η , and the length of the lamp beam ℓ within the field of view of the detector as

$$S = \left\{ F\sigma[X] \right\} \left\{ \epsilon T\eta \right\} \ell = C[X] \tag{1}$$

where the proportionality "constant" C relating the atom or radical concentration [X] to the count rate is

$$C = \{ F\sigma \} \{ \epsilon T\eta \} \ \ell \tag{2}$$

An inspection of the quantities on the right-hand side of Equation (2) reveals that all are constants with the exception of the lamp flux F. Thus, if the absolute concentration [X] is independently established and the lamp flux F (or a quantity proportional to F) is monitored continuously during both laboratory calibration and flight, then C is uniquely determined. In practice, during calibration S is determined as a function of [X] for a fixed flux to verify linearity (the optical depth within the fluorescence chamber at line center for a typical calibration or stratospheric measurement is $< 10^{-6}$), and C is plotted as a function of F for a fixed [X] to verify linearity of the overlap integral of the lamp resonance line and the absorption line of the fluorescing species.

After analysis and calibration of the instrument in the laboratory, the detection module is removed unaltered from the flow reactor and fitted with a flow nacelle to insure laminar flow around and through the instrument as shown in Figure 2. Details of the nacelle are discussed elsewhere (Anderson, 1976).

In order to establish the background count from sources other than resonance fluorescence during flight, gas is added to the flow at the throat of the instrument to chemically eliminate the atom or radical of interest, thus providing a count rate in the absence and the presence of the fluorescing species without altering the mechanical configuration of the instrument in any way. In the case of O(³P), cis-2-butene is added to determine the background, and in the case of OH, HCl is added. The gas-addition system is programmed before flight to add gas at predetermined intervals.

RESULTS AND DISCUSSION

Atomic Oxygen

The laminar flow-through/resonancefluorescence technique was first used for the investigation of ground-state O(³P) atomic

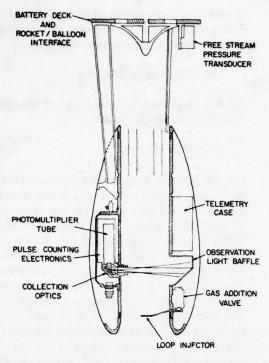


Figure 2. Detection module as housed in the flight nacelle.

oxygen in the stratosphere. An instrument configured as shown in Figure 2 was suspended from a stabilized high-altitude parachute which was dropped from a balloon. Two flights were made, the first on 25 November 1974, descending from an altitude of 40 kilometers, and the second on 7 February 1975 from an altitude of 43 kilometers. The launch and deployment were in the vicinity of Palestine, Texas (32°N) at solar zenith angles of 56° and 51° respectively. Figure 3 presents the results of both flights, along with a theoretically calculated midlatitude model for a solar zenith angle of 55° (Liu, 1976). Although a thorough discussion of the model and of the agreement between theory and experiment is beyond the scope of this paper, several observations may be drawn from Figure 3.

a. Rather good agreement is apparent between the model and the measurements below 40 kilometers. Above that altitude, rather less O(³P) is measured than is calculated. Of course, a simultaneous measurement of the in-situ concentration of O₃ would be crucial in determining whether the observed low

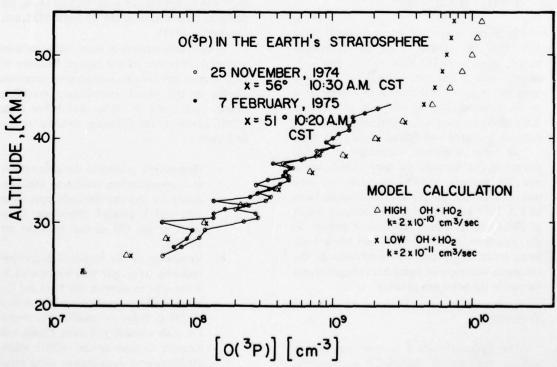


Figure 3. The atomic-oxygen concentration on 25 November 1974 and 7 February 1975 in the earth's stratosphere, compared with model calculations.

 $O(^3P)$ concentration above 40 km is a reflection of a low $O(^3P)$ -to- O_3 ratio or of a depression in total odd oxygen $(O(^3P) + O_3)$.

concentration above 40 km is a reflection of a low $O(^3P)$ -to- O_3 ratio or of a depression in total odd oxygen $(O(^3P) + O_3)$.

- b. There is significant structure in the atomic oxygen profile below about 30 km. Although the mean value of O(³P) was similar during both flights, local variations up to a factor of six are apparent in the low-altitude data.
- c. The measurement technique should be able to detect atoms in the part-pertrillion range under flight conditions.

The high-altitude limit of the experiments was determined by the peak altitude of the balloon chosen for the flights, and the low-altitude limit was determined by consideration of the recombination of O(³P) in the three-body reaction

$$O + O_2 + M \rightarrow O_3 + M$$

which, in the absence of solar ultraviolet radiation after the sample enters the instrument throat, converts $O(^3P)$ back to O_3 . This low-altitude limit is not insurmountable: it has now been demonstrated that there is no contribution to the detector counting rate from atmospheric Rayleigh-backscattered sunlight, so the detection axis can be moved to the plane of the entry port.

In order to prevent formation of atomic oxygen in the beam of the lamp (which would alter the apparent ambient concentration) care was taken to limit the photon flux from the lamp to 5×10^{10} photons/sec in the resonance triplet at 130.4 nm. At typical velocities of descent on the parachute of 10^4 cm/sec, and for a lamp beam width of 1.5 cm, no contribution to the resonance-fluorescence signal from oxygen atoms formed in the beam was possible.

Hydroxyl

The hydroxyl radical is now regarded as perhaps the central radical in stratospheric chemistry. Not only is it responsible for the direct catalytic recombination of O₃ and O(³P), it also links together the hydrogen and nitrogen radical systems via the recombination reaction

$$OH + NO_2 + M \rightarrow HNO_3 + M$$

and it is responsible for liberating free chlorine from HCl through the reaction

$$OH + HC1 \rightarrow C1 + H_2$$

(see, for example, Stolarski and Cicerone, 1974; Wofsy and McElroy, 1974; and Rowland and Molina, 1975). Figure 4 presents data taken on 22 April 1971 between the altitudes of 45 and 70 km at a solar zenith angle of 86°, and on 18 July 1975 at an altitude of 40 km and a solar zenith angle of 80°. In both cases, collisional deactivation of the A state of OH was calculated using a bimolecular quenching-rate constant for molecular nitrogen of 2 × 10⁻¹¹ cm³ sec⁻¹ (Becker et al., 1972; Hooymayers and Alkemade, 1967) and for molecular oxygen of 6 × 10-11 cm³ sec⁻¹ (Hooymayers, 1967), both of which are significantly larger than the 1 × 10⁻¹¹ cm³ sec-1 value adopted for both N2 and O2 in the previous presentation of the 22 April 1971 data (Anderson, 1971).

A full interpretation of these results requires a careful treatment of the diurnal behavior of OH, because the radical concentration decreases rapidly in the period immediately preceding sunset, particularly at 50 km and below (Liu, 1976). However, the following conclusions can be drawn:

- a. Hydroxyl is present in the stratosphere at a concentration similar to that predicted by theory, although both more data and a detailed theoretical treatment of the OH diurnal behavior are lacking.
- b. Variability in the hydroxyl concentration may be greater than anticipated. It is essential to monitor the H₂O and O₃ concentrations simultaneously with that of OH in order to establish the reason for such variability. Future flights will measure all three species with a multiple-instrument arrangement using separate detectors on a common airframe.

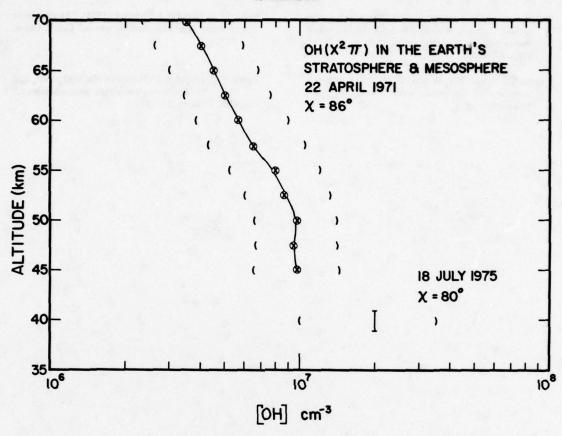


Figure 4. Comparison between hydroxyl concentrations measured using rocket and using balloon techniques. Parentheses indicate estimated experimental uncertainties.

REFERENCES

Anderson, J.G. (1971), "Rocket measurement of OH in the mesosphere," J. Geophys. Res. 76, 7820.

Anderson, J.G. and F. Kaufman (1972), "Kinetics of the reaction OH + NO₂ + M → HNO₃ + M," Chem. Phys. Lett. 16, 375.

Anderson, J.G. (1975), "The absolute concentration of O (³P) in the earth's stratosphere," Geophys. Res. Lett. 2, 231.

Anderson, J.G. (1976), "The absolute concentration of OH (X $^{2}\pi$) in the earth's stratosphere," Geophys. Res. Lett. 3, 165.

Barth, C.A. (1966), "Nitric oxide in the upper atmosphere," Ann. Geophys. 22, 198.

Barth, C.A., C.W. Hord, J.B. Pearse, K.K. Kelly, G.P. Anderson, and A.I. Stewart (1971), "Mariner 6 and 7 ultraviolet spectrometer experiments: Upper atmosphere data," J. Geophys. Res. 76, 2113.

Becker, K.H., D. Haaks, and T. Tatarczyk (1972), "Monitoring of radicals by a tunable dye laser," Z. Naturforsch. 27, 1520.

Clyne, M.A.A. and H.W. Cruse (1972), "Atomic resonance fluorescence spectrometry for rate constants of rapid biomolecular reactions," J.C.S. Farad. Trans. (2) 68, 1281.

Golden, D.M., F.P. DelGreco and F. Kaufman (1963), "Experimental oscillator strength of OH $^2\Sigma^{-2}\pi$ by a chemical method," J. Chem. Phys. 39, 3034.

Goody, R.M. (1964), Atmospheric Radiation I - Theoretical Basis, Oxford Univ. Press, London.

Hooymayers, H.P. and C.T.J. Alkemade (1967), "Quenching of excited hydroxyl ($^2\Sigma^+$, v'=0) radicals in flames," J. Quant. Spec. Rad. Transf. 7, 405

Liu, S.C. (1976), private communication.

- Morse, F.A. and F. Kaufman (1965), "Determination of ground state (O, N and H) by light absorption and measurements of oscillator strengths," J. Chem. Phys. 42, 1785.
- Rowland, F.S. and M.J. Molina (1975), "Chlorofluoromethanes in the environment," Revs. Geophys. Space Phys. 13, 1.
- Stolarski, R.S. and R.J. Cicerone (1974), "Stratospheric chlorine: a possible sink for ozone," Can. J. Chem. 52, 1610.
- Wofsy, S.C. and M.B. McElroy (1974), "HO_x, NO_x and ClO_x: Their role in atmospheric photochemistry," Can. J. Chem. 52, 1582.

STRATOSPHERIC HALOGEN MEASUREMENTS AND IN-SITU DETERMINATION OF ACCURACY OF NITRIC ACID MEASUREMENTS

A. LAZRUS, B. GANDRUD, AND R. WOODARD National Center for Atmospheric Research* Boulder, Colorado

W. SEDLACEK

Los Alamos Scientific Laboratory Los Alamos, New Mexico

ABSTRACT: This presentation covers two distinct subjects. The efficiency of IPC-1478 filters in the collection of stratospheric nitric acid vapor has been determined by in-situ controlled exposures, and a calibrated curve is presented. Recent measurements of stratospheric hydrogen chloride are also discussed.

HYDROGEN NITRATE

In February 1971, we measured nitric acid at 25 kilometers using two separate air-filtration samplers, one containing a regular IPC-1478 filter and one a base-impregnated filter. They both gave the same results, thus providing the basis for our continued use of neutral IPC-1478 filters for determining HNO3 throughout the CIAP program. Since that time, however, two developments have suggested that their collection efficiency might not be adequate. First, between 21 and 30 km, which is where the HNO3 exists in highest concentration, our measurements have been consistently less than those obtained by infrared spectroscopy. Second, some indirect evidence obtained by W. Sedlacek suggested our data collection at lower altitudes was not efficient.

Our approach has been to determine efficiencies under in-situ sampling conditions. The filters we are using (see Figure 1) are segmented into four sectors separated from each other by thin barriers of Silastic resin. IPC-1478 filters are composed of cellulose fibers impregnated with dibutoxyethylphthalate. One-half the filter is then further impregnated with tetrabutylammonium hydroxide. Two-sixths of the filter are masked during sampling to provide contamination controls for the basic and regular portions of the filter. A balloon flight in which the sampler

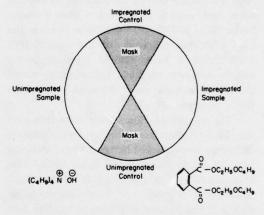


Figure 1. Segmented and impregnated IPC-1478 filter used for balloon sampling.

doors did not open was used to confirm the reliability of these contamination controls as blank corrections.

The efficiency determination consisted of three parts. First, four sets of completely base-impregnated filters, each containing two in tandem, were flown on several flights of the WB-57F aircraft. In each case, no HNO₃ passed beyond the first filter. It is important to know that the face velocity of air passing through the aircraft filters is an order of magnitude higher than through the balloon filters, and therefore represents our most difficult conditions in terms of collection efficiency. Laboratory tests indicated

^{*} The National Center for Atmospheric Research is sponsored by the National Science Foundation.

LAZRUS, GANDRUD, WOODWARD AND SEDLACEK

the extent to which the face velocity was decreased by the presence of the second filter in tandem. In-situ tests, in which the speed of the WB-57F was varied on three separate flights, confirmed that this decrease in face velocity did not observably alter the collection efficiency for HNO₃. Lab experiments further show that the pressure drop of the filter is not measurably changed by the impregnation procedure. The evidence thus demonstrates the high efficiency of the base-impregnated filters for HNO₃ collection.

The segmented filters were next flown on four balloons between 60 and 90 thousand feet. There was no systematic difference between the HNO₃ measurements made on the neutral sectors and those made on the basic sectors. If one therefore assumes the mean value is the true one, then the mean relative error between the impregnated and neutral sectors of a given balloon-borne filter is 12%. The data thus confirm the high collection efficiency of the neutral IPC-1478 filters in balloon-borne sampling during our measurement program. This sampling covers the altitude region where the main body of the HNO₃ layer exists.

The segmented filters were then flown on the WB-57F aircraft. In this case no consistent difference was observed between the neutral and basic filter collections below 1 ppbm HNO3. This is illustrated in Figure 2. The data for concentrations above 1 ppbm are shown expanded in Figure 3. The percent efficiency at the high face velocities encountered in aircraft sampling (about 0.92 km/min) appears to be a function of the amount of HNO3 collected on the paper. According to Figure 3, the collection efficiency for the highest concentrations we have encountered during our general sampling is about 65%. Usually, however, the HNO₃ concentrations we have encountered are in the collection-efficiency range of 75-100%.

We now plan to republish our data with the necessary correction. From the viewpoint of stratospheric modelers, the validity of the data of most interest (i.e., above 21 km) has been confirmed by our recent results. Similarly, the low HNO₃ concentrations in the region of loweraltitude aircraft sampling are confirmed. The principal effect of the correction will be to make the concentration gradient more gradual at the bottom of the main HNO₃ layer.

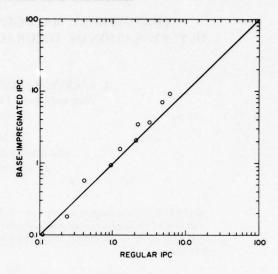


Figure 2. HNO₃ concentrations determined by base-impregnated IPC-1478 filter paper compared with those determined by neutral paper. Units are 10⁻⁹ HNO₃/g air.

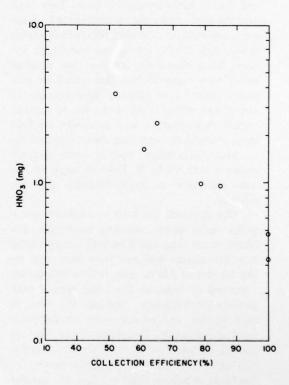


Figure 3. Collection efficiency (%) as a function of HNO₃ per sample (mg).

LAZRUS, GANDRUD, WOODWARD AND SEDLACEK

HYDROGEN CHLORIDE

The stratospheric hydrogen chloride measurements were made using the segmented filters. The basic portion is assumed to collect HCl plus particulate chloride, while the neutral portion collects only particulate chloride. The amount of chlorine collected is determined by a standard test in which chloride ion displaces thiocyanate ion from mercuric thiocyanate. The thiocyanate then forms a red complex with ferric alum. The chloride measurements have been independently confirmed by W. Sedlacek using neutron activation. Since the latter method determines total chlorine, we can conclude that there is no large contribution from species other than chloride, except possibly from compounds which could convert to chloride during sampling. Since ClO is at most a sixth of the HCl at 30 km, and diminishes rapidly with decreasing altitude according to current models, it is improbable that our results are appreciably affected by this material. Our worst errors are estimated at 30%.

Figure 4 shows the chloride results. The concentrations increase with altitude, suggesting an in-situ stratospheric source. Similarly, the concentrations increase at higher latitudes.

Particulate chloride may represent a sink for gaseous stratospheric halogens. As is shown in

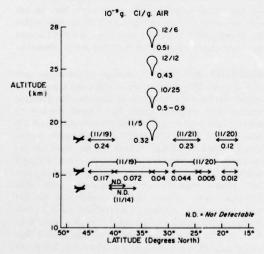


Figure 4. Stratospheric hydrogen chloride reported as 10-9 g Cl/g air. Points of balloon symbols indicate sampling altitudes. Length of arrows indicates latitude range per filter collection. Longitude is approximately 95°W.

Figure 5, however, the amounts of particulate chloride in our samples were sporadic and low. Since the highest particulate concentrations appear at 24.5 and 27 km, at an altitude considerably higher than that of the usual aerosol layer, it is very likely that they represent a sampling artifact. It is quite possible that Clwould not be retained in stratospheric sulfuricacid aerosol after sampling, because of its high vapor pressure at surface temperatures. We are now checking this possibility in the laboratory, since it may mean that our present technique cannot determine the stratospheric particulate chloride. C.S. Kiang, visiting NCAR from Clark College, is attempting to determine the maximum HCl content at stratospheric temperatures under equilibrium conditions in stratospheric sulfate aerosol (believed to be about 70% H₂SO₄). We are also considering the option of keeping our samples cold.

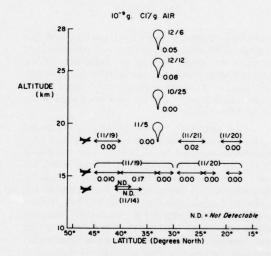


Figure 5. Stratospheric particulate chloride reported as 10:9g Cl/g air.

Several preliminary measurements of stratospheric bromine were made by neutron-activation analysis of the extracts of segmented filters flown on the WB-57F aircraft. The results are shown in Table 1. The concentrations appear to be larger at the higher altitude, though the data are too sparse to draw a firm conclusion.

Our attempt to determine the collection efficiency for HCl during a series of flights in November 1974 was unsuccessful, partly because we flew at low altitudes and partly because of

LAZRUS, GANDRUD, WOODWARD AND SEDLACEK

Table 1. Stratospheric Bromine Measurements

Latitude	Impregnated Filter*	Neutral Filter*	HBr*
17-19N	6.5	3.4	3.1
21-24N	7.5	3.3	4.2
24-29N	7.6	2.4	5.2
29-33N	9.6	4.0	5.6
33-40N	7.3	4.4	2.9
40-45N	9.4	8.0	1.4
17-20N	12.7	1.7	11.0
40-45N	12.6	5.6	7.0
	17-19N 21-24N 24-29N 29-33N 33-40N 40-45N 17-20N	Latitude Filter* 17-19N 6.5 21-24N 7.5 24-29N 7.6 29-33N 9.6 33-40N 7.3 40-45N 9.4 17-20N 12.7	Latitude Filter* Filter* 17-19N 6.5 3.4 21-24N 7.5 3.3 24-29N 7.6 2.4 29-33N 9.6 4.0 33-40N 7.3 4.4 40-45N 9.4 8.0 17-20N 12.7 1.7

*Units: 10-12g Br/g air.

equipment failure. In February 1975 a new series of efficiency tests is being attempted with the

aircraft. These will be followed in April by analogous balloon-borne experiments. The collection efficiencies of our measurements for both stratospheric aerosol and nitric acid have now been checked in a fairly direct manner, and we hope soon to complete the picture with similar results for stratospheric hydrogen chloride.

ACKNOWLEDGMENT

This work was performed as part of a joint research venture with the Energy Research and Development Administration, and is related to the Climatic Impact Assessment Program of the Department of Transportation.

TRACE-GAS CONCENTRATION MEASUREMENTS

DISCUSSION

GELINAS: About a year and a half ago I worked on a diurnal model of the NO_x species, and unfortunately I reported my results only in the proceedings of the IAMAP/IAPSO Melbourne conference of January 1974. So there are a couple of points that I would like to make for those who might not have heard some of the results of that work.

First, factors of 20 in the variability of NO are not surprising when variable transport rates of N_2O_5 are included in a diurnal kinetic model. When the flux of N_2O_5 into or out of a very local region is varied, NO can change easily by factors of 20 and perhaps by factors up to 100. In this regard, N_2O_5 is a sequesterer, as Halstead Harrison liked to say, for NO. NO₃ is also a crucial element in this diurnal mechanism. The variability seen among the one-dimensional models is thus not surprising. Such models have to be applied with particular care because they are really not designed to account for these local variations in transport.

My second point has to do with the controversial NO₂ data of Brewer et al., which were also presented at Melbourne. Our kinetic model does in fact reveal some of the same general characteristics for NO₂. Our NO₂ concentration increases from a low value just after sunrise to a high value around noon, may decline somewhat in the afternoon, may increase again just before sunset, and then rises quickly after sunset.

It is going to take very precisely directed mechanistic studies to deal properly with local variables, such as NO and NO₂.

CRUTZEN: Ackerman mentioned NO_2 mixing ratios of 3×10^{-9} in the troposphere. John Noxon has done extensive measurements of NO_2 in the troposphere. At

his observatory in the Rocky Mountains, when the wind is blowing from the west, the $\mathrm{NO_x}$ background mixing ratio never goes above 10^{-10} . His data on $\mathrm{NO_2}$ in the stratosphere generally agree with those reported here by C.T. McElroy et al. However, he doesn't find the diurnal variation which they do, and he suggests that water-vapor absorption is also present at one of the absorption wavelengths they use.

C.T. McELROY: My co-worker Jim Kerr has made other measurements at different wavelength triplets that do not include that possible water-vapor line. In one case he got qualitative agreement which was well within the experimental accuracy. Therefore, we don't accept the water-vapor explanation for what we're observing.

JOHNSTON: Bob Gelinas's reminder of the importance of N2O5 and NO3 prompts me to point out some of our recent results, even though Rick Graham, the graduate student who obtained them, has begged me not to commit him until he has completed interpreting all the data. But I think it's important, and some people haven't heard it, though I have written most of the modelers. In the photolysis of NO₃, there is a threshold wavelength below which you can only get NO + O2, and that path completes another catalytic cycle that destroys ozone. Above that threshold you can get NO₂ + O, which completes a do-nothing cycle. I think we have good data now that show that NO₃ photolysis does not give NO with a quantum yield any greater than 10%, but it does give NO₂ with a substantial, but as yet unmeasured, quantum yield.

WATSON: Are your observed oxygen-atom concentrations consistent with theory? How do you hope to observe OH by the resonance-lamp technique when its cross-section is so much weaker than that of O?

TRACE-GAS CONCENTRATION MEASUREMENTS

J. ANDERSON: Both of those are very good questions. The Wallops Island ozonesonde flight of the same day demonstrated that the ozone profile was typical of winter. The ratio of the observed O and O₃ concentrations agrees with the Chapman theory, though the lower part of the profile gives more atomic oxygen than theory would predict.

The answer to the second question is that the resonance absorption cross-section for O has a value of about 3 \times 10⁻¹³. The most-allowed transition for OH

has a cross-section of 5×10^{-17} . However, the flux from the lamp in the case of oxygen atoms is limited by the optical depth, which is of course proportional to the oscillator strength. That is not a problem in the case of the OH lamp, and the detectability of both OH and O is some 5×10^5 per cubic centimeter.

There is another problem with OH; its transition has a lifetime in the microsecond range, so that you have to be careful of quenching in the lower stratosphere.

HETEROGENEOUS PROCESSES AND THE CHEMISTRY OF AEROSOL FORMATION IN THE UPPER ATMOSPHERE

A.W. CASTLEMAN, JR., * R.E. DAVIS, I.N. TANG, AND J.A. BELL

Department of Applied Science Brookhaven National Laboratory Upton, New York

ABSTRACT: Heterogeneous processes of potential importance in the stratosphere may be classified into five categories. These include charge exchange between ions and aerosols, the production of trace species, surface catalytic effects, adsorption of trace species, and the formation of new aerosol particles. Each of these is assessed with regard to its significance for the chemical and physical processes operating in the stratosphere.

Particular attention is given to the formation mechanisms responsible for the stratospheric aerosol layer. Under certain conditions, sulfur compounds are known to contribute to aerosol formation, but the basic mechanism leading to the production of sulfuric acid and other sulfate aerosols has not been well established. Experiments have been performed in this laboratory to elucidate some important reaction steps in the mechanism of sulfuric-acid aerosol formation. Specifically, the oxidation of SO₂ by the OH radical, and the reaction of SO₃ and H₂O, have been studied and are described here. In addition, experimental results on the gas-to-particle conversion arising from reactions of SO₂ and nitrogen oxides under stratospheric conditions are presented. This paper discusses the results of these kinetic studies and the likelihood of particle formation under various atmospheric conditions.

INTRODUCTION

Knowledge of the chemistry of upperatmospheric aerosols is still quite rudimentary, so it is not surprising that there is a paucity of quantitative information regarding the latter's role in the chemistry of gaseous species occupying these regions. We have recently undertaken a study examining the various possible heterogeneous mechanisms and processes which may occur; this examination has led to a determination of those likely to be important. These assessments have shown which mechanisms should be incorporated into modeling calculations of the behavior of trace atmospheric constituents, and which processes warrant further attention in laboratory studies.

In the broad contexts of heterogeneous processes in the upper atmosphere, there are five major areas to be considered: charge exchange, production of trace species, catalytic effects, adsorption of trace species, and development of new surfaces. This paper is divided into two

sections. The first addresses the importance of heterogeneous processes to stratospheric chemistry; it discusses the first four of these areas. A second section is devoted to the development of new surfaces; it deals mainly with the formation of sulfate aerosols in the stratosphere.

ASSESSMENT OF THE IMPORTANCE OF HETEROGENEOUS PROCESSES TO STRATOSPHERIC CHEMISTRY

Charge Exchange

The stratosphere contains approximately 10^3 ion pairs cm⁻³, distributed variously with altitude and latitude. Ion concentrations are established by the balance between the rates of formation and of destruction. The latter is the result of two processes; it includes recombination of negative and positive ions, and the process of ion charge exchange with free surfaces provided by aerosol particles.

^{*}Dr. Castleman, to whom correspondence should be addressed, is now with the Department of Chemistry and CIRES of the University of Colorado, Boulder, Colorado 80309.

Studies show that, to a good approximation, aerosols probably maintain a charge distribution according to the relationship (Keefe et al., 1959)

$$\frac{N_{\pm}}{N_0} = 2e^{-p^2q^2/2rkT}$$

where N_{\pm} is the number concentration of aerosols (negatively or positively charged) with p charges and radius r, while N_0 is the total number concentration of uncharged aerosols. The symbols q, k, and T denote the charge of the electron, Boltzmann constant, and absolute temperature, respectively.

The rate of change of ion concentration, n, is given (Bricard and Pradel, 1966) by

$$\frac{dn}{dt} = Q - \alpha n^2 - n[\beta N]$$

where t is time, Q ion production rate, α recombination coefficient for negative and positive ions, and β coefficient of ion attachment to aerosols.

Under stratospheric conditions,

$$10^{-7} \le \alpha \le 10^{-6}$$
 and $10^{-6} \le \beta \le 10^{-4}$

from which it follows that

$$\frac{\text{ion recombination}}{\text{charge exchange}} \geqslant \frac{\alpha n}{\beta N} \geqslant 1.0$$

The processes of ion recombination and charge exchange could be of about equal importance only in regions where the stratospheric aerosol concentration is at a maximum; elsewhere in the upper atmosphere, the process of charge-exchange with aerosols is of only secondary importance.

Production of Trace Species

There are several situations where aerosols have been thought to play a role in the production of trace species in the upper atmosphere. These include the production of aerosols composed of condensed metal-oxide vapors resulting from the ablation of meteors, the possible role of

aerosols in the production of the sodium layer of 93 km, and the production of HCl from the reaction of H_2SO_4 and NaCl. We have previously considered the first two possibilities (Castleman, 1974) and shown that the second is of no importance.

The possibility of HCl production from the reaction of H_2SO_4 and NaCl was calculated; the results are plotted in Figure 1. Based on thermodynamic considerations, there is a strong likelihood that this reaction forms appreciable quantities of HCl in the stratosphere. It is almost certain that either the supply of NaCl (sea salt) aerosols, the kinetics of the surface reaction, or both, limit HCl production. Clearly the kinetics of this reaction warrants study.

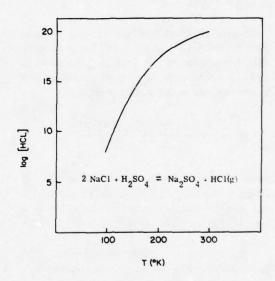


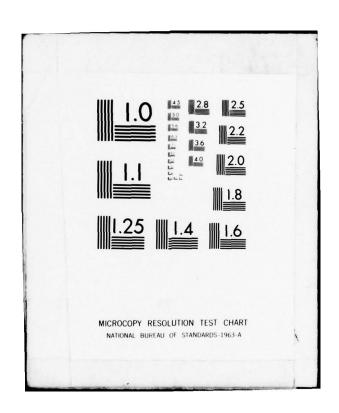
Figure 1. Concentration of HCl as a function of temperature in the equilibrium between NaCl and H₂SO₄.

Surface Catalytic Effects

There are three possible ways in which aerosol surfaces may play a role in affecting the gas-phase concentration of chemically reactive species. These include the destruction of reactive intermediates such as free radicals which normally are important in gas-phase reactions, a catalytic influence on reactions between stable gas-phase constituents, and the stabilization of a product molecule in the condensed state which readily dissociates in the gas phase.

TRANSPORTATION SYSTEMS CENTER CAMBRIDGE MASS
PROCEEDINGS OF THY CONFERENCE ON THE CLIMATIC IMPACT ASSESSMENT -- ETC. (1) F/G 4/2 AUG 76 T M HARD, A J BRODERICK UNCLASSIFIED TSC-0ST-75-38 N/L 6 OF 6 AD A069982 END DATE FILMED DTIC

4D-A068 982



Studies show that, to a good approximation, aerosols probably maintain a charge distribution according to the relationship (Keefe et al., 1959)

$$\frac{N_{\pm}}{N_0} = 2e^{-p^2q^2/2rkT}$$

where N_{\pm} is the number concentration of aerosols (negatively or positively charged) with p charges and radius r, while N_0 is the total number concentration of uncharged aerosols. The symbols q, k, and T denote the charge of the electron, Boltzmann constant, and absolute temperature, respectively.

The rate of change of ion concentration, n, is given (Bricard and Pradel, 1966) by

$$\frac{dn}{dt} = Q - \alpha n^2 - n[\beta N]$$

where t is time, Q ion production rate, α recombination coefficient for negative and positive ions, and β coefficient of ion attachment to aerosols.

Under stratospheric conditions,

$$10^{-7} \le \alpha \le 10^{-6}$$
 and

$$10^{-6} \le \beta \le 10^{-4}$$

from which it follows that

$$\frac{\text{ion recombination}}{\text{charge exchange}} \geqslant \frac{\alpha n}{\beta N} \geqslant 1.0$$

The processes of ion recombination and charge exchange could be of about equal importance only in regions where the stratospheric aerosol concentration is at a maximum; elsewhere in the upper atmosphere, the process of charge-exchange with aerosols is of only secondary importance.

Production of Trace Species

There are several situations where aerosols have been thought to play a role in the production of trace species in the upper atmosphere. These include the production of aerosols composed of condensed metal-oxide vapors resulting from the ablation of meteors, the possible role of

aerosols in the production of the sodium layer of 93 km, and the production of HCl from the reaction of H₂SO₄ and NaCl. We have previously considered the first two possibilities (Castleman, 1974) and shown that the second is of no importance.

The possibility of HCl production from the reaction of H₂SO₄ and NaCl was calculated; the results are plotted in Figure 1. Based on thermodynamic considerations, there is a strong likelihood that this reaction forms appreciable quantities of HCl in the stratosphere. It is almost certain that either the supply of NaCl (sea salt) aerosols, the kinetics of the surface reaction, or both, limit HCl production. Clearly the kinetics of this reaction warrants study.

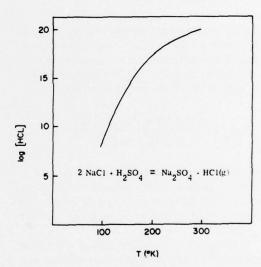


Figure 1. Concentration of HCl as a function of temperature in the equilibrium between NaCl and H₂SO₄.

Surface Catalytic Effects

There are three possible ways in which aerosol surfaces may play a role in affecting the gas-phase concentration of chemically reactive species. These include the destruction of reactive intermediates such as free radicals which normally are important in gas-phase reactions, a catalytic influence on reactions between stable gas-phase constituents, and the stabilization of a product molecule in the condensed state which readily dissociates in the gas phase.

In order to assess the possible importance of the first and second processes, we extended the calculations of Klein (1973) and Johnston (1973). The well-known Eley-Rideal mechanism was chosen to provide a basis for discussion. In making the calculations, a binary reaction between an adsorbed molecule A and a gas-phase species at concentration [B] was assumed to occur. Furthermore, A and B were considered to react on the surface, and product C to desorb.

By equating the rate of adsorption of A (rate constant k₁) with the rate of removal by reaction (rate constant k₂), the following relation for fraction of the surface covered is obtained:

$$\theta = \frac{k_1[A]}{k_1[A] + k_2[B]}$$

Taking the gas-phase molecular velocity of A and B to be $\approx 4 \times 10^4$ cm sec⁻¹, and the probability that A will stick, and B react, on collision as f_1 and f_2 respectively, the approximate overall conversion rate on the surface is given by

$$R_{s} = \frac{4 \times 10^{4} \pi r^{2} N f_{1} f_{2}[A][B]}{\left\{f_{1}[A] + f_{2}[B]\right\}}$$

Here, N is the number density of aerosols of radius r. The radii of the particles of interest are not greatly different from several tenths of a micron. Furthermore, as a maximum, we take $f_1 = 1$.

Taking the ratio of the surface rate to the gas-phase rate of conversion (rate constant k_g), we obtain

$$\frac{R_s}{R_g} \le \frac{10^{-4} f_2 N}{k_g \{[A] + f_2[B]\}}$$

Five cases may be identified: $f_2[B] \gg [A]$; $f_2[B] \approx [A]$; $f_2 \ll 1$, $[B] \approx [A]$; $[A] \approx [B]$, $f_2 \approx 1$; and $[B] f_2 \ll [A]$. All may be generalized by the relationship

$$\frac{R_s}{R_g} \leqslant \frac{10^{-4} \text{Nf}}{k_g[B]} \quad ,$$

where for the five cases respectively, it can be

easily shown that f = 1, 1/2, f_2 , 1/2 f_2 , and f_2 [B]/[A]. At this point, specific systems are not under discussion and the choice of [A] and [B] is arbitrary; therefore, the fifth case need not be considered. Furthermore, within the uncertainty of the approximations, factors of two are immaterial and only the two cases $f = \{1, f_2\}$ are of consequence. Note that the constant $f_2 \le 1$.

As discussed earlier, within the region between the tropopause and stratopause, $N \lesssim 1$ cm⁻³; at higher elevations $N \lesssim 10^{-3}$ cm⁻³. The inverse of the product $k_g[B]$ is related to the relaxation time for the reaction of A (taken as the minor constituent). As pointed out by Klein (1973) and Johnston (1973), for the case of very fast gas-phase reactions, $R_s/R_g \ll 1$, and the effects of surfaces are negligible.

In fact, for the stratosphere, even if appropriate catalytic surfaces were available at the reported total aerosol number concentrations, surface reactions could be significant only for cases in which the gas-phase reactions have relaxation times $\geq 10^4$ sec. At much higher altitudes, surface reactions could be important only if the homogeneous reactions have relaxation times longer than 10^7 sec.

There are some cases which may fulfill this criterion. For instance (Johnston, 1973), the recombination reaction of ozone on some metaloxide surfaces occurs with nearly unit efficiency. Therefore, if present in appreciable concentrations, metal-oxide aerosols could have some effect on the ozone levels in the upper atmosphere. Other possible surface reactions which may be of some importance are

$$H_2O + N_2O_5 \rightarrow 2HNO_3$$

(Klein, 1973; Johnston, 1973) and

$$SO_2 + [oxidant] \rightarrow SO_3$$
.

The ratios of the surface rate to the gas-phase rate are given in Table 1 for these reactions, as well as for others that may be of marginal importance.

Similar analyses have been made for the case of reactions involving the free radicals HO₂, OH, CH₃O, Cl, O, CH₃, and H. The results are given in Table 2. The gaseous reactants and product

Table 1. Gas-Phase Characteristic Times, and Ratios of Surface Rates to Gas-Phase Rates, for Stratospheric Reactions of Interest

Reactants	Products	Gas-Phase τ, sec	R_s/R_g
N ₂ O ₅ , H ₂ O	2 HNO ₃	>107	>103
NO_2, O_3	NO_3, O_2	≈10 ⁵	≈10
CH_3O_2 , NO	CH_3O, NO_2	≈10⁴	≈1
03,0	2 O ₂	2×10^6	200
NO, O ₃	NO_2, O_2	≈10 ⁵	≈10

molecules are given in columns 2 and 3, respectively. In all cases, the gas-phase reaction rate is far greater than that for the surface reaction, even considering unit reaction efficiency upon collision. At first glance, this might be used as evidence to discount the role of aerosol surfaces in affecting the reactions involving free radicals. However, this conclusion must be modified for those cases in which a cyclic gas-phase reaction consumes a free radical, but leads to its regeneration in a related subsequent step. In such situations, the aerosol surface could possibly play a role in terminating the reactant, and thereby have an appreciable effect on the gas-phase "catalytic" cycle as well.

Adsorption of Trace Species

Another surface process to be considered is that of the adsorption of trace species. In all upper-atmosphere situations very small concentrations of the species of interest are involved, and it is doubtful that their concentration on surfaces could ever approach a significant fraction of a monolayer, say, much less several monolayers. An exception might be the case of SO_3 , which could perhaps become adsorbed on surfaces prior to its reaction to form H_2SO_4 . (This is considered to be in the domain of the subject area covered in the next section.)

As for the other species, their maximum potential concentration on surfaces can then be calculated by assuming a monolayer coverage on existing aerosols. The various distributions observed allow an approximate surface area per unit volume to be calculated. Subsequent calculations suggest that aerosol surfaces can retain no more than about 10⁷ molec cm⁻³ of noncondensables.

FORMATION OF SULFATE AEROSOLS IN THE STRATOSPHERE

Sulfur compounds are known to be an important constituent of atmospheric aerosols, but the basic chemical conversion and aerosol-formation mechanisms are not well established. Under some conditions reactions may occur on surfaces, in which case the sulfate products serve only to modify the size distribution of the pre-existing particles. In other situations, the aerosol formation may be initiated by homogeneous gas-phase reactions; attendant clustering reactions may subsequently lead to nucleation and, therefore, the formation of new particles.

New sulfuric acid particle formation may then be viewed as being comprised of three primary steps:

Table 2. Maximum R_e/R_g for the Important Atoms and Free Radicals in the Stratosphere at 20 km

Atoms or Free Radicals	Gaseous Reactants	Products	Gas-Phase τ , sec	R_s/R_g
но2.	03	OH∙, O ₂	530	5.3×10^{-2}
он•	03	HO_2 , O_2	10	1 × 10 ⁻³
CH ₃ O·	02	CH ₂ O∙, HO ₂ ∙	0.16	1.6×10^{-5}
Cl·	03	CIO+, O2	1 × 10 ⁻²	1 × 10 ⁻⁶
0.	02	03	2.5×10^{-3}	2.5×10^{-7}
СН₃•	O ₂	СН ₃ О₂•	5.8 × 10 ⁻⁴	5.8×10^{-8}
н•	02	HO ₂ ·	1.7×10^{-6}	1.7×10^{-10}

- oxidation of SO2
- reaction of SO₃ with water to form H₂SO₄
- clustering of H₂SO₄ and H₂O molecules to form prenucleation embryos, followed by the heteromolecular nucleation process

We present here the results of our recent studies on each of these aspects of the formation process.

Oxidation of SO2

In earlier studies (Wood et al., 1975; Castleman et al., 1976) we showed that the hydroxyl radical was an important reactant responsible for the oxidation of SO₂. Appropriate steady-state photolysis experiments were performed in our laboratory to measure the rate constants for the following:

$$OH + SO_2 \underset{k_{1r}}{\overset{k_1}{\rightleftharpoons}} HSO_3^*$$
 (1)

$$HSO_3* + M \xrightarrow{k_2} HSO_3 + M$$
 . (2)

The overall reaction is given by

$$SO_2 + OH + M \stackrel{k_3}{\rightarrow} HSO_3 + M$$
, (3)

where M is a third body. The third-order rate constant, k₃, is given by

$$k_3 = \frac{k_1 k_2}{k_{1r} + k_2 [M]}$$

Experiments were carried out over the pressure range 20 to 1000 torr and the temperature range -20° to 24°C. A plot of k₃-1 versus pressure was found to be linear in accordance with the above relationship.

A least-squares analysis of the data obtained at 24°C gave 7.1×10^{-13} cm³ molec⁻¹ sec⁻¹ for k_1 . The ratio of k_1k_2/k_{1r} is 1.6×10^{-31} cm⁶ molec⁻² sec⁻¹. The effective bimolecular rate constant measured at 760 torr and 24°C with N_2 as the third body is 6.0×10^{-13} cm³ molec⁻¹

sec⁻¹; this is in exact agreement with the value recently reported by Cox (1974/5).

Temperature studies yielded an activation energy of -2.8 kcal/mole for the termolecular reaction (3). A value of 1.7×10^{-12} cm³ molec⁻¹ sec⁻¹ is obtained as the effective bimolecular rate constant, k_3 [M], for the stratospheric conditions (220°K at 15 km elevation) to be used in later calculations.

Reactions of NO2 with SO2

Because of interest in both the NO_x and the sulfur cycles in the atmosphere, the possibility of coupling between these cycles was examined in exploratory experiments for the $(NO_2 + SO_2 + H_2O)$ system. These experiments were performed in a 14-liter glass reaction vessel which could be cooled to stratospheric temperatures (-50°C) by a methanol bath. A Pyrex window allowed irradiation of the flowing reactant, and aerosol formation was monitored by a condensation-nuclei counter.

In the dark, no aerosol formation was observed. Irradiation of NO2 in nitrogen carrier gas, and of NO₂ + H₂O in carrier, also gave no product. Irradiation of SO₂ in carrier at high relative humidity did produce some aerosols. Addition of NO₂ (under the same conditions) considerably enhanced the aerosol formation. For another series of photochemical experiments, the effect of individual constituents upon aerosol production was investigated by maintaining a constant concentration of one of the constituents (either SO2 or NO2) and observing the aerosol production as a function of addition of the other reactant. A plot of aerosol concentration versus SO2 addition at constant NO2 (14 ppm) was found to be essentially linear above ≈ 2 ppm. Other experiments were made in which the SO₂ was held constant at 15 ppm and the aerosol concentration monitored as a function of NO2 addition. These data showed aerosol formation to result at concentrations above 1 ppm NO2, and to be independent of the NO2 concentration at values above 9 ppm.

These results are consistent with either of two mechanisms: the SO₂ becomes photoexcited and reacts with NO₂ to form an aerosol, or NO₂ is photodissociated and the O atom reacts competitively with NO₂ and with SO₂ to form SO₃.

In order to elucidate the mechanism, aerosol formation was studied as a function of irradiation wavelength and intensity. Glass cut-off filters were used to establish that wavelengths less than 380 nm were responsible for the particle production. Aerosol number did not increase linearly with light intensity. Rather, the percentage increase of number concentration diminished as the intensity was raised.

The wavelength dependence of the aerosol formation indicates that photodissociation of NO₂ to NO + O could be an important process in the enhancement of SO₂ oxidation by NO₂. In other experiments, either oxygen or NO was added in order to scavenge the O atoms. Addition of either reactant at the part-per-thousand level reduced the observed aerosol formation, suggesting that O atoms play a role in a homogeneous gas-phase initiating process.

Efforts to sample the aerosol product with a thermal precipitator were unsuccessful. However, some sampling was successfully implemented by placing grids directly in the product stream. The collected material was examined by electron microscopy, and a small number of particles $\approx 1~\mu m$ in size were observed. This material was unstable to the electron beam and behaved as if it were liquid. In addition, shadowing of the grids showed that the surface had a uniform covering of material $\approx 50~nm$ in diameter. The collected material has not yet been definitely characterized and analyzed.

A second measure of the aerosol size was obtained using a Sinclair (described in Sinclair, 1972) portable diffusion battery. This instrument consists of several stainless-steel discs of varied thickness mounted in series. Each disc contains several thousand accurately sized and collimated holes; as the sample flows through this assembly, particles are deposited according to size on the walls of the holes. Sinclair has calculated the loss of particles as a function of distance along the assembly for particles of different sizes. The data obtained in the present study indicated that all the aerosol particles were under 30 nm and most were under 20 nm in diameter.

The Reaction of Water with SO 3

Following the gas-phase oxidation of SO₂ to SO₃, two alternate reaction channels are envi-

sioned for the conversion of SO_3 to H_2SO_4 : one involves a direct gas-phase reaction with H_2O , and the other involves a surface reaction as SO_3 is scavenged by a pre-existing aerosol particle. The former process has the potential for new particle formation, while the latter would merely serve to alter the size spectrum of the pre-existing aerosol distribution. An assessment of the importance of these competing processes depends upon knowledge of the gas-phase reaction rate, and we have undertaken the necessary measurements to fulfill this need.

The reaction rate of the homogeneous gasphase reaction

$$H_2O + SO_3 \stackrel{M}{\rightarrow} H_2SO_4$$
 (or analogous adducts),

where M is a third body, has been measured by fast-flow techniques. Details of the apparatus as well as the investigation have been published previously (Castleman et al., 1976). At a total pressure of 1.3 Torr and a temperature of 300K, and with N_2 as the carrier gas, the value obtained for the pseudo-bimolecular rate constant is $(9.1 \pm 2.0) \times 10^{-13}$ cm³ molec⁻¹ sec⁻¹.

The observed rate for the reaction of SO₃ and H2O is surprisingly fast. If the reaction were termolecular at 1.3 torr, the apparent threebody rate constant would be 2.2 × 10-29 cm6 molec-2 sec-1. This is much faster than would be expected, since the formation of H2SO4 would be likely to proceed via a four-center intermediate complex. However, the reproducibility of the data, and the correspondences obtained by varying several different experimental parameters, indicated that the reaction was taking place in the gas phase. (It has been suggested that the observed reaction product (m/e = 98) may not be molecular H2SO4 but an adduct H2O·SO3. Definitive proof of this possibility must await a detailed structural study, but indirect evidence for the existence of an adduct with a small binding energy has been obtained and will be reported elsewhere.)

Subsequently, preliminary experiments were performed and acid-water clusters were observed. These clusters are expected to serve as the prenucleation embryos in the heteromolecular nucleation (Castleman, 1974) of the gas-phase molecules to sulfuric-acid aerosols.

Formation of H₂SO₄ Aerosols

If the SO_3 molecules formed from SO_2 oxidation were totally scavenged by pre-existing particles before reacting with H_2O to form H_2SO_4 , there would be no possibility that new particles could be formed from the heteromolecular nucleation of sulfuric acid in a moist environment. Consequently, the oxidation of SO_2 in the atmosphere would serve only to modify the size spectra already existing. Alternatively, if the rate of reaction with water vapor is faster than the maximum rate of scavenging by particles, H_2SO_4 molecules will form and there is a potential for the nucleation of sulfuric-acid aerosols.

If complete accommodation of the molecules colliding with a surface is assumed, the maximum SO_3 removal rate by existing particles may be estimated from the collision frequency. Likewise, the reaction rate given for SO_3 and water vapor may be used to assess the rate of SO_3 consumption by direct reaction to H_2SO_4 . Utilizing our data, we estimate the ratio of the gas-phase to the particle-removal processes to be 1.5×10^5 under stratospheric conditions.

With our recent results for the oxidation of SO_2 via OH, the possibility of the heteromolecular nucleation of H_2SO_4 being an important process in the stratosphere can be assessed. In setting up the steady-state model for the stratosphere, the SO_2 concentration was taken as 1 ppb and [OH] as 10^6 molec cm⁻³. Particle scavenging was assumed to be the only removal process for gaseous H_2SO_4 . This leads to a steady-state H_2SO_4 partial pressure of 2.3×10^{-9} torr.

The theory of heteromolecular nucleation is not sufficiently advanced to permit quantitative consideration of the nucleation of H₂SO₄ - H₂O solutions. Nevertheless, the likelihood of particle formation can be preliminarily assessed from a knowledge of the supersaturation ratio of the vapor species, compared to that for the stable condensed phase. In almost all cases, nucleation occurs for supersaturations in the range 5-7, and rarely do supersaturation ratios exceed 20; at such high values, nucleation to the condensed phase always results.

Experimentally determined vapor pressures over aqueous solutions of sulfuric acid are not

available for the temperature and composition range of stratospheric interest. The calculations by Vermeulen and Gmitro (Gmitro and Vermeulen, 1964) are probably the most extensive source of extrapolated data currently available, and have been employed in making the following estimates. If a typical stratospheric temperature of -50°C is taken, a 70% $\rm H_2SO_4$ solution is in equilibrium with a partial pressure of 5.02×10^{-14} torr $\rm H_2SO_4$, and 8.16×10^{-4} torr $\rm H_2O$. The latter represents a mixing ratio of 6×10^{-6} for $\rm H_2O$, which is slightly higher than the accepted 1-3 ppm.

On the basis of the above analyses, the supersaturation value is greater than 104 and it is likely that nucleation of H2SO4 will occur in the stratosphere, thereby contributing to the production of new sulfuric-acid aerosols. Note that here the value of the supersaturation has been calculated with respect to the stable condensed phase, and the scavenging of the acid molecules by pre-existing particles has already been taken into consideration. Clearly the estimates must be refined as the development of the molecular theory of nucleation progresses. Furthermore, the possibility that the newly formed Aitken-size particles might coagulate with the pre-existing atmospheric aerosols must be considered in assessing specific situations.

CONCLUSIONS

The results of our assessment of the importance of heterogeneous chemistry to stratospheric processes indicate that the following items warrant attention in laboratory studies:

- the rate of formation of HCl from the NaCl · H₂SO₄ reaction.
- the rate of HNO₃ formation from N₂O₅ and H₂O contained in sulfuric-acid aerosols.
- the potential for the catalytic destruction of O₃ on pre-existing metal-oxide surfaces.
- the termination reactions of the free radicals HO₂, OH, and Cl on aerosol surfaces.
- the role of HNO₃ vapor in promoting the nucleation of the ternary system involving H₂SO₄ and H₂O, and the

related possibility that such ternary solutions partially contribute to a limitation of the vapor-phase concentration of HNO₃.

the oxidation of SO₂ by oxidants adsorbed on particle surfaces.

ACKNOWLEDGMENTS

This research was performed under the auspices of the U.S. Energy Research and Development Administration and was partially financed by the Department of Transportation under an interagency agreement.

REFERENCES

- Bricard, J. and J. Pradel (1966), "Electric charge and radioactivity of naturally occurring aerosol," in Aerosol Science, ed. C.N. Davies, Academic Press, 87-109.
- Castleman, A.W., Jr. (1974), "Nucleation processes and aerosol chemistry," Space Sci. Revs. 15, 547.
- Castleman, A.W., Jr., R.E. Davis, H.R. Munkelwitz, I.N. Tang and W.P. Wood (1976), "Kinetics of association reactions pertaining to H₂SO₄ aerosol formation," in *Proceedings of the Symposium on Chemical Kinetics Data for the Upper and Lower Atmospheres* (Warrenton, VA), pub. Wiley for Int. J. Chem. Kinet., NY, 629.

- Cox, R.A. (1974/75), "The photolysis of nitrous acid in the presence of carbon monoxide and sulfur dioxide," J. Photochem. 3, 291.
- Gmitro, J.I. and i. Vermeulen (1964), "Vapor-liquid equilibria of aqueous sulfuric acid," AlChE J. 10, 740.
- Johnston, H. (1973), University of California, Berkeley: private communication.
- Keefe, D., P.J. Noland and T.A. Rich (1959), "Charge equilibrium in aerosols according to the Boltzmann law," Proc. Royal Irish Acad. 60A, 6.
- Klein, R. (1973), National Bureau of Standards: private communication.
- Sinclair, D. (1972), "A portable diffusion battery," Amer. Ind. Hyg. Ass. J. 33, 729.
- Wood, W.P., A.W. Castleman, Jr. and I.N. Tang (1975), "Mechanisms of aerosol formation from SO₂," J. Aerosol. Sci. 6, 367.

CAN IONS CONTRIBUTE TO STRATOSPHERIC AEROSOL FORMATION?

VOLKER A. MOHNEN

Atmospheric Sciences Research Center State University of New York at Albany Albany, New York

ABSTRACT: The available mechanisms for particle initiation and growth in the stratosphere are reviewed, and the possible roles of ions in these mechanisms are examined. It is concluded that the average ion population does not significantly influence aerosol formation processes in the unperturbed stratosphere.

AEROSOL INITIATION

Aerosol can be introduced into the stratosphere (1) by direct transport from the troposphere (including volcanic injection), (2) as a result of downward flux of meteoritic material, or (3) by gas-to-particle conversion processes occurring in the stratosphere. The most widely accepted explanation for the existence of a sulfate particle layer in the stratosphere ("Junge layer") is that most of the sulfate is produced in situ by the oxidation of sulfur dioxide into sulfuric acid, which then undergoes a phase transition to yield sulfuric-acid droplets, It is believed today that gaseous sulfur compounds (mainly sulfur dioxide) reach the lower stratosphere both by continual diffusional transport and by sporadic, direct volcanic injections. There is, furthermore, very good evidence indicating that the variability in the sulfate concentration in the lower stratosphere is due to volcanic activity. The principal initiating reaction responsible for sulfur dioxide's eventual oxidation to sulfuric acid in the stratosphere is thought to be:

$$SO_2 + OH + M \xrightarrow{k} HSO_3 + M$$

with $k = (2 \text{ to } 5) \times 10^{-31} \text{ cm}^6 \text{ sec}^{-1}$

(Davis and Klauber, 1975; Castleman, 1974). Other initiating reactions involving $O(^3P)$, $O_2(^1\Delta)$, HO_2 , NH_3 , CH_3O_2 , direct photooxidation, etc. have been dismissed since they do not significantly contribute to sulfuric-acid formation.

The subsequent steps HSO₃ → H₂SO₄ have not been identified and established yet and, until proven otherwise, the initiating step $SO_2 + OH$ is assumed to be rate-determining for the formation of surfuric acid.

The gas-to-particle conversion process (phase transition) for sulfuric acid can be initiated via two main mechanisms:

- Homogeneous, heteromolecular nucleation
 - as binary system H₂SO₄ + H₂O
 - as ternary or multicomponent system such as H₂SO₄ + HNO₃ + H₂O
 - as "ion nucleation"
- Heterogeneous, heteromolecular nucleation
 - on the surface of preexisting "sulfate particles" (radius $> 0.1 \mu m$)
 - on the surface of preexisting Aitken particles (radius > 500 nm)
 - on the "surface" of ions (ion growth).

Further growth into the particle size range typically found in the "Junge layer" (0.1 < R < 1 μ m) occurs via heteromolecular condensation. The relative importance of these two conversion processes cannot be established with certainty at present from experimental data gathered in the stratosphere or deduced from laboratory experiments.

Various models have been developed which focus on one or several critical physical and/or chemical processes in an attempt to explain

MOHNEN

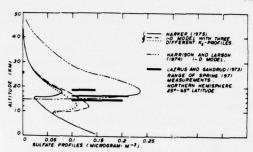


Figure 1. Stratospheric surfate profiles for two models, together with actual measurements.

Harker profiles

Chemistry of the stratosphere has reached steady state. Sulfur dioxide mixing ratio fixed at 0.2 ppbv and $[SO_2]/[SO_4^-] = 3.3$ at the tropopause. Three different vertical K_Z profiles are used (all within the range indicated in Figure 2).

Case 1: tropopause fixed at 15 km (K_z from Wofsy and McElroy)

Case 2: tropopause fixed at 10 km (K_z from Chang)

Case 3: tropopause fixed at 10 km (K_z from Hays and Olivero)

Sources:

A.B. Harker (1975), J. Geophys. Res. 80, 3399.

J. Chang (1974), in Proceedings of the Third Conference on CIAP, Dept. of Transportation, DOI-TSC-OST-75-14, 330-341.

P.B. Hays and J.J. Olivero (1970), Planet. Space Sci. 18, 1729.

S.C. Wofsy and M.B. McElroy (1973), J. Geophys. Res. 78, 2619.

Harrison and Larson profile

Sulfur dioxide mixing ratio fixed at 1 ppbv and $[SO_4^-] = 0$ at the tropopause. Tropopause fixed at 15 km, K_z constant (5000 cm 2 s $^{-1}$) above tropopause. Specifies 3×10^8 molecules cm $^{-2}$ s $^{-1}$ upward flux of SO_2 through tropopause.

Source:

H. Harrison and T. Larson (1974), J. Geophys. Res. 79, 3095-3097.

Lazrus and Gandrud measurements

Aircraft measurements of sulfate concentrations for spring 1971. Bars indicate the approximate range of SO_{4}^{-} at 15, 17, and 19 km altitudes (25°-65° latitude).

Source:

A.L. Fazrus and B.W. Gandrud (1973), "Progress Report on Systematic Study of Stratospheric Aerosol," NCAR, Boulder, CO.

It should be noted that both of the models imply a gas-to-particle conversion process:

$$SO_2 + OH \xrightarrow{(M)} HSO_3 \xrightarrow{?} H_2SO_4 (gas)$$

They do not, however, specify the aerosol-formation process itself.

experimentally well-established features of the stratospheric sulfate layer. For example:

- One-dimensional diffusion models combined with gas-phase chemical kinetics but disregarding phase-transition processes (Harrison and Larson, 1974, and Harker, 1975).
- Homogeneous and heterogeneous nucleation and condensation models combined with limited chemical kinetics but disregarding transport processes (Kiang et al., 1973; Stauffer et al., 1973; Yue et al., 1975; Hofmann et al., 1975).

Both types of models in turn rely heavily upon stratospheric chemical-modeling efforts that predict the concentration of trace constituents such as OH. Furthermore, crucial assumptions have to be made in both types of model as to physical and chemical state of the atmosphere.

Figure 1 shows the results from diffusion models and their sensitivity to changes of boundary conditions (tropopause height, concentration of sulfur compounds near the tropopause, etc.) and vertical eddy-diffusion profiles (see Figure 2). Also included in Figure 1 is the approximate range of stratospheric sulfate measurements as reported by Lazrus and Gandrud (1973) for spring 1971. Through changing those uncertain atmospheric parameters, the model can be "adjusted" to agree with experimental observations. The models predict steady-state maximum sulfate concentrations of 0.08 to $0.27 \mu g \text{ m}^{-3}$ (ambient) or, more accurately, the predictions

MOHNEN

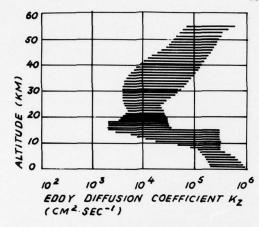


Figure 2. Range of vertical diffusion coefficients used in models. Horizontal bars indicate the range of K₂.

Sources

- J. Chang (1974), in Proceedings of the Third Conference on CIAP, Dept. of Transportation, DOT-TSC-OST-74-15, 330-341.
- P.J. Crutzen (1974), Can. J. Chem. 52, 1569-1581.
- E. Hesstvedt (1974), Can. J. Chem. 52, 1592-1598.
- D.M. Hunten (1974), quoted in A.J. Grobecker, S.C. Coroniti, and R.H. Cannon, Jr. (1974), Report of Findings: The Effects of Stratospheric Pollution by Aircraft, Climatic Impact Assessment Program, U.S. Dept. of Transportation, DOT-TST-75-50.
- T. Shimazaki and T. Ogawa (1974), J. Geophys. Res. 79, 3411-3423.
- R.W. Stewart and M.I. Hoffert (1975), J. Atmos. Sci. 32, 195-210.
- R.C. Whitten and R.P. Turco (1974), AIAA J. 12, 1110-1117.
- S.C. Wofsy and M.B. McElroy (1973), J. Geophys. Res. 78, 2610-2624.

are for sulfuric acid concentrations of 5.1×10^7 molecules cm⁻³ (at 18 km), 1.8×10^8 molecules cm⁻³ (at 12 km), 2.2×10^8 molecules cm⁻³ (at 12 km), and 1.9×10^8 molecules cm⁻³ (at 17.5 km). These sulfuric-acid molecules are assumed (without specifying the conversion process) to be converted immediately into the condensed phase.

Some basic results of model calculations dealing with gas-to-particle conversion processes

are shown in Figure 3. There are several crucial assumptions in these model calculations which have not yet been fully verified by laboratory measurements. They all influence the rate of formation of new particles - for example, vapor pressure over binary or ternary solutions, or surface tension of embryonic droplets. However, order-of-magnitude estimates can be made, and, in conjunction with sensitivity tests, a confidence limit for the accuracy of predictions can be set (Kiang et al., 1975). In general, those model predictions eliminate the "classical" binary phase-transition process of H₂SO₄ + H₂O as a mechanism responsible for aerosol formation. The critical sulfuric acid concentration required for homogeneous binary nucleation would be of the order of 3.7×10^8 molecules cm⁻³. This concentration is higher than the maximum concentration attainable in the stratosphere under steady-state conditions, as predicted by diffusion models. Underlying these models is the assumption that the vapor pressure over pure sulfuric acid solution is 10⁻⁶ Torr (at 25°C), one of the lowest reported in the literature. Conditions for nucleation will be even less favorable for higher vapor pressures. More likely, the H2SO4 molecules will condense on preexisting particles as indicated in Figure 3. Even if the available total surface area per cubic centimeter decreases from 4.5×10^{-8} cm² cm⁻³ (Castleman et al., 1975) to 4.5×10^{-9} cm² cm⁻³ (corresponding to $0.03 \mu g$ m-3), homogeneous binary nucleation doesn't play a dominant role. Another aerosol formation mechanism is suggested by the fact that some of the preexisting stratospheric aerosol comes from extraterrestrial sources. Newkirk and Eddy (1964) have estimated the relative concentration of meteoritic debris in aerosols (at 20 km) and concluded that, over a size range of 0.1 to 2 µm radius, it represents less than 10%. A completely "particle-free" (R > 0.1 μ m) stratosphere is therefore an unreasonable assumption.

Most likely, however, the gas-to-particle conversion will occur via ternary nucleation involving $H_2SO_4 + HNO_3 + H_2O$. This process assumes that an $\approx 70\%$ $H_2SO_4 + \approx 10\%$ $HNO_3 + \approx 20\%$ H_2O solution constitutes an optimum mixture for which the total vapor pressure of droplets is drastically reduced. If the estimated thermodynamic parameters entering the ternary system (vapor-pressure and surface-tension data) are correct, then this aerosol formation mechanism

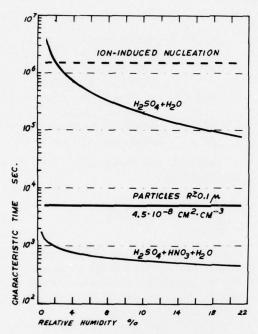


Figure 3. Characteristic times for binary and ternary nucleation and for heterogeneous condensation on preexisting particles as function of relative humidity. (Temperature, -55°C; altitude, ≤ 20 km.)

H₂SO₄ + H₂O curve

Equilibrium water-vapor pressure, 3×10^{-2} Torr; actual water-vapor mixing ratio, 3.5 ppmv. Rate of formation of H_2SO_4 from SO_2 :

$$-\frac{d[SO_2]}{dt} = k \cdot [SO_2][OH][M] \rightarrow \frac{d[H_2SO_4]}{dt}$$

[SO₂] $\lesssim 0.2$ ppby; [OH] = 6×10^5 cm⁻³; k = 3×10^{-31} cm⁶ s⁻¹; [M] = 1.85×10^{18} cm⁻³. Therefore, production rate for H_2SO_4 is $c_B \approx 125$ molecules cm⁻³. Composition of stable embryonic droplet $\approx 80\%$ H_2SO_4 , $\approx 20\%$ H_2O . Critical size of stable embryo: 60-70 nm. Vapor pressure of H_2SO_4 over pure solution 10^{-6} Torr. H_2SO_4 gas-phase concentration required for the binary nucleation process to occur is $\approx 3.7 \times 10^8$ molecules cm⁻³ (at 1% relative humidity, decreasing with increasing relative humidity). For further details, see G.K. Yue, C.S. Kiang, V.A. Mohnen, and E. Danielsen (1975), "The Interaction of Atmospheric Sulfur Compounds with Cloud and Precipitation Elements," interim report to NSF, Atmospheric Sciences Research Center Pub. No. 365, State Univ. of N.Y., Albany, NY.

$$H_2SO_4 + HNO_3 + H_2O$$
 curve

All parameters are the same as in the binary system. Critical composition of stable embryonic droplet is $75\%~H_2SO_4$, $10\%~HNO_3$, $20\%~H_2O$. Under those conditions, the partial vapor pressures for this ternary system are estimated to be 10^{-13} , 10^{-9} , and 10^{-7} Torr respectively. The minimum concentration of H_2SO_4 required for this ternary homogeneous nucleation process is of the order of 2×10^5 molecules cm⁻³ (for 1% relative humidity). For further details see "The Interaction of Atmospheric Sulfur Compounds with Cloud and Precipitation Elements" cited above.

Particles

It is assumed that the preexisting "Junge layer" contains 0.3 μg m⁻³ of particulate matter with an average size of R $\approx 0.1~\mu m$, a particle density of $\rho = 2~g$ cm⁻³, and a total number concentration of around 40 cm⁻³. This leads to a total surface area per unit volume of A = 4.5 \times 10⁻⁸ cm² cm⁻³. Deposition of H₂SO₄ molecules on these preexisting particles ("condensation") is proportional to the surface area (this condition is fulfilled for all particles with R < 0.3 μ m). The sticking coefficient is assumed to be one. The characteristic time is then defined by

$$\tau_{\text{particle}} \approx \left(\frac{kT}{2\pi m} \right)^{-1/2} \times A^{-1}$$

where

k: Boltzmann constant

T: absolute temperature

m: mass of impinging gas molecule, here H₂SO₄

 $A = \frac{3x}{R\rho} \times 10^{-8} \text{ cm}^2 \text{ cm}^{-3}$

χ: particulate matter concentration in μg m⁻³

 ρ : density in g cm⁻³

R: particle radius in micrometers

(Note that $\tau_{\text{particle}} \approx A^{-1}$, so a tenfold decrease in specific surface area will result in a tenfold increase in characteristic time.) (For further information, see the report cited above.)

Definition of characteristic time:

 $\tau_{\text{nucleation}} = \frac{\text{Minimum H}_{2}\text{SO}_{4} \text{ concentration}}{\text{required for homogeneous}}$ $\frac{\text{nucleation}}{\text{Production rate of H}_{2}\text{SO}_{4}}$

would be favored against any other process put forth to date. Current information seems to indicate sufficiently high HNO₃ and H₂O concentrations in the stratosphere. The critical concentration of H₂SO₄ required for this ternary nucleation process is less than 10⁵ molecules cm⁻³. This rather low concentration for aerosol initiation would warrant a constant source for

MOHNEN

stratospheric particles. This $\rm H_2SO_4$ concentration is also at least one order of magnitude lower than required by Hofmann et al. (1975) for their proposed heterogeneous-condensation model. It involves Aitken nuclei diffusing from the troposphere into the stratosphere and encountering a gaseous sulfuric acid layer (106 $\rm H_2SO_4$ molecules cm⁻³ max) between 16 and 22 km altitude. Condensation of $\rm H_2SO_4$ on those Aitken particles then leads to particle sizes and concentration profiles as found in the "Junge layer."

IONS

The above attempt to summarize the current opinions on stratospheric aerosol formation processes constitutes a necessary prerequisite for critically assessing the role of ions in this important aspect of stratospheric chemistry. It has become obvious that most of our understanding of stratospheric aerosol formation leans heavily on model predictions. Models have not yet been fully validated for the stratosphere, and hence contain physical and/or chemical parameters that might be quite different from reality.

Our understanding of stratospheric ion chemistry is incomplete; it is mostly derived from laboratory experiments and ionospheric research work, and not yet validated by stratospheric in-situ measurements. It is within this framework of uncertainty that the role of ions in stratospheric chemistry (aerosol formation) is being discussed and compared — on a competitive basis — with homogeneous and heterogeneous reactions of the electrically neutral atmosphere.

The formation and nature of ions of atmospheric importance has been summarized by Mohnen (1971, 1974) and Ferguson (1975). The evolution and final composition of atmospheric ions strongly depend upon their collisional interaction with the neutral atmosphere, and thus become a function of altitude (and temperature). The equilibrium concentration of ions is governed by a budget equation:

$$\frac{dn^{(+ \text{ or } -)}}{dt} = q - \alpha n^{+} \cdot n^{-} - n^{(+ \text{ or } -)}$$

$$\cdot \int_{R_{min}}^{R_{max}} \beta(R) \cdot f(R) dR$$
(1)

where:

n^(+ or -): ion concentration q: ion formation rate

α: recombination coefficient for positive and negative ions

 $\beta(R)$: ion annihilation coefficient with

atmospheric aerosol f(R): aerosol size-distribution function

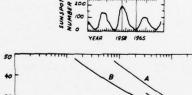
R: radius of aerosol particles

Zikmunda and Mohnen (1972) have evaluated the integral

$$\int_{R_{min}}^{R_{max}} \beta(R) \cdot f(R) dR$$

for the stratosphere and found it to be much smaller than the ion loss due to recombination for the unperturbed stratospheric particle load. The ion formation rate q, derived from cosmic radiation, is shown in Figure 4.

Typical values between 20 and 50 ion pairs cm⁻³ sec⁻¹ can be expected within the altitude range of 10-20 km, with a maximum around 12 km. The recombination coefficient is of the



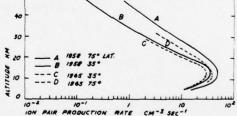


Figure 4. Recent history of solar sunspot activity, and calculated cosmic-ray-induced ion-pair production rates.

Sources:

R.D. Hake, E.T. Pierce, and W. Viezee (1973), "Stratospheric Electricity," final rept. on Project 1724, Stanford Research Inst., Menlo Park, CA.

H.V. Neher (1971), J. Geophys. Res. 76, 1637-1651.

M.A. Ruderman and J.W. Chamberlain (1975), Planet. Space Sci. 23, 247-268.

order of 1 × 10-6 cm³ sec-1, which leads to average ion equilibrium concentrations $n = (q/\alpha)$ $\exp (1/2)$ of $4400 < (q/\alpha) \exp (1/2) < 7000$ ions cm⁻³. Actual measurements in the stratosphere (summarized by Hake (1973)) reveal ion profiles that follow the ionization profile and fall within the concentration range of 1000 to at most 10,000 ions cm⁻³. To assess the possible role of ions, we will assume two ion concentration values, $n = 1000 \text{ cm}^{-3}$ and $n = 5000 \text{ cm}^{-3}$, and thus cover minimum and average conditions. The average lifetime (e-1 value) of ions in the stratosphere thus becomes 1000 s and 200 s respectively. As mentioned earlier, the chemical composition of ions depends upon the gas composition and the "reactivity" of these molecules with particular ion species. The average stratospheric concentration profiles for gases, particles (large particles and condensation nuclei or "Aitken particles"), and ions are illustrated in Figure 5. Conceivably, ions can alter their chemical nature as they collide with neutral gas molecules. From this emerges the concept of initial ions → intermediate ions → terminal ions. The boundary condition, that there is a limited average lifetime for ions, determines the minimum concentration level for which ion-molecule interactions can occur. Assuming an ion-molecule reaction-rate constant of 5 × 10-10 cm³ sec-1 fixes this lowest trace-gas concentration at 3 X 106 molecules cm-3 (for a 1000-s average ion lifetime), as indicated in Figure 5. For a more detailed consideration, measured reaction-rate constants for a specific ion-molecule process should be used. Those rate constants available to date have been compiled by Ferguson (1975).

Our current understanding of the nature of positive ions at 20 km altitude, as derived from measured reaction-rate constants and measured and/or estimated stratospheric molecular concentrations (Table 1), is that the terminal ion is predominantly of the type $H_3O^+ \cdot (H_2O)_n$ with $n = 4 \ (\approx 0.4\%), n = 5 \ (\approx 35\%), n = 6 \ (\approx 60.6\%),$ and n = 7 (4%). One can expect, due to the high collision frequency, nitrogen molecules to be also clustered about these terminal ions. One of the unresolved problems in stratospheric ion chemistry concerns the amount of gaseous ammonia present in the stratosphere, which is of interest because it reacts via proton transfer with the hydronium ion to form mixed clusters of the type NH₄ (NH₃)_m·(H₂O)_n (this type of ion constitutes the predominant terminal-ion core in the lower troposphere). If the ammonia concentration in the stratosphere is below 3×10^6 , then no collisional interaction occurs, on the average.

For negative ions, the transition from initial ions to terminal ions is considerably more complicated than that for positive ions and involves almost every molecular species listed in Figure 5. The *simplified* ion evolution sequence valid in the stratosphere is currently thought to be (Ferguson, 1975):

Electron
$$\rightarrow O_{2}^{-} \xrightarrow{[O_{2}]} O_{4}^{-} \xrightarrow{(H_{2}O)_{1,2}} O_{2}^{-} \cdot (H_{2}O)_{1,2}$$

$$[H_{2}O] \longrightarrow O_{2}^{-} \cdot (H_{2}O)_{n} \xrightarrow{[O_{3}]} O_{3}^{-} \cdot (H_{2}O)_{m}$$

$$[CO_{2}] \longrightarrow 10^{-6} \text{s} \qquad CO_{3}^{-} \cdot (H_{2}O)_{k} \xrightarrow{[NO_{2}]} NO_{3}^{-} \cdot (H_{2}O)_{i}$$

$$[HNO_{3}] \longrightarrow 1 \text{s} \qquad NO_{3}^{-} \cdot (H_{2}O)_{j} \quad [clustered molecules]$$

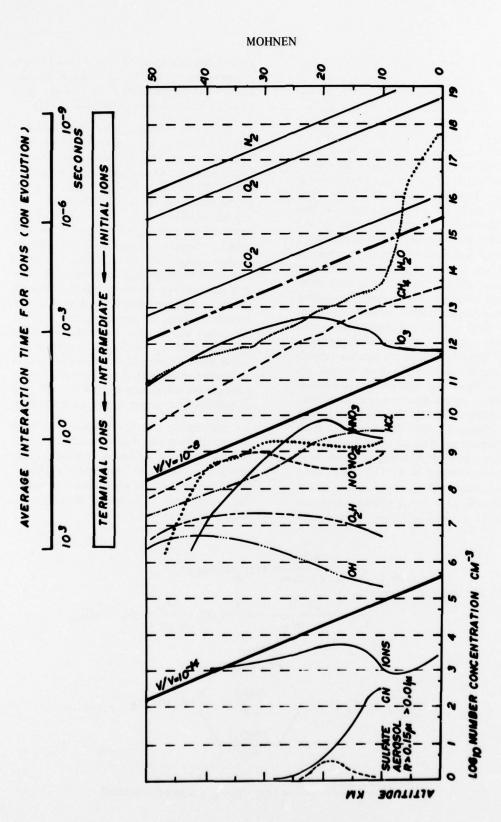


Figure 5. Ion interaction times, and profiles of atmospheric constituents.

Table 1. Average Conditions in Stratosphere (20 km altitude)

Trace Gas	Trace-Gas Concentration (molecules cm ⁻³)	Characteristic Ion Interaction Time ^f (seconds)	No. of Collisional Interactions During Average Lifetime of Ion ^g	
			For 1000 Ions cm ⁻³	For 5000 Ions cm ⁻³
O2ª	3.9×10^{17}	5 × 10 ⁻⁹	2 × 10 ¹¹	4 × 10 ¹⁰
CO ₂ a	5.9×10^{14}	2.9×10^{-6}	3.4×10^{8}	6.8×10^{7}
H ₂ O ^a	1013	2 × 10 ⁻⁴	5×10^{6}	105
O ₃ a	2.5×10^{12}	8×10^{-4}	1.3×10^{6}	2.6×10^{5}
NO ₂ ^a	1.5×10^{9}	0.75	1.3×10^{3}	2.6×10^{2}
NOa	5 × 10 ⁸	4	250	50
HNO ₃ a	5 × 10 ⁹	0.4	2.5×10^{3}	500
N ₂ O ₅	4×10^6	500	2	<u> </u>
NO ₃	10 ⁵	2×10^{4}	_	_
HCl ^a	2 × 10 ⁹	1	1000	200
CIO.	2×10^{7}	100	10	2
ОН	6 × 10 ⁵	3.3×10^{3}	(0.3)	
O ₂ H	2×10^{7}	100	10	. 2
O(³ P)	3×10^{5}	6.7×10^{3}	(0.15)	
CH ₃ O ₂	1×10^{7}	200	5	1
U	nknown:			
SO ₂ ^b	$< 3.7 \times 10^8$	<5	<200	<40
H ₂ SO ₄ c	$>10^5$ but $<10^8$	<20	<50	<10
NH3 ^d	<<3.10 ⁹	<<1	<<1000	<<200
Particles ^e		2.5×10^3	_	-

a Average of all measured values.

Sources: C.E. Junge (1974), in Proceedings of the International Conference on Structure, Composition and General Circulation of the Upper and Lower Atmospheres and Possible Anthropogenic Perturbations, pub. IAMAP, 85-97.

A.B. Harker (1975), J. Geophys. Res. 80, 3399-3401.

H. Harrison and T. Larson (1974), J. Geophys. Res. 79, 3095-3097.

^b Based on 0.2 ppbv, as assumed by Junge, Harrison and Larson, and Harker for model calculations.

^c Based on an average total sulfate content of 0.25 $\mu g/m^3$ (ambient) collected as aerosol.

^d Value from C.B. Farmer (1974), Can. J. Chem. 52, 1544-1559.

e Ion annihilation time defined as $\tau = 1/\beta N$, where β is the attachment coefficient of ions to particles ($\beta = 10^{-5}$ cm³ s⁻¹ for $R \approx 0.1~\mu m$) and N is the total number of particles (here 40 cm⁻³). Source: J. Zikmunda and V.A. Mohnen (1972), Meteor. Rundschau 25, 10-14.

f Characteristic interaction time is defined by $\tau_c = 1/([\text{trace-gas concentration}] \times \text{rate constant})$. A typical ion-molecule rate constant of 5×10^{-10} cm³ sec is used. It is assumed that temporary or permanent attachment of the trace-gas molecule to the ion occurs, or in some instances an ion-molecule reaction (see text).

g The lifetime τ of ions is defined as follows: dn⁺/dt = $-\alpha$ n⁺n⁻, where n⁺, n⁻ are the concentrations of positive and negative ions/cm³ respectively, and α is the recombination coefficient, here assumed to be of the order of 10^{-6} cm³ s⁻¹. $\tau = 1/\alpha$ n. $\tau \approx 1000$ s for 1000 ions cm⁻³ and ≈ 200 s for 5000 ions cm⁻³.

ION NUCLEATION

Ion-induced nucleation is a well-established laboratory phenomenon in atmospheric sciences, although it does not play any major role in cloud physics in the *lower* part of the troposphere. Ion nucleation occurs principally at a supersaturation ratio *lower* than is required for homogeneous nucleation, because of the reduction in the free-energy barrier.

In the stratosphere, ion nucleation can occur only via heteromolecular nucleation, i.e., nucleation involving two or more gaseous components such as $H_2SO_4 + H_2O$ or $H_2SO_4 + HNO_3 + H_2O$, since the supersaturation ratio normally never reaches (or exceeds) 3.8, the value required for nucleation in a *pure* water system.

The simplified equation describing the free energy for the formation of embryos in a binary (or ternary, with the addition of items in parentheses) system is:

$$\Delta G = -[A] \cdot kT \cdot \ln \frac{P_{[A]}}{P_{[A]}^{\infty}}$$

$$-[B] \cdot kT \cdot \ln \frac{P_{[B]}}{P_{[B]}^{\infty}}$$

$$-\left([C] \cdot kT \cdot \ln \frac{P_{[C]}}{P_{[C]}^{\infty}}\right)$$

$$+4\pi r^{2}\sigma + \frac{Q^{2}}{2r(1-1/\epsilon)}$$
(2)

where:

[A], [B], ([C]): Molecular number concentration; for example, number of molecules of water, sulfuric acid, (nitric acid)

P[A], P[B], (P[C]): Actual partial pressure

of component A, B, (C) above the

 $P_{[A]}^{\infty}$, $P_{[B]}^{\infty}$, $(P_{[C]}^{\infty})$: Saturation partial pressure of A, B, (C) above the mixture

Q: Ion charge, normally one elementary charge

r: Cluster radius

e: Dielectric constant

A general solution of this ion-induced heteromolecular nucleation process as a function of relative humidity is not yet available. However, Castleman and Tang (1972) have extensively studied ion nucleation in a pure water system (unimolecular), and some of their general conclusions can be applied here: The steadystate concentrations of ion clusters do not increase continuously from the small hydrates up to and including the critical (stable) embryo as the supersaturation ratio increases. The existence of a continuously increasing concentration is not a prerequisite to ion clusters' participation in the nucleation process. Conceivably, the free-energy barrier for nucleation can be different for different ion species irrespective of their sign (positive or negative). The structure and bonding of the small ion clusters are the physical and chemical factors leading to the different macroscopically observable values of supersaturation ratios required for different ions. It becomes obvious from the work of Castleman and Tang that the single term $Q/r(1-1/\epsilon)$ cannot adequately describe binary or ternary ion-nucleation systems, and is at the most suitable for obtaining order-of-magnitude estimates.

Keeping these constraints in mind, Wiendl (1974) has estimated the ΔG values (from equation 2) for the clustering of H₂SO₄ + H₂O around ions. The important conclusion that can be derived from this study is that these cluster ions (as found by Castleman (1974) in the pure-water system) do not increase continuously in size up to and including the stable embryo. One can also deduce from Wiendl's results that under stratospheric conditions, the number of H2SO4 molecules clustered to the (positive or negative) ions must be less than three: Wiendl calculated the H₂SO₄+H₂O ion-cluster distribution for 25°C, relative humidity 50%, Ptotal = 760 Torr, PH2SO4 = 10-11 Torr (actual partial pressure; the saturation vapor pressure over pure H₂SO₄ solution was assumed to be 10⁻⁶ Torr), and found that the most probable ion cluster contains two H₂SO₄ molecules with 4 to 12 water molecules attached (peaking at $n_{H_2O} = 9$).

Kiang and Stauffer (1973) have obtained order-of-magnitude estimates for *ion*-induced nucleation rates (based on equation (2)) in the

binary H₂SO₄ + H₂O system and found the minimum H2SO4 concentration required for ion nucleation to be a factor of ten lower than that required without ions, i.e., under stratospheric conditions of the order of 3×10^7 molecules cm⁻³ (at 1% relative humidity, decreasing with increasing relative humidity; see the text to Figure 3). When calculating the characteristic time for ion-induced binary nucleation, one must keep in mind that it depends on the number of ions available: Once the H2SO4 concentration required for ion nucleation has been reached, all ions will simultaneously become "stable embryos" and grow into larger particles. Therefore, the total number of stable embryos is limited to the number of ions present. The size of these critical embryos is in the range of 0.4 to 0.8 nm. Assuming $r_{embryo} = 0.5$ nm leads to a specific surface area of $A = 3 \times 10^{-11}$ cm² cm⁻³ for 1000 ions cm⁻³ and 1.5×10^{-10} cm² cm⁻³ for 5000 ions cm⁻³. This yields (see the text to Figure 3), for 1000 ions cm⁻³,

$$\tau_{\text{ion}} = \left(\frac{kT}{2\pi m_{\text{H}_2\text{SO}_4}}\right)^{-1/2} \times A^{-1} = 6 \times 10^6 \text{ s}$$

and for 5000 ions cm⁻³,

$$\tau_{\rm ion} = 1.2 \times 10^6 \, \rm s$$

The relative-humidity dependence of τ_{ion} matters because it affects the size of the critical (stable) ion embryo, but changes between 1 < r.h. < 20% are not expected to cause a change of more than one order of magnitude in τ_{ion} . Comparing these characteristic times for ioninduced nucleation with the characteristic time for the H₂SO₄+H₂O ion-free system (Figure 3) forces us to the conclusion that ion-induced nucleation does not play a dominant role in stratospheric nucleation. Except at very low humidities, it constitutes the least likely mechanism, and yields orders-of-magnitude higher characteristic times than the condensation process on preexisting particles. If, under perturbed stratospheric conditions, the ion density locally and/or regionally increased by more than one order of magnitude, then ions could compete with the homogeneous binary nucleation. But in order for ion nucleation to become the dominant phase-transition mechanism, a very low atmospheric total particle load (less than 10⁻⁹ cm² cm⁻³) would also have to be postulated.

Whether or not the postulated ternary nucleation process involving H_2SO_4 ($\approx 70\%$) + HNO_3 ($\approx 10\%$) + H_2O ($\approx 20\%$) exists is still uncertain. Unlike the case of the H_2SO_4 + H_2O system, there are as yet no experimental data – from either laboratory simulation experiments or thermodynamic data on vapor pressures – on this ternary system. However, as far as ion involvement is concerned, this unresolved problem has little consequence for the two conclusions made so far on ion-induced nucleation:

- 1. The minimum H₂SO₄ concentration required for the ternary nucleation is of the order of 105 cm⁻³ under stratospheric conditions. During its average lifetime (200-1000 s), an ion would not collide with any H2SO4 molecules, and, therefore, ion nucleation in the stratosphere would have to be treated as a unimolecular process involving H2O only and requiring supersaturation ratios (with respect to water) in excess of 3.8. In principle, for any ion-induced nucleation process involving one or more molecular species (of low volatility) in addition to water, one must postulate that the molecular species is (are) clustered to the ion. This requires a minimum of concentration of at least 3×10^6 molecules cm⁻³. Should the stratospheric concentration of H2SO4 be below this level (as it would be if the ternary H₂SO₄ (70%) + HNO₃ (10%) + H₂O (20%) system exists, since the equilibrium vapor pressure over a mixed-solution droplet of this composition is < 10⁻⁶ Torr), then ion-induced nucleation would not occur at all.
- 2. The boundary condition for ion nucleation is that only as many stable embryos can be formed as there are ions present. This automatically establishes and *limits* the characteristic time $\tau_{\rm ion}$ to $> 10^6$ seconds for ion densities normally present in the *unperturbed* stratosphere.

ION GROWTH

The existence of ion growth is an experimentally well-documented fact in the lower part of the troposphere: Electrical-mobility measurements of small ions seem to correlate well with the "age" of ions; a longer interaction time with the neutral gaseous environment yields lower mobility values. This phenomenon is, of course, easily explainable with the concept of ion evolution (Figure 5), i.e., collisional interaction with various trace gases of lower and lower concentration as the lifetime of the ion increases (Mohnen. 1974). Typical mobility measurements in the lower troposphere reveal a broad, continuous "spectrum" peaking around 1.2 cm² V⁻¹ s⁻¹. The initial ion mobility is usually in excess of 2 cm² V-1 s-1. While ion-mobility measurements do not relate uniquely to the mass of ions, they nevertheless are a good indicator for obtaining some information on the average ion mass. Figure 6 shows these ion-mobility measurements for the stratosphere, ranging from 0.5 to 1.5 cm² V⁻¹ s⁻¹ at 20 km. Whether this spread is real or exhibits artifacts of individual instruments is subject to some debate. Only a very few mobility data are available from the stratosphere. If we assume that the terminal stratospheric positive ion is of the type $H_3O^+ \cdot (H_2O)_n$, with n = 6 and 7 (at 20 km), we get a single mobility value of around 1.75 cm² V⁻¹ s⁻¹ for stp (Mohnen, 1974).

A deviation towards lower values would be indicative of molecules clustered to this core ion. The most likely candidate is, of course, N₂. (Although its clustering ability is very low, the high collision frequency would still allow for some attachment.) In the attempt to assess the existence and importance of ion growth in the stratosphere, simple model calculations based on laboratory measurements are again inadequate. To date, two mechanisms by which ions can grow have been observed:

The usual ion-molecule cluster development, where the cluster size and the nature of clustered molecules reflect

 and are in a pseudo-equilibrium with —
 the surrounding gaseous environment.
 Each molecule is held within the cluster by hydrogen bonding and/or electro

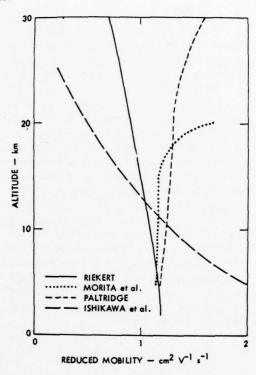


Figure 6. Deduced profiles of positive ion mobility.

Source:

- R.D. Hake, E.T. Pierce, and W. Viezee (1973), "Stratospheric Electricity," final rept. on Project 1724, Stanford Research Inst., Menlo Park, CA.
 - static forces. Cluster growth is limited by the free-energy barrier for nucleation.
 - 2. Chemical reactions that occur between clustered molecules, or chemical reactions between ion clusters and impinging gas molecules whereby the reactant product is incorporated into the ion cluster. Virtually no information is available on this type of ion chemistry except from laboratory experiments by Kadlacek (1974) where ion growth was established in a system containing air and variable amounts of water vapor, ammonia, and sulfur dioxide. The ions that were mass-identified and mobility-analyzed were in general

$$NH_4^+ \cdot (NH_3)_n \cdot (H_2O)_m$$

and

$$NH_4^+ \cdot (NH_3)_i \cdot (H_2O)_j \cdot$$

$$[(NH_3)_2 \cdot SO_2]_k$$

where n,m = functions of [NH₃],[H₂O]. Individual mobility peaks were observed, ranging from 2.46 cm² V⁻¹ s^{-1} (for $NH_4^+ \cdot (NH_3)_{2,3}$) down to 1.17 cm² V⁻¹ s⁻¹ (for NH₄+(NH₃)_{3.4}). $[(NH_3)_2 \cdot SO_2]_4$) and lower. At the same time, some evidence of particle formation of size ≥2.5 nm radius was obtained, the total number of particles being, however, at least two orders of magnitude lower than the ion concentration. For these types of ion-molecule reactions, there appears to exist no energy barrier to cluster growth. As these "crystal-like structured" clusters develop, the addition of more mass enhances the stability of the cluster (Castleman, 1974). McLaren et al. (1974) have determined reaction enthalpies for (NH₃)₂·SO₂ of -45 Kcal mole-1 and -34 Kcal mole-1 in the presence and absence respectively of water vapor.

In a system containing air, ammonia, and hydrochloric acid, Coffey and Mohnen (1972) have found particles to be produced at ammonia concentrations as low as 100 parts per trillion. In the absence of ions, particle formation ceased. They postulated an overall ion reaction scheme NH₄+(NH₃)_i+(H₂O)_i + n HCl → particles as being responsible for the described phenomena. Fehsenfeld (1975) has found, however, that the postulated ion-molecule reaction is endothermic. at least for all i < 3 and j < 2. The exact mechanism of this ion-induced aerosol-formation process is therefore not known at this time. Growth processes involving negative ions and leading to particle formation have not been reported to date - which does not, however, exclude their existence. Conceivably there are other atmospheric trace gases, particularly reactive hydrocarbons, ozone, and oxides of nitrogen, that could undergo a chemical transformation after attachment to the ion cluster and cause it to grow slowly into a larger and more stable complex. The conditions are favorable for such processes in the lower part of the troposphere. (Most of the trace gases mentioned above are present in concentrations exceeding 10^{10} molecules cm⁻³ and hence allow for at least 10^3 collisional interactions during the average lifetime of ions.) But not even there does the average ion grow beyond a mass corresponding to $\approx 1.2 \text{ cm}^2 \text{ V}^{-1} \text{ s}^{-1}$. Ions having a mobility lower than $0.5 \text{ cm}^2 \text{ V}^{-1} \text{ sec}^{-1}$ constitute less than 5% of the total ion population.

In the stratosphere the concentration levels of trace gases, such as NH3, SO2, and reactive hydrocarbons, are considerably lower. As mentioned above in the section entitled "Ions," the average positive or negative ion will not collisionally interact with any molecular constituents having a concentration of less than 3×10^6 molecules cm⁻³. Although the NH₃ concentrations in the stratosphere have not been measured yet, current estimates from various investigators (Crutzen, 1975) tend to be less than 5×10^7 molecules cm⁻³ (20 km). If this is the case, then ion growth due to the (NH₃)₂·SO₂ complex (the only mass-spectrometrically-identified iongrowth process reported to date) is very unlikely to occur in the stratosphere, since it first requires the formation of NH₄ (NH₃)_n core ions. This latter is achievable only if [NH₃] > 10⁹ molecules cm-3. For the same reason, one can exclude the ion-induced NH3-HCl particle formation reaction. Any chemical reaction between OH and ions is also unlikely to occur. (See Table 1 and Figure 5 for the concentration range of OH.)

One can conclude that ion growth leading to larger, more complex, and more stable ions, and eventually to particle formation, is *not* favored in the *unperturbed* stratosphere.

Even if there were yet-undiscovered chemical reaction mechanisms by which ions could grow into particles that are stable *after* the recombination process, their final fate would be coagulation with preexisting particles rather than condensational growth into large "sulfate particles":

$$\tau_{\text{coagulation}} = \frac{1}{K_{1,2}N_1}$$

where

 $K_{1,2}\colon$ coagulation coefficient $\approx\!10^{\text{-}6}~\text{cm}^3$ · $\text{sec}^{\text{-}1}$ for $R_2\approx50~\text{nm}$

N₁: preexisting particles ≥ 1 cm⁻³ for R₁ $\geq 0.1 \mu m$

and thus

$$\tau_{\rm coagulation}$$
: $\lesssim 10^6 {\rm s}$

This characteristic time has to be compared with the characteristic time for condensational growth,

$$\tau_{\rm c} = \left(\frac{{\rm kT}}{2\pi {\rm m}_{\rm H_2SO_4}}\right)^{-1/2} \times {\rm A}^{-1}$$

$$= 2.3 \times 10^8 \,{\rm s}$$

for $A = 2.5 \times 10^{-13}$ cm² cm⁻³ (0.5-nm radius and 100 particles cm⁻³). We assumed here that only a fraction of the total ion population can grow into stable particles (100 cm⁻³). Ion growth mechanisms cannot therefore be responsible for the formation of the "Junge layer."

CONCLUSION AND ACKNOWLEDGMENT

This assessment of the role of ions in aerosol formation in the stratosphere is based on numerous assumptions, model predictions, deductions from processes occurring in other parts of the atmosphere, and, last but not least, rough order-of-magnitude estimates. With those limitations in mind, one can conclude that the impact of the average stratospheric ion population on aerosol-formation processes in the unperturbed stratosphere is not significant.

This work was supported by National Science Foundation Grant DES74-23-856.

REFERENCES

- Castleman, A.W. (1974), "Nucleation processes and aerosol chemistry," Space Sci. Rev. 15, 547-589.
- Castleman, A.W. and I.N. Tang (1972), "Role of small clusters in nucleation about ions," J. Chem. Phys. 57, 3629-3638.

- Castleman, A.W., Jr., R.E. Davis, H.R. Munkelwitz, I.N. Tang, and W.P. Wood (1975), "Kinetics of association reactions pertaining to H₂SO₄ aerosol formation," in *Proceedings of the Symposium on Chemical Kinetics Data for the Upper and Lower Atmosphere* (Warrenton, VA), John Wiley (for Int. J. Chem. Kinet.), New York, 629-640.
- Coffey, P. and V.A. Mohnen (1972), "Ion induced large cluster formation," Bull. Am. Phys. Soc. (Ser. II) 17, 392.
- Crutzen, P. (1975), personal communication.
- Davis, D.D. and Gary Klauber (1975), "Atmospheric gas phase oxidation mechanisms for the molecule SO₂," in Proceedings of the Symposium on Chemical Kinetics Data for the Lower and Upper Atmosphere (Warrenton, VA), John Wiley (for Int. J. Chem. Kinet.), New York, 543-556.
- Fehsenfeld, F.C. (1975), personal communication.
- Ferguson, E.E. (1975), "Ion chemistry of the normal earth's stratosphere," section 5.4 of CIAP Monograph 1, Dept. of Transportation, DOT-TST-75-51, 5-43-5-55.
- Hake, R.D., E.T. Pierce, and W. Viezee (1973), "Stratospheric Electricity," final rept. of Project 1724, Stanford Research Institute (Menlo Park, CA).
- Harker, A.B. (1975), "The formation of sulfate in the stratosphere through the gas phase oxidation of sulfur dioxide," J. Geophys. Res. 80, 3399-3401.
- Harrison, H. and T. Larson (1974), "The oxidation of SO₂ in the stratosphere," J. Geophys. Res. 79, 3095-3097.
- Hofmann, D.J., J.M. Rosen, J.M. Kiernan, and J. Laby (1975), "Stratospheric Aerosol Measurements IV: Global Time Variations of the Aerosol Burden and Source Consideration," Univ. of Wyoming, Dept. of Physics and Astronomy, Tech. Report GM-29.
- Kadlacek, J.A. (1974), "Ion Molecule Reactions of Atmospheric Importance," Interim Report to NSF, ASRC Pub. No. 263, Atmospheric Sciences Research Center, State Univ. of N.Y., Albany.
- Kiang, C.S. and D. Stauffer (1973), "Chemical nucleation theory for various humidities and pollutants," Faraday Symposium 7, 26-33.
- Kiang, C.S., D. Stauffer, V.A. Mohnen, J. Bricard, and D. Vigla (1973), "Heteromolecular nucleation theory applied to gas-to-particle conversion," Atm. Environ. 7, 1279-1283.
- Kiang, C.S., R.D. Cadle, and G.K. Yue (1975), "H₂SO₄-HNO₃-H₂O ternary aerosol formation mechanism in the stratosphere," Geophys. Res. Lett. 2, 41-44.

- Lazrus, A.L. and B.W. Gandrud (1973), "Progress Report on Systematic Study of Stratospheric Aerosol," National Center for Atmospheric Research (Boulder, CO).
- McLaren, E., A. Yencha, J. Kushnir, and V.A. Mohnen (1974), "Some new thermal data and interpretations for the system SO₂-NH₃-H₂O-O₂" Tellus **26**, 1-2.
- Mohnen, V.A. (1971), "Discussion of the formation of major positive and negative ions up to the 50 km level," Pure Appl. Geophys. 84, 141-153.
- Mohnen, V.A. (1974), "Formation, nature and mobility of ions of atmospheric importance," presented at Fifth International Conference on Atmospheric Electricity, Garmisch-Partenkirchen, Sept. 2-7, 1974.
- Newkirk, G., Jr. and J.A. Eddy (1964), "Light scattering by particles in the upper atmosphere," J. Atm. Sci. 21, 35-60.

- Stauffer, D., V.A. Mohnen, and C.S. Kiang (1973), "Heteromolecular condensation theory applied to particle growth," Aerosol Sci. 4, 461-471.
- Wiendl, E. (1974), "Structure of liquid H₂SO₄-H₂O clusters around ions: Thermodynamic theory," presented at the Fifth International Conference on Atmospheric Electricity, Garmisch-Partenkirchen, Sept. 2-7, 1974.
- Yue, G.K., C.S. Kiang, V.A. Mohnen, and E. Danielsen (1975), "The Interaction of Atmospheric Sulfur Compounds with Cloud and Precipitation Elements," interim rept. to NSF, Atmospheric Sciences Research Center, State Univ. of N.Y.—Albany, Report No. 365.
- Zikmunda, J. and V.A. Mohnen (1972), "Ion annihilation by aerosol particles from ground level to 60 km height," Meteorologische Rundschau 25, 10-14.

ENERGY EXCHANGE OF AEROSOLS IN THE STRATOSPHERE

GIORGIO FIOCCO*

Istituto di Fisica Università di Roma Rome, Italy

GERALD GRAMS

National Center for Atmospheric Research**
Boulder, Colorado

ALBERTO MUGNAI

Istituto di Fisica Università di Firenze Florence, Italy

ABSTRACT: The energetic equilibrium of small particles in the stratosphere is summarized, and is shown to be relevant to the perturbed stratosphere.

The energetic equilibrium of small particles in the earth's atmosphere has been considered in some detail by Fiocco, Grams, and Visconti (1975) and by Fiocco, Grams, and Mugnai (1976), hereafter referred to as FGV and FGM, respectively. In this paper those results are summarized and shown to be of particular relevance to the perturbed stratosphere. Aerosols absorb energy from the solar and planetary radiation fields, exchange energy by collisions with the ambient gas, and emit thermal radiation. If changes in phase are possible, particles also lose or acquire latent heat during phase change. Interactions with the radiation field vary significantly with the size and refractive index of the particles and with the spectral density and anisotropy of the radiation. The heat exchanged through collisions is a function of the temperature and density of the ambient gas and of the temperature of the particles. Thus, equilibrium conditions for a given particle size and composition will vary with altitude, as well as with the time of day, season, and planetary albedo. The equation for equilibrium is

where $P_{A_{\odot}}$ is the solar radiation power absorbed by the particle, $P_{A_{pla}}$ is the planetary radiation power absorbed by the particle, P_E is the thermal power radiated by the particle, and P_C is the power lost by the particles because of collisions with the ambient gas.

In evaluating $P_{A_{\odot}}$, we have included both the directly incident solar radiation and the solar radiation backscattered by the surface-atmosphere system because of its albedo, A. $P_{A_{pla}}$ takes into account the thermal radiation emitted by the surface, and the absorption and emission by atmospheric gases (principally O_3 , H_2O , and CO_2).

As a result of the equilibrium described by Eq. 1, the particle temperature, T_p , can be substantially different from the ambient gas temperature, T_g . FGV found the effect to be large above 60 km, with differences $T_p - T_g$ in excess of 100K calculated for the 90-km region in daytime. Differences of this magnitude could account for a substantial increase in the sublimation rates of certain species (Fiocco and Visconti, 1973), for a reduction in the regions of existence of ice particles in the mesosphere, and possibly for an increase in the catalytic efficiency of aerosols in atmospheric chemistry.

$$P_{A_{\odot}} + P_{A_{pla}} - P_{E} - P_{C} = 0$$
 (1)

^{*}Part of this research was carried out while Dr. Fiocco was a Visiting Senior Fellow of the Advanced Study Program, National Center for Atmospheric Research.

^{**}The National Center for Atmospheric Research is sponsored by the National Science Foundation.

The relative contributions of the different terms in the equation of energetic equilibrium were found to vary with altitude and particle size. Each of the terms in Eq. 1 is shown in Figure 1 (taken from FGM) for the altitude interval from 0 to 60 km. These results refer to spherical particles of 0.3 µm radius; in the calculations, the complex refractive index of the particles was specified as a function of the wavelength of the incident radiation, using the model proposed by Ivlev and Popova (1973). The curves in Figure 1 show that significant changes can occur in the fraction of energy absorbed from the radiation field that goes directly into the sensible heat of the ambient gas via molecular collisions. The effectiveness of the particles for heating and cooling the ambient gas varies for different size ranges and at different heights, and it cannot be assumed that all the energy absorbed from the radiation field will heat the local gas.

In Eq. 1, the collisional term P_C leads directly to local heating of the gas surrounding the aerosol particles. Although the energy

emitted by the particles, $P_{\rm E}$, can be reabsorbed by the atmosphere, most of this absorption is likely to take place at large distances from the stratospheric aerosol layer. Contributions from the $P_{\rm E}$ term have not been included in the present calculations.

In Figure 1 the atmospheric conditions are for 45° N July (summer) and 45° N January (winter), as specified in the U.S. Standard Atmosphere Supplements, 1966; the midday results were obtained for albedo values A = 0.3 for the summer and A = 0.5 for winter, representing the average seasonal conditions at 45° N (Raschke et al., 1973). Heating will ensue at all altitudes during the daytime; however, relatively small negative values are obtained in the lower stratosphere under nighttime conditions. Thus, we would expect the sign of the daily average heating rates to be positive throughout the entire region in which the stratospheric aerosol is located.

Figure 2 shows daily average heating rates as a function of size and altitude for summer and

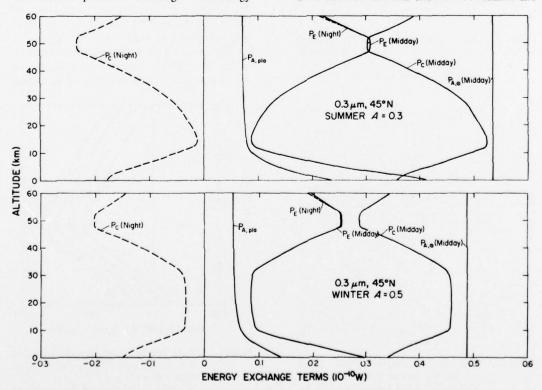


Figure 1. Behavior of energy-exchange terms in Eq. 1 for aerosols with a radius of 0.3 μm (from FGM, 1976).

winter at 45° N. Figure 3 also shows daily average heating rates for the 15° N annual atmosphere as specified in the *U.S. Standard Atmosphere Supplements*, 1966, and for different values of the albedo. Large variations of the heating rate as a function of height, particle radius, and albedo are evident; it is apparent that particles with a radius of about $0.5~\mu m$ would be the most active in heating the ambient gas. In the region of the atmosphere around the stratopause, the aerosols would almost always remove heat, although their concentrations at those heights are normally so small that the process would not be important. In the lower stratosphere where the photochemical heating terms are minimal and where

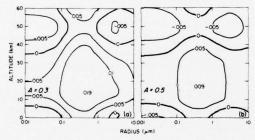


Figure 2. Daily average heating rates (degrees Kelvin per day) for aerosols with a mass mixing ratio of 10^{-9} grams per gram of air for 45° N for (a) summer A = 0.3 and (b) winter with A = 0.5.

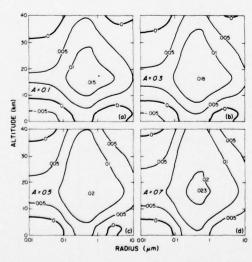


Figure 3. Daily average heating rates (degrees Kelvin per day) for aerosols with a mass mixing ratio of 10^{-9} grams per gram of air for the 15° N annual atmosphere with (a) A = 0.1, (b) A = 0.3, (c) A = 0.5, and (d) A = 0.7.

the aerosols are abundant, aerosols always add heat. The heat exchange varies with albedo; thus a coupling mechanism exists between the surface and the stratosphere which may have effects on the stratospheric climate.

Figures 2 and 3 emphasize the effect of particle size by assuming a monodisperse aerosol. We have also considered a properties aerosol having a power-law size-distribution function in the size interval $r = 0.01 \mu m$ to $r = 10 \mu m$, of the form $dN/d \log r = Cr^{-3}$, where N is the total number of particles with radius less than r and C is the concentration constant that results in a mass mixing ratio of 10^{-9} g (g air)⁻¹.

Figure 4 shows the daily average heating rate for this size distribution as a function of height for different values of the albedo and for the conditions of Figure 3. Figures 2, 3, and 4 apply to a constant aerosol mass mixing ratio, $\nu = 10^{-9}$ g (g air)⁻¹. In the lower troposphere, concentrations often exceed that value; in most other regions, however, they are normally lower. Regarding stratospheric aerosols, it is known that the aerosol mass concentration is variable, and that it often exceeds the above value – especially after major volcanic eruptions.

The distribution with longitude and latitude of the stratospheric temperature increase that was observed after the eruption of Mt. Agung

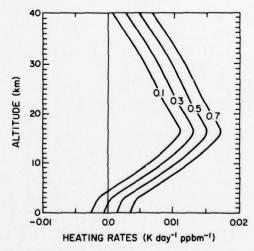


Figure 4. Daily average heating rates (degrees Kelvin per day) for a polydisperse aerosol with a mass mixing ratio of 10⁻⁹ grams per gram of air for the 15°N annual atmosphere and the indicated values of A (see text for details)

(Newell, 1971) is shown in Figure 5. The geographical distribution of temperature differences is highly correlated with the albedo contours published by Raschke et al. (1973), which we have reproduced in Figure 6. Thus, the association of increased heating rates with increased albedo points to a radiative coupling mechanism between troposphere and stratosphere.

The above study was limited to aerosols characterized by the complex refractive index model of Ivlev and Popova (1973). While this model has a more realistic representation of the spectral variability of the complex refractive index than those used by other investigators to date, we plan to make additional calculations

using complex refractive indexes for a number of different solution acceptate that have special significance for the stratospheric aerosol layer, such as sulfuric acid droplets and particles of volcanic ash.

REFERENCES

Fiocco, G., G. Grams, and A. Mugnai (1976), "Energy exchange and temperature of aerosols in the earth's atmosphere (0-60 km)," submitted to J. Atmos. Sci.

Fiocco, G., G. Grams, and G. Visconti (1975), "Equilibrium temperature of small particles in the upper atmosphere (50-110 km)," J. Atmos. Terr. Phys., 37, 1327-1337.

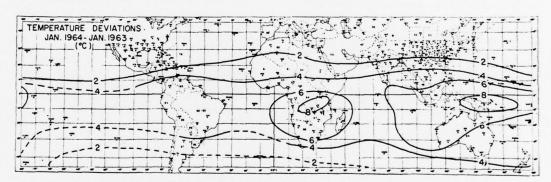


Figure 5. Increase of temperature in January 1964 compared to January 1963 (from Newell, 1971)

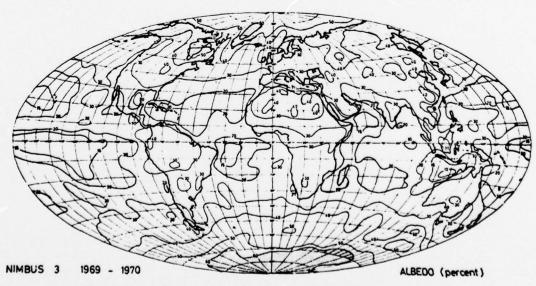


Figure 6. Annual albedo of the earth-atmosphere system (from Raschke et al., 1973).

- Fiocco, G., and G. Visconti (1973), "On the seasonal variation of upper atmospheric sodium," J. Atmos. Terr. Phys. 35, 165-171.
- Ivlev, L.S., and S.I. Popova (1973), "The complex refractive indices of substances in the atmosphericaerosol dispersed phase," Izv. Atmos. and Oceanic Phys. 9, 1034-1043.
- Newell, R.E. (1971). "The global circulation of atmospheric pollutants," Sci. Am. 224, 32-42.
- Raschke, E., T.H. Vonder Haar, W.R. Bandeen, and M. Pasternak (1973), "The annual radiation balance of the earth-atmosphere system during 1969-70 from Nimbus 3 measurements," J. Atmos. Sci. 30, 341-364.

THEORIES OF AEROSOL CHEMISTRY AND OPTICS

DISCUSSION

CICERONE: I would like to make several points. First, I'd like to add something to a chart that Dr. Castleman presented, in which he compared the rates of reaction of certain radicals, atoms, and other gas-phase constituents to possible reaction rates with surfaces. For some problems, such as the chlorine chain, where we don't seem to know of any other chain-terminating steps besides removal from the stratosphere, I think we have to be a little more careful, and compare surface reaction rates to the rate of removal from the stratosphere instead of the rates of other gas-phase reactions.

Second, in regard to Friend's paper, SO₂ is a highly soluble gas, and ground-level sources of such gases have

a hard time competing with fairly large sources injected into the stratosphere. There are some similarities between the sulfur cycle and the odd-nitrogen and odd-chlorine cycles.

Finally, Farmer's ground-level measurements of HCl were a factor of two or three below the levels that others have reported for HCl, 1 ppm. Donald Stedman, a colleague of mine, believes there's a good chance that the previous measurements of HCl at ground level are really upper limits, because of the probability of particle-to-gas conversion in the inlet systems of those various workers' instruments. So I don't think Farmer's values should be criticized on the basis of the previous measurements.

LIDAR OBSERVATIONS OF THE STRATOSPHERIC AEROSOL: SUMMARY OF RESULTS AND A CALIBRATION-ERROR ASSESSMENT

P.B. RUSSELL, W. VIEZEE, R.D. HAKE, JR., AND R.T.H. COLLIS

Stanford Research Institute

Menlo Park, California

ABSTRACT: Under CIAP support, SRI made 30 nighttime stratospheric lidar observations between October 1972 and March 1974, a period when volcanic contributions to the stratospheric aerosol were at a minimum. Profiles of scattering ratio consistently indicated the presence of a quasi-permanent aerosol layer near 20 km, which displayed considerable variation, at one time apparently correlated with a sudden stratospheric warming. The maximum observed particulate backscattering coefficient was only 10 to 20% of the molecular backscattering coefficient, indicating a substantial reduction, compared with lidar observations shortly after the 1963 Agung volcanic eruption. The overall decline in lidar-observed scattering ratio between 1964 and mid-1974 is shown to agree with measurements by balloon-borne particle counters, twilight photometers, and aircraft filter samplers made during the same period. Lidar-inferred turbidity values were also considerably less than those obtained by searchlight in 1964-1965. A comparative experiment indicated good agreement between lidar- and aircraft-inferred particle mass concentrations, when these were linked by means of a realistic optical model of the sampled particles.

Results from a series of balloon measurements and several lidar/balloon comparative experiments carried out elsewhere are analyzed, to estimate the errors introduced into lidar-measured profiles by the "clean-air" calibration procedure. The analysis indicates that, during the nonvolcanic period, midlatitude lidar profiles extending below 10 km would usually have underestimated the scattering ratio R by less than 10% of $R_{\rm max}-1$, and in all cases by less than 20% of $R_{\rm max}-1$. If, however, lidar profile analysis had been restricted to altitudes above 15 km, the mixing-ratio minimum usually observed near the tropopause during the nonvolcanic period would have been excluded from analysis, and larger underestimations could frequently have resulted.

INTRODUCTION

During the 18-month period between October 1972 and March 1974, SRI made a series of 30 nighttime observations of the stratospheric aerosol using a ground-based ruby lidar (laser radar) located in Menlo Park, California. The equipment and procedures used in those observations, as well as the primary data obtained, are described by Russell et al. (1974a, 1976a). This paper summarizes the data and compares them to a number of other stratospheric aerosol measurements made by lidar and other observational methods. In addition, as a means of indicating the validity and information content of the lidar observations, results are presented from (1) an experiment in which a common stratospheric volume was sampled by the SRI lidar and an aircraft-borne sampler, and (2) an analysis of balloon-measured profiles of stratospheric particle number. The latter analysis is intended specifically to provide an estimate of probable errors introduced into lidar measurements by the "clean-air" calibration procedure.

RESULTS FROM THE SRI/CIAP LIDAR OBSERVATION PROGRAM

Average Vertical Profile and Temporal Variations

A fundamental quantity that expresses lidar measurements of particulate content is the "scattering ratio," defined as

$$R(z) \equiv \left(f_{p}(z) + f_{m}(z)\right) / f_{m}(z)$$
$$= 1 + f_{p}(z) / f_{m}(z), \tag{1}$$

where $f_p(z)$ and $f_m(z)$ are, respectively, the particulate and molecular backscattering coefficients at altitude z. Scattering ratios in excess of unity indicate the presence of particulate matter in the atmosphere, and measure its ability to backscatter light from the laser transmitter relative to the backscattering strength of the local atmospheric gases. The solid line shown in Figure 1 is the error-weighted average profile of scattering ratio for all of the SRI/CIAP lidar

observations that extended down to an altitude of 10 km or below. (Scattering-ratio profiles that did not extend as low as 10 km have been excluded from the average because, as shown in the calibration-error section below, it is likely that the "clean-air" calibration procedure introduced appreciable underestimation into these profiles.) Included in the average are 16 profiles, measured on dates between June 1973 and March 1974. The maximum in scattering ratio near 20 km indicates the presence of the "Junge" layer of stratospheric particles, which was evident in all of our observations. Note, however, that the maximum backscattering coefficient of the particles averaged only about 10% of the backscattering coefficient of the local gas molecules (see Section B below).

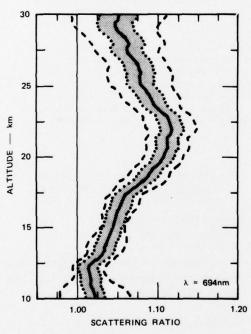


Figure 1. Average vertical profile of scattering ratio observed over central California coast, June 1973 - March 1974. Solid line is error-weighted mean of 16 observations. Dotted lines indicate typical experimental uncertainty in a single profile. Dashed lines indicate standard deviation of observations included in data set.

The dotted lines in Figure 1 indicate the typical observational uncertainty $(\pm 1\sigma)$ in any single measured profile. The dashed lines indicate the standard deviation of the 16 profiles included

in the data set. If the variability among measured profiles were due entirely to observational errors, the dotted and dashed curves would approximately coincide. The fact that the spread between the dashed curves consistently exceeds the spread between the dotted curves indicates that during the 10-month period of averaged observations there was quite a bit of real, natural variability in scattering ratio profiles. This variability in the stratospheric aerosol, even during "background" (i.e., nonvolcanic) conditions, has, of course, been noted in many other recent studies.

A particularly interesting example of this type of variability was noted near the time of the major sudden stratospheric warming of January 1973 (before lidar profiles had been extended down to 10 km). As described in detail by Russell et al. (1976a), vertical movements of the scattering-ratio peak between December 1972 and March 1973 were well correlated with reversals of the local zonal wind that accompanied development of the sudden warming (Quiroz, 1975).

Comparison to Other Observations

Figure 2 presents a comparison of the SRI (June 1973-March 1974) average profile of scattering ratio and average profiles obtained in two previous lidar studies. Profile FGSW is the average profile observed by Fox et al. (1973) over the Pacific Ocean in August 1971, using an airborne dye lidar (wavelength $\lambda = 585$ nm). (The profile has been converted to a ruby wavelength ($\lambda = 694$ nm) for this comparison, assuming fp $\propto \lambda^{-1}$.) Profile GF is the average of 66 scattering ratio profiles measured by Grams and Fiocco (1967) in Massachusetts during 1964-65, using a ground-based ruby lidar.

The most obvious difference between the 1964-65 profile and the more recent ones is the size of the scattering ratios. Grams and Fiocco observed an average peak value of f_p/f_m (i.e., (R-1)) of nearly 90%, while the profiles of the early 1970's display peak values of only 10 to 20%. (The CIAP-supported lidar measurements made prior to October 1974 by Northam et al. (1974) and Fernald et al. (1974) yielded scattering ratios similar to those in the SRI profile.) In addition, there is a significant difference in the shapes of the profiles. In 1964-65, the peak in

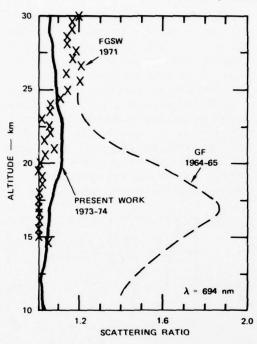


Figure 2. Average vertical profiles of scattering ratio observed in three lidar studies of the stratospheric aerosol between 1964 and 1974.

average scattering ratio was at 17 km, whereas in the early 1970's it was typically above 20 km. Both of these changes in scattering-ratio profiles are evidently attributable to the gradual removal of particles from the major eruption of the volcano Agung on Bali in March 1963, and other major eruptions that occurred through May 1970 (see, e.g., Cronin, 1971).

The overall decline of scattering ratio between 1964 and mid-1974, as observed by a number of stratospheric lidar groups in both hemispheres, is illustrated in Figure 3, which also includes some comparison data obtained by other observational methods. Considering that each of the four methods observes a different measure of stratospheric particulate content, at a variety of measurement locations, there is good mutual agreement in depicting the overall trend. Numerous short-term variations, superimposed on the general trend, are evident in the data obtained with all four measurement techniques, especially the twilight photometry data, for which the measurement frequency was the highest. Some of the major short-term variations are

evidently associated with (and lag somewhat behind) the times of major volcanic eruptions, as indicated by the vertical lines in Figure 3d.

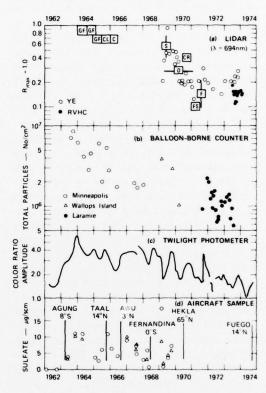


Figure 3. Comparison of stratospheric aerosol measurements made by four independent techniques between 1962 and 1974. (a) Maximum ratio of particulate to gaseous backscattering fp/fm, as observed by a number of lidar groups. GF: Grams and Fiocco (1967), Massachusetts; CL: Collis and Ligda (1966), California; C: Clemesha et al. (1966), Jamaica; S: Schuster (1970), Colorado; CR: Clemesha and Rodrigues (1971), Brazil; O: Ottway (1972), Jamaica; FS: Frush and Schuster (unpublished), Colorado; F: Fox et al. (1973), Hawaii and Bermuda; YE: Young and Elford (1975), Australia; RVHC: present work, California. (b) Number of particles (radius ≥ 0.15 µm) above tropopause as measured by photoelectric particle counter (Hofmann et al., 1972, 1973, 1974a, b, 1975). (c) Color-ratio amplitude, as measured by twilight photometer at Weissenau, Germany, through October 1967; then at Bedford, Massachusetts (Volz, 1970, 1974). (d) Mass of sulfate per standard cubic meter (scm), as collected on aircraftborne filters (Castleman, 1974).

It is also of interest to compare measurements of stratospheric turbidity (i.e., the ratio of particulate to molecular-Rayleigh extinction β_p/β_m) over the decade beginning shortly after the Agung eruption and ending before the volcanic activity of late 1974. However, deriving a turbidity profile from a lidar observation requires the use of a particulate backscatter-toextinction ratio, which has never been directly measured for the stratospheric aerosol. In spite of this, it is possible to make a realistic conversion from backscatter to extinction by using an optical model of the stratospheric aerosol that is consistent with measurements (both remote- and direct-sampling) made near the time and location of the lidar observations. On the basis of a number of recently published results (see Russell et al. (1974a) for details), we have adopted the optical model shown in Table 1. We emphasize that this is only a model, and that it may require modification to incorporate recent measurement data on the stratospheric aerosol of the early 1970's. Moreover, it is highly likely that revisions will be required to describe accurately the new post-volcanic aerosol. Nevertheless, the model of Table 1 is consistent with a number of measurements made in the non-volcanic period, and is probably suitable for use with lidar measurements made during that time (see also Cadle and Grams, 1975; Pinnick et al., 1975).

Table 1. An Optical Model of the Stratospheric Aerosol (based on nonvolcanic conditions in the early 1970's)

COMPOSITION:

Aqueous solution of sulfuric acid (75% H₂SO₄ by mass)

SIZE DISTRIBUTION: Deirmendjian* Haze H

SHAPE:

Spherical

CHARACTERISTICS IMPLED BY THE ABOVE:

Specific gravity = 1.63

Refractive index = 1.42 - 0 i = 700nm Backscatter-to-extinction ratio = 0.013 sr^{-1}

The solid line in Figure 4 is the profile of stratospheric turbidity (i.e., the ratio of particulate to molecular-Rayleigh extinction) obtained from the scattering-ratio profile of Figure 2 by using the model backscatter-toextinction ratio and converting to a wavelength λ of 550 nm (assuming $f_p \propto \lambda^{-1}$). Also shown are two previous profiles, obtained by searchlight measurements in 1964-65 and late 1970 (Elterman, 1968; Elterman et al., 1973). Again, the two previous profiles greatly exceed the 1973-74 one, and their shape differs, with both previous profiles having peaks below 20 km.

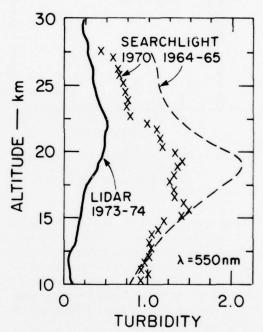


Figure 4. Vertical profiles of stratospheric turbidity (ratio of particulate to gaseous (Rayleigh) extinction) obtained from searchlight and lidar measurements between 1964 and 1974.

Lidar/Aircraft Comparative Experiment

In addition to the pure lidar measurement aspect of the SRI program, there was a second aspect, which included participation in several comparative experiments, in which aircraft and lidar data were jointly acquired. This section summarizes results of one of the comparative experiments, the details of which are given by Russell et al. (1974a, 1976a).

See Deirmendjian (1969)

In the first comparative experiment, a WB-57F aircraft flew over the lidar site and collected a filter sample of stratospheric particles. This sample was subsequently analyzed in the laboratory, yielding a particle composition of concentrated aqueous sulfuric acid, in agreement with the optical model given in Table 1. Therefore, we used the optical model to derive an expected backscattering coefficient from the mass of collected particles. Figure 5 shows a comparison between the particulate-backscattering coefficient inferred from aircraft observations and the lidar-measured value at the flight altitude. On 26 July, the actual date of the overflight, the agreement between lidar and aircraft values is good (that is, within each other's error bars). (It is also good on the previous two dates, which simply indicates small day-to-day variation of the particulatebackscattering coefficient near the date of the overflight). Moreover, if a particle acidity of 60% (a possible value) is assumed in the optical

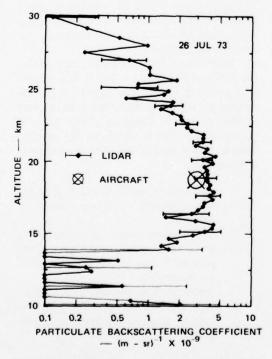


Figure 5. Comparison of lidar-measured particulate backscattering coefficient with computed value based on aircraft mass-sampler measurement. The computation assumes the particle optical and physical characteristics of the Table 1 model.

model, near-perfect agreement is obtained between the lidar-measured and aircraft-inferred particulate-backscattering coefficients on 26 July (see Russell et al. (1974a, 1976a) for details).

ERROR ASSESSMENT OF THE "CLEAN-AIR" CALIBRATION PROCEDURE

As with any experimental technique, lidar measurements of the stratospheric aerosol are subject to a number of experimental uncertainties, the most important of which derive from the following four items:

- 1. The "clean-air" or "molecular-layer" calibration procedure;
- 2. The choice of a gas-density profile for use in computing scattering ratios;
- The choice of a particulate-extinction profile for the same purpose;
- The choice of an optical model for converting lidar-measured backscattering to other quantities.

The last three items have been treated in some detail in recent reports by our group and others. As regards item 2, there is near-universal recommendation that a concurrently-measured (e.g., by radiosonde), rather than a modeled, profile or molecular density be used. Regarding item 3, it seems clear that a particulateextinction profile considerably less than the Elterman (1968) measurements of 1964-65 was appropriate for use in the nonvolcanic period of the early 70's. And as for item 4, realistic optical models have been recommended by Cadle and Grams (1975), Pinnick et al. (1975), and the preceding section of this paper. On the other hand, a comprehensive assessment of the probable errors introduced by the "clean-air" calibration procedure has not appeared in the literature (see, however, Young and Elford (1975) for one approach). Therefore, this section addresses this question, primarily on the basis of two sets of data acquired under CIAP funding: (1) an extensive set of balloon-borne measurements made by the University of Wyoming, and (2) several simultaneous lidar/balloon comparative experiments made by the NASA-Langley and University of Wyoming groups.

Error Analysis

The "clean-air" calibration procedure consists of renormalizing any given scattering-ratio profile in order to force the minimum ratio in the profile to equal unity (i.e., the value it would assume if particulate backscattering at that level were negligible). Therefore we begin by deriving expressions for the errors that will be introduced into lidar-derived scattering ratios by this renormalization if the minimum scattering ratio in fact somewhat exceeds 1.00. To quantify the argument, suppose that at the altitude z_0 of minimum scattering ratio, the ratio of particulate to molecular backscattering, defined as

$$\rho(z) \equiv f_{p}(z)/f_{m}(z) = R(z) - 1$$
 , (2)

has the value

$$\rho(z_0) = \rho_{\min},\tag{3}$$

rather than its assumed value of zero. Given this assumption, it can readily be shown that the resulting errors in scattering ratio at any altitude z are given by

$$E_{R}(z) \equiv R(z) - R'(z) = R'(z)\rho_{min},$$
 (4)

where (in this section) unprimed quantities are actual values, and primed quantities are those obtained from a lidar measurement as a result of normalizing the scattering-ratio profile to force $R'(z_0)=1.00$. As can be seen, the error is given by a quantity normally available in a lidar measurement (R'(z)) multiplied by ρ_{\min} , where ρ_{\min} cannot be measured in a lidar experiment, but is in fact assumed to equal zero. Thus, the determination of probable values for the errors given by Eq. (4) becomes simply the determination of the probable value of ρ_{\min} at the particular minimum level z_0 for a given lidar profile.

Balloon Data

Values of ρ_{\min} , the difference between true and assumed minimum scattering ratio, can be determined only by reference to a representative set of data on the stratospheric aerosol that are independent of the lidar data, but that can be

easily related to lidar scattering ratios. Such a set of data is provided by the University of Wyoming's measurements of stratospheric particle number, obtained by balloon-borne photoelectric particle counter (Hofmann et al., 1972, 1973, 1974a). These data are obtained as vertical profiles, with vertical resolution and range comparable to those of lidar-measured profiles. Moreover, the balloon measurements can be related to lidar measurements by using the results of several comparative lidar/balloon experiments (Northam et al., 1974; Remsberg and Northam, 1975, 1976).

A typical balloon profile, taken from a recent CIAP report (Hofmann et al., 1973) is shown in Figure 6a. The profile gives the number of particles with radius $>0.15 \mu m$, as a function of altitude z. The University of Wyoming group has acquired a large number of such profiles, from stations in both hemispheres. The profile in Figure 6a was measured at Laramie, Wyoming; it is characteristic in showing a peak at about $18 \, km$, a minimum near the tropopause, and a dropoff above the main stratospheric peak, which trails off nearly to zero somewhere between 25 and 30 km.

By dividing it by an air-mass-density profile, the profile in Figure 6a can readily be converted to a profile of number mixing ratio, or particle number per milligram of air. The result obtained in this manner is shown in Figure 6b. The mixing-ratio profile is similar to the particle-number profile, but it has three characteristic differences:

- The peak is broader and at a higher mean altitude (≈21 km instead of 18 km).
- The minimum near the tropopause is quite a bit smaller, with respect to the peak value, than the one in the absolutenumber profile.
- Above the peak, the mixing-ratio profile does not tail off to zero nearly as quickly as does the absolute-number profile.

These three characteristic differences result in a mixing-ratio profile that has a shape very similar to many profiles of scattering ratio obtained in the nonvolcanic period of the early 1970's by our and other stratospheric lidar groups.

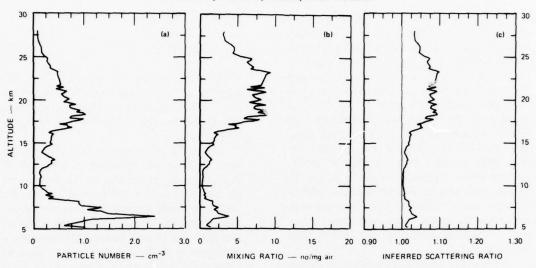


Figure 6. Vertical profiles of aerosol structure obtained from a single University of Wyoming balloon flight over Laramie, Wyoming, 16 September 1972. (a) Number of particles with radius greater than 0.15 μm, measured by balloon-borne photoelectric particle counter. (b) Mixing ratio (number of particles per mg of air), computed from particle number profile in Figure 6a. (c) Scattering ratio (1 + [particulate backscattering ÷ gaseous backscattering]), computed from mixing-ratio profile in Figure 6b using an assumed effective particulate backscattering cross-section of 4.7 × 10¹¹ cm²sr⁻¹.

This similarity of particle mixing-ratio and scattering-ratio profiles is to be expected if the ratio $\sigma_{\rm p}$ of particulate backscattering to balloon-measured particle number is approximately independent of height for any given observation. In fact, several comparative lidar/balloon experiments made during the nonvolcanic period not only demonstrated that the ratio $\sigma_{\rm p}$ was approximately constant with height, but also yielded several values for the ratio itself (Northam et al., 1974; Remsberg and Northam, 1975, 1976). The value

$$\sigma_p = 4.7 \times 10^{-11} \text{cm}^2 \text{sr}^{-1} \ (\lambda = 694 \text{ nm}) \ (5)$$

may be taken as representative, with a variability among observations (i.e., standard deviation) of about 30% of this value. This value may be used to convert the mixing-ratio profile of Figure 6b to a profile of inferred scattering ratio, as shown in Figure 6c. For the particular observation shown, the maximum inferred scattering ratio is about 10% greater than 1.00, corresponding to a maximum mixing ratio of about 10 particles per mg of air (cf. Figure 6b). Thus the conversion factor of Eq. (5) is rather easy to remember —

one particle of radius $\gtrsim 0.15~\mu m$) per mg corresponds to about one percentage point of scattering ratio.

For the particular balloon profile shown in Figures 6a through 6c, the minimum in scattering ratio occurs near 10 or 11 km, and is very close to 1.00, differing by less than 1%. Since 2% is a current typical experimental uncertainty in lidar-measured scattering ratio, we can say that, for this particular example, the particulate-backscattering coefficient at the level of minimum scattering ratio was truly negligible compared to the molecular-backscattering coefficient. In other words, there was a clean level, suitable for lidar calibration, at 10-11 km on this date.

However, aerosol behavior is known to be quite variable, and thus the minimum observed over Laramie on 16 September 1972 is shown merely as an example, and should not be taken as representative. To judge properly the representativeness of this example, it is necessary to repeat this type of analysis for a number of observations, spread over a period of time — or, in other words, to build up a climatology of the behavior of the minimum in scattering ratio. Such an extended analysis was performed by Russell et al.

(1974b), using as input a set of balloon data gathered at Laramie over a period of 22 months and tabulated in a series of CIAP reports. The resulting values of ρ_{min} , which were based on the conversion factor given by Eq. (5), showed that use of the "clean-air" calibration procedure on lidar measurements made at the time and location of the balloon soundings would have introduced into scattering-ratio profiles a negative error (cf. Eq. (4)) that was typically less than 0.02, provided that the range of profile analysis included altitudes as low as 10 km. If, however, the lidar analysis had been restricted to altitudes above 15 km, or if profiles had been normalized above the major peak, then a larger error, frequently exceeding 0.04, would have been introduced.

It should be noted that the results of Russell et al. (1974b) depend directly on the value of the conversion factor σ_p , for which there is appreciable variability (or uncertainty) among observations (see Eq. (5) and the accompanying discussion). It is therefore desirable to obtain a measure of the calibration error that is independent of any specific value for σ_p . This can be done from the balloon data, provided that errors are expressed as fractions of the maximum value of profiled quantities. For example, let us define

$$\epsilon_{\rm p}(z) \equiv \left[\rho(z) - \rho'(z)\right] / \rho_{\rm max}.$$
 (6)

(For any given profile, $\epsilon_{\rho}(z)$ is the error in $\rho'(z)$ at altitude z, expressed as a fraction of the maximum value of ρ in the profile.) Since

$$\rho(z) - \rho'(z) = R(z) - R'(z),$$
 (7)

we have from Eq. (4)

$$\epsilon_{\rho}(z) = R'(z) \rho_{\min}/\rho_{\max}$$
 (8)

Then, assuming the σ_p is independent of height, one can readily show that

$$\rho_{\min}/\rho_{\max} = r_{\min}/r_{\max}, \tag{9}$$

where r_{min} and r_{max} are the minimum and maximum mixing ratios in the balloon-observed profile. If we then define

$$s \equiv r_{\min}/r_{\max}, \tag{10}$$

we have, by Eq. (8),

$$\epsilon_{\rho}(z) = R'(z) s,$$
 (11)

which is independent of the value of σ_p but depends only on the assumption (verified by the lidar/balloon experiments) that σ_p is approximately independent of altitude in any given observation.

From Eq. (11) we see that the probable error in R'(z) - 1, expressed as a fraction of $R_{max} - 1$, can be assessed on the basis of the typical behavior of s, the ratio of minimum to maximum mixing ratios in balloon-observed profiles. Values of s obtained from balloon profiles measured over Laramie during a 22-month period are shown in Figure 7a. Most of the values fall below 0.08, which implies (using Eq. (11) and typical nonvolcanic values of $R'(z) \le 1.2$) typical errors in lidar-measured scattering ratios of less than 10% of the peak value of R - 1. However, there is a definite seasonal dependence to the balloon data (cf. Hofmann et al., 1974b) such that in and around March of both 1972 and 1973 the s values (ratios of minimum to maximum mixing ratios) become somewhat larger - increasing to as much as 18%.

Figure 8 shows the altitudes at which the mixing-ratio minima of Figure 7a occurred. Most of the minima fall between 5 and 10 km, with a few falling above the peak, near 30 km. (Note that minima tend to occur above the peak in the springtime, when the clean region normally observed near the tropopause becomes somewhat dirtier). These data show that, in order to observe most of the minima shown in Figure 7a, lidar observations would have had to extend below 10 km, possibly down to 5 km. In the past, however (for a number of experimental reasons), stratospheric lidar observations typically have not been extended as low as 5 km, and thus it is necessary to investigate the behavior of the mixing-ratio minima within the restricted altitude ranges used in a number of lidar observations.

Figure 7b shows the s-values obtained within the portion of the balloon profiles extending above 10 km (as well as the values obtained in Figure 7a for the unrestricted minima). Most of the s-values for the partial profiles exceed the values for the complete profiles. However, most of the values remain below 0.10, and all are less

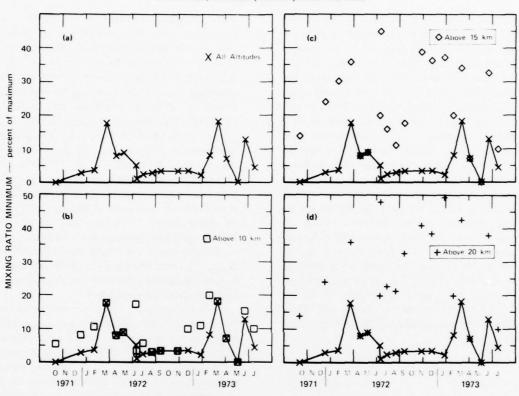


Figure 7. Minimum values of particle-number mixing-ratio profiles measured by University of Wyoming balloons over Laramie, Wyoming, October 1972 - July 1973. X, minimum value in complete profile; p, minimum value above 10 km; p, minimum value above 15 km; +, minimum value above 20 km. All values are expressed as percentage of maximum value in complete profile.

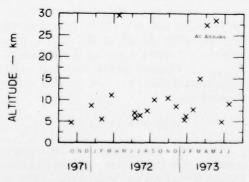


Figure 8. Altitudes of mixing-ratio minima shown in Figure 7a.

than 0.20, implying errors in lidar-observed scattering ratio (cf. Eq. (11)) of less than 12% and 24%, respectively, of $R_{max}-1$. Figure 7c shows s-values obtained within the portion of the balloon profiles above 15 km. In this case the

s-values become appreciably larger, frequently exceeding 0.30. These values indicate that if the "clean-air" calibration procedure had been employed on lidar profiles restricted to altitudes above 15 km, the resulting errors in scattering ratio would frequently have exceeded 30% of $R_{max} - 1. \label{eq:resulting}$

Figure 7d shows s-values obtained when analysis is restricted to the altitude range above 20 km, to indicate errors that would be introduced if the frequently-observed minimum above the major peak were used for normalization in all seasons. Again, the errors are quite large, frequently falling in the 30%-50% range. It should, however, be noted that these errors may be somewhat overestimated, because often the balloon data stop below 30 km; if they had extended higher, it is probable that a smaller minimum would have been encountered. This matter is illustrated in Figure 9, which shows the

altitudes of mixing-ratio minima in the altitude range above 20 km. Points circled in Figure 9 indicate minima that occurred at the highest altitude from which balloon data were received. Numerous lidar and balloon observations of the 25-to-30-km region indicate that mixing ratios (and scattering ratios) typically decrease with increasing height in this region. However, in a significant number of cases, balloon data were available above 28 km, and the s-value still exceeded 20%. And in a number of other cases, indicated by the four non-circled crosses near 22 km, the mixing-ratio minimum occurred at an altitude at which the peak usually occurs. In these cases, the mixing ratio never really decreased above the usual peak altitude, but remained essentially constant, or actually increased. This type of behavior, while atypical, has also been noted in some of the SRI lidar observations (Russell et al., 1974a, 1975a) and several times in the data of Young and Elford (1975). (See also profile FGSW in Figure 2 of this paper.)

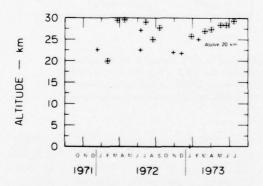


Figure 9. Altitudes of mixing-ratio minima above 20 km shown in Figure 7d. Circled points indicate minima that occurred at highest altitude of balloon data.

Error Summary

The balloon data used in the above analysis apply strictly only to the times shown, and to one location, Laramie, Wyoming, at 42°N. The Laramie location was chosen as being the balloon-launch site at which aerosol behavior best approximated that at the latitude (37.5°N) of the SRI lidar observations. The balloon data indicate that, during the nonvolcanic period, the mixing-ratio minimum typically occurred in the

altitude region near (not necessarily at) the tropopause, and that pre-Fuego lidar observations should have been extended down to altitudes of 10 km or below in order to observe as frequently as possible the true minimum in scattering ratio. Lidar observations with lower bounds of 10 km or less would have typically underestimated scattering ratios by less than 10% of the peak value of R-1. However, there appears to be a definite seasonal variation in the balloon data (Hofmann et al., 1974b), and underestimations of 20% of $R_{max} - 1$ could have been encountered in the springtime. Lidar normalizations conducted at altitudes of 15 km or above would frequently have missed the balloon-measured mixing-ratio minimum and introduced errors sometimes exceeding 30% of R_{max} - 1, thus leading to a significant underestimation of true scattering ratios and particulate backscattering coefficients.

Similar analyses could be performed on balloon data from other launch sites to estimate lidar errors in nearby geographical areas. (Eleven stations, ranging from 85°N to the South Pole, were used in the University of Wyoming global monitoring program.) By the same token, more recent balloon data, acquired after the late-1974 volcanic intrusion, would be required to estimate accurately the "clean-air" calibration errors appropriate to the new postvolcanic stratosphere. Since values of $R_{max} - 1$ have increased dramatically (by a factor of ≈10) in the new postvolcanic period (e.g., McCormick and Fuller, 1975; Fegley and Ellis, 1975; Remsberg and Northam 1976; Russell et al., 1975b), it is expected that errors, expressed as a fraction of R_{max} - 1, would be smaller than those in the nonvolcanic period, but this remains to be demonstrated.

ACKNOWLEDGMENTS

The stratospheric lidar observations described in this paper were supported by the Climatic Impact Assessment Program of the U.S. Department of Transportation through NASA Ames Research Center. The data summary, comparison with previous observations, and error assessment of the "clean-air" calibration procedure were supported by Stanford Research Institute through internal research funds. We are grateful to W. Sedlacek and D. Briehl for making

their aircraft data available prior to publication, and to J. Rosen for providing the University of Wyoming reports on stratospheric balloon data. The format of Figure 3, and much of the data therein, are adopted from the publication of Fox et al. (1973).

REFERENCES

- Cadle, R.D., and Grams, G.W. (1975), "Stratospheric aerosol particles and their optical properties," Rev. Geophys. Space Phys. 13, 475-501.
- Castleman, A.W., Jr. (1974), "Nucleation processes and aerosol chemistry," Space Sci. Rev. 15, 547-589.
- Clemesha, B.R., G.S. Kent, and R.W.H. Wright (1966), "Laser probing of the lower atmosphere," Nature 237, 328-329.
- Clemesha, B.R., and S.N. Rodrigues (1971), "The stratospheric scattering profile at 23° south," J. Atmos. Terr. Phys. 33, 1119-1124.
- Collis, R.T.H., and M.G.H. Ligda (1966), "Note on tidar observations of particulate matter in the stratosphere," J. Atmos. Sci. 23, 255-257.
- Cronin, J.F. (1971), "Recent volcanism and the stratosphere," Science 172, 847-849.
- Deirmendjian, D. (1969), Electromagnetic Scattering on Spherical Polydispersions, American Elsevier, New York, 290 pp.
- Elterman, L. (1968), "UV, Visible and IR Attentuation for Altitudes to 50 km, 1968," AFCRL-68-0153, Environmental Research Paper No. 285, Air Force Cambridge Research Laboratory, Bedford, MA.
- Elterman, L., R.B. Toolin, and J.D. Essex (1973), "Stratospheric aerosol measurements with implications for global climate," Appl. Opt. 12, 330-337.
- Fegley, R.W., and H.T. Ellis (1975), "Lidar observation of a stratospheric cloud layer in the tropics," Geophys. Res. Letters 2, 139-141.
- Fernald, F.G., C.L. Frush, and B.G. Schuster (1974), "Airborne lidar measurements of the distribution of stratospheric aerosols," in *Proceedings of the Third Conference on the Climatic Impact Assessment Program* (Cambridge, MA), U.S. Dept. of Transportation, DOT-TSC-OST-74-15, 318-322.
- Fox, R.J., G.W. Grams, B.G. Schuster, and J.A. Weinman (1973), "Measurements of stratospheric aerosols by airborne laser radar," J. Geophys. Res. 78, 7789-7801.

- Grams, G.W. (1966), "Optical Radar Studies of Stratospheric Aerosols," thesis, Dept. of Meteorology, Mass. Inst. of Tech., 133 pp.
- Grams, G.W., and G. Fiocco (1967), "Stratospheric aerosol layer during 1964 and 1965," J. Geophys. Res. 72, 3523-3542.
- Hofmann, D.J., J.M. Rosen, T.J. Pepin, and J.L. Kroening (1972), "Global monitoring of stratospheric aerosol, ozone, and water vapor," Progress Report dated June 1972, Dept. of Physics and Aston., Univ. of Wyoming, Laramie, Wyoming.
- Hofmann, D.J., J.M. Rosen, T.J. Pepin, and J.L. Kroening (1973), "Global monitoring of stratospheric aerosol, ozone, and water vapor," Progress Reports dated April and June 1973, Dept. of Physics and Astron., Univ. of Wyoming, Laramie, Wyoming.
- Hofmann, D.J., J.M. Rosen, T.J. Pepin, and J.L. Kroening (1974a), "Global monitoring of stratospheric aerosol, ozone, and water vapor," Progress Report dated February 1974, Dept. of Physics and Astron., Univ. of Wyoming, Laramie, Wyoming.
- Hofmann, D.J., J.M. Rosen, T.J. Pepin, and R.G. Pinnick (1974b), "Stratospheric aerosol measurements I: Time variations at northern midlatitudes," J. Atmos. Sci. 32, 1446-1456.
- McCormick, M.P., and W.H. Fuller, Jr. (1975), "Lidar measurements of two intense stratospheric dust layers," Appl. Opt. 14, 4-5.
- Northam, G.B., J.M. Rosen, S.H. Melfi, T.J. Pepin, M.P. McCormick, D.J. Hofmann, and W.H. Fuller, Jr. (1974), "Dustsonde and lidar measurements of stratospheric aerosols: a comparison," Appl. Opt. 13, 2416-2421.
- Ottway, M.T. (1972), "Laser radar observations of the 20-km aerosol layer," presented at the Fourth Conference on Laser Atmospheric Studies, Tucson, Ariz.
- Pinnick, R.G., J.M. Rosen, and D.J. Hofmann (1975), "Stratospheric aerosol measurements III: Optical model calculations," J. Atmos. Sci. 33, 304-314.
- Quiroz, R.S. (1975), "The stratospheric evolution of sudden warmings in 1969-74 determined from measured infrared radiation fields," J. Atmos. Sci. 32, 211-224.
- Remsberg, E.E., and G.B. Northam (1975), "A Comparison of Dustsonde and LIDAR Measurements of Stratospheric Aerosols," Final Report, Interagency Agreement DOT-AS-20062, NASA Langley Research Center, Hampton, VA 23665.

- Remsberg, E.E., and G.B. Northam (1976), "A comparison of dustsonde and LIDAR measurements of stratospheric aerosols," in this volume.
- Russell, P.B., W. Viezee, and R.D. Hake, Jr. (1974a), "Lidar Measurements of Stratospheric Aerosols over Menlo Park, California; October 1972 - March 1974," Final Report, SRI Project 2217, Stanford Research Institute, Menlo Park, CA.
- Russell, P.B., W. Viezee, R.D. Hake, Jr., and R.T.H. Collis (1974b), "Credibility and significance of lidar observations of the stratospheric aerosol," presented at the Sixth Conference on Laser Atmospheric Studies, 3-6 September, Sendai, Japan.
- Russell, P.B., W. Viezee, R.D. Hake, Jr., and R.T.H. Collis (1976a), "Lidar observations of the nonvolcanic stratospheric aerosol: California, October 1972 - March 1974," Quart. J. Roy. Meteor. Soc. 102, 619-639.

- Russell, P.B., W. Viezee, and R.D. Hake, Jr. (1976b), "Lidar observations of the post-Fuego stratospheric aerosol," Final Report, SRI Project 4019, Stanford Research Institute, Menlo Park, California 94025.
- Schuster, B.G. (1970), "Detection of tropospheric and stratospheric aerosol layers by optical radar (lidar)," J. Geophys. Res. 75, 3123-3132.
- Young, S.A., and W.G. Elford (1975), "Laser observations of stratospheric aerosols at Adelaide (35°S), 1969-73," Internal Report ADP 119, Dept. of Physics, Univ. of Adelaide, Adelaide, Australia.
- Volz, F.E. (1970), "On dust in the tropical and midlatitude stratosphere from recent twilight measurements," J. Geophys. Res. 75, 1641-1646.
- Volz, F.E. (1974), "Stratospheric background aerosol from twilight data" (draft manuscript).

A COMPARISON OF DUSTSONDE AND LIDAR MEASUREMENTS OF STRATOSPHERIC AEROSOLS

ELLIS E. REMSBERG AND G. BURTON NORTHAM

Environmental and Space Sciences Division NASA Langley Research Center Hampton, Virginia

ABSTRACT: This paper describes the results and analysis of an experiment to compare the stratospheric aerosol profiles as measured by a balloon-borne in-situ particle counter and by the backscattered light from a ground-based laser radar (lidar) operating at a wavelength of 694.3 nm. The profiles agree within the experimental errors for particles with radii greater than $0.25~\mu m$ and for altitudes between 15 and 28 km.

Following the calibration tests, the lidar was used to monitor the stratospheric aerosols at Hampton, Virginia. Enhanced backscatter appeared sporadically in November and December of 1974 over Hampton; scattering ratios averaged over altitude increments of 450 meters range from 1.10 at 20 km in early November to 3.3 at 17 km on December 18. This enhanced backscattering is attributed to the aerosols associated with the eruption of the Fuego volcano in Guatemala in mid-October.

INTRODUCTION

Various measurement techniques are being used to characterize the natural level and variability of the stratospheric aerosol as a part of the DOT Climatic Impact Assessment Program (CIAP). Northam et al. (1974) reported on an initial comparative experiment at Laramie, Wyoming in 1972 using lidar backscatter returns and a University of Wyoming dustsonde measurement. That particular experiment indicated relative agreement between the two methods, but further refinements in the lidar were deemed desirable.

Improvements in the Langley Research Center 48-inch lidar system were made and another comparative experiment was conducted on May 7-8, 1974, at San Angelo, Texas. This particular site was chosen because it was near the site of a more comprehensive stratospheric measurements program - the balloon LACATE (Lower Atmospheric Composition and Temperature Experiment) tests. The first part of this paper describes the results and analysis of an experiment designed to compare the stratospheric aerosol profiles as measured by a balloon-borne in-situ particle counter and by the backscattered light from a ground-based laser radar (lidar) operating at a wavelength of 694.3 nm. The second part of the paper presents the results and analysis of the lidar data obtained at Hampton, Virginia from October 1974 to February 1975. The enhancement in backscattering observed during this period corresponds to the arrival of the stratospheric dust associated with the mid-October eruptions of Volcan de Fuego in Guatemala.

MEASUREMENT TECHNIQUES

The pulsed lidar system measures aerosol plus molecular backscatter from the lower stratosphere, while the balloon-borne dustsonde detects aerosols in situ as the balloon ascends. The dustsonde provides an indication of both aerosol size distribution and aerosol concentration as a function of altitude. Independent knowledge of the molecular density is supplied by a balloon-borne radiosonde, and this information enables one to separate molecular and aerosol contributions in the laser backscatter signal. The dust-sonde and the lidar systems, and data reduction techniques, are described and discussed by Northam et al. (1974).

DUSTSONDE-LIDAR COMPARISONS

The time line for the lidar data and the dustsonde and temperature-sonde launches for the San Angelo comparative measurements is shown in Table 1. Over 800 laser soundings were made, and the data obtained with the dustsonde and thermistor are examined along with the concurrent laser firings.

Table 1. San Angelo Measurements on May 7-8, 1974

	Initial Time (MDT)	Number of Shots
LIDAR Sou	indings:	
May 7	2035	50
-	2102	50
	2223	60
	2333	300
May 8	0122	70
	0158	100
	0236	130
	0328	100
Dustsonde:		
May 8	0200	(1)
Temperatur	e Sonde:	
May 7	2330	(1)

Figures 1 through 3 present aerosol return data for 100 shots at 0330-0400 MDT on the morning of May 8, 1974. These laser firings coincide most closely with the ascent through the lower stratosphere of the University of Wyoming dustsonde (launch 0200 MDT). Figures 2 and 3 illustrate the scattering ratio and aerosol backscattering function profiles, respectively, for the data shown in Figure 1. A scattering ratio of 1.0 would correspond to no aerosol; any excess would then be representative of the aerosol loading only. Error bars represent the 95% confidence interval for the mean of the data.

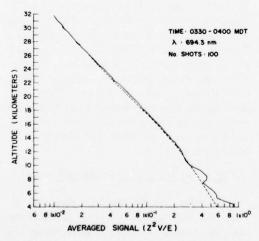


Figure 1. Range-corrected lidar return, San Angelo, Texas, May 8, 1974. Solid line, average range-corrected return signal; broken line, calculated range-corrected lidar return signal expected from the molecular atmosphere.

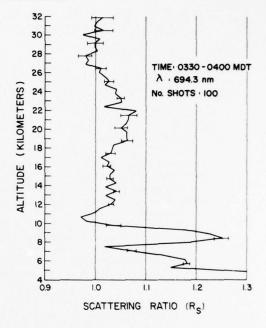


Figure 2. Scattering-ratio profile, San Angelo, Texas, May 8, 1974.

Northam et al. (1974) discuss the lidar equation and its subsequent use in the calculation of scattering ratio R_s and the aerosol backscattering function f_a .* The scattering-ratio profile in Figure 2 is the result of averaging returns over altitude increments of 0.45 km, which are comparable with the vertical resolution available from the dustsonde on this launch. Since each range bin for the lidar data covers an altitude of 15 meters, this represents a 30-point average in altitude. The total-backscatter profile is normalized to the molecular profile between 28 and 31 km. This normalization process gives the scattering-ratio R_s profile shown in Figure 2. A bulge in the R_s profile occurs between 18

^{*} The symbols used in this paper will be:

R.	scattering ratio
R _s f _a σ _a N _m σ _m Ri	aerosol backscattering function
$\sigma_{\mathbf{a}}$	aerosol-backscatter cross-section
N _a	aerosol number density
Nm	molecular number density
σm	molecular-backscatter cross-section
Rí	gradient Richardson number
Z	range from lidar
V	voltage
E	transmitted energy per pulse
λ	wavelength
r	particle radius

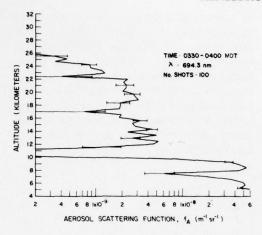


Figure 3. Aerosol backscattering-function profile, San Angelo, Texas, May 8, 1974.

and 24 km; its peak value is only 1.07, which indicates relatively low aerosol content.

A scattering ratio of less than 1.0 exists at 11 kilometers in Figure 2. This may be a result of two systematic effects. It is possible that the rawinsonde temperature profile applied to the calculation of molecular densities was in error. However, a deviation in scattering ratio of 0.03 would represent an error of 6K in measured temperature, an unusually large error. It is more likely that this scattering-ratio minimum is a result of normalizing the total-backscatter profile to the expected backscatter calculated for the molecular atmosphere between 28 and 31 km. In this particular profile the 11-km minimum would have been more appropriate for the normalization. Further discussion on this topic will appear later in this report.

Figure 3 is a plot of aerosol backscattering function $f_a(m^{-1}sr^{-1})$, a quantity directly proportional to the aerosol concentration or number density, if the aerosol characteristics such as size distribution, composition or index of refraction, and particle shape remain constant with altitude. This quantity f_a is defined as the product of backscatter cross-section $\sigma_a(m^2sr^{-1})$ and particle concentration $N_a(m^{-3})$.

In Figures 4 and 5 the f_a profile is compared directly with particle counts (N_a) measured with the Wyoming dustsonde. The comparison in Figure 4 for particles greater than 0.15 μ m in radius gives best agreement in the 20-km region when one particle/cm³ corresponds to a value of

 $f_a = 4 \times 10^{-9} \, \mathrm{m}^{-1} \, \mathrm{sr}^{-1}$. Agreement is not within the error bars of the two techniques above about 22 km. Figure 5 shows the comparison for particles with radii greater than 0.25 μ m. The correlation in Figure 5 is even better, especially at the higher altitudes, indicating that the lidar wavelength, 694.3 nm, may exhibit sensitivity to the particle size distribution with height. Particles with radii greater than 0.25 μ m exhibit correspondence when 1 particle/cm³ is equivalent to $f_a = 1.8 \times 10^{-8} \, \mathrm{m}^{-1} \, \mathrm{sr}^{-1}$.

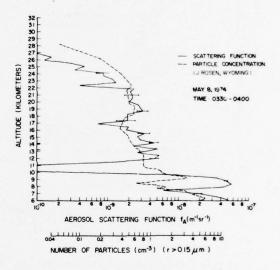


Figure 4. Comparison of LIDAR and dustsonde profiles for particles with radii greater than 0.15 µm.

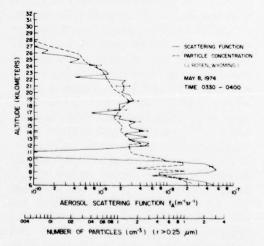


Figure 5. Comparison of LIDAR and dustsonde profiles for particles with radii of greater than 0.25 μm.

Figure 6 presents a comparison between the particle profile used in Figure 5 and 300 laser firings taken earlier on May 7-8 (2330-0115 MDT) at San Angelo. Features are still roughly the same except for a continually changing cirrus structure at 9 km during that night.

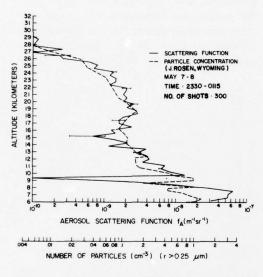


Figure 6. Comparison of LIDAR and dustsonde profiles for 300 laser firings and particles greater than $0.25~\mu m$ radius.

Figure 7 shows the mixing-ratio profile data from Rosen (1974) for particles greater than 0.15 µm and greater than 0.25 µm in radius from the San Angelo experiments. Russell et al. (1975) show that the mixing-ratio profiles, for particles with radii 0.15 µm and greater, have a minimum at tropopause altitudes (near 10 km for the Laramie data); they therefore justify clean-air normalization at those heights. However, the May 8 data reported herein, Figures 4 and 5, indicate a better lidar-dustsonde profile agreement for particles greater than 0.25 µm in radius. This trend is examined further in Figure 7. For the larger particles a minimum appears above the 20-km layer, whereas the mixing-ratio profile for the smaller particles displays minima of comparable magnitude at 12-16 km and at 28 km. Thus for this set of observations on May 8, it is slightly preferable to normalize the data to air densities at the higher altitude, 28 km. This altitude also corresponds to the maximum height of the rawinsonde profile. Consequently, all of the data in this paper are normalized at the higher altitudes. In order to make such an extrapolation for this larger quantity of data, however, it seems important to re-evaluate mixing-ratio minima in light of the findings of Russell et al. (1975). The normalization process does not in itself insure that no aerosol exists at regions of scattering-ratio minima, but the systematic errors involved are in most cases much less than 20%.

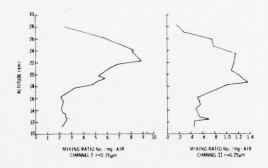
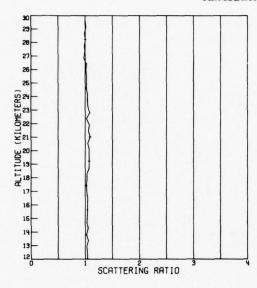


Figure 7. Aerosol mixing-ratio profiles for determining clean-air calibration regions, San Angelo, Texas, May 8, 1974.

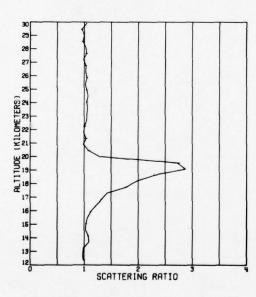
TEMPORAL AEROSOL MEASUREMENTS AT HAMPTON, VIRGINIA

With the confidence gained from the San Angelo comparison experiments, data were taken using the Langley 48-inch lidar from October 1974 to February 1975 at Hampton, Virginia. The temporal variations in those data are presented in the following section of this paper. To emphasize the changes that have occurred in the aerosol load during 1974, a scattering-ratio profile from the May 7-8 San Angelo comparative experiment is shown in Figure 8a on a reduced scattering-ratio scale. Figure 8b displays a similar profile for January 2, 1975 on the same scale. The marked increase is believed to be due to a large dust incursion from the mid-October eruptions of Volcan de Fuego in Guatemala (Meinel and Meinel, 1975). Observations at Hampton, Virginia were being conducted both before (serving as a baseline) and during the enhancement of the dust layer.

The temporal variation of this dust layer is illustrated in Figure 9. These plots display relative aerosol column densities for the indicated



a. May 7, 1974.



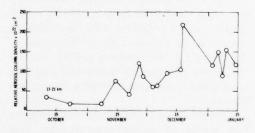
b. January 2, 1975.

Figure 8. Scattering-ratio profiles.

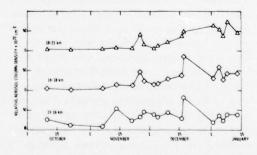
altitudes. Quantities on the ordinates represent summations over 1-km increments of $(\overline{R}_s(Z)-1)\,N_m(z)$, where $\overline{R}_s(z)$ is the average scattering ratio and $N_m(z)$ is the molecular number density in cm⁻³. Thus in Figure 10 the relative aerosol column density applies to an 8-km-deep column of 1-cm² cross-section. The quantity on the

ordinate is then equivalent to (σ_a/σ_m) $N_a(z)$, where σ_a and σ_m are aerosol and molecular cross-sections, respectively, and $N_a(z)$ is the aerosol number density.

Figure 9a illustrates the temporal variation in the total stratospheric aerosol burden between 13 and 21 km through January. The significant variability in the aerosol is shown in more detail in Figure 9b. A dust layer of as-yet-unexplained origin was present at 15 km on October 10, the first night that the lidar was operational at Hampton after the San Angelo experiment. The first indications of more significant enhancement are on November 14 in the 13-16 km region and on the 26th of November (McCormick and Fuller, 1975) at 17 to 20 km. However, aerosolburden fluctuations continued until December 18, when a strong return from all three altitude regions contributed to the maximum observed aerosol burden. A peak scattering ratio of 3.3 was present at 17 km on December 18. During January the low-level aerosol features subsided, but the 16 to 21 km regions exhibited a single consistently strong layer (typical of the data shown in Figure 8b) as though the "Junge layer"



a. Total loading.



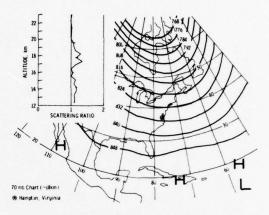
b. Loading for three altitude ranges.

Figure 9. Variations of aerosol loading for Hampton, Virginia (1974-75).

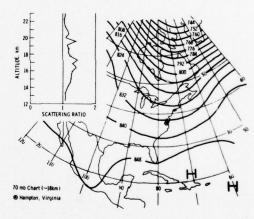
had become reestablished. Whereas lines have been used to connect the data points in Figure 9, it is quite possible that fluctuations between adjacent observations exist. For instance, no data were taken on 24 and 25 November, but visual observations of striated dust layers did occur at sunset on those days. Lidar data were recorded only on November 22, 26, and 28 during that period.

A more detailed evaluation of the aerosol variability in Figure 10 can be made by considering data for December 5, 10, and 17, where the column load exhibits a slowly increasing trend. In Figure 10 complementary plots of scattering ratio and 70-mb circulation patterns are presented for the three dates. On both December 5 and 10, R, values do not exceed 1.4 and the flow patterns are predominantly west-to-east over Virginia. However, on December 17 the flow shifted to a strong southwesterly pattern with substantial confluence of the isolines (flow considered parallel to lines of constant height) over Virginia. The corresponding R_s profile displays a marked increase and, in fact, on the night of December 18 the largest observed aerosol loading occurred. This sequence indicates that the dust was being transported from latitudes south of Virginia and is consistent with the postulated volcanic source in Guatemala (15°N latitude). If the Fuego volcanic source is correct, the latitudinal spread of the dust had already resulted in more uniform dust amounts during January over Virginia.

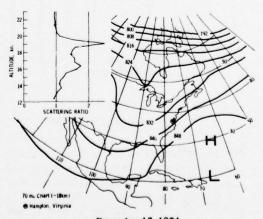
Investigations of the effects of the temperature profile on aerosol structure have been conducted and, as shown in Figures 11a and 11b, a positive correlation exists between temperature inversions and increases in aerosol concentration. However, in Figure 11c no inversion was present in the low-resolution rawinsonde temperature data even though significant dust loads were present. Of course, the vertical structuring that occurs can be due to strong vertical wind shear as well as to the temperature gradients. The gradient Richardson number, Ri, a measure of turbulent exchange, includes both of these effects. Reliance on Ri to relate aerosol structure to turbulence requires comparable spatial measures of both temperature and wind, requiring a data transmission rate that is normally not reported for rawinsondes. The scattering-ratio data in Figure 11 have been averaged over ten points in altitude (150 meters) to emphasize any real aerosol structure.



a. December 5, 1974.

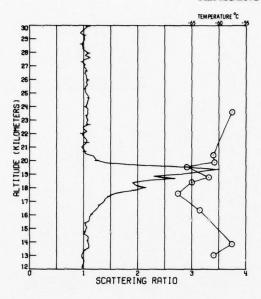


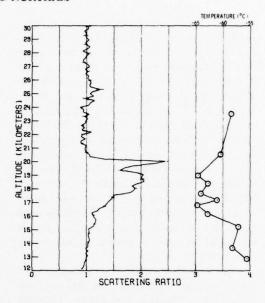
b. December 10, 1974.



c. December 17, 1974.

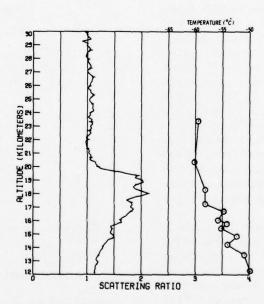
Figure 10. Scattering-ratio profiles and circulation patterns.





a. January 2, 1975.

b. January 9, 1975.



c. January 14, 1975.

Figure 11. Effect of temperature on aerosol structure.

In Figure 11b a significant scattering ratio appears at 25 km and is of a greater magnitude than the peak values observed in May at 20 km. Although this data has not been properly corrected for intervening atmospheric extinction,

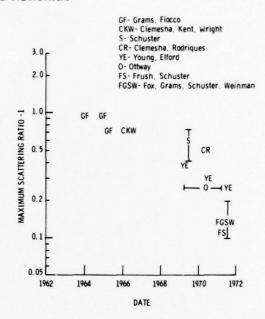
once the latter has been included a more thorough analysis of the features at 25 km can be achieved.

For the scattering-ratio profiles obtained since October 1974 it is tempting to apply the

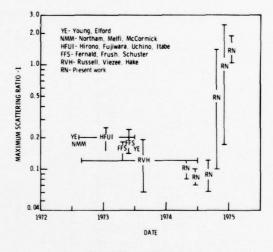
calibration factors reported in Figures 4 and 5 relating aerosol backscattering function and particle concentration. In this way one could derive particle-concentration profiles from the lidar data. However, the two profile conversion factors at San Angelo, Texas (Figures 4 and 5) are appropriate to an aerosol layer composed of particles whose composition and size distribution are very different from those of the present enhanced aerosol. In fact, dust sonde measurements made in December 1974 at Wyoming indicate that the size distribution also varies with altitude in the stratosphere; the conversion factor would then vary with altitude. Thus, in order to relate present aerosol backscatter to particle concentration, another intercomparison experiment would be necessary.

The long-term trends in the magnitude of the 20-km layer are shown in the following two figures. (See Clemesha et al. (1966), Clemesha and Rodriques (1971), Fernald et al. (1974), Fox et al. (1973), Grams and Fiocco (1967), Hirono et al. (1974), Northam et al. (1974), Russell (1975), Schuster (1970), and Young and Elford (1975).) A history of average maximum scattering ratio for the 20-km region is plotted in Figure 12a. On the ordinate is listed maximum scattering-ratio minus one $(R_s - 1.0)$. This graph is an accumulation of observations by various lidar groups over a ten-year period. Vertical bars on the symbols indicate the range of values recorded, while horizontal bars show the period of time over which backscatter measurements were obtained. The general decline of aerosol content has continued since the Agung volcanic event in March of 1963.

Figure 12b indicates that the number of measurements has increased during the time that the CIAP program has been going on, although not all groups have been funded by the Department of Transportation. Minimum measured values are represented by scattering ratios of 1.05 to 1.10. Among the observations reported in this paper (which are plotted as code RN), minimal values existed at Hampton, Virginia in March and October 1974 and at San Angelo, Texas in May 1974. Dramatic increases then occurred in November and December at Hampton, though the variability was still high, as is evidenced by the large vertical brackets. January levels had settled down to more consistently high readings with



a. For 1962-1972.



b. For 1972-1975, the CIAP time frame.

Figure 12. History of average maximum scattering ratio for the 20-km region.

magnitudes even greater than the 1964-65 data of Grams and Fiocco (1967). Of course, the data of Grams and Fiocco were obtained in Massachusetts and Alaska and were begun some nine months after the eruption of Mount Agung. F.E. Volz of the Air Force Cambridge Research Laboratories observed dust over Boston from

Fuego about five weeks after its major eruptions (Volz, 1975). While average scattering ratios reported by Grams and Fiocco (1967) were no higher than 2.2, larger quantities of dust probably existed earlier. Also, both the data of Grams and Fiocco and the data presented in the present paper have been averaged over comparable altitude increments (about 0.5 km) in order to prevent any bias. Therefore, the intensity of the Fuego eruption appears to have been less than that of Mount Agung. Additional lidar data, not plotted during this post-Fuego period, are becoming available; these include the data of Fernald and Frush at the National Center for Atmospheric Research (NCAR) and the measurements by Fegley of the National Oceanic and Atmospheric Administration (NOAA) at the Mauna Loa Observatory in Hawaii.

SUMMARY AND CONCLUSIONS

The dustsonde and lidar comparative experiments indicate good correlation between the two measurement techniques for the background or minimum aerosol loading present in May 1974 over San Angelo, Texas.

The following points emerge from the analysis of the lidar observations from October 1974 to February 1975 at Hampton, Virginia:

- Onset of increased scattering was first observed at Hampton, Virginia on November 14, 1974;
- Substantial enhancement was observed at 19 km on November 26, 1974 but scattering ratios continued to be quite variable through December:
- The maximum scattering ratio of 3.3 was observed at 17 km on December 18, 1974 (the profile was obtained by averaging over 450 meters).
- The large-scale circulation pattern indicates the source of the dust to be from latitudes south of Virginia.
- Conversion factors between the aerosol backscatter and particle concentration, as determined at San Angelo, Texas, do not apply to the present enhanced aerosol layers.

ACKNOWLEDGMENTS

The comparative measurements were conducted jointly with Dr. J. Rosen of the University of Wyoming. Circulation charts were supplied by the Upper Air Branch of the National Oceanic and Atmospheric Administration, and rawinsonde data for determining air-density profiles were provided by J. Brewton of the Weather Service at Wallops Island, Virginia.

The lidar facility was supported by W. H. Fuller, Jr. of the Langley Research Center and W. Hunt, F. Diehl, and C. Bartusiak of Wyle Laboratories. Carolyn Jones of LTV Corporation conducted the data reduction and computer software programming.

This work was partially supported by a Department of Transportation contract DOT-AS-20062.

REFERENCES

- Clemesha, B.R., G.S. Kent, and R.W.H. Wright (1971), "Laser probing of the lower atmosphere," Nature 209, 184-185.
- Clemesha, B.R. and S.N. Rodriques (1971), "The stratospheric scattering profile at 23° South," J. Atm. Terrest. Phys. 33, 1119-1124.
- Fernald, F.G., C.L. Frush, and B.G. Schuster (1974), "Airborne lidar measurements of the distribution of stratospheric aerosols," in *Proceedings of the Third Conference on the Climatic Impact Assessment Program* (Cambridge, Mass.), U.S. Dept. of Transportation, DOT-TSC-OST-74-15, 318-322.
- Fox, R.J., G.W. Grams, B.G. Schuster, and J.A. Weinman (1973), "Measurements of stratospheric aerosols by airborne laser radar," J. Geophys. Res. 78, 7789-7801.
- Grams, G. and G. Fiocco (1967), "Stratospheric aerosol layer during 1964 and 1965," J. Geophys. Res. 72, 3523-3542.
- Hirono, M., M. Fujiwara, O. Uchino, and T. Itabe (1974), "Observations of stratospheric aerosol layers by optical radar," Can. J. Chem. 52, 1560-1568.
- Meinel, A.B. and M.P. Meinel (1975), "Stratospheric dust-aerosol event of November 1974," Science 188, 477-8.

- McCormick, M.P. and W.H. Fuller, Jr. (1975), "LIDAR measurements of two intense stratospheric dust layers," Appl. Opt. 14 (1), 4-5.
- Northam, G.B., J.M. Rosen, S.H. Melfi, T.J. Pepin, M.P. McCormick, D.J. Hofmann, and W.H. Fuller, Jr. (1974), "A comparison of dustsonde and LIDAR measurements of stratospheric aerosols," Appl. Opt. 13 (10), 2416-2421.
- Rosen, J.M. (1974), "Dustsonde and Ozone Support for the LACATE Experiment," Final Progress Report for Grant NSG 1009, Department of Physics and Astronomy, University of Wyoming, Laramie, WY.
- Russell, P.B., W. Viezee, R.D. Hake, Jr. and R.T. Collis (1975), "LIDAR observations of the stratospheric aerosol: Summary of results and a calibration-error assessment," in this volume.
- Schuster, B.G. (1970), "Detection of tropospheric and stratospheric aerosol layers by optical radar (LIDAR)," J. Geophys. Res. 75, 3123-3132.
- Volz, F.E. (1975), "Volcanic twilights from the Fuego eruption," Science 189, 48-58.
- Young, S.A. and W.G. Elford (1975), "Laser Observations of Stratospheric Aerosols at Adelaide (35°S), 1969-73," Report ADP 119, Dept. of Physics, University of Adelaide, Adelaide, Australia.

RECENT MEASUREMENTS OF AITKEN NUCLEI IN THE LOWER STRATOSPHERE

J. PODZIMEK

University of Missouri Rolla, Missouri

J.B. HABERL

General Electric Company Pittsfield, Massachusetts

W.A. SEDLACEK

Los Alamos Scientific Laboratory Los Alamos, New Mexico

ABSTRACT: Evaluation of the 1974 aircraft measurements of Aitken nuclei (AN) in the lower stratosphere showed that the mean concentration of AN at the tropopause level is between several hundred and one thousand nuclei per cm³, and that at altitudes above 18 km the AN concentration is only several tens of nuclei per cm³. Flights over the Rocky Mountains and over Texas during a well-developed jet-stream situation indicate an increased AN concentration at the 18-km level and strong fluctuations. A negative correlation between ozone and AN concentration was found above Houston and above the Gulf of Mexico at altitudes above 17 km on November 18 and 21, 1974. The possible reasons for the sudden changes of ozone and AN concentration along the aircraft path at the 18-km level are briefly discussed.

INTRODUCTION

The purpose of this report is to evaluate AN measurements performed in 1974 as a part of CIAP, using the new GE stratospheric AN counter. The instrument, named SANDS (Stratospheric Aitken Nuclei Detection System) was flown on a WB-57F aircraft up to an altitude of 20 km. This report is based on the results of twelve successful flights made in the months of March, April, May, and November 1974. These flights were designed to check the ability of the instrument (which was calibrated twice during this period) to measure the vertical profiles and the spatial distribution of AN concentrations in the lower stratosphere over the Rocky Mountains, Texas and the Gulf of Mexico. The results of several successful flights in 1975 will be described later.

THE INSTRUMENT: ITS DESCRIPTION, CALIBRATION, AND INSTALLATION IN THE AIRCRAFT

The GE SANDS instrument consists of an instrument unit, a pressurization unit, a cockpit-mounted control box, and a sampling-probe

assembly. Air samples are standardized in the pressurization unit to near-sea-level conditions before the nuclei are measured in the instrument unit

The pressurizer employs two holding chambers which alternate every two seconds in preparing and delivering the standardized air samples. Each holding chamber is first purged with air at ambient conditions; then it is sealed and clean air is added to raise the pressure to standard conditions.

The sample air enters the instrument unit (shown in Figure 1), passes through a cylindrical condenser (electrostatic precipitator), and then enters the cloud-chamber assembly. The cloud-chamber assembly includes humidifier components, cloud-chamber optical elements, a photo-multiplier tube, and a rotary air valve. Detection of AN is achieved by a cyclic adiabatic expansion which causes water droplets to form upon the nuclei. The droplets are sensed by the light they scatter in an illuminated dark-field cloud chamber. The cycling rate is 2.5 samples per second, which yields essentially continuous, real-time concentration data. When size measurements are desired, a programmed series of pre-

cipitating voltages are applied to the condenser. The consequent decrease in measured nuclei concentration is manually analyzed for size information.

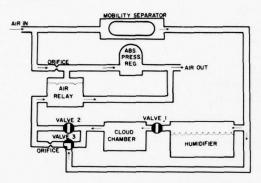


Figure 1. The SANDS instrument unit.

Since the system was designed for unattended operation, it contains automatic rangeswitching circuits which select the proper scale from the following ranges: 0-100, 100-300, 1000-3000, 3000-10,000, and 300-1000, 10,000-60,000 particles per cm³. The output data is in the form of analog voltages (+5V full scale) which continuously signal primary parameters (nuclei count, range, precipitation voltage step) as well as a number of secondary parameters (ambient pressure and temperature, expansion pressure, sample temperature, etc.). These voltages are sent to a flight-recording system (magnetic tape) provided in the aircraft. A more detailed description of the SANDS was published by Haberl (1975).

Preliminary calibration of the SANDS was performed by comparison with a Pollak counter using room-air nuclei diluted to various concentrations. The calibration was rechecked after six test flights and various laboratory operations; it showed no detectable shift. The functioning of the counter at stratospheric conditions was investigated at the Los Alamos Scientific Laboratory. Final calibration was performed twice in the laboratories of the Graduate Center for Cloud Physics Research at the University of Missouri-Rolla. It was based on a comparison with the UMR Aitken nuclei counter (Kassner et al., 1968). Comparison of the mentioned counters yielded the following results:

On the basis of a regression analysis, the mean correlation factor for seven different kinds

of aerosols (room air, sodium chloride, silver iodide, propane residual nuclei, nichrome, and gold) was approximately 0.90. The strongest correlation was found for propane residual nuclei and gold particles (0.970; 0.932) and the weakest correlation was found in the case of room-air and sodium chloride particles (0.855; 0.876). Analysis of electron micrographs of the aerosols used for the calibration showed the following mean sizes (diameters) of particles: $0.025 \,\mu\text{m}$ for gold, $0.05 \,\mu\text{m}$ for room air, $0.06 \,\mu\text{m}$ for nichrome-wire nuclei, and $0.13 \,\mu\text{m}$ for sodium chloride.

The ratio between estimated standard error and the concentration of AN served as a measure of the expected deviations of the measured data from the theoretically-assumed linear relationship. The ratio depends on the AN concentration range and on the nature of the nuclei; it amounted to several percent in the case of gold and nichrome aerosol and to several tens of percent for sodium chloride particles.

The SANDS instrument was installed in the nose section of the fuselage of the WB-57F aircraft. Sample air entered through two 1.5inch-diameter probes which extended three feet in front of the aircraft. The stratospheric air flowed continuously through a short air duct (SANDS intake tube) to the exhaust tube in the aft section of the aircraft nose. In this way, the velocity of the air in the duct was very close to that of the aircraft. Air which was necessary for pressurization of the sample came from the engine bleed. It was necessary to tap into the bleed air supply prior to passing through the pressure regulators (pressure maintained at one atmosphere) in order to have sufficient pressure at higher altitudes.

RESULTS OF THE MEASUREMENTS WITH THE SANDS

The AN concentrations measured by the SANDS follow the general trend of the vertical profiles found by Junge et al. (1961) and Rosen (1974) (see Figure 2). However, at an altitude above 18.0 km, the concentrations are about one order of magnitude higher than those found by Junge et al. This does not necessarily mean that Junge's measurements were characterized by particle losses in the instrument, as some authors suggested (Remsberg, 1972). The higher counts

of AN in the stratosphere might be explained more easily by the intense generation of AN by jet aircraft near the tropopause, which are exchanged into the higher stratosphere by bulk transport. The lower AN counts of Rosen (1974) could have been caused by the different supersaturation in his counter.

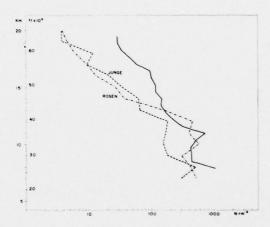


Figure 2. Comparison of the mean AN concentrations measured by SANDS over New Mexico, by Junge et al. (1961) over South Dakota, and by Rosen (1974) over Wyoming.

Vertical Profiles

Vertical profiles of AN concentrations were plotted from the aircraft ascents on March 5, April 10, May 5, 22, and 31, and November 18, 1974. The general features of those measurements were higher counts below the tropopause (several hundred to 1,000 cm⁻³) and a steep decrease in AN concentration above the tropopause. This decrease was strongly expressed during the ascents in April and May by comparison with the flights in March and November 1974 (see Figures 3 and 4). At altitudes above 50,000 feet, the mean AN concentration usually reached values between 20 and 100 nuclei per cm3. During several ascents, a distinct stratification of the measured AN counts was found above 50,000 feet; the layers with higher AN concentrations had thicknesses of several hundred to thousands of feet (Figure 4). During the November 18 flight (Figure 4) simultaneous measurements of ozone concentration were performed; they showed a mean negative correlation

of AN counts and ozone concentration above 17 km. The ozone concentrations measured by the instrument of Dr. Rosen and Dr. Hoffman are plotted in relative units, in which 10 means approximately 35 nanobars of ozone partial pressure at 25°C.

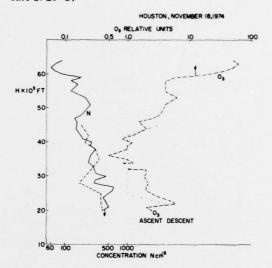
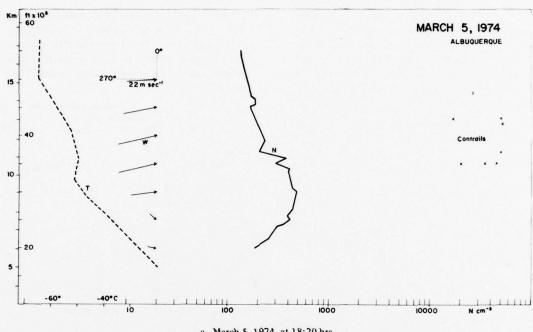


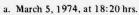
Figure 4. Vertical profile of AN and ozone concentrations over Houston, Texas on November 18, 1974 at 20:50 hrs GMT.

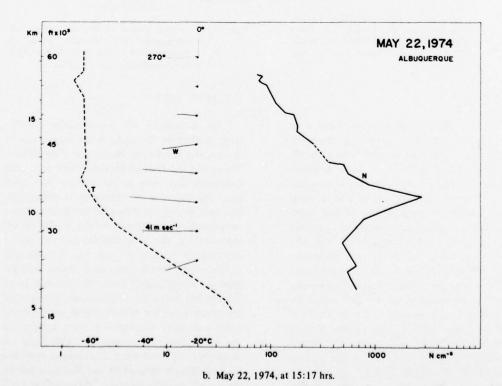
Rawinsonde ascent at 12:00 hrs.

Horizontal Flights

Six horizontal AN concentration profiles were plotted on the basis of the measurements made above the Rocky Mountains, New Mexico, Texas, and the Gulf of Mexico. There is a strong indication that even at the altitude of 62,000 feet, the influence of orography is measurable, and that the higher ridges of the Rocky Mountains seem to contribute to the mixing of air masses from the troposphere and the lower stratosphere as well (Figure 5a). A horizontal profile of the May 5 flight made above the New Mexico mountains and above the plains of Texas (Figure 5b) shows that high mountains stimulate the transport of the AN into higher stratospheric levels and form stratospheric wave patterns to the leeward of the mountains. The flight of November 21 southward of Houston over the Gulf of Mexico (Figure 6) was characterized by steady AN counts of around 100 nuclei per cm⁻³ at an altitude of 60,000 feet. However, southward of the latitude $\phi \approx 26^{\circ}$ N the record showed







Vertical profiles of AN concentrations over Albuquerque, New Mexico. In both cases the rawinsonde ascent was at $12:00\ hrs\ GMT$. Figure 3.

suddenly strong fluctuations, with AN concentrations often surpassing 200 counts per cm³. The AN variations were almost perfectly negatively correlated with ozone variations. This case seems to be a unique example of a direct relationship between AN and ozone concentrations, which might be interpreted in terms of possible stratospheric air exchange, or of the injection of pollutants into higher stratospheric levels.

Intercepts of Trails of Jet Aircraft

On several flights the pilots intentionally passed through the trails made by their airplanes and through the trails of commercial airplanes around the tropopause level. Those qualitative investigations showed (Figure 3a) that in a "fresh" trail AN concentrations can be as high as 20,000 cm⁻³. Interceptions of jet-engine exhaust were usually characterized by a decreased concentration of small ions (i.e., decreased electrical conductivity). However, for the time being no attempt has been made to draw quantitative conclusions from these measurements. Jet-engine exhaust trails generate a highly concentrated AN layer, which, mainly in areas covered by the lanes of commercial air transport, represent a constant potential source of air pollution in the lower stratosphere. Despite the fact that little is known about the nature of the nuclei, a valid hypothesis would be that there is an intense exchange of particles over mountainous areas.

Estimates of the Size Spectrum of the Stratospheric AN

Assuming charge equilibrium and the applicability of Boltzmann's Law for the distribution of charges on different sizes of aerosol particles (e.g., Rich, 1959), one can estimate the size spectrum of stratospheric AN in the following way: Stratospheric aerosol passes through a cylindrical condenser, where different voltages are imposed to drive the electrically charged particles to the appropriate electrode. The percentage of removed AN versus the applied voltage is converted into the number of AN (with an assumed particle mobility) that will be totally precipitated at certain voltages. Despite the uncertainties related to the assumptions made, and the low accuracy of the AN concentration readings, an attempt was made to evaluate several measurements made during the flights of November 1974.

The flight of November 15 over Texas showed that integrated AN concentration can be roughly expressed as an exponential function of the radii of AN. For this reason, the number of particles larger than a certain size was plotted in relative units (see Figure 7a), assuming that each AN carries a charge. A curve similar to that of November 15 was found six days later at the altitude of 18.2 km, approximately 10 minutes before the AN concentration started to fluctuate (Figure 7b).

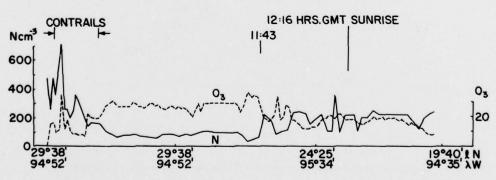
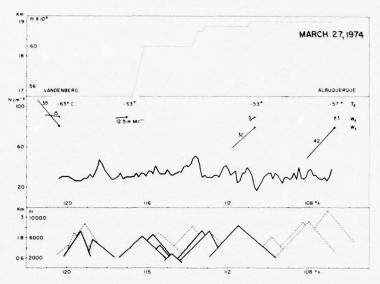
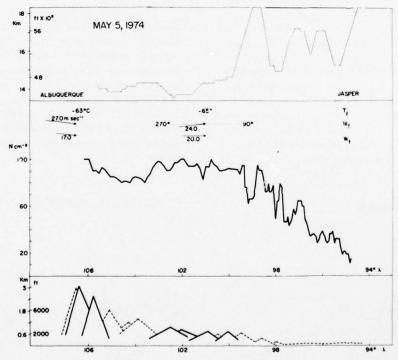


Figure 6. Horizontal profile of AN concentrations along the flight path south of Houston over the Gulf of Mexico, on November 21, 1974, 10:27 to 12:43 hrs GMT. Ozone concentrations are roughly evaluated in relative units.

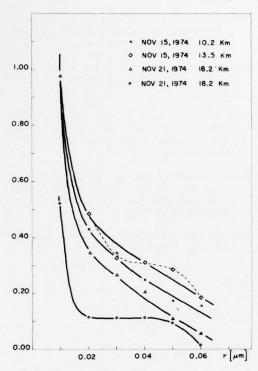


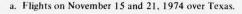
a. Flight path between Vandenburg (CA) and Albuquerque on March 27, 1974, 20:50 to 22:50 hrs GMT.

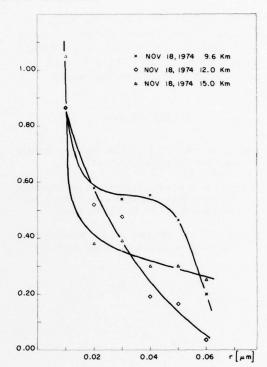


b. Flight path between Albuquerque and Jasper (TX) on May 5, 1974, 8:42 to 12:00 hrs GMT.

Figure 5. Horizontal profile of AN concentrations. In the upper part of the figure is the flight altitude; T_f is the temperature at the flight level; W_f is the wind vector at the flight level; W_t is the wind vector at the tropopause level; Ncm⁻³ are Aitken-nuclei concentrations. In the lower part of the figure are the mean altitudes of the mountains along the flight path (unbroken line signifies mountains within 15 miles of the path on the south, broken in esignifies the same on the north).







b. Flight on November 18, 1974 over Houston.

Figure 7. Rough estimates of AN size distribution at different altitudes.

Unlike the AN size spectra of November 15 and 21, the spectrum of nuclei measured during the aircraft ascent over Houston on November 18 (Figure 7b) had the following features: Two different groups of particles were found at the altitude of 9.6 km. One, with particles with radii larger than 0.04 μ m, represented almost 60% of the total AN concentration; the other had particle radii less than 0.01 μ m. The curve at the tropopause level had a shape similar to those of the curves of November 15. However, at an altitude of 15.0 km there was a sudden change in AN size distribution; more than 25% of the measured AN had radii larger than 0.06 μ m.

The mentioned method, its accuracy, and the deduced size spectra of AN could be subjected to criticism. However, there seems to be one possible explanation of the different shapes of the curves of November 18 and the curves deduced from the measurements of November 15 and 21. Because the curves of November 18 are characterized by a relatively high precipitation of

particles with radii greater than $0.04 \mu m$, one might hypothesize that their presence at an altitude of 15.0 km over the Houston area could be related to the eruption of the Guatemalan volcano Fuego (McCormick et al., 1974; Volz, 1975).

ACKNOWLEDGMENTS

The authors wish to thank S.C. Coroniti and J. Sturm from the U.S. Department of Transportation for their advice and support in this work and P. Christman, R. McPherson, L.F. Gil, D. Koonce, S. Shults, and E. Podzimek for their technical assistance. Also, they are grateful to E. Danielson, from NCAR, for making available all meteorological data for the flights of the first half of 1974. Last, but not least, the authors highly appreciate the flight planning and technical assistance of P. Guthals and the many unnamed pilots, navigators, and technicians of the USAF 58th Weather Reconnaissance Squadron

stationed at Kirtland AFB and the NASA Johnson Space Center, Houston. Without their unfailing readiness to help, and without the financial support of the Office of Naval Research, this investigation would not have been possible.

REFERENCES

- Haberl, J.B. (1975), "Stratospheric Aitken nuclei counter," Rev. Sci. Instrum. 4, 443-447.
- Kassner, J.L., Jr. (1968), "Experimental and Theoretical Studies of Nucleation Phenomena," Rept. to NSF, No. GA-428, GCCPR, Univ. of Mo.-Rolla.
- Junge, C.E., C.W. Chagnon, and J.E. Manson (1961), "Stratospheric aerosols," J. Meteor. 18, 81-108.

- McCormick, M.P. and W.H. Fuller, Jr. (1975), "Lidar measurements of two intense stratospheric dust layers," Appl. Opt. 14 (1), 4-5.
- Remsberg, E. (1972), "Discrepancies in stratospheric Aitken nuclei counts," J. Geophys. Res. 77, 6014-6016.
- Rich, T.A., L.W. Pollak, and A.L. Metnieks (1959), "Estimation of average size of submicron particles from the number of all and uncharged particles," Geof. Pura Appl. 44, 233-241.
- Rosen, J.M. and D.J. Hofmann (1974), "Recent Measurements of Condensation Nuclei from Ground Level to 25 km," Rept. No. CN-2, University of Wyoming, Laramie, WY.
- Volz, F.E. (1975), "Volcanic twilights from the Fuego Eruption," Science 189, 48-49.

IN-SITU MEASUREMENTS AT LARAMIE, WYOMING OF THE RECENT INCREASE IN STRATOSPHERIC AEROSOL

D.J. HOFMANN AND J.M. ROSEN

Department of Physics and Astronomy
University of Wyoming
Laramie, Wyoming

ABSTRACT: Recent balloon soundings of the stratospheric aerosol by photoelectric particle counters are compared with earlier ones. It is suggested that the observed increase in late 1974, and a similar one in late 1971, may require explanations other than the identified volcanic eruptions.

The University of Wyoming's Atmospheric Research Group has continued to make measurements of the stratospheric aerosol for the Climatic Impact Assessment Program (CIAP) through 1974, although on a greatly reduced scale. The balloon soundings made with the Wyoming dustsonde have been continued at the Laramie station on a seasonal basis. While the extensive measurements obtained during the first two and one-half years of the program revealed a general decay of aerosol particles following an apparent increase in late 1971, recent observations indicate that the stratospheric aerosol has once again undergone a substantial increase in late 1974. However, as with the 1971 increase, it is again not clear that the new increase is associated with a particular volcanic eruption.

Observations of this increase are now numerous; they apparently began with enhanced twilights observed over Mexico and Arizona by Meinel and Meinel (private communication) in November. These observations were subsequently confirmed through lidar detection of two stratospheric particle layers by the NASA and NCAR groups. In addition, pilots flying the RB-57 for the November CIAP mission also reported visible dust layers in the stratosphere.

Although in-situ dustsonde measurements of the two extensive layers observed by lidar were not carried out until December 10, it is of interest to note that a sounding at Laramie on October 8 had already revealed a new layer in the lower stratosphere. The observations follow.

Figure 1 (central box) shows the total number of aerosol particles having diameters greater than 0.3 μ m per cm² column of strato-

sphere above 20 km, above 15 km and above the local tropopause, at Laramie, Wyoming, as a function of time from late 1971 to late 1974. The last two points are the soundings of October 8 and December 10. Notice that the increasing trend which began in October is larger than would be expected from a "normal" extrapolated seasonal variation. The integrated aerosol was observed to have a value of 3.2×10^6 particles/cm² column above the tropopause on December 10, 1974. This is about 50% higher than the increase observed in December 1971. The December 1971 level may have been higher, however, since maximum twilight effects had already been noticed in October of that year by Volz. The latter event could not be readily related to volcanic activity. We thus submit that the recent event, which apparently already had begun in October, is similar to the 1971 event, and may not be due solely to the volcanic activity of Fuego on Guatemala in October as has been proposed by several observers.

Figure 1 (lower box) also shows the concentration ratio (N > 0.3 μ m)/(N > 0.5 μ m), and gives an indication of changes in the aerosol size distribution. The gradual increase in the ratio, indicating a trend towards smaller particles, reached a peak in April 1974, and now appears to be declining. The last point shown (for the 10 December sounding) is somewhat misleading, since one of three layers observed in that sounding consisted of very small particles (ratio \approx 16) while the other two layers indicated relatively large particles (ratio \approx 3). The resulting average ratio of about 5 for the sounding is thus not as representative as one would like, since

HOFMANN AND ROSEN

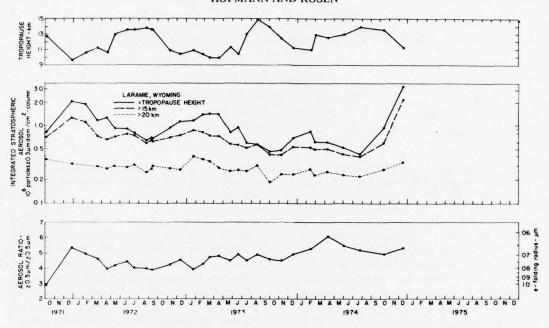


Figure 1: Tropopause height, integrated aerosol, and aerosol ratio as functions of time obtained at Laramie during the CIAP measurements.

most of the new particles were somewhat larger than those generally observed over the past two years. This will be described in more detail later.

The top box in Figure 1 gives the tropopause height, which has shown an excellent anticorrelation with total aerosol in the past. Since the tropopause heights for the 8 October sounding and the sounding before that on 23 July were not much different, the increase observed in October was not due to the normal seasonal variation but rather to a new aerosol layer.

Figure 2 shows the vertical aerosol distribution (diameters greater than 0.3 µm) for the July 23, October 8 and December 10 soundings. As indicated earlier, the increase in total aerosol in October was due mainly to the layer at 130 mb. This layer had a ratio of concentrations of about 3.5. In December, a layer was again observed at 130 mb, with additional higher layers at 82 mb and 60 mb as shown in Figure 2. However, the layer at 130 mb was now found to have a very steep size distribution, with a concentration ratio of about 16, while the two upper layers had a relatively flat size distribution (ratio ≈3). Figure 3 shows these features by comparing the vertical distributions of particles having diameters greater than $0.3 \,\mu m$ and greater than $0.5 \,\mu m$ for the December sounding. Notice that the larger particles were essentially absent in the lower layer. For this reason, during the night previous to the sounding, the NCAR lidar, being relatively insensitive to small particles, did not detect the lower layer, while it clearly saw the upper two (Fernald, private communication). Thus, the lower layers observed on the October and the December soundings are probably not one and the same, unless the characteristic aerosol particle size somehow changed through a process such as evaporation. It appears more plausible to explain this observation in terms of multiple sources, probably of a different nature. At this writing, analysis of particles collected in the layers by the Los Alamos group has not been completed, so the composition of the particles is not yet known. If they are sulfates, as has been the case in the past, they were probably formed from sulfur-bearing gases. Since the time constant for growth of sulfate particles to the relatively large size observed is thought to be at least one-half year, it is doubtful that volcanic activity in October could result in extensive sulfate aerosol layers in early December unless they were directly injected as such. Furthermore, the suggestion that the general nature of the

HOFMANN AND ROSEN

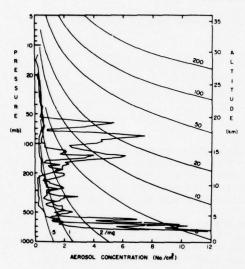


Figure 2. Three aerosol (d ≥ 0.3 μm) soundings at Laramie. Reading from left to right at the 15-km level, the dates are July 23, 1974, Cctober 8, 1974 and December 10, 1974.

stratospheric aerosol was already changing prior to the eruption of Fuego makes this eruption even less plausible as the only source of the layers.

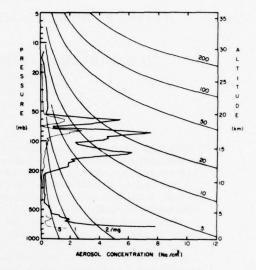


Figure 3. The vertical distribution of two aerosol size ranges at Laramie on December 10, 1975. The thick and thin lines represent particles with diameters greater than 0.3 and 0.5 μ m, respectively.

It is the hope of the Wyoming group that enough observations of this event have been made so that the various research methods can be compared and a reasonable explanation can be constructed.

ION AND AEROSOL MEASUREMENT IN THE STRATOSPHERE

HARUJI ISHIKAWA, YASUHIRO MORITA, AND MASUMI TAKAGI

Research Institute of Atmospherics Nagoya University Toyokawa, Japan

ABSTRACT: Simultaneous measurements of atmospheric small ions, condensation nuclei (CN), and aerosols (with diameters of $>0.3 \mu m$) have been made with balloons in cooperation with University of Wyoming, in a cooperative Japan-US program of work, sponsored by the CIAP program of DOT.

This work has included a balloon flight at Sanriku, Japan in October 1973 and two at Laramie, Wyoming in May-June 1974. Simultaneous concentration profiles of small ions, CN and aerosols have been obtained on a single balloon.

Comparisons between small ions and CN, and between small ions and aerosols, indicate reasonable agreement of their gross profile structures and the theoretically deduced profiles that assume ion equilibrium state in the stratosphere and troposphere; on the other hand, closer comparison of profile details often indicated contrary results. Accumulation of simultaneously measured data on ions and aerosols in the stratosphere is concluded to be very important for exploring the relationship of atmospheric electricity to aerosol problems.

INTRODUCTION

It is a generally accepted concept of research in atmospheric electricity that under fair-weather conditions there is an electrical balance between production and loss of small ions, over appropriate scales of time and space. Ion production in the stratosphere is thoroughly controlled by cosmic rays, whose intensities are believed to be constant with time, except for abnormal solar events. Ion dissipation in the stratosphere is controlled by recombination between small ions and by attachment of small ions to aerosols. The latter mechanism applies mainly to the submicron size range (involving CN), and is supposed to be less important in the large particle size range (aerosols with diameters of $> 0.3 \,\mu\text{m}$). Junge et al. (1961) made measurements of Aitken nuclei (AN, thought to be roughly equivalent to CN) and large aerosol particles in the stratosphere and compared their concentration profiles. As a result, they attached considerable importance to the simultaneous measurement of AN and large aerosol particles for the study of the nature and distribution of stratospheric and tropospheric aerosols.

Measurement of aerosol particles throughout the whole size range, from micron through submicron to very small, may be most properly made with the combination of a neutral particle counter (an optical dust-particle counter along with an optical CN counter) and an atmospheric small-ion counter. Under prevailing ion-equilibrium conditions, the concentration of small ions (including electric conductivity) is a convenient parameter, containing information about the concentration of submicron aerosols (including very small sizes) in the troposphere and stratosphere, and it is especially useful for surveying the secular variation of the global distribution of pollutants for the 1970's (Cobb and Wells, 1970).

SIMULTANEOUS MEASUREMENT OF ION AND AEROSOL

Cooperative simultaneous measurements of ions and aerosol in the stratosphere were made for the first time at Sanriku Balloon Launching Site (Sanriku, Iwate, Japan), of the Research Institute of Space and Aeronautical Science, University of Tokyo, using a 5000-cubic-meter balloon. Sent up with the balloon were the atmospheric electrical conductivity meter of the Gerdien condenser type, which was developed by Nagoya University for estimating submicronaerosol concentration in the stratosphere, and the optical-dust particle counter which was developed by the University of Wyoming for the measurement of concentration of aerosols with

diameters of $> 0.3 \,\mu\text{m}$. The balloon was launched on Oct. 10, 1973; it drifted eastwards over the Pacific ocean while floating at 26 km above sea surface.

After 330 minutes of measurement of conductivity in level flight, the balloon was cut off from the payload by a command signal sent from the launching site, and the payload parachuted to the sea surface. The next two simultaneous measurements of ion and aerosol were made at the University of Wyoming's Laramie balloon launching site (Laramie, Wyoming), where the twin-balloon technique was used to keep the ascending and descending speeds of the payload system almost the same. It is in this way possible to check the validity of the balloon measurements, by whether the upward leg and downward leg profiles coincide. Payloads (all instruments loaded on a metal frame) hanging down from two plastic balloons (about 3000 cubic meters each) were launched on May 27 and May 30, 1974. After about 100 minutes of flight in the air, one of the twin balloons was cut off from the payload system at maximum altitude (17 mb on May 27, and 14 mb on May 30), and the payload, suspended from the remaining balloon, descended at roughly the same speed it had ascended. Comparison between the ascent and

descent profiles for each item of the measurement (ion, aerosol, etc.) indicated reasonable agreement, and this was thought to guarantee the validity of the balloon measurement. On May 27 we flew the ionization chamber for ionization measurement, the Gerdien condenser for electrical conductivity (Nagoya University), the CN optical counter for condensation nuclei measurement, and sensors for ozone, temperature, and pressure (University of Wyoming). On May 30 we replaced the ionization chamber (Nagoya University) with an optical-dust particle counter (University of Wyoming) that counts aerosols with diameters of $> 0.3 \, \mu \text{m}$, and left the other items of the measurements unchanged.

Figure 1 shows a positive-polar-conductivity profile obtained during the ascending period of the flight on May 30, 1974; it represents a typical exponential conductivity increase with altitude.

Simultaneous measurements of small-ion concentration and conductivity on several balloon flights in the past years have indicated that the mobility of small ions usually takes nearly the same value of 1.3×10^{-4} m²/vol sec, when the mobility value calculated from the measured values of concentration and conductivity is reduced to the value at ground level. This calculation is done by assuming mobility to be

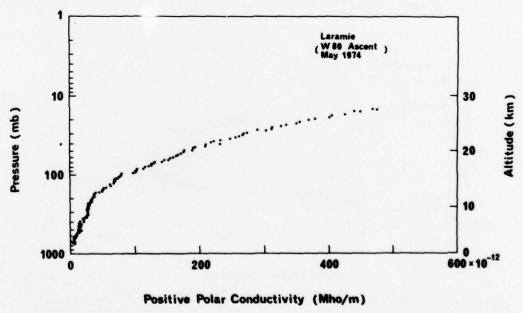


Figure 1. Positive electric polar conductivity profile. (Flight W80, ascent, Laramie, Wyoming, May 30, 1974.)

inversely proportional to air density (Morita, 1973). This evidence is thought to be experimental support for the theory that the size distribution of small ions is constant in the troposphere and lower stratosphere up to about 20 km in altitude.

It appears to be reasonable to assume that the trend of variations of the mobility value with altitude, whose validity is confirmed up to 20 km, can be extended up to 30 km without producing serious errors. In accordance with this idea, we calculated the profile of small-ion concentration using measured conductivity values and calculated experimental values for small-ion mobility. The result for the small-ion concentration profile is shown in Figure 2, along with the profile for aerosols with diameters of $> 0.3 \, \mu \text{m}$, obtained with the optical dust-particle counter. The two profiles are the result of simultaneous measurements made aloft on a balloon system sent up on Oct. 10, 1973.

Figure 3 shows the small-ion concentration profile, calculated in the same way as that of Figure 2. Also shown in Figure 3 is the condensation-nuclei profile measured with the optical CN counter. The two profiles in Figure 3 represent the results obtained from simultaneous

measurement of conductivity and aerosols (including CN) made on a balloon launched on May 30, 1974.

RESULTS

If the concentration profiles shown in Figure 2 for small ions and aerosol particles with diameters of $> 0.3 \,\mu m$ are compared, a highconcentration layer of large aerosol particles, with a laminar structure of concentration fluctuations superposed on it, is found to extend to about 9 km altitude from the lowermost part of the atmosphere. Corresponding to this, smallion concentration decreases steeply from 9 km downward towards the lowermost atmosphere. A similar trend appears when the concentration profiles of small ions and condensation nuclei are compared, as indicated in Figure 3. A condensation-nuclei layer of high concentration, with strong concentration fluctuations superposed on it, is found to extend to 12-13 km altitude from the bottom of the atmosphere. Corresponding to this, a very steep decrease in small-ion concentration is found from about 16 km altitude downward towards the bottom of the atmosphere, with a step decrease at 12 km altitude. Further

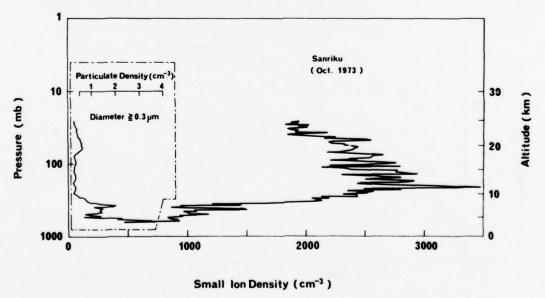


Figure 2. Small-ion density profile deduced from electric conductivity measurement (Nagoya University) and aerosol-particle profile ($d > 0.3 \,\mu\text{m}$) obtained with an optical dust-particle counter (University of Wyoming). (Flight S73 ascent, Sanriku, Iwate, Oct. 10, 1973.)

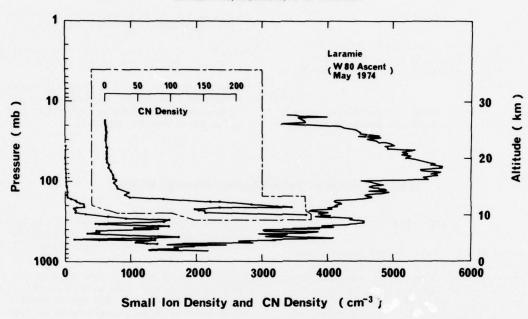


Figure 3. Small-ion density profile deduced from electric-conductivity measurements (Nagoya University) and condensation-nuclei density profile obtained with CN optical counter (University of Wyoming). (Flight W80, ascent, Laramie, Wyoming, May 30, 1974.)

examination was made of the large-aerosolparticle profile which was obtained simultaneously with the condensation-nuclei profile on the May 30, 1974 balloon flight shown in Figure 3. The thickness of the lowermost high-concentration layer for large aerosol particles was found to be 12-13 km from the ground level, and few differences were found between the condensationnuclei and large-aerosol profiles. It is very reasonable, as a manifestation of a gross general trend of atmospheric electricity, to see that a considerable decrease in the layered structure of small-ion concentration is really very closely correlated with a high-concentration layer of condensation nuclei and with a high-concentration layer of large aerosol particles, and that both these layers are distributed over the same altitudes, from ground to 12-16 km in the troposphere and lower stratosphere. Comparison of concentration profiles of small ions, condensation nuclei, and large aerosol particles, if it is made in great detail, often shows contrary relations - for example, a decrease in small-ion concentration often shows very clear correspondence with a decrease in concentration of condensation nuclei and/or large aerosol particles etc. Possible causes might be found in instrumentation problems and/or in the real geophysics of atmospheric electricity. For example, if the instruments for concentration measurement of small ions and of condensation nuclei work best for different sizedistribution ranges, we could not expect to measure condensation nuclei which have less electrical activity to contribute to small-ion equilibrium establishment in the stratosphere. If small-ion equilibrium does not hold in the stratosphere over the scale of space and time appropriate to our measuring instruments, we would obtain another complicated relationship between small ions and condensation nuclei. If, on the other hand, the origins of condensation nuclei and large aerosol particle formation are different and independent of each other, we would observe another contrary correlation between small ions and large aerosol particles in the stratosphere.

In view of the complexity of the present problems, the accumulation of sufficient data from simultaneous measurements of ions and aerosols throughout the whole size-distribution range is concluded to be very important for the exploration of the potential application of atmospheric electricity to aerosol problems in the submicron size range in the stratosphere.

REFERENCES

- Cobb, W.E. and H.J. Wells (1970), "The electrical conductivity of oceanic air and its correlation to global atmospheric pollution," J. Atmos. Sci. 27, 814-819.
- Junge, C.E. (1961), "Vertical profiles of condensation nuclei in the stratosphere," J. Meteor. 18, 501-509.
- Junge, C.E., C.W. Chagnon, and J.E. Manson (1961), "Stratospheric aerosols," J. Meteor. 18, 81-108.
- Junge, C.E., and J.E. Manson (1961), "Stratospheric aerosol studies," J. Geophys. Res. 66, 2163-2182.
- Morita, Y. (1973), "Studies on the temporal and spatial variations of atmospheric electric parameters and their relation to atmospheric pollution," Proc. Res. Inst. Atmos. Nagoya U. 20A, 39-51.

AEROSOL AND ION CONCENTRATION MEASUREMENTS

DISCUSSION

(UNIDENTIFIED): Nearly everybody measures small-particle concentrations by water supersaturation in adiabatic expansion chambers using a standard technique. These particles have been called "Aitken nuclei." Could you please tell me what advantage we gain in measuring "Rosen nuclei" with the new technique just described?

ROSEN: As far as our environmental tests go, there is no difference between using water and using alcohol. We use alcohol primarily because it doesn't evaporate at the high altitudes. Water, of course, would give us quite a few problems. In fact, we wouldn't be able to obtain measurements at the altitudes we do. It seems to make no difference whether you use water or alcohol or whatever.

(UNIDENTIFIED): Dr. Podzimek, the size distribution you showed seemed to trail off, at least as I read it from your plot on log-probability paper. The smallest size you show is about 1/100 of a micron, and there's very little of the mass of the Aitken nuclei in that range. Do you think the fact that your distribution goes quickly toward zero at that size accurately reflects the ambient stratosphere, or might this be an instrumental effect?

PODZIMEK: We did apply the Fuchs electrical-mobility method to measure the size distribution of small particulates. Of course, the theory behind this technique is very primitive. I would be more suspicious that there are some deficiencies in the theory, before I began to

blame the instrument. If I understood your question correctly, I guess I would say that the size distribution might be realistic, but the absolute numbers are not.

HALE: I'd like to briefly mention the result of a measurement that may relate to the nucleation of particles in the stratosphere. This was an electricalconductivity measurement made in the south of France in collaboration with Ackerman and the Belgian group; we measured electrical conductivity through a sunset period. At a solar zenith angle of about 85°, the conductivity due to the positive ions began to increase, and it grew by a factor of 3 in a period of about an hour. Since that period is too short for the ion density to change appreciably, we believe that the ion mobility was increasing, and thus that in the daytime the ion mobility is very small, indicating that in sunlight the positive ions are large aggregates. During this same time frame the negative conductivity decreased by a factor of three and at night the negative and positive ion conductivities were about the same, indicating that there were only small ions present. I also attribute the large daytime negative conductivity to the possibility of ultraviolet photodetachment of electrons from negatively charged aggregates.

(UNIDENTIFIED): Recent papers by Kiang and Hamill and their co-workers show that it is thermodynamically possible that some small but significant amounts of nitric acid could be dissolved in sulfuric acid particles in the stratosphere, and this would lower the freezing point of the dreplets and make it more likely that they are liquid in the stratosphere.

PUBLICATIONS OF THE CLIMATIC IMPACT ASSESSMENT PROGRAM

Report of Findings: The Effects of Stratospheric Pollution by Aircraft, by A.J. Grobecker, S.C. Coroniti, and R.H. Cannon, Jr. (1975). U.S. Department of Transportation Rept. No. DOT-TST-75-50. (Available from NTIS as AD-A005458, at \$19.25.)

The Natural Stratosphere of 1974, edited by E.R. Reiter, E. Bauer, and S.C. Coroniti (1975). Volume 1 of the CIAP monograph series. U.S. Department of Transportation Rept. No. DOT-TST-75-51. (Available from NTIS as PB246318, at \$41.75.)

Propulsion Effluents in the Stratosphere, edited by J.M. English, R.C. Oliver, and A.K. Forney (1975). Volume 2 of the CIAP monograph series. U.S. Department of Transportation Rept. No. DOT-TST-75-52. (Available from NTIS as PB246319, at \$12.00.)

The Stratosphere Perturbed by Propulsion Effluents, edited by G.D. Robinson, H. Hidalgo, and R. Greenstone (1975). Volume 3 of the CIAP monograph series. U.S. Department of Transportation Rept. No. DOT-TST-75-53. (Available from NTIS as PB249684, at \$15.00.)

The Natural and Radiatively Perturbed Troposphere, edited by C.E. Leith, H. Hidalgo, and N. Sundararaman (1975). Volume 4 of the CIAP monograph series. U.S. Department of Transportation Rept. No. DOT-TST-75-54. (Available from NTIS as PB249316, at \$16.25.)

Impacts of Climatic Change on the Biosphere, Volume 5 of the CIAP monograph series (1975). U.S. Department of Transportation Rept. No. DOT-TST-75-55.

Part 1 – Ultraviolet Radiation Effects, edited by D.S. Nachtwey, M.M. Caldwell, R.H. Biggs, P. Cutchis, and J.J. Gwiazdowski. Chapters 1-3 available from NTIS as PB247724 (\$16.25); chapters 4-7 available as PB247725 (\$18.75).

Part 2 - Climatic Effects, edited by J. Bartholic, R.E. Jensen, M.M. Caldwell, P. Cutchis, and J.J. Gwiazdowski. Available from NTIS as PB247726, at \$13.00.

Economic and Social Measures of Biologic and Climatic Change, edited by R.C. d'Arge, G. Daly, and C.W. Patten (1975). Volume 6 of the CIAP monograph series. U.S. Department of Transportation Rept. No. DOT-TST-75-56. (Available from NTIS as PB247727, at \$32.75.)

Proceedings of the Survey Conference (Feb. 15-16, 1972), edited by A.E. Barrington (1972). Climatic Impact Assessment Program, U.S. Department of Transportation Rept. No. DOT-TSC-OST-72-13. (Available from NTIS as PB212427, at \$9.25.)*

Proceedings of the Second Conference on the Climatic Impact Assessment Program (Nov. 14-17, 1972), edited by A.J. Broderick (1973). U.S. Department of Transportation Rept. No. DOT-TSC-OST-73-4. (Available from NTIS as PB221166, at \$11.75.)*

Proceedings of the Third Conference on the Climatic Impact Assessment Program (Feb. 26 - Mar. 1, 1974), edited by A.J. Broderick and T.M. Hard (1974). U.S. Department of Transportation Rept. No. DOT-TSC-OST-74-15. (Available from NTIS as ADA003846, at \$15.00.)*

^{*}A limited supply of the CIAP Proceedings is still available from Dr. Thomas M. Hard at the Transportation Systems Center.

LIST OF REGISTRANTS

Marcel Ackerman Institut d'Aéronomie Spatiale 3 avenue Circulaire B 1180 Brussels, Belgium

Eric Allen SUNY Atmospheric Science Research Center 1400 Washington Ave. Albany, NY 12222

Frederick N. Alyea Department of Meteorology MIT Cambridge, MA 02139

J.G. Anderson Space Physics Research Lab University of Michigan Ann Arbor, MI 48105

Larry G. Anderson Environmental Science Dept, GM Research Laboratories Warren, MI 48090

R. Rox Anderson Harvard Medical School Massachusetts General Hospital Boston, MA 02114

Etienne Arijs Institut d'Aéronomie Spatiale 3 Ringlaan 1180 Brussels, Belgium

Randolph W. Ashby Edwards AFB, CA 93523

Thomas E. Ashenfelter NOAA Air Resources Laboratory 8060 13th St. Silver Spring, MD 20910

Robert W. Atherton Systems Control, Inc. 1801 Page Mill Rd. Palo Alto, CA 94304

Walter Baginsky Air Force Cambridge Research Labs Hanscom AFB Bedford, MA 01731

Donald W. Bahr General Electric Co. 6576 Branford Ct. Cincinnati, OH 45236

Charles E. Baker NASA Lewis Research Center 21000 Brookpark Road Cleveland, OH 44135 Harold N. Ballard Atmospheric Sciences Lab White Sands Missile Range, NM 88002

Emanuel M. Ballenzweig (AEQ-220) DOT Federal Aviation Administration 800 Independence Ave., SW Washington, DC 20591

William R. Bandeen NASA Goddard Space Flight Center Greenbelt, MD 20771

Morton L. Barad Air Force Cambridge Research Labs Hanscom AFB Bedford, MA 01731

John L. Barnes Department of Engineering UCLA Los Angeles, CA 90024

Neal M. Barr The Boeing Company Renton, WA 98124

Marcel Barrère
ONERA
29, ave, de la Division Leclerc
92320 Châtillon-sur-Bagneux, France

Joan B, Barriage (AEQ-2) DOT Federal Aviation Administration 800 Independence Ave., SW Washington, DC 20591

William C. Bartley Science & Technology Policy Office National Science Foundation 1800 G St., NW Washington, DC 20550

Arthur Bass Flow Research, Inc. 1 Broadway Cambridge, MA 02142

E. Karl Bastress Arthur D. Little, Inc. Acorn Park Cambridge, MA 02140

Ernest Bauer Institute for Defense Analyses 400 Army-Navy Drive Arlington, VA 22202

P. C. Beadle British Aircraft Corp. Filton House, Filton Bristol, England BS99 7AR James Bell Dept. of Applied Science Brookhaven National Laboratory Upton, NY 11973

A. Belmont Control Data Box 1249 Minneapolis, MN 55440

Robert S, Berens Boston Air Pollution Control Commission 31 State St. Boston, MA 02109

Daniel Berger Temple School of Medicine 3322 N. Broad Street Philadelphia, PA 19140

A. L. Berlad
Department of Mechanics
State University of New York at Stony Brook
Stony Brook, NY 11794

G. T. Best Air Force Cambridge Research Labs Hanscom AFB Bedford, MA 01731

R. H. Biggs Fruit Crops Department University of Florida Gainesville, FL 32611

F. G. Blake Science and Technology Policy Office National Science Foundation 1800 G St., NW Washington, DC 20550

H. Blau Environmental Research and Technology 696 Virginia Rd. Concord, MA 01742

William S. Blazowski Air Force Aero Propulsion Lab Wright-Patterson AFB, OH 45433

M. H. Bortner GE Space Sciences Laboratory P. O. Box 8555 Philadelphia, PA 19101

William J. Borucki NASA Ames Research Center Moffett Field, CA 94035

B. W. Boville
Atmospheric Environment Service
4905 Dufferin St.
Downsview, Ontario M3H 5T4, Canada

Edward George Bowen Embassy of Australia 1601 Massachusetts Avenue, NW Washington, DC 20036

Frank A. Bower E. I. du Pont de Nemours & Co. Freon Products Lab, Chestnut Run Wilmington, DL 19898

Guy Brasseur Institut d'Aéronomie Spatiale 3 avenue Circulaire 1180 Brussels, Belgium

Anthony J. Broderick (641) DOT Transportation Systems Center Kendall Square Cambridge, MA 02142

Charles M. Brown U.S. Naval Research Laboratory Washington, DC 20375

Edmond A. Brun President, COVOS 93, bd. du Montparnasse 75006 Paris, France

Charles E. Brunot Environmental Protection Agency Fourth and M Sts., SW Washington, DC 20460

John A, Busterud Council on Environmental Quality 722 Jackson Place, NW Washington, DC 20006

Richard D. Cadle NCAR P. O. Box 3000 Boulder, CO 80303

George E. Caledonia Physical Sciences Inc. 18 Lakeside Office Park Wakefield, MA 01880

Linwood B. Callis NASA Langley Research Center Hampton, VA 23365

Robert H. Cannon, Jr. Chairman, Department of Engineering California Institute of Technology Pasadena, CA 91103

Charles O. Cary (AIA-1) Federal Aviation Administration 800 Independence Ave., SW Washington, DC 20591 A. W. Castleman, Jr. Dept, of Chemistry University of Colorado Boulder, CO 80302

R. E. Center AVCO Everett Research Labs 2385 Revere Beach Parkway Everett, MA 02149

William Chameides Space Physics Research Lab University of Michigan Ann Arbor, MI 48105

Julius S. Chang Lawrence Livermore Laboratory P. O. Box 808 Livermore, CA 94550

M. L. Chanin Service d'Aéronomie CNRS 91370 Verrières-le-Buisson, France

E. T. Chesworth Ionosphere Research Laboratory Pennsylvania State University University Park, PA 16802

D. Chleck Panametrics Inc. 221 Crescent Street Waltham, MA 02154

Ralph J. Cicerone Space Physics Research Lab. University of Michigan Ann Arbor, MI 48105

Clayton Clark Utah State University Logan, UT 84322

Alan E. Clarke U. K. Department of Industry Room 610, Monsanto House 10-18 Victoria Street London, England SW1 HONQ

Shepard A. Clough (OPI) Air Force Cambridge Research Labs Hanscom AFB Bedford, MA 01731

Dale Compton NASA Ames Research Center Moffett Field, CA 94035 René V. Cormier Air Force Cambridge Research Labs Hanscom AFB Bedford, MA 01731

Samuel C. Coroniti (TST-46) Deputy Manager, CIAP Department of Transportation 2100 Second St., SW Washington, DC 20590

Owen R, Coté Air Force Cambridge Research Labs Hanscom AFB Bedford, MA 01731

Edward C. Creutz National Science Foundation 1800 G St., NW Washington, DC 20550

George W. Crosse British Embassy 3100 Massachusetts Ave., NW Washington, DC 20008

Thomas J. Crowley Dept. of Geology (CLIMAP) Brown University Providence, RI 02912

Paul J. Crutzen National Center for Atmospheric Research P. O. Box 3000 Boulder, CO 80303

Derek M. Cunnold Dept. of Meteorology MIT Cambridge, MA 02139

Pythagoras Cutchis Institute for Defense Analyses 400 Army-Navy Drive Arlington, VA 22202

R. J. Cvetanović National Research Council of Canada Ottawa, Ontario K1A 0R9, Canada

Ralph C. d'Arge Dept. of Economics The University of Wyoming Laramie, WY 82071

Eric Davies Rolls-Royce Aero Engines, Inc. 375 Park Avenue New York, NY 10022 Douglas D. Davis Dept. of Chemistry University of Maryland College Park, MD 20742

Robert E. Dean Aeronautical Systems Division Wright-Patterson AFB, OH 45433

Edward C. DeFabo USDA Plant Physiology Institute Beltsville, MD 20705

Thomas C. Degges Visidyne, Inc. 19 Third Ave. Burlington, MA 01803

D. Deirmendjian The Rand Corp. 1700 Main Street Santa Monica, CA 90406

F. P. DelGreco (OPR) Air Force Cambridge Research Labs Hanscom AFB Bedford, MA 01731

Edmond M. Dewan (LKC) Air Force Cambridge Research Labs Hanscom AFB Bedford, MA 01731

Noreen A, Dimond (LKC) Air Force Cambridge Research Labs Hanscom AFB Bedford, MA 01731

Clement Dousset Aérospatiale 37 bd. Montmorency Paris, France

William H. Duewer Lawrence Livermore Laboratory P. O. Box 808 Livermore, CA 94550

Maurice W. Dumais DOT Transportation Systems Center Kendall Square Cambridge, MA 02142

H. Frank Eden National Science Foundation Washington, DC 20550

Ralph G. Eldridge The Mitre Corp. Westgate Research Park McLean, VA 22101 Hugh W. Ellsaesser (L-142) Lawrence Livermore Lab P. O. Box 808 Livermore, CA 94550

Louis Elterman Air Force Cambridge Research Labs Hanscom AFB Bedford, MA 01731

James R. Engel Block Engineering, Inc. 19 Blackstone St. Cambridge, MA 02139

Ronald C. Englade Visidyne, Inc. 19 Third Ave. Burlington, MA 01803

J. Morley English Department of Engineering UCLA Los Angeles, CA 90024

W. F. J. Evans Atmospheric Environment Service 4905 Dufferin St. Downsview, Ontario M3H 5T4, Canada

Neil H. Farlow NASA Ames Research Center Moffett Field, CA 94035

Crofton B. Farmer Jet Propulsion Laboratory 4800 Oak Grove Drive Pasadena, CA 91103

James A. Fay
Dept, of Mechanical Engineering
MIT
Cambridge, MA 02139

R. Boyd Ferris ICAO 1080 University St. Montreal, Quebec, Canada

J. D. Few ARO, Inc. Arnold Engineering Development Center Tullahoma, TN 37389

Giorgio Fiocco Istituto di Fisica Università di Roma Rome, Italy

A. K. Forney (AFS-141)
DOT Federal Aviation Administration
800 Independence Ave., SW
Washington, DC 20591

Daryl E. Freeman Air Force Cambridge Research Labs Hanscom AFB Bedford, MA 01731

James P. Friend Dept. of Chemistry Drexel University Philadelphia, PA 19104

Alvin F. Futtrell (ARD-410) Federal Aviation Administration 2100 Second St., SW Washington, DC 20590

Charles C. Gallagher Air Force Cambridge Research Labs Hanscom AFB Bedford, MA 01731

John S. Garing (OP) Air Force Cambridge Research Labs Hanscom AFB Bedford, MA 01731

David Garvin (B152) Chemistry Building National Bureau of Standards Washington, DC 20234

Robert Gelinas Science Applications, Inc. P. O. Box 34 Pleasanton, CA 94566

Ali Ghovanlou MITRE Westgate Research Park McLean, VA 22101

Frank W. Gibson Air Force Cambridge Research Labs Hanscom AFB Bedford, MA 01731

John C. Gille National Center for Atmospheric Research P. O. Box 3000 Boulder, CO 80303

Forrest R. Gilmore R & D Associates P. O. Box 3580 Santa Monica, CA 90403

André Girard ONERA 29, ave. de la division Leclerc 92320 Châtillon-sur-Bagneux, France Howard Goldberg DGA International, Inc. 1225 19th St., NW Washington, DC 20036

Arnold Goldburg The Boeing Company P. O. Box 3999 Seattle, WA 98124

A. Goldman Dept. of Physics Denver University Denver, CO 80210

D. Golomb Air Force Cambridge Research Labs Hanscom AFB Bedford, MA 01731

R. E. Good Air Force Cambridge Research Labs Hanscom AFB Bedford, MA 01731

Philip Goodman Panametrics Inc. 221 Crescent St. Waltham, MA 02154

Gerald W. Grams
National Center for Atmospheric Research
P. O. Box 3000
Boulder, CO 80303

Donald D. Grantham Air Force Cambridge Research Labs Hanscom AFB Bedford, MA 01731

Carlton R. Gray MIT Draper Laboratory 75 Cambridge Pkwy. Cambridge, MA 02142

Richard S. Greenfield National Science Foundation 1800 G Street, NW Washington, DC 20550

Reynold Greenstone (AEQ-10) ORI, Inc. Federal Aviation Administration 800 Independence Ave., SW Washington, DC 20591

L. R. Greenwood (MS 217) NASA Langley Research Center Hampton, VA 23665 Alan J. Grobecker Manager, CIAP Department of Transportation 2100 Second St., SW Washington, DC 20590

Thomas J. Gross
Energy Research and Development Administration
Washington, DC 20545

Paul R, Guthals (MS 514) Los Alamos Scientific Laboratory P. O. Box 1663 Los Alamos, NM 87544

Joseph J. Gwiazdowski Department of Transportation 2100 Second St., SW Washington, DC 20590

J. Brooks Haberl General Electric Co. 100 Plastics Ave. Pittsfield, MA 01201

L. C. Hale Ionosphere Research Laboratory The Pennsylvania State University University Park, PA 16802

L. A. Hall Air Force Cambridge Research Labs Hanscom AFB Bedford, MA 01731

Robert F. Hampson, Jr. National Bureau of Standards Washington, DC 20234

Frederick A. Hanser Panametrics, Inc. 221 Crescent St. Waltham, MA 02154

Thomas M, Hard (641) DOT Transportation Systems Center Kendall Square Cambridge, MA 02142

Charles R, Hauer National Science Foundation 1800 G Street Washington, DC 20550

Julian Heicklen Ionosphere Research Laboratory The Pennsylvania State University University Park, PA 16802

Dr. Heinsheimer Atmospherics 7 John's Canyon Rd, Rolling Hills, CA 90274 Wayne S. Hering Air Force Cambridge Research Labs Hanscom AFB Bedford, MA 01731

Henry Hidalgo Institute for Defense Analyses 400 Army-Navy Drive Arlington, VA 22202

Henry B. Hinckley Union Carbide / MCA P. O. Box 8361 S. Charlestown, WV 25303

E. David Hinkley (183-30) Jet Propulsion Laboratory 4800 Oak Grove Drive Pasadena, CA 91103

Martin I. Hoffert Division of Applied Science New York University New York, NY 10003

Herbert S, Hoffman (LKC) Air Force Cambridge Research Labs Hanscom AFB Bedford, MA 01731

David J. Hofmann Dept, of Physics and Astronomy University of Wyoming Laramie, WY 82070

Joseph W. Howell 6512 Lily Dhu Lane Falls Church, VA 22044

Frank P. Hudson (1721) Sandía Laboratories P. O. Box 5800 Albuquerque, NM 87115

R. E. Huffman Air Force Cambridge Research Labs Hanscom AFB Bedford, MA 01731

John R. Hummel Ionosphere Research Laboratory Pennsylvania State University University Park, PA 16801

Donald M. Hunten Kitt Peak National Observatory 950 N. Cherry Ave, Tucson, AR 85717

Haruji Ishikawa Research Institute of Atmospherics Nagoya University Toyokawa Aichi, Japan 442 Tomizo Itoh Institute of Space and Aeronautical Science University of Tokyo 4-6-1, Komaba, Meguro-ku Tokyo, Japan 153

Ruprecht Jaenicke Max Planck-Institut Saar str. 23 D65 Mainz, Germany

Brian D. Jarman Institute for Defense Analyses 400 Army-Navy Drive Arlington, VA 22202

Ray E., Jensen NOAA Environmental Studies Service Center Texas A & M University College Station, TX 77843

René Joatton Aérospatiale France 37 boulevard Montmorency 75018 Paris, France

D. D. Job GTE Labs, Inc. 40 Sylvan Rd. Waltham, MA 02154

Harold S. Johnston Dept. of Chemistry University of California Berkeley, CA 94720

Richard Eric Jones Ministry of Transport CAPR, 8th Floor Tower C Place de Ville Ottawa, Ontario K1A 0N8, Canada

Sheldon L. Kahalas Mt. Auburn Research Assoc. Inc. 385 Elliot St. Newton, MA 02164

Arthur J. Kantor Air Force Cambridge Research Labs Hanscom AFB Bedford, MA 01731

D. Katayama Air Force Cambridge Research Labs Hanscom AFB Bedford, MA 01731

Frederick Kaufman Dept, of Chemistry University of Pittsburgh Pittsburgh, PA 15260 Ryuma Kawamura Institute of Space and Aeronautical Science University of Tokyo 6-1 Komaba-4, Meguro-ku Tokyo, Japan 153

Thomas W. Kelly Air Force Cambridge Research Labs Hanscom AFB Bedford, MA 01731

Gerard L. Kernan Irish Development Agency St. Martin's House Waterloo Rd. Dublin 4, Ireland

James King, Jr. NASA Headquarters 600 Independence Ave., SW Washington, DC 20546

I. L. Kofsky Photometrics Inc. 442 Marrett Rd. Lexington, MA 02173

Charles E. Kolb Aerodyne Research, Inc. 20 South Ave. Burlington, MA 01803

Bernard Laporte French Military Mission 1228 Alton Pl., NW Washington, DC 20016

Ronald Lau Systems Control Inc. 1801 Page Mill Rd. Palo Alto, CA 94304

Vernon J. Laurie (RD-687) Environmental Protection Agency 401 M Street, SW Washington, DC 20460

Allan Lazrus National Center for Atmospheric Research P. O. Box 3000 Boulder, CO 80303

Francis J. LeBlanc Air Force Cambridge Research Labs Hanscom AFB Bedford, MA 01731

Richard L. Lehman
National Oceanic and Atmospheric Administration
Department of Commerce
Washington, DC 20034

C. E. Leith
National Oceanic and Atmospheric Administration
Department of Commerce
Washington, DC 20034

Hiram Levy II NOAA Geophysical Fluid Dynamics Laboratory Princeton University P. O. Box 308 Princeton, NJ 08540

Erwin A. Lezberg NASA Lewis Research Center 21000 Brookpark Rd. Cleveland, OH 44135

Edward Lilley Harvard Observatory 60 Garden St. Cambridge, MA 02138

Carl Lindström Swedish Embassy 600 New Hampshire Ave., NW Washington, DC 20037

Ernest V. Loewenstein 57 Hyde St. Newton, MA 02161

Max Loewenstein (245-5) NASA Ames Research Center Moffett Field, CA 94035

Carl Lorenzen
Department of Oceanography
University of Washington
Seattle, WA 98195

D. J. Lovell Barton Rd. Stow, MA 01775

Iver A. Lund Air Force Cambridge Research Labs Hanscom AFB Bedford, MA 01731

Frank E. Lundin, Jr. Food and Drug Administration 5600 Fishers Lane Rockville, MD 20852

Frederick M. Luther Lawrence Livermore Laboratory P. O. Box 808 Livermore, CA 94550

Michael C. MacCracken (L-142) Lawrence Livermore Laboratory P. O. Box 808 Livermore, CA 94550 Eleanor J. Macdonald University of Texas Cancer Center – M.D.A. Houston, TX 77025

Gordon J. F. MacDonald Department of Earth Sciences Dartmouth College Hanover, NH 03755

Lester Machta NOAA Air Resources Laboratory 8060 Thirteenth St. Silver Spring, MD 20910

Jerry D. Mahlman NOAA Geophysical Fluid Dynamics Laboratory Princeton University Box 308 Princeton, NJ 08540

Harvey L. Malchow MIT Draper Laboratory 75 Cambridge Pkwy. Cambridge, MA 02142

R. Carroll Maninger (L-340) Lawrence Livermore Laboratory P. O. Box 808 Livermore, CA 94550

Oscar P. Manley Visidyne, Inc. 19 Third Ave. Burlington, MA 01803

Howard Margolis Department of Political Science MIT Cambridge, MA 02139

Frederick F. Marmo DOT Transportation Systems Center Kendall Square Cambridge, MA 02142

Ronald J. Massa Dynatrend Inc. 131 Middlesex St. Burlington, MA 01803

John Mastenbrook Naval Research Laboratory Washington, DC 20375

John McAuley British Embassy 3100 Massachusetts Ave. Washington, DC 20008

C. Thomas McElroy Dept. of Physics University of Toronto Toronto, Ontario M5S 1A7, Canada Robert A. McClatchey Air Force Cambridge Research Labs Hanscom AFB Bedford, MA 01731

John C, McConnell York University 9700 Keele St. Downsview, Ontario M3J 1P3, Canada

Mike McGhan Utah State University Logan, UT 84321

W. K. McGregor ARO, Inc. Arnold Engineering Development Center Tullahoma, TN 37389

Paul Meakin Central Research and Development Dept. E. I. du Pont de Nemours & Co. Wilmington, DL 19898

Lawrence R. Megill National Science Foundation 1800 G. St., NW Washington, DC 20550

Frederick A. Meister (APD-1) DOT Federal Aviation Administration 800 Independence Ave., SW Washington, DC 20591

Valentin Meleshko Main Geophysical Observatory 7 Karbysheva Leningrad, USSR

Brig. Gen. Martin Menter (Ret.) National Academy of Sciences 2101 Constitution Ave., NW Washington, DC 20418

Tom Mikus Dept. of Mechanical Engineering MIT Cambridge, MA 02139

Alvin J. Miller Upper Air Branch NOAA National Weather Service 5200 Auth Rd. Washington, DC 20233

Réné H. Miller Dept. of Aeronautics MIT Cambridge, MA 02139

William J. Miller AeroChem Research Labs P. O. Box 12 Princeton, NJ 08540 Yale Mintz Dept, of Meteorology UCLA Los Angeles, CA 90024

Mario J. Molina Dept. of €hemistry University of California Irvine, CA 92664

Yasuhiro Morita Research Institute of Atmospherics Nagoya University Toyokawa Aichi, Japan 442

James M. Morris DOT Transportation Systems Center Kendall Square Cambridge, MA 02142

H. Moses Air Force Cambridge Research Labs Hanscom AFB Bedford, MA 01731

Walter J. Moxim NOAA Geophysical Fluid Dynamics Lab Princeton University P. O. Box 308 Princeton, NJ 08540

Richard W. Munt Environmental Protection Agency 2565 Plymouth Rd. Ann Arbor, MI 48105

Edmond Murad (LKB) Air Force Cambridge Research Labs Hanscom AFB Bedford, MA 01731

David G. Murcray Denver Research Institute University of Denver Denver, CO 80210

Robert G. Murgatroyd British Meteorological Office 12 London Rd. Bracknell, Berks RG12 2SZ, England

D. Stuart Nachtwey (DD7) NASA Johnson Space Center Houston, TX 77058

Richard Nadile Air Force Cambridge Research Labs Hanscom AFB Bedford, MA 01731 Rocco S, Narcisi (LKD) Air Force Cambridge Research Labs Hanscom AFB Bedford, MA 01731

Murali Natarajan NASA Lewis Research Center 21000 Brookpark Rd. Cleveland, OH 44135

Arthur W. Nelson Pratt & Whitney Aircraft Division United Technologies 400 Main St. East Hartford, CT 06108

Capt. Jack H. Nelson Office of Naval Research 495 Summer St. Boston, MA 02210

Reginald E. Newell Dept. of Meteorology MIT Cambridge, MA 02139

Marcel Nicolet Institut d'Aéronomie Spatiale 3, avenue Circulaire B-1180 Brussels, Belgium

Franklin E. Niles US Army Ballistics Research Lab Aberdeen Proving Ground, MD 21005

George F. Nolan Air Force Cambridge Research Labs Hanscom AFB Bedford, MA 01731

G. Burton Northam (401A) NASA Langley Research Center Langley Field Hampton, VA 23665

Toshihiro Ogawa Geophysics Research Laboratory University of Tokyo Hongo, Bunkyo-ku Tokyo, Japan

Robert C. Oliver Institute for Defense Analyses 400 Army-Navy Drive Arlington, VA 22202

J. J. Olivero Ionosphere Research Laboratory Pennsylvania State University University Park, PA 16802 Robert R. O'Neil Air Force Cambridge Research Labs Hanscom AFB Bedford, MA 01731

Fritz Ostherr Dynatrend Inc. 131 Middlesex St. Burlington, MA 01803

Hans-Karl Paetzold University of Cologne Albertus-Magnus-Platz D-500 Köln 41, West Germany

Jae H. Park College of William & Mary Williamsburg, VA 23185

Deran Pashayan (RD-684) Office of Research and Development EPA 401 M St., SW Washington, DC 20460

C. K. Patel (4E-436) Bell Labs Holmdel, NJ 07733

M. A. Pathak Harvard Medical School Massachusetts General Hospital Boston, MA 02114

James W. Patmore Systems Control, Inc. 1801 Page Mill Road Palo Alto, CA 94304

Clarence W. Patten ORI 4506 Duncan Drive Annandale, VA 22003

John F. Paulson (LKB) Air Force Cambridge Research Labs Hanscom AFB Bedford, MA 01731

Rudolf Penndorf 148 Oakland Street Wellesley Hills, MA 02181

Theodore J. Pepin
Dept. of Physics and Astronomy
University of Wyoming
Laramie, WY 82070

Porter J. Perkins NASA Lewis Research Center 21000 Brookpark Rd. Cleveland, OH 44135 Millard Fillmore Perry Perry Associates, Inc. R. D. #2, Rosewood Lane Cumberland, RI 02864

Steve A. Piacsek Naval Research Laboratory Washington, DC 20375

Josef Podzimek Cloud Physics Research Center University of Missouri Rolla, MO 65401

Charles Polk
Dept, of Electrical Engineering
University of Rhode Island
Kingston, RI 02881

John A. Polutchko Dynatrend, Inc. 131 Middlesex Street Burlington, MA 01803

Jean-Pierre Pommereau CNRS 91370 Verrières-le-Buisson, France

I. G. Poppoff (245-10) NASA Ames Research Center Moffett Field, CA 94035

A. L. Powell Office of Naval Research 495 Summer St. Boston, MA 02210

Jerome Pressman Pressman Enterprises 4 Fessenden Way Lexington, MA 02173

Ronald G. Prinn Dept. of Meteorology MIT Cambridge, MA 02139

Larry A. Pugh The Ohio State University 174 W. 18th Ave. Columbus, OH 43210

Larisa Rakipova Main Geophysical Observatory 7 Karbysheva Leningrad, USSR

V. Ramanathan NASA Langley Research Center Hampton, VA 23665 K. Narahari Rao Physics Department The Ohio State University Columbus, OH 43210

Odell F. Raper Jet Propulsion Laboratory 4800 Oak Grove Dr. Pasadena, CA 91103

Elmar R. Reiter Dept. of Atmospheric Science Colorado State University Fort Collins, CO 80523

Ellis E. Remsberg NASA Langley Research Center Hampton, VA 23665

Ray T. Reynolds NASA Ames Research Center Moffett Field, CA 94035

Edward Ricco Environics Branch Air Force Weapons Lab Kirtland AFB, NM 87117

Brian A. Ridley
Department of Chemistry
York University
4700 Keele Street
Downsview, Ontario M3J 1P3, Canada

James M. Rosen
Dept. of Physics and Astronomy
University of Wyoming
Laramie, WY 82070

Norman W. Rosenberg Air Force Cambridge Research Labs Hanscom AFB Bedford, MA 01731

Laurence S, Rothman Air Force Cambridge Research Labs Hanscom AFB Bedford, MA 01731

F. Sherwood Rowland Dept. of Chemistry University of California Irvine, CA 92664

Richard A. Rudey NASA Lewis Research Center 21000 Brookpark Rd. Cleveland, OH 44135 R. W. Rummel Trans World Airlines, Inc. 605 Third Avenue New York, NY 10016

Philip B. Russell Stanford Research Institute 333 Ravenswood Ave, Menlo Park, CA 94025

Edward S. Sarachik Center for Earth and Planetary Physics Harvard University Cambridge, MA 02138

Howard F. Savage (245-5) NASA Ames Research Center Moffett Field, CA 94035

Robert N. Schainker Systems Control Inc. 1801 Page Mill Road Palo Alto, CA 94304

H. I. Schiff
Dept. of Chemistry
York University
4700 Keele St.
Downsview, Ontario M3J 1P3, Canada

Michael E. Schlesinger Dept, of Meteorology UCLA Los Angeles, CA 90024

Marion F. Schuler HSS Inc. 2 Alfred Circle Bedford, MA 01730

C. John Scott
Bristol Engine Division
Rolls Royce (1971) Ltd.
P. O. Box 3
Filton, Bristol BS12 7QE, England

William A. Sedlacek (MS 514) Los Alamos Scientific Labs P. O. Box 1663 Los Alamos, NM 87544

John E. A. Selby Air Force Cambridge Research Labs Hanscom AFB Bedford, MA 01731

Bach Sellers Panametrics Inc. 221 Crescent Street Waltham, MA 02154 Edmund Sellman (AEQ-200) Federal Aviation Administration 800 Independence Ave., SW Washington, DC 20591

Ralph Shapiro Air Force Cambridge Research Labs Hanscom AFB Bedford, MA 01731

Ramesh D. Sharma Physics Department MIT Cambridge, MA 02139

Alan W. Shaw Utah State University Logan, UT 84322

Eric P. Shettle Air Force Cambridge Research Labs Hanscom AFB Bedford, MA 01731

T. Shimazaki NASA Ames Research Center Moffett Field, CA 94035

Ven H. Shui AVCO Everett Research Labs. 2385 Revere Beach Parkway Everett, MA 02149

Robert Silberglied Museum of Comparative Zoology Harvard University Cambridge, MA 02138

Ronald Smelt Lockheed Aircraft Corp. Box 551 Burbank, CA 91520

Henry J. P. Smith Visidyne Inc. 19 Third Ave. Burlington, MA 01803

Marvin L. Smith (KBA-1B) Pratt & Whitney Aircraft United Technology 400 Main St. East Hartford, CT 06108

Cdr. William L. Smith (Code 465) Office of Naval Research 800 N. Quincy St, Arlington, VA 22217 Igor Sobolev Kaiser Aluminum & Chemical Corp. P. O. Box 870 Pleasanton, CA 94566

Deborah F, Sola ORI, Inc. 800 Independence Ave., SW Washington, DC 20591

J. R. Soulen Pennwalt, Inc. 900 First Ave. King of Prussia, PA 19406

Kenneth C. Spengler American Meteorological Society 45 Beacon St. Boston, MA 02108

R. Scott Stahr Eastern Airlines, Inc. c/o Miami International Airport Miami, FL 33148

A. T. Stair, Jr. Air Force Cambridge Research Labs Hanscom AFB Bedford, MA 01731

Kenneth J. Stein Aviation Week 1221 Ave. of the Americas New York, NY 10020

C. G. Stergis Air Force Cambridge Research Labs Hanscom AFB Bedford, MA 01731

Charles B. Stewart Boeing Commercial Airplane Company P. O. Box 3707 Seattle, WA 98124

Richard W. Stewart NASA Goddard Institute for Space Studies 2880 Broadway New York, NY 10025

Richard S. Stolarski (MS 624) NASA Goddard Space Flight Center Greenbelt, MD 20771

William E. Stoney
Deputy Director
Office of the Director of Defense Research and Engineering
The Pentagon (3E 1044)
Washington, DC 20301

Darrell F. Strobel (Code 7750) Naval Research Laboratory Washington, DC 20375 Richard L. Strombotne (TST-46) Department of Transportation 400 Seventh St., SW Washington, DC 20590

J. C. Sturm DOT Transportation Systems Center Kendall Square Cambridge, MA 02142

Simeon R. Stutter Bristol Engine Division Rolls Royce (1971) Ltd. P. O. Box 3 Filton, Bristol BS12 7QE, England

Jack A. Suddreth NASA Headquarters 600 Independence Ave., SW Washington, DC 20546

Edward M. Sullivan NASA Langley Research Center Hampton, VA 23665

Walter Sullivan The New York Times Times Square New York, NY 10036

N. Sundararaman ORI, Inc. 800 Independence Ave., SW Washington, DC 20591

Walter C. Swan (MS 77-12) Boeing Commercial Airplane Company P. O. Box 3707 Seattle, WA 98124

Mary Ann Sweeney (Org. 5241) Sandia Laboratories P. O. Box 5800 Albuquerque, NM 87115

William Swider Air Force Cambridge Research Labs Hanscom AFB Bedford, MA 01731

Akira Takeishi Japan Air Lines, Ltd. 655 Fifth Ave. New York, NY 10022

Sanzo Takezawa Air Force Cambridge Research Labs Hanscom AFB Bedford, MA 01731

Raja K. Tallamraju High Altitude Engineering Laboratory University of Michigan Ann Arbor, MI 48105 Yoshio Tanaka Air Force Cambridge Research Labs Hanscom AFB Bedford, MA 01731

Ming H, Tang (RT) NASA Headquarters 600 Independence Ave., SW Washington, DC 20546

Ogden Tanner 51 Lambert Rd. New Canaan, CT 06840

Raymond L. Taylor Physical Sciences Inc, 18 Lakeside Office Park Wakefield, MA 01880

Timothy F. Thomas Air Force Cambridge Research Labs Hanscom AFB Bedford, MA 01731

S. G. Tilford (7146) Naval Research Laboratory Washington, DC 20375

Takao Tohmatsu Faculty of Science University of Tokyo Bunkyo-ku Tokyo 113, Japan

C. N. Touart Air Force Cambridge Research Labs Hanscom AFB Bedford, MA 01731

Richard Tousey (7140) U.S. Naval Research Laboratory Washington, DC 20375

Daniel Trainor AVCO Everett Research Labs 2385 Revere Beach Parkway Everett, MA 02149

S. C. Traugott Martin Marietta Laboratories 1450 S. Rolling Rd. Baltimore, MD 21227

Charles C. Troha (ARD-510) DOT Federal Aviation Administration 2100 Second St., SW Washington, DC 20590

A. F. Tuck (Met 020) UK Meteorological Office London Rd. Bracknell, Berks RG12 2SZ, England Richard Turco R&D Associates 525 Wilshire Blvd. Santa Monica, CA 90403

Paul F. Twitchell Office of Naval Research 495 Summer St. Boston, MA 02210

Robert L. Underwood TRW, Inc. 10880 Wilshire Blvd. Los Angeles, CA 90024

Frederick Urbach, M.D. Skin & Cancer Hospital 3322 N. Broad St. Philadelphia, PA 13140

Douglas I, Vickery British Aircraft Corporation Filton House, Filton Bristol, England BS99 7AR

Herbert Viebrock (ML) EPA Environmental Research Center Research Triangle Park, NC 27711

Bill Viezee Stanford Research Institute 333 Ravenswood Ave. Menlo Park, CA 94025

Jerome Vigil Block Engineering Inc. 19 Blackstone St. Cambridge, MA 02139

Frederic E. Volz Air Force Cambridge Research Labs Hanscom AFB Bedford, MA 01731

C. W. von Rosenberg, Jr. AVCO Everett Research Labs 2385 Revere Beach Pkwy. Everett, MA 02149

F. O. Vonbun NASA Headquarters 600 Independence Ave., SW Washington, DC 20546

R. K. R. Vupputuri Atmospheric Environment Service 4905 Dufferin St. Downsview, Ontario M3H 5T4, Canada

Stacy Walters Space Physics Research Lab. University of Michigan Ann Arbor, MI 48105 Ronald E. Waltz Visidyne, Inc. 19 Third Ave. Burlington, MA 01803

Anthony B. Wassell Rolls-Royce (1971) Ltd. P. O. Box 31 Derby, Derbyshire DE2 8BJ, England

Robert T. Watson Jet Propulsion Laboratory 4800 Oak Grove Drive Pasadena, CA 91103

L. H. Weeks Air Force Cambridge Research Labs Hanscom AFB Bedford, MA 01731

James A. Weinman Dept. of Meteorology University of Wisconsin Madison, WI 53706

William T. Westfield (ARD-550) DOT Federal Aviation Administration 2100 Second St., SW Washington, DC 20590

Raymond Wexler NASA Goddard Space Flight Center Greenbelt, MD 20771

Cynthia K. Whitney MIT Draper Laboratory 75 Cambridge Pkwy. Cambridge, MA 02142

R. C. Whitten NASA Ames Research Center Moffett Field, CA 94035

George F. Widhopf The Aerospace Corporation 2350 E. El Segundo Blvd. El Segundo, CA 90245

Herbert L. Wiser (RD-672) Environmental Protection Agency 401 M St., SW Washington, DC 20460

Lawrence B, Woolaver HSS Inc. 2 Alfred Circle Bedford, MA 01730 G. Wijntjes Block Engineering 19 Blackstone Street Cambridge, MA 02139

Howard B. Winkler Dynatrend Inc. 131 Middlesex St. Burlington, MA 01803

Steven C. Wofsy Center for Earth and Planetary Physics Harvard University Cambridge, MA 02138

Albert D. Wood Office of Naval Research 495 Summer St. Boston, MA 02210

Neil M. Woodroffe Embassy of Australia 1601 Massachusetts Ave., NW Washington, DC 20036

Mao-Fou Wu Environmental Research & Technology 696 Virginia Road Concord, MA 01742

Donald J. Wuebbles (L-142) Lawrence Livermore Laboratory P. O. Box 808 Livermore, CA 94550

Samuel Yee Air Force Cambridge Research Labs Hanscom AFB Bedford, MA 01731

Kouichi Yoshino Air Force Cambridge Research Labs Hanscom AFB Bedford, MA 01731

Robert A. Young IntraSpace International P. O. Box 1691 Boulder, CO 90307

J. Ronald V. Zaneveld Oregon State University Corvallis, OR 97331

Samuel P. Zimmerman Air Force Cambridge Research Labs Hanscom AFB Bedford, MA 01731

DETAILED AUTHOR INDEX FOR ALL CIAP CONFERENCE PROCEEDINGS

Ackerman, M.	III 254, IV 438	Corrin, M.	II 57
Alyea, F.N.	III 403	Cotton, G.	IV 405
Anderson, L.B.	II 263	Cox, F.W.	II 194
Anderson, J.G.	IV 366, 458	Creutz, E.C.	IV 25
Anderson, R.J., Jr.	III 582	Crocker, T.D.	III 593
Arakawa, A.	I 194	Cropper, M.I.	IV 104
Bahr, D.W.	IV 109	Crutzen, P.J.	1 80, II 154, IV 264
Baluteau, JP.	II 99	Cunnold, D.M.	III 403
Barker, D.B.	II 86, III 184, IV 432	Danielsen, E.F.	III 83
Barkstrom, B.R.	IV 224	d'Arge, R.C.	III 564, IV 97
Barnes, J.L.	III 573	Davidson, D.L.	II 180
Barrett, E.W.	II 34	Davies, R.E.	III 523, IV 66
Bartholic, J.F.	II 394, III 498	Davis, D.D.	II 126, III 124, IV 372
Bauer, E.	II 254, IV 354	Davis, R.E.	IV 470
Bell, F.W.	III 612	Deaven, D.	III 83
Bell, J.A.		Delattre, P.	III 168
Berger, D.	IV 470	Dewan, E.M.	III 91
	III 523		
Biggs, R.H.	II 394, III 498, IV 62	Dickinson, R.E.	I 148
Birch, J.R.	III 197	Dütsch, H.U.	II 106
Birks, J.	II 340	Dyer, A.J.	II 407
Black, G.	II 144	Ehhalt, D.H.	III 153
Blamont, J.	II 407	Ellsaesser, H.W.	III 273
Blasing, T.J.	III 550	English, J.M.	III 16, IV 118
Bloxam, R.M.	IV 454	Erdmann, R.C.	1 251
Blum, H.F.	II 373, III 536	Evans, W.F.	IV 412
Bortner, M.H.	III 117	D.L. D	
Borucki, W.J.	III 342, IV 332	Fabian, P.	III 103
Boughner, R.E.	IV 224	Farmer, C.B.	II 65, III 234, IV 449
Boville, B.W.	IV 55	Fernald, F.G.	III 318
Brewer, A.W.	III 257, 271, IV 454	Ferrar, T.A.	III 593
Bricard, J.	III 168	Ferris, R.B.	IV 25
Brun, E.A.	IV 25, 45	Ferry, G.V.	III 310
Broderick, A.J.	II 13, III 67	Few, J.D.	II 214
Brooks, J.N.	II 86, III 184, IV 432	Fiocco, G.	IV 492
Bruin, J.T.	IV 417	Fischer, S.D.	II 126, IV 372
Bussoletti, E.	II 99	Fleming, J.W.	III 197
Cadle, R.D.	I 130, II 57	Fontanella, JC.	III 217, 254
Caldwell, M.M.	II 388, III 482	Forney, A.K.	I 24, II 169
Calkins, J.	III 505	Friend, J.P.	I 71
Callis, L.B.	IV 224	Frimout, D.	III 254
Campbell, W.F.	III 482	Fritts, H.C.	III 550
Cannon, R.H.	I 1, IV 25	Frush, C.L.	III 318
Castleman, A.W., Jr.		Gal-Chen, T.	III 450
Chang, J.S.	II 338, III 323, 330, IV 175	Gandrud, B.W.	III 161, IV 465
Cicerone, R.J.	IV 280	Garvin, D.	II 114, IV 391
Collis, R.T.H.	IV 497	Gilmore, F.R.	IV 354
Conti, R.J.	II 263	Girard, A.	III 217, 254
Cooper, C.F.	III 550	Goldman, A.	II 86, III 184, 246, IV 432
Coroniti, S.C.	II 13	Goldstein, H.W.	III 117
colonia, o.c.	11 13	Column, II.W.	III II 7

Good, R.E.	II 247	Leith, C.E.	IV 195
Gramont, L.	III 247 III 217	Lem, H.Y.	III 310
Grams, G.	IV 492	Léna, P.	II 99
Green, A.E.S.	III 518	Lephardt, J.O.	II 126
Greenspan, L.	II 22	Libby, W.F.	III 103
Grissom, J.L.	II 99	Loewenstein, M.	III 213, IV 422, 425
Grobecker, A.J.	12, II 2, 407, 416, III 1, IV 2	London, J.	II 154
Grobman, J.	I 25, III 49	Louisnard, N.	III 217, 254
		Lueb, R.H.	III 153
Haberl, J.B.	IV 519	Luther, F.M.	III 437, IV 242
Hake, R.D., Jr.	III 303, IV 497	MacCracken, M.C.	
Hall, R. Halsey, L.H.	III 298 III 498	MacDonald, G.J.	II 298, III 437, IV 183 IV 25
		Machado, E.S.	IV 372
Hampson, R.F., Jr Hanser, F.A.	III 129, IV 398	Machta, L.	II 47, IV 405
Harries, J.E.	II 78, III 197	Madelaine, G.	III 168
Hasegawa, S.	II 78, III 197	Mahlman, J.D.	I 186, II 321, IV 132
Hass, W.	IV 405		
		Manabe, S.	I 186
Heath, D.F.	1 226	Margitan, J.J.	IV 366
Heck, W.	III 102	Marten, A.	II 99
Heidt, L.E.	III 153	McConnell, J.C.	IV 417
Herman, B.M.	III 422	McElroy, C.T.	III 257, 271, IV 454
Herron, J.T.	II 126	McElroy, M.B.	I 260, II 154, IV 286
Hesstvedt, E.	II 285	McGregor, W.K.	II 214
Hilst, G.R.	II 351	Megill, L.R.	11 146, III 193
Hofmann, D.J.	II 23, III 284, IV 527	Meister, F.A.	IV 25
Hogan, P.	III 124	Mintz, Y.	I 194, IV 201
Hoshizaki, H.	II 263	Mo, T.	III 518
Hudson, F.P.	I 115, II 237	Mohnen, V.A.	IV 478
Huie, R.E.	II 126	Moriarty, A.	III 124
Hunten, D.M.	IV 147	Morita, Y.	IV 530
Hurn, R.W.	II 194	Morris, M.S.	III 70
Ingebo, R.D.	III 49	Moss, D.G.	III 197
Ishikawa, H.	IV 530	Mugnai, A.	IV 492
Ivlev, L.S.	III 143	Murcray, D.G.	II 86, III 184, 246, IV 432
		Murcray, F.H.	II 86, III 184, 246, IV 432
Jensen, R.E.	IV 87	Murgatroyd, R.J.	IV 25, 39
Johnston, H.S.	I 90, II 340, 407, III 264, 323, IV 156	Muller, C.	III 254
		Nachtwey, D.S.	IV 79
Katayama, A.	I 194	Narcisi, R.	II 57
Kattenhorn, D.	IV 156	Neely, J.	II 180
Kaufman, F.	II 154, IV 366	Neill, G.F.	III 197
Kellogg, W.	II 407	Newell, R.E.	I 165
Kernan, G.L.	IV 118	Newson, R.L.	III 461
Kerr, J.B.	III 257, 271, IV 412	Nicolet, M.	1 44, II 154, IV 292
Knipling, E.B.	II 379	Nikolsky, G.A.	III 143
Komhyr, W.	IV 405	Northam, G.B.	IV 509
Kondratyev, K.Ya		Norton, R.H.	IV 449
Kosters, J.J.	III 184, IV 432		
Kroening, J.L.	II 23	Oak Ridge Systems E	
Kuhn, P.M.	II 34	Oliver, R.C.	IV 335
Kurylo, M.J.	IV 391	Paddock, J.P.	III 213
Lazrus, A.L.	III 161, IV 465	Panofsky, H.	III 102
Leach, J.F.	III 70	Parton, W.J.	III 550

D			
Payne, W.A.	II 126	Starr, C.	I 251
Pepin, T.J.	II 126, III 284	Steber, W.C., Jr.	II 1
Peskin, H.M.	II 404	Stief, L.J.	II 126
Phillips, N.A.	III 403	Stocker, R.N.	III 184
Pierce, E.T.	II 57	Stolarski, R.S.	IV 280
Podzimek, J.	IV 519	Stone, N.W.B.	II 78, III 197
Pokrovsky, O.M.	IV 254	Stone, P.H.	III 475
Pollack, J.B.	III 457	Stoner, W.	III 550
Poppoff, I.G.	I 217, III 213	Stoney, W.E.	IV 24
Porter, W.R.	IV 104	Sundararaman, N.	IV 234
Pinnick, R.G.	III 298	Swann, N.R.W.	III 197
Prinn, R.G.	III 403	Takagi, M.	IV 530
Prusaczyk, J.E.	II 126	Tang, I.N.	IV 470
Ramanathan, V.	IV 224	Taylor, T.D.	III 376
Rao, K.N.	III 173	Telegadas, K.	II 47
Raper, O.F.	II 65, III 234, IV 449	Tohmatsu, T.	IV 58
Reiter, E.R.	II 407, III 79	Toon, O.B.	III 457
Remsberg, E.E.	IV 509	Toth, R.A.	II 65, III 234
Ridley, B.A.	II 146, III 193, IV 417	Tuck, A.F.	IV 303
Roper, N.	III 153	Turco, R.P.	IV 332
Rosen, J.M.	II 23, III 284, 298, IV 527	Underwood, R.L.	II 230
Rosenberg, N.W.	III 91	Urbach, F.	III 523, IV 66
Rummel, R.W.	I 34, IV 25, 127		
Russell, P.B.	III 303, IV 497	Van Allen, J.	III 184, 246
Sakamoto, C.		Venkateswaran, S.V.	III 428
Savage, H.F.	III 539	Viezee, W.	III 303, IV 497
Schainker, R.B.	III 213, IV 422, 425	Vogh, J.W.	II 194
	III 575	Vupputuri, R.K.R.	III 390
Schiff, H.I.	II 146, III 193, 216, IV 417	Wardle, D.I.	IV 412
Schiff, R.L.	II 126, IV 372	Wardman, P.	III 70
Schmidt, S.C.	III 246	Warneck, P.	I 162
Schindler, R.A.	II 65, III 234	Warshaw, M.	II 363
Schlesinger, M.	V 201	Washington, W.M.	II 358
Schneider, S.H.	III 450	Watson, R.T.	IV 372
Schreuder, G.F.	III 550	Welge, K.H.	II 146
Schuster, B.G.	III 318	Wexler, A.	II 22
Sedlacek, W.A.	IV 465, 519	Whitten, G.	II 340, IV 156
Seiber, B.L. Seizinger, D.E.	II 214	Whitten, R.C.	III 342, IV 332, 425
Sekera, Z.	II 194	Widhopf, G.F.	III 376, IV 316
	I 140	Williams, M.R.	II 173
Sellers, B. Shaw, A.W.	III 129, IV 398	Williams, W.J.	II 86, III 184, 246, IV 432
Sheldon, D.R.	II 146, III 193	Wofsy, S.C.	III 359, IV 286
Shimazaki, T.	II 369	Wong, W.W.	II 126
Shipera, A.	II 291	Wood, B.J.	II 144
Sincer P	II 34	Woodard, R.	IV 465
	III 137	Wuebbles, D.J.	II 291
Steen W.B.	III 482	Yamamoto, G.	II 407
Storodensk M.A.	IV 254	Yung, Y.L.	IV 286
Stage: T.C.	II 144		
1000 7 M	III 550	Zahniser, M.S.	IV 366
	£ 243	Zich, J.	III 550
	III 550	Zimmerman, S.P.	II 247

INDEX OF FIRST AUTHORS, THIS VOLUME

Ackerman	438	Loewenstein 422	, 425
Anderson	366, 458	Luther	242
Bahr	109	MacCracken	183
Bauer	354	MacDonald (panel)	25
Biggs	62	Machta	405
Bloxam	454	Mahlman	132
Boville	55	Meister (panel)	25
Brun (panel)	25	Mintz	201
Brun	45	Mohnen	478
Callis	224	Murcray	432
Cannon (panel)	25	Murgatroyd (panel)	25
Castleman	470	Murgatroyd	39
Chang	175	Nachtwey	79
Creutz (panel)	25	Nicolet	292
Crutzen	264	Oliver	335
d'Arge	97	Podzimek	519
English	118	Remsberg	509
Evans	412	Ridley	417
Farmer	449	Rummel (panel)	25
Ferris (panel)	25	Rummel	127
Fiocco	492	Russell	497
Garvin	391	Sellers	398
Grobecker	1	Stolarski	280
Hofmann	527	Stoney (panel)	24
Hunten	147	Sundararaman	234
Ishikawa	530	Tohmatsu	58
Jensen	87	Tuck	303
Johnston	156	Urbach	66
Kondratyev	254	Watson	372
Lazrus	465	Whitten	332
Leith	195	Widhopf	316
		Wofsy	286

The complete author index to the four volumes of CIAP conference proceedings begins on page 551.

	S T.			č	£ .	= 1	2	Ē				, ·	Þ.	Ē					20	•					2	K	5	ī	£ "	P				*				
C Measures	7. Fig.			inches	inches	leet	yards	miles				square inches	square yards	square miles	acres				ounces	spunod	short tons				fluid ounces	pints	quarts	gallons	cubic feet	cubic yards				Fahrenheit	temperature	9.6 22 28	1.	
trsions from Metri	Multiply by	LENGTH		5.0	4.0	3.3	-	9.0		AREA		91.0			2.5		MASS (mainht)	THE MENT OF THE	0.035	2.2			VOLUME		0.03	2.1	1.06	97.0	*	1.3		TEMBERATIIRE (ATTENTAL	THAILDHE ISSEED	9/5 (then	900 35)	986	100	•
Approximate Conversions from Metric Measures	When You Know	١		millimeters	centimeters	meters	meters	kilometers				Square centimeters	Square meters	square kilometers	hectares (10,000 m			1	grams	kilograms	tonnes (1000 kg)			1	milliliters	liters	liters	liters	cubic meters	cubic meters		101		Celsius	temperature		2 8 8	
	Symbol			Ē	5	E	E	5			•	1 6.	'E	5	2				•	f kg	-				Ē	-	-		ີ∈ິ	È				o,			1 4	•
EZ :	zz t	z 	oz	1111			81		1111		91		ST IIII		• 1		EI	111111	1			0		6		8				9		11111		•		z	' wa	,
' ' 'l	Til	' ' ' 	Ţ''	'	Ί.	1.	7	T	"	""	1	6	Ί΄	"	1"	''	5	' '	Ϊ	'' '	'l'	' ' •	'I'	"	' '		' ' 3	'1	<u>'</u>	1'	'	' ' ;	•	171	' 'I		' ' ' ' inche	1
	Symbol					E	E	E	Ē			2	cm.	ΈÑ	~ E	2				. S	? -				Ē	Ē	Ē	-	-	-	_'	È	È		٥	,		
Measures	To Find					Centimeters	Centimeters	meters	kilometers				Square centimeters	square meters	Square kilometers	hectares				kiloorams	Tonnes				milliliters	milliliters	milliliters	liters	liters	liters	liters	cubic meters	cubic meters		Colsius	temperature		
rersions to Metric Measures	Multiply by		LENGTH			2.5	93	6.0	1.6	4064	AUEA		0.0	60.0	2.6	0.4		MASS (weight)		0.45	60		VOLUME		•	15	8	0.24	0.47	6.95	3.8	0.03	6.0	TEMPERATURE (exact)	5/9 (after	subtracting 32)		
Approximate Conversions	When You Know					inches	feet	yards	miles		l		square inches	Square reed	square miles	acres		=	-	pounds	short tons	(2000 lb)			teaspoons	tablespoons	fluid cunces	sdno	pints	quarts	gallons	cubic feet	copic yards	TEMP	Fahrenheit	temperature		
	1					•		P	ē			-	27	-	2 6				,						ds	Thep	fl 02		K	16	3.	13						

END

DATE FILMED O-80

DTIC